Daqing Yang
Douglas L. Kane *Editors*

Arctic Hydrology, Permafrost and Ecosystems

Springer

Arctic Hydrology, Permafrost and Ecosystems

Daqing Yang • Douglas L. Kane
Editors

Arctic Hydrology, Permafrost and Ecosystems

Springer

Editors
Daqing Yang
Watershed Hydrology and Ecology
Research Division
Water Science and Technology Directorate
Environment and Climate Change Canada
Victoria, BC, Canada

Douglas L. Kane
Water and Environmental Research Center
Institute of Northern Engineering
University of Alaska Fairbanks
Fairbanks, AK, USA

ISBN 978-3-030-50928-6 ISBN 978-3-030-50930-9 (eBook)
https://doi.org/10.1007/978-3-030-50930-9

This Springer imprint is published by the registered company Springer Nature Switzerland AG
The registered company address is: Gewerbestrasse 11, 6330 Cham, Switzerland

Preface

The Arctic is an integrated system (physical, biological, and chemical) with its elements closely linked by its atmosphere, ocean, and land. The Arctic system has experienced significant changes over the past several decades. To better understand the changes, causes, and consequences, it is important to regularly review and update the research progress of the Arctic system science. This book, drawing on the most recent research results across the circumpolar regions, provides a comprehensive, up-to-date assessment of the key terrestrial components of the Arctic system, i.e., hydrology, permafrost, and ecology. The chapters written by the leading (invited) scholars carefully examine Arctic climate variability/change, large river hydrology, lakes and wetlands, snow cover and ice processes, permafrost characteristics, vegetation/landscape changes, and the future trajectory of Arctic system evolution. The discussions cover the fundamental features and processes of the Arctic system, with a special focus on the critical knowledge gaps, i.e., the interactions and feedbacks among water, permafrost, and ecosystems, such as snowpack and permafrost changes and their impacts on basin hydrology and ecology, river flow, geochemistry, and energy fluxes to the Arctic Ocean, and the structure and function of Arctic ecosystem in response to changes in climate, hydrology, and permafrost conditions.

This book focuses on Arctic hydrology, permafrost, and ecosystem, and their key elements and components. There are different definitions for the Arctic. A common delineation of the Arctic is the Arctic Circle. This definition ignores large regions that experience the Arctic conditions but are outside this latitudinal margin. On the basis of different components of the Arctic system, some alternative boundaries have been suggested and used, such as North of 60° N, temperature isotherms, permafrost distribution, tundra and taiga snow regions, vegetation pattern or the tree line, and areas of surface water convergence and drainage into the Arctic Ocean. In the recent Arctic Freshwater Synthesis program, the Arctic is defined as the land areas contributing to the Arctic Freshwater System.

The scope of the chapters in the book covers the broader northern regions in consideration of many factors and elements of climate system, hydrology system, permafrost, and ecosystems across the high latitudes. There are some variations in terms of Arctic region among the sections of this book, depending on the Arctic system component of interest. We adopt a loose definition for the Arctic, because

Arctic system is closely linked and the interaction among the hydrology, permafrost, and ecosystem do occur within and outside of the traditional definition of the Arctic. Relative to a strict Arctic boundary, a broader definition (allowing some degree of flexibility) is a better way to provide the space necessary for comprehensive presentations and discussions of the connections among the sub-systems of the Arctic. For example, the freshwater-related chapters (Chaps. 6–13, 24–26) cover almost all the land areas with rivers directly or indirectly contributing flows to the Arctic Ocean and the northern seas. The source areas of the large watersheds expand to the mid-latitude regions, e.g., about 45 N in Siberia. Some large Arctic rivers pass through prairies (e.g., the Saskatchewan River that joins the Nelson River) and steppes (e.g., the Ob) in their upper courses. The climate-related subjects (Chaps. 1–4), such as the precipitation and evaporation chapters, discuss climatic datasets for the northern regions above 45 N, so as to cover the entire watersheds draining into the Arctic Ocean. The ecosystem chapters (Chaps. 18–23) also present regional analyses and results of phenology for the broad northern Eurasian continent.

Based on recent progress in our understanding of the complex interactions across the Arctic system, this book comprises 5 Parts, with 30 chapters, to systematically review, synthesize, and assess some major features and the changes in the system components; it also describes key processes and cross-system interactions within the changing Arctic environment.

Part I: Arctic Climate and Greenland (Chaps. 1 through 5) discusses key elements of Arctic climate system changes and their impacts on hydrology and ecosystems. Among the five chapters in this Part, Walsh (Chap. 1) addresses the critical issue of Arctic amplification of global warming and related climatic processes, including feedbacks associated with the loss of sea ice and snow cover, increase of atmospheric moisture, and the vertical temperature structure of the Arctic atmosphere. Precipitation plays a significant role in water/energy cycles and affects ecosystem function over the northern regions. Ye et al. (Chap. 2) provide a comprehensive overview of northern precipitation research, introduce existing and forthcoming data sources and their challenges across the Arctic, describe precipitation distribution characteristics, and discuss past changes and future predictions. Snow cover is most closely related with precipitation and temperature features in the cold climates. Brown et al. (Chap. 3) focus on regional snow cover changes and its impact on northern hydrology, and discuss future snow cover conditions. Zhang et al. (Chap. 4) review and synthesize evaporation processes and changes over the northern regions and watersheds, and highlight some important results from in situ observations over various land cover types, and large-scale land surface modeling and remote sensing analyses. Mernild et al. (Chap. 5) provide a review and update of glacier/ice sheet hydrology and their contributions to sea-level change and ocean circulation. They demonstrate the capability of the SnowModel/HydroFlow model framework and present key results of Greenland snow/ice melt processes and runoff contribution to sea level rise.

Part II: Hydrology and Biogeochemistry (Chaps. 6 through 13) focuses on issues of watershed hydrology, biogeochemistry, and water quality. The eight chapters cover important topics and research aspects. Rawlins et al. (Chap. 6) provide an overview of recent progress in Arctic hydrology research, particularly

the Freshwater Integration (FWI) within the Arctic Community-wide Hydrologic Analysis and Monitoring Program. They also discuss large-scale flow variability/trends and possible causes due to climate impact and human effect, and specifically examine discharge regimes and changes for the Lena and Yukon rivers. Shrestha et al. (Chap. 7) survey the range of hydrologic extremes occurring in Arctic rivers, including winter low flows, river ice-jam breakup spring floods, snowmelt peak spring/early summer flows, and in some instances, rainfall floods in summer. They conclude that climatological drivers mainly influence these extreme conditions, and in particular, warming climate and enhanced precipitation may cause substantial changes in the magnitude, variability, and timing of the extreme events. Peters et al. (Chap. 8) review research programs/progresses of environmental flows for the northern permafrost regions with a focus on North America. The main topics include cold regions hydro-ecology, history, and application of environmental flows in the northern regions, environmental flow guidelines and policy in the Arctic states, and riverine monitoring in northern regimes to support environmental flow frameworks. Yang et al. (Chap. 9) present qualitative assessment of large-scale snowcover data from remote sensing and Yukon river discharge response to seasonal snow cover changes. Yang et al. (Chap. 10) report northern river water temperatures and thermal regimes through data analysis and hydrologic modeling. O'Donnell et al. (Chap. 11) summarize the state of research linking watershed hydrology and biogeochemical cycling (organic carbon, nitrogen, phosphorus, and trace elements) in Arctic rivers, and how these processes are changing in response to changing climate and disturbance regimes, e.g., permafrost thaw and wildfire. Young et al. (Chap. 12) examine Arctic wetlands and lake-dynamics and climate change impacts, including snow and ice regimes and their changes. Yang et al. (Chap. 13) focus on river ice processes and changes through network observations, remote sensing, and modeling approaches across the northern regions and large watersheds.

Part III: Permafrost and Frozen Ground (Chaps. 14 through 17) examines permafrost processes and their impacts/linkages to regional/watershed hydrologic characteristics and changes. The four chapters review and describe key subjects of northern permafrost and hydrology. Yoshikawa and Kane (Chap. 14) describe permafrost classification, formation, and distribution of taliks and pingos over the northern regions. Zhao et al. (Chap. 15) review permafrost observation networks/programs and datasets, ground temperature variations, active layer changes, effect of snow cover on ground thermal regimes, ground ice distribution, carbon storage in frozen ground, and InSAR applications in the northern regions. Hiyama et al. (Chap. 16) discuss regional/basin scale permafrost-hydrology linkages and feedback processes, particularly the relationship between permafrost coverage and streamflow regime, detection of permafrost thawing trends from long-term streamflow data, determination of permafrost groundwater age, and water balance of northern permafrost basins. Kurylyk and Walvoord (Chap. 17) use field examples to discuss key processes and conditions that control groundwater dynamics in permafrost settings, and present an up-to-date synthesis of the

mathematical representation of heat transfer and groundwater flow in northern landscapes.

Part IV: Ecosystem Change and Impact (Chaps. 18 through 23) talks about the main features and changes in the northern ecosystem and its components. It has six chapters to present and discuss recent research and results. Ueyama et al. (Chap. 18) synthesize tower greenhouse gas and energy flux measurements in Alaska and Siberia, and combine in situ observations with remote sensing data. Delbart (Chap. 19) discusses spring season phenology of the large boreal ecosystems across the northern regions, including a remote sensing green-up retrieval and its validation with ground observations of the plant phenology. Kim et al. (Chap. 20) use satellite observations of vegetation greenness (EVI), sun-induced chlorophyll fluorescence (SIF), and gross primary productivity (GPP) to clarify regional patterns and recent variations in vegetation growth over the Arctic Boreal Vulnerability Experiment (ABoVE) domain. Kim et al. (Chap. 21) describe recent research in boreal forest ecosystem of Alaska, such as field survey and satellite observation of aboveground biomass, spatiotemporal variation in leaf area index, latitudinal gradients of phenology and winter–spring soil CO_2 emission, and successional changes in CO_2 and energy balance after forest fires. Young-Robertson et al. (Chap. 22) review recent work of northern ecohydrology of Interior Alaskan subarctic, and discover hydrological processes that are dominated by soil moisture storage in areas with permafrost and by ecological processes in areas without permafrost. Xu and Yang (Chap. 23) summarize a new development of watershed ecohydrology investigation, i.e., long-term discharge and NDVI (Normalized Difference Vegetation Index) data analysis for the Yukon river, and a strong seasonal consistency between NDVI and discharge, particularly during the early growing season.

Part V: Cross-System Linkage and Integration (Chaps. 24 through 30) aims to bring the above sections and discussions into the Arctic system framework, i.e., to examine the questions of system connection and integrations, and identify knowledge gaps and future research needs. Of the eight chapters in this Part, Shiklomanov et al. (Chap. 24) synthesize our knowledge and recent research results of river freshwater input into the Arctic Ocean, including regional flux and its change over space and time. They point out that Pan-Arctic river discharge changes (increases) were especially pronounced during the last 30 years, associated with most intense climate warming over the northern hemisphere and significant declines in sea ice extent over the Arctic Ocean. They also demonstrate great potential of the (remote sensed) sea surface salinity products in understanding the impact and linkage of river discharge to the coastal surface water salinity, and the variability in the Arctic Ocean freshwater system. Yang et al. (Chap. 25) present an overview of thermal regime and river heat/energy flux to the Arctic Ocean through data analysis and hydrological models across the Arctic domain. They also compare the results between the Siberian and North American Arctic watersheds/regions, and discuss the differences and changes in water temperature and heat flux due to climate variation and human effect. The other four chapters in this section concentrate on models and their applications that deal with the core issues of integration and interaction among Arctic water, permafrost, and ecosystems.

Park et al. (Chap. 26) assess various hydrologic models and their applications across the Arctic large watersheds, including the VIC and CHAGE model simulations of changes in key processes of the Arctic hydrology system, and provide important recommendations for further development and improvement of cold region hydrologic models. Li Z. et al. (Chap. 27) review regional climate models (RCM) design and performance in the high latitudes, and specifically discuss some key topics, such as the regional climate modeling in Canada, convection-permitting RCMs, and challenges and needs for future RCM development over the northern regions. Li Y. et al. (Chap. 28) showcase the evaluation of the retrospective, 4-km high-resolution simulation by the Weather Research Forecasting (WRF), and examine the dynamically downscaled regional climate change over western Canada, especially the Mackenzie River Basin (MRB) and Saskatchewan River Basin (SRB). Yi and Yuan (Chap. 29) focus on the terrestrial ecosystem models, in particular, the responses of boreal forest ecosystems and permafrost to climate change and disturbances. They describe a terrestrial ecosystem model with dynamic organic soil module (DOS-TEM) and its unique freezing–thawing algorithm, and present key results of its applications in boreal forests of Alaska. Finally, Saito et al. (Chap. 30) address the future trajectory of the Arctic climate system, i.e., a major issue for necessary adaptation to anticipated climate impacts at local (water security, hydropower, infrastructure, and human health) to global scale (greenhouse gas releases and sea-level rise). They highlight projections of changes in Arctic water cycle: precipitation, evapotranspiration, snow, river discharge, surface- and groundwater, and permafrost. They also discuss key uncertainties in model projections arising from the future emission scenarios and across-model differences, and emphasize critical gaps, challenges, and directions in Arctic environment research.

In summary, this book and its chapters with the most recent update of Arctic system status and its change provide Arctic residents, indigenous peoples, governments, and industries with important knowledge for adapting to climate warming. The information of datasets, models, and remote sensing advancement and capability are also useful for the regional/national research projects and assessment activities, such as those carried out regularly by the IPCC, the Arctic Council AMAP program, Climate and the Cryosphere (CliC), and Global Water and Energy Exchanges (GEWEX) Projects of the World Climate Research Programme (WCRP).

Editors
Victoria, Canada — Daqing Yang
Fairbanks, USA — Douglas L. Kane

The original version of the book was revised: The affiliation of the volume editor "Daqing Yang" has been updated. The correction to the book is available at https://doi.org/10.1007/978-3-030-50930-9_31

Acknowledgements

This book, with 30 chapters by more than 85 co-authors from 12 countries, is the outcome of international collaboration over past few years. As the editors, we are deeply thankful to the authors for their outstanding contribution and sincere dedication to Arctic hydrology, permafrost, and ecosystem research. Review and revision are the critical processes to ensure manuscript quality, and we greatly appreciate the reviewers of all chapters. Their valuable comments and suggestions have resulted in distinctive improvements in many chapters after necessary revisions by the authors. We would also like to thank many organizations and publishers who have permitted the use and inclusion of the unique illustrations and images with proper citations. We greatly appreciate the strong support and encouragement from the Watershed Hydrology and Ecology Research Division, Environment and Climate Change Canada; and Water and Environmental Research Center, the University of Alaska Fairbanks. We sincerely thank the editors and production coordinators at Springer, particularly Juliana Pitanguy and Ram Prasad Chandrasekar, for their effective work and deep commitment to produce this book to serve the international northern research community at large.

Finally, Dr. Rikie Suzuki, Japan Agency for Marine-Earth Science and Technology, was a key member of the editing team in the initial phase of the project during 2016–2017. He made important contributions to the book structure and content, including identification and invitation to key authors to take the lead on certain chapters. Rikie passed away in spring 2017 after fighting cancer bravely for many years. His research achievement in northern ecosystems has been extensively cited/reflected in many parts of the book. We are very grateful to have had the opportunity of working with him on this book project. We, together with the co-authors of the chapters, would like to dedicate this book to our dear colleague and close friend Rikie Suzuki.

Contents

Part I
Arctic Climate and Greenland

Arctic Climate Change, Variability, and Extremes

1

John E. Walsh

Abstract

Global warming over the past half century has been amplified in the Arctic, especially in the cold season. Other Arctic indicators, especially those of the cryosphere, show signals consistent with the warming of the past half century. This Arctic amplification of the warming arises from a number of processes in the climate system, including the feedbacks associated with the loss of sea ice and snow, the increase of atmospheric moisture, and the vertical temperature structure of the Arctic atmosphere. Ocean heat fluxes into the Arctic from the North Atlantic and North Pacific also appear to have contributed to the Arctic warming through a reduction of sea ice. Internal variability, which played a major role in Arctic warming during the early twentieth century, appears to have been a minor contributor to the more recent warming, which has also been associated with unprecedented extremes of Arctic temperature and sea ice. There is evidence for increased moisture content of the Arctic atmosphere and corresponding impacts on episodes of extreme warmth. The recent variations of Arctic temperature and associated variables fit well with the simulations of Arctic climate by global and regional climate models. Projected changes include a continued warming of the Arctic even under moderate mitigation scenarios, and an increase of Arctic precipitation consistent with the higher temperatures and atmospheric humidities.

J. E. Walsh (✉)
International Arctic Research Center, University of Alaska, 2160 Koyukuk Drive, Fairbanks, AK 99775, USA
e-mail: jewalsh@alaska.edu

D. Yang and D. L. Kane (eds.), *Arctic Hydrology, Permafrost and Ecosystems*,
https://doi.org/10.1007/978-3-030-50930-9_1

1.1 Introduction

While the subject of this volume is Arctic hydrology, temperature is a primary driver of many of the variations and trends in hydrology, especially in high latitudes where phase transitions between the solid and liquid phases of water are prominent and pervasive. Temperature's reach in the Arctic extends to changes in sea ice, snow cover, permafrost, glaciers and the Greenland Ice Sheet, with corresponding impacts on the ocean. Even the Arctic's dynamical connection to midlatitude climate and weather is related to temperature through the latitudinal dependence of warming and cooling, as discussed in Sect. 1.3.

Systematically compiled records of Arctic temperatures extend back only about 100 years, although the record lengths are shorter in some areas and extremely sparse over the high latitude oceans. Earlier expeditions and whaling activity provided occasional observations for specific marine locations, but these observations do not permit robust detection of changes. Inferences about Arctic temperatures over time periods longer than about 100 years are based on paleoclimatic reconstructions from proxy data (tree rings, sediments, diatoms, ice cores), some of which are heavily weighted toward the warm season. One such reconstruction by Kaufman et al. (2009) showed that the Arctic slowly cooled for much of the past 2000 years, consistent with earth-sun orbital changes, until a recent warming over the past 150 years or so. The warming is confirmed by instrumental data (e.g., Bekyraev et al. 2010) and is most striking in the past 50–60 years. As stated by the IPCC (2013), "Warming of the climate system is unequivocal, and since the 1950s, many of the observed changes are unprecedented over decades to millennia." The Arctic has warmed at about twice the global rate over the past 50–60 years, a pattern known as Arctic amplification. This warming is apparent in Fig. 1.1, which

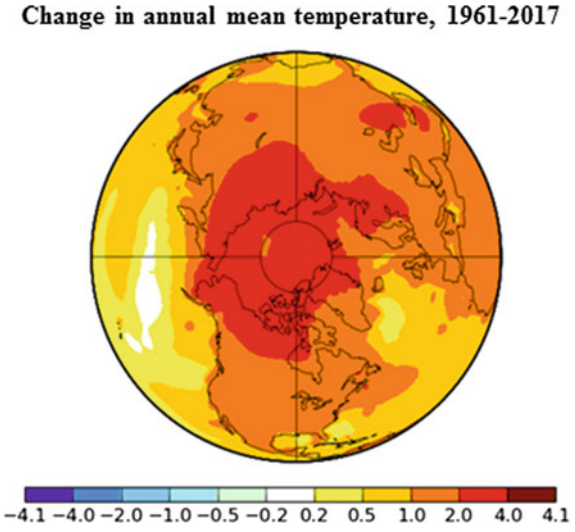

Fig. 1.1 Changes in Arctic temperatures over 1961–2017, based on linear trends of annual temperatures at each location. *Source* NASA GISTEMP (http://data.giss.nasa.gov/gistemp/maps/)

shows the spatial pattern of the change of the annual mean temperature since 1961. The warming is between 2 and 4 °C over most of the Arctic. In middle latitudes, the warming is generally greater over land, where it ranges from 1 to 2 °C than over the ocean. The subarctic land areas of Eurasia and North America have warmed by more than 2 °C since 1961.

The recent Arctic warming varies seasonally, with the strongest warming in autumn and winter and the weakest warming in summer (Fig. 1.2). The seasonal warming since 1960 exceeds 4 °C in some areas: Alaska and northwest Canada in winter, and the central Arctic Ocean in autumn and winter. It must be noted, however, that the lack of instrumental data from the Arctic Ocean in the 1960s and 1970s introduces a reliance on interpolation over the Arctic Ocean. Nevertheless, a pattern of Arctic amplification is apparent in all seasons in Fig. 1.2, with the

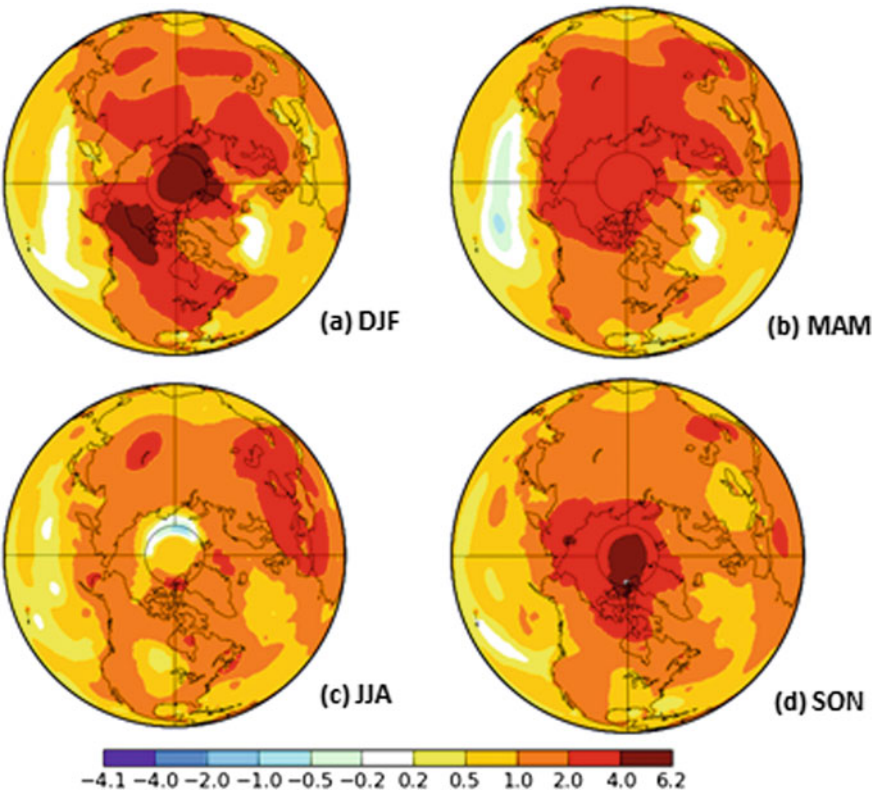

Fig. 1.2 Changes in Arctic temperatures by season over 1961–2017, based on linear trends of temperatures at each location. Seasons are **a** winter (Dec–Feb), **b** spring (Mar–May), **c** summer (Jun–Aug), and **d** autumn (Sep–Nov). *Source* NASA GISTEMP (http://data.giss.nasa.gov/gistemp/maps/)

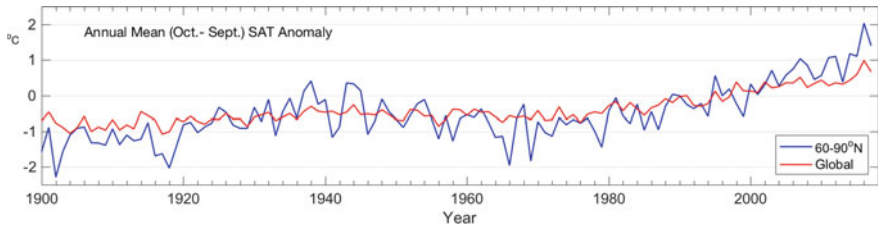

Fig. 1.3 Arctic (blue) and global (red) air temperatures, 1900–2017. *Source* NOAA Arctic Report Card (2017), http://www.arctic.noaa.gov/Report-Card/Report-Card-2017

exception of the immediate polar cap (70–90°N) during summer, when the thermal inertia of the Arctic Ocean and its sea ice limits the warming. It should also be noted that the summer warming over northern land areas corresponds to a rate of more than 2 °C per century, which is two orders of magnitude larger than the Arctic's longer-term rate of summer cooling deduced by Kaufman et al. (2009).

While the Arctic has warmed more than the rest of the globe in recent decades, variability is also greater in the Arctic. Figure 1.3 shows that this greater variability characterizes temperature swings over interannual, multiyear, and multidecadal timescales. In particular, the Arctic also warmed at a greater rate than the global mean in the early twentieth century and it cooled at a greater rate in the middle twentieth century. This greater variability complicates the attribution of recent changes, as the importance of internal variability relative to external forcing is greater in the Arctic than in lower latitudes. For this reason, several recent evaluations of global climate model simulations under greenhouse forcing have found that the emergence of the anthropogenic warming signal occurs later in the Arctic (around the present decade) than in other parts of the world (Kattsov and Sporyshev 2006; Hawkins and Sutton 2009). Nevertheless, it is apparent from Fig. 1.3 that (1) the Arctic is warmer now than at any time since 1900, (2) the most recent years (2015–2017) are the warmest in the entire instrumental record, and (3) the 1998–2012 "hiatus" in global warming (red curve in Fig. 1.3) was not evident in the Arctic.

1.2 Temperature-Related Changes

The recent Arctic warming has been accompanied by a rapid loss of sea ice, especially during the warm season. September sea ice extent during the past 5–10 years was approximately 50% of the mean for the 1979–2000 period. (Consistent measurements by satellite passive microwave sensors began in 1979). The recent decline is unprecedented in the satellite record and in paleo reconstructions spanning more than 1400 years (Kinnard et al. 2011). The recent reduction of sea ice has been much less in winter and spring than in summer and autumn, resulting

in a sea ice cover that is largely seasonal. The increasingly seasonal ice cover contrasts with the Arctic Ocean's predominantly multiyear ice pack of the pre-2000 decades. The seasonality of Arctic sea ice loss is highlighted here because it has direct relevance to the interpretation of the drivers as well as the impacts of Arctic temperature change, as discussed in the following two sections.

When compared to the reductions in ice extent, the percentage reductions of ice volume and thickness are even greater. Ice thickness decreased by more than 50% from 1958–1976 to 2003–2008 (Kwok and Rothrock 2009), and the percentage of the March ice cover made up of thicker multiyear ice (ice that has survived a summer melt season) decreased from 75% in the mid-1980s to 45% in 2011 (Maslanik et al. 2001). Laxon et al. (2013) indicate an even greater decrease of 64% in autumn sea ice volume from 2003–08 to 2012.

Changes in other cryospheric variables, including terrestrial snow cover, permafrost, glaciers, and the Greenland Ice Sheet, are summarized in the most recent *Snow, Water, Ice and Permafrost in the Arctic*, a synthesis report published recently by the Arctic Monitoring and Assessment Programme (AMAP 2017). Figure 1.4 is a plot of time series of key Arctic variables from the AMAP report. The changes in these other variables are consistent with the warming Arctic in recent decades. Because the primary focus of the present paper is the Arctic warming, we refer the reader to the AMAP report for additional information on recent changes in other components of the Arctic's physical system.

1.3 Attribution

Recent attribution studies have attempted to explain why, prior to the recent warming, the Arctic warmed at a greater rate than the global mean in the early twentieth century and cooled at a greater rate in the mid-twentieth century. Fyfe et al. (2013) used a series of controlled model experiments to deduce the contributions of various forcings (including solar, volcanic, and anthropogenic) as well as internal variability. Fyfe et al. show the contribution of these various factors to Arctic temperature trends during three periods of the twentieth century. Natural variability made a positive contribution before 1939 but opposed the emerging Greenhouse Gas (GHG) contribution during the mid-twentieth century. In the last third of the century, GHG is the dominant contributor to warming. There were also small contributions to low-frequency Arctic temperature variations from the oceanic deep circulation in the Atlantic Ocean, the Atlantic Multidecadal Oscillation. Miles et al. (2014) and Kravtsov et al. (2014) provide further discussion of the role of multidecadal Atlantic variability and other manifestations of low-frequency variations.

Given the prominence of Arctic amplification in the historical temperature records, a key question is: What are the relative contributions of various feedbacks to Arctic warming? While these feedbacks are notoriously difficult to untangle in observational data, the feedbacks have been evaluated using the more

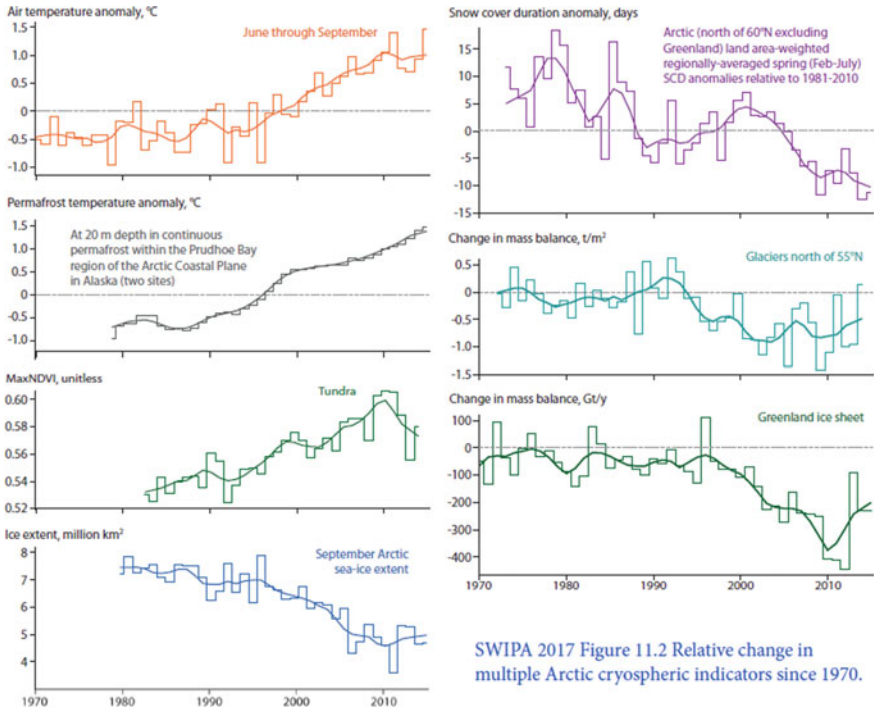

Fig. 1.4 Annual values of indicators of Arctic change from AMAP (2017). Left column (from top): Arctic summer air temperature (June–September), permafrost temperatures on the North Slope of Alaska; tundra vegetative greenness (maximum Normalized Difference Vegetation Index); September pan-Arctic sea ice extent. Right column (from top): February–July anomalies of snow cover duration on land north of 60°N; the mass balance of glaciers north of 55°N; the mass balance of the Greenland ice sheet. See Chap. 11 of AMAP (2017) for details

comprehensive information from global climate model simulations (Pithan and Mauritsen 2014). As shown in Fig. 1.5, the two largest feedbacks are the surface albedo (snow and ice) feedback and the lapse rate feedback, both of which are positive in the Arctic. The Planck effect and the water vapor feedback are also positive in the Arctic, ranking third and fourth, respectively, followed by the direct radiative effect of increased CO_2 concentrations. The largest (and only substantial) negative feedback in the Arctic is ocean heat transport, which decreases as the Arctic warms in the models. This negative feedback contrasts with the apparent positive contribution of ocean heat influxes to the recent Arctic warming. Figure 1.5 compares the various feedbacks and shows how the magnitude of each feedback varies among the major global climate models. In the following sections, we address several of the key processes underlying the stronger feedbacks.

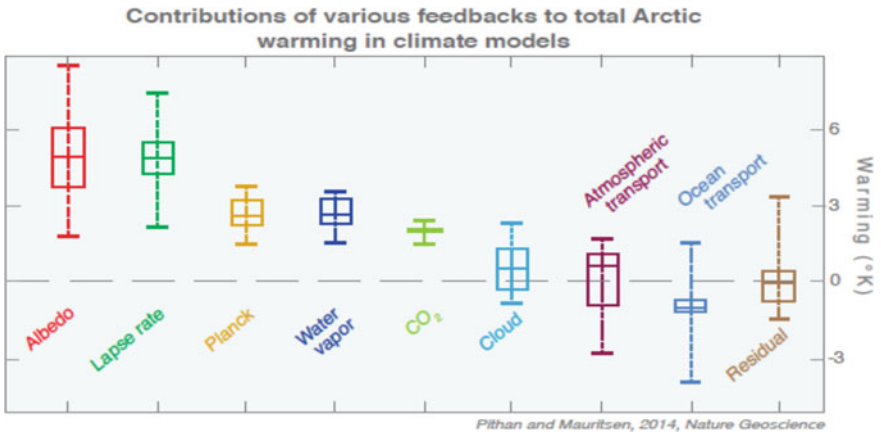

Fig. 1.5 Contributions of various feedbacks to total Arctic warming in CMIP5 global climate models Source: Pithan and Mauritsen (2014, Nature Geosci. Fig. 1.3)

The feedbacks described above were evaluated from a general framework provided by global climate model simulations. A more tangible example is provided by the recent Arctic warming and associated sea ice loss, the explanation of which has become one of the grand challenges of Arctic research (Kattsov et al. 2010). Three temperature-related factors have been identified as contributors to the accelerated sea ice loss of the post-2000 period, so the post-2000 warming and sea ice loss can serve as an illustrative example of the key feedbacks in Fig. 1.5. The three factors are:

- the albedo-temperature feedback triggered by a loss of sea ice
- increased downwelling longwave radiation resulting from increases in atmospheric moisture
- an increase in poleward heat transports in the atmosphere and the ocean

Although these three factors can be interdependent (e.g., increased humidity and/or poleward heat transports can lead to warming that drives a loss of sea ice), they are discussed sequentially in the following sections in order to provide structure to the presentation.

1.3.1 The Albedo-Temperature Feedback

Figure 1.5 shows the change of Arctic temperature over 1961–2017 as a function of latitude and calendar month. The warming is strongest over the latitudes of the Arctic Ocean and during the autumn and winter. On the other hand, the loss of sea ice reduces the warming during spring and summer by enabling greater

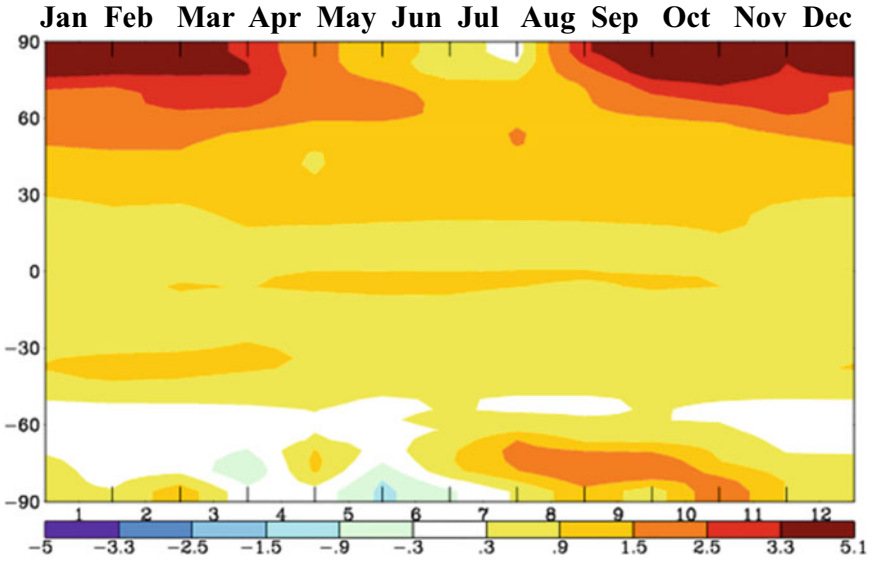

Fig. 1.6 Changes of zonal mean air temperature (°C) over the period 1961–2017. Changes are differences between starting and ending values of linear trend lines. *Source* NASA Goddard Institute for Space Studies, https://data.giss.nasa.gov/gistemp/seas_cycle/

oceanic absorption of the incoming solar radiation during these seasons. The additional heat absorbed by the ocean is released back to the atmosphere during autumn and early winter (Perovich and Richter-Menge 2009), contributing to the warming in those seasons. Figure 1.6 shows a clear signal of this seasonality of changes in the surface heat fluxes.

1.3.2 Increased Atmospheric Humidity and Associated Downwelling Radiation

The air's water vapor-holding capacity increases exponentially with temperature. If the atmosphere's relative humidity does not change substantially, the actual humidity will increase with climate warming. This increase in humidity has important thermodynamic implications because water vapor is a strong greenhouse gas, which will further increase the downward longwave radiation to the surface. A loss of sea ice will result in increased surface moisture fluxes to the atmosphere and hence increased atmospheric humidity, which then increases the downwelling radiation and warming of the surface (Francis and Hunter 2006). This "water vapor feedback" can be expected to amplify the surface warming in the Arctic. The model experiments by Pithan and Mauritsen (2014) support this expectation, as shown in Fig. 1.5, as do the reanalysis- and model-derived results of Bintanja and van der Linden (2013)

Observational data analyses confirm that humidity in the Arctic has increased in recent years (Screen and Simmonds 2010; Serreze et al. 2012). Consistent with the seasonality of sea ice loss, the increase of humidity has been found to be largest in the autumn months (Cohen et al. 2013). More recently, associations between regional increases in humidity and atmospheric warming have been identified (Cullather et al. 2016; Alexeev et al. 2017). Ghatak and Miller (2013) also show that increased water vapor has made a much greater contribution to the increased downwelling longwave flux and Arctic warming in winter than in summer, consistent with the seasonality of the Arctic warming in Fig. 1.6.

1.3.3 Increased Poleward Transports by the Ocean and Atmosphere

Poleward heat and moisture transports, which are key processes in the Arctic's energy budget (Serreze and Barry 2014), are achieved by the atmospheric circulation (winds). Ocean currents also account for a substantial portion of the heat transport into the Arctic. The greatest inflow of oceanic heat occurs in the North Atlantic. Interannual, decadal, and multidecadal variations of North Atlantic Ocean heat inflow to the Arctic Ocean are superimposed on a warming trend (Polyakov et al. 2010, 2011). This combination of trend and variability has been manifest as a series of increasingly warm inflow pulses. One such pulse occurred in 2005–2006, preceding the 2007 sea ice loss event, which may have been responsible for an acceleration of the albedo-temperature feedback in the Arctic (Perovich and Richter-Menge 2009).

Pacific Ocean water enters the Arctic through Bering Strait. The heat content of this water has also increased over the past decade (Woodgate et al. 2012). Serreze et al. (2016) show that this increased heating has reduced the coverage and thickness of sea ice in the Chukchi, East Siberian, and Beaufort Seas. The thinning has made the ice more responsive to the winds that drive the Beaufort gyre, increasing the transport of the warmer Pacific water to the deeper Arctic Ocean from the continental shelves (Shimada et al. 2006). The additional melt of sea ice then enhances the albedo-temperature feedback. The greatest recent loss of sea ice has been in the Pacific sector, pointing to the importance of Pacific Water inflow for the Arctic energy budget.

As the atmosphere in lower latitudes becomes warmer and moister, poleward transports of atmospheric heat as well as moisture should increase if there are no major changes in the atmospheric circulation. A time series of the poleward transports computed using an atmospheric reanalysis displays a peak in the 2005–2006 time period, after which the summers showed increases in retreat of Arctic sea ice (Alexeev et al. 2017). The recent increase in the moisture content of the Arctic atmosphere (Sect. 1.3.2) is likely attributable to a combination of increased poleward transports and local evaporation. The relative contributions of these two changes to the increased temperature of the Arctic remain to be determined.

1.4 Arctic Warming's Impacts on Middle Latitudes

The extent to which Arctic warming impacts the large-scale atmospheric circulation and middle latitudes is an active research topic. Several mechanisms have been proposed for linkages between the Arctic and the midlatitude circulation. The first is an Arctic-warming induced effect on geopotential height and the jet stream. To the extent that an amplified Arctic warming alters the pole-to-equator temperature gradient, an impact of Arctic warming on the jet stream is indeed plausible. Blocking patterns in the jet stream have been invoked in this linkage, and the role of the stratosphere in the linkage is gaining increasing traction in the atmospheric dynamics community (Overland et al. 2020). A second mechanistic linkage involves Eurasian snow cover, which also impacts the temperatures of the lower troposphere and the pressure gradients aloft (Cohen et al. 2007). We summarize these mechanistic linkages in the following two subsections.

1.4.1 Impacts on Geopotential Heights and Blocking Events

In order to illustrate the scale of Arctic thermal anomalies that may impact upper-level pressures, Fig. 1.7 extends the analysis of Overland and Wang (2010) by showing the longitudinally averaged) temperature anomalies for October–November 2012–2017 as a function of altitude (pressure) poleward of 50ºN. Figure 1.8 shows that the strongest warming during this six-year period was surface-based. The location of this surface-based warming in the Arctic implicates sea ice loss in the warming, The zonally averaged warming poleward of about 75ºN in Fig. 1.7 exceeds 3.5 °C close to the surface and 1.5 °C when averaged over the lowest 200 hPa (about 2 km) By contrast, the warming in the middle troposphere of the Arctic is typically 0.5–1.5 °C.

Heating of the lower atmosphere results in thermal expansion, which increases the thickness (depth) of the air column between two pressures and increases the pressures aloft (i.e., thermal expansion "lifts" the pressure surfaces). Figure 1.8 shows that pressures have indeed increased aloft above the latitudes of warming in the Arctic during the autumns of 2012–2017. The changes in the north–south gradients of the pressure in the upper atmosphere result in changes in the zonal (west-to-east) winds, for which the speed at any altitude is proportional to the equatorward pressure gradient at that altitude. Because the changes in Fig. 1.8 reduce the normal equatorward gradient of pressure, the zonal winds weaken.

The jet stream's meanders, consisting of troughs (southward dips) and ridges (northward bulges), become stronger as the west-to-east component of the wind speed decreases. The troughs in the jet stream represent southward intrusions of cold polar air masses into middle latitudes, while ridges represent poleward excursions of warmer air. Jet stream waves with longer wavelengths and larger amplitudes tend to propagate more slowly. Accordingly, an amplified pattern is generally associated with persistent anomalies, often associated with extreme

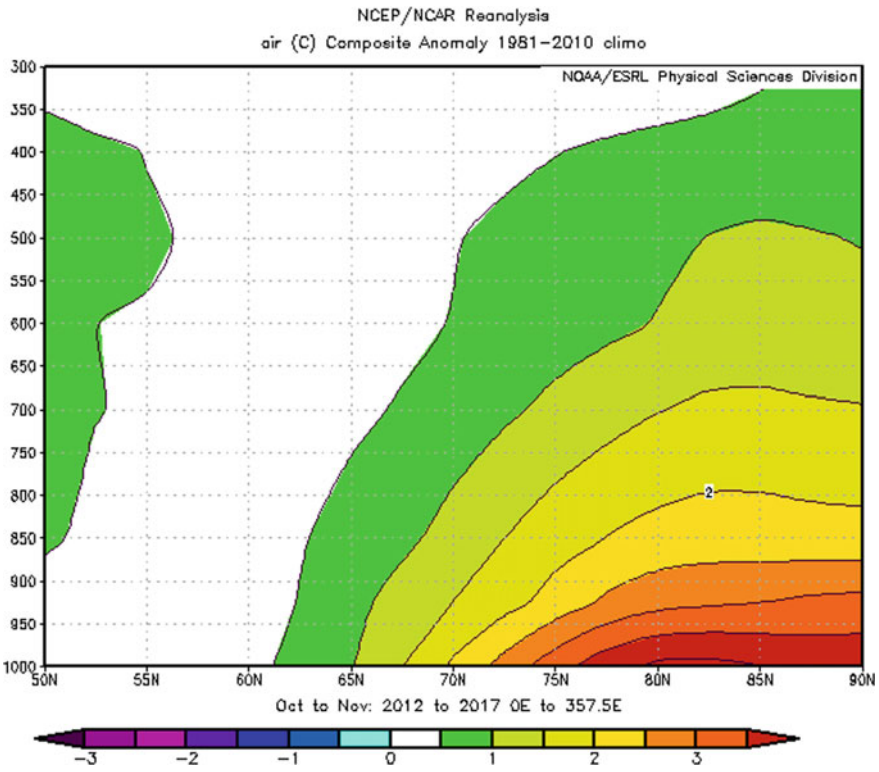

Fig. 1.7 Latitude-height cross-section of the departures from mean (1981–2010) of the zonally averaged air temperatures (°C) during October–November of 2012–2017. *Source* NOAA Earth System Research Laboratory, https://www.esrl.noaa.gov/psd/cgi-bin/data/composites/printpage.pl

weather, in middle latitudes. Francis and Vavrus (2012) found evidence of decreased zonal wind speeds and increased wave amplitudes in winter and autumn of the post-1979 period. The changes are especially apparent in the Atlantic hemisphere. They are consistent with Arctic-amplified warming that favors poleward extensions of ridges and with extended periods of anomalous weather in middle latitudes. Such periods are termed "blocking" episodes, as the highly amplified waves (often with embedded closed pressure centers) tend to block the normal eastward propagation of the upper-atmospheric waves that control the evolution of surface weather systems. However, subsequent work has shown that conclusions about recent changes in wave activity are sensitive to the metric of waviness and the choice of the geographical region (e.g., Screen and Simmons 2013; Barnes 2013; Barnes and Screen 2015; Overland et al. 2016; Screen et al. 2018). Screen et al. (2015) also showed that the warming of the cold Arctic air masses that move equatorward during cold air outbreaks will outweigh the effects of changes in the frequency of cold air outbreaks through the twenty-first century.

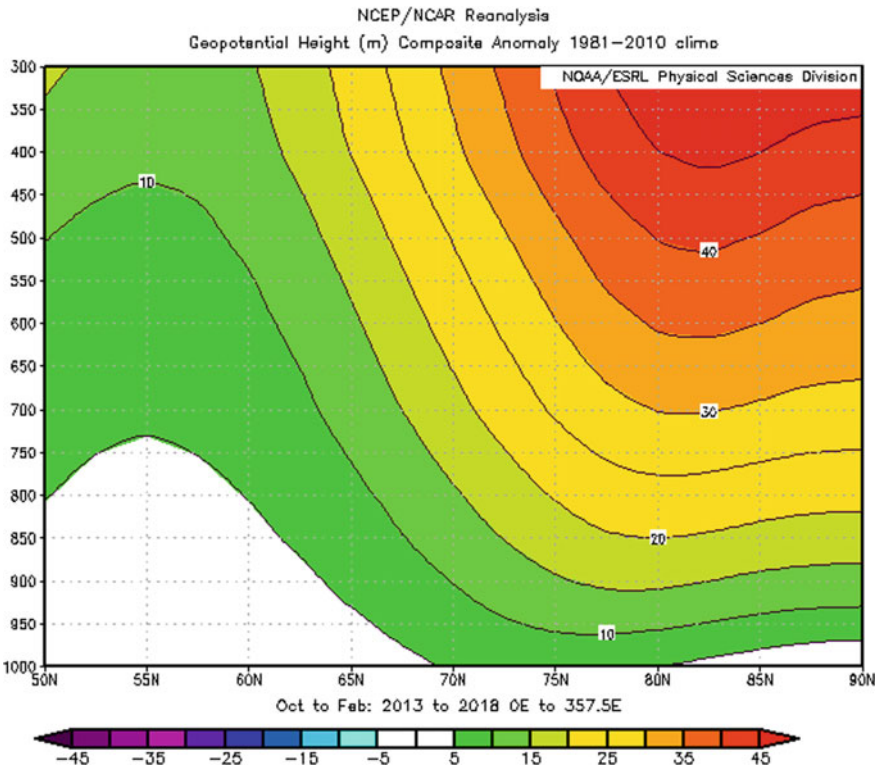

Fig. 1.8 Latitude-height cross-section of the departures from mean (1981–2010) of the zonally averaged geopotential height (m) during October–November of 2012–2017. A northward increase of the change of geopotential height implies a decrease of the west-to-east wind speed. *Source* NOAA Earth System Research Laboratory, https://www.esrl.noaa.gov/psd/cgi-bin/data/composites/printpage.pl

This warming of the cold air masses has been shown to already be underway by Kanno et al. (2016) in a study based on historical (reanalysis) data. Moreover, even when frequent cold air outbreaks occur during a midlatitude winter, the Arctic outbreaks may be manifestations of internal variability that is associated with forcing from other regions, e.g., the tropics (Hartmann 2015; Abdillah et al. 2018).

1.4.2 The Arctic-Midlatitude Connection via Terrestrial Snow Cover

On the basis of both observational data analyses and model simulations, reduced Arctic sea ice during autumn favors an increase of snow cover over Eurasia (Liu et al. 2012; Cohen et al. 2013). This type of association is physically plausible

because an increase of open water during autumn enhances the supply of moisture to the atmosphere. Autumn sea ice/snow cover are indeed correlated with wintertime snow cover, atmospheric circulation and air temperature. For example, observational data analysis shows that a reduction of *autumn* sea ice coverage by 1 million km^2 corresponds to an increase of 3–12% in *winter* snow cover over eastern Asia, parts of Europe, eastern Asia, and the northern United States (Liu et al. 2012). A climate model's sea ice sensitivity experiments (Honda et al. 2009) showed a pattern of temperature anomalies consistent with these observational results. The associated atmospheric circulation anomaly pattern corresponds to the negative phase of the Arctic Oscillation, in which the Arctic is warmer than normal and middle-latitude land areas are colder than normal. These anomalies are associated with an increased frequency of blocking, in agreement with the results described in Sect. 1.4.1.

Cohen et al. (2013) presented an analysis of observational data, showing statistically significant trends in Jul–Sep Arctic mean air temperature, September fractional sea ice coverage, autumn Arctic tropospheric moisture, October Eurasian snow cover, and the Dec–Feb Arctic Oscillation index. The relationship between these significant trends forms the basis of Cohen et al.'s proposed linkage between the Arctic, its autumn sea ice, and midlatitude wintertime anomalies. The linkage across seasons (autumn ice/snow vs. winter Arctic Oscillation) is arguably the most tenuous link in the causal chain. Dynamical linkages involving stratosphere-troposphere are now emerging to explain the across-season correlation between the high-latitude surface state during autumn and the wintertime circulation of the atmosphere (e.g., Kim et al. 2014; Overland et al. 2020). However, in view of our limited understanding of the underlying mechanisms, Arctic-midlatitude linkages remain an active research topic (Francis 2017).

1.5 Changes in Extremes

Changes in extremes often have greater impacts on ecosystems, infrastructure, and humans than changes in climatic means (CCSP 2008; IPCC 2012). Historical data from Alaska show recent trends toward less frequent cold extremes and more frequent warm extremes (Fig. 1.9). By contrast, there is no systematic trend in extremes of heavy precipitation at the same Alaskan stations (Fig. 1.9c). As discussed elsewhere in this volume, however, precipitation measurements at weather observing stations are subject to heterogeneities to a greater extent than are measurements of temperature.

On the pan-Arctic scale, Matthes et al. (2015) showed widespread decreases in extreme cold spells, although there are small areas of increases in cold spells in Siberia. Changes in extreme warm spells were found to be generally small throughout the Arctic except in Scandinavia, where increases of up to 2.5 days per decade have occurred. Long cold spells (cold events lasting more than 15 days) have almost completely disappeared since 2000.

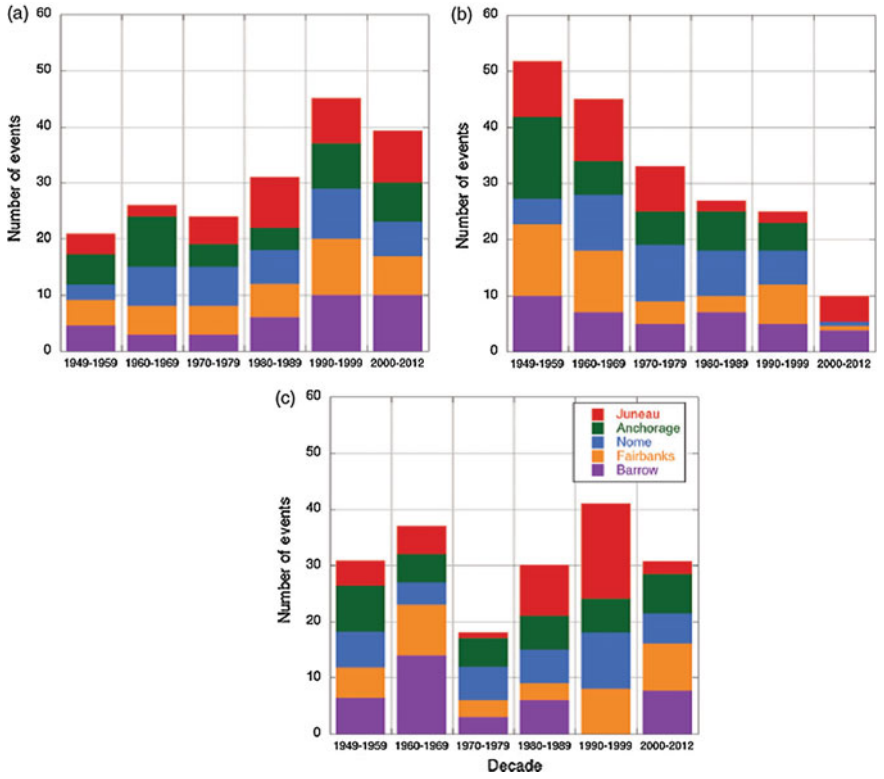

Fig. 1.9 Decadal distributions of **a** extreme high daily maximum temperatures **b** extreme low daily minimum temperatures, and **c** extreme 3-day precipitation amount for the period 1949–2012 at five first-order weather stations in Alaska. Each station is assigned a color (legend in Panel **c**). The bars for 2000–2012 have been adjusted to represent the number of events over 10 years (Bieniek and Walsh 2017)

A type of extreme event with major impact in the Arctic is freezing rain, or rain-on-snow events, which are dependent on temperature in the sense that they are favored by air temperatures close to 0 °C in the lowest kilometer. As larger areas of the Arctic experience more frequent wintertime temperatures approaching (or exceeding) 0 °C, these events can be expected to become more frequent. Hansen et al. (2014) examined the recent occurrence of such events in Svalbard and concluded that the likely increase of the frequency of rain-on-snow events has implications for wildlife, infrastructure, transportation, and other human activities. Studies of freezing rain events in other parts of the Arctic are needed for a pan-Arctic assessment of ongoing changes in icing events.

Cyclones in the Arctic represent another temperature-sensitive type of extreme event, as cyclones form and track in the zones of greatest baroclinicity (horizontal temperature gradient). While individual cyclones have been investigated, (e.g.,

Simmonds and Rudeva 2012; Parkinson and Comiso 2013), comprehensive data-based studies of storms over the pan-Arctic domain and evaluations of historical trends in subarctic storminess have not provided compelling evidence of trends (USGCRP 2014). There are some indications from models of a northward shift in the storm tracks over the North Atlantic Ocean, but the Northern Hmisphere shows a less spatially coherent poleward shift in storm tracks (Collins et al. 2013, their Fig. 12.20).

1.6 Future Projections

According to state-of-the-art global climate models, the recent Arctic warming is projected to continue. Warming depends on the global emission scenario, as shown in Fig. 1.10. Under RCP 8.5, which is the RCP emission scenario being tracked most closely by present emissions, the increase of the annual mean temperature over 60–90°N is approximately 10 °C by the end of the twenty-first century. For the RCP 2.6 scenario, which requires substantial negative global emissions (i.e., carbon uptake) by 2100, the warming averaged over 60–90°N is between 3 and 4 °C. The substantial difference between the business-as-usual and the mitigation scenarios emerges primarily after mid-century, indicating that several decades of future Arctic warming are already "locked into" the system (Overland et al. 2014). The projected warming resembles the observed warming (Figs. 1.1 and 1.2) in two notable respects: (1) the spatial pattern of the warming shows a strong polar amplification, and (2) the projected warming is largest in winter and autumn, and smallest in summer. Moreover, the rate of pan-Arctic warming of the past 50–60 years, 2–4 °C per half century (Fig. 1.1), is generally consistent with the model simulations.

While the consistency between the recent and projected Arctic warming lends credibility to the model simulations, uncertainty must be kept in mind. As summarized by Hodson et al. (2013), three sources of uncertainty apply to changes such as those mapped in Fig. 1.10: (1) internal variability, (2) across-model differences, and (3) the dependence on emission scenario. While (3) is acknowledged by the presentation of different panels for different scenarios and (2) by the use of stippling to indicate model agreement (or lack thereof), internal variability confounds the expected temperatures for any particular year or even decade. Excursions from the mean have characterized the historical Arctic temperature record, as shown in Fig. 1.3 and discussed in Sect. 1.1, and will almost certainly continue to do so in the future. Nevertheless, the aggregate of the model simulations suggests that these excursions will be relative to higher mean temperatures in the future.

Figure 1.11 shows the corresponding projections of future (2081–2100) precipitation, expressed as percentage changes from the averages for the 1986–2005 period. In both the low- and high-emission scenarios, Arctic precipitation increases. The percentage increases under RCP 8.5 are quite high, exceeding 20% over the subarctic land areas and exceeding 40% over the Arctic Ocean. Only the equatorial Pacific Ocean has a comparable percentage increase. The actual increases (e.g., mm

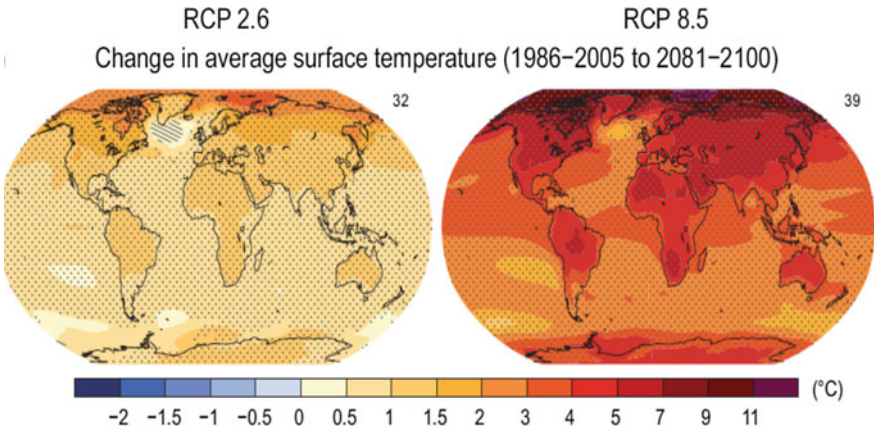

Fig. 1.10 Changes of surface air temperature (°C) projected by the CMIP5 climate models for the period 2081–2100 relative to 1986–2005. Left and right panels are for RCP 2.6 (extreme mitigation) and RCP 8.5 (business-as-usual) emission scenarios. Stippling indicates regions where the multi-model mean change exceeds two standard deviations of internal variability and where at least 90% of the models agree on the sign of the change. The number of models is indicated above and to eight of each map. *Source* IPCC (2013, Fig. SPM.8)

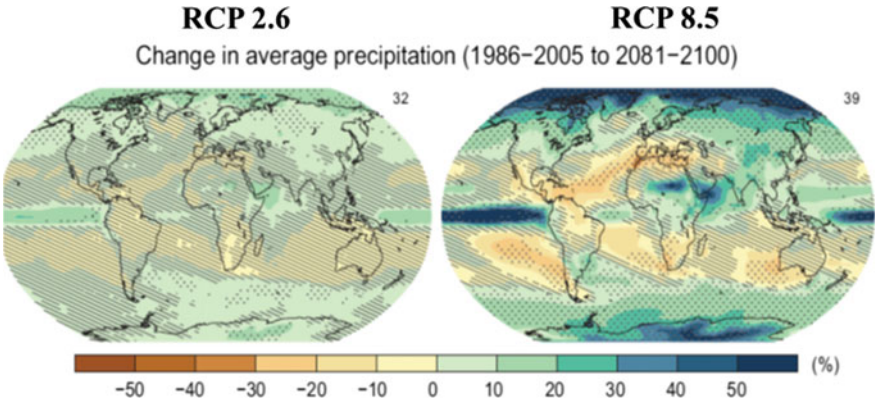

Fig. 1.11 Percentage change in annual mean precipitation projected by the CMIP5 climate models for the period 2081–2100 relative to 1986–2005. Left and right panels are for RCP 2.6 (extreme mitigation) and RCP 8.5 (business-as-usual) emission scenarios. Stippling indicates regions where the multi-model mean change exceeds two standard deviations of internal variability and where at least 90% of the models agree on the sign of the change. The number of models is indicated above and to eight of each map. *Source* IPCC (2013, Fig. SPM.8)

per year) are smaller in the Arctic than areas such as the tropical Pacific because the base-level (1986–2010) amounts are much smaller in the Arctic. Nevertheless, the projected increase of Arctic precipitation is one of the more robust signals in the

global model projections of climate change. The extent to which these increases of precipitation will be offset by other hydrologic changes in high latitudes is one of the central issues of Arctic change and will be addressed in later chapters of this volume.

1.7 Conclusion

Several conclusions about Arctic temperatures emerge from the survey provided here. First, the Arctic warming of recent decades is unambiguous. The warming is further supported by corresponding changes in other components of the Arctic system. Second, there is no longer much "debate" about the emergence of Arctic amplification (Serreze and Francis 2006; Serreze et al. 2009), which is now unmistakable in the pattern of recent air temperature change. Furthermore, there have been recent advances in establishing the relative importance of the processes and feedbacks contributing to Arctic amplification. For example, the albedo-temperature feedback is detectable and is almost certainly a contributor to the recent loss of sea ice. Other notable factors in the recent Arctic-amplified warming and loss of sea ice are the increases in atmospheric water vapor and the poleward heat transports, especially in the ocean.

While the evidence for Arctic warming is unambiguous, there are remaining diagnostic challenges. These challenges pertain to the following fundamental questions:

- Are Arctic warming and sea ice loss irreversible in a climate system in which multiyear multidecadal variability is known to have been prominent in the past? The fact that the recent Arctic warming and loss of sea ice are, according to some reconstructions, unprecedented in the past 1400–2000 years suggests at least the possibility that a threshold may have indeed been crossed.
- What is the role of cloudiness in ongoing and future changes of the Arctic system? Despite its important effect on air temperatures, cloudiness has received relatively little attention in diagnostic evaluations of historical (observed) and future (model-based) Arctic change. Given the role of the Arctic surface as a moisture source for the atmosphere and its clouds, hydrology will need to be a key consideration in addressing this question.
- What are the key dynamical mechanisms underlying the atmospheric "blocking" response to Arctic warming? The answer to this question has implications for the seasonal-to-decadal predictability of severe winters in middle latitudes.
- How robust are the associations between variations of sea ice, Eurasian snow cover and the atmospheric circulation? What are the hydrological implications of these associations?
- How will the atmospheric circulation change in response to Arctic-amplified global warming? These changes will have first-order impacts on the poleward transports of heat and moisture. While future changes in these transports are not presently known, they are highly relevant to Arctic hydrology.

Climate models are unanimous in predicting that the Arctic will warm and that its precipitation will increase by the end of the present century. However, on shorter timescales of years to decades, the Arctic is notorious for its internal or natural variability, so much so that the signal of greenhouse warming emerges above the "noise" of climate variability more slowly than in the tropics, as discussed in Sect. 1.1. Moreover, climate model experiments show that even under external forcing scenarios consistent with ongoing increases of greenhouse gases, the likelihood of an increase of Arctic sea ice over any particular 10-year period is about 30% (Kay et al. 2011). If models are capturing the key Arctic feedback processes and their timescales, it would therefore not be surprising if there is a pause or a reprieve from the Arctic warming and sea ice loss over several years or a decade. Such a pause would undoubtedly have hydrologic implications as well, so the trajectory of the Arctic hydrologic budget must be viewed in a framework of uncertainty that depends strongly on the timescale.

Acknowledgments The preparation of this paper was supported by the Climate Program Office of the National Oceanic and Atmospheric Administration through Grants NA15OAR4310169 and NA17OAR4310160.

References

Abdillah MR, Kanno Y, Iwasaki T (2018) Strong linkage of El Niño-Southern Oscillation to polar cold air mass in the Northern Hemisphere. Res Lett, Geophys in press

Alexeev VA, Walsh JE, Ivanov VV, Semenov VA, Smirnov AV (2017) Warming in the Nordic Seas, North Atlantic storms and thinning Arctic sea ice. Env Res Lett 12:084011. https://doi.org/10.1088/1748-9326/aa7a1d

AMAP (2017) Snow, water, ice and permafrost in the Arctic (SWIPA): Climate Change and the Cryosphere - 2017. Arctic Monitoring and Assessment Programme (AMAP), Oslo, Norway, xiv+269 pp. ISBN 978-82-7971-101-8

Barnes EA (2013) Revisiting the evidence linking Arctic amplification to extreme weather in middle latitudes. Geophys Res Lett 40:4734–4739

Barnes EA, Screen JA (2015) The impact of Arctic warming on the midlatitude jet-stream: Can it? Has it? Will it? WIREs Climate Change 6:277–286

Bekryaev RV, Polyakov IV, Alexeev VA (2010) Role of polar amplification in long-term surface air temperature variations and modern Arctic warming. J Climate 23:3888–3906

Bieniek PA, Walsh JE (2017) Atmospheric circulation patterns associated with monthly and daily temperature and precipitation extremes in Alaska. Int J Climatol 37:208–217

Bintanja R, van der Linden EC (2013) The changing seasonal climate in the Arctic. Nat Sci Rep 3:1556. https://doi.org/10.1038/srep01556

CCSP (2008) Weather and climate extremes in a changing climate. In: Karl TR, Meehl GA, Miller CD, Hassol SJ, Waple AM, Murray WL (eds) Synthesis and assessment product 3.3. U. S. Climate Change Science Program (CCSP)

Cohen J, Furtado JC, Barlow MA, Alexeev VA, Cherry JC (2013) Arctic warming, increasing snow cover and widespread boreal winter cooling. Environ Res Lett 7(014007):1–8

Cohen J, Barlow M, Kushner P, Saito K (2007) Stratosphere–troposphere coupling and links with Eurasian land-surface variability. J Climate 20:5335–5343

Collins M, Knutti R, Arblaster J, Dufresne J-L, Fichefet T, Friedlingstein P, Gao X, Gutowski WJ, Johns T, Krinner G, Shongwe M, Tebaldi C, Weaver AJ, Wehner M (2013) Long-term Climate change: projections, com-mitments and irreversibility. In: Stocker TF, Qin D, Plattner G-K,

Tignor M, Allen SK, Boschung J, Nauels A, Xia Y, Bex V, Midgley PM (eds) Climate change 2013: the physical science basis. Contribution of working group i to the fifth assessment report of the intergovernmental panel on climate change. Cambridge University Press, Cambridge, United Kingdom and New York, NY, USA

Cullather RL, Lim Y-K, Boisvert LN, Brucker L, Lee JN, Nowicki SMJ (2016) Analysis of the warmest Arctic winter, 2015-2016. Geophys Res Lett 43:10808–10816. https://doi.org/10.1002/2016GL071228

Francis JA (2017) Why are Arctic linkages to extreme weather still up in the air? Bull Amer Meteor Soc 96:2551–2557

Francis JA, Hunter E (2006) New insight into the disappearing Arctic sea ice. Eos Trans Amer Geophys Union 87:509–524

Francis JA, Vavrus SJ (2012) Evidence linking Arctic amplification to extreme weather in mid-latitudes. Geophys Res Lett 39:L06801. https://doi.org/10.1029/2012GL051000

Fyfe JC, von Salzen K, Gillett NP, Arora VK, Flato G, McConnell JR (2013) One hundred years of Arctic surface temperature variation due to anthropogenic influence. Nat Sci Rep 3:2645. https://doi.org/10.1038/srep02645

Ghatak D, Miller J (2013) Implications for Arctic amplification of changes in the strength of the water vapour feedback. J Geophys Res 118. https://doi.org/10.1002/jgrd.50578

Hansen BB, Isaksen K, Benestad RE, Kohler J, Pedersen AO, Loe LE, Coulson SJ, Larsen JO, Varpe O (2014) Warmer and wetter winters: Characteristics and implications of an extreme weather event in the High Arctic. Env Res Lett 9:114021

Hartmann D (2015) Pacific sea surface temperature and the winter of 2014. Geophys Res Lett 42:1894–1902. https://doi.org/10.1002/2015GL063083

Hawkins E, Sutton R (2009) The potential to narrow uncertainty in regional climate predictions. Bull Amer Meteor Soc 90:1095–1107

Hodson DLR, Keeley SPE, West A, Ridley J, Hawkins E, Hewitt HT (2013) Identifying uncertainties in Arctic climate change projections. Clim Dyn 40:2849–2865

Honda M, Inoue J, Yamane S (2009) Influence of low Arctic sea ice minima on anomalously cold Eurasian winters. Geophys Res Lett 36(L08707). https://doi.org/10.1029/2008gl037079

IPCC (2013) Summary for policymakers. In: Stocker TF, Qin D, Plattner G-K, Tignor M, Allen SK, Boschung J, Nauels A, Xia Y, Bex V Midgley PM (eds) Climate change 2013: the physical science basis. Contribution of working group i to the fifth assessment report of the intergovernmental panel on climate change. Cambridge University Press, Cambridge, United Kingdom and New York, NY, USA

IPCC (2012) Managing the risks of extreme events and disasters to advance climate change adaptation. In: Field CB, Barros V, Stocker TF, Qin D, Dokken DJ, Ebi KL, Mastrandrea MD, Mach KJ, Plattner G-K, Allen SK, Tignor M, Midgley M (eds) A special report of working groups I and II of the intergovernmental panel on climate change. Cambridge University Press

Kanno Y, Abdillah MR, Iwasaki T (2016) Long-term trend of cold air mass amount below a designated potential temperature in Northern and Southern Hemisphere winters using reanalysis data sets. J Geophys Res-Atmos 121:10,1398-10.152. https://doi.org/10.1002/2015jd024635

Kattsov VM, Ryabinin VE, Overland JE, Serreze MC, Visbeck M, Walsh JE, Meier W, Zhang X (2010) Arctic sea-ice change: A grand challenge of climate science. Ann Glaciol 56 (200):1115–1121

Kattsov VM, Sporyshev PV (2006) Timing of global warming in IPCC AR4 AOGCM simulations. Geophys Res Lett 33:L23707. https://doi.org/10.1029/2006GL027476

Kaufman DS, Schneider DP, McKay NP, Ammann CM, Bradley RS, Briffa KR, Miller GH, Otto-Bliesner BL, Overpeck JT, Vinther VM, Arctic Lakes 2 K Project (2009) Recent warming reverses long-term Arctic cooling. Science 325(1):236

Kay JE, Holland MM, Jahn A (2011) Inter-annual to multi-decadal Arctic sea ice extent trends in a warming world. Geopys Res Lett 38:L15708

Kim B-M, and Coauthors (2014) Weakening of the stratospheric polar vortex by Arctic sea-ice loss. Nat Commun 4:4646. https://doi.org/10.1038/ncomms5646

Kinnard C, Zdanowicz CM, Fisher DA, Isaksson E, De Vernal A, Thompson LG (2011) Reconstructed changes in Arctic sea ice over the past 1,450 years. Nature 479:509–512

Kravstov S, Wyatt MG, Curry JA, Tsonis AS (2014) Two contrasting views of multidecadal climate variability in the twentieth century. Geophys Res Lett 41:6881–6888

Kwok R, Rothrock DA (2009) Decline in Arctic sea ice thickness from submarine and ICESat records: 1958-2008. Geophys Res Lett 36:L15501

Laxon SW, Giles KA, Rideout AL, Wingham DJ, Willatt R, Cullen R, Kwok R, Schweiger A, Zhang J, Haas C, Hendricks S, Krishfield R, Kurtz N, Farrell S, Davidson M (2013) CryoSat-2 estimates of Arctic sea ice thickness and volume. Geophys Res Lett 40. https://doi.org/10.1002/grl.50193

Liu J, Curry AJ, Wand H, Song M, Horton RM (2012) Impact of declining sea ice on winter snowfall. Proc Nat Acad Sci 109:4074–4079

Maslanik J, Stroeve J, Fowler C, Emery W (2001) Distribution and trends in Arctic sea ice age through spring 2011. Geophys Res Lett 38:L13502. https://doi.org/10.10029/2011GL047735

Matthes H, Rinke A, Dethloff K (2015) Recent changes in Arctic summer temperature extremes: warm and cold spells during winter and summer. Env Res Lett 20:114020. https://doi.org/10.1088/1748-9326/10/11/114020

Miles MW, Divine DV, Furevik T, Jansen E, Moros M, Ogilvie AEJ (2014) A signal of persistent multidecadal variability in Arctic sea ice. Geophys Res Lett 41:463–469

Overland JE, Ballinger TJ, Cohen J, Francis J, Hanna E, Jaiser R, Kim B-M, Kim S-J, Krettschmer M, Petrescu E, Ukita J, Vihma T, Walsh JE, Wan M, Zhang X (2020) How does Arctic environmental change influence midlatitude weather events? J Clim, in prep

Overland JE, Dethloff K, Francis JA, Hall RJ, Hanna E, Kim SJ, Screen JA, Shepherd TG, Vihma T (2016) Nonlinear response of mid-latitude weather to the changing Arctic. Nature Clim Change 6(11):992–999. https://doi.org/10.1038/nclimate3121

Overland JE, Wang M, Walsh JE, Stroeve JC (2014) Future Arctic climate changes: adaptation and mitigation timescales. Earth's Future 2:68–74

Overland JE, Wang M (2010) Large-scale atmospheric circulation changes are associated with the recent loss of Arctic sea ice. Tellus 62A:1–9

Parkinson CL, Comiso JC (2013) On the 2012 record low sea ice cover: combined impact of preconditioning and an August storm. Geophys Res Lett 40:1356–1361

Perovich D, Richter-Menge J (2009) Loss of sea ice in the Arctic. Ann Rev Mar Sci 1:417–441

Pithan F, Mauritsen T (2014) Arctic amplification dominated by temperature feedbacks in contemporary climate models. Nat Geosci 7:181–184

Polyakov IV, Alexeev VA, Bhatt US, Polyakova EI, Zhang X (2010) North atlantic warming: fingerprints of climate change and multidecadal variability. Clim Dyn 34:439–457

Polyakov, I.V., and 20 Co-authors, 2011: Fate of early 2000s Arctic warm water pulse. *Bull. Amer. Meteor. Soc., 92*, 561–566

Screen JA, Deser C, Smith DM, Zhang X, Blackport R, Kushner PJ, Oudar T, McCusker KE, Sun L (2018) Consistency and discrepancy in the atmospheric response to Arctic sea ice loss across climate models. Nat Geosci 11(3):155–163. https://doi.org/10.1038/s41561-018-0059-y

Screen JA, Deser C, Sun L (2015) Reduced risk of North American cold extremes due to continued Arctic sea ice loss. Bull Amer Meteor Soc 96:1489–1503. https://doi.org/10.1175/BAMS-D-14-00185.1

Screen JA, Simmonds I (2013) Exploring links between Arctic amplification and mid-latitude weather. Geophys Res Lett 40:959–964

Screen JA, Simmonds I (2010) The central role of diminishing sea ice in recent Arctic temperature amplification. Nature 464:1334–1337

Serreze MC, Barrett AP, Stroeve J (2012) Recent changes in tropospheric water vapor over the Arctic as assessed from radiosondes and atmospheric reanalyses. J Geophys Res-Atmos 117: D10104. https://doi.org/10.1029/2011jd017421

Serreze MC, Barrett AP, Stroeve JC, Kindig DN, Holland MM (2009) The emergence of surface-based Arctic amplification. The Cryosphere 3:11–19
Serreze MC, Barry RG (2014) The arctic climate system (2nd Ed.). Cambridge University Press, Cambridge, UK, 404 pp
Serreze MC, Crawford AD, Stroeve JC, Barrett AP, Woodgate RA (2016) Variability, trends, and predictability of seasonal sea ice retreat and advance in the Chukchi Sea. J Geophys Res-Oceans 121:7,308–7,325
Serreze MC, Francis JA (2006) The Arctic amplification debate. Clim Change 76:241–264
Shimada K, Kamoshida T, Itoh M, Nishino S, Carmack E, McLaughlin F, Zimmerman S, Proshutinsky A (2006) Pacific Ocean inflow: influence on catastrophic reduction of sea ice cover in the Arctic Ocean. Geophys Res Lett 33:L08605
Simmonds I, Rudeva I (2012) The great Arctic cyclone of August 2012. Geophys Res Lett 39: L23709. https://doi.org/10.1029/2012GL
USGCRP (2014) Highlights of climate change impacts in the United States. In: Melillo JM, Richmond TC, Yohe G (eds) U.S. global change research program (GCRP). Washington, DC
Woodgate RA, Weingartner TJ, Lindsay R (2012) Observed increases in Bering strait oceanic heat fluxes from the Pacific to the Arctic from 2001 to 2011 and their impacts on the Arctic Ocean water column. Geophys Res Lett 39(24):L24603

Dr. John E. Walsh is the Chief Scientist of the International Research Center and President's Professor of Global Change at the University of Alaska, Fairbanks, USA. He is also an emeritus faculty member of the University of Illinois. He has been involved in Arctic research and education for more than 40 years. His more recent research has addressed Arctic climate and weather variability, with an emphasis on the drivers of cryospheric variations over seasonal to multidecadal timescales. He has served as lead author for assessment reports of the Intergovernmental Panel on Climate Change, the Arctic Monitoring and Assessment Programme, and the U.S. National Climate Assessment. He has also co-authored a textbook, Severe and Hazardous Weather. He received a B.S. in Mathematics from Dartmouth College and a Ph.D. in Meteorology from the Massachusetts Institute of Technology.

Precipitation Characteristics and Changes

2

Hengchun Ye, Daqing Yang, Ali Behrangi, Svetlana L. Stuefer, Xicai Pan, Eva Mekis, Yonas Dibike, and John E. Walsh

Abstract

Precipitation over the Arctic region plays a significant role in the water and energy cycle that sustains the Arctic's unique ecosystem. Although a cold climate with strong seasonality in temperature and moisture predominates, there is large spatial variation due to the heterogeneity of the landscape and atmospheric processes that control local weather and climate. Long-term historical synoptic records exist for some regions providing very valuable information on how precipitation has been changing, yet there are many challenges to overcome. Inconsistency in instrumentation and measurement techniques, undercatch due to weather conditions and precipitation types,

H. Ye (✉)
College of Natural and Social Sciences, California State University, 5151 State University Drive, Los Angeles, CA 90032, USA
e-mail: hye2@calstatela.edu

D. Yang · Y. Dibike
Environment and Climate Change Canada, Watershed Hydrology and Ecology Division, Victoria, BC, Canada
e-mail: daqing.yang@canada.ca

Y. Dibike
e-mail: yonas.dibike@canada.ca

A. Behrangi
Department of Hydrology and Atmospheric Sciences and Department of Geosciences, University of Arizona, Tucson, AZ, USA
e-mail: behrangi@email.arizona.edu

S. L. Stuefer
Water and Environment Research Center, University of Alaska Fairbanks, Fairbanks, AK, USA
e-mail: sveta.sturfer@alaska.edu

D. Yang and D. L. Kane (eds.), *Arctic Hydrology, Permafrost and Ecosystems*,
https://doi.org/10.1007/978-3-030-50930-9_2

uneven spatial and temporal distribution of station locations, and the reliability of remote sensing products all have to be considered. Research on Arctic precipitation is mostly focused on a specific continent or geographical or political region using very diverse perspectives and approaches. Here we draw from many of these and remote sensing to piece together studies that illustrate a broader picture of Arctic precipitation conditions and reveal emerging and/or diverging patterns of change. This chapter will (1) introduce existing and forthcoming sources of data and their corresponding challenges across the Arctic; (2) describe the distribution of precipitation characteristics including total amount, intensity, and frequency over major land areas and the oceans; and (3) demonstrate past changes and future predictions in these precipitation characteristics and their extremes. This will provide a fairly comprehensive knowledge repository and a strong foundation to promote and inspire future research development on precipitation over the Arctic region.

2.1 Introduction

Arctic precipitation is one of the main drivers of terrestrial Arctic hydrologic processes. With rapid warming in high latitudes, major changes in water and energy cycles and ecosystem of the region are expected, sometimes with greater amplitude due to the unique feedbacks in the cryosphere environment (e.g., Lau et al. 2013; Smith et al. 2005; Solomon 2007; Stuefer et al. 2017; Ye et al. 2016a). Arctic precipitation is also a principal source of feedback within the climate system as the albedo contrast between snow-covered and snow-free surfaces affects the surface energy balance and resulting hydrologic processes. Snow can also be an efficient thermal isolator separating the underlying surface from the atmosphere above, and thus, for example, determining the conditions for persistence or decay of permafrost. In addition, other cryospheric components, such as sea ice, can also play a role in precipitation feedback. For example, a decrease in sea ice would cause an

X. Pan
Institute of Soil Science, Chinese Academy of Sciences, Nanjing, China
e-mail: xicai.pan@issas.ac.cn

E. Mekis
Environment and Climate Change Canada, Meteorological Research Division, Toronto, ON, Canada
e-mail: eva.mekis@canada.ca

J. E. Walsh
International Arctic Research Center, University of Alaska, Fairbanks, AK, USA
e-mail: jewalsh@alaska.edu

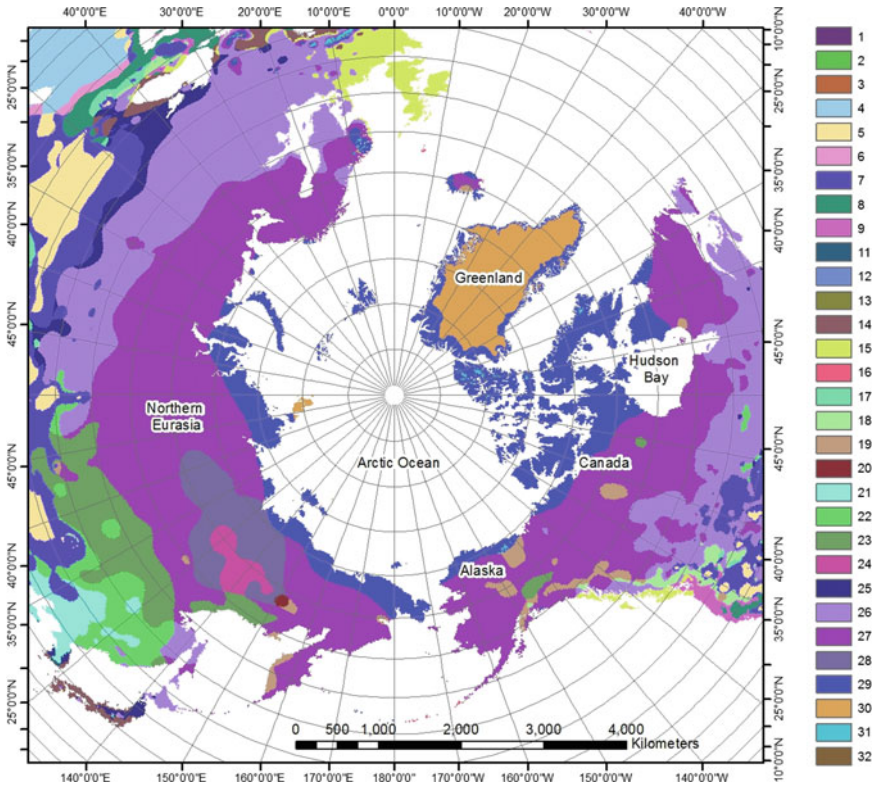

Fig. 2.1 Köppen's climate regimes north of 45° N based on Peel et al. (2007) updated dataset. Color codes used in this chapter are BWk (5), Cfb (15), Dsc (19), Dwc (23), Dwd (24), Dfa (25), Dfb (26), Dfc (27), Dfd (28), ET (29), and EF (30)

increase in Arctic precipitation because of the potential for increased local evaporation (Kopeca et al. 2015).

The largest continuous land surface over the Arctic north of 45° N is northern Eurasia, followed by Canadian territories and Alaska. The climate regimes are dominantly cold climate (D) with strong seasonality in moisture and temperature. Based on Koppen's classification updated by Peel et al. (2007) the climate includes cold-without dry season-cold summer (Dfc) over northern areas, cold-without dry season-warm summer over southern areas (Dfb), and Tundra (ET) along the arctic coast and high elevations (Fig. 2.1). Polar Frost (ET) climate prevails over Greenland. Along the west coast of Eurasia, it has temperate-without dry season-warm summer (Cfb) and other seasonal variations of cold climate along the west coast. Cold-winter dry-cold summer (Dwc), cold-winter dry-warm summer (Dwb), and cold-winter dry-hot summer (Dwa) are found over the east coast of northern Eurasia (Fig. 2.1). Cold dry-summer cold-winter (Dsc) climate class

occurs in northern Canada and Alaska. There are also some patches of cold desert (BWk) over the southern edges of northern Eurasia and western Canada.

Historical precipitation records are available mostly from the former Soviet Union, Canada, Alaska, and northern European countries with varying data record lengths and distribution densities, thus most research has focused on these three large land areas. However, accurate measurements of precipitation are challenging due to the multiphases and wide range of intensity in this extreme environment (Rawlins et al. 2007). Researchers, engineers, stakeholders, and the general public need to be aware of the precipitation data biases and limitations.

2.2 Precipitation Data and Quality

Precipitation records over the Arctic region include historical synoptic weather stations or research stations operated by various governments and local agencies' monitoring sites, snow measurement stations using rulers or snow telemetry, drifting stations over the Arctic Ocean ice surface, and (in recent decades) remote sensing products. Each country has its own history and unique ways of collecting data, especially in earlier years. While surface station data have been available for more than a century, they can contain large errors in high latitudes for two main reasons: (1) the precipitation gauge network is often sparse and discontinuous in most regions (a substantial decrease in the number of high-latitude precipitation stations since 1990 has exacerbated this limitation) and (2) precipitation measurement must be bias-corrected to account for wetting loss and gauge undercatch due to strong wind and/or blowing snow (Goodison et al. 1998; Yang et al. 2001; Sturm and Stuefer 2013). The bias correction factors, which are largest for solid precipitation, can be as high as 300% (Fuchs et al. 2001) depending on the choice of correction method. Walsh et al. (2008) and others have found that estimates of Arctic regional mean precipitation from several observational sources show considerable scatter, and the observational estimates based on gauge-adjusted station data are considerably larger than other observational estimates. Thus different methods of bias correction have been developed for specific types of instrumentation and for different regions (Goodison et al. 1992). Moreover, for many stations, it may be necessary to join observations to produce longer time series of rainfall and snowfall for trend analysis due to stations' relocation. In order to avoid artificial discontinuity affecting the trend, adjustment using overlapping periods and/or homogeneity testing can be applied. The annual and seasonal trends before and after adjustments show that the trends computed from the adjusted data present a more consistent regional pattern than do trends computed from unadjusted observations (Vincent and Mekis 2009).

2.2.1 Historical Data of Surface Observations

Arctic Ocean

Drifting ice stations over the Arctic Ocean and adjacent Siberian seas was set up by the Russian Arctic and Antarctic Research Institute during 1950–1991. These operated ice camps reported position, surface weather, atmospheric soundings, solar radiation, and snow conditions. Observations were made throughout the Arctic basin with a spatial resolution dependent on the movement of the drifting ice floes on which the stations were located. At all the drifting stations, precipitation was measured using a shielded Tretyakov precipitation gauge mounted on a geodesic frame, with the orifice at 2 m high. Measurements were made at 0600 and 1800 h (local time) using the volumetric method (Colony et al. 1998).

The Tretyakov gauges were tested against the WMO reference at 11 stations in 7 countries. The intercomparison data collected at these sites for more than 3 winter seasons represent a great variety of climate, terrain, and exposure. The relationship of Tretyakov gauge catch efficiency to wind speed and air temperature was developed by Yang et al. (1995) and Goodison et al. (1998) and has been used to improve data accuracy. The majority of the drifting station data were collected in climatologically uniform regions (Colony et al. 1998), since the ice stations tended to be clustered in the central part of the Arctic Ocean (Fig. 2.2) (Yang 1999). Figure 2.3 presents the overall mean monthly gauge-measured precipitation and bias corrections for the drifting stations operated from 1957 to 1990 (Yang 1999). It shows that monthly gauge-measured precipitation ranged from 5 to 20 mm, with the minimum in April and the maximum in July. Monthly correction for wind-induced undercatch varied from 3 to 11 mm, or about a 20–100% increase in the gauge-measured amounts. The relative increase of monthly precipitation (ratio of monthly correction to monthly measured value) is much higher in the cold season (September to May) than in the warm season (June to August), mainly due to the higher wind-induced gauge undercatch for snow and also the smaller amount of absolute precipitation in the cold season. Overall, monthly precipitation was increased by 50–90%, i.e., from 5–20 mm to 10–30 mm, due to the bias correction; it was even doubled for winter months of low precipitation.

The seasonal cycle of the bias-corrected precipitation is different from the gauge-measured data. The monthly maximum shifted from July to September; this seasonal pattern was reported by Legates and Willmott (1990) and is also in general agreement with most GCM simulations (Walsh et al. 1998). Quantitatively, the amount of the bias-corrected monthly precipitation is lower than Legates and Willmott (1990) for most of the months; this discrepancy may have been caused by using different datasets and by the different bias correction methods applied in the studies.

Annual corrections for wind-induced biases ranged from 50 mm to 170 mm and the annual correction for trace precipitation events varied from 10 mm to 30 mm. The bias correction raised the annual precipitation to 200–500 mm (from 100 mm–300 mm based on gauge records) for the drifting stations, an increase of 40–90%;

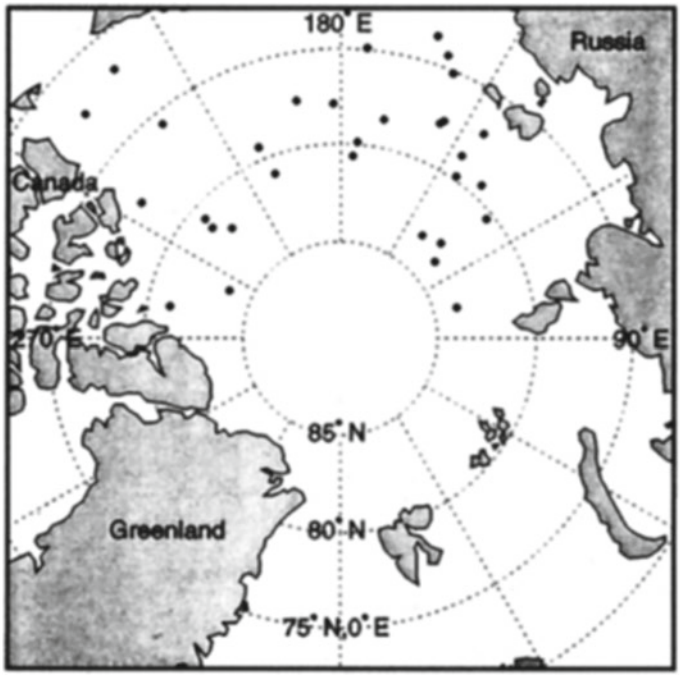

Fig. 2.2 Annual mean position of the Arctic Ocean drifting stations during 1957–1990 (Yang 1999)

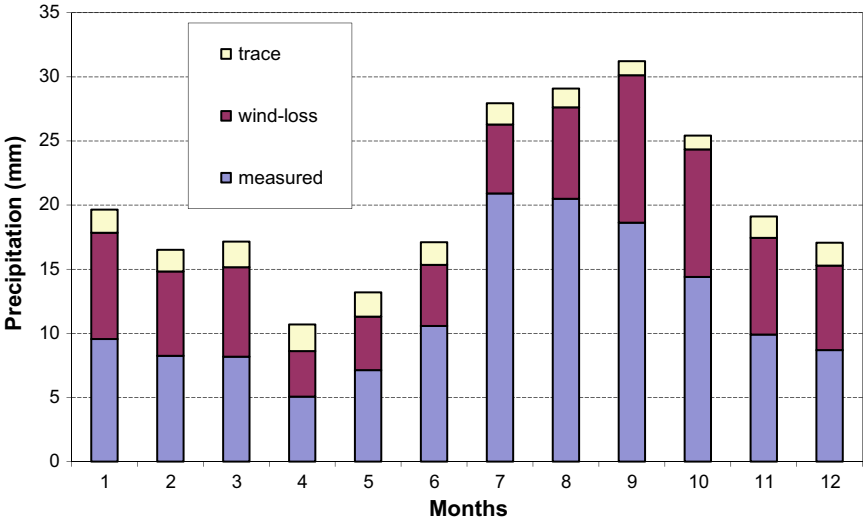

Fig. 2.3 The overall mean monthly gauge-measured precipitation and bias corrections for all drifting stations during 1957–1990 (Yang 1999)

consequently, the long-term mean annual precipitation is estimated to be 260 mm (from 150 mm) for the Arctic Ocean.

Alaska

Unlike other regions, precipitation data collection networks in Alaska were concurrently developed by different agencies to address each agency's specific needs and projects (Kane and Stuefer 2015). The precipitation data in Alaska were primarily collected by (1) the National Oceanic and Atmospheric Administration (NOAA) National Weather Service (NWS), (2) the NRCS Snow Telemetry (SNOTEL), (3) the United States Geological Survey (USGS), and (4) the Alaska Department of Transportation and Public Facilities (ADOT&PF). In addition to federal and state agencies, private industry and academia collect precipitation data in remote regions for environmental research projects. Each agency has its own protocol and site configurations for precipitation data collection. The use of collected precipitation data for climate change research was not a priority (or consideration) at the time when these networks were established. More recent initiatives, such as NOAA's U.S. Climate Reference Network (USCRN), were designed to fill the gap and support climate change research. The current USCRN network includes 21 first-order NWS stations in Alaska, which are commonly used for climate research.

Canada

The National Climate Data Archive of Environment Canada has daily rainfall gauge and snowfall ruler data. The Meteorological Service of Canada (MSC) has used a number of different gauges for measuring rainfall over the past 150 years (Metcalfe et al 1997). There are two Adjusted Precipitation for Canada-Daily datasets, the APC1-Daily, introduced in mid-1990 and the APC2-Daily, the second generation that extended the datasets to 2007 in order to provide more accurate precipitation amounts for trend analyses (Mekis and Vincent 2011a, b).

Precipitation accumulation with less than 1 mm has issues with quality due to a significant amount of trace precipitation which was not consistently defined, for example, difficulty in observation, conversion on metric system around 1977–78, etc. (Mekis 2005; Mekis and Vincent 2011a, b). Fresh snowfall measured with snow ruler in Canada adds another layer of complexity to the observations due to the spatial and temporal variation of snow water equivalent. Adjustment factors for snow density variation ranging from more than 1.5 over the Maritimes to less than 0.8 over southern-central British Columbia (Mekis and Brown (2010), allow estimates of SWE for all long-term climate stations in Canada.

Northern Eurasia

The network of stations in Russia began with 23 sites in 1850 and grew to 552 primary and secondary observing stations (including Finland and Poland) in 1890 (Groisman et al. 1991). There were 11,000 stations measuring precipitation during the 1980s over the USSR but these decreased drastically in the following decades. There were changes in gauges, installation standards, measurement practices, and relocation of stations that occurred at different times. Bias correction methods were

developed to minimize the impact of these changes (Groisman et al. 1991; Groisman and Rankova 2001). The monthly precipitation records of 622 stations are available for international users from the National Snow and Ice Data Center, Boulder, Colorado (Ye 2001; Serreze and Etringer 2003).

Precipitation daily record data over Russia were collected by the Russian Federal Service for Hydrometeorology and Environmental Monitoring (Roshydromet). Post-processing was done by the All-Russian Institute for Hydrometeorological Information and is also available from the NOAA data archive. An earlier version is available from the Carbon Dioxide Center (Bulygina and Razuvaev 2012). Again, the changes in precipitation gauge types and observation practices may have impacted the quality of the data. Various quality control methods were used depending on their instruments and observation practices to adjust for undercatch in solid and liquid precipitation measurements. Overall, the quality of data for climate change study is better starting in 1966 due to the consistency of instrumentation and quality control methods (Groisman et al. 1991). The most commonly used dataset available is the daily precipitation data from Daily Temperature and Precipitation Data for 518 Russian Meteorological Stations archived at the Carbon Dioxide Information Analysis Center (Bulygina and Razuvaev 2012).

Pan-Arctic

Uncertainties exist in the estimation of precipitation climatology over the high-latitude regions mainly due to sparse observation networks, space-time discontinuities of precipitation data, and biases of gauge observations. Of these factors, biases in gauge measurements, such as wind-induced undercatch, wetting loss (water adhesive to the surface of the inner walls of the gauge that cannot be measured by the volumetric method), evaporation loss (water lost by evaporation before the observation is made), and underestimation of trace precipitation amounts (Goodison et al. 1998), are particularly important, because they affect all types of precipitation gauges, especially those used in the cold regions. The WMO experiment has developed bias correction procedures for many precipitation gauges commonly used around the world, including those used in the high-latitude countries (Goodison et al. 1998). These bias correction methods have been applied in the high-latitude regions (including the Arctic Ocean drifting station records) and resulted in significantly higher estimates of precipitation (Yang et al. 1998; Yang 1999). Based on the regional applications of the WMO bias correction methods, Yang et al. (2005) expanded the analyses to the pan-Arctic scale, using available long-term daily data collected at locations above 45° N across national boundaries. The major advantage of this approach is the capability of examining the discontinuity of precipitation records across national borders.

Bias corrections for the observed daily precipitation over northern land have been conducted using daily meteorological data of precipitation, temperature, and wind speed. A consistent bias correction procedure was applied to quantify the biases of wind-induced undercatch, wetting losses, and trace precipitation amount on a daily basis. Its impacts on the precipitation climatologies were investigated by

using a subset of the global daily data, 4802 stations located north of 45° N with data records longer than 15 years during 1973–2004.

The corrections have increased the gauge-measured monthly precipitation significantly by up to 22 mm for winter months and by about 10 mm during the summer season. Wind-induced gauge undercatch is the largest error, but wetting loss and trace precipitation are also important particularly in the low precipitation regions. Relatively, the correction factors (CF = corrected/measured precipitation) are small in summer (less than 10%) and very large in winter (up to 80–120%) because of the increased effect of wind on gauge undercatch of snowfall. The CFs also vary over space, particularly in the snowfall season. The spatial patterns of CF are different from the measured and corrected precipitation especially in winter, with low CFs (20–40%) over the higher mid-latitudes and very high values (over 100%) along the windy Arctic coasts of low precipitation. Significant CF differences were also found across the USA/Canada borders mainly due to difference in catch efficiency between the national standard gauges. This inconsistency affects climate analyses over large regions, such as the Arctic as a whole (Fig. 2.4).

The impact of bias corrections on long-term precipitation changes over the northern regions was examined by calculating monthly trends for measured and corrected precipitation for the selected stations with records longer than 25 years during 1973–2004. Bias corrections generally enhance the long-term trends of monthly precipitation—indicating underestimation of precipitation changes,

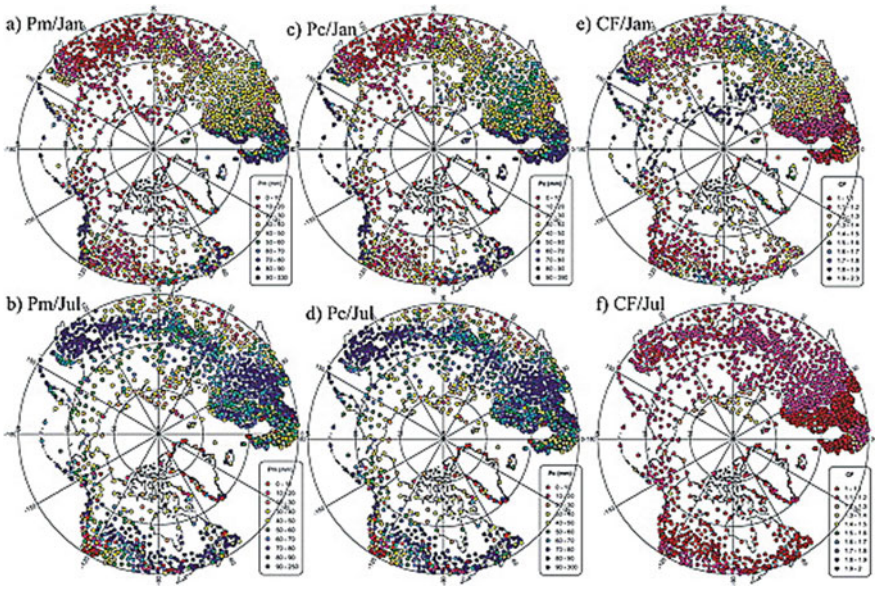

Fig. 2.4 Monthly mean gauge-measured (Pm) and bias-corrected (Pc) precipitation, and correction factor (CF) for January and July (Yang et al. 2005)

particularly for the regions with large changes, over the northern regions. These results clearly point to a need to utilize bias-corrected precipitation estimates to provide a better understanding of the Arctic freshwater budget and its change.

2.2.2 Remote Sensing Precipitation Products

During the last four decades space-borne sensors have enabled precipitation estimation with full areal coverage that can complement point measurements by gauge stations. Furthermore, they can provide complete coverage over both land and ocean, the latter of which is impossible through in situ network. However, remote sensing estimates also contain large uncertainties, especially in high latitudes where they still do not cover the entire high latitudes (e.g., Behrangi et al. 2012). Nevertheless, remote sensing of precipitation is an active area of research and development and significant progress has been made by improving both sensors and retrieval methods (e.g., Skofronick-Jackson et al. 2017).

Overall, four major types of sensors for precipitation estimation are infrared (IR) and microwave (MW) imagers and sounders, and more recently radars. IR data often lack a strong correlation with precipitation at fine spatiotemporal scales and show major limitations, especially for warm rain events (Behrangi et al. 2009). MW-based precipitation retrieval is more physical than IR-based as MW sensors sense hydrometeors in the entire atmosphere and capture bulk emission from liquid water at low frequencies and scattering by ice particles at high frequencies (Wilheit 1986). However, challenges such as insufficient sensitivity of sensors to light rain and snowfall, poor understanding of precipitation microphysics, unknown surface emissivity over snow and frozen land (Ferraro et al. 2013), problems in distinguishing light rain from clouds (Berg et al. 2006; Lebsock and L'Ecuyer 2011), and dependence of retrievals on prior knowledge of precipitation phase (Liu 2008) pose difficulties in MW-based retrieval of precipitation in high latitudes (Petty 1997). Radars typically provide the most direct and fine-scale observation of precipitation intensity. The 13.8 GHz Precipitation Radar (PR) aboard the Tropical Rainfall Measuring Mission (TRMM; Kummerow et al. 1998) has allowed advanced retrievals of moderate to intense rainfall over tropics (37° S–37° N) since 1997. However, it has no coverage in high latitudes and its sensitivity ($\sim$17 Dbz) makes it poorly suited to retrieve light rain and snowfall (Short and Nakamura 2000; Behrangi et al. 2012).

Combining multiple sensors (e.g., IR, MW) aboard multiple platforms is a popular means to enhance accuracy or spatiotemporal resolution of precipitation estimates (e.g., Hsu et al. 1997; Sorooshian et al. 2000; Kuligowski 2002; Huffman et al. 2007; Behrangi et al. 2010). Due to lack of quality precipitation products and geographical coverage of geostationary IR, several of the current combined products do not cover regions poleward of latitude 60 or 65 degrees in both hemispheres. The most popular combined products with global (90° S–90° N) coverage are (1) the Global Precipitation Climatology Project (GPCP; Huffman et al. 1997; Adler et al. 2003, 2016) which uses a combination of space-borne sensors over land

and ocean and gridded in situ observations from the Global Precipitation Climatology Centre (GPCC; Schneider et al. 2017) for monthly bias adjustment over land, and (2) the Climate Prediction Center (CPC) Merged Analysis of Precipitation (CMAP) product (Xie and Arkin 1997) which provides gridded global monthly estimates of precipitation using many of the same datasets as GPCP, plus Microwave Sounding Unit data. Furthermore, the method of merging the individual data sources in CMAP is different from GPCP.

During the last 15 years several new capabilities have emerged that can help improve retrieval of precipitation in high latitudes. These are mainly the launch and operation of CloudSat (Stephens 2008), the Global Precipitation Measurement (GPM) mission (Skofronick-Jackson et al. 2017), and the Gravity Recovery and Climate Experiment (GRACE) (Tapley et al. 2004).

CloudSat

The 94 GHz (W band) Cloud Profiling Radar (CPR) aboard CloudSat with a minimum detectable signal of ~ -28 dBZ was launched in 2006. The high sensitivity of CloudSat allows for detection and estimation of light rainfall, drizzle, and snowfall that is often missed by other sensors (Behrangi et al. 2012, 2014a) thus CloudSat has enabled assessing the performance of several existing products in high latitudes. Figure 2.5 shows the contribution of light precipitation to total precipitation occurrence and amount over high-latitude ocean in the Northern Hemisphere. For example, it shows that at 65° N and higher latitudes, more than 70% of total precipitation occurs at intensities less than 0.5 mm/hr which sum up to about 15% and 40% of total precipitation amount at $\sim$65° N and 80° N,

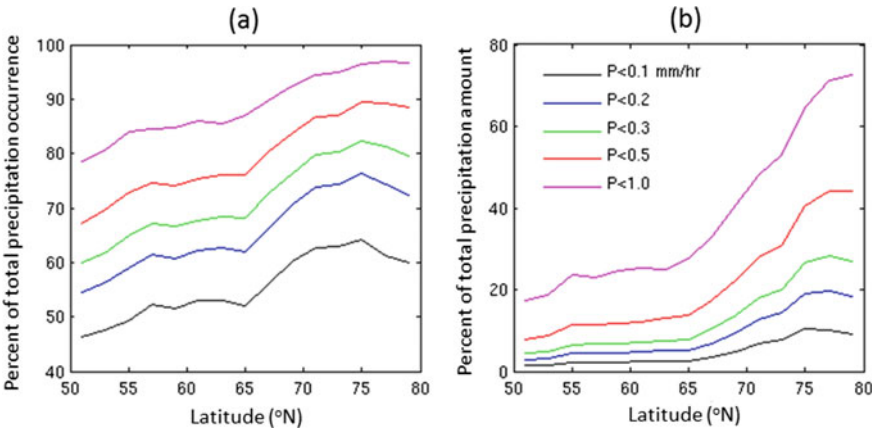

Fig. 2.5 Contribution of light precipitation to **a** total precipitation occurrence and **b** total precipitation amount over high-latitude ocean. Light precipitation is defined as precipitation rate below threshold P shown in legend of panel (**b**). Precipitation rates are obtained by accumulating rain, mixed phase, and snow intensities from four years (2007–2010) of CloudSat rain and snow products

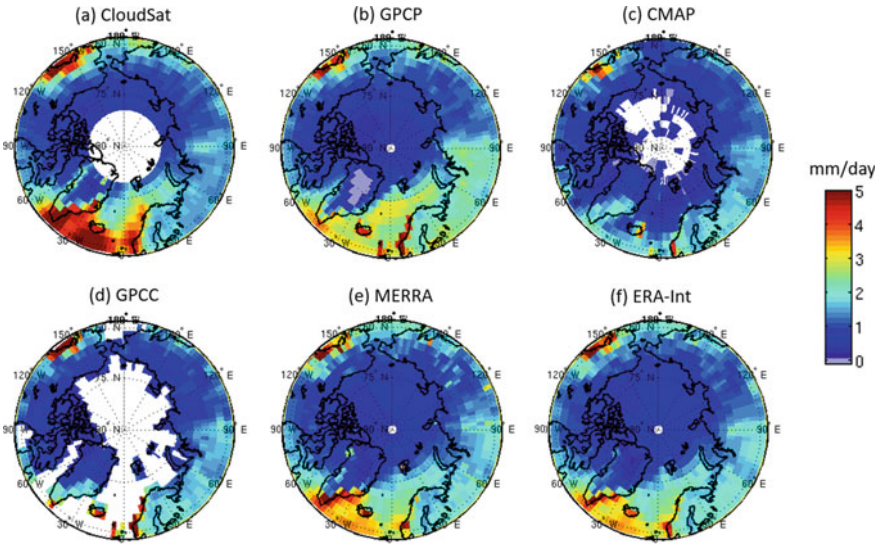

Fig. 2.6 Maps of four-year (2007–2010) averaged precipitation rates (mm/day) constructed from CloudSat, GPCP, CMAP, GPCC, MERRA, and ERA-Interim over land and ocean north of latitude 57°. Missing or non-reported data are shown in white. The figure is from Behrangi et al. (2016) with modifications

respectively. Note that 0.5 mm/hr typically exceeds the sensitivity of most of the precipitation sensors prior to CloudSat.

Figure 2.6 shows maps of four-year (2007–2010) averaged precipitation rates (mm/day) north of latitude 57° N constructed from CloudSat, GPCP, CMAP, GPCC, and two popular reanalysis products: the Modern-Era Retrospective Analysis (MERRA; Bosilovich et al. 2011) and European Center for Medium-Range Weather Forecasting (ECMWF) global atmospheric reanalysis (ERA-Interim; Dee et al. 2011). GPCC is based on gauge observations so reports no ocean data, suggesting that satellite data is critical to fill the observational gaps. Despite the general agreement in their seasonal patterns, several interesting features can be observed from Fig. 2.6. For example, based on CloudSat estimates, the highest precipitation rates are in the North Atlantic up to the coast of Greenland and along the southern coast of Alaska. This is not clearly seen in GPCP and CMAP. Furthermore, over the Atlantic south of 70° N, CloudSat reports average precipitation about or greater than 5 mm/day and shows a noticeable precipitation gradient around 70° N over the Atlantic Ocean. These features are not well produced in GPCP and reanalysis show less precipitation intensity than CloudSat.

Table 2.1 shows the annual (2007–2010) precipitation rates from the products shown in Fig. 2.6, separately over land and ocean. As can be seen GPCC has the lowest and GPCP has the highest annual rates. GPCC full product used here does not include gauge corrections, while GPCP uses a gauge correction based on the

Table 2.1 Summary of annual (2007–2010) precipitation rate of products over land and ocean north of latitude 57° (shown in Fig. 2.6)

Products	Annual precipitation rate (mm/year)	
	NH land	NH ocean
CloudSat	478	684
GPCP	557	692
CMAP	433	330
GPCC	447	_
MERRA	553	653
ERA-Interim	528	641

Legates climatology (Legates and Willmott 1990) that may result in overestimation of precipitation, especially over Eurasia and western Siberia, based on previous studies (Behrangi et al. 2014b, 2016). Furthermore, in estimating precipitation from CloudSat, an experimental product is used for rainfall over land.

GPM

The GPM core observatory satellite was launched in February 2014 and carries two important instruments for precipitation estimation: (1) the Dual-frequency Precipitation Radar (DPR) with Ku/Ka (13.6/35.5 GHz) bands and (2) the GPM Microwave Imager (GMI) which has 13 channels with frequencies ranging from 10 to 183 GHz (Draper et al. 2015). These instruments cover ~60° S-N, extending TRMM's coverage (~37° S-N) to higher latitudes. The better sensitivity of the GPM DPR (~0.2 mm/hr) relative to the single Ku frequency TRMM PR (~0.5 mm/hr), four additional high-frequency channels on the GMI, and advanced retrieval techniques (Kummerow et al. 2015, 2016) have added new capabilities to detect and quantify snowfall and rainfall everywhere, including polar regions. This is an important advancement, as the Passive Microwave precipitation retrievals used to be significantly low or missing over frozen surfaces in the pre-GPM era (Behrangi et al. 2014a). Initial analysis of the latest GPM products have shown that the accuracy of GPM PMW products has improved in high latitudes (Kummerow et al. 2016). It should be noted that the products are currently under development and evaluation. In the near future the products will not only include the GPM post-launch era, but will also be available for earlier periods by applying the latest retrieval methods to the constellation of low Earth-orbiting sensors.

GRACE

The GRACE mission (Tapley et al. 2004) has retrieved mass variations within the Earth with high accuracy since 2002. Recent studies have shown that GRACE observations are valuable for precipitation estimation in cold regions (Swenson 2010; Boening et al. 2012; Behrangi et al. 2017). Precipitation accumulation can be calculated using GRACE Terrestrial Water Storage Anomaly (TWSA) estimates based on the mass conservation principle, dictating that any change in one component of the water balance must be compensated for by the same amount collectively in the other components (e.g., Dingman 2008). The application of this

concept over cold regions in high latitudes can leverage recent advances in estimating TWSA from GRACE (e.g., through mascons solution; Watkins et al. 2015), low uncertainties in remotely sensed ET in cold regions, and runoff observations to provide observational constraints on basin- and grid-level precipitation estimates. By applying this method over Eurasia, Behrangi et al. (2016) showed that GPCP precipitation rates over Eurasia are almost twice those estimated by CloudSat and GRACE. This is consistent with previous findings of Behrangi et al. (2014b; via water vapor convergence) and Swenson (2010), and is likely related to overcorrection for gauge undercatch in GPCP. This overestimation can also be seen in Fig. 2.6. Behrangi et al. (2017) also used a similar concept and compared GRACE-based precipitation accumulation with GPCP and a few other products over large endorheic basins in the Tibetan Plateau. While the results matched fairly well in summer, GPCP showed ~30% bias compared to GRACE estimates in winter, when accurate precipitation retrieval is more difficult. It was also shown that GRACE can provide valuable insights on gauge undercatch correction factors that otherwise are often difficult to assess (Behrangi et al. 2018).

2.3 Precipitation Characteristics Over the Arctic

Due to extremely low air temperatures, trace precipitation (less than the minimum measurable amount for a given gauge) is very common (Yang et al. 1988). Thus, accounting for trace precipitation is important over vast parts of the Arctic, where precipitation amounts are very low and the sum of all trace amounts becomes a significant portion of total precipitation. Including trace events may increase the amount of precipitation by up to an additional 20% (Mekis 2005). The number of days with precipitation below 1 mm is averaged at about 51 and 69% of total wet days in winter and summer respectively and contributes to about 13 and 5.2% of their corresponding seasonal precipitation total on average.

Precipitation estimates in terrestrial Arctic regions vary from over 1,000 mm at the southern coast of Greenland, western Scandinavia, and the northeastern Pacific with amounts decreasing to about 300 mm in Northern Siberia and Northern Canada to the lowest total precipitation of <150 mm over Northern Greenland and the northern Canadian Arctic archipelago (Serreze and Hurst 2000). Over the Arctic Ocean, annual precipitation is estimated to be 260 mm (about 60–100% in snow), based on records from drifting stations after bias corrections increases 40–90%; Yang et al.1995; Goodwin et al. 1988).

In addition, there is very strong seasonality in precipitation characteristics over the Arctic given the large land coverage that consists of diverse climate regimes. For example, over Northern Eurasia, precipitation is lowest in winter (about 84 mm), followed by spring (98 mm). The highest occurs in summer (205 mm), followed by fall (143 mm). In general, winter and spring precipitation shows a longitudinal pattern of wetter along both coasts and drier inland. Western European Russia receives about 150 mm and this decreases to about 100 mm in western

Siberia, 50 mm or lower over northeastern Siberia and then increases again along the coast of eastern Siberia (Fig. 2.7a, b). There is also a strong localized precipitation of up to 600 mm along the east shore of the Black Sea, possibly related to Lake Effect snow and orographic lifting (Korzun 1984; Lydolph 1977; Ye 2001, 2016a, b). Summer and fall precipitation have a latitudinal pattern of higher in the south and lower toward the north (Fig. 2.7c, d).

The number of wet days (including days with 0.1 mm or higher daily precipitation total) is highest in winter of up to 60 days or more over northern European Russia and northwestern Siberia. Fall has the second highest number of wet days and spatial patterns resembling that of the winter season (Fig. 2.7e, h). The area-averaged value is about 40 days in winter and fall. Spring and summer have

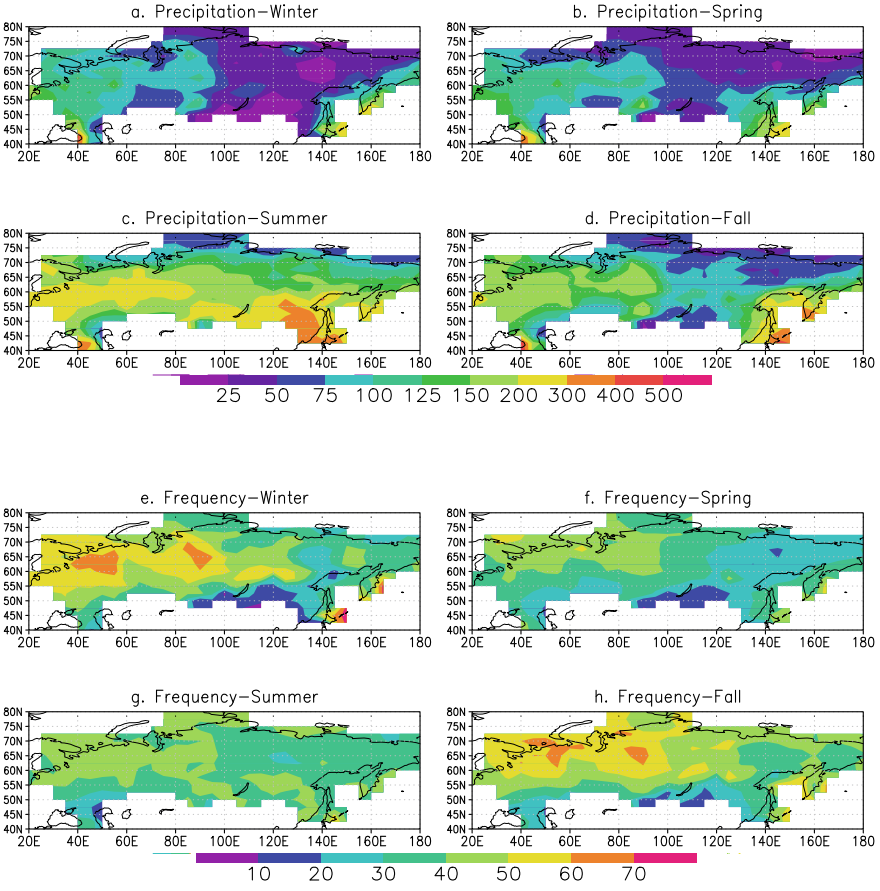

Fig. 2.7 Geographical distributions of seasonal precipitation total (mm) and frequency (wet days) based on 1966–2010 (Ye et al. 2016a)

similar distributions of low wet days of mean 32 days and 37 days respectively (Fig. 2.7f, g).

As a result, summer has the highest daily precipitation intensity of 5.4 mm/day with a well-defined zonal distribution decreasing toward the north, followed by the fall of 3.7 mm/day. Fall and spring have similar patterns of daily precipitation intensity distribution with spring having a slightly lower precipitation intensity of 3.0 mm/day. Winter has the lowest daily intensity of only 2 mm/day (Fig. 2.8). For all seasons, the highest intensities are found in the wet regions along the east shore of the Black Sea and along the southeastern coast near the Pacific Ocean. From Figs. 2.7 and 2.8, one can clearly see that there are very different precipitation characteristics between winter and summer. Winter precipitation is made up of very frequent low-intensity events while summer features more sporadic but intense precipitation. Spring and fall precipitation characteristics lie between those of winter and summer but with an evident zonal pattern more characteristic of summer precipitation intensity rather than the longitudinal pattern that characterizes winter precipitation intensity.

The entire state of Alaska is located north of 45° N, defined in this book as the southern boundary of the pan-Arctic hydrologic region. The climate within the state of Alaska ranges from maritime on Alaska's southeast coast to Arctic in the region north of the Brooks Range. Alaska is commonly separated into several climate zones that are useful in describing precipitation distribution across the state: Arctic, Interior, West Coast, Aleutians, Cook Inlet, and Alaska Southeast Coast (Shulski and Wendler 2007; Kane and Stuefer 2013).

Precipitation distribution in Alaska is controlled by the state's large geographic extent, proximity to the oceans, and extreme topographic gradients—from sea level to the highest peak of North America (Denali 6,190 m). Mean total precipitation

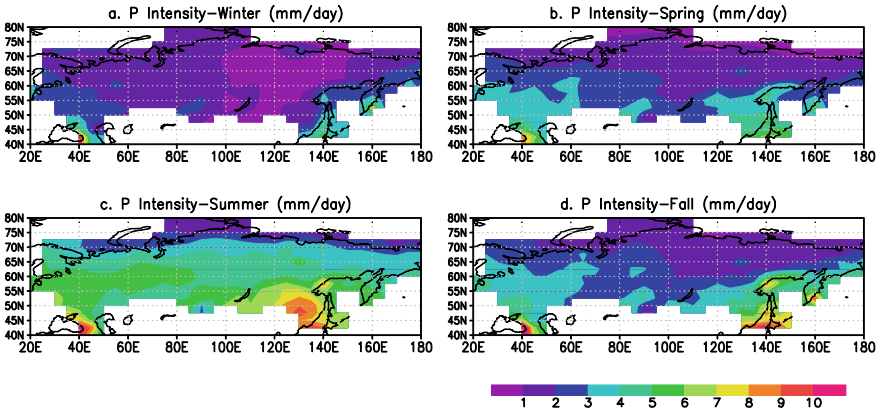

Fig. 2.8 Geographical distribution of mean seasonal precipitation intensity based on 1966–2010 (mm/day) (Ye et al. 2016a)

has large spatial variation from 3,000 mm in Alaska Southeast Coast to 250 mm in Arctic Coastal Plain (Kane and Stuefer 2013).

Precipitation frequency is much higher in the southern portions of the state in comparison to the Interior and Arctic regions. The mean annual statistics on the number of days with precipitation above 2.5 mm can serve as a metric that shows high variability in frequency across Alaska. For example, Barrow (Arctic) has 11 days a year with precipitation above 2.5 mm, 31 days for Fairbanks (Interior), and 143 days for Kodiak (Alaska Southeast Coast) (Shulski and Wendler 2007).

Seasonally, the frequency of precipitation (number of days with precipitation) in the Arctic and Interior Alaska regions is highest in July–August and lowest in April. The percentage of precipitation falling as solid on the Arctic Coastal Plain is on average about 60%, ranging from 40 to 88% (Stuefer and Kane 2016; Stuefer, Kane, and Liston 2013). The intensity of precipitation in Arctic Alaska is highest during summer months due to warmer air temperatures and ice-free coastal seas that allow air masses to hold more moisture (Shulski and Wendler 2007). Alaska Southeast Coast and Aleutians have extreme precipitation later in the year, during fall and winter. The largest 1-day precipitation event in Alaska—382 mm—was recorded on 10 October 1986 in Seward (Alaska Southeast Coast); this information supersedes the previous record for Angoon station (Brettschneider and Trypaluk 2014). For comparison, the largest 1-day precipitation event of 87 mm occurred in Fairbanks (Interior) on 12 August 1967 (Perica et al. 2012), resulting in historical flooding of Fairbanks and led to the construction of the flood control facilities around the city.

a. Changes in Precipitation Characteristics Based on Historical Records

Studies of observed precipitation trends in the terrestrial Arctic suggest that the magnitude and direction of trends very much depend on the specific region considered and the particular period of analysis. In general, warming over the Arctic region is associated with upward trends in total precipitation and extremes, however the magnitude and direction of trend may vary with the selected time period (e.g., Alexander et al. 2006; Bieniek et al. 2014; Tebaldi et al. 2006). It is estimated that total precipitation over the Arctic in the past century increased at a rate of about 1% per decade (ACIA 2005). The exception is for summer, when precipitation may have been decreasing in many regions (Dirmeyer et al. 2013; Ye et al. 2016a). The decrease is estimated at about 0.79 mm/year over the terrestrial pan-Arctic during 1989–2005 based on ERA-Interim data (Rawlins et al. 2010).

Canada has seen significant increases in precipitation, especially northern Canada including the Canadian Arctic Archipelago (Mekis and Vincent 2011a, b; Vincent et al. 2015; Rapaic et al. 2015). An increase in precipitation total in spring over British Columbia and the Canadian Prairies has been accompanied by increasing air temperature (Jarujareet 2016; Martin 2017). Although no significant changes in total wet days over British Columbia have been found, significant decreases in snowfall days and frozen rain days were found (Montenegro 2015). A study over Southeast Canada suggests that decreases in wet days during summer and fall occur as air temperature increases (Chamnansiri 2016).

Positive trend in total precipitation in Alaska Arctic Coastal stations was found during more recent decades 1981–2012 (Bieniek et al. 2014). During this period, an increase in October and November monthly precipitation was the most pronounced, i.e., November precipitation increase was 7.4 mm from 1981 to 2012.

Regional analysis of three gridded datasets (GPCC, CRU, and UDEL) in Alaska Arctic supports an increasing trend in total precipitation during 1980–2010 time period (McAfee et al. 2014). Total precipitation in Utqiaġvik (former Barrow, Arctic) shows no significant decrease during 1950–2010, (McAfee et al. 2013). Similarly, total change in mean accumulated precipitation in Utqiaġvik was reported as −1.7 mm from 1949 to 2012, with largest decrease of −2.3 mm observed in summer (Bieniek et al. 2014).

Precipitation total over Eurasia in general has been increasing in winter (Ye 2001) but not changing much in other seasons (Ye et al. 2016a). This is in general consistent with the observation that increasing atmospheric water vapor associated with higher air temperature is related to higher precipitation efficiency in winter and lower precipitation efficiency in summer (Ye et al. 2014).

Most evident is increasing precipitation extremes over Northern Eurasia (Groisman et al. 2005; Zolina et al. 2010). The daily intensity is about 1–3% per degree of air temperature increase in all seasons (Ye et al. 2015, 2016a) over northern Eurasia. Over Canada, 2/3 of regions have shown increases in extreme rainfall amount (Shephard et al. 2014). It appears that increasing higher intensity precipitation is accompanied by decreasing lower intensity precipitation (Ye et al. 2015).

Convective precipitation appears to be increasing at the expense of non-convective precipitation (Ye et al. 2016b, 2017). The transitional seasons of spring and fall have become summer-like by the late 1980s when occurrence of convective precipitation outnumbered non-convective precipitation (Ye et al. 2017). Increasing extremes and daily intensity are occurring in the convective precipitation events which are getting stronger and more frequent (Ye et al. 2017). Changes in atmospheric water vapor or specific humidity appear to be key to changes in precipitation characteristics (Ye and Fetzer 2009; Ye et al. 2014, 2017).

2.4 Extreme Precipitation: Case Studies

a. An Alaska Example in the twenty-first century

Extreme precipitation events can have major consequences for ecosystems, infrastructure, and humans. The frequency and intensity of extreme precipitation events have been increasing in much of the world, and the increase of the highest percentiles of daily precipitation amounts have exceeded the increases in the median amounts in many areas (IPCC 2013; USGCRP 2014). However, there have been few studies of extreme precipitation in the Arctic. A recent study (Lader et al. 2017) used regional dynamical downscaling with the Weather Research and Forecasting Model (WRF) to investigate projected twenty-first-century changes of extreme precipitation over Alaska. The forcing data used for the downscaling

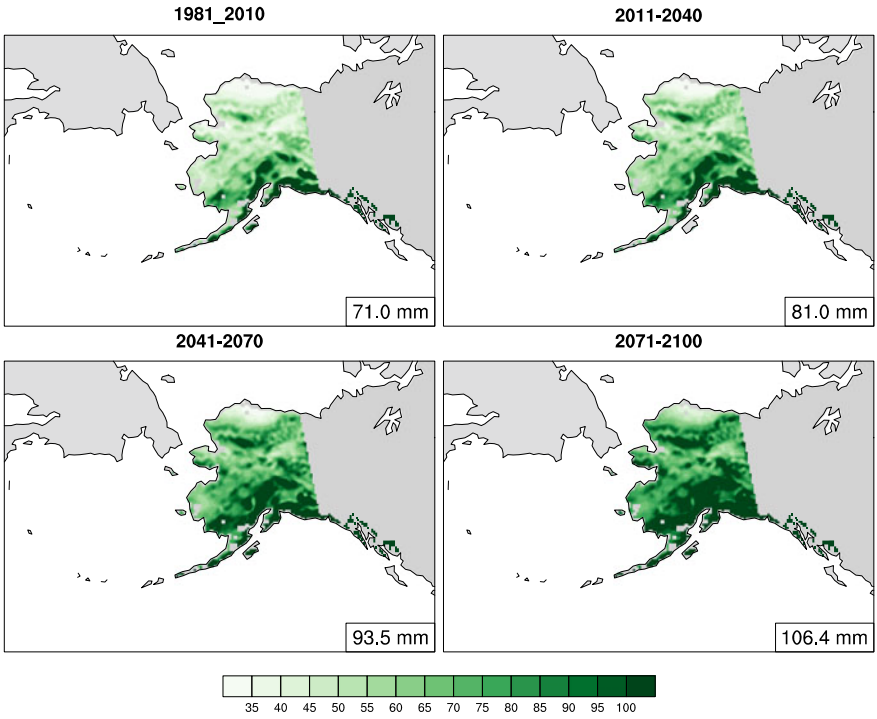

Fig. 2.9 30-year means of the annual maximum consecutive 5-day precipitation (mm). The statewide average is located at the bottom right

simulations included the ERA-Interim reanalysis and GFDL-CM3 climate model output for a historical period (1976–2005), and GFDL-CM3 RCP8.5 for the future (2006–2100). A quantile mapping procedure was used to bias-adjust the distributions of the daily precipitation simulated for a historical period.

In the model simulation, the statewide average of the annual mean accumulation increases from 79.3 cm yr^{-1} during the base period (1981–2010) to 121.2 cm yr^{-1} by 2071–2100 (Fig. 2.9), an increase of 53%. The changes to extreme precipitation are similarly dramatic. The average annual count of heavy precipitation days ($\geq$ 10 mm) and very heavy precipitation days ($\geq$ 20 mm) increases by 66% and 101%, respectively (Table 2.1). The average annual maximum 1-day (Table 2.1) and 5-day (Fig. 2.1) precipitation amounts are also projected to increase by more than 50% by the end of the century. The greatest relative change by percentage is expected for the Brooks Range and locations further north. The average annual maximum number of consecutive wet days ($\geq$ 1.0 mm) is projected to increase by 23%, whereas the number of consecutive dry days is projected to decrease by 21% (Table 2.1). This does not necessarily mean that the threat for severe drought would

decrease, however, because higher temperatures would lead to greater daily evapotranspiration.

There is also an apparent connection between diminishing sea ice and extreme precipitation across western Alaska. The average daily sea ice extent during March, when the climatological maximum annual extent is reached, extends well south in the Bering Sea to between St. Paul Island and the Aleutians from 2011–2040, but this line recedes into the Chukchi Sea from 2071–2100. Coincident with these losses of sea ice is an increasing trend for greater extreme precipitation, first for the Aleutians and southwest Alaska from 2041–2070, and then for the Bering Strait and northwest Alaska from 2071–2100 (Table 2.2). Possible mechanisms for this relationship include shifting storm tracks and dynamics along the ice edge, and greater local evaporation in areas where sea ice has been replaced by open water (Kopec et al. 2015).

One of the few studies to examine corresponding trends in station data aggregated by climate divisions (Bieniek and Walsh 2017) did not find a significant increase in heavy precipitation events over Alaska during the 1920–2012 period. Similarly, Perica et al. 2012 reported lack of significant trends in annual precipitation maxima time series, used to update precipitation frequency estimates in the state of Alaska. This finding may well be a consequence of the precipitation measurement network, which is not only sparse over Alaska but is subject to the measurement errors and lack of bias-correction that limit the reliability of precipitation data for the Arctic (Yang et al. 2005).

b. Under Reporting of Daily P_{max}

To investigate the impact of bias-correction on precipitation extremes, a subset of 1329 stations with over 15-year records within the period 1973–2004 were extracted from the bias-corrected daily precipitation dataset of Yang et al. (2005). A quality control was applied for extracting daily precipitation maximum in each year; a year was rejected if the fraction of missing data exceeded 5%.

The mean yearly gauge-measured daily maximum precipitation Pm_{max} at the sites ranges from 18 to 167 mm with a mean value of 53 mm over the northern regions. The spatial patterns of the mean values are characterized by low daily maximum precipitation in the near-polar region and west coast of Europe, moderate daily maximum precipitation along latitude 60ºN in Eurasia and along the lower latitude than 60° N in North America, and high daily maximum precipitation interspersing in the lower latitude than 60° N of Eurasia and the coasts of Pacific Ocean (Fig. 2.10a). Underestimation of the gauge-measured daily maximum precipitation over the northern regions is significant (Fig. 2.10b). The mean yearly corrected daily maximum precipitation Pc_{max} ranges from 20 to 185 mm with a mean value of 59 mm over the northern regions. Despite the general agreement in the spatial pattern of the gauge-measured daily maximum precipitation extremes, and the corrected precipitation extremes, several regional features can be identified in Fig. 2.10a, b. For example, the bias correction does not change the pattern of the precipitation extreme distribution, and the high precipitation maxima (>60 mm/d) are mainly concentrated in western northern Eurasia. The increased

Table 2.2 The median (Med), 90th percentile (90P), 99th percentile (99P), maximum (Max) and annual total of daily precipitation (mm) averaged over successive 30-year periods for the nearest downscaled grid cell to selected **cities** in Alaska. Values are for model grid cells containing stations

Station		Precipitation (mm)				
		Median	90th % ile	99th % ile	Max daily	Annual mean
Barrow	1981–2010	0.07	1.73	6.99	24.62	217.72
	2011–2040	0.10	2.06	8.04	30.67	263.93
	2041–2070	0.12	2.69	9.77	28.67	335.84
	2071–2100	0.19	3.58	12.28	34.68	439.88
Nome	1981–2010	0.06	4.66	17.47	43.43	541.55
	2011–2040	0.12	5.61	21.10	48.52	661.58
	2041–2070	0.15	7.02	25.23	62.91	825.44
	2071–2100	0.24	8.62	29.77	93.62	1022.17
McGrath	1981–2010	0.35	5.59	16.50	39.34	683.52
	2011–2040	0.50	6.36	18.72	50.56	794.53
	2041–2070	0.61	7.62	21.61	88.60	944.63
	2071–2100	0.65	7.82	25.02	90.53	1010.98
Fairbanks	1981–2010	0.18	4.02	13.62	45.37	495.86
	2011–2040	0.21	4.62	16.39	68.76	582.42
	2041–2070	0.26	5.48	18.80	97.92	696.25
	2071–2100	0.33	6.22	21.27	65.54	797.80
Anchorage	1981–2010	0.21	5.79	18.49	65.77	686.93
	2011–2040	0.21	6.77	22.25	54.11	796.59
	2041–2070	0.19	7.42	25.09	64.39	879.51
	2071–2100	0.20	8.86	28.51	102.48	1024.03
Juneau	1981–2010	1.37	14.18	32.88	92.07	1747.05
	2011–2040	1.25	15.16	35.72	144.02	1816.60
	2041–2070	0.86	16.77	41.80	137.88	1963.05
	2071–2100	1.16	20.54	47.72	163.74	2353.02

amounts/percentages of precipitation extremes show a noticeable gradient from low latitude to the north polar Ocean (or coast) in Fig. 2.10c, d, for instance, along Urals (the longitude 60° E). Since these spatial patterns in daily maximum precipitation are mainly influenced by rainfall regimes and snowfall distributions, they are slightly different from general precipitation maps for the northern latitudes (Legates 1995; Adam and Lettenmaier 2003; Fekete et al. 2004).

Apart from the impact of regional climate patterns, the underestimation of gauge-measured daily maximum precipitation is also influenced by gauge catch efficiency. For instance, the catch efficiency of the Canadian Nipher snow gauge is much higher than the US NWS 8-inch standard gauge particularly for high wind speeds (Yang et al. 2005). Here we selected 480, 55, and 167 sites in Russia, the

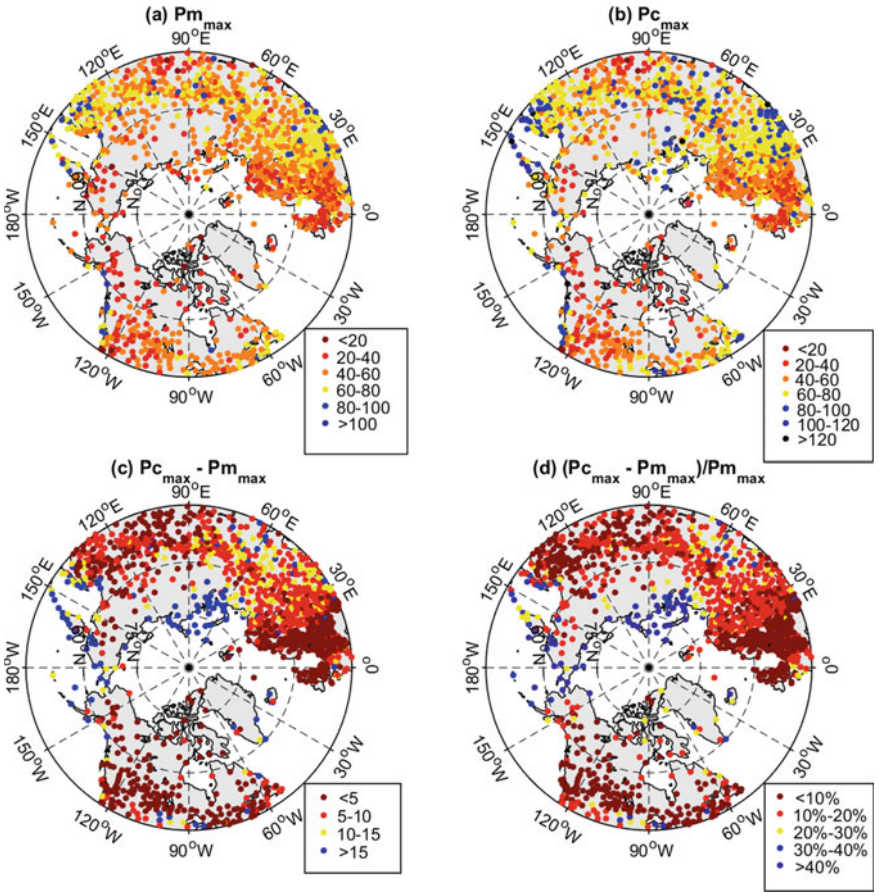

Fig. 2.10 Average of daily maximum precipitation for measured (**a**) and bias-corrected (**b**) data, respectively; average bias corrections of daily maximum precipitation (**c**); mean relative correction (**d**)

United States, and Canada, respectively, and impacts of gauge catch efficiency are shown by comparing minimum, maximum, and mean values of measured and corrected daily maximum precipitation at the sites in Fig. 2.11. Generally, the median values of minimum Pm_{max} and Pc_{max} are all no more than 20 mm in the three countries, while the median values of maximum Pm_{max} and Pc_{max} in Russia are much higher than the other two. This is mainly attributed to the regional climate difference. In addition, the United States and Canada are in the same region with comparable maximum and mean Pc_{max}, although maximum and mean Pm_{max} are all smaller in the United States. This indicates the correction factors play a significant role due to difference gauge catch efficiencies.

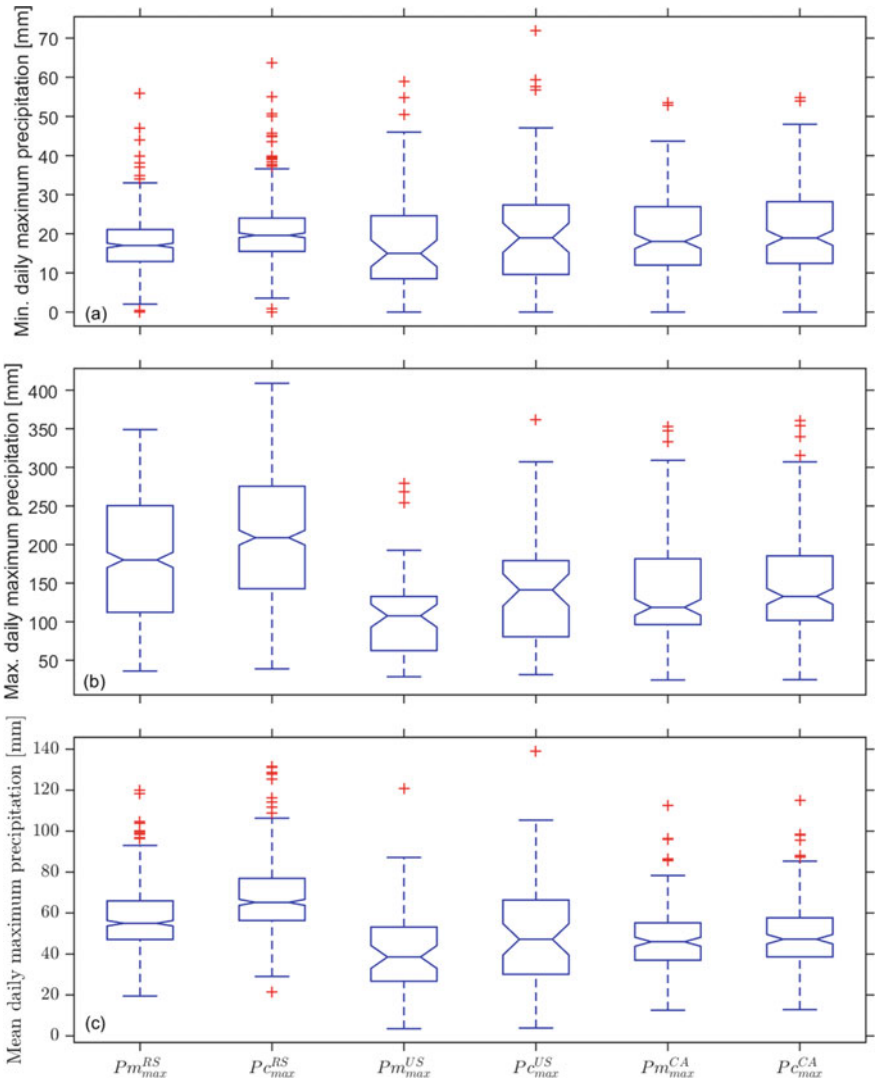

Fig. 2.11 Statistics of minimum (**a**), maximum (**b**), and mean (**c**) values of measured and corrected daily maximum precipitation at the sites in Russia, the United States, and Canada using different types of gauges. RS: Russia; US: United States; CA: Canada

2.5 Future Projection by Climate Models

Using state-of-the-art GCMs within the framework of CMIP5 to systematically quantify projected Arctic precipitation trends, Bintanja and Selten (2014) showed that the projected increases in Arctic precipitation over the twenty-first century,

which peak in late autumn and winter, are due mainly to strongly intensified local surface evaporation, and only to a lesser degree to enhanced moisture inflow from lower latitudes. They also demonstrated that Arctic precipitation will continue to increase and possibly even accelerate in the twenty-first century with Arctic mean precipitation sensitivity of 4.5% increase per degree of temperature warming which is much larger than the global value (of 1–3%). Using a subset of the IPCC AR4 GCMs, Kattsov et al. (2007) have also showed that precipitation over the Arctic Ocean and its terrestrial watersheds, including the Ob, the Yenisey, the Lena, and the Mackenzie will increase through the twenty-first century, showing much faster percentage increases than global mean precipitation. The precipitation changes over the Arctic Ocean have also exhibited pronounced seasonality, with the strongest relative increase in winter and fall, and the weakest in summer (Kattsov et al. 2007). These are in general consistent with results for historical data records.

Based on the nine GCMs examined in the CMIP3, Rawlins et al (2010) calculated precipitation trends over the terrestrial Arctic basins during the 1950–2049 period ranging from 0.24 to as much as 0.92 mm/year, with the multi-model mean trend at 0.65 mm/year. Modeled results have also showed overall increases in snowfall and SWE associated with a projected increase in cold season precipitation in northeastern Eurasia and northern Canada, while they show decreases in more southerly locations where warming effects dominated, with the −10 and −20 °C late twentieth-century winter air temperature isotherm lines representing the transition boundaries for snowfall (Krasting et al. 2013; Deser et al. 2010) and SWE (Raisanen 2008) respectively.

Based on an ensemble-mean scenario, Barrow et al. (2014) have reported that the largest end-of-century increases in precipitation of 20–25% wetter are projected to occur in northern and eastern areas of Canada, while in more southerly regions precipitation increases are likely to be between 0 and 10% above 1961–1990 baseline conditions. They also observed large seasonal and spatial differences with projected increases in summer precipitation and decreases in winter precipitation in northern Canada while the reverse is true for the southern prairie provinces and British Columbia.

Summarizing various studies on projected changes in Canadian precipitation, Bush et al. (2016) concluded that, while projections of precipitation change are generally less robust and exhibit greater variability among models than those for temperature, increases in precipitation are projected for the majority of the country and for all seasons, the exception being parts of southern Canada where a decline in precipitation in summer and fall is projected.

After assessing projected changes to 1-, 2-, 3-, 5-, 7-, and 10-day annual maximum precipitation amounts over Canada, Mladjic et al. (2011) presented evidence that, while the Canadian Regional Climate Model (CRCM) underestimates precipitation extremes over most of Canada, when evaluated against observed changes, the northern Canadian climatic regions generally exhibit the highest percentage change in 20-, 50-, and 100-year return levels of precipitation extremes. Moreover, statistical frequency analysis of projected precipitation over the different regions of Canada by Mailhot et al (2010) suggests that daily and multi-day extreme

precipitation events will be more intense and frequent in a future climate for all regions except the prairie provinces. In some regions (e.g., west coast of British Columbia), the return period associated with a given precipitation intensity in historical climate will decrease by a factor of five over the 2080–2100 period.

2.6 Concluding Remarks and Future Research

While precipitation represents one of the largest water fluxes in Arctic terrestrial hydrology, it is one of the most challenging variables to quantify at watershed scale due to the cold snow-dominated environment, limited in situ data, and heterogeneity of the landscape (e.g., Rawlins, et al. 2007). Similarly, Arctic terrestrial precipitation trends are inherently difficult to detect given snowfall measurement challenges resulting from gauge undercatch of solid precipitation, sparsely distributed observations, low precipitation amounts, and the scarcity of long-term records (Serreze and Hurst 2000; Adam and Lettenmaier 2003; Yang et al. 2005). The compounding effects of elevation on precipitation in topographically complex regions of the Arctic, where the distribution of observing stations is biased toward low elevations and coastal regions is also a factor.

Surface precipitation observation technologies are moving away from manual observations to automated stations. Joining manual and auto gauge observations are essential for the creation of longer time series. In order to avoid artificial discontinuity affecting the trend, proper transfer functions, adjustment using overlapping periods, and/or homogeneity testing should be applied. Further research is required for precipitation type and snowfall amount observations from in situ operational automatic stations.

Over the last four decades the emergence of remotely sensed data has enabled advances in retrieving precipitation rate, frequency, and spatial distribution over both land and ocean. The more recent instruments such as CloudSat, GPM core observatory, and GRACE together with advances in retrieval methods have provided added information that can further refine or constrain precipitation estimates in cold regions including high latitudes in the northern hemisphere. Other experiments such as the World Meteorological Organization (WMO) Solid Precipitation Intercomparison Experiment (SPICE) project (2013–2016) (Rasmussen et al. 2012; Kochendorfer et al. 2017) have also enhanced bias correction of in situ data in various climate regimes. These recent datasets collectively provide an unprecedented opportunity to advance estimation of precipitation amount, distribution, and changes in high latitudes, especially in the northern hemisphere where signals of change are robust. Therefore, more research in exploiting remote sensing techniques for measuring high-latitude precipitation and evapotranspiration should be pursued.

There are still systematic differences between precipitation in climate model simulations for the historical periods and considerable across-model scatter for future scenarios. While the range between individual model simulations is

substantial, it is noteworthy that a comparable scatter exists even among different observational data (ACIA 2005). Research on examining climate model CMIP5' simulation on different types of precipitation show models overestimate non-convective precipitation and underestimate convective precipitation (Kusunoki and Arakawa 2015). One way to address these shortcomings is through the use of an Arctic regional climate system model that allows increased horizontal and vertical resolution and improved model physics that are optimized for polar regions (Maslowski et al. 2011).

Related to extreme short-duration rainfall projections, Zhang et al. (2017) state that it is challenging because of our poor understanding of its past and future behavior. The characterization of past changes is severely limited by the availability of observational data. Climate models, including typical regional climate models, do not directly simulate all extreme rainfall producing processes, such as convection. Recently developed convection-permitting models are better at simulating extreme precipitation, but this type of simulation is not yet widely available due to computational cost and possible uncertainties. Until better methods are available, the evidence observed from historical records and the relationship of the atmosphere's water-holding capacity with temperature still provide guidance for planners in extratropical regions, albeit with large uncertainties.

References

Adam JC, Lettenmaier DP (2003) Adjustment of global gridded precipitation for systematic bias. J Geophys Res 108(D9): 4257. https://doi.org/10.1029/2002JD002499

Adler RF et al (2003) The version-2 global precipitation climatology project (GPCP) monthly precipitation analysis (1979-present). J Hydrometeorology 4:1147–1167

Adler RF, Gu G, Huffman GJ (2012) Estimating climatological bias errors for the global precipitation climatology project (GPCP). J Appl Meteorol Climatol 51:84–99

Adler RF, Gu G, Sapiano M, Wang J-J, Huffman GJ (2017) Global precipitation: means, variations and trends during the satellite era (1979–2014). Surv Geophys 38:679–699

Alexander LV, et al. (2006) Global observed changes in daily climate extremes of temperature and precipitation. J Geophys Res 111:D05109. https://doi.org/10.1029/2005JD006290

Arctic Climate Impact Assessment (ACIA) (2005) Arctic climate impact assessment. Cambridge Univ. Press, New York, 1042 pp

Barrow E, Maxwell B, Gachon P (2004) Climate variability and change in Canada; past, present and future. Meteorological Service of Canada Environment Canada, Toronto

Behrangi A, Gardner A, Reager JT, Fisher JB, Yang D, Huffman GJ, Adler RF (2018) Using GRACE to estimate snowfall accumulation and assess gauge undercatch corrections in high latitudes. J Clim 31:8689–8704

Behrangi A, Gardner AS, Reager JT, Fisher JB (2017) Using GRACE to constrain precipitation amount over cold mountainous basins. Geophys Res Lett 44:219–227

Behrangi A et al (2016) Status of high-latitude precipitation estimates from observations and reanalyses. J Geophys Res: Atmos 121:4468–4486

Behrangi A, Imam B, Hsu KL, Sorooshian S, Bellerby TJ, Huffman GJ (2010) REFAME: rain estimation using forward-adjusted advection of microwave estimates. J Hydrometeorology 11:1305–1321

Behrangi A, Hsu K-I, Imam B, Sorooshian S, Huffman GJ, Kuligowski RJ (2009) PERSIANN-MSA: a precipitation estimation method from satellite-based multispectral analysis. J Hydrometeorology 10:1414–1429

Behrangi A, Lebsock M, Wong S, Lambrigtsen BH (2012) On the quantification of oceanic rainfall using spaceborne sensors. J Geophys Res 117:D20105

Behrangi A, Tian Y, Lambrigtsen BH, Stephens GL (2014a) What does CloudSat reveal about global land precipitation detection by other spaceborne sensors? Water Resour Res 50:4893–4905

Behrangi A, Wong S, Mallick K, Fisher JB (2014b) On the net surface water exchange rate estimated from remote-sensing observation and reanalysis. Int J Remote Sens 2170–2185

Berg W, L'Ecuyer T, Kummerow C (2006) Rainfall climate regimes: the relationship of regional TRMM rainfall biases to the environment. J Appl Meteorol Climatol 45:434–454

Bieniek PA, Walsh JE, Thoman RL, Bhatt US (2014) Using climate divisions to analyze variations and trends in Alaska temperature and precipitation. J Clim 27(8):2800–2818. https://doi.org/10.1175/JCLI-D-13-00342.1

Bieniek PA, Walsh JE (2017) Atmospheric circulation patterns associated with monthly and daily temperature and precipitation extremes in Alaska. Int J Climatol 37:208–217

Bintanja R, Selten FM (2014) Future increases in Arctic precipitation linked to local evaporation and sea-ice retreat. Nature 509:479–482. https://doi.org/10.1038/nature13259

Boening C, Lebsock M, Landerer F, Stephens GL (2012) Snowfall-driven mass change on the East Antarctic ice sheet. Geophys Res Lett 39:L21501

Bosilovich MG, Robertson FR, Chen J (2011) Global energy and water budgets in MERRA. J Clim 24:5721–5739

Brettschneider B, Trypaluk C (2014) Reexamination of the Alaska 1-Day record rainfall. Bull Am Meteor Soc 95(8):1249–1256. https://doi.org/10.1175/BAMS-D-13-00027.1

Brown RD, Braaten RO (1998) Spatial and temporal variability of Canadian monthly snow depths, 1946–1995. Atmos Ocean 36(1):37–54. https://doi.org/10.1080/07055900.1998.9649605

Bulygina ON, Razuvaev VN (2012) Daily temperature and precipitation data for 518 Russian meteorological stations. Carbon Dioxide Information Analysis Center, Oak Ridge National Laboratory, U.S. Department of Energy, Oak Ridge, Tennessee

Bush EJ, Loder JW, James TS, Mortsch LD, Cohen SJ (2014) An overview of Canada's changing climate. In: Lemmen DS (ed) Warren FJ. Canada in a changing climate, Sector Perspectives on Impacts and Adaptation, pp 23–64

Chamnansiri N (2016) Changes in precipitation characteristics associated with air temperature, dew point temperature and relative humidity over southeastern Canada during 1977–2015. MA thesis, California State University, Los Angeles. http://hdl.handle.net/10211.3/173880

Collins M et al (2013) Long-term climate change: projections, commitments and irreversibility. In Stocker TF et al (eds) Climate change 2013: the physical science basis. Cambridge University Press, 1029–1136

Colony R, Randinov V, Tanis FR (1998) Measurements of precipitation and snow pack at Russian north pole drifting stations. Polar Record 34(188):3–14

Dee DP et al (2011) The ERA-interim reanalysis: configuration and performance of the data assimilation system. Q J R Meteorol Soc 137:553–597

Deser C, Tomas R, Alexander M, Lawrence D (2010) The seasonal atmospheric response to projected Arctic sea ice loss in the late 21st century. J Clim 23:333–351. https://doi.org/10.1175/2009JCLI3053.1

Dingman SL (2008) Physical hydrology, 2nd edn. Waveland Press, Long Grove, IL, p 646

Dirmeyer PA, Jin Y, Singh B, Yan X (2013) Trends in land–atmosphere interactions from CMIP5 simulations. J Hydrometeorology 14(3):829–849

Donat MG, Lowry AL, Alexander LV, O'Gorman PA, Maher N (2017) Addendum: More extreme precipitation in the world's dry and wet regions. Nat Clim Change 7(2):154–158

Draper DW, Newell DA, Wentz FJ, Krimchansky S, Skofronick-Jackson GM (2015) The Global Precipitation Measurement (GPM) Microwave Imager (GMI): Instrument Overview and Early On-Orbit Performance. IEEE J Sel Top Appl Earth Obse Remote Sens 8(7):3452–3462

Fekete BM, Vörösmarty CJ, Roads JO, Willmott CJ (2004) Uncertainties in precipitation and their impacts on runoff estimates. J Clim 17:294–304

Ferraro RR et al (2013) An Evaluation of Microwave Land Surface Emissivities Over the Continental United States to Benefit GPM-Era Precipitation Algorithms. IEEE Trans Geosci Remote Sens 51:378–398

Førland EJ, Hanssen-Bauer I (2003) Past and future climate variations in the Norwegian Arctic: overview and novel analysis. Polar Res 22(2):113–124. https://doi.org/10.1111/j.1751-8369.2003.tb00102.x

Fuchs T, Rapp J, Rubel F, Rudolf B (2001) Correction of synoptic precipitation observations due to systematic measuring errors with special regard to precipitation phases. Phys Chem Earth Part B 26:689–693

Goodison BE, Louie PYT, Yang D (1998) WMO solid precipitation measurement intercomparison. Rept 67:212 pp. World Meteorological Organization, Geneva

Goodison BE, Louie PYT, Yang D (1988) WMO solid precipitation measurement intercomparison, final report, WMO/TD-No. 872, WMO, Geneva, 212 pp

Groisman PY, Rankova EY (2001) Precipitation trends over the Russian permafrost-free zone: removing the artfacts of pre-professing. Inter J Climatol 21:657–678

Groisman PY, Knight RW, Easterling DR, Karl TR (2005) Trends in intense precipitation in climate record. J Climate 18:1326–1350

Groisman PYa, Koknaeva VV, Belokrylova TA, Karl TR (1991) Overcoming biases of precipitation measurement: a history of the USSR experience. Bull Amer Meteor Soc 72:1725–1733. https://doi.org/10.1175/1520-0477(1991)072%3c1725:OBOPMA%3e2.0CO;2

Groisman PYa, Sun B, Vose RS, Lawrimore JH, Whitfield PH, Serreze MC, Razuvaev V, Alekseev G (2003) Contemporary Climate Changes in High Latitudes of the Northern Hemisphere: Daily Time Resolution. In Proceedings of the 14th symposium on global change and climate variations, 1–10. Long Beach, CA: American Meteorological Society

Hsu KL, Gao XG, Sorooshian S, Gupta HV (1997) Precipitation estimation from remotely sensed information using artificial neural networks. J Appl Meteorol 36:1176–1190

Huffman GJ et al (2001) Global precipitation at one-degree daily resolution from multisatellite observations. J Hydrometeorology 2:36–50

IPCC (2013) Climate Change 2013: The Physical Science Basis. Report of Working Group I of the Intergovernmental Panel on Climate Change. Cambridge University Press, Cambridge, U.K

Jarujareet P (2016) Precipitation trends under a warming climate in British Columbia, Canada, from 1950–2010. MA Thesis, California State University, Los Angeles. http://hdl.handle.net/10211.3/173903

Kane DL, Stuefer SL (2013) Challenges of Precipitation Data Collection in Alaska. 19th International Northern Research Basins Symposium and Workshop Southcentral Alaska, USA —August 11–17, 2013

Kattsov VM et al (2007) Simulation and Projection of Arctic Freshwater Budget Components by the IPCC AR4 Global Climate Models. J of Hydrometeorology 8(3):571–589

Kochendorfer J, Nitu R, Wolff M, Mekis E, et al. (2017) Errors and adjustments for single-Alter shielded and unshielded weighing gauge precipitation measurements from WMO-SPICE. Hydrol Earth Syst Sci Discuss. https://doi.org/10.5194/hess-2016-684, in review

Kopec BG, eng X, Michel FA, Posmentier ES (2015) Influence of sea ice on Arctic precipitation. Proc Natl Acad Sci 113(1):46–51. https://doi.org/10.1073/pnas.150463133

Korzun VI (Editor-in-Chief) (1978) World water balance and water resources of the earth. Unesco Press, Paris, pp 663

Krasting JP, Broccoli AJ, Dixon KW, Lanzante JR (2013) Future changes in northern hemisphere snowfall. J Clim 26(20):7813–7828

Kuligowski RJ (2002) A self-calibrating real-time GOES rainfall algorithm for short-term rainfall estimates. J Hydrometeorology 3:112–130
Kummerow C, Barnes W, Kozu T, Shiue J, Simpson J (1998) The Tropical Rainfall Measuring Mission (TRMM) sensor package. J Atmo Oceanic Technol 15:809–817
Kummerow CD, Randel D, Petkovic V (2016) Results from GPM GPROF V4 and improvements planned for V5, 8th IPWG and 5th IWSSM joint workshop bologna, 3–7 October, 2016. http://www.isac.cnr.it/~ipwg/meetings/bologna-2016/Bologna2016_Posters/P1-20_Kummerow.pdf
Kummerow CD, Randel DL, Kulie M, Wang N, Ferraro R, Munchak SJ, Petkovic V (2015) The evolution of the Goddard profiling algorithm to a fully parametric scheme. J Atmos Oceanic Technol 32:2265–2280
Kusunoki S, Arakawa O (2015) Are CMIP5 models better than CMIP3 models in simulating precipitation over East Asia? J Clim 28:5601–5621
Lader R, Walsh JE, Bhatt US, Bieniek PA (2017) Projections of twenty-first-century climate extremes for Alaska via dynamical downscaling and quantile mapping. J Appl Meteor Climatol 56:2393–2409. https://doi.org/10.1175/JAMC-D-16-0415.1
Lau WK, Wu MHT, Kim KM (2013) A canonical response of precipitation characteristics to global warming from CMIP5 models. Geophys Res Lett 40:3163–3169
Lebsock MD, L'Ecuyer TS (2011) The retrieval of warm rain from CloudSat. J Geophys Res 116: D20209
Legates DR, Willmott CJ (1990) Mean seasonal and spatial variability in gauge-corrected, global precipitation. Internat J Climatol 10:111–127
Legates DR (1995) Global and terrestrial precipitation: a comparative assessment of existing climatologies. Int J Climatol 15:237–258
Liu G (2008) Deriving snow cloud characteristics from CloudSat observations. J Geophys Res 113:D00A09
Lydolph PE (1977) Climates of the Soviet Union. World survey of climatology volume 7, Elsevier Scientific Publishing Company, Amstrerdam-Oxford-New York
Mailhot A, Kingumbi A, Talbot G, Poulin A (2010) Future changes in intensity and seasonal pattern of occurrence of daily and multi-day annual maximum precipitation over Canada. J Hydrol 388(3):173–185
Maslowski W, Cassano J, Gutowski W, Lettenmaier D (2011) Regional arctic climate system model (RACM) - development and selected results, geophysical research abstracts, 13, EGU2011-9648, 2011, EGU General Assembly
Metcalfe JR, Routledge B, Devine K (1997) Rainfall measurement in Canada: changing observational methods and archive adjustment procedures. J. Clim 10:92–101
McAfee S, Guentchev G, Eischeid J (2013) Reconciling precipitation trends in Alaska: 1. Station-based analyses. J Geophys Rese 118:7523–7542. https://doi.org/10.1002/jgrd.50572
McAfee S, Guentchev G, Eischeid J (2014) Reconciling precipitation trends in Alaska: 2. Gridded data analyses. J Geophys Res. https://doi.org/10.1002/2014jd022461
Mekis É (2005) Adjustments for trace measurements in Canada. In 15th conference on applied climatology, Savannah, Georgia, USA, June, J3.7 (pp 20–24)
Mekis É, Vincent LA (2011) An overview of the second generation adjusted daily precipitation dataset for trend analysis in Canada. Atmos.–Ocean, 49, 163–177, https://doi.org/10.1080/07055900.2011.583910
Mekis É, Brown R (2010) Derivation of an adjustment factor map for the estimation of the water equivalent of snowfall from ruler measurements in Canada. Atmos Ocean 48(4):284–293
Mekis E, Vincent LA (2011b) An overview of the second generation adjusted daily precipitation dataset for trend analysis in Canada. Atmos Ocean 49:163–177
Mladjic B, Sushama L, Khaliq MN, Laprise R, Caya D, Roy R (2011) Canadian RCM projected changes to extreme precipitation characteristics over Canada. J Clim 24(10):2565–2584
Montenegro F (2015) A look into changes in precipitation types linked with surface air temperature over British Columbia, Canada 1953–2005. MA thesis, California State University, Los Angeles. http://hdl.handle.net/10211.3/133589

Pendergrass AG, Lehner F, Sanderson BM, Xu Y (2015) Does extreme precipitation intensity depend on the emissions scenario? Geophys Res Lett 42:8767–8774
Peel MC, Finlayson BL, McMahon TA (2007) Updated world map of the Köppen –Geiger climate classification. Hydrol Earth Syst Sci 11:1633–1644
Perica S, Kane D, Dietz S, Maitaria K, Martin D, Pavlovic S, Roy I (2012) NOAA Atlas 14: Precipitation- frequency atlas of the United States, Alaska. www.nws.noaa.gov/oh/hdsc/PF_documents/Atlas14_Volume7.pdf
Ponce M (2017) Detecting climate change over Canadian prairies. MA thesis at California State University, Los Angeles http://hdl.handle.net/10211.3/192086
Räisänen J (2008) Warmer climate: less or more snow? Clim Dyn 30:307–319. https://doi.org/10.1007/s00382-007-0289-y
Rapaić M, Brown R, Markovic M, Chaumont D (2015) An evaluation of temperature and precipitation surface-based and reanalysis datasets for the Canadian Arctic, 1950–2010. Atmos Ocean 53(3):283–303
Rasmussen R, Baker B, Kochendorfer J (2012) How well are we measuring snow: The NOAA/FAA/NCAR winter precipitation test bed. Bull Amer Mete Soc 93:811–829
Rawlins MA, Fahnestock M, Frolking S, Vörösmarty CJ (2007) On the evaluation of snow water equivalent estimates over the terrestrial Arctic drainage basin. Hydrol Process 21:1616–1623
Rawlins MA et al (2010) Analysis of the arctic system for freshwater cycle intensification: Observations and expectations. J Clim 23:5715–5737
Scaff L, Yang D, Li Y, Mekis E (2015) Inconsistency in precipitation measurements across the Alaska-Yukon border. The Cryosphere 9:2417–2428
Schneider U, Finger P, Meyer-Christoffer A, Rustemeier E, Ziese M, Becker A (2017) Evaluating the hydrological cycle over land using the newly-corrected precipitation climatology from the global precipitation climatology centre (GPCC). Atmosphere 8:52
Serreze MC, Etringer AJ (2003) Precipitation charactersitics of the Eurasian Arctic Drainage system. Inter J Climatol 23:1267–1291
Serreze MC, Hurst CM (2000) Representation of mean Arctic precipitation from NCEP-NCAR and ERA reanalyses. J Clim 13:182–201
Shephard MW, Mekis E, Morris RJ, Feng Y, Zhang X, Kilcup K, Fleetwood R (2014) Trends in canadian short-duration extreme rainfall: including an intensity–duration–frequency perspective. Atmos Ocean 52(5):398–417
Short DA, Nakamura K (2000) TRMM radar observations of shallow precipitation over the tropical oceans. J Clim 13:4107–4124
Shulski M, Wendler G2 (2007) Climate of Alaska. University of Alaska Press
Skofronick-Jackson G et al (2017) The global precipitation measurement (GPM) mission for science and society. Bull Am Meteor Soc 98:1679–1695
Smith LC, Sheng Y, MacDonald GM, Hinzman LD (2005) Disappearing arctic lakes. Science 308:1429
Solomon S et al (2007) Technical summary, in climate change 2007: the physical science basis. In: S. Solomon et al (ed) Contribution of working group I to the fourth assessment report of the intergovernmental panel on climate change. Cambridge Univ. Press, Cambridge, UK, pp 20–91
Sorooshian S, Hsu KL, Gao X, Gupta HV, Imam B, Braithwaite D (2000) Evaluation of PERSIANN system satellite-based estimates of tropical rainfall. Bull Am Meteor Soc 81:2035–2046
Stephens GL et al (2008) CloudSat mission: performance and early science after the first year of operation. J Geophys Res: Atmos 113:D00A18
Stuefer SL, Kane DL (2016) Snow retention for increased water supply of shallow arctic lakes. Cold Reg Sci Technol 123(March):32–43. https://doi.org/10.1016/j.coldregions.2015.11.011
Stuefer SL, Kane DL, Liston GE (2013) In situ snow water equivalent observations in the US arctic. Hydrol Res 44(1):21. https://doi.org/10.2166/nh.2012.177
Stuefer SL, Arp C, Kane DL, Liljedahl A (2017) Recent extreme runoff observations from coastal Arctic watersheds in Alaska. Water Resour Res 53(11):9145–9163

Sturm M, Stuefer SL (2013) Wind-blown flux rates derived from drifts at arctic snow fences. J Glaciol 213(59):21–34. https://doi.org/10.3189/2013JoG12J110
Swenson S (2010) Assessing high-latitude winter precipitation from global precipitation analyses using GRACE. J Hydrometeorology 11:405–420
Tapley BD, Bettadpur S, Ries JC, Thompson PF, Watkins MM (2004) GRACE measurements of mass variability in the earth system. Science 305:503–505
Tebaldi C, Arblaster JM, Hayhoe K, Meehl GA (2006) Going to the extremes: an intercomparison of model-simulated historical and future changes in extreme events. Clim Change 79:185–211. https://doi.org/10.1007/s10584-006-9051-4
USGCRP (2014) US national climate assessment, 2014: global climate change impacts in the United States. US.Global Change Research Program, Washington, DC. http://nca2014.globalchange.gov/downloads
Vincent LA, Mekis E (2009) Discontinuities due to joining precipitation station observations in Canada. J Appl Meteorol Climatol 48(1):156–166
Vincent LA, Zhang X, Brown RD, Feng Y, Mekis E, Milewska EJ, Wan H, Wang XL (2015) Observed trends in Canada's climate and influence of low-frequency variability modes. J Clim 28(11):4545–4560
Vincent LA, Mekis E (2006) Changes in daily and extreme temperature and precipitation indices for Canada over the twentieth century. Atmos Ocean 44(2):177–193
Vincent LA, Wang XL, Milewska EJ, Wan H,Yang F, Swail V (2012) A second generation of homogenized Canadian monthly surface air temperature for climate trend analysis. J Geophys Res: Atmos 117(D18). https://doi.org/10.1029/2012jd017859
Walsh JE, Kattsov V, Portis D, Meleshko V (1988) Arctic precipitation and evaporation: model results and observational estimates. J. Clim 11(1):72–87
Walsh JE, Kattsov V, Portis D, Meleshko V (1998) Arctic precipitation and evaporation: model results and observational estimates. J Clim 11:72–87
Watkins MM, Wiese DN, Yuan D-N, Boening C, Landerer FWCJB (2015) Improved methods for observing Earth's time variable mass distribution with GRACE using spherical cap mascons. J Geophys Res: Solid Earth 120:2648–2671
Wilheit TT (1986) Some comments on passive microwave measurement of rain. Bull Am Meteor Soc 67:1226–1232
Xie P, Arkin PA (1997) Global precipitation: A 17-Year monthly analysis based on gauge observations, satellite estimates, and numerical model outputs. Bull Am Meteor Soc 78:2539–2558
Yang D et al (2001) Compatibility evaluation of national precipitation gage measurements. J Geophys Res: Atmos 106:1481–1491
Yang D, Goodison BE, Metcalfe JR, Golubev VS, Elomaa E, Gunther TH, Bates R, Pangburn TC, Hanson L, Emerson D, Copaciu V, Milkovic J (1995) Accuracy of Tretyakov precipitation gauge: results of WMO Intercomparison. Hydrol Process 9(8):877–895
Yang D (1999) An improved precipitation climatology for the arctic ocean. Geophys Res Lett 26 (11):1625–1628
Yang D, Kane D, Zhang Z (2005) Bias corrections of long-term (1973–2004) daily precipitation data over the northern regions. Geophys Res Lett 32:L19501. https://doi.org/10.1029/2005GL024057
Yang D, Goodison BE, Metcalfe JR, Golubev VS, Bates R, Pangburn T, Hanson CL (1998) Accuracy of NWS 8″ standard nonrecording precipitation gauge: results and application of WMO intercomparison. J Atmos Oceanic Technol 15(1):54–68
Ye H, Cohen J (2013) Shortening snowfall season associated with increasing air temperature over northern Eurasia. Environ ResLett 8(2013)014052. http://stacks.iop.org/1748-9326/8/014052
Ye H (2001) Characteristics of winter precipitation variation over Northern Central Eurasia and their connections to sea surface temperatures over the Atlantic and Pacific oceans. J Clim 14:3140–3155

Ye H (2008) Changes in frequency of precipitation types associated with surface air temperature over Northern Eurasia during 1936-90. J Clim 21:5807–5819. https://doi.org/10.1002/joc.1741
Ye H, Fetzer EJ (2010) Atmospheric moisture content associated with surface air temperatures during northern Eurasian summer. Int J Climatol 30(10):1463–1471. https://doi.org/10.1002/joc.1991
Ye H, Fetzer EJ, Wong S, Behrangi A, Olsen ET, Cohen J, Lambrigtsen BH, Chen L (2014) Impact of increased water vapor on precipitation efficiency over northern Eurasia. Geophys Res Lett 41:2941–2947. https://doi.org/10.1002/2014GL,059830
Ye H, Fetzer EJ, Wong S, Yang D, Lambrigtsen BH (2015) Increasing atmospheric water vapor and higher daily precipitation intensity over Northern Eurasia. Geophys Res Lett 42 https://doi.org/10.1002/2015GL066104
Ye H, Fetzer EJ, Behrangi A, Wong S, Lambrigtsen BH, Wang CY, Cohen J, Gamelin BL (2016a) Increasing daily precipitation intensity associated with warmer air temperatures over Northern Eurasia. J Clim 29:623–636
Ye H, Fetzer EJ, Wong S, Lambrigtsen BH, Wong T, Chen L, Dang V (2016b) More frequent showers and thunderstorm events under a warming climate: evidence observed over Northern Eurasia from 1966–2000. Clim Dyn, 13 pp. https://doi.org/10.1007/s00382-016-3412-0
Ye H, Fetzer EJ, Wong S, Lambrigtsen BH (2017) Rapid decadal convective precipitation increase during the last three decades of the 20th century. Sci Adv 3:1600944
Zhang X, Harvey KD, Hogg WD, Yuzyk TR (2001) Trends in Canadian streamflow. Water Resour Res 37:987–998 https://doi.org/10.1029/2000WR900357
Zhang X, Zwiers FW, Li G, Wan H, Cannon AJ (2017). Complexity in estimating past and future extreme short-duration rainfall. Nat Geosci 10(4):255–259
Zolina, O, Simmer C, Gulev SK, Kollet S (2010) Changing structure of European precipitation: longer wet periods leading to more abundant rainfalls. Geophys Res Letts 37:L06704. https://doi.org/10.1029/2010GL042468

Dr. Hengchun Ye is the Associate Dean of Natural and Social Sciences at California State University, Los Angeles, USA. She was a Professor and Department Chair in the Department of Geosciences and Environment and the PI for NASA DIRECT-STEM at the Cal State LA. Her research focuses on hydroclimatology and climate change. Her research expertise is in changing precipitation characteristics (intensity, frequency, and type), durations of wet and dry days, and snow (snowfall season length and accumulation) and its connections to atmospheric water vapor, atmospheric circulation patterns, and sea surface temperatures. She received her Ph.D. in Climatology at the University of Delaware and held tenure-track positions at the University of Idaho and Emporia State University before she took an associate professor position at Cal State LA.

Dr. Daqing Yang is a Research Scientist at the Watershed Hydrology and Ecology Research Division, Environment and Climate Change Canada. He is also Affiliate Research Professor at the International Arctic Research Center, Univ. of Alaska Fairbanks. Over the past 25 years, he has conducted cryosphere system research in China, Canada, Japan, USA, and Norway. His primary research activities/interests include cold region hydrology and climate, particularly Arctic large river streamflow regime and change, snow cover and snowfall measurements, climate change and human impact to regional hydrology, and applications of remote sensing in cold regions. He has served as journal editor and subject editor for IAHS publications (cold region hydrology, northern research basin water balance, and cold/mountain region hydrological systems under climate change), and WMO technical reports (solid precipitation measurement intercomparison and integrated global observing strategy cryosphere theme). He also contributed as review and/or author to the IPCC Reports, and the Arctic Council's Snow, Water, Ice and Permafrost in the Arctic (SWIPA 2017 and follow up) assessment. His current research focuses on investigating the impacts of climate variability/change and human activities on hydrologic system across the broader northern regions.

Dr. Ali Behrangi is an Associate Professor in the Department of Hydrology and Atmospheric Sciences and also Department of Geosciences, University of Arizona, USA. His research interest and activities are in various aspects of cloud-precipitation and hydrologic studies: Retrieval, diagnostic evaluation, and uncertainty analysis of precipitation products, extreme weather event analysis, and hydrologic simulations. In the last 7 years, he has had a greater focus on remote sensing of precipitation in cold regions, where he has also utilized CloudSat, GRACE, reanalyses, and other new observations. He currently leads a project to improve GPCP in high latitudes. He received his Doctoral degree in Civil Engineering at University of California, Irvine and was a postdoctoral scholar at California Institute of Technology (Caltech). He was with NASA JPL as Scientist for more than 5 years (2013–2018), before he joined the University of Arizona.

Dr. Svetlana L. Stuefer is an Associate Professor at the Department of Civil and Environmental Engineering and Water and Environmental Research Center at the University of Alaska Fairbanks, Alaska, USA. Her specialization is in the cold region's hydrology with an emphasis on the snow and ice-related processes. She received her Ph.D. from the Russian State Hydrometeorological University, St. Petersburg, Russia. She joined the Water and Environmental Research Center at the University of Alaska Fairbanks in 2003 as a Postdoctoral Fellow. Her research can be viewed at ORCID https://orcid.org/0000-0003-0740-8335.

Dr. Xicai Pan is a Professor in the State Key Laboratory of Soil and Sustainable Agriculture, Institute of Soil Science, Chinese Academy of Sciences, in Nanjing, China. He studies soil and terrestrial environmental physics and associated ecosystem services. His research includes investigations of key processes affecting cold region hydrology and the sustainability of agricultural ecosystems. He received his doctoral degree in Environmental Physics at the Heidelberg University in Germany, and was a Postdoctoral Fellow at the University of Saskatchewan in Canada.

Dr. Eva Mekis is a Physical Scientist in the Meteorological Research Division of Environment and Climate Change Canada in Toronto, Ontario, Canada. She graduated and received her Doctoral degree in Meteorology at the Eötvös Loránd University in Budapest (Hungary). Since arriving in Canada as an NSERC Postdoctoral fellow, she spent over 20 years dealing with precipitation-related issues. Her main research interest includes the development of precipitation data adjustment and homogenization procedures and the analysis of precipitation-related climate indices and trends. She developed and maintaining the first and second generation of the Adjusted Historical Canadian Climate Data (AHCCD) precipitation database used by thousands of applications and users. Recently, her focus shifted toward the automated precipitation observations including observation data flow, quality control, catch efficiency assessment, and transfer function development.

Dr. Yonas Dibike is a Research Scientist at Environment and Climate Change Canada, Watershed Hydrology and Ecology Research Division at the University of Victoria. His research interests include hydrological, hydrodynamic, and transport modeling as well as hydro-climate analysis and climate change impact studies in cold region watersheds. He also holds adjunct faculty appointment at McMaster University, and the University of Victoria in Canada. He is the author/co-author of numerous (70) scientific articles that have appeared in a variety of peer-reviewed journals and conference proceedings. He is actively involved in Departmental and University-based researches and has co-supervised several graduate students and post-doctoral fellows.

Dr. John E. Walsh is the Chief Scientist of the International Research Center and President's Professor of Global Change at the University of Alaska, Fairbanks, USA. He is also an emeritus faculty member of the University of Illinois. He has been involved in Arctic research and education for more than 40 years. His more recent research has addressed Arctic climate and weather variability, with an emphasis on the drivers of cryospheric variations over seasonal to multidecadal timescales. He has served as lead author for assessment reports of the Intergovernmental Panel on Climate Change, the Arctic Monitoring and Assessment Programme, and the U.S. National Climate Assessment. He has also co-authored a textbook, Severe and Hazardous Weather. He received a B.S. in Mathematics from Dartmouth College and a Ph.D. in Meteorology from the Massachusetts Institute of Technology.

Snow Cover—Observations, Processes, Changes, and Impacts on Northern Hydrology

3

Ross Brown, Philip Marsh, Stephen Déry, and Daqing Yang

Abstract

This chapter presents an overview of Arctic terrestrial snow cover and hydrology starting with the factors contributing to variability and change in large-scale snow cover extent and snow water equivalent (SWE), then moves to the local scale for a discussion of the processes and interactions responsible for the spatial distribution and physical properties of Arctic snow cover, most notably the roles of blowing snow and vegetation interactions. Snowmelt and runoff processes are subsequently covered with particular attention on liquid water infiltration through the snowpack and soil layers. The chapter concludes with an overview of Arctic snow observing systems, estimates of current and projected trends in Arctic snow cover extent and SWE, and potential hydrologic implications of the projected changes in snow cover. A key message from the Chapter is that the

R. Brown (✉)
Environment and Climate Change Canada, Climate Research Division, Montreal, QC, Canada
e-mail: rdbrown@videotron.ca

P. Marsh
Department of Geography and Environmental Studies, Wilfrid Laurier University, Waterloo, ON, Canada
e-mail: pmarsh@wlu.ca

S. Déry
Environmental Science Program, University of Northern British Columbia, Prince George, BC, Canada
e-mail: sdery@unbc.ca

D. Yang
Environment and Climate Change Canada, Watershed Hydrology and Ecology Division, Victoria, BC, Canada
e-mail: daqing.yang@canada.ca

D. Yang and D. L. Kane (eds.), *Arctic Hydrology, Permafrost and Ecosystems*,
https://doi.org/10.1007/978-3-030-50930-9_3

response of Arctic snow cover and snow hydrology to a changing climate is complex due to the numerous linkages and feedbacks within the coupled snow–soil–vegetation system.

3.1 Introduction

Seasonal snow covers the Arctic for 7 to 10 months of the year and through its unique physical properties (high reflectivity and low thermal conductivity) and water storage plays critical roles in energy and water exchanges at scales from local to global (Brown et al. 2017). For example, at the local scale, large energy inputs during the May to June melt period mean that ~80% of the total Arctic snow water storage melts over a period of a few weeks, generating a rapid pulse of fresh water into upland lakes and watersheds with effects on lake ice melt, hydrology, ground thermal regime and permafrost, carbon cycling, and many ecosystem services. At the hemispheric scale, the maximum annual amount of water stored in the seasonal snowpack over land areas north of 60° N, excluding Greenland, is estimated to average ~1700−1750[1] km^3. This represents ~50% of the mean annual freshwater discharge into the Arctic Ocean (Syed et al. 2007) and has important implications for the global hydrological cycle and the ocean's thermohaline circulation (Carmack et al. 2016).

The amount of snow that falls in the terrestrial Arctic is a net result of a complex series of atmospheric, oceanic, and land surface processes and interactions that include proximity to moisture, latitude, and elevation. Combined, these determine the duration of the snowfall season and the total amount of snowfall. For example, in Fig. 3.1a the important control of latitude on seasonal air temperatures is clearly visible in the strong zonal gradient in the mean duration of the snow cover season, while proximity to ocean and elevation are clear factors in the more regional distribution of mean annual maximum accumulation (Fig. 3.1b).

Once on the ground, terrain and vegetation take over as the most important factors in determining the spatial variability in Arctic snow accumulation and snow properties (Pohl and Marsh 2006; Marsh et al. 2010; Assini and Young 2012; Clark et al. 2013; Rees et al. 2014; Homan and Kane 2015) due to frequent wind redistribution of snow (Pomeroy et al. 1997; Déry and Yau 2002; Sturm and Stuefer 2013). The tundra and taiga environments (Fig. 3.1c) cover the largest areas of the Arctic land region and are the focus of this chapter. Snow cover stratigraphy and properties vary considerably between these environments because of the different climates and vegetation covers. The snow cover is also subject to year-to-year and multi-decadal variations in climate linked to atmospheric and oceanic circulation,

[1]Arctic annual maximum season snow water storage estimated from the GlobSnow version 2 product (Takala et al. 2011) and the Liston and Hiemstra (2011) 10-km Arctic snow cover reconstruction.

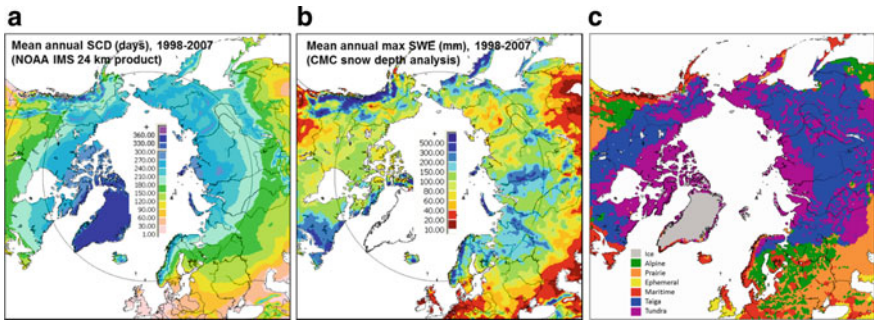

Fig. 3.1 **a** Mean annual snow cover duration from the NOAA IMS-24 daily snow cover analysis, **b** estimated mean annual maximum snow water equivalent (mm) from the CMC operational snow depth analysis for snow seasons 1998 to 2007, and **c** the snow cover climate classification proposed by Sturm et al. (1995)

ice cover, and local moisture sources such as polynyas (e.g. Boon et al. 2010). Additional complexity is added by the fact that Arctic snow cover is responding to multiple drivers and feedbacks linked to polar amplification of global warming (Brown et al. 2017).

3.2 Drivers of Arctic Snow Cover Change

There is growing evidence that the Arctic environment is experiencing a rapid transition away from its twentieth-century state in response to rapid human-induced warming occurring at more than twice the rate of the global average (Box et al. 2019). The response of Arctic snow cover to this period of rapid change is complex as snow cover responds to multiple environmental drivers and feedbacks (see Table 3.1). Changes in these drivers and associated feedbacks interact to produce spatially, temporally, and seasonally varying responses in Arctic snow cover. For example, the observed widespread trend of increasing shrubbiness of arctic tundra (Myers-Smith et al. 2011, 2015) allows more snow to be trapped in shrub patches, providing more insulation and warming of the ground. This results in significant changes to snowmelt and hydrology (Marsh et al. 2010), as well as complex changes to soil temperature and active layer depth. Increased snow accumulation in some regions of the Arctic in response to increasing winter precipitation is playing an important role in observed trends toward permafrost warming and deepening of the active layer in several regions of the Arctic (e.g. Park et al. 2014, 2015; Sannel et al. 2015). However, in other regions, snowfall and the depth of snow on the ground is decreasing (Lesack et al. 2014; Mann 2018), with poorly described impacts on permafrost. A summary of the some of the main drivers of Arctic snow cover change and their hydrological impacts is provided in Table 3.1.

Table 3.1 Summary of important drivers of Arctic snow cover change and their hydrological impacts

Driver	Observed change	Impacts on snow cover	Feedbacks	Hydrological implications
Warming air temperatures	The Arctic is warming at more than twice the global rate over the past 50 years due to a number of processes and feedbacks that amplify warming over high latitudes	Decrease in snow cover duration, the snow accumulation period, and the fraction of total precipitation falling as snow. Warming affects snow properties and thermodynamics through temperature dependencies in turbulent energy exchanges, incoming longwave radiation, snow metamorphism, and snow albedo. It also impacts the frequency of winter thaw and rain-on-snow events that contribute to ice layer development and changes in snow cover properties	Less snow cover provides positive radiative feedbacks to the climate system. Changes in snow cover timing may enhance or retard permafrost warming	Earlier spring melt and a relatively less important snowmelt contribution to total runoff. A shift in the timing of snowmelt to earlier in the season (less incoming solar radiation) reduces the potential for high-melt rates
Increasing precipitation	Human-induced warming, loss of ice cover, and enhanced poleward atmospheric moisture transport are contributing to increased atmospheric moisture and increasing precipitation over Arctic land areas of ~1.5–2%/decade. Evidence of increasing precipitation extremes in some regions	Changes in seasonal snow accumulation amount and snow properties. In some regions of the Arctic, increases in snowfall rates are sufficient to offset the impact of reductions in the length of the snow accumulation period and contribute to increasing annual maximum accumulations	Positive feedbacks to melting snow from latent heat and cloud cover. Changes in the seasonal snow depth distribution may enhance or retard permafrost warming	Increased risk of rapid melt and rain-on-snow events

(continued)

Table 3.1 (continued)

Driver	Observed change	Impacts on snow cover	Feedbacks	Hydrological implications
Changing vegetation	Extensive evidence of shrub expansion over the Arctic but changes are neither uniform nor simple	Increased plant mass provides greater potential to trap snow, increases the insulating properties of the snowpack, and changes the melt season energy budget	Provides mostly positive feedbacks to soil warming and plant growth.	Changed melt dynamics, increased snow water storage, and melt
Increased downwelling longwave radiation (DLR)	DLR has increased at a rate of ~ 2 W m^{-2} per decade in response to a number of factors including increasing atmospheric moisture and temperature, cloud cover, and the concentration of greenhouse gases in the atmosphere	DLR is important for high latitude snow cover because it is the main energy source for much of the year, and has a direct impact on cryospheric processes such as snow sublimation, ice growth, and snowmelt	Warmer snowpacks contribute to earlier melt and to permafrost warming	Warmer snowpack and earlier snowmelt
Light absorbing particles (LAP)	LAP is a collective term for various impurities in the snowpack of which black carbon is one of the main contributors. The deposition rate of LAP varies spatially and temporally but is generally declining with the switch to cleaner-burning fuels	LAP affects melt rates through a reduction of surface reflectance. In areas with perennial snow, such as glaciers, LAP accumulates over successive melt seasons during periods of extended melt loss, decoupling the albedo effect from atmospheric deposition	Snow darkening from LAP is estimated to provide a positive surface temperature feedback of 3–6 K near the snowline	Contributes to more rapid spring melt rates

(continued)

Table 3.1 (continued)

Driver	Observed change	Impacts on snow cover	Feedbacks	Hydrological implications
Changing atmospheric circulation	There is some evidence that Arctic atmospheric circulation may be changing in response to warming and sea ice loss, although the attribution to global warming is still highly uncertain	Impacts vary regionally, e.g. weakening of westerly winds and more persistent weather patterns such as the prolonged blocking patterns observed over the eastern Canadian Arctic and Greenland from 2007 have contributed to enhanced summer melt of snow and ice over the region	Snow cover can influence atmospheric variability through various feedback mechanisms such as the dynamic link between autumn snow depth anomalies over Siberia and changes in the surface-based Arctic Oscillation	Multi-decadal variability in snow accumulation, melt, and the hydrological regime

3.3 Snow Hydrology in Arctic Regions—Processes and Interactions

Snow hydrology is defined as the "*study of the factors that control the accumulation, melting and runoff of water from seasonal snowpacks over the surface of the earth*" (Principles of Snow Hydrology, D.R. DeWalle and A. Rango 2011). In the Arctic terrestrial environment, snow hydrology will also include the melting of snow from perennial snowpacks that can cover a large portion of the watershed, and control streamflow over the entire summer period (Marsh and Woo 1981). The science of Arctic snow hydrology is more complex than in the mid-latitudes because the snow cover is part of a coupled snow–vegetation–soil–hydrology system with multiple linkages and feedbacks (Brown et al. 2017). While many of the processes are interlinked, the definition provided by DeWalle and Rango remains a convenient framework for presenting and discussing key concepts and processes in Arctic snow hydrology. This definition can be rephrased in the following three basic questions: (1) how much snow has accumulated on the ground and vegetation, and how is it distributed over a hydrological unit such as a small basin (**the mass balance**); (2) when and at what rate does snow melt/refreeze (**the energy balance**); and (3) what happens to the meltwater released by the snowpack (**surface/subsurface flow, infiltration, runoff routing**). An excellent overview of current understanding and modelling of Arctic hydrology is provided by Krogh et al (2017).

3.3.1 Snow Accumulation Processes

The basic mass balance equation for a seasonal snowpack is (King et al. 2008):

$$\mathrm{dM/dt} = \mathrm{P} \pm \mathrm{E} - \mathrm{Runoff} \tag{3.1}$$

where dM/dt is the snowpack mass change rate, P is the accumulated solid precipitation rate, E is the loss/gain rate from evaporation and sublimation, and Runoff is the mass loss rate from melted snow.

In the absence of measurements of pre-melt SWE, which is often the case in many Arctic watersheds, knowledge of the amount and phase of precipitation, sublimation, and winter melt events from warm periods or from rain-on-snow events is critical for estimating the accumulated snowfall. A detailed discussion of precipitation measurement issues in Arctic environments is provided in Chap. 2. The key points to note are (1) solid precipitation is difficult to measure accurately in high wind environments and typically results in the undercatch of actual precipitation; (2) the high Arctic is characterized by frequent trace events that may not be registered by precipitation gauges, again resulting in underestimates of actual precipitation; and (3) estimates of precipitation from atmospheric reanalyses exhibit large spread and tend to exhibit warm-moist biases over the Arctic (Rapaic et al. 2015). Knowledge of precipitation phase is also extremely important for realistic

snow cover simulations and for diagnosing the formation of ice layers that can impede the infiltration of meltwater in the spring melt period (Harder and Pomeroy 2013). There are numerous empirical approaches for estimating precipitation phase such as the commonly used assumption of liquid–solid transition at a threshold air temperature of 0 °C. However, empirical relationships vary significantly with location (Jennings et al. 2018) and physically based phase partitioning methods incorporating both air temperature and humidity information introduce less uncertainty into snowpack simulations (Harder and Pomeroy 2013). Precipitation phase can be estimated from hourly synoptic reports of precipitation types and intensities if these are available.

Mass losses/gains from evaporation/condensation and sublimation are included in the "E" term of Eq. (3.1). In Arctic environments, this term is dominated by sublimation losses (the direct transfer of water from the solid to vapour phases to the atmosphere) during blowing snow events or during late winter when radiation increases and relative humidity is very low. Unlike most other surfaces, Arctic snow remains mobile over much of the winter and can be displaced large distances if near-surface winds exceed its threshold for transport, inducing blowing, and drifting snow. At relatively low wind speeds ($\sim$7–10 m s^{-1}), snow grains bounce along the surface in ballistic trajectories in a process termed saltation (Pomeroy and Gray 1990). As wind speeds increase, turbulent motions in the atmosphere suspend snow particles such that turbulent suspension then dominates horizontal mass transport (Pomeroy and Gray 1992). Both snow saltation and suspension accompany blowing snow, with only the latter causing a noticeable reduction in atmospheric visibility at 2 m above the surface. High winds erode snow in exposed locations such as ridge tops, while decelerating winds deposit snow in gullies, the lee sides of hills with slope greater than approximately 9 degrees, topographic depressions, shrub and forest patches, snow fences along northern roads, and buildings. Thus blowing snow is a primary driver of snowpack heterogeneity in windy Arctic environments (Déry et al. 2004; Liston 2004; Freudiger et al. 2017). This spatial variability in snowpack conditions leads to non-uniform snowmelt patterns and thus a lagged hydrological response with late-lying snowdrifts feeding critical meltwater during dry summertime conditions (Pohl et al. 2006; Sturm et al. 2001; Freudiger et al. 2017).

During wind transport, sublimation is typically enhanced owing to the relatively large exposed surface area of the snow particles. Sublimation requires a net input of thermal energy to initiate the phase change, subsaturated air (relative to an ice surface), and turbulent motions in the atmosphere (Déry et al. 1998). Blowing snow sublimation is an important term in the surface water budget of snowy and windy regions, leading to estimated losses of $\sim$20–30% of winter snowfall (Pomeroy et al. 1997; Déry and Yau 2002; Strasser et al. 2008). It is unclear how climate warming will affect blowing snow sublimation as the process is influenced by air temperature, wind speed, and humidity as well as winter melting and rain-on-snow events that limit the availability of snow particles to be entrained in the atmosphere. In addition, diminished snowpacks yield shorter snow seasons during which wind transport may occur; however, if winter storms intensify in a warmer world, there is

then the potential for increased wind transport of snow. Warmer (but subfreezing) air temperatures may also enhance the sublimation process yielding further losses of precipitation at the surface. Further research is needed to assess the potential impacts of climate warming on blowing and drifting snow.

In taiga regions with an open coniferous forest cover, the sublimation of snow intercepted by the vegetation canopy is an important mass loss term that can account for ~15–20% of total snowfall (Ellis et al. 2010; Krogh et al. 2017). The canopy (and snow accumulation on the canopy) also have important influences on the snowpack energy budget (see Sect. 3.3.2.3). The process of canopy snow interception and unloading is complex involving interactions between meteorology (air temperature, wind speed, incoming solar radiation), snowfall properties (density, crystal type, liquid water content), and vegetation characteristics (tree type, stand density, leaf area index). Bartlett and Verseghy (2015) reviewed a number of snow interception and unloading parameterizations and found none were very satisfactory at estimating the fraction of the canopy covered with snow. However, a single parameter unloading model based on wind speed at the canopy top gave consistent canopy albedo results across a number of sites and tree types.

In Arctic watersheds exposed to high winds, the processes of blowing snow transport and sublimation, and canopy interception and sublimation generate strong spatial variations in snow cover related to vegetation cover and terrain. For example, Table 3.2 shows mean winter snow mass fluxes over a small Arctic watershed simulated by the Cold Regions Hydrological Model (CRHM) (Krogh et al. 2017). Key points to note are (1) the transport of snow out of the more exposed upper tundra region (−35 mm/yr), (2) the higher canopy sublimation loss from the forest (88 mm/yr), (3) the large transport of blowing snow into gullies (316 mm/yr), and the large spatial variability in end-of-winter SWE (67–475 mm).

Table 3.2 CRHM simulated mean winter mass fluxes for a subset of Hydrological Response Units in the Havikpak Creek basin, NWT (from Krogh et al. 2017). The estimated mean annual snowfall for the basin is 191 mm

Hydrological Response Unit	End-of-the-winter SWE (mm)	Blowing snow transport (mm/yr)	Blowing snow sublimation (mm/yr)	Sublimation from canopyinterception (mm/yr)	Sublimation from the snow surface (mm/yr)
Upper Tundra	67	−35	76	0	23
Closed Shrubs	158	0	0	7	22
Forest	68	0	0	88	35
Upper Gully/Drift	475	316	0	4	20

3.3.2 Snowmelt Processes

3.3.2.1 Snowpack Energy Balance

When and how much snow melts is influenced by the energy balance of the snowpack. Neglecting horizontal energy transfers, blowing snow and a vegetation canopy for the moment, the basic volume energy balance for a simplified snow layer over permafrost is shown schematically in Fig. 3.2 and defined by Boike et al. (2003) as

$$Q_n + Q_h + Q_e + Q_r = \Delta H_s + \Delta H_g + \Delta H_l + Q_m \quad (3.2)$$

where Q_n, the net radiation balance for both short and longwave radiation, is given by

$$Q_n = (Q + q)(1 - \alpha) + L\downarrow - L\uparrow \quad (3.3)$$

with Q and q the incoming direct and indirect solar radiation, respectively, α the surface albedo, and $L\downarrow$ and $L\uparrow$ the downwelling longwave and surface emitted longwave radiation, respectively. Q_h and Q_e are the turbulent fluxes of sensible and latent heat, and Q_r is the heat flux from rain. The terms on the right-hand side are the change in thermal energy stored in the snow (ΔH_s) and soil (ΔH_g), and the change in heat from freezing water in the active layer (ΔH_l). The mass and energy

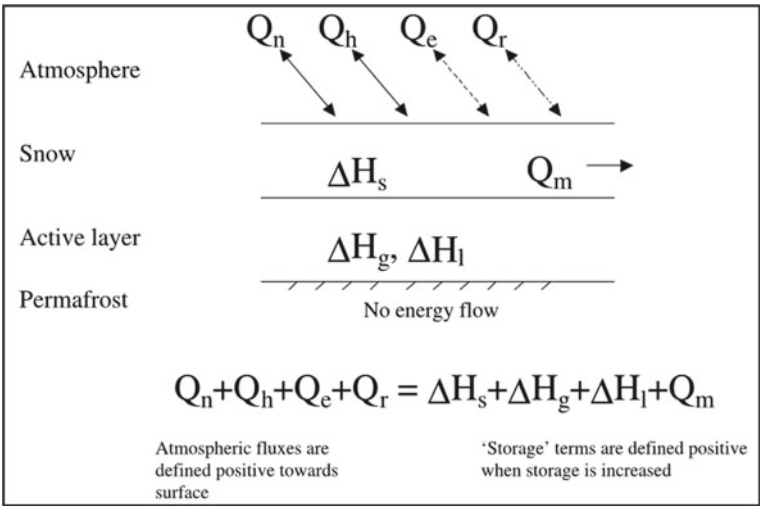

Fig. 3.2 Schematic diagram of the energy balance of an Arctic snowpack from Boike et al. (2003). Note that the "no energy flow condition" occurs at the depth of zero annual amplitude, which is typically located ~10–20 m within the permafrost layer

budgets are linked through the latent heat of the snowpack, Q_m, that determines how much snow melts when $Q_m > 0$. The amount of melt is given by

$$\text{Melt} = Q_m / (\rho_w L_f) \tag{3.4}$$

where ρ_w is the density of water and L_f is the latent heat of fusion for ice. Condensation onto the snowpack can be an important energy source for melting during winter thaws events as it releases the latent heat of vapourization, which is about 7.5 times larger than L_f. Note that Melt in Eq. 3.4 refers to the energy required to melt the entire snowcover, not the amount of melt that occurs at the surface of the pack, or the amount of runoff from the base of the snowcover.

Physical snowpack models solve Eq. (3.2) over single or multiple layers with varying degrees of sophistication depending on the application. For example, physical snowpack models developed for avalanche risk prediction such as *CROCUS* (Vionnet et al. 2012) have a focus on simulating the evolution of snow crystal structure and internal layers linked to snow instability on sloping terrain in mid-latitude mountain environments. This contrasts with models such as *SnowModel* (Liston and Elder 2006) developed for use in Arctic environments that have a stronger emphasis on arctic processes such as blowing snow and snow–shrub interactions.

For more detailed explanations and definitions of each of the terms in Eq. (3.2) and the methods used to solve them the reader is referred to King et al. (2008), Ellis et al. (2010), and Essery et al. (2013). The following sections will deal more with the practical aspects of running physical snow models, and some of the key areas of uncertainty in the physical process parameterizations. The basic variables required to solve the energy and mass balance are at least hourly values of near-surface air temperature, atmospheric pressure, relative humidity (or vapour pressure), precipitation amount and phase, wind speed, and incoming solar and longwave radiation. The automatic weather stations used in standard meteorological observing networks measure most of these variables at hourly intervals, with the exception of precipitation phase and incoming short (Q + q) and longwave radiation (L↓) that are more likely to only be measured at research sites. L↓ plays a key role in the evolution of the snowpack thermal state over the Arctic winter and is an important energy source for snowmelt, particularly during cloudy conditions. L↓ can be estimated from surface air temperature and humidity, with greater accuracy achieved with the addition of information on cloud cover (Juszak and Pellicciotti 2013; Ebrahimi and Marshall 2015) and vertical profiles of atmospheric air temperature and humidity (Raddatz et al. 2013). Adjustments are required for radiating bodies in the sky field of view such as steep slopes and vegetation canopy that augment L↓ (Sicart et al. 2006).

Incoming solar radiation (Q + q) is the dominant driver of snowmelt under clear sky conditions and there is a wide array of surface and satellite-based methods for estimating incoming solar radiation (Liang et al. 2010). Snowpack modellers at research sites typically use measured values for all components required, while for non-research locations modellers frequently turn to atmospheric reanalyses to

obtain internally consistent variables for driving snowpack models, with temporal and spatial interpolation provided by statistical or dynamical downscaling. In regions with strong spatial and vertical variability in snow cover and driving variables, more sophisticated downscaling approaches may be required (e.g. Liston and Hiemstra 2011). Care is required when using atmospheric reanalyses as these may not be homogeneous (i.e. from changing data streams over time) and tend to exhibit warm and moist biases over high latitudes (Rapaic et al. 2015).

Horizontal advection of sensible and latent heat occurs at two scales: regional scale advection when a large-scale air mass moves over a region (e.g. a winter thaw event), and local-scale advection arising from patches of bare ground where snow has melted preferentially (Shook and Gray 1997). We will concentrate here on the local-scale advection that is important in areas characterized by highly uneven snow accumulation (Neumann and Marsh 1998). Such advection is a critical factor in the timing of basin snowmelt (Marsh and Pomeroy 1996). A number of approaches have been taken to estimate the evolution of patchy snow cover and the resulting additional sensible heat provided for melting snow (see review of methods in Harder et al. 2019). These initially concentrated on the local advection of sensible heat and developed empirical relationships for estimating areal averaged heat flux via an advection efficiency term that varied with snow-covered area (e.g. Marsh and Pomeroy 1996). More recent work (Harder et al. 2017, 2019) has highlighted the importance of latent heat flux advection from upwind wet surfaces when Q_e is the same order of magnitude as sensible heat advection. This finding underscores the need to take account of the "spatial arrangement of surface features, meteorological conditions, soil properties, and antecedent conditions" (Harder et al. 2017) when simulating snowmelt in Arctic environments. Harder et al. (2019) provide an initial one-dimensional framework for estimating sensible and latent heat advection to melting snow that contains a more physically realistic treatment of the processes. However, they note that there are a number of uncertainties in the individual process parametrizations that need to be constrained. They also note that a number of energy balance snowpack models provide good estimates of SWE depletion during the melt season without taking account of patchy snow or local advection, which suggests that these models are compensating for the role of local-scale advection. However, the details of this compensation, or the times when such models work well, versus work poorly, are not well understood.

3.3.2.2 Snow Metamorphism and Influence on Snow Physical Properties

When snowflakes reach the surface, they are subject to a range of mechanical and thermodynamic processes that transform them into the bonded grains that make-up the snowpack. This process, termed snow metamorphism, is driven by mass exchanges between ice, vapour, and liquid water (see Jordan et al. 2008 for more detail). The type of snowflakes, their density, and the environmental conditions during snowfall or blowing snow events determine the initial properties of a new snow layer, and a snowpack typically contains several distinct layers related to different snowfall events (Colbeck 1991). There are international standards and best

practices for the observing (Pielmeir and Schneebli 2003) and classification (Fierz et al. 2009) of snow on the ground.

Air temperature, wind speed, and precipitation were found to be three key climate variables for differentiating seasonal snow cover characteristics such as depth, stratigraphy, and bulk density across northern hemisphere land areas (Sturm et al. 1995, 2010—Fig. 3.1c). The two major classes of Arctic snow cover are tundra and taiga. In the tundra environment, the snowpack is shallow across wind swept areas ($< \sim 40$ cm depth, Derksen et al. 2009), while areas of shrub patches, stream channels, and steep hill slopes, collect wind blown snow, and the snowpack can be 1 to 10 m in depth. All Arctic snowpacks are characterized by a strong vertical temperature gradient through the snow layer over most of the snow season, and a resulting large vertical vapour pressure gradient that drives the transfer of mass from the warmer to the colder regions of the snowpack. This process, described as **temperature gradient metamorphism**, leads to the development of depth hoar layers that typically have larger grain sizes, low density, and low strength (Woo and Marsh 2017).

The presence of depth hoar decreases the thermal conductivity of the snowpack and reinforces the insulating role of snow, which is critical for subnival habitat (Jones et al. 2001) and the ground thermal regime (Barrere et al. 2017). The simplified energy balance schemes employed in many climate and hydrological models do not take account of vertical vapour diffusion and are hence unable to simulate realistic vertical density profiles in Arctic climates dominated by depth hoar formation (Barrere et al. 2017; Domine et al. 2018). This results in unrealistic estimates of snowpack thermal conductivity and heat transfer to the soil layer (Slater et al. 2017). Wind slab is another common feature of tundra snow cover formed by the mechanical fragmentation, sintering, and packing of blowing snow by strong winds. In a traverse across the tundra from Fairbanks, Alaska to Baker Lake, Canada, Derksen et al. (2009) were able to differentiate four types of wind slab based on hardness and noted depth hoar layers whose texture indicated wind slab origins. Linkages between depth hoar and wind slab were considered a key element in understanding the stratigraphy observed on the traverse, as wind slabs can be converted into depth hoar, while depth hoar can be eroded and reconstituted as wind slab (Derksen et al. 2009). Depth hoar is also a prominent feature of snow cover in the taiga snow environment but the lower surface wind speeds under forest canopies limit the formation of wind slab and results in a less dense snowpack (Pomeroy and Brun 2001; Pomeroy et al. 1998). Recent observations by Domine et al. (2018) suggest that the presence of depth hoar in Arctic snowpacks is influenced by soil moisture and wind conditions at the start of the snow season. The combination of low soil moisture with high wind speeds after snow-onset reduces the temperature gradient in the snowpack and prevents depth hoar formation. Snowpack bulk density exhibits an approximately linear increase over the snow season (Fig. 3.3) with relatively low interannual variability and can be readily modelled as a function of snow depth, day of year, and snow climate class (Sturm et al. 2010). The lower bulk density of snow cover at the taiga site (Fort Reliance) in Fig. 3.3 is evident compared to the other two tundra sites.

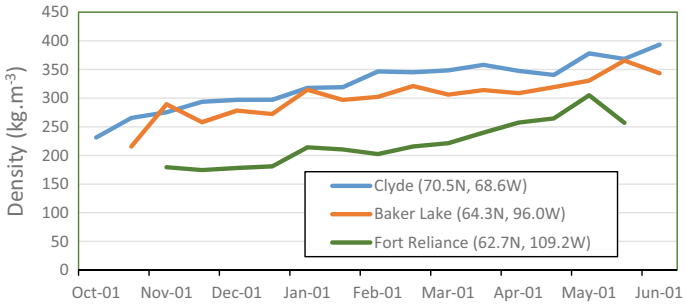

Fig. 3.3 Seasonal variation in mean snowpack bulk density (kg m^{-3}) at three northern Canadian sites along a southwest-to-northeast transect from Fort Reliance (taiga region) in the west to Clyde (tundra region) in the east. The values are averaged bulk densities computed from bi-weekly manual snow surveys carried out over 1965–1994. Clyde and Baker Lake are both classified as tundra in the Sturm et al. (1995) snow climate classification, but Clyde has a deeper mean maximum snowpack (56 cm) than Baker Lake (22 cm)

Snow metamorphism influences the optical properties of snow cover such as albedo, which decreases with increasing grain size (Woo and Marsh 2017). The initial albedo of fresh snowfall is typically high ($\sim$0.90) but decreases rapidly over a short period to values of $\sim$0.80–0.85 in response to the fast destruction of fresh snow crystals. Snowpack albedo undergoes further gradual reduction over the snow season, with periodic short-lived albedo refresh from snowfall events. Snowpack albedo is also influenced by the accumulation of dust, and in forested areas by leaf litter, both of which are concentrated on the snow surface during the melt period. The progressive accumulation of impurities on the melt surface is especially important in areas with perennial snow cover undergoing a period of extended mass loss. The seasonal change in snow albedo is relatively small compared to the areal changes in albedo driven by changes in snow-covered area (Shook et al. 1993). Figure 3.4 highlights the strong sensitivity of albedo to shallow snow accumulations and the relative insensitivity of snow albedo to major melt events that took place in early February. Essery et al. (2013) evaluated a number of physical and empirically based parameterizations for estimating snowpack albedo and found that prognostic representations of snow albedo typically resulted in better snowpack simulations.

The presence of liquid water in the snowpack from melt events or rain, and subsequent refreezing, is a strong driver of changes in snowpack grain size and properties such as density and albedo through the process of melt–freeze metamorphism (Woo and Marsh 2017). The presence of ice layers in the snowpack impacts runoff, affects gas exchanges with the atmosphere and can impede the foraging ability of ungulates such as caribou (Brown et al. 2017). There is evidence from some regions of the Arctic that the frequency of winter thaw and rain-on-snow events is increasing in response to warming (Brown et al. 2017; Langlois et al. 2017). These regions tend to be coastal climates with relatively warmer winter

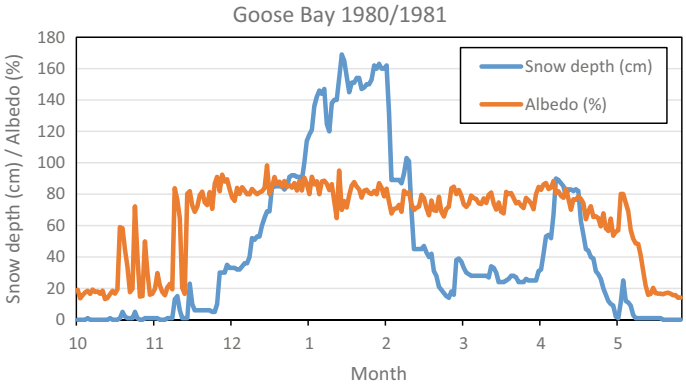

Fig. 3.4 Daily snow depth (cm) and albedo (%) over the 1980–81 snow season at Goose Bay, Labrador

temperatures and higher snow accumulations (e.g. Scandinavia, Baffin Island, Alaska, and Kamchatka). There is no clear evidence of widespread increases in thaw events over the Arctic as winter thaws and rain-on-snow events are relatively rare synoptic-scale events (Cohen et al. 2015), and their potential frequency of occurrence is offset to some extent by declining snow cover. Wang et al. (2016) showed that failure to take account of changes in snow season timing can generate apparent increasing trends in melt- and thaw-related phenomena.

3.3.2.3 Snow–Vegetation Processes

Snow and vegetation interact dynamically at many levels with the types and extent of the interactions varying with the vegetation height and characteristics. In tundra environments characterized by low vegetation and high winds, patches of shrubs play a major role in the trapping of blowing snow, the physical properties of the snowpack, and the energy budget during the melt period when shrubs emerge from the snowpack. Endrizzi and Marsh (2010) and Marsh et al. (2010) demonstrated differences in albedo and snow depth between an alder shrub patch and a nearby upland tundra site and used two different snow models to demonstrate the ability to model these contrasting Arctic sites. Domine et al. (2015) found that in tundra areas with shrubs (willow), snow depths were greater but snow density, thermal conductivity, and specific surface area were all significantly lower than on herb tundra. The combined effects of increased snow accumulation and increased thermal resistance of the snowpack result in warmer winter soil temperatures, an important positive feedback from increasing shrub growth in the Arctic. Marsh et al. (2010) observed higher spring melt rates over shrub sites following shrub emergence due to the combined effects of decreased albedo and additional longwave energy contributed by shrub stems. The increased snow accumulation and more rapid spring melt accompanying Arctic shrubification contributes to the intensification of the Arctic freshwater cycle (Rawlins et al. 2010).

In the taiga region that comprises approximately 20% of the global land surface area, the vegetation canopy influences energy transfers at the snow surface by shading of incoming solar radiation, by reducing wind speed at the surface, by providing an additional source of downwelling longwave radiation, and by limiting nocturnal heat loss from a reduced sky view factor. The snow intercepted by the canopy plays two important roles: (1) it modifies the albedo of the forest cover and (2) it influences the magnitude and direction of sensible and latent heat fluxes at the surface because the canopy is cooler and wetter with a snow cover (Pomeroy and Harding 2008). The attenuation of incoming solar radiation is the dominant effect of dense coniferous forests: Pomeroy and Harding (2008) indicate that the subcanopy net radiation of a mature conifer stand is one-tenth of above-canopy values during the snowmelt period. Thus, snow under a dense forest canopy melts later and at a lower rate than open areas. Most physical snowpack models include some treatment of canopy processes, but these differ widely and contribute to a larger spread in simulations over forested versus open sites (Essery et al. 2009).

3.3.3 Snow Runoff Processes

Snowmelt runoff in the Arctic is greatly impacted by numerous snowpack properties that are not typically found in more temperate snowpacks, including:

(1) a *highly heterogenous snow cover* with snow depths that range from a few cm to many metres over lateral distances of only tens of metres. Such heterogeneity is the result of frequent and extreme blowing snow, interacting with terrain and vegetation;
(2) a variable snow density, with density ranging from less than 100 kg/m^3 to over 600 kg/m^3 within a single vertical snow profile. This range in density results from a combination of temperature gradient metamorphism resulting in depth hoar formation near the base of the snowpack; densification due to blowing snow and equitemperature metamorphism near the top of the snowpack, and compaction of snow in deep snowdrifts; and
(3) extremely cold snow and soil temperatures (Marsh and Woo 1987, Marsh and Pomeroy 1996, 1999). This results in the freezing of large quantities of meltwater within the snow and soil.

This combination of factors impacts the rate of water flow though the snowpack and the time it takes meltwater to reach the base of the snowpack. The net result is that the timing and magnitude of meltwater availability at the base of the snowpack varies dramatically, and over small horizontal distances (Marsh and Pomeroy 1999). Perennial snow patches are important contributors to melt-fed wetlands (Chap. 12) and have been observed to be losing their perennial status over the Canadian Arctic Archipelago in recent decades (Woo and Young 2014) with important impacts for wetland hydrology and ecology.

3.3.3.1 Water Infiltration into Snow

Over most regions of the Arctic, the winter is characterized by many months of below freezing air temperature, with little or no melt or rain. As a result, the snowcover is dry, containing no liquid water and the pores are filled only with air (Marsh 2005). Typically atmospheric conditions change from cold, below 0 °C winter conditions to a rapid rise in air temperatures to >0 °C over a very short period of time (Marsh et al. 2010). This rapid transition initiates the start of the brief spring snowmelt period. In addition to air temperatures rising above freezing, solar radiation increases rapidly and there are often brief periods of light rainfall. The overall result is a rapid increase in liquid water availability at the surface of the snowpack. This water then infiltrates into the snowcover, filling the air-filled pores with water. The downward water flux only occurs when pore water content is above the irreducible water content (Jordan et al. 2008). At this point liquid water percolates into the snowcover and a wetting front develops that separates wet snow from dry snow below. Above the wetting front the snow is wet and isothermal at 0 °C. The layer immediately below the wetting front is dry with a temperature below 0 °C. As in many types of porous media, preferential flow paths develop as the wetting fronts move downward (Marsh and Woo 1984a; Jordan et al. 2008). In snow, these preferential flow paths are often referred to as flow fingers (Fierz et al. 2009).

Numerous studies have described these features in snow [Seligman (1936), U.S. Army (1956), Marsh and Woo (1984a), Kattelmann (1985), Albert et al. (1999), Schneebeli (1995), and Waldner et al. (2004)]. One of the effects of flow fingers is to concentrate water into a smaller cross-sectional area than would occur with a uniform wetting front. For example, Marsh and Woo (1984a) and Kattelmann and Dozier (1999) showed that flow fingers carry upwards of 70% of the total flow through only 20% of the horizontal cross-sectional area. The result is that water can move more quickly downward through the snowcover than if wetting fronts were uniform without flow paths. The hydrological result is that flow fingers alter the lag time between melt and runoff (Marsh and Woo 1984b; Bøggild 2000). This is especially true in deep snowpacks where flow fingers are able to route water from the snow surface to the base of the snowpack much quicker than if flow through the pack was uniform (Marsh and Woo 1985). Owing to their effect on flow, flow fingers also have implications for solute release from snow (Marsh and Pomeroy 1999; Pomeroy et al. 2006).

A unique characteristic of Arctic snowcovers is that they are typically very cold at the end of winter, and do not warm significantly prior to the start of snowmelt. This is especially true in the high Arctic (Marsh and Woo 1987) where snow may be as cold as −20 °C at the base of a 2 m deep snowpack at the start of melt. Near the Arctic treeline, the snow is typically much warmer, often −5 °C at the base of a 2 m deep snowcover. With snow temperatures well below freezing, meltwater that infiltrates into the snowcover will freeze within the snowcover. Freezing may occur in the pore spaces, as horizontal ice layers, or as vertical ice fingers (Marsh and Woo 1984a; Leroux 2018). This freezing is extremely important in warming the snow to 0 °C from the release of latent heat. As there is always a layer of wet snow,

isothermal at 0 °C, at the top of the snowcover, energy cannot travel through this upper wet zone of the snow cover through conduction. The only process to move energy into the snowcover, warming the snow below the upper isothermal layer is through the freezing of meltwater, and the release of latent heat. This energy is then conducted downward into the cold dry snow below. This freezing of meltwater can greatly slow the movement of meltwater to the base of the snowcover and can delay runoff. The duration of the delay is dependent on: snow depth, porosity, and temperature. The combination of ice layers, flow fingers, basal ice, and freezing of meltwater greatly complicates prediction of snowmelt runoff in the Arctic. To date, few meltwater runoff models include these processes although Marsh and Woo (1984b) demonstrated modelling of ice layers and flow fingers, while recent progress in simulating internal ice layers has been reported by Wever et al. (2016) and Leroux (2018).

The wetting of the snowpack is also responsible for marked changes in snow grains through the process of wet snow metamorphism (Brun 1989) that leads to crystal growth (Marsh 1987) and rounding from mass transfer driven by melting from more convex surfaces and refreezing of water on less convex or concave surfaces (Jordan et al. 2008). The process of wet snow metamorphism and frequent freezing and thawing of liquid water in the snowpack influences the capillary pressure and drainage rate, but this process has yet to be studied in detail and is a source of uncertainty in current snowmelt models (Leroux and Pomeroy 2019).

3.3.3.2 Soil Infiltration

Prior to liquid water reaching the snowpack base, the conduction of heat from freezing of ice in the snow is able to warm the soil considerably. The extent of warming prior to water reaching the soil, and prior to the ground becoming snow free, plays a significant role in controlling soil infiltration. Once meltwater reaches the base of the snowcover, it is available to either infiltrate the soil or runoff laterally as overland flow if the soil infiltration capacity is low.

Infiltration of meltwater into frozen soils is very dependent on the soil type and soil temperature (Zhao and Gray 1999). Marsh and Woo (1993) showed that for a high Arctic site with very cold mineral soils, soil infiltration was very limited, typically less than 25 mm of water. Once the infiltration capacity was filled, water ponded at the base of the snowcover, and was able to flow laterally as saturated flow. Typically, the later flow is laminar, but Kattelmann (1985) showed that in warm snowcovers, turbulent flow occurs in some cases. However, if the soil was still below 0 °C, this ponded water would freeze to form basal ice (Woo et al. 1982). Basal ice layers as thick as 70 cm were reported by Woo et al. (1982) in a snow pit excavated at the bottom of a long slope. For warmer Arctic soils with a high organic content, the infiltration is typically much higher (Quinton and Marsh 1999). In these cases, the infiltration capacity was typically larger than the total snowcover SWE, and basal ice does not form.

With sufficient heat transfer, the soil may reach 0 °C before the site becomes snow free. Once snow free, the ground continues to warm, and a distinct unfrozen later at the top of the soil forms, with a frozen later at depth. This frozen layer is

typically saturated, with zero infiltration capacity. Lateral subsurface flow ("suprapermafrost groundwater") is often the dominant runoff mechanism (Krogh et al. 2017). The depth of thaw has an important control on the rate of subsurface flow as the hydraulic conductivity of organic soils exhibits an exponential decline in hydraulic conductivity with depth (Carey et al. 2007; Quinton and Marsh 1999). The depth of thaw or active layer thickness (ALT) controls both ground heat transfer and available soil water storage capacity for late summer, and winter snow cover (depth, thermal conductivity) has a strong influence on ALT, which is a nice example of the close coupling between snow cover, the ground thermal regime, and hydrology in the Arctic. Modelling infiltration into frozen soils remains extremely challenging, but progress in developing numerical models of snowmelt infiltration and macropore flow is being made (Mohammed et al. 2018).

3.3.3.3 Lateral Flow to Stream Channels

Lateral flow of meltwater in sloping snowpacks is a well-known phenomenon (Marsh and Woo 1985; Kattelman and Dozier 1999; Quinton et al. 2004; Eriksson et al. 2013) that arises when the vertical energy gradients driving flow are disrupted, enabling lateral energy gradients to drive flow. Anything that creates a hydraulic conductivity contrast in the snowpack can impede vertical flow and promote lateral flow such as boundaries between different snow layers, or the presence of an impermeable ice layer (Woo et al. 1982; Marsh and Woo 1985). Lateral flow can be an important source of direct stream snowmelt contributions during rain-on-snow (ROS) events; Eriksson et al. (2013) found that lateral flow generated up to 12% of streamflow during one ROS event. Lateral flows can also contribute to wet snow avalanches as local concentrations of liquid water decrease shear strength and increase strain rate (McClung and Schaerer 2006).

The hydrologic importance of lateral flow in snow depends on the length of the lateral flowpaths and the quantities of transmitted water. For example, ice layers frequently contain holes (Kattelmann and Dozier 1999), which means water is only routed laterally for short distances before being diverted into vertical channels (Marsh and Woo 1985). Although the occurrence of lateral flow in snow is well known, Eriksson et al. (2013) conclude that few studies have investigated its potential velocities, flow rates, and impacts on hillslope and catchment-scale hydrologic processes. Tracer experiments carried out by Eriksson et al. (2013) demonstrated that rain and melt water can travel at speeds of up to a metre per hour along layers within the snowpack. In many cases lateral flow took place along almost imperceptible boundaries in snowpack properties without impervious layers. The probability of lateral flow occurring within the snowpack becomes less likely as the snowpack becomes saturated and stratigraphic boundaries are destroyed, but flow over a basal ice layer can occur in all snowpack conditions. In very steep terrain, lateral flows dominate vertical flows as observed by Hetrick et al. (2016).

3.3.4 Snow Choked Channels and Slush Flows

Another unique snowmelt runoff component of upland Arctic streams, especially in the continuous permafrost zone, is that streamflow typically ceases during the winter as there is no source of water. The only exception is for streamflow below large lakes. In addition, blowing snow is able to accumulate in the stream channels. As Woo and Saurial (1981) showed, in the High Arctic, snow was many metres deep in typical stream channels, with deeper drifts common. These drifts are often of high density. Such accumulation of snow in stream channels is common across the Arctic, but is poorly documented. Woo and Sauriol (1981) documented the process of liquid water accumulating within these snow choked channels, although the impact of these processes on the timing and magnitude of spring melt runoff has not been documented. However, the general effects are to delay snowmelt runoff from one to two weeks and contribute to the development of large ponds upstream of snow dams. As the snow dams are over-topped, they are rapidly eroded and melted, resulting in much higher peak flows than would normally be expected. No hydrologic models include these processes, and as a result, modelling of snowmelt streamflow is not currently possible.

3.4 Snow Chemistry/Water Quality

Snowflakes in the atmosphere are very effective scavengers of aerosol particles and absorbers of trace gases, which means that solid precipitation arriving at the ground contains a number of impurities and contaminants. On the ground, snow metamorphic processes, photochemical reactions and melt events influence the concentration, storage, and cycling of these contaminants (Grannas et al 2013; Bartels-Rauch et al. 2014). Bartels-Rausch et al. (2014) provide a detailed review of the physical processes and chemical reactivity in surface snow. Projected warming of the Arctic will affect the uptake and cycling of contaminants through changes in the liquid/solid fraction of precipitation, and the partitioning equilibria of contaminants between gas phase and snow and ice (Grannas et al. 2013). However, a number of major gaps in the current understanding of snow chemistry processes (Domine et al. 2013; Bartels-Rausch et al. 2014) limit the ability to model the potential impact of warming on contaminant cycling. Recent modelling efforts by Costa et al. (2018) have been able to successfully simulate the transport and reallocation of solutes within the snow matrix.

3.5 Arctic Snow Observing Systems

Observing snow in the Arctic environment faces a number of challenges. Firstly, surface measurement sites are sparsely distributed, and the harsh environment poses challenges for both manual and automated measurements. In situ measurements may also be unrepresentative of the prevailing snow cover due to local influences related to the location and exposure of the measurement site. Secondly, space-based observations are limited by daylight and cloud cover for visible satellites, while passive microwave estimates of snow depth and SWE over Arctic areas are more challenging in regions with extensive depth hoar (Derksen et al. 2005; Mortimer et al. 2020), and in areas with large numbers of lakes (Duguay et al. 2005; Derksen et al. 2009). Yang et al. (2007) showed that weekly SWE data/products derived from microwave remote sensing technology were useful in understanding snowmelt process and runoff changes in the Arctic over large watersheds such as the Ob and Yenisei, and Lena.

Tables 3.3 and 3.4 present summaries of commonly used in situ and remotely sensed methods for monitoring the presence and physical properties of snow cover such as depth, water equivalent, and albedo. Measurement methods have differing accuracies (Smith and Fierz 2019) and spatial and temporal scales, which need to be taken into account when evaluating snow cover products and model output. Standards for variable names and units are provided in the *International Classification for Seasonal Snow on the Ground* (Fierz et al. 2009). When working with Arctic snow cover datasets it is important to be aware of the characteristics and limitations of the data sources used. For example, point snow depth measurements made at Arctic sites in Canada are often made over open terrain near airports that may not be representative of the snow cover in the prevailing land cover and terrain. These data have been found to underestimate the landscape peak winter snow accumulation and to melt off snow too quickly in the spring (Brown et al. 2003). Hydrologic applications assimilating data from multiple sources must be especially aware of the different spatial and temporal scales involved. A review of the state of the Arctic in situ and remotely sensed snow monitoring capabilities (Brown et al. 2017) concluded that while the past decade had seen a major increase in the availability of reanalysis snow products, as well as rapid development of a number of new technologies for measuring snow at point-to-local scales, there has been relatively little progress in monitoring snow depth and snow water equivalent from satellites. One area of promise is synthetic aperture radar, which is ideally suited for estimating depth and SWE over the dry snowpacks found over large areas of the Arctic (Brown et al. 2017). However, the development of robust SWE retrievals is a major challenge as snow microstructure influences the multi-frequency response of radar backscatter to SWE. Thus, the radar response from two snowpacks with the same SWE but differing snow stratigraphy (for example, rounded grains associated with taiga snow versus the predominantly faceted grains associated with tundra snow) will be strongly influenced by different volume scattering interactions.

Table 3.3 Summary of commonly used methods for measuring in situ snow depth and/or SWE. See Kinar and Pomeroy (2015) for a comprehensive review of snow measurement methods and technologies

Method	Manual (M)/ Auto (A)	Variable	Spatial scales (area of footprint)	Temporal Scales	Comments	References
Ruler/stake	M	Snow Depth	~1–25 m^2 depending on number of stakes or sample points	Daily	Average of 3–5 point measurements; three fixed stakes used in Russia and Former Soviet Union	Smith and Fierz (2019)
Snow depth sensor (sonic, laser)	A	Snow Depth	~1 m^2 for sonic sensor @ 2 m above snow surface; <5 mm for laser	15 min	Area seen by ultrasound sensor varies with height above the snow surface. Zero depth drift a common source of error	Smith and Fierz (2019)
Snow corer	M	SWE	~1–5 × 10^3 m^2	Weekly, bi-weekly	5–10 observations along transect of 100–500 m. Common errors are loss of snow from the corer, and non-penetration of basal ice layers.	Smith and Fierz (2019)
Snow pillow	A	SWE	~3 m^2	Continuous	Most common errors are bridging and zero drift	Smith and Fierz (2019)
Snowpit	M	Depth, density, and SWE stratigraphy	~3 m^2	Discrete (as required)	Loss of coarse-grained snow from sampler can lead to underestimation of snow density	Smith and Fierz (2019)
Passive gamma	A	SWE	~40 m^2 at 2 m above the snow surface for passive gamma	Continuous	Gamma sensors are influenced by the amount of soil moisture present at the time that the soil freezes and are sensitive to mid-season changes in soil moisture	Choquette et al. (2008); Smith et al. (2017)
Terrestrial Laser Scanning (TLS)	A	Snow depth	~0.1 to 0.3 m^2 @ 1 km range (footprint is a function of range and terrain slope)	Discrete (as required)	Requires a stable platform and proper georegistration of snow-free and snow-covered scans to get reliable results	Deems et al. (2013)

Table 3.4 Summary of commonly used remotely sensed methods for monitoring arctic snow cover

Method	Variable	Resolution	Temporal scales	Comments	References
Optical satellite (e.g. MODIS, VIIRS)	Snow cover fraction, snow cover extent, snow albedo, time of snow cover onset, and snow-off	~500 m	Continuous for geostationary satellites, daily for polar-orbiting satellites	Coverage limited by winter darkness, cloud cover, and dense forest cover	Riggs et al. (2017)
Passive microwave satellite	Snow depth and/or SWE, time of snow cover, and melt onset	~25 km	Daily	Not limited by cloud cover or darkness. Most SWE retrievals lose signal for SWE values >~ 150 mm. SWE typically biased high over regions with shallow, cold snow with extensive depth hoar. Incorporation of surface snow depth observations in SWE retrievals improves performance over shallow Arctic snowpacks	Takala et al. (2011) Derksen et al. (2010) Mortimer et al. (2020)
Aerial Photogrammetry	Snow depth	~5 cm @ 100 m elevation above surface for UAV	Discrete (usually peak accumulation)	Requires a snow-free scene and precise georegistration	Michele et al. (2016)
Airborne LiDAR	Snow Depth	~0.2 to 0.3 m @ 1 km elevation above surface	Discrete (usually peak accumulation)	Requires a snow-free scene and precise georegistration	Deems et al. (2013)

(continued)

Table 3.4 (continued)

Method	Variable	Resolution	Temporal scales	Comments	References
GRACE	Terrestrial water storage	~300 km	10–30 days	SWE must be separated from total storage, which requires estimates of the non-snow terms from observations or land surface models. SWE estimates are unaffected by forest canopy and variable snow grain size and are not limited by deep snow conditions	Rowlands et al. (2005), Frappart et al. (2011), Forman et al. (2012)

MODIS Moderate Resolution Imaging Spectroradiometer, VIIRS Visible Infrared Imaging Radiometer Suite, GRACE Gravity Recovery and Climate Experiment, UAV Unmanned Aerial Vehicle, LiDAR Light Detection and Ranging

3.6 The Current State of Arctic Snow Cover—Historical Variability and Trends

Documenting the current state and historical variability of Arctic snow cover faces a number of challenges related to the large spatial variation in snow cover, sparse surface observations, and limitations of satellite monitoring systems. There is higher confidence in snow cover variables more closely controlled by air temperature such as dates of snow cover onset and snow-off, and snow cover duration, and generally strong agreement in snow cover trends between different data sources in the spring period (Brown et al. 2010; Mudryk et al. 2015). There is much larger dataset spread in annual maximum SWE than snow cover duration or extent, with the highest spread over tundra regions (Mudryk et al. 2015).

Special attention must be given to data homogeneity when analysing trends in snow cover. Inhomogeneities can be introduced from a number of sources including changes in instrumentation, changes in site characteristics (e.g. growing vegetation), changes in observing practices, technological bias (e.g. from increasing satellite coverage and resolution over time), and shifts in the distribution and density of surface observations over time. Snow cover reconstructions from snow models driven by atmospheric reanalyses are sensitive to well-documented inhomogeneities in many of the reanalyses. Multi-dataset approaches such as blending can increase confidence in trend estimates and provide some idea of the relative levels of uncertainty (Mudryk et al. 2018).

Surface observations and satellite data provide a fairly consistent picture of declining snow cover by 2–4 days per decade over the past ~40 years with stronger reductions in the spring period and over high latitudes and elevations consistent with polar amplification of warming and enhanced albedo feedbacks (Brown et al. 2017). Declines in Arctic spring snow cover are typically associated with earlier snowmelt (Serreze et al. 2000; Yang et al. 2003, 2007; Ye and Cohen 2013).

Significant declines in autumn snow cover (later snow cover onset) are observed in areas such as the Canadian eastern Arctic that have experienced rapid sea ice loss, an extension of the open water period, and delayed freeze-up (Langen et al. 2018). Reported increases in Eurasian snow cover in the snow-onset period from the NOAA-CDR dataset (e.g. Cohen et al. 2012) are not consistent with other snow cover products (Brown and Derksen 2013; Mudryk et al 2015; Hori et al. 2017) and observed warming of Arctic temperatures which show evidence of enhanced warming in both the fall and spring periods (Fig. 3.5). Arctic spring (June) snow cover extent is currently estimated to be decreasing at a rate of −13.6% per decade in spite of a number of recent years with above-average winter snow accumulation (Mudryk et al. 2019).

Trends in annual maximum snow accumulation are more uncertain and vary regionally, by elevation and between different data sources, but with a consensus for declining maximum snow accumulation (SWEmax) of ~−4% per decade when averaged over pan-Arctic land areas (Brown et al. 2017). Increasing snowfall has

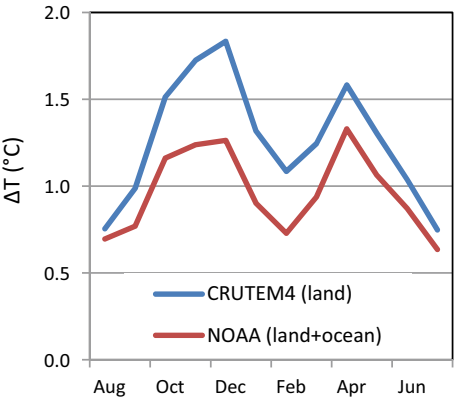

Fig. 3.5 Seasonal character of recent warming over the Arctic (difference between 2006–2015 average and 1951–2010 average) from two datasets, CRUTEM4 (Jones et al. 2012) and NOAA version 4.01 (Karl et al. 2015)

been documented over northern Canada and Siberia (Kononova 2012; Vincent et al. 2015) but the increases need to more than compensate for a shortened snow accumulation period to generate increased maximum snow depth or SWE. In Canada, the available evidence points to widespread reductions in surface snow accumulations at Arctic sites (Lesack et al. 2013; Lesack et al. 2014; Vincent et al. 2015). However, Brown et al. (2019) found evidence of a latitudinal dependence in SWEmax trends from snow surveys in Canada, with some of the more northern sites exhibiting significant increases in SWEmax in agreement with observations from Russia (Bulygina et al. 2011).

3.7 Projected Changes in Arctic Snow Cover

As noted previously, Arctic terrestrial snow cover is part of a tightly coupled soil–climate–vegetation–soil–hydrology system with multiple interactions and feedbacks that responds to a number of environmental drivers. Current global climate and earth system models include physical snowpack models and are able to account for many of the important processes and feedbacks involved in simulating the snow cover response to a warmer climate. However, they do not include dynamic snow–vegetation interactions related to Arctic greening or browning (Phoenix and Bjerke 2016), the representation of snow processes in the vegetation canopy is rudimentary (Bokhorst et al. 2016) contributing to large model spread in the representation of snow albedo feedbacks (Thackeray et al. 2018), and the representation of heat transfer through the snow–soil system is unrealistic in many models (Slater et al. 2017).

Nonetheless, climate and earth system models represent a physically based, internally consistent approach for constructing snow cover change scenarios for the Arctic that provide some indication of the large-scale changes in the duration and maximum amount of snow accumulation. Projected changes in Arctic snow cover from the CMIP5 model ensemble for two emission scenarios representing business

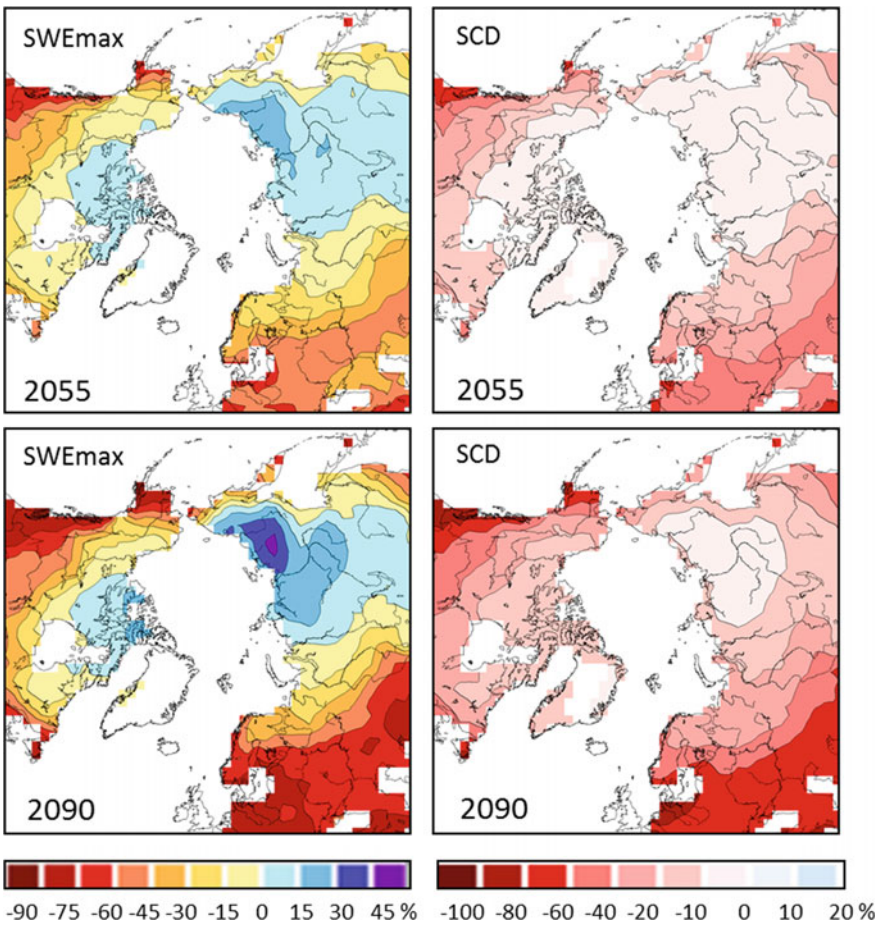

Fig. 3.6 Left: 2055 and 2090 projected median % change in annual maximum monthly SWE (SWEmax) from 16 CMIP5 GCMs for the RCP8.5 scenario (2046–2065 and 2081–2100 minus 1986–2005). Right: same for annual snow cover duration (SCD). After Brown et al. (2017)

as usual (RCP8.5) and efforts to limit emissions (RCP4.5) were provided in Brown et al. (2017) for the mid- and end of twenty-first-century time periods. The model spread was captured by presenting the median and the upper and lower quartile projections from the 16-model ensemble following the IPCC (2013) *Atlas of Global and Regional Climate Projections*. The median model projected changes for annual SCD and SWEmax for 2055 and 2090 for RCP8.5 are reproduced in Fig. 3.6. All regions of the Arctic are projected to undergo reductions in snow season length with the relative magnitude decreasing moving northward. A relative decrease of 10–20% of annual SCD may seem small but this represents 30–60 days less snow cover over higher latitudes. The areas of the Arctic at highest risk of rapid snow

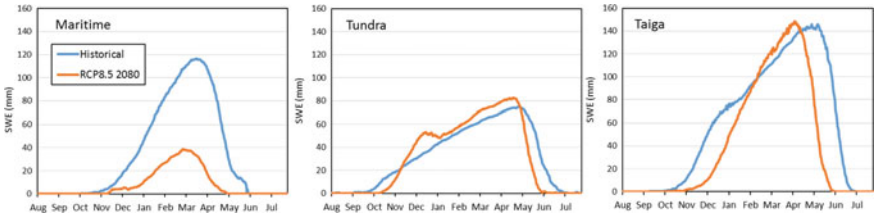

Fig. 3.7 Projected change in average seasonal snowpack SWE for three different snow climate regions of the Arctic from CanESM2 historical and RCP8.5 simulations. Snow cover is modelled with the CLASS 2.7 land surface scheme snow model described in Bartlett et al. (2006)

cover loss are the warmest sectors with relative high winter precipitation which includes regions such as Scandinavia, Alaska, Baffin Island, and the Pacific coast of the Russian Arctic.

The large-scale response of Arctic snow cover to projected warming and moistening involves non-linear interactions between warming (shortened snow season, reduced solid fraction of total precipitation) and increasing precipitation as originally pointed out by Räisänen (2008). This gives rise to the contrasting pattern of projected SWEmax change seen in Fig. 3.6 where the coldest regions of the Arctic are projected to have increased snow accumulation (increases in snowfall are sufficient to offset warming effects on snow season and solid fraction), while the warmer regions of the Arctic such as Scandinavia and Alaska, are projected to experience large relative decreases in SWEmax from reductions in the solid fraction of precipitation (Shi and Wang 2015; Bintanja and Andry 2017).

The consequences of projected warming and increased precipitation on seasonal snowpack are shown in Fig. 3.7 for three different climate regions of the Arctic. The results highlight key elements of the snow cover response: a universal shortening of the period with snow cover and advancement of the date of maximum SWE, large relative declines of SWE in the shoulder seasons, increased snow accumulation rates over the taiga and tundra regions, a higher sensitivity of SWEmax to warming in the warmer maritime regions of the Arctic, and the relative insensitivity of SWEmax to projected climate change over the boreal and taiga regions. More recent climate change simulations using a high resolution spatially distributed Arctic hydrological model incorporating projected changes in vegetation over a small headwater basin at the tundra–taiga transition in northwestern Canada (Krogh and Pomeroy 2019) revealed an important intensification of hydrological processes with maximum peak snow accumulation increasing 70% with an earlier and larger (130%) peak spring streamflow. The snow cover response was mostly driven by projected climate change, with increasing vegetation cover playing an important role through reduced blowing snow redistribution and sublimation.

The magnitude and temporal evolution of the projected SCD changes averaged over the Arctic are strongly dependent on the emission scenario used. The RCP4.5 results presented in Brown et al. (2017) show evidence of Arctic annual SCD losses

stabilising at a new equilibrium level about 10% lower than current values by the end of the twenty-first century while the RCP8.5 results show accelerating losses in snow cover throughout the twenty-first century.

3.8 Hydrological Implications of a Changing Arctic Snow Cover

The response of Arctic hydrologic systems to change in snow cover generated from the combined influence of the environmental drivers listed in Table 3.1 is complex because snow cover is part of a coupled snow–soil–vegetation system. This complexity was clearly demonstrated by Shi and Wang (2015) who showed that although the start of spring snowmelt was occurring dramatically earlier in the western Canadian Arctic, spring streamflow in a headwater basin was delayed. This unexpected change in runoff is likely related to changes in end-of-winter snowcover, active layer thickness, and shrub expansion, however, additional research is needed to both verify the controlling processes and establish whether current hydrologic models are able to accurately simulate these key interactions controlling streamflow.

Warming and increased precipitation are expected to contribute to more frequent extreme hydroclimatic events such as winter thaw and rain-on-snow events (Ye et al. 2008; Cohen et al. 2015; Langlois et al. 2017). These have potential to influence the snowpack energy budget by modifying surface albedo and snow density, can generate rapid runoff (Pedersen et al. 2015), and can create ice layers within the snowpack that influence snowmelt percolation during the melt period. There is evidence from a number of sources of increasing ice layer content in Arctic snowpacks (Johansson et al. 2011; Chen et al. 2013; Langlois et al. 2017).

Another important issue for Arctic snow hydrology is the large-scale transition underway from permanent to seasonal snow cover in cold regions of the Arctic, and from a nival to more pluvial dominated runoff regimes in warmer sectors of the Arctic such as Scandinavia and southern Alaska (Vihma et al. 2016). This transition is associated with a relative increase in winter flows (Tan et al. 2011), a relative decline in the contribution of the spring freshet to total runoff (Ahmed 2015), and the emergence of new streamflow regimes in response to more frequent large summer and fall rainfall events (Spence et al. 2011, 2015; DeBeer et al. 2016). The loss of perennial snow patches in tundra regions will have a major impact on support of wetlands and streamflow during the summer season, especially in dry polar desert environments (Woo and Young 2014). The projected advancement of the date of peak snowmelt seen in Fig. 3.7 has important consequences for melt rates and extreme spring melt events in the Arctic as earlier dates are associated with a lower net radiation for driving the melt process (Musselman et al. 2017). Climate model simulations project most areas of the Arctic to transition to pluvial dominated precipitation regimes before the end of the twenty-first century (Bintanja and Andry 2017).

References

Ahmed R (2015) MSc thesis, UVic. Spatio-temporal variation in the spring freshet of major circumpolar Arctic river systems

Albert M, Koh G, Perron F (1999) Radar investigations of melt pathways in a natural snowpack. Hydrol Process 13(18):2991–3000

Assini J, Young KL (2012) Snow cover and snowmelt of an extensive High Arctic wetland: spatial and temporal seasonal patterns. Hydrol Sci J 57(4):738–755

Barrere M, Domine F, Decharme B, Morin S, Vionnet V, Lafaysse M (2017) Evaluating the performance of coupled snow–soil models in SURFEXv8 to simulate the permafrost thermal regime at a high Arctic site. Geoscientific Model Dev 10(9):3461–3479

Bartels-Rausch T, Jacobi H-W, Kahan TF, Thomas JL, Thomson ES, Abbatt JPD, Ammann M et al (2014) A review of air–ice chemical and physical interactions (AICI): liquids, quasi-liquids, and solids in snow. Atmos Chem Phys 14(3):1587–1633

Bartlett PA, MacKay MD, Verseghy DL (2006) Modified snow algorithms in the Canadian Land Surface Scheme: Model runs and sensitivity analysis at three boreal forest stands. Atmos Ocean 44(3):207–222

Bartlett PA, Verseghy DL (2015) Modified treatment of intercepted snow improves the simulated forest albedo in the Canadian Land Surface Scheme. Hydrol Process 29(14):3208–3226

Bintanja R, Andry O (2017) Towards a rain-dominated Arctic. Nat Clim Change 7(4):263

Bøggild CE (2000). Preferential flow and melt water retention in cold snow packs in west-greenland. In: Paper presented at the 12th Northern Res. Basins/Workshop (Reykjavik, Iceland–Aug 23rd–27th 1999). Hydrol Res 31(4–5):287–300

Boike J, Roth K, Ippisch O (2003) Seasonal snow cover on frozen ground: energy balance calculations of a permafrost site near Ny-Ålesund, Spitsbergen. J Geophys Res: Atmos 108 (D2)

Bokhorst S, Pedersen SH, Brucker L, Anisimov O, Bjerke JW, Brown RD, Ehrich D, Essery RL, Heilig A, Ingvander S, Johansson C (2016) Changing Arctic snow cover: A review of recent developments and assessment of future needs for observations, modelling, and impacts. Ambio 45(5):516–537

Boon S, Burgess DO, Koerner RM, Sharp MJ (2010) Forty-seven years of research on the Devon Island ice cap, Arctic Canada. Arctic 63:13–29. https://doi.org/10.2307/40513366

Box J et al (2019) Key Indicators of Arctic Climate Change: 1971-2017. Environ Res Lett. https://doi.org/10.1088/1748-9326/aafc1b

Brown RD, Brasnett B, Robinson D (2003) Gridded North American monthly snow depth and snow water equivalent for GCM evaluation. Atmos Ocean 41(1):1–14

Brown R, Derksen C, Wang L (2010) A multi-data set analysis of variability and change in Arctic spring snow cover extent, 1967–2008. J Geophys Res 115:D16111. https://doi.org/10.1029/2010JD013975

Brown RD, Derksen C (2013) Is Eurasian October snow cover extent increasing? Environ Res Lett 8:024006. https://doi.org/10.1088/1748-9326/8/2/024006

Brown R, Vikhamar-Schuler D, Bulygina O, Derksen C, Luojus K, Mudryk L, Wang L, Yang D (2017) Arctic terrestrial snow cover. Chapter 3 in: Snow, water, ice and permafrost in the arctic (SWIPA) 2017, pp. 25–64, Arctic Monitoring and Assessment Programme (AMAP), Oslo, Norway

Brown R, Fang B, Mudryk L (2019) Update of Canadian historical snow survey data and analysis of snow water equivalent trends, 1967–2016. Atmosphere-Ocean 57(2):149–156

Brun E (1989) Investigation on wet-snow metamorphism in respect of liquid-water content. Ann Glaciol 13:22–26

Bulygina ON, Groisman PY, Razuvaev VN, Korshunova NN (2011) Changes in snow cover characteristics over Northern Eurasia since 1966. Environ Res Lett 6(4). https://doi.org/10.1088/1748-9326/6/4/045204

Carey SK, Quinton WL, Goeller NT (2007) Field and laboratory estimates of pore size properties and hydraulic characteristics for subarctic organic soils. Hydrol Process: Int J 21(19):2560–2571

Carmack EC, Yamamoto-Kawai M, Haine TW, Bacon S, Bluhm BA, Lique C, Melling H, Polyakov IV, Straneo F, Timmermans ML, Williams WJ (2016) Freshwater and its role in the Arctic Marine System: Sources, disposition, storage, export, and physical and biogeochemical consequences in the Arctic and global oceans. J Geophys Res: Biogeosci 121(3):675–717

Chen W, Russell DE, Gunn A, Croft B, Chen WR, Fernandes R, Zhao H et al (2013) Monitoring habitat condition changes during winter and pre-calving migration for Bathurst Caribou in northern Canada. Biodiversity 14(1):36–44

Choquette Y, Lavigne P, Nadeau M, Ducharme P, Martin JP, Houdayer A, Rogoza J (2008) GMON, a new sensor for snow water equivalent via gamma monitoring. In: Proceedings Whistler 2008 International Snow Science Workshop September 21–27, 2008 (p 802)

Clark M, Gurnell AM, Milton EJ, Seppälä M, Kyöstilä M (2013) Remotely-sensed vegetation classification as a snow depth indicator for hydrological analysis in sub-arctic Finland. Fennia-Int J Geograph 163(2):195–216

Cohen JL, Furtado JC, Barlow MA, Alexeev VA, Cherry JE (2012) Arctic warming, increasing snow cover and widespread boreal winter cooling. Environ Res Lett 7(1):014007

Cohen, J., H. Ye, and J. Jones, 2015. Trends and variability in rain-on-snow events. Geophys. Res. Lett., 42, doi:10.1002/2015GL065320

Colbeck SC (1991) The layered character of snow covers. Rev Geophys 29(1):81–96

Costa D, Pomeroy J, Wheater H (2018) A numerical model for the simulation of snowpack solute dynamics to capture runoff ionic pulses during snowmelt: The PULSE model. Adv Water Resour 122:37–48

DeBeer CM, Wheater HS, Carey SK, Chun KP (2016) Recent climatic, cryospheric, and hydrological changes over the interior of western Canada: a review and synthesis. Hydrol Earth Syst Sci 20(4):1573–1598. https://doi.org/10.5194/hess-20-1573-2016

Deems JS, Painter TH, Finnegan DC (2013) Lidar measurement of snow depth: a review. J Glaciol 59:467–479

Derksen C, Walker A, Goodison B (2005) Evaluation of passive microwave snow water equivalent retrievals across the boreal forest/tundra transition of western Canada. Remote Sens Environ 96(3–4):315–327

Derksen C, Silis A, Sturm M, Holmgren J, Liston GE, Huntington H, Solie D (2009) Northwest Territories and Nunavut snow characteristics from a subarctic traverse: Implications for passive microwave remote sensing. J Hydrometeorol 10(2):448–463

Derksen C, Toose P, Rees A, Wang L, English M, Walker A, Sturm M (2010) Development of a tundra-specific snow water equivalent retrieval algorithm for satellite passive microwave data. Remote Sens Environ 114(8):1699–1709

Déry SJ, Taylor PA, Xiao J (1998) The thermodynamic effects of sublimating, blowing snow in the atmospheric boundary layer. Bound-Layer Meteorol 89(2):251–283

Déry SJ, Yau MK (2002) Large-scale mass balance effects of blowing snow and surface sublimation. J Geophys Res - Atmos 107(D23):4679. https://doi.org/10.1029/2001JD001251

Déry SJ, Crow WT, Stieglitz M, Wood EF (2004) Modeling snow-cover heterogeneity over complex Arctic terrain for regional and global climate models. J Hydrometeorol 5:33–48

DeWalle DR, Rango A (2011) Principles of snow hydrology. Cambridge University Press

Domine F, Bock J, Voisin D, Donaldson DJ (2013) Can we model snow photochemistry? Problems with the current approaches. J Phys Chem A 117(23):4733–4749

Domine F, Barrere M, Sarrazin D, Morin S, Arnaud L (2015) 2015: Automatic monitoring of the effective thermal conductivity of snow in a low Arctic shrub tundra. The Cryosphere 9:1265–1276. https://doi.org/10.5194/tc-9-1265-2015

Domine F, Belke-Brea M, Sarrazin D, Arnaud L, Barrere M, Poirier M (2018) Soil moisture, wind speed and depth hoar formation in the Arctic snowpack. J Glaciol 64(248):990–1002

Duguay CL, Green JE, Derksen C, English MI, Rees A, Sturm MA, Walker A (2005) Preliminary assessment of the impact of lakes on passive microwave snow retrieval algorithms in the Arctic. In: 62nd Eastern snow conference proceedings, 2005 Jun 7

Ebrahimi S, Marshall SJ (2015) Parameterization of incoming longwave radiation at glacier sites in the Canadian Rocky Mountains. J. Geophys. Res. Atmos. 120:12536–12556. https://doi.org/10.1002/2015JD023324

Ellis CR, Pomeroy JW, Brown T, MacDonald J (2010) Simulation of snow accumulation and melt in needleleaf forest environments. Hydrol Earth Syst Sci 14(6):925–940

Endrizzi S, Marsh P (2010) Observations and modeling of turbulent fluxes during melt at the shrub-tundra transition zone 1: point scale variations. Hydrol Res 41(6):471–491

Essery R, Rutter N, Pomeroy J, Baxter R, Stähli M, Gustafsson D, Barr A, Bartlett P, Elder K (2009) SNOWMIP2: An evaluation of forest snow process simulations. Bull Am Meteor Soc 90(8):1120–1136

Essery R, Morin S, Lejeune Y, Ménard CB (2013) A comparison of 1701 snow models using observations from an alpine site. Adv Water Resour 55:131–148

Eiriksson D, Whitson M, Luce CH, Marshall HP, Bradford J, Benner SG, McNamara JP (2013) An evaluation of the hydrologic relevance of lateral flow in snow at hillslope and catchment scales. Hydrol Process 27(5):640–654. https://doi.org/10.1002/hyp.9666

Fierz C, Armstrong RL, Durand Y, Etchevers P, Greene E, McClung DM, Nishimura K, Satyawali PK, Sokratov SA (2009) The international classification for seasonal snow on the ground. IHP-VII Technical Documents in Hydrology N°83, IACS Contribution N°1, UNESCO-IHP, Paris

Forman BA, Reichle RH, Rodell M (2012) Assimilation of terrestrial water storage from GRACE in a snow-dominated basin. Water Resour Res 48:W01507. https://doi.org/10.1029/2011WR011239

Frappart F, Ramillien G, Famiglietti JS (2011) Water balance of the Arctic drainage system using GRACE gravimetry products. Int J Remote Sens 32:431–453

Freudiger D, Kohn I, Seibert J, Stahl K, Weiler M (2017) Snow redistribution for the hydrological modeling of alpine catchments, WIRES Water, e1232, https://doi.org/10.1002/wat2.1232

Grannas AM, Bogdal C, Hageman KJ, Halsall C, Harner T, Hung H, Kallenborn R, Klán P, Klánová J, Macdonald RW, Meyer T (2013) The role of the global cryosphere in the fate of organic contaminants. Atmos Chem Phys 13(6):3271–3305

Harder P, Pomeroy J (2013) Estimating precipitation phase using a psychrometric energy balance method. Hydrol Process 27(13):1901–1914

Harder P, Pomeroy JW, Helgason W (2017) Local-scale advection of sensible and latent heat during snowmelt. Geophys Res Lett 44(19):9769–9777

Harder P, Pomeroy JW, Helgason WD (2019) A simple model for local scale sensible and latent heat advection contributions to snowmelt. Hydrol Earth Syst Sci 23:1–17. https://doi.org/10.5194/hess-23-1-2019

Hetrick HF, Marshall HP, Bradford JH, McNamara JP, Eiriksson D (2016) Quantifying the role of lateral flow of water in a sloped mountainous snowpack: spatiotemporal patterns in soil moisture and snowmelt. AGUFM, 2016, pp C51D-0686

Homan JW, Kane DL (2015) Arctic snow distribution patterns at the watershed scale. Hydrol Res 46(4):507–520

Hori M, Sugiura K, Kobayashi K, Aoki T, Tanikawa T, Kuchiki K, Niwano M, Enomoto H (2017) A 38-year (1978–2015) Northern Hemisphere daily snow cover extent product derived using consistent objective criteria from satellite-borne optical sensors. Remote Sens Environ 191:402–418

IPCC (2013) Annex I: Atlas of Global and Regional Climate Projections [van Oldenborgh GJ, Collins M, Arblaster J, Christensen JH, Marotzke J, Power SB, Rummukainen M and Zhou T (eds)]. In: Climate Change 2013: The Physical Science Basis. Contribution of Working Group I to the Fifth Assessment Report of the Intergovernmental Panel on Climate Change [Stocker TF, Qin D, Plattner G-K, Tignor M, Allen SK, Boschung J, Nauels A, Xia Y, Bex V

and Midgley PM (eds)]. Cambridge University Press, Cambridge, United Kingdom and New York, NY, USA
Jennings KS, Winchell TS, Livneh B, Molotch NP (2018) Spatial variation of the rain–snow temperature threshold across the Northern Hemisphere. Nature Commun 9(1):1148
Johansson C, Pohjola VA, Jonasson C, Callaghan TV (2011) Multi-decadal changes in snow characteristics in sub-Arctic Sweden. Ambio 40(6):566–74
Jones HG, Pomeroy JW, Walker DA, Hoham RW eds (2001) Snow ecology: an interdisciplinary examination of snow-covered ecosystems. Cambridge University Press
Jones PD, Lister DH, Osborn TJ, Harpham C, Salmon M, Morice CP (2012) Hemispheric and large-scale land surface air temperature variations: an extensive revision and an update to 2010. J Geophys Res 117:D05127. https://doi.org/10.1029/2011JD017139
Jordan R, Albert M, Brun E (2008) Physical processes within the snow cover and their parameterization. Chapter 2 in: Armstrong R, Brun E (eds) Snow and climate: physical processes, surface energy exchange and modeling. Cambridge University Press, pp 12–69
Juszak I, Pellicciotti F (2013) A comparison of parameterizations of incoming longwave radiation over melting glaciers: model robustness and seasonal variability. J Geophys Res: Atmos 118 (8):3066–3084
Karl Thomas R, Arguez Anthony, Huang Boyin, Lawrimore Jay H, McMahon James R, Menne Matthew J, Peterson Thomas C, Vose Russell S, Zhang Huai-Min (2015) Possible artifacts of data biases in the recent global surface warming hiatus. Sci Expr. https://doi.org/10.1126/science.aaa5632
Kattelmann RC (1985) Macropores in snowpacks of Sierra Nevada. Ann Glaciol 6:272–273. https://doi.org/10.3189/1985AoG6-1-272-273
Kattelmann R, Dozier J (1999) Observations of snowpack ripening in the Sierra Nevada, California, USA. J Glaciol 45(151):409–416
Kinar NJ, Pomeroy JW (2015) Measurement of the physical properties of the snowpack. Rev Geophys 53(2):481–544
King J, Pomeroy J, Gray DM, Fierz C, Föhn P, Harding R, Jordan R, Martin E, Plüss C (2008) Snow-atmosphere energy and mass balance. Chapter 3 in: Armstrong R, Brun E (eds) Snow and climate: physical processes, surface energy exchange and modeling. Cambridge University Press, pp 70–124
Kononova NK (2012) The influence of atmospheric circulation on the formation of snow cover on the north eastern Siberia. Ice Snow 1(117):38–53 (in Russian with English summary)
Krogh SA, Pomeroy JW, Marsh P (2017) Diagnosis of the hydrology of a small arctic basin at the tundra-taiga transition using a physically based hydrological model. J Hydrol 550:685–703
Krogh SA, Pomeroy JW (2019) Impact of future climate and vegetation on the hydrology of an arctic headwater basin at the tundra-taiga transition. J Hydrometeorol 20(2):197–215
Langen PL, Brown R, Grenier P, Barrette C, Chaumont D, Derksen C, Hamilton J, Ingeman-Nielsen T, Howell S, James T, Lavoie D, Marchenko S, Olsen SM, Rodehacke CB, Sharp M, Smith SL, Stendel M, Tonboe RT (2018) In adaptation actions for a changing arctic: perspectives from the baffin bay/davis strait region. Arctic Monitoring and Assessment Programme (AMAP), pp 39–76
Langlois A, Johnson CA, Montpetit B, Royer A, Blukacz-Richards EA, Neave E, Dolant C, Roy A, Arhonditsis G, Kim DK, Kaluskar S (2017) Detection of rain-on-snow (ROS) events and ice layer formation using passive microwave radiometry: a context for Peary caribou habitat in the Canadian Arctic. Remote Sens Environ 189:84–95
Leroux NR (2018) Mass and heat flow through snowpacks. PhD Thesis, University of Saskatchewan, Saskatoon, Canada. 162 pp
Leroux NR, Pomeroy JW (2019) Simulation of capillary pressure overshoot in snow combining trapping of the wetting phase with a nonequilibrium Richards Equation model. Water Resour Res 55(1):236–248. https://doi.org/10.1029/2018WR022969

Lesack LF, Marsh P, Hicks FE, Forbes DL (2013) Timing, duration, and magnitude of peak annual water-levels during ice breakup in the Mackenzie Delta and the role of river discharge. Water Resour Res 49(12):8234–8249
Lesack LFW, Marsh P, Hicks FE, Forbes DL (2014) Local spring warming drives earlier river-ice breakup in a large Arctic delta. Geophys Res Lett 41(5):1560–1567
Liang S, Wang K, Zhang X, Wild M (2010) Review on estimation of land surface radiation and energy budgets from ground measurement, remote sensing and model simulations. IEEE J Sel Top Appl Earth Obs Remote Sens 3(3):225–240
Liston GE (2004) Representing subgrid snow cover heterogeneities in regional and global models. J Clim 17:1381–1397
Liston GE, Elder K (2006) A distributed snow-evolution modeling system (SnowModel). J Hydrometeorol 7(6):1259–1276
Liston GE, Hiemstra CA (2011) The changing cryosphere: Pan-Arctic snow trends (1979–2009). J Clim 24(21):5691–5712
Mann P (2018) Spatial and temporal variability of the snow environment in the Western Canadian Arctic. MSc Thesis, Wilfrid Laurier University, Waterloo, Canada. 83 pp
Marsh P (1987) Grain growth in a wet arctic snow cover. Cold Reg Sci Technol 14(1):23–31
Marsh P, Woo MK (1981) Snowmelt, glacier melt, and high arctic streamflow regimes. Can J Earth Sci 18(8):1380–1384. https://doi.org/10.1139/e81-127
Marsh P, Woo MK (1984a) Wetting front advance and freezing of meltwater within a snow cover. Observations in the Canadian Arctic. Water Resour Res 16:1853–1864
Marsh P, Woo MK (1984b) Wetting front advance and freezing of meltwater within a snow cover. 2 A simulation model. Water Resour Res 16:1865–1874
Marsh P, Woo MK (1985) Meltwater movement in natural heterogeneous snow covers. Water Resour Res 21(11):1710–1716
Marsh P, Woo M (1987) Soil heat flux, wetting front advance and ice layer growth in cold, dry snow covers. Proceedings, snow property measurements workshop, pp 497–524
Marsh P, Woo MK (1993) Infiltration of meltwater into frozen soils in a continuous permafrost environment. In Proceedings of the sixth international conference on permafrost, vol 1. Beijing: South China University of Technology Press, pp 443–448
Marsh P, Pomeroy JW (1996) Meltwater fluxes at an arctic forest-tundra site. Hydrol Process 10 (10):1383–1400
Marsh P, Pomeroy JW (1999) Spatial and temporal variations in snowmelt runoff chemistry, Northwest Territories Canada. Water Resour Res 35(5):1559–1567
Marsh, P., 2005. Water flow through snow and firn. In *Encyclopedia of Hydrological Sciences* (Vol. 4, Part 14, pp. 97–123). Chichester, England: John Wiley & Sons, Ltd
Marsh P, Bartlett P, MacKay M, Pohl S, Lantz T (2010) Snowmelt energetics at a shrub tundra site in the western Canadian Arctic. Hydrol Process 24(25):3603–3620
McClung D, Schaerer PA (2006) The avalanche handbook. The Mountaineers Books, Seattle, Washington
Michele CD, Avanzi F, Passoni D, Barzaghi R, Pinto L, Dosso P, Ghezzi A, Gianatti R, Vedova GD (2016) Using a fixed-wing UAS to map snow depth distribution: an evaluation at peak accumulation. The Cryosphere 10(2):511–522
Mohammed AA, Kurylyk BL, Cey EE, Hayashi M (2018) Snowmelt infiltration and macropore flow in frozen soils: overview, knowledge gaps, and a conceptual framework. Vadose Zone J 17(1):1–15
Mortimer C, Mudryk L, Derksen C, Luojus K, Brown R, Kelly R, Tedesco M (2020) Evaluation of long-term Northern Hemisphere snow water equivalent products. The Cryosphere 14:1579–1594. https://doi.org/10.5194/tc-14-1579-2020
Mudryk LR, Derksen C, Kushner PJ, Brown R (2015) Characterization of Northern Hemisphere snow water equivalent datasets, 1981–2010. J Clim 28(20):8037–8051

Mudryk LR, Derksen C, Howell S, Laliberté F, Thackeray C, Sospedra-Alfonso R, Vionnet V, Kushner PJ, Brown R (2018) Canadian snow and sea ice: historical trends and projections. The Cryosphere 12(4):1157–1176

Mudryk L, Brown R, Derksen C, Luojus K, Decharme B, Helfrich S (2019) Terrestrial snow cover. NOAA Arctic Report Card 2019. https://arctic.noaa.gov/Report-Card/Report-Card-2019

Musselman KN, Clark MP, Liu C, Ikeda K, Rasmussen R (2017) Slower snowmelt in a warmer world. Nat Clim Change 7(3):214

Myers-Smith IH, Forbes BC, Wilmking M, Hallinger M, Lantz T, Blok D, Tape KD, Macias-Fauria M, Sass-Klaassen U, Lévesque E, Boudreau S, Ropars P, Hermanutz L, Trant A, Collier LS, Weijers S, Rozema J, Rayback SA, Schmidt NM, Schaepman-Strub G, Wipf S, Rixen C, Ménard CB, Venn S, Goetz S, Andreu-Hayles L, Elmendorf S, Ravolainen V, Welker J, Grogan P, Epstein HE, Hik DS (2011) Shrub expansion in tundra ecosystems: dynamics, impacts, and research priorities. Environ Res Lett 6:045509

Myers-Smith IH, Elmendorf SC, Beck PSA, Wilmking M, Hallinge M, Blok D, Tape KD, Rayback SA, Macias-Fauria M, Forbes BC, Speed JDM, Boulanger-Lapointe N, Rixen C, Lévesque E, Schmidt NM, Baittinger C, Trant AJ, Hermanutz L, Collier LS, Dawes MA, Lantz TC, Weijers S, Jørgensen RH, Buchwal A, Buras A, Naito AT, Ravolainen V, Schaepman-Strub G, Wheeler JA, Wipf S, Guay KC, Hik DS, Vellend M (2015) Climate sensitivity of shrub growth across the tundra biome. Nat Clim Change 5:887–891

Neumann N, Marsh P (1998) Local advection of sensible heat in the snowmelt landscape of Arctic tundra. Hydrol Process 1560:1547–1560

Park H, Sherstiukov AB, Fedorov AN, Polyakov IV, Walsh JE (2014) An observation-based assessment of the influences of air temperature and snow depth on soil temperature in Russia. Environ Res Lett 9(6):064026

Park H, Fedorov AN, Zheleznyak MN, Konstantinov PY, Walsh JE (2015) Effect of snow cover on pan-Arctic permafrost thermal regimes. Clim Dyn 44(9–10):2873–2895

Pedersen SH, Liston GE, Tamstorf MP, Westergaard-Nielsen A, Schmidt NM (2015) Quantifying episodic snowmelt events in arctic ecosystems. Ecosystems 18(5):839–856

Phoenix GK, Bjerke JW (2016) Arctic browning: extreme events and trends reversing arctic greening. Glob Change Biol 22(9):2960–2962

Pielmeier C, Schneebeli M (2003) Developments in the stratigraphy of snow. Surv Geophys 24(5–6):389–416

Pohl S, Marsh P (2006) Modelling the spatial–temporal variability of spring snowmelt in an arctic catchment. Hydrol Process 20(8):1773–1792

Pohl S, Marsh P, Liston GE (2006) Spatial-temporal variability in turbulent fluxes during spring snowmelt. Arct Antarct Alp Res 38(1):136–146

Pomeroy JW, Gray DM (1990) Saltation of snow. Water Resour Res 26(7):1583–1594

Pomeroy JW, Gray DM (1992) Steady-state suspension of snow. J Hydrol 136(1–4):275–301

Pomeroy JW, Marsh P, Gray DM (1997) Application of a distributed blowing snow model to the Arctic. Hydrol Process 11(11):1451–1464

Pomeroy JW, Gray DM, Shook KR, Toth B, Essery RLH, Pietroniro A, Hedstrom N (1998) An evaluation of snow accumulation and ablation processes for land surface modelling. Hydrol Process 12(15):2339–2367

Pomeroy JW, Brun E (2001) Physical properties of snow. In: Jones HG, Pomeroy WJ, Walker DA, Hoham RW (eds) Snow ecology: an interdisciplinary examination of snow-covered ecosystems. Cambridge University Press, Cambridge, UK, pp 45–118

Pomeroy JW, Jones HG, Tranter M, Lilbæk G (2006) Hydrochemical processes in snow-covered basins. Encyclopedia of hydrological sciences

Pomeroy JW, Harding RJ (2008) Boreal forest. Section 3.5.5. In: Armstrong R, Brun E (eds) Snow and climate: physical processes, surface energy exchange and modeling. Cambridge University Press, pp 109–115

Quinton WL, Marsh P (1999) A conceptual framework for runoff generation in a permafrost environment. Hydrol Process 13(16):2563–2581

Quinton WL, Carey SK, Goeller NT (2004) Snowmelt runoff from northern alpine tundra hillslopes: major processes and methods of simulation. Hydrol Earth Syst Sci 8(5):877–890
Raddatz RL, Asplin MG, Papakyriakou T, Candlish LM, Galley RJ, Else B, Barber DG (2013) All-Sky Downwelling Longwave Radiation and Atmospheric-Column Water Vapour and Temperature over the Western Maritime Arctic. Atmos Ocean 51(2):145–152
Räisänen J (2008) Warmer climate: less or more snow? Clim Dyn 30(2–3):307–319
Rapaic M, Brown R, Markovic M, Chaumont D (2015) An evaluation of temperature and precipitation surface-based and reanalysis datasets for the Canadian Arctic, 1950–2010. Atmos Ocean 53(3):283–303. https://doi.org/10.1080/07055900.2015.1045825
Rawlins MA, Steele M, Holland MM, Adam JC, Cherry JE, Francis JA, Ya Groisman P et al (2010) Analysis of the Arctic system for freshwater cycle intensification: observations and expectations. J Clim 23(21):5715–5737. https://doi.org/10.1175/2010JCLI3421.1
Rees A, English M, Derksen C, Toose P, Silis A (2014) Observations of late winter Canadian tundra snow cover properties. Hydrol Process 28(12):3962–3977
Riggs GA, Hall DK, Román MO (2017) Overview of NASA's MODIS and visible infrared imaging radiometer suite (VIIRS) snow-cover earth system data records. Earth Sys Sci Data 9 (2):765–777
Rowlands DD, Luthcke SB, Klosko SM, Lemoine FG, Chinn DS, McCarthy JJ, Cox CM, Anderson OB (2005) Resolving mass flux at high spatial and temporal resolution using GRACE intersatellite measurements. Geophys Res Lett 32(4)
Sannel ABK, Hugelius G, Jansson P, Kuhry P (2015) Permafrost Warming in a Subarctic Peatland – Which Meteorological Controls are Most Important? Permafrost Periglac Process. https://doi.org/10.1002/ppp.1862
Schneebeli M (1995) Development and stability of preferential flow paths in a layered snowpack. IAHS Publ-Ser Proc Rep-Int Assoc Hydrol Sci 228:89–96
Seligman, G., 1936. Snow structure and ski fields: being an account of snow and ice forms met with in nature, and a study on avalanches and snowcraft. Macmillan and Company, limited
Serreze MC, Walsh JE, Chapin EC, Osterkamp T, Dyugerov M, Romanovsky V, Oechel WC, Morison J, Zhang T, Barry RG (2000) Observational evidence of recent change in the northern high latitude environment. Clim Change 46:159–207
Shi HX, Wang CH (2015) Projected 21st century changes in snow water equivalent over Northern Hemisphere landmasses from the CMIP5 model ensemble. The Cryosphere 9(5):1943–1953
Shook K, Gray DM, Pomeroy JW (1993) Temporal variation in snowcover area during melt in prairie and alpine environments. Hydrol Res 24(2–3):183–198
Shook K, Gray DM (1997) Synthesizing shallow seasonal snow covers. Water Resour Res 33 (3):419–426
Sicart JE, Pomeroy JW, Essery RLH, Bewley D (2006) Incoming longwave radiation to melting snow: observations, sensitivity and estimation in northern environments. Hydrol Process 20 (17):3697–3708
Slater AG, Lawrence DM, Koven CD (2017) Process-level model evaluation: a snow and heat transfer metric. The Cryosphere 11:989–996. https://doi.org/10.5194/tc-11-989-2017
Smith CD, Kontu A, Laffin R, Pomeroy JW (2017) An assessment of two automated snow water equivalent instruments during the WMO Solid Precipitation Intercomparison Experiment. The Cryosphere 11(1):101–116
Smith C, Fierz C (2019) Measurement of snow. In: Preliminary 2018 edition of the CIMO Guide (WMO-No.8). https://www.wmo.int/pages/prog/www/IMOP/publications/CIMO-Guide/Prelim_2018_ed/Preliminary-2018-edition.html (Chapter link provided in table under MEASUREMENT OF CRYOSPHERIC VARIABLES)
Spence CH, Kokelj SV, Ehsanzadeh EG (2011) Precipitation trends contribute to streamflow regime shifts in northern Canada. In: Yang D, Marsh P, Gelfan A (eds) Cold regions hydrology in a changing climate. IAHS Publication, Int Assoc Hydrological Sciences, Wallingford, pp 3–8

Spence C, Kokelj SV, Kokelj SA, McCluskie M, Hedstrom N (2015) 2015: Evidence of a change in water chemistry in Canada's subarctic associated with enhanced winter streamflow. J Geophys Res-Biogeosci 120:113–127
Strasser U, Bernhardt M, Weber M, Liston GE, Mauser W (2008) Is snow sublimation important in the alpine water balance? The Cryosphere 2:53–66
Sturm M, Holmgren J, Liston GE (1995) A seasonal snow cover classification system for local to global applications. J Clim 8(5):1261–1283
Sturm M, Liston GE, Benson CS, Holmgren J (2001) Characteristics and growth of a snowdrift in Arctic Alaska, USA. Arct, Antarct Alp Res 33(3):319–329
Sturm M, Taras B, Liston GE, Derksen C, Jonas T, Lea J (2010) Estimating snow water equivalent using snow depth data and climate classes. J Hydrometeorol 11(6):1380–1394
Sturm M, Stuefer S (2013) Wind-blown flux rates derived from drifts at arctic snow fences. J Glaciol 59(213):21–34
Syed TH, Famiglietti JS, Zlotnicki V, Rodell M (2007) Contemporary estimates of Pan-Arctic freshwater discharge from GRACE and reanalysis. Geophys Res Lett 34:L19404. https://doi.org/10.1029/2007GL031254
Takala M, Luojus K, Pulliainen J, Derksen C, Lemmetyinen J, Kärnä JP, Koskinen J, Bojkov B (2011) Estimating northern hemisphere snow water equivalent for climate research through assimilation of space-borne radiometer data and ground-based measurements. Remote Sens Environ 115(12):3517–3529
Tan A, Adam JC, Lettenmaier DP (2011) Change in spring snowmelt timing in Eurasian Arctic rivers. J Geophys Res: Atmos 116:D03101. https://doi.org/10.1029/2010JD014337
Thackeray CW, Qu X, Hall A (2018) Why do models produce spread in snow albedo feedback? Geophys Res Lett 45:6223–6231. https://doi.org/10.1029/2018GL078493
US Army Corps of Engineers (1956). Snow hydrology: summary report of the snow investigations. Portland Oregon, 437 p
Vihma T, Screen J, Tjernström M, Newton B, Zhang X, Popova V, Deser C, Holland M, Prowse T (2016) The atmospheric role in the Arctic water cycle: A review on processes, past and future changes, and their impacts. J Geophys Res Biogeosci 121:586–620. https://doi.org/10.1002/2015JG003132
Vincent LA, Zhang X, Brown RD, Feng Y, Mekis E, Milewska EJ, Wan H, Wang XL (2015) Observed trends in Canada's climate and influence of low-frequency variability modes. J Clim 28:4545–4560. https://doi.org/10.1175/JCLI-D-14-00697.1
Vionnet V, Brun E, Morin S, Boone A, Faroux S, Le Moigne P et al (2012) The detailed snowpack scheme Crocus and its implementation in SURFEX v7.2. Geosci Model Dev 5:773–791. https://doi.org/10.5194/gmd-5-773-2012
Waldner PA, Schneebeli M, Schultze-Zimmermann U, Flühler H (2004) Effect of snow structure on water flow and solute transport. Hydrol Process 18(7):1271–1290
Wang L, Toose P, Brown R, Derksen C (2016) Frequency and distribution of winter melt events from passive microwave satellite data in the pan-Arctic, 1988–2013. The Cryosphere 10 (6):2589
Wever N, Würzer S, Fierz C, Lehning M (2016) Simulating ice layer formation under the presence of preferential flow in layered snowpacks. The Cryosphere 10(6):2731–2744
Woo MK, Sauriol J (1981) Effects of snow jams on fluvial activities in the High Arctic. Phys Geogr 2(1):83–98
Woo MK, Heron R, Marsh P (1982) Basal ice in high arctic snowpacks. Arct Alp Res 14(3):251–260
Woo M-K, Young KL (2014) Disappearing semi-permanent snow in the High Arctic and its consequences. J Glaciol 60:192–200
Woo MK, Marsh P (2017) Snow distribution and snowpack characteristics. Chapter 40, Singh VP (ed) Handbook of applied hydrology, Second Edition Hardcover. McGraw Hill

Yang D, Robinson D, Zhao Y, Estilow T, Ye B (2003) Streamflow response to seasonal snow cover extent changes in large Siberian watersheds. J Geophys Res 108(D18):4578. https://doi.org/10.1029/2002JD003149

Yang D, Zhao Y, Armstrong R, Robinson D, Brodzik M-J (2007) Streamflow response to seasonal snow cover mass changes over large Siberian watersheds. J Geophys Res 112:F02S22 https://doi.org/10.1029/2006jf000518

Ye H, Cohen J (2013) A shorter snowfall season associated with higher air temperatures over northern Eurasia. Environ Res Lett 8(2013)014052:7 pp https://doi.org/10.1088/1748-9326/8/1/014052

Ye H, Yang D, Robinson D (2008) Winter rain on snow and its association with air temperature over northern Eurasia. Hydrol Process 22:2728–2736. https://doi.org/10.1002/hyp.7094

Zhao L, Gray DM (1999) Estimating snowmelt infiltration into frozen soils. Hydrol Process 13 (12–13):1827–1842

Mr. Ross Brown is a recently retired climate scientist from the Climate Research Division of Environment and Climate Change Canada (ECCC), with more than 30 years of experience investigating variability and change in snow cover, and over 70 publications as lead or co-author in refereed journals and proceedings. He was the lead author of the Arctic terrestrial snow cover chapter in the Arctic Council's Snow, Water, Ice and Permafrost in the Arctic (SWIPA) 2017 assessment report, and a contributing author for several Intergovernmental Panel on Climate Change (IPCC) Assessment Reports between 1995 and 2013. He graduated from McGill University in 1980 with an M. Sc. in Physical Geography with specialization in climatology. He is currently working part-time for ECCC until December 2020, and is located at the Ouranos Climate Change Consortium in Montreal where he has collaborated in Ouranos projects since 2005, most notably the ArcticNet Integrated Regional Impact Studies for the Canadian Arctic.

Dr. Philip Marsh is a Professor and Canada Research Chair in Cold Regions Water Science. He is located in the Department of Geography and Environmental Studies, and the Cold Regions Research Centre, at Wilfrid Laurier University in Waterloo, Ontario, Canada. He has carried out Arctic research for 45 years. Although much of his research has focussed on snow hydrology, his research has addressed a wide range of Arctic hydrological processes and issues. During this period, his research program has integrated field observations, remote sensing, and physics-based modeling. His research has focussed on improving our understanding of Arctic hydrology, and applying it to understanding climate change and the impacts of developments such as hydroelectric, road, and hydrocarbon development. He is an Editor for The Cryosphere and a Canadian Delegate to the International Arctic Science Committee. He received his B.A. in Geography from York University, and M.Sc. and Ph.D. in Geography from McMaster University.

Dr. Stephen Déry is Professor in the Environmental Science and Engineering undergraduate program and the Natural Resources and Environmental Studies graduate program at the University of Northern British Columbia (UNBC), Prince George, BC. He also holds the NSERC/Rio Tinto Senior Industrial Research Chair in Climate Change and Water Security with a 5-year program of research focused on the Nechako Watershed. His background is in atmospheric science, hydrometeorology, and applied mathematics, and he has degrees from York University (B.Sc. and M.Sc.) and McGill University (Ph.D.). He has completed postdoctoral positions at the Lamont-Doherty Earth Observatory of Columbia University, New York and held a Visiting Research Scientist position at Princeton University in New Jersey. He investigates the consequences of climate change and water management on the water cycle of northern and alpine regions. A major aspect of this research is to better monitor, understand, and project the water balance and streamflow trends in major watersheds such as the Fraser based on observational data and numerical simulations.

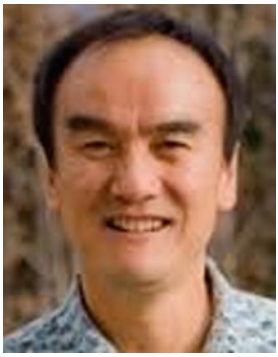

Dr. Daqing Yang is a Research Scientist at the Watershed Hydrology and Ecology Research Division, Environment and Climate Change Canada. He is also Affiliate Research Professor at the International Arctic Research Center, Univ. of Alaska Fairbanks. Over the past 25 years, he has conducted cryosphere system research in China, Canada, Japan, USA, and Norway. His primary research activities/interests include cold region hydrology and climate, particularly Arctic large river streamflow regime and change, snow cover and snowfall measurements, climate change and human impact to regional hydrology, and applications of remote sensing in cold regions. He has served as journal editor and subject editor for IAHS publications (cold region hydrology, northern research basin water balance, and cold/mountain region hydrological systems under climate change), and WMO technical reports (solid precipitation measurement intercomparison and integrated global observing strategy cryosphere theme). He also contributed as review and/or author to the IPCC Reports, and the Arctic Council's Snow, Water, Ice and Permafrost in the Arctic (SWIPA 2017 and follow up) assessment. His current research focuses on investigating the impacts of climate variability/change and human activities on hydrologic system across the broader northern regions.

Evaporation Processes and Changes Over the Northern Regions

4

Yinsheng Zhang, Ning Ma, Hotaek Park, John E. Walsh, and Ke Zhang

Abstract

Evapotranspiration (ET) is a key component in global water and energy cycles. This chapter presents and discusses recent research advances about ET over northern regions and watersheds. ET in northern regions tends to increase with the decrease of latitude. The largest ET typically appears in the forest ecosystem, while the grasslands and shrublands have small ET. While the seasonal variations in ET are usually high, the interannual variability in annual ET is usually low over the Arctic regions. Sublimation from snow cover accounts for about 15–25% of winter precipitation. Many factors, such as soil moisture, vegetation type and productivity, and ecosystem features affect ET over northern regions. In addition, precipitation plays a key role in impacting ET. ET is more sensitive to precipitation in the early growing season than in the late growing season. Furthermore, changes in freeze–thaw processes due to warming also affect land surface conditions and the ET processes. During 1983–2005, ET

Y. Zhang (✉) · N. Ma
Institute of Tibetan Plateau Research, Chinese Academy of Sciences, Beijing, China
e-mail: yinshengzhang@icloud.com; yszhang@itpcas.ac.cn

N. Ma
e-mail: ningma@itpcas.ac.cn

H. Park
Japan Agency for Marine-Earth Science and Technology (JAMSTEC), Yokohama, Japan
e-mail: park@jamstec.go.jp

J. E. Walsh
International Arctic Research Center, University of Alaska, Fairbanks, AK, USA
e-mail: jewalsh@alaska.edu

K. Zhang
College of Hydrology and Water Resources, Hohai University, Nanjing, China
e-mail: kzhang@hhu.edu.cn

D. Yang and D. L. Kane (eds.), *Arctic Hydrology, Permafrost and Ecosystems*,
https://doi.org/10.1007/978-3-030-50930-9_4

increased significantly in the Arctic region with a rate of 3.8 mm decade-1 because of regional warming and vegetation greening. Such an increase in ET may exert significant impacts on the regional hydrology and water resources. Advanced models can simulate past ET change over the large northern watersheds. Remote sensing has provided new ET data and information that support climate and hydrology research and applications. There is a key question: Will Arctic landscapes become wetter or drier as climate changes? According to global models and data analyses, annual ET has increased over the northern regions. In the future, summer PE is projected to decrease much of Canada, increase over Alaska, decrease over the western and northern Eurasian subarctic, and increase over parts of northeastern Russia. Over most of these areas, the sign of the projected change is not robust across the models at the 95% confidence level. Many factors contribute to the uncertainty in the projected changes in Arctic surface wetness. There is certainly a need to better quantify and narrow the uncertainties in global models in the northern regions.

4.1 Introduction

Evapotranspiration (ET) refers to the amount of water vapor evaporated from the unit area of the land surface during a unit of time and consists of evaporation from canopy-intercepted water, evaporation from soil (E), and transpiration from plants (T). ET is a key component in global water and energy cycles. On average, more than 60% of global land precipitation is returned to the atmosphere through terrestrial ET (Oki and Kanae 2006). ET as latent heat flux consumes roughly 50% of the solar radiation absorbed by the Earth's surface (Trenberth et al. 2009). ET affects climate through a wide range of feedbacks to air temperature, humidity, and precipitation (Shen et al. 2015; Shukla and Mintz 1982; Zeng et al. 2017). Accurate estimation of ET is therefore fundamental to not only elucidating how the hydrological cycle responds to climate change but also to regional drought monitoring and water resources management (Fisher et al. 2017; Ma et al. 2019). However, investigating ET is challenging because of its complex interactions across the soil–vegetation–atmosphere interface (Katul et al. 2012; Matheny et al. 2014; Zhang et al. 2014). Historically, ET was related (via linear or nonlinear scaling with soil moisture) to direct measurements of its conceived maximum value, i.e., pan evaporation (Brutsaert 2013). However, neither water-limited nor energy-limited land surface ET acts as pan evaporation (Brutsaert 1982). With recent advances in instrumentations and data storage, a better understanding of ET from various land covers has been reported through the use of in situ flux observations (e.g., Baldocchi et al. 2004; Fischer et al. 2013; Ma et al. 2014; Mackay et al. 2007; Wilson and Baldocchi 2000). These studies have significantly contributed to our knowledge of regional hydrological regimes and their complex feedback mechanisms between land and atmosphere (Baldocchi 2014).

Because transpiration from plants (T) links the water and carbon cycles, it is used to calculate carbon assimilation by terrestrial vegetation, so estimating T fluxes is a major focus in climate and ecology studies (Evaristo et al. 2015; Jasechko et al. 2013; Kool et al. 2014; Wei et al. 2017). As T process directly correlates with plant growth and the carbon cycle (Scott et al. 2006), quantitative estimation of T in the total evapotranspiration (T/ET) has long been acknowledged to play a crucial role in water resource management, yield estimation, water cycle, and climate change, from plot scale to global scale (Schlesinger and Jasechko 2014; Scott and Biederman 2017; Xiao et al. 2018). There is, however, a considerable discrepancy among global T/ET estimations by different methods. For example, the results of a combination of wide ranging, remotely sensed observations showed that approximately 80% of the annual land ET is attributed to T (Miralles et al. 2011). Wei et al. (2017) quantified the global T/ET with a leaf area index (LAI)-based ET partitioning algorithm and concluded that T accounts for 57% of ET. The distinct isotope effects of T and E based on the isotopic analysis of a global dataset of large lakes and rivers showed that T represents 80–90% of terrestrial ET (Jasechko et al. 2013), although this estimate was challenged by Coendersgerrits et al. (2014). The results of isotope mass budget-based simulations suggested that the transpired fraction of ET accounts for approximately 60% of the annual land ET (Good et al. 2015). There are also great challenges in the state-of-the-art land surface models and remote sensing models in representing the ratio of T to ET. Maxwell and Condon (2016) argued that partitioning ET is connected to water table depth and they found that including lateral groundwater flow in the model increases transpiration partitioning from 47 ± 13 to 62 ± 12%. This aspect was recently also acknowledged in Chang et al. (2018), in which terrain-driven lateral water flows spread out soil moisture to a wider range along hill slopes with an optimum subrange from the middle to upper slopes, where soil evaporation was more suppressed by the drier surface than T due to plant uptake of deep soil water, thereby enhancing T/ET. In terms of remote sensing models, large errors in representing the components of ET also exist in Moderate Resolution Imaging Spectroradiometer (PM-MODIS), the Priestley–Taylor Jet Propulsion Laboratory model (PT-JPL), and the Global Land Evaporation Amsterdam Model (GLEAM), which shows root-mean-square-error of 90–114% for soil evaporation and 54–114% for transpiration (Talsma et al. 2018).

This chapter reviews recent research and results of ET from various land surfaces (including different vegetation types) and also across large regions and watersheds. Specifically, it discusses ET process, pattern, and variabilities over space and time, such as regional/basin ET, its change, and impact to water balance. It also demonstrates model estimates/simulation of large-scale ET over the arctic domain and selected watersheds, highlights remote sensing development in ET estimation, and global model analysis of the net moisture flux (P-E) and its change across the northern regions.

4.2 ET Distribution and Variability

Atmospheric conditions, such as wind speed and saturation deficit, are dominant factors in determining ET variability. Zhang et al. (2003) summarized that daily mean evaporation over the Tibetan Plateau varied within the range of 0.3–3.5 mm on the permafrost surface, and regional differences in evaporation were strongly related to surface soil moisture. Locally, topography and its influence on surface soil moisture was found to control evaporation systematically. The seasonality of evaporation in permafrost regions is dominated by freeze–thaw cycles at the surface; evaporation from the melting permafrost surface is up to 4–7 times greater than that from the frozen ground. In forested terrain, the interception of precipitation can reduce daily evaporation by 60–70%. Sublimation from the snow surface observed at Tianshan Mountains and eastern Tibetan Plateau was in the range of 0.2–1.0 mm d^{-1}. Mu et al. (2009) investigated the spatial pattern of evapotranspiration for the pan-Arctic domain and found large annual ET variability during 2000–2006 among the regional biomes. The largest annual ET rates occur over forests, while the lowest rates occur over grasslands and scrublands; annual ET rates for savanna and cropland areas are generally intermediate. Ecosystem processes in high-latitude boreal and tundra biomes are strongly constrained by low solar irradiance and freezing temperatures for much of the year, so that seasonal patterns in plant photosynthesis (GPP) and ET correspond closely and are generally confined to a relatively narrow growing season. The interannual variability in estimated annual ET is relatively low although the seasonal variation is high over the Arctic, which reflects the dominance of cold temperature constraints on boreal Arctic ecosystem processes (Fig. 4.1).

Variation in evapotranspiration is influenced by all ecosystem parameters and processes, such as soil moisture content, vegetation productivity, and ecosystem nutrient and water budgets. The partitioning of available energy into evapotranspiration (latent heat flux) and sensible heat flux at a vegetation surface also affects aspects of weather and climate. As ET consists of soil evaporation, and transpiration from plants, the soil moisture, and biological feature are key factors to determine ET variation. Zhang et al (2005) demonstrated that E is more sensitive to surface soil moisture than T. The former takes water from a very thin soil layer and moves it to the atmosphere; the latter transfers water from the soil through root–stalk–leaf mechanisms and may take water from a thicker soil layer. Therefore, T is anticipated to be more independent of soil moisture variations than E. Figure 4.2 shows the relationship between E/Ep (Ep is potential evaporation) and the surface soil moisture. E/Ep increased almost linearly with ground surface moisture when the volumetric water content was less than 30% but varied little when moisture content beyond that level. This suggests that soil evaporation was constrained by the deficiency of available water when soil moisture was less than the critical value of 30%, illustrating the primary controls of soil water status on the soil evaporation.

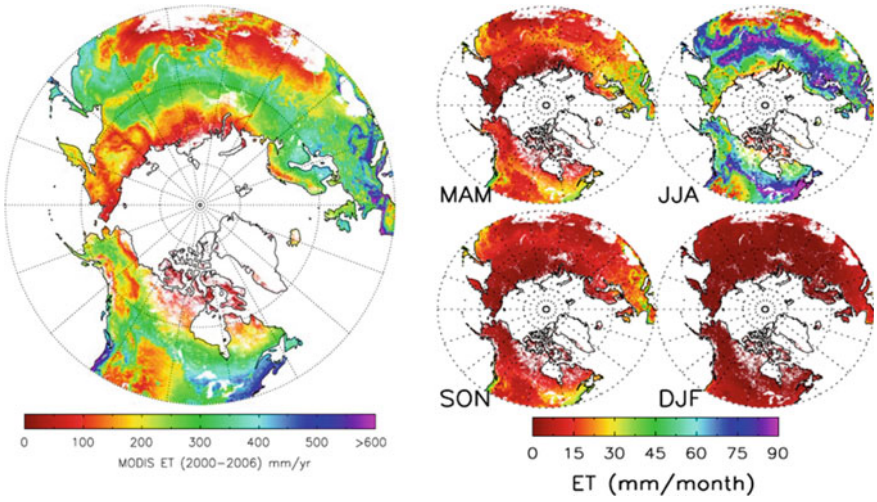

Fig. 4.1 Spatial pattern of mean annual and seasonal ET during 2000–2006 for the pan-Arctic domain (Mu et al. 2009)

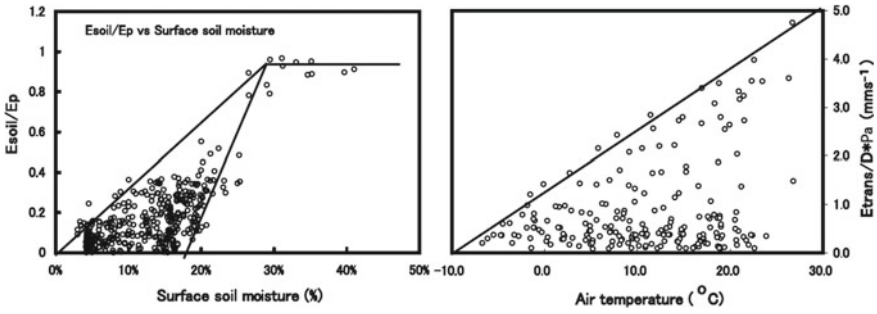

Fig. 4.2 Relationships between (left) E/Ep and surface moisture and (right) leaf conductance (Etrans/D * Pa, mms-2) and air temperature. D, leaf-to-air specific deficit; Pa, air density (After Zhang et al. (2005) for sparse grassland in northeastern Mongolia)

Transpiration rates are determined by two parameters: leaf conductance and leaf-to-air specific deficit (D). While it is impossible to present leaf conductance because of no CO_2 concentration data were collected, the right panel of Fig. 4.2 shows the ratio of Etrans/D * Pa (D is the leaf-to-air specific deficit and Pa is air density), which implies a leaf conductance value, plotted against air temperature. The plots show that transpiration increased as temperatures increased. When temperatures became warm, higher leaf conductance allowed water uptake if soil moisture was low but higher than wilting point (2.8–4.1% in the root zone). Lower temperatures, lower D, and higher humidity accompany precipitation events, so

plant transpiration decreased as soil evaporation approached to potential evapotranspiration (Fig. 4.2).

Projected increases in air temperature and precipitation due to climate change in Arctic wetlands could dramatically affect ecosystem function. As a consequence, it is important to define controls on evapotranspiration, i.e., the major pathway of water loss from the system. Liljedahl et al. (2011) quantified the multi-year controls on midday Arctic coastal wetland evapotranspiration, measured with the eddy covariance method at two vegetated, drained thaw lake basins near Barrow, Alaska. Variations in near-surface soil moisture and atmospheric vapor pressure deficits were found to have nonlinear effects on midday evapotranspiration rates. Data collections near Barrow over 3 years showed that vapor pressure deficits (VPD) near 0.3 kPa appeared to be an important hydrological threshold, allowing latent heat flux to persistently exceed sensible heat flux (Fig. 4.3). Dry (compared to wet) soils increased bulk surface resistance (water-limited). Wet soils favored ground heat flux and therefore limited the energy available to sensible and latent heat flux (energy-limited). Thus, midday evapotranspiration was suppressed from both dry and wet soils but through different mechanisms. They also found that wet soils (ponding excluded) combined with large VPD, resulted in an increased bulk surface resistance and therefore suppressing evapotranspiration below its potential rate (Priestley-Taylor coefficient < 1.26). This was likely caused by the limited ability of mosses to transfer moisture during large atmospheric demands. Ultimately, in addition to net radiation, the various controlling factors on midday evapotranspiration (i.e., near-surface soil moisture, atmospheric vapor pressure, and the limited ability of saturated mosses to transfer water during high VPD) resulted in an average evapotranspiration rate of up to 75% of the potential evapotranspiration rate. These multiple limitations on midday evapotranspiration rates have the potential to moderate interannual variation of total evapotranspiration and reduce excessive water loss in a warmer climate. Combined with the prevailing maritime winds and projected increases in precipitation, these curbing mechanisms will likely prevent extensive future soil drying and hence maintain the presence of coastal wetlands.

Evapotranspiration dominates hydrological processes on the Arctic Coastal Plain for a couple of months after snowmelt until soil moisture declines (Kane et al. 2000, 2008). The majority of studies on ET in the Arctic tundra focus on whole-ecosystem fluxes, with rates of approximately 1–3 mm day^{-1} (Liljedahl et al. 2011; Mendez et al. 1998). However, a whole-ecosystem approach to determining ET rates does not allow for quantifying the variability in fluxes associated with the heterogeneous landscape (Oren et al. 2006), particularly on the Arctic Coastal Plain (Oechel et al. 1998). Further, a whole-ecosystem approach does not allow for partitioning ET into its components of evaporation and transpiration. Spatial heterogeneity in soil moisture, soil temperature, and plant composition likely affect how ET is partitioned into evaporation and transpiration in the Arctic Coastal Plain (Oberbauer and Dawson 1992). It is critical to understand the partitioning of evapotranspiration because environmental processes control evaporation and transpiration differently (Jasechko et al. 2013). While both respond to surface energy, atmospheric demand, and soil water availability (Betts et al. 1999;

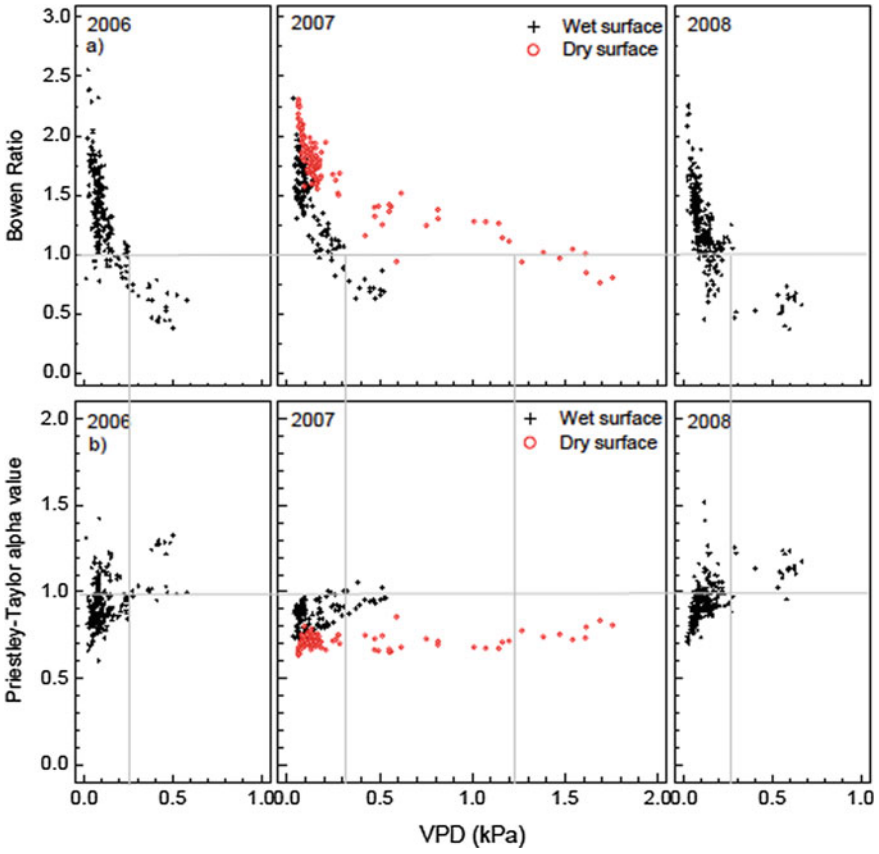

Fig. 4.3 The relationship between mean hourly air vapor pressure deficit (VPD) and **a** Bowen ratio (β) or **b** Priestley–Taylor α during differing soil moisture conditions at the BE site, 2006–2008. Dry soils represent a soil water potential <−0.13 MPa at 10 cm depth. The vertical dashed lines represent the identified critical value of VPD. VPDs above this threshold resulted in a <1 and a Priestley–Taylor near or above 1. The identified VPD thresholds were 0.25 (2006), 0.31 (2007), and 0.28 kPa (2008) for wet soils and 1.19 kPa for dry soils (2007). (© Liljedahl et al. 2011, distributed under the Creative Commons Attribution 3.0 License. use with permission from the authors)

Calder 1998), evaporation is a physical process but transpiration is a plant physiological process controlled by stomata (Wullschleger et al. 1998).

On the tundra surface near Barrow, Alaska, Raz-Yaseef et al. (2017) found that variation in environmental conditions and plant community composition, driven by micro-topographical features, has a significant influence on ET. ET had high variability across the field site, i.e., the fluxes were highest over mosses and open water, lower from grasses and sedges (65% of those from mosses and open water), and lowest over bare ground and lichens (50% of those from mosses and open water) (Fig. 4.4).

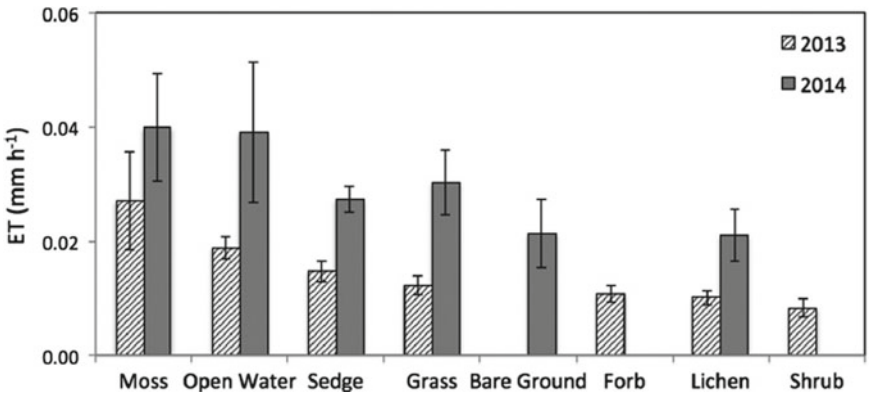

Fig. 4.4 Two years ET measured with the portable chamber. Values are averages for each plant type and for open water; bars denote standard deviation (After Raz-Yaseef et al. 2017)

Among plant types, ET from moss and inundated areas was more than twice that from other plant types. ET from troughs and low polygonal centers was significantly higher than that from high polygonal centers. ET also varied seasonally, with peak fluxes of 0.14 mm h^{-1} in July. Diurnal fluctuations in incoming solar radiation and plant processes produced a diurnal cycle in ET. Observed patterns with projections for the impact of permafrost degradation on polygonal structure suggest that micro-topographic changes associated with permafrost thaw have the potential to alter the tundra ecosystem ET (Young-Robertson et al. 2018). Yuan et al. (2010) examined the impacts of precipitation seasonality and ecosystem types on ET quantified by eddy covariance towers from 2002 to 2004 in three ecosystems (grassland, deciduous broadleaf forest, and evergreen needle leaf forest) in the Yukon River Basin, Alaska. The annual precipitation changed greatly in both magnitude and seasonal distribution through the three investigated years. Observations and model results showed that ET was more sensitive to precipitation scarcity in the early growing season than in the late growing season, which was the direct result of different responses of ET components to precipitation in different seasons. The results demonstrated the importance of seasonal variations of precipitation in regulating annual ET and overshadowing the function of annual precipitation. Comparison of ET among ecosystems over the growing season indicated that ET was largest in deciduous broadleaf, intermediate in evergreen needle leaf, and lowest in the grassland ecosystem. These ecosystem differences in ET were related to differences in successional stages and physiological responses.

Sublimation from snow surface has been identified as an important hydrological process at high altitudes and in high-latitude regions, involving complex mass and energy exchanges. In the Colorado Frontal Ranges, measurements from snow evaporation pans indicated that net sublimation for the 5-month winter period from December to April was 135 mm (Meiman and Grant 1974). Berg (1986) estimated

sublimation losses from snow cover to be 30–51% of precipitation over a 2-year period from 1973 to 1975. Kattelmann and Elder (1991) estimated sublimation from snow to be 18% of total precipitation over 2 years in the Sierra Nevada. In the subarctic region, several studies have shown that sublimation from snow cover is a non-negligible hydrological component that also affects river discharge and regional water resources. In western Canada, sublimation from snow during the winter season consumed from 15 to 40% of seasonal snowfall (Woo et al. 2000) and 12 to 33% of annual snowfall (Pomeroy and Li 1997). Suzuki et al. (2002) estimated that sublimation from snow cover in eastern Siberia was significant at 25.6% of precipitation from October to April. However, these estimations were derived from modeling and lack of observational verification. Subarctic ground surfaces are dominantly covered by subalpine and boreal forests. The impact of forests on snow cover has been extensively investigated via accumulation and melting processes. An increase of 30–45% in seasonal snow accumulation was measured after the removal of the evergreen forest (Pomeroy and Gray 1995; Pomeroy and Li 1997). Pomeroy et al. (1998) also found that snow water equivalent (SWE) generally increases with evergreen canopy density in boreal forests. Simulation models for snowmelt under a forest canopy have been developed to examine the relationship between snowmelt and forest density (Barry et al. 1990; Yamazaki and Kondo 1992; Wigmosta et al. 1994). Canopy density is important in controlling snow ablation timing and rates because tree height and canopy properties control the transmission of solar radiation (Davis et al. 1997; Ni et al. 1997).

Leydecker and Melack (1999) discussed the sensitivity of sublimation over a short time scale using snow surface roughness, instrument height, and wind speed and demonstrated that wind speed was the critical variable for determining sublimation and that doubling wind speed can triple the sublimation. Zhang et al. (2008) demonstrated that when the wind speed is less than 2. 0 m s^{-1}, the saturation deficiency is predominant in determining sublimation, and sublimation increases significantly when the wind speed is above 2.0 m s^{-1}. The variation in vapor transfer coefficient versus wind speed can be deduced (Fig. 4.5). This result shows that the vapor transfer coefficient for the snow surface is larger under low wind and decreases sharply as wind speed increases. However, the vapor transfer coefficient is nearly constant when the monthly mean wind speed is above 2.0 m s^{-1}. The impact of the coefficient on the sublimation rate is not so clear. Daily sublimation shows a tendency toward correlation with the vapor transfer coefficient (Fig. 4.5). The values of 20.3–21.6% of total snowfall lost to sublimation compares favorably with snow cover lost due to sublimation of 25.6% in eastern Siberia (Suzuki et al. 2002), or 12–33% of annual snowfall in Canada (Pomeroy and Li 1997).

Snow cover models were used to quantify sublimation. Sexstone et al. (2018) demonstrated that snow sublimation rates corresponding to climate-warming simulations remained unchanged or slightly increased but total sublimation losses decreased by up to 6% because of a reduction in snow-covered area and duration. Seasonally snow-covered forests in western North America have experienced substantial disturbance from mountain pine beetle (Dendroctonus ponderosae) and

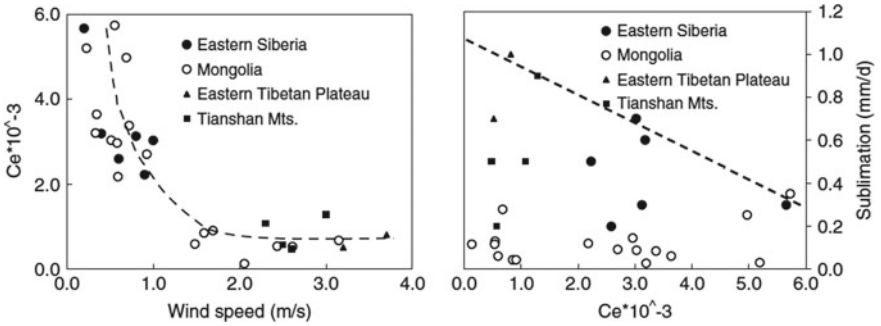

Fig. 4.5 Vapor transfer coefficient versus wind speed (left) and daily sublimation versus the vapor transfer coefficient (right) (Zhang et al. 2008)

spruce beetle (Dendroctonus rufipennis) outbreaks (Potter and Conkling 2016), which have resulted in widespread tree mortality and thus changes to forest structure that are particularly relevant to canopy and surface sublimation processes. Field studies that have focused on measuring SWE in both unimpacted and disturbed forests have inferred decreasing (e.g., Boon 2012; Pugh and Small 2012) as well as steady or increasing (e.g., Biederman et al. 2014; Harpold et al. 2014) net sublimation fluxes in the presence of disturbance. In contrast, distributed watershed modeling studies considering beetle-induced forest mortality (Penn et al. 2016) have generally reported decreased evapotranspiration but have not specifically focused on the sublimation component of evapotranspiration. Although changes to snow accumulation and melt processes from climate warming have been studied widely (Musselman et al. 2017a, b), the response of sublimation to climate change has received little investigation. As a result, specific knowledge gaps remain including how the components of sublimation will individually and collectively respond to changes in forcing mechanisms, in addition to changing snow accumulation and melt dynamics. Process-based snow models that can integrate responses and feedbacks of the snow energy balance offer the ability to evaluate sublimation responses to these changing land cover and climate conditions, which is critically important for the understanding of the water balance in snow-dominated regions.

4.3 Climate Warming and ET Change

The terrestrial cryosphere covers approximately 66 million km^2 ($\sim$52.5%) of the global land area where water is either permanently or seasonally frozen. Each year, most of the terrestrial cryosphere undergoes a seasonal transition between predominantly frozen and non-frozen (i.e., thawed) landscape conditions; these transitional events are relatively abrupt and analogous to a biospheric and hydrological

on/off switch between active ecosystem processes during the growing season and largely dormant conditions during the seasonal frozen period. The cold temperatures and seasonal frozen conditions pose strong constraints to vegetation productivity; surface hydrological processes, surface energy fluxes, and land–atmosphere trace gas exchange in these regions. In seasonally frozen environments, vegetation photosynthetic activity and associated ET are constrained by low temperatures and chemical unavailability of water as a result of being frozen.

Recent warming has altered freeze–thaw (FT) processes in the northern regions, resulting in substantial changes in terrestrial ecological and hydrological processes, including generally earlier onset and lengthening of potential vegetation growing seasons, thawing and degradation of permafrost, earlier spring snowmelt and increased groundwater to stream discharge from permafrost thawing. Warming and associated lengthening of the potential growing season has led to positive impacts on ecosystems of more cold-limited regions of the northern high latitudes, including increases in vegetation structure, greenness, productivity, and net CO_2 exchange. Recent warming trends also have been associated with negative ecosystem impacts within more water-limited regions of the northern latitudes by increasing water stress, which has been attributed to be a major cause of recent vegetation browning and productivity reductions, higher tree mortality rates, and increasing fire frequency.

Seasonal transitions of the landscape between predominantly frozen and thawed conditions are analogous to a biospheric and hydrological on/off switch, with marked differences in ET, vegetation productivity, and other biological activity between largely dormant winter and active summer conditions. By analyzing independent FT and ET records derived from satellite remote sensing, Zhang et al. (2011) investigated changes in FT seasons and ET from 1983 to 2006 and their connections in the northern cryosphere. They found that annual ET shows predominantly negative correlations with the timing of primary seasonal thaw (T_{thaw}) but has positive correlations with the timing of primary seasonal freeze (T_{freeze}) in most areas of the domain (Fig. 4.6). The correlations between annual ET and Tthaw are generally higher than that between ET and Tfreeze, indicating that the onset of the non-frozen season has a relatively larger impact on annual ET than its cessation. This is likely because incident solar radiation available for evaporation is generally higher during the spring Tthaw period than the autumn Tfreeze period; the Tthaw period also coincides with the general onset of the active growing season in northern, boreal, and Arctic environments, whereas vegetation photosynthetic activity and transpiration is reduced in autumn when plants are transitioning to winter dormancy (Kimball et al. 2004). Annual ET is positively correlated with the annual number of non-frozen days (DNF) over most of the domain, with stronger correlations at higher latitudes than in lower latitude areas.

In contrast to the prevailing pattern, some regions in the southern portion of the Arctic region show positive correlations between annual ET and Tthaw (Fig. 4.6a), where earlier than the normal onset of non-frozen period corresponds with less-than-normal annual ET. Almost all of these regions are located in areas where ET is predominantly limited by water supply. This suggests that an advancing

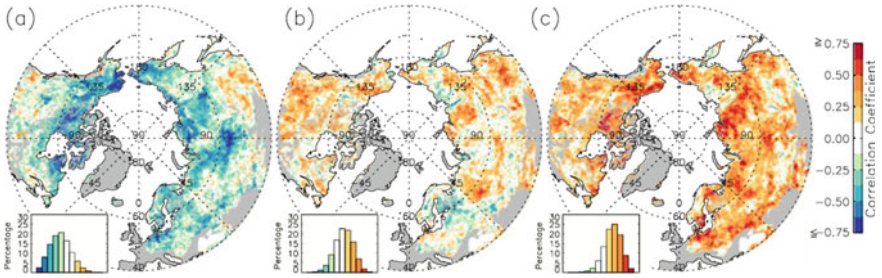

Fig. 4.6 Correlation maps **a** between annual ET and Tthaw, **b** between annual ET and Tfreeze and **c** between annual ET and DNF from 1983 to 2006; the insets show the frequency distributions of corresponding correlation coefficients, (Zhang et al. 2011)

non-frozen period may not promote additional increases in annual ET in these water supply-limited regions.

At northern high latitudes, cold temperatures and limited photoperiod largely constrain the potential growing season to a relatively brief period during the spring and summer months. Vegetation is largely dormant during the winter frozen period and coupled with frozen temperatures, seasonally low solar radiation loads, and limited day length strongly constrain ET. Low temperatures also inhibit plant photosynthesis and respiration by decreasing enzyme activity and protein synthesis in plant cells (Raich and Schlesinger 1992). Because transpiration is a consequence of plant photosynthesis, the constraint of low temperatures on photosynthesis also functions as a constraint on ET. Low temperatures also restrict photosynthesis and canopy gas exchange by limiting water supply and mobility in roots and xylem, leading to canopy stomatal closure (Woodward and Kelly 1997). Moreover, the atmospheric capacity to hold moisture increases exponentially with increasing temperature according to the well-known Clausius–Clapeyron relationship. Low temperatures, therefore, suppress ET by reducing atmospheric moisture demand. In addition, vegetation in cold boreal and Arctic regions are well adapted to the characteristic harsh environmental conditions and recover photosynthesis and respiration at relatively high rates following snowmelt and the new release of water in the landscape (Havranek and Tranquillini 1995; Suni et al. 2003; Kimball et al. 2004). Earlier onset of springtime thaw facilitates earlier photosynthesis and transpiration and generally enhances plant growth and transpiration when plant-available moisture is not limiting. During later stages of the non-frozen season in autumn, plants begin to enter the stage of senescence and dormancy, coinciding with seasonal reductions in temperatures, solar radiation, and photoperiod; thus, plant photosynthesis and transpiration are substantially reduced. After several months of vigorous ET, surface water storage accessible to vegetation would be substantially depleted without sufficient recharge. As a result, an extended non-frozen period in autumn would have less impact on ET than a similar extension in the spring.

The results of the positive response of ET to an advancing and lengthening non-frozen season vary spatially and are even reversed in warmer, southern regions of the domain where water supply is a leading constraint for ET (Zhang et al. 2011). These results also are consistent with recent reports indicating increasing regional water stress (Angert et al. 2005; Schindler and Donahue 2006; Hogg et al. 2008) and associated vegetation browning and productivity reduction (Goetz et al. 2005; Zhang et al. 2009; Beck et al. 2011), higher tree mortality rates (Kurz et al. 2008; Mantgem et al. 2009), and increasing fire frequency (Westerling et al. 2006).

4.4 Regional/Basin ET and Impact on Water Balance

ET plays an important role in linking the water, energy, and carbon cycles and represents over 60% of precipitation over the global land area (Oki and Kanae 2006). A better understanding of recent changes in the Arctic regions requires linking ET with other hydrological components including precipitation and river discharge. Precipitation and river discharge measurements are currently available from Arctic observation networks (Yang et al. 2005; McClelland et al. 2004). Evapotranspiration (ET) is highly heterogeneous both spatially and temporally due to strong vegetation canopy control on transpiration. Relatively sparse measurements of these variables across the northern high latitudes make an accurate assessment of ET a challenge. Remotely sensed data, especially from polar-orbiting satellites, provide relatively frequent and spatially contiguous monitoring of surface biophysical variables affecting ET, including albedo, biome type, and vegetation density. Satellite-based ET products have been produced at regional and global scales with varying accuracy (Suzuki et al. 2018; Zhang et al. 2009; Cleugh et al. 2007; Mu et al. 2007; Fisher et al. 2008).

Zhang et al. (2009) developed an evapotranspiration (ET) algorithm driven by satellite remote sensing inputs, including AVHRR GIMMS NDVI, MODIS land cover, and NASA/GEWEX solar radiation and albedo, and regionally corrected NCEP/NCAR Reanalysis daily surface meteorology. The algorithm was used to assess spatial patterns and temporal trends in ET over the pan-Arctic basin and Alaska from 1983 to 2005 (Fig. 4.7). The annual ET patterns are spatially complex but show generally reduced ET with increasing latitude. The spatial pattern of ET also corresponds to distributions of the major biome types. Boreal forest regions have the highest annual ET (277.35 ± 68.89 mm yr^{-1}) among the three major biome types followed by grassland (248.40 ± 76.94 mm yr^{-1}) and Arctic tundra (158.98 ± 37.61 mm yr^{-1}) c water bodies resolved by the 1-km resolution global land cover classification cover only 6.4% of the pan-Arctic domain, they are distributed across a wide geographic range, with relatively large magnitude and spatial variation in annual ET (410.35 ± 142.58 mm yr^{-1}) relative to vegetated land areas. Meanwhile, both the GPCP and GPCC sources show similar multiyear mean annual precipitation patterns; though the GPCP precipitation rates are much larger, averaging 1.31 (±0.38) times the GPCC precipitation rates. Both precipitation datasets

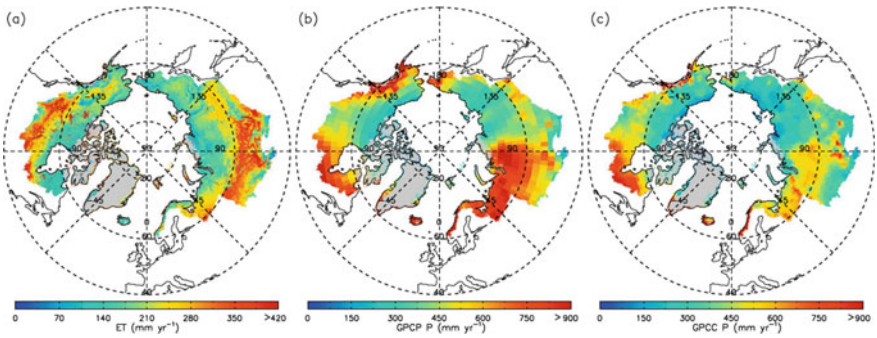

Fig. 4.7 Maps of multi-year (1983–2005) mean annual calculated ET **a** and precipitation derived from **b** GPCP and **c** GPCC sources (Zhang et al. 2009)

show portions of Southern Alaska, Northeastern Canada near Hudson Bay, and Western Eurasia having the largest precipitation, with relatively arid polar tundra areas showing the least precipitation.

The pan-Arctic region has a small positive trend in annual P for the 1983–2005 period (Fig. 4.8), indicated by both GPCP (7.4 mm decade-1) and GPCC (4.3 mm decade-1) sources, while ET shows a significant positive trend of 3.8 mm decade-1 for this period coinciding with regional warming (Trenberth et al. 2007) and vegetation greening trends (e.g., Goetz et al. 2005; Zhang et al. 2008). On average, ET represents 44.4% (±1.6) and 54.7% (±1.8) of P for the pan-Arctic domain relative to the GPCP and GPCC sources, respectively. Both P and ET show positive trends so the net effect on P–ET is reduced and annual P–ET shows an insignificant wetting trend indicated by both GPCP and GPCC data. Both GPCP- and GPCC-derived results show P–ET interannual variability of approximately ±6% relative to the long-term mean. Time series plots of annual P–ET anomalies for the domain show that the years 1984–1985, 1995–1996, 1998–2001, and 2003 are dry relative to the long-term mean. Both regional average P and ET show seasonal changes during the 23-year period (Table 4.1). The GPCP and GPCC data show positive regional P trends in spring, summer, and autumn, with slightly decreasing P trends in winter. The ET results show significant ($P < 0.1$) positive trends for all four seasons, with the largest ET increases in spring and summer, similar to P. These results suggest that regional warming and associated lengthening of the seasonal non-frozen period are promoting increases in annual ET, while positive P trends during this period are counteracting these evaporative water losses and associated changes to the annual water balance. On a seasonal basis, larger positive trends in P relative to ET in spring, summer, and autumn imply that the pan-Arctic domain is becoming wetter during the growing season. In contrast, decreasing P and slightly positive ET trends indicate that the pan-Arctic domain is becoming drier during the winter period.

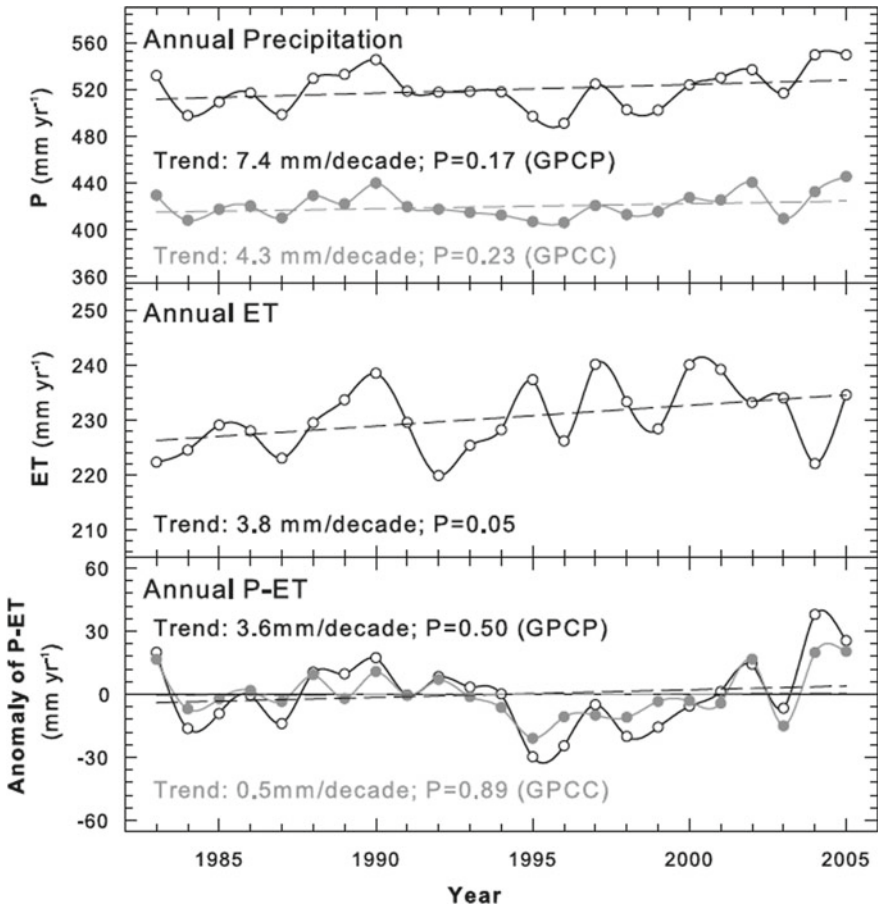

Fig. 4.8 Annual time series of precipitation (P) derived from GPCP and GPCC data sources; ET derived from the NDVI-based ET algorithm, and corresponding annual P–ET anomalies from the long-term (23-year) mean. Dashed lines show linear trends for the time series. The two P series from GPCP and GPCC sources are highly correlated ($r = 0.91$; $p < 0.001$). The resulting P–ET anomalies are also highly correlated ($r = 0.89$; $p < 0.001$). (Zhang et al. 2009)

Similar interannual changes were found by Suzuki et al. (2018) for the Mackenzie River, the Lena River, and the Yukon River basin. Comparisons were made among monthly precipitation (**P**) from GLDAS-2 and river runoff (R) for each river basin (Fig. 4.9). The maximum monthly **P** occurred in July for the Lena and Mackenzie River basins and in June or July for the Yukon River basin. The Lena River exhibits the largest amount of river runoff (**R**), followed by the Yukon River and the Mackenzie River. The peak value of **R** occurred in June for all three rivers. Using monthly climatology of river runoff data, the peak snowmelt occurs between April and June, accounting for approximately 40%, 36%, and 28% of the annual R

Table 4.1 Trends of annual precipitation, ET, and P–ET from 1983 to 2005 for the three primary regional biome types and North American and Eurasian portions of the pan-Arctic domain (Zhang et al. 2009)

Continent	Biome type	Area (10^6 km^2)	P trend (mm de^{-1})		ET trend (mm de^{-1})	P-ET trend (mm de^{-1})	
			GPCP	GPCC		GPCP	GPCC
North American	Tundra	3.9	19.80**	8.77	2.81*	16.99*	5.97
	Forest	2.69	−7.97	−11.9*	−3.06	−4.90	−8.84
	Grassland	0.72	5.03	5.12	6.54*	−1.52	−1.42
Eurasia	Tundra	6.21	12.83**	8.70*	2.72	10.11*	5.98
	Forest	4.91	2.53	6.27	6.94**	−4.41*	−0.68
	Grassland	1.96	−9.99	−6.05	4.71*	−14.70	−10.77

* $p < 0.10$
** $p < 0.05$

in the Lena River, Yukon River, and Mackenzie River basins, respectively. E increased steadily from 2002 to 2016 with slopes of 1.2–4.1 mm y^{-1}. The increase in E from GLDAS-2 dataset can explain most of the decrease in water storage. Thus, evapotranspiration driven by increasing summer temperatures may be the primary factor controlling water storage. This suggests that future warming might further decrease the water storage at high latitudes in the Arctic circumpolar region.

Evapotranspiration of the major Arctic river basins simulated by a land surface model, CHANGE (Park et al. 2011), shows larger interannual variability, with large regional differences (Fig. 4.10), representing differences in climate, soil, vegetation, and landscape. Interestingly, the interannual variability of ET is larger in relatively warm basins (i.e., Ob and Mackenzie) than cold (Yenisey and Lena). A considerable area of the latter is underlaid by permafrost relative to the first. The recent warming temperature derives the warming of permafrost and thereby wetting soil that reduces moisture stress to ET. In other words, the wetted soil decreases the variability of ET under the warming temperature (Ohta et al. 2014). In reality, observations have identified the expansion of thermokarst lake resulted from permafrost degradation in the eastern Siberia (Ulrich et al. 2017), and consecutive positive anomalies of soil moisture were observed at the same region in the recent decade due to abnormally high winter precipitation (Iijima et al. 2010).

The four major basins show an increasing trend of ET over the period of 1979–2015 (Fig. 4.10). However, the trends evidently indicate large regional differences; the Siberian basins have significantly high increasing rates of ET (+0.72–+1.01 mm yr^{-1}) compared to Mackenzie. The significant increases in the Siberian basins are due to the recent warming temperature under the wetted soil moisture mentioned above because the temperature is a major deriving factor of ET (Park et al. 2008). The warming temperature also derives increases in vegetation biomass, so that the increased leaf area enhances transpiration and canopy interception to precipitation water. In contrast, the higher leaf area reduces solar radiation reaching

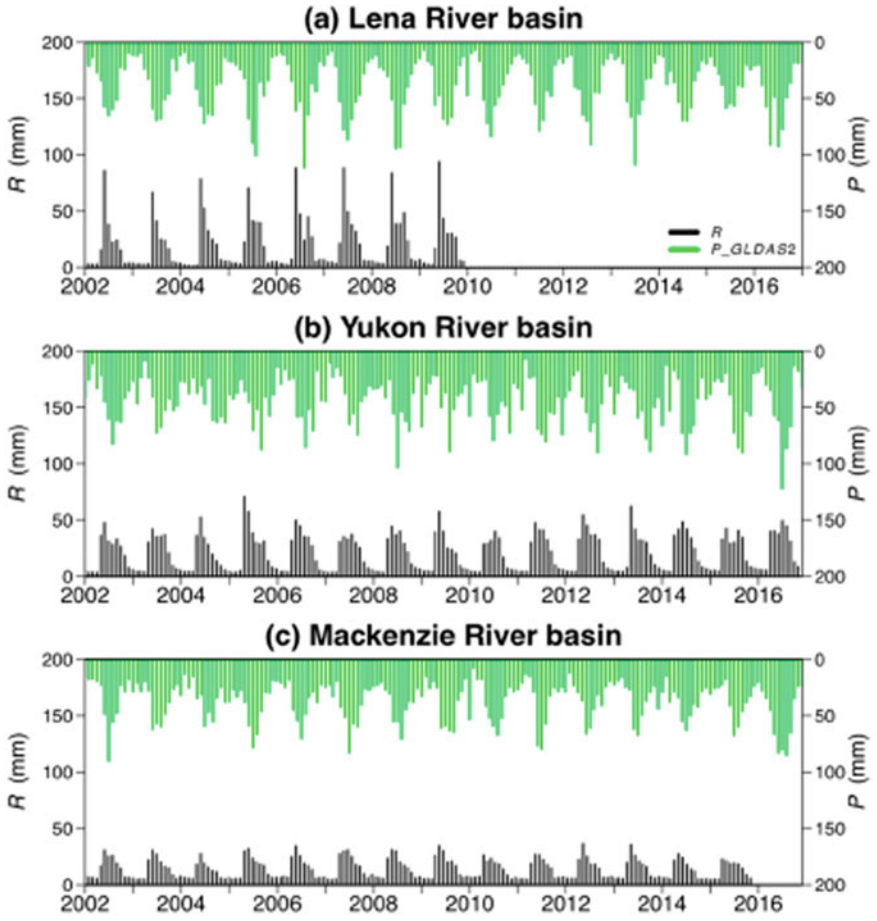

Fig. 4.9 Temporal variations in monthly water balance components from 2002 to 2016 in the **a** Lena River basin, **b** Yukon River basin, and **c** Mackenzie River basin (Suzuki et al. 2018, open access, no special permission is required to reuse all or part of the article published by MDPI, including figures and tables)

on soil surface and thereby less soil evaporation. However, most soil evaporation occurs in the spring season when solar radiation is the strongest, and leaf opening is not initiated (Park et al. 2008). In the Mackenzie River, warming was consistent with Siberia, while there was soil drought due to less precipitation during the recent period (Park et al. 2013). It suggests that the lower ET in the Mackenzie River for the recent decade is likely because of the influence of the drought. The comparison of ET between the river basins concludes that the differences in regional ETs mainly resulted from different climate and soil moisture conditions.

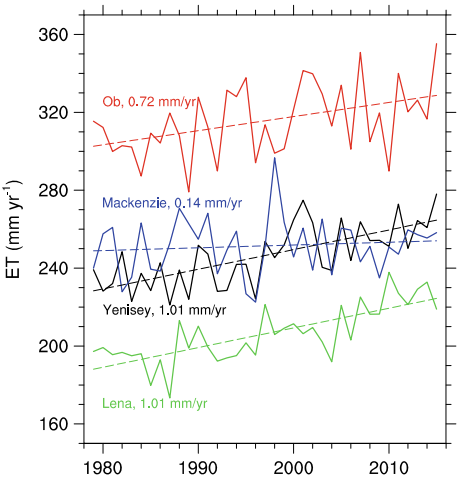

Fig. 4.10 Interannual variability of ET in the Arctic major river basins, simulated by a land surface model CHANGE using WATCH forcing dataset. The dot lines and numbers represent the ET trend in individual river basins

4.5 The Net Surface Moisture Flux (P-E)

Great hydrologic consequences are arising from the variations in the net surface moisture flux, which is the difference between precipitation (P) and evapotranspiration (E), over the large region and watersheds. For simplicity, here we use E to represent evapotranspiration over terrestrial surfaces and evaporation over ocean surfaces. In this respect, a key underlying question is: Will Arctic landscapes become wetter or drier as climate changes? Over the ocean, a corresponding question is: Will the ocean surface gain or lose freshwater to the atmosphere? While scaling issues complicate the answer to these questions, the fundamental uncertainty surrounds the surface moisture budget and the relationship P and E. If P (including both rain and snow) exceeds E over a period of time, the excess goes into runoff or storage. If E exceeds P, the surface moisture deficit leads to drying over land unless there is sufficient recharge from below. A drying surface leads to decreased water supplies, increased wildfire risk, and moisture stress on vegetation, all of which have consequences for terrestrial ecosystems and human activities. Over the ocean, the consequences of an imbalance of P and E will be a change of the near-surface stratification.

The trajectory of Arctic surface wetness is confounded by observations of decreasing soil moisture in the Arctic (Hinzman et al. 2013) and in subarctic Swedish basins where precipitation has been increasing (Destouni and Varrot 2014). Earth system model results also show a reduction in wetland extent in higher latitudes, largely associated with permafrost thaw (Avis et al. 2011). The most comprehensive assessment of trends of P-E based on historical data and model simulations appears to be that of Rawlins et al. (2010), who used a variety of precipitation datasets, atmospheric reanalyses, land surface model output, and global climate models. Rawlins et al. (2010) used various approaches, such as

average of nine global climate models (GCMs), average of five land surface models (LSMs), the surface energy balance and remote sensing (RS) method, the Variable Infiltration Capacity (VIC) model, and the ERA-Interim reanalysis, to synthesizing data, and found increases of E over Arctic terrestrial regions in recent decades. More generally, Rawlins et al. also found that trends of P, P-E, and river discharge were generally positive in the observational data, for which record lengths ranged from 20 to 50 years. However, trends of P-E, computed as differences between historical P datasets and satellite-derived (AVHRR GIMMS) E, showed no significant trend. The nine global climate models examined by Rawlins et al. (2010) showed statistically significant trends of terrestrial pan-Arctic P-E over the period 1950–1999 in eight of the nine cases, and in all nine cases for the period 1950–2049. Trends for the historical period were smaller than for the future period in the climate model output. All results were for annual means. The positive trends in annual mean P-E contrast with the expectation that longer and warmer summers will increase E sufficiently to favor summer drying. Anticipated increases of high-latitude wildfire activity (Partain et al. 2016; Flannigan et al. 2015) are consistent with this expectation, highlighting the mixed picture of future surface wetness trends in the Arctic. For the Arctic marine areas, Bintanja and Selton's (2014) analysis of model output found that increased open water drove an increase of E that, in turn, was a major contributor to future increases of P over the Arctic Ocean in climate model simulations. However, compelling demonstrations of increases of E over the Arctic Ocean based on historical data are generally lacking.

For the future, one of the earlier examinations of pan-Arctic hydrology changes projected by climate models found that Arctic P-E increased in model simulations of the twenty-first century (Kattsov et al. 2007), implying a wetter Arctic surface in the future. However, that study presented changes in only the annual pan-Arctic P-E and did not consider differences between ocean and land areas nor between different terrestrial subregions. Model-based studies summarized below are unanimous in projecting future increases of river discharge in the Arctic. The coarse resolution of these models and their rudimentary treatment of permafrost and vegetative processes make it questionable to base conclusions about Arctic surface wetness trends on results from these simulations. A more recent evaluation of 25 CMIP5 global climate model projections, although global rather than the Arctic in scope, distinguished summer and winter changes of E (Laine et al. 2014). The results presented by Laine et al. (2014) highlight the challenge of assessing future changes in high-latitude surface wetness. As shown in Fig. 4.11 (Laine et al. 2014), The projected changes of P and E show the expected pattern, with increases of E over Arctic land areas, primarily during summer, and strong increases over the subarctic seas during winter in areas of sea ice loss (consistent with Bintanja and Selten 2014). However, the middle panels of Fig. 4.11 show that changes of P-E over the Arctic are much less spatially coherent and less robust than changes of P and E separately. In particular, summer P-E is projected to decrease much of Canada, increase over Alaska, decrease over the western and northern Eurasian subarctic, and increase over parts of northeastern Russia, including Chukotka. Over most of these areas, the sign of the projected change is not robust across the models at the

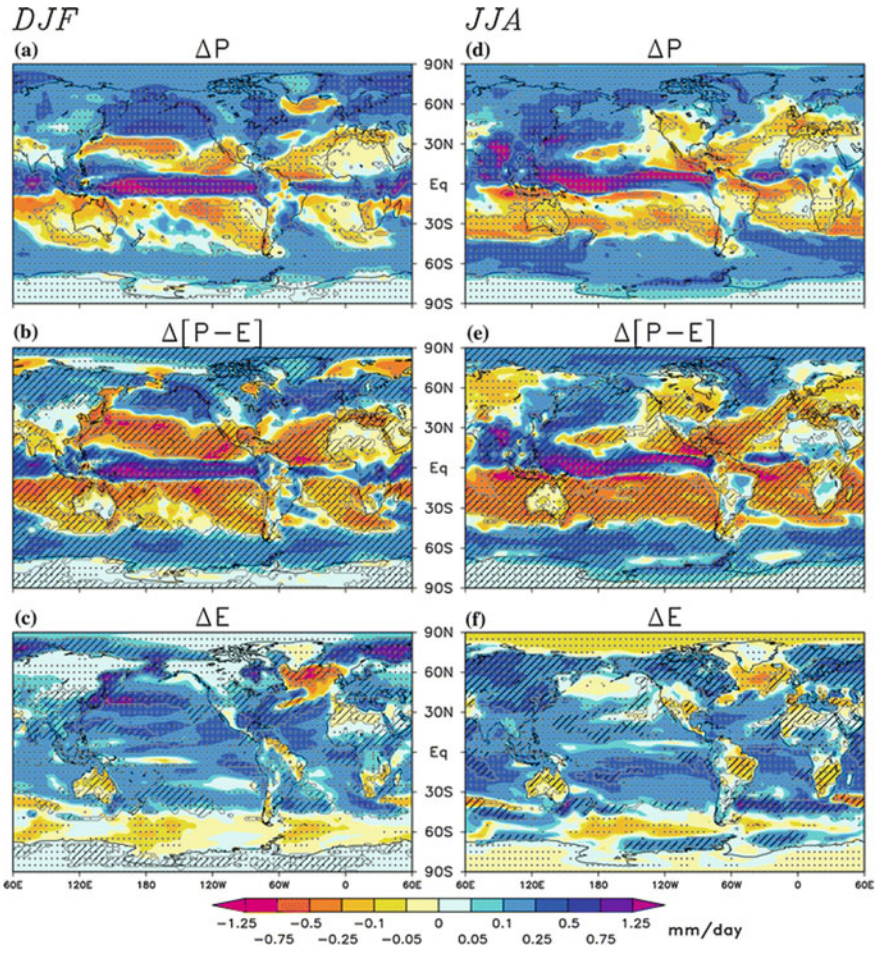

Fig. 4.11 25-model mean changes in precipitation P (upper panels), P-E (middle panels), and evapotranspiration E (lower panels) for Dec–Feb (left panels) and Jun–Aug (right panels). In dotted regions, the sign of change is robust among the different models at the 95% confidence level. Hatching in middle and lower panels indicates where a change in P-E is dominated by P and E, respectively (Laine et al. 2014, with open access)

95% confidence level. Figure 4.11e's spatial pattern over high-latitude land areas is very consistent with the projected changes in soil moisture obtained by Dirmeyer et al. (2013) using 15 of the same models. Dirmeyer et al. (2013) showed reductions of summer soil moisture over northern Canada and north-central Russia but not over Alaska and eastern Siberia, from the preindustrial to the twentieth century. However, decreases of summer soil moisture do spread to southern and central

Alaska in the twenty-first century (Dirmeyer et al. 2013). The results of these two studies highlight the uncertainty in the trajectory of surface wetness in Arctic land areas in the present generation of global climate models.

River discharge data, which can be viewed as proxies for P-E integrated over river basins, generally show increases from the mid-twentieth century to the early 2000s, with varying degrees of statistical significance (Yang et al. 2004a, b; Shiklomanov and Lammers 2009; Overeem and Syvitski 2010; Holmes et al. 2013; Bring and Destouni 2014). Model-based studies consistently show that projected changes in atmospheric forcing will drive twenty-first-century increases in high-latitude river discharge (e.g., Vliet et al. 2013; Koirala et al. 2014; Bring et al. 2015).

Various factors contribute to the uncertainty in the projected changes in Arctic surface wetness. Internal variability, which can affect trends over decadal and multidecadal timescales, is clearly one consideration. However, studies such as those of Rawlins et al. (2010), Laine et al. (2014) and Dirmeyer et al. (2013) have utilized multimodel ensembles that tend to average out internal variations, and these studies indeed contained robust signals in the future changes of P and E, although not the hydrologically critical difference, P-E. Across-model differences in process formulations, especially the formulations in the terrestrial modules, almost certainly are key contributors to the uncertainty. Because of their coarse ($\sim$100–200 km) resolution, global climate models are often unable to resolve terrain and vegetation variations that characterize the Arctic landscape. The terrestrial modules of many global models include crude treatments of permafrost, with an inadequate representation of soil horizons and resolution of the changing active layer. Important differences in Arctic vegetation such as tundra types (e.g., heath vs. tussock), forest composition, and effects of small lakes and ponds are generally not well considered. Also not included in most global models are local topography, subgrid-scale vegetation distributions, and permafrost hydrology, which are all important determinants of soil moisture, drainage, and, to at least some extent, land surface evaporation.

4.6 Conclusion and Discussion

Evapotranspiration (ET) is a key component in global water and energy cycles. In the northern regions where water is either permanently or seasonally frozen, ET is influenced by both hydrological and thermal conditions of the land surface through complex physical processes and feedbacks to the surrounded environment. This chapter presents and discusses recent research advances about the ET in northern regions. ET in northern regions tends to increase with the decrease of latitude. The largest ET typically appears in the forest ecosystem, while the grasslands and shrublands have the small ET. While the seasonal variations in ET are usually high,

the interannual variability in annual ET is usually low over the Arctic regions, reflecting the dominance of cold temperature constraints on northern ecosystem processes. It should be noted that the sublimation from snow cover accounts for about 15% (in Siberia) to 25% (in western Canada) of winter precipitation. This is certainly a non-negligible hydrological component that affects the end of winter snow mass, river discharge, and regional water resources across the broad northern regions. Many factors, such as soil moisture, vegetation type, and productivity, and ecosystem features affect ET over the northern regions. In addition, precipitation plays a key role in impacting ET. ET is more sensitive to precipitation in the early growing season than in the late growing season. Furthermore, changes in freeze–thaw processes due to warming also affect land surface conditions and the ET processes. Such an effect is different between the southern and northern parts of the Arctic because of the water supply in the soil. Therefore, annual ET shows positive correlations with the timing of primary seasonal thaw in the northern Arctic region, in which soil water is relatively large. This is because the earlier onset of springtime thaw facilitates earlier photosynthesis and transpiration and generally enhances plant growth and transpiration when plant-available moisture is high. However, the reverse relationship is witnessed in the southern Arctic regions where the water supply is usually limited. From 1983 to 2005, ET increased significantly in the Arctic region with a rate of 3.8 mm decade^{-1} because of regional warming and vegetation greening. Such an increase in ET may exert significant impacts on the regional hydrology and water resources. Advanced models can simulate past ET change over the large northern watersheds. Remote sensing has proved new ET data and information that support climate and hydrology research and applications. It should be noted that most available ET studies in the Arctic region rely heavily on the models and/or satellite observations, while the ground measurements of ET in such a harsh but hydroclimatically important regions are yet extremely sparse. It is therefore highly recommended that the community should focus more on improving our understanding of ET processes and its feedbacks to climate by integrating a wide range of in situ observations and physical-based modeling approach. Finally, it is a key underlying question: Will Arctic landscapes become wetter or drier as climate changes? Global models suggest increases of E over Arctic terrestrial regions in recent decades. Rawlins et al. also found that trends of P, P-E, and river discharge were generally positive in the observational data. For the future, summer P-E is projected to decrease much of Canada, increase over Alaska, decrease over the western and northern Eurasian subarctic, and increase over parts of northeastern Russia. Over most of these areas, the sign of the projected change is not robust across the models at the 95% confidence level. Many factors contribute to the uncertainty in the projected changes in Arctic surface wetness. There is certainly a need to quantify and narrow the uncertainties in global models over the large northern regions.

References

Angert A, Biraud S, Bonfils C, Henning CC, Buermann W, Pinzon J, Tucker CJ, Fung I (2005) Drier summers cancel out the CO_2 uptake enhancement induced by warmer springs. Proc Natl Acad Sci USA 102(31):10823–10827

Avis CA, Weaver AJ, Meissner KJ (2011) Reduction in areal extent of high-latitude wetlands in response to permafrost thaw. Nat Geosci 4(7):444–448

Baldocchi D (2014) Measuring fluxes of trace gases and energy between ecosystems and the atmosphere - the state and future of the eddy covariance method. Glob Change Biol 20 (12):3600–3609

Baldocchi DD, Xu LK, Kiang N (2004) How plant functional-type, weather, seasonal drought, and soil physical properties alter water and energy fluxes of an oak-grass savanna and an annual grassland. Agric For Meteorol 123(1):13–39

Barry R, Prévost M, Stein J, Plamondon AP (1990) Simulation of snowmelt runoff pathways on the Lac Laflamme watershed. J Hydrol 113(1–4):103–121

Beck PSA, Horning N, Goetz SJ, Loranty MM, Tape KD (2011) Shrub Cover on the North Slope of Alaska: a circa 2000 Baseline Map. Arct Antarct Alp Res 43(3):355–363. https://doi.org/10.1657/1938-4246-43.3.355

Berg NH (1986) Blowing snow at a Colorado Alpine site: measurements and implications. Arct Alp Res 18(2):147–161

Betts AK, Ball JH, Viterbo P (1999) Basin-scale surface water and energy budgets for the Mississippi from the ECMWF reanalysis. J Geophys Res Atmos 104(D16):19293

Biederman JA, Brooks PD, Harpold AA, Gochis DJ, Gutmann E, Reed DE et al (2014) Multiscale observations of snow accumulation and peak snowpack following widespread, insect-induced lodgepole pine mortality. Ecohydrology 7:150–162. https://doi.org/10.1038/nclimate219810.1002/eco.1342

Bintanja R, Selten FM (2014) Future increases in Arctic precipitation linked to local evaporation and sea-ice retreat. Nature 509(7501):479–482

Boon S (2012) Snow accumulation following forest disturbance. Ecohydrology 5:279–285. https://doi.org/10.1002/eco.212

Bring A, Asokan SM, Jaramillo F, Jarsjö J, Levi L, Pietroń J, Prieto C, Rogberg P, Destouni G (2015) Implications of freshwater flux data from the CMIP5 multimodel output across a set of Northern Hemisphere drainage basins. Earths Future 3(6):206–217

Bring A, Destouni G (2014) Arctic climate and water change: model and observation relevance for assessment and adaptation. Surv Geophys 35(3):853–877

Brutsaert W (1982) Evaporation into the atmosphere: theory, history, and applications. Springer, New York

Brutsaert W (2013) Use of pan evaporation to estimate terrestrial evaporation trends: the case of the Tibetan Plateau. Water Resour Res 49(5):3054–3058

Calder IR (1998) Water use by forests, limits and controls. Tree Physiol 18(8–9):625–631. https://doi.org/10.1093/treephys/18.8-9.625

Chang L-L, Dwivedi R, Knowles J, Fang Y-H, Niu G-Y, D Pelletier J, Rasmussen C, Durcik M, Barron-Gafford G, Meixner T (2018) Why do large-scale land surface models produce a low ratio of transpiration to evapotranspiration? J Geophys Res: Atmos

Cleugh HA, Leuning R, Mu Q, Running SW (2007) Regional evaporation estimates from flux tower and MODIS satellite data. Remote Sens Environ 106(3):285–304. https://doi.org/10.1016/j.rse.2006.07.007

Coendersgerrits AMJ, Ent RJVD, Bogaard TA, Wangerlandsson L, Hrachowitz M, Savenije HHG (2014) Uncertainties in transpiration estimates. Nature 506(7487):E1

Davis RE, Hardy JP, Ni W, Woodcock C, McKenzie JC, Jordan R, Li X (1997) Variation of snow cover ablation in the boreal forest: a sensitivity study on the effects of conifer canopy. J Geophys Res Atmos 102(D24):29389–29395. https://doi.org/10.1029/97jd01335

Destouni G, Verrot L (2014) Screening long-term variability and change of soil moisture in a changing climate. J Hydrol 516(1):131–139
Dirmeyer PA, Jin Y, Singh B, Yan X (2013) Trends in land-atmosphere interactions from CMIP5 simulations. J Hydrometeorology 14(3):829–849
Evaristo J, Jasechko S, Mcdonnell JJ (2015) Global separation of plant transpiration from groundwater and streamflow. Nature 525(7567):91
Fischer M, Trnka M, Kučera J, Deckmyn G, Orság M, Sedlák P, Žalud Z, Ceulemans R (2013) Evapotranspiration of a high-density poplar stand in comparison with a reference grass cover in the Czech-Moravian Highlands. Agric For Meteorol 181:43–60
Fisher JB, Melton F, Middleton E, Hain C, Anderson M, Allen R, Mccabe MF, Hook S, Baldocchi D, Townsend PA (2017) The future of evapotranspiration: Global requirements for ecosystem functioning, carbon and climate feedbacks, agricultural management, and water resources. Water Resour Res 53(4):2618–2626
Fisher JB, Tu KP, Baldocchi DD (2008) Global estimates of the land–atmosphere water flux based on monthly AVHRR and ISLSCP-II data, validated at 16 FLUXNET sites. Remote Sens Environ 112(3):901–919. https://doi.org/10.1016/j.rse.2007.06.025
Flannigan MD, Wotton BM, Marshall GA, de Groot WJ, Johnston J, Jurko N, Cantin AS (2015) Fuel moisture sensitivity to temperature and precipitation: climate change implications. Clim Change 134(1–2):59–71
Goetz S, Bunn A, Fiske G, Houghton R (2005) Satellite-observed photosynthetic trends across boreal North America associated with climate and fire disturbance. Proc Nat Acad Sci USA 102(38):13521–13525
Good, S.P., Noone, D. and Bowen, G. (2015) WATER RESOURCES. Hydrologic connectivity constrains partitioning of global terrestrial water fluxes. Science 349(6244), 175–177
Harpold AA, Biederman JA, Condon K, Merino M, Korgaonkar Y, Nan TC et al (2014) Changes in snow accumulation and ablation following the Las Conchas Forest Fire, New Mexico, USA. Ecohydrology 7:440–452. https://doi.org/10.1002/eco.1363
Havranek WM, Tranquillini W (1995) 5–physiological processes during winter dormancy and their ecological significance. Ecophysiology of coniferous forests. p 95–124
Hogg EH, Brandt JP, Michaelian M (2008) Impacts of a regional drought on the productivity, dieback, and biomass of western Canadian aspen forests. Can J For Res 38(6):1373–1384. https://doi.org/10.1139/x08-001
Hinzman LD, Deal CJ, McGuire AD, Mernild SH, Polyakov IV, Walsh JE (2013) Trajectory of the Arctic as an integrated system. Ecol Appl 23(8):1837–1868
Holmes RM, Coe MT, Fiske GJ, Gurtovaya T, Mcclelland JW, Shiklomanov AI, Spencer RGM, Tank SE, Zhulidov AV (2013) Climate change impacts on the hydrology and biogeochemistry of arctic rivers. Wiley, Ltd
Iijima Y, Fedorov AN, Park H, Suzuki K, Yabuki H, Maximov TC, Ohata T (2010) Abrupt increases in soil temperatures following increased precipitation in a permafrost region, central Lena River basin. Russia Permafrost Periglac Process 21:30–41
Jasechko S, Sharp ZD, Birks SJ, Yi Y, Fawcett PJ (2013) Terrestrial water fluxes dominated by transpiration. Nature 496(7445):347
Mendez J, Hinzman LD, Kane DL (1998) Evapotranspiration from a wetland complex on the arctic coastal plain of Alaska. Nordic Hydrol 29(4–5):303–330
Kane DL, Hinzman LD, Gieck RE, Mcnamara JP, Youcha EK, Oatley JA (2008) Contrasting extreme runoff events in areas of continuous permafrost, Arctic Alaska. Hydrol Res 39(4):287–298
Kane DL, Hinzman LD, Mcnamara JP, Zhang Z, Benson CS (2000) An overview of a nested watershed study in Arctic Alaska. Nordic Hydrol 31(4–5):245–266
Kattelmann R, Elder K (1991) Hydrologic characteristics and water balance of an Alpine Basin in the Sierra Nevada. Water Resour Res 27(7):1553–1562

Kattsov VM, Walsh JE, Chapman WL, Govorkova VA, Pavlova TV, Zhang X (2007) Simulation and projection of arctic freshwater budget components by the IPCC AR4 global climate models. J Hydrometeorology 8(3):571–589. https://doi.org/10.1175/jhm575.1

Katul, GG, Oren R, Manzoni S, Higgins C, Parlange MB (2012) Evapotranspiration: a process driving mass transport and energy exchange in the soil-plant-atmosphere-climate system. Rev Geophys 50(3)

Kimball JS, Mcdonald KC, Running SW, Frolking SE (2004) Satellite radar remote sensing of seasonal growing seasons for boreal and subalpine evergreen forests. Remote Sens Environ 90 (2):243–258. https://doi.org/10.1016/j.rse.2004.01.002

Koirala S, Hirabayashi Y, Mahendran R, Kanae S (2014) Global assessment of agreement among streamflow projections using CMIP5 model outputs. Environ Res Lett 9(9):064017

Kool D, Agam N, Lazarovitch N, Heitman JL, Sauer TJ, Bengal A (2014) A review of approaches for evapotranspiration partitioning. Agric For Meteorol 184(1):56–70

Kurz, WA, Dymond, CC, Stinson, Rampley, GJ, Neilson, ET (2008) Mountain pine beetle and forest carbon feedback to climate change. Nature 45:987–990. https://doi.org/10.1038/nature06777

Laîné A, Nakamura H, Nishii K, Miyasaka T (2014) A diagnostic study of future evaporation changes projected in CMIP5 climate models. Clim Dyn 42(9–10):2745–2761

Leydecker A, Melack JM (1999) Evaporation from snow in the central Sierra Nevada of California. Hydrol Res 30(2):81–108

Liljedahl AK, Hinzman LD, Harazono Y, Zona D, Tweedie CE, Hollister RD, Engstrom R, Oechel WC (2011) Nonlinear controls on evapotranspiration in arctic coastal wetlands. Biogeosciences 8(11):3375–3389

Ma N, Szilagyi J, Zhang Y, Liu W (2019) Complementary-relationship-based modeling of terrestrial evapotranspiration across China during 1982–2012: validations and spatiotemporal analyses. J Geophys Res: Atmos 124. https://doi.org/10.1029/2018JD029580

Ma N, Wang N, Zhao L, Zhang Z, Dong C, Shen S (2014) Observation of mega-dune evaporation after various rain events in the hinterland of Badain Jaran Desert, China. Sci Bull 59(2):162–170

Mackay DS, Ewers BE, Cook BD, Davis KJ (2007) Environmental drivers of evapotranspiration in a shrub wetland and an upland forest in northern Wisconsin. Water Resour Res 43(3): W03442

Mantgem PJV, Stephenson NL, Byrne JC, Daniels LD, Franklin JF, Fule PZ, Harmon ME, Larson AJ, Smith JM, Taylor AH (2009) Widespread increase of tree mortality rates In the Western United States. Science 323(5913):521–524

Matheny AM, Bohrer G, Stoy PC, Baker IT, Black AT, Desai AR, Dietze MC, Gough CM, Ivanov VY, Jassal RS (2014) Characterizing the diurnal patterns of errors in the prediction of evapotranspiration by several land-surface models: an NACP analysis. J Geophys Res Biogeosci 119(7):1458–1473

Maxwell RM, Condon LE (2016) Connections between groundwater flow and transpiration partitioning. p 377

McClelland JW (2004) Increasing river discharge in the Eurasian Arctic: Consideration of dams, permafrost thaw, and fires as potential agents of change. J Geophys Res 109(D18). https://doi.org/10.1029/2004jd004583

Meiman JR, Grant LO (1974) Snow-air interactions and management on mountain watershed snowpack. In: Environmental Research Center. Colorado State University, Fort Collins, pp 3–5

Miralles DG, De Jeu RAM, Gash JH, Holmes TRH, Dolman AJ (2011) Magnitude and variability of land evaporation and its components at the global scale. Hydrol Earth Syst Sci 15(3):967–981

Mu Q, Heinsch FA, Zhao M, Running SW (2007) Development of a global evapotranspiration algorithm based on MODIS and global meteorology data. Remote Sens Environ 111(4):519–536. https://doi.org/10.1016/j.rse.2007.04.015

Mu QZ, Jones LA, Kimball JS, McDonald KC, Running SW (2009) Satellite assessment of land surface evapotranspiration for the pan-Arctic domain. Water Resour Res 45(20)
Musselman KN, Clark MP, Liu CH, Ikeda K, Rasmussen R (2017a) Slower snowmelt in a warmer world. Nat Clim Change 7:214–219. https://doi.org/10.1038/nclimate3225
Musselman KN, Clark MP, Liu CH, Ikeda K, Rasmussen R (2017b) Slower snowmelt in a warmer world. Na Clim Change 7:214–219. https://doi.org/10.1038/nclimate3225
Ni W, Li X, Woodcock CE, Roujean JL, Davis R E (1997) Transmission of solar radiation in boreal conifer forests: measurements and models. J Geophys Res Atmos 102(D24):29555–29566. https://doi.org/10.1029/97jd00198
Oberbauer S, Dawson T (1992) Water relations of Arctic vascular plants Physiological ecology of arctic plants: implications for climate change
Oechel WC, Vourlitis GL, Hastings SJ, Ault RP, Bryant P (1998) The effect of water table manipulation and elevated temperature on the net CO2 flux of wet sedge tundra ecosystem. Glob Change Biol 4(1):77–90
Ohta T, Kotani A, Iijima Y, Maximov T, Ito S, Hanamura M, Kononov A, Maximov A (2014) Effects of waterlogging on water and carbon dioxide fluxes and environmental variables in a Siberian larch forest. Agri For Meteorol 188:64–75
Oki T, Kanae S (2006) Global Hydrological Cycles and World Water Resources. Science 313 (5790):1068
Oren R, HSIEH C-I, Stoy P, Albertson J, Mccarthy HR, Harrell P, Katul GG (2006) Estimating the uncertainty in annual net ecosystem carbon exchange: spatial variation in turbulent fluxes and sampling errors in eddy-covariance measurements. Glob Change Biol 12(5):883–896
Overeem I, Syvitski JPM (2010) Shifting discharge peaks in Arctic rivers, 1977–2007. Geogr Ann 92(2):285–296
Park H, Yamazaki T, Yamamoto K, Ohta T (2008) Tempo-spatial characteristics of energy budget and evapotranspiration in the eastern Siberia. Agric For Meteorol 148:1990–2005
Park H, Iijima Y, Yabuki H, Ohta T, Walsh J, Kodama Y, Ohata T (2011) The application of a coupled hydrological and biogeochemical model (CHANGE) for modeling of energy, water, and CO2 exchanges over a larch forest in eastern Siberia. J Geophys Res 116:D15102. https://doi.org/10.1029/2010JD015386
Park H, Walsh J, Fedorov AN, Sherstiukov AB, Iijima Y, Ohata T (2013) The influence of climate and hydrological variables on opposite anomaly in active-layer thickness between Eurasian and North American watersheds. Cryosphere 7:631–645
Partain JL Jr, Alden S, Strader H, Bhatt US, Bieniek PA, Brettschneider BR, Walsh JE, Lader RT, Olsson PQ, Rupp TS (2016) An Assessment of the role of anthropogenic climate change in the alaska fire season of 2015. Bull Am Meteor Soc 97(12):S14–S18
Penn CA, Bearup LA, Maxwell RM, Clow DW (2016) Numerical experiments to explain multiscale hydrological responses to mountain pine beetle tree mortality in a headwater watershed. Water Resour Res 52(4):3143–3161. https://doi.org/10.1002/2015wr018300
Pomeroy JW, Gray DM (1995) Snowcover accumulation, relocation and management. Sci Rep 7:134. Natl Hydrol Res Inst Environ Can, Saskatoon, Canada
Pomeroy JW, Li L (1997) Development of the prairie blowing snow model for application in climatological and hydrological models. Proc W Snow Conf 65:186–197
Pomeroy JW, Parviainen J, Hedstrom N, Gray DM (1998) Coupled modelling of forest snow interception and sublimation. Hydrol Process 12(15):2317–2337
Potter KM, Conkling BL (2016) Forest health monitoring: national status, trends, and analysis 2015 (Gen Tech Rep SRS-213). Asheville, NC: US Department of Agriculture, Forest Service, Southern Research Station
Pugh E, Small E (2012) The impact of pine beetle infestation on snow accumulation and melt in the headwaters of the Colorado River. Ecohydrology 5:467–477. https://doi.org/10.1002/eco.239
Raich JW, Schlesinger WH (1992) The global carbon dioxide flux in soil respiration and its relationship to vegetation and climate. Tellus 44(2):81–89

Rawlins MA, Steele M, Holland MM, Adam JC, Cherry JE, Francis JA, Groisman PY, Hinzman LD, Huntington TG, Kane DL (2010) Analysis of the arctic system for freshwater cycle intensification: observations and expectations. J Clim 23(21):5715–5737

Raz-Yaseef N, Young-Robertson J, Rahn T, Sloan V, Newman B, Wilson C, Torn MS (2017) Evapotranspiration across plant types and geomorphological units in polygonal Arctic tundra. J Hydrol 553:816–825

Schindler DW, Donahue W (2006) A case study of the Saskatchewan river system. In: Fifth Biennial Rosenberg International Forum on Water Policy

Schlesinger WH, Jasechko S (2014) Transpiration in the global water cycle. Agric For Meteorol 189–190(6):115–117

Scott RL, Biederman JA (2017) Partitioning evapotranspiration using long-term carbon dioxide and water vapor fluxes. Geophys Res Lett 44

Scott RL, Huxman TE, Cable WL, Emmerich WE (2006) Partitioning of evapotranspiration and its relation to carbon dioxide exchange in a Chihuahuan Desert shrubland. Hydrol Process 20 (15):3227–3243

Shen M, Piao S, Jeong SJ, Zhou L, Zeng Z, Ciais P, Chen D, Huang M, Jin CS, Li LZ (2015) Evaporative cooling over the Tibetan Plateau induced by vegetation growth. Proc Natl Acad Sci USA 112(30):9299–9304

Shiklomanov AI, Lammers RB (2009) Record Russian river discharge in 2007 and the limits of analysis. Environ Res Lett 4(4):045015

Shukla J, Mintz Y (1982) Influence of Land-Surface Evapotranspiration on the Earth's Climate. Science 215(4539):1498–1501

Suni T, Berninger F, Markkanen T, Keronen P, Rannik l, Vesala T (2003) Interannual variability and timing of growing-season CO2 exchange in a boreal forest. J Geophys Res Atmos 108 (D9). https://doi.org/10.1029/2002jd002381

Suzuki K, Ohata T, Kubota J, Vasilenko N, Zhuravin S, Vulinsy V (2002) Winter hydrological processes in the Mogot experimental watershed, in the southern mountainous taiga, Eastern Siberia. In: Proceedings of the 6th water resources symposium, Tokyo, 525–530

Suzuki K, Matsuo K, Yamazaki D, Ichii K, Iijima Y, Papa F, Yanagi Y, Hiyama T (2018) Hydrological variability and changes in the Arctic circumpolar tundra and the three largest Pan-Arctic river basins from 2002 to 2016. Remote Sens 10(3):402. https://doi.org/10.3390/rs10030402

Sexstone GA, Clow DW, Fassnacht SR, Liston GE, Hiemstra CA, Knowles JF, Penn CA (2018) Snow sublimation in mountain environments and its sensitivity to forest disturbance and climate warming. Water Resour Res 54:1191–1211. https://doi.org/10.1002/2017WR021172

Talsma CJ, Good SP, Jimenez C, Martens B, Fisher JB, Miralles DG, Mccabe MF, Purdy AJ (2018) Partitioning of evapotranspiration in remote sensing-based models. Agric For Meteorol s 260–261:131–143

Trenberth KE, Fasullo J, Dai A, Qian T, Smith L (2007) Estimates of the global water budget and Its annual cycle using observational and model data. J Hydrometeorology 8(4):758–769. https://doi.org/10.1175/jhm600.1

Trenberth KE, Fasullo JT, Kiehl J (2009) Earth's global energy budget. Bull Am Meteor Soc 90 (3):311–323

Ulrich M, Matthes H, Schirrmeister L, Schutze J, Park H, Iijima Y, Fedorov AN (2017) Differences in behavior and distribution of permafrost-related lakes in Central Yakutia and their response to climatic drivers. Water Resour Res 53. https://doi.org/10.1002/2016WR109267

Vliet MTHV, Franssen WHP, Yearsley JR, Ludwig F, Haddeland I, Lettenmaier DP, Kabat P (2013) Global river discharge and water temperature under climate change. Glob Environ Change-Hum Policy Dimensions 23(2):450–464

Wei Z, Yoshimura K, Wang L, Miralles DG, Jasechko S, Lee X (2017) Revisiting the contribution of transpiration to global terrestrial evapotranspiration. Geophys Res Lett 44:2792–2801

Westerling AL (2006) Warming and earlier spring increase Western U.S. forest wildfire activity. Science 313(5789):940–943. https://doi.org/10.1126/science.1128834

Wigmosta MS, Vail LW, Lettenmaier DP (1994) A distributed hydrology-vegetation model for complex terrain. Water Resour Res 30(6):1665–1679
Wilson KB, Baldocchi DD (2000) Seasonal and interannual variability of energy fluxes over a broadleaved temperate deciduous forest in North America. Agric For Meteorol 100(1):1–18
Woo M-K, Marsh P, Pomeroy JP (2000) Snow, frozen soils and permafrost hydrology in Canada, 1995–1998. Hydrol Process 14:1591–1611
Woodward FI, Kelly CK (1997) Plant functional types: towards a definition by environmental constraints. p 47–65
Wullschleger SD, Meinzer FC, Vertessy RA (1998) A review of whole-plant water use studies in tree. Tree Physiol (8–9):8–9
Xiao W, Zhongwang W, Wen X (2018) Evapotranspiration partitioning at the ecosystem scale using the stable isotope method—A review. Agric For Meteorol 263:346–361
Yamazaki T, Kondo J (1992) The snowmelt and heat balance in snow-covered forested areas. J Appl Meteorol 31(11):1322–1327
Yang D, Ye B, Kane D (2004a) Streamflow changes over Siberian Yenisei River Basin. J Hydrol 296(1–4):59–80. https://doi.org/10.1016/j.jhydrol.2004.03.017
Yang D, Kane D, Zhang Z, Legates D, Goodison B (2005) Bias corrections of long-term (1973–2004) daily precipitation data over the northern regions. Geophys Res Lett 32(19):n/a–n/a. https://doi.org/10.1029/2005gl024057
Yang D, Ye B, Shiklomanov A (2004b) Discharge characteristics and changes over the Ob river watershed in Siberia. J Hydrometeorol 5:595–610
Young-Robertson JM, Naama RY, Cohen LR, Brent N, Thom R, Victoria S, W C, W SD (2018) Evaporation dominates evapotranspiration on alaska's arctic coastal plain. Arct Antarct Alp Res 50(1)
Yuan W, Liu S, Liu H, Randerson JT, Yu G, Tieszen LL (2010) Impacts of precipitation seasonality and ecosystem types on evapotranspiration in the Yukon River Basin, Alaska. Water Res Res 46(2). https://doi.org/10.1029/2009wr008119
Zeng Z, Piao S, Li LZX, Zhou L, Ciais P, Wang T, Li Y, Lian X, Wood EF, Friedlingstein P (2017) Climate mitigation from vegetation biophysical feedbacks during the past three decades. Nat Clim Change 7(6):432–436
Zhang K, Kimball JS, Kim Y, Mcdonald KC (2011) Changing freeze-thaw seasons in northern high latitudes and associated influences on evapotranspiration. Hydrol Process 25(26):4142–4151
Zhang K, Kimball JS, Mu Q, Jones LA, Goetz SJ, Running SW (2009) Satellite based analysis of northern ET trends and associated changes in the regional water balance from 1983 to 2005. J Hydrol 379(1):92–110
Zhang Q, Manzoni S, Katul G, Porporato A, Yang D (2014) The hysteretic evapotranspiration—Vapor pressure deficit relation. J Geophys Res Biogeosci 119(2):125–140
Zhang Y, Ohata T, Kang E, Yao T (2003) Observation and estimation of evaporation from the ground surface of the cryosphere in eastern Asia. Hydrol Process 17:1135–1147
Zhang Y, Munkhtsetseg E, Kadota T, Ohata T (2005) An observational study of ecohydrology of a sparse grassland at the edge of the Eurasian cryosphere in Mongolia. J Geophys Res: Atmos 110. D14103. https://doi.org/10.1029/2004JD005474
Zhang Y, Ishikawa M, Ohata T, Oyunbaatar D (2008) Sublimation from thin snow cover at the edge of the Eurasian cryosphere in Mongolia. Hydrol Process 22:3564–3575

Yinsheng Zhang is a Professor of Hydrology and Physical Geography in the Institute of Tibetan Plateau Research, Chinese Academy of Sciences (ITPCAS). He received his Ph.D. with a major in physical geography from Lanzhou Institute of Glaciology and Geocryology, Chinese Academy of Sciences in 1994. Prior to joining ITPCAS in 2009, He was a Senior Research Scientist at the Institute of Observational Research for Global Change, Japan Agency for Marine-Earth Science and Technology for more than 10 years. He is particularly interested in land surface hydrological processes in the cold regions and has carried out extensive fieldwork to monitor the hydrological processes in the Tibetan Plateau, Eastern Eurasia, Mongolia, etc. He has been the PI for six research projects from the National Natural Sciences Foundation of China (NSFC), Ministry of Science and Technology (MOST) of China, and Chinese Academy of Sciences. He has authored and co-authored more than 90 papers in peer-reviewed journals and book chapters. He was awarded as "Excellent Graduate Advisor of Chinese Academy of Sciences" in 2018.

Ning Ma is a Postdoc Researcher at the Institute of Tibetan Plateau Research, Chinese Academy of Sciences. He received his B.S. with a major of Geographical Sciences and M.S. with a major of Earth System Sciences from the Department of Earth and Environmental Sciences, Lanzhou University in June 2010 and December 2012, respectively. He received his Ph.D. from the Institute of Tibetan Plateau Research, Chinese Academy of Sciences in June 2017. His research interests include land surface processes, hydrological processes, and climate change in cold and arid regions. He has authored and co-authored more than 30 publications in peer-reviewed journals and he was also selected as an award winner of "Hundred Excellent PhD theses of Chinese Academy of Sciences" in 2018. The overall goal of his research is to improve our systematic understanding of the evapotranspiration processes and its response to climate and land cover changes through applications of an integrated research approach consisting of field data analysis and process-based modeling.

Dr. Hotaek Park is a Senior Scientist at JAMSTEC. He earned his Ph.D. at Graduate School of Bioagricultural Sciences, Nagoya University in 2000. Then, he worked at two Japanese Institutes as postdoctoral fellowship and joined the position of JAMSTEC research scientist in 2007. He is an expert on hydrology, biogeochemistry, and climate researches in cold regions, with interests in evaluating changes in land surface processes under climate changes and predicting future changes using land surface model, remote sensing data, reanalysis products, in site observations, and model outputs. He has the author/co-author of numerous scientific articles that have published on a variety of peer-reviewed journals, conference proceedings, and books. His recent research is focused on assessing impacts of changing snow and permafrost on hydrological processes in the context of climate variability and interactions between declining Arctic sea ice and terrestrial ecohydrologic processes coupling models of land–atmosphere–ocean processes.

Dr. John E. Walsh is the Chief Scientist of the International Research Center and President's Professor of Global Change at the University of Alaska, Fairbanks, USA. He is also an emeritus faculty member of the University of Illinois. He has been involved in Arctic research and education for more than 40 years. His more recent research has addressed Arctic climate and weather variability, with an emphasis on the drivers of cryospheric variations over seasonal to multidecadal timescales. He has served as lead author for assessment reports of the Intergovernmental Panel on Climate Change, the Arctic Monitoring and Assessment Programme, and the U.S. National Climate Assessment. He has also co-authored a textbook, Severe and Hazardous Weather. He received a B.S. in Mathematics from Dartmouth College and a Ph.D. in Meteorology from the Massachusetts Institute of Technology.

Ke Zhang is a Professor of Hydrology and Water Resources in College of Hydrology and Water Resources at Hohai University, China. He received his Ph.D. in Ecohydrology in 2009 from University of Montana, USA and his Master's in Hydrology and Water Resources from Hohai University, China. Prior to joining Hohai University, he worked as a research scientist and research associate at University of Oklahama and Harvard University for five years. His research interest includes hydrological modeling, hydrometeorology, ecohydrology, land surface remote sensing and modeling, and climate change. He has published more than 90 articles in peer-reviewed journals, authored 6 book chapters, and presented more than 60 research papers in national and international conferences. He has frequently served as reviewers for more than more than 30 international journals. He also serves as associate editor for Journal of Hydrology, Frontiers in Earth Science, and Water Science and Engineering, and editorial board member for Environmental Modelling & Software, Scientific Reports, and Hydrology Research.

Greenland Ice Sheet and Arctic Mountain Glaciers

5

Sebastian H. Mernild, Glen E. Liston, and Daqing Yang

Abstract

This chapter provides a review and update of meltwater and Arctic hydrology, and the impact of glacier and ice sheet mass balance contributions to sea-level rise and ocean circulation. It highlights the recent work and results of large-scale modeling of Greenland climate, glaciers, and ice caps and Greenland Ice Sheet (GrIS) mass balances, and Greenland spatiotemporal freshwater runoff to the surrounding oceans and seas (spatiotemporal runoff simulations based on SnowModel/HydroFlow generated individual drainage catchments for Greenland (n = 3,150), each with an individual flow network). The mass balance for the GrIS was close to equilibrium during the relatively cold 1970s and 1980s and lost mass rapidly as the climate warmed in the 1990s and 2000s. Since 2003, the average annual GrIS mass loss rate was 250–300 $km^3\ yr^{-1}$ (equal to 250–300 $Gt\ yr^{-1}$). This represents a GrIS

S. H. Mernild (✉)
Nansen Environmental and Remote Sensing Center, Thormøhlens Gate 47, 5006 Bergen, Norway
e-mail: sebastian.mernild@nersc.no; smernild@gmail.com

Faculty of Engineering and Science, Western Norway University of Applied Sciences, Sogndal, Norway

Direction of Antarctic and Sub-Antarctic Programs, Universidad de Magallanes, Punta Arenas, Chile

Geophysical Institute, University of Bergen, Bergen, Norway

G. E. Liston
Cooperative Institute for Research in the Atmosphere (CIRA), Colorado State University, Fort Collins, CO, USA
e-mail: glen.liston@colostate.edu

D. Yang
Environment and Climate Change Canada, Watershed Hydrology and Ecology Division, Victoria, BC, Canada
e-mail: daqing.yang@canada.ca; daqing.yang@gmail.com

D. Yang and D. L. Kane (eds.), *Arctic Hydrology, Permafrost and Ecosystems*,
https://doi.org/10.1007/978-3-030-50930-9_5

loss rate equivalent to a eustatic sea-level rise contribution of 1.1 mm SLE yr^{-1}, compared to a mean estimated global sea-level rise of 3.3 ± 0.4 mm SLE yr^{-1} from 1993 to 2009, and an average 4.8 mm SLE yr^{-1} for 2013–2018. Not only has the GrIS lost mass, the land- and marine-terminating outlet glaciers on the periphery of the GrIS have undergone rapid mass and area changes over the recent decades. For example, for the last decade (2000–2010) the average simulated Greenland runoff was 572 ± 53 km^3 yr^{-1} (1.6 ± 0.2 mm SLE yr^{-1}), where the simulations indicated that 69% of the runoff to the surrounding seas originated from the GrIS and 31% came from the land area.

5.1 Introduction

The Greenland ice sheet (GrIS) is the largest reservoir of permanent snow and ice in the Arctic (*c.* 7.4 m sea-level equivalent [SLE]), and it is highly sensitive to ongoing climatic variations and changes (e.g., Hanna et al. 2012; Box and Colgan 2013). Since 1979, satellite observational studies (Mote 2007; Steffen et al. 2008; Tedesco et al. 2011, 2017) have demonstrated that the GrIS melt extent has increased, and that the melt extent is very sensitive to climate changes, with record melt extent in 2012 (Nghiem et al. 2012; Hall et al. 2013). Further, GrIS melt from 1960 to 1972 was simulated by Mernild et al. (2011a), which indicated an average decrease in melt extent of 6%; during 1973–2010, however, average melt extent increased by 13%, with the record melt in 2012 (Hanna et al. 2014). The simulated trends in melt extent were similar to the smoothed trend of the AMO index (Atlantic Multidecadal Oscillation) (Mernild et al. 2011a). The trend in simulated melt extent since 1972 also indicated that the melt period increased by an average of two days yr^{-1} since 1972, including an extended melting period for the GrIS of about 70–40 days and 30 days in the spring and autumn, respectively.

The exceptional 2012 melt event (July 12) was simulated by SnowModel in Hanna et al. (2014), showing that surface melt covered 90% of the GrIS surface area, which concurs with the 95–98% melt extent from Nghiem et al. (2012) and Hall et al. (2013). This widespread melt event during the satellite era was forced by a blocking high-pressure feature in the mid-troposphere forming a heat dome over Greenland that led to the widespread surface melting (Hanna et al. 2014; Keegan et al. 2014).

The changes in the GrIS melting regime (extent and duration) can produce substantial differences in surface albedo and energy and moisture balances, and may establish a positive feedback mechanism, because wet (i.e., below the dry snow line) snow absorbs up to three times as much incident solar energy as dry, non-melting snow (Steffen 1995). An altered melt regime can, for example, influence the ice sheet's surface mass balance (SMB), supraglacial lake volumes, snowmelt and ice melt runoff, ice surface velocity, and subglacial sliding processes. One would expect that increasing annual ablation would cause increasing mean annual ice-flow velocity, because of the increasing volume of lubricating surface meltwater reaches

the ice–bedrock interface (Joughin et al. 2008). However, for a land-terminating sector of the GrIS, it has been shown that a higher average annual ablation does not necessarily lead to an increase in annual ice velocities (van der Wal et al. 2008).

5.2 Greenland Ice Sheet

5.2.1 Greenland Ice Sheet Surface Hydrological Conditions

Mechanisms that link climate, surface hydrology, internal drainage, and ice dynamics are poorly understood, and numerical ice sheet models do not simulate these changes realistically (Nick et al. 2009). From 1960 to 2010, the GrIS surface hydrological conditions, net accumulation (precipitation minus evaporation and sublimation), runoff, and SMB (Fettweis et al. 2008; Hanna et al. 2008; Ettema et al. 2009; Mernild and Liston 2012), were influenced climatically first by decreasing air temperature (1960–mid-1980s) and then by increasing air temperature and net precipitation (mid-1980s–present; Cappelen 2013). The associated increase in surface runoff leads to enhanced SMB loss. Overall, for the GrIS, since the early 1990s to the late 2000s, the amount of runoff to adjacent seas explains about half of the recent annual GrIS mass loss (Rignot and Kanagaratnam 2006; van den Broeke et al. 2009), with iceberg calving generating the other half (Straneo et al. 2013). During 2009–2012, however, freshwater runoff has been estimated to explain around two-thirds of the mass loss of the GrIS (Enderlin et al. 2014). For the GrIS, subtracting the average surface runoff from the net precipitation yielded a surface mass gain, with an average annual GrIS SMB of 156 ± 82 km^3 yr^{-1} (1960–2010), varying from 220 ± 86 km^3 yr^{-1} in 1970–1979 to 86 ± 72 km^3 yr^{-1} in 2000–2010 (Mernild and Liston 2012). Mernild et al. further projected, on average, a GrIS SMB mass loss after 2040—indicating that the GrIS *tipping point* (defined to be the point where the GrIS continuously face a negative SMB value; Bamber et al. 2009) will occur after 2040, based on the IPCC A1B scenarios; the values were in the same range as projections by Fettweis et al. (2008) and Pattyn et al. (2018).

While, on average, the GrIS surface was gaining mass (1960–2010; with a positive SMB) and closely following mean temperature fluctuations; the overall mass balance for the GrIS was close to equilibrium during the relatively cold 1970s and 1980s and lost mass rapidly as the climate warmed in the 1990s and 2000s, with no indications of deceleration (Rignot et al. 2008; Tedesco et al. 2017). Since 2003, the average annual GrIS mass loss rate was 250–300 km^3 yr^{-1} (equal to 250–300 Gt yr^{-1}); in particular, from April 2010 to April 2011, the ice sheet cumulative loss rate was 430 Gt yr^{-1}: 70% larger than the 2003–2009 average annual loss rate. This represents a GrIS loss rate equivalent to a eustatic sea-level rise contribution of 1.1 mm SLE yr^{-1} (where 362.5 Gt yr^{-1} = 1 mm SLE yr^{-1}), compared to a mean estimated global sea-level rise of 3.3 ± 0.4 mm SLE yr^{-1} from 1993 to 2009 (Church et al. 2013). According to the European Space Agency (ESA), the global mean sea-level rise was 4.8 mm SLE yr^{-1} for 2013–2018 (http://www.esa.int).

In addition to the sea-level contribution, the increase in GrIS runoff (in net amount and duration), and in iceberg calving (in mass loss) are important for ocean density changes and the thermohaline circulation (e.g., Rahmstorf et al. 2005), specifically to the Atlantic Meridional Overturning Circulation (AMOC) and its impact on the climate system (Bryden et al. 2005). Over the past four decades, through the analysis of long-term hydrographic records, the system of overflow and entrainment that ventilates the deep Atlantic has steadily changed, which led to the sustained and widespread freshening of the deep ocean (Dickson et al. 2002).

The AMOC may be sensitive to changes in salinity based on GrIS runoff and calving; freshening of surface waters in the northern North Atlantic inhibits deep convection that feeds the deep southward branch of the AMOC (e.g., Rahmstorf 1995). The AMOC carries warm upper waters into far-northern latitudes and returns cold deep waters southward to the southern hemisphere. This heat transport contributes substantially to the climate of continental Europe and the Northern North Atlantic region (Hanna et al. 2008), for example, any slowdown in the circulation due to the increasing terrestrial freshwater flux could have important implications for climate change (Bryden et al. 2005). This pathway between the GrIS and North Atlantic/European climate could be a key linkage in a broader climate feedback via ocean circulation, though the extent to which GrIS-induced climate change would, in turn, alter the GrIS is not known.

5.2.2 Greenland Area Changes

Not only has the GrIS lost mass but it has also faced area recession (Kargel et al. 2011). The land- and marine-terminating outlet glaciers on the periphery of the GrIS have undergone rapid area changes over the last decades (e.g., Howat and Eddy 2011), during which a transition occurred from stability and small fluctuations in marine-terminating glacier frontal positions (1972–1985) to moderate widespread recession in the southeast and western parts of the GrIS (1985–2000), followed by an accelerated net recession in all regions of the ice sheet (2000–2010) (Howat and Eddy 2011). For 2000–2010, the mean net recession rate for frontal positions of GrIS marine-terminating outlet glaciers was 0.11 km yr^{-1}, for 210 outlet glaciers (Howat and Eddy 2011). Box and Decker (2011) measured area changes of 39 widest GrIS marine-terminating glaciers based on Moderate Resolution Imaging Spectroradiometer (MODIS) data, between 2000 and 2010. Overall, for the 39 glaciers, they exposed a cumulative net area of 1,368 km^2. The recession in GrIS cover for the last decades for both land- and marine-terminating margins caused changes in the surface albedo and subsequent changes in the energy balance. This climate–ice sheet pathway may establish a positive feedback mechanism and an increase in GrIS melting, for example, due to more surface energy absorption.

5.3 Glacier and Ice Cap Changes

Half of the estimated global glacier and ice cap (GIC) surface area, and two-thirds of the GIC volume, are located in the circumpolar Arctic region (Radić and Hock 2010). This makes studies of SMB and volume changes in northern latitude GIC essential because of their contribution to global sea-level rise. However, few GIC SMB observations exist. SMB observations from around 25 GICs in the circumpolar Arctic (Alaska, Arctic Canada, Greenland, Iceland, and Svalbard) have been published for 2001–2010 (WGMS 2013), where Box et al. (2018), using up to 44 GIC, estimated the global sea-level contribution from Arctic land ice (1971–2017). This subset represents only a minor fraction of the Arctic's several thousand GICs. Furthermore, very few GIC has uninterrupted annual records covering at least two or more decades. Even though GICs account for less than 1% of all water on Earthbound in glacier ice, their increasing retreat and mass loss due to iceberg calving and runoff may have dominated the glacial component of the global eustatic sea-level rise during the past century (Radić and Hock 2011; Box et al. 2018). The Arctic Monitoring and Assessment Program (AMAP) identified the Arctic as the largest regional source of land ice to global sea-level rise (2003–2014; AMAP 2017).

The GIC mass balance observations have shown an overall increase in mass loss (Dyurgerov 2010; Cogley 2012; WGMS 2013; Box et al. 2018), heading toward more negative annual SMB during the first 15 years (2001–2016) of the first decade in the twenty-first century. For example, Gardner et al. (2011) showed that Canadian Arctic Archipelago GIC had recently lost 61 ± 7 Gt yr^{-1} ice in the period 2004–2009. In East Greenland (peripheral to the GrIS), GICs have also lost mass and faced area recession. A study by Mernild et al. (2015a, b), based on satellite observations of 35 GICs in East Greenland, determined a mean areal recession of around 1% per year, indicating that GICs overall have lost 27 ± 24% of their area since 1986. Furthermore, five GICs have melted away, and GICs, on average, have faced a volume recession of one-third since 1986 (Mernild et al. 2015a, b). Specific GICs in East Greenland might be significantly out of equilibrium with the present-day climate and will likely lose at least 70% of their current area and 80% of its volume, even in the absence of further climate changes. Temperature records from coastal stations in East Greenland suggest that recent GIC area and volume losses are out of equilibrium and not merely a local phenomenon; they are indicative of glacier changes in the broader region (Mernild et al. 2011b). Globally, GICs will shed around one-quarter of their present-day volume if they are to reach a size in equilibrium with the present-day climate (Mernild et al. 2013), indicating that Greenland GIC area and volume adjustment lag behind the current climatic forcing (Cogley 2012).

At present, GIC mass losses are raising the mean global sea level by approximately 1.0 mm SLE yr^{-1}). This is about one-third of the total rate of sea-level rise inferred from satellite altimetry, with ocean thermal expansion and ice sheet mass loss accounting for most of the remainder (e.g., Cazenave and Llovel 2010). It has

been suggested that GIC SMB losses are expected to dominate the cryospheric contribution to sea-level rise between now and 2100 (Cogley 2012) and that the GIC derived sea-level rise will continue to increase in the future (Dyurgerov and Meier 2005; Meier et al. 2007), with the largest contribution from Arctic circumpolar GICs in Arctic Canada and Alaska.

5.4 Recent Model Development—A Runoff Routing Model (HydroFlow)

Liston and Mernild (2012) developed a gridded linear reservoir runoff routing model (HydroFlow) to simulate the linkages between runoff production from land-based snowmelt and ice melt processes and the associated freshwater fluxes to downstream areas and surrounding oceans. HydroFlow was specifically designed to account for the glacier, ice sheet, and snow-free and snow-covered land applications. Its performance was verified for a test area in southeast Greenland (Figs. 5.1 and 5.2) that contains the Mittivakkat Glacier (formerly known as Midtluagkat Gletscher (26.2 km^2 in 2011); 65°41′N, 37°48′W), the local glacier in Greenland with the longest observed time series of mass balance and ice-front fluctuations. The time evolution of spatially distributed grid cell runoff required by HydroFlow (Liston and Mernild 2012) was provided by the SnowModel (Liston and Elder 2006a; Mernild et al. 2006), i.e., the snow evolution modeling system, driven with observed atmospheric data, for the years 2003 through 2010 (Liston and Mernild 2012). In general, the HydroFlow simulated runoff variations and peaks reproduced available discharge observations from the Mittivakkat Glacier (r^2 = 0.77 and 0.63), both in time and volume (Fig. 5.3). For 2003 and 2010, the difference between simulated and observed runoff was ~12,000 m^3 (analog to a mean discharge difference of 0.14 m^3 s^{-1}) and ~2,200 m^3 (0.03 m^3 s^{-1}), respectively, where positive numbers mean the model is overestimating observed values, and vice versa. Comparison of simulated and observed peak runoff values indicate a maximum difference of ~267,000 m^3 (analog to a maximum discharge difference of 3.10 m^3 s^{-1}) for 2003 and ~453,000 m^3 (5.25 m^3 s^{-1}) for 2010 (Fig. 5.3). Overall, for the two analyzed years, HydroFlow was able to reproduce mean and peak control values within acceptable limits (Liston and Mernild 2012).

Figure 5.3 display the within-catchment runoff variability by plotting the hydrographs at locations A1–A4 for 2003 and 2010 within the Mittivakkat Glacier catchment. Consistent with the model formulation, the hydrographs for both 2003 and 2010 increased in volume and runoff period downstream as the flow network progressed down basin from point A1–A4. This occurs in response to both decreasing elevation and increasing drainage area. Further, seasonal runoff variations were similar for all four locations, with the most pronounced being at the outlet (A4) and the least pronounced being upstream (A1).

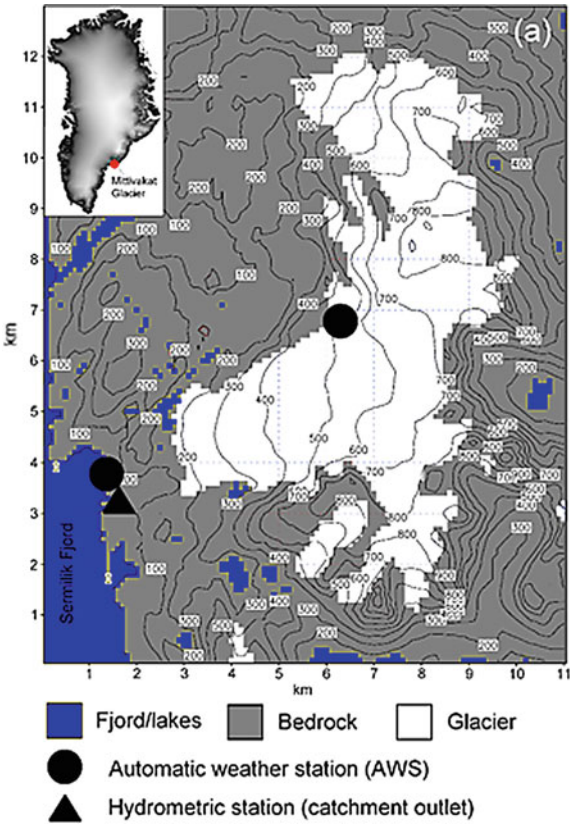

Fig. 5.1 The Mittivakkat Glacier simulation domain, in southeast Greenland (around 10–12 km northwest of the settlement Tasiilaq), with topography (100-m contour interval) and land cover characteristics. Also shown are the two automatic weather stations, Station Nunatak (515 m a.s.l.) and Station Coast (25 m a.s.l.), and the hydrometric station at the A4 catchment outlet (for locations of the different catchment outlets see Fig. 5.2). The inset figure indicates the general location of the Mittivakkat Glacier region (red dot) in southeast Greenland. The domain coordinates can be converted to UTM by adding 548 km to the west–east origin (easting) and 7281 km to the south–north origin (northing) and converting to meters (Mernild and Liston 2012, © American Meteorological Society. Used with permission)

The simulated runoff values at the B1, A4, C1, and D1 catchment outlets (Fig. 5.3), display the spatial variation in coastal runoff contributions from these primary catchments that drain into Sermilik Fjord, Southeast Greenland. At regional scales, the spatial variation in runoff was closely associated with variations in glacier cover, size of the drainage area, and travel distance within each catchment (Fig. 5.3). The watersheds upstream of outlets A4 and C1 produced the greatest runoff contribution to Sermilik Fjord.

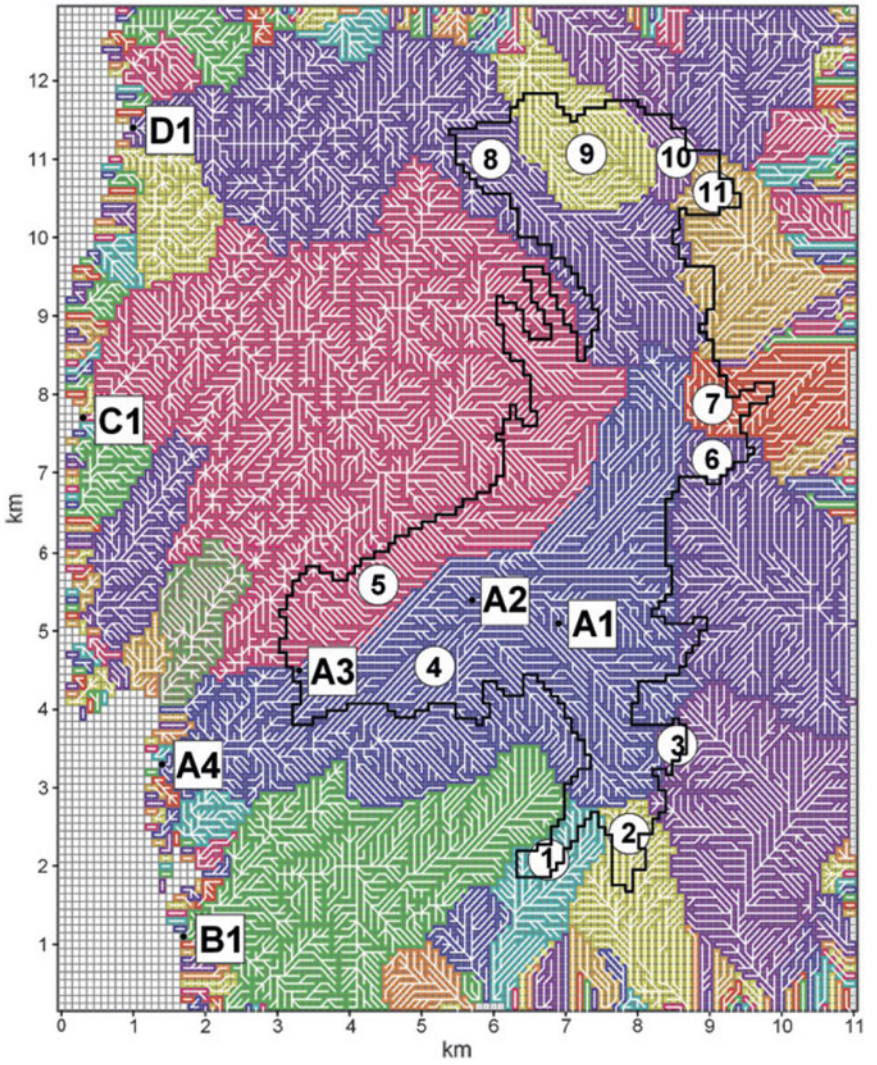

Fig. 5.2 Mittivakkat Glacier complex (represented by the bold black line) and simulation domain including individual glacier basins (Area 1–11) (represented by different colors), stream/river flow network (represented by white lines), and locations B1, A4, C1, D1, A3, A2, and A1 for the simulated hydrographs

The 2003–2010 mean cumulative annual discharge (m^3) into Sermilik Fjord from catchment outlets B1, A4, C1, and D1 is illustrated in Fig. 5.3. Figure 5.4 displays the mean cumulative annual discharge (m^3) from all the catchment outlets along the eastern coast of the simulation domain (they all feed into Sermilik Fjord) for 2003 and 2010. The dominance of the B1, A4, C1, and D1 outlets are clear in

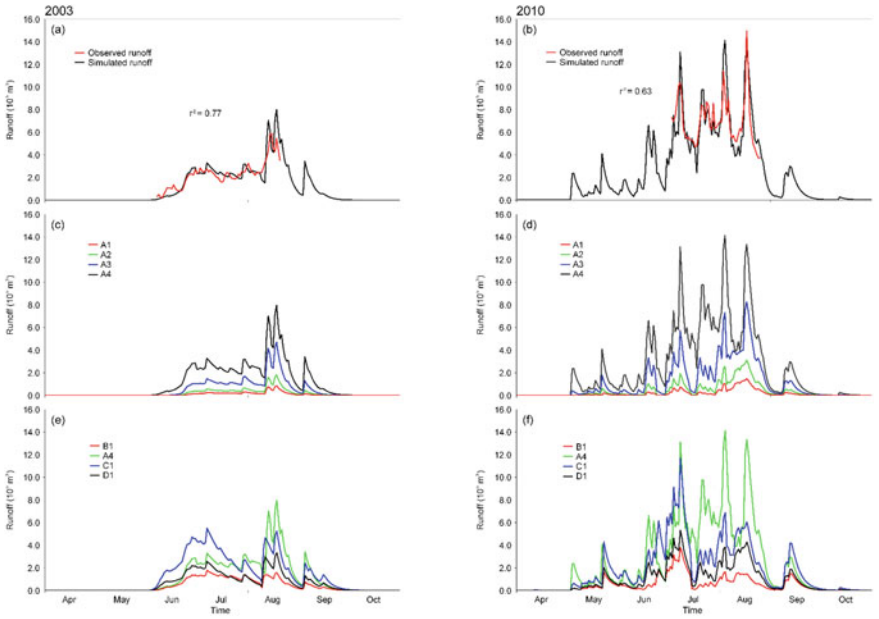

Fig. 5.3 **a** Observed and simulated runoff at the location for 2003 (the year with the second-lowest cumulative runoff); and **b** 2010 (the year with the highest cumulative runoff) (r^2 = square of the linear correlation coefficient), the observation period is shorter than the simulation period; **c**, **d** simulated hydrographs at different locations upstream for outlet A4; and **e**, **f** simulated hydrographs at outlets B1, A4, C1, and D1 to the Sermilik Fjord (for outlet locations see Fig. 5.2) (Mernild and Liston, 2012, © American Meteorological Society. Used with permission)

Fig. 5.4. The percentage of total annual discharge represented by the B1, A4, C1, and D1 outlets is also shown. In 2003 and 2010, 84% and 90%, respectively, of the eastern coastal discharge came from outlets B1, A4, C1, and D1. Averaged over the 2003–2010 simulation period, outlets B1, A4, C1, and D1 contributed approximately 90% of the annual discharge ($128.9 \pm 34.1 \times 10^6$ m^3 yr^{-1} with a standard deviation of $\pm 34.1 \times 10^6$ m^3 yr^{-1}) to Sermilik Fjord. Taken individually, the average contributions from C1 ($38.5 \pm 22.2 \times 10^6$ m^3 yr^{-1}) and A4 ($40.9 \pm 13.7 \times 10^6$ m^3 yr^{-1}) were each approximately 30% of the total, and contributions from B1 ($14.7 \pm 5.8 \times 10^6$ m^3 yr^{-1}) and D1 ($22.4 \pm 8.0 \times 10^6$ m^3 yr^{-1}) were each approximately 15% of the total. For the watersheds, without glacier cover (these comprised approximately 90% of the catchments) the cumulative annual discharge to the ocean was relatively low, in the range of 1.0×10^4 to 1.0×10^5 m^3 y^{-1}. This uneven spatial distribution of runoff to the ocean (Fig. 5.4) is expected to occur throughout East Greenland where the strip of land between the GrIS and ocean contains thousands of individual glaciers, ice caps, and ice-free areas peripheral to the Ice Sheet.

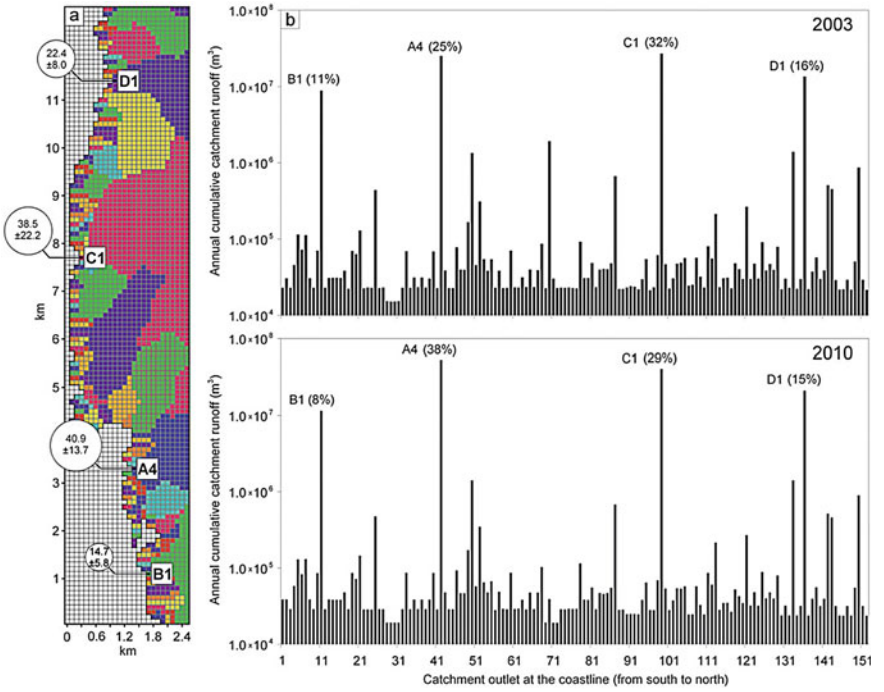

Fig. 5.4 **a** 2003–10 mean and standard deviation of annual simulated cumulative runoff to the Sermilik Fjord from catchment outlets D1, C1, A4, and B1 (10^6 m^3 y^{-1}); and **b** spatial runoff distribution to Sermilik Fjord for 2003 and 2010. The percentages indicate the fraction of annual discharge into Sermilik Fjord from outlets D1, C1, A4, and B1. Note the ordinate logarithmic scale (Mernild and Liston 2012, © American Meteorological Society. Used with permission)

One source of uncertainty in the HydroFlow simulations results from processes occurring within the watershed of interest that are not included in the modeling system. While the improvements included in HydroFlow can be thought of as a step forward in runoff simulations for snowmelt and ice melt on glaciers, ice sheets, and snow-covered land, there are still numerous water-transport-related processes that are not explicitly included in the model simulations. HydroFlow, for example, as with most other models, omits processes such as temporal variations in (1) englacial bulk water storage and release, including drainage from glacial surges and drainage of glacial-dammed water (long-term build-up of storage followed by short-term release); (2) melt contributions from internal glacial deformation, geothermal heat, basal sliding, and the internal drainage system as it evolves during the melt season; (3) englacial water flow between neighboring catchments; and 4) open channel streamflow routing. In addition, SnowModel is not a dynamic glacier model, and routines for simulating changes in the glacier area, size, surface elevation, and

seasonal variations in the internal drainage system, are not yet represented within the modeling system.

Uncertainty in the simulated runoff discharges also occurs as a result of over-simplifications of the processes represented within the modeling system and due to simplified representations of the atmospheric forcing (e.g., air temperature and precipitation). At present, physically based glacier runoff models are simple representations of a complex natural system (e.g., Hock and Jansson 2005). But with the HydroFlow routines for estimating drainage area, watershed divides, the flow-accumulation network, the time evolution and spatial distribution of different water transport mechanisms, and the runoff transient times, we are now able to provide information about the temporal and spatial variability in runoff at each point within the catchment, including the watershed outlet and at every watershed, large and small, within the simulation domain. A further advantage of this spatially distributed modeling approach is that it also allows detailed analyses of within-watershed runoff-related processes such as those associated with solute transport and sediment erosion and accumulation (Hasholt and Mernild 2006). While good model performance at gauging stations does not ensure good performance at sites upstream of those stations (Refsgaard 1997), the nested watersheds within the simulation domain considered herein have similar physical and climatological conditions as the outlets of the main catchments. Therefore, we also expect similar behavior in them. In addition, the physically based representations contained within MicroMet (Liston and Elder 2006b) and SnowModel make them appropriate tools to simulate rainwater, snowmelt, and ice melt fluxes, and it is also appropriate to use their outputs to drive HydroFlow, for both gauged and ungauged basin applications. At the largest scale, the combination of MicroMet, SnowModel, and HydroFlow provides the ability to estimate the time evolution and spatial distribution of runoff into adjacent oceans.

5.5 Greenland Freshwater Runoff

5.5.1 Regional Runoff Distribution

Mernild and Liston (2012) examined the GrIS surface mass balance conditions, including GrIS and Greenland surface runoff, the spatial distribution of Greenland runoff to the adjacent seas, and their changes from 1960 to 2010. They coupled the HydroFlow runoff routing model with SnowModel. They ran the coupled modeling system over the GrIS and all surrounding land and peripheral glaciers and ice caps for the period 1960 through 2010, using a 5-km grid and outputting daily hydrological variables. HydroFlow divided all of Greenland, including the GrIS, into individual drainage basins (Fig. 5.5) and simulated the associated grid connectivity —its water routing network—within each individual watershed; in total, there were $n = 3{,}150$ individual drainage catchments. SnowModel and HydroFlow were forced with observed meteorological data, and the overall trends and annual

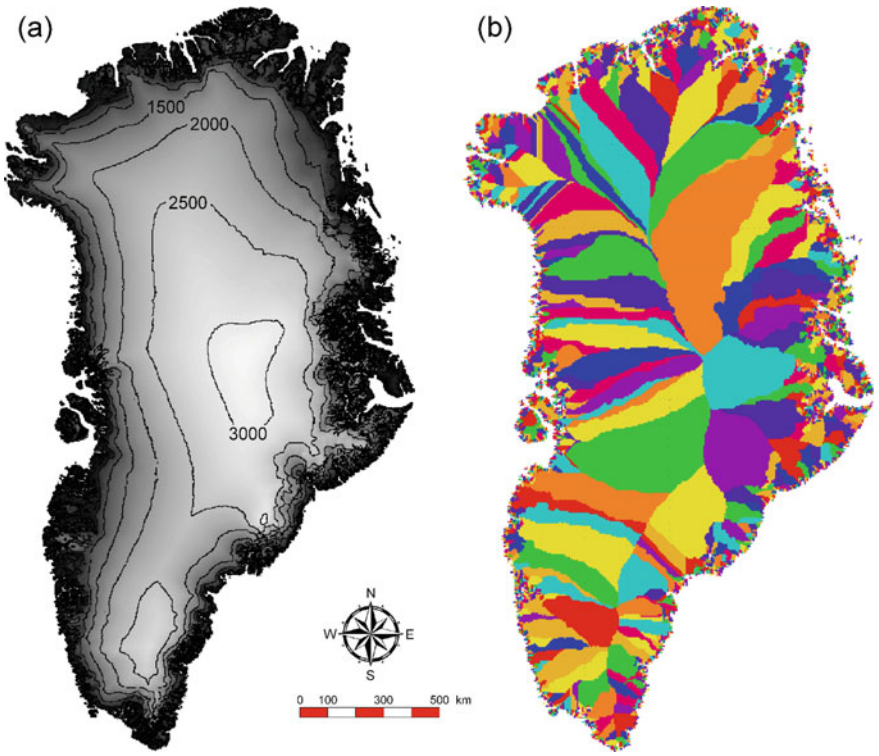

Fig. 5.5 **a** Greenland; and **b** simulated individual Greenland drainage basins (represented by multiple colors)

variability in air temperature and runoff were related to both variations and trends in the Atlantic Multidecadal Oscillation (AMO) index (e.g., Folland et al. 1986; Schlesinger and Ramankutty 1994; Kerr 2000; Chylek et al. 2009, 2010) to illustrate the impact from regional weather systems and the impacts from major episodic volcanic eruptions as part of an effort to understand the runoff response to natural forcing. They further examined whether the spatial runoff distribution from the warmest decade on record (2001–10) (Hansen et al. 2010) was different from the runoff distribution from both the average of 1960–69 and the average of 1960–2010.

5.5.2 Climate and GrIS Mass Balance

From 1960 to 2010, the Greenland mean summer air temperature and mean annual air temperature (MAAT) increased an average of 1.9 and 1.2 °C, respectively. The last decade (2000–2010) has been the warmest decade on record (Hansen et al.

2010). However, before the mid-1980s, the trend in mean summer temperature correlates significantly with MAAT and was in the antiphase, meaning JJA was on average increasing while MAAT was on average decreasing, and hereafter the trends were in phase and increasing. Since the mid-1980s, mean summer temperature and MAAT increased an average of 1.5º and 2.2 °C, respectively (Mernild et al. 2011a). Hanna et al. (2008) found an increase in coastal Greenland summer temperatures by 1.8 °C during 1991–2006.

The overall variations in SnowModel simulated mean summer temperature explain the variance significantly, with the smoothed trends of the AMO index. A similar condition between summer temperature and AMO variations was confirmed by Hanna et al. (2012). From 1960 to the mid-1970s, the smoothed AMO index, on average, decreased, and thereafter, it increased through 2010, corresponding with the trend in simulated mean summer temperature for Greenland. Chylek et al. (2010) showed that Arctic temperatures were highly correlated with the AMO index, suggesting the Atlantic Ocean as a possible source of Arctic climate variability. This was also the case for the simulated Greenland MAAT for which the explained variance was significant for the periods after the mid-1980s (1986–2010) and before that time (1960–1985); however, the latter period had a higher r^2-value that explained more of the variance (Mernild and Liston 2012).

Figure 5.6 presents time series (1960–2010) of simulated GrIS surface hydrological conditions: net precipitation (precipitation minus evaporation and sublimation), surface runoff, and SMB on an annual basis for the calendar year (1 January–31 December). GrIS mass gain (accumulation) was calculated as positive and mass loss (ablation) was considered negative. The average 1960–2010 simulated GrIS net precipitation was 489 ± 53 km^3 yr^{-1}, varying from 456 ± 46 km^3 yr^{-1} in 1960–1969 to 516 ± 38 km^3 yr^{-1} in 2000–2010. The simulated average GrIS net precipitation was just below the range of recently reported average net precipitation values, and these studies all reported similar annual average increasing precipitation trends to those simulated by SnowModel (Box et al. 2006; Hanna et al. 2005, 2008; Fettweis 2007; Fettweis et al. 2008; Ettema et al. 2009). Averaged for the GrIS, 85% of the SnowModel simulated precipitation fell as snow, with the rest falling as rain.

On a decadal time scale, the GrIS SMB decadal variability ranged from 220 ± 86 km^3 yr^{-1} in 1970–1979 to 86 ± 72 km^3 yr^{-1} in 2000–2010. The simulations showed the largest (most positive) SMB near the beginning of the simulation period, with a subsequent mass loss as temperatures and runoff increased. For the GrIS, during 1960–2010 the accumulation zone covered an average of 90% of the total GrIS area, and the ablation zone an average of 10%. In contrast, the simulated area generating surface runoff covered an average of 12% and surface melt an average of 15% of the GrIS (Mernild and Liston 2012). A maximum SnowModel simulated ablation zone width of 125 km occurred in the southwest region of the GrIS and was almost as wide for the northeast GrIS. In contrast, the narrowest ablation zone had a maximum width of 10–20 km and occurred in both the northwest and the southeast regions of the GrIS, a distribution predominantly following elevation changes and the spatial variability in precipitation. Therefore,

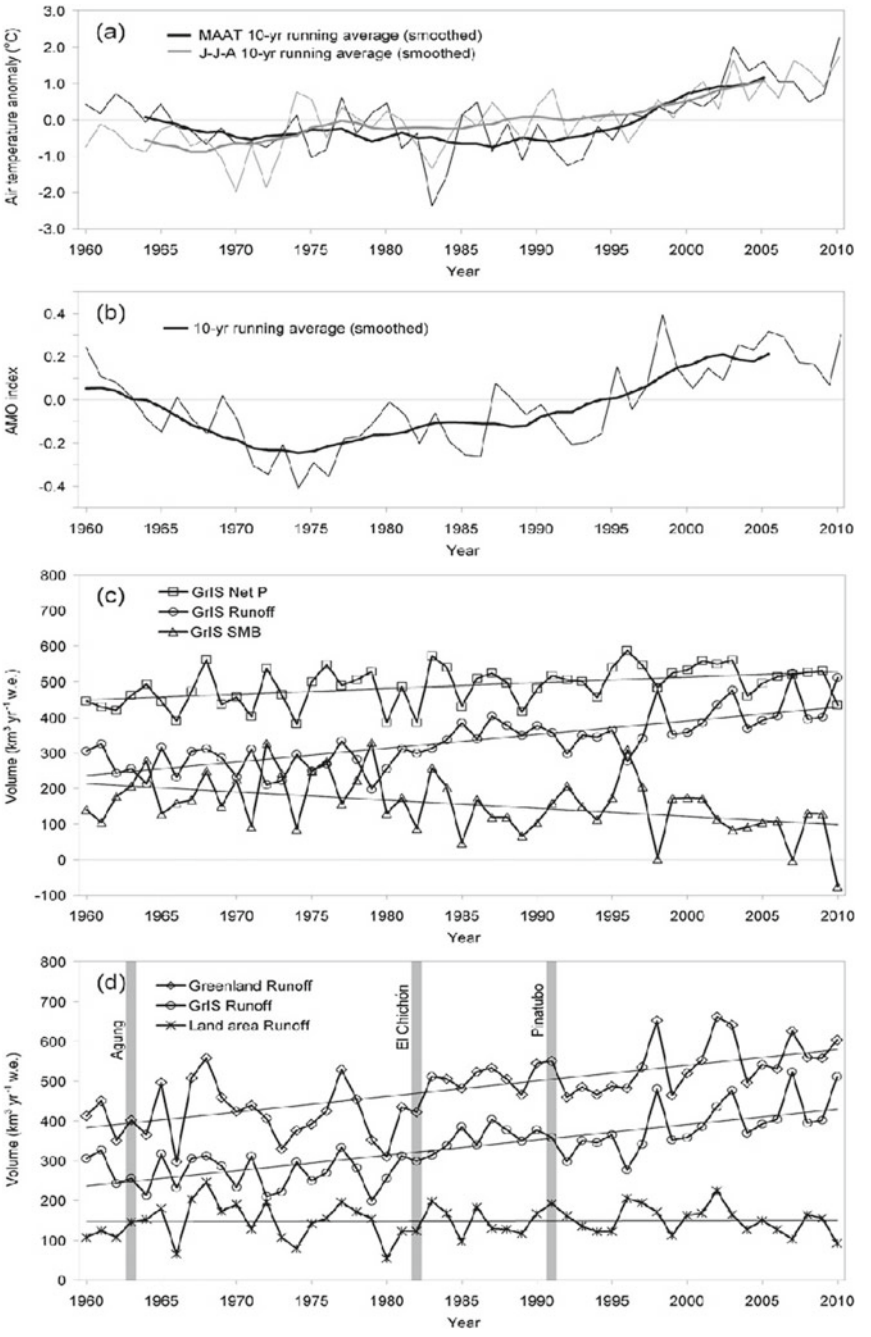
(a)
MAAT 10-yr running average (smoothed)
J-J-A 10-yr running average (smoothed)
Air temperature anomaly (°C)
Year
(b)
10-yr running average (smoothed)
AMO index
Year
(c)
GrIS Net P
GrIS Runoff
GrIS SMB
Volume (km³ yr⁻¹ w.e.)
Year
(d)
Greenland Runoff
GrIS Runoff
Land area Runoff
Agung
El Chichón
Pinatubo
Volume (km³ yr⁻¹ w.e.)
Year

◀

Fig. 5.6 **a** Simulated mean summer (JJA) and mean annual air temperature (MAAT) Greenland anomaly time series for 1960–2010; **b** unsmoothed and smoothed (10-yr running average) Atlantic multidecadal oscillation (AMO) index; **c** GrIS simulated net precipitation *P*, surface mass balance (*SMB*), and surface runoff *R* time series for 1960–2010; and **d** simulated surface GrIS runoff, land strip area (area outside the GrIS) runoff, and Greenland runoff time series for 1960–2010. The Agung (1963; Bali), El Chichón (1982; Mexico), and Mt. Pinatubo (1991; Philippines) volcanic eruptions are marked in **d**

the widest ablation zones occurred in relatively low precipitation regions, and the narrowest zones occurred in the high precipitation areas. The spatial variability in simulated GrIS ablation zones was in general agreement with Ettema et al. (2009).

5.5.3 Spatial and Temporal Distributions and Trends

Figure 5.6 presents the time series of simulated Greenland runoff (1960–2010) and individual runoff contributions from the GrIS and from the land area—including thousands of glaciers and ice caps—located between the ice sheet and the surrounding oceans. The 1960–2010 average, simulated Greenland runoff was 481 ± 85 km^3 yr^{-1} (in a sea-level perspective 1.3 ± 0.2 mm SLE yr^{-1}), varying from 413 ± 56 km^3 yr^{-1} (1.1 ± 0.2 mm SLE yr^{-1}) in 1960–69 to 572 ± 53 km^3 yr^{-1} (1.6 ± 0.2 mm SLE yr^{-1}) in 2000–10, following the trends in air temperature and precipitation (Fig. 5.6a, c).

Regionally, the average Greenland 1960–2010 simulated runoff to the adjacent seas was greater in the western half of Greenland, 263 km^3 yr^{-1} (equals 55% of the total Greenland runoff), than in the eastern half of Greenland, 218 km^3 yr^{-1} (45%) (indicating an insignificant regional difference). The average Greenland 1960–2010 simulated runoff to the adjacent seas was greatest from the south part (88 km^3 yr^{-1}) and southwest part (82 km^3 yr^{-1}) and lowest from the east part (45 km^3 yr^{-1}) and southeast sector (49 km^3 yr^{-1}) (1960–2010). The regional distribution of runoff to the surrounding oceans appears to be in general agreement with Lewis and Smith (2009).

The runoff simulations indicated that 69% of the runoff to the surrounding seas originated from the GrIS and 31% came from the land area. For the land area, the trend in simulated runoff was constant (Fig. 5.6d), with an average runoff of 148 ± 41 km^3 yr^{-1}. A possible explanation for this is because the glaciers and ice caps are already melting all summer, and an enhanced melt season and melt extent were therefore not possible. In contrast, simulated GrIS runoff, on average, has increased 3.9 km^3 yr^{-1} since 1960, and there has been an enhanced surface melt extent (Fettweis et al. 2011; Mernild et al. 2011a).

The impact on runoff variability during 1960–2010, due to major episodic volcanic eruptions such as Agung (1963), El Chichón (1982), and Mt. Pinatubo (1991) (Fig. 5.6d), and in the years immediately after do not appear to be systematic. For the year immediately after Agung and Pinatubo, simulated annual

runoff values decreased, and they increased after El Chichón. The simulated Greenland runoff variations appear to be due to a combination of annual variations in both temperature and precipitation that are controlled by factors other than volcanic activity. Hanna et al. (2005) stated that global dust veils generated by volcanic activity might cool the polar regions and suppress ice sheet melt, but clearly, there are other aspects of the climate system that may offset the volcanic signal. In contrast, the general climate forcing conditions captured by variations in the smooth AMO index time series can be traced in the overall Greenland runoff pattern (Fig. 5.6d). In general, years with positive AMO index equaled years with relatively high Greenland simulated runoff volume (and relatively high mean summer temperatures), and years with negative AMO index had low runoff volume, with a significantly explained variance ($r^2 = 0.73$, $p < 0.01$) between the AMO index and Greenland runoff.

Generally, relatively high average surface runoff values were simulated for the southwest and southeast regions of Greenland, and sporadic high values were simulated in the north region with maximum values of 4–6 m water equivalent (w.e.) yr^{-1}. Elsewhere, the runoff was less with the lowest values in the northeast and northwest regions of less than 0.5 m w.e. yr^{-1}. This spatial simulated surface runoff distribution is largely in agreement with values from Lewis and Smith (2009). This regional pattern in surface runoff can be largely explained by the spatial distribution of precipitation, since snowfall (end-of-winter accumulation) and surface runoff are negatively correlated through surface albedo, snow depth, and snow characteristics (e.g., snow cold content) (Hanna et al. 2008; Ettema et al. 2009). For dry precipitation regions (west and northeast Greenland), the relatively low end-of-winter snow accumulation melts relatively fast during spring warmup. After the winter snow accumulation (albedo 0.50–0.80) has ablated, the ice surface albedo (0.40) promotes a stronger radiation driven ablation and surface runoff, owing to the lower ice albedo. For wet precipitation regions (southeast and northwest Greenland) the relatively high end-of-winter snow accumulation, combined with frequent summer snowfall precipitation events, keeps the albedo high. Therefore, in wet regions, it generally takes a longer time to melt the snowpack compared to dry regions before ablating the underlying glacier ice. For glaciers, ice caps, and the GrIS, snowpack retention and refreezing processes suggest that regions with relatively high surface runoff are synchronous with the relatively low end-of-winter snow accumulation because more meltwater was retained in the thicker snowpack, reducing runoff to the internal glacier drainage system (e.g., Hanna et al. 2008; Reijmer et al. 2012; Machguth et al. 2018).

For the GrIS itself, 87% of the GrIS runoff increase was due to increases in melt extent, 18% was due to increases in melt duration, and a reduction of 5% occurred because of a decrease in melt rates (87% + 18% – 5% = 100%). For the land area surrounding the GrIS, the weak increase in runoff to the surrounding oceans over the period 1960–2010 was due to a 0% change in melt extent, with a 108% increase due to an increase in melt duration and a runoff reduction of 8% due to a decrease in melt rates (0% + 108% – 8% = 100%). In summary, the strong increase in GrIS runoff was largely due to increases in melt extent, while the relatively small increase

in land area runoff was mainly due to changes in melt duration. This and the air temperature increases further suggest that the increase in discharge from Greenland to the surrounding oceans is primarily the result of increasing air temperatures that allow the melt to occur over more area of the GrIS. In addition, our analysis suggests that increases in the GrIS melt extent play a relatively larger role in the simulated runoff increases than do the melt rate and melt duration changes.

5.6 Model Limitations and Future Research Topics

In MicroMet, only one-way atmospheric coupling was provided, where the meteorological conditions were prescribed at each time step. In the natural system, the atmospheric conditions would be adjusted in response to changes in surface conditions and properties (Liston and Hiemstra 2011). Due to the use of the 5-km horizontal grid increments, snow transport, and blowing-snow sublimation processes (usually produced by SnowTran-3D in SnowModel) were excluded from the simulations because blowing snow does not typically move completely across 5-km distances. Static sublimation was, however, included in the model integrations. In HydroFlow, the generated catchment divides and flow network was controlled by the digital elevation model (DEM), i.e., exclusively by the surface topography and not by the development of the glacial drainage system. The role of GrIS bedrock topography on controlling the potentiometric surface and the associated meltwater flow direction was assumed to be a secondary control on discharge processes (Cuffey and Paterson 2010).

An example of the HydroFlow generated catchment divides and flow network is illustrated in detail in Figs. 5.2 and 5.5. Because the DEM is time-invariant, no changes though feedbacks from a thinning ice, ice retreat, and from changes in hypsometry will influence the catchment divides and the flow network patterns, including the glacial drainage system. Changes in runoff over time are therefore solely influenced by the climate signal and the surface snow and ice cover conditions (runoff was generated from gridded inputs from rain, snowmelt, and ice melt), not by the glacial drainage system. In HydroFlow, the meltwater flow velocities were gained from dye tracer experiments conducted both through the snowpack (in early and late summer) and through the englacial and subglacial environments (Mernild et al. 2006).

5.7 Summary and Potential Research Topics

We have investigated the impact of changes in Greenland weather and climate conditions on surface hydrological processes and runoff for the 50-year period 1960–2010. This included quantifying the spatial distribution and trends of meltwater and freshwater runoff into the adjacent seas from the GrIS and the land, ice

cap, and glacier areas between the GrIS and surrounding oceans. The merging of observed atmospheric forcing datasets with SnowModel—a snow and ice evolution system—and HydroFlow—a runoff routing system—allowed a detailed (5 km, daily) analysis and mapping of spatial variations in Greenland discharge to the adjacent seas and provided insights into the regional distribution of runoff features and quantities. Individual drainage catchments (n = 3,150), each with an individual flow network, were estimated for Greenland before simulating runoff to down flow areas and the surrounding oceans. Given the severe dearth of Greenland discharge observations, runoff simulations are crucial for understanding Greenland spatial and temporal runoff variations; this runoff explains half of the recent mass loss of the GrIS (van den Broeke 2009). Overall, Greenland has warmed and the runoff has increased during the last 50 years with the greatest runoff increase occurring in southwest Greenland and lower runoff increases occurring in northeast Greenland.

The spatial runoff distributions show greater hydrological activity in southwest Greenland and lowest for the northeast Greenland region, supporting the hypothesis that discharges into the adjacent seas are greatest in regions where snowfall (end-of-winter snow accumulation) is generally low and discharge is least in regions where snowfall is high. These processes and relationships are crucial for understanding the spatial distribution of runoff and its contribution to the surrounding oceans, and the linkages among a changing climate and the associated changes in runoff magnitudes and distributions. The Greenland simulations showed distinct regional (scale) runoff variability throughout the simulation domain.

Runoff magnitudes, the spatial patterns from individual Greenland catchments, and their changes through time (1960–2010) were simulated in an effort to understand runoff variations to adjacent seas and to illustrate the capability of SnowModel (a snow and ice evolution model) and HydroFlow (a runoff routing model) to link variations in the terrestrial runoff with ocean processes and other components of Earth's climate system.

Significant increases in air temperature, net precipitation, and surface runoff lead to enhanced and statistically significant Greenland ice sheet (GrIS) surface mass balance (SMB) loss. Total Greenland runoff to the surrounding oceans increased 30%, averaging 481 $\pm$ 85 $km^3\ yr^{-1}$. Averaged over the period, 69% of the runoff to the surrounding seas originated from the GrIS and 31% came from outside the GrIS from rain and melting glaciers and ice caps. The runoff increase from the GrIS was due to an 87% increase in melt extent, 18% from increases in melt duration, and a 5% decrease in melt rates (87% + 18% − 5% = 100%). In contrast, the runoff increase from the land area surrounding the GrIS was due to a 0% change in melt extent, a 108% increase in melt duration, and an 8% decrease in melt rate. In general, years with positive AMO index equaled years with relatively high Greenland runoff volume and vice versa. Regionally, a runoff was greater from western than eastern Greenland. Since 1960, the data showed pronounced runoff increases in west Greenland, with the greatest increase occurring in the southwest and the lowest increase in the northwest.

GIC and GrIS mass balance and runoff observations and modeling have expanded over the last several decades as the demand to understand and describe complicated physical atmosphere–snow–ice–water processes and interactions has increased. Even though over the last decades we have gained information about GIC and the GrIS surface mass balance, runoff, and mass balance conditions, there is still research to be conducted with the purpose of identifying, monitoring, quantifying, and determining processes, variabilities, and interactions regarding hydrological processes and the water balance related to GIC and the GrIS.

GIC are reservoirs of water, and our knowledge about future GIC mass balance and runoff projections is limited. In addition to already published GIC model studies, research that quantifies future runoff conditions would improve our understanding of individual GIC behavior: Such a study would be the first to quantify, for example, the runoff *Tipping Points* for GIC. After the occurrence of the runoff *Tipping Point,* the annual GIC runoff amount will, on the average, decline as reductions in glacier areas outweigh the effect of glacier melting (AMAP 2011). Such future simulations will also be able to help answer questions such as: within what range of years can we expect the runoff *Tipping Point* to occur for individual GIC?

We also need to better understand the link between the freshwater flux (and the HydroFlow spatiotemporal simulated runoff variability) and the hydrographic conditions near the GrIS glacier–ocean boundaries. This could be done, for example, for Ilulissat Icefjord, West Greenland, and Sermilik Fjord, Southeast Greenland, using, for example, quasi-continuous water salinity and temperature observations obtained by ringed seals near tidewater glacier margins. Instrumented seals provide a platform to examine the impacts from terrestrial freshwater on the otherwise inaccessible waters beneath the dense ice melangé within the first 0–10 km of a glacier's calving front (Mernild et al. 2015a, b).

The spatiotemporal distribution of freshwater runoff from Greenland is expected to have an effect on the North Atlantic oceanic conditions, including the AMOC (Rahmstorf et al. 2005), and their impacts on the climate system (Bryden et al. 2005). The HydroFlow modeling tool is capable of providing the missing connection between terrestrial water fluxes and ocean circulation features such as the AMOC. Historically, the representation of Greenland freshwater discharge into the oceans has been either non-existent or unrealistically simplistic. For example, ocean models have traditionally placed the freshwater runoff flux directly into the mid-ocean areas (Weijer et al. 2012) rather than accurately accounting for the spatial and temporal distributions of actual Greenland runoff.

References

AMAP (2011) Snow, water, ice, and permafrost in the arctic (SWIPA): climate change and the cryosphere. Arctic monitoring and assessment programme (AMAP). Oslo. Norway. Xii +538 pp

AMAP (2017) Snow, water, ice and permafrost in the arctic (SWIPA) 2017. Arctic monitoring and assessment programme (AMAP), Oslo, Norway. xiv+269 pp

Bamber, J. L., Steig, E., and Dahl-Jensen, D. 2009. What is the tipping point for the Greenland Ice Sheet. C15, Nuuk Climate Days, Changes of the Greenland Cryosphere Workshop & The Arctic Freshwater Budget International Symposium. Nuuk, Greenland, 25–27 August 2009

Box JE, Bromwich DH, Veenhuis BA, Bai L-S, Stroeve JC, Rogers JC, Steffen K, Haran T, Wang S-H (2006) Greenland ice sheet surface mass balance variability (1988–2004) from calibrated Polar MM5 output. J Clim 19:2783–2800

Box JE, Colgan W (2013) Greenland Ice sheet mass balance reconstruction. Part III: Marine ice loss and total mass balance (1840–2010). J Clim 26:6990–7002

Box J, Colgan W, Bert, Wouters B, Burgess D, O'Neel S, Thomson L, Mernild SH (2018) Global sea-level contribution from arctic land ice: 1971 to 2017. Accepted Environ Res Lett

Box JE, Decker DT (2011) Greenland marine-terminating glacier area changes: 2000–2010. Ann Glaciol 52:91–98

Bryden HL, Longworth HR, Cunningham SA (2005) Slowing of the Atlantic meridional overturning circulation at 25°N. Nature 438:655–657

Cappelen J (ed) (2013) Weather and climate data from Greenland 1958–2012—observation data with description. DMI Technical Report 13-11, Copenhagen, 23.

Cazenave A, Llovel W (2010) Contemporary Sea Level Rise. Ann Rev Mar Sci 2:145–173. https://doi.org/10.1146/annurev-marine-120308-081105

Church JA, Clark PU, Cazenave A, Gregory JM, Jevrejeva S, Levermann A, Merrifield MA, Milne GA, Nerem RS, Nunn PD, Payne AJ, Pfeffer WT, Stammer D, Unnikrishnan AS (2013) Sea level change. In: Stocker TF, Qin D, Plattner G-K, Tignor M, Allen SK, Boschung J, Nauels A, Xia Y, Bex V, Midgley PM (eds) Climate change 2013: the physical science basis. Contribution of working group i to the fifth assessment report of the intergovernmental panel on climate change. Cambridge University Press, Cambridge, United Kingdom and New York, NY, USA

Chylek P, Folland CK, Lesins G, Dubey MK (2010) Twentieth century bipolar seesaw of the Arctic and Antarctic surface air temperatures. Geophys Res Lett 37:L08703. https://doi.org/10.1029/2010GL042793

Chylek P, Folland CK, Lesins G, Dubey MK, Wang M (2009) Arctic air temperature change amplification and the Atlantic multidecadal oscillation. Geophys Res Lett 36:L14801. https://doi.org/10.1029/2009GL038777

Cogley JG (2012) The future of the world's glaciers. In: Henderson-Sellers A, McGuffie K (eds) The future of the world's climate, 197–222. Elsevier, Amsterdam

Cuffey KM, Paterson WSB (2010) The physics of glaciers. Fourth Edition. Elsevier, pp 693

Dickson B, Yashayaey I, Meincke J, Turrell B, Dye S, Holfort J (2002) Rapid freshening of the deep North Atlantic Ocean over the past four decades. Nature 416:832–837

Dyurgerov MB (2010) Data of glaciological studies—Reanalysis of glacier changes: From the IGY to the IPY, 1960–2008. Publication 108, Institute of Arctic and Alpine Research, 116 pp

Dyurgerov MB, Meier MF (2005) Glaciers and the changing earth system: a 2004 snapshot, occas. Paper 58, 117 pp. Institute of Arctic and Alpine Research, Boulder, Colorado

Enderlin EM, Howat IM, Jeong S, Hoh M-J, van Angelen JH, van den Broeke MR (2014) An improved mass budget for the Greenland ice sheet. Geophys Res Lett 41(3):866–872

Ettema J, van den Broeke MR, van Meijgaard E, van den Berg WJ, Bamber JL, Box JE, Bales RC (2009) Higher surface mass balance of the Greenland ice sheet revealed by high-resolution climate modeling. Geophys Res Lett 36:L125

Fettweis X (2007) Reconstruction of the 1979–2006 Greenland ice sheet surface mass balance using the regional climate model MAR. The Cryosphere 1:21–40

Fettweis X, Hanna E, Gallee H, Huybrechts P, Erpicum M (2008) Estimation of the Greenland ice sheet surface mass balance during 20th and 21st centuries. The Cryosphere 2:117–129

Fettweis X, Tedesco M, van den Broeke MR, Ettema J (2011) Melting trends over the Greenland ice sheet (1958–2009) from spaceborne microwave data and regional climate models. The Cryosphere 5:359–375

Folland CK, Palmer T, Parker DE (1986) Sahel rainfall and worldwide sea temperatures. Nature 320:602–607

Gardner AS, Moholdt G, Wouters B, Wolken GJ, Burgess DO, Sharp MJ, Cogley JG, Braun C, Labine C (2011) Sharply increased mass loss from glaciers and ice caps in the Canadian Arctic Archipelago. Nature 473(7347):357–360

Hall DK, Comiso JC, DiGirolamo NE, Shuman CA, Box JE, Koenig LS (2013) Variability in the surface temperature and melt extent of the Greenland ice sheet from MODIS. Geophys Res Lett 40(10):2120–2144

Hanna E, Fettweis X, Mernild SH, Cappelen J, Ribergaard M, Shuman C, Steffen K, Wood L, Mote T (2014) Atmospheric and oceanic climate forcing of the exceptional Greenland Ice Sheet surface melt in summer 2012. Int J Climatol 34:1022–1037. https://doi.org/10.1002/joc.3743

Hanna E, Huybrechts P, Janssens I, Cappelen J, Steffen K, Stephens A (2005) Runoff and mass balance of the Greenland ice sheet: 1958–2003. J Geophys Res 110:D13108

Hanna E, Huybrechts P, Steffen K, Cappelen J, Huff R, Shuman C, Irvine-Fynn T, Wise S, Griffiths M (2008) Increased runoff from melt from the Greenland ice sheet: a response to global warming. J Clim 21:331–341

Hanna E, Mernild SH, Cappelen J, Steffen K (2012) Recent warming in Greenland in a long-term instrumental (1881–2012) climatic context. Part 1: Evaluation of surface air temperature records. Environ Res Lett 7:045404

Hansen J, Ruedy R, Sato M, Lo K (2010) Global surface temperature change. Rev Geophys 48: RG4004

Hasholt B, Mernild SH (2006) Glacial erosion and sediment transport in the Mittivakkat Glacier catchment, Ammassalik island, southeast Greenland, 2005. IAHS 306:45–55

Hock R, Jansson P (2005) Modeling glacier hydrology. Anderson MG, McDonnell J (eds), Enzyclopedia of Hydrologcial Sciences, vol 4. John Wiley & Sons, Ltd, pp 2647–2655

Howat IM, Eddy A (2011) Multi-decadal retreat of Greenland's marine-terminating glaciers. J Glaciol 57:389–396

Joughin I, 7 others (2008) Continued evolution of Jakobshavn Isbrae following its rapid speedup. J Geophys Res 113(F4):F04006. https://doi.org/10.1029/2008JF001023

Keegan KM, Albert MR, McConnell JR, Baker I (2014) Climate change and forrest fires synergistically drive widesperad melt events of the Greenland Ice Sheet. Proc Nat Acad Sci 111 (22):7964–7967

Kargel JS, Ahlstrøm AP, Alley RB, Bamber JL, Benham TJ, Box JE, Chen C, Christoffersen P, Citterio M, Cogley JG, Jiskoot H, Leonard GJ, Morin P, Scambos T, Sheldon T, Willis I (2011) Brief communication Greenland's shrinking ice cover: "fast times" but not that fast. The Cryosphere 6:533–537. https://doi.org/10.5194/tc-6-533-2012

Kerr RA (2000) A North Atlantic climate pacemaker for the centuries. Science 288:1984–1985

Lewis SM, Smith LC (2009) Hydrological drainage of the Greenland ice sheet. Hydrol Process 23:2004–2011. https://doi.org/10.1002/hyp.7343

Liston GE, Elder K (2006a) A distributed snow-evolution modeling system (SnowModel). J Hydrometeorol 7:1259–1276

Liston GE, Elder K (2006b) A meteorological distribution system for high-resolution terrestrial modeling (MicroMet). J Hydrometeorol 7:217–234

Liston GE, Hiemstra CA (2011) The changing cryosphere: Pan-Arctic snow trends (1979–2009). J Clim 24:5691–5712

Machguth, M., Box, J. E., Fausto, R. S., and Pfeffer, W. T. 2018. Editorial: Melt Water Retention Processes in Snow and Firn on Ice Sheets and Glaciers: Observations and Modeling. *Front. Earth Sci.*, doi.org/10.3389/feart.2018.00105

Meier MF, Dyurgerov MB, Rick UK, O'Neel S, Pfeffer WT, Anderson RS, Anderson SP, Glazovsky AF (2007) Glaciers dominate eustatic sea-level rise in the 21st century. Science 317:1064–1067

Mernild SH, Holland DM, Holland D, Rosing-Asvid A, Yde JC, Liston GE, Steffen K (2015a) Freshwater flux and spatiotemporal simulated runoff variability into Ilulissat Icefjord, West Greenland, linked to salinity and temperature observations near tidewater glacier margins

obtained using instrumented ringed seals. J Phys Oceanogr 45(5):1426–1445. https://doi.org/10.1175/JPO-D-14-0217.1

Mernild SH, Knudsen NT, Lipscomb WH, Yde JC, Malmros JK, Jakobsen BH, Hasholt B (2011a) Increasing mass loss from Greenland's Mittivakkat Gletscher. The Cryosphere 5:341–348. https://doi.org/10.5194/tc-5-341-2011

Mernild SH, Lipscomb WH, Bahr DB, Radić V, Zemp M (2013) Global glacier retreat: A revised assessment of committed mass losses and sampling uncertainties. The Cryosphere 7:1565–1577

Mernild SH, Liston GE (2012) Greenland freshwater runoff. Part II: Distribution and trends, 1960–2010. J Clim 25(17):6015–6035

Mernild SH, Liston GE, Hasholt B, Knudsen NT (2006) Snow distribution and melt modeling for Mittivakkat Glacier, Ammassalik Island, Southeast Greenland. J Hydrometeorol 7:808–824

Mernild SH, Mote TL, Liston GE (2011b) Greenland ice sheet surface melt extent and trends, 1960–2010. J Glaciol 57(204):621–628. https://doi.org/10.3189/002214311797409712

Mernild SH, Malmros JK, Yde JC, de Villiers S, Wilson R, Hanna E, Knudsen NT (2015) Glacier changes in the circumpolar Arctic and sub-Arctic, mid-1980s to late-2000s/2011. Geografisk Tidsskrift – Danish J Geogr 115(1):39–56. https://doi.org/10.1080/00167223.2015.1026917

Mote TL (2007) Greenland surface melt trends 1973–2007: evidence of a large increase in 2007. Geophys Res Lett 34(22):L22507. https://doi.org/10.1029/2007gl031976

Nghiem S, Hall D, Mote T, Tedesco M, Albert M, Keegan K, DiGirolamo N (2012) The extreme melt across the Greenland ice sheet in 2012. Geophys Res Lett 39:L20502. https://doi.org/10.1029/2012GL053611

Nick FM, Vieli A, Howat IM, Joughin I (2009) Large-scale changes in Greenland outlet glacier dynamics triggered at the terminus. Nat Geosci 2(2):110–114

Pattyn F, Ritz C, Hanna E, Asay-Davis X, DeConto R, Durand G, Favier L, Fettweis X, Goelzer H, Golledge NR, Munneke PK, Lenaerts JTM, Nowicki S, Payne AJ, Robinson A, Seroussi H, Trusel LD, van den Broeke M (2018) The Greenland and Antarctic ice sheets under 1.5 °C global warming. Nat Clim Change 1–9.https://doi.org/10.1038/s41558-018-0305-8

Radić V, Hock R (2010) Regional and global volumes of glaciers derived from statistical upscaling of glacier inventory data. J Geophys Res 115:F01010. https://doi.org/10.1029/2009JF001373

Radić V, Hock R (2011) Regionally differentiated contribution of mountain glaciers and ice caps to future sea-level rise. Nat Geosci 4:91–94

Rahmstorf S (1995) Bifurcations of the Atlantic thermohaline circulation in response to changes in the hydrological cycle. Nature 378:145–149

Rahmstorf S, Coauthors (2005) Thermohaline circulation hysteresis: a model intercomparison. Geophys Res Lett 32:L23605. https://doi.org/10.1029/2005GL023655

Refsgaard JC (1997) Parameterisation, calibration and validation of distributed hydrological models. J Hydrol 198:69–97

Reimer CH, van den Broeke M, Ettema J, Stap LB (2012) Refreezing on the Greenland ice sheet: a comparison of parameterizations. The Cryosphere 6(4):743–762. https://doi.org/10.5194/tc-6-743-2012

Rignot E, Box JE, Burgess E, Hanna E (2008) Mass balance of the Greenland ice sheet from 1958 to 2007. Geophys Res Lett 35:L20502.

Rignot E, Kanagaratnam P (2006) Changes in the velocity structure of the Greenland Ice Sheet. Science 311:986–990

Schlesinger ME, Ramankutty N (1994) An oscillation in the global climate system of period 65–70 years. Nature 367:723

Straneo F, Heimbach P, Sergienko O, Hamilton G, Catania G, Griffies S, Hallberg R, Jenkins A, Joughin I, Motyka R, Pfeffer WT, Price SF, Rignot E, Scambos T, Truffer M, Veili A (2013) Challenges to understanding the dynamic response of Greenland's marine terminating glaciers to oceanic and atmospheric forcing. BAMS 8:1131–1144. https://doi.org/10.1175/BAMS-D-12-00100.1

Steffen K (1995) Surface energy exchange at the equilibrium line on the Greenland ice sheet during onset of melt. Ann Glaciol 21:13–18

Steffen K, 6 others (2008) Rapid changes in glaciers and ice sheets and their impacts on sea level. In: Abrupt climate change. Reston, VA, US Geological Survey, 29–66. (US Climate Change Science Program: Synthesis and Assessment Product 3.4.)

Tedesco M, Box JE, Cappelen J, Fausto RS, Fettweis X, Hansen K, Mote T, Sasgen I, Smeets CJPP, van As D, van de Wal RSW, Velicogna I (2017) Greenland ice sheet. Arctic Report Card 2017. https://www.arctic.noaa.gov/Report-Card

Tedesco M, 7 others (2011) The role of albedo and accumulation in the 2010 melting record in Greenland. Environ Res Lett 6:014005. https://doi.org/10.1088/1748-9326/6/1/014005

van den Broeke MR, Bamber J, Ettema J, Rignot E, Schrama E, van de Berg WJ, van Meijgaard E, Velicogna I, Wouters B (2009) Partitioning recent Greenland mass loss. Science 326:984–986

van de Wal RSW, Boot W, van den Broeke MR, Smeets CJPP, Reijmer CH, Donker JJA, Oerlemans J (2008) Large and rapid velocity changes in the ablation zone of the Greenland ice sheet. Science 321:111–113

Weijer W, Maltrud ME, Hecht MW, Dijkstra HA, Kliphuis MA (2012) Response of the Atlantic Ocean circulation to Greenland Ice Sheet melting in a strongly-eddying ocean model. Geophys Res Lett 39:L09606

World Glacier Monitoring Service (WGMS) 2013. Glacier mass balance bulletin 2010–2011 (Bulletin No 12) Zemp M, Nussbaumer SU, Naegeli K, Gärtner-Roer I, Paul F, Hoelzle M, Haeberli W, ICSU (WDS)/IUGG (IACS)/UNEP/UNESCO/WMO, Zurich, Switzerland, 106 pp, Publication based on database version. https://doi.org/10.5904/wgms-fog-2013-11

Dr. Sebastian H. Mernild is Director and Full Professor in Climate Change and Glaciology, at the Nansen Environmental and Remote Sensing Center (also known as the Nansen Center) in Bergen, Norway. Mernild is also a Lead Author on IPCC AR6 WG1, and was a Contributing Author on IPCC AR5 WG1. His research centers on local, regional, and global modeling using a wide variety of atmospheric and terrestrial models and observations with a specific focus on understanding and simulating climate change interactions related to snow, glacier ice mass balance for the Greenland Ice Sheet and mountain glaciers, and freshwater runoff (the hydrological cycle) in Arctic, Antarctic, Patagonia, and the Andes. He received his Doctoral degree in climate change, glaciology, and hydrology focusing on Greenland conditions from the University of Copenhagen, Denmark. He worked in the US for more than 6 years at the International Arctic Research Center, University of Alaska Fairbanks (2006–2009), and at Los Alamos National Laboratory in New Mexico (2009–2013), and 3 years at Centro de Estudios Científicos (CECs) in Valdivia, Chile (2013-2016). Since 2016, he has been at the Nansen Center in Bergen. Mernild is also a Lead Author on IPCC AR6 WG1, and was a Contributing Author on IPCC AR5 WG1.

Dr. Glen E. Liston is a Senior Research Scientist at the Cooperative Institute for Research in the Atmosphere (CIRA), Colorado State University. He is the author of the most widely tested and applied meteorological, snow-evolution, blowing snow, and snow data assimilation modeling system in the world: MicroMet, SnowModel, SnowTran-3D, and SnowAssim. On October 18, 2011, the "Liston Glacier" in the Dry Valleys of Antarctica was named for him by the U.S. Board on Geographic Names for his work on Antarctic glacier and ice sheet melt processes. He has spent over 71 months (5.9 years) on cold regions field-research expeditions around the world. He has over 145 refereed journal publications on snow-related topics.

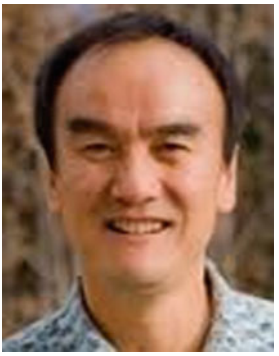

Dr. Daqing Yang is a Research Scientist at the Watershed Hydrology and Ecology Research Division, Environment and Climate Change Canada. He is also Affiliate Research Professor at the International Arctic Research Center, Univ. of Alaska Fairbanks. Over the past 25 years, he has conducted cryosphere system research in China, Canada, Japan, USA, and Norway. His primary research activities/interests include cold region hydrology and climate, particularly Arctic large river streamflow regime and change, snow cover and snowfall measurements, climate change and human impact to regional hydrology, and applications of remote sensing in cold regions. He has served as journal editor and subject editor for IAHS publications (cold region hydrology, northern research basin water balance, and cold/mountain region hydrological systems under climate change), and WMO technical reports (solid precipitation measurement intercomparison and integrated global observing strategy cryosphere theme). He also contributed as review and/or author to the IPCC Reports, and the Arctic Council's Snow, Water, Ice and Permafrost in the Arctic (SWIPA 2017 and follow up) assessment. His current research focuses on investigating the impacts of climate variability/change and human activities on hydrologic system across the broader northern regions.

Part II
Hydrology and Biogeochemistry

Regional and Basin Streamflow Regimes and Changes: Climate Impact and Human Effect

6

Michael Rawlins, Daqing Yang, and Shaoqing Ge

Abstract

Many large northern rivers contribute significant amount of freshwater and energy from land to the Arctic Ocean. Due to climate warming and human effect, basin hydrology changed very significant over the past decades. This chapter reviews the research progress of regional flow regimes and changes, and the results of watershed hydrology analyses, including climate impact and influence of human activities, particularly dam regulation. This chapter is closely linked with other chapters of basin snow cover hydrology, and freshwater and heat fluxes into the Arctic Ocean.

6.1 Introduction

Many large northern rivers contribute significant amount of freshwater and energy from land to the Arctic Ocean (Fig. 6.1 and table). Due to recent strong climate warming in the Polar Regions, arctic hydrology system and its key elements have significantly changed. It is important to point out that several community-based

M. Rawlins
Department of Geosciences, University of Massachusetts – Amherst, Amherst, MA, USA
e-mail: rawlins@geo.umass.edu

D. Yang (✉)
Watershed Hydrology and Ecology Division, Environment and Climate Change Canada, Victoria, Canada
e-mail: Daqing.Yang@canada.ca; daqing.yang@gmail.com

S. Ge
American Water, Camden, New Jersey, USA
e-mail: geshaoqing@gmail.com

D. Yang and D. L. Kane (eds.), *Arctic Hydrology, Permafrost and Ecosystems*,
https://doi.org/10.1007/978-3-030-50930-9_6

River Basin	Discharge ($km^3\ yr^{-1}$)
Lena	532
Yenisey	630
Ob	530
Yukon	205
Mackenzie	309
HJUB*	714
Pan-Arctic	~5250

*Hudson, James & Ungava Bays gauged area only

Fig. 6.1 Large rivers in the northern regions (Froman et al. 2000) and their flow contribution to the Arctic Ocean (Shiklomanov and Shiklomanov 2003)

efforts have advanced our understanding of arctic hydrologic processes and its interactions/linkage to atmosphere and ocean. These investigations have provided new knowledge on key processes, feedbacks, responses in water cycle elements including streamflow regimes and how they have responded to climate warming. For example, coordinated efforts such as the Arctic Community-wide Hydrologic Analysis and Monitoring Program (Arctic CHAMP) catalyzed the necessary research in order to construct a holistic understanding of arctic hydrology, with a major focus on watershed hydrology. Under Arctic CHAMP a targeted subset of projects such as the National Science Foundation Freshwater Integration (FWI) have brought a wealth of knowledge regarding the Arctic's large-scale freshwater budget (Serreze et al. 2006), linkages between land–surface hydrology and nutrient fluxes (McClelland et al. 2007; Frey and Smith 2003), the dynamics of freshwater transfer between the atmosphere, river systems and Arctic Ocean (Rawlins et al. 2009a), and anticipated changes in the water cycle through the twenty-first century (Holland et al. 2007). From 2002 to 2007 FWI project teams published over 100 peer-review journal articles and guided the research of more than 2 dozen undergraduate and graduate students.

In the FWI several community-based "capstone" study activities were designed and executed to improve system-level understanding of the arctic freshwater system. One study drawing together observations over land, in the atmosphere, and the oceans found increases in atmospheric water vapor, poleward moisture transport, and net precipitation over the last century, pointing to an acceleration of the hydrologic cycle (White et al. 2007). In another study, key relationships between storages and fluxes including streamflow and associated feedbacks within the system were explored (Francis et al. 2009). Their heuristic approach provided a rich assessment of the many physical and biological interactions and feedbacks within the arctic system. For example, as permafrost becomes thinner, the subpermafrost groundwater can contribute more water readily to streamflow, or can promote surface drainage. In a contemporary budget analysis of the pan-Arctic freshwater system, Serreze et al. (2006) synthesized terrestrial and oceanic observations, insights gained from the ERA-40 reanalysis, and land surface and ice-ocean models. They found that total freshwater input to the Arctic Ocean is dominated by river discharge. They also concluded that the Arctic atmosphere, land surface, and ocean are in the midst of pronounced change, while acknowledging that our understanding of the Arctic freshwater system is still far from complete. In another capstone study, an international group of researchers synthesized observations and model data to answer one of several fundamental questions posed during the FWI, namely, is the freshwater cycle accelerating or "intensifying"? (Rawlins et al. 2010). Intensification is defined as an increase in the amount of freshwater flowing through branches of the atmosphere-land-ocean system, and is an expected manifestation of a warming climate, related to the atmosphere's ability to hold more moisture as it warms. The analysis documented that, with few exceptions, precipitation, evapotranspiration, and river discharge fluxes drawn from observations and from general circulation models (GCMs) exhibited positive trends, with the broad-scale increases providing early evidence that the Arctic FWC is experiencing intensification. Results of other studies from the 22 individual FWI projects over a variety of scales and domains within the atmospheric, oceanic, and land-based branches of the Arctic hydrologic cycle were summarized in Vörösmarty et al. (2008).

Hydrologic models applicable to studies of arctic streamflow and river discharge range from simple water balance models to lumped parameter models and large-scale distributed 3D models. To capture the high prevalence of wet surficial soils and surface water, hydrology models operating across the high northern latitudes typically include the seasonal thawing and freezing of soils. Recognition that seasonal changes in soil water and ice content are an important component of Arctic hydrology (Woo et al. 2008) has led to the modification and development of numerical climate/land surface/hydrological models that incorporate the key processes (Cherkauer et al. 2003; Nicolsky et al. 2007; Niu and Yang 2006; Rawlins et al. 2013; Ganji et al. 2017). The inclusion of freezing soils in model simulations will typically increase the ratio of runoff relative to precipitation and produce greater amounts of surface runoff following snowmelt compared with a model simulation that lacks this detail, often resulting in runoff that compares more

favorably with observations (Niu and Yang 2006; Ganji et al. 2017). Outputs from simulations from general circulation models (GCMs) have been used to project how runoff and streamflow in the arctic may respond as the climate warms (Kattsov et al. 2007; Holland et al. 2007; Wu et al. 2005).

6.2 Large-Scale Flow Variability/Trends and Possible Causes

Of the myriad changes occurring across the terrestrial arctic system, few contain as clear a signal of hydrological cycle intensification as the dramatic rise in river discharge from the Eurasia landmass. Drawing on long-term records of river discharge from the six largest Eurasian rivers to the Arctic Ocean, Peterson et al. (2002) documented the increase in average annual discharge of 7% from 1936 to 1999. The trend is consistent with river discharge increases predicted by GCMs (Miller and Russell 1992; Shiklomanov and Shiklomanov 2003; Kattsov et al. 2007), suggesting a possible response to atmospheric warming. Correlation between Eurasian river discharge and the North Atlantic Oscillation (NAO) suggests that the rivers are responding to changes in large-scale hemispheric climate patterns. From 1950 to 2004, river discharge averaged across the pan-Arctic basin exhibits a significant, positive trend of 0.23 mm year^{-2} (5.3 km^3 year^{-2}), significant at the 90% confidence level (Rawlins et al. 2010). Despite this large increase in annual river flow, relatively equal numbers of significant positive and negative trends were reported for maximum daily discharge (Shiklomanov et al. 2007). Changes in snowpack water are consistent with the increase in river discharge from Eurasia (Troy et al. 2012). While there is no strong evidence for increased maximum daily discharge from the Eurasian pan-Arctic, data from the same rivers suggest an overall pattern of increasing minimum daily flows (or "low flows") throughout the region (Smith et al. 2007). Minimum flow increases were documented in summer as well as winter and in nonpermafrost as well as permafrost terrain. Analysis of a subset of the stations in south central Russia suggests that the flow increases since 1985 are largely unprecedented in the instrumental record. Analysis of daily and seasonal discharge changes through the region must be view cautiously, as dams, particular large ones in the Yenisey basin, can confound interpretation of trends (Ye et al. 2003, Yang et al. 2004a, b; Shiklomanov and Lammers 2009).

Attribution for the increasing river discharge from Eurasia has focused on the flux of moisture into the Eurasian basin, the seasonal storage of snow and associated river runoff, and the role of permafrost thaw in subsurface hydrology. Impacts from fires and dams are relatively small compared to the magnitude of annual discharge increase from Eurasia (McClelland et al. 2004). Mass flux data from the NCEP-NCAR reanalysis points to an increase in atmospheric moisture transport into the Eurasian basin of 15.6% from the 1940s to 2000, with the net moisture transport increase commensurate with the increase in river discharge

(Zhang et al. 2013). Consistent with model projections (Kattsov et al. 2007; Wu et al. 2005), increases in cold season precipitation have been reported, primarily across northern Eurasia (Bring and Destouni 2013; Bulygina et al. 2009; Ye et al. 1998; Frey and Smith 2003; Rawlins et al. 2006). Annual total precipitation for the three largest basins (Ob, Yenisei, and Lena) exhibits no significant trend over the period 1936–1999 (Berezovskaya et al. 2004). However, there is general agreement in the sign of changes in annual precipitation and river discharge among a collection of the region's smaller basins (Pavelsky and Smith 2006). Aggregate annual discharge from the Ob, Yenesey, and Lena basins is positively correlated with cold season precipitation between 1966 and 1999, illustrating the strong influence seasonal snow accumulation plays in the annual total discharge flux (Rawlins et al. 2009a, b). In situ observations synthesized with snowpack dynamics simulated by a hydrological model explain approximately 67% of the observed discharge trend (Troy et al. 2012). More solid precipitation leads to higher terrestrial runoff, particularly in areas underlain by permafrost. Using data from atmospheric reanalysis and the Gravity Recovery and Climate Experiment (GRACE), Landerer et al. (2010) concluded that increases in terrestrial water storage and river discharge across Eurasia were linked with upward trends in atmospheric moisture flux as manifested in increased winter precipitation. Record high annual discharge from the six largest Arctic-draining Eurasian rivers in 2007 was due in part to anomalously high net precipitation, strong positive anomalies in late winter snow water equivalent (Rawlins et al. 2009b), and runoff across the northern part of the basin (Shiklomanov and Lammers 2009). Summer flooding and high mean annual discharge in the middle Lena River in recent years have been linked to more frequent intrusions of storms in Siberia (Gautier et al. 2018). Taken together these studies further the notion that rising freshwater export from the region is a manifestation of additional moisture transport into the region and water movement due to precipitation, snowmelt, and thawing of ground ice.

Degrading ground ice in permafrost landscapes may be leading to an increase soil infiltration, subsurface water movement, stream network interconnectivity, and shift in water storage from lakes to increased baseflow (Smith et al. 2007). Mobilization of water through permafrost thaw has been identified as a factor in the observed rise in winter (low flow) discharge in parts of the Arctic (St. Jacques and Sauchyn 2009; Smith et al. 2007; Walvoord and Striegl 2007). Significant increases in baseflow have been documented for 20 of 23 subbasins in the NWT of Canada, with 2 subbasins showing a significant trend in annual discharge (St. Jacques and Sauchyn 2009). Groundwater flow increases inferred from winter (Jan 1–Mar 31) discharge in twenty-one streamflow gaging stations in the Yukon River basin were not accompanied by upward trends in annual flow (Walvoord and Striegl 2007). The increase in winter discharge and decrease in the ratio of maximum to minimum monthly discharge in the middle and lower part of the Lena River basin reflect the controls permafrost exerts on winter discharge (Gautier et al. 2018; Ye et al. 2003, 2009). Rising groundwater inputs to streams is supported by evidence of ancient carbon in arctic rivers (Vonk et al. 2013), with thawing permafrost supplying soil organic carbon to inland waters. While the total mass of water released via

permafrost thaw is thought to be too small to explain much of long-term rise in annual discharge from Eurasia, relative to other potential drivers, changes observed in arctic streamflow records point to the mobilization of subsurface water in recent decades.

Models are useful tools to examine and explain the process changes in large-scale and watershed hydrology. In recent decades land surface and hydrological models have been adapted to capture the seasonal freezing and thawing of soils over the northern high latitudes, a key process contributing to the relatively high runoff-precipitation ratios typically seen throughout the region. The Variable Infiltration Capacity (VIC) model includes an improved its representation of cold land processes, and the effects of surface storage in lakes and wetlands (Cherkauer et al. 2003). It was used to examine the land surface water fluxes from an off-line VIC simulation and ERA-40 reanalysis for the pan-Arctic land area (Su et al. 2006). In a study using measured streamfllow, satellite-based snow cover extent, observed dates of lake freeze-up and break-up, and permafrost maximum active-layer thickness, the VIC model was able to reproduce a range of hydrologic processes across the pan-Arctic domain (Su et al. 2005). Troy et al. (2012) used VIC to study how interactions between winter precipitation and temperature drove changes in snowpack water, which was manifested in the modeled runoff trends consistent with the increase in river discharge from Eurasia. The Community Land Model (CLM) has also been used extensively to investigate Arctic hydrological processes controlling runoff and river discharge flux (Niu and Yang 2006; Slater et al. 2007; Lawrence and Slater 2010; Lawrence et al. 2015). Models which are suitably physically scaled and tailored specifically for studies of the Arctic freshwater cycle are most useful for understanding connections among processes controlling runoff generation and river discharge export. The PWBM simulates all major elements of the arctic water cycle, including snowfall and storage, sublimation, transpiration, and surface evaporation (Rawlins et al. 2003, 2013). It is forced with meteorological data, and simulations are at an implicit model daily time step. Snowpack dynamics are simulated with a multi-layer snow model that accounts for wind compaction, change in density due to fresh snowfall, and depth hoar development with time. The PWBM has been used to investigate causes behind the record Eurasian discharge in 2007 (Rawlins et al. 2009b); to corroborate remote sensing estimates of surface water dynamics (Schroeder et al. 2010); and to quantify present and future water cycle changes around Nome, Alaska (Clilverd et al. 2011). Soil temperature dynamics are simulated by a 1-D nonlinear heat equation with phase change (Rawlins et al. 2013). Simulations when coupled to a dynamic soil carbon model capture the influence of snow cover and soil thermal dynamics on the seasonal and spatial variability in soil carbon dioxide respiration (Yi et al. 2015). Simulations for the periods 1996–1999 and 2066–2069 for a location in central Alaska illustrate the potential for drier soils in the presence of increases in active-layer thickness, annual total precipitation, and winter snowfall (Rawlins et al. 2013).

Table 6.1 Physical characteristics for the five major rivers of the Arctic

River name	Drainage area (1000 Km^2)	River length (Km)	Annual discharge (Km^3)	Mean annual temperature (°C)	Mean yearly precipitation (mm)	Snowfall percent (%)	Mean max. SWE (mm)
Ob	2,990	4,400	404	0.4	523	47	95
Yenisei	2,580	3,650	603	−4.3	467	47	87
Lena	2,490	3,490	525	−7.8	373	44	123
Yukon	1,790	3,000	333	−5.1	385	44	103
Mackenzie	850	5,470	210	−3.3	395	42	92

6.3 Basin Hydrology Regimes and Changes—Lena and Yukon Rivers

There are large variations in climate, permafrost, hydrology, and human activities across the arctic regions and watersheds (Table 6.1). For example, the permafrost coverage is more than 75% for the Lena river and less the 20% for the Ob basin (Fig. 6.2); there are more than 10 dams in the Yenisey river and only one in the Lena basin. Because of these factors and climate variation across the northern regions, streamflow regimes are very different among the large rivers (see more in

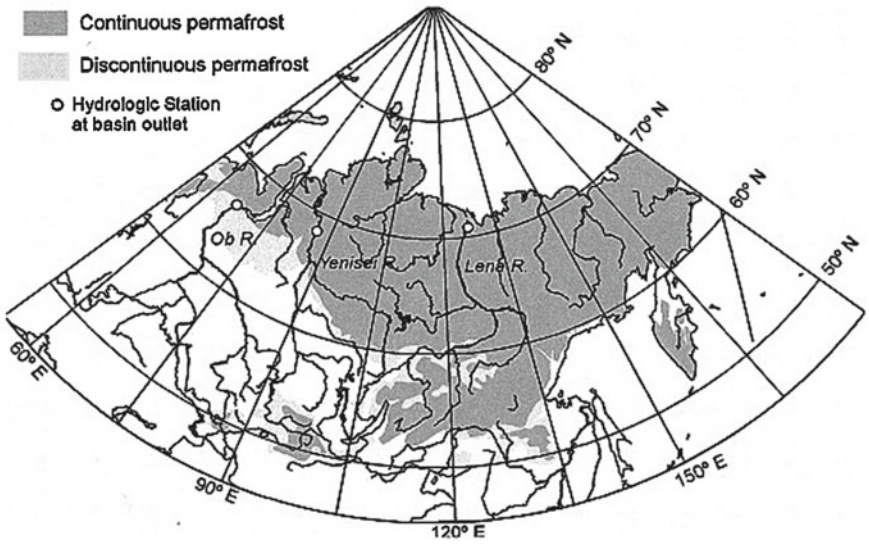

Fig. 6.2 Permafrost distribution for the Lena, Yenisei, and Ob rivers and the locations of gauging stations at the basin outlets (Yang et al. 2002)

Chap. 24). Many studies analyzed long-term flow data to investigate basin hydrological regimes and changes (Ye et al. 2003; Yang et al. 2002, 2004a, b; Ge et al. 2012; Woo et al. 2008; Majhi and Yang 2008), as this is the only way to explain and understand flow variations and changes. Here we highlight two studies on watershed flow regimes and changes, i.e., the Lena and Yukon rivers. The goal is to systematically examine and quantify discharge processes and interactions among the subbasins and their downstream effect, including regional climate variation and dam impact.

6.3.1 Lena River

The Lena River is one of the largest rivers in the Arctic. It originates from the Baikal Mountains in the south central Siberian Plateau and flows northeast and north, emptying into the Arctic Ocean via the Laptev Sea (Fig. 6.3). The drainage area of the Lena basin is about 2,430,000 km^2, approximately 78–93% of which is underlain by permafrost (Zhang et al. 1999). The Lena River contributes 524 km^3 of freshwater per year, or about 15% of the total freshwater flow into the Arctic Ocean (Shiklomanov et al. 2000; Prowse and Flegg 2000). The drainage is covered mainly by forest (84%), shrub (9%), grassland (3%), cropland (2%), and wetland (1%) (Revenga et al. 1998). Basin total population is about 2.3 million people, with one city (Yakutsk) having a population of more than 100,000. Compared with other large Siberian rivers, such as the Ob and Yenisei Rivers, the Lena basin has less human activities and much less economic development. There is only one large reservoir (capacity greater than 25 km^3) in west Lena basin that was built during the late 1960s.

Since the late 1930s hydrological observations in the Siberian regions, such as discharge, stream water temperature, river-ice thickness, dates of river freeze-up and break-up, have been carried out systematically by the Russian Hydrometeorological Services, and the observational records were quality controlled and archived by the same agency (Shiklomanov et al. 2000). Some discharge data are now available from the R-ArcticNet (v. 2.0) (A database of pan-Arctic river discharge, www.r-arcticnet.sr.unh.edu/main.html) for the period from 1936 to 1999. Ye et al. (2003) examined discharge regime and change for the three major subbasins (i.e., the Aldan/station B, Upper Lena/station C, and Vilui valley/stations D–F) and at the Lena basin outlet (station A) (Fig. 6.1), and determined impact of dams on the streamflow hydrology across the basin, through comparisons and reconstruction of monthly data.

Discharge seasonal cycle near the Aldan's outlet (station B in Fig. 6.1) shows a very low flow (320–1230 m^3/s) during November to April and a high runoff (3630–19,470 m^3/s) season from May to October, with the maximum discharge usually in June due to snow cover melt (Fig. 6.4a). Trend analysis of the monthly flow during 1942–1999 reveals an increase in the Aldan basin in most months (Fig. 6.4a), with the total trends over this period between 150 and 300 m^3/s from December to April, or increase by about 50–120%. Streamflow also increased in November by

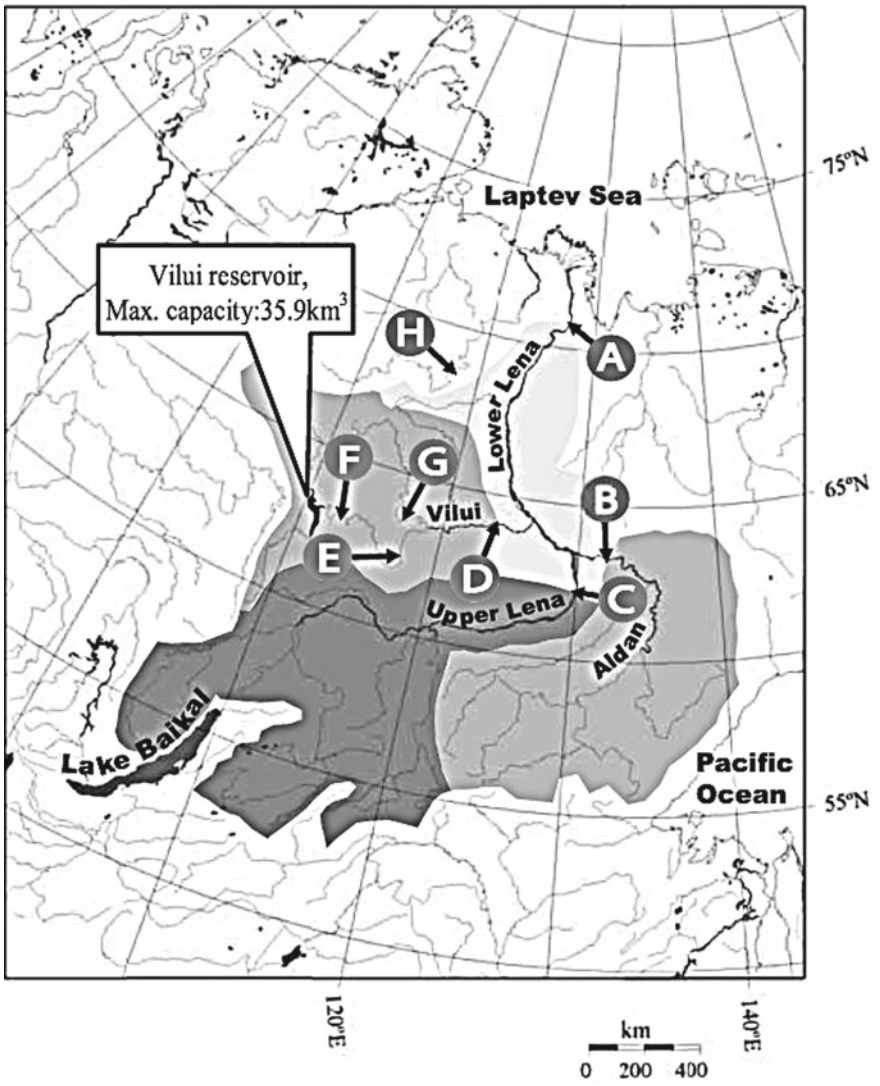

Fig. 6.3 The Lena River watershed and locations of key hydrological stations. Also shown are subbasin boundaries and reservoir location/information. Figure modified from Ye et al. (2003)

1520 m/s (125%) and in May by 3430 m^3/s (35%). These positive changes are statistically significant at 90–99% confidence. On the other hand, relatively weak increases in monthly flows were detected during the high flow season, i.e., June (7%), July (3%), September (8%), and October (14%), while a decreasing trend by 11% was discovered in August. As the result of the monthly streamflow changes, yearly mean discharge shows a visible upward trend, 740 m^3/s (or 14% rise), over

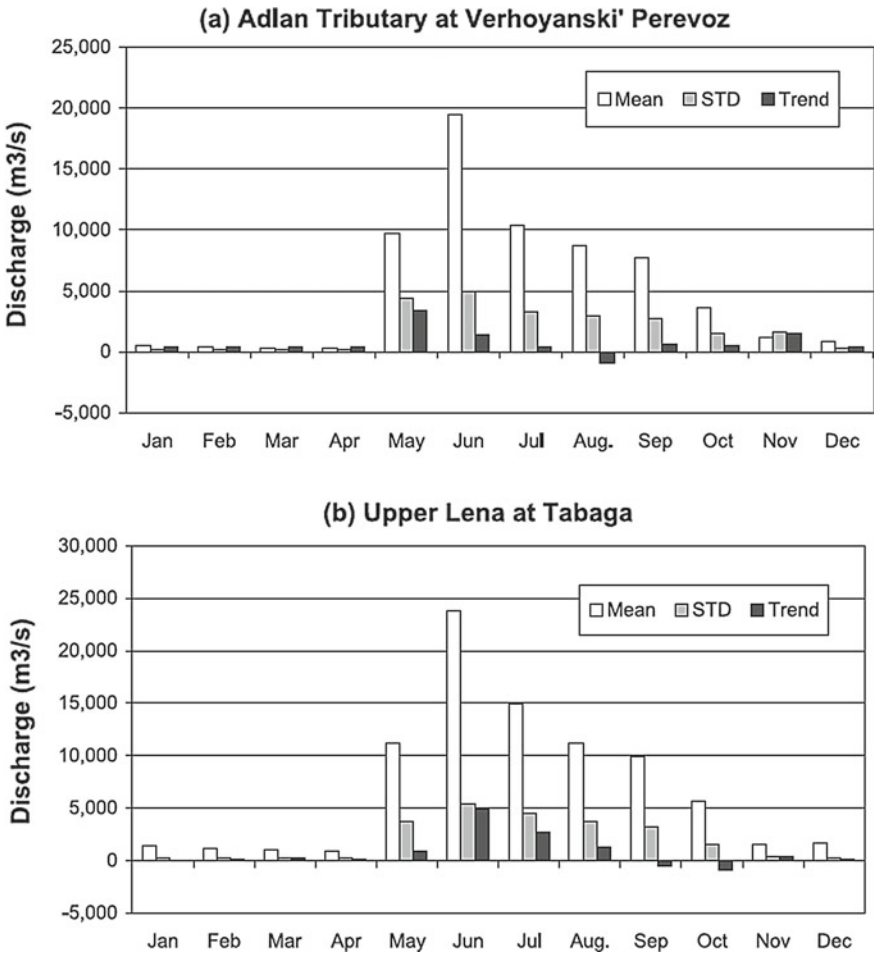

Fig. 6.4 Long-term mean monthly discharge, standard deviation, and trend for **a** the Aldan tributary and **b** the upper Lena basin (Ye et al. 2003)

the period 1942–1999. Positive runoff trends in winter, spring, and summer seasons and a negative trend in fall season have been reported for the Arctic rivers in other studies (Yang et al. 2002, 2004a, b; Ye et al. 2009). These changes in seasonal streamflow characteristics over the Aldan regions indicate a hydrologic regime shift toward early snowmelt and higher summer flow due to regional warming and permafrost degradation in the southern parts of Siberia, where permafrost is the warmest and already discontinuous (Pavlov 1994).

Upper Lena region monthly flows show a regime similar to that of the Aldan tributary, with the high flows from 5640 to 23,880 m^3/s during May to October and

lows around 900–1610 m^3/s during November to April (Fig. 6.4b). The upper Lena region is larger than the Aldan tributary; both its high- and low-flow values are higher relative to those for the Aldan subbasin. The ratio of highest flow (in June) to lowest flow (in April) is only 26 over the upper Lena, though the ratio between June and May discharge remains the same as for the Aldan catchment. The higher cold season base flows in the upper Lena may indicate warmer winter conditions and less permafrost over this region. The interannual variation of the upper Lena basin monthly streamflow is very similar to the Aldan regions, i.e., high standard deviations in summer and low in winter.

Changes in monthly streamflow over the upper Lena are characterized by negative trends in September and October and positive trends during November to August (Fig. 6.4b). The decreasing trends during 1942–1999, about 5% in September and 15% for October, are statistically less significant (confidence lower than 80%). However, the upward trends are strong and statistically significant (confidence greater than 80%) over most winter months, i.e., increases by 22% for November, 7% for December, 2% for January, and 13–21% during February to April. Over summer season, streamflows rise by 7% in May, 20% in June, 18% in July, and 11% in August. These positive changes are statistically significant at 80–95% confidence for both June and July, and less significant for May and August (40–50% confidence). Annual discharge at the Tabaga station shows an upward trend (1120 m^3/s, or 11%) during 1942–1999 due mainly to streamflow increases in the summer months.

In the 1960s, a large reservoir was built at the upper Vilui valley near Chernyshevskyi (112150W, 62450N). The rock-filled dam, 75 m high and 600 m long, was completed in 1967. The maximum reservoir capacity is 35.9 km^3, about 7% of total annual runoff (524 km^3) of the Lena River, or 1.8 times total discharge (20 km^3) at the Chernyshevskyi station in the Vilui valley. The reservoir reached its designed stage during the spring of 1972, with the total reservoir area exceeding 2100 km^2 (Kane 1997). The reservoir, primarily for electric power generation, had the capability to regulate the monthly to seasonal streamflow processes. Comparison of the long-term mean flow in the Vilui valley between the pre-dam and post-dam periods demonstrate very significant changes. At the Chernyshevskyi station, monthly streamflow has been increased by about 400–600 m^3/s (about 11–110 times the pre-dam discharge) during November to April. Streamflow has been reduced by 1400 m^3/s (80%) in May and 2300 m^3/s (70%) in June. July discharge has increased by 300 m^3/s (40%), and small changes (less than 25%) were observed during August to October (Fig. 6.5a). The Suntan station, about 350 km downstream of the Chernyshevskyi dam, experienced similar changes in monthly mean streamflow (Fig. 6.5b). However, at the Hatyrik-Homo stations located 900 km downstream of the dam, the difference in May mean discharges has been substantially reduced due perhaps to increased runoff contribution in the post-dam period from other unregulated areas within the Vilui valley. The impact of the reservoir regulation is most obvious during winter months and also in June, since mean monthly flow in June was reduced by 2200 m^3/s (or 28%) during the post-dam period (Fig. 6.5c).

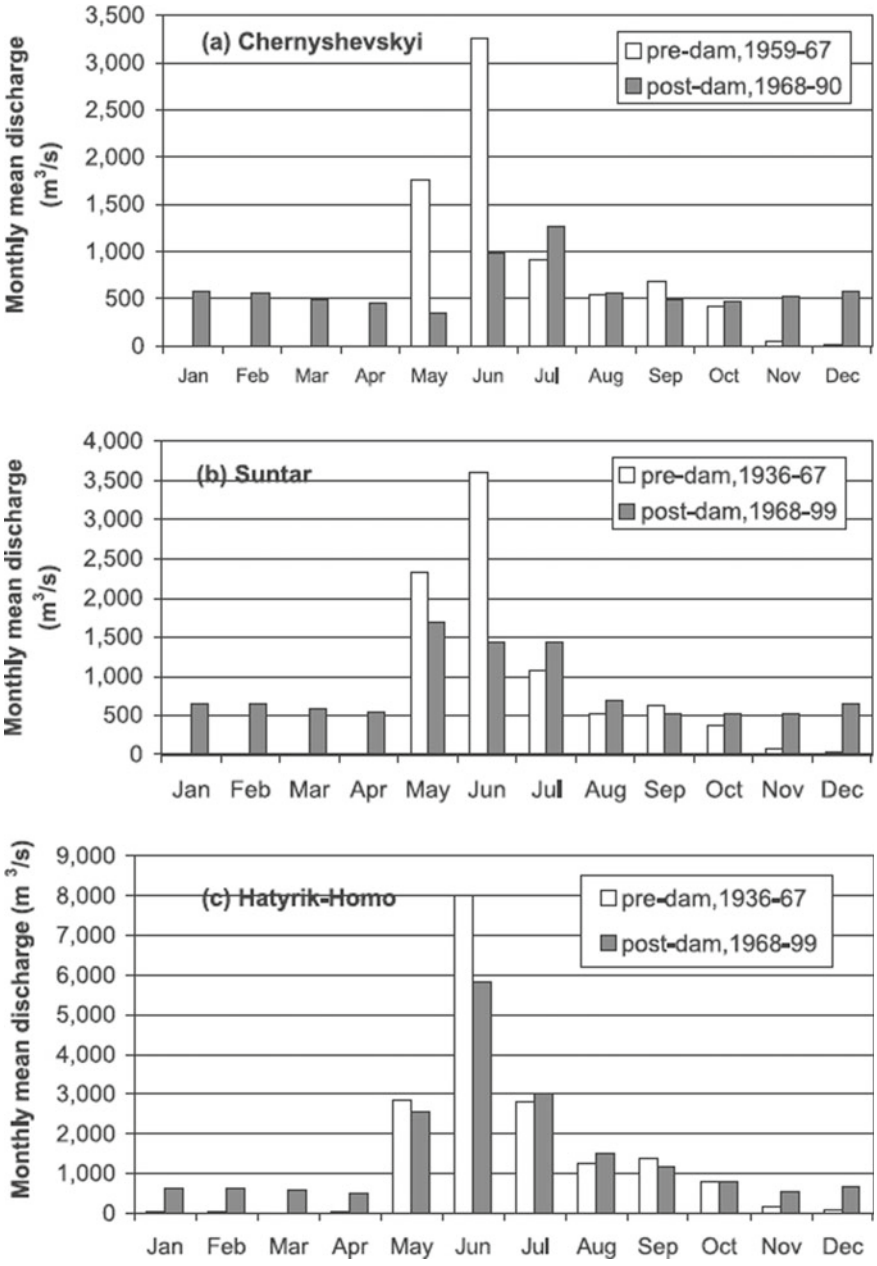

Fig. 6.5 Comparison of long-term mean monthly discharge at the three stations in the Vilui valley between the pre-dam and post-dam periods (Ye et al. 2003)

Discharge seasonal cycle at the Kusur station near the basin outlet (station A in Fig. 6.1) shows a low-flow period during November to April and a high runoff season from June to October, with the maximum discharge usually in June due to snowmelt floods (Fig. 6.6). As discussed in Chaps. 16 and 17, permafrost conditions affect the flow regime over the northern regions. The Lena River basin, mostly underlain by continuous permafrost (78–93%), has a very low winter flow and a very high peak flow in June, about 50–55 times greater than the minimum discharge. Monthly runoff variation is usually small (22–32%) in the cold season and large (15–115%) in summer months due to floods induced by snowmelt and heavy rainfall storms.

Trend analysis of the observed monthly discharge records at the Kusur station shows significant changes in streamflow characteristics. During 1942–1999, discharge at this location has significantly (95–99% confidence) increased by 20–90% in the low-flow season (November to April). This increase demonstrates the combined effect of human influence and natural changes. Aldan basin (station B) base flow slightly increased during the recent decades (Fig. 6.4a), while the upper Lena (stations C) had little changes in winter flow (Fig. 6.4b). More important, the Chernyshevskyi reservoir released water in winter season (November–April), leading to flow increase at the basin outlet. Furthermore, April flow is the lowest in a year. Comparisons of this low flows over the Lena regions/subbasins show little changes over the upper Lena region, a weak increase in the Aldan subbasin, and very strong rises in both the Vilui valley and at the Lena basin outlet (Fig. 6.7). The consistence of the increasing trends over the Vilui and at Lena basin mouth may suggest a downstream transfer of the reservoir impact to the northern Lena regions.

To better understand and quantify the effect of reservoir regulation on monthly and seasonal discharge distributions at the basin outlet, Ye et al. (2003) used statistical methods to determine the relationship of upstream and downstream flows

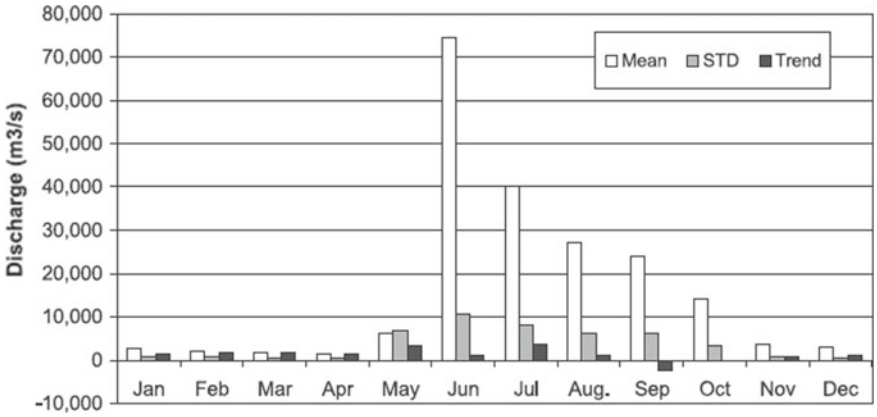

Fig. 6.6 Long-term mean monthly discharge, standard deviation, and trend at the Lena basin outlet (Kusur station). Figure modified from Ye et al. (2003)

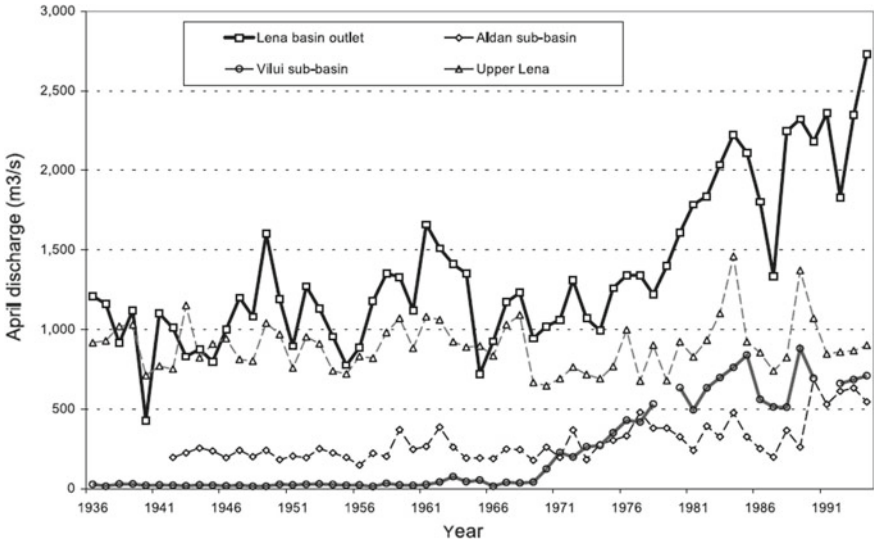

Fig. 6.7 Comparison of April discharge records among the Lena regions/subbasins, 1936–1994 (Ye et al. 2003)

for the pre-dam period, so as to reconstruct (or naturalize) downstream flow data for the basin. Three stations were chosen (Verhoyanski Perevoz at the Aldan subbasin/station B; Tabaga at the upper Lena/station C; and Suhana at the adjacent Olenek River/station H) located in the unregulated areas to represent the natural discharge conditions (Fig. 6.1). A stepwise regression was used to select input variables. To consider the routing time of flow within the basin, time lags of 0–2 months between the downstream and upstream monthly flows were applied in the stepwise regression. The results show a strong (statistically significant at 90% confidence) 1-month-lagged correlation, and a weak 2-month-lagged correction between the downstream station (Kusur) and upstream natural flows during the pre-dam period from 1942 to 1967. Routing time up to 2 months has been reported for large Arctic river basins (Arora and Boer 1999). The lagged correlations found here reflect the time of flow routing within the Lena River basin.

Based on the results of analysis, five input variables were inlcluded in the monthly regression model, i.e., monthly flows at stations Verhoyanski Perevoz (station B), Tabaga (station C), and Suhana (station H), and 1-month-ahead monthly flows at stations Tabaga and Verhoyanski Perevoz. The multi regression approach wan then use to obtain the best (least squares) relationships for every month. Statistical tests of the developed relationships show that they are significant at 95–99% confidence, indicating close relationships among the upstream and downstream flows. The relationships were good for most months, except for May when the linear regression underestimated streamflow perhaps because of the

impact of river ice. An exponential model was then chosen for this month, which generated better results.

Reconstructed monthly flow data usually reflect smoothed natural variability and change. Comparisons of the reconstructed vs. the observed records for the pre-dam periods show good agreements for most months, with the difference generally being less than 15%. Comparison between monthly streamflow regimes and trends derived from the observed and reconstructed monthly data show that reconstructed long-term mean discharges are lower (by 120–1740 m^3/s or 5–30%) than the observed data during November to May, and are higher (by 200–3700 m^3/s or 2–5%) from June to October (Fig. 6.8).

Using the reconstructed monthly data, Ye et al. (2003) generated the annual discharge time series and compared with the observed data. The results show that the naturalized yearly flows are higher since the mid-1970s. Although both the observed and reconstructed yearly records have increasing trends during 1942–1999, the rate of increase is much higher for the reconstructed data, i.e., 2499 m^3/s versus 1218 m^3/s (Fig. 6.9). This result is reasonable, as, relative to the observed data, the reconstructed monthly flows have higher trends during most of the high flow months, and these higher monthly trends transfer into a higher trend in yearly flow. It is important to emphasize that this remarkable difference identified in the yearly flow trends may demonstrate that reservoir regulations not only impact monthly/seasonal flow regimes, but also affect yearly flow characteristics at the basin scale.

Recent update of flow data analysis for the period 1936–2017 for the Lena Kusur station (Hu et al. 2019) shows similar flow patterns, i.e., small difference in mean flows between the pre- and post-dam periods, but significant changes in monthly flows over time. Monthly discharge increased in most months, particular in May

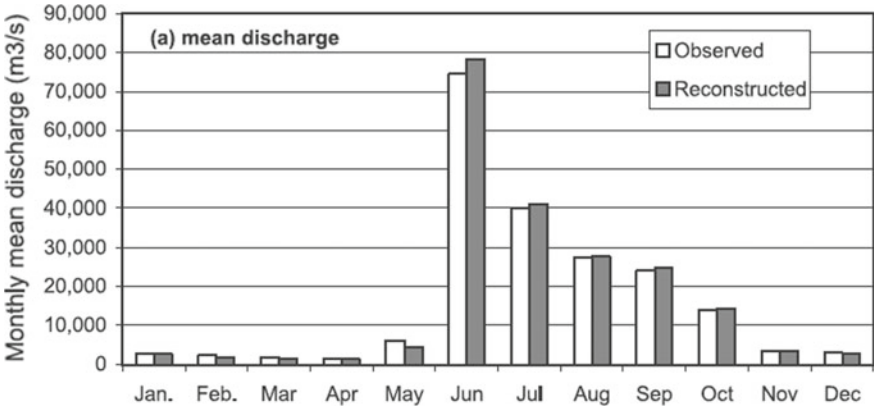

Fig. 6.8 Comparisons of **a** monthly mean discharges between observed and reconstructed records at the Lena basin outlet (Ye et al. 2003)

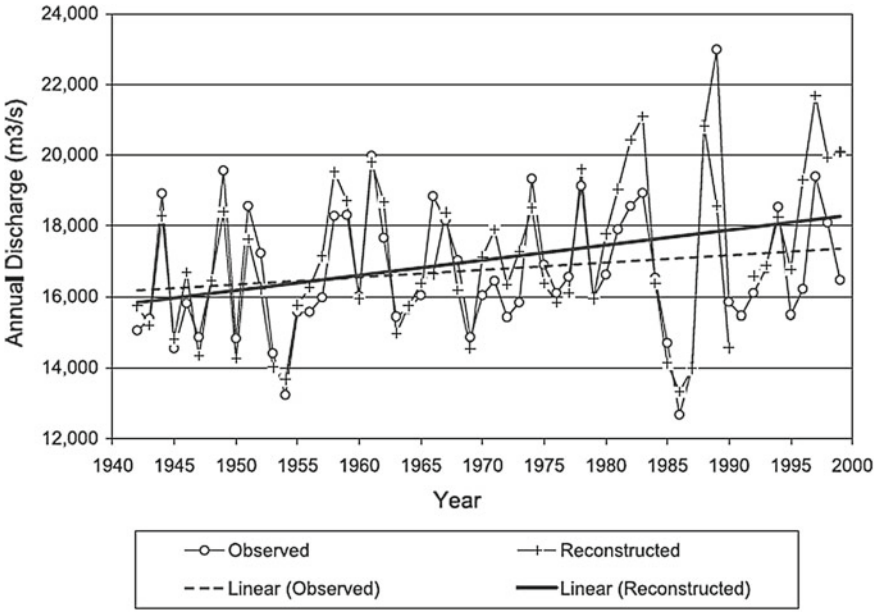

Fig. 6.9 Comparisons of annual discharge and its trend between observed and reconstructed records at the Lena basin outlet, 1936–1999. Figure modified from Ye et al. (2003)

and decrease in June. This change in the early summer season confirms the results reported by Ye et al. (2003), i.e., a shift of snowmelt timing and runoff toward early summer.

6.3.2 Yukon River

The Yukon River Basin (Fig. 6.10) is located in northwestern Canada and central Alaska. The Yukon River is the fourth largest drainage basin in North America with an area of 331 005 mile^2 (857,300 km^2) and has an average annual discharge of 226,014 ft^3/s (6400 m^3/s) (Brabets et al. 2000; Brabets and Walvoord 2009). It begins at the Llewellyn Glacier in Canada and flows through the Teslin River, which is one of the main tributaries for the Yukon River; it continues generally westward through Alaska and empties into the Bering Sea. There are three basic runoff patterns throughout the Yukon River Basin: lake runoff, snowmelt runoff, and glacier runoff (Brabets et al. 2000). Rainfall runoff is not obvious because of low precipitation in summer of the Alaska interior (Shulski and Wendler 2007) and the great extent of the basin.

The data sets used in this study include discharge, basin mean air temperature, and precipitation. For discharge data, because other discharge stations do not have continuous discharge data, four key stations with a common data period of

Fig. 6.10 The Yukon River Basin and distribution of selected stream-gauging and climatic stations in the basin

1977–2017 (Table 6.1) have been selected for analyses. The distribution of these US Geological Survey stations is shown in Fig. 6.10. Temperature and precipitation data are from the Alaska Climate Research Center (ACRC, http://climate.gi.alaska.edu) at the University of Alaska Fairbanks. The monthly air temperature and precipitation data from five climate stations within (and closest to) the Yukon River Basin have an overlapping period (1977–2017) with discharge data.

The interannual fluctuations of the Yukon River are high, with the highest flow in 2005 (275 459 ft^3/s; 7800 m^3/s) and lowest (174 661 ft^3/s; 4946 m^3/s) in 1978. Trend analysis indicates an increase of annul flow by 16,355 ft^3/s (463 m^3/s; 7.1% increase) over the 1977–2017 period, with confidence level above 96%. Following the high discharge event in 2005 (784 400 ft^3/s or 22 200 m^3/s, there were two high annual flows in 2012 and 2017, with discharge of 259,269 ft^3/s (or 7,339 m^3/s) and 270,108 ft^3/s (or 7,649 m^3/s), respectively.

As indicated in Fig. 6.11, Stevens Village annual flow has increased by 10,693 ft^3/s (303 m^3/s, or 8.8% increase) over the period of 1977–2017, with confidence level above 97%. Yukon River has low flow with small variations in winter (November–April) and high flow with large variations in summer (May–October). The upper basin above the Stevens Village contributes the most flow to the discharge at the Pilot Station (Fig. 6.11). Therefore, the flow at Stevens Village Station has major influence on the flow at the Pilot Station. In comparison, the flows at Eagle and Nenana stations are much smaller and hence, have a smaller impact on

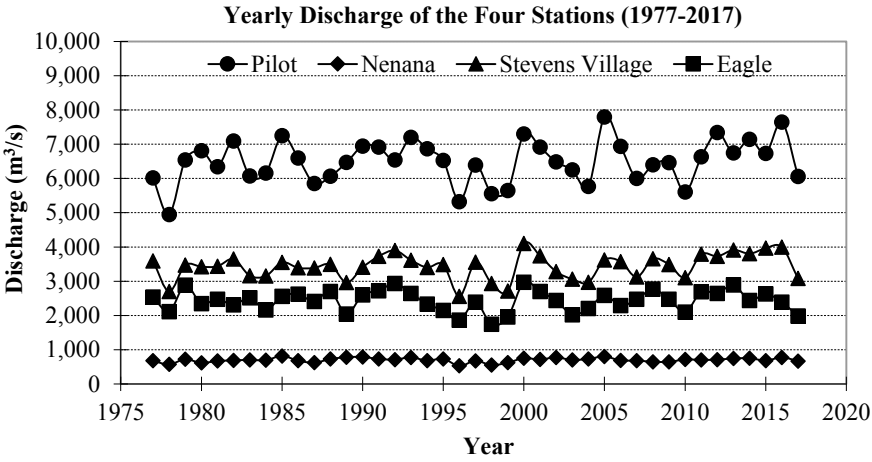

Fig. 6.11 Yearly discharge records at four gauging sites in the Yukon River during 1977–2017

the basin flow. Stevens Village Station has the highest flow value per square mile (0.59 $ft^3/s/mi^2$; 0.0065 $m^3/s/km^2$) and Tanana River at Nenana Station has 0.53 $ft^3/s/mi^2$ (0.0058 $m^3/s/km^2$).

Discharge patterns have changed over the seasons in the basin during the 1977–2017 period (Fig. 6.12). The flow at Eagle Station has increased slightly from January to March; it decreased from June to August, especially in June by 34,206 ft^3/s (969 m^3/s, or 16.1%). Flow has increased by over 14% from September to December. The flow in November and December has increased by 8,624 ft^3/s (244 m^3/s) and 4,278 ft^3/s (121 m^3/s), respectively, with confidence level above 90%. Flow at the Stevens Village Station decreased very slightly in February and March. It increased significantly by 70,488 ft^3/s (1,996 m^3/s or 33%) in May, with confidence level above 95%. The flow between September and December has increased by 16.2%–30.7% with confidence level above 95%. In June, the flow has decreased by 68,272 ft^3/s (1,933 m^3/s, or 20.6%), with confidence level of 86%.

Flow at the Nenana Station has slight increase from January to March. In April, it has increased by 1,872 ft^3/s (53 m^3/s, or 19.0%), due to warmer spring; discharge has shown increase between July and November, especially for October, the flow has increased by 3,360 ft^3/s (95 m^3/s, or 19.8%) with confidence level above 90%. June and December has not shown much change. Discharge at Pilot Station has increase in all months, except for June and July which have decreased by 55,944–58,664 ft^3/s (1,584–1,661 m^3/s, or above 10%) due to a warmer spring. The flow in April has increased by 5,184 ft^3/s (147 m^3/s, or 11.0%), with confidence level above 93%. In May, the flow has significantly increased by 148,520 ft^3/s (4,206 m^3/s, or 48.0%), with confidence level above 97%. The October flow has increase by 65,132 ft^3/s (1,844 m^3/s, or 24.8%), with confidence level above 95%.

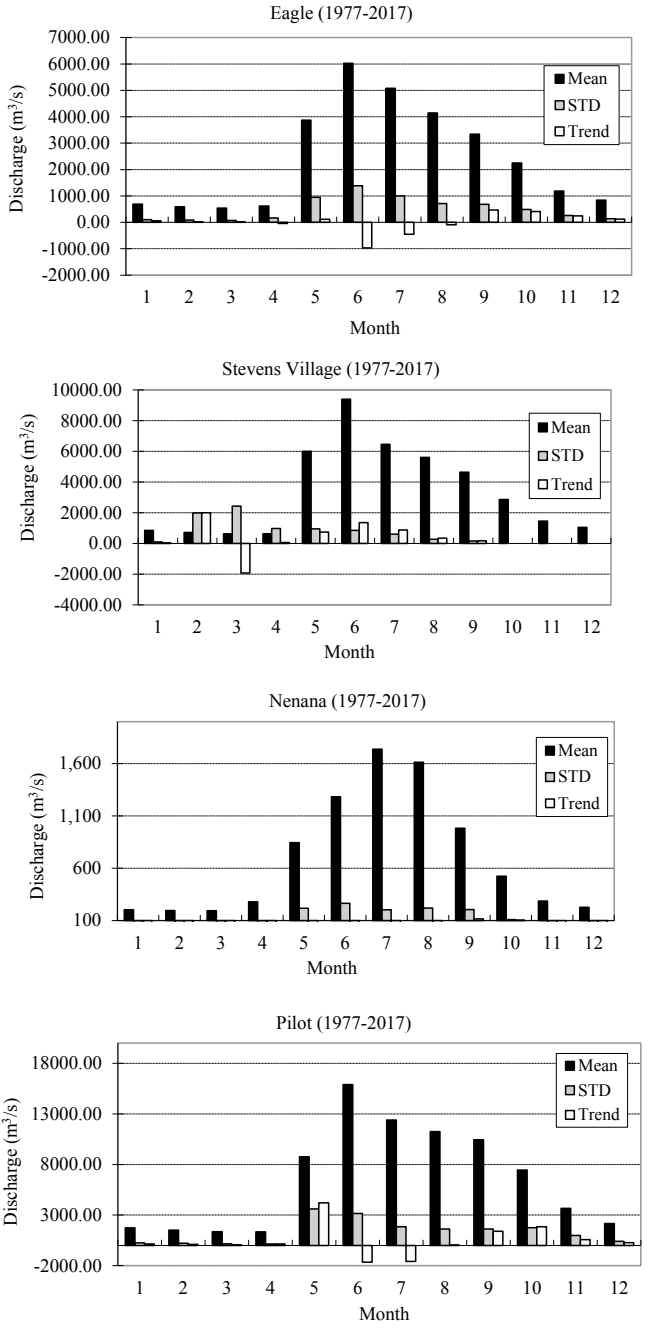

Fig. 6.12 Mean monthly discharge, standard deviation (STD), and trend at four stations in the Yukon River Basin (1977–2017)

Daily discharge analyses show high variations during the warm season (May to October) and very low base flow during the cold season (November to April). The 10-year-average peak daily flows slightly decreased at Pilot, Stevens Village, and Nenana stations (Fig. 6.13). The peak flow at Eagle Station increased by 123,355 ft^3/s (3,493 m^3/s), with a timing shifting to 3 days earlier due to early warming in spring.

6.4 Future Research Needs

Measurements of geophysical quantities such as precipitation, soil moisture, streamflow, and active-layer thickness are sparse across time and space over the northern high latitudes. Small local populations and harsh cold season conditions hinder the gathering of important data useful to advancing understanding of fundamental physical processes controlling streamflow generation and export to coast margins. Within arctic river basins, melt of snow stored over winter provides the bulk of annual river flow. In situ measurement of snowfall is challenged by the undercatch of snowfall in standard gauges due to wind effect and other systematic biases (Yang et al. 2005). The improved monitoring of rainfall that has been achieved over tropical regions has not been realized over the northern high latitudes. Microwave retrievals of precipitation have higher uncertainties over land compared to the ocean, and scattering algorithms must also account for the low snow water contents, the unique characteristics of ice particles, and similarities (Stephens and Kummerow 2007; Ehrlich et al. 2007). The use of higher frequency channels used in radiometers (e.g. Advanced Microwave Sounding Unit-B (AMSU-B), Special Sensor Microwave Imager/Sounder (SSM/IS)) has been proposed to better account for scattering by ice particles. Quantifying snow storage over large arctic watersheds is feasible only through the use of remotely sensed data validated in field campaigns. Estimates of the water equivalent in snowpacks can be obtained using microwave remote sensing (Chang et al. 1987), though the microwave response of snow is very sensitive to density differences arising due to snow crystal size (Foster et al. 1999). Campaigns which simultaneously employ satellite and aircraft remote sensing with field measurements have led to improvements of algorithms for retrieving snow and frozen soil information from active and passive microwave sensors (Cline et al. 2003), though challenges remain (Foster et al. 1999).

Improvements in model representations of cold land processes that influence streamflow can be achieved through use of measured data which provide more accurate parameterizations for vegetation cover, soil properties (texture, carbon content, and conductivity), surface water extent and other key landscape characteristics. At fine spatial scales local landscape factors become essential parametrizations in hydrological modeling. A deeper understanding of changes in subsurface runoff is being made possible through recent advances in mapping of permafrost active-layer thickness from remote sensing (Widhalm et al. 2017; Jia

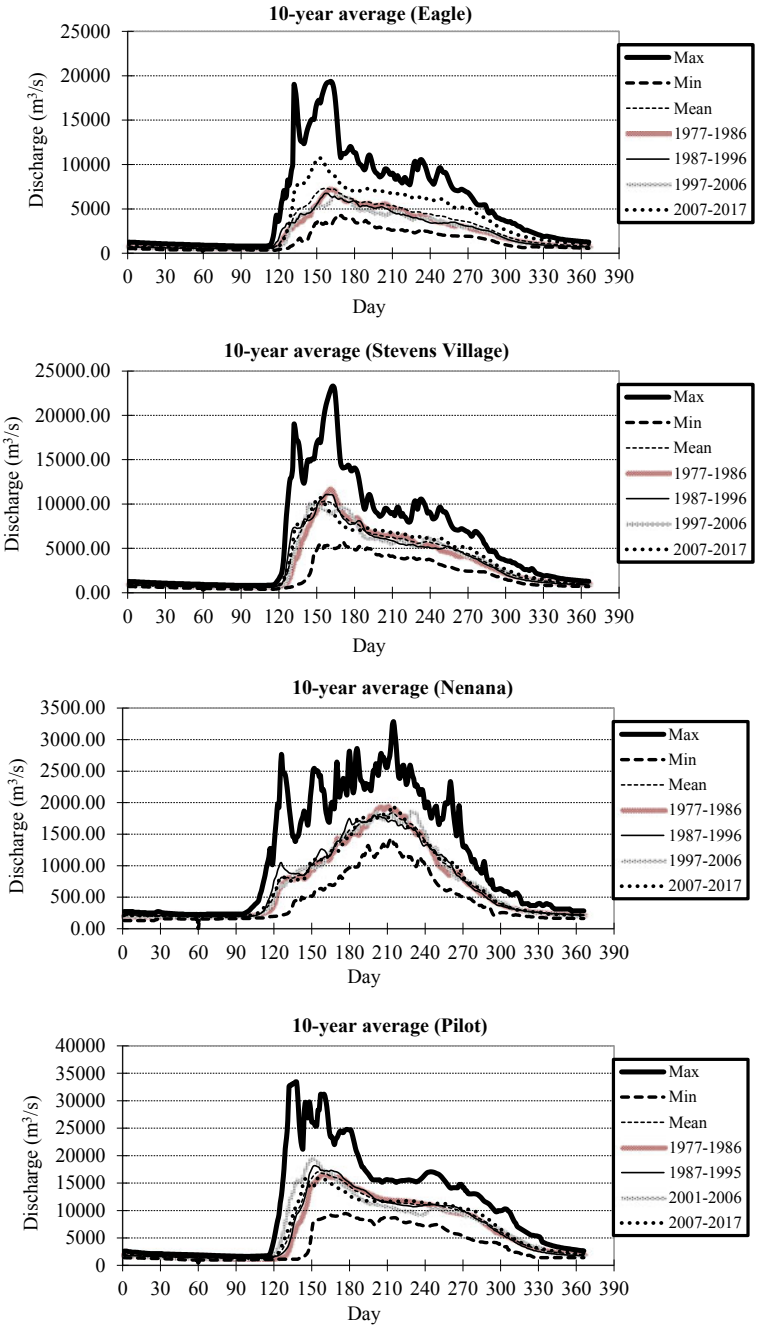

Fig. 6.13 Mean daily discharge and change at four major stations in the Yukon River Basin (1977–2017)

et al. 2017). New high resolution digital elevation models for the Arctic (ArcticDEM 2018) will aid the derivation of surface flow networks and open water areas (Turcotte et al. 2001). New data sets for inundated area and wetland extent derived from satellite remote sensing retrievals (Smith 1997; Schroeder et al. 2010; Du et al. 2016) will improve quantitative estimates of runoff and associated carbon cycle dynamics. Composite runoff fields (Fekete et al. 2002) drawn from measured data merged with simulated runoff at high spatial resolution can provide discharge estimates for unmonitored rivers. Model simulations that produce streamflow should also take into account the effects of lakes, groundwater dynamics, and river routing to accurately capture the strong seasonal hydrological dynamics common to arctic environments. Priority research goals guiding future field campaigns should include the quantification of surface water extents and their connections with surface meteorology; linkages between surface and subsurface flows; and the amount and timing of lateral transports of waterborne materials across the region.

River discharge is typically estimated using measurements of flow velocity together with knowledge of riverbed geometry. In recent decades there has been a sharp decline in the number of arctic rivers actively being monitored (Shiklomanov et al. 2002), consistent with the broad decline of globally available discharge information (Alsdorf et al. 2007; Vörösmarty et al. 2002). The decline in monitored area has raised uncertainties in estimates of freshwater, geochemical, and sediment delivery to the ocean. Satellite remote sensing has the potential to fill this gap. By taking advantage of power-law relationships that relate river flow width, mean depth, and mean velocity to discharge, absolute discharge flux may be derived solely from multiple satellite images of a river, with no ground-based or a priori information (Gleason and Smith 2014a). The method show great promise, though discharge estimates for braided rivers tend to be underestimated by the methodology (Gleason et al. 2014b). Improvements in the characterization of discharge for rivers wider than 50–100 m may also be possible from data returned by the Surface Water and Ocean Topography (SWOT) mission when it becomes operational after planned launch in 2020 (Pavelsky et al. 2014). Remote sensing holds the potential to estimate the temperature of river water entering coastal margins (Ngiem et al. 2014). A combination of measured data, modeling, and remote sensing products can provide energy fluxes linked with the freshwater cycle. Improvements in the monitoring and numerical modeling of streamflow and associated materials exports will complement coordinated field programs that deploy remote sensing assets (e.g. Arctic-COLORS) with a goal of characterizing the influence of streamflow inputs on aquatic biogeochemistry in coastal regions. The research community is well poised to employ biogeochemical modeling to understand currency exports across ungaged/unmonitored regions. Strong positive linear relationship between DOC concentration and CDOM absorption have been observed, presenting the potential to use optical remote sensing measurements to improve understanding of DOM dynamics in fluvial systems.

References

Alsdorf DE, Rodriguez E, Lettenmaier DP (2007) Measuring surface water from space. Rev Geophys 45(2). https://doi.org/10.1029/2006rg000197

ArcticDEM (2018) Polar geospatial center. https://www.pgc.umn.edu/data/arcticdem/

Arora VK, Boer GJ (1999) A variable velocity flow routing algorithm for general circulation models. J Geophys Res 104(D24):30, 965–979

Berezovskaya S, Yang D, Kane DL (2004) Compatibility analysis of precipitation and runoff trends over the large Siberian watersheds. Geophys Res Lett 31(21). https://doi.org/10.1029/2004gl021277

Brabets TP, Wang B, Meade RH (2000) Environmental and hydrologic overview of the Yukon River Basin, Alaska and Canada: U.S. In: Geological survey water-resources investigations report, vol 99–4204, p 106

Brabets TP, Walvoord MA (2009) Trends in streamflow in the Yukon River Basin from 1944 to 2005 and the influence of the Pacific Decadal Oscillation. J Hydrol 371(1–4):108–119

Bring A, Destouni G (2013) Hydro-climatic changes and their monitoring in the Arctic: observation-model comparisons and prioritization options for monitoring development. J Hydrol 492:273–280

Bulygina ON, Razuvaev VN, Korshunova NN (2009) Changes in snow cover over Northern Eurasia in the last few decades. Environ Res Lett 4(4):045026

Chang AT, Foster JL, Hall DK (1987) Nimbus-7 SMMR derived global snow cover parameters. Ann Glaciol 9:39–44

Cherkauer KA, Bowling LC, Lettenmaier DP (2003) Variable infiltration capacity cold land process model updates. Glob Planet Chang 38(1–2):151–159

Clilverd HM, White DM, Tidwell AC et al (2011) The sensitivity of northern groundwater recharge to climate change: a case study in northwest Alaska. JAWRA J Am Water Resour Assoc 47(6):1228–1240

Cline D, Elder K, Davis B, Hardy J, Liston GE, Imel D, Yueh SH, Gasiewski AJ, Koh G, Armstrong RL, Parsons M (2003) Overview of the NASA cold land processes field experiment (CLPX-2002). In: Microwave remote sensing of the atmosphere and environment III. Apr 30, vol 4894. International Society for Optics and Photonics, pp 361–373

Du J, Kimball JS, Jones LA, Watts JD (2016) Implementation of satellite based fractional water cover indices in the pan-Arctic region using AMSR-E and MODIS. Remote Sens Environ 184:469–481. https://doi.org/10.1016/j.rse.2016.07.029

Ehrlich A, Bierwirth E, Istomina L, Wendisch M (2007) Combined retrieval of Arctic liquid water cloud and surface snow properties using airborne spectral solar remote sensing. Atmos Meas Tech 10(9):3215

Fekete BM, Vörösmarty CJ, Grabs W. (2002) High-resolution fields of global runoff combining observed river discharge and simulated water balances. Glob Biogeochem Cycles 16(3)

Francis JA, White DM, Cassano JJ, Gutowski WJ, Hinzman LD, Holland MM, Steele MA, Vorosmarty CJ (2009) An arctic hydrologic system in transition: feedbacks and impacts on terrestrial, marine, and human life. J Geophys Res: Biogeosci 114(G4). https://doi.org/10.1029/2008jg000902

Frey KE, Smith LC (2003) Recent temperature and precipitation increases in West Siberia and their association with the Arctic Oscillation. Polar Res 22(2):287–300

Forman SL, Maslowski W, Andrews JT, Lubinski D, Steele M, Zhang J, Lammers R, Peterson B (2000) Researchers explore Arctic freshwater's role in ocean circulation. EOS Trans Am Geophys Union 81(16):169–174

Foster JL, Hall DK, Chang AT et al (1999) Effects of snow crystal shape on the scattering of passive microwave radiation. IEEE Trans Geosci Remote Sens 37(2):1165–1168. https://doi.org/10.1109/36.752235

Ganji A, Sushama L, Verseghy D et al (2017) On improving cold region hydrological processes in the Canadian Land Surface Scheme. Theoret Appl Climatol 127(1–2):45–59. https://doi.org/10.1007/s00704-015-1618-4

Gautier E, Dépret T, Costard F et al (2018) Going with the flow: hydrologic response of middle Lena River (Siberia) to the climate variability and change. J Hydrol 557:475–488. https://doi.org/10.1016/j.jhydrol.2017.12.034

Ge S, Yang D, Kane D (2012) Yukon River Basin long-term (1977–2006) hydrologic and climatic analysis. Hydrol Process. https://doi.org/10.1002/hyp.9282

Gleason CJ, Smith LC (2014) Toward global mapping of river discharge using satellite images and at-many-stations hydraulic geometry. Proc Natl Acad Sci 111(13):4788–4791. https://doi.org/10.1073/pnas.1317606111

Gleason CJ, Smith LC, Lee J (2014b) Retrieval of river discharge solely from satellite imagery and at-many-stations hydraulic geometry: sensitivity to river form and optimization parameters. Water Resour Res 50(12):9604–9619

Holland MM, Finnis J, Barrett AP et al (2007) Projected changes in Arctic Ocean freshwater budgets. J. Geophys. Res 112:G04S55. https://doi.org/10.1029/2006jg000354

Hu D, Kang S, Xu M (2019) Climate change and its impacts on discharge in Lena River Basin of Arctic regions during 1936–2017. J Glaciol Geocryol (Accepted)

Jia Y, Kim JW, Shum CK, Lu Z, Ding X, Zhang L, Erkan K, Kuo CY, Shang K, Tseng KH, Yi Y (2017) Characterization of active layer thickening rate over the northern Qinghai-Tibetan plateau permafrost region using ALOS interferometric synthetic aperture radar data, 2007–2009. Remote Sens 9(1):84

Kane DL (1997) The impact of Arctic hydrologic perturbations on Arctic ecosystems induced by climate change, in global change and Arctic terrestrial ecosystems. Ecol Stud Ser 124:63–81

Kattsov VM, Walsh JE, Chapman WL et al (2007) Simulation and projection of Arctic freshwater budget components by the IPCC AR4 global climate models. J Hydrometeorol 8(3):571–589. https://doi.org/10.1175/JHM575.1

Landerer FW, Dickey JO, Güntner A (2010) Terrestrial water budget of the Eurasian pan-Arctic from GRACE satellite measurements during 2003–2009. J Geophys Res: Atmos (1984–2012) 115(D23)

Lawrence DM, Slater AG (2010) The contribution of snow condition trends to future ground climate. Clim Dyn 34(7–8):969–981

Lawrence DM, Koven CD, Swenson SC et al (2015) Permafrost thaw and resulting soil moisture changes regulate projected high-latitude CO_2 and CH_4 emissions. Environ Res Lett 10 (9):094011

Majhi I, Yang D (2008) Streamflow characteristics and changes in Kolyma basin in Siberia. J Hydrometeorol 9:267–279

McClelland JW, Holmes RM et al (2004) Increasing river discharge in the Eurasian Arctic: consideration of dams, permafrost thaw, and fires as potential agents of change. J Geophys Res: Atmos 109(D18). https://doi.org/10.1029/2004jd004583

McClelland JW, Stieglitz M, Pan F et al (2007) Recent changes in nitrate and dissolved organic carbon export from the upper Kuparuk River, North Slope, Alaska. J Geophys Res: Biogeosci 112(G4). https://doi.org/10.1029/2006jg000371

Miller JR, Russell GL (1992) The impact of global warming on river runoff. J Geophys Res: Atmos 97(D3):2757–2764

Nghiem SV, Hall DK, Rigor IG, Li P, Neumann G (2014) Effects of Mackenzie River discharge and bathymetry on sea ice in the Beaufort Sea. Geophys Res Lett 41(3):873–879. https://doi.org/10.1002/2013gl058956

Nicolsky DJ, Romanovsky VE, Alexeev VA et al (2007) Improved modeling of permafrost dynamics in a GCM land-surface scheme. Geophys Res Lett 34(8). https://doi.org/10.1029/2007GL029525

Niu GY, Yang ZL (2006) Effects of frozen soil on snowmelt runoff and soil water storage at a continental scale. J Hydrometeorol 7(5):937–952. https://doi.org/10.1175/JHM538.1

Pavelsky TM, Smith LC (2006) Intercomparison of four global precipitation data sets and their correlation with increased Eurasian river discharge to the Arctic Ocean. J Geophys Res: Atmos 111(D21)

Pavelsky TM, Durand MT, Andreadis KM, Beighley RE, Paiva RC, Allen GH, Miller ZF (2014) Assessing the potential global extent of SWOT river discharge observations. J Hydrol 519:1516–1525. https://doi.org/10.1016/j.jhydrol.2014.08.044

Pavlov AV (1994) Current change of climate and permafrost in the Arctic and subarctic of Russia. Permafr Periglac Process 5:101–110

Peterson BJ, Holmes RM, McClelland JW et al (2002) Increasing river discharge to the Arctic Ocean. Science 298(5601):2171–2173. https://doi.org/10.1126/science.1077445

Prowse TD, Flegg PO (2000) Arctic river flow: a review of contributing areas. In: Lewis EL et al (ed) The freshwater budget of the Arctic Ocean: proceedings of the NATO advanced research workshop, pp 269–280

Rawlins MA, Lammers RB, Frolking S, Fekete BM, Vorosmarty CJ (2003) Simulating pan-Arctic runoff with a macro-scale terrestrial water balance model. Hydrol Process 17(13):2521–2539

Rawlins MA, Willmott CJ, Shiklomanov A et al (2006) Evaluation of trends in derived snowfall and rainfall across Eurasia and linkages with discharge to the Arctic Ocean. Geophys Res Lett 33(7). https://doi.org/10.1029/2005gl025231

Rawlins MA, Steele M, Serreze MC et al (2009a) Tracing freshwater anomalies through the air-land-ocean system: a case study from the Mackenzie river basin and the Beaufort Gyre. Atmos Ocean 47(1):79–97

Rawlins MA, Serreze MC, Schroeder R et al (2009b) Diagnosis of the record discharge of Arctic-draining Eurasian rivers in 2007. Environ Res Lett 4. https://doi.org/10.1088/1748-9326/4/4/045011

Rawlins MA, Steele M, Holland MM et al (2010) Analysis of the Arctic system for freshwater cycle intensification: observations and expectations. J Clim 23(21):5715–5737

Rawlins MA, Nicolsky DJ, McDonald KC et al (2013) Simulating soil freeze/thaw dynamics with an improved pan-Arctic water balance model. J Adv Model Earth Syst 5(4):659–675

Revenga C, Murray S, Abramovitz J et al (1998) Watersheds of the world: ecological value and vulnerability. World Resource Institute and Worldwatch Institute, Washington, D. C

Schroeder R, Rawlins MA, McDonald KC et al (2010) Satellite microwave remote sensing of North Eurasian inundation dynamics: development of coarse-resolution products and comparison with high-resolution synthetic aperture radar data. Environ Res Lett 5 (1):015003. https://doi.org/10.1088/1748-9326/5/1/015003

Serreze MC, Barrett AP, Slater AG et al (2006) The large-scale freshwater cycle of the Arctic. J Geophys Res: Ocean 111(C11). https://doi.org/10.1029/2005jc003424

Shiklomanov IA, Shiklomanov AI, Lammers RB et al (2000) The dynamics of river water inflow to the Arctic Ocean. In: Lewis EEL et al (ed) The freshwater budget of the Arctic ocean: proceedings of the NATO advanced research workshop, pp 281–296

Shiklomanov AI, Lammers RB, Vörösmarty CJ (2002) Widespread decline in hydrological monitoring threatens pan-Arctic research. Eos Trans Am Geophys Union 83(2):13–17. https://doi.org/10.1029/2002EO000007

Shiklomanov IA, Shiklomanov AI (2003) Climatic change and the dynamics of river runoff into the Arctic Ocean. Water Resour 30(6):593–601. https://doi.org/10.1023/B:WARE.0000007584.73692.ca

Shiklomanov AI, Lammers RB, Rawlins MA et al (2007) Temporal and spatial variations in maximum river discharge from a new Russian data set. J Geophys Res: Biogeosci 112(G4)

Shiklomanov AI, Lammers RB (2009) Record Russian river discharge in 2007 and the limits of analysis. Environ Res Lett 4(4):045015
Shulski M, Wendler G (2007) The climate of Alaska. University of Alaska Press, Fairbanks, p 143
Slater AG, Bohn TJ, McCreight JL et al (2007) A multimodel simulation of pan-Arctic hydrology. J Geophys Res: Biogeosci 112(G4)
Smith LC (1997) Satellite remote sensing of river inundation area, stage, and discharge: a review. Hydrol Process 11:1427–1439. https://doi.org/10.1002/(SICI)1099-1085(199708)11:10%3c1427:AID-HYP473%3e3.0.CO;2-S
Smith LC, Pavelsky TM, MacDonald GM et al (2007) Rising minimum daily flows in northern Eurasian rivers: a growing influence of groundwater in the high-latitude hydrologic cycle. J Geophys Res: Biogeosci 112(G4). https://doi.org/10.1029/2006jg000327
St Jacques JM, Sauchyn DJ (2009) Increasing winter baseflow and mean annual streamflow from possible permafrost thawing in the Northwest Territories, Canada. Geophys Res Lett 36(1). https://doi.org/10.1029/2008gl035822
Stephens GL, Kummerow CD. (2007) The remote sensing of clouds and precipitation from space: a review. J Atmos Sci 64(11):3742–3765
Su F, Adam JC, Bowling LC, Lettenmaier DP (2005) Streamflow simulations of the terrestrial Arctic domain. J Geophys Res: Atmos 110(D8)
Su F, Adam JC, Trenberth KE, Lettenmaier DP (2006) Evaluation of surface water fluxes of the pan-Arctic land region with a land surface model and ERA-40 reanalysis. J Geophys Res: Atmos 111(D5)
Troy TJ, Sheffield J, Wood EF (2012) The role of winter precipitation and temperature on northern Eurasian streamflow trends. J Geophys Res: Atmos 117(D5)
Turcotte R, Fortin JP, Rousseau AN, Massicotte S, Villeneuve JP (2001) Determination of the drainage structure of a watershed using a digital elevation model and a digital river and lake network. J Hydrol 240(3–4):225–242. https://doi.org/10.1016/S0022-1694(00)00342-5
Vonk JE, Mann PJ, Davydov et al (2013) High biolability of ancient permafrost carbon upon thaw. Geophys Res Lett 40(11):2689–2693. https://doi.org/10.1002/grl.50348
Vörösmarty C, Askew A, Grabs W, Barry RG, Birkett C, Döll P, Goodison B, Hall A, Jenne R, Kitaev L, Landwehr J (2002) Global water data: a newly endangered species. Eos Trans Am Geophys Union 82(5):54–58. https://doi.org/10.1029/01EO00031
Vörösmarty C, Hinzman L, Pundsack J (2008) Introduction to special section on changes in the arctic freshwater system: identification, attribution, and impacts at local and global scales. J Geophys Res: Biogeosci 113(G1). https://doi.org/10.1029/2007jg000615
Walvoord MA, Striegl RG (2007) Increased groundwater to stream discharge from permafrost thawing in the Yukon River basin: Potential impacts on lateral export of carbon and nitrogen. Geophys Res Lett 34(12)
White D, Hinzman L, Alessa L et al (2007) The arctic freshwater system: changes and impacts. J Geophys Res: Biogeosci 112(G4). https://doi.org/10.1029/2006jg000353
Widhalm B, Bartsch A, Leibman M, Khomutov A (2017) Active-layer thickness estimation from X-band SAR backscatter intensity. Cryosphere 11(1):483
Woo MK, Kane DL, Carey SK, Yang D (2008) Progress in permafrost hydrology in the new millennium. Permafr Periglac Process 19(2):237–254
Wu P, Wood R, Stott P (2005). Human influence on increasing Arctic river discharges. Geophys Res Lett 32(2). https://doi.org/10.1029/2004gl021570
Yang D, Kane D, Hinzman L et al (2002) Siberian Lena River hydrologic regime and recent change. J Geophys Res 107(D23):4694. https://doi.org/10.1029/2002JD002542
Yang D, Zhao Y, Armstrong R, Robinson D, Brodzik MJ (2007) Streamflow response to seasonal snow cover mass changes over large Siberian watersheds. J Geophys Res: Earth Surf 112(F2)
Yang D, Ye B, Kane DL (2004a) Streamflow changes over Siberian Yenisei river basin. J Hydrol 296(1–4):59–80
Yang D, Ye B, Shiklomanov A (2004b) Discharge characteristics and changes over the Ob River watershed in Siberia. J Hydrometeorol 5(4):595–610

Yang D, Kane D, Zhang Z, Legates D, Goodison B (2005) Bias corrections of long-term (1973–2004) daily precipitation data over the northern regions. Geophys Res Lett 32(19). https://doi.org/10.1029/2005gl024057

Ye H, Cho HR, Gustafson PE (1998) The changes in Russian winter snow accumulation during 1936–83 and its spatial patterns. J Clim 11(5):856–863. https://doi.org/10.1175/1520-0442(1998)011%3c0856:TCIRWS%3e2.0.CO;2

Ye B, Yang D, Kane DL (2003) Changes in Lena River streamflow hydrology: human impacts versus natural variations. Water Resour Res 39(7):1–14. https://doi.org/10.1029/2003WR001991

Ye B, Yang D, Zhang Z, Kane DL (2009) Variation of hydrological regime with permafrost coverage over Lena Basin in Siberia. J Geophys Res: Atmosp 114(D7)

Yi Y, Kimball JS, Rawlins MA et al (2015) The role of snow cover affecting boreal-arctic soil freeze–thaw and carbon dynamics. Biogeosciences 12(19):5811–5829

Zhang T, Barry RG, Knowles K (1999) Statistics and characteristics of permafrost and ground-ice distribution in the Northern Hemisphere. Polar Geogr 23(2):132–154

Zhang X, He J, Zhang J et al (2013) Enhanced poleward moisture transport and amplified northern high-latitude wetting trend. Nat Clim Change 3(1):47–51. https://doi.org/10.1038/NCLIMATE1631

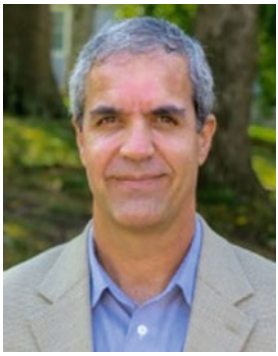

Michael A. Rawlins is Associate Director of the Climate System Research Center, and Extension Associate Professor, Department of Geosciences, College of Natural Sciences, University of Massachusetts in Amherst. His research advances understanding of the hydrology and biogeochemistry of Arctic environments, such as how climate processes influence terrestrial water and carbon cycles and the ways in which warming, permafrost thaw, and hydrological cycle intensification are impacting life across the northern high latitudes. His research engagements in recent years have resulted in synthetic publications that leverage in situ observations, numerical models, and remote sensing data. Through this work, he seeks to advance knowledge of water, energy, and carbon cycling across the earth's land, atmosphere, and ocean domains. Most recently, he has investigated the recent and potential future change in the Arctic's freshwater cycle and its connections with warming across the region. His research has helped build on the prevailing the theory that the Arctic's freshwater cycle will accelerate or "intensify" as an expected manifestation of climate warming. In recent years, his research has focused principally on advancing knowledge of how a warming climate is impacting permafrost and, in turn, the export of carbon and other nutrients from river systems of the northern high latitudes.

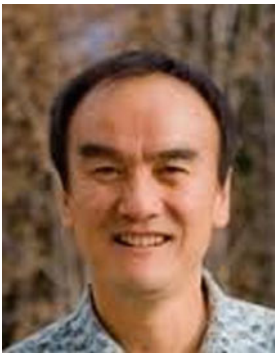

Dr. Daqing Yang is a Research Scientist at the Watershed Hydrology and Ecology Research Division, Environment and Climate Change Canada. He is also Affiliate Research Professor at the International Arctic Research Center, Univ. of Alaska Fairbanks. Over the past 25 years, he has conducted cryosphere system research in China, Canada, Japan, USA, and Norway. His primary research activities/interests include cold region hydrology and climate, particularly Arctic large river streamflow regime and change, snow cover and snowfall measurements, climate change and human impact to regional hydrology, and applications of remote sensing in cold regions. He has served as journal editor and subject editor for IAHS publications (cold region hydrology, northern research basin water balance, and cold/mountain region hydrological systems under climate change), and WMO technical reports (solid precipitation measurement intercomparison and integrated global observing strategy cryosphere theme). He also contributed as review and/or author to the IPCC Reports, and the Arctic Council's Snow, Water, Ice and Permafrost in the Arctic (SWIPA 2017 and follow up) assessment. His current research focuses on investigating the impacts of climate variability/change and human activities on hydrologic system across the broader northern regions.

Dr. Shaoqing Ge is an Engineer in the Engineering Department of American Water and works on buried infrastructure management and water system comprehensive planning studies. His areas of expertise include hydro-climate analysis of watersheds, Prestressed Concrete Cylinder Pipe (PCCP), numerical analysis, pipeline management, asset risk assessment, forensic study of asset failures, and hydraulic analysis of water distribution systems. He received a B.S. in Civil Engineering from China University of Petroleum, an M.S. in Hydraulic Structural Engineering from China Institute of Water Resources and Hydropower Research, an M.S. in Civil Engineering from University of Alaska Fairbanks, and a Ph.D. in Civil Engineering from Virginia Tech. He now serves as a Trustee in the Distribution and Plant Operations Division of AWWA, and the Chair of the Planning Committee for the AWWA Water Infrastructure Conference 2020.

Hydrologic Extremes in Arctic Rivers and Regions: Historical Variability and Future Perspectives

7

Rajesh R. Shrestha, Katrina E. Bennett, Daniel L. Peters, and Daqing Yang

Abstract

This chapter provides an overview on the range of hydrologic extremes occurring in Arctic Rivers, consisting of extreme low winter flows; river-ice jam breakup spring floods; snowmelt-driven peak spring/early summer flows; and in some instances, rainfall-driven peak flows in summer. These extreme conditions are mainly influenced by climatological drivers, and in particular, warming climate and enhanced wetness is causing substantial changes in the magnitude, variability and timing of extreme events. The most prominent historical changes in the Arctic include increasing trends in mean annual flow and winter low flow, and earlier timing of peak flow, which are attributable to warming temperature and increasing precipitation, and resulting changes in snowpack storage. Winter low flow is further enhanced by permafrost degradation as it promotes increased soil infiltration and subsurface water movement. Snowmelt-driven annual maximum flow, primarily, has been decreasing, consistent with increased warming and decreased snowpack. Secondary peak flow events in late summer, driven by extreme summer rainfall and possibly enhanced by glacial melt, have been occurring more frequently in some areas of the Arctic, exceeding

R. R. Shrestha (✉) · D. L. Peters · D. Yang
Watershed Hydrology and Ecology Research Division, Environment and Climate Change Canada, University of Victoria, Victoria, BC, Canada
e-mail: rajesh.shrestha@canada.ca

D. L. Peters
e-mail: daniel.peters@canada.ca

D. Yang
e-mail: daqing.yang@canada.ca; daqing.yang@gmail.com

K. E. Bennett
Los Alamos National Lab, Applied Terrestrial, Energy and Atmospheric Modeling, Computational Earth Science Earth and Environmental Sciences, Los Alamos, NM, USA
e-mail: kbennett@lanl.gov

D. Yang and D. L. Kane (eds.), *Arctic Hydrology, Permafrost and Ecosystems*,
https://doi.org/10.1007/978-3-030-50930-9_7

snowmelt-driven peak flow events. There is also evidence of nonstationary changes in streamflow extremes, such as increasing recurrence intervals of snowmelt-driven floods of a particular magnitude. Future projections indicate continued and enhanced warming, and strong increases in the high-latitude precipitation leading to enhanced annual flows and low flows. Future changes in peak flow remain unclear as peak flow could either increase or decrease depending on the region and interactions between precipitation change and temperature increases. Alterations in hydrologic extremes in the Arctic will have major social and economic implications; thus, focused research aimed at understanding, predicting, and projecting the Arctic streamflow extremes is recommended.

Keywords

Future projection · Historical trend · Low flow · Nonstationarity · Peak flow · River-ice breakup flood · Summer rainfall flood

7.1 Introduction

Hydrologic regimes in the Arctic environment are characterized by a range of extreme conditions: extreme low flows in winter under an ice cover; spring floods due to river-ice breakup and snowmelt; snowmelt-driven peak flows during spring/early summer; summer low flows following the recession of peak flow; and in rare instances, rainfall-driven peak flows later in the summer. These extreme conditions are influenced by various climatological and landscape drivers and controls, and the gradual and step changes in these factors are affecting the magnitude, timing, and duration of extreme events.

The most prominent hydrologic extreme event in the Arctic is the spring/early summer (typically May-June-July) peak flow from snowpack melt. Due to cold climatic conditions, snowpack accumulates over the winter when losses in the form of evapotranspiration and sublimation are small. Thus, peak discharge from snowmelt can be expected every year. Additionally, the presence of permafrost in the Arctic and subarctic limits near-surface storage, and therefore is a poor buffer for snowmelt-generated runoff (Kane et al. 2008). On the other hand, landscape controls, such as wetlands (Zakharova et al. 2011) and glaciers (Striegl et al. 2007; Aiken et al. 2014), and their connectivity to hydrologic systems, also influence the magnitude and timing of the peak flows. While these climatological and physiographic factors control snow accumulation and melt processes, snowmelt often occurs at a slow rate due to the variable contributing area of meltwater runoff (Buttle et al. 2016). The melt area is dependent on the temperature gradient within the basin, and the magnitude and timing of the peak flow depend on a number of

factors, including snowpack depth and travel time for the meltwater from different parts of the basin to reach to basin outlet.

The dominant contribution from snow accumulation and melt processes to the peak flows extends to permafrost-free headwaters of large northern river systems (e.g., the Lena, Ob, Yenisei, and Mackenzie Rivers). Rainfall-driven floods in these large northern rivers are unlikely because low-pressure systems conveying summer rainfall extend across only a portion of these basins, which is insufficient to generate annual peak flow (Woo et al. 2008). However, rain-on-snow (ROS) events can play a role in amplifying the snowmelt-driven peak flow. Specifically, higher net radiation input during warmer rainfall events and, to a smaller extent, turbulent heat exchange between rainfall and snowpack can lead to a faster snowmelt and runoff (Mazurkiewicz et al. 2008). Above normal air temperatures and ROS events may also lead to mid-winter snowmelt runoff, early winter river-ice breakup and ice-jam flooding (discussed later) (e.g., Janowicz 2010). Further, ROS events in the fall and winter snow accumulation could impact the snow characteristics and permafrost conditions, e.g., icing the snowpack and warming the soil surface (Putkonen and Roe 2003; Rennert et al. 2009; Hansen et al. 2014; Cohen et al. 2015).

Historically, summer rainfall-generated peak flows in the Arctic have been found to be rare, and typically occur only in the small coastal catchments (e.g., Kane et al. 2003, 2008; Dugan et al. 2009) where the summer rainfall rates could exceed snow ablation rates (Woo et al. 2008). Specifically, such events follow intense summer rainfall events and generate localized peak flow responses that could be larger than the snowmelt peaks, and aided by factors such as limited subsurface storage due to shallow permafrost/active layer depths and steep slopes in the basin. For instance, an extreme summer flood event occurred in the Upper Kuparuk River catchment (drainage area 142 km^2) (discussed later) on the northern slope of Alaska in response to a 50-h, 80 mm rainfall event in July 1999, with the peak flow exceeding snowmelt peak discharge for 1993–2001 (Kane et al. 2003).

Low flows in cold climate regions occur either during winter ice-covered season or summer open-water season (Peters et al. 2014). During the lengthy winter period, sub-freezing temperatures inhibit rainfall events and prevent snowmelt. Baseflow from groundwater sustains low flow discharge (Woo and Thorne 2014) with a larger contribution from deep groundwater flow via the subpermafrost zone (Clark et al. 2001; Walvoord et al. 2012). Additionally, river-ice can modify flow through the reduction of in-channel flow area, phase-change storage into the ice cover, and hydraulic storage in the channel. These modifications can lead to substantial flow reductions such that a period of low flow develops, which is characterized by lower discharge than typically occurring in late winter when flow contributions from the terrestrial and groundwater systems are already at a minimum (Beltaos and Prowse 2008). Northern rivers can also experience low flow conditions in late summer months following the recession of snowmelt-driven flow, which may be interrupted by rainfall and local glacier melt events (Woo and Thorne 2016). Generally, summer low flow exceeds the winter low flow in Arctic river basins. For large northern rivers, discharge gradually declines after snowmelt peaks to a winter low flow minimum, with no distinct summer low flow.

In addition to the discharge-related extreme events, cold regions of the world are also affected by river-ice breakup that has the potential of generating extremely high water level events (Ward 1989). River-ice breakup results when the driving forces acting on ice cover exceed the resisting forces operating to keep it intact, under a broad spectrum of conditions, ranging from thermal (or overmature) to dynamic (or premature) (Beltaos and Prowse 2008). Thermal breakup is defined as the warming temperature-driven deterioration of the ice-cover thickness and strength that encompasses a variety of processes associated with thermal deterioration, including initial fracture, movement, fragmentation, transport, jamming, and final clearance of the ice (Beltaos 2003). Typically, thermal breakup occurs under mild weather conditions that results in low spring runoff and protracted melt, and there is no dramatic rise in water level. In contrast, dynamic breakup typically occurs under severe weather conditions, including large rain events and rapid snowmelt runoff, and results in a rapid increase in channel flow while the ice is still intact (Beltaos 2003, 2014). Snowmelt that moves northward in concert with flow is a major factor contributing to dynamic breakup in the north-draining rivers. This advancing floodwave fractures and then fragments the ice cover that may eventually lead to an ice-jam. This temporarily raises the river level to flood stage due to significant resistance and obstruction of the ice to the intense freshet flow. In certain ecosystems, such as deltaic floodplains, ice jamming in combination with a large spring freshet is often the only mechanism capable of inundating elevated wetlands (Peters et al. 2016). In general, a higher river stage occurs under the influence of ice than under open-water conditions for the same flow magnitude (Gray and Prowse 1992; Beltaos 2014). Dynamic breakups occasionally occur during the mid-winter period, which is also referred to as mid-winter breakup, such as observed in Alaska and the Yukon (Janowicz 2010; Newton et al. 2016). Readers are referred to Beltaos (2003, 2014) for more details on river-ice breakup.

Hydrologic extremes in Arctic environments are changing in response to a warming climate and changes in precipitation and snow regimes. Enhanced warming in the Arctic, which is almost twice as large as global temperature average (Serreze and Barry 2011), is affecting different components of the hydrologic systems with linkages to hydrologic extremes, such as reductions in the magnitude, duration, and extent of snow cover; enhanced permafrost thaw; changes in the precipitation–evaporation balance (Larsen et al. 2014; Bring et al. 2016); and transitions toward rain-dominated regimes (Bintanja and Andry 2017). Furthermore, enhanced poleward moisture transport (Zhang et al. 2013; Vihma et al. 2016) propagates into increased precipitation, which in turn causes increased annual streamflow across the Eurasian and North American river basins (Peterson et al. 2002; Yang et al. 2004; Wu et al. 2005; McClelland et al. 2006; St. Jacques and Sauchyn 2009; Overeem and Syvitski 2010; Zhang et al. 2013). Annual streamflow increases are occurring even with the decreases in snow storage for some of these Arctic river systems, implying an increasing role of rainfall on streamflow, with potential contributions from ground ice melt from permafrost thaw and glacial melt.

Changes in precipitation and temperature regimes can have major implications on hydrologic extremes (Tan et al. 2011; Shi et al. 2015). Increased winter precipitation implies more snow storage and greater water input in the basin, thus the potential for more intense floods. In contrast, warmer temperatures tend to moderate floods by reducing the fraction of winter precipitation that is stored as snow and shortening the period over which snow storage can occur (Shrestha et al. 2017). Warmer temperatures also lead to an earlier snowmelt peak discharge (Barnett et al. 2005, 2008), with the magnitude of peak streamflow determined by the interactions between precipitation and temperature changes. For instance, large atmospheric moisture transport to the Arctic in 2007 resulted in the record high river discharge across several large Eurasian Rivers (Shiklomanov and Lammers 2009; Rawlins et al. 2009; Zhang et al. 2013). However, this event did not lead to record peak monthly discharge in the Lena and Yenisei Rivers (See Fig. 7.4; Overeem and Syvitski 2010).

Warmer temperatures also affect snowfall–rainfall partitioning, with linkages to Arctic hydrologic extremes. For instance, winter rainfall can promote ROS events, which have been found to be increasing in the recent years (Rennert et al. 2009; Liston and Hiemstra 2011; Hansen et al. 2014; Bokhorst et al. 2016). As stated previously, ROS events could play a role in amplifying the snowmelt-driven peak flow. There are also indications that warming may reduce the frequency and intensity of spring ice-jam flooding (Beltaos et al. 2006), while increasing the occurrence of mid-winter river-ice breakup events (Beltaos 2002). Furthermore, winter ROS events can trigger mid-winter breakup events and ice-jam floods, as observed in the Klondike River in Yukon during the winter of 2002–2003 (Janowicz 2010). Further implications of a warming climate on Arctic hydrologic extremes may include decreased summer low flows (Matti et al. 2016) and summer drought events with increased evapotranspiration (Bring et al. 2016). However, glacier melt and increased summer precipitation could sustain or even enhance the summer low flows.

Permafrost degradation associated with the warming temperatures also has implications on streamflow extremes. Specifically, thawing permafrost can lead to increases in subsurface flow pathways, soil moisture volume, and groundwater recharge (Bense et al. 2009). The magnitude and extent of these changes are affected by a number of factors that interact with permafrost, such as the changes in precipitation regime, changes in snow depths, the onset and disappearance of snow cover as well as the presence of organic matter and vegetation (Bokhorst et al. 2016). Specifically, increases in rainfall and ROS events reduce snow depths and snow cover durations as well as increase soil moisture that leads to shifts in the permafrost regime. Snow insulates the ground during winter and provides a blanket over the permafrost that inhibits the penetration of cold temperatures deep into the near-surface soils (Riseborough 1990; Myers-Smith and Hik 2013). Reductions in snow cover extent and duration can lead to increased permafrost as snow-free conditions increase, but that could be partially offset by increasing temperatures. On the other hand, changes in the soil moisture regime coupled with shifts in snow cover and depth can lead to increases or decreases in permafrost, depending on the

moisture content and phase (liquid or solid form such as ice wedges), changes in the thermal conductivity, and latent heat content of the soil (Romanovsky et al. 2010). Additionally, organic materials and shrub growth also affect the response of permafrost to changing snow and moisture regimes (Myers-Smith et al. 2015), e.g., by partially capturing blowing snow and increasing snow depth with the shrub growth (Liston and Hiemstra 2011).

Climate change also affects winter low flows regimes. As the soil water movement becomes more active and the fraction of winter rainfall increases, winter low flow will also increase (Smith et al. 2007), as has been observed in the rivers across the Pan-Arctic (Rennermalm et al. 2010; Tananaev et al. 2016). Additionally, permafrost thawing increases a catchment's water storage capacity, and could decrease the annual maximum discharge (Matti et al. 2016). Consequently, the ratio of maximum to minimum discharge could be used as a diagnostic tool to evaluate the changing influence of permafrost on hydrologic regimes (Ye et al. 2009).

Given these climate-induced changes in the hydrologic regimes, such as the shifts in the magnitude and frequency of extreme events, it has become essential to consider the changes in the context of nonstationarity (Milly et al. 2008). For instance, using nonstationary extreme value analysis, Bennett et al. (2015) identified time-dependent changes in the distribution of spring streamflow extremes for watersheds in the interior region of boreal Alaska. The consideration of nonstationarity is especially relevant in the context of projected enhanced warming and amplified moisture fluxes to the Arctic region (Serreze and Barry 2011; Van Oldenborgh et al. 2013; Zhang et al. 2013), and significant future changes in the extreme flow regimes (Hirabayashi et al. 2013; Shevnina et al. 2017; Shkolnik et al. 2018). Finally, extreme events are rare by nature and thus the methodology and approaches to determine changes in events must be carefully considered in order to assess impacts correctly and present reliable results for decision-making purposes (Zhang and Zwiers 2013).

This chapter provides a review of historical extreme events in the Arctic that are associated with river discharge and water level, as well as a perspective on potential future changes. In Sect. 7.2.1, a review of the previous studies on mean flow, low flow, and peak flow magnitude and timing is provided. Section 7.2.2 provides an updated trend analysis for two important North American rivers, the Mackenzie and Yukon Rivers. Section 7.2.3 discusses a case study on rainfall-driven summer flood event in Alaska. Section 7.2.4 discusses characteristics of extremes associated with river-ice. Section 7.2.5 illustrates the treatment of streamflow extremes in the stationary and nonstationary frameworks with a case study for coastal Alaska. Section 7.3 provides a perspective on potential future changes in extreme hydrologic events. Lastly, Sect. 7.4 provides a summary of key findings and outlines research gaps and challenges, as well as future research needs and directions.

7.2 Historical Changes/Trends in Extremes

7.2.1 Review of Previous Studies on Streamflow Extremes for Major Pan-Arctic Rivers

Trend analyses results from previous studies (most recent study for each river) focused on the Kolyma, Lena, Yenisey, and Ob Rivers in Eurasia, and the Mackenzie and Yukon Rivers in North America are compiled in this section. Figure 7.1 shows the location, and Table 7.1 summarizes the published results for these major rivers. Mean annual flow together with three extreme flow measures (annual maximum daily flow, date of occurrence of annual daily maximum flow, and annual minimum daily flow) are considered. For several of these basins, trend analyses for multiple stations are available. In such cases, the results are summarized as a count of stations with significant trends out of the total number of stations (Table 7.1). Also included are the results for multiple stations aggregated to a single flow time series.

The summaries of positive and negative trends at different statistical significance levels (5% ($p \leq 0.05$) and 10% ($p \leq 0.10$)) are presented. Note that published studies present trends for different time periods, thus reflecting the response to different periods of long-term climate forcing (e.g., temperature and precipitation) and their changes, as well as short-term variability (i.e., Arctic Oscillation, Pacific Decadal Oscillation and El Niño Southern Oscillation). Some of the compiled results are for different stations (upstream or downstream), and/or flow conditions (naturalized or observed) for the same river, which could produce different trends.

Nevertheless, generally consistent patterns emerge across the Pan-Arctic. For instance, in the case of mean annual flow, most studies found increasing trend or no trend ($p \leq 0.05$ or $p \leq 0.10$), with no significantly decreasing trends with the exception of 2 out of 100 stations in Lena basin studied by Tananaev et al. (2016). Furthermore, Zhang et al. (2013) found an upward discharge trend for the Lena, Yenisey, and Ob Rivers for the period 1948–2008. The record 2007 high discharge in these rivers (Rawlins et al. 2009; Shiklomanov and Lammers 2009) is a part of this increasing trend, which as previously mentioned, occurred in response to unusually large atmospheric moisture transport in 2006–2007 over Eurasia (Zhang et al. 2013).

In the case of annual maximum flow, both increasing and decreasing trends were reported, but decreases seem to be more prevalent for these Arctic Rivers and tributaries. Exceptions are Yenisey and Lena Rivers, where significant increases were documented. Shiklomanov et al. (2007) suggested that the increasing trend ($p \leq 0.05$) for the Yenisey River during 1960–2001 could be partly due to reservoir filling in 1960s, while strong warming during spring across the southern and central parts may have contributed to more intense snowmelt and higher peak discharge increases in the Lena basin. Indeed, temperature increases play a dominant role in spring snowmelt timing and thus snowmelt peak discharge. This is

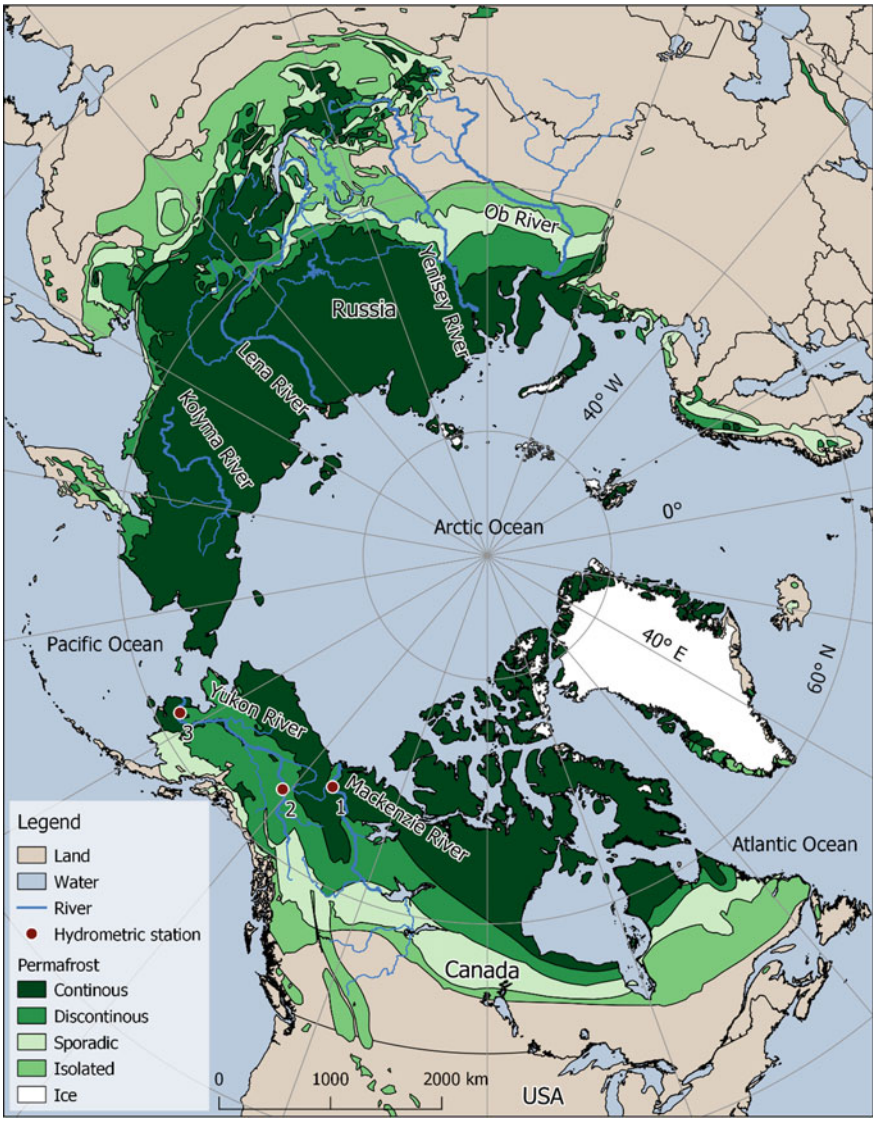

Fig. 7.1 Map showing the six large northward flowing rivers summarized in Table 7.1 (Kolyma, Lena, Yenisey, Ob, Mackenzie, and Yukon). Red dots indicate the location of three hydrometric stations: (1) Mackenzie River at Arctic Red Station; (2) Yukon River at Eagle Station, and (3) Yukon River at Pilot Station; for which trend analyses were updated in this study

reflected in the earlier timing of snowmelt discharge across the Pan-Arctic rivers and tributaries with many significant trends. Overall, the generally consistent patterns of decreasing peak flows and earlier timing are in agreement with the

Table 7.1 Summary of previous studies on streamflow trends for major Pan-Arctic Rivers

River/region	Reference	Study period	Trends			
			Mean annual flow	Maximum flow	Maximum flow timing	Minimum flow
Kolyma (Observed)	Chapter 24	1936–2015	+NS10 (1)			
Kolyma (Downstream gauge)	Shiklomanov et al. (2007)	1940–2001 1950–2001 1960–2001		−NS10 (1) −NS10 (1) −NS10 (1)	−−(1) −−(1) −NS10 (1)	
Kolyma (Aggregation of flows from natural tributaries)	Shiklomanov et al. (2007)	1940–2001 1950–2001 1960–2001		−NS10 – −NS10	−NS10 – −NS10	
Lena (Observed)	Chapter 24	1936–2015	++1 (1)			
Lena (Downstream gauge)	Shiklomanov et al. (2007)	1940–2001 1950–2001 1960–2001		−NS10 (1) −NS10 (1) −NS10 (1)	−NS10 (1) −NS10 (1) −NS10 (1)	
Lena (Aggregation of flows from small natural tributaries)	Shiklomanov et al. (2007)	1940–2001 1950–2001 1960–2001		++ +NS10 +NS10	-NS10 −− −NS10	
Lena + Eastern Siberia (multiple natural tributaries)	Smith et al. (2007)	1958–1989				*+46 (212);* *−17 (212)*
Lena (multiple stations)	Tananaev et al. (2016)	Varying periods between 1925 and 2013	++29 (100); –2 (100)	++6 (105); – 3 (105)		++30 (55); –2 (55)
Yenisey (Naturalized)	Chapter 24	1936–2015	++1 (1)			
Yenisey (Downstream gauge)	Shiklomanov et al. (2007)	1940–2001 1950–2001 1960–2001		+NS10 (1) +NS10 (1) ++(1)	+NS10 (1) −NS10 (1) −NS10 (1)	
Yenisey (Aggregation of flows from small natural tributaries)	Shiklomanov et al. (2007)	1940–2001 1950–2001 1960–2001		– −− −−	−− −− −NS10	

(continued)

Table 7.1 (continued)

River/region	Reference	Study period	Trends			
			Mean annual flow	Maximum flow	Maximum flow timing	Minimum flow
Yenisey (multiple natural tributaries)	Smith et al. (2007)	1958–1989				*+29 (234); −24 (234)*
Ob (Observed)	Chapter 24	1936–2015	+NS10			
Ob (Downstream gauge)	Shiklomanov et al. (2007)	1940–2001 1950–2001 1960–2001		+NS10 (1) +NS10 (1) +NS10 (1)	+NS10 (1) −NS10 (1) −NS10 (1)	
Ob (Aggregation of flows from small natural tributaries)	Shiklomanov et al. (2007)	1940–2001 1950–2001 1960–2001		−NS10 −NS10 −NS10	−NS10 −NS10 −NS10	
Mackenzie + Peel	Déry et al. (2016)	1964–2013	+NS05			
Mackenzie	Yang et al. (2015)	1973–2011	+NS10 (1)	−NS10 (1)	−NS10 (1)	+NS10 (1)
Mackenzie and tributaries	St. Jacques and Sauchyn (2009)	Varying periods between 1939 and 2007	+9 (23)			+20 (23) January–March mean flow
Yukon (Canadian Portion)	Déry et al. (2016)	1964–2013	+NS05 (1)			
Yukon and other rivers in Alaska	Bennett et al. (2015)	1954/1964–2013		−3 (8)		+3 (8)
Pelly (Yukon tributary)	Burn et al. (2010)	1957–2006		−1 (1)	−NS05 (1)	

++(− −) indicate increasing (decreasing) trends at 5% significance level; +(−) indicate increasing (decreasing) trends at 10% significance level. NS05 and NS10 signify no significant trends at the 5 and 10% significance levels, respectively. Blank cells mean no analysis for that variable was performed in the cited study. The numbers in the trend columns are the number of stations with statistically significant trends (out of total number of stations); numbers in italics signify number of monthly minimums (number of months) with statistically significant trends; and no number in parenthesis is given when the data from multiple stations are aggregated

expectation that climate warming would lead to smaller snowpack and earlier melt, which in turn would lead to earlier timing and smaller magnitude of peak flows.

Mostly increasing trends were found for winter minimum flow. Specifically, although some of the sub-basins studied by Smith et al. (2007) and Tananaev et al. (2016) showed decreases in winter minimum flow, the number of sub-basins with increases were higher than those with decreases. The winter low flow change is mainly controlled by winter temperature changes. As discussed earlier, warmer winter temperatures promote increased infiltration and subsurface water movement, which together with increased rainfall would drive the winter low flow increases.

7.2.2 Case Study: Streamflow Trend Analysis for the Mackenzie and Yukon Rivers

This section summarizes trend analyses for the Mackenzie and Yukon Rivers (Fig. 7.1) with records extended up to 2016. The most downstream stations were considered to assess the changes in total fluxes. The Mackenzie River at Arctic Red Station incorporates fluxes from the majority of the basin before flowing through channels of the Mackenzie delta. In the case of the Yukon River, since the downstream station (Pilot Station) has a number of years with missing values, an upstream station (Eagle Station) was also included to consider consistency of the trends. Annual mean flow, maximum flow magnitude and timing, and the 7-day mean minimum flow were considered. The latter was considered instead of 1-day minimum flow because of the difficulties in obtaining reliable low flow measurements during the ice season (Hamilton 2008). The non-parametric Mann–Kendall test (Kendall 1955) was employed to detect trends at the 5% and 10% significance levels, with iterative pre-whitening (Zhang and Zwiers 2004) used to remove the effects of serial correlation.

Figure 7.2 displays the results of monotonic trend analyses of the mean and extreme flow fluxes for the Mackenzie River. The trend results for all four streamflow variables are small and insignificant ($p \leq 0.10$) and corroborated with previous studies that used different periods (Table 7.1). Specifically, similar to Yang et al. (2015) for 1973–2011, there is a weak increasing tendency in mean flow over 1973–2016 (Fig. 7.2a) within a small coefficient of variation (CV = 0.10). The 7-day minimum daily flow (which occurs in winter months) has a CV of 0.19 over the study period and a weak tendency of increase during 1973–2016 (Fig. 7.2b). This change in flow amount is very small and statistically insignificant. In the case of maximum daily flow, the trend is a small non-significant ($p \leq 0.10$) decrease. The maximum flow has CV = 0.14, but a wide range with flows of 15,800 m^3/s to 35,000 m^3/s occurring in 1995 and 1992, respectively. These two periods corresponded to the lowest snowpack in 1994/1995 and the highest snowpack in 1991/1992 (Yang et al. 2015). The ratio of maximum to minimum flow declined by about 12%, which although not significant ($p \leq 0.10$), is indicative of permafrost degradation in the basin. The timings of the annual maximum flow, which occurs between late spring to early summer, vary between 226 and 280 days starting from

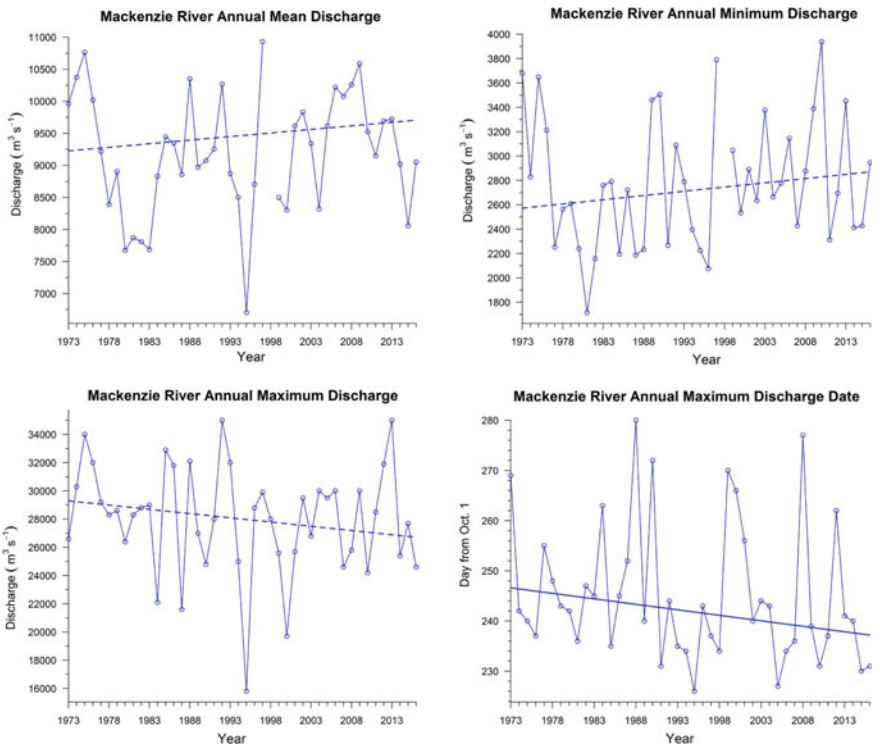

Fig. 7.2 Streamflow trends for the Mackenzie River at Arctic Red hydrometric station. Solid trend lines indicate statistically significant trends ($p \leq 0.05$), and dashed lines indicate insignificant trends. No other significant trends at $p \leq 0.10$ were obtained

October 1st. Peak timing advanced significantly ($p \leq 0.05$) by about ten days over the period 1973–2016, indicative of the earlier snowmelt occurring in the basin.

The results for the Yukon River (Fig. 7.3) are also consistent with previous studies that used different periods (Table 7.1). Corroborating with these studies, the magnitude of trends for all four variables are small and non-significant. Nevertheless, the directions of trends match, which are also in general agreements for the same variables for other basins. Specifically, the mean annual flow shows non-significant increases for both Yukon-Eagle and Yukon-Pilot Stations over 1977–2016, with small variability (CV of 0.12 and 0.08, respectively), which is consistent with the analysis by Déry et al. (2016) (Fig. 7.3a). The 7-day low flows have weak increasing tendencies for both stations (Fig. 7.3b), and small variability (CV of 0.14 and 0.12, respectively). The direction of increasing trend matches with the Bennett et al. (2015) study for the Yukon River at Eagle Station, with key differences being the use of annual minimums 1954–2013 period, and significance level ($p \leq 0.10$). In the case of annual maximum flow, non-significant trends were discerned, which are of increasing and decreasing tendencies, and CV of 0.25 and

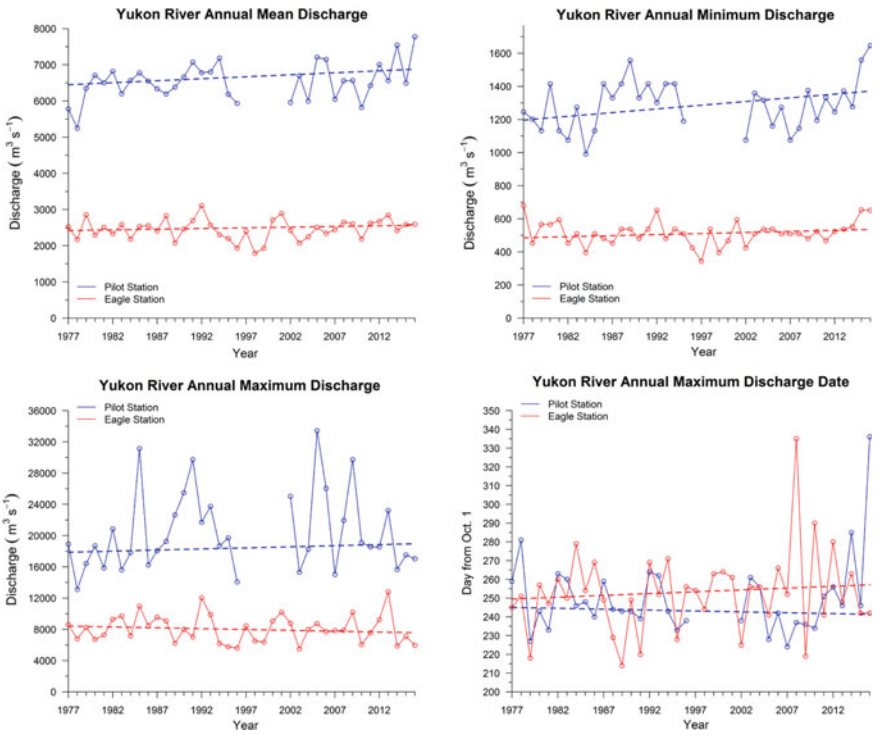

Fig. 7.3 Streamflow trends for the Yukon River at the two stations, Eagle and Pilot Station. Dashed line indicates insignificant trend; no significant trends at $p \leq 0.10$ were obtained

0.22 for Yukon River at Eagle and Pilot Stations, respectively (Fig. 7.3c). The non-significant increasing trend for the annual maximum flow contrasts with decreasing maximum flow for most basins. In this case, missing data spanning 1997–2000 could have played a part, as the maximum flows for this period are relatively smaller at the Eagle Station. With regard to maximum to minimum flow ratio, there is a weak declining trend for the Eagle Station and no trend for the Pilot Station, suggesting limited influence of permafrost change.

Trends in the timing of the maximum flows are non-significant and in opposite directions for the two stations, with the ranges of 214–335 and 224–336 days for the Yukon River at Eagle and Pilot Stations, respectively (Fig. 7.3d). The increasing (albeit non-significant) trend for the Eagle Station contradicts with the expected trend of earlier snowmelt and earlier maximum flow with the warming climate. Additionally, peak flows at the beginning of September for both stations (Eagle Station: 2008; Pilot Station: 2016) are later than the expected occurrence of early summer. A closer examination of the Eagle Station streamflow revealed occurrences of multiple summer peaks, with secondary peaks later in the summer of 2010 and 2012. Such late summer secondary peaks were also observed in the Pilot

Station in 2014 (not shown), suggesting a possible influence of summer rainfall. Furthermore, portions of the Yukon Basin are experiencing extensive melting of alpine glaciers and perennial snow fields (Striegl et al. 2007), with discharge for rivers directly influenced by glacial meltwater typically peaking later in the summer (Aiken et al. 2014). These factors complicate the diagnosis of winter snowmelt-driven streamflow timing trends.

Overall, the trend analysis results from this and other studies align with the expectation for a warming climate and increased wetness. Specifically, the increasing tendencies in the mean annual flow (although not all significant) is consistent with increased wetness across the Pan-Arctic basins that tend to overshadow the effects of increased warming, thus increased evapotranspiration. The increased wetness also plays a role in higher winter low flows, which is enhanced by increased temperatures, thus higher proportion of rainfall. In the case of annual maximum flow, which is conditional upon the evolution of seasonal snowpack, the mostly decreasing peak flow magnitude (again not all significant) is consistent with increased warming and decreased snowpack. This corroborates with a recent study (Musselman et al. 2017), which suggested slower snowmelt and smaller peak flow in a warmer climate. Furthermore, earlier snowmelt-driven peak flow is an obvious change arising from warming temperatures.

7.2.3 Case Study: Rainfall-Driven Extreme Flow in Arctic

Historically over the Alaskan Arctic, annual peak floods occur following snowmelt when the snowpack that has accumulated over 8–9 months typically melts in 7–14 days. The shallow active layer, which freezes and thaws each year over the continuous permafrost, has limited subsurface storage within the 40–60 cm active layer depth. Rainfall-generated floods in the Arctic are rare and seldom documented. In July 1999, a summer flood was recorded on the Upper Kuparuk River (Fig. 7.4) in response to a 50-h duration rainfall event that produced a watershed average runoff in excess of 80 mm (Fig. 7.5). Prevailing atmospheric conditions allowed moist air to move northward over areas of little or no vertical relief from the North Pacific Ocean to the Arctic Ocean. Cyclogenesis occurred along the quasi-stationary front separating maritime and continental air masses along the arctic coast. This low-pressure system propagated inland southward over the 142-km^2 headwater basin of the Kuparuk River in the northern foothills of the Brooks Range; a treeless area underlain by continuous permafrost. This research catchment was instrumented with a stream-gauging station, two major and six minor meteorological stations, for a total of eight precipitation gauges. The peak instantaneous flow was estimated at 100 m^3/s and was about three times greater than any previously measured flood peak. Typically for Alaska North Slope, the ratio of runoff volume to snowmelt volume is near 0.67 or greater and the ratio of cumulative summer runoff and rainfall averages around 0.5 or greater. For the storm discussed here the runoff ratio was 0.73. These high runoff ratios are due to the role

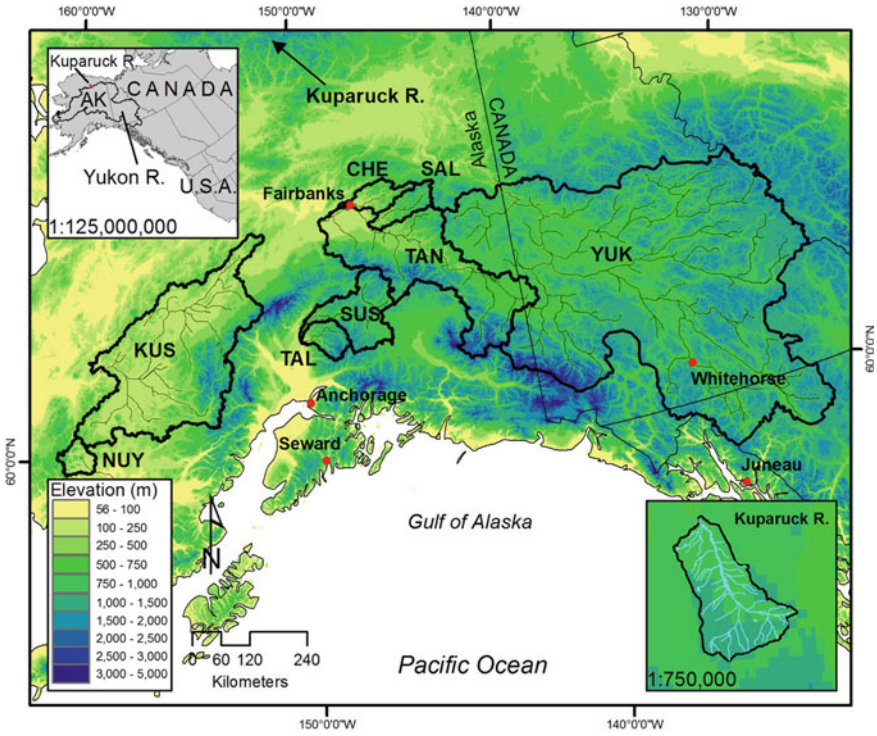

Fig. 7.4 Map of river basins in central Interior and western Alaska. YUK = Yukon, CHE = Chena, SUS = Susitna, TAN = Tanana, TAL = Talkeetna, KUS = Kuskokwim, and NUY = Nuyakuk rivers. Also shown is the Kuparuck River basin (lower right inset) and the study site location in North America (top left inset)

of permafrost in limiting the potential subsurface storage and the steep slopes of this headwater basin.

Although the data reported in this section are of a short duration for the flooding period, a general understanding of the hydrologic and meteorological processes of this nested grouping of Arctic basins is evolving. It is comprehensible that, for the headwater basins in the foothills, rainfall-generated runoff events will produce flood magnitudes that far exceed those generated during snowmelt. From the precipitation data collected to date, it is also evident that the foothills receive significantly greater amounts of precipitation than the lower coastal areas, and the higher the foothills the greater the annual precipitation received. This combined with the high-gradient topography and continuous permafrost promotes a significant and rapid runoff response to snowmelt and summer precipitation, hence a relatively high flood risk over this region. Further details on the Kuparuk River rainfall-driven event are available in Kane et al. (2003), and additional discussion on the rainfall-driven extreme flow events are available in Kane et al. (2008) and Dugan et al. (2009).

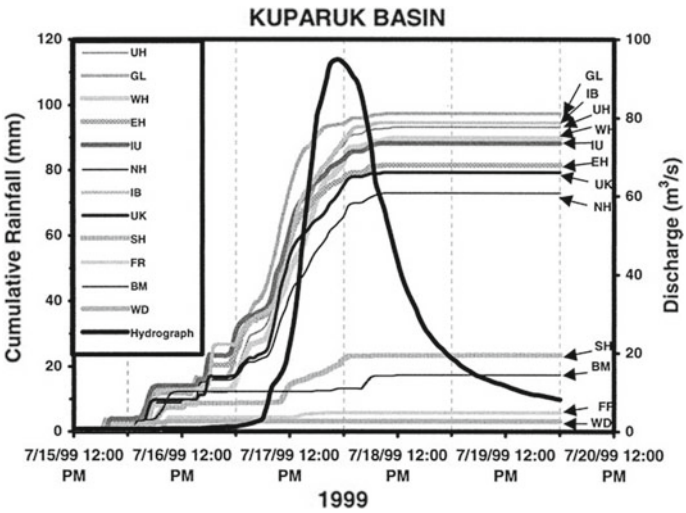

Fig. 7.5 Cumulative rainfall at eight headwater rain gauges and four other gauges between the Upper Kuparuk River catchment and the coast. The dark line represents the hourly mean discharge for the storm; note that the hourly mean discharge is slightly less at the time of the peak than the instantaneous peak of 100 m^3/s (kane et al. 2003). ©American Meteorological Society. Used with permission

7.2.4 Case Study: River-Ice Breakup Floods

River-ice breakup and associated ice-jams generally dominate the generation of annual high water levels throughout the Arctic regions of Canada. A recent study across Canada found that ~32% of the rivers were dominated by annual extreme peak water levels generated under river-ice breakup, ~45% open-water, and ~23% mixed conditions for the current climate regime (von der Wall 2011) (Fig. 7.6). This flood-generating process is most pronounced in sub-regions possessing the combined effects of low relief and a cold, dry arctic climate (Buttle et al. 2016). For instance, the south to north spring breakup season in the Mackenzie River basin is on average ~8 weeks but can last up to three months. Patterns in both breakup events and calculated time lags between events indicate that in general both the duration and variability of events increases downstream in the basin, likely due to increasing contributing areas, and the occurrence of ice-jamming events (de Rham et al. 2008a).

For the Mackenzie River at Arctic Red Station (Fig. 7.1), river-ice breakup-influenced peak water levels for discharges ranging from 20,000 to 30,000 m^3/s have been found to be 2–10 meters higher than during ice-free period (Fig. 7.7). Goulding et al. (2009) concluded that for this river reach, the severity of peak breakup stage was mostly influenced by upstream discharge (driver) and the balance between upstream and downstream ice melt, while timing was related to ice

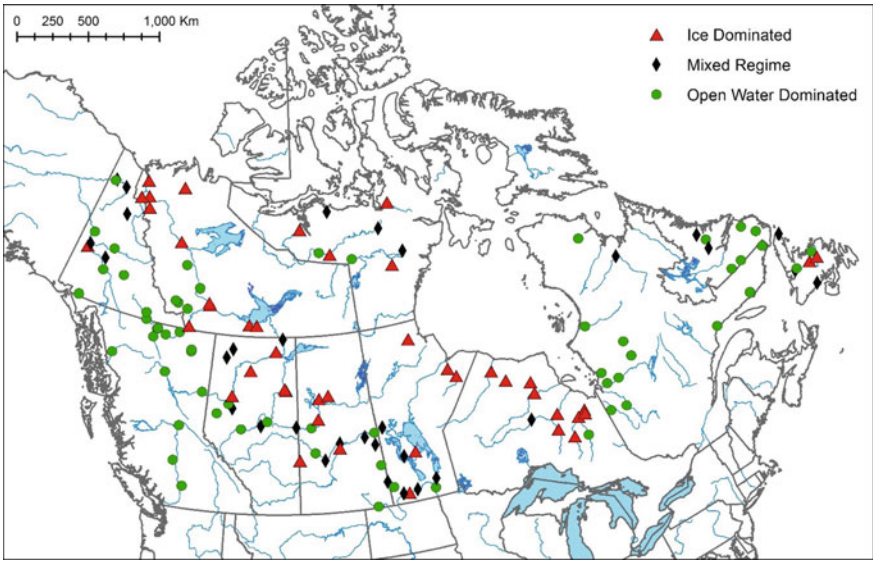

Fig. 7.6 Distribution of peak-water level regimes across Canada for available hydrometric stations. Modified from von der Wall (2011)

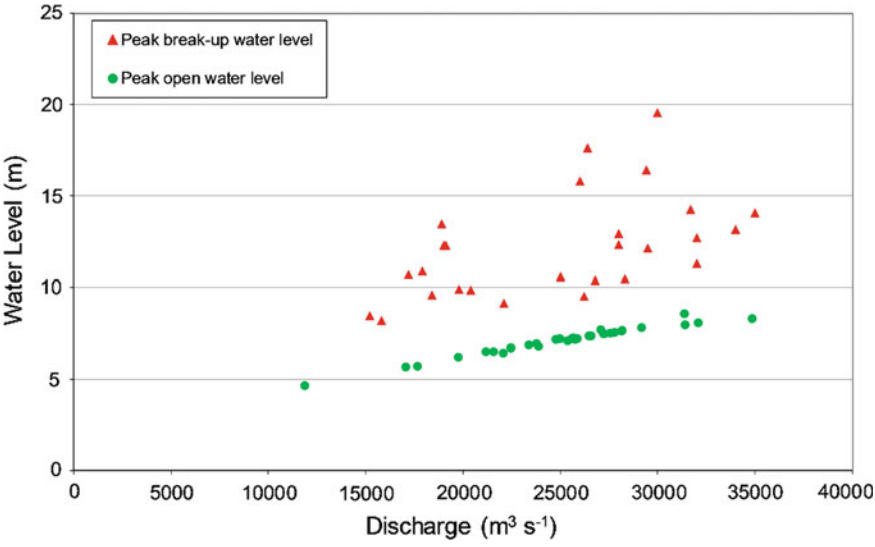

Fig. 7.7 Open-water and ice-influenced peak water levels versus discharge at the Mackenzie River at Arctic Red River hydrometric station for the years 1972–2006. Modified from Goulding et al. (2009), von der Wall (2011)

conditions in the delta and the rise of the hydrograph. They found that there were trends toward a longer pre-breakup melt interval, lower peak discharge, lower rate of rise in discharge, and thinner ice thickness, and higher freeze-up stage, with greater variability of these controls and breakup severity in the most recent decade.

Similar to the issue of defining flood frequencies for different hydrologic processes (e.g., snowmelt and rainfall), flood frequency analysis in cold regions of the world must be based not only on discharge records, but also consider the occurrence of extreme backwater level conditions produced by ice jamming. To this end, de Rham et al. (2008b) carried out flood frequency analysis of the maximum annual nominal water depths during the spring breakup and open-water season for 28 hydrometric stations in the Mackenzie River over 1913–2002. They found that the return periods of peak water levels for 13 stations were dominated by spring breakup events, including the Mackenzie-Arctic Red Station, while open-water return periods dominated 14 stations. At sites where discharge during the spring breakup is greater than one quarter of the peak annual discharge, nominal water depths can be expected to exceed those occurring during the peak annual discharge event. Furthermore, for river reaches dominated by spring breakup extremes, the ratios of ice covered to open-water return periods generally increase with increasing return periods. In addition, de Rham et al. (2008a) carried out trend analysis for the timing of spring breakup events and found significantly earlier trends ($p \leq 0.10$) of about 1 day/decade in upstream portions of the major tributaries of the Mackenzie Basin over the period 1970–2002. A similar trend was also found for the Canadian portion of the Yukon River (Janowicz 2010). Additionally, the study by von der Wall (2011) noted that the timing of ice-influenced peak water levels and ice breakup have generally been occurring earlier since the late 1960s across Canada. A related change is the shortened duration and decreased thickness of the river-ice cover, as observed in five major Siberian rivers (Shiklomanov and Lammers 2014).

Also of interest is the role of large reservoirs in the ice-influenced extremes. For example, in the headwaters of the Mackenzie River basin on the Peace River, the combined effects of i) higher than naturally occurring fall freeze-up stage due to reservoir releases and ii) declining spring snowpack depth in key trigger tributaries have played a role in reduced frequency of ice-jam flood events (Beltaos 2014, 2017). Interestingly, a small flow release over a 10-day period from the Peace River headwater reservoir was shown to be an effective approach for enhancing an ice-jam flood 1000 km downstream in the Peace–Athabasca Delta, resulting in approximately 0.25 m higher backwater level on the lower river mainstem (Prowse et al. 2002). This “real life” case study suggests that a properly timed reservoir release can be used as an adaptation strategy to offset anthropogenic effects on extreme events.

7.2.5 Case Study: Nonstationary Frequency Analysis of Maximum Streamflow

The case study using Generalized Extreme Value (or GEV) approach (see Box 7.1) for eight streamflow stations in Alaska demonstrates the stationary and nonstationary distributions of maximum streamflow extremes. The streamflow stations analyzed here span a range of climatic and physiographic conditions, extending from the central Interior region of Alaska near Fairbanks, southwest to the village of Dillingham, and east to the town of Eagle near the Yukon Territory, Canada. Only the gauges with more than 40 years of data were considered, with years ranging from 1954 to 2013 for six of the eight stations, and 1964–2013 for the Tanana and Talkeetna river systems (Fig. 7.4). The sites are a sample of Interior Arctic stations exhibiting both glacial and snowmelt influences (glacial–nival, i.e., Susitna, Talkeetna River basins), and snowmelt and rainfall influences (nival–rainfall, i.e., Chena, Salcha River basins). The Yukon River at Eagle Station covers the largest watershed area, and trend analysis for this station is presented in Sect. 7.2.3.

A statistical approach based on physically plausible relationships was used to evaluate the distribution of the spring time (April-May-June) maximum streamflow extremes for these basins, with both stationary and nonstationary distributions considered for each station. To test the goodness-of-fit of the distributions and determine if the GEV fit of the model candidates was appropriate, Kolmogorov–Smirnov (K–S) test was employed. Hence, the stationary (S: Susitna, Kuskokwim, Yukon-Eagle, Tanana), linear nonstationary (LNS: Talkeetna, Nuyakuk, Chena), and simple nonlinear nonstationary (NLNS1: Salcha) models were selected (Fig. 7.8). Stationary results are indicative of no trend in the system. The nonstationary GEV model can also consider the effects of large-scale climate variability with the Pacific North American pattern, the Arctic Oscillation, the Pacific Decadal Oscillation, and the El Niño–Southern Oscillation indices used as potential covariates (see Bennett et al. 2015). Alternatively, seasonal precipitation and temperature, which drive the maximum streamflow, could be used as covariates for the evaluation of nonstationary GEV distribution, as demonstrated by Shrestha et al. (2017). Readers are referred to Cannon (2010) for more details on these methods.

The results show a range of responses, from stationary (no change) to highly nonstationary (large change) across the study region. The nonstationary return periods (2, 5, 10, 20, 50, and 100 year) shown in Fig. 7.8 illustrate the magnitude of changes in extreme value statistics over time. For example, in the Salcha system, a spring time maximum streamflow of almost 800 m^3/s in the 1950s has a 10% recurrent probability (10-year return period) but, by 2013, the same flow magnitude has a recurrent probability of 98% (50-year return period). In other words, the 10-year spring return flow value has decreased by approximately 150 m^3/s in the Salcha system over the 60-year period, 1954–2013.

The nonstationary changes could be attributed to a number of factors, such as changes in high elevation snow and glaciers (Talkeetna), and/or early loss of

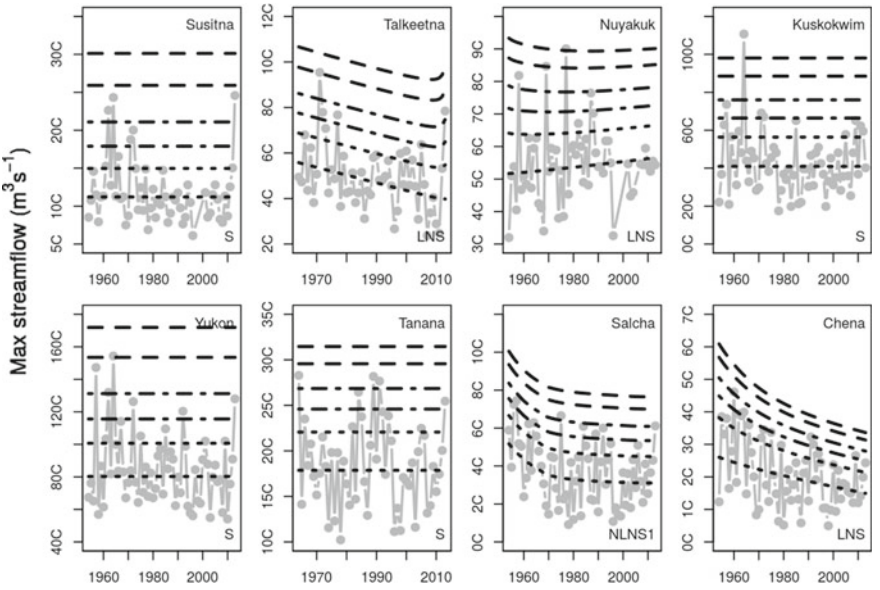

Fig. 7.8 GEV results for maximum streamflow in April-May-June for the eight river basins in Alaska: Susitna, Talkeetna, Nuyakuk, Kuskokwim, Yukon (Yukon-Eagle), Tanana, Salcha, and Chena. The results are shown for Stationary (S), Linear Nonstationary (LNS), and simple Nonlinear Nonstationary (NLNS1) models. Grey circles and lines illustrate the observed streamflow maximums for the season. Dashed lines show 2, 5, 10, 20, 50, and 100 year return intervals, based on the GEV fits. Time interval (x-axis) is relative to length of record and y-axis scale is shown in 100 s (C). This figure is modified from Bennett et al. (2015)

snowpack (Chena and Salcha). Seasonal and annual maximum streamflow declines for the Susitna, Talkeetna, Salcha, and Chena River basins are also supported by non-parametric trend results (Bennett et al. 2015). On the other hand, systems such as the Yukon River at Eagle Station may be experiencing multiple effects and can result in opposing changes in the system, changes that could very well cancel out in terms of streamflow volume or timing changes, thus resulting in the stationary GEV.

Overall, the methods employed in this case study provide a framework for a regime-based evaluation of stationary to nonstationary extreme events, and relating them to particular processes that are impacted by climate change or variability. Likewise, directional changes are not likely to be consistent across regions; rather they are more likely to be consistent between climate regimes. Therefore, river systems must be examined carefully to clearly separate regimes and processes operating across expansive basins in the north.

Box 7.1. A Generalized Extreme Value Approach for Evaluating the Distribution of Streamflow Extremes The Generalized Extreme Value (GEV) approach is grounded in the theory of extremal limits. The theory states that block maxima drawn from sufficiently long series will approach the GEV distribution asymptotically at large sample sizes (Coles 2001). This provides justification for making inferences about return periods of extremes for finite sample sizes. The GEV-based approach to estimating trends in streamflow extremes can also incorporate nonstationarity, thus allowing inferences to be made about changes in the frequency and magnitude of maximum and minimum flows (Milly et al. 2008; Salas and Obeysekera 2014; Cheng et al. 2014).

The GEV approach described in this case study utilizes the R-project's GEVcdn package as described in Cannon (2010). The GEV cumulative distribution function can be expressed as

$$F(x,\theta) = \exp\left[-\left\{1+\xi\left(\frac{x-\mu}{\sigma}\right)\right\}^{-1/\xi}\right] \quad \text{for } \xi \neq 0, 1+\xi\left(\frac{x-\mu}{\sigma}\right) > 0 \tag{7.1}$$

$$F(x,\theta) = \exp\left[-\exp\left\{-\left(\frac{x-\mu}{\sigma}\right)\right\}\right] \quad \text{for } \xi = 0 \tag{7.2}$$

where $\theta = (\mu, \sigma, \xi)$ are the location (μ), scale ($\sigma > 0$), and shape (ξ) parameters of the GEV distribution. Based on the shape parameter, which characterizes the distribution's tail, the GEV can assume three types: (I) $\xi = 0$ light-tailed or Gumbel type; (II) $\xi > 0$ heavy-tailed or Fréchet type; and (III) $\xi < 0$ bounded tail or Weibull type. From Eqs. (7.1) to (7.2), the extreme streamflow quantile x_τ can be obtained:

$$x_\tau = \mu - \frac{\sigma}{\xi}\left[1-\{-\log(\tau)\}^{-\xi}\right],\ \xi \neq 0 \tag{7.3}$$

$$x_\tau = \mu - \sigma\log\{-\log(\tau)\},\ \xi = 0 \tag{7.4}$$

where quantile x_τ is a function of exceedance probability p: $G(x_\tau) = p = 1-\tau$ with $0 < p < 1$, and the annual maximum x_τ corresponds to the return period $T = 1/\tau$.

For stationary models all parameters of the GEV distribution are assumed constant. In the case of nonstationary models, one or more parameters of the GEV distribution can be allowed to vary with time, e.g., by including covariates that are time-dependent. The covariates could simply be time itself or the hydro-climatic variables that drive the extremes. Additionally, the GEV

analysis approach allows determining the form of the relationship (or if there is indeed evidence of a nonstationary relationship) that best fits the streamflow data. More details on the applications of the nonstationary GEV method for evaluating the distribution of streamflow extremes are available in Bennett et al. (2015) and Shrestha et al. (2017).

7.3 Projected Future Changes

As noted earlier in the chapter, future climate projections indicate continued enhanced warming and strong increases in high-latitude precipitation (Collins et al. 2013; Vihma et al. 2016). Specifically, December-February and June-August mean temperatures over the Arctic are projected to increase by 10 (6) and 5 (4 °C) under the Representative Concentration Pathway RCP8.5 (4.5) scenarios by the end of the twenty-first century (Coupled Model Intercomparison Project, Phase 5, CMIP5, multi-model mean for 2081–2100 relative to 1986–2005 averages) (Van Oldenborgh et al. 2013). In the case of precipitation over the Arctic land, mean precipitation for October-March and April-September is projected to increase by 60 (35%) and 25 (20%) under the RCP8.5 (RCP4.5) scenarios by the end of the twenty-first century (Van Oldenborgh et al. 2013). Extreme temperature and precipitation is anticipated to increase by 2–3 times the mean values in Alaska, indicating larger and more frequent extreme events for the Arctic than those described for mean conditions (Bennett and Walsh 2015). The implications of these changes include an increase in fraction of winter rainfall, a reduction in snowfall fractions and extent, and an increase in ROS events. Specifically, Bintanja and Andry (2017) projected that the snowfall fraction would reduce to below 50% for much of the Arctic (except for Greenland) by the end of century (RCP8.5 forcing multi-model means). This would also lead to an increased frequency and areal extent of ROS events in many parts of the Arctic (Rennert et al. 2009; Hansen et al. 2014; Jeong and Sushama 2018). In terms of snowpack, decreased snow cover extent but increased maximum snow water equivalent are projected to occur (Callaghan et al. 2011; Thackeray et al. 2016). Further, in response to not only to warming, but also to changes in snow cover, which exerts a control on the underlying soil, Arctic permafrost is projected to undergo substantial degradation. Specifically, the CMIP5 models projected substantial loss of permafrost by the end of century ranging from 51 ± 13% for RCP4.5 and 81 ± 12% for RCP8.5 (CMIP5 multi-model mean for 2080–2099 relative to 1986–2005 averages) diagnosed near-surface permafrost area (Collins et al. 2013).

These changes in precipitation, temperature, and consequent changes in snow and permafrost could be expected to lead to considerable changes in the streamflow extremes. For instance, recent global/Pan-Arctic scale studies (Koirala et al. 2014; Schewe et al. 2014; Bring et al. 2017) projected enhanced annual flows and low flows for the future climate scenarios, while peak flow could increase or decrease depending on the region, and changes in temperature and precipitation in a climate model. In terms of extreme value distribution, a recent analysis by Hirabayashi et al. (2013) found that the 100-year return period flood event of the twentieth century would become more frequent for the Yukon, Mackenzie, Yenisey, and Lena Rivers, and less frequent for Ob River by the end of twenty-first century. Implications of these changes in peak flow could be an increase in the annual maximum flood area across the Arctic (Shkolnik et al. 2018). In general, the projected future changes in annual flow and low flow in the Arctic region tend to follow historical trends. In the case of maximum flows, the declining trends could either continue or reverse, depending on the interactions of temperature and precipitation changes.

A warming climate may also bring significant shifts to the dominant flood generation mechanism in rivers, such as a shift from an ice-breakup-dominated flood regime to a mixed or to an open-water peak flow-dominated flood regime. For example, Beltaos et al. (2006) projected a two to four weeks reduction in the ice-cover season and depletion of the winter snowpack by mid-winter thaws in headwater tributaries of the Mackenzie River basin, leading to a severe reduction in the frequency of spring ice-jam flooding in the Peace–Athabasca Delta. Furthermore, with potentially thinner river-ice cover under a warmer climate (Beltaos and Prowse 2008), hydraulic obstruction to the passage of the spring freshet would be reduced, thus producing reduced water levels associated with the river-ice breakup and reducing the severity of the spring ice-jam floods (Prowse et al. 2010). Overall, decreases in the severity and/or occurrence of ice-jam-induced floods have the potential to lessen inundation of floodplain regions (Beltaos 2017), lengthen dry intervals—if not replaced by open-water extreme flow events—and increase the likelihood of degrading riparian aquatic ecosystems (Peters et al. 2016). Additionally, stream air–temperature gradients over large basins, which are known to be a good proxy for the timing of spring melt/breakup conditions (Bonsal and Prowse 2003), are projected to change in the future climate. Specifically, Prowse et al. (2010) discussed that for the north-flowing rivers, enhanced downstream warming compared to headwaters will lead to a decrease in temperature gradients from the river headwaters to mouth. This change in temperature gradient, together with the changes in magnitude of the spring runoff and ice-cover thickness, will have implications on the driving and resisting forces for river-ice breakup.

7.4 Conclusion and Recommendation

Due to enhanced warming and amplified moisture fluxes, the characteristics of hydrologic extremes in the Arctic are changing rapidly—with substantial alterations in the magnitude, variability and timing of events. Overall, the historical trends align with the expectation of a warming climate and increased poleward moisture transport. Specifically, increasing trends in mean annual flow are consistent with the increased wetness across the Pan-Arctic basins that tend to overshadow the effects of increased warming, thus increased evapotranspiration. Increasing precipitation, especially winter precipitation, plays an important role in increasing winter low flow trends, as warming enhances the proportion of rainfall. Winter low flow is further enhanced by the permafrost loss as it promotes increased soil infiltration, subsurface water movement, and connections to stream networks. In the case of annual maximum flow, which is conditional on the seasonal snowpack accumulation and melt, mostly decreasing trends in peak flow magnitude have been observed, which is consistent with the increased warming and decreased snowpack. Furthermore, earlier timing of snowmelt-driven peak flow is an expected change with warming. The change in precipitation regime, i.e., extreme summer rainfall, has been found to be causing more frequent secondary peak flow events in late summer in some areas of the Arctic. Such events could be enhanced by glacier melt, and the secondary peaks could exceed the snowmelt-driven peak flows.

There is also evidence of nonstationary changes in the snowmelt-driven streamflow extremes, such as increasing recurrence interval of floods of a particular magnitude, or decreasing magnitude of floods of a given return period. These alterations are in line with decreasing snowpack depth and earlier snowmelt, hence smaller snowmelt-driven peak flows. The directional changes are not likely to be consistent across regions; rather they are more likely to be consistent between climate regimes. Therefore, a careful analysis on river systems must be carried out to clearly separate regimes and processes operating across expansive basins in the north.

Future projections indicate continued enhanced warming and strong increases in high-latitude precipitation, and mostly continuation of the historical trends in extremes, such as enhanced annual flows and low flows. The peak flows could either increase or decrease depending on the region, as well as interactions of future precipitation, temperature, and snow storage. On the other hand, nonstationary changes in the peak streamflow extremes have been projected to occur in the future climate, with a potential to decrease the recurrence intervals of historical floods. These results reinforce the need for nonstationary analysis of streamflow extremes.

It is also important to consider the social and economic implications of the climate-driven shifts in extremes. The infrastructure in the Arctic is one of the main areas of vulnerability. The development in the Far North (Arctic and subarctic) is progressing at a rapid pace, such as the development of hydroelectric water resources (Cherry et al. 2017; Sturm et al. 2017), and their design and operation need to take into account projected changes in the extremes. For instance, while

increased low flow could augment water supply needs in the winter, the shift in timing together with the potential increase in magnitude of peak flow could lead to situations where built hydraulic structures are inadequate to cope with the shifts, and result in frequent and widespread flooding. The increased risk associated with flooding could threaten other infrastructure as well as operational services, such as mines, roads, railways, bridges, pipelines, and settlements located nearby (Instanes et al. 2016). This could potentially require costly construction of new flood protection infrastructure as well as modifying/reconstructing existing dams, bridge crossings and pipeline, etc. Also associated with the warming climate is the permafrost degradation and threats to infrastructure it poses. Particularly, temperature increases will affect the stability of the frozen embankments and water-retaining structures, and likely to increase the construction and operational costs (Instanes et al. 2005). Further, infrastructure designed for frozen soils that become unfrozen may collapse, leading to economic loss either in the redesign or abandonment (Instanes et al. 2016). On the other hand, while the potential decrease in the severity of ice-jam flood may not impact the infrastructure directly, the thinner and shorter duration of river-ice cover may impact winter transport over the river-ice roads.

Also associated with these changes are the challenges in terms of observing, understanding, mitigating, and adapting to these impacts. In particular, it may not be possible to extrapolate or transfer the likely impacts across different river basins. Thus, an enhanced monitoring network together with development of robust decision support system tailored for an individual river basin will be needed. There is also a need to better address major research gaps for improved understanding of potential changes in Arctic streamflow extremes, e.g., basin scale hydrologic modeling studies that incorporate key processes such as permafrost change. Currently, impact studies in most Arctic regions are limited to global/Pan-Arctic wide studies, which provide a basic understanding of the large-scale climate-driven changes, but are often not designed to represent the finer details of the hydrologic extremes. Hence, focused research on hydrologic modeling and analysis of extreme events at a river basin/regional scale is recommended. The Arctic region is vast, with limited observational data and selected research focus. As such, many extreme events go unrecorded, and it becomes challenging to attribute changes in extremes to a specific cause. In this respect, satellite-based observations could provide new avenues for evaluating and attributing hydrologic changes in the Arctic, including the extreme events.

References

Aiken GR, Spencer RGM, Striegl RG, Schuster PF, Raymond PA (2014) Influences of glacier melt and permafrost thaw on the age of dissolved organic carbon in the Yukon River basin. Glob Biogeochem Cycles 28:525–537. https://doi.org/10.1002/2013GB004764

Barnett TP, Adam JC, Lettenmaier DP (2005) Potential impacts of a warming climate on water availability in snow-dominated regions. Nature 438:303–309. https://doi.org/10.1038/nature04141

Barnett TP, Pierce DW, Hidalgo HG, Bonfils C, Santer BD, Das T, Bala G, Wood AW, Nozawa T, Mirin AA, Cayan DR, Dettinger MD (2008) Human-induced changes in the hydrology of the western United States. Science 319:1080–1083. https://doi.org/10.1126/science.1152538

Beltaos S (2003) Threshold between mechanical and thermal breakup of river ice cover. Cold Reg Sci Technol 37:1–13

Beltaos S (2014) Comparing the impacts of regulation and climate on ice-jam flooding of the Peace-Athabasca Delta. Cold Reg Sci Technol 108:49–58. https://doi.org/10.1016/j.coldregions.2014.08.006

Beltaos S (2002) Effects of climate on mid-winter ice jams. Hydrol Process 16:789–804. https://doi.org/10.1002/hyp.370

Beltaos S (2017) Frequency of ice-jam flooding of Peace-Athabasca Delta. Can J Civ Eng 45:71–75. https://doi.org/10.1139/cjce-2017-0434

Beltaos S, Prowse T (2008) River-ice hydrology in a shrinking cryosphere. Hydrol Process 23:122–144. https://doi.org/10.1002/hyp.7165

Beltaos S, Prowse T, Bonsal B, MacKay R, Romolo L, Pietroniro A, Toth B (2006) Climatic effects on ice-jam flooding of the Peace-Athabasca Delta. Hydrol Process 20:4031–4050. https://doi.org/10.1002/hyp.6418

Bennett KE, Cannon AJ, Hinzman L (2015) Historical trends and extremes in boreal Alaska river basins. J Hydrol 527:590–607. https://doi.org/10.1016/j.jhydrol.2015.04.065

Bennett KE, Walsh JE (2015) Spatial and temporal changes in indices of extreme precipitation and temperature for Alaska. Int J Climatol 35:1434–1452. https://doi.org/10.1002/joc.4067

Bense VF, Ferguson G, Kooi H (2009) Evolution of shallow groundwater flow systems in areas of degrading permafrost. Geophys Res Lett 36. https://doi.org/10.1029/2009gl039225

Bintanja R, Andry O (2017) Towards a rain-dominated Arctic. Nat Clim Change 7:263–267. https://doi.org/10.1038/nclimate3240

Bokhorst S, Pedersen SH, Brucker L, Anisimov O, Bjerke JW, Brown RD, Ehrich D, Essery RLH, Heilig A, Ingvander S, Johansson C, Johansson M, Jónsdóttir IS, Inga N, Luojus K, Macelloni G, Mariash H, McLennan D, Rosqvist GN, Sato A, Savela H, Schneebeli M, Sokolov A, Sokratov SA, Terzago S, Vikhamar-Schuler D, Williamson S, Qiu Y, Callaghan TV (2016) Changing Arctic snow cover: a review of recent developments and assessment of future needs for observations, modelling, and impacts. Ambio 45:516–537. https://doi.org/10.1007/s13280-016-0770-0

Bonsal BR, Prowse TD (2003) Trends and variability in spring and autumn 0 C-isotherm dates over Canada. Clim Change 57:341–358. https://doi.org/10.1023/A:1022810531237

Bring A, Fedorova I, Dibike Y, Hinzman L, Mård J, Mernild SH, Prowse T, Semenova O, Stuefer SL, Woo M-K (2016) Arctic terrestrial hydrology: a synthesis of processes, regional effects, and research challenges. J Geophys Res Biogeosci 121:2015JG003131. https://doi.org/10.1002/2015jg003131

Bring A, Shiklomanov A, Lammers RB (2017) Pan-Arctic river discharge: prioritizing monitoring of future climate change hot spots. Earths Future 5:72–92. https://doi.org/10.1002/2016EF000434

Burn DH, Sharif M, Zhang K (2010) Detection of trends in hydrological extremes for Canadian watersheds. Hydrol Process 24:1781–1790. https://doi.org/10.1002/hyp.7625

Buttle JM, Allen DM, Caissie D, Davison B, Hayashi M, Peters DL, Pomeroy JW, Simonovic S, St-Hilaire A, Whitfield PH (2016) Flood processes in Canada: regional and special aspects. Can Water Resour J Rev Can Ressour Hydr 41:7–30. https://doi.org/10.1080/07011784.2015.1131629

Callaghan TV, Johansson M, Brown RD, Groisman PY, Labba N, Radionov V, Barry RG, Bulygina ON, Essery RLH, Frolov DM, Golubev VN, Grenfell TC, Petrushina MN, Razuvaev VN, Robinson DA, Romanov P, Shindell D, Shmakin AB, Sokratov SA, Warren S, Yang D (2011) The changing face of Arctic snow cover: a synthesis of observed and projected changes. AMBIO J Hum Environ 40:17–31. https://doi.org/10.1007/s13280-011-0212-y

Cannon AJ (2010) A flexible nonlinear modelling framework for nonstationary generalized extreme value analysis in hydroclimatology. Hydrol Process 24:673–685. https://doi.org/10.1002/hyp.7506

Cheng L, AghaKouchak A, Gilleland E, Katz RW (2014) Non-stationary extreme value analysis in a changing climate. Clim Change 127:353–369. https://doi.org/10.1007/s10584-014-1254-5

Cherry JE, Knapp C, Trainor S, Ray AJ, Tedesche M, Walker S (2017) Planning for climate change impacts on hydropower in the Far North. Hydrol Earth Syst Sci 21:133–151

Clark ID, Lauriol B, Harwood L, Marschner M (2001) Groundwater contributions to discharge in a permafrost setting, Big Fish River, NWT, Canada. Arct Antarct Alp Res 33:62–69

Cohen J, Hengchun Y, Justin J (2015) Trends and variability in rain-on-snow events. Geophys Res Lett 42:7115–7122. https://doi.org/10.1002/2015GL065320

Coles S (2001) An introduction to statistical modeling of extreme values. Springer Science & Business Media

Collins M, Knutti R, Arblaster J, Dufresne J, Fichefet T, Friedlingstein P, Gao X, Gutowski W, Johns T, Krinner G, Shongwe M, Tebaldi C, Weaver A, Wehner M (2013) Long-term climate change: projections, commitments and irreversibility. In: Stocker T, Qin D, Plattner G, Tignor M, Allen S, Boschung J, Nauels A, Xia Y, Bex V, Midgley P (eds) Climate change 2013: the physical science basis. contribution of working group I to the fifth assessment report of the intergovernmental panel on climate change. Cambridge University Press, pp 1029–1136

de Rham LP, Prowse TD, Beltaos S, Lacroix MP (2008a) Assessment of annual high-water events for the Mackenzie River basin, Canada. Hydrol Process 22:3864–3880. https://doi.org/10.1002/hyp.7016

de Rham LP, Prowse TD, Bonsal BR (2008b) Temporal variations in river-ice break-up over the Mackenzie River Basin, Canada. J Hydrol 349:441–454. https://doi.org/10.1016/j.jhydrol.2007.11.018

Déry SJ, Stadnyk TA, MacDonald MK, Gauli-Sharma B (2016) Recent trends and variability in river discharge across northern Canada. Hydrol Earth Syst Sci 20:4801–4818. https://doi.org/10.5194/hess-20-4801-2016

Dugan HA, Lamoureux SF, Lafrenière MJ, Lewis T (2009) Hydrological and sediment yield response to summer rainfall in a small high Arctic watershed. Hydrol Process 23:1514–1526. https://doi.org/10.1002/hyp.7285

Goulding HL, Prowse TD, Bonsal B (2009) Hydroclimatic controls on the occurrence of break-up and ice-jam flooding in the Mackenzie Delta, NWT, Canada. J Hydrol 379:251–267. https://doi.org/10.1016/j.jhydrol.2009.10.006

Gray D, Prowse T (1992) Snow and floating ice. In: Maidment DR (ed) Handbook of hydrology

Hamilton S (2008) Sources of uncertainty in Canadian low flow hydrometric data. Can Water Resour J Rev Can Ressour Hydr 33:125–136. https://doi.org/10.4296/cwrj3302125

Hansen BB, Isaksen K, Benestad RE, Kohler J, Pedersen ÅØ, Loe LE, Coulson SJ, Larsen JO, Varpe Ø (2014) Warmer and wetter winters: characteristics and implications of an extreme weather event in the high Arctic. Environ Res Lett 9:114021. https://doi.org/10.1088/1748-9326/9/11/114021

Hirabayashi Y, Mahendran R, Koirala S, Konoshima L, Yamazaki D, Watanabe S, Kim H, Kanae S (2013) Global flood risk under climate change. Nat Clim Change 3:816–821. https://doi.org/10.1038/nclimate1911

Instanes A, Anisimov O, Brigham L, Goering D, Khrustalev LN, Ladanyi B, Larsen JO (2005) Chapter 16: infrastructure: buildings, support systems, and industrial facilities. Arct Clim Impact Assess

Instanes A, Kokorev V, Janowicz R, Bruland O, Sand K, Prowse T (2016) Changes to freshwater systems affecting Arctic infrastructure and natural resources. J Geophys Res Biogeosci 121:567–585

Janowicz JR (2010) Observed trends in the river ice regimes of northwest Canada. Hydrol Res 41:462–470. https://doi.org/10.2166/nh.2010.145

Jeong DI, Sushama L (2018) Rain-on-snow events over North America based on two Canadian regional climate models. Clim Dyn 50:303–316. https://doi.org/10.1007/s00382-017-3609-x

Kane DL, Hinzman LD, Gieck RE, McNamara JP, Youcha EK, Oatley JA (2008) Contrasting extreme runoff events in areas of continuous permafrost, Arctic Alaska. Hydrol Res 39:287–298. https://doi.org/10.2166/nh.2008.005

Kane DL, McNamara JP, Yang D, Olsson PQ, Gieck RE (2003) An extreme rainfall/runoff event in Arctic Alaska. J Hydrometeorol 4:1220–1228. https://doi.org/10.1175/1525-7541(2003)004%3c1220:AEREIA%3e2.0.CO;2

Kendall MG (1955) Rank correlation methods. Charles Griffin, London, UK

Koirala S, Hirabayashi Y, Mahendran R, Kanae S (2014) Global assessment of agreement among streamflow projections using CMIP5 model outputs. Environ Res Lett 9:064017. https://doi.org/10.1088/1748-9326/9/6/064017

Larsen JN, Anisimov OA, Constable A, Hollowed AB, Maynard N, Prestrud P, Prowse TD, Stone JMR (2014) Polar regions. In: Barros VR, Field CB, Dokken DJ, Mastrandrea MD, Mach KJ, Bilir TE, Chatterjee M, Ebi KL, Estrada YO, Genova RC, Girma B, Kissel ES, Levy AN, MacCracken S, Mastrandrea PR, White LL (eds) Climate change 2014: impacts, adaptation, and vulnerability. Part B: regional aspects. contribution of working group II to the fifth assessment report of the intergovernmental panel of climate change. Cambridge University Press, Cambridge, United Kingdom and New York, NY, USA, pp 1567–1612

Liston GE, Hiemstra CA (2011) The changing cryosphere: pan-Arctic snow trends (1979–2009). J Clim 24:5691–5712. https://doi.org/10.1175/JCLI-D-11-00081.1

Matti B, Dahlke HE, Lyon SW (2016) On the variability of cold region flooding. J Hydrol 534:669–679. https://doi.org/10.1016/j.jhydrol.2016.01.055

Mazurkiewicz AB, Callery DG, McDonnell JJ (2008) Assessing the controls of the snow energy balance and water available for runoff in a rain-on-snow environment. J Hydrol 354:1–14. https://doi.org/10.1016/j.jhydrol.2007.12.027

McClelland JW, Déry SJ, Peterson BJ, Holmes RM, Wood EF (2006) A pan-Arctic evaluation of changes in river discharge during the latter half of the 20th century. Geophys Res Lett 33

Milly P, Betancourt J, Falkenmark M, Hirsch R, Kundzewicz Z, Lettenmaier D, Stouffer R (2008) Stationarity is dead: whither water management? Science 319:573–574. https://doi.org/10.1126/science.1151915

Musselman KN, Clark MP, Liu C, Ikeda K, Rasmussen R (2017) Slower snowmelt in a warmer world. Nat Clim Change 7:214–219. https://doi.org/10.1038/nclimate3225

Myers-Smith IH, Elmendorf SC, Beck PS, Wilmking M, Hallinger M, Blok D, Tape KD, Rayback SA, Macias-Fauria M, Forbes BC (2015) Climate sensitivity of shrub growth across the tundra biome. Nat Clim Change 5:887

Myers-Smith IH, Hik DS (2013) Shrub canopies influence soil temperatures but not nutrient dynamics: an experimental test of tundra snow–shrub interactions. Ecol Evol 3:3683–3700

Newton B, Prowse T, de Rham L (2016) Hydro-climatic drivers of mid-winter break-up of river ice in western Canada and Alaska. Hydrol Res 358

Overeem I, Syvitski JPM (2010) Shifting discharge peaks in Arctic rivers, 1977–2007. Geogr Ann Ser Phys Geogr 92:285–296. https://doi.org/10.1111/j.1468-0459.2010.00395.x

Peters DL, Caissie D, Monk WA, Rood SB, St-Hilaire A (2016) An ecological perspective on floods in Canada. Can Water Resour J Rev Can Ressour Hydr 0:1–19. https://doi.org/10.1080/07011784.2015.1070694

Peters DL, Monk WA, Baird DJ (2014) Cold-regions hydrological indicators of change (CHIC) for ecological flow needs assessment. Hydrol Sci J 59:502–516. https://doi.org/10.1080/02626667.2013.835489

Peterson BJ, Holmes RM, McClelland JW, Vörösmarty CJ, Lammers RB, Shiklomanov AI, Shiklomanov IA, Rahmstorf S (2002) Increasing river discharge to the Arctic ocean. Science 298:2171–2173. https://doi.org/10.1126/science.1077445

Prowse T, Shrestha R, Bonsal B, Dibike Y (2010) Changing spring air-temperature gradients along large northern rivers: implications for severity of river-ice floods. Geophys Res Lett 37: L19706. https://doi.org/10.1029/2010GL044878

Prowse TD, Peters D, Beltaos S, Pietroniro A, Romolo L, Töyrä J, Leconte R (2002) Restoring ice-jam floodwater to a drying delta ecosystem. Water Int 27:58–69. https://doi.org/10.1080/02508060208686978

Putkonen J, Roe G (2003) Rain-on-snow events impact soil temperatures and affect ungulate survival. Geophys Res Lett 30. https://doi.org/10.1029/2002gl016326

Rawlins MA, Steele M, Serreze MC, Vörösmarty CJ, Ermold W, Lammers RB, McDonald KC, Pavelsky TM, Shiklomanov A, Zhang J (2009) Tracing freshwater anomalies through the air-land-ocean system: a case study from the Mackenzie river basin and the Beaufort Gyre. Atmos Ocean 47:79–97. https://doi.org/10.3137/OC301.2009

Rennermalm AK, Wood EF, Troy TJ (2010) Observed changes in pan-arctic cold-season minimum monthly river discharge. Clim Dyn 35:923–939. https://doi.org/10.1007/s00382-009-0730-5

Rennert KJ, Roe G, Putkonen J, Bitz CM (2009) Soil thermal and ecological impacts of rain on snow events in the circumpolar Arctic. J Clim 22:2302–2315. https://doi.org/10.1175/2008JCLI2117.1

Riseborough DW (1990) Soil latent heat as a filter of the climate signal in permafrost. In: Proceedings of the fifth canadian permafrost conference, Collect Nordicana Citeseer, pp 199–205

Romanovsky VE, Smith SL, Christiansen HH (2010) Permafrost thermal state in the polar Northern Hemisphere during the international polar year 2007–2009: a synthesis. Permafr Periglac Process 21:106–116

Salas J, Obeysekera J (2014) Revisiting the concepts of return period and risk for nonstationary hydrologic extreme events. J Hydrol Eng 19:554–568. https://doi.org/10.1061/(ASCE)HE.1943-5584.0000820

Schewe J, Heinke J, Gerten D, Haddeland I, Arnell NW, Clark DB, Dankers R, Eisner S, Fekete BM, Colón-González FJ, Gosling SN, Kim H, Liu X, Masaki Y, Portmann FT, Satoh Y, Stacke T, Tang Q, Wada Y, Wisser D, Albrecht T, Frieler K, Piontek F, Warszawski L, Kabat P (2014) Multimodel assessment of water scarcity under climate change. Proc Natl Acad Sci 111:3245–3250. https://doi.org/10.1073/pnas.1222460110

Serreze MC, Barry RG (2011) Processes and impacts of Arctic amplification: a research synthesis. Glob Planet Change 77:85–96. https://doi.org/10.1016/j.gloplacha.2011.03.004

Shevnina E, Kourzeneva E, Kovalenko V, Vihma T (2017) Assessment of extreme flood events in a changing climate for a long-term planning of socio-economic infrastructure in the Russian Arctic. Hydrol Earth Syst Sci 21:2559–2578. https://doi.org/10.5194/hess-21-2559-2017

Shi X, Marsh P, Yang D (2015) Warming spring air temperatures, but delayed spring streamflow in an Arctic headwater basin. Environ Res Lett 10:064003

Shiklomanov AI, Lammers RB (2009) Record Russian river discharge in 2007 and the limits of analysis. Environ Res Lett 4:045015. https://doi.org/10.1088/1748-9326/4/4/045015

Shiklomanov AI, Lammers RB (2014) River ice responses to a warming Arctic—recent evidence from Russian rivers. Environ Res Lett 9:035008. https://doi.org/10.1088/1748-9326/9/3/035008

Shiklomanov AI, Lammers RB, Rawlins MA, Smith LC, Pavelsky TM (2007) Temporal and spatial variations in maximum river discharge from a new Russian data set. J Geophys Res Biogeosci 112:G04S53. https://doi.org/10.1029/2006jg000352

Shkolnik I, Pavlova T, Efimov S, Zhuravlev S (2018) Future changes in peak river flows across northern Eurasia as inferred from an ensemble of regional climate projections under the IPCC RCP8.5 scenario. Clim Dyn 50:215–230. https://doi.org/10.1007/s00382-017-3600-6

Shrestha RR, Cannon AJ, Schnorbus MA, Zwiers FW (2017) Projecting future nonstationary extreme streamflow for the Fraser River, Canada. Clim Change 1–15. https://doi.org/10.1007/s10584-017-2098-6

Smith LC, Pavelsky TM, MacDonald GM, Shiklomanov AI, Lammers RB (2007) Rising minimum daily flows in northern Eurasian rivers: a growing influence of groundwater in the high-latitude hydrologic cycle. J Geophys Res Biogeosci 112:G04S47. https://doi.org/10.1029/2006jg000327

St. Jacques J-M, Sauchyn DJ (2009) Increasing winter baseflow and mean annual streamflow from possible permafrost thawing in the Northwest Territories, Canada. Geophys Res Lett 36: L01401. https://doi.org/10.1029/2008gl035822

Striegl RG, Dornblaser MM, Aiken GR, Wickland KP, Raymond PA (2007) Carbon export and cycling by the Yukon, Tanana, and Porcupine rivers, Alaska, 2001–2005. Water Resour Res 43:W02411. https://doi.org/10.1029/2006WR005201

Sturm M, Goldstein MA, Parr C (2017) Water and life from snow: a trillion dollar science question. Water Resour Res 53:3534–3544

Tan A, Adam JC, Lettenmaier DP (2011) Change in spring snowmelt timing in Eurasian Arctic rivers. J Geophys Res Atmospheres 116

Tananaev NI, Makarieva OM, Lebedeva LS (2016) Trends in annual and extreme flows in the Lena River basin, Northern Eurasia. Geophys Res Lett 43:2016GL070796. https://doi.org/10.1002/2016gl070796

Thackeray CW, Fletcher CG, Mudryk LR, Derksen C (2016) Quantifying the uncertainty in historical and future simulations of Northern Hemisphere Spring snow cover. J Clim 29:8647–8663. https://doi.org/10.1175/JCLI-D-16-0341.1

Van Oldenborgh GJ, Collins M, Arblaster J, Christensen JH, Marotzke J, Power SB, Rummukainen M, Zhou T, Stocker T, Qin D (2013) Annex I: atlas of global and regional climate projections. Clim Change 1311–1393

Vihma T, Screen J, Tjernström M, Newton B, Zhang X, Popova V, Deser C, Holland M, Prowse T (2016) The atmospheric role in the Arctic water cycle: a review on processes, past and future changes, and their impacts. J Geophys Res Biogeosci 121:2015JG003132. https://doi.org/10.1002/2015jg003132

von der Wall SJ (2011) An assessment of the river ice break-up season in Canada. Thesis

Walvoord MA, Voss CI, Wellman TP (2012) Influence of permafrost distribution on groundwater flow in the context of climate-driven permafrost thaw: example from Yukon Flats Basin, Alaska. United States, Water Resour Res, p 48

Ward R (1989) Hydrology of floods in Canada: a guide to planning and design. Ott Natl Res Counc Can

Woo M, Thorne R (2016) Summer low flow events in the Mackenzie river system. Arctic 69:286–304. https://doi.org/10.14430/arctic4581

Woo M-K, Kane DL, Carey SK, Yang D (2008) Progress in permafrost hydrology in the new millennium. Permafr Periglac Process 19:237–254. https://doi.org/10.1002/ppp.613

Woo M-K, Thorne R (2014) Winter flows in the Mackenzie Drainage system. Arctic 67:238–256

Wu P, Wood R, Stott P (2005) Human influence on increasing Arctic river discharges. Geophys Res Lett 32:L02703. https://doi.org/10.1029/2004GL021570

Yang D, Shi X, Marsh P (2015) Variability and extreme of Mackenzie river daily discharge during 1973–2011. Quat Int 380–381:159–168. https://doi.org/10.1016/j.quaint.2014.09.023

Yang D, Ye B, Kane DL (2004) Streamflow changes over Siberian Yenisei river basin. J Hydrol 296:59–80

Ye B, Yang D, Zhang Z, Kane DL (2009) Variation of hydrological regime with permafrost coverage over Lena Basin in Siberia. J Geophys Res Atmospheres 114. https://doi.org/10.1029/2008jd010537

Zakharova EA, Kouraev AV, Biancamaria S, Kolmakova MV, Mognard NM, Zemtsov VA, Kirpotin SN, Decharme B (2011) Snow cover and spring flood flow in the Northern Part of Western Siberia (the Poluy, Nadym, Pur, and Taz Rivers). J Hydrometeorol 12:1498–1511

Zhang X, He J, Zhang J, Polyakov I, Gerdes R, Inoue J, Wu P (2013) Enhanced poleward moisture transport and amplified northern high-latitude wetting trend. Nat Clim Change 3:47–51. https://doi.org/10.1038/nclimate1631

Zhang X, Zwiers FW (2013) Statistical indices for the diagnosing and detecting changes in extremes. Extremes in a changing climate. Springer, Dordrecht, pp 1–14

Zhang X, Zwiers FW (2004) Comment on "Applicability of prewhitening to eliminate the influence of serial correlation on the Mann-Kendall test" by Sheng Yue and Chun Yuan Wang. Water Resour Res 40:W03805. https://doi.org/10.1029/2003WR002073

Dr. Rajesh R. Shrestha is a Research Scientist at the Watershed Hydrology and Ecology Research Division, Environment and Climate Change Canada, and holds an Adjunct Professor appointment at the University of Victoria. His current research focuses primarily on assessing the impacts of climate variability and change on hydrologic systems, including methods to characterize interactions and uncertainties in hydrologic projections, and nonstationarity of extreme events. He is active in the development and application of snow and hydrologic models, and observation-based and statistically downscaled climate data products.

Dr. Katrina Eleanor Bennett is a hydrologist interested in changes to water resources that impact human and ecological systems. She completed her Ph.D. from the International Arctic Research Center at the University of Alaska Fairbanks in 2014. She has worked on the influences of climate change and climate variability on the hydrology of northern and forested watersheds in Alaska and Canada, and US southwestern systems of the Colorado River and Rio Grande basins. Her research interests are primarily hydrological modeling, remote sensing of solid and liquid water in the soils, air and on the ground, changes in the land surface (forests, vegetation, fire) and associated impacts to the hydrologic regime, and the quantification of uncertainty and sensitivity in hydrologic estimates. She is currently a Research Scientist, Applied Terrestrial Energy and Atmospheric Modeling Team Leader, and LANL Early Career scientist awardee in the Los Alamos National Laboratory's Earth and Environmental Sciences Division.

Dr. Daniel L. Peters is a Research Scientist within the Watershed Hydrology & Ecology Research Division of Environment and Climate Change Canada. His role is to investigate the effects of climate variability/change and development (e.g., flow regulation, water abstraction) on the hydrology of river, lake, wetland, and delta systems in Canada. He is also involved in research linking hydrology to aquatic ecology, such as developing rapid assessment tools for environmental flow approaches. He has provided Technical Expertise to the Canadian Environmental Assessment Agency, Parks Canada Agency, and UNESCO WHC/IUCN. He is the Past President of the Canadian Geophysical Union—Hydrology Section, an Associate Editor of the Canadian Water Resources Journal, and has published more than 40 papers in peer-reviewed journals. He holds an Associate Professor (limited term appointment) in the Geography Department at the University of Victoria (BC) where he taught Hydrology for 10 years and supervises graduate students.

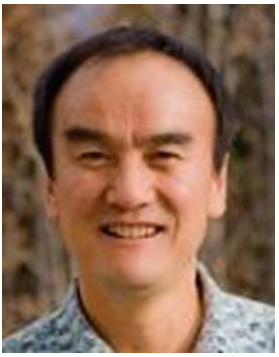

Dr. Daqing Yang is a Research Scientist at the Watershed Hydrology and Ecology Research Division, Environment and Climate Change Canada. He is also Affiliate Research Professor at the International Arctic Research Center, Univ. of Alaska Fairbanks. Over the past 25 years, he has conducted cryosphere system research in China, Canada, Japan, USA, and Norway. His primary research activities/interests include cold region hydrology and climate, particularly Arctic large river streamflow regime and change, snow cover and snowfall measurements, climate change and human impact to regional hydrology, and applications of remote sensing in cold regions. He has served as journal editor and subject editor for IAHS publications (cold region hydrology, northern research basin water balance, and cold/mountain region hydrological systems under climate change), and WMO technical reports (solid precipitation measurement intercomparison and integrated global observing strategy cryosphere theme). He also contributed as review and/or author to the IPCC Reports, and the Arctic Council's Snow, Water, Ice and Permafrost in the Arctic (SWIPA 2017 and follow up) assessment. His current research focuses on investigating the impacts of climate variability/change and human activities on hydrologic system across the broader northern regions.

Overview of Environmental Flows in Permafrost Regions

8

Daniel L. Peters, Donald J. Baird, Joseph Culp, Jennifer Lento, Wendy A. Monk, and Rajesh R. Shrestha

Abstract

River ecosystems have adapted to a natural range of variability in magnitude, timing, duration, and predictability of key hydrograph components, such as high- and low-flow periods. However, the timing, magnitude, and variability of cold region flow regimes are changing in response to a warming climate, water abstraction, and building of impoundments. Changes in water quantity flowing down a river at a given time have the potential to adversely and/or positively affect habitat conditions and sustainability of ecological diversity within both the

D. L. Peters (✉) · R. R. Shrestha
Watershed Hydrology and Ecology Research Division, Environment and Climate Change Canada, University of Victoria, Victoria, BC, Canada
e-mail: daniel.peters@canada.ca

R. R. Shrestha
e-mail: rajesh.shrestha@canada.ca

D. J. Baird · W. A. Monk
Watershed Hydrology and Ecology Research Division, Environment and Climate Change Canada, University of New Brunswick, Fredericton, NB, Canada
e-mail: djbaird@unb.ca

W. A. Monk
e-mail: wmonk@unb.ca

J. Culp
Watershed Hydrology and Ecology Research Division, Environment and Climate Change Canada, University of Wilfrid Laurier, Waterloo, ON, Canada
e-mail: jculp@wlu.ca

J. Lento
Canadian Rivers Institute, University of New Brunswick, Fredericton, NB, Canada
e-mail: jlento@gmail.com

D. Yang and D. L. Kane (eds.), *Arctic Hydrology, Permafrost and Ecosystems*,
https://doi.org/10.1007/978-3-030-50930-9_8

river and associated riparian and floodplain zones. There is a growing need to incorporate environmental flow assessments in the management of permafrost regions in response to changing flow regimes in order to preserve these diverse ecosystems. Environmental flows are defined as the quantity, timing, and quality of freshwater flows and levels necessary to sustain aquatic ecosystems. The goal of this Chapter is to present an overview of environmental flows for permafrost regions, with a focus on North America where information is most readily available. This goal is achieved via a review of (i) cold regions hydro-ecology, (ii) history and application of environmental flows internationally, (iii) environmental flow guidelines and policy in Arctic states, and (iv) riverine monitoring in northern regimes to support environmental flow frameworks. Several key recommendations to address knowledge and data gaps to better manage natural resources are provided.

Keywords

Environmental flows · Permafrost regions · Cold regions hydro-ecology · Natural flow regime · Altered flow · Arctic

8.1 Introduction

Hydrological regimes of the permafrost regions, especially the Arctic, have become an increasing area of interest because of the region's enhanced susceptibility to climate variability and change (Bring et al. 2016; Bush et al. 2019; Box et al. 2019), as well as encroaching development for the utilization and extraction of resources (e.g., oil, gas, hydropower: Gautier et al. (2011), Instanes et al. (2016)). Not only are the timing and magnitude of major cold region hydrological processes (snow, ice, permafrost) sensitive to a warming climate, but large-scale alterations of flow regimes via damming of rivers and water abstraction have been shown to be potentially significant disruptors of natural flow regimes and related aquatic ecosystems of Arctic and subarctic rivers (Prowse et al. 2004; Wrona et al. 2006). For example, the construction of impoundments has dramatically altered the seasonality of large Eurasian rivers draining into the Arctic Ocean (Ye et al. 2003; McClelland et al. 2004; Yang et al. 2004a). Although some large river systems originate in more southern latitudes, such as the Mackenzie River in North America, impacts from sufficiently large flow alterations in distant headwater and mid-watershed regions may be carried to northern areas prior to reaching the Arctic Ocean.

The seminal natural flow paradigm proposed by Poff et al. (1997) established explicit linkages between the flow regime and lotic ecosystem structure, function, and diversity (Statzner and Higler 1986; Poff et al. 1997). Riverine communities are adapted to variability in magnitude, timing, duration, and predictability of key hydrograph components, such as high- and low-flow periods (Jowett and Duncan

1990; Dunbar et al. 2010). Previous studies have explored the significance of these and other key variables for hydro-ecological research and environmental flow recommendations (e.g., Monk et al. 2008; Peters et al. 2012). Recent hydro-ecological research has focused on two important questions: (i) *How much water does a river need to sustain the aquatic ecosystem?* (Richter et al. 1997) and (ii) *How do we identify the ecologically important components of flow regimes to improve flow management of rivers?* (Wood et al. 2000; Poff 2002; Boulton 2003; Lake 2003; Monk et al. 2006).

Historically, environmental flow needs (EFN) research focused on specific local-scale protection goals of maintaining minimum instream flows to sustain fish species of commercial and/or sporting interest (Arthington et al. 2006). However, given their narrow target focus, these protection goals often fail to protect all components of the river and floodplain ecosystem, many of which are strongly influenced by temporal variation in streamflow and high-water flood generation mechanisms (Richter et al. 1996; Poff et al. 1997; Lytle and Poff 2004; Monk et al. 2012). This is especially true for cold-climate countries where flow regimes are typically characterized by winter low flows during the ice-covered period, extreme peak water levels generated with the influence of ice jamming during the spring ice breakup, followed by high spring/summer flows during the open-water period (Leclerc et al. 2003; Monk et al. 2011; Buttle et al. 2016; Peters et al. 2016).

Environmental flows (EF) are defined as the quantity, timing, and quality of freshwater flows and levels necessary to sustain aquatic ecosystems (Arthington et al. 2006). With increasing development pressures and projected climate change impacts on the timing and magnitude of water availability (Instanes et al. 2016), there is a growing need to explicitly incorporate environmental flows into water sustainability frameworks for cold regions of the globe in order to sustain the diverse ecosystems (e.g., Peters et al. 2014). The goal of this Chapter is to present an overview of environmental flows for permafrost regions, with a focus on North America, which to our knowledge has not been completed.

8.2 Cold Regions Hydro-Ecology

Sustainable management of freshwater ecosystems requires a paired approach combining our understanding of the relationships among key drivers, pressures and stressors, and their impact on the ecosystem components that we monitor with the development of target indices to monitor these changes. Peters et al. (2014) recently developed the Cold regions Hydrological Indicators of Change (CHIC) approach that explicitly recognizes the ice-covered and open-water seasons for climate change impacts and environmental flow assessments. Subsequently, Peters et al. (2016) provided an overview of the ecological aspects of floods in Canada. Material from these two papers was updated below to provide the reader with the necessary background on the hydrology and ecology of subarctic and Arctic regions that cover large areas of landscape influenced by permafrost and river ice processes (Fig. 8.1).

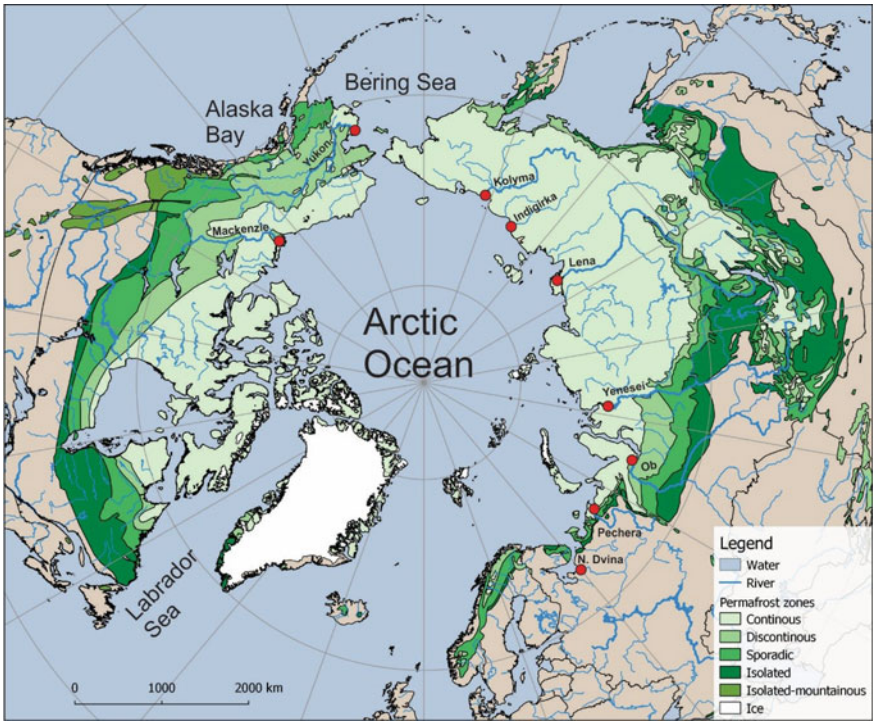

Fig. 8.1 Circumpolar map of regions affected by permafrost. Lighter shades of green indicate higher percentages of permanently frozen ground. Map based on shapefiles provided by NSIDC (2018). Major circumpolar deltas are noted with red dots

8.2.1 Ice-Covered Period

The hydrologic regime of cold region rivers is governed by temperature-controlled processes that influence the timing, duration, and magnitude of flow and water levels related to the formation, growth, and ablation of the annual snow and ice cover (Ashton 1986; Gray and Prowse 1993). As synthesized by Prowse (2001a, b), river-ice processes have a major effect on bio-geo-chemical processes, especially the spring breakup of the river-ice cover, which can lead to extreme ice-jam induced flooding (e.g., Beltaos 1995; Prowse and Culp 2003). The influence of ice should therefore be explicitly considered in the assessment and development of environmental flows (Peters et al. 2014).

Even before ice begins to form on river reaches, the biological system begins to adjust to declining flows, reduction of solar radiation (i.e., shortening of day length) and cooling waters (Prowse 2001a). Winter conditions present a substantial challenge to the survival of aquatic species, such as fish, because winter flows and ice formation reduce the availability of habitat (Cunjak 1996; Cunjak et al. 1998).

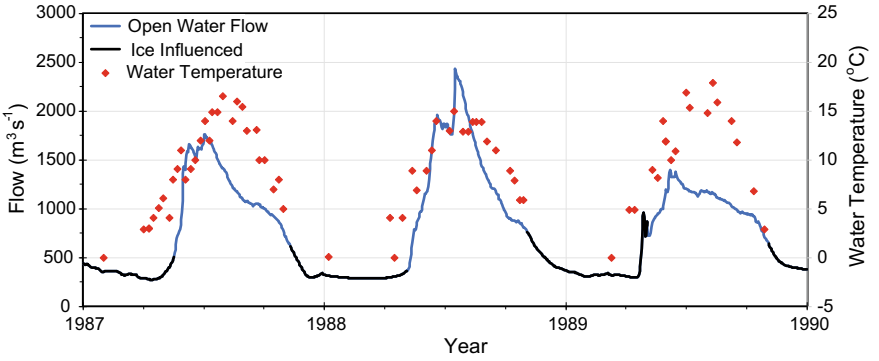

Fig. 8.2 Streamflow during the ice-influenced and open-water seasons for the Yukon River at Carmacks (Station 09AH001) during the years 1987–1989 obtained from ECCC (2018). Also shown are streamflow temperatures extracted from Yang and Peterson (2017). Location of the river highlighted in Fig. 8.1

An example of typical seasonal variation in streamflow conditions for a large river is shown in Fig. 8.2 for a reach of the Yukon River in North America, typifying changes from the late spring open-water conditions through late autumn freeze-up to stable winter ice cover, and ultimately followed by river ice breakup in the spring. Floating ice is thus a key component of freshwater river systems found in permafrost zones of the world, as it creates and controls aquatic habitats and related biological productivity and diversity. It is worth noting that the latter is even more strongly influenced by longer ice periods in smaller and more northern rivers.

River ice-cover formation starts with the cooling of surface waters to ~0 °C, leading to the development of ice crystals, and the formation of border ice along the banks of the channel where flow velocity and turbulence are negligible (Hicks 2009). Frazil ice particles will grow and accumulate to form floating pans that freeze together and collect along border ice—all of which can be enhanced by low flow conditions and riffles where cold air is entrained by turbulence (Simpkins and Hubert 2000). Fish that inhabit pools may be buffered from low flows (Dare et al. 2002), but the accumulation of frazil ice in pools can be significant and force fish to exit these habitats (Komadina-Douthwright et al. 1997). Frazil ice within the main flow can cause physical and physiological damage to fish species through gill abrasion and plugging (Brown et al. 1994).

Hydraulic properties defining fish habitat may also be affected by anchor ice formed by frazil ice particles that adhere to bed material. By artificially raising the riverbed, anchor ice can create backwaters with reduced water velocities, which may result in water diversion into other parts of the channel/floodplain network (Prowse and Gridley 1993; Stickler and Alfredsen 2005). Biota, particularly fish eggs and developing embryos, may be affected by the freezing of the bed material and by the restriction of substrate inflow (e.g., Walsh and Calkins 1986; Calkins 1989; Power et al. 1993). Macroinvertebrates, a key source of food for

overwintering fish, can also be affected by freezing conditions with anchor ice found to be implicated in winter-long declines in invertebrate abundance (Martin et al. 2001).

The congestion of surface ice floes and the resulting cessation of their downstream movement can occur at tight bends or a channel narrowing. With bridging of the ice cover, incoming ice floes may accumulate edge to edge with the upstream progression of the ice front by juxtaposition and/or maybe swept under the existing ice cover, resulting in hydraulic ice thickening. Establishment of an ice cover decreases the flow conveyance by decreasing channel cross-sectional area, reducing flow velocity and increasing flow resistance due to the presence of an enlarged wetted perimeter, resulting in increased water levels and displacement of water into channel storage behind the ice cover (Prowse 2001a; Hicks 2009). On the other hand, ice growth and hydraulic storage of water behind the accumulating ice can substantially decrease flow in downstream reaches (Moore et al. 2002; Prowse and Carter 2002).

Ice-influenced stage increases have been found to be important for supplying water to aquatic habitats located along channel margins and the floodplain (Paschke and Coleman 1986; Burn 1993), providing side- and off-channel pond habitat for some fish species (e.g., Komadina-Douthwright et al. 1997); whereas restricted access to bank habitat and overwintering survival of fish was found in a region with low winter flows that lacked the presence of an ice cover (Mitro et al. 2003). Declining flows under the ice cover can result in less hyporheic flow and an increased presence of lower dissolved oxygen groundwater, which can cause mortality of incubating eggs and larvae (Bradford and Heinonen 2008). The restriction of reaeration due to ice cover and oxidation of organic material may further increase rates of dissolved oxygen depletion over the long winter period (Chambers et al. 1997).

Continued ice growth can lead to an increasing portion of the river channel margins completely freezing to the bed. In shallow streams or connecting channels, this can lead to the concentration of flow within only the deepest and/or highest velocity zones, and complete freezing unless there is enough winter flow from lakes and ponds or recharge from groundwater (Prowse 2001a). Complete or partial freezing to the bed can be beneficial to connected lake systems by preventing drainage (e.g., Pohl et al. 2009; Lesack and Marsh 2010). Streamflow in small creeks may cease completely due to the freezing of soil down to the permafrost, preventing subsurface flow from reaching the channel (Woo 1986). For instance, all gauged streams in the Canadian Archipelago have been shown to exhibit zero flow during the winter due to cold temperatures and permafrost (Spence and Burke 2008).

Changing ice conditions have been cited as a major reason for the instream movement of some fish species throughout the winter (Cunjak and Randall 1993). The movement of gravel beds in association with ice formation, ice breakups, and high flows may also negatively impact fish eggs by washing them out, subjecting them to mechanical abrasion, or by decreasing wetted area and thereby exposing the

eggs to desiccation or freezing. Ice processes thus need to be taken into consideration in the design of fish-stream habitat enhancement (Linnansaari et al. 2009).

8.2.2 Ice Breakup Period

In colder climates, river ice breakup is typically a spring event when air temperatures increase above 0 °C causing the melting of the snowpack and initiating significant runoff to river systems. (Beltaos et al. 2003). Moderate increases inflow and a thermally deteriorated ice cover together pose little resistance to the passage of flow (Gray and Prowse 1993); whereas the interaction of a large flood wave with an intact and mechanically strong ice cover can result in a dynamic river ice breakup, jamming of ice pieces, posing increased resistance and/or obstruction to flow and leading to extremely high river stage. Figure 8.3a, b illustrate the dramatic effect of dynamic breakup processes on river stage as compared to peak open-water flow conditions for a Mackenzie River near the mouth and channels of the downstream Mackenzie Delta complex (Fig. 8.1), where the presence of ice jams produced backwater levels several meters higher than those for the same discharge under open water conditions.

Ice-influenced flooding has been established to be essential for the periodic replenishing of water to floodplain areas, such as perched wetland basins in cold regions deltas in the Mackenzie River Basin (Peters et al. 2006; Goulding et al. 2009; Lesack and Marsh 2010). As exemplified by this river basin, analysis of cold regions flood regimes should not be solely based on open-water discharge records, as traditionally done (e.g., Burn et al. 2016), and instead requires specific attention to extreme water levels influence by ice processes. This is especially the case for Arctic rivers in which annual high-water flood levels are driven by river ice breakup mechanism (e.g., ~50% of Canadian Arctic streams; von de Wall et al. 2009).

Although difficult to predict, it has been established that the severity of ice-jam flooding is dependent on the antecedent fall freeze-up level, ice conditions, and prevailing climate (snowpack accumulation and melt rate) that generated the spring flows (Beltaos 1995). Large development projects within the watershed that alter key characteristics of the river flow regime, such as storage and release of water for the generation of hydroelectricity and water abstraction for mining activities, may affect the occurrence and/or severity of such flood events (Beltaos 1995; Peters et al. 2016). Moreover, ice-jam flood frequency and intensity are likely to be significantly altered under climate warming scenarios in response to warming air temperatures that are projected to shorten the snow accumulation period and lead to occasional mid-winter melt events that deplete the snowpack water (Beltaos et al. 2006). A good example in North America is the Williston hydroelectric reservoir in the headwaters of Peace River tributary of the Mackenzie Basin.

Compared to more southern regions, high-latitude regions experience shorter ice-free periods; ranging from approximately 90 days in the high Arctic to ~180 days in more southern regions. As illustrated by the Yukon River hydrograph in Fig. 8.2, peak annual flows typically occur during the open-water season

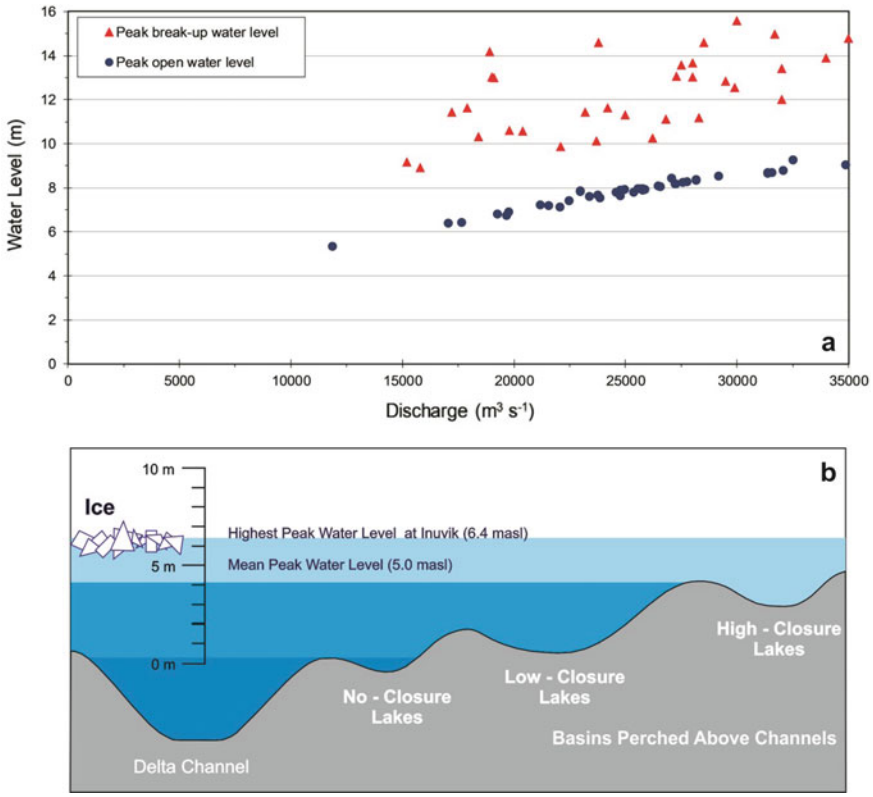

Fig. 8.3 **a** Open-water and ice-influenced peak water levels versus discharge at the Mackenzie River at Arctic Red River (ECCC Station 10LC014) for the years 1972–2015. (modified from Goulding et al. (2009) and von de Wall et al. (2010)). **b** Classification of wetland/lake basins in the downstream circumpolar Mackenzie Delta according to surface water connectivity on East Channel near Inuvik (10LC002). Ice jam generated floodwaters are responsible for flooding the highly elevated, perched basins (Modified from Emmerton et al. (2007) in Prowse et al. (2011)). Location of Mackenzie River Delta highlighted in Fig. 8.1

in response to annual snowmelt and/or rainfall runoff. For example, based on an assessment of stations from the Regional Hydrometric Basin Network (RHBN; see Fig. 8.5a for network) for Canada, Burn et al. (2016) identified the dominant flow regime as "nival," while Monk et al. (2011) classified three dominant peak flow regime timings (standard weeks starting May 27th, June 17th, and July 1st) for the Arctic region. In Alaska, high-gradient headwater basins are dominated by summer floods, while snowmelt drives flooding in basins on low-gradient coastal plains (Kane et al. 2008).

8.2.3 Open-Water Period

Open-water floods occur when the river flow exceeds the bankfull discharge, which also represents the channel-forming discharge (Leopold 1994), and spills river water onto the adjacent floodplains (Peters et al. 2016). For North American rivers, the bankfull discharge commonly approximates the maximum flow that is reached on average every 2 years (Leopold 1994), and possibly up to 5 years for some channels that are widened by ice scour (Kellerhals and Church 1980; Polzin and Rood 2006). The magnitude, frequency, duration, and timing of floods are of particular importance in river ecosystems (e.g., productivity, response to habitat availability, etc.) (Poff et al. 1997).

The role of ice scouring and the volume of spring meltwater in sediment erosion, transport, and yield are well established (Prowse and Culp 2003; Forbes and Lamoureux 2005). The physical structure of habitats is largely defined by flood processes within the channel and between the channel and floodplain. Floods play an important role in the delivery of food and energy to streams, especially to small streams where the amount of sunlight is limited and energy come from allochthonous sources (i.e., nutrients, terrestrial plant debris composed of leaves, needles, and twigs, etc.) from the nearby floodplain/riparian habitat during high-water events (Hynes 1975). This energy flux from the drainage basin is critical for aquatic invertebrates and fungal populations, which in turn provide the basic diet for many species of fish. In recognition that floods are crucial to the food web dynamics of rivers, (Junk et al. 1989) put forward the "flood pulse concept," a conceptual framework that highlights the importance of annual floods in linking terrestrial sources of nutrient and organic matter to stream productivity in shaping ecosystem structure and contributing to a healthy river ecosystem. The flood pulse and accompanying river ice influences erosional and depositional processes and results in unique styles of sediment transport, deposition, and riverbank erosion. Flow variability shapes ecological communities through taxon-specific responses and associated adaptation of key biological traits to flow variability along the hydrological connectivity gradient (Poff et al. 1997; Lake 2000). For example, in the case of invertebrates, overall community-level taxon richness often peaks at intermediate hydrological connectivity and disturbance where generalist and specialist taxa coexist (Ward and Stanford 1983; Tockner et al. 2000).

Although Arctic streams seem inhospitable due to extremes in environmental conditions, fish and other aquatic organisms have adapted to cold waters, streamflow variability, disturbances, and brief summers that provide seasonal habitat used during various species life cycles. In the Arctic and elsewhere, varying flow magnitude and connectivity are needed by fish for migration, spawning, incubation, and rearing (Klein 2016; Heim et al. 2016). There are conservatively 99 species of freshwater and diadromous fish in the Arctic, with about a third represented by salmonids, most of which are important in various fisheries (Reist et al. 2006; Lento et al. 2019) For instance, the deltas of the Colville River in Alaska's north slope and the Mackenzie River in northwestern Canada (see Fig. 8.1 for locations), are known

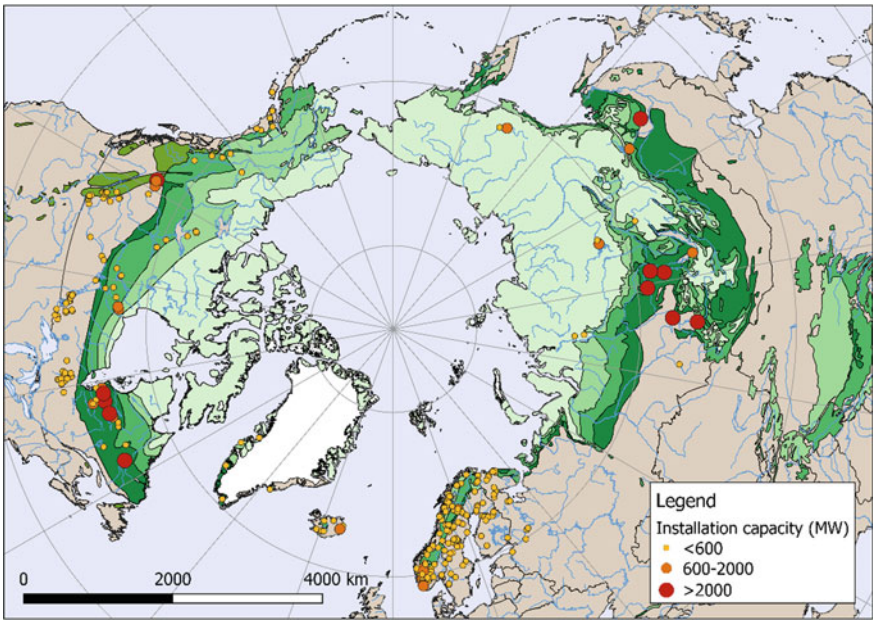

Fig. 8.4 Hydroelectric facilities in ice-dominated river systems (Data presented in map updated from AMAP (2012))

to support large populations of Arctic Cisco that represent principal sources of commercial fish (Bickman et al. 1989).

A key lesson learned from riverine studies in Norway is that the ecology in high-latitude rivers can be vulnerable to even small changes in the water flow and other impacts from development, such as hydropower. As illustrated in Fig. 8.4, more than 80 GW of hydroelectricity is already generated in permafrost regions. Hydroelectric power production has the potential to expand rapidly in response to a warming climate ensuring increased availability of water from an enhanced melt of glaciers and snowmelt, plus thawing of permafrost. Increased availability for hydropower generation is expected to last for several decades in many areas, but the eventual loss of key cryosphere components, such as glaciers, will limit future energy generation (AMAP 2012).

With the growing demand for water consumption and use associated with the increasing development of northern areas, and potentially changing background levels in water availability (as projected from current consensus on the long-term effects of global climate change; Larsen et al. (2014)), there is an urgent need to establish an environmental flow framework that will protect riverine and floodplain ecosystems in permafrost regions. However, this could be a challenge given the large geographic area that encompasses a range of climatic and landscape controls on hydrology, geomorphology, and aquatic ecology.

8.3 Environmental Flows Science

A key question frequently posed to riverine scientists is "how much water does a river need?", in other words, what is the required environmental flow to sustain the aquatic ecosystem (Richter et al. 1997). Initially referred to as instream flow needs (IFN), research toward answering this question focused on the protection goal of maintaining minimum instream flows to sustain fish species of interest (Arthington et al. 2006). The concept of sustaining fisheries of interest by supporting an IFN first appeared in the 1940s in the United States (Arthington et al. 2006). IFN recommendations were initially based on an assumption that "river health" (see Karr (1999)) issues were associated with low flow magnitude and that the river ecosystem would be preserved if flow rates could be maintained above a critical level (Acreman and Dunbar 2004).

Minimum flow approaches have been shown to be inadequate because the complex adaptations of the biota, such as fish and macro invertebrates, are strongly influenced by predictable temporal variations in flow (Richter et al. 1996; Poff et al. 1997; Lytle and Poff 2004). In addition to low flow periods, annual flood flows have been shown to be critical to the maintenance of the fluvial ecosystem (Richter et al. 1996; Peters et al. 2016). This is especially true for cold-climate countries, such as the circumpolar regions, where flow regimes are characterized by winter ice and low flow conditions and high spring/summer flow periods (Leclerc et al. 2003; Monk et al. 2011).

As concerns evolved beyond protecting fish species to encompass the river ecosystem, the number of EF methods has proliferated to >200 documented (Arthington et al. 2006). A detailed review of methods and frameworks for producing EF recommendations is beyond the scope of this paper and is available in the literature (Jowett 1997; Arthington 1998; Arthington et al. 2004, 2006; Acreman and Dunbar 2004; Anderson et al. 2006; Smakhtin and Anputhas 2006; Bradford and Heinonen 2008; Poff et al. 2010; Linnansaari et al. 2013). Ideally, EF management methods provide the water flows and levels needed to sustain freshwater and estuarine ecosystems and balance these needs with those of society and development.

Environmental flow regime assessments can be grouped into four core categories (Tharme 2003): (i) hydrological, (ii) hydraulic rating, and (iii) habitat simulation, and elements of each are captured in (iv) holistic methodologies (Table 8.1). The simplest EF methods are based on hydrological flow indices, which employ a desktop computer approach using historical streamflow to establish strategic, broad-scale EF levels. Pyrce (2004) stated that the most frequently used hydrological EF methods were (i) the Tennant (1976) method (percentage of mean annual flow), (ii) the seasonal and annual 7Q10 (one in 10-year, 7-day mean low flow), (iii) the monthly Q50 (flow equaled or exceeded 50% of the time), and (iv) the monthly Q90. With due caution, these desktop approaches have been widely promoted (e.g., Smakhtin and Anputhas 2006; Mathews and Richter 2007).

Table 8.1 Approaches used to estimate environmental flows (EF)

Method	Purpose & scope	Examples of methods
Hydrological	• EF recommendations (indices) made using simple desktop methods primarily using hydrological data (historical or simulated daily or weekly or monthly flow records) to set a "safe" flow abstraction • Rapid, non-resource intensive method, providing low-resolution EF estimates intended to maintain ecological features • Whole rivers, applicable for regional assessments • Appropriate at the water resource planning level development, or in low risk situations where used as a primary flow target	• The most widely used hydrological method is the (Tennant 1976) and the second most widely used method include various flow duration exceedance percentiles (e.g., Q_{95}, Q_{75}), or single low flow indices (e.g., $7Q_{10}$, $7Q_2$) • Range of Variability Approach (RVA; Richter et al. (1997)) and indicators of Hydrological Alteration (IHA; Richter et al. (1996)) are recently applied methods where protection of natural seasonality and variability of flows to maintain ecosystem is the primary objective • Prescriptive Standard (Richter et al. 2012) of natural flow abstraction to e.g., 20% when no foreseeable EF • Cold Regions Hydrological Indicators of Change (CHIC; Peters et al. (2014)) recognizes influence of ice on flows
Hydraulic rating	• EF determined from assessment of change in hydraulic variable(s) as a function of discharge (Jowett 1997) • Threshold (breakpoint) where significant reductions in habitat quality occur with decrease in discharge is identified—assumed to maintain ecosystem integrity • River reach specific and fish focused applications	• Hydraulic variables (e.g., river stage or maximum depth or wetted perimeter typically measured across riffle) used to assess habitat factors known/assumed to be limiting to target aquatic biota • The most commonly used method is the "wetted perimeter method" that predicts wetted area of a cross-section as a function of flow at a location in the river (Tharme 2003) • Low-resolution hydraulic methods superseded by more advanced habitat modeling or holistic methods
Habitat simulation	• EF based on detailed analyses of the suitability of physical habitat vs flow using integrated hydrological, hydraulic and biological response data • The results usually take the form of habitat-discharge curves to predict optimum flows for target species, e.g., fish • Study site/river segment scale	• Flow is typically modelled using data on hydraulic depth, velocity, channel slope, substratum type, cross-section shape, etc., collected at multiple cross-sections within a study reach • The Physical Habitat Simulation Model (Bovee et al. 1998) is the preeminent modeling platform

(continued)

Table 8.1 (continued)

Method	Purpose & scope	Examples of methods
	• Representative assumption in scaling up	• More recent methods are RIVER2D (Blackburn and Steffler 2003) and Generalized Habitat models (e.g., STATHAB; Lamoureux and Jowett (2005)
Holistic frameworks	• Designed to evaluate entire ecosystem riverine processes requirements: e.g., fluvial geomorphology, aquatic biota, riparian zone, floodplain, etc. • Critical flow criteria identified for some or all major components of the riverine ecosystem -not limited to single species protection • The basis for most approaches is a systematic construction of a modified flow regime which defines features of the flow regime to achieve particular ecological, geomorphological, water quality, social objectives • Flexible in using available data, high confidence in answers obtained • Whole rivers, applicable for regionalization	• Advanced holistic methods routinely utilize several of the tools found in hydrologic, hydraulic and habitat rating methods, e.g., Instream Flow Incremental Method (Bovee et al. 1998) • The natural regime of the river is the fundamental guide, flows that maintained the "entire panoply of species," and key features of this regime are identified and adequately incorporated into the modified flow regimes • A wide range of holistic methodologies have been developed and applied in Australia, South Africa, United Kingdom, and Canada • Ecological Limits of Hydrological Alteration (ELOHA; Poff et al. (2010)); Building Block Methodology (BBM; King and Louw (1998), Tharme and King (1998)); Downstream Response to Imposed Flow Transformations (DRIFT; Brown and King (2000), King et al. (2003))

Adapted from Karim et al. (1995), Tharme (2003), Arthington et al. (2004), Pyrce (2004), Acreman and Dunbar (2004), Golder Associates Ltd (2005), Linnansaari et al. (2013), and Peters et al. (2012)

Since the initial 2007 Brisbane Declaration, the international community has progressively embraced the term environmental flows (EF) as essential for freshwater ecosystem health and human well-being, which was recently expanded to include all aspects of the aquatic ecosystem. More inclusively, EF are now defined as the "*quantity, timing, and quality of freshwater flows and levels necessary to sustain aquatic ecosystems which, in turn, support human cultures, economies, sustainable livelihoods, and well-being. In this definition, aquatic ecosystems include rivers, streams, springs, riparian, floodplain and other wetlands, lakes, coastal waterbodies, including lagoons and estuaries, and groundwater-dependent ecosystems*" (Arthington et al. 2018). The term provides an inclusive definition for the science of flow management in the context of the protection of natural ecosystems and water use needs among all stakeholders, including Indigenous groups.

The natural flow paradigm, which explicitly recognizes temporal and magnitude variability of water conditions, is now an established approach in the management and basic study of riverine ecosystems, allowing assessment of the ecological implications of deviations from the reference regime as a result of water diversion, storage, abstraction, and/or additions (Poff et al. 1997; Lytle and Poff 2004; Peters et al. 2012). Richter et al. (1996) identified a set of 33 annual hydro-ecological variables, known as the Indicators of Hydrologic Alteration (IHA), which represent ecologically important flow-regime components, such as timing and magnitude of peak flows. The set of IHA variables quantify five ecologically significant facets of the flow regime: (i) magnitude of monthly water conditions; (ii) magnitude and duration of extreme water conditions; (iii) timing of annual extreme water conditions; (iv) frequency and timing of high and low pulses; and (v) rate and frequency of flow reversals. Although the IHA approach has been applied internationally, it does not explicitly consider the effect of ice on water conditions. Peters et al. (2014) and Alfredsen (2017) addressed this obvious gap for applications in cold regions via the identification of ice-affected indicators for Canada and Norway, respectively (Table 8.2). Overall, these sets of ecologically relevant statistics of water conditions provide a framework to compare natural to altered flow regimes to assess the degree of perturbation to aquatic flow conditions.

More elaborate and costly processes for developing EF recommendations to protect multiple ecosystem components include the Instream Flow Incremental Method (IFIM; Bovee et al. (1998)), where the water requirements for the flow regime itself, water quality, riparian vegetation, channel maintenance, and fish habitat are individually determined, and subsequently integrated into an EF recommendation. The use of habitat simulation approaches, such as the Physical Habitat Simulation Model (PHABSIM; Bovee et al. (1998)), has increased as a preferred tool in North America (Annear et al. 2009). Considered more defensible (Dunbar and Acreman 2001), extensive site-specific biotic/abiotic data are required to establish EF levels for target species (typically fish) at relatively small spatial scales (i.e., <1-km river length).

Holistic EF approaches that address the water requirements of the entire river ecosystem (Arthington et al. 1992, 2004) rather than the needs of select taxa (e.g., fish or invertebrates) within a segment of a river channel and/or the entire watershed river system have increasingly gained recognition internationally. Holistic approaches are typically multidisciplinary and complex in nature and employ many of the hydrological, hydraulic, and habitat simulation tools, with elements incorporated in an IFIM type framework. For instance, the "bottom-up" Building Block Methodology (BBM) was developed to provide guidance on sustainable use of South Africa's river water (King and Louw 1998) and the "top-down" Downstream Response to Imposed Flow Transformations (DRIFT) iterative approach was developed to provide flow scenarios/descriptive summaries of flow alteration consequence in Australia (King et al. 2003). As holistic approaches evolve, they are

Table 8.2 List of ecologically relevant cold regions hydrological indicators of change (CHIC)

Period	Hydro-ecological variables	Example of ecological influence
Annual	Monthly median flow magnitude	Availability and temporal variability of suitable aquatic and riparian habitat
	Baseflow value	Shorter-term availability of aquatic and riparian habitat during low flow period
	Mean 90-day minimum flow magnitude	Seasonal low flows affect availability of aquatic and riparian habitat
	Mean 90-day maximum flow magnitude	Seasonal high flows influence availability of aquatic and riparian habitat
	Rise rate	Stress and habitat recovery relating to rising water levels
	Fall rate	Stress and habitat recovery relating to falling water levels
	Number of hydrograph reversals	Habitat availability and connectivity relating to water level range
	Number of low pulses/year	Occurrence of potentially stressful low flow conditions
	Median duration of low pulses	Duration of potentially stressful low flow conditions
	Number of high pulses/year	Occurrence of potentially stressful high flow conditions
	Median duration of high pulses	Duration of potentially stressful high flow conditions
	Number of zero flow days	Extreme loss of aquatic habitat availability and connectivity
	Spring Freshet initiation date	Freshet represents the primary driving annual hydrological event for most systems
	Flow magnitude on day of freshet initiation	Flows that structure aquatic habitat availability and channel morphology through substrate scour and ice-jam flooding
Open water	1-day minimum open-water flow magnitude	Short-term extreme low flow conditions affect habitat availability
	Date of 1-day minimum open-water flow	Timing of short-term extreme low flow conditions can influence aquatic spawning
	1-day maximum open-water flow magnitude	Short-term extreme high flow conditions affect availability and connectivity of habitat
	Date of 1-day maximum open-water flow	Timing of short-term extreme high flow conditions can influence ecological processes cued to water availability
	Duration of open-water period	Critical for photosynthetic production and oxygenation
Ice affected	Date of freeze-up	Timing of winter ice formation can reduce habitat availability and alter distribution
	Magnitude of flow at freeze-up	Magnitude of flow at time of freeze-up can be directly related to loss of shallow water habitat and reduced contaminants dilution

(continued)

Table 8.2 (continued)

Period	Hydro-ecological variables	Example of ecological influence
	Date of breakup	Timing related to habitat availability and cues for spawning
	Magnitude of flow at breakup	Magnitude related to ecological processes including habitat availability
	Duration of ice-influenced period	Duration of under ice conditions including effects of solar radiation, thermal regime change and oxygen levels
	1-day minimum ice-influenced flow magnitude	Availability of habitat and stressful conditions for aquatic taxa relating to ice conditions
	Date of 1-day ice-influenced minimum flow	Timing of winter low flows related to habitat availability
	1-day maximum ice-influenced flow magnitude	Availability of habitat and stressful conditions for aquatic taxa relating to ice conditions
	Date of 1-day ice-affected maximum flow	Timing of winter low flows related to habitat availability
	Peak water level during ice period	Related to habitat availability especially channel connectivity
	Date of peak water level during ice period	Timing important for connectivity
	Flow magnitude on day of ice-influenced peak water level	Related to habitat availability especially channel connectivity

Modified from Richter et al. (1996) and Monk et al. (2012)

considering more than the environmental needs of the watershed and moving to incorporate social and cultural needs.

Most recently, a group of international scientists proposed the Ecological Limits of Hydrologic Alteration (ELOHA; Poff et al. (2010)) framework for developing broad EF standards based on the synthesis of available regional data, models, and expert knowledge in five key steps: (i) hydrologic baseline, (ii) river typing, (iii) flow alteration assessment, (iv) flow alteration–ecological response definition, and (v) policy implementation. The ELOHA framework does not prescribe a specific hydrological assessment tool and a scientifically challenging step is the development of flow–ecological relationships (Kendy et al. 2009; Poff et al. 2010).

The most northerly application of the ELOHA is the current EF project on the lower Saint John River basin in eastern Canada ($\sim$45° N Latitude) where the estuary floodplain is influenced by ice-jam flooding (Monk et al. 2017). Although located south of permafrost zones, lessons learned from the development of an EF framework for this more southern cold regions river can be applied to northern regions. A relevant example is the multi-jurisdictional action plan led by Wood Buffalo National Park (WBNP 2019) to address environmental flows within the Peace-Athabasca Delta (Mackenzie River headwaters) as part of a response to

several UNESCO World Heritage Committee recommendations to ensure state of the environmental assessment (SEA) identified outstanding universal values are maintained for generations to come.

8.4 Environmental Flows Policies and Guidelines in Northern Regions

Non-consuming water projects that store/release and/or divert flow (e.g., hydroelectric power generation, flow diversion), as well as abstractions that consume water (e.g., mining and agriculture), have the potential to adversely affect riverine and riparian habitat conditions needed to support fish, invertebrates, mammals, waterfowl, and other aquatic related organisms, unless sufficient amounts of water are maintained in the channel during appropriate periods of the year. EF requirements (i.e., water management framework) vary depending on whether the objective is to maintain an existing ecosystem, restore or upgrade it to a prescribed or desired state. As a general rule, the closer to a natural flow status, the more water will need to be allocated for the ecosystem, and the higher the EF will be. In many nations, water is a state-owned natural resource, and the state has an obligation to manage it for the public good, including protecting freshwater environments. Internationally, several legal principles support the direct and indirect protection of EF.

Arctic states, comprising Finland, Sweden, Norway, Kingdom of Denmark (including Greenland), Iceland, Canada, the United States of America, and the Russian Federation, have adopted environmental impact assessments (EIA) and SEA provisions in their national legal systems (Koivurova 2005). Arctic states are thus, in theory, obligated to carry out environmental assessments for overarching policies, plans, and programmes that could potentially harm their Arctic environments (Azcárate et al. 2013). Importantly, the Arctic states agreed in the early 1990 s, through the Espoo Convention (UNECE 1991) to carry out EIA on planned development projects taking place in transboundary river basins. There are several large river systems that cross Arctic states, such as the Yukon River originating in Canada and flowing through the USA prior to discharging into the Bering Sea at the Yukon–Kuskokwim Delta (see Fig. 8.1). The implementation of SEA in the Arctic has been limited by the discretion left to states to decide what are significant impacts (Hildén and Furman 2001; Bastmeijer and Koivurova 2008). Azcárate et al. (2013) articulated that EF should be a key component of SEA.

A scan of the international literature revealed a wide range of EF policies, guidelines, and recommended methodologies for subarctic and Arctic regions (Tables 8.1 and 8.3). What further complicates the synthesis of EF information is that several large river systems flow from southern to northern latitudes, with some cases having headwaters emanating outside of permafrost regions and across jurisdictions. An example is the second largest river in North America: the Mackenzie River Basin drains an area of $\sim$1.8 million km^2 that originates

Table 8.3 Environmental flow guidelines for the Arctic States

Jurisdiction	Policy/guideline
USA	
Alaska	• Fish and Game Act requires "manage, protect, maintain, improve and extend the fish, game and aquatic plant resource of the state in the interest of the economy and general well-being of the state" (Klein 2016) • 1980 Water Law amended to allow protection of instream flows in rivers and water levels in lakes—commonly known as Alaska instream flow law • Burden is on applicant to choose and defend the EFN approach used • Alaska Dept. of Fisheries & Game used hydrologic-based approaches, such as historical flow with the Tennant (1976), combined with fish use information to quantity EFN for fish • Reservation of water follow instructions and State of Alaska Instream Flow Handbook (DNR 1985) • Fish habitat permits are issued by Department of Natural Resources as one of the tools to retain sufficient amounts of water in lotic and lentic fish-bearing systems
Canada	
	• Consideration of e-Flows falls under the Federal Department of Fisheries and Oceans (DFO) mandate • 2013 developed a national framework for assessing ecological flow requirements to support fisheries (DFO 2013)—provides advice on the management of the flow regimes and water levels required to maintain the ecological functions that sustain fisheries associated with that water body and its habitat • 2019 Modernization of Fisheries Act to incorporate indigenous considerations and restore the previous prohibition against the harmful alteration, disruption or destruction of fish habitat (DFO 2019) • DFO has participated in the developed e-Flows guidelines with several provinces and territories
Yukon	• Yukon Waters Act water licensing process provides for the conservation, development and utilization of waters. Government water inspectors conduct proactive enforcement and compliance monitoring programs to help eliminate or reduce the risks associated with water use • No explicit information on EFN available
Northwest Territories	• Federal Department of Fisheries and Ocean (DFO) drafted a guideline for winter water withdrawal in 2005, which allowed a 5% instantaneous reduction from natural flow (Cott et al. 2005) • The guideline was revised, however, in 2010 and no fixed allowable reduction was described (DFO 2010) • The current assessment is carried out on a case-by-case basis and if withdrawal is allowed, the recommendation is typically 5–10% of the instantaneous flow by the time of withdrawal
Nunavut	• Nunavut Water Board has responsibilities and powers over the regulation, use and management of water • NWB seeks to protect, manage and regulate freshwaters in Nunavut by incorporating Inuit Qaujimajatuqangit and scientific knowledge in decision-making • No information on EFN available

(continued)

Table 8.3 (continued)

Jurisdiction	Policy/guideline
British Columbia	• 2016 BC Water Sustainability Act, which includes both surface and subsurface water use, has a provision for assessing risk and identifying where cautionary measures could be taken or additional analysis needed, including developing site-specific environmental flow needs thresholds • Framework recognizes fish and non-fish bearing streams, open-water versus ice covered periods, and size of stream (see Lewis et al. 2004) • Key aspects of the natural hydrograph should be maintained by restricting hydrologic alterations to within a percentage-based range around natural or historic flow variability (DFO 2013) • A stream, or specific flow periods, deemed to be at Risk Management • Level 1: Sufficient natural water availability for the proposed withdrawal period and cumulative water withdrawals are below specified threshold—can range from 5 to 15% of the natural or naturalized flow, with the more conservative threshold for streams or flow periods that are naturally flow sensitive • Level 2: Aquatic environment is flow-limited for the proposed withdrawal period; or cumulative water withdrawals are greater than a specified threshold of concern—5–20% of the natural flow • Level 3: Aquatic environment may be very flow-limited for the proposed period of withdrawal; or that cumulative water withdrawals are greater than a specified threshold of concern—5% for the most flow sensitive to greater than 20% cumulative withdrawals in a low sensitivity scenario. More rigorous review of the potential risk and/or comprehensive approval/license terms and conditions are likely • Special Consideration: Presence of sensitive species or habitats may require "special consideration" or species-specific information which would be taken into consideration with the risk management level • Use of mean annual discharge for characterizing flow sensitivity has a precedence in BC (e.g., BC Modified Tennant method in Hatfield et al. (2003) and is supported by BC specific studies
Alberta	• Alberta's Water Act and Water for Life Strategy support and encourage establishment of EF. A holistic approach to aquatic management to ensure resources are maintained, restored and enhanced is outlined in the Strategy for the Protection of the Aquatic Environment • Level 1: Alberta desktop method for determining EF is used in the absence of having site-specific information that could otherwise be used to establish an environmental flow (Locke and Paul 2011). The guideline prescribes the greater of either – A 15% instantaneous reduction from natural flow or the lesser of either the natural flow or the Q80 natural flow based on a weekly or monthly (depending on the availability of hydrology data) time step – No water abstractions are allowed for the lowest flows that occur up to 20% of the time, and for the remaining 80% of the time, up to 15% of the natural flow can be withdrawn – Preserves the quantity and natural fluctuations of flow • Level 2: EF have been determined in a number of large-scale projects based on multi-year, site-specific studies (Clipperton et al. 2003; Goater et al. 2007; Ohlson et al. 2010). The approach in these projects has been holistic, using multiple environmental criteria and a range of different

(continued)

Table 8.3 (continued)

Jurisdiction	Policy/guideline
	methodologies for assessment and incorporation into a water management framework. For instance, a framework establishes weekly management triggers and water withdrawal limits to enable proactive management of mineable oil sands water use from the Athabasca River
Saskatchewan	• Saskatchewan watershed security agency—any use which will consume greater than 5 cubic decameters will require an approval • No information on EFN available
Manitoba	• 2003 Water Strategy for the future—holistic approach to protect water to support and maintain ecosystems while meeting the water needs. Water allocation regime is based on the Water Rights Act • Guiding principles based on concept of sustaining native aquatic resources and ecosystem processes (Manitoba Government 2008; Golder Associates Ltd., 2005) • Level 1: Tennant (1976) or Tessman (1979) method recommended as a first approach to determine instream flow needs for fish • Level 2: Instream Flow Incremental Methodology (IFIM, Bovee (1982) recommended for sites with development. 2-dimensional and RIVER2D modeling has been applied on Assiniboine River to develop flow regime to sustain fish populations • Provincial Instream Flow Method for intermittent streams—based on median flow of the 7-week period beginning with the first week of April
Ontario	• Ministries of Natural Resources and of the Environment oversee hydropower development and water use related flow, respectively. Greater than 50,000 L of water per day requires permit to take water • There is currently no EFN guideline and various rules have been used • A number of approaches were applied in the three pilot projects. These included hydrological, hydraulic rating and habitat simulation approaches • Incorporation of e-Flows into Conservation Authority management plans
Quebec	• Le ministre du Développement durable, de l'Environnement et des Parcs oversees EF • The promoter of a project must justify the IFN method (hydrological, hydraulic, habitat simulation) chosen and Faune et Parcs Quebec must approve the method (FPQ 1999) • Level 1: An "ecohydrological method" (Belzile et al. 1997; Bérubé et al. 2002) has been described to determine conservation flows in the rivers of southern Québec to protect fish habitat • Level 2: 2-D habitat modeling approach used along with complementary holistic methods to determine hydrological regime at upstream diversion to conserve spawning habitat of fish (Boudreau et al. 2004)
Labrador	• Newfoundland and Labrador Department of Environment and Conservation • "low quartile of mean monthly lows method" has been suggested (i.e., Q25 of MMF; Rollings 2011)
Iceland	• Iceland in the process of implementing the Water Framework Directive
Finland	• European Union Water Framework Directive (EUWFD 2018) requires that the hydrology and connectivity of watercourses are guaranteed.

(continued)

Table 8.3 (continued)

Jurisdiction	Policy/guideline
	Waterbodies should be restored to meet 'Good Ecological Status', implying slight deviations from natural conditions • Finland 2011 Water Act has provisions for protection of fish • Range of no obligations to mandated minimum flows exist for hydropower dams (Hellsten et al. 2017) • Survey by Linnansaari et al. (2013) reported use of dynamic definition of e-Flows and that in some cases, fish habitat modeling based on relationship of flows, water depth, substrate and quality/quantity of habitat
Denmark (Greenland)	• No information on EFN readily available
Sweden	• Environmental law in Sweden dictates that measures should be implemented to safeguard riverine ecosystems (SEPA 2018) • Mandates owners of power stations set aside minimum flows corresponding to >5 and <20% of production value if motivated by gains in ecological values • Minimum flow requirements generally do not include seasonal variation in flow. If any variability is incorporated, it typically reflects higher summer flows and lower winter flows • Environmental objective "Flourishing Lakes and Streams," set by the Swedish Parliament (SEO 2008), states that 'the natural flows and water levels in today's unexploited and virtually unspoiled streams are maintained, and the flows in streams affected by regulation are adjusted wherever possible to the needs of biological diversity' • Sweden has four large, free-flowing rivers (Torne, Kalix, Pite, and Vindel rivers) that are declared national rivers and protected from hydroelectric development under environmental law (Renöfält et al. 2010)
Norway	• Transparency rule in legislation regarding environmental flow releases—requires the hydropower company to document that the correct amount of water is released • No nationwide environmental flow guideline has been established • As a general rule, the Q95 is used for summer and winter seasons • More water is required for rivers that have a special "National salmon river" status or where species of special concern exist • Habitat simulation methods are commonly used for the case-by-case evaluations. Recently, a holistic BBM method was applied in Norway (Alfredsen et al. 2012, 2017)
Russia	• No information on EFN readily available

thousands of kilometers upstream in the Rocky Mountains (latitude 52° N) prior to discharging through the >10,000 km^2 Mackenzie Delta floodplain in the Beaufort Sea (latitude 69° N). Another example is the largest river in Asia: the Ob River basin ($\sim$3 million km^2) encompassing most of Western Siberia and the Altai Mountains (headwaters in Kazakhstan, China, and Mongolia), drains predominantly Russian terrain prior to discharging into the Gulf of Ob in the Kara Sea, the world's largest estuary (see Fig. 8.1). In both these river systems, the impact on the

natural flow regime from operating large reservoirs for storage/release of mountain water to generate hydropower can be traced thousands of kilometers downstream and into permafrost regions (Yang et al. 2004b; Gibson et al. 2006; Peters and Buttle 2010).

Although the country of Russia comprises a significant portion of the Arctic, information on EF was not readily available from internet searches (Table 8.3). Other Arctic states, including Finland, Sweden, Norway, Iceland, and Denmark (excluding Greenland), are signed on to the European Union (EU) Water Framework Directive (WFD), which mandates monitoring and assessment of freshwater biota to achieve good ecological status in all waterbodies (e.g., Acreman and Ferguson (2010)). These authors note that within the assessment framework of the WFD, there is no explicit use of the term EF; however, achieving hydrological regimes that are ecologically appropriate has been identified as an essential component of meeting WFD targets. Furthermore, management and restoration to improve the ecological status of river ecosystems that have undergone alteration require implementing an EF (Acreman and Ferguson 2010). Most EU countries have a recommendation based on the WFD for setting an EF regime, but some countries determine environmental flow guidelines on a case-by-case basis.

In Canada, consideration of EF generally falls under the Federal Department of Fisheries and Oceans (DFO) mandate and Fisheries Act, with an obvious primary focus on fish and the protection or restoration of fish habitat. The Fisheries Act was modernized in June 2019 to incorporate Indigenous considerations and to restore the previous prohibition against the harmful alteration, disruption or destruction of fish habitat (DFO 2019). In 2013, DFO developed a national framework for assessing ecological flow requirements to support fisheries (DFO 2013), which provides advice on the management of the flow regimes and water levels required to maintain the ecological functions that sustain fisheries associated with that water body and its habitat. DFO has participated in the development of EF guidelines with several provinces and territories. For example, DFO was extensively involved in the research and consultation for the development of EF guidelines—triggers and thresholds for water abstraction associated with oil sands mining—for the lower Athabasca River surface water quantity management framework (GoA 2014). This framework protects a key headwater sub-basin river of the Mackenzie Basin from cumulative water withdrawal to support human and ecosystem needs, while considering an acceptable balance between social, environmental, and economic interest.

The Canadian Arctic region covers the Yukon, Northwest Territories, Nunavut, Quebec, and Labrador; while the permafrost and subarctic regions extend south into the northern regions of the Provinces. As outlined in Table 8.3, there is a range of EF considerations across Canadian jurisdictions, from none to multi-tiered approaches, but there is a general intent to protect water resources from anthropogenic impacts on rivers. With some exceptions, territorial and provincial legislation protects water resources using relatively general description (e.g., reference to protection of aquatic biota/ habitat), without specifying the means to determine EF. In general, overarching rules describe that alterations must be sustainable,

should not cause significant adverse effects to the watercourse, and that "some" amount of water is required in a river to maintain a healthy aquatic habitat (Linnansaari et al. 2013). This philosophy also extends to lakes, where DFO oversees projects that are identified to significantly affect lake habitats, such as a whole lake or partial lake destruction as a result of diamond mining in northern regions that require "fish-out" programs. EF guidelines, if these exist, tend to be recommendations or "best advice" to the regulator. A jurisdiction to highlight is the Province of British Columbia that adopted a new Water Sustainability Act in 2016, which specifically protects surface waters and EF, including groundwater connected to adjacent channels. In this provincial act, non- and fish-bearing streams are recognized, with three levels of EF methods outlined (BC 2016; see Table 8.3).

Alaska has been at the forefront of riverine protection with the amendment of their Water Act to allow for the protection of instream flows in rivers and water levels in lakes—commonly known as the Alaska instream flow law. Similar to other jurisdictions in North America, the burden is on the applicant to choose and defend the EF approach applied. The Fish and Game Act requires the Alaska Department of Fish and Game to "manage, protect, maintain, improve and extend the fish, game and aquatic resources of the state in the interested of the economy and general well-being of the state". Alaska has an open EF presence with the annual publication of instream flow protection activity reports (e.g., Klein (2016)).

Environmental flow frameworks presented in the literature are typically designed for river systems for which there remains flowing water at any given time. However, Linnansaari et al. (2013) pointed out that it should also be recognized that defining EF requirements could be very different in perennial (flows continuously all year) versus temporary (flows only for a part of the year) streams and rivers. As outlined in earlier sections and covered in Buttle et al. (2012), temporary flow systems are prominent in the Arctic regions where permafrost limits subsurface pathways of baseflow and channels may freeze solid over the long, cold winter months. A framework for the assessment of EF requirements for ecosystem protection in permafrost regions should thus be based upon and accompanied by a well-designed monitoring program that explicitly considers cold region processes, which enables periodic refinement via an adaptive management process, especially if one wishes to consider rapidly changing climate conditions (non-stationarity baseline) in high latitudes.

8.5 Riverine Monitoring in the Northern Regions

Environmental monitoring is a requisite in the detection, understanding, and evaluation of changes in the physical, ecological, and geochemical environment. As such, monitoring is explicitly recognized as a critical component of a SEA and EF assessment process. Repeated and long-term monitoring is also necessary for understanding the causes and consequences of rapid change and longer-term trends, while supporting sustainable resource development in northern areas. The Arctic

and subarctic are vast and sparsely populated regions. The remoteness and harsh conditions increase operating costs and challenges associated with establishing monitoring infrastructure and ensuring sufficient geographic coverage (Mallory et al. 2018). Although indirect methods exist, such as remote sensing approaches, environmental monitoring fundamentally relies on actual observations in the field to establish baseline conditions and identify areas of vulnerability as compared to a reference state.

8.5.1 Hydrometric

The flow regime is a primary determinant of the structure and function of aquatic and riparian ecosystems for streams and rivers (Poff et al. 1997). Thus, a primary dataset required for carrying out an EF assessment is hydrological information in the form of discharge ($m^3\ s^{-1}$) and stage (m), with the latter convertible to depth (m) if bathymetry is available for a river reach of interest. Furthermore, baseline hydrologic data are needed by water resource agencies and water users for planning/management, as well as hydrological modeling. Figure 8.5a shows the location and distribution of hydrometric stations with daily observations (e.g., daily mean, maximum, minimum) for areas draining to the Arctic Ocean to the north, Bering Sea and Gulf of Alaska to the west, and Labrador Sea to the East available from federal government agencies—Water Survey of Canada (WSC 2018) and United States Geological Survey (USGS 2018).

In Canada, hydrometric stations are identified as "natural" or "regulated." It can be seen in Fig. 8.5a that the majority of regulated rivers systems are located below 60° N latitude. However, as previously stated, for the purpose of EF, one should consider large development projects from outside the immediate permafrost regions as hydrological alterations of sufficient magnitude may be propagated downstream to the mouth of the river entering the Arctic Ocean. For instance, the most downstream hydrometric station near the mouth of the Mackenzie River is labeled as "regulated" in recognition of hydropower reservoir operations more than 2000 km upstream in the Peace River sub-basin that has been shown to not only affect the river mainstream (Peters and Prowse 2001) but also the water level regime of the downstream Lake Athabasca (Peters et al. 2006) and Great Slave Lake (Gibson et al. 2006).

Notably, the density of hydrometric stations decreases markedly from the southern headwaters to more northern portions of the Canadian Arctic drainage basins. Laudon et al. (2017) noted in that ~40% of far northern hydrological research catchments have been closed since the year 2000. An evaluation of the Canadian National Hydrometric network by Coulibaly et al. (2013) concluded that the majority of the Arctic region does not meet World Meteorological Organization standards (WMO 2008). In the adjacent state of Alaska, Klein (2016) highlighted that although the state has 40% of the US surface water outflow, the paucity of hydrometric stations (323 with >5 years of data) limits the State's ability to account for, identify and acquire reserve flows. Overall, the paucity of the North American

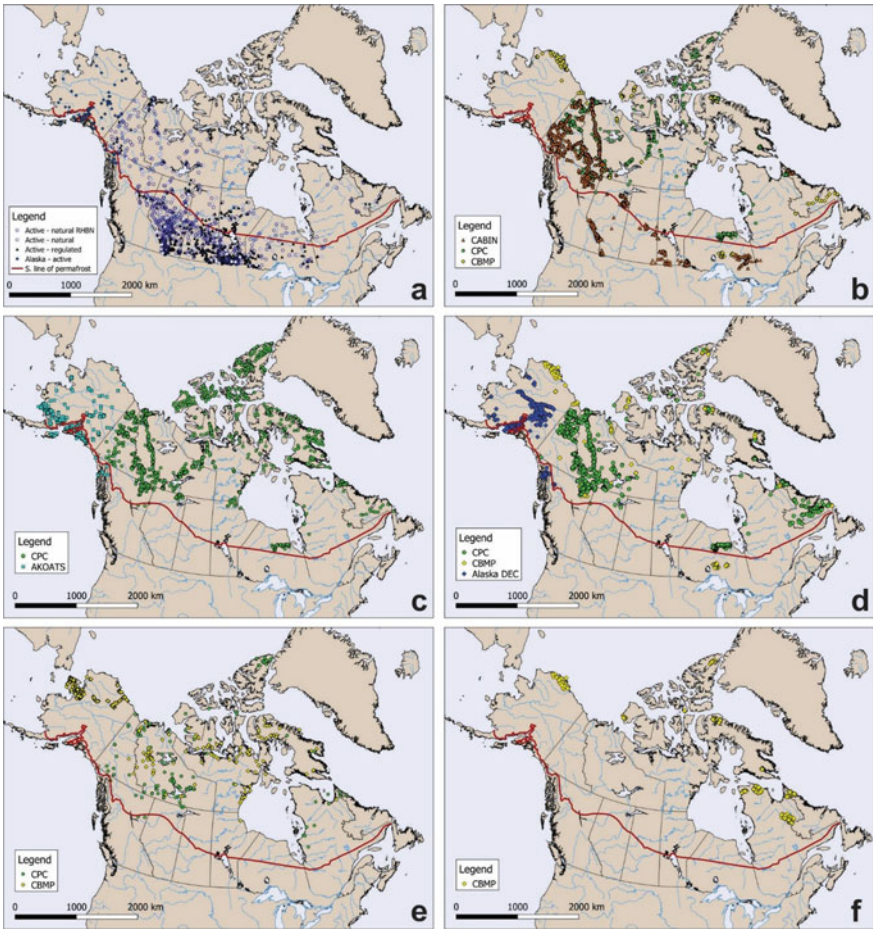

Fig. 8.5 Location of select monitoring in North American areas draining to the Arctic Ocean to the north, the Bering Sea and Gulf of Alaska to the west, and Labrador Sea to the East (i.e., areas above 58° N Latitude). **a** Hydrometric (ECCC 2018; USGS 2018), **b** benthic macroinvertebrate (CPC 2015; CABIN 2019; Lento et al. 2019), **c** water temperature (CPC 2015; AKOATS 2017), **d** water quality (ADEC 2010; CPC 2015; Lento et al. 2019), **e** fish (CPC 2015; Lento et al. 2019), and **f** diatoms (Lento et al. 2019)

hydrometric network across the Arctic diminishes societies' ability to detect, understand, and predict the water resource responses changing climate and human perturbations, especially on remote Arctic Islands (e.g., Spence and Burke 2008). In recognition of this, key stations were reintroduced to the network on two of these islands and added near the Mackenzie Delta during the International Polar Year Program.

Either because of a lack of adequate baseline hydrological data or the need to simulate the effects of climate change and/or development scenarios, models are used to estimate daily streamflow to obtain flow regime characteristics. On streams with limited or no streamflow data, using hydrologic models to simulate long-term or seasonal flow characteristics is difficult and highly uncertain, with limited ability to simulate key hydrological indicators (e.g., Shrestha et al. 2014). In particular, key to modeling flow regime characteristics is the proper representation of frozen-ground/permafrost processes. Frozen-ground algorithms are especially important for simulating the spring freshet when the ground is still frozen, subsequent active layer development, and baseflow from groundwater that sustains low flows (Woo et al. 2014; Woo and Thorne 2016). A number of hydrologic models have been developed that explicitly represent the water and energy balance over snow and frozen ground, such as the Variable Infiltration Capacity (VIC; Andreadis et al. 2009), Pan-Arctic Water Balance Model (PWBM; Rawlins et al. 2013) and Cold Regions Hydrological Model (CRHM; Pomeroy et al. 2007). However, the use of hydrologic models with frozen-ground/permafrost processes are computationally expensive for large basins (Shrestha et al. 2019a). Further limiting hydrologic modeling is the lack of high-resolution topographic and wetland classification information. Limited observation data, such as the sparse permafrost and meteorological monitoring networks in the high latitudes (Smith et al. 2010; Mekis and Vincent 2011; Vincent et al. 2012), pose challenges for calibrating/validating hydrologic models and simulated flow timing/magnitude uncertainty, especially during the ice-covered low flow period (Hamilton 2008). Given these challenges, it is not surprising that the Arctic and subarctic regions have received relatively limited focus in terms of hydrologic modeling studies. Specifically, in contrast to other regions of the world, hydrologic impact studies are conducted using sophisticated high-resolution hydrologic models, there is still a need to rely on coarse resolution global or pan-Arctic models for the high-latitude regions (Shrestha et al. 2019). Readers are referred to another chapter in this book by Park et al. (2021) entitled "*Cold Region Hydrologic Models*" for an overview and a more thorough discussion on this technical subject.

Given climate-induced changes in the hydrologic regimes, such as the shifts in the magnitude and frequency of extreme events, it has become essential to consider the changes in the context of non-stationarity (Milly et al. 2008; 2015). Case studies and discussion of this latter topic are presented in another chapter of this book entitled "*Changing Hydrologic Extremes in Arctic Rivers and Regions*" by (Shrestha et al. 2021). For instance, using non-stationary extreme value analysis, Bennett et al. (2015) identified time-dependent changes in the distribution of spring streamflow extremes for watersheds in the interior region of boreal Alaska. The consideration of non-stationarity is especially relevant in the context of projected enhanced warming and amplified moisture fluxes to the Arctic region (Serreze and Barry 2011; van Oldenborgh et al. 2013; Zhang and Zweirs 2013), and significant future changes to streamflow regimes, particularly in extremes (Hirabayashi et al. 2013; Shevnina et al. 2017; Shkolnik et al. 2018). Extreme hydrological events are

relatively rare by nature, but important in shaping the aquatic environment, and thus the methodology and approaches to determine changes in extreme events must be carefully considered in order to assess impacts correctly and present reliable results for decision-making purposes (Zhang and Zweirs 2013).

8.5.2 Ecological

EF frameworks, such as the ELOHA (Poff et al. 2010), include the synthesis of existing hydrologic and ecological databases from many rivers within a user-defined region. In the high latitudes of North America, an ELOHA type EF assessment may be feasible as background aquatic ecology related monitoring has been carried out by federal, territorial and regional governments, academia, and non-governmental organizations that have a wide variety of mandates. Figure 8.5b–f present the meta coverage of macroinvertebrate, water temperature, water chemistry, diatoms, and fish monitoring sites that have been assembled from information obtained by (i) Alaska Online Temperature (AKOATS 2017), (ii) Canadian Aquatic Biomonitoring Network (CABIN 2019), (iii) Canadian Polar Commission report on the State of Environmental Monitoring in Northern Canada (CPC 2015), and (iv) the Canadian contribution to the Circumpolar Biodiversity Monitoring Program (CBMP) (Culp et al. 2012; Lento et al. 2019). Note that the sampling locations shown in these figures are a mixture of spot and continuous monitoring, for which the former will provide good information on species presence/composition and the latter the ability to examine change over time.

Environmental data, such as the ones presented in Fig. 8.5, are essential for the development of scientifically defensible and empirically testable relationships between flow alteration and ecological/water quality responses. A good indicator of stream health is the composition of bottom-dwelling (benthic) invertebrates (e.g., snails, amphipods, and aquatic larvae of insects such as mayflies, caddisflies, and dragonflies). An example is the Canadian Ecological Flow Index (CEFI; Armanini et al. 2011, 2012) that summarized the flow sensitivity preferences for benthic macroinvertebrates (BMI) in a range of river systems across Canada. Combined with the CHIC variables discussed above, CEFI provides a basis for hypothesis development and testing of aquatic response to hydrological alterations. Although the number of BMI sampling and monitoring sites has grown since the early 2000s with programs such as the CABIN, large extents of Arctic drainage areas remain to be sampled/monitored for BMI (Fig. 8.5b).

Scientific uncertainty exists in establishing the relationship between flow alteration and ecological responses, in part because of the potential confounding of hydrologic alteration with other important environmental stressors (e.g., water temperature and chemistry). Water temperature and chemistry are collected as part of the CABIN protocol, which is predominantly based on a single annual sampling campaign. Figure 8.5c, d, present the distribution of water temperature and water quality observation sites as reported by CPC (2015) and AKOATS (2017), while

Fig. 8.5e, f show the reported monitoring of fish and diatoms, which are sparse in comparison to other environmental information (CPC 2015; Lento et al. 2019).

The metadata collected and presented in Fig. 8.5 clearly demonstrate that while there is substantial monitoring in Canada's North, gaps in coverage are present for a number of key parameters that are important in the context of resource development, climate change, and EF assessments. As highlighted by CPC (2015), another concern is the short-term duration of many monitoring programs. Baseline information is fundamental in any analysis, and detecting change requires long-term monitoring, with the required duration and frequency-dependent on the parameter (e.g., hydrometric requires daily observations over 20+ years). Current monitoring efforts in cold regions of North American would benefit from greater coordination and collaboration, both logistically and operationally, in support of longer-term planning and strategic direction (CPC 2015; Lento et al. 2019). As exemplified by Armanini et al. (2012), a good example would be the co-location of long-term hydrometric stations, which provide a primary measure of historical variability and change and development effect on EF indicators (e.g., CHIC), with biological monitoring sites such as CABIN.

An important step to address knowledge gaps is the Arctic Freshwater Biodiversity Monitoring Plan framework outlined in 2012 for improving circumpolar monitoring efforts as part of CBMP (see Culp et al. 2012). The framework addresses freshwater biodiversity priorities in the Canadian and circumpolar Arctic relating to conducting research and monitoring of water quality, quantity, and ecosystem health while addressing primary issue areas: (i) identify the impacts of climate change/variability on Arctic lakes and river ecosystems to inform adaptation planning/mitigation actions and responsible resource development; (ii) freshwater quality monitoring through collaborative efforts to assess status and trends of aquatic ecosystem health; (iii) develop environmental indicators that can be used to measure the status and trends of environment state; and (iv) relate contaminant levels and trends to ecosystem health (CBMP 2019). As part of the implementation of this plan, the CBMP Freshwater Group (CBMP-Freshwater) completed the first State of Arctic Freshwater Biodiversity Report (Lento et al. 2019), which assessed status and trends in freshwater biodiversity from across the circumpolar region, identified gaps in monitoring efforts, and provided advice for future monitoring to improve coordination and harmonization of monitoring efforts. The results and advice stemming from this report can play a key role in supporting the development of EF indicators for the permafrost regions.

8.5.3 Remotely Sensed Information

Data from remote sensing could assist in supplementing monitoring coverage in underrepresented areas for certain parameters, especially difficult to access, high-latitude regions of the circumpolar Arctic. For example, SAR satellite sensors (e.g., Radarsat 2 interferometry) have been used to map and monitor ice conditions on Arctic rivers (e.g., Mackenzie River Delta; van der Sanden et al. 2012). On the

near horizon is the Surface Water and Ocean Topography (SWOT; launch 2021) mapping satellite that has the aim to partially fill the large spatial gap in hydrometric monitoring (Biancamaria et al. 2016). The surface water elevation, extent and slope measurements from space by SWOT will enable the estimation of surface water storage changes, and when coupled with simple hydraulic equations, models and/or conventional measurement allow the hydrological community to infer streamflow in ungauged regions. Pre-launch calibration/validation of SWOT surface water products are currently underway at select sites in Canada (e.g., Peace-Athabasca Delta, northern lakes and wetlands; Pietroniro et al. 2019) and Alaska (e.g., Yukon River; Altenau et al. 2017) using an airborne analogue AirSWOT. Furthermore, satellite sensors have been used to evaluate water quality indicators: chlorophyll-a, colored dissolved organic matters, Secchi disk depth, turbidity, total suspended sediments, water temperature, total phosphorus, dissolved oxygen, biochemical oxygen demand, and chemical oxygen demand (Gholizadeh et al. 2016).

8.6 Conclusions, Future Needs and Recommendations

In light of the projected climate change and increased development in the high latitudes of the globe, the goal of this chapter was to present an overview of environmental flows for permafrost regions, with a focus on North America. In its simplest form, environmental flows (EF) are defined as the quantity, timing, and quality of freshwater flows and levels necessary to sustain aquatic ecosystems. Although there no nationwide frameworks for establishing EF flows in the USA, as was recently developed in Canada, Alaska has incorporated EF into water licensing of projects. For the most part, where information was available, countries that comprise the Arctic states have indirectly considered (e.g., European Water Framework Directive) or are in the process of considering EF guidelines within their water-related regulations. Given the commonality of governing cold regions processes and changes to hydrological regimes, a recommendation is that Arctic states pool their hydro-ecological knowledge to enhance the collective ability to address the projected growing need for applying EF Frameworks in the permafrost regions which have received considerably less attention than more southern regions.

A primary source of data needed to initiate even the most basic EF methods/assessments is hydrometric data in the form of daily flows and water level/depths. The good news is that hydrometric data of varying length exist to describe flow regimes. However, there is a need to augment the hydrometric network density in North America, especially in the more remote locations nearer the Arctic Coast and Islands, as to provide local reference sites prior to and post development.

Of greater concern for EF is the likelihood of not being able to assess responses to change due to the following factors: (i) ecological baseline monitoring has not been carried out until relatively recently in comparison to hydrometric monitoring; (ii) available data may not be “fit for purpose” with limited or lack of co-located

ecological and hydrological monitoring sites; and (iii) lack of temporal sequence data as sites may have been rarely visited. These factors limit the potential of developing basic ecological predictive models for cold regions that are necessary to inform decision-makers overseeing the development of northern regions. Future research should focus on enhancing our understanding of flow-ecology relationships to better manage important natural resources in a region that is heavily influenced by snow and ice for extended periods.

A recommendation is for a study to be carried out to assess hydro-ecological sites that are currently co-located (i.e., an ongoing collection of a combination of hydrometric, water quality, macroinvertebrate, and fish) and identify key regions that require such sites. Based on information gathered from this study, a network of "supersites" that will provide regional baselines/reference information should be developed. An initial network would also take advantage of existing remotely accessible infrastructure that is maintained by governments and academics. Engagement of communities to grow the monitoring network into local areas of high interest should be also considered. Given the remoteness and vast area, there is a need to develop and cost-share adaptive monitoring focused on criteria developed in cooperation with stakeholder groups and Indigenous peoples. There is also a need to develop a management framework for EF which embraces a range of possible climate warming scenarios.

Lastly, a permafrost region framework for the assessment of EF requirements for ecosystem protection should be based upon and accompanied by a well-designed monitoring program that explicitly considers cold region processes, which enables periodic refinement via an adaptive management process, especially if one wishes to consider rapidly changing climate conditions (non-stationarity baseline) in high latitudes.

Acknowledgments Cydne Potter provided valuable assistance expertise in drafting maps contained in this chapter. We wish to thank the Editors of this book, Daqing Yang and Douglas Kane, for the invitation to contribute and for helpful reviews that have improved this chapter. Support for the production of this chapter was provided by Environment and Climate Change Canada.

References

Acreman MC, Dunbar MJ (2004) Defining environmental river flow requirements—A review. Hydrol Earth Syst Sci 8:861–876. https://doi.org/10.5194/hess-8-861-2004

Acreman MC, Ferguson AJD (2010) Environmental flows and the European water framework directive. Freshw Biol 55:32–48. https://doi.org/10.1111/j.1365-2427.2009.02181.x

ADEC (2010) Alaska Department of Environmental Conservation, Water Quality Standards, Assessment and Restoration Program. https://dec.alaska.gov/water/water-quality/map/

AKOATS (2017) Alaska Online Aquatic Temperature Site, Alaska Center for Conservation Science. University of Alaska Anchorage. https://accs.uaa.alaska.edu/aquatic-ecology/akoats/

Alfredsen K (2017) An assessment of ice effects on indices for hydrological alteration in flow regimes. Water 9:914. https://doi.org/10.3390/w9120914

Alfredsen K, Harby A, Linnansaari T, Ugedal O (2012) Development of an inflow-controlled environmental flow regime for a Norwegian river. River Res Appl 28:731–739. https://doi.org/10.1002/rra.1550

Altenau EH, Pavelsky TM, Moller D, Lion C, Pitcher LH, Allen GH, Bates PD, Calmant S, Durand M, Smith LC (2017) AirSWOT measurements of river water surface elevation and slope: Tanana River, AK. Geophys Res Lett 44:181–189. https://doi.org/10.1002/2016GL071577

AMAP (2012) Arctic climate issues 2011: Changes in Arctic Snow, water, ice and permafrost. SWIPA 2011 overview report. Arctic Monitoring and Assessment Programme (AMAP), Oslo, Sweden

Anderson KE, Paul AJ, McCauley E, Jackson LJ, Post JR, Nisbet RM (2006) Instream flow needs in streams and rivers: the importance of understanding ecological dynamics. Front Ecol Environ 4:309–318. https://doi.org/10.1890/1540-9295

Andreadis KA, Storck P, Lettenmaier DP (2009) Modeling snow accumulation and ablation processes in forested environments. Water Resour Res 45:W05429. https://doi.org/10.1029/2008WR007042

Annear T, Lobb D, Coomer C, Woythal M, Hendry C, Estes C, Williams K (2009) International instream flow program initiative: a status report of state and provincial fish and wildlife agency instream flow activities and strategies for the future. Instream Flow Council, Cheyenne, Wyoming, USA

Armanini DG, Horrigan N, Monk WA, Peters DL, Baird DJ (2011) Development of a benthic macroinvertebrate flow sensitivity index for Canadian rivers. River Res Appl 27:723–737. https://doi.org/10.1002/rra.1389

Armanini DG, Monk WA, Tenenbaum DE, Peters DL, Baird DJ (2012) Influence of runoff regime type on a macroinvertebrate-based flow index in rivers of British Columbia (Canada). Ecohydrology 5:414–423. https://doi.org/10.1002/eco.234

Arthington AH (1998) Comparative evaluation of environmental flow assessment techniques: review of holistic methodologies. Land and Water Resources Research and Development Corporation (LWRRDC), Canberra, Australia

Arthington AH, Bunn SE, Pusey BJ, Blühdorn DR, King JM, Day JA, Tharme RE, O'Keeffe JH (1992) Development of an holistic approach for assessing environmental fl ow requirements of riverine ecosystems. In: Pigram JJ, Hooper BP (eds) Proceeding of an international seminar and workshop on water allocation for the environment. The Center for Water Policy Research. University of New England, Armidale, Australia, pp 69–76

Arthington AH, Tharmes RE, Brizga SO, Pusey BJ, Kennard MJ (2004) Environmental flow assessment with emphasis on holistic methodologies. In: Welcomme RL, Petr T (eds) Proceeding of the second international symposium on the management of large rovers for fisheries. Food and Agriculture Organization of the United Nations & The Mekong River Commission, Phnom Penh, Kingdom of Cambodia, pp 37–56

Arthington AH, Bunn SE, Poff NL, Naiman RJ (2006) The challenge of providing environmental flow rules to Sustain river ecosystems. Ecol Appl 16:1311–1318. https://doi.org/10.1890/1051-0761

Arthington AH, Bhaduri A, Bunn SE, Jackson SE, Tharme RE, Tickner D, Young B, Acreman M, Baker N, Capon S, Horne AC, Kendy E, McClain ME, Poff NL, Richter BD, Ward S (2018) The Brisbane declaration and global action agenda on environmental flows. Front Environ Sci 6. https://doi.org/10.3389/fenvs.2018.00045

Ashton GD (1986) River and lake ice engineering. Water Resources Publication

Azcárate J, Balfors B, Bring A, Destouni G (2013) Strategic environmental assessment and monitoring: Arctic key gaps and bridging pathways. Environ Res Lett 8:044033. https://doi.org/10.1088/1748-9326/8/4/044033

Bastmeijer K, Koivurova T (2008) Theory and practice of transboundary environmental impact assessment. Martinus Nijhoff Publishers, Boston, Massachusetts, USA

BC (2016) British Columbia water sustainability act. https://www2.gov.bc.ca/gov/content/environment/air-land-water/water/laws-rules/water-sustainability-act

Beltaos S (1995) River ice jams. Water Resources Publication, Littleton, Colorado, USA

Beltaos S, Ismail S, Burrell BC (2003) Midwinter breakup and jamming on the upper Saint John River: a case study. Can J Civil Engin 30:77–88. https://doi.org/10.1139/l02-062

Beltaos S, Prowse T, Bonsal B, MacKay R, Romolo L, Pietroniro A, Toth B (2006) Climatic effects on ice-jam flooding of the peace-athabasca delta. Hydrol Process 20:4031–4050. https://doi.org/10.1002/hyp.6418

Belzile L, Bérubé P, Hoang VD, Leclerc M (1997) Méthode écohydrologique de détermination des débits réservés pour la protection des habitats du poisson dans les rivières du Québec. Joint Report INRS-Eau—Groupe conseil Génivar to Québec's Ministry of Environment and to Department of Fisheries and Oceans Canada, Report INRS-Eau 494

Bennett KE, Cannon AJ, Hinzman L (2015) Historical trends and extremes in boreal Alaska river basins. J Hydrol 527:590–607. https://doi.org/10.1016/j.jhydrol.2015.04.065

Bérubé P, Leclerc M, Belzile L (2002) Presentation of an ecohydrological method for determining the conservative flow for fish habitats in Quebec's rivers (Canada). In: Proceedings of the 4th IAHR international symposium on ecohydraulics. Capetown, South Africa, p 23

Biancamaria S, Lettenmaier DP, Pavelsky TM (2016) The SWOT mission and its capabilities for land hydrology. In: Cazenave A, Champollion N, Benveniste J, Chen J (eds) Remote sensing and water resources. Springer International Publishing, Cham, Switzerland, pp 117–147

Bickman JW, Carr SS, Hanks BG, Burton DW, Gallaway BJ (1989) Genetic analysis of population variation in the arctic cisco (Coregonus autumnalis) using electrophoretic, flow cytometric, and mito-chondrial DNA restriction analyses. Biological Papers of the University of Alaska 24

Blackfurn J, Steffler PM (2003) River2D: two-dimensional depth averaged model of river hydrodynamics and fish habitat. University of Alberta, Edmonton, Alberta, Canada

Boudreau P, Leclerc M, Secretan Y (2004) Centrale eastmain-1-a et dérivation rupert Rapport sectoriel. Simulation des habitats de reproduction piscicole de la riviere rupert avec hydrosim/modeleur. Report to Hydro-Québec and to the Société d'Énergie de la Baie James prepared by Institut National de Recherche Scientifique. Rapport INRS-ETE #R-732. Québec, Québec, Canada

Boulton AJ (2003) Parallels and contrasts in the effects of drought on stream macroinvertebrate assemblages. Freshw Biol 48:1173–1185. https://doi.org/10.1046/j.1365-2427.2003.01084.x

Bovee KD (1982) A guide to stream habitat analysis using the instream flow incremental methodology. Instream Flow Information Paper 12. United States Fish and Wildlife Service, Fort Collins, Colorado, USA

Bovee KD, Lamb BL, Bartholow JM, Stalnaker CB, Taylor J, Henriksen J (1998) Analysis using the instream flow incremental methodology. United States Geological Survey (USGS)

Box JE, Colgan WT, Christensen TR, Schmidt NM, Lund M, Parmentier F-JW, Brown R, Bhatt US, Euskirchen ES, Romanovsky VE, Walsh JE, Overland JE, Wang M, Corell RW, Meier WN, Wouters B, Mernild S, Ard JM, Pawlak J, Olsen MS (2019) Key indicators of Arctic climate change: 1971–2017. Environm Res Lett 14:045010. https://doi.org/10.1088/1748-9326/aafc1b

Bradford MJ, Heinonen JS (2008) Low flows, instream flow needs and fish ecology in small streams. Can Water Resour J 33:165–180. https://doi.org/10.4296/cwrj3302165

Bring A, Fedorova I, Dibike Y, Hinzman L, Mård J, Mernild SH, Prowse T, Semenova O, Stuefer SL, Woo M-K (2016) Arctic terrestrial hydrology: a synthesis of processes, regional effects, and research challenges. J Geophys Res: Biogeosci 121:621–649. https://doi.org/10.1002/2015JG003131

Brown C, King J (2000) Environmental flow assessments for rivers. A summary of the DRIFT process. Southern Waters Information Rep. 01/00. Southern Waters, Cape Town, South Africa

Brown RS, Stanislawski SS, Mackay WC (1994) Effects of frazil ice on fish. In: Prowse TD (ed) Proceedings of the workshop on environmental aspects of river ice. National Hydrology Research Institute, Saskatoon, Saskatchewan, Canada, pp 261–278

Burn CR (1993) Stage-discharge relations in the Mackenzie Delta during winter and development of intrusive ice in lake-bottom sediments. In: Proceedings of the 6th international permafrost conference. University of Technology Press, Beijing. Wushan Guangzhou, South China, pp 60–65

Burn DH, Whitfield PH, Sharif M (2016) Identification of changes in floods and flood regimes in Canada using a peaks over threshold approach. Hydrol Process 30:3303–3314. https://doi.org/10.1002/hyp.10861

Bush E, Gillett N, Bonsal B, Cohen S, Derksen C, Flato G, Greenan BJW, Sherperd M, Zhang X (2019) Executive summary. In: Canada's climate change report. Environment and Climate Change Canada, Ottawa, Ontario, Canada

Buttle JM, Boon S, Peters DL, Spence C, Meerveld HJ (Ilja) van Whitfield PH (2012) An overview of temporary stream hydrology in Canada. Can Water Resour J 37:279–310. https://doi.org/10.4296/cwrj2011-903

Buttle JM, Allen DM, Caissie D, Davison B, Hayashi M, Peters DL, Pomeroy JW, Simonovic S, St-Hilaire A, Whitfield PH (2016) Flood processes in Canada: regional and special aspects. Can Water Resour J 41:7–30. https://doi.org/10.1080/07011784.2015.1131629

CABIN (2019) Canadian aquatic biomonitoring network. https://www.canada.ca/en/environment-climate-change/services/canadian-aquatic-biomonitoring-network.html

Calkins DJ (1989) Winter habitats of Atlantic salmon, brook trout, brown trout and rainbow trout. CRREL Special Rep. 89–34, US Army Cold Regions Research and Engineering Laboratory, Hanover, New Hampshire, USA

CBMP (2019) Circumpolar biodiversity monitoring program—Freshwater. https://www.caff.is/freshwater

Chambers PA, Scrimgeour GJ, Pietroniro A (1997) Winter oxygen conditions in ice-covered rivers: the impact of pulp mill and municipal effluents. Can J Fish Aquat Sci 54:2796–2806. https://doi.org/10.1139/f97-188

Clipperton GK, Koning CW, Locke A, Mahoney JM, Quazi B (2003) Instream flow needs determinations for the South Saskatchewan River Basin, Alberta, Canada. Alberta Environment and Sustainable Resource Development, Government of Alberta, Edmonton, Alberta, Canada

Cott PA, Monita DMA, Majewski AR, Hanna BW, Bourassa KJ (2005) Application of the NWT winter water withdrawal protocol with bathymetric profiles of select small lakes in the Mackenzie delta region. Canadian manuscript report fisheries aquatic science, vol 2731, Fisheries and Oceans Canada

Coulibaly P, Samuel J, Pietroniro A, Harvey D (2013) Evaluation of Canadian national hydrometric network density based on WMO 2008 standards. Can Water Resour J 38:159–167. https://doi.org/10.1080/07011784.2013.787181

CPC (2015) State of environmental monitoring in Northern Canada. Canadian Polar Commission (CPC), Ottawa, Ontario, Canada

Culp J, Lento J, Goedkoop W, Power M, Rautio M, Christoffersen K, Guðbergsson G, Lau D, Liljaniemi P, Sandøy S, Svoboda M (2012) Developing a circumpolar monitoring framework for Arctic freshwater biodiversity. Biodiversity 13:215–227. https://doi.org/10.1080/14888386.2012.717526

Cunjak RA (1996) Winter habitat of selected stream fishes and potential impacts from land-use activity. Can J Fish Aquat Sci 53:267–282. https://doi.org/10.1139/f95-275

Cunjak RA, Randall RG (1993) In-stream movements of young Atlantic salmon (Salmo salar) during winter and early spring. In: Gibson RJ, Cutting RE (eds) Production of juvenile Atlantic salmon, Salmo salar, in natural waters. Special Publication of the Can J Fish Aquat Sci, Ottawa, Ontario, Canada, pp 43–51

Cunjak RA, Prowse TD, Parrish DL (1998) Atlantic salmon (Salmo salar) in winter: "the season of parr discontent"? Can J Fish Aquat Sci 55:161–180. https://doi.org/10.1139/d98-008

Dare MR, Hubert WA, Gerow KG (2002) Changes in habitat availability and habitat use and movements by two trout species in response to declining discharge in a regulated river during winter. North Am J Fish Manag 22:917–928. https://doi.org/10.1577/1548-8675

DFO (2010) Department of fisheries and oceans protocol for winter water withdrawal from ice-covered waterbodies in the Northwest Territories and Nunavut. Department of Fisheries and Oceans

DFO (2013) Framework for assessing the ecological flow requirements to support fisheries in Canada. Canadian Science Advisory Secretariat Science Advisory Report 2013/017 Department of Fisheries and Oceans

DFO (2019) Introducing Canada's modernized fisheries act. https://www.dfo-mpo.gc.ca/campaign-campagne/fisheries-act-loi-sur-les-peches/introduction-eng.html

DNR (1985) State of Alaska instream flow handbook: a guide to reserving water for instream use. Alaska Department of Natural Resources (DNR), Division of Land and Water Management, Water Management Section, Anchorage, Alaska, USA

Dunbar MJ, Acreman MC (2001) Applied hydro-ecological science for the twenty first century. In: Acreman MC (ed) Hydro-ecology: linking hydrology and aquatic ecology. IAHS Press, Centre for Ecology and Hydrology, Wallingford, United Kingdom, pp 1–17

Dunbar MJ, Pedersen ML, Cadman D, Extence C, Waddingham J, Chadd R, Larsen SE (2010) River discharge and local-scale physical habitat influence macroinvertebrate LIFE scores. Freshw Biol 55:226–242. https://doi.org/10.1111/j.1365-2427.2009.02306.x

ECCC (2018) HYDAT water survey data products. https://www.canada.ca/en/environment-climate-change/services/water-overview/quantity/monitoring/survey/data-products-services.html

Emmerton CA, Lesack LFW, Marsh P (2007) Lake abundance, potential water storage, and habitat distribution in the Mackenzie River Delta, western Canadian Arctic. Water Resour Res 43. https://doi.org/10.1029/2006wr005139

EUWFD (2018) European Union water framework directive. http://ec.europa.eu/environment/water/water-framework/info/intro_en.htm

Forbes AC, Lamoureux SF (2005) Climatic controls on streamflow and suspended Sediment transport in three large middle Arctic catchments, Boothia Peninsula, Nunavut, Canada. Arct Antarct Alp Res 37:304–315. https://doi.org/10.1657/1523-0430(2005)037%5b0304:ccosas%5d2.0.co;2

FPQ (1999) Politique de débits réservés écologiques pour la protection du poisson et de ses habitats. Direction de la faune et des habitats, Faune et Parcs Québec (FPQ), Québec City, Québec, Canada

Gautier DL, Bird KJ, Charpentier RR, Grantz A, Houseknecht DW, Klett TR, Moore TE, Pitman JK, Schenk CJ, Schuenemeyer JH, Sørensen K, Tennyson ME, Valin ZC, Wandrey CJ (2011) Chapter 9 Oil and gas resource potential north of the Arctic Circle. Geol Soc Lond Mem 35:151–161. https://doi.org/10.1144/m35.9

Gholizadeh MH, Melesse AM, Reddi L (2016) A comprehensive review on water quality parameters estimation using remote sensing techniques. Sensors (Basel) 16. https://doi.org/10.3390/s16081298

Gibson JJ, Prowse TD, Peters DL (2006) Hydroclimatic controls on water balance and water level variability in Great Slave Lake. Hydrol Process 20:4155–4172. https://doi.org/10.1002/hyp.6424

GoA (2014) Surface water quantity management framework for the lower Athabasca River. Alberta Environment and Sustainable Resource Development, Government of Alberta, Edmonton, Alberta, Canada

Goater L, Koning CW, Locke A, Mahoney JM, Paul AJ (2007) Aquatic environment impact ratings: a method for evaluating SSRB flow scenarios—Red Deer River case study. Alberta Environment and Sustainable Resource Development, Government of Alberta, Alberta, Canada

Golder Associates Ltd (2005) Technical review of current methods for instream flow needs and related science gaps: hydrology and hydraulic models for the major agricultural regions of Canada. Environment Canada, Gatineau, Quebec, Canada

Goulding HL, Prowse TD, Beltaos S (2009) Spatial and temporal patterns of break-up and ice-jam flooding in the Mackenzie Delta, NWT. Hydrol Process 23(2):654–2670. https://doi.org/10.1002/hyp.7251

Gray DM, Prowse TD (1993) Snow and floating ice, Chapter 7. In: Maidment D (ed) Handbook of hydrology. McGraw-Hill, New York, USA, pp 7.1–7.58

Hamilton S (2008) Sources of uncertainty in Canadian low flow hydrometric data. Can Water Resour J 33:125–136. https://doi.org/10.4296/cwrj3302125

Hatfield T, Lewis A, Ohlson D, Bradford M (2003) Development of instream flow thresholds as guidelines for reviewing proposed water uses. Victoria, British Columbia, Canada

Heim KC, Wipfli MS, Whitman MS, Arp CD, Adams J, Falke JA (2016) Seasonal cues of Arctic grayling movement in a small Arctic stream: the importance of surface water connectivity. Environm Biol Fish 99:49–65. https://doi.org/10.1007/s10641-015-0453-x

Hellsten S, Koljonen S, Vehanen T, Olin S, Aronsuu K, Jormola J (2017) Applying environmental flow in Finland. In: Nordic conference 2017: towards a better implementation of the WFD from a Nordic perspective. Scandic Lerkendal, Trondheim, Findland

Hicks F (2009) An overview of river ice problems: CRIPE07 guest editorial. Cold Reg Sci Technol 55:175–185. https://doi.org/10.1016/j.coldregions.2008.09.006

Hildén M, Furman ER (2001) Assessment across borders stumbling blocks and options in the practical implementation of the Espoo convention. Environ Impact Assess Rev 21:537–551

Hirabayashi Y, Mahendran R, Koirala S, Konoshima L, Yamazaki D, Watanabe S, Kim H, Kanae S (2013) Global flood risk under climate change. Nat Clim Change 3:816–821

Hynes HBN (1975) The stream and its valley. Verhandlungen des Internationalen Verein Limnologie 19:1–15

Instanes A, Kokorev V, Janowicz R, Bruland O, Sand K, Prowse T (2016) Changes to freshwater systems affecting Arctic infrastructure and natural resources. J Geophys Res: Biogeosci 121:567–585. https://doi.org/10.1002/2015JG003125

Jowett IG (1997) Instream flow methods: a comparison of approaches. Regul Rivers: Res Manag 13:115–127. https://doi.org/10.1002/(SICI)1099-1646(199703)13:2%3c115:AID-RRR440%3e3.0.CO;2-6

Jowett IG, Duncan MJ (1990) Flow variability in New Zealand rivers and its relationship to in-stream habitat and biota. NZ J Mar Freshwat Res 24:305–317. https://doi.org/10.1080/00288330.1990.9516427

Junk W, Bayley PB, Sparks RE (1989) The flood pulse concept in river-floodplain systems. Can Spec Publ J Fish Aquat Sci 106:110–127

Kane DL, Hinzman LD, Gieck RE, McNamara JP, Youcha EK, Oatley JA (2008) Contrasting extreme runoff events in areas of continuous permafrost, Arctic Alaska. Hydrol Res 39:287–298. https://doi.org/10.2166/nh.2008.005

Karim K, Gubbels ME, Goulter IC (1995) Review of determination of instream flow requirements with special application to Australia. Water Resour Bull 31:1063–1077

Karr JR (1999) Defining and measuring river health. Freshw Biol 41:221–234. https://doi.org/10.1046/j.1365-2427.1999.00427.x

Kellerhals R, Church M (1980) Comment on 'Effects of channel enlargement by river ice processes on bankfull discharge in Alberta, Canada' by D. G. Smith. Water Resour Res 16:1131–1134. https://doi.org/10.1029/WR016i006p01131

Kendy E, Sanderson JD, Olden JD, Aspe CD, DePhilip MM, Haney JA, Zimmerman JKH (2009) Application of the ecological limits of hydrologic alteration (ELOHA) in the United States. In: Proceedings from the international conference on implementing environmental water allocations. Port Elizabeth, South Africa

King J, Louw D (1998) Instream flow assessments for regulated rivers in South Africa using the building block methodology. Aquat Ecosyst Health Manag 1:109–124. https://doi.org/10.1016/S1463-4988(98)00018-9

King J, Brown C, Sabet H (2003) A scenario-based holistic approach to environmental flow assessments for rivers. River Res Appl 19:619–639

Klein J (2016) Instream flow protection in Alaska 2015. Special publication 16–09, Alaska Department of Fish and Game, Anchorage, Alaska, USA

Koivurova T (2005) Environmental protection in the Arctic and Antarctic: can the polar regimes learn from each other? Int J Leg Inform 33:204–218

Komadina-Douthwright SM, Caissie D, Cunjak RA (1997) Winter movement of radio-tagged Atlantic salmon (Salmo salar) kelts in relation to frazil ice in pools of the Miramichi River. In: Canadian technical report of fisheries and aquatic sciences, vol 2161, pp 1–66

Lake PS (2000) Disturbance, patchiness, and diversity in streams. J N Am Benthol Soc 19:573–592. https://doi.org/10.2307/1468118

Lake PS (2003) Ecological effects of perturbation by drought in flowing waters. Freshw Biol 48:1161–1172. https://doi.org/10.1046/j.1365-2427.2003.01086.x

Lamoureux SF, Jowett IG (2005) Generalized instream habitat models. Can J Fish Aquat Sci 62:7–14

Larsen JN, Anisimov OA, Constable A, Hollowed AB, Maynard N, Prestrud P, Prowse TD, Stone JMR (2014) Polar regions. In: Barros VR, Field CB, Dokken DJ, Mastrandrea MD, Mach KJ, Bilir TE, Chatterjee M, Ebi KL, Estrada YO, Genova RC, Girma B, Kissel ES, Levy AN, MacCracken S, Mastrandrea PR, White LL (eds) Climate change 2014: impacts, adaptation, and vulnerability. Part B: regional aspects. Contribution of Working Group II to the fifth assessment report of the intergovernmental panel on climate change. Cambridge University Press, Cambridge, United Kingdom and New York, USA, pp 1567–1612

Laudon H, Spence C, Buttle J, Carey SK, McDonnell JJ, McNamara JP, Soulsby C, Tetzlaff D (2017) Save northern high-latitude catchments. Nat Geosci 10:324–325. https://doi.org/10.1038/ngeo2947

Leclerc M, Saint-Hilaire A, Bechara J (2003) State-of-the-art and perspectives of habitat modelling for determining conservation flows. Can Water Resour J 28:135–151. https://doi.org/10.4296/cwrj2802135

Lento J, Goedkoop W, Culp J, Christoffersen K, Fefilova E, Guðbergsson G, Liljaniemi P, Ólafsson JS, Sandøy S, Zimmerman C, Christensen T, Chambers P, Heino J, Hellsten S, Kahlert M, Keck F, Laske S, Lau DCP, Lavoie I, Levenstein B, Mariash H, Rühland K, Saulnier-Talbot E, Schartau AK, Svenning M (2019) State of Arctic freshwater biodiversity report. Conservation of Arctic Flora and Fauna International Secretariat, Akureyri, Iceland

Leopold LB (1994) A view of the river. Harvard University Press, Cambridge, Massachusetts, USA

Lesack LFW, Marsh P (2010) River-to-lake connectivities, water renewal, and aquatic habitat diversity in the Mackenzie River Delta. Water Resour Res 46. https://doi.org/10.1029/2010wr009607

Lewis A, Hatfield T, Chillibeck B, Roberts C (2004) Assessment methods for aquatic habitat and instream flow characteristics in support of applications to dam, divert, or extract water from streams in British Columbia. Report prepared for the British Columbia Ministry of Sustainable Resource Management and the British Columbia Ministry of Water, Land and Air Protection, British Columbia, Canada

Linnansaari T, Alfredsen K, Stickler M, Arnekleiv JV, Harby A, Cunjak RA (2009) Does ice matter? Site fidelity and movements by Atlantic salmon (Salmo salar L.) parr during winter in a substrate enhanced river reach. River Res Appl 25:773–787. https://doi.org/10.1002/rra.1190

Linnansaari T, Monk WA, Baird DJ, Curry RA (2013) Review of approaches and methods to assess environmental flows across Canada and internationally. DFO Canadian science advisory secretariat research document 2012/039. Department of Fisheries and Oceans, Ottawa, Ontario, Canada

Locke A, Paul AJ (2011) A desk-top method for establishing environmental flows in Alberta rivers and streams. Alberta Environment and Sustainable Resource Development, Government of Alberta, Edmonton, Alberta, Canada

Lytle DA, Poff NL (2004) Adaptation to natural flow regimes. Trends Ecol Evol 19:94–100. https://doi.org/10.1016/j.tree.2003.10.002

Mallory ML, Gilchrist HG, Janssen M, Major HL, Merkel F, Provencher JF, Strøm H (2018) Financial costs of conducting science in the Arctic: examples from seabird research. Arctic Sci 4:624–633. https://doi.org/10.1139/as-2017-0019

Manitoba Government (2008) Manitoba water stewardship annual report 2007–2008. Accessed June 2020 http://www.manitoba.ca

Martin MD, Brown RS, Barton DR, Power G (2001) Abundance of invertebrates in winter seasonal changes and effects of river ice. Can Field Nat 115:68–74

Mathews R, Richter BD (2007) Application of the indicators of hydrologic alteration software in environmental flow setting[1]. JAWRA J Am Water Resour Assoc 43:1400–1413. https://doi.org/10.1111/j.1752-1688.2007.00099.x

McClelland JW, Holmes RM, Peterson BJ, Stieglitz M (2004) Increasing river discharge in the Eurasian Arctic: consideration of dams, permafrost thaw, and fires as potential agents of change. J Geophys Res: Atmos 109. https://doi.org/10.1029/2004jd004583

Mekis É, Vincent LA (2011) An overview of the second generation adjusted daily precipitation dataset for trend analysis in Canada. Atmos Ocean 49:163–177. https://doi.org/10.1080/07055900.2011.583910

Milly PCD, Betancourt J, Falkenmark M, Hirsch RM, Kundzewicz ZW, Lettenmaier DP, Stouffer RJ (2008) Stationarity is dead: whither water management? Science 319:573–574. https://doi.org/10.1126/science.1151915

Milly PCD, Betancourt J, Falkenmark M, Hirsch RM, Kundzewicz ZW, Lettenmaier DP, Stouffer RJ, Dettinger MD, Krysanova V (2015) On critiques of "Stationarity is Dead: Whither Water Management?". Water Resour Res 51:7785–7789. https://doi.org/10.1002/2015WR017408

Mitro MG, Zale AV, Rich BA (2003) The relation between age-0 rainbow trout (oncorhynchus mykiss) abundance and winter discharge in a regulated river. Can J Fish Aquat Sci 60:135–139

Monk WA, Wood PJ, Hannah DM, Wilson DA, Extence CA, Chadd RP (2006) Flow variability and macroinvertebrate community response within riverine systems. River Res Appl 22:595–615. https://doi.org/10.1002/rra.933

Monk WA, Wood PJ, Hannah DM, Wilson DA (2008) Macroinvertebrate community response to inter-annual and regional river flow regime dynamics. River Res Appl 24:988–1001. https://doi.org/10.1002/rra.1120

Monk WA, Peters DL, Curry RA, Baird DJ (2011) Quantifying trends in indicator hydroecological variables for regime-based groups of Canadian rivers. Hydrol Process 25:3086–3100. https://doi.org/10.1002/hyp.8137

Monk WA, Peters DL, Baird DJ (2012) Assessment of ecologically relevant hydrological variables influencing a cold-region river and its delta: the Athabasca River and the Peace-Athabasca Delta, northwestern Canada. Hydrol Process 26:1827–1839. https://doi.org/10.1002/hyp.9307

Monk WA, Compson ZG, Armanini DG, Chaumel I (2017) Proposed holistic environmental flows framework for the Saint John River with a focus on operations at the Mactaquac Generating Station. Mactaquac Aquatic Ecosystem Report Series 2017-035, Fredericton, New Brunswick, Canada

Moore RD, Hamilton AS, Scibek J (2002) Winter streamflow variability, Yukon Territory, Canada. Hydrol Process 16:763–778. https://doi.org/10.1002/hyp.372

NSIDC (2018) National snow and ice data center. https://nsidc.org/cryosphere/sotc/permafrost.html

Ohlson D, Long G, Hatfield T (2010) Phase 2 framework committee report of the Lower Athabasca River. Report prepared by Compass Resource Management and Solander Ecological Research, Edmonton, Alberta, Canada

Park H, Dibike Y, Su F, Wu X (2021) Cold Region Hydrologic Models. In: Yang D, Kane DL (eds) Arctic hydrology, permafrost, and ecosystem: linkages and interactions, accepted in this book

Paschke NW, Coleman HW (1986) Forecasting the effects on river ice due to the proposed Susitna hydroelectric project. In: Proceedings of the cold regions hydrology symposium. American Water Resources Association, Bethesda, Madison, USA, pp 557–563

Peters DL, Buttle JM (2010) The effects of flow regulation and climatic variability on obstructed drainage and reverse flow contribution in a Northern river–lake–Delta complex, Mackenzie basin headwaters. River Res Appl 26:1065–1089. https://doi.org/10.1002/rra.1314

Peters DL, Prowse TD (2001) Regulation effects on the lower Peace River, Canada. Hydrol Process 15:3181–3194. https://doi.org/10.1002/hyp.321

Peters DL, Prowse TD, Pietroniro A, Leconte R (2006) Flood hydrology of the Peace-Athabasca Delta, northern Canada. Hydrol Process 20:4073–4096. https://doi.org/10.1002/hyp.6420

Peters DL, Baird DJ, Monk WA, Armanini DG (2012) Establishing standards and assessment criteria for ecological instream flow needs in agricultural regions of Canada. J Environ Qual 41:41–51. https://doi.org/10.2134/jeq2011.0094

Peters DL, Monk WA, Baird DJ (2014) Cold-regions Hydrological Indicators of Change (CHIC) for ecological flow needs assessment. Hydrol Sci J 59:502–516. https://doi.org/10.1080/02626667.2013.835489

Peters DL, Caissie D, Monk WA, Rood SB, St-Hilaire A (2016) An ecological perspective on floods in Canada. Can Water Resour J 41:288–306. https://doi.org/10.1080/07011784.2015.1070694

Pietroniro A, Peters DL, Yang D, Fiset J-M, Saint-Jean R, Fortin V, Leconte R, Bergeron J, Siles G, Trudel M, Garnaud C, Matte P, Smith LC, Gleason CJ, Pavelsky TM (2019) Canada's contributions to the SWOT mission—Terrestrial hydrology (C-SWOT-TH). Can J Remote Sens, in press

Poff NL (2002) Ecological response to and management of increased flooding caused by climate change. Philos Trans Ser A, Math Phys Eng Sci 360:1497–1510. https://doi.org/10.1098/rsta.2002.1012

Poff NL, Allan JD, Bain MB, Karr JR, Prestegaard KL, Richter BD, Sparks RE, Stromberg JC (1997) The natural flow regime. Bioscience 47:769–784. https://doi.org/10.2307/1313099

Poff NL, Richter BD, Arthington AH, Bunn SE, Naiman RJ, Kendy E, Acreman M, Apse C, Bledsoe BP, Freeman MC, Henriksen J, Jacobson RB, Kennen JG, Merritt DM, O'Keeffe JH, Olden JD, Rogers K, Tharme RE, Warner A (2010) The ecological limits of hydrologic alteration (ELOHA): a new framework for developing regional environmental flow standards. Freshw Biol 55:147–170. https://doi.org/10.1111/j.1365-2427.2009.02204.x

Pohl S, Marsh P, Onclin C, Russell M (2009) The summer hydrology of a small upland tundra thaw lake: implications to lake drainage. Hydrol Process 23:2536–2546. https://doi.org/10.1002/hyp.7238

Polzin ML, Rood SB (2006) Effective disturbance: Seedling safe sites and patch recruitment of riparian cottonwoods after a major flood of a mountain river. Wetlands 26:965–980. https://doi.org/10.1672/0277-5212(2006)26%5b965:edsssa%5d2.0.co;2

Pomeroy JW, Gray DM, Brown T, Hedstrom NR, Quinton WL, Granger RJ, Carey SK (2007) The cold regions hydrological model: a platform for basing process representation and model structure on physical evidence. Hydrol Process 21:2650–2667. https://doi.org/10.1002/hyp.6787

Power G, Cunjak RA, Flannagan J, Katopodis C (1993) Biological effects of river ice. In: Prowse TD, Gridley NC (eds). Environmental aspects of river ice. task force on environmental aspects of river ice. National Hydrology Research Institute, Saskatoon, Saskatchewan, Canada

Prowse TD (2001a) River-ice ecology.I: hydrologic, geomorphic, and water-quality aspects. J Cold Reg Eng 15:1–16. https://doi.org/10.1061/(ASCE)0887-381X(2001)15:1(1)

Prowse TD (2001b) River-ice ecology. II: biological aspects. J Cold Reg Eng 15:17–33. https://doi.org/10.1061/(ASCE)0887-381X(2001)15:1(17)

Prowse TD, Carter T (2002) Significance of ice-induced storage to spring runoff: a case study of the Mackenzie River. Hydrol Process 16:779–788. https://doi.org/10.1002/hyp.371

Prowse TD, Culp JM (2003) Ice breakup: a neglected factor in river ecology. Can J Civil Eng 30:128–144. https://doi.org/10.1139/l02-040

Prowse TD, Gridley NC (eds) (1993) Environmental aspects of river ice. In: Task force on environmental aspects of river ice. National Hydrology Research Institute, Saskatoon, Saskatchewan, Canada

Prowse TD, Wrona FJ, Power G (2004) Dams, reservoirs and flow regulation. In: Threats to water availability in Canada. NWRI Scientific Assessment Report Series No. 3 and ACSD Science Assessment Series No. 1., Environment Canada, Burlington, Ontario, Canada, pp 9–18

Prowse T, Alfredsen K, Beltaos S, Bonsal BR, Bowden WB, Duguay CR, Korhola A, McNamara J, Vincent WF, Vuglinsky V, Anthony KMW, Weyhenmeyer GA (2011) Effects of changes in Arctic lake and river ice. Ambio 40:63–74. https://doi.org/10.1007/s13280-011-0217-6

Pyrce R (2004) Hydrological low flow indices and their uses. Trent University, Watershed Science Centre, Peterborough, Ontario, Canada

Rawlins MA, Nicolsky DJ, McDonald KC, Romanovsky VE (2013) Simulating soil freeze/thaw dynamics with an improved pan-Arctic water balance model. J Adv Model Earth Syst 5:659–675. https://doi.org/10.1002/jame.20045

Reist JD, Wrona FJ, Prowse TD, Power M, Dempson JB, Beamish RJ, King JR, Carmichael TJ, Sawatzky CD (2006) General effects of climate change on Arctic fishes and fish populations. Ambio 35:370–380. https://doi.org/10.1579/0044-7447(2006)35%5b370:geocco%5d2.0.co;2

Renöfält BM, Jansson R, Nilsson C (2010) Effects of hydropower generation and opportunities for environmental flow management in Swedish riverine ecosystems. Freshw Biol 55:49–67. https://doi.org/10.1111/j.1365-2427.2009.02241.x

Richter BD, Baumgartner JV, Powell J, Braun DP (1996) A method for assessing hydrologic alteration within ecosystems. Conserv Biol 10:1163–1174. https://doi.org/10.1046/j.1523-1739.1996.10041163.x

Richter B, Baumgartner J, Wigington R, Braun D (1997) How much water does a river need? Freshw Biol 37:231–249. https://doi.org/10.1046/j.1365-2427.1997.00153.x

Richter BD, Davis MM, Apse C, Konrad C (2012) A presumptive standard for environmental flow prediction. River Res Appl 28:1312–1321. https://doi.org/10.1002/rra.1511

Rollings KW (2011) Hydrological low flow indices for the protection of fish and fish habitat in Newfoundland and Labrador. In: 64th Canadian water resources association national conference. St. John's Newfound Land, Canada, p 11

SEO (2008) Swedish environmental objectives—No time to los. Swedish Environmental Objectives Council, Sweden

SEPA (2018) The Swedish environmental code. Swedish Environmental Protection Agency. http://www.swedishepa.se/Guidance/Laws-and-regulations/The-Swedish-Environmental-Code/

Serreze MC, Barry RG (2011) Processes and impacts of Arctic amplification: a research synthesis. Glob Planet Change 77:85–96. https://doi.org/10.1016/j.gloplacha.2011.03.004

Shevnina E, Kourzeneva E, Kovalenko V, Vihma T (2017) Assessment of extreme flood events in a changing climate for a long-term planning of socio-economic infrastructure in the Russian Arctic. Hydrol Earth Syst Sci 21:2559–2578. https://doi.org/10.5194/hess-21-2559-2017

Shkolnik I, Pavlova T, Efimov S, Zhuravlev S (2018) Future changes in peak river flows across northern Eurasia as inferred from an ensemble of regional climate projections under the IPCC RCP8.5 scenario. Clim Dyn 50:215–230. https://doi.org/10.1007/s00382-017-3600-6

Shrestha RR, Peters DL, Schnorbus MA (2014) Evaluating the ability of a hydrologic model to replicate hydro-ecologically relevant indicators. Hydrol Process 28:4294–4310. https://doi.org/10.1002/hyp.9997

Shrestha RR, Cannon AJ, Schnorbus MA, Alford H (2019) Climatic controls on future hydrologic changes in the subarctic River basin in Canada. J Hydrometeorol (in press). https://doi.org/10.1175/jhm-d-18-0262.1

Shrestha RR, Bennett KE, Peters DL, Yang D (2021) Hydrological Extremes in Artic Rivers and Regions. In: Yang D, Kane DL (eds) Arctic hydrology, permafrost, and ecosystem: linkages and interactions, accepted in this book

Simpkins DG, Hubert WA (2000) Drifting invertebrates, stomach contents, and body conditions of juvenile rainbow trout from fall through winter in a wyoming tailwater. Trans Am Fish Soc 129:1187–1195. https://doi.org/10.1577/1548-8659(2000)1291187:DISCAB%3e2.0.CO;2

Smakhtin V, Anputhas M (2006) An assessment of environmental flow requirements of Indian river basins. International Water Management Institute (IWMI), Colombo, Sri Lanka

Smith SL, Romanovsky VE, Lewkowicz AG, Burn CR, Allard M, Clow GD, Yoshikawa K, Throop J (2010) Thermal state of permafrost in North America: a contribution to the international polar year. Permafr Periglac Process 21:117–135. https://doi.org/10.1002/ppp.690

Spence C, Burke A (2008) Estimates of Canadian Arctic Archipelago runoff from observed hydrometric data. J Hydrol 362:247–259. https://doi.org/10.1016/j.jhydrol.2008.08.019

Statzner B, Higler B (1986) Stream hydraulics as a major determinant of benthic invertebrate zonation patterns. Freshw Biol 16:127–139. https://doi.org/10.1111/j.1365-2427.1986.tb00954.x

Stickler M, Alfredsen K (2005) Factors controlling anchor ice. In: Anon (ed) Proceedings from the13th workshop on the hydraulics of ice covered rivers. Committee on River Ice Processes and the Environment, Hanover, New Hampshire, USA

Tennant DL (1976) Instream flow regimens for fish, wildlife, recreation and related environmental resources. Fisheries 1:6–10. https://doi.org/10.1577/1548-8446(1976)001%3c0006:IFRFFW%3e2.0.CO;2

Tessman SA (1979) Environmental assessment. Technical Appendix E. In: Reconnaissance elements—Western Dakotas regions of South Dakota study. Water Resources Research Institute, South Dakota State University, Brookings, South Dakota, USA

Tharme RE (2003) A global perspective on environmental flow assessment: emerging trends in the development and application of environmental flow methodologies for rivers. River Res Appl 19:397–441

Tharme RE, King J (1998) Development of the Building Block Methodology for instream flow assessments, and supporting research on the effects of different magnitude flows on riverine ecosystems. Water Research Commission Report No. 576/1/98

Tockner K, Malard F, Ward JV (2000) An extension of the flood pulse concept. Hydrol Process 14:2861–2883. https://doi.org/10.1002/1099-1085(200011/12)14:16/17%3c2861:AID-HYP124%3e3.0.CO;2-F

UNECE (1991) Convention on Environmental Impact Assessment in Transboundary Contexts (the Espoo Convention). United Nations Economic Commission for Europe

USGS (2018) United states geological survey. https://www.usgs.gov/products/data-and-tools/data-and-tools-topics/water

van der Sanden JJ, Geldsetzer T, Short N, Brisco B (2012) Advanced SAR applications for Canada's cryosphere (Freshwater Ice and Permafrost). Natural Resources Canada, Ottawa, Ontario, Canada

van Oldenborgh GJ, Collins M, Arblaster J, Christensen JH, Marotzke J, Power SB, Rummukainen M, Zhou T (2013) Annex I: atlas of global and regional climate projections. In climate change 2013: the physical science basis. In: Stocker TF, Qin D, Plattner G-K, Tignor M, Allen SK, Boschung J, Nauels A, Xia Y, Bex V, Midgley PM (eds) Contribution of Working Group I to the fifth assessment report of the intergovernmental panel on climate change. Cambridge University Press, Cambridge, United Kingdom, pp 1311–1393

Vincent LA, Wang XL, Milewska EJ, Wan H, Yang F, Swail V (2012) A second generation of homogenized Canadian monthly surface air temperature for climate trend analysis. J Geophys Res: Atmos 117. https://doi.org/10.1029/2012jd017859

von de Wall S, de Rham LP, Prowse TD (2009) Open water and ice-induced extreme water levels on Canadian rivers. In: Young KL, Quinton W (eds) Proceedings of the 17th international northern research Basins symposium and workshop. York University, Iqaluit-Pang-nirtung-Kuujjaq, Nunavut, Canada, Toronto, pp 337–347

von de Wall S, de Rham LP, Prowse TD (2010) The river ice break-up season in Canada: Variations in water levels and timing. In: Proceedings of the 67th Eastern Snow conference, pp 5–15

Walsh M, Calkins D (1986) River ice and salmonids. In: Proceedings of the 4th workshop on hydraulics of river ice. US Army Cold Regions Research and Engineering Laboratory, Hanover, New Hampshire, USA, pp D-4.1–D-4.26

Ward JV, Stanford JA (1983) The intermediate disturbance hypothesis: an explanation for biotic diversity in bance hypothesis. In: Fontaine, Bartell, SM (eds) In dynamics of lotic ecosystems. Ann Arbor Science Publishers, Ann Arbor, Michigan, USA, pp 347–356

WBNP (2019) Development of a multi-jurisdiction action plan to protect the World Heritage Values of Wood Buffalo National Park. https://www.pc.gc.ca/en/pn-np/nt/woodbuffalo/info/action

WMO (2008) Guide to hydrological practices. In: Hydrology—From measurement to hydrological information, vol I. World Meteorological Organization, Geneva, Switzerland

Woo M (1986) Permafrost hydrology in North America. Atmos Ocean 24:201–234. https://doi.org/10.1080/07055900.1986.9649248

Woo M, Thorne R (2016) Summer low flow events in the Mackenzie river system. Arctic 69:286–304. https://doi.org/10.14430/arctic4581

Woo M-K, Thorne R, Giguère N (2014) Winter flows in the Mackenzie drainage system. Arctic 67:238–256

Wood PJ, Agnew MD, Petts GE (2000) Flow variations and macroinvertebrate community responses in a small groundwater-dominated stream in south-east England. Hydrol Process 14:3133–3147. https://doi.org/10.1002/1099-1085(200011/12)14:16/17%3c3133:AID-HYP138%3e3.0.CO;2-J

Wrona FJ, Prowse TD, Reist JD, Hobbie JE, Lévesque LMJ, Vincent WF (2006) Climate impacts on arctic freshwater ecosystems and fisheries: background, rationale and approach of the Arctic climate impact assessment (ACIA). Ambio 35:326–329. https://doi.org/10.1579/0044-7447(2006)35%5b326:cioafe%5d2.0.co;2

WSC (2018) Water survey of Canada. https://www.canada.ca/en/environment-climate-change/services/water-overview/quantity/monitoring/survey.html

Yang D, Peterson A (2017) River water temperature in relation to local air temperature in the Mackenzie and Yukon Basins. Arctic 70:47–58. https://doi.org/10.14430/arctic4627

Yang D, Ye B, L. Kane D (2004a) Streamflow changes over Siberian Yenisei River Basin. J Hydrol 296:59–80. https://doi.org/10.1016/j.jhydrol.2004.03.017

Yang D, Ye B, Shiklomanov A (2004b) Discharge characteristics and changes over the Ob river Watershed in Siberia. J Hydrometeorol 5:595–610. https://doi.org/10.1175/1525-7541

Ye B, Yang D, Kane DL (2003) Changes in Lena River streamflow hydrology: human impacts versus natural variations. Water Resour Res 39. https://doi.org/10.1029/2003wr001991

Zhang X, Zweirs FW (2013) Statistical indices for the diagnosing and detecting changes in extremes. In: AghaKouchak A, Easterling E, Hsu K, Schubert S, Sorooshian S (eds) Extremes in a changing climate: detection, analysis and uncertainty. Springer, Dordrecht, pp 1–14

Dr. Daniel L. Peters is a Research Scientist within the Watershed Hydrology & Ecology Research Division of Environment and Climate Change Canada. His role is to investigate the effects of climate variability/change and development (e.g., flow regulation, water abstraction) on the hydrology of river, lake, wetland, and delta systems in Canada. He is also involved in research linking hydrology to aquatic ecology, such as developing rapid assessment tools for environmental flow approaches. He has provided Technical Expertise to the Canadian Environmental Assessment Agency, Parks Canada Agency, and UNESCO WHC/IUCN. He is the Past President of the Canadian Geophysical Union—Hydrology Section, an Associate Editor of the Canadian Water Resources Journal, and has published more than 40 papers in peer-reviewed journals. He holds an Associate Professor (limited term appointment) in the Geography Department at the University of Victoria (BC) where he taught Hydrology for 10 years and supervises Graduate students.

Dr. Donald J. Baird is a Research Scientist at Environment and Climate Change Canada's Water Science and Technology Directorate, and is also a Research Professor at the University of New Brunswick in the Department of Biology, located on the Fredericton campus. He has 30+ years of experience in the area of aquatic ecology, publishing over 150 papers and 4 books. His main research interests focus on ecological risk assessment, and the development of new methods for ecosystem observation, including eDNA approaches. He has served as a science advisor and external reviewer for WHO-Water, Ramsar, UNDP, and WWF-Canada.

Dr. Joseph Culp is a Senior Research Scientist with Environment and Climate Change Canada (ECCC) and a Research Professor at Wilfrid Laurier University. His research investigates the impacts of multiple stressors on aquatic systems including the combined effects of nutrients, sediments and chemical stressors on taxonomic, and trait composition of stream benthos. Currently, he focuses on investigating benthic biodiversity and ecological function of northern and Arctic rivers. He is international co-lead of the Arctic Council's, Circumpolar Biodiversity Monitoring Program, Freshwater Monitoring Group, is a Past President of the Society of Freshwater Science, and regularly serves on national and international review panels.

Dr. Jennifer Lento is a Research Scientist at the Canadian Rivers Institute and Department of Biology at the University of New Brunswick (Fredericton). Her primary research interests are focused on Arctic freshwater ecology, specifically structural and functional community response to environmental drivers in the Arctic. This has included assessment of the biotic response to permafrost thaw slumping in the Northwest Territories, Canada, and latitudinal trends in Arctic freshwater biodiversity. Since 2010, she has acted as the Science Coordinator and alternate Canadian representative for the international Freshwater Steering Group of the Circumpolar Biodiversity Monitoring Program, part of the Conservation of Arctic Flora and Fauna, a working group of the Arctic Council. Through this group, she led the development of a circumpolar freshwater biodiversity database and the recent completion of the first State of Arctic Freshwater Biodiversity Report.

Dr. Wendy A. Monk is a Research Scientist in the Watershed Hydrology and Ecology Research Division with Environment and Climate Change Canada, based at the Canadian Rivers Institute, and also holds a Visiting Research Professor position in the Faculty of Forestry and Environmental Management at the University of New Brunswick (Fredericton). With more than 15 years of interdisciplinary experience, her research focuses on the spatial and temporal integration of hydrology, aquatic ecology, and geospatial analyses within freshwater ecosystems. The primary focus of her research is to develop novel tools by integrating new monitoring and data approaches to isolate and understand the impact of individual stressors within complex multiple stressor environments. Her research and collaborations include the creation of a national hydrological regime classification, extensive analysis of flow-ecology relationships leading to the development of flow stressor-specific diagnostic indices, the first application of a watershed-scale holistic environmental flows framework in Canada, and the integration of new genomics-based approaches for multiple stressor assessments.

Dr. Rajesh R. Shrestha is a Research Scientist at the Watershed Hydrology and Ecology Research Division, Environment and Climate Change Canada, and holds an Adjunct Professor appointment at the University of Victoria. His current research focuses primarily on assessing the impacts of climate variability and change on hydrologic systems, including methods to characterize interactions and uncertainties in hydrologic projections, and nonstationarity of extreme events. He is active in the development and application of snow and hydrologic models, and observation-based and statistically downscaled climate data products.

Yukon River Discharge Response to Seasonal Snow Cover Change

9

Daqing Yang, Yuanyuan Zhao, Richard Armstrong, Mary J. Brodzik, and David Robinson

Abstract

We used remotely sensed Snow Water Equivalent (SWE) and Snow Cover Extent (SCE) data to investigate streamflow response to seasonal snow cover change over the Yukon watershed. We quantified the seasonal cycles and variations of snow cover (both SWE and SCE) and river streamflow, and identified a clear correspondence of river discharge to seasonal snow cover change. We also examined and compared the weekly mean streamflow with the weekly basin SWE and SCE. The results revealed a strong relationship between streamflow and snow cover change during the spring melt season. This relationship provides a practical procedure of using remotely sensed snow cover information for snowmelt runoff estimation over the large northern watersheds.

D. Yang (✉)
Watershed Hydrology and Ecology Division, Environment and Climate Change Canada, Victoria, BC, Canada
e-mail: Daqing.Yang@canada.ca; daqing.yang@gmail.com

Y. Zhao
Department of Mathematics and Statistics, University of Alaska Fairbanks, Fairbanks, AK 99775, USA
e-mail: yuanyuanzhao17@gmail.com

R. Armstrong · M. J. Brodzik
National Snow & Ice Data Center/CIRES, University of Colorado, Boulder, CO 80309-0449, USA
e-mail: rlx@nsidc.org

M. J. Brodzik
e-mail: brodzik@nsidc.org

D. Robinson
Department of Geography & NJ Agricultural Experiment Station, Rutgers University, Piscataway, NJ 08854-8054, USA
e-mail: david.robinson@rutgers.edu

D. Yang and D. L. Kane (eds.), *Arctic Hydrology, Permafrost and Ecosystems*,
https://doi.org/10.1007/978-3-030-50930-9_9

Analyses of extreme (high/low) streamflow cases (years) and basin snow cover conditions indicate an association of high (low) flood peak with high (low) maximum SWE. Comparative analyses of weekly basin SWE versus SCE, peak snowmelt floods, and climatic variables (temperature and winter precipitation) show consistency among basin SWE, SCE, and temperature, but there is some incompatibility between basin SWE and winter precipitation. The inconsistency suggests uncertainties in determination of basin winter snowfall amounts and limitations in applications of the SWE retrieval algorithm over large watersheds/regions with different physical characteristics. Overall, the results of this analysis demonstrate that the SWE and SCE data/products derived from remote sensing technology are useful in understanding seasonal streamflow variations in the northern regions.

9.1 Introduction

River discharge is an important element of freshwater budget for the Arctic Ocean and the high-latitude seas. The amount and variation of this freshwater inflow critically affect the salinity and sea ice formation, and may also exert significant control over global ocean circulation (Aagaard and Carmack 1989). Snow cover is a main component of global cryosphere system. Snow cover significantly affects atmosphere, hydrology, permafrost, and ecosystem in the high-latitude regions. Snow cover melt and associated floods are the most important hydrologic event of the year in the northern river basins (Woo 1986; Kane et al. 2000). Recent investigations document snowmelt has started earlier over the recent decades in the northern regions, such as Canada, Alaska, and Siberia, associated with warming in winter and spring seasons (Brabets et al. 2000; Serreze et al. 2000; Whitfield and Cannon 2000; Lammers et al. 2001; Zhang et al. 1999; Ye et al. 2003; Yang et al. 2002, 2014a, b). Studies also demonstrate that the timing and magnitude of northern river streamflow are strongly allied with cold season snow cover storage and subsequent melt (Cao et al. 2002; Yang et al. 2003, 2007). The changes in snowmelt runoff pattern may indicate a hydrologic regime shift over the high latitudes (Serreze et al. 2002; Yang et al. 2002, 2014a, b).

Snow depth data have been routinely collected at the operational networks in the United States and Canada. As a result of differences and changes in methods of observations and data-processing procedures, these data are subject to uncertainties and inconsistency over time and space, particularly across national borders. The operational networks in the northern regions are very sparse. It is therefore a challenge to combine regional snow data to generate basin snow information or gridded products for the high-latitude regions or large watersheds (Robinson 1989; Dyer and Mote 2006). Dyer (2008) used snow depth and discharge data to analyze patterns of snow volume and discharge in major North American watersheds (including the Yukon basin), and found, through statistical analysis, that snow

accumulation during late fall and winter is useful to predict spring discharge particularly in the cold Yukon basin and Mackenzie watersheds. Dyer (2008) pointed out that Snow Water Equivalent (SWE) and snow density data should be used to better define the snow accumulation and melt processes; however, reliable SWE and density estimates are difficult to obtain, especially for the continental-scale watersheds in the northern regions. Our knowledge of large-scale snowmelt processes and their interaction with climatic change and variation is incomplete, particularly for the northern regions with insufficient ground-based observations. This limits our ability of understanding past changes and predicting future characteristics of the hydrology system under a warming climate in the high-latitude regions.

Remotely sensed snow data have been very useful to cold region climate and hydrology investigations. For instance, the NOAA weekly snow cover dataset (maps) over the Northern Hemisphere permits quantitative assessments of changes and variations in regional snow extent (Robinson et al. 1993; Serreze et al. 1993; Clark et al. 1997; Frei and Robinson 1999b; Robinson and Frei 2000), and they are useful for hydrologic and snowmelt runoff models (Rango 1996, 1997; Rango and Shalaby 1999). Yang et al. (2003) used the weekly NOAA Snow Cover Extent (SCE) data to study streamflow hydrology in the large Siberian rivers, and discovered that SCE could predict spring discharge with the acceptable accuracy. In addition, long-term SWE data have been derived from the passive microwave sensors (Chang et al. 1987; Chang 1997; Armstrong and Brodzik 2001, 2002). Their potential utility for large-scale hydrology and climate studies in the high-latitude regions has not been fully evaluated. This chapter assesses the compatibility of the passive microwave SWE data over the Yukon watershed, and examines the streamflow response to snow cover change particularly during the spring melt season. The objective is to determine the potential of using remotely sensed snow cover information to enhance our capability of snowmelt runoff modeling over the large northern regions with continuous and discontinuous permafrost. Changes in seasonal snow cover conditions may have significantly contributed to the ground surface temperature increase. The influence of seasonal snow cover on soil temperature, soil freezing, thawing processes, and permafrost has considerable impact on carbon exchange between the atmosphere and the ground and on the hydrologic cycle in cold regions/cold seasons (Zhang 2005). The methods and results of this analysis should improve our understanding of hydrologic effects of a shrinking cryosphere.

9.2 Basin, Datasets, and Methods

The Yukon has a drainage area of 840 000 km^2. It is 3185-km long, with 1149 km in Canada. The Yukon River rises from the Atlin Lake and flows northwest to Fort Yukon, and then turns southwest and enters the Bering Sea (Fig. 9.1). Its major tributaries are the Teslin, Pelly, White, Stewart, Porcupine, Tanana, and Koyukuk rivers. The Yukon basin consists of 37% rolling topography and gentle slopes, 24%

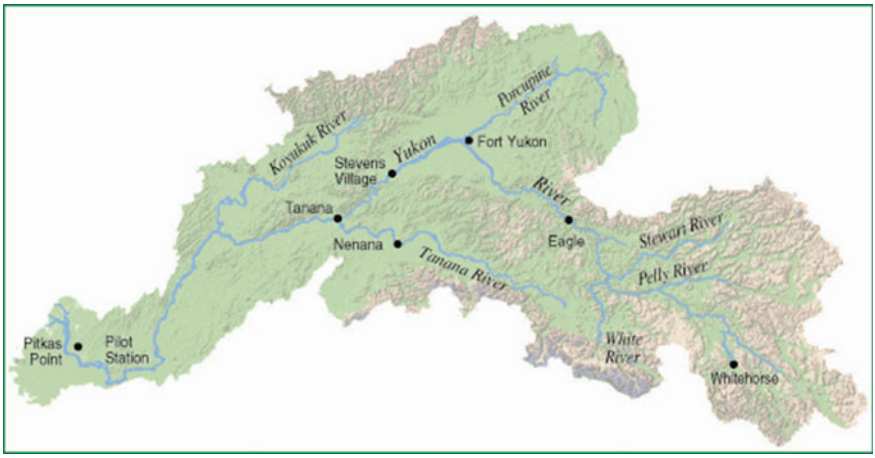

Fig. 9.1 The Yukon River basin and its tributaries

low mountains 20% plains and low mountains, 17% moderately high rugged mountains, and 2% extremely high rugged mountains. The Yukon River is one of the largest rivers in the northern regions. It contributes 203 km^3 $year^{-1}$ freshwater to the Bering Sea. It is the fifth-largest river in terms of annual total discharge in the northern regions. Hydrologic conditions and its changes in the Yukon River significantly affect regional biological and ecological systems. The US Geological Survey and Environment Canada maintain a hydrologic network in the Yukon River basin. In this study, long-term daily discharge records collected at the basin outlet station (the Pilot station, 61°56′10″N 162°53′0″W, near the river mouth) during 1975–2001 are used for analyses. Large dams and reservoirs were built in the northern regions for power generation, flood control, and irrigation. Studies show that reservoirs' regulation alters hydrologic regimes particularly in the regulated sub-basins (Ye et al. 2003; Yang et al. 2004a, b). There are no large dams in the Yukon basin; discharge data collected over this basin are reliable indicators of climate change and variation. The USGS produced a report to document the major hydrologic patterns within the basin (Brabets et al. 2000). Ge et al. (2012) examined Yukon basin hydrologic and climatic changes and variations. Yang et al. (2014b) calculated heat flux for the Yukon River.

Maps of snow extent and SWE derived from passive microwave satellite data (Scanning Multichannel Microwave Radiometer (SMMR) and Special Sensor Microwave Radiometer (SSMI)) for the Northern Hemisphere have been produced at the National Snow and Ice Data Center (NSIDC) (Armstrong and Brodzik 2001, 2002) using a modified version of the Chang et al. (1987) algorithm. The validation data set used in the Armstrong and Brodzik (2002) study was a topographically consistent subset of data from the 'Former Soviet Union Hydrological Surveys' (FSUHS) (Haggerty and Armstrong 1996). This subset (45–60 north latitude 25–45 east longitude) contains a high station density (approximately one transect per

100-km grid cell) and is primarily composed of non-complex terrain (grassland steppe) with maximum elevation differences of less than 500 m. The validation results indicated a general tendency for the algorithms to underestimate SWE in the range of 5–25 mm, particularly as forest cover density begins to exceed 30–40%. Regional maps and products have also been developed in Canada from the SMMR and SSM/I data, and used for analyses of snow cover variations over space and time (Walker and Goodison 1993; Derksen et al. 2000; Walker and Silis 2002). The algorithm by Armstrong and Brodzik (2002) is not able to consistently detect wet snow, only night time or early morning ('cold') orbits are used in most analysis, so as to reduce the chance that wet snow is present. Oelke et al. (2003) applied these SWE data for the active layer depth modeling in the Arctic and produced reasonable results. This analysis derived and applied daily SWE data for the Arctic watersheds as part of the effort to examine the large-scale seasonal and inter-annual variations of snow cover and its linkage with river flows (Yang et al. 2003, 2007).

In addition, the NOAA weekly snow cover maps based on visible data are quite reliable to map Snow Cover Extent (SCE) at many times and in many regions including the high latitudes. Mapping frequency and spatial resolution increased with the introduction of daily Interactive Multisensor Snow and Ice Mapping System (IMS) maps in June 1999. However, a lower resolution weekly map has continued to be generated from the IMS and is used in this analysis (Robinson 2003). This pseudo-weekly map involved taking high-resolution IMS grid cells for the fifth map of a week (continuing the weekly NOAA calendar) and determining whether more than 38% (determined from a comparison of both products that were produced independently during 2-year evaluation period) of the 64 IMS cells within a coarse resolution weekly cell were snow covered. If so, the coarse cell was considered snow covered (the 38% value was). Intercomparisons of visible, microwave, and station data derived weekly snow maps suggest strong agreement between the three, though admittedly lower in mountainous regions and near the periphery of the snowpack. The SCE maps have been widely used for hydrologic and climatic analyses in the cold regions, such as development of basin snow cover depletion curves (Rango 1996, 1997), study of streamflow response to snow changes in large northern rivers (Yang et al. 2003), input snow cover data to regional hydrologic and snowmelt runoff models (Rango 1997), and validation of climate model performance (Frei and Robinson 1999a; Yang et al. 1999).

This analysis used the daily EASE-Grid brightness temperature data from NSIDC (nsidc.org/data/nsidc-0032) to run the SWE algorithm (Armstrong and Brodzik 2001, 2002; Brodzik and Knowles 2002), for cold passes without the vegetation corrections, and produced daily SWE data for the northern regions including the Yukon watershed. The basin-mean SWE time-series have been generated from the daily records by averaging all pixels in the watershed. The weekly data have been generated by averaging the 7 day basin-mean SWE record during 1988–2001. On the basis of these weekly records, we examine the seasonal changes of snow cover mass, by defining the SWE climatology based on weekly statistics, determining the dates of snow cover formation/disappearance and duration of snow cover/snow-free days, and quantifying the rates of snow cover

mass change during the accumulation and melt seasons. We also derive weekly discharge time-series from the daily streamflow data collected near the basin outlet, and use the weekly data to describe the seasonal streamflow characteristics, including discharge regime, rates of streamflow rise, and peak flow during the melt period. We calculate the weekly correlation of streamflow with basin SWE, and determine the consistency between SWE and streamflow changes over the seasons. Furthermore, we identify extreme snowmelt streamflow cases and examine their correspondence with basin snow cover conditions. These analyses characterize the weekly relationship between snowmelt runoff and basin SWE changes for the Yukon River. In addition to streamflow and snow cover data, basin-mean weekly precipitation and temperature time-series during 1966–1998 have been created based on gridded global data sets (Jones 1994), and used to investigate the compatibility of SWE/SCE data with climate variables and to explain the streamflow response to seasonal snow cover changes.

It is important to note that the approach of this analysis is not a complete water budget calculation; rather, we focus on the major terms in basin water budget, i.e., SWE, winter precipitation, and streamflow. We relate snow cover data (SWE and SCE) with streamflow data measured near the basin outlet, since discharge represents the integrated response of basin hydrology to climate influence. To be compatible with discharge data, we need basin-mean snow and climate data for our analysis. To generate basin-averaged data, it is necessary to define the basin boundary. A river network grid by Fekete et al. (2001) was used over the Yukon basin and overpaid onto the gridded snow and climate data. All the grids inside the basin and those with more than 50% within the basin boundary were counted as the basin grids and used to produce basin averages. A simple average was calculated without taking into account topography effects on snow, precipitation, and temperature distributions. Similar approach has been applied for other large watersheds in North America and Siberia (Yang et al. 2003; Dyer 2008). Given the large size of the Yukon watershed and the focus of this analysis on the consistency examination of various data, the use of basin average is effective and appropriate.

9.3 Basin Hydro-Climatic Regime

To understand the climatic and hydrologic regime of the Yukon basin, we present the basin-mean temperature, precipitation, snow cover, and discharge data. The weekly timescale is used for accurate discussions of the seasonal cycles of basin hydrology and climate, particularly for snow cover and streamflow. Figure 9.2 shows the basin-mean weekly temperature regime. The basin is cold, with mean temperatures between −10 and −20 °C, during weeks 42–14; and it is relatively warm during weeks 20–38, when mean temperatures vary from 0 to 12 °C. Basin temperatures rise from −10 °C to near 0 °C during weeks 15–19, and decline from 0 to −10 °C during weeks 39–41. The inter-annual fluctuations in winter temperatures are significantly greater (ranging from −35 to −5 °C) than the differences in the

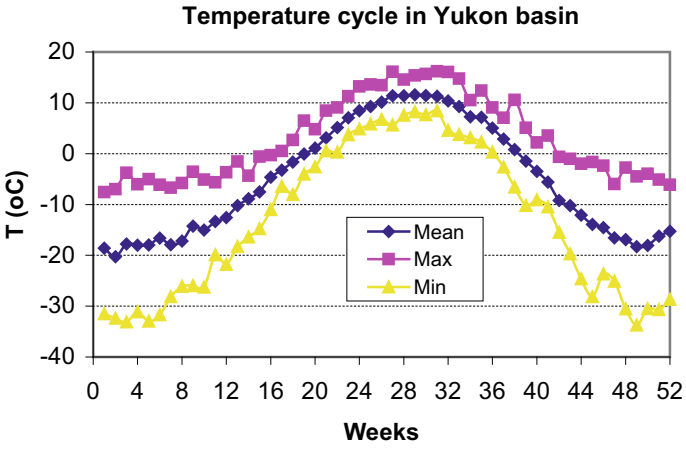

Fig. 9.2 Basin-mean weekly temperature in (T, °C) for the Yukon watershed, 1966–2002

summer temperatures (ranging from 8 to 15 °C). During the period 1966–2002, Yukon basin-mean annual air temperature is about −5.1 °C (SD = 0.98 °C), with the lowest annual air temperature of −6.8 °C in 1974, and the highest being −2.9 °C in 1993. Similar to other northern regions, Yukon basin has experienced a significant ($\alpha = 0.05$ level) warming trend (0.03 °C/year) during 1966–2002.

Similar to temperatures, a strong seasonal cycle exists for precipitation over the Yukon basin (Fig. 9.3). Precipitation is high (10–15 mm) during the warm season (weeks 21–43) and low (5–10 mm) during the winter season (weeks 44–20). During the period of 1988–2002 ($n = 15$), the mean annual total precipitation in Yukon basin is 384.6 mm (SD = 37.7 mm). The lowest annual precipitation is

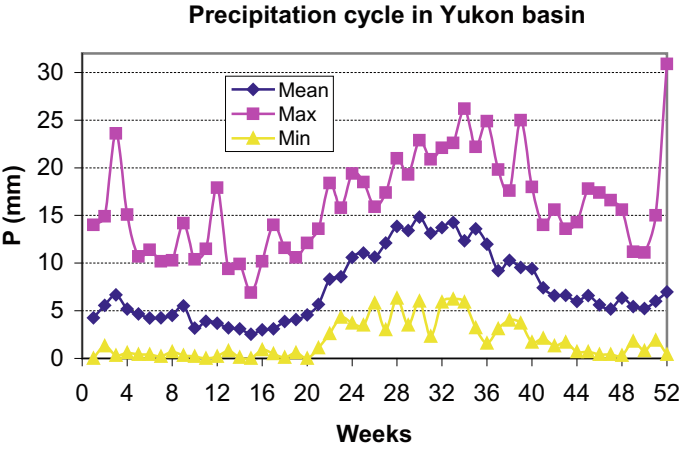

Fig. 9.3 Basin-mean weekly precipitation (P, mm) over the Yukon watershed, 1988–2002

312.3 mm in 1999, and the highest annual precipitation is 442.0 mm in 1994. The mean annual total snowfall (defined as the precipitation during the period when basin-mean air temperature is below 0 °C) is 180.4 mm (or 47% of the yearly total precipitation). The lowest annual snowfall is 102.3 mm in 1998, and the highest annual snowfall is 258.9 mm in 1992. Winter precipitation is generally lower than summer precipitation over the Yukon basin. On the 52nd week of 1999 and the 3rd week of 2000, weekly precipitation was about 31 and 24 mm, respectively; they were unusually higher for winter season perhaps due to strong snowfall events over the lower parts of the basin. No significant trends were found for yearly total precipitation and annual total snowfall for the study period 1988–2002.

Figures 9.4 and 9.5 show the basin weekly Snow Cover Percent (SCP) and SWE cycles. They illustrate snow accumulation during weeks 37–44, when basin SCE rises from 10 to 90%; a complete snow cover (100% SCE) during weeks 44–16; snowmelt during weeks 17–24, when SCE drops from 90 to 10% over the basin; and a minimum SCE of 5–10% in summer (weeks 25–36) due to glacier and snow cover in the high elevations. The SCE data show significant inter-annual variations. For the maximum SCE case, we see 100% SCE lasting during weeks 40–24, a fast melt in 2–3 weeks during weeks 25–28, a higher minimum SCE of 20–30% in the mid-summer, and an early snow accumulation during weeks 36–40. On the other hand, for the minimum SCE case, we observe a 100% snow cover during the weeks 50–16, a slow snowmelt in weeks 17–22, almost snow-free during weeks 24–39, and a late snow accumulation in weeks 40–48.

Similar pattern exists for the SWE (Fig. 9.5). Snowpack accumulates during weeks 38–4, reaches a stable state during weeks 5–16, with the mean max SWE of 90–100 mm around weeks 8–12. Snowpack starts to shrink slightly after the peak SWE. Snow cover melts during weeks 16–22, with SWE dropping from the peak to

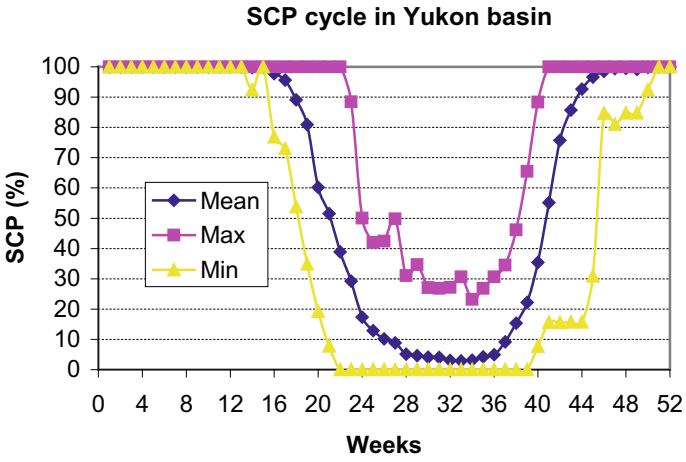

Fig. 9.4 Basin-mean weekly snow cover percentage (SCP, %) over the Yukon watershed, 1966–2002

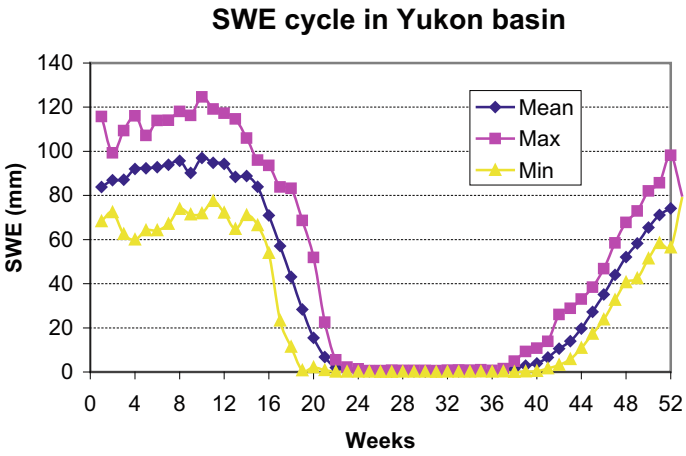

Fig. 9.5 Basin-mean weekly snow water equivalent (SWE, mm) over the Yukon watershed, 1988–2001

near 0 mm at week 23. Basin becomes snow-free during weeks 23–37, when the average SCE is about 5%, with max being as high as 30%, due to glaciers and snow cover in the high elevations. SWE condition varies among the years, for instance, the peak SWE range from 60–70 to 110–120 mm. The rate and length of snowmelt season also varies greatly, depending on the spring temperature and amount of peak SWE. A shorter melt season usually suggests a faster melt of snow cover due to late onset of melt associated with higher temperatures during late spring. During the period of 1988–2002, the mean peak SWE in Yukon basin is about 106 mm (SD = 130 mm). The lowest and highest peak SWEs are 81 mm in 1991 and 125 mm in 1998, respectively. No significant trends were found for the SCP or SWE over the study period 1988–2002.

The seasonal cycle of discharge near the basin outlet is illustrated in Fig. 9.6. It generally shows low flows during November–April (weeks 45–17), highest flow in June (weeks 22–24) due to snowmelt runoff, high flow in summer (weeks 25–40) due to glacier melt, and recession of flow in fall season (weeks 40–44). Streamflow of the Yukon River peaks at weeks 22–24 (or mid-June), when the basin is covered by a small patchy snowpack, i.e., approximately 4% SCE and 1 mm SWE over the watershed. The basin SWE amounts are very low at the time of peak streamflow, perhaps reflecting a long lag of streamflow response to snowmelt and flow routing within the large watershed. On the other hand, it should be noted that the SWE algorithm is more appropriate for the temperature gradient typical of a deep and dry snowpack. SWE will decrease in the presence of even small amount of liquid water, as soon as the cold passes start observing liquid water, since the emission from the water effectively reduces the temperature gradient. The SWE may fall off much faster than the real melt rate.

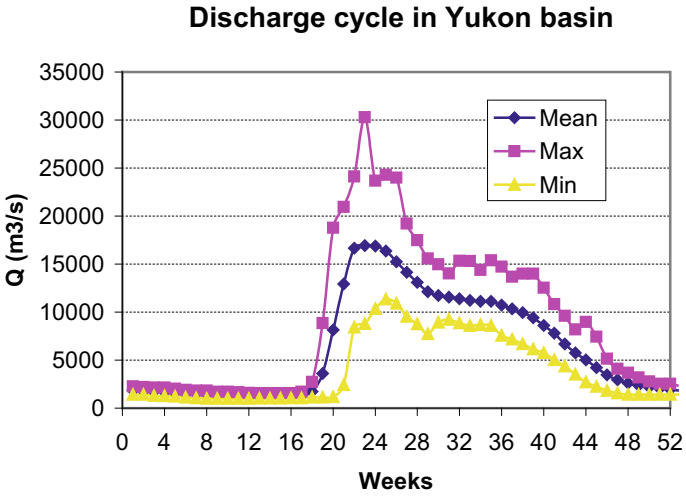

Fig. 9.6 Mean weekly discharge (m^3/s) near the basin outlet, 1975–1996

Streamflow decreases at the end of the snowmelt season, although heavy rainfall events and glacier melt in mid-summer generate secondary floods over the basin. The inter-annual variations of weekly streamflow are generally small in the cold season and large over summer months mainly due to rainfall storm activities and associated streamflow fluctuations. It also indicates noticeable differences in streamflow characteristics between years mainly due to different climate and snow conditions over the basin. The annual peak discharge in Yukon basin is 19 178 m^3/s, with the lowest and highest peak discharge being 12 969 m^3/s in 1978, and 30 299 m^3/s in 1985, respectively. It is important to note that the year having the highest annual flow was the same year for the highest peak flow, and the year with the lowest annual flow also has the lowest peak flow. This indicates that the peak flow in spring and summer dominates the annual flow. No significant changes were found for peak discharge or annual total discharge during the study period.

9.4 Compatibility of Basin Snow Cover Data

Temperature and precipitation are the main factors affecting snow cover characteristics including accumulation and melt processes. To understand the winter snow-mass budget, we compare basin SWE with the Accumulated Precipitation (AP) over the period when the basin-mean weekly temperatures are below 0 °C. The AP may include some rainfall events in early spring and late fall seasons particularly over the southern parts of the watersheds. The contribution of rainfall events is small to the winter total precipitation.

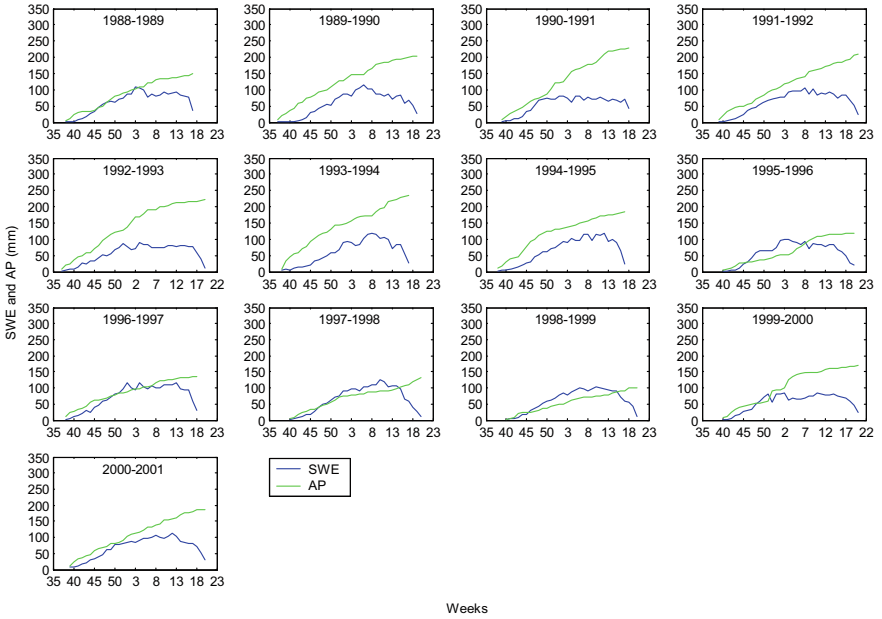

Fig. 9.7 Comparisons of basin snow water equivalent (SWE, mm) with winter Accumulated Precipitation (AP, mm) from 1988/1989 to 2000/2001 (Zhao 2004)

Figure 9.7 shows significant variation in the AP among the years. Both the high and low AP winters were associated with similar SWE amounts, although in most years basin SWE is generally less than the AP during the snow cover season. It is interesting to note that the amounts of maximum SWE are closer to AP in low snowfall winters, and much less than AP in high snowfall winters. These results are consistent with the saturation in the temperature gradient with the modeling work by Chang et al. (1987). It is reasonable to expect that basin maximum SWE should be generally close to winter total snowfall amount. The lack of correspondence of the basin SWE to AP variation indicates some inconsistency between the SWE and precipitation data. This is not completely unexpected given the large biases in snowfall data over the high-latitude regions (Yang et al. 1998, 2005; Yang and Ohata 2001) and limitations in remote sensing snow cover algorithm, including the issue of saturation (Walker and Goodison 1993; Armstrong and Brodzik 2001). In addition, sublimation loss from snowpack over winter is another factor contributing to the uncertainty in SWE and AP compatibility. As discussed in Chaps. 3 and 4, many studies reported that sublimation from the snow surface accounts for up to 1/3 of total accumulation in the northern regions (Benson 1982; Liston and Sturm 1998, 2004). Sublimation over large basins and regions is difficult to determine through direct measurements. Snow models taking into account the blowing and drifting snow processes can provide reasonable estimate of regional winter sublimation

amount (Liston and Sturm 1998, 2002). The ratios of maximum basin SWE versus AP are 37–120% (mean 77%) for the Yukon River. The ratios close to 100% reflect less difference between the SWE and AP.

The inter-annual variations in the SWE/AP ratios are mainly due to fluctuations in snowfall amounts and temperatures over the winter season. The low (high) ratios are found associated with high (low) AP and warm (cold) winter. It is important to note that the Yukon basin SWE was greater than the AP for several winters (i.e., 1995–1996, 1996–1997, 1997–1998, and 1998–1999). This unexpected result indicates uncertainties in the SWE and AP estimations over the region. There might be possible SWE algorithm saturation, as the basin-average SWE never exceeded 100 mm, regardless of winter precipitation variation. In addition, precipitation gauge undercatch of snowfall is also a factor, since studies (Yang et al. 1998, 2005; Benning and Yang 2005) found underestimation of yearly precipitation by 25–50% over Alaska. In addition, determination of timing of snow cover accumulation is also a challenge. In this analysis, basin-mean temperatures at 0 C were used to estimate the beginning date (week) of snow cover formation, i.e., the starting point for AP. Given the very large size of the watershed, basin-mean temperatures do not always represent the thermal conditions over the entire basin, particularly during spring and fall transition periods. Sub-basin scale analyses might be necessary to better examine the compatibility between basin SWE and winter precipitation.

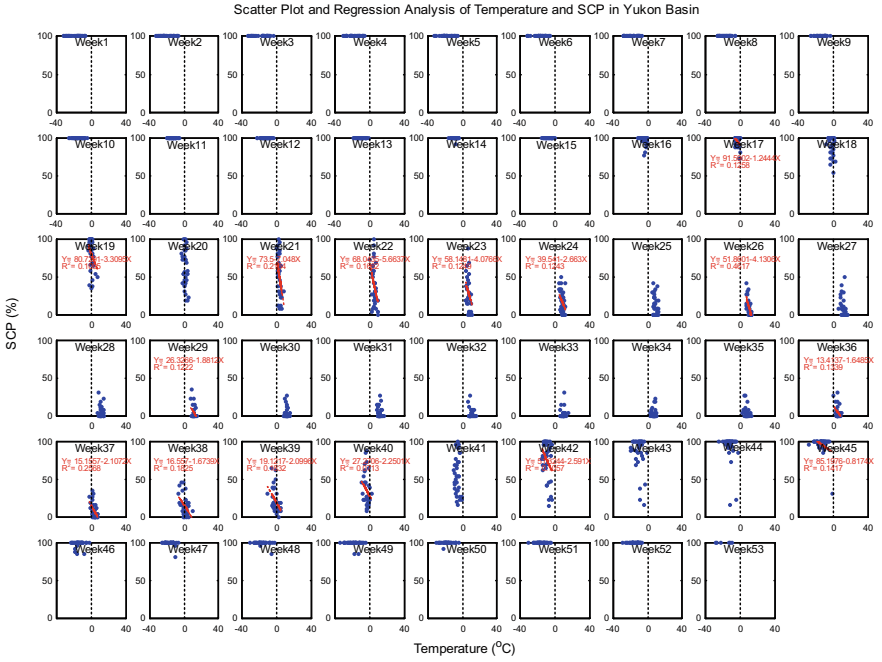

Fig. 9.8 Scatter plots and regression equations of basin weekly SCP (%) versus weekly air temperature (°C) for the 53 weeks in a year during 1966–2001 (Zhao 2004)

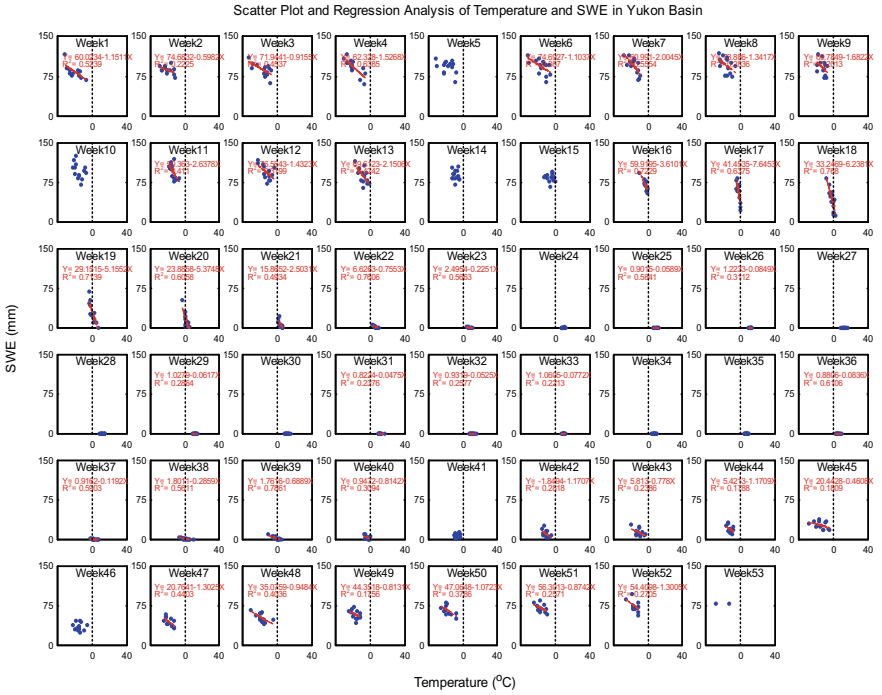

Fig. 9.9 Scatter plots and regression equations of basin weekly SWE (mm) versus weekly air temperature (°C) for the 53 weeks in a year during 1988–2001 (Zhao 2004)

To examine and quantify the impact of temperature on basin snow cover conditions, a linear regression is applied to the temperature and SCE/SWE data sets for each week in a year. Figures 9.8 and 9.9 present the scatter plots of (snow cover percent or SCE) SCP versus temperature and SWE versus temperature for the 53 weeks. The regression functions and R^2 are displayed in the plots for the weeks with significant relationships. The results generally show that the snow cover changes as a function of temperature. The basin SCP and SWE are the highest in the beginning of the year when temperatures are very cold between −15 and −20 C. Both SCP and SWE decrease in spring from very high to very low in a short time period when basin-mean temperatures are around 0 C. The basin is almost snow-free in the short summer season except in the mountain regions with glaciers and snow cover all year around. Snow cover forms when temperatures drop back to around 0 C in fall and continues to accumulate over the fall–winter seasons. Regression analyses identify strong negative correlations between basin SCP/SWE and temperature, particularly when temperatures are close to 0 C during the snow accumulation and melt seasons (Figs. 9.8 and 9.9). These correlations demonstrate the association of (high) low SWE/SCP with (low) high temperatures.

9.5 Weekly Relation Between Streamflow and Basin SWE

The seasonal changes of the basin SWE and streamflow in each individual year are displayed in Fig. 9.10. They clearly indicate a general response of river runoff to seasonal snow cover changes, i.e., an association of high discharge with low SCE and SWE during summer, a decrease in discharge associated with increasing SCE and SWE in fall, an association of low streamflow with high SCE and SWE during the cold season, and an increase in discharge associated with decreasing SCE and SWE during the spring melt periods. They also show the inter-annual variations in both SWE and streamflow. Relative to the basin SWE, streamflow varies much more between years. For instance, the Yukon River peak streamflow was high (23 000 m^3/s) in 1991 and low (18 000 m^3/s) in 1996, while the maximum basin SWE was low (about 75 mm) in 1991 and high (about 90 mm) in 1996. A similar peak SWE was found for 1988, 1989, 1990, 1994, 1995, and 2001, while the spring peak flow differs significantly among these years, particularly between 1994 (low flow) and 2001 (high flow). This discrepancy between basin snow cover and streamflow variations may suggest uncertainties in basin SWE data perhaps due to algorithm limitations (Armstrong and Brodzik 2002), particularly for the mountain regions within the Yukon basin.

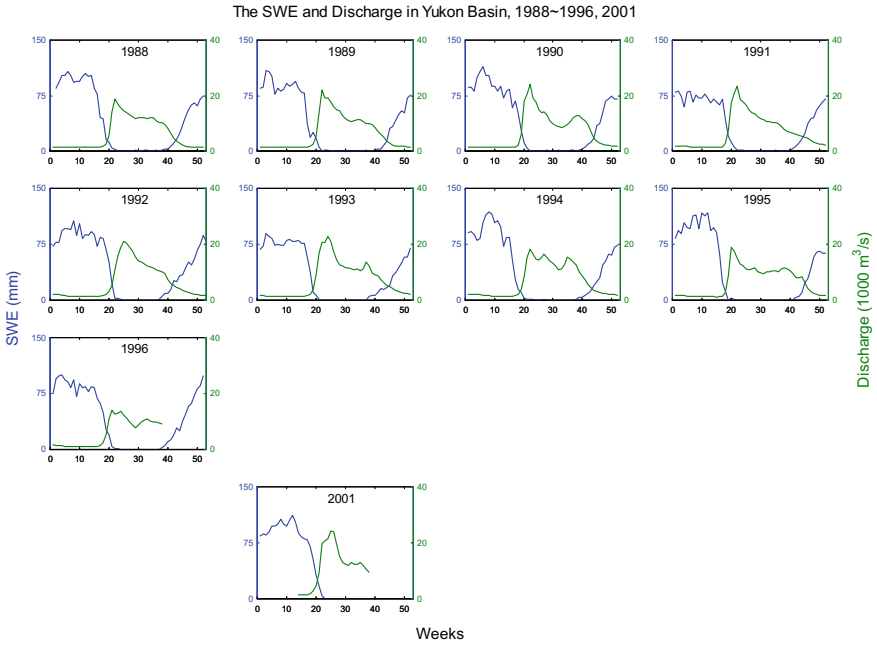

Fig. 9.10 Comparisons of basin Snow Water Equivalent (SWE, mm) with river discharge (Q, m^3/s) during 1988–1996 and 2001 (Zhao 2004)

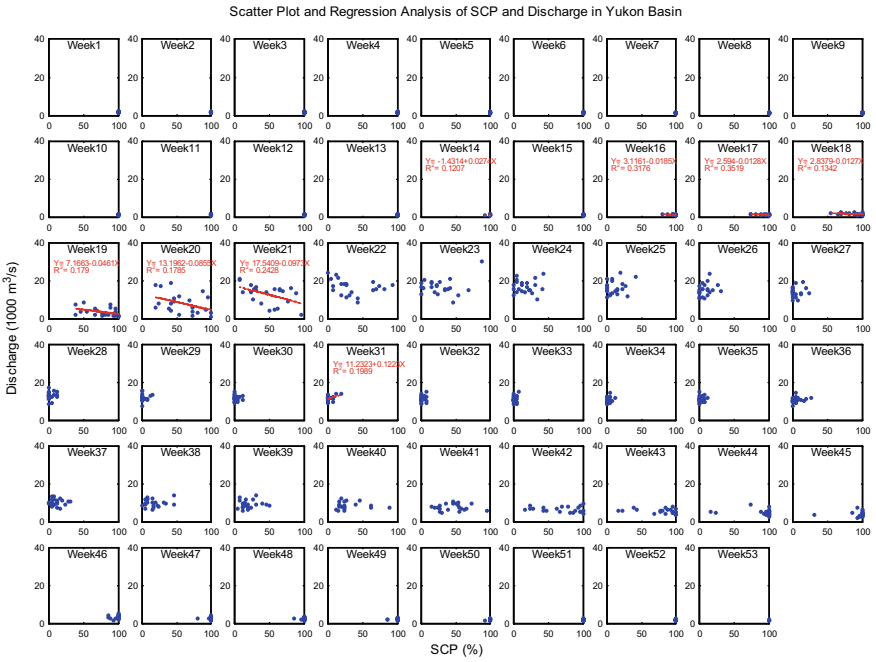

Fig. 9.11 Scatter plots and regression equations of weekly discharge (Q, m^3/s) versus weekly basin Snow Water Equivalent (SWE, mm) for the 53 weeks in a year, 1988–2001 (Zhao 2004)

To quantify the response of river streamflow to basin snow cover variation, we examine and compare the weekly mean streamflow with the weekly basin SWE for the study period 1988–1999. The results generally confirm a meaningful relationship between the streamflow and SWE during the spring melt season over the Yukon watershed (Fig. 9.11). In the early melt period (weeks 16–18), basin SWE reduces from 120 to 50 mm. Most of the meltwater is stored in ponds, lakes, and river valleys. River ice breaks up around this time in the upper parts of the basin, but streamflow at the basin outlet does not show a clear response due to ice jams in the river valleys. As snowmelt progresses (weeks 19–21), SWE decreases from 70 to 20 mm, releasing more water to satisfy the surface storage within the basin. During weeks 22–24, river channels open up in the downstream parts of the watershed and discharge near the basin mouth starts to rise and reach the maximum. This response of streamflow to snowmelt is reflected by a negative correlation between streamflow and basin SWE in weeks 19–21. In the late melt period (weeks 23–25), streamflow response to snowmelt weakens due to reduced snowmelt runoff contribution. The results of regression analyses are shown in Fig. 9.11. They explain 30–70% of streamflow variability, although they are statistically significant at 85–95% confidence. It is useful to derive these relationships, as they suggest a practical procedure of using remotely sensed SWE information for snowmelt runoff estimation over the large northern watersheds.

9.6 Extreme Streamflow and Associated Snow Condition

The basin snow cover and discharge data show that weekly snow cover and snowmelt peak flows vary significantly among years. To better understand the variability in snowmelt runoff, it is useful to examine extreme streamflow and its association with the snow cover condition, such as the peak accumulation and melt process. Two sample years of highest and lowest streamflow cases were selected, i.e., peak flows during the snowmelt season of 13 900 m^3/s in 1996 and 24 110 m^3/s in 1990. Figure 9.12 compares the SCE and SWE data with the extreme streamflow for the two years. It shows that, for the SCE, a similar process (rate) of snow cover depletion during the early melt season (weeks 17–20) between the two years, and a slower melt and longer SCE recession for the low flow year during the late melt season (weeks 21–25) (Fig. 9.12a). The peak snow accumulation over the basin is about 115 mm for the high flow year of 1990 and 100 mm for the low flow year of 1996, indicating higher (lower) flows associated with higher (lower) basin SWE. The melt patterns were very similar between the two extreme years, with the snowmelt beginning around week 16 and ending around week 21. The timing of the peak flow was 1 week earlier in the low flow year than the high flow year; the shape of the spring hydrograph is sharp (with a single high peak) in the high flow year and flat (with two low peaks) in the low flow year. It is important to note that the difference in peak SWE was only 15 mm, while the peak spring flow difference was about 10 210 m^3/s (Fig. 9.12b). The difference in peak flows is much higher than the difference in basin SWE between the extreme years. This seems to suggest inconsistency between basin SWE and streamflow. In addition to the winter maximum SWE over the basin, other factors such as temperature, precipitation, soil moisture condition, and ground thaw processes during the melt periods also affect snowmelt processes and influence the timing and magnitude of peak snowmelt floods.

9.7 Summary and Conclusion

Validation and evaluation of available remotely sensing products are important to develop our capability of observing and monitoring the earth system from the space. This analysis applied remotely sensed SWE, SCE, and gridded climatic data to investigate snowmelt runoff response to seasonal snow cover change over the Yukon watershed. It defined the seasonal cycles and variations of snow cover and river streamflow, and identified a clear correspondence of river streamflow to seasonal snow cover change, i.e., an association of low streamflow with high snow cover mass during the cold season and an increase in discharge associated with a decrease of snow cover extent and SWE during the melt periods. It also examined the compatibility of the basin SWE data with the SCE, peak snowmelt floods, and climatic variables (temperature and winter precipitation), and found consistency among the basin SWE, SCE, and temperature. On the other hand, it detected

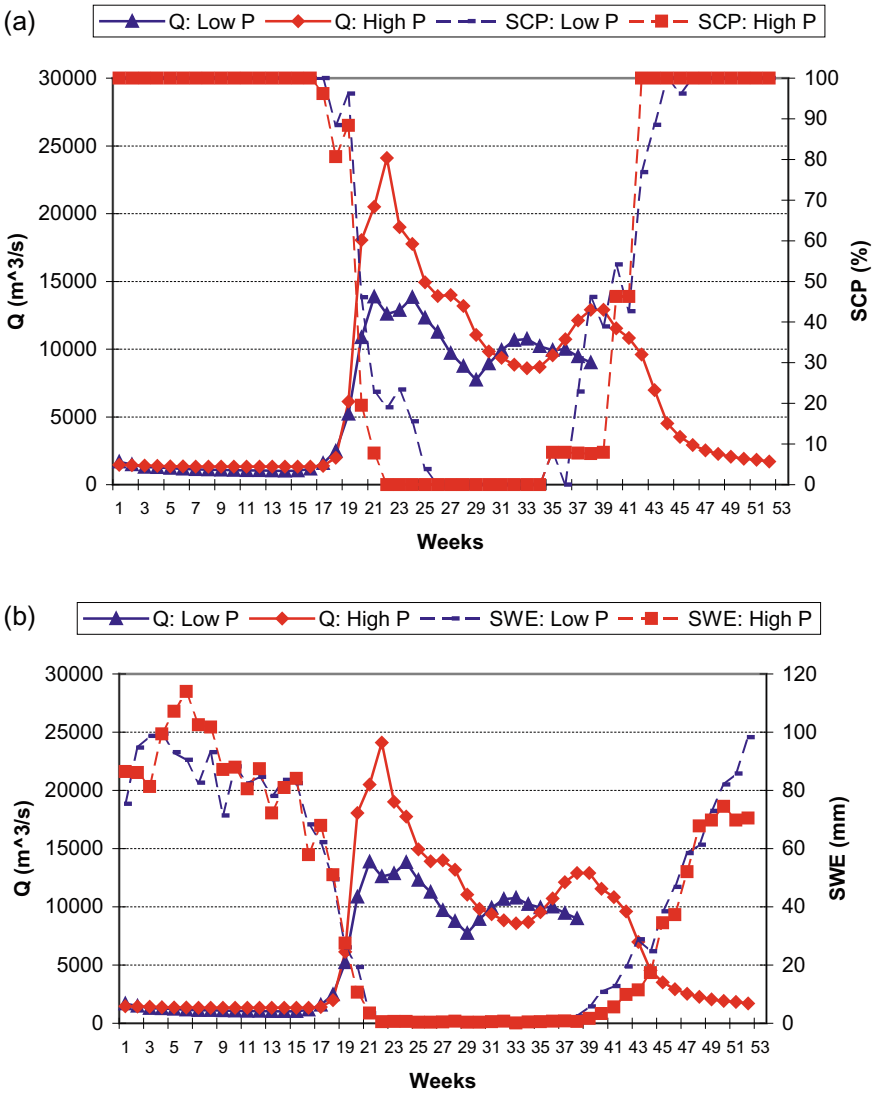

Fig. 9.12 Comparison of extreme discharge (Q, m^3/s) cases with SCP (**a**) and SWE, (**b**) over the Yukon watershed (Zhao 2004)

incompatibility between basin SWE and winter precipitation, suggesting limitations in SWE retrieval algorithm and uncertainties in the determination of basin winter snowfall amounts.

To quantify the relation between river streamflow and basin snow cover variations, we compared the weekly mean streamflow with the weekly basin SWE for the study period. The results revealed a meaningful linkage between streamflow and

basin SWE during the spring melt season, and developed a statistically significant weekly streamflow–SWE relationship. It is important to explore these relationships, as they improve our understanding of the most important arctic hydrologic process —snowmelt peak floods—and they also suggest practical procedures of using remotely sensed snow cover information for snowmelt runoff forecasting over the large northern watersheds with insufficient ground observations. Furthermore, analyses of extreme (high/low) streamflow cases (years) and basin snow cover conditions indicate a general association of high (low) flow peak with high (low) maximum SWE over the basin, although some inconsistencies exist between extreme flow and basin SWE. These results point to a need to further search for the best snowmelt–streamflow relationship, and to develop the most useful snowmelt runoff forecasting methods for the large northern rivers. There are uncertainty and saturation problems in the SWE algorithms (Clifford 2010). There is good improvement in passive microwave SWE algorithms, including the AMSR-E (Kelly 2009; RSSJ) that includes adjustments for shallow show and a dynamic density model.

The results of this analysis demonstrate that remote sensing snow cover data are useful in understanding streamflow characteristics and changes in the arctic regions with a very sparse observational network. The methods and results of this investigation are important to seasonal hydrologic forecasting, snowmelt model, and process studies. They improve our understanding of the spatial and temporal variability of high-latitude snow cover and its contribution to river runoff in the northern rivers. Snow depth and water equivalent data obtained by ground observations are also useful to better understand snowmelt and runoff processes (Dyer 2008; Brown et al 2010). Long-term snow observations particularly over the Siberian regions have been found valuable for cold region climate studies (Ye et al. 1998; Armstrong and Brodzik 2001). There is a need to investigate the compatibility of the SWE with in situ snow cover observations at sub-basins scales for more detailed analyses of snow–runoff relationship. It is also necessary to integrate remote sensing and ground-based snow datasets for land surface process modeling and simulation of hydrologic change over the cold regions.

References

Aagaard K, Carmack EC (1989) The role of sea ice and other fresh water in the arctic circulation. J Geophys Res 94(C10):14485–14498

Armstrong RL, Brodzik MJ (2001) Recent Northern Hemisphere snow extent: a comparison of data derived from visible and microwave sensors. Geophys Res Lett 28(19):3673–3676. https://doi.org/10.1029/2000GL012556

Armstrong RL, Brodzik MJ (2002) Hemispheric-scale comparison and evaluation of passive microwave snow algorithms. Ann Glaciol 34:38–44

Benning J, Yang D (2005) Adjustment of daily precipitation data at Barrow and Nome Alaska for 1995–2001. Arct Antarct Alp Res 37(3):267–283

Benson CS (1982) Reassessment of winter precipitation on Alaska's Arctic Slope and measurement on the flux of wind blown snow report. Geophysical Institute of the University of Alaska, Fairbanks, AK, p 26

Brabets T, Wang B, Meade R (2000) Environmental and hydrologic overview of the Yukon river basin, Alaska and Canada, USGS. Water-Resour Investig Rep 99–4204:106

Brodzik MJ, Knowles KW (2002) EASE-grid: a versatile set of equal-area projections and grids. In: Goodchild M (ed) Discrete global grids. National Center for Geographic Information & Analysis, Santa Barbara, CA. http://www.ncgia.ucsb.edu/globalgrids-book/ease grid/

Brown R, Brasnett B, Robinson D (2010) Gridded North American monthly snow depth and snow water equivalent for GCM evaluation. Atmos Ocean. https://doi.org/10.3137/ao.410101

Cao Z, Wang M, Proctor B, Strong G, Stewart R, Ritchie H, Burnford J (2002) On the physical processes associated with the water budget and discharge of the Mackenzie basin during the 1994/95 water year. Atmos Ocean 40(2):125–143

Chang ATC (1997) Snow parameters derived from microwave measurements during the BOREAS winter field campaign. J Geophys Res 102(D24):29663–29671

Chang ATC, Foster JL, Hall DK (1987) Nimbus 7 SMMR derived global snow cover parameters. Ann Glaciol 9:39–44

Clark MP, Serreze MC, Robinson DA (1997) Atmospheric controls on Eurasian snow extent. Int J Climatol 19(1):27–40

Clifford D (2010) Global estimates of snow water equivalent from passive microwave instruments: history, challenges and future developments. Int J Remote Sens 3707–3726. https://doi.org/10.1080/01431161.2010

Derksen C, LeDrew E, Goodison B (2000) Temporal and spatial variability of North American prairie snow cover (1988–1995) inferred from passive microwave-derived snow water equivalent imagery. Water Resour Res 36(1):255–266

Dyer JL (2008) Snow depth and streamflow relationships in large North American watersheds. J Geophys Res 113:D18113. https://doi.org/10.1029/2008JD010031

Dyer JL, Mote TL (2006) Spatial variability and trends in snow depth over North America. Geophys Res Lett 33:L16503. https://doi.org/10.1029/2006GL027258

Fekete BM, Vörösmarty CJ, Lammers RB (2001) Scaling gridded river networks for macroscale hydrology: development, analysis, and control of error. Water Resour Res 37(7):1955–1967

Frei A, Robinson DA (1999a) Northern Hemisphere snow extent: regional variability 1972–1994. Int J Climatol 19(14):1535–1560

Frei A, Robinson DA (1999b) Evaluation of snow extent and its variability in the atmospheric model intercomparison project. J Geophys Res 103(D8):8859–8871

Ge S, Yang D, Kane D (2012) Yukon river basin long-term (1977–2006) hydrologic and climatic analysis. Hydrol Process. https://doi.org/10.1002/hyp.9282

Haggerty CD, Armstrong RL (1996) Snow trends within the Former Soviet Union. Eos 77(46): [Abstract] Fall Meeting Supplement, F191

Jones PD (1994) Hemispheric surface air temperature variations: a reanalysis and an update to 1993. J Clim 7:1794–1802

Kane DL (1997) The impact of Arctic hydrologic perturbations on Arctic ecosystems induced by climate change. In: Global change and Arctic terrestrial ecosystems, ecological studies, vol 124. Springer, New York, pp 63–81

Kane DL, Hinzman LD, McNamara JP, Zhang Z, Benson CS (2000) An overview of a nested watershed study in Arctic Alaska. Nord Hydrol 4(5):245–266

Kelly REJ (2009) The AMSR-E snow depth algorithm: description and initial results. J Remote Sens Soc Jpn 29(1):307–317. (GLI/AMSR Special Issue)

Lammers R, Shiklomanov A, Vorosmarty C, Fekete B, Peterson B (2001) Assessment of contemporary arctic river runoff based on observational discharge records. J Geophys Res 106 (D4):3321–3334

Liston GE, Sturm M (1998) A snow-transport model for complex terrain. J Glaciol 44:498–516

Liston GE, Sturm M (2002) Winter precipitation patterns in Arctic Alaska determined from a blowing-snow model and snow-depth observations. J Hydrometeorol 3:646–659

Liston GE, Sturm M (2004) The role of winter sublimation in the Arctic moisture budget. Nord Hydrol 35(4):325–334

Oelke C, Zhang T, Serreze MC, Armstrong RL (2003) Regional-scale modeling of soil freeze/thaw over the Arctic drainage basin. J Geophys Res 108(D10):4314. https://doi.org/10.1029/2002JD002722

Rango A (1996) Spaceborne remote sensing for snow hydrology applications. Hydrol Sci J 41 (4):477–494

Rango A (1997) Response of areal snow cover to climate change in a snowmelt-runoff model. In: Walsh JE (eds) International symposium on representation of the cryosphere in climate and hydrological models, vol 25, Victoria, British Columbia. Annals of Glaciology, Cambridge, UK, pp 232–236

Rango A, Shalaby AI (1999) Current operational applications of remote sensing in hydrology. Operational hydrology report, No. 43. World Meteorological Organization (WMO), Geneva, p 73

Robinson DA (1989) Construction of a United States historical snow data base. In: Proceedings of eastern snow conference, vol 45, pp 50–59

Robinson DA (2003) Recent variability of Northern Hemisphere snow cover. In: Preprints: seventh conference on polar meteorology and oceanography, paper 13.12. American Meteorological Society, Hyannis, MA, p 6

Robinson DA, Frei A (2000) Seasonal variability of Northern Hemisphere snow extent using visible satellite data. Prof Geogr 52(2):307–314

Robinson DA, Dewey KF, Heim RR Jr (1993) Global snow cover monitoring: an update. Bull Am Meteor Soc 74:1689–1696

Serreze MC, Maslanik JA, Scharfen G, Barry RG (1993) Interannual variations in snow melt over arctic sea ice and relationships to atmospheric forcings. In: Proceedings of the 3rd international symposium on remote sensing of snow and ice, vol 17. Annals of Glaciology, Boulder, CO, pp 327–331

Serreze MC, Walsh JE, Chapin EC, Osterkamp T, Dyugerov M, Romanovsky V, Oechel WC, Morison J, Zhang T, Barry RG (2000) Observation evidence of recent change in the northern high-latitude environment. Clim Change 46:159–207

Serreze MC, Bromwich DH, Clark MP, Etringer AJ, Zhang T, Lam-mers RB (2002) The large scale-hydro-climatology of the terrestrial arctic drainage system. J Geophys Res 107:8160. https://doi.org/10.1029/2001JD000919

Walker AE, Goodison BE (1993) Discrimination of a wet snow cover using passive microwave satellite data. Ann Glaciol 17:307–311

Walker AE, Silis A (2002) Snow-cover variations over the Mackenzie River basin, Canada, derived from SSM/I passive-microwave satellite data. Ann Glaciol 34:8–14

Whitfield P, Cannon A (2000) Recent climate moderated shifts in Yukon hydrology. Water resources in extreme environments, AWRA. Anchorage, Alaska, pp 257–262

Woo M-K (1986) Permafrost hydrology in North America. Atmos Ocean 24(3):201–234

Yang D, Ohata T (2001) A bias corrected Siberian regional precipitation climatology. J Hydrometeorol 2(1):122–139

Yang D, Goodison BE, Benson CS, Ishida S (1998) Adjustment of daily precipitation at 10 climate stations in Alaska: application of WMO intercomparison results. Water Resour Res 34(2):241–256

Yang ZL, Dickinson RE, Hahmann AN, Niu G-Y, Shaikh M, Gao X, Bales RC, Sorooshian S, Jin J (1999) Simulation of snow mass and extent in general circulation models. Hydrol Process 13(12/13):2097–2113

Yang D, Kane D, Hinzman L, Zhang X, Zhang T, Ye H (2002) Siberian Lena river hydrologic regime and recent change. J Geophys Res 107(D23):4694. https://doi.org/10.1029/2002JD00254

Yang D, Robinson D, Zhao Y, Estilow T, Ye B (2003) Streamflow response to seasonal snow cover extent changes in large Siberian watersheds. J Geophys Res 108(D18):4578. https://doi.org/10.1029/2002JD003149
Yang D, Ye B, Kane D (2004a) Streamflow changes over Siberian Yenisei river basin. J Hydrol 296:59–80
Yang D, Ye B, Shiklomanov A (2004b) Streamflow characteristics and changes over the Ob river watershed in Siberia. J Hydrometeorol 5(4):595–610
Yang D, Kane D, Zhang Z, Legates D, Goodison B (2005) Bias-corrections of long-term (1973–2004) daily precipitation data over the northern regions. Geophys Res Lett 32:L19501. https://doi.org/10.1029/2005GL024057
Yang D, Zhao Y, Armstrong R, Robinson D, Brodzik M-J (2007) Streamflow response to seasonal snow cover mass changes over large Siberian watersheds. J Geophys Res 112:F02S22. https://doi.org/10.1029/2006jf000518
Yang D, Shi X, Marsh P (2014a) Variability and extreme of Mackenzie River daily discharge during, 1973–2011. Quat. Int. https://doi.org/10.1016/j.quaint.2014.09.023
Yang D, Marsh P, Ge S (2014b) Heat flux calculations for Mackenzie and Yukon Rivers. Polar Sci. https://doi.org/10.1016/j.polar.2014.05.001
Ye H, Cho H, Gustafson PE (1998) The changes in Russian winter snow accumulation during 1936–1983 and its spatial patterns. J Clim 11:856–863
Ye B, Yang D, Kane D (2003) Changes in Lena river streamflow hydrology: human impacts versus natural variations. Water Resour Res 39(8):1200. https://doi.org/10.1029/2003WR001991
Zhang T (2005) Influence of the seasonal snow cover on the ground thermal regime: an overview. Rev Geophys 43:RG4002. https://doi.org/10.1029/2004RG000157
Zhang T, Barry RG, Knowles K, Heginbottom JA, Brown J (1999) Statistics and characteristics of permafrost and ground-ice distribution in the Northern Hemisphere. Polar Geogr 23(2):132–154
Zhang X, Harvey KD, Hogg WD, Yuzyk TR (2001) Trends in Canadian streamflow. Water Resour Res 37:987–998
Zhao Y (2004) Snow runoff assessment for five large northern watersheds. MS thesis. University Alaska Fairbanks

Dr. Daqing Yang is a Research Scientist at the Watershed Hydrology and Ecology Research Division, Environment and Climate Change Canada. He is also Affiliate Research Professor at the International Arctic Research Center, Univ. of Alaska Fairbanks. Over the past 25 years, he has conducted cryosphere system research in China, Canada, Japan, USA, and Norway. His primary research activities/interests include cold region hydrology and climate, particularly Arctic large river streamflow regime and change, snow cover and snowfall measurements, climate change and human impact to regional hydrology, and applications of remote sensing in cold regions. He has served as journal editor and subject editor for IAHS publications (cold region hydrology, northern research basin water balance, and cold/mountain region hydrological systems under climate change), and WMO technical reports (solid precipitation measurement intercomparison and integrated global observing strategy cryosphere theme). He also contributed as review and/or author to the IPCC Reports, and the Arctic Council's Snow, Water, Ice and Permafrost in the Arctic

(SWIPA 2017 and follow up) assessment. His current research focuses on investigating the impacts of climate variability/change and human activities on hydrologic system across the broader northern regions.

Yuanyuan Zhao P.E., is a civil engineer and a resident of Fairbanks Alaska. Her research interests are varied; she has studied streamflow response to snow cover changes in large northern river watersheds in the early 2000s for her graduate study in hydrology. She also conducted analysis of Alaska oil production cycles in resource economics. Currently, she is pursuing a Ph.D. in mathematics, studying control, and inverse problem on quantum graphs. She is a recipient of the National Science Foundation Graduate Study Fellowship.

Dr. Richard L. Armstrong is a Senior Research Scientist at the National Snow and Ice Data Center (NSIDC), Associate Professor (Adjunct) at Department of Geography, Associate Director for the Cryospheric and Polar Processes Division, and Council of Fellows of the Cooperative Institute for Research in Environmental Sciences (CIRES), University of Colorado in Boulder. His research has covered a variety of relevant topics, including (1) evaluation of fluctuations of glaciers and seasonal snow cover as indicators of climate change, (2) assessments of the individual contribution of melting seasonal snow and glacier ice to the water resources of high mountain basins, (3) passive microwave satellite remote sensing of snow, ice and frozen ground, (4) validation and cross-calibration of satellite sensor data to assure quality time series data in support of accurate climate change detection, (5) former director of various relevant field projects including Blue Glacier Mass Balance Project, Mount Olympus, University of Washington and San Juan Avalanche Project, San Juan Mountains, University of Colorado. He is also the Principal Investigator for the USAID-funded CHARIS project (Contribution to High Asian Runoff from Ice and Snow) 2013–2019.

Dr. Mary J. Brodzik received the B.A. (summa cum laude) degree in mathematics from Fordham University, New York, NY, USA, in 1987. Her experience includes software development, validation, and verification on Defense Department satellite command and control, and satellite tracking systems. Since 1993, she has been with the National Snow and Ice Data Center (NSIDC) and with the Cooperative Institute for Research in Environmental Sciences, University of Colorado, Boulder, CO, USA, where she is currently a Senior Associate Scientist. At NSIDC, she has implemented software systems to design, produce, and analyze snow and ice data products from satellite-based visible and passive microwave imagery. She has contributed to the NSIDC data management and software development teams for the NASA Cold Lands Processes Experiment and Operation IceBridge. She is managing the operational production of the EASE-Grid 2.0 Earth Science Data Record of satellite passive microwave data, including over 100 years of observations from SMMR, SSM/I-SSMIS, AMSR-E, and SMAP. She is currently working to produce enhanced-resolution, near real-time snow water equivalent products. She has used MODIS snow products to derive the first systematically derived global map of the world's glaciers. She has developed snow and glacier ice melt models to better understand the contribution of glacier ice melt to major rivers with headwaters in High Asia. Her research interests include optical and passive microwave sensing of snow, remote sensing data gridding schemes, and effective ways to visualize science data. She is a member of IEEE and the IEEE Geoscience and Remote Sensing Society.

Dr. David Robinson is a Distinguished Professor in the Department of Geography at Rutgers, The State University of New Jersey, and also the New Jersey State Climatologist. As a physical geographer and climatologist, his research interests run the spatial gamut from global to local, with an underlying theme being the development of a better understanding of the climate system. The majority of his published research has focused on hemispheric and regional snow cover dynamics and interactions of snow cover with other climate elements. This includes maintaining an internationally recognized database of Northern Hemisphere snow extent throughout the satellite era; information that is used in his Global Snow Lab's research endeavors, efforts of others, and contributions to national and international climate assessments. He has been a member of the National Academy of Sciences' Board on Atmospheric Sciences and Climate, is past president of the American Association of State Climatologists, is a Fellow of the American Meteorological Society, and has received the Lifetime Achievement award of the American Association of Geographers.

Arctic River Water Temperatures and Thermal Regimes

10

Daqing Yang, Hoteak Park, Amber Peterson, and Baozhong Liu

Abstract

Water temperature has an important impact on many aspects of basin hydrology and ecology. In the northern regions, the investigation of river thermal regimes and their changes over space and time is a challenge due to data limitations. This chapter determines the water temperature regimes and its changes at several locations within the Yukon, Mackenzie River, and Lena watersheds, and examines their relationship with air temperature. Yukon and Mackenzie Rivers have distinct water temperature dynamics. They remain near zero from freeze-up in the fall to ice break-up in the spring, and reach their peak temperature during mid-summer. For the locations examined, peak mean monthly water temperatures ranged from 9 to 15 °C, and mean July air temperatures ranged from 13 to 16 °C. The lags between water and air temperatures ranged from 1 to 40 days. The largest lag was found at the Great Bear River monitoring location, since water temperature at this site is strongly influenced by the heat storage of Great Bear Lake. Tests of three models, i.e., linear regression, logical regression

D. Yang (✉)
Watershed Hydrology and Ecology Division, Environment and Climate Change Canada, Victoria, BC, Canada
e-mail: Daqing.Yang@canada.ca; daqing.yang@gmail.com

H. Park
Japan Agency for Marine-Earth Science and Technology, Research Institute for Global Change, Yokohama, Kanagawa, Japan
e-mail: park@jamstec.go.jp

A. Peterson
University of Saskatchewan, Global Institute of Water Security, Saskatoon, SK, Canada
e-mail: apeterson@usask.ca

B. Liu
Occidental Petroleum, Fulshear, TX, USA
e-mail: baozhongliu@gmail.com

D. Yang and D. L. Kane (eds.), *Arctic Hydrology, Permafrost and Ecosystems*,
https://doi.org/10.1007/978-3-030-50930-9_10

(s-shape), and the physically based air2stream model, show that the air2stream model provided the best results, followed by logical regression. Linear regression gave the poorest result. Model estimates of water temperature from air temperature were slightly improved by the inclusion of discharge data. The water temperature sampling regimes had a considerable effect on model performance; long-term data provide a more robust test of a model. Comparisons of mean monthly water temperatures suggest significant spatial variability and some inconsistency between upstream and downstream sites, mainly due to difference in data collection schemes. Similar to the VIC model, the CHANGE model can simulate large basin water temperature pattern over the arctic regions as a whole. With this capability, it might be possible to reconstruct the water temperature records for the northern rivers without past observations. This review clearly demonstrates the need to improve water temperature monitoring in the northern regions.

10.1 Introduction

River thermal conditions influence biological and ecological processes within the basin and near the coastal regions. Water temperature is the direct measure of a river's physical and thermal conditions. Stream temperatures vary with atmospheric condition, topography, streamflow, and heat transfer processes (Caissie 2006), and they generally follow air temperature on a seasonal time scale (Sinokrot and Stefan 1993). Due to climate change and human impacts, stream temperatures have warmed by several degrees over many regions in USA, Australia, and Russia (Webb and Nobilis 1995; Liu et al. 2005; van Vliet et al. 2011). Warmer water temperatures have become an important concern for watershed biology and aquatic species (Lowney 2000). In the high latitude regions, water temperature and discharge significantly affect the freeze-up/and break-up processes, thickness of river ice, and thermal erosion along the riverbanks. Marsh and Prowse (1987) examined the influence of stream heat on overlying ice cover of the Liard River, and reported large spatial and temporal variations in water temperatures and heat fluxes. Costart et al. (2003) found water temperature and discharge as the main factors for thermal erosion of the frozen riverbanks in the Lena basin. Liu et al. (2005) and Yang et al. (2005), using the long-term water temperature records over the Lena basin, discovered significant trends in river thermal conditions as the results of regional climate warming and human impacts, particularly reservoir regulation. Lammers et al. (2007) analyzed water temperature data across Siberia and calculated heat energy for the large rivers, and reported a consistent increase in the decadal maximum temperature for the basins in the European part of Russia. In a study of river temperature in 32 monitoring stations in 7 unique drainage basins around Cook Inlet in Alaska, Kyle and Brabets (2001) found river temperature increases affect fish quantity, well-being, and disease. King et al. (2016), using field observations in

summer season and modeling approach, examined water temperature controls in the low arctic rivers of Alaska.

Many studies have derived relationships between air and water temperatures over large regions and basins (Davies 1975; Webb and Nobilis 1995; van Vliet et al. 2011). Liu et al. (2005), for example, found positive correlations between the Lena basin mean monthly air and water temperatures during the warm season. Lammers et al. (2007), however, did not detect river temperature rising with air temperature across the Russian Arctic, and they noticed that river energy flux was not coupled closely to water temperature and discharge. They also found a significant decrease in the aggregated energy flux from the three largest Russian rivers, i.e., the Ob, Yenisey, and Lena. This result is not expected, given the recent warming trends across the Siberian region, but perhaps related with reservoir regulation in these basins, as studies show that dam regulation alters downstream discharge and water temperature regimes over Siberia (Yang et al. 2004a, b; Ye et al. 2003; Liu et al. 2005).

Due to data limitation in the northern regions, it is a challenge to investigate river thermal regimes and their changes over space and time. Yang et al. (2014) analyzed the long-term water temperature and discharge records collected near the basin outlets of the Yukon and Mackenzie Rivers, quantifying the seasonal cycles of discharge, water temperature, and heat flux for the basins. Based on future changes in air temperature and discharge, water temperature projections by models suggest a moderate increase in water temperature in the Yukon and Mackenzie River basins (van Vliet et al. 2011). Park et al. (2017) carried out water temperature and discharge simulations with an advanced LSM/hydrological model for the pan-Arctic large rivers. This chapter reviews recent work and progress on water temperature analyses and modeling over the northern regions. The main objectives are to characterize water temperature regimes for the large rivers, and to examine the relationship between water and air temperatures across the northern regions. This synthesis is useful in understanding hydrologic conditions in the northern regions. It is also important for regional hydrology and climate change investigations, including basin energy balance calculations, and atmosphere–land–water interactions.

10.2 Stream Temperature Observations and Data

Since the late 1930s hydrological observations in the Siberian regions, such as discharge, stream water temperature, river-ice thickness, dates of river freeze-up and break-up, have been carried out systematically by the Russian Hydrometeorological Services, and the observational records were quality controlled and archived by the same agency (Shiklomanov et al. 2002). According to the standard procedures for hydrometeorological observations in the former USSR (State Hydrologic Institute 1961), stream temperatures were observed at the regional hydrologic stations three times a month (10th, 20th, and 30th day), and

measurements were taken twice (at 8:00 A.M. and 8:00 P.M.) on each observation day. The observations were made near the river bank with flowing water deeper than 0.3–0.5 m. For small rivers and rivers with offshore bars, measurements were taken at a location along the deepest channel. Occasionally, two measurements were taken, respectively, near bank and at the deepest channel to ensure the consistency of observations at different locations. Stream temperature observations usually start at the beginning of spring while the rivers are ice-covered and water temperatures are close to 0 C, and observations stop in fall season 3–5 days after the rivers freeze-up. During observations, a thermometer (installed inside a cup) was placed at 0.3–0.5 m below the water surface for 5–8 min, and the cup was retrieved carefully for a quick recording of temperatures. For certain temperature readings, such as those below 2 C, a minor adjustment was applied according to the last thermometer calibration.

Quality of water temperature observations and their representativeness to mean river water temperatures are important for analyses of river thermal regime and change. Studies have shown that local conditions, such as topographic and vegetation effects, and groundwater recharge, influence temperature observations in small streams (Caissie 2006; Sinokrot and Stefan 1993). For large rivers, lateral and vertical mixing of water is often very strong particularly during the high discharge periods, and groundwater advection is relatively insignificant (Caissie 2006; Sinokrot and Stefan 1993). Although there are sometimes small vertical variations in water temperatures, water temperature observations taken near shore and near surface in large rivers are generally representative of the mean water temperature. A study in the Mackenzie basin concluded that water temperatures measured at a depth of 1 m below the water surface were reasonably representative of the flow passing the observation sites (Mackay and Mackay 1975). Water temperature data have been considered as reliable indicators of river thermal conditions, and used for determinations of river heat content over the Mackenzie basin in Canada (Mackay and Mackay 1975) and in large regions of the former USSR, including Siberia. Lammers et al. (2007) developed a river temperature data set covering 20 gauges in 17 unique Arctic Ocean drainage basins in the Russian pan-Arctic (ART-Russia). The warm (open water) season 10-day time step data (decades) were collected from Russian archival sources for the period 1929–2003, with most data falling in the range from the mid-1930s to the early 1990s.

Water temperature was not an element routinely measured in the USA and Canada hydrometric networks. Relative to the Siberian regions, water temperature observations were short and sporadic in northern Canada and USA. Kyle and Brabets (2001) produced a river temperature dataset for 32 monitoring stations in 7 unique drainage basins around Cook Inlet in Alaska. These time series cover 1 to 14 years of records in basins ranging from 1.8 to 31,000 km^2. Yang and Peterson (2017) recently compiled stream temperature data from several locations within the Yukon and Mackenzie Basins (Fig. 10.1). They also collected air temperature, streamflow, and water level data for these sites (Table 10.1). In the Yukon Basin, water temperature was monitored on the Yukon River at Carmacks, and on the Klondike River above Bonanza Creek (Brabets et al. 2000). For the Mackenzie

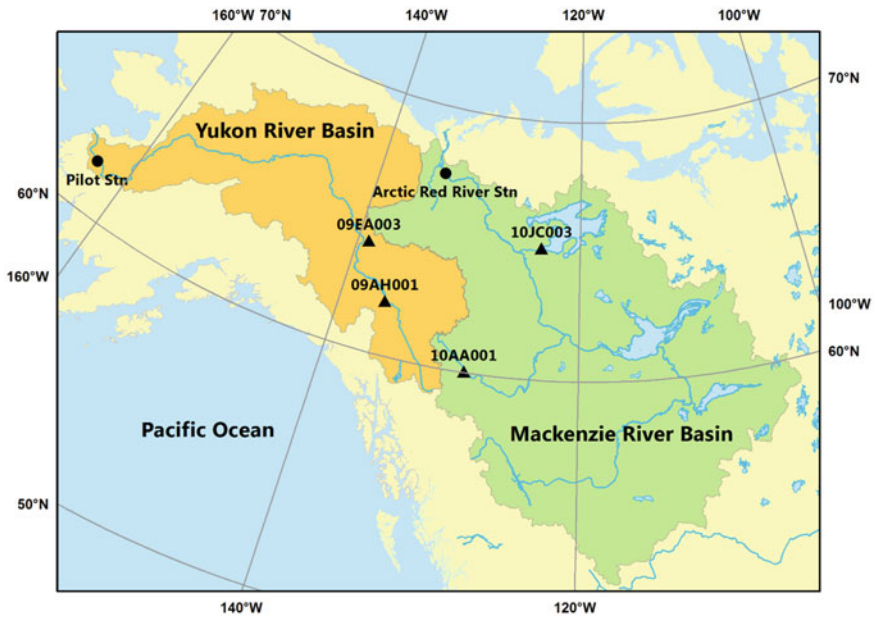

Fig. 10.1 Map of water temperature monitoring locations in Yukon and Mackenzie rivers. Triangles symbolize the four stations examined in detail for this study. The circles are stations representing outflow from the Mackenzie and Yukon River Basins (Yang et al. 2014)

Basin, water monitoring occurred on the Liard River and the Great Bear River. These monitoring locations represent two distinct types of water temperature data. The first type is high-frequency short-term data. For the Great Bear River and Klondike River, water temperatures were recorded at sub-daily intervals for 3–4 years. Water temperature data for the Great Bear River and the Klondike River were provided by the Water Survey of Canada and NWS/NOAA, respectively. The other two sites are examples of the second data type; low-frequency long-term data. Water temperature has been monitored on the Liard River and Yukon River at Carmacks on a bi-weekly (every 2 weeks) basis for decades, as part of the Pacific-Yukon Long-term Trend Monitoring (PYLTM) study. The data for these locations, as well as many others in the program, are available at http://aquatic.pyr.ec.gc.ca/webdataonlinenational/. Measurements from this program are considered to be instantaneous, and observation time in a day was also variable. Discharge and water level data for the rivers were obtained from the Canadian hydrometric database (https://wateroffice.ec.gc.ca/). Air temperature data were obtained from nearby weather stations operated by the Meteorological Service of Canada. The quality-controlled data were downloaded from the Canadian national climate archive (http://climate.weather.gc.ca/). The mean daily air temperature was determined as the average of the daily maximum and minimum temperatures.

Table 10.1 Summary of water temperature, air temperature, and flow data for each monitoring station

Stations		Water temperature			Air temperature	
Name and ID	Comments	Years	Frequency	Source	Measurement	Station and distance
Great Bear River (10JC003)	• 3 km from outlet of Great Bear Lake	2002–2003 2012–2013	Tri-hourly	WSC	Daily mean	Deline CS (15 km N)
Klondike River above Bonanza Creek (KLNQ9 & 09EA003)		2010–2012	Hourly	NWS	Daily mean	Dawson (15 km E)
Liard River at Upper Crossing (10AA001)		1991–2013	Bi-weekly 14:00 ± 4 h	PYLTM Study	Daily mean	Watson Lake (11 km NE)
Yukon River at Carmacks (09AH001)		1980–1996	Bi-weekly 13:30 ± 3 h	PYLTM Study	Daily mean	Carmacks (3 km NW)
Mackenzie River at Arctic Red River (10LC014)	• Representative of basin outflow	1950–2010	Long-term Mean monthly	Yang et al. (2014)	Climate normals 1981–2010	Fort McPherson (100 km W)
Yukon River at Pilot Station (15565447)	• Representative of basin outflow	1975–2010	Long-term Mean monthly	Yang et al. (2014)	Climate normals 1981–2010	Bethel Airport (160 km S)

10.3 Water Temperature Regimes and Changes

Water temperature data were collected mostly at different time intervals across the northern regions. This section, based on the available water temperature observations and publications, describes water temperature process over the open water season. It also defines the monthly mean water temperatures for some selected locations in the Yukon, Mackenzie, and Lena watersheds.

The Lena River has long-term (1950–1992) stream temperature, air temperature, and discharge data. These data provide good opportunity to investigate the stream temperature changes and its relationship with air temperature. The Siberian Lena River is one of the largest rivers flowing into the Arctic Ocean. It originates from the Baikal Mountains in the south central Siberian Plateau and flows northeast and north, entering into the Arctic Ocean via the Laptev Sea. It composes of three sub-basins: the Aldan tributary, the Upper Lena sub-basin, and the Vilui tributary. The Aldan tributary occupies the southeast corner of the Lena basin, close to the Pacific Ocean. The mountains and Aldan plateau that surround the Aldan valley are the water sources to the tributary. Human activities in this region are insignificant, with one dam built in 1967 in the Vilui sub-basin. The Upper Lena sub-basin covers the mountain regions in the southwest corner of the Lena catchment. It contributes 42% of the basin total flow. The Vilui tributary, located in the west Lena basin, contributes only 9% of the yearly total runoff in the Lena River.

Liu et al. (2005) described the stream temperature regimes over the various parts of the Lena watershed, and documented significant changes due to reservoir regulation and natural variations/changes. Their results revealed consistent warming trends across the entire Lena River basin in the early open water season. This may indicate a response to earlier snowmelt over the Lena River watershed. Trend results also demonstrate regional characteristics in long-term water temperature changes over the open water season. The Aldan tributary has warming (cooling) trends in the first (second) half of the open water season, leading to a stream temperature regime shift toward early open water season. The upper Lena River shows warming trends in the early open water season, and cooling trends over the mid-late season. The maximum stream temperature usually occurs on August 10 in the Upper Lena River while it is July 20 in the Aldan tributary. Liu et al. (2005) attributed this difference to the local climatic difference. Their results also showed that the stream temperatures at the Lena basin outlet are up to 8 °C colder than those over the southern sub-basins. This suggests that the latitudinal difference in climatic variables, such as air temperature, may be the major control on stream temperature regime.

Liu et al. (2005) also found that the reservoir regulation has a strong influence on the regional water temperature regime and change in the regulated sub-basin. For the downstream Vilui valley, the reservoir acts as a warm source in May and June, and a cold source in July and August. Relative to the pre-dam condition, post-dam mean water temperatures at the Suntar station have increased by 2–5 °C in the early open water season, and decreased by 2–3 °C in the mid-open water season. As a

result, the seasonal cycle of water temperature has shifted toward an earlier warm season. Generally, the water released from the reservoir has increased (reduced) the downstream water temperatures in the Vilui valley during the early (mid) open water season, and the reservoir has not significantly influenced downstream water temperatures in the late open water season, such as the Lena basin outlet (Yang et al. 2005).

It is important to point out significant variations in water temperature patterns across Siberia. Long-term data collections (1929–2003) at 20 gauges in 17 river basins in the Russian Arctic (ART-Russia) show that individual decadal temperatures ranged from 0 °C at all stations to 25.3 °C with a mean of 9.4 °C. Decadal river discharge ranged from 0 to 15.1 $km^3\ d^{-1}$ and the overall mean value was 0.32 km^3 (Lammers et al. 2007). For the Yenisey River outlet, discharge peaks first (around early June) and temperature tends to peak later, with the maximum temperature of 17 C in mid-August.

Yang and Peterson (2017) recently examined water temperature features at several locations in the Yukon and Mackenzie rivers (Fig. 10.1). Figure 10.2 shows water temperature, air temperature, and flow observations from the Klondike River, above the Bonanza Creek. This site represents a typical northern river, in terms of its seasonal dynamics. Water temperature data were collected at the Klondike River monitoring site during 2010–2012. Daily average water and air temperatures ranged from 0 to 13 °C and −47 to 21 °C, respectively. Between freeze-up in the fall and break-up in the spring, water temperature stays fairly constant at ~0 °C. After ice break-up, water temperature rises to reach a maximum around mid-summer. Water temperature then follows a decreasing trend until freeze-up. Water temperature can vary by more than a few degrees within a single day which is why hourly water temperature shows more variability than daily data. Water temperature is also much less variable than air temperature, due to its slow heating and cooling. There is a lag of about a week between water and air temperatures during break-up period. Flow rate is lowest during winter months when river is iced over, and peak flows occur due to upstream and localized ice jam/snowmelt and rainfall events. The Klondike River data also show the discharge effect on water temperature at the seasonal scale. Discharge and water level at this site are quite low. Peak annual flows ranged from 200 to 400 m^3/s; and flow was less than 50 m^3/s in the late fall and winter months. Water level ranged from 0.5 to 2.5 m. The lag between air and water temperature changes seasonally. For example, Fig. 10.2 shows that from spring to mid-summer daily air temperatures are, on average, 5 °C warmer than water temperatures, whereas from late summer to fall mean daily water and air temperatures are nearly identical. The increased response of water temperature to air temperature in the fall may be due to the shallow water level and reduced flow. Observations from Klondike River also revealed that the lag between air and water temperature changes seasonally (Fig. 10.2). For example, from spring to mid-summer daily air temperatures are on average 5 °C warmer than water temperatures, while from late summer to fall mean daily water and air temperatures are nearly identical. The increased response of water temperature to air temperature in the fall may be due to the shallow water level and reduced flow.

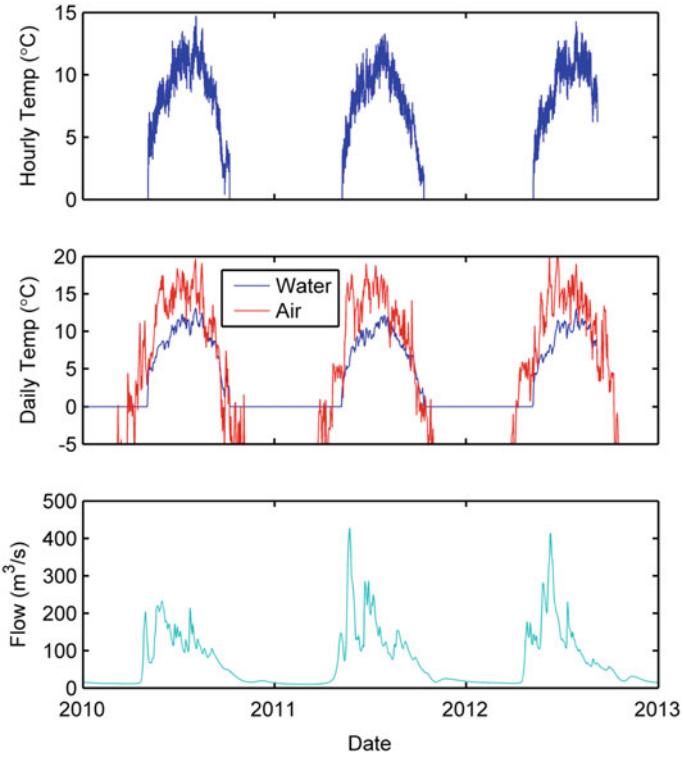

Fig. 10.2 Klondike River (09EA003) hourly water temperature, average daily air temperature, water temperature, and flow

Figure 10.3 presents the water temperature, air temperature, and discharge from the Great Bear River monitoring station. This monitoring site is unique, only 3 km downstream from an extremely large lake; Great Bear Lake (area of $\sim$31000 km^2). The lake has a strong influence on the water temperature and flow dynamics of this river, and many of its features are different from the Klondike River. Firstly, flow and water level are fairly constant throughout the year. Maximum flow was 700 m^3/s, and minimum flow was only 525 m^3/s, because water level of the lake may only change by 20–30 cm during a single year (Johnson 1975). Secondly, water temperature lags air temperature by about a month (Fig. 10.3). This is unusual for rivers and is caused, in this case, by the heat storage of the Great Bear Lake. At this location, the Great Bear River is late in breaking-up in the spring and freezing-up in the fall. Although air temperature is well below freezing in November, the river does not freeze until the temperature of the lake is reduced. Due to the size of Great Bear Lake, this process takes a considerable amount of time.

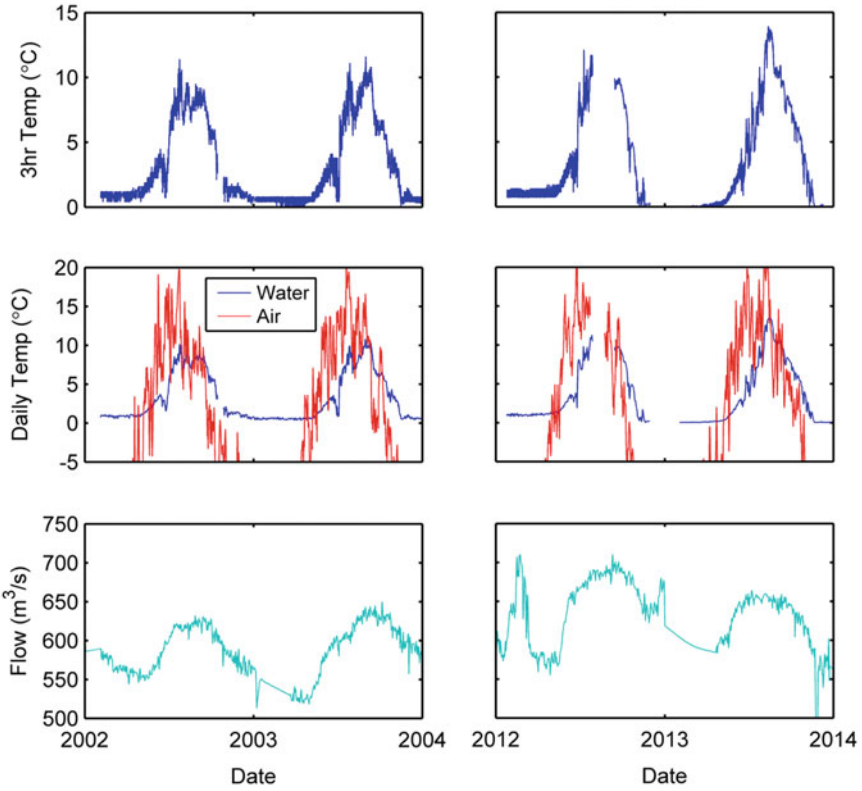

Fig. 10.3 Great Bear River (10JC003) three-hourly water temperature, average daily air temperature, water temperature, and flow

Also of interest is a water temperature drop of a few degrees near the end of June, as seen in both the daily and three hour data (Fig. 10.3). It is evident for all years in the record, but is strongest for 2002 and 2003. At this time of the year, the prevailing wind is from the east, heading toward the mouth of the river. Lake overturn may not be the cause of the temperature drop. Instead, it is more likely that lake ice is flowing down the river at this period. The melt of lake ice begins in May, but it is not until mid-July when the lake is completely ice free (Johnson 1975; Rouse et al. 2008; Kang et al. 2012). The arm of the lake with the mouth of the Great Bear River, Keith Arm, becomes ice free in late June/early July (Woo et al. 2007). This timing is consistent with the water temperature drop.

Figure 10.4 displays the data for the Liard River at Upper Crossing from 1991 to 2013. During this time, water temperature ranged from 0 to 17 °C. Air temperature generally varied from −20 to 20 °C, with the minimum and maximum of −38 °C and 25 °C, respectively. Peak discharge ranged from 1000 to 3000 m^3/s; while winter flow was about 100 m^3/s with water level ranging from 2 to 8 m. The

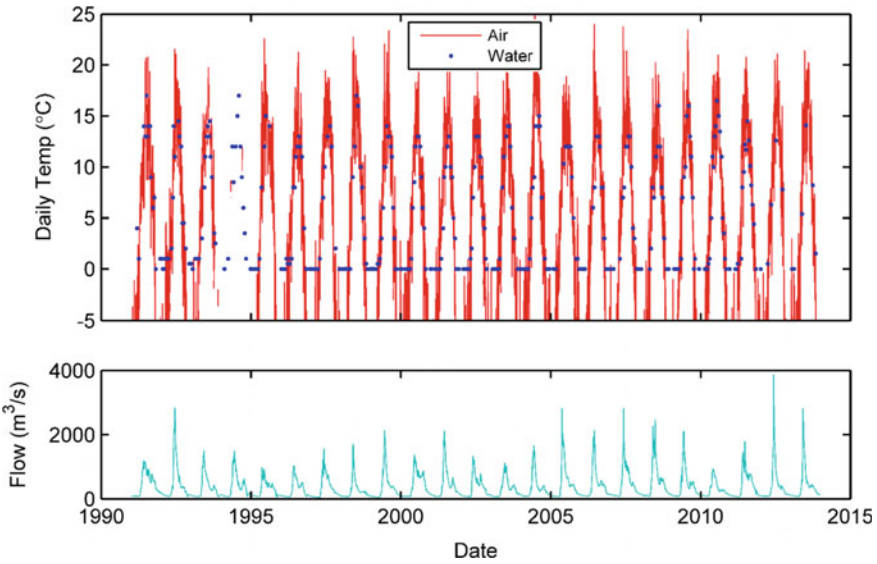

Fig. 10.4 The Liard River (10AA001) bi-weekly water and air temperatures, and average daily flow (Yang and Peterson 2017, with public sector information licensed under the Open Government Licence v3.0, http://www.nationalarchives.gov.uk/doc/open-government-licence/version/3/)

long-term records are useful to examine interannual variation and change of water and air temperatures. To reveal the details of air and water temperature relationship, a zoomed in look at the record during 2009–2011 is given in Fig. 10.5. Air and water temperatures have a larger lag in the rising limb, than the falling limb. Similar to the Klondike River, seasonal differences in flow and water depth may be responsible for this.

The data for the Yukon River at Carmacks station during 1981–1996 show water temperature ranged from 0 to 19 °C. Air temperature generally varied from −25 to 20 °C, with the minimum and maximum of −52 °C and 36 °C, respectively (Fig. 10.6). Peak flows at this location ranged from 1000 to 3000 m^3/s, with the minimum flow of 230 m^3/s. For this site, discharge does not seem to affect the water temperature and air temperature correlation.

10.4 Monthly Mean Water Temperatures for Yukon and Western Canada Rivers

Monthly mean is a standard time scale for climatic and hydrological analyses. To relate and compare water and air temperatures over the northern basins, their monthly means for the 4 sites are shown in Fig. 10.7. For the two PYLTM sites, the

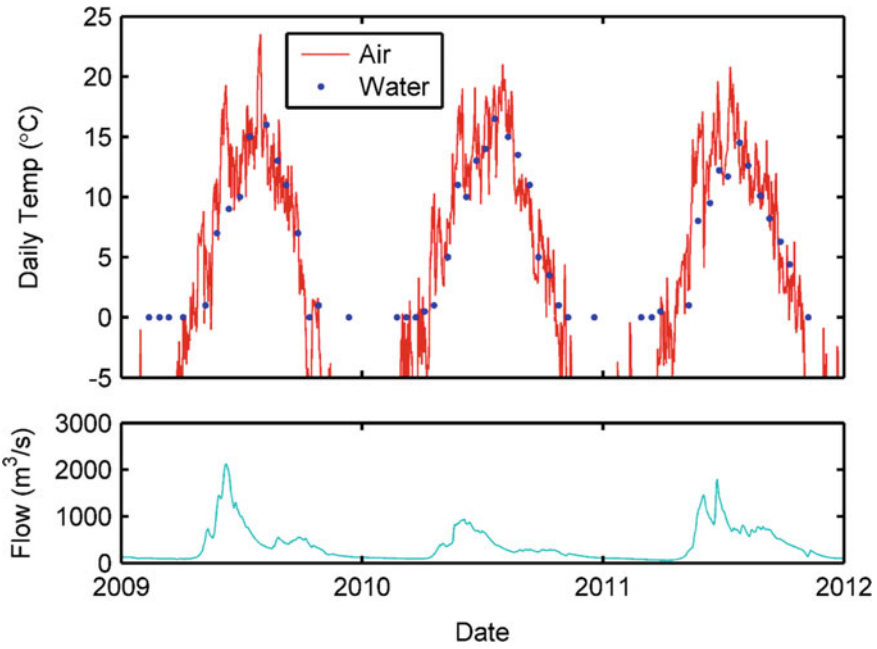

Fig. 10.5 The Liard River (10AA001) air and water temperatures and flow measurements during 2009–2011

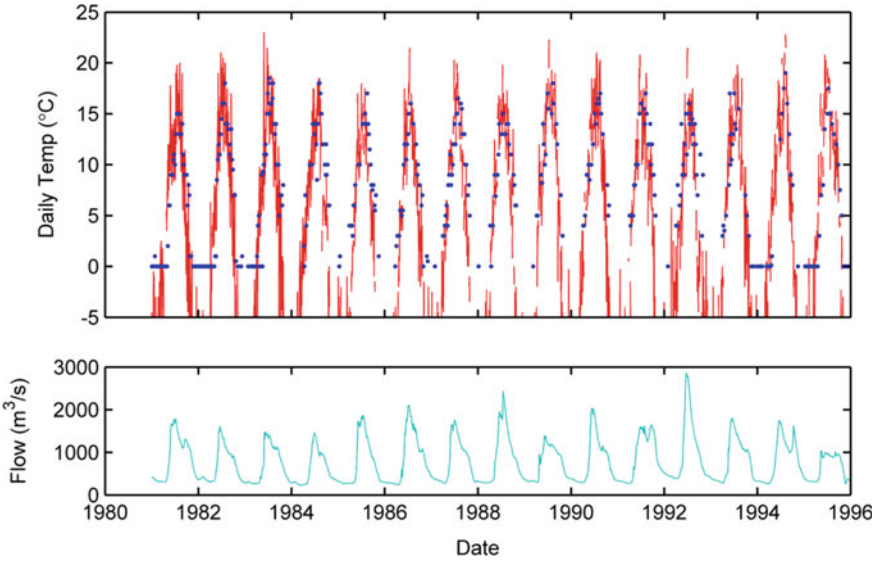

Fig. 10.6 Yukon River at Carmacks (09AH001) bi-weekly water temperature, daily air temperature, and daily flow during 1981–1996 (Yang and Peterson 2017, with public sector, information licensed under the Open Government Licence v3.0, http://www.nationalarchives.gov.uk/doc/open-government-licence/version/3/)

number of measurements used to calculate a single monthly mean ranged from 11 to 22, with the average being 17. The monthly average for the high-frequency short-term datasets was calculated using ~90 measurements. Monthly air temperature peaks in July. Water temperature also usually peaks in July, but July and August generally have similar monthly averages. A few conclusions can be made from the figure. At the monthly timescale water temperature and air temperature follow similar seasonal patterns. This suggests that air temperature has either a strong direct or indirect control on water temperature. Secondly, the larger optimum lags for the Yukon (09AH001) and Great Bear (10JC003) Rivers are evident on a monthly scale. Lastly, for the monitored sites on the Yukon (09AH001) and Liard (10AA001) Rivers, a relatively small difference is seen between monthly air and water temperatures, relative to the other two sites. It is possible that this is due to water temperature sampling frequency. Water temperature samples for these two PYLTM sites were taken at an average of 2 pm LST, with a standard deviation of 3–4 h. The majority of these samples may therefore represent water temperatures warmer than the daily average. Comparison among the datasets indicates that the spatial variability of air and water temperatures is perhaps mainly due to the differences in sampling regimes. For example, the mean July air temperature at Klondike River is the same as the Yukon River, and higher than the Liard River, even though it is located at a higher latitude. The datasets cover different and almost non-overlapping time periods. The Klondike River data covers the years 2010–2012, while the Yukon River at Carmacks and the Liard River have observations for 1980–1996 and 1991–2013, respectively.

Monthly mean water temperatures for the outlets of the Mackenzie and Yukon River Basins are presented in Fig. 10.7. The monthly means were developed from a low temporal resolution long-term data record (Yang et al. 2014). The July average water temperatures of the Yukon River at the Pilot Station and the Mackenzie River at the Arctic Red River Station were about 17 °C and 16 °C, respectively (Yang et al. 2014). At the Pilot Station monthly mean water temperature during the open water season is generally a few degrees higher than the local mean monthly air temperature. The Arctic Red River Station exhibits similar characteristics. This is different relative to the other four monitoring stations where mean water temperature is generally lower than local air temperature during the open water season (Fig. 10.7). It is important to note that the discharge at the four monitoring stations is considered low with respect to the total discharge from the Yukon and Mackenzie Basins. For example, at the Pilot Station and Arctic Red River Station, the average June flow rates are 16,000 and 20,000 m^3/s (Yang et al. 2014), respectively. Of the four stations analyzed in Yang and Peterson (2017), Yukon River at Carmacks had the highest flow with a June average of 1500 m^3/s, which only accounts for up to 10% of the outflow of the Yukon River at the Pilot Station. Discharge is strongly related to the size of the contributing area. The Pilot Station and Arctic Red River Station have large contributing areas, with all water from the Yukon and Mackenzie basins exiting through these two channels. Relative to these two stations, the four monitoring locations examined by Yang and Peterson (2017), had small contributing areas. In case of big rivers and high discharge, such as those near the

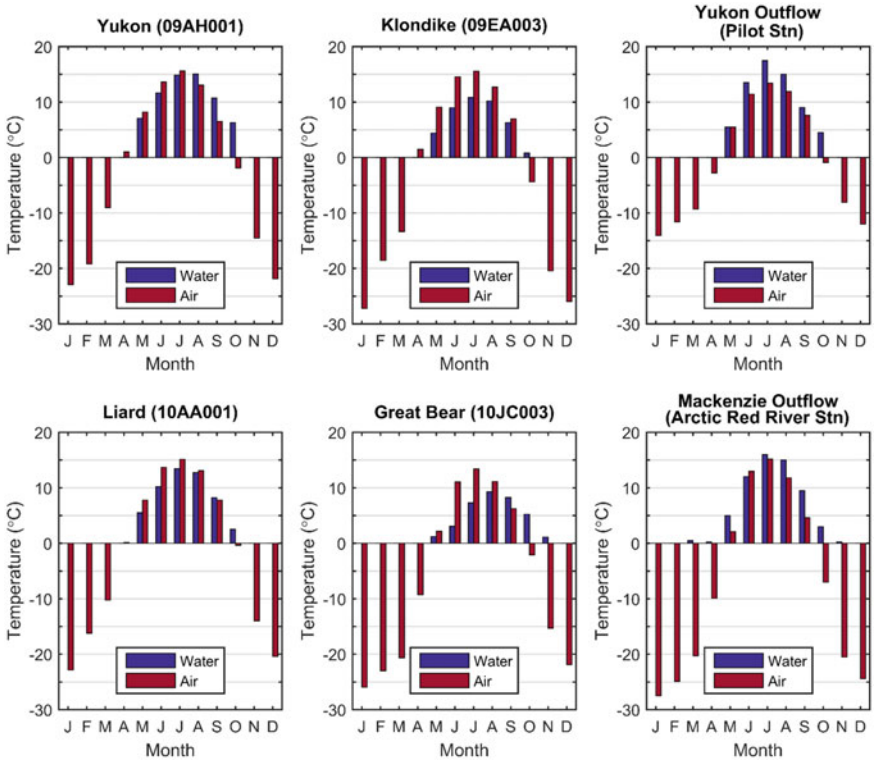

Fig. 10.7 Comparison of mean monthly air and water temperatures for the monitoring sites, arranged into Yukon (top) and Mackenzie (bottom) River Basin from most upstream (left) to most downstream (right). The monthly means for the outlet stations are also provided (Yang et al. 2014)

outlets of large basins, local air temperature may not be a good predictor for water temperatures. The use of air/water temperatures of upstream tributaries may be a potential consideration for estimating water temperatures at the Pilot Station or Arctic Red River Station.

The water temperatures from the Pilot Station and Arctic Red River Station are significantly warmer than the upstream stations. The spatial variability of water temperature over the Lena River Basin in Siberia shows water temperature at the basin outlet to be several degrees cooler than the upstream sub-basins (Liu et al. 2005). Water temperature data in Russia are long term and more consistent in terms of monitoring duration and frequency than the sites in Canada, and the pattern of water temperature decreasing with latitude toward the basin outlet was observed. The quality and frequency of water temperature measurements across the Yukon and Mackenzie watersheds have been inconsistent, which may have led to the different results from other studies for Siberia. In addition, water temperature over the Mackenzie and Yukon basins are monitored by several different agencies for

various purposes, and therefore lack the benefits of a unified network. In particular, the time of the measurement, frequency, and monitoring duration is not consistent among the sites. Measurement depth and position from shore are also likely not consistent, and may contribute to the variation in results.

10.5 Water Temperature Models and Analyses

There are different approaches to examine water and air temperatures relationship over the northern regions, including statistical regression and physically based models. In terms of regression analyses, the water temperature (Tw) observations can be fit with three different models using air temperature (T_A) and discharge (Q) as input variables. The first model is a simple linear regression equation:

$$T_w = m \cdot T_A + n \cdot Q + b; \tag{10.1}$$

where m, n, and b are fitted coefficients. Air temperature and discharge are considered in this model, as a comprehensive study of river water temperatures (van Vliet et al. 2011) found, for a sample size of 157 monitoring stations from all over the globe, 87% of water temperature estimates were improved by considering discharge in addition to air temperature.

The second method is a nonlinear regression model (Mohseni et al. 1998), where water temperature is estimated as an s-shape function of air temperature. This function was modified by van Vliet et al. (2011) to include discharge data. The equation is given as:

$$T_w = \mu + \frac{\alpha - \mu}{1 + \exp(\gamma(\beta - T_A)} + \frac{n}{Q}; \gamma = \frac{4 \cdot \tan\theta}{\alpha - \mu}; \tag{10.2}$$

where μ and α are the lower and upper bound of water temperature, respectively; θ is the angle at the inflection point; β is the air temperature at the inflection point; and n is a fitted coefficient. The lag time between air and water temperatures needs to be considered. The Pearson correlation coefficient (R) can be used to evaluate the strength of the linear association and determine the optimum time lag in days. The regression models (Eqs. 10.1–10.2) can be used if only air temperature data are available, i.e., by removing any terms containing Q. The regression equations (Eqs. 10.1–10.2) are purely statistical. Although these models may be able to simulate past water temperatures, they are not physically based. Because of this, their suitability for estimating water temperature into the future, particularly under a changing climate, is questioned (Toffolon and Piccolroaz 2015).

The third model is the air2stream model (Toffolon and Piccolroaz 2015). This method is considered to be a physically based model that uses calibrated parameters. The full equation of the model, utilizing both air temperature and discharge data, is:

$$\frac{dT_w}{dt} = \frac{1}{\delta}\left\{a_1 + a_2 \cdot T_A - a_3 \cdot T_w + \theta\left[a_5 + a_6 \cdot \cos\left(2\pi\left(\frac{t}{t_y} - a_7\right)\right) - a_8 T_w\right]\right\};$$
$$\delta = \theta^{a_4}; \theta = \frac{Q}{Q}; \tag{10.3}$$

where $a_1 - a_8$ are calibrated coefficients, t is time, and t_y the number of time units in a year. The five parameter version utilizing only air temperature measurements is given as:

$$\frac{dT_w}{dt} = a_1 + a_2 T_A - a_3 T_w + a_6 \cos\left[2\pi\left(\frac{t}{t_y} - a_7\right)\right] \tag{10.4}$$

The fourth model is the process model based on the heat exchange at the air–water interface, simultaneously considering the inflow of heat and water from upstream or tributaries (van Vliet et al. 2011; Park et al. 2017). The surface water energy balance is described as

$$\rho C_p \frac{\partial(T_w A)}{\partial t} = \Phi w_x + \rho C_p Q_{trb} \frac{\partial T_{trb}}{\partial x} \tag{10.5}$$

where ρ is the density of water (kg m^{-3}), C_p is the specific heat capacity of water (J kg^{-1} $°C^{-1}$), A is the cross-sectional area of the river at distance x (m^2), Φ is the heat flux at the air–water interface (J m^{-2} s^{-1}), w_x is stream width at distance x (m), Q_{trb} is the discharge from tributaries or upstream (m^3 s^{-1}), ΔT_{trb} is the difference in temperature from tributaries or upstream, and t is time (s). The net heat flux at the air–water interface is calculated as the summation of the different heat flux components (Wunderlich and Gras 1967) as:

$$\Phi = (\Phi_s - \Phi_{rs}) + (\Phi_a - \Phi_{ar}) + \Phi_{\text{evap}} + \Phi_{\text{cond}} + \Phi_{\text{back}} \tag{10.6}$$

where Φ_s is shortwave solar radiation (J m^{-2} s^{-1}), Φ_{rs} is reflected shortwave radiation (J m^{-2} s^{-1}), Φ_a is longwave atmospheric radiation (J m^{-2} s^{-1}), Φ_{ar} is reflected atmospheric radiation (J m^{-2} s^{-1}), Φ_{evap} is evaporative heat flux (J m^{-2} s^{-1}), Φ_{cond} is the conductive or convective heat flux (J m^{-2} s^{-1}), and Φ_{back} is blackbody radiation from the water surface (J m^{-2} s^{-1}). To calculate Φ_{rs}, we assumed that the albedo of open water is 0.12, and that of ice cover is 0.8. This treatment was possible because the model included the snow effect on the change in ice thickness (Park et al. 2017).

Model performance can be evaluated by the root mean square error (RMSE) and Nash-Sutcliffe efficiency (NSE). The RMSE, also referred to as the standard deviation of errors, quantifies the spread of data from the estimated values. For a normally distributed dataset, 68% of the errors are within ± RMSE. The NSE is a measure of the predictive power of a model. A NSE of 1 indicates a perfect match

between the modeled and observed data, while a negative NSE means the average observed value is a better estimate than the model.

Liu et al. (2005) found a strong positive correlation between the basin mean monthly air and water temperatures during the warm season for the Lena River. Yang and Peterson (2017) report a linear association between air and water temperatures for different lag times (Fig. 10.8) for Yukon and Mackenzie rivers. The Klondike and Great Bear River show two very different patterns. The correlation between water and lagged air temperature quickly decreases as lags longer than 1 d are considered for the Klondike River. The Great Bear River has the opposite pattern where the correlation starts low, but as longer lags are considered increases. The optimum lag of 40 d for the Great Bear River site is synonymous with Fig. 10.3, which shows a large consistent lag for the entire open water season. The data for the Klondike River shows differences in lag that are dependent on season. However, when considering all the open water data, the optimum lag is 1 d. For the Yukon and Liard Rivers, the optimum lag times were 14 d and 1 d, respectively. For these low-frequency long-term datasets, the relationship between correlation and lag time is seen to be very noisy (Fig. 10.8). The Klondike and Great Bear monitoring sites, which are the high-frequency short-term datasets, show a smooth relationship. The differences are likely due to sampling frequency. In particular, the low-frequency long-term datasets had fewer data points available to be used in determining optimum lag, and the instantaneous measurements were not always collected at the same time each day.

Scatterplots of water temperature versus optimally lagged air temperature are shown in Fig. 10.9. Water temperature measurements from the two PYLTM sites fall along distinct lines, indicating a resolution of 1 °C. The high-frequency

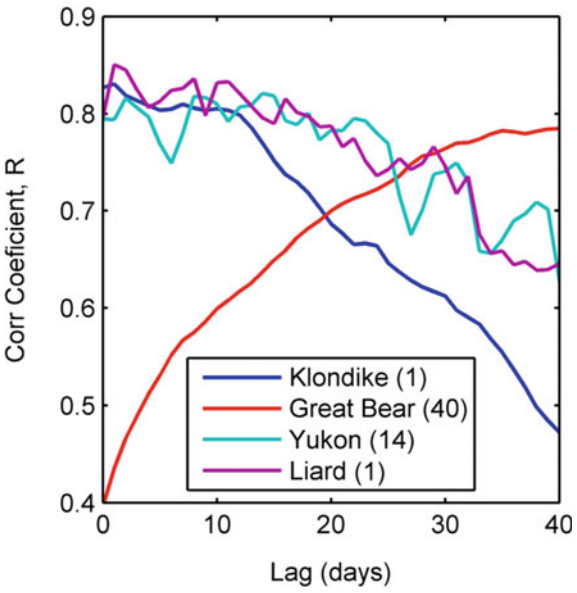

Fig. 10.8 Linear correlation between air and water temperature during open water season. The optimum lag time is given in brackets

datasets, although over a short time period, still provide more water temperature measurements than those from long-term low-frequency measurements of the PYLTM study. The relationship between water temperature and air temperature follows a linear trend at three of the four monitoring sites examined. The Great Bear River shows a curved trend. Low water temperatures in May–June, represent the period where the Great Bear River is ice free, but the lake remains frozen. When water temperature for this period is compared against a lagged air temperature of 40 d, poor correlation is seen (Fig. 10.9); flat relationship for lagged air temperatures of <0 °C). Correlation for Great Bear River is stronger during the other open water months when lagged air temperature is >0 °C.

Yang and Peterson (2017) tested water temperature models at four monitoring stations in Yukon and west Canada. The results show that the air2stream model (Toffolon and Piccolroaz 2015) generally gave a superior fit, over the s-shape and linear regression models. The inclusion of discharge data into the water temperature

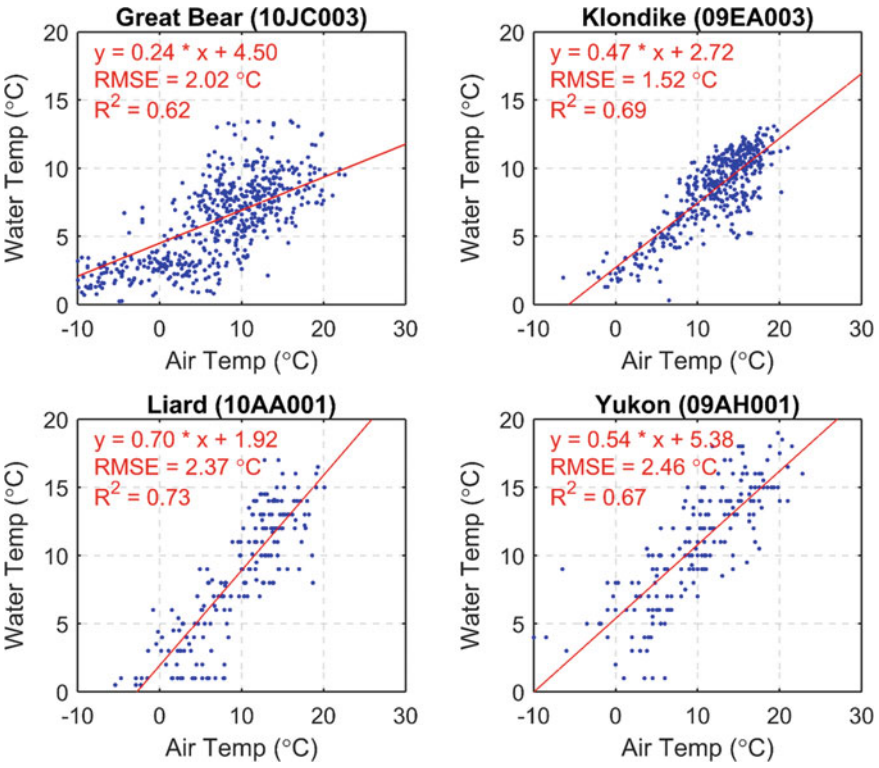

Fig. 10.9 Linear relationship between air and water temperatures at the optimum lag for the four monitoring stations (Yang and Peterson 2017, with public sector information licensed under the Open Government Licence v3.0, http://www.nationalarchives.gov.uk/doc/open-government-licence/version/3/)

models was also examined. The results were found to be improved through the inclusion of discharge data. However, the improvement was often small (difference in RMSE <0.15 °C) and only air temperature data may be necessary. Of all four sites, water temperature estimates for the Klondike River were improved most by the inclusion of discharge data. This is expected, as the correlation between water and air temperature change was seasonally affected by discharge variations.

The water temperature models provided the best fit to water temperature observations from the Klondike River (RMSE = 1.13 °C; NSE = 0.91). Great Bear River had the second best performance metrics (RMSE = 1.37 °C; NSE = 0.81), followed by the Liard River (RMSE = 1.69 °C; NSE = 0.84), and Yukon River (RMSE = 2.10 °C; NSE = 0.82). The differences in performance among the sites may be due to a number of factors. Important considerations are the length of the monitoring period and the water temperature sampling regime. The Klondike River and Great Bear River monitoring stations were high-frequency short-term datasets. These contained 3–4 years of water temperature observations. Longer time periods may show larger variations in river flow, as well as air and water temperature. Sampling regimes for the Klondike River and Great Bear River were 1 h and 3 h, respectively. The Liard River and Yukon River locations had low-frequency long-term datasets, having an instantaneous measurement once in every 2 weeks for 15–20 years. An average of the sub-daily data likely provides a more representative daily average water temperature, as opposed to the instantaneous measurements from the PYLTM study.

It is important to note that the linear regression model cannot be used to predict water temperature in the winter. In particular, only the s-shape and air2stream models are able to predict a winter water temperature of 0 °C. In this study water temperature was modeled from air temperature and flow data. Accuracy of water temperature estimates may also be improved by considering seasonally based relationships. It can be seen from the Klondike River data (Fig. 10.2) that under lower discharge rates during late summer/fall, water temperature is similar to air temperature. The relationship between water temperature and air temperature shows seasonal hysteresis. This is most visible in the Great Bear River data, although also evident for the PYLTM monitoring sites.

A water temperature model based on the surface water energy exchange simulated water temperature in the Arctic rivers for many years (Park et al. 2017). Figure 10.10 compares seasonal and interannual variations in simulated T_w and observations at the mouths of the four major Arctic rivers; the model results indicated a good performance, realistically simulating both the seasonal variation in the rising and falling limbs of T_w at most stations and the T_w variability among years. In particular, the modeling framework that included river-ice processes captured the timing of the start ($T_w \geqq 0$ °C) and end ($T_w < 0$ °C) of the river-ice cover quite well. However, the model slightly overestimated early spring T_w in most river basins. In nature, broken river ice gradually melts in spring as it flows down the river. This increases both albedo and latent heat, causing T_w to rise later in the spring than in rivers without an ice pack. The model assumed that the broken ice immediately melts; this assumption was likely associated with the overestimation.

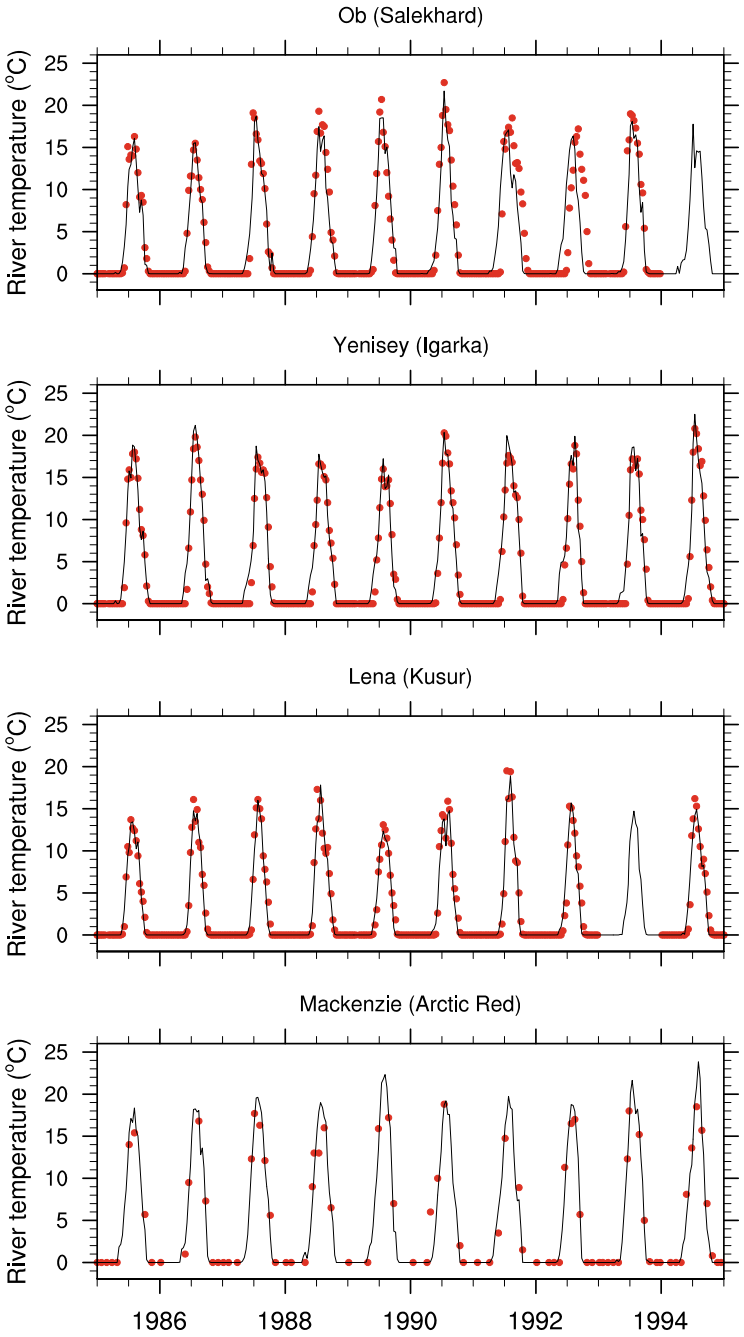

Fig. 10.10 Comparison of modeled river water temperature (lines) against observations (dots) recorded at the outlet stations of the major Arctic river basins. The simulation results displayed here were averaged over 10 days, corresponding to the observation records (Park et al. 2017). ©American Meteorological Society. Used with permission

The inclusion of both surface energy exchanges and heat advection from upstream or tributaries through the river network resulted in a significant improvement in model simulation of the timing and magnitude of the peak summer temperature (Fig. 10.10). The model raised summer temperature by about 1–6 °C relative to previous results that did not consider the impacts of heat exchange and advection (Park et al. 2016). A noticeable rise in temperature was also found along the falling limb of T_w at all stations (Fig. 10.10). The improvement in model performance was reflected by the comparisons of statistical values to the previous CHANGE model results; root mean square error (RMSE) and mean bias (BIAS) for all stations were smaller, while the correlation coefficients were larger than the previous model values (Park et al. 2016). For example, the absolute BIAS for all stations was less than 1 °C, which was comparable to the absolute values of 0.2 ∼ 2.4 °C at key stations for three Siberian rivers (Ob, Yenisey Olenek) documented by van Vliet et al. (2011). Furthermore, the improved model simulation was demonstrated using the Nash coefficient (NASH) to test the bias in modeled T_w, with all stations having values greater than 0.85, which exceeded the previous values in Park et al. (2016), indicating very good simulations. On the other hand, the simulated summer maximum T_w for the Arctic Red station of the Mackenzie River was slightly higher than observations (Fig. 10.10). This station collected relatively few observations around the summer peaks, which may be one cause of the overestimation.

To examine the changes in water temperature over the arctic basins, the CHANGE simulated daily T_w at all Arctic river mouths was averaged by the flow volume weighting of individual river basins over an annual scale (Park et al. 2017). Figure 10.11 displays the time series of annual anomalies in T_w, and the integrated Q and averaged T_a for the period 1979–2013. Water temperature measured at the river mouths reflects the aggregated influences on the river thermal regime of topography, meteorology, and hydrology within the basin. Therefore, T_a was averaged for the entire grid of the Arctic rivers. T_w increased (0.16 °C dec^{-1}, $p < 0.001$), as did T_a (0.45 °C dec^{-1}, $p < 0.001$), over the period 1979–2013. Relatively stronger increases in T_w were apparent after 2000 when the warming in the model forcing T_a data was very large. Annual T_w anomalies showed interannual variations similar to T_a over the study period ($r = 0.69$, $p < 0.001$), while the correlation between T_w and Q was lower ($r = 0.20$, $p > 0.1$). These correlation statistics indicate the major influence of T_a on the interannual variations of T_w. The lower correlation between T_w and Q does not mean that the influence of Q on T_w was trivial. The increase in Q has the reverse impact on T_w due to the high heat capacity of water, reducing the relative contribution of T_a to T_w.

The trends in annual mean T_w and T_a, and total Q, over the Arctic sea drainage regions are compared in Table 10.2 (Park et al. 2017). Statistically significant increases of T_w ($p < 0.01$) were found in Eurasian basins (i.e., Barents, Kara, Laptev, and East Siberia), which was consistent with the significant warming of T_a ($p < 0.02$). Q also increased in all Eurasian basins, except for the Barents. The increase in Q was significant in early spring (Holmes et al. 2015) when T_a remains around the freezing point, thereby lowering the negative impact of Q on T_w.

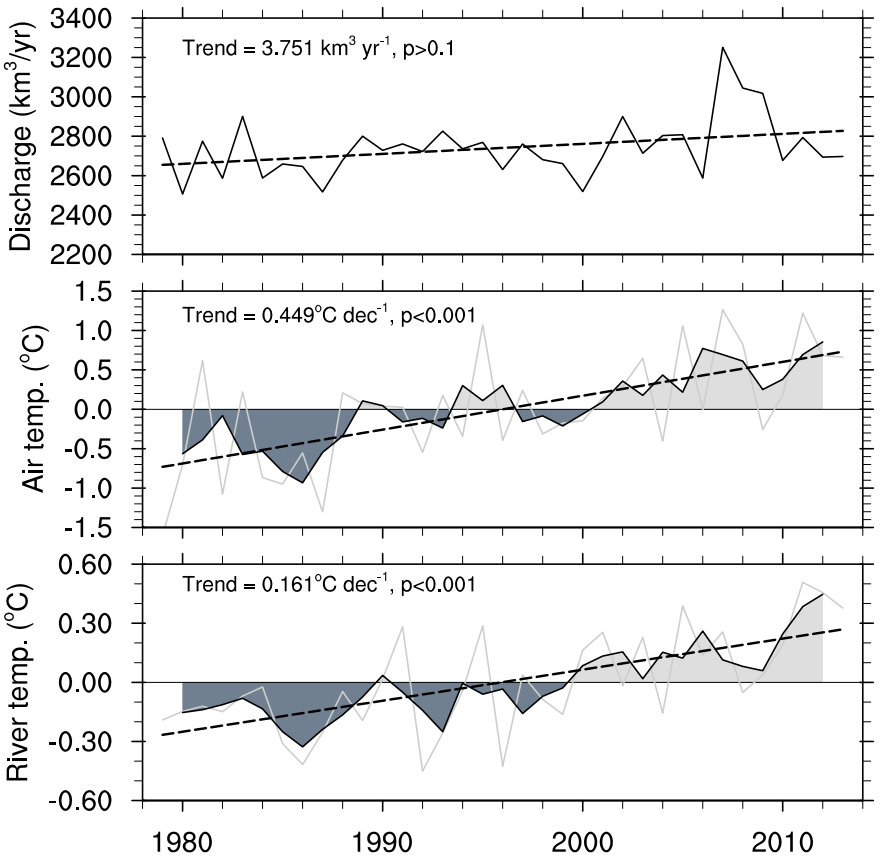

Fig. 10.11 Interannual variability and trend (dashed lines) in (top) annual total discharge, (middle) annual air temperature anomaly averaged over the pan-Arctic mainland, and (bottom) annual average river temperature at the outlets of Arctic rivers. In the middle and bottom, the dark lines represent 3-yr running means of the annual anomalies (light gray lines) of the variables (Park et al. 2017). ©American Meteorological Society. Used with permission

CHANGE model estimated positive T_w trends (0.15 $\sim$ 0.22 °C dec^{-1}) for the four Eurasian basins, which were comparable to the T_w trends ranging from −0.31 to +0.22 °C dec^{-1} derived from observations during 1929–2003 at 20 river mouths of Eurasian basins (Lammers et al. 2007). Although the comparisons include different data period and regions/basins, the trends in T_w estimated by CHANGE model strongly suggest a link with the warming T_a during the recent decade. The T_w trends in the North American basins, including the Chukchi basin, were low relative to the Eurasian basins. However, unexpected T_w cooling (−0.01 °C dec^{-1}, $p > 0.1$) was found in the Beaufort basin (Table 10.2), which deviated from the T_a warming (0.33 °C dec^{-1}, $p < 0.03$). Intermittently larger negative T_a anomalies appeared in

Table 10.2 Trend values of annual mean water temperature and air temperature and annual discharge in each river sea basin defined in Fig. 10.1 during the study period of 1979–2013. The annual mean water temperature was averaged by the flow volume weighting of rivers within individual sea basins. Variable p represents the probability value of the trend

Sea basin	Water temperature		Air temperature		Discharge	
	Trend (°C decade^{-1})	P	Trend (°C decade^{-1})	P	Trend (km^3 decade^{-1})	P
Barents	0.22	<0.005	0.49	<0.004	−0.33	>0.100
Kara	0.16	<0.005	0.40	<0.020	13.47	>0.100
Laptev	0.20	<0.001	0.48	<0.002	17.92	<0.050
East Siberia	0.15	<0.003	0.48	<0.001	8.17	<0.050
Chukchi	0.04	>0.100	0.29	<0.050	2.45	>0.100
Beaufort	0.01	>0.100	0.33	<0.030	1.35	>0.100
Archipelago	0.06	>0.100	0.74	<0.001	5.92	>0.100

spring and summer during 1999–2010 over the Beaufort basin (Park et al. 2017). Considering the strong sensitivity of T_w to T_a (Yang and Peterson 2017), it is possible that the spring and summer T_a anomalies likely account for some portion of the negative T_w trend.

10.6 Summary and Future Needs

In the Lena basin, water temperature conditions are similar over the Aldan and upper Lena regions. However, stream temperatures at the Lena basin outlet are up to 8 C colder than those over the southern sub-basins. This suggests the latitudinal difference in climatic variables, such as air temperature, as a major control on stream temperature regime. Warming in stream temperatures has been discovered at the Lena basin outlet during the early and mid-June. River discharge also increased in this peak flow period (Ye et al. 2003). As a result, the heat flux has increased in June by 23% over the Lena basin.

Water temperature data across the Mackenzie and Yukon River basins are lacking, particularly in terms of high resolution, long-term records. Limited data collections were available for 2 sites (Klondike River and Great Bear River) with high resolution, short-term data, i.e., sub-daily water temperature records for a few years. The Klondike River had a water temperature regime typical of low flow northern rivers, and demonstrated how seasonal flow patterns may impact air temperature–water temperature correlations. The water temperature regime of the Great Bear River monitoring location was strongly influenced by the heat storage of Great Bear Lake, representing an example of strong upstream (lake) control. Water temperature measured during the PYLTM program contained low resolution, long-term records, i.e., bi-weekly measurements over decades. The data at these sites generally captured the annual water temperature cycle, and appeared to match

air temperature well. However, it was found that the instantaneous water temperature measurements may not represent the daily average.

The characteristics of the two different datasets strongly influenced data analysis and model performance. The association between water and air temperatures for each monitoring site was investigated. Uncertainty in the correlation between air–water temperature and lag time was seen for the low-frequency, long-term datasets, but not the high-frequency, short-term datasets. Comparison of the water temperature regimes (monthly means) among sites indicate that due to different data periods, it is not easy to develop clear conclusions of the spatial variability of water temperature over large basin. The performances of several water temperature models were examined using air temperature and flow data as inputs. Model performance was slightly improved by including discharge. The best fits were found for the high-frequency, short-term datasets. The Air2stream, the physically based model with calibrated parameters, performed better than the statistical regression models. The CHANGE model can simulate large basin water temperature patterns over the arctic regions as a whole. With this capability, it might be possible to reconstruct the water temperature records for the northern rivers without past observations.

Water temperature is very important to many applications and relatively easy to measure. Unfortunately water temperature has not been systematically observed at the northern operational and research networks in Canada and USA. In the Mackenzie and Yukon rivers, water temperature data were traditionally taken in conjunction with water/sediment samples. Water temperature over the Mackenzie and Yukon basins have been monitored by several different agencies for various purposes, and therefore lack the benefits of a unified network. In particular, the time of the measurement, frequency, and monitoring duration were not consistent among sites. Measurement depth and position from shore were also most likely not consistent. Water temperature directly impacts many aspects of basin hydrology and ecology. In a warming climate over the high latitudes, there is an urgent need to improve water temperature observations in the northern regions. One option is to explore the use of remote sensing of river (Cherkauer et al. 2005, Handcock et al. 2006) and lake (Bussières and Schertzer 2003) temperatures in combination with near real time in situ data acquisition in the high-latitude watersheds.

References

Brabets TP, Wang B, Meade RH (2000) Environmental and hydrologic overview of the Yukon River Basin, Alaska and Canada. U.S. Geological Survey Water-Resources Investigations Report 99–4204, 106 pp

Bussières N, Schertzer WM (2003) The evolution of AVHRR-derived water temperature over lakes in the Mackenzie Basin and hydrometeorological applications. J Hydrometeorol 4:660–672

Caissie D (2006) The thermal regime of rivers: a review. Freshw Biol 51(8):1389–1406. https://doi.org/10.1111/j.1365-2427.2006.01597.x

Cherkauer KA, Burges SJ, Handcock RN, Kay JE, Kampf SK, Gillespie AR (2005) Assessing satellite-based and aircraft-based thermal infrared remote sensing for monitoring Pacific Northwest River temperature. J Am Water Resour Assoc 41(5):1149–1159

Costart F, Dupeyrat L, Gautier E, Carry-Gailhardis E (2003) Fluvial thermal erosion investigation along a rapid eroding river bank: application to the Lena river (central Siberia). Earth Surf Proc Land 29:1349–1359. https://doi.org/10.1002/esp.592

Davies KF (1975) Mackenzie river input to the Beaufort Sea, Water Survey of Canada. Beaufort Sea technical report #15. Department of the Environment, Calgary, pp 38–62

Handcock RN, Gillespie AR, Cherkauer KA, Kay JE, Burges SJ, Kampf SK (2006) Accuracy and uncertainty of thermal-infrared remote sensing of stream temperatures at multiple spatial scales. Remote Sens Environ 100:427–440

Holmes RM, Shiklomanov AI, Tank SE, McClelland JW, Tretiakov M (2015) River discharge. Arctic Report Card 2015. In: Jeffries MO, Richter-Menge J, Overland JE (eds) NOAA Tech. Doc., 60–65. Available online at ftp://ftp.oar.noaa.gov/arctic/documents/ArcticReportCard_full_report2015.pdf

Johnson L (1975) Physical and chemical characteristics of Great Bear Lake, Northwest territories. J Fish Res Board Can 32:1971–1987

Kang KK, Duguay CR, Howell SEL (2012) Estimating ice phenology on large northern lakes from AMSR-E: algorithm development and application to Great Bear Lake and Great Slave Lake, Canada. Cryosphere 6:235–254. https://doi.org/10.5194/tc-6-235-2012

King TV, Neilson BT, Overbeck LD, Kane DL (2016) Water temperature controls in low arctic rivers. Water Resour Res 52(6):4358–4376

Kyle RE, Brabets TP (2001) Water temperature of streams in Cook Inlet Basin, Alaska, and implications for climate change. U.S. geological survey water resource investment report 01-4109, 24 pp

Lammers RB, Pundsack JW, Shiklomanov AI (2007) Variability in river temperature, discharge, and energy flux from the Russian pan-Arctic landmass. J Geophys Res 112:G04S59. http://dx.doi.org/10.1029/2006JG000370

Liu B, Yang D, Ye B, Berezovskaya S (2005) Long-term open water season stream temperature variations and changes over Lena river basin in Siberia. Glob Planet Change 48(1–3):96–111. https://doi.org/10.1016/j.gloplacha.2004.12.007

Lowney CL (2000) Stream temperature variation in regulated rivers: evidence for a spatial pattern in daily minimum and maximum magnitudes. Water Resour Res 36(10):2947–2955. https://doi.org/10.1029/2000WR900142

Mackay JR, Mackay DK (1975) Heat energy of the Mackenzie river. In: Further hydrologic studies in the Mackenzie valley, Canada (Environmental-Social Committee Northern Pipelines). Task force on northern oil development report, Ottawa, Information Canada, pp 1–23

Marsh P, Prowse TD (1987) Water temperature and heat flux at the base of river ice covers. Cold Reg Sci Technol 14:33–50

Mohseni O, Stefan HG, Erickson TR (1998) A nonlinear regression model for weekly stream temperatures. Water Resour Res 35(12):3723–3733. https://doi.org/10.1029/98WR01877

Park H, Yoshikawa Y, Oshima K, Kim Y, Ngo-Duc T, Kimball JS, Yang D (2016) Quantification of warming climate-induced changes in terrestrial Arctic river ice thickness and phenology. J Clim 29(5):1733–1754. https://doi.org/10.1175/jcli-d-15-0569.1

Park H, Yoshikawa Y, Yang D, Oshima K (2017) Warming water in Arctic terrestrial rivers under climate change. J Hydrometeorol 18(7):1983–1995. https://doi.org/10.1175/jhm-d-16-0260.1

Rouse WR, Blanken PD, Bussières N, Oswald CJ, Schertzer WM, Spence C, Walker AE (2008) An investigation of the thermal and energy balance regimes of Great Slave and Great Bear Lakes. J Hydrometeorol 9:1318–1333. https://doi.org/10.1175/2008JHM977.1

Shiklomanov AI, Lammers RB, Vorosmarty CJ (2002) Widespread decline in hydrological monitoring threatens pan-Arctic research. EOS Trans AGU 83(2):13–17

Sinokrot BA, Stefan HG (1993) Stream temperature dynamics: measurement and modeling. Water Resour Res 29(7):2299–2312. https://doi.org/10.1029/93WR00540

State Hydrologic Institute (1961) Recommendation on methods of compiling data on water resources, vol. 9, Thermal and Ice Conditions on Rivers (in Russian), St. Petersburg, 207 pp
Toffolon M, Piccolroaz S (2015) A hybrid model for river water temperature as a function of air temperature and discharge. Environ Res Lett 10:114011. https://doi.org/10.1088/1748-9326/10/11/114011
van Vliet MT, Ludwig HF, Zwolsman JJG, Weedon GP, Kabat P (2011) Global river temperatures and sensitivity to atmospheric warming and changes in river flow. Water Resour Res 47: W02544. http://dx.doi.org/10.1029/2010WR009198
Webb BE, Nobilis F (1995) Long term water temperature trends in Austrian rivers. Hydrol Sci J 40 (1):83–96. https://doi.org/10.1080/02626669509491392
Woo MK, Modeste P, Martz L, Blondin J, Kochtubajda B, Tutcho D, Gyakum J et al (2007) Science meets traditional knowledge: water and climate in the Sahtu (Great Bear Lake) Region, Northwest Territories, Canada. Arctic 60(1):37–46
Wunderlich WO, Gras R (1967) Heat and mass transfer between a water surface and the atmosphere. . Water Resources Research Laboratory Rep. 14, Tennessee Valley Authority, 270 pp
Yang D, Peterson A (2017) Water temperature characteristics and relationship with air temperature, Northern Canadian rivers. Arctic 70(1):47–58
Yang D, Ye B, Kane D (2004a) Streamflow changes over Siberian Yenisei River Basin. J Hydrol 296(1–4):59–80. https://doi.org/10.1016/j.jhydrol.2004.03.017
Yang D, Ye B, Shiklomanov A (2004b) Discharge characteristics and changes over the Ob river watershed in Siberia. J Hydrometeorol 5:595–610
Yang D, Liu B, Ye B (2005) Stream temperature changes over Lena River Basin in Siberia. Geophys Res Lett 32:L05401. https://doi.org/10.1029/2004GL021568
Yang D, Marsh P, Ge S (2014) Heat flux calculations for Mackenzie and Yukon Rivers. Polar Sci 8:232–241. https://doi.org/10.1016/j.polar.2014.05.001
Ye B, Yang D, Kane D (2003) Changes in Lena River streamflow hydrology: human impacts versus natural variations. Water Resour Res 39(7):1200. http://dx.doi.org/10.1029/2003WR001991

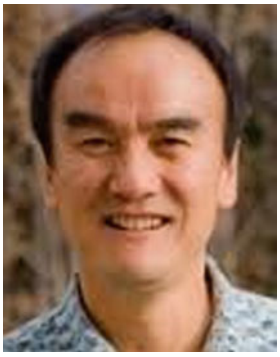

Dr. Daqing Yang is a Research Scientist at the Watershed Hydrology and Ecology Research Division, Environment and Climate Change Canada. He is also Affiliate Research Professor at the International Arctic Research Center, Univ. of Alaska Fairbanks. Over the past 25 years, he has conducted cryosphere system research in China, Canada, Japan, USA, and Norway. His primary research activities/interests include cold region hydrology and climate, particularly Arctic large river streamflow regime and change, snow cover and snowfall measurements, climate change and human impact to regional hydrology, and applications of remote sensing in cold regions. He has served as journal editor and subject editor for IAHS publications (cold region hydrology, northern research basin water balance, and cold/mountain region hydrological systems under climate change), and WMO technical reports (solid precipitation measurement intercomparison and integrated global observing strategy cryosphere theme). He also contributed as review and/or author to the IPCC Reports, and the Arctic Council's Snow, Water, Ice and Permafrost in the Arctic (SWIPA 2017 and follow up) assessment. His current research focuses on investigating the impacts of climate variability/change and human activities on hydrologic system across the broader northern regions.

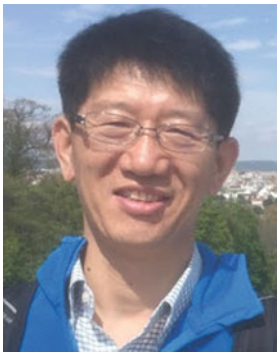

Dr. Hotaek Park is a Senior Scientist at JAMSTEC. He earned his Ph.D. at Graduate School of Bioagricultural Sciences, Nagoya University in 2000. Then, he worked at two Japanese Institutes as postdoctoral fellowship and joined the position of JAMSTEC research scientist in 2007. He is an expert on hydrology, biogeochemistry, and climate researches in cold regions, with interests in evaluating changes in land surface processes under climate changes and predicting future changes using land surface model, remote sensing data, reanalysis products, in site observations, and model outputs. He is the author/co-author of numerous scientific articles that have published on a variety of peer-reviewed journals, conference proceedings, and books. His recent research is focused on assessing impacts of changing snow and permafrost on hydrological processes in the context of climate variability and interactions between declining Arctic sea ice and terrestrial ecohydrologic processes coupling models of land–atmosphere–ocean processes.

Ms. Amber Peterson is the Data Manager for the Global Institute for Water Security at the University of Saskatchewan. She received an M.Sc. in Civil Engineering from the University of Saskatchewan and participated in Environment Canada's Federal Student Work Experience Program. Her research interests include soil moisture variability and scaling, modeling cold regions hydrology, and data management.

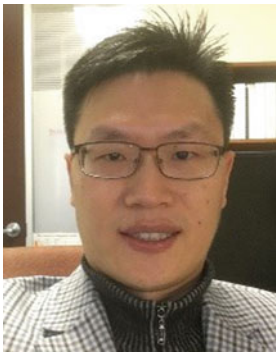

Mr. Baozhong Liu is a PE in Petroleum Engineer registered in Texas and living in Houston TX. He has earned a master's degree in Hydrology during his graduate studies with Dr. Daqing Yang as his academic advisor, and he also earned a master's degree in Petroleum Engineering, both from the University of Alaska Fairbanks (UAF) in 2001–2007. During his graduate studies in hydrology, he focused on investigating the impact of reservoir regulation on the downstream water temperature in the Lena River basin. He published three journal papers with the help of Dr. Yang. After his graduation from the UAF in 2007, he has been working in the oil and gas industry, with a focus on the development of unconventional resources in the Permian Basin, which employs horizontal drilling and hydraulic fracturing as major technologies. He is a member of Society of Petroleum Evaluation Engineers (SPEE). He is still interested in hydrology, i.e., to investigate the usage and cycling of water used in the oil and gas industry.

11 Changing Biogeochemical Cycles of Organic Carbon, Nitrogen, Phosphorus, and Trace Elements in Arctic Rivers

Jonathan O'Donnell, Thomas Douglas, Amanda Barker, and Laodong Guo

Abstract

Streams and rivers are critical components of Arctic watersheds, functioning as corridors for the movement of water, carbon, and other solutes from headwater streams to larger rivers, estuaries, and the Arctic Ocean. Recent climate change in the Arctic has altered stream and river discharge, temperature, and biogeochemical processes. In this chapter, we summarize the state of research linking watershed hydrology and biogeochemical cycling in Arctic rivers, and how these processes are changing in response to changing climate and disturbance regimes (e.g., permafrost thaw, wildfire). The chapter is divided into three main sections. First, we examine hydrologic controls on stream and river chemistry, including the roles of spring snowmelt and subsurface hydrology as mediated by permafrost characteristics. Second, we summarize recent findings from the literature that describe biogeochemical processes in Arctic rivers, with particular focus on the cycling of organic carbon, nitrogen and phosphorus species, and a suite of trace elements. Third, we identify

J. O'Donnell (✉)
National Park Service, Arctic Network, Anchorage, AK, USA
e-mail: jaodonnell@nps.gov

T. Douglas
U.S. Army Cold Regions Research and Engineering Laboratory, Fort Wainwright, AK, USA
e-mail: Tom.Douglas@erdc.dren.mil

A. Barker
U.S. Army Cold Regions Research and Engineering Laboratory, Fort Wainwright, AK, USA
e-mail: amanda.j.barker@usace.army.mil

L. Guo
School of Freshwater Sciences, University of Wisconsin-Milwaukee, Milwaukee, WI, USA
e-mail: guol@uwm.edu

D. Yang and D. L. Kane (eds.), *Arctic Hydrology, Permafrost and Ecosystems*,
https://doi.org/10.1007/978-3-030-50930-9_11

uncertainties and current gaps in our knowledge of biogeochemical processes in Arctic rivers and recommend steps forward to address these uncertainties.

11.1 Introduction

The Arctic region is characterized by extreme climatologic and physiographic conditions not found elsewhere on Earth (Hinzman et al. 2005). Air temperatures can vary as much as 70 °C between winter and summer and sunlight shifts from total darkness to continuous sunlight. Air temperatures in the Arctic are warming at a faster rate than temperate and tropical regions at lower latitudes and much research is focused on the responses of Arctic systems to this rapid warming and associated changing seasonality (Larsen et al. 2014). Of particular concern is the response of Arctic ecosystems to changing disturbance regimes, including changing hydrology and increasing river discharge, wildfire frequency and severity, and permafrost thaw (Turetsky et al. 2011; Schuur et al. 2015; Walvoord and Kurylyk 2016). Warming and disturbance can alter biogeochemical cycles in both terrestrial and aquatic ecosystems. Recent research has focused on biogeochemical feedbacks from terrestrial ecosystems to the atmosphere and climate system (e.g., Schuur et al. 2015), but there is also considerable interest in the response of aquatic ecosystems to changing conditions in the Arctic, including streams and rivers draining high-latitude watersheds (e.g., Vonk et al. 2015a).

Arctic rivers and streams are important corridors for the movement of water, carbon (C), other nutrients, and a variety of other solutes from headwater streams to larger rivers, estuaries, and ultimately, the Arctic Ocean. The chemical composition of streams and rivers in the Arctic varies considerably across space and time, as dictated by a variety of factors including landscape characteristics (vegetation, lithology), watershed hydrology, latitudes, and in-stream processes (Guo et al. 2004a; Neff et al. 2006; Holmes et al. 2012; Douglas et al. 2013; Pokrovsky et al. 2016, 2018). Arctic river chemistry typically exhibits strong seasonal patterns, with significant differences observed between the peak flows of spring snowmelt and base flow conditions during summer and winter (e.g., Finlay et al. 2006; Guo et al. 2012). Recent work has documented long-term changes in Arctic stream and river chemistry over the past 40–50 years, indicating climate and landscape change may be altering the concentration and flux of various solutes, although specific pathways and mechanisms are not well understood and could be seemingly contradictory (Frey and Smith 2005; Striegl et al. 2005; Toohey et al. 2016; Lung et al. 2018). Given the rapid pace of change in the Arctic, many uncertainties remain regarding the dynamics and trajectory of river chemistry and biogeochemical processes (McGuire et al. 2009).

In this chapter, we summarize riverine sources and transport of chemical species and their biogeochemical processes in Arctic watersheds with a focus on the major biogeochemical compounds of greatest impact in watershed processes. These

include dissolved organic carbon (DOC), nutrients (nitrogen (N) and phosphorus (P)), dissolved silica, and selected trace elements (iron, strontium, uranium, and mercury). We review recent findings from the literature that document how the cycling of these constituents are changing in response to climate change and disturbance in the Arctic and identify knowledge gaps that limit our ability to project how river biogeochemical cycles will be affected in a warmer future.

11.2 Hydrologic Controls on Arctic River Biogeochemistry

11.2.1 Spring Melt Runoff Processes as Major Drivers of Arctic Watershed Biogeochemistry

One unique aspect of Arctic watersheds is the spring snowmelt runoff (freshet). In a short time window in May or June (often in less than 2 weeks), much of the yearly surface water discharge runs from the land through river channels to the sea (Kane et al. 1989; McNamara et al. 1997, 2008; Bowling et al. 2003; Holmes et al. 2012). A white, snow-covered landscape is converted rapidly to a brown and eventually green one (Fig. 11.1). During the spring snowmelt period, discharge is often at peak yearly values and there is a significant dilution of river solutes, yet stream water concentrations of dissolved organic C (DOC) and other nutrients like ammonium (NH_4^+), phosphate (PO_4^{3-}), and nitrate (NO_3^-) reach their highest levels of the year due to hydrologic "flushing" (e.g., Hornberger et al. 1994; Finlay et al. 2006; Raymond et al. 2007; Cai et al. 2008a, b; Guo et al. 2004a, 2012; Douglas et al. 2013).

The snowmelt period is dynamic across a range of spatial scales. For instance, at the macro-scale, the timing of peak snowmelt varies longitudinally within a watershed, with the lower reaches of the river snow-free by mid-June and starting to Greenup, while headwater reaches are still snow-covered and just beginning to melt (Fig. 11.2). As a result, the timing of melt-driven changes in stream and river chemistry varies within an individual watershed. At the micro-scale, carbon (C), nutrients, major elements, and trace metals in the snowpack become constituents in meltwater. An "ionic pulse" of solutes moves downward into the pool at the base of the snowpack (Tranter et al. 1986; Rember and Trefry 2004; Douglas et al. 2017). Elevated solute concentrations before snowmelt are partially caused by ion exclusion from the quasi-liquid water layer, a disordered microthin layer on snow grain surfaces (Dominé and Shepson 2002). As snow and ice crystals approach 0 °C the snow grains start to metamorphose into rounded melt grain clusters. Larger molecules or ions (like sulfate (SO_4^{2-}) and some metals) present as impurities on the snow or ice crystal surface undergo preferential elution compared to smaller ions like chloride (Cragin and McGilvary 1995). As a consequence, DOC, SO_4^{2-}, NO_3^-, lead (Pb), and mercury (Hg) concentrations in the early pulse of snowmelt water that moves across the landscape typically exceed bulk snowpack values (Williams and Melack 1991; Douglas et al. 2017). Though vegetation, soils, and atmospheric deposition are the dominant sources of nutrients, major ions, and trace

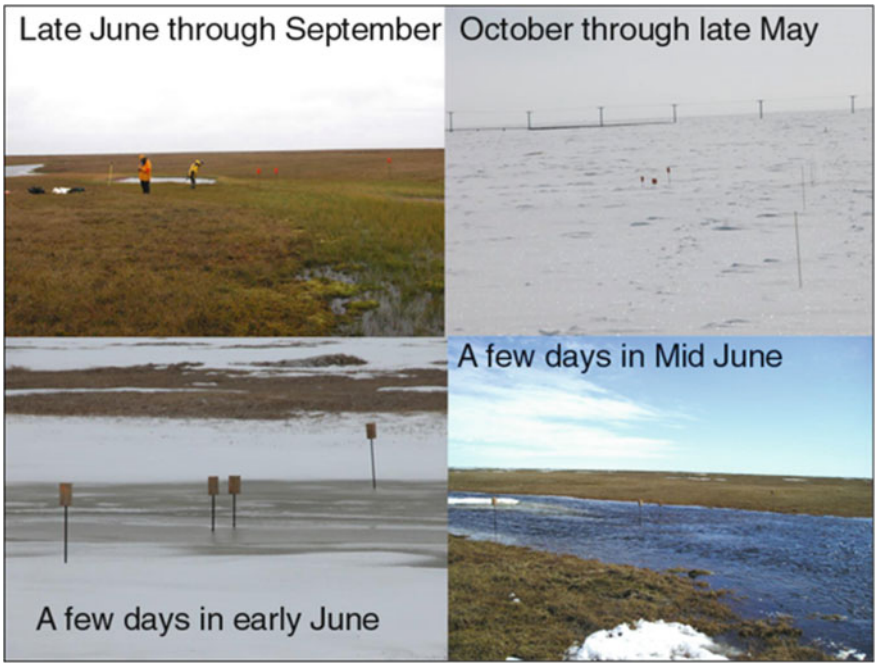

Fig. 11.1 Photographs of a small watershed near Utqiaġvik, Alaska, representing the major seasons and seasonal transitions in Arctic watersheds. Most of the Arctic is snow-covered for up to 8 months of the year. The spring melt period includes a dramatic flux of surface water and biogeochemical compounds that is active for only a few weeks. Photos by T. Douglas

metals in river waters (Rember and Trefry 2004; Cai et al. 2008a; Barker et al. 2014) the snowpack is a source of some chemical species (e.g., Pb, SO_4^{2-}; Douglas and Sturm 2004).

In most Arctic locations, the surface soils of the seasonally thawed active layer are frozen during spring melt, which limits infiltration of snowmelt water into surface soils depending on the previous year's soil moisture and snow water equivalent (Gray et al. 2001), in addition to a variety of other factors including the presence of preferential pathways (Stähl et al. 2004), soil aggregates (Koren et al. 1999), and abundance of air-filled macropores (Niu and Yang 2006). Where permafrost is present, soils and bedrock can be frozen to a depth of up to 300 m. As such, groundwater discharge to surface waters is negligible during snowmelt and the nutrient load in runoff is predominantly controlled by the vegetation cover and soil type (Judd and Kling 2002; Hobbie and Gough 2004). Decaying plant litter and shallow organic-soil horizons at the base of the snowpack are the major sources of DOC and nutrients to river flows during this period (Fig. 11.3). Snowmelt has been found to contain up to 60% of the annual DOC export from major Arctic rivers (Guo et al. 2007; Raymond et al. 2007). This C, leached from vegetation and

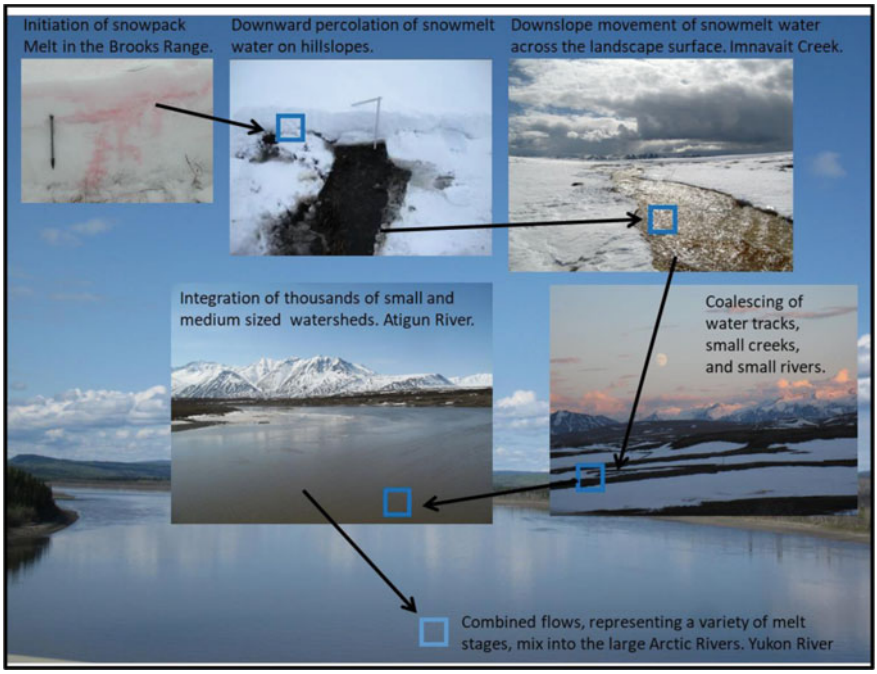

Fig. 11.2 A series of photos, taken within 2 days of one another, exhibiting the different scales and the delayed timing of spring melt across a broad geographical range. Each blue box represents a hydrologic source to the larger system it feeds. Note that in the upstream mountains and on hillslopes snowmelt is just starting while lower elevation small streams are beginning to flow and reach a peak discharge and, at the regional scale, the Yukon River (large background photo) is snow and ice-free and has initiated Greenup. Photos by T. Douglas

surface organic-soil layers, is of the modern age (Neff et al. 2006; Guo and Macdonald 2006) and close to a third of the DOC pool may be biologically labile (Holmes et al. 2008) and over 90% of chromophoric DOM can be photochemically degraded (e.g., Cory et al. 2014) although only a small fraction of soil organic C can be leached out during permafrost thaw (Xu et al. 2009; Gao et al. 2018).

11.2.2 Seasonally Frozen Ground and Permafrost as Controls on Arctic River Biogeochemistry

As noted above, many Arctic watersheds are underlain by permafrost, earth material such as soil, organic matter, or bedrock that has remained below 0 °C for at least two consecutive years. In most cases, permafrost has remained frozen for hundreds to thousands of years. However, recent warming in the Arctic has caused permafrost to warm and thaw (Jorgenson et al. 2006; Romanovsky et al. 2010). This has important consequences for watershed hydrology and the chemical composition

Fig. 11.3 Photos of Imnavait Creek north of the Brooks Range in the Alaskan Arctic during peak spring melt flow (left) and in early fall (right). Note the dark brown color of the water during spring melt which is attributable to the heavy load of particulate organic C, decayed vegetation, and mineral particles. For most of the year, this watershed is a small trickle roughly a few meters wide (fall photo). Photos by T. Douglas

of rivers (Frey and McClelland 2009; Walvoord et al. 2012). Permafrost properties, including thermal and hydraulic characteristics, are important for controlling depth and velocity of subsurface flow paths that contribute to streamflow. The active layer is the shallow surface vegetation and soil above the permafrost that thaws and refreezes on an annual basis (Fig. 11.4). Seasonally thawing of the active layer governs depths of subsurface flow paths during the summer (i.e., the supra-permafrost aquifer; Lamontagne-Halle et al. 2018) and consequently influences leaching and mobilization of solutes from soil horizons.

In the continuous permafrost zone (>90% of the land area underlain by permafrost), groundwater discharge from deep, sub-permafrost aquifers to surface waters is limited (Fig. 11.5). In this area, the permafrost is hundreds of meters thick. By contrast, in the discontinuous permafrost zone to the south (50–90% of the land area underlain by permafrost) the permafrost is warmer and less thick (10–100 m), groundwater discharge is higher and can comprise a larger fraction of river discharge (Walvoord and Striegl 2007). Within the discontinuous zone, slope and aspect can drive the spatial extent of permafrost with north-facing slopes and valley bottoms underlain by permafrost and south-facing slopes and ridge tops are often permafrost-free. Headwater catchments that vary with permafrost extent also exhibit striking variations in discharge patterns and chemical composition (Maclean et al. 1999). The hydrologic mixing of waters from shallow supra-permafrost and deep sub-permafrost aquifers is a key determinant of spatial and temporal variability in stream water chemistry (O'Donnell et al. 2012, 2016). Thermokarst, or the subsidence of the ground surface following the thawing of ice-rich permafrost (Loranty et al. 2018), can also alter stream and river chemistry (Bowden et al. 2008). However, yields and fluxes of C, nutrients, and trace elements via lateral transport from soils to streams, rivers, and the Arctic Ocean during permafrost thaw and coastal erosion are poorly understood although laboratory studies have mimicked

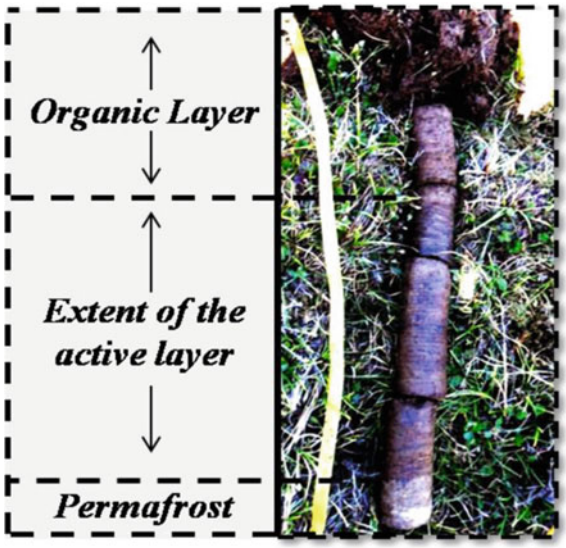

Fig. 11.4 The surface vegetation (dark brown mass) in an 80-cm-long SIPRE core collected in early spring. Note the lighter colored material toward the base of the core. This region, comprised of small (1–2 cm) layers of transition zone ice, is the boundary between the seasonally thawed active layer and the top of the near-surface permafrost. Photos by A.J. Barker

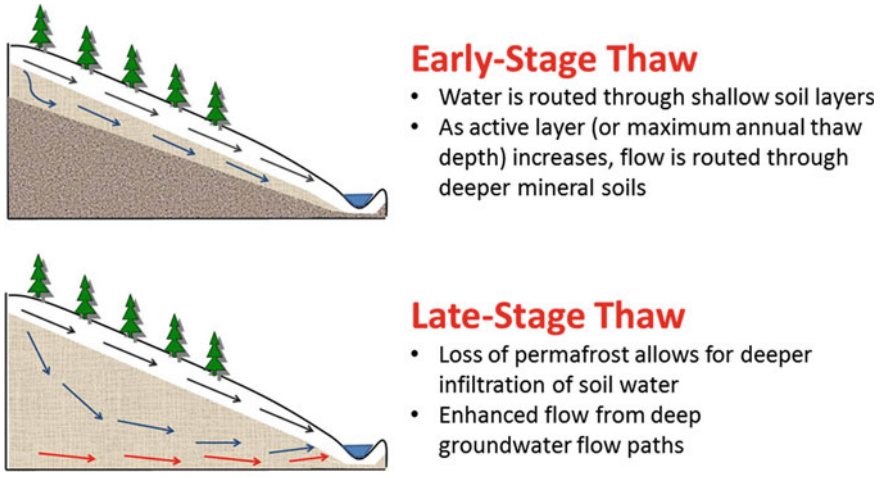

Fig. 11.5 A conceptual model of subsurface hydrologic change associated with thawing permafrost (adapted from Walvoord and Kurylyk 2016)

the permafrost–water interactions and quantified their yields and fluxes of C and nutrients (Dou et al. 2008; Xu et al. 2009; Gao et al. 2018). Much uncertainty exists regarding the effects of permafrost thaw on river chemistry under a warming climate (Liao and Zhuang 2017). Recent findings on this topic are highlighted below.

11.3 Major Chemical Species/Components in the Arctic Stream and River Waters

11.3.1 Dissolved Organic Carbon

DOC is a critical component of aquatic ecosystems and the Arctic C cycle as it functions to regulate water quality and nutrient availability and serves as a substrate for microbially mediated reactions (Cole et al. 2007; Tranvik et al. 2009). DOC can also influence photochemical reactions and interactions with trace metals and organic pollutants, altering their fate, transport, and bioavailability/toxicity (Chin et al. 1997; Aiken et al. 2011; Philippe and Schaumann 2014). Increases in DOC concentration have contributed to the browning of surface waters in some high-latitude regions (Roulet and Moore 2006), affecting the photic zone and rates of primary productivity. In the Arctic, DOC in rivers is sensitive to watershed hydrology (Striegl et al. 2005; O'Donnell et al. 2010, 2012), permafrost presence (Maclean et al. 1999; Frey and McClelland 2009; Olefeldt et al. 2014), active layer thickness (O'Donnell et al. 2016; Harms et al. 2016), wetland extent, and permafrost soil properties (O'Donnell et al. 2016).

Soils of the northern circumpolar permafrost region store approximately 1300 petagrams (Pg) of organic C (Hugelius et al. 2014). As a result, high-latitude rivers tend to have higher DOC concentrations (Finlay et al. 2006) than temperate or tropical rivers (Hope et al. 1994). Regardless of sources, the flux of C in Arctic rivers represents an important component of the high-latitude C budget (McGuire et al. 2009), and the magnitude of this flux is expected to change under projected warming and disturbance scenarios (Frey and Smith 2005; Striegl et al. 2005; Kicklighter et al. 2013). Moreover, inland waters can release C to the atmosphere through microbial and photochemical processes (Kling et al. 1991; Cory et al. 2014), which can function as a positive feedback to the climate system. By incorporating DOC into terrestrial ecosystem and earth system models, it is possible to better constrain C sources and sinks in the Arctic and globally (Kicklighter et al. 2013; Wu et al. 2014).

DOC in rivers is chemically complex, reflecting a broad gradient of compounds ranging in molecular size, structure, and decomposability/reactivity (Xu and Guo 2017). Scientists have developed a variety of analytical techniques to characterize the composition and reactivity of dissolved organic matter (DOM), including bulk measurements of concentration (DOC, dissolved organic N (DON)), optical measurements (ultraviolet (UV)–visible absorbance and fluorescence), chemical fractionation, and high-resolution mass spectroscopy (e.g., FTICR-MS) among others.

In the Arctic rivers, DOM composition varies across space and time, as determined by hydrology and landscape features. Most rivers are dominated by hydrophobic organic acids (e.g., humic and fulvic acids) during the open-water period, which tends to be highly aromatic compounds derived from organic-rich wetland soils (Striegl et al. 2005; Spencer et al. 2008; O'Donnell et al. 2010). During winter or in groundwater-dominated systems, DOM is comprised primarily of low-molecular weight aliphatic compounds and tends to more N-rich (O'Donnell et al. 2012). DOM composition reflects and integrates processing in both the terrestrial (e.g., microbial transformation, sorption to mineral soils) and aquatic ecosystems (e.g., photo-oxidation), and is closely linked to its bio-lability (Holmes et al. 2008). In general, DOM lability is higher in high-latitude rivers than other biomes and tends to decrease with increasing stream size or order (Vonk et al. 2015b). In addition, DOM liability is highly related to chemical composition, molecular size, and specific degradation pathways (e.g., photochemical vs biological degradation; Xu and Guo 2018).

In the Arctic, the majority of riverine DOC is derived from terrestrial sources (Wauthy et al. 2018). The decomposition of plant litter, organic soils, and mineral-associated soil organic matter can drive production of DOC, which is then, transported from terrestrial to aquatic ecosystems through runoff and subsurface flow paths. Recent work has also documented the importance of permafrost thaw on the delivery of ancient DOC to river networks (e.g., Spencer et al. 2015). However, DOC transported in Arctic rivers is mostly contemporary, especially the high-molecular weight (>1 lDa) DOC fraction (Benner et al. 2004; Guo and Macdonald 2006; Raymond et al. 2007) or much younger than both particulate organic C (POC) pool and river sediment (Guo et al. 2007). This indicates riverine DOC derived from old permafrost soil is limited although pre-aged POC derived from permafrost has been measured in Arctic rivers (Guo et al. 2004a, b, 2007). In addition, the ^{14}C ages among DOC, POC, and river sediment changed across different rivers and sampling season, and the relative contributions of DOC from modern primary production and ancient soil organic C also varied with rivers (Fig. 11.6). Young DOC but extremely old POC observed in Arctic rivers are consistent with the experimental results that only a small fraction (<2%) of permafrost TOC is water-soluble and can be released into the DOC pool during permafrost interactions with aquatic environments (Guo et al. 2007; Dou et al. 2008; Xu et al. 2009; Gao et al. 2018).

Given the large stores of permafrost OC in the Arctic terrestrial ecosystem, warming and thawing could potentially release significant amounts of DOC into Arctic waterways should permafrost soils be thawed and flushed into aquatic environments even though only a small fraction of total soil organic C can be released into water-extractable phase (Xu et al. 2009; Gao et al. 2018). Within the soil-derived DOC pool, the aromatic components can be readily decomposed photochemically (Cory et al. 2014) while bio-labile organic acids (e.g., acetate, Ewing et al. 2015) and other carbohydrates and protein-like components can be rapidly degraded microbially regardless of their radiocarbon (^{14}C) ages (Vonk et al. 2013, 2015b; Xu and Guo 2018; Gao et al. 2018). Evidence from ^{14}C

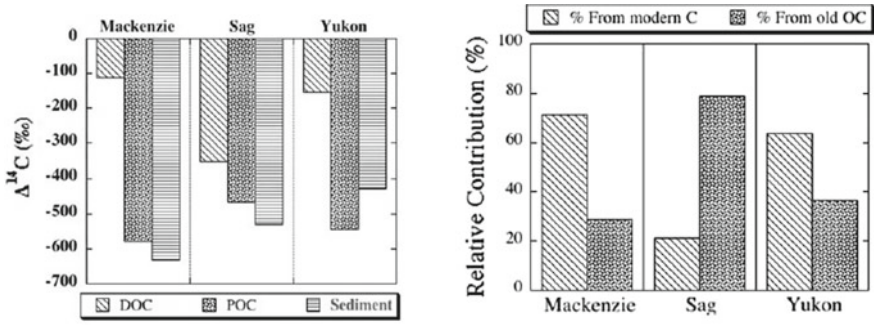

Fig. 11.6 Changes in $\Delta^{14}C$ values (or ^{14}C ages) among DOC, POC and river sedimentary organic carbon pool in the Mackenzie, Sag (Sagavanirktok) and Yukon Rivers (left panel) and relative contributions of DOC from modern primary production and ancient soil organic C in different Arctic rivers, including the Mackenzie, Sagavanirktok (Sag), and Yukon Rivers (right panel, from Guo et al. 2007)

measurements indicates permafrost-derived old DOC is not an important component of the DOC pool in higher order rivers (Guo and Macdonald 2006; Guo et al. 2007; Raymond et al. 2007; O'Donnell et al. 2014; Aiken et al. 2014). This is consistent with the consistently low DOC yields of soil-OC in different aged permafrost (up to 16,000 years BP) from northern Alaska (Guo et al. 2007; Dou et al. 2008; Xu et al. 2009; Gao et al. 2018). Therefore, DOC in Arctic rivers should be mostly derived from surface soil and contemporary terrestrial primary production enhanced by warming, and autochthonous sources of DOC to rivers, include stream periphyton, are generally a minor component of DOC pool in Arctic watersheds (e.g., Mann et al. 2015). However, the contribution of autochthonous DOC to Arctic rivers can be greatly underestimated due to its ^{14}C reservoir effect or old dissolved inorganic C (DIC) ^{14}C ages (Guo et al., *unpublished data*).

DOC concentration and DOM composition vary across watersheds that differ with respect to landscape and subsurface properties. In the Yukon River basin of Alaska and Canada, DOC concentration and flux vary among watersheds according to watershed hydrogeologic characteristics and source water contribution to streamflow (Striegl et al. 2007; O'Donnell et al. 2010). Blackwater streams (i.e., streams dominated by hydrologic and C inputs from wetlands) have high DOC concentrations relative to glacially fed or groundwater-dominated streams. Further, blackwater streams tend to have higher concentrations of aromatic DOM (i.e., high specific ultraviolet absorbance, or $SUVA_{254}$; Weishaar et al. 2003) compared to glacially fed or groundwater-dominated streams which tend to have higher concentrations of low-molecular weight organic acids and aliphatic compounds. Permafrost thermal state (e.g., ground temperatures, rates and timing of seasonal thaw, and active layer thickness) and hydraulic properties (e.g., parent material, ground ice content) also influence spatial patterns of DOC in streams and rivers (Olefeldt et al. 2014; Harms et al. 2016; O'Donnell et al. 2016; Fig. 11.7). More generally,

Fig. 11.7 Arctic rivers drain watersheds that vary with respect to soil and bedrock characteristics and permafrost mineralogy and ground-ice content. In the Alaskan Arctic, watersheds are mostly commonly underlain by ice-poor bedrock (top left), coarse-grained glacial till (top middle), ice-rich, fine-grained glaciolacustrine deposits (top left), ice-rich Pleistocene loess (yedoma; lower left), sand (lower middle), and volcanic deposits (lower right). These watershed properties strongly influence the hydrology and chemical composition of streams and rivers (O'Donnell et al. 2016)

watershed properties that convey water through runoff and shallow subsurface flow paths (supra-permafrost flow; Fig. 11.5) typically yield larger concentrations of DOC in surface waters. Alternately, watersheds that allow for more groundwater discharge from sub-permafrost aquifers typically yield low concentrations of DOC in surface waters.

DOC concentration and flux are highly sensitive to recent warming in high-latitude regions. Numerous measurements and studies have focused on the flux of C in large Arctic rivers and estuaries (Dittmar and Kattner 2003; Raymond et al. 2007; Holmes et al. 2008; Spencer et al. 2008; Guo et al. 2012), given the importance of these riverine fluxes as components of regional-scale terrestrial budgets (McGuire et al. 2010; Kicklighter et al. 2013) and the large C stores in permafrost (Hugelius et al. 2014). In the Yukon River basin discharge-normalized DOC flux has decreased over the past 40 years (Striegl et al. 2005), likely due to permafrost thaw and associated increases in groundwater discharge to streamflow (Walvoord & Striegl 2007). Thawing of permafrost exposes more mineral soils to weathering and provides the potential for extensive physical stabilization (i.e., adsorption) and retention of DOC by soils, reducing the flux to rivers (Kawahigashi et al. 2004, 2006). On the other hand, warming could also increase primary production (e.g., higher plants) in Arctic terrestrial ecosystems, enhancing the release of contemporary DOC to Arctic rivers since river DOC has been found mostly contemporary in all major Arctic rivers (e.g., Benner et al. 2004; Guo and Macdonald 2006; Raymond et al. 2007). Total yearly DOC export has also declined in the much smaller Kuparuk River in northern Alaska, likely due to the decreases in discharge during the spring snowmelt period (McClelland et al. 2007) or possibly

due to the increases in baseflow (e.g., Walvoord and Striegl 2007; O'Donnell et al. 2012). However, DOC flux has increased by nearly 40% in the much larger Mackenzie River in northwest Canada, with much of the change occurring during autumn and winter flow (Tank et al. 2016). This appears to be influenced by permafrost and hydrological conditions and higher rates of plant production, but the exact mechanisms driving this change are still unclear. The different responses to the two terrain types to climate warming and associated disturbances may be driven by geomorphologic characteristics. Model simulations indicate that DOC loading from terrestrial ecosystems to Arctic rivers has increased in recent decades due to the increased water yields (Kicklighter et al. 2013). These seemingly contradictory observations and conclusions between different studies on the increased and decreased DOC fluxes remain to be verified. Future changes in riverine DOC flux will likely depend on the balance of factors that promote DOC production, loss, and hydrologic transport.

Once in a stream or river DOC can undergo in-stream processing which modifies lateral C fluxes from terrestrial ecosystems to the Arctic Ocean. In the northern permafrost region, DOC concentrations vary considerably across the continuum of soils, streams, and larger rivers (O'Donnell et al., unpublished data; Fig. 11.8). DOM composition strongly determines its fate and reactivity along the river reaches. While aromatic and humic-like DOM components are preferentially decomposed through photochemical pathways, carbohydrates and protein-like DOM components are somewhat resistant to photochemical degradation but preferentially utilized by microorganisms (Cory et al. 2014; Xu et al. 2018; Xu and Guo 2018). For example, recent work by Cory et al. (2014) has documented the importance of photo-oxidation of CDOM and DOC by sunlight in the water column of Arctic streams. Complete oxidation of DOC by sunlight and microorganisms results in the release of CO_2 from surface waters to the atmosphere, whereas partial oxidation results in the chemical transformation of the DOC pool prior to transport to downstream ecosystems. In many cases, rates of photo-oxidation outpace rates of DOC mineralization by aquatic microbial communities depending on the DOM composition. Further, the chemical alteration of DOC by sunlight can stimulate microbial mineralization of the residual DOC pool through the production of more bio-labile compounds (Ward et al. 2017). River ecosystems can also function to retain DOC, reducing the flux of C to downstream ecosystems or to the atmosphere. Some evidence suggests that benthic biofilm communities in streams and rivers can function to retain DOC through adsorption processes (Battin et al. 2016).

11.3.2 Major Nutrients: Nitrogen and Phosphorus

N and P are essential nutrients that can govern C-cycle processes, such as rates of primary production and microbial process rates in terrestrial and aquatic ecosystems (Elser et al. 1990; Vitousek and Howarth 1991; Heimann and Reichstein 2008). N occurs in various forms in stream ecosystems, including particulate N, dissolved organic N (DON, e.g., amino acids, proteins, etc.), and dissolved inorganic N (DIN:

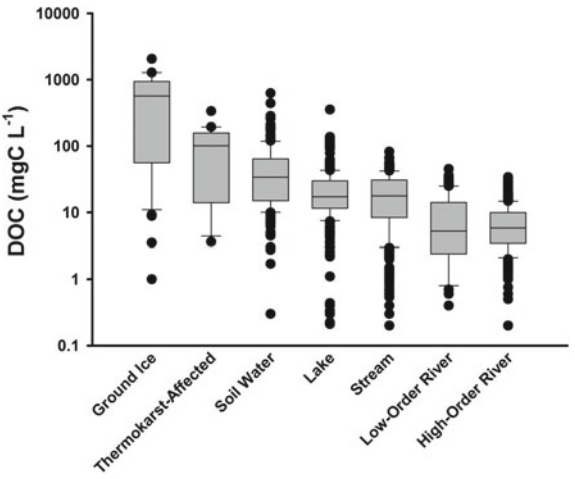

Fig. 11.8 DOC concentrations from different sites (approximately 2500 samples) across the Arctic along the continuum from permafrost soils to large rivers (O'Donnell et al., *unpublished data*)

NO_3^-, nitrite (NO_2^-), and NH_4^+). N-containing compounds can cycle between these various forms through microbially mediated reactions, which are typically controlled by reduction–oxidation (redox) state and availability (Hedin et al. 1998). N can also be assimilated by aquatic vegetation, including benthic algae, moss, phytoplankton, and macrophytes. While P typically limits primary productivity in aquatic systems, increased availability of inorganic N can directly limit or co-limit primary production in some systems (Grimm and Fisher 1986). Some microbial processes, such as nitrification (conversion of NH_4^+ to NO_3^-) and denitrification (conversion of NO_3^- to nitrous oxide (N_2O) and dinitrogen gas (N_2)) can result in the loss of N from the system to the atmosphere. N_2O is a greenhouse gas, and emission of N_2O from aquatic ecosystems can function as positive feedback to the climate system (Beaulieu et al. 2010).

In addition, the abundance, chemical speciation, and export fluxes of nutrients from rivers can be linked to changes in permafrost dynamics, vegetation/land cover, hydrological conditions, and human disturbance in river basins and changes in the ecosystem. Humans have dramatically altered the global N cycle (Vitousek et al. 1997), primarily through N fertilization of agricultural lands and through altering rates of atmospheric deposition. In undisturbed regions of the Arctic, the primary inputs of N to watersheds are through fixation of atmospheric N_2 by N-fixing organisms (e.g., boreal feather mosses) and atmospheric deposition. While terrestrial ecosystems retain a significant fraction of these N inputs, some are released to streams and rivers (Vitousek and Reiners 1975).

Some research indicates that boreal watersheds are losing N, as fluvial N fluxes exceed watershed inputs (Jones et al. 2005). Compared to other forms of N, NO_3^- is highly mobile and can be readily transported via runoff and subsurface flow paths to surface waters, and is often the dominant form of DIN and even TDN in high-latitude streams and rivers (Petrone et al. 2006). Indeed, in the Chena River of interior Alaska, DIN accounted for 60 ± 15% of the total N while DON and

particulate-N comprised 30 ± 8 and 10 ± 9%, respectively (Cai et al. 2008b). However, in the upper Yukon River, DON is the predominant N species, followed by particulate N and then DIN (Guo et al. 2004a, b). The same is true for the lower Yukon River with DON being the major N species (Guo et al. 2012). The predominance of DON in Arctic river waters is consistent with those derived from the leaching of different-aged permafrost soils in northern Alaska (Gao et al. 2018). Under warmer climatic conditions, increased mineralization of soil organic N pools may also increase production and transport of inorganic N to streams and rivers. Still, there are large uncertainties with respect to the fate of N in high-latitude watersheds in response to warming and disturbance (e.g., permafrost thaw; Frey and McClelland 2009). Sources of uncertainty include changing magnitude and seasonality of runoff and river discharge, the release of permafrost nitrogen, and rates of soil and in-stream N processing.

Wildfire, permafrost thaw, and erosional processes are three primary disturbance processes that may alter stream and river chemistry. Wildfires reduce terrestrial N stocks, but also temporarily reduce N retention by vegetation and soil microbial communities. Evidence from the boreal region indicates that wildfire may increase NO_3^- concentrations in headwater streams (Betts and Jones 2009). Wildfire can accelerate rates of permafrost thaw (O'Donnell et al. 2011), and thaw waters are typically enriched with DIN (Ewing et al. 2015). Recently, Ping et al (2011) reported that total N fluxes through coastal erosion along the Alaska Beaufort Sea coastal line could reach 7.76 ± 1.31 10^9 g-N/year during 1950–2000. On the other hand, based on laboratory leaching experiments, different aged permafrost with TN contents ranging from 500 to 12,000 μg-TN can produce soluble DIN, including NO_3^-, NO_2^-, and NH_4^+, varying from 12 to 41 μg-N/g-soil, and DON between 8 and 116 μg-N/g-soil (Gao et al. 2018). Yields of DON from soil TN were only 0.9–3.4% while yields of DIN from TN varied from 0.3 to 2.3% depending on specific soil (Gao et al. 2018). Nevertheless, the overall TDN released from soil can be enormous should permafrost thaw. Within the soil TDN pool, DON is the dominant N species followed by NH_4 and NO_3 and NO_2.

There are three primary sources of P to stream ecosystems, including soil/mineral leaching, anthropogenic input, and atmospheric deposition. Erosion and sedimentation through changes in watershed land use or disturbance can load P into aquatic systems. In soils, most P is found in particulate forms where organic or inorganic P complexes with mineral particles, such as iron (Fe), aluminum (Al), or manganese (Mn) hydroxides (Schlesinger and Bernhardt 2013). Permafrost soil leaching experiments show that yields of PO_4^{3-} from soil ranged from 0.6 to 6 μg-P/g-soil or 0.12 to 1.2% of the total P in soil, while yields of dissolved organic P (DOP) were 1.1–8.1 μg-P/g-soil or 1.2–2.9% of total organic P (Gao et al. 2018). Decomposition of soil organic matter by microbes can also release P, both as DOP and mineralized forms (e.g., PO_4^{3-}). Weathering of parent materials, such as limestone or volcanic deposits, can also contribute P to stream ecosystems. P cycling in streams is controlled by both abiotic processes (e.g., sorption–desorption reactions between surface water and sediments) and biological processes (decomposition of organic matter, assimilation, and immobilization in microbial biomass;

Hendricks and White 2000). In most Arctic streams, P is the primary limiting nutrient governing primary production (Peterson et al. 1985). For example, long-term P fertilization of the Kuparuk River near the Toolik Field Station in northern Alaska has altered stream ecosystem function, leading to enhanced moss and algal productivity, invertebrate production, and fish production (Slavik et al. 2004). In many Arctic streams and rivers, N and P concentrations are very low, and in many cases below detection limits (e.g., O'Donnell et al. 2015). However, given that permafrost soils store large amounts of N and P (Harden et al. 2012; Ewing et al. 2015), warming and disturbance will likely increase both N and P inputs to streams from soils (e.g., Frey et al. 2007; Bowden et al. 2008) although yields of soluble N and P from permafrost are generally low (Gao et al. 2018), driving bottom-up effects on food web dynamics due to the overall large store in the northern high-latitude regions.

Overall, studies of the detailed chemical speciation of nutrients for Arctic rivers are somewhat limited. In contrast to rivers with significant anthropogenic influences such as the Mississippi, where PO_4^{3-} is the predominant P species (Cai and Guo 2009), >80–90% of total P was measured in the >0.4 μm particulate phase in the upper Yukon River, followed by DOP, leaving PO_4^{3-} mostly below the detection limit (Guo et al. 2004a, b). Similarly, particulate organic P is also the predominant P species in the Lower Yukon River (Guo et al. 2012). In the Chena River, particulate P is the dominant P species, especially during the spring freshet, comprising on average 74 ± 10% of the total P while DIP and DOP comprised 19 ± 9% and 7 ± 4% of the total P, respectively (Cai et al. 2008b; Fig. 11.9). A low abundance of dissolved P species in Arctic rivers is likely derived from the high surface reactivity of P or high values of partition coefficient between dissolved and particulate phases (e.g., Lin and Guo 2016). More studies are needed to better understand the transformation of P between dissolved and particulate, and between inorganic and organic P species during soil leaching and transport from land to waterways.

11.3.3 Dissolved Silica

Silicon (Si) is the second most abundant element in the Earth's crust and a critical nutrient for diatoms in aquatic environments (De La Rocha et al. 1998), in addition to being essential to plant productivity and C cycling (Cornelis et al. 2011). Dissolved Si (DSi) exists in river waters as a result of weathering of Si-containing solid phases. In some Arctic rivers, dissolved silica responds differently than other solutes to permafrost dynamics in Arctic river systems. For example, Guo et al. (2004a, b) showed that thawing of the active layer and thus leaching of deeper soil horizon and riverbank erosion gave rise to higher orthosilicic acid ($Si(OH)_4$) and DIC but lower DOC, DOP, and PO_4^{3-} concentrations. Controls on DSi and nutrient exports (when normalized to watershed size) are also different across constituents. For instance, DSi fluxes are primarily governed by latitude (or temperature) and chemical weathering, whereas both N and P fluxes are regulated largely by

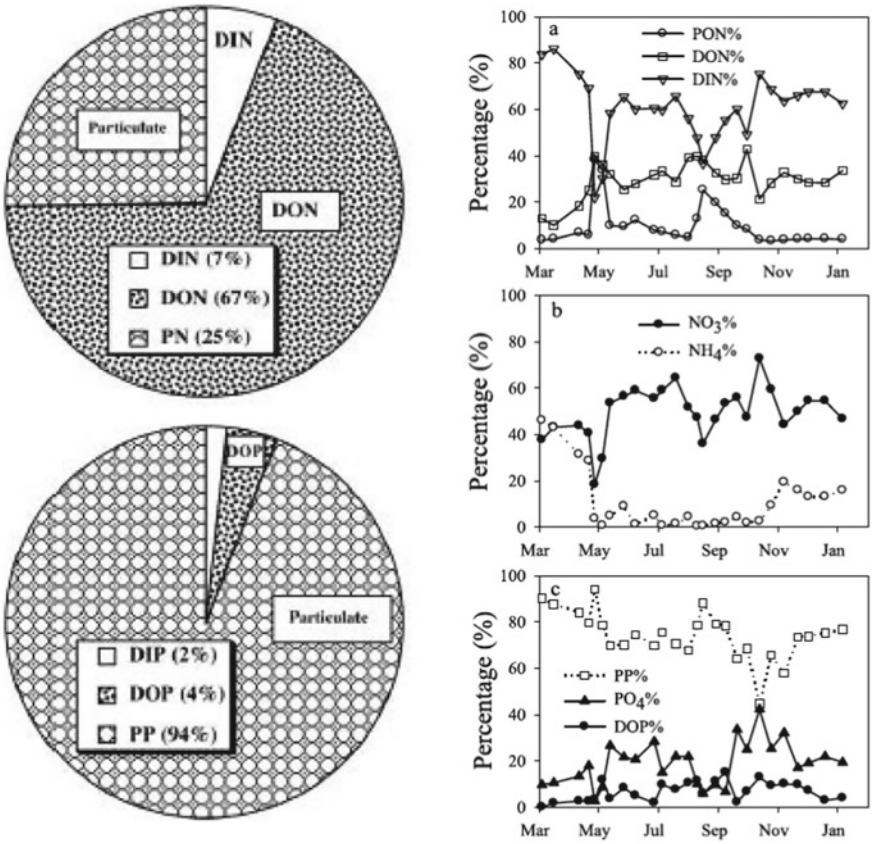

Fig. 11.9 Examples of chemical speciation of N and P in the upper Yukon River (left, from Guo et al. 2004a, b) and Chena River (right panel; from Cai et al. 2008b)

anthropogenic influences or human disturbances (Guo et al. 2004a, b). In comparison with DOC and DIC, the concentration of DSi have been shown to be negatively correlated with DOC concentration, but positively correlated to conductivity and DIC, indicating that $Si(OH)_4$ had a similar source function as DIC but different from DOC and other nutrients, especially during the snowmelt and early ice opening in the Yukon River Basin (Guo et al. 2004a, b).

DSi, as a proxy for silicate mineral weathering, can be used to identify the relative sources of major ions and trace metals in watersheds. As the seasonal thaw expands downward in a given summer thaw season the deeper thawed soils are increasingly comprised of a material that is only exposed to chemical or physical weathering for months or even days per year (Keller et al. 2007, 2010; Douglas et al. 2013; Barker et al. 2014; Fig. 11.10). At the local scale, this is also associated with an oxidation/reduction front that moves downward into the thawed soil

horizon over time. This oxidation/reduction front has major ramifications for the fate and transport of trace elements and nutrients in permafrost watersheds because solubility is often controlled largely by oxidation state and pH (Kimbrough et al. 1999; Barker et al. 2014). Silicate minerals can also be exposed to weathering when the thaw front reaches formerly frozen permafrost soil mineral horizons, leading to the direct release of DSi species into soil solution and local surface waters. Any future expanse of the active layer and degradation of permafrost is expected to impact concentrations of DSi in Arctic river systems (Guo et al. 2004a, b; Holmes et al. 2012; Pokrovsky et al. 2013).

Element cycling in the Arctic is expected to change as a result of increasing air temperatures (Alfredsson et al. 2016) through the expanse of the active layer, degradation of permafrost, and altering of vegetation and snow cover (Tape et al. 2006; Pokrovsky et al. 2013; Vaughan 2013). These changes will likely yield increased concentrations of dissolved Si in Arctic surface waters and the enrichment of the light Si stable isotope (Pokrovsky et al. 2013). Eventually, the formation of new wetlands and expansion of existing wetlands is expected to occur with increasing air temperatures, which have been shown to increase biological fixation and reduce the export of DSi (Sannel and Kuhry 2011). Any decrease in the amount of DSi that is transported to the Arctic Ocean as a result of riverine export will

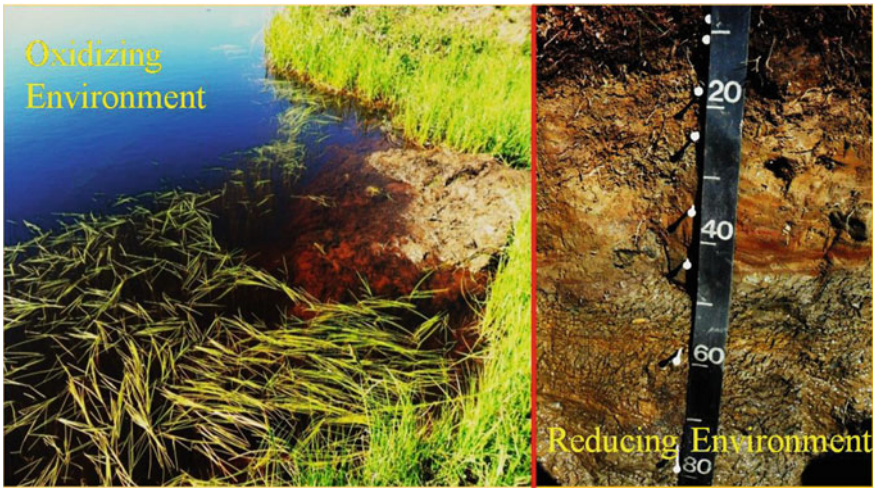

Fig. 11.10 Photographs identifying oxidation and reduction zones in permafrost in the Imnavait Creek watershed north of the Brooks Range in the Alaskan Arctic. Left: the edge of a tundra pond where surface conditions are oxidizing but anaerobic, low pH, and photochemically limited reducing conditions are likely to present at the base of the water column and in the pond sediments. Right: a cross section of a pit excavated in mid-summer with a jackhammer. The seasonal thaw at this time was roughly 45 cm. Note the zone of oxidized Fe just above the seasonal thaw line. Also, note the reduced Fe (grey and gleyed) from 50 to 80 cm depth. This is likely active layer soils that were frozen at the time of the picture that denote a reducing environment. Photos by A. J. Barker

likely result in disturbances to marine biological life and C cycling (Alfredsson et al. 2016). Therefore, the effect of climate change on Arctic terrestrial systems with respect to DSi transport is complex and may yield varying feedback responses.

11.3.4 Trace Metals

Metals comprise a major fraction of soil, surface water, and sediment on Earth and play a significant role in hydro-biogeochemical reactions in the environment. In rivers, metals partition between phases and the fate, transport, mobility, and speciation of metals are controlled by a variety of site-specific environmental parameters, predominantly pH, oxidation state, temperature, soil moisture, hydraulic conductivity, soil type, dissolved oxygen, presence of organic materials/clay minerals, wind, and the presence/concentrations of other competing elements (Loretta and Li 2001; Knechtenhofer et al. 2003; Dinis and Fiúza 2006; Pachana et al. 2010; Liao et al. 2017). A summary of key biogeochemical weathering processes and their associated impact on watersheds is summarized in Table 11.1. In Arctic ecosystems, there are additional landscape-scale controls on the reaction chemistry of metals in rivers (e.g., extreme temperature variations, varying oxidation–reduction conditions seasonally in the subsurface (Fig. 11.10), and the presence of permafrost and seasonally thawed surface soils).

Increasing air temperatures, permafrost thaw, and projected shifting of permafrost boundaries have the potential to affect the fate and transport of metals to surface waters as a result of the unique chemical reactions that occur in the subsurface. Understanding metal reactions directly at the permafrost-active layer boundary can be complicated because there often exist sharp redox transitions,

Table 11.1 Major biogeochemical weathering processes are identified with associated landscape-scale watershed implications. The multiple processes act in concert but are largely seasonally, spatially, and temporally independent of one another

Biogeochemical weathering processes	Implications to watershed
Oxidation/reduction	• Directly affects metal(loid) mobility/toxicity • Redox gradients often present in the subsurface (permafrost-active layer boundary)
Precipitation/dissolution	• Acts as a control on species activity in solution
Adsorption/desorption	• Contributes to fate and transport of species in surface waters • Soil organic matter often coats mineral surfaces in watersheds • Integral to heterogeneous surface reactions
Complexation	• Drives formation of metal ligand complexes • Important for nutrient availability
Microbial activity	• Often consumes or produces CO_2 • Contributes to a variety of element cycles (C, N, O, P, Fe, Mn, etc.) • Primary driver of organic matter decomposition

surface charge gradients, and phase changes (liquid/ice). In the near-surface environment, metals (particularly Fe and Mn) can have multiple oxidation states and thus act as electron donors or acceptors depending on local geochemical conditions. This can impact microbial communities and C speciation/cycling but C cycle processes can, in turn, control metals fate and transport (Pokrovsky and Schott 2002; Page et al. 2013; Stolpe et al. 2013; Salvadó et al. 2015; Emerson et al. 2015; Trusiak et al. 2018). Additionally, seasonal changes and annual freeze–thaw cycles inherent to Arctic freshwater processes influences metal transport to surface waters (Barker et al. 2014; Pokrovsky et al. 2016) and metal cycling in Arctic thaw ponds (Loiko et al. 2017; Pokrovsky et al. 2018; Raudina et al. 2018). As such, the chemical environment of metals in Arctic rivers tends to be highly heterogeneous, dependent on a variety of site-specific factors, and constantly undergoing a transformation. In an attempt to decrease the complexities of measuring permafrost-active layer dynamics, metals (e.g., strontium (Sr), Fe, Mn, and Al) have been employed as geochemical tracers to infer changes within Arctic watersheds and scale to the landscape watershed scale (Rember and Trefry 2004; Keller et al. 2010; Barker et al. 2014; Lehn et al. 2017).

Riverine sediment environments are a unique chemical setting for trace metal studies, particularly in Arctic ecosystems. Riverine sediments are composed of fine-grained materials that offer excellent surface capacity for metals to chemically and physically sorb or bind, including clay minerals (Ilgen and Trainor 2011; Cai et al. 2014), colloids (Pachana et al. 2010), organic matter (humic and fulvic acids; Sklodowski et al. 2006; Clemens and Ma 2016), Fe oxides (Yin et al. 2016), and Mn oxides (Gunawardana et al. 2015). Unlike surface water and soil systems, sediment environments tend to be more reducing and contain lesser amounts of dissolved oxygen (Morford and Emerson 1999). As a result, metal speciation, mobility, and accumulation are affected by deposition, burial, interaction, and re-suspension in aquatic sediment systems. In particular, metal(loid)s have been shown to accumulate in reducing environments (Kimbrough et al. 1999; Barker et al. 2014; Ilgen et al. 2014) and sediments have been shown to stabilize reduced metals (Miao et al. 2006). Mobilization of sediment as a result of natural disruption events (i.e., snowmelt, wind, rain events, increased turbidity), can result in the transport of metals to the water column and subsequent migration downstream (Kaplan et al. 1995; Pachana et al. 2010). As a result, riverine fate and transport of metals are often controlled by sediment acting as a source, a sink, and a reaction surface for environmental systems. This can have both positive and negative effects on Arctic ecosystems since certain metals (e.g., copper, chromium, and zinc) provide essential nutrients for in-country foods (Horowitz and Elrick 1987; Kabata-Pendias 2010), while others (i.e., mercury (Hg) and cadmium) are toxic even in trace amounts (Schuster et al. 2018). Within the context of Arctic ecosystem processes outlined above, we discuss the role and response of metals in Arctic C cycle processes. We focus on Fe, Sr, uranium (U), and Hg because they represent a ubiquitous element in earth's crust (Fe), a tracer used to distinguish between silicate and carbonate weathering reactions in soils (Sr), a long-lived radioactive element (U), and a toxic metal of concern because it bioaccumulates in the environment (Hg).

11.3.4.1 Iron and the Arctic Carbon Cycle

Fe is the most abundant element on Earth and the fourth most abundant element in the Earth's crust, by mass. As such, Fe has significant importance to life and plays an integral role in biogeochemical reactions. Fe exists in multiple valence states, ranging from -2 to +6, but in the near-surface, it is found primarily as divalent Fe (Fe(II)) or trivalent Fe ((Fe(III)). Fe(II) and Fe(III) readily form complexes with other species, which can act as catalysts in biogeochemical reactions, sinks for organic C, and facilitate electron transfer (Williams and Scherer 2004; Lalonde et al. 2012; Frey and Reed 2012; Page et al. 2013; Trusiak et al. 2018). Fe redox cycling is complex and is intricately tied to the presence of organic C and microbial activity and can vary even within one watershed since reduced Fe tends to accumulate at the permafrost-active layer boundary and oxidized Fe found generally in near-surface environments (Barker et al. 2014; Fig. 11.10).

In the Arctic, the C cycle is a significantly important process due to the abundance of C stored currently frozen in permafrost (Tarnocai et al. 2009; Hugelius et al. 2014) and the risk of CO_2 and CH_4 release if air temperatures continue to increase and permafrost thaws and degrades (Vincent et al. 2017). Fe plays a role in the overall Arctic C cycle, contributing both positive and negative permafrost-C feedbacks to the climate. Fe acts as a sink for organic C due to its reactivity and large surface area (Salvadó et al. 2015), thereby stabilizing C in soil and decreasing the potential for degradation and release of CO_2 (Lalonde et al. 2012; Yang et al. 2017). However, various microbial communities active in Arctic soil systems have been shown to use Fe(II) or Fe(III) as energy sources depending on the community composition (Emerson et al. 2015), leading to substantial positive feedback to climate change by the direct release of CO_2 and potentially CH_4 into the atmosphere (Yang et al. 2017). Additionally, two recent studies have focused on the chemical oxidation of DOC mediated by reduced Fe in anoxic soil waters in the Arctic through the production of hydroxyl radical (•OH), which is a highly reactive oxidant (Page et al. 2013; Trusiak et al. 2018). Therefore, the presence of Fe in soils and soil waters contributes to both the production and consumption of CO_2. A simplified schematic showing the overall role of Fe in the Arctic C cycle is shown in Fig. 11.11. Fe can act as a sink for organic C, energy source for microbial reduction and oxidation, and contribute to the formation of •OH thereby oxidizing organic C. Investigating Fe redox cycling is critical to understanding the fate of C in the Arctic, particularly with projected warming and thawing of permafrost soils.

The chemical speciation of Fe and thus its fate and transport from streams/rivers to the Arctic Ocean are also related to permafrost and C dynamics. Stolpe et al. (2013) have shown that during spring freshet when DOM and Fe abundance is the highest, dissolved Fe is mostly complexed with DOM and present almost exclusively in the form of nanocolloids or the <4 nm size fractions in small Alaska rivers. In contrast, during late summer/early fall when DOM is low in abundance, the molecular size spectra of dissolved Fe show two peaks: one associated with nanocolloids derived from the complexation of Fe with and DOM, and the other with large sized colloids ranging from 10 to 50 nm derived from the formation of Fe oxide/hydroxide which could be removed through coagulation from the

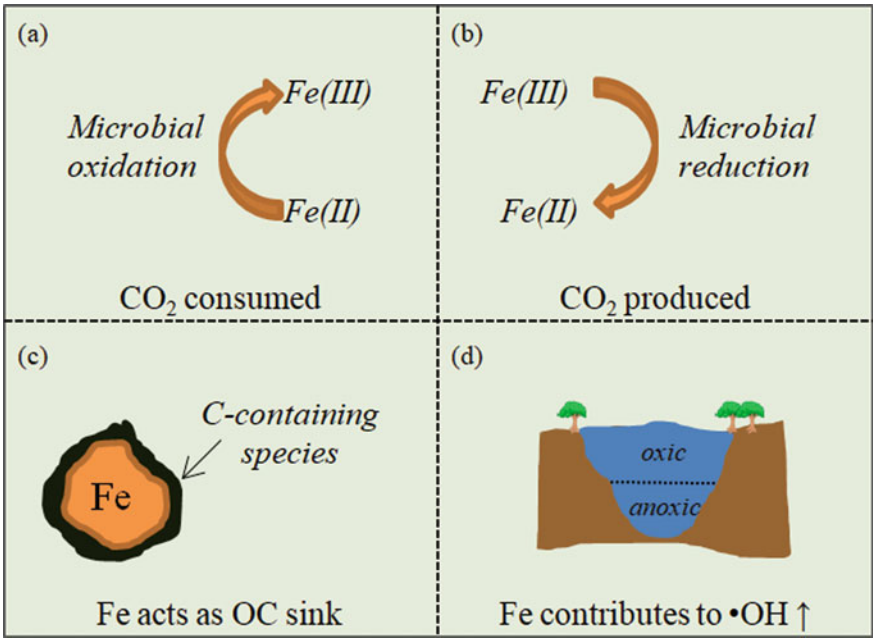

Fig. 11.11 A simplified schematic diagram showing the roles of Fe in the C cycle of Arctic soils and soil pore waters **a** CO_2 is consumed during microbial oxidation of Fe, **b** CO_2 is produced during microbial reduction of Fe, **c** Fe can act as a sink with organic C through precipitation, complexation, and sorption reactions, and **d** reduced Fe plays a role in the formation of hydroxyl radical in anoxic soil waters, which is a highly reactive oxidant for C or metals oxidation

dissolved phase. Similar metal size spectra were also observed for Cr and other trace elements in small Alaska rivers based on the analysis using flow field-flow fraction coupled online with ICP-MS (Stolpe et al. 2013). In addition, Pokrovsky et al (2018) found freeze–thaw cycles of Arctic thaw ponds remove colloidal metals and generate low-molecular weight organic matter in boreal rivers in Siberia.

11.3.4.2 Sr and U Isotopes as Geochemical Tracers

The use of isotopes as environmental tracers for biogeochemical processes in the Arctic has become increasingly popular in recent years to determine trace element dynamics, quantify variations between varied source materials, monitor active layer deepening, and characterize seasonal changes in geochemical processes in watersheds. Since these processes are also the main drivers of C-cycle processes in soils and watersheds isotope studies can be used to infer C cycle processes. Specifically, radiogenic isotopes of Sr (^{87}Sr and ^{86}Sr; Guo et al. 2004b; Bagard et al. 2013; Douglas et al. 2013; Stevenson et al. 2016, 2018; Lehn et al. 2017) and U (^{238}U and ^{234}U) (Koch et al. 2013; Ewing et al. 2015; 2016; Hindshaw et al. 2018) have been applied to understand seasonal geochemical weathering reactions and rates in

permafrost environments. Radiogenic Sr ratios are a function of their source in the near-surface environment resulting from weathering of primary materials and, as such, they are useful for predicting preferential weathering and hydrological flow paths (Stevenson et al. 2016; Keller et al. 2010; Douglas et al. 2013). Conversely, U isotope activity ratios ($^{234}U/^{238}U$) tend to be a function of water residence times (e.g., groundwater versus surface water) and studies have shown that longer water residence times translate to higher $^{234}U/^{238}U$ activity ratios. Permafrost systems can complicate this measurement because uranium isotopic enrichment can also be affected by ice residence time in addition to water residence time (Hindshaw et al. 2018). A study by Ewing et al. (2015) showed that $^{234}U/^{238}U$ ratios were higher for waters sourced from older permafrost thawing compared to younger permafrost. This established U isotope ratios as tracers for identifying the likely sources of soil and organic materials in watersheds.

11.3.4.3 Mercury Bioaccumulation and Release in the Arctic

Hg is a naturally occurring toxic element that is of increasing concern in Arctic ecosystems due to the large stocks of Hg currently stored in the northern permafrost region, and the sensitivity of permafrost Hg to thaw and mobilization (Ci et al. 2018; Schuster et al. 2018). Hg can bioaccumulate in terrestrial and aquatic food webs and has been found in foods across the Arctic region (Jæger et al. 2009). Hg can accumulate in Arctic snow and is present in snowmelt runoff due to the long-range atmospheric transport, oxidation, and subsequent deposition onto the snow surface (Douglas and Sturm 2004; Douglas et al. 2005, 2017; Driscoll et al. 2013; Agnan et al. 2018). The interaction of Hg and organic matter can drive the production of methylmercury (MeHg), which is a neurotoxin that strongly bioaccumulates and biomagnifies in nature (Schartup et al. 2013). MeHg is highly mobile in aquatic systems and is relatively lipid-soluble, making it an ideal species to accumulate in bio (Rice et al. 2014). Since MeHg production, retention, and mobilization are largely controlled by the presence of organic species in soils or water Hg is intimately associated with the C cycle.

Projected future permafrost degradation, particularly the dramatic loss of near-surface permafrost over the next decades (Pastick et al. 2015), will expose soil organic C that is currently bound to Hg and stored frozen. Once exposed, microbial activity can decompose organic matter, releasing CO_2 in the process. Any Hg bound to the soil organic matter is also expected to be released into the environment during permafrost thaw and organic matter liberation (Schuster et al. 2018). Once released, the Hg can interact with both DOM and soil organic matter and form MeHg in watersheds (French et al. 2014). Similar observations in Arctic and sub-Arctic permafrost thaw ponds have already been reported by MacMillan et al. (2015) showing that high MeHg concentrations were correlated with high inputs of organic matter and microbial activity. Organic C affects Hg cycling and bioaccumulation in the environment and permafrost degradation is expected to impact the fate of Hg. However, the magnitude of that impact on the environment remains to be determined and further work is needed to quantify potential human health concerns.

11.4 Conclusions and Knowledge Gaps

Despite the growing body of literature documenting the response of Arctic stream and river biogeochemistry to warming and disturbance, there are still many challenges and uncertainties for the scientific community. In this chapter, we discuss some of these uncertainties and directions for future research, including (1) thermokarst effects (2) changing seasonality, (3) altered watershed hydrology, and (4) timing and magnitude of changes across Arctic landscapes.

The effects of thermokarst and thermal erosional processes on stream and river biogeochemistry represent a critical uncertainty for Arctic researchers. Much of the uncertainty regarding thermokarst is due to the complex, three-dimensional nature of the problem, and the difficulty in predicting the initiation and extent of thermokarst features across the landscape. Whereas many land surface models can now simulate one-dimensional permafrost thaw via active layer thickening, measuring and modeling thermokarst represents a true challenge to the scientific community. Thermokarst can develop across a variety of landscape types and in a variety of modes, including thaw slumps, slope failures, pits, scarps, gullies, and expanding lake margins. Some evidence indicates thermokarst and thermal erosion features may function as a large source of C and nutrients to streams. Other studies have documented that permafrost degradation via thermokarst can enhance riverine fluxes of water, sediment, organic C, nutrients, and trace metals. Still, the persistence and spatial extent of these thermokarst impacts are not clear and require more long-term monitoring and intensive research to better constrain.

As noted above, Arctic streams and rivers exhibit strong seasonal patterns with respect to flows and chemical composition. Under a warming Arctic, changing seasonality represents another key uncertainty that could impact hydrologic and biogeochemical processes in stream and river ecosystems. Evidence indicates many components of northern watersheds are already changing, including the timing and magnitude of snowmelt, the extent of the ice-free season, increase groundwater discharge to surface water (Lamontagne-Halle et al. 2018). In some cases, perennial streams may shift to ephemeral states in response to changing water balance and longer open-water seasons. Tracking the impacts of changing seasonality on river biogeochemical processes will take a considerable, multidisciplinary effort, linking remote sensing, field-based, and modeling approaches.

Changing watershed and subsurface hydrology in Arctic regions represents another key uncertainty and an important area of current and future research. The timing and magnitude of precipitation are likely to change, which may alter runoff to surface water and thawing rates in near-surface soils. Warming and disturbance (wildfire, permafrost thaw) can dramatically alter watershed hydrology and the delivery of water and solutes to stream and river channels. Spatial differences in permafrost characteristics across watersheds, including ground ice content, hydraulic properties, and lithology, all influence the hydrologic and biogeochemical response to warming and thawing. Recent advances in airborne and ground-based geophysical techniques have improved characterizations of subsurface properties in permafrost

landscapes. Groundwater models have also been improved in recent years through the incorporation of freeze–thaw processes. Still, much work is still needed to establish conceptual and quantitative linkages between changing hydrologic conditions, permafrost dynamics, and biogeochemical responses in surface waters.

Predicting the timing and magnitude of change represents yet another key uncertainty and knowledge gap for Arctic river systems. The response of the biogeochemistry of C species, nutrients, and trace elements in Arctic aquatic ecosystems to warming and permafrost thaw should have different extents and time-dependent features, and thus different impacts on ecosystems. In addition, changes in river biogeochemistry are also distinct across Arctic rivers that draining different watershed types (O'Donnell et al. 2016; Lung et al. 2018). Therefore, comprehensive time-series observations in different watersheds across different latitudes are needed to better understand the evolution in C, nutrients, and trace elements biogeochemistry in Arctic rivers in a changing climate. Further, a more process-based understanding of biogeochemical processes that span the terrestrial–aquatic interface will strengthen our understanding of the mechanisms driving change. Large-scale studies of river biogeochemistry and the seasonality of flows and fluxes form the basis for statistical models of the export of DOC, other nutrients, major elements, and trace metals, but for predictions, we need physically based models, and these require an understanding of snow and chemical processes that occur at a much smaller scales.

References

Agnan Y, Douglas TA, Helmig D et al (2018) Mercury in the Arctic tundra snowpack: temporal and spatial concentration patterns and trace gas exchanges. Cryosphere 12:1939–1956

Aiken GR, Hsu-Kim H, Ryan JN (2011) Influence of dissolved organic matter on the environmental fate of metals, nanoparticles, and colloids. Environ Sci Technol 45:3196–3201

Aiken GR, Spencer RG, Striegl RG et al (2014) Influences of glacier melt and permafrost thaw on the age of dissolved organic carbon in the Yukon River basin. Glob Biogeochem Cycles 28(5):525–37

Alfredsson H, Clymans W, Hugelius G et al (2016) Estimated storage of amorphous silica in soils of the circum-Arctic tundra region. Glob Biogeochem Cycles 30:479–500

Bagard M-L, Schmitt A-D, Chabauc F et al (2013) Biogeochemistry of stable Ca and radiogenic Sr isotopes in a larch-covered permafrost-dominated watershed of Central Siberia. Geochim Cosmochim Acta 114(1):169–187

Barker AJ, Douglas TA, Jacobson AD et al (2014) Late season mobilization of trace metals in two small Alaskan arctic watersheds as a proxy for landscape scale permafrost active layer dynamics. Chem Geol 381:180–93

Battin TJ, Besemer K, Bengtsson MM et al (2016) The ecology and biogeochemistry of stream biofilms. Nat Rev Microbiol 14(4):251

Beaulieu JJ, Tank JL, Hamilton SK et al (2010) Nitrous oxide emission from denitrification in stream and river networks. P Natl Acad Sci USA 15:201011464

Benner R, Benitez-Nelson B, Kaiser K et al (2004) Export of young terrigenous dissolved organic carbon from rivers to the Arctic Ocean. Geophys Res Lett 31(5). https://doi.org/10.1029/2003gl019251

Betts EF, Jones JB Jr (2009) Impact of wildfire on stream nutrient chemistry and ecosystem metabolism in boreal forest catchments of interior Alaska. Arct Antarct Alp Res 41(4):407–417

Bowden WB, Gooseff MN, Balser A et al (2008) Sediment and nutrient delivery from thermokarst features in the foothills of the North Slope, Alaska: potential impacts on headwater stream ecosystems. J Geophys Res-Biogeosci 113:G2. https://doi.org/10.1029/2007JG000470
Bowling LC, Kane DL, Gieck RE et al (2003) The role of surface storage in a low-gradient Arctic watershed. Water Resour Res 39(4). https://doi.org/10.1029/2002wr001466
Cai Y, Guo L, Douglas TA (2008a) Temporal variations in organic carbon species and fluxes from the Chena River, Alaska. Limnol Ocean 53(4):1408–1419
Cai Y, Guo L, Douglas T et al (2008b) Seasonal variations in nutrient concentrations and speciation in the Chena River, Alaska. J Geophys Res-Biogeosci 113(G030035). https://doi.org/10.1029/2008jg000733
Cai Y, Guo L (2009) Abundance and variation of colloidal organic phosphorus in riverine, estuarine, and coastal waters in the northern Gulf of Mexico. Limnol Oceanogr 54. https://doi.org/10.4319/lo.2009.54.4.1393
Cai L, Tong M, Wang X et al (2014) Influence of clay particles on the transport and retention of titanium dioxide nanoparticles in quartz sand. Environ Sci Technol 48(13):7323–7332
Chin Y-P, Aiken GR, Danielsen KM (1997) Binding of pyrene to aquatic and commercial humic substances: the role of molecular weight and aromaticity. Environ Sci Technol 31:1630–1635. https://doi.org/10.1021/es960404k
Ci Z, Peng F, Xue X et al (2018) Temperature sensitivity of gaseous elemental mercury in the active layer of the Qinghai-Tibet Plateau permafrost. Environ Pollut 238:508–515
Clemens S, Ma JF (2016) Toxic heavy metal and metalloid accumulation in crop plants and foods. Annu Rev Plant Biol 67:489–512
Cole JJ, Prairie YT, Caraco NF et al (2007) Plumbing the global carbon cycle: integrating inland waters into the terrestrial carbon budget. Ecosystems 10:172–185
Cornelis J-T, Delvaux B, Georg RB et al (2011) Tracing the origin of dissolved silicon transferred from various soil-plant systems towards rivers: a review. Biogeosciences 8:89–112
Cory RM, Ward CP, Crump BC et al (2014) Sunlight controls water column processing of carbon in arctic fresh waters. Science 345:925–928. https://doi.org/10.1126/science.1253119
Cragin JH, McGilvary R (1995) Can inorganic chemical species volatilize from snow? Biogeochemistry of seasonally snow-covered catchments. IAHS publ. no. 228
De La Rocha CL, Brzezinski MA, DeNiro MJ et al (1998) Silicon-isotope composition of diatoms as an indicator of past oceanic change. Nature 395:680–683
Dinis M, Fiúza A (2006) Modeling the transport and fate of contaminants in the environment: soil, water and air. In: Simeonov L, Chirila E (eds) Chemicals as intentional and accidental global environmental threats. Springer Publishing, New York, pp 469–476
Dittmar T, Kattner G (2003) The biogeochemistry of the river and shelf ecosystem of the Arctic Ocean: a review. Mar Chem 83:103–120. https://doi.org/10.1016/S0304-4203(03)00105-1
Dominé F, Shepson PB (2002) Air-snow interactions and atmospheric chemistry. Science 297:1506–1510. https://doi.org/10.1126/science.1074610
Dou F, Ping CL, Guo L et al (2008) Estimating the impact of seawater on the production of soil water-extractable organic carbon during coastal erosion. J Environ Qual 37:2368–2374. https://doi.org/10.2134/jeq2007.0403
Douglas TA, Sturm M (2004) Arctic haze, mercury and the chemical composition of snow across northwestern Alaska. Atmos Environ 38(6):805–20
Douglas TA, Sturm M, Simpson WR et al (2005) Elevated mercury measured in snow and frost flowers near Arctic sea ice leads. Geophys Res, Lett, p 32
Douglas TA, Blum JD, Guo L et al (2013) Hydrogeochemistry of seasonal flow regimes in the Chena River, a subarctic watershed draining discontinuous permafrost in interior Alaska (USA). Chem Geol 335:48–62
Douglas TA, Sturm M, Blum JD et al (2017) Pulse of mercury and major ions in snowmelt runoff from a small arctic Alaska watershed. Environ Sci Technol 51(19):11145–55
Driscoll CT, Mason RP, Chan HM et al (2013) Mercury as a global pollutant: sources, pathways, and effects. Environ Sci Technol 47:4967–4983

Elser JJ, Marzolf ER, Goldman CR (1990) Phosphorus and nitrogen limitation of phytoplankton growth in the freshwaters of North America: a review and critique of experimental enrichments. Can J Fish Aquat Sci 47(7):1468–1477

Emerson D, Scott J, Benes J et al (2015) Microbial iron oxidation in the Arctic tundra and the implications for biogeochemical cycling. Appl Environ Microb 8:AEM-02832

Ewing SA, O'Donnell JA, Aiken GR et al (2015) Long-term anoxia and release of ancient, labile carbon upon thaw of Pleistocene permafrost. Geophys Res Lett 42(24):10–730

Ewing SA, Paces JB, O'Donnell JA et al (2016) Uranium isotopes and dissolved organic carbon in loess permafrost: modeling the age of ancient ice. Geochim Cosmochim Acta 152:143–165

Finlay J, Neff J, Zimov S, Davydova A, Davydov S (2006) Snowmelt dominance of DOC in high-latitude watersheds: implications for characterization and flux of river DOC. Geophys Res Lett 33(l10401)

French TD, Houben AJ, Desforges J-PW et al (2014) Dissolved organic carbon thresholds affect mercury bioaccumulation in Arctic Lakes. Environ Sci Technol 48:3162–3168

Frey KE, Smith LC (2005) Amplified carbon release from vast West Siberian peatlands by 2100. Geophys Res Lett 32(9)

Frey KE, McClelland JW (2009) Impacts of permafrost degradation on arctic river biogeochemistry. Hydrol Process 23(1):169–182

Frey PA, Reed GH (2012) The ubiquity of iron. ACS Chem Biol 7:1477–1481

Frey KE, McClelland JW, Holmes RM et al (2007) Impacts of climate warming and permafrost thaw on the riverine transport of nitrogen and phosphorus to the Kara Sea. J Geophys Res-Biogeosci 112(G4)

Gao L, Zhou Z, Reyes A, Guo L (2018) Yields and characterization of dissolved organic matter from different-aged soil in northern Alaska. J Geophys Res Biogeosci 123(7):2035–2052. https://doi.org/10.1029/2018JG004408

Gray DM, Toth B, Zhao L et al (2001) Estimating areal snowmelt infiltration into frozen soils. Hydrol Process 15:3095–3111

Grimm NB, Fisher SG (1986) Nitrogen limitation in a Sonoran Desert stream. J North Am Benthol Soc 5(1):2–15

Gunawardana C, Egodawatta P, Goonetilleke A (2015) Adsorption and mobility of metals in build-up on road surfaces. Chemosphere 119:1391–8

Guo L, Macdonald RW (2006) Source and transport of terrigenous organic matter in the upper Yukon River: evidence from isotope (δ13C, Δ14C, and δ15 N) composition of dissolved, colloidal, and particulate phases. Glob Biogeochem Cycles 20(2):GB2011. https://doi.org/10.1029/2005gb002593

Guo L, Zhang JZ, Guéguen C (2004a) Speciation and fluxes of nutrients (N, P, Si) from the upper Yukon River. Glob Biogeochem Cycles 18(1):GB1038. https://doi.org/10.1029/2003gb002152

Guo L, Semiletov I, Gustafsson Ö et al (2004b) Characterization of Siberian Arctic coastal sediments: Implications for terrestrial organic carbon export. Glob Biogeochem Cycles 18(1):GB1036. https://doi.org/10.1029/2003gb002087

Guo L, Ping CL, Macdonald RW (2007) Mobilization pathways of organic carbon from permafrost to arctic rivers in a changing climate. Geophys Res Lett 34(13):L13603. https://doi.org/10.1029/2007GL030689

Guo L, Cai Y, Belzile C, Macdonald RW (2012) Sources and export fluxes of inorganic and organic carbon and nutrient species from the seasonally ice-covered Yukon River. Biogeochemistry 107(1–3):187–206

Harden JW, Koven CD, Ping CL et al (2012) Field information links permafrost carbon to physical vulnerabilities of thawing. Geophys Res Lett 39(15)

Harms TK, Edmonds JW, Genet H et al (2016) Catchment influence on nitrate and dissolved organic matter in Alaskan streams along a latitudinal gradient. J Geophys Res-Biogeosci 121:350–369. https://doi.org/10.1002/2015JG003201

Hedin LO, von Fischer JC, Ostrom NE et al (1998) Thermodynamic constraints on nitrogen transformations and other biogeochemical processes at soil–stream interfaces. Ecology 79 (2):684–703
Heimann M, Reichstein M (2008) Terrestrial ecosystem carbon dynamics and climate feedbacks. Nature 451(7176):289
Hendricks SP, White DS (2000) Stream and groundwater influences on phosphorus biogeochemistry. In: Jones JB, Mulholland PJ (eds) Streams and ground waters. Academic Press, San Diego, pp 221–235
Hindshaw RS, Aciego SM and Tipper ET (2018) Li and U isotopes as a potential tool for monitoring active layer deepening in permafrost dominated catchments. Front. Earth Sci 6 (102):17
Hinzman LD, Bettez ND, Bolton WR et al (2005) Evidence and implications of recent climate change in northern Alaska and other arctic regions. Clim Chang 72:251–298
Hobbie SE, Gough L (2004) Litter decomposition in moist acidic and non-acidic tundra with different glacial histories. Oecologia 140:113–124
Holmes RM, McClelland JW, Raymond PA et al (2008) Lability of DOC transported by Alaskan rivers to the Arctic Ocean. Geophys Res Lett 35(3). https://doi.org/10.1029/2007gl032837
Holmes RM, McClelland JW, Peterson BJ et al (2012) Seasonal and annual fluxes of nutrients and organic matter from large rivers to the arctic ocean and surrounding seas. Estuaries Coasts 35 (2):369–382
Hope D, Billett MF, Cresser MS (1994) A review of the export of carbon in river water: fluxes and processes. Environ Pollut 84:301–324. https://doi.org/10.1016/0269-7491(94)90142-2
Hornberger GM, Bencala KE, McKnight DM (1994) Hydrological controls on dissolved organic carbon during snowmelt in the Snake River near Montezuma, Colorado. Biogeochemistry 25:147–165
Horowitz AJ, Elrick KA (1987) The relation of stream sediment surface area, grain size and composition to trace element chemistry. Appl Geochem 2(4):437–51
Hugelius G, Strauss J, Zubrzycki S et al (2014) Estimated stocks of circumpolar permafrost carbon with quantified uncertainty ranges and identified data gaps. Biogeosciences 11:6573–6593. https://doi.org/10.5194/bg-11-6573-2014
Ilgen AG, Trainor TP (2011) Sb (III) and Sb (V) sorption onto Al-rich phases: hydrous Al oxide and the clay minerals kaolinite KGa-1b and oxidized and reduced nontronite NAu-1. Environ Sci Technol 46(2):843–51
Ilgen AG, Majs F, Barker AJ, Douglas TA, Trainor TP (2014) Oxidation and mobilization of metallic antimony in aqueous systems with simulated groundwater. Geochim Cosmochim Acta 1(132):16–30
Jæger I, Hop H, Gabrielsen GW (2009) Biomagnification of mercury in selected species from an Arctic marine food web in Svalbard. Sci Total Environ 407(16):4744–51
Jones JB Jr, Petrone KC, Finlay JC et al (2005) Nitrogen loss from watersheds of interior Alaska underlain with discontinuous permafrost. Geophys Res Lett 32(2)
Jorgenson MT, Shur YL, Pullman ER (2006) Abrupt increase in permafrost degradation in Arctic Alaska. Geophys Res Lett 33:L02503. https://doi.org/10.1029/2005GL024960
Judd KE, Kling GW (2002) Production and export of dissolved C in arctic tundra mesocosms: the roles of vegetation and water flow. Biogeochemistry 60:213–234
Kabata-Pendias A (2010) Trace elements in soils and plants, 4th edn. Taylor & Francis, Boca Raton
Kane DL, Hinzman LD, Benson CS, Everett KR (1989) Hydrology of Imnaviat Creek, an arctic watershed. Ecography 12:262–269. https://doi.org/10.1111/j.1600-0587.1989.tb00845.x
Kaplan DI, Bertsch PM, Adriano DC (1995) Facilitated transport of contaminant metals through an acidified aquifer. Groundwater 33(5):708–17
Kawahigashi M, Kaiser K, Kalbitz K et al (2004) Dissolved organic matter in small streams along a gradient from discontinuous to continuous permafrost. Glob Chang Biol 10(9):1576–86

Kawahigashi M, Kaiser K, Rodionov A et al (2006) Sorption of dissolved organic matter by mineral soils of the Siberian forest tundra. Glob Change Biol 12(10):1868–77
Keller K, Blum JD, Kling GW (2007) Geochemistry of soils and streams on surfaces of varying ages in Arctic Alaska. Arct Antarct Alp Res 39:84–98
Keller K, Blum JD, Kling GW (2010) Stream geochemistry as an indicator of increasing permafrost thaw depth in an arctic watershed. Chem Geol 273(1–2):76–81
Kicklighter DW, Hayes DJ, McClelland JW et al (2013) Insights and issues with simulating terrestrial DOC loading of Arctic river networks. Ecol Appl 23:1817–1836. https://doi.org/10.1890/11-1050.1
Kimbrough DE, Cohen Y, Winer AM et al (1999) A critical assessment of chromium in the environment. Crit Rev Environ Sci Tech 29(1):1–46
Kling GW, Kipphut GW, Miller MC (1991) Arctic lakes and streams as gas conduits to the atmosphere: implications for tundra carbon budgets. Science 251(4991):298–301
Knechtenhofer L, Xifra I, Scheinost AC et al (2003) Fate of heavy metals in a strongly acidic shooting range-soil: small-scale metal distribution and its relation to preferential water flow. J Plant Nutr Soil Sci 166:84–92
Koch JC, Ewing SA, Striegl R et al (2013) Rapid runoff via shallow throughflow and deeper preferential flow in a boreal catchment underlain by frozen silt (Alaska, USA). Hydrogeol J 21(1):93–106
Koren V, Schaake J, Mitchell K et al (1999) A parameterization of snowpack and frozen ground intended for NCEP weather and climate models. J Geophys Res 104(D16):19569–19585
Lalonde K, Mucci A, Ouellet A et al (2012) Preservation of organic matter in sediments promoted by iron. Nature 483(7388):198–200
Lamontagne-Halle P, McKenzie JM, Kurylyk BL et al (2018) Changing groundwater discharge dynamics in permafrost regions. Environ Res Lett 13:084017
Larsen JN, Anisimov OA, Constable A et al (2014) Polar regions. In: Climate change 2014, impacts, adaptation, and vulnerability, part B: regional aspects. Contribution of working group II to the fifth asessment report of the intergovernmental panel on climate change, pp 1567–1612
Lehn GO, Jacobson AD, Douglas TA et al (2017) Constraining seasonal active layer dynamics and chemical weathering reactions occurring in North Slope Alaskan watersheds with major ion and isotope (δ34SSO4, δ13CDIC, 87Sr/86Sr, δ44/40Ca, and δ44/42Ca) measurements. Geochim Cosmochim Acta 217:399–420
Liao C, Zhuang Q (2017) Quantifying the role of permafrost distribution in groundwater and surface water interactions using a three-dimensional hydrological model. Arct Antarct Alp Res 49:81–100
Liao P, Li W, Jiang Y et al (2017) Formation, aggregation, and deposition dynamics of NOM-iron colloids at anoxic–oxic interfaces. Environ Sci Technol 12235–12245
Lin P, Guo L (2016) Dynamic changes in the abundance and chemical speciation of dissolved and particulate phosphorus across the river-lake interface in southwest Lake Michigan. Limnol Oceanogr 61:771–789
Loiko SV, Pokrovsky OS, Raudina TV et al (2017) Abrupt permafrost collapse enhances organic carbon, CO2, nutrient and metal release into surface waters. Chem Geol 471:153–65
Loranty M et al (2018) Changing ecosystem influences on soil thermal regimes in northern high-latitude permafrost regions. Biogeosciences 15:5287–5313
Loretta YL, Li F (2001) Heavy metal sorption and hydraulic conductivity studies using three types of bentonite admixes. J Environ Eng 10:420–429
Lung JYSLY, Tank SE, Spence C et al (2018) Seasonal and geographic variation in dissolved carbon biogeochemistry of rivers draining to the Canadian Arctic Ocean and Hudson Bay. J Geophys Res Biogeosci. https://doi.org/10.1029/2018JG004659
Maclean R, Oswood MW, Irons JG et al (1999) The effect of permafrost on stream biogeochemistry: a case study of two streams in the Alaskan (USA) taiga. Biogeochemistry 47:239–267

MacMillan GA, Girard C, Chételat J et al (2015) High methylmercury in Arctic and subarctic ponds is related to nutrient levels in the warming eastern Canadian Arctic. Environ Sci Technol 49:7743–7753

Mann PJ, Eglinton TI, McIntyre CP et al (2015) Utilization of ancient permafrost carbon in headwaters of Arctic fluvial networks. Nat Commun 6:7856

McClelland JW, Stieglitz M, Pan F et al (2007) Recent changes in nitrate and dissolved organic carbon export from the upper Kuparuk River, North Slope, Alaska. J Geophys Res Biogeosci 112(G4). https://doi.org/10.1029/2006jg000371

McGuire AD, Anderson L, Christensen TR et al (2009) Sensitivity of the carbon cycle in the Arctic to climate change (review). Ecol Monogr 79(4):523–555

McGuire AD, Hayes DJ, Kicklighter DW et al (2010) An analysis of the carbon balance of the Arctic Basin from 1997 to 2006. Tellus B 62:455–474. https://doi.org/10.1111/j.1600-0889.2010.00497.x

McNamara JP, Kane DL, Hinzman DL (1997) Hydrograph separations in an arctic watershed using mixing model and graphical techniques. Water Resour Res 33:1707–1719. https://doi.org/10.1029/97WR01033

McNamara JP, Kane DL, Hobbie JE, Kling GW (2008) Hydrologic and biogeochemical controls on the spatial and temporal patterns of nitrogen and phosphorus in the Kuparuk River, arctic Alaska. Hydrol Process 22(17):3294–3309

Miao S, DeLaune RD, Jugsujinda A (2006) Influence of sediment redox conditions on release/solubility of metals and nutrients in a Louisiana Mississippi River deltaic plain freshwater lake. Sci Total Environ 371(1–3):334–43

Morford JL, Emerson S (1999) The geochemistry of redox sensitive trace metals in sediments. Geochim Cosmochim Acta 63(11–12):1735–50

Neff JC, Finlay JC, Zimov SA et al (2006) Seasonal changes in the age and structure of dissolved organic carbon in Siberian rivers and streams. Geophys Res Lett 33. https://doi.org/10.1029/2006GL028222

Niu G-Y, Yang Z-L (2006) Effects of frozen soil on snowmelt runoff and soil water storage at a continental scale. J Hydrometeorol 7(5):937–952

O'Donnell JA, Aiken GR, Kane ES, Jones JB (2010) Source water controls on the character and origin of dissolved organic matter in streams of the Yukon River basin, Alaska. J Geophys Res: Biogeosci 115(G3). https://doi.org/10.1029/2009jg001153

O'Donnell JA, Harden JW, McGuire AD et al (2011) The effect of fire and permafrost interactions on soil carbon accumulation in an upland black spruce ecosystem of interior Alaska: implications for post-thaw carbon loss. Glob Chang Biol 17(3):1461–74

O'Donnell JA, Aiken GR, Walvoord MA, Butler KD (2012) Dissolved organic matter composition of winter flow in the Yukon River basin: implications of permafrost thaw and increased groundwater discharge. Global Biogeochem Cycles 26(4). https://doi.org/10.1029/2012gb004341

O'Donnell JA, Aiken GR, Walvoord MA et al (2014) Using dissolved organic matter age and composition to detect permafrost thaw in boreal watersheds of interior Alaska. J Geophys Res-Biogeosci 119:2155–2170. https://doi.org/10.1002/2014JG002695

O'Donnell JA, Aiken GR, Butler KD et al (2015) Chemical composition of rivers in Alaska's Arctic network, 2013–2014. Natural Resource Data Series, NPS/ARCN/NRDS – 2015/809. National Park Service. Fort Collins, Colorado. Published Report-2222958

O'Donnell JA, Aiken GR, Swanson DK et al (2016) Dissolved organic matter composition of Arctic rivers: linking permafrost and parent material to riverine carbon. Glob Biogeochem Cycles 30:1811–1826. https://doi.org/10.1002/2016GB005482

Olefeldt D, Persson A, Turetsky MR (2014) Influence of the permafrost boundary on dissolved organic matter characteristics in rivers within the boreal and taiga plains of western Canada. Environ Res Lett 9:035005

Pachana K, Wattanakornsiri A, Nanuam J (2010) Heavy metal transport and fate in the environmental compartments. NU Int J Sci 7(1):1–1

Page SE, Kling GW, Sander M et al (2013) Dark formation of hydroxyl radical in Arctic soil and surface waters. Environ Sci Technol 47(22):12860–7

Pastick NJ, Jorgenson MT, Wylie BK, Nield SJ, Johnson KD, Finley AO (2015) Distribution of near-surface permafrost in Alaska: Estimates of present and future conditions. Remote Sens Environ 168:301–15

Peterson BJ, Hobbie JE, Hershey AE et al (1985) Transformation of a tundra river from heterotrophy to autotrophy by addition of phosphorus. Science 229:1383–1386. https://doi.org/10.1126/science.229.4720.1383

Petrone KC, Jones JB, Hinzman LD et al (2006) Seasonal export of carbon, nitrogen, and major solutes from Alaskan catchments with discontinuous permafrost. J Geophys Res-Biogeosci 111(G2)

Philippe A, Schaumann GE (2014) Interactions of dissolved organic matter with natural and engineered inorganic colloids: a review. Environ Sci Technol 48:8946–8962

Ping C.-L, Michaelson GJ, Guo L et al (2011) Soil carbon and material flux across the eroding coastline of the Beaufort Sea, Alaska. J Geophys Res: Biogeosci 116(G02004). https://doi.org/10.1029/2010jg001588

Pokrovsky OS, Schott J (2002) Iron colloids/organic matter associated transport of major and trace elements in small boreal rivers and their estuaries (NW Russia). Chem Geol 190:141–179

Pokrovsky OS, Reynolds BC, Prokushkin AS et al (2013) Silicon isotope variations in Central Siberian rivers during basalt weathering in permafrost-dominated larch forests. Chem Geol 355:103–116

Pokrovsky OS, Manasypov RM, Loiko SV et al (2016) Trace element transport in western Siberian rivers across a permafrost gradient. Biogeosciences 13(6):1877–900

Pokrovsky OS, Karlsson J, Giesler R (2018) Freeze-thaw cycles of Arctic thaw ponds remove colloidal metals and generate low-molecular-weight organic matter. Biogeochemistry 137 (3):321–336

Raudina TV, Loiko SV, Lim A et al (2018) Permafrost thaw and climate warming may decrease the CO 2, carbon, and metal concentration in peat soil waters of the Western Siberia Lowland. Sci Total Environ 634:1004–23

Raymond PA, McClelland JW, Holmes RM et al (2007) Flux and age of dissolved organic carbon exported to the Arctic Ocean: a carbon isotopic study of the five largest rivers. Global Biogeochem Cycles 21. https://doi.org/10.1029/2007GB002934

Rember RD, Trefry JH (2004) Increased concentrations of dissolved trace metals and organic carbon during snowmelt in rivers of the Alaskan Arctic. Geochim Cosmochim Acta 68(3):477–489

Rice KM, Walker EM Jr, Wu M et al (2014) Environmental mercury and its toxic effects. J Prev Med Public Health 47(2):74–83

Romanovsky VE, Smith SL, Christiansen HH (2010) Permafrost thermal state in the polar Northern Hemisphere during the international polar year 2007–2009: a synthesis. Permafrost Periglac 21:106–116. https://doi.org/10.1002/ppp.689

Roulet N, Moore TR (2006) Environmental chemistry: browning the waters. Nature 444:283–284

Salvadó JA, Tesi T, Andersson A et al (2015) Organic carbon remobilized from thawing permafrost is resequestered by reactive iron on the Eurasian Arctic Shelf. Geophys Res Lett 42 (19):8122–30

Sannel ABK, Kuhry P (2011) Warming induced destabilization of peat plateau/thermokarst lake complexes. J Geophys Res 116:G03035

Schartup AT, Mason RP, Balcom PH et al (2013) Methylmercury production in estuarine sediments: role of organic matter. Environ Sci Technol 47:695–700

Schlesinger WH, Bernhardt ES (2013) Biogeochemistry: an analysis of global change. Academic Press, Cambridge

Schuster PF, Schaefer KM, Aiken GR et al (2018) Permafrost stores a globally significant amount of mercury. Geophys Res Lett 45(3):1463–71

Schuur EAG, McGuire AD, Schadel C et al (2015) Climate change and the permafrost carbon feedback. Nature 520:171–179

Skłodowski P, Maciejewska A, Kwiatkowska J (2006) The effect of organic matter from brown coal on bioavailability of heavy metals in contaminated soils. Nato science series SS IV Ear, vol 3, pp 299–307

Slavik K, Peterson BJ, Deegan LA et al (2004) Long-term responses of the Kuparuk River ecosystem to phosphorus fertilization. Ecology 85(4):939–54

Spencer RG, Aiken GR, Wickland KP et al (2008) Seasonal and spatial variability in dissolved organic matter quantity and composition from the Yukon River basin, Alaska. Glob Biogeochem Cycles 22(4). https://doi.org/10.1029/2008gb003231

Spencer RG, Mann PJ, Dittmar T et al (2015) Detecting the signature of permafrost thaw in Arctic rivers. Geophys Res Lett 42(8):2830–5

Stähl M, Bayard D, Wydler H et al (2004) Snowmelt infiltration into alpine soils visualized by dye tracer technique. Arct Anarct Alp Res 36:128–135

Stevenson EI, Aciego SM, Chutcharavan P et al (2016) Insights into combined radiogenic and stable strontium isotopes as tracers for weathering processes in subglacial environments. Chem Geol 429:33–43

Stevenson R, Pearce CR, Rosa E et al (2018) Weathering processes, catchment geology and river management impacts on radiogenic (^{87} Sr/^{86} Sr) and stable ($\delta^{88}/^{86}$ Sr) strontium isotope compositions of Canadian boreal rivers. Chem Geol 486:50–60

Stolpe B, Guo L, Shiller AM, Aiken GR (2013) Abundance, size distributions and trace-element binding of organic and iron-rich nanocolloids in Alaskan rivers, as revealed by field-flow fractionation and ICP-MS. Geochim Cosmochim Acta 105:221–239

Striegl RG, Aiken GR, Dornblaser MM et al (2005) A decrease in discharge-normalized DOC export by the Yukon River during summer through autumn. Geophys Res Lett 32(21):L21413

Striegl RG, Dornblaser MM, Aiken GR et al (2007) Carbon export and cycling by the Yukon, Tanana, and Porcupine rivers, Alaska, 2001–2005. Water Resour Res 43(2). https://doi.org/10.1029/2006wr005201

Tank SE, Striegl RG, McClelland JW et al (2016) Multi-decadal increases in dissolved organic carbon and alkalinity flux from the Mackenzie drainage basin to the Arctic Ocean. Environ Res Lett 11(5):054015

Tape K, Sturm M, Racine C (2006) The evidence for shrub expansion in Northern Alaska and the Pan-Arctic. Glob Chang Biol 12:686–702

Tarnocai C, Canadell JG, Schuur EAG et al (2009) Soil organic carbon pools in the northern circumpolar permafrost region. Glob Biogeochem Cycles 23:1–11

Toohey RC, Herman-Mercer NM, Schuster PF et al (2016) Multidecadal increases in the Yukon River Basin of chemical fluxes as indicators of changing flowpaths, groundwater, and permafrost. Geophys Res Lett 43:12120–12130. https://doi.org/10.1002/2016GL070817

Tranter M, Brimblecombe P, Davies TD et al (1986) The composition of snowfall, snowpack and meltwater in the Scottish highlands-evidence for preferential elution. Atmos Environ 20:517–525

Tranvik LJ, Downing JA, Cotner JB et al (2009) Lakes and reservoirs as regulators of carbon cycling and climate. Limnol Oceanogr 54:2298–2314

Trusiak A, Treibergs LA, Kling GW et al (2018) The role of iron and reactive oxygen species in the production of CO2 in arctic soil waters. Geochim Cosmochim Acta 224:80–95

Turetsky MR, Kane ES, Harden JW et al (2011) Recent acceleration of biomass burning and carbon losses in Alaskan forests and peatlands. Nat Geosci 4:27–31

Vaughan DG (2013), Observations: cryosphere. In: Stocker TF et al (eds) Climate change 2013: the physical science basis. Contribution of working group I to the fifth assessment report of the intergovernmental panel on climate change. Cambridge Univ. Press, Cambridge

Vincent WF, Lemay M, Allard M (2017) Arctic permafrost landscapes in transition: towards an integrated Earth system approach. Arct Sci 3:39–64

Vitousek PM, Howarth RW (1991) Nitrogen limitation on land and in the sea: how can it occur? Biogeochemistry 13(2):87–115

Vitousek PM, Reiners WA (1975) Ecosystem succession and nutrient retention: a hypothesis. Bioscience 25(6):376–81

Vitousek PM, Aber JD, Howarth RW et al (1997) Human alteration of the global nitrogen cycle: sources and consequences. Ecol App 7(3):737–50
Vonk JE, Mann PJ, Davydov S et al (2013) High biolability of ancient permafrost carbon upon thaw. Geophys Res Lett 40:2689–2693. https://doi.org/10.1002/grl.50348
Vonk JE, Tank SE, Bowden WB et al (2015a) Reviews and syntheses: effects of permafrost thaw on arctic aquatic ecosystems. Biogeosciences 23:7129–7167
Vonk JE, Tank SE, Mann PJ et al (2015b) Biodegradability of dissolved organic carbon in permafrost soils and aquatic systems: a meta-analysis. Biogeosciences 12:6915–6930. https://doi.org/10.5194/bg-12-6915-2015
Walvoord MA, Striegl RG (2007) Increased groundwater to stream discharge from permafrost thawing in the Yukon River basin: potential impacts on lateral export of carbon and nitrogen. Geophys Res Lett 34. https://doi.org/10.1029/2007GL030216
Walvoord MA, Kurylyk BL (2016) Hydrologic impacts of thawing permafrost—a review. Vadose Zone J 15:vzj2016.01.0010
Walvoord MA, Voss CI, Wellman TP (2012) Influence of permafrost distribution on groundwater flow in the context of climate-driven permafrost thaw: example from Yukon Flats Basin, Alaska, United States. Water Resour Res 48:7524. https://doi.org/10.1029/2011W011595
Ward CP, Nalven SG, Crump BC et al (2017) Photochemical alteration of organic carbon draining permafrost soils shifts microbial metabolic pathways and stimulates respiration. Nat Commun 8(1):772
Wauthy M, Rautio M, Christoffersen KS et al (2018) Increasing dominance of terrigenous organic matter in circumpolar freshwaters due to permafrost thaw. Limnol Oceanogr Lett 3(3):186–98
Weishaar JL, Aiken GR, Bergamaschi BA et al (2003) Evaluation of specific ultraviolet absorbance as an indicator of the chemical composition and reactivity of dissolved organic carbon. Environ Sci Technol 37(20):4702–8
Williams MW, Melack JM (1991) Solute chemistry of snowmelt and runoff in an Alpine Basin, Sierra Nevada. Water Resour Res 27:1575–1588. https://doi.org/10.1029/90WR02774
Williams AGB, Scherer MM (2004) Spectroscopic evidence for Fe(II)-Fe(III) electron transfer at the iron oxide-water interface. Environ Sci Technol 38(18):4782–4790
Wu HC, Peng TR, Moore D et al (2014) Modeling dissolved organic carbon in temperate forest soils: TRIPLEX-DOC model development and validation. Geosci Model Dev 7:867–881
Xu HC, Guo L (2017) Molecular size-dependent abundance and chemical composition of dissolved organic matter in river, lake and sea waters. Water Res 117:115–126. https://doi.org/10.1016/j/waters.2017.04.006
Xu HC, Guo L (2018) Intriguing changes in molecular size and composition of dissolved organic matter induced by microbial degradation and self-assembly. Water Res 135:187–194. https://doi.org/10.1016/j.watres.2018.02.016
Xu C, Guo L, Dou F, Ping CL (2009) Potential DOC production from size-fractionated Arctic tundra soils. Cold Reg Sci Technol 55:141–150. https://doi.org/10.1016/j.coldregions.2008.08.001
Xu H, Guan D, Lin H, Guo L (2018) Contrasting effects of photochemical and microbial degradation on Cu(II) binding with fluorescent DOM from different origins. Environ Pollut 239:205–214
Yang Z, Yang S, Van Nostrand JD et al (2017) Microbial community and functional gene changes in Arctic tundra soils in a microcosm warming experiment. Front Microbiol 8:1741
Yin H, Tan N, Liu C et al (2016) The associations of heavy metals with crystalline iron oxides in the polluted soils around the mining areas in Guangdong Province, China. Chemosphere 161:181–9

Dr. Jonathan O'Donnell is an Ecologist with the National Park Service's Arctic Inventory and Monitoring Network in Anchorage, Alaska. His research focuses on carbon cycling in terrestrial and aquatic ecosystems in Arctic and boreal regions, and how climate and disturbance may alter the fate of carbon. He received his Doctoral and Master's degrees from the Department of Biology & Wildlife at the University of Alaska Fairbanks.

Dr. Thomas A. Douglas is a Senior Scientist and Research Geochemist at the U.S. Army's Cold Regions Research and Engineering Laboratory in Fairbanks, Alaska. He uses geochemical tracers to investigate environmental processes occurring in the snowpack, on sea ice, and in cold regions soil and water. Many of his current projects are focused on predicting the response of permafrost to climate warming and the biogeochemical processes occurring in permafrost soils. This work combines remote sensing, geophysics, extensive site measurements, coring and laboratory measurements, and geospatial analyses to link terrain properties with soil and vegetation characteristics. He holds a Master's degree in Geology from the University of Alaska Fairbanks and a Ph.D. in Earth Sciences from Dartmouth College and is an Affiliate Faculty Member in the Department of Chemistry and Biochemistry at the University of Alaska Fairbanks.

Dr. Amanda Barker is a Research Chemist in the Biogeochemical Sciences Branch at the U.S. Army Cold Regions Research and Engineering Laboratory (CRREL) in Fairbanks, Alaska, USA. Her research interests include fate and transport of elements in the environment, permafrost-active layer dynamics, and analytical tools for bulk- and micro-scale geochemical characterization. He received her Doctoral degree in Environmental Chemistry at the University of Alaska Fairbanks.

Dr. Laodong Guo is a Professor in the School of Freshwater Sciences at the University of Wisconsin Milwaukee. His major research focus is on the biogeochemical cycling of carbon, nutrients (N, P, and Si), and trace elements (also radionuclides) in aquatic environments including high-latitude rivers. He received his Doctoral degree in Chemical Oceanography at Texas A&M University, College Station. Before coming to UWM, he was a faculty member at the University of Southern Mississippi (2005–2012) and University of Alaska Fairbanks (2000–2005).

Arctic Wetlands and Lakes-Dynamics and Linkages

12

Kathy L. Young, Laura Brown, and Yonas Dibike

Abstract

Arctic wetlands can occur as isolated patches with areas of 1–10 km^2, or they can cover extensive areas in the landscape. Wetlands exert a strong influence on the hydrological cycle as they can both store and release water to streams, other wetlands (ponds) and replenish groundwater reserves. Arctic landscapes are also rich with lakes and their occurrence depends on geology, geomorphic or anthropogenic setting. Like ponds, lake sustainability over time depends on inputs exceeding losses. Hence, their capacity to hold water and the nature of shifting storage capacity especially in light of climate warming (shifts in precipitation/evaporation), or stream/river connectivity, together with growing expansion of mining, oil development are critical issues for northern ecosystems and communities. To survive over time, a wetland or lake needs positive water storage to maintain a high degree of saturation (wetland) or storage capacity (lake). Snow is particularly important, and for Arctic wetlands and lakes, it is the total winter snow accumulation that is of major hydrological consequence. Summer rainfall in most permafrost areas is not high, and often is insufficient to match evaporation rates in lakes. However, the frequency and duration of rainfall can be important for arctic wetlands. Climate warming has been tied to an increase in ground thaw, resulting in both the loss of lakes/ponds and expansion

K. L. Young (✉)
Department of Geography, York University, Toronto, ON, Canada
e-mail: klyoung@yorku.ca

L. Brown
Department of Geography, University of Toronto Mississauga, Mississauga, ON, Canada
e-mail: lc.brown@utoronto.ca

Y. Dibike
Environment and Climate Change Canada, Watershed Hydrology and Ecology Division, Victoria, BC, Canada
e-mail: yonas.dibike@canada.ca

D. Yang and D. L. Kane (eds.), *Arctic Hydrology, Permafrost and Ecosystems*,
https://doi.org/10.1007/978-3-030-50930-9_12

of ponds/lakes depending on permafrost conditions. The timing of ice cover on lakes can affect evaporation, where shallower lakes that experience bed-fast ice during the winter become ice-free sooner in the warm season, which leads to longer open-water seasons and greater amounts of evaporation. Northern lakes have shown shifts towards shorter ice cover duration during the cold seasons, resulting in longer open-water seasons. Lake ice modelling suggests continued shifts towards earlier break-up and later freeze-up may be expected.

12.1 Importance and Linkages to Other Elements

A wetland is defined as 'lands saturated for most parts of the growing season to allow the development of hydric soils, or support of hydrophytes or prolonged flooding up to a depth of 2 m' (National Wetlands Working Group 1988). For hydrological purposes, wetlands can be subdivided into bogs, fens and inundated lands, which include marshes/swamps and ponds. Bogs obtain water supply mainly from the atmosphere (rain, snow, fog) and shed water to their surroundings whereas fens usually receive lateral drainage from surface and subsurface sources. Marshes and swamps (the latter have an abundance of trees) are located along the shores, being inundated for various durations by river, lake or sea water. Ponds are water bodies arbitrarily distinguished from lakes using a depth criterion of never reaching 2 m depth. Arctic wetlands occur as isolated patches with areas of 1–10 km^2, or they cover extensive areas in the landscape (Woo and Young 2006). Patchy wetlands are particularly common in the High Arctic. Extensive wetlands are commonly encountered on coastal and interior plains. Wetlands exert a strong influence on the hydrological cycle (Bullock and Acereman 2003), as they can both store and release water to streams, other wetlands (ponds) and replenish groundwater reserves. Their structure and function can shift in response to climate warming/variability (e.g., Hayashi et al. 2004; Young and Abnizova 2011), from infrastructure installations (runways, roads, bridges, oil pads), or artificial drainage due to agricultural needs (Arnalds et al. 2016).

Arctic landscapes are rich with lakes, and their occurrence depends on geology, geomorphic or anthropogenic setting (Woo 2012). There are bedrock-type lakes, ones shaped by volcanic activity (crater lakes, lava dammed lakes), glaciers, or alluvial and shoreline lakes (Woo 2012). Thermokarst lakes in permafrost areas and oriented lakes are also common and exhibit high to moderate ground ice contents (Vincent et al. 2013; Ulrich et al. 2017). Large lakes >500 km^2 are also found throughout the circumpolar Arctic. One of the largest above the Arctic Circle is Lake Taymyr (lat. 74.1°N, 4560 km^2, average depth of 2.5 m) in northern Russia (Vincent et al. 2013). Large, deep lakes in Canada's North include Great Bear Lake (65–67°N, area of 31,153 km^2, average depth of 76 m). Artificial lakes (e.g., reservoirs) are often created by human activity and support hydro-electric power or water for consumption. Like ponds, lake sustainability over time depends on inputs

exceeding losses. Hence, their capacity to hold water and the nature of shifting storage capacity especially in light of climate warming (shifts in precipitation/evaporation), or stream/river connectivity, together with growing expansion of mining, oil development are critical issues for northern ecosystems and community members (Rouse et al. 2008; Woo 2012; Vincent et al. 2013; Chen et al. 2014; Ulrich et al. 2017).

12.2 Key Processes and Features

Hydrologic processes are the primary reason for the existence of wetlands and natural lakes, because even if a physiographic and geologic setting favourable for formation of a wetland or lake exists, hydrologic conditions must be such that water will persist long enough for a wetland or lake to form (Winter 1988; Woo 2012).

12.2.1 Water Balance

To survive over time, a wetland or lake needs a positive water storage to maintain a high degree of saturation (wetland) or storage capacity (lake), necessitating the water inputs exceed water losses.

$$\begin{matrix} \textit{Storage Change} & \textit{Inputs} & \textit{Losses} \\ \dfrac{\mathrm{d}S}{\mathrm{d}t} = [P(Sn+R)+Q_{\mathrm{in}}] - [E+Q_{\mathrm{out}}] \end{matrix} \tag{12.1}$$

Here, $\mathrm{d}S/\mathrm{d}t$ is change in storage during time interval $\mathrm{d}t$, P is precipitation and includes both snowfall (water equivalent) (Sn) and rainfall (R). Q_{in} are inputs into the wetland or lake system from surface and subsurface routes. Losses of water from wetlands and lakes include evaporation *(E)* from open water and adjacent wet areas (wetland, shallow lake) which tend to expand and shrink over a summer season, and water losses to groundwater or surface runoff from the wetland/lake (Q_{out}). Table 12.1 (updated from Woo and Young 2012) presents values of water balance components for selected wetlands and lakes across the Arctic. The period of study ranges from one to several years.

12.2.2 Water Sources

Water for wetlands and lakes is derived from direct precipitation, snow and ground ice melt in the wetlands, spillage of lakes (for wetlands) and rivers, coastal inundation, meltwater and groundwater inflows from nearby hillslopes, or from upstream catchments. If near a glacier, lakes and wetlands can receive ice melt inputs (Björnsson 2010; Woo 2012). Snow is particularly important and for Arctic

Table 12.1 Components of water balance for selected wetlands and lakes in Subarctic, Low Arctic and High Arctic in Canada and Alaska (all values in mm) (updated from Woo and Young 2012)

Basin	Site description	Year	*Sn*	*R*	$P = Sn + R$	Q_{out}	*E*	d*S*/d*t*	Q_{out}/P
Subarctic Pelletier Wetland—patterned fen, 54°48'N, 66°49'W (Quinton and Roulet 1998)	Pool-ridge moss-peat complex; Open-closed lichen woodland (0.242 km^2)	?	268	211	479	196	181	NA	0.38
Subarctic Peat Plateau, 61°18' 48.9'N, 121°18"22.7"W (Wright et al. 2008)	Raised bog, treed plateau (black spruce, moss, lichen) 22 km^2	2004 29 Mar–4 Jun 2005 29 Apr–8 Jun	222 206, plus ground icemelt of 162	53 63	275 269	238 213	56 67	143 152 (as soil moisture change)	0.86 0.79
Low Arctic Putuligayuk Watershed, Coastal Plain, Alaska, 70°N, 148°45'W (Bowling et al. 2003)	Tundra sedge/shrub (471 km^2)	1999 2000 2001	81 117 93	172 146 NA	253 263 NA	49 87 56	188 161 NA	–2 –25 NA	0.19 0.33 NA
Low Arctic Coastal Plain, Prudhoe Bay, Alaska 70°26'n, 148°53'W (Rovansek et al. 1996)	Tundra sedge/shrub (0.224 km^2)	1992 1993	NA NA	NA NA	50.2 70.5	NA NA	165 201	–111 –114	NA NA
High Arctic Muskox Fen, Ellesmere Is., 79°58', 84°28'W (Glenn and Woo 1997)	Sedge meadow (3700 m^2)	1993 13 May to 8 Aug	47	34	81	$15 = Q_{in} - Q_{out}$	118	–22	0.18 (0.28 for the melt period)

(continued)

Table 12.1 (continued)

Basin	Site description	Year	*Sn*	*R*	*P* = *Sn* + *R*	Q_{out}	*E*	d*S*/d*t*	Q_{out}/P
High Arctic Vendom Fiord, 78°03'N, 82°12'W, (Marsh and Woo 1977)	Tundra pond (800 m^2) in a 0.5 km^2 catchment	1975 6 Jul–17 Aug	NA	30	NA	NA	27	3	NA
High Arctic Intensive Watershed, Devon Island, 75°33'N, 84°40'W, (Rydén 1977)	Coastal wetland (0.12 km^2) with 63% vegetated and bare soil, 12% water, 25% bedrock	1972 1973 1974 *Mean* *SDev.*	132 111 169 *137* *29*	36 73 35 *48* *22*	168 184 204 *184* *18*	66 83 101 *83* *18*	69 110 65 *81* *24*	1 –50 4 *–15* *30*	0.39 0.45 0.50
High Arctic Eastwind Lake, 80°08'N, 85°35'W, (Woo and Guan 2006)	Tundra ponds P1 (1080 m^2) P2 (2056 m^2) P3 (1494 m^2) P4 (1211 m^2) P5(2104 m^2)	2005 12 Jun–11 Aug (post-melt)	NA	28	NA	NA	 155 163 157 159 156	 –106(–21) –70(–65) –130(+1) –140(+10) –70(–58)	NA
High Arctic Creswell Bay, 72°43'N, 94°15'W, (Abnizova and Young 2010)	Ponds (areas in m^2): moraine (149) plateau (1074) coastal (1386) bedrock (646) moraine (149) plateau (1074) coastal (1386) bedrock (646)	Post-snowmelt 2005 12 Jun–25 Aug 2006 12 Jun–11 Aug	NA NA	41 68	NA NA	NA NA	 15 73 123 56 10 64 95 38	 –17(–8) –301(–254) –286(–202) –129(–88) –1 (–2) –183(–151) –319(–276) –107(–87)	NA NA
High Arctic Polar Bear Pass, 75°43'N 98°W (Young et al. 2017)	Pond (7245 m^2) lying below a late-lying snowbed-wet meadow continuum	Post-Snowmelt 2007 26 Jun–30 Jul 2008 24 Jun- 17 Aug	NA NA	8.4 74	NA NA	NA NA	144 120	–78[–47] –56[+13]	NA NA

(continued)

Table 12.1 (continued)

Basin	Site description	Year	*Sn*	*R*	*P* = *Sn* + *R*	Q_{out}	*E*	d*S*/d*t*	Q_{out}/P
	Sedge Moss Fen (74,093 m^2) lying below a late-lying snowbed	2009 25Jun-23 Aug	NA	89	NA	NA	104	–28.5[+17]	NA
		Post-Snowmelt 2007 26 Jun–30 Jul	NA	8.4	NA	0.6	102	73[–87]	NA
		2008 18 Jun-31 Aug	NA	74	NA	2.0	91	149[+15]	NA
		2009 27Jun-23 Aug	NA	89	NA	2.0	73	158[+15]	NA
High Arctic Polar Bear Pass, 75°43'N 98°W Young (2019)	Eastern Watershed including plateau, slopes and vegetated wetland (102.6 km^2)	2012 (5 Jun–23 Aug)	72	52	124	109	139	–125	0.89
		2013 (20 Jun–8 Aug)	83	23	106	118	39	–52	1.11

P = precipitation; *Sn* = snowfall in snow water equivalent; *R* = rainfall; Q_{out} = runoff or lateral outflow; *E* = evaporation; d*S*/d*t* = change in storage

Note that for storage change of Eastwind Lake and Creswell Bay, the first number is measured d*S*/d*t* and the second in round brackets () is the difference between calculated and measured d*S*/d*t*. For storage change at Polar Bear Pass (pond, wet meadow), the second number in square brackets [] is the error or residual term (see Young et al. 2017)

wetlands and lakes, it is the total winter snow accumulation rather than snowfall of individual events that is of major hydrological consequence. Aside from low snow years (Bouchard et al. 2013), generally, melting of winter snow replenishes storage deficits at the beginning of a new hydrological year so that wetlands start off with saturated conditions for plant growth and both lakes and wetlands can have adequate storage to buffer against summer drought. As seen in Table 12.1, snow accumulation is highest in subarctic catchments (Payette et al. 2004; Quinton and Roulet 1998; Wright et al. 2008), typically >200 mm per year and this decreases northward to around 100 mm in a given year on the Alaskan Coastal Plain (Bowling et al. 2003) and the Arctic Archipelagoes, reflecting the drier and colder environments of the Low and High Arctic. There are local variations. For instance, in a warm and dry polar oasis of the Canadian High Arctic (Glenn and Woo 1997; Woo and Guan 2006), snowpacks of <100 mm are the norm (Assini and Young 2012; Young et al. 2013), while wetlands in cold and dry polar deserts often capture more (100–200 mm) (Abnizova and Young 2010).

Snow depth on frozen lakes is influenced by wind redistribution, snow metamorphism and the timing of the ice formation (with snow accumulation typically beginning on land prior to ice formation) (Brown and Duguay 2010). Due to strong winds in winter, a portion of the snowfall is blown off of lakes, though it can accumulate in sheltered margins (Woo 2012). For the Alaskan Arctic Coast Plain, Sturm and Liston (2003) found that the snow depth on lake ice was ~60% less than on land, but was 21% denser (in 2000 and 2002), while in the nearby Kuparuk Basin (in spring 1997) snow depth averaged 28% less on lakes than on land. In the Churchill vicinity, Brown and Duguay (2011) and Gunn et al. (2015) found a lower ratio of on-ice snow depths of 10–30% of that measured at nearby on-shore weather stations. On the contrary, Hunting Camp Lake, Bathurst Island (Young et al. 2018) was shown to have a higher SWE than the surrounding tundra, likely as a result of the local topographic setting of the lake. The influence of warm water below a lake's ice cover favours the formation of depth hoar in the lower layers of the snow cover, when the ice is not blown free of snow (Adams 1976; Sturm and Liston 2003; Leppäranta 2015). Surface runoff and suprapermafrost groundwater from the direct catchment are critical water sources for lakes, especially if the catchment area is larger than the lake area.

With long, cold winters, the bulk of the Arctic snowpack only melts in the spring, corresponding roughly with the arrival of sustained above-freezing air temperatures. The timing and duration of snowmelt is crucial in wetland systems because they define when and how much water becomes available for surface storage, infiltration and for runoff. For lakes, runoff generally lags after runoff generation from Arctic slopes (Woo 2012). Melt begins earlier in the subarctic than in the Low and High Arctic. Quinton and Roulet (1998) noted that melt started at the end of April for a ridge-pool fen in subarctic Quebec, while snowmelt typically commences in mid-May for wetlands in the Low Arctic (Rovansek et al. 1996) and in many polar oases of the High Arctic (Rydén 1977; Glenn and Woo 1997; Woo and Guan 2006). Polar oases are typically located in intermontaine areas, sheltered from prevailing low-pressure systems. They frequently have warmer springs and

higher solar radiation receipt than polar desert sites, even ones located at the same or lower latitudes (Woo and Young 1997). There is, however, much variability in the amount, timing and duration of melt, from year-to-year and from site-to-site even within a small area owing to local wind-topographic interactions in the High Arctic, or wind-vegetation interactions in the Low Arctic and the subarctic.

Summer rainfall in most permafrost areas is not high, and is often insufficient to match evaporation rates in lakes (Woo 2012). However, the frequency and duration of rainfall are important in the summer water budget, especially for the ponds and wet meadows that do not receive reliable lateral inflows (Woo and Young 2014; Young et al. 2006). Steady inputs of rainfall over a summer season appear to be more useful in satisfying evaporative demand, sustaining wetland storage and connectivity between wetland elements (peat bogs, fens) (Quinton and Roulet 1998) than long stretches of drought punctuated by heavy rainfall. However, late-summer rainfall can help to recharge ponds and wet meadows to snowmelt-season levels (Abnizova and Young 2010; Woo and Guan 2006), possibly offsetting any detrimental effects of low snow storage the following year (Bouchard et al. 2013). Like snowfall (melt), rainfall inputs decline as latitude increases with subarctic regions receiving much more summer precipitation (rainfall) than high arctic locations (see Table 12.1, Kane and Yang 2004). On a meso-scale, wetlands/lakes in polar oases receive less rain than polar desert sites (Woo and Young 1997).

The existence of most patchy wetlands and the maintenance of a high degree of saturation in extensive wetlands depend upon near surface and subsurface inflows, including water from lateral flooding of riparian and littoral zones (Woo and Young 2003), spillage from lakes (Roulet and Woo 1986a), slope drainage (Rovansek et al. 1996), glacier runoff (including outburst floods) (Björnsson 2010) and meltwater from late-lying snowbeds (Young and Lewkowicz 1988). Woo and Guan (2006) found that meltwater inflow from upslope was the main water source responsible for filling high arctic ponds in spring, a finding similar to that of Bowling et al. (2003) and Rovansek et al. (1996) for the Alaskan Arctic Coastal Plain, and Wright et al. (2008) for subarctic wetlands. Hayashi et al. (2004) indicate that meltwater drainage from peat plateaus into subarctic fens is effective in lowering the albedo, thereby enhancing the ablation of ice in the fen and the underlying frozen peat. Paquette et al. (2015) noted that shallow water hillslope inflows (rills and water tracks), which flow across dark, sunlight-absorbing soil is effective in developing a seasonal moat for Ward Hunt Lake (perennial lake ice) though ice totally disappeared here in 2011 and 2012. Groundwater inputs failed to be important for maintaining the saturated status of a high arctic pond-wet meadow landscape on Bathurst Island (see Table 12.1, Young et al. 2017). In contrast, the discharge of groundwater from deep-seated (e.g., sub-permafrost) sources provides steady water supply to some wetlands in the discontinuous permafrost areas, particularly in carbonate terrain. Moreover, in discontinuous regions, sub-permafrost groundwater is a water source to some lakes and not others depending on their topographic position in the landscape (see Fig. 12.1 and Woo 2012).

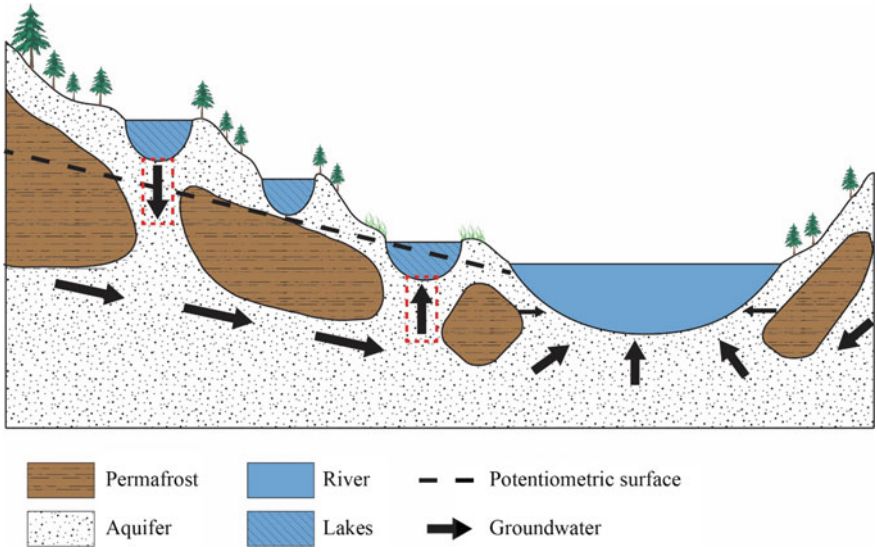

Fig. 12.1 In discontinuous regions, sub-permafrost groundwater is a water source to some lakes and not others, depending on their topographic position in the landscape. Diagram modified after Chen et al. (2014)

Riparian wetlands and lakes are usually flooded by high flows associated with annual river breakups. However, spring flood does not necessarily lead to complete inundation of all wetlands or lakes in a large delta. For example, only 60% of the Colville delta is flooded in any given year (Walker and Hudson 2003). For the Ob River delta, this exchange of water (river-lake) can be higher (90% of the delta) (Woo 2012). The presence of river ice jams amplifies the magnitude of floods which is crucial to flooding wetlands/lakes perched above regular river stage, such as the Peace-Athabasca Delta (Prowse and Conly 1998; Peters et al. 2006), or wetlands/lakes separated from river channels by levees, such as the Mackenzie Delta (Marsh and Hey 1989). In addition, episodic storm surges can produce backwater effects that raise the river stage to drown deltaic wetlands and lakes, as happened in the Mackenzie Delta (Marsh and Schmidt 1993). Ice events in the Lena Delta can play a significant role as well. Fedorva et al. (2013) report that ice jams may not only cause a sharp increase of the Bykovskaya branch water level, but can also block runoff entirely on the Olenekskaya and sometimes, on the Turnatskaya branches. On a much more local scale, Young (2008) reported that deep snow and ice in a mountain stream channel blocked meltwater inflow to a low-lying riparian zone causing the wetland to dry out before the snow dam was finally released and the wetland was flooded. In Iceland, glacial outburst floods (jökulhaups) can flood outwash plains (sandur-singular; sandar-plural), the extent being defined by the type of jökulhaup (Björnsson 2010). During eruptions, volcanic ash can elevate streambeds and sandar levels allowing subsequent heavy rainfall or glacial

Fig. 12.2 Heavy rainfall and glacial meltwater inputs flood a sandur and breech a levee spilling water into a low-lying, lush wet meadow in South-east Iceland. Photograph taken late August, 2014 by K. L. Young

meltwater inputs to overflow stream banks and breech levees flooding low-lying, lush wet meadows (Fig. 12.2).

In the subarctic, Canadian Shield lakes demonstrate the importance of catchment runoff to lake storage capacity. Mielko and Woo (2006) indicated three different flow pathways into lakes. They include fast flow delivery from upland bedrock areas adjacent to lakes, slower flow from soil-filled valleys and bottomlands and meltwater detained in depressions, which may either evaporate or infiltrate to groundwater before entering the lake at a later time. In addition to runoff from direct catchment areas, inflow from upstream areas can occur. For example, Great Slave Lake in NWT receives over 80% of its water from rivers that flow into the lake, notably from the extensive Slave River. Inflow, however, is meagre for headwater lakes, and for lakes in semi-arid catchments. Here the position of the lake in the landscape (semi-arid) may be an important factor, as upstream lakes may deprive lower lakes from storage replenishment (Woo 2012).

The importance of ground ice contribution varies depending on ice content in the frozen soil and the depth of seasonal thaw. Woo and Guan (2006) indicated that ground ice melt was not an important source of water to their cluster of tundra ponds despite the presence of massive ground ice in the vicinity. Elsewhere in the

High Arctic, Young and Woo (2000) reported that ground ice melt can be important to patchy wetlands, and Young et al. (2017) found that it serves to maintain saturation in a wet meadow offsetting evaporation, especially during warm, dry years. Abnizova and Young (2010) also noted that ground ice melt elevated an arctic pond level during a dry, warm year. Roulet and Woo (1986b) and Wright et al. (2008) determined ice melt to be significant in a low arctic fen and at a subarctic peat bog, but much of the moisture in the wetland soil froze back as ground ice in the winter. In a recent study evaluating the expansion of young thermokarst lakes in the Central Yakutsk region, Fedorov et al. (2014) demonstrated that ground ice melting in the water balance of young thermokarst lakes was significant, accounting for up to one-third of the total water input. This was confirmed by morphological changes in the lakes.

Ground ice melting can also contribute to the rapid drainage of thermokarst lakes (Marsh et al. 2009; Jones and Arp 2015). Jones and Arp (2015) monitored the catastrophic collapse of a thermokarst lake in the Alaskan Arctic Coastal Plain and proposed that the early summer weather conditions (cooler temperatures with higher than normal rainfall and snowmelt) primed the lake for drainage along an ice-wedge network (Jones and Arp 2015).

12.2.3 Wetland and Lake Storage

There is a misconception that wetlands in arctic regions are an effective modulator of flow due to their storage capacity (Winters 1988). Subsurface storage capacity is limited to the active layer, a seasonally frozen and thawed zone overlying the permafrost. Within this zone is a peat layer which ubiquitously covers most wetlands. The top part of the peat layer, known as the acrotelm, is generally porous and has high hydraulic conductivity, in contrast to the lower compacted section, known as the catotelm with high density, lower porosity and restricted hydraulic conductivity. The hydraulic conductivity, a measure of how easily water can be transmitted through the medium, decreases exponentially downward from ground surface (Quinton et al. 2008). Consequently, most subsurface water storage and movement occur in the acrotelm and through the living plant mat of the wetlands.

Arctic wetland storage undergoes large changes in the course of a year. The seasonal freeze-thaw depth in wetlands is shallower than their adjacent uplands due to the effective insulation property of thawed (and especially dry) peat (Carey and Woo 1998). Freezing of the active layer converts most of its water into ground ice for winter storage. Where groundwater supply is sustained, such as in subarctic fens, descent of the freezing front forces some water to break through the frozen cap and spread above ground to freeze as icing (Price and FitzGibbon 1987). In hilly terrain, the merging of seasonally frozen ground with an impervious base like permafrost or rock creates pressure in the unfrozen groundwater upslope, causing the water to seek exit to the ground surface (Carey 1973). In addition to icing, surface storage in winter includes ice in the many pools, ponds and lakes, and snow that falls and stays on them.

The arrival of spring replenishes wetland storage typically with ample snow meltwater. Surface storage in the thaw season is afforded by numerous depressions of different sizes on the wetland surface. They range from inconspicuous undulations and small rills, the troughs between earth hummocks and tussocks, cracks along the rims of ice-wedge polygons, pools of patterned bogs and fens, to the tundra ponds and shallow depressions on flood plains, deltas and coastal zones. Subsurface storage switches from icy frozen soil with extremely low liquid storage capacity to a thawed state that can accommodate water inputs. However, it is often the surface rather than the subsurface component of storage that holds the bulk of water. In summer, storage is drawn down mainly by evaporation. It is chiefly in the dry season with a deepened thaw layer and a low water table that arctic wetlands offer adequate capacity to absorb and retain water from rain and lateral inflow. The stored water is then released gradually to outflow, lost to evaporation or freezes in situ if energy levels start to decline (late summer, early fall).

Lake storage increases as snowmelt runoff arrives, although the outlet of Arctic lakes can often still be blocked by snow and ice, further increasing the storage (and possibly flooding low-lying areas) until the blockage dissipates or is eroded (FitzGibbon and Dunne 1981; Woo et al. 1981; Meilko and Woo 2006). Meilko and Woo (2006), focussing on lakes in the NWT, highlight the three primary factors that raise lake storage levels enough to generate outflow: the rate of delivery, where runoff can lead to increased storage at a faster rate than the rate of evaporation from the lake can reduce the storage; the antecedent lake storage conditions; and the ratio of catchment to lake area, where a large basin-to-lake area would likely contribute enough runoff to balance the lake evaporation. Along the Arctic Coastal Plain, Alaska, the difference in ice-out timing between lakes with contrasting ice regimes can impact both storage and evaporation, as precipitation rarely exceeds landscape-evapotranspiration here (Arp et al. 2015). Arp et al. (2015) found that bed-fast ice lakes had between 110 and 130 days of being ice-free, transition-type lakes (100–110 days) and floating ice lakes only 80–90 days.

12.2.4 Evaporation

The intensity of evaporation depends on the availability of water and energy, the surface to air vapour pressure gradient and the intensity of turbulent motion. Surface cover (percentage open water and bare or vegetated land) and vegetation type (woody, vascular or non-vascular plants) further modify evaporation rates in wetlands. Between the termination of the main snowmelt season and the end of summer, much water in wetlands is lost to evaporation (Winters 1988). When snow disappears from a wetland, the freshly exposed surface has high moisture content. Ample available moisture and large input of energy in May and June enable high evaporation in the immediate post-melt period (Young and Labine 2010). Plant growth adds to transpiration loss but lichens and mosses, being non-transpiring, especially when dry (Kershaw and Rouse 1971). Evaporation declines when wetlands become drier and solar radiation becomes lower in the later parts of summer.

Deviations from this seasonal trend are due to changes in the weather and in wetland storage status (Young and Woo 2000; Macrae et al. 2014).

Table 12.2 presents evaporation rates and ranges for selected wetlands across the Arctic. As suggested by the reported values, bogs tend to have lower rates than fens and ponds have the highest rates. The advection of heat to the wet surface augments evaporation (Marsh and Bigras 1988) as do the summers with warmer and drier conditions than normal. The length of the evaporation season is a major consideration, being longer in the subarctic than the Low and High Arctic. Taking these factors into account, evaporation rate for the same wetland can vary greatly between years.

Lake evaporation in Arctic landscapes is largely controlled by the duration of ice coverage and the open-water season. In the open-water season, much radiation can be absorbed owing to radiation penetration due to the transparency of water and the low albedo of water (0.1). The heat absorbed in the water causes a lag in freeze-back in relation to the land in the fall, and evaporation rates are higher than the adjacent lands with larger lakes having higher evaporation losses than smaller lakes (Rouse et al. 2008). Small lakes can be subject to the effects of advection from the surrounding land (Marsh and Bigras 1988; Bello and Smith 1990; Oswald et al. 2008) (see Table 12.2). Evaporation from small lakes typically exhibits a diurnal pattern as radiation input is important in water losses (Woo 2012) but for large lakes, ones with extremely large surface areas (e.g., Great Slave Lake), synoptic scale systems (wind speed, vapour pressure differences) are key for driving evaporation.

Thermokarst lakes cover up to 25–40% of lowland arctic landscapes, including coastal plain regions of Alaska and Siberia (Arp et al. 2012). Estimation of the evaporative loss from 13 lakes during the full open-water season (ice-out to ice-on) in 2013 averaged 174 mm and ranged from 102 to 232 mm (Arp et al. 2015). This wide range of variation in one summer was best explained by considering lake depth relative to ice thickness (i.e., ice regime). A longer study indicated that over a two-year period (2012–2014), lakes that had bed-fast ice in the winter had earlier ice-off dates, which led to greater daily evaporation losses during the open-water season (1.7–2.3 mm/d) compared to evaporation from nearby lakes with floating ice regimes (0.4–1.1 mm/d) (see Table 3, Arp et al. 2015). In central Yakutia, Fedorov et al. (2014) report that the main output components of the lake water balances are sublimation from the snowpack (including catchment), and evaporation from the open-water season. Sublimation generally accounts for 16% of the snowpack, and summer potential evaporation (May to September) can vary from 202 to 403 mm, close to the weather station at Yakutsk (439 mm).

12.2.5 Lateral Outflow

The delivery of water within and from an Arctic wetland is strongly seasonal. A freshet is common in the spring due to rapid melting of snow accumulated over the long Arctic winter. The modes of surface runoff include overland flow on

Table 12.2 Rates of daily evaporation (mm d^{-1}) from selected locations in permafrost regions (updated from Woo and Young 2012)

Location	Wetland type	Period	Evaporation	References
High Arctic				
Hot Weather Ck., Ellesmere Island	Sedge-moss fen	7 Jun–8 Aug, 1993	0.5–3.8	Glenn and Woo (1997)
Eastwind Lake, Ellesmere Island	Pond Wet meadow	10 Jun–10 Aug, 1993	1.0–4.6 1.0–4.0	Woo and Guan (2006)
Vendom Fiord, Ellesmere Island	Pond	6 Jul–17 Aug, 1975	0.6[a]	Marsh and Woo (1977)
Resolute, Cornwallis Island	Patchy wetland	29 Jun–8 Aug, 1997 (cool and wet) 14 Jun–8 Aug, 1998 (warm and dry)	1.7[a] 2.6[a]	Young and Woo (2003)
Creswell Bay, Somerset Island	Sedge-moss fen Pond Sedge-moss fen Pond	July 2005 July 2006 July 2007 July 2008	1.4[a] 1.8[a] 1.5[a] 2.2[a]	Abnizova and Young (2010)
Polar Bear Pass, Bathurst Island	Sedge-moss fen Pond Sedge-moss fen Pond Sedge-moss fen Pond Sedge-moss fen Pond	July 2012 July 2013	0.4–4.0 (3.0[a]) 0.5–5.9 (4.2[a]) 0.2–3.1 (1.6[a]) 0.8–4.8 (2.6[a]) 0.4–3.6 (2.2[a]) 0.3–4.5 (2.6[a]) 0.3–3.9 (1.7[a]) 0.4–3.4 (1.9[a])	Young and Labine (2010) Young (2009)
Low Arctic				
Lone Gull or Kiggavik, Keewatin	Sedge meadow	22 Jun–1 Aug, 1983	2.2–7.3 (4.5[a])	Roulet and Woo (1986a, b)
Prudhoe Bay, Alaska	Pond	9 Jun–14 Sep, 1992 29 May–11 Sep, 1993	2.0[a] 2.1[a]	Rovansek et al. (1996)
Putuligayuk River, Alaska	Pond	10 Jun–15 Sep, 1999 17 Jun–13 Sep, 2000	1.9[a] 1.8[a]	Bowling et al. (2003)
Mackenzie River Delta, NWT	Pond (NRC Lake) Pond (Dishwater Lake) subject to heat advection	7 Jun–31 Aug, 1984 9 Jun–1 Sep, 1985	2.9[a] 2.8[a] 2.5[a] 3.9[a] 4.1[a]	Marsh and Bigras (1988)

(continued)

Table 12.2 (continued)

Location	Wetland type	Period	Evaporation	References
		16 Jun–2 Sep, 1986 15 Jun–11 Sep, 1982 15 Jun–1 Sep, 1983 7 Jun–29 Aug 1984 9 Jun–27 Aug, 1985	4.6[a] 3.9[a]	
Coastal Wetlands, Barrow, Alaska	Two thawed lakes, poorly drained, wet meadow tundra	1999–2003 (311 days)[b] 2006–2008 (46 days)[b]	0–4.7 (1.5)[a] 0.2–3.4 (1.8)[a]	Liljedahl et al. (2011)
Lena River Delta, Siberia		July 21 to Aug 21, 2008 July 21 to Aug 21, 2008	1.8[a] ± 1.0 1.0[a] ± 0.7 1.4[a] ± 0.7	Muster et al. (2012)
	Wet Sedge Dry tundra Water	July 21 to Aug 21, 2008		
		Aug 22 to Sept 14, 2008 Aug 22 to Sept 14, 2008 Aug 22 to Sept 14, 2008	0.8[a] ± 0.4 1.4[a] ± 0.9 0.7[a] ± 0.4	Muster et al. (2012)
	Wet Sedge Dry tundra Water			
SE Iceland 63°54.639'N 17°40.995'W	Sandur (bare ground) Wet meadow tundra	June 5 to Aug 30, 2016 June 5 to Aug 30, 2016	0.1–5.8 (2.1)[a] 0.1–6.9 (2.3)[a]	Scheffel (2018), unpublished MSc. Thesis
Arctic Coastal Plain, Alaska	13 Thermokarst Lakes –Bed-fast –Fice	Summer 2012–2014	1.7–2.3 0.4–1.1	Arp et al. (2015)
Subarctic				
Hudson Bay Lowland, Manitoba	Wet fen Dry fen	Summer	3.1[a] 2.6[a]	Lafleur (1990)
Schefferville, Quebec	String fen	24 May–18 Jul, 1997	4.5[a]	Quinton and Roulet (1998)
Scotty Creek, NWT	Peat plateau	29 Mar–4 Jun, 2004 19 Apr–8 Jun, 2005	0.8[a] 1.3[a]	Wright et al. (2008)
Washkugaw Ck., Ontario	Marsh/swamp	28 May–16 Aug, 1985	1–7 (3.0[a])	Woo and diCenzo (1989)

[a]indicates daily mean, otherwise the numbers indicate the range of daily evaporation during the study period;[b]indicates that evapotranspiration measurements began shortly after snowmelt ended and went until Aug 31 of the study year; ±indicates standard deviation

wetland surfaces, spillage from ponds and lakes as they become full, and channelled flow in rills, gullies and streams that cut through the wetland. These modes of flow often alternate or merge with each other within a wetland. Overland outflow and spillage take place when storage is filled to capacity (Woo and Young 2006) and water spills over vegetated borders and pond rims. Flooding of arctic wetlands recurs every spring when substantial snowmelt cannot be absorbed into storage by the frozen ground. Channelled flow is facilitated by frost cracks in the permafrost landscape, as noted by Abnizova and Young (2008) in the High Arctic. Fluvial and thermo-erosion along frost cracks enlarge the channels (Fortier et al. 2007; Boike et al. 2008) to enhance wetland drainage, resulting in a nonlinear soil moisture conditions (Godin et al. 2015) and a transition from wet to drier vegetation (Perreault et al. 2015). In an extreme case, thermokarst and erosion by running water carve new channels in ice-rich permafrost and catastrophically drain the ponds impounded by the permafrost rim (Marsh et al. 2009). Other landscape alterations leading to drainage include meander encroachment on lake or pond shorelines (Eisner et al. 2009).

Subsurface drainage of wetlands includes vertical seepage and lateral flow. Infiltration is facilitated by the highly permeable nature of the acrotelm. Deep percolation depends on properties of the substrate, being retarded by the catotelm, limited by large ice content and restricted by fine grained mineral soils or bedrocks that underlie the peat. Much water can seep into coarse soils and flow out of the wetland where the hydraulic gradient is steep (e.g., Abnizova and Young 2010). In the Lena Delta, Fedorova et al. (2013) found that much river water could infiltrate into a talik under the river bed of the Lena Delta. Flows in the Sardakhskaya branch decreased from more than 11,000 m^3/s near Gogolevsky Island (in the central delta), to 11 m^3/s at the branch outlet. They hypothesized that there was a hydraulic connection between flow in the river and the talik beneath it, that is, there was outflow to the talik in summer and inflow to the river in winter. On a much smaller scale, Young and Woo (2000) indicated the loss of runoff to a deeply thawed gravelly section of a patchy groundwater fen during a warm season (1998). Subsurface lateral flow increases after snowmelt as the ground begins to thaw. When the water table resides in the acrotelm, much of the flow moves through its organic soil matrix. Soil pipes are also common in the peat. They effectively convey water from wetlands to creeks (Woo and Dicenzo 1988) and their presence can lead to widespread thermokarsting on some river terraces (Seppälä 1997). For a subarctic wetland, Wright et al. (2009) found that subsurface flow is nearly as important as snowmelt runoff from a raised bog to a fen. Since then, Connon et al. (2014) have shown that land-cover change, moving from land types that facilitate storage to ones producing runoff were the most important in generating streamflow, accounting for 31–67 mm versus 9 mm for ground ice melt and baseflow (0.6–6.8 mm) in terms of basin water budgets. Young et al. (2017) found that the groundwater flow pattern in a low-gradient wet meadow reflected inputs of meltwater from an upslope late-lying snowbed, summer rains and evaporation demands but in the context of seasonal water budgets, groundwater inflow/outflow were negligible. Subsequently, groundwater inflow from the wet meadow to an adjacent

tundra pond was minimal, highlighting the continuing importance of snowmelt and summer precipitation in recharging selected high arctic wet meadows and ponds.

Connectivity of flow pathways is important in the generation of wetland outflows. Spring freshet is the prime time for storage recharge, and once accomplished, surplus waters can be shed from the wetland. Although the overall snow cover pattern is similar between years, slight changes in snow distribution alter the runoff pathways and linkages within a wetland (pond to pond, pond to wet meadow etc.). The prevalence of frozen grounds in all wetlands during snowmelt encourages flooding and overland flow, offering strong connectivity within the wetland and with non-wetland zones in the catchment, thereby allowing easy transfer of water and nutrients (Thompson and Woo 2009).

Within a large wetland complex, some areas generate runoff; others receive it or convey it out of the basin. Quinton et al. (2003) identified several hydrological functions in a subarctic continental wetland: permafrost plateaus that generate runoff, flat bogs that store water and channel fens that carry water out of the wetland. Flow connection among the peat plateaus, the bogs and the fens change in the course of the thaw season. Outflow from the wetland is high when these various components are linked to tap the runoff generated in large parts of the wetland, as it often occurs in the snowmelt season.

As summer advances, continued evaporation and drainage gradually dries the wetlands. The water table subsides, surface ponds shrink and surface flow connectivity diminishes, causing substantial reduction in wetland outflow. Revival of flow connection across various parts of the wetland depends on heavy rain events or episodic glacial outburst floods, or storm surges to fill the storage and expand the wet spots. Such seasonal enlargement and contraction of wet areas are commonly observed in Arctic wetlands (Bowling et al. 2003). The *fill-and-spill* mechanism appropriately describes the expansion and contraction of surface ponding and flow connectivity (Woo 2012: pp. 296–297). Ponds expand as they are filled, especially shallow ones with low shorelines. Spillage of individual ponds occurs when their levels reach the elevations of their outlet lips. Overflow provides runoff that establishes linkages among ponds and integrates the wetland drainage network. The *fill-and-spill* principle also applies to subsurface flow as the ground thaws. Differential thaw rates within a wetland give rise to an uneven frost table with many troughs and depressions that temporarily withhold suprapermafrost groundwater from drainage. Wright et al. (2009) found that spatial and temporal variations in active layer thaw create subsurface sills that prevent subsurface flow in a subarctic wetland. When sufficient water is accumulated, subsurface flow occurs as water spills over the frozen sill.

12.2.6 Streamflow from Wetlands and Lakes

The wetland streamflow is the average seasonal rhythm of discharge of rivers draining arctic wetlands (Woo 1988). The magnitude and timing of seasonal discharge reflect the processes of water inputs and losses, storage retention and release,

and winter freeze and spring thaw. Wetland rivers emerge from their winter dormancy of no flow or low flow when the snowmelt season arrives. The initiation of streamflow in arctic wetland catchments lags behind snowmelt by one to two weeks (Bowling et al. 2003; Quinton and Roulet 1998; Young et al. 2010), with the delay being more extended for large rivers and in cold and cloudy springs (Young and Woo 2000). The delay is attributed to the time needed for the meltwater (1) to percolate the snowpack to reach the ground, including the possibility of refreezing in the cold snow to form ice lenses and basal ice (Marsh and Woo 1984a, b), (2) to satisfy wetland storage requirements, such as filling topographic depressions, (3) to travel across the wetland as overland flow and through the shallow thawed acrotelm, (4) to clear the channels within the wetland which are usually infilled with snow and ice that block the flow (Woo and Heron 1987; Young 2008). Spring peak discharges are attained when the wetland drainage network is connected for flow delivery, and peaks are magnified by snow and ice breakup events in the channels. For some large wetland rivers, peak discharge may not occur until over a week after the end of the main snowmelt season.

Subsequently, discharge recedes as evaporation intensifies and storage declines. Streamflow can rise again in periods of intense or protracted summer rain or glacial outburst floods (Iceland). However, with an increased storage status, including those drained artificially (Iceland, Arnalds et al. 2016) the wetland becomes more effective in attenuating stormflow than it does with the spring freshet. Depending on antecedent moisture conditions and the amount of rainfall, arctic wetlands may or may not show discharge response in the rainy period. By early winter, streamflow ceases or if the river is fed by groundwater, baseflow continues under an ice cover.

Lake storage generally results in a more uniform and delayed outflow, reducing the effect of short-term fluctuations from upstream of the lake and extending the period of outflow from the lake. Streamflow from outlet-dammed lakes (e.g., Woo et al. 1981) can be abrupt when the obstruction is removed, with steep peaks and fast streamflow before tapering off. Streamflow from large natural lakes (e.g., Great Slave Lake and Great Bear Lake) can have a substantial effect on river flow, resulting in a prolacustrine flow regime rather than the typical nival regimes seen in arctic streamflow (Woo et al. 2018).

12.3 Recent Research Highlights

12.3.1 Climate Change

There is now compelling evidence of rising atmospheric temperatures at a planetary scale, and the greatest increases has been recorded at high northern latitudes (IPCC 2014). Global circulation models predict that the most severe ongoing warming will be in the Arctic, with temperatures up to 8 °C above present values by the end of the twenty-first century (Vincent et al. 2013). Arctic wetlands are not escaping the effects of this warming (e.g., Macrae et al. 2014; Woo and Young 2014) and

climate change modelling reveals further future changes (Avis et al. 2011), though changes can and will vary across arctic landscapes. For example, in the Hudson Bay Lowlands (HBL), Macrae et al. (2014) studying the fate of surface water bodies (ponds and lakes) in relation to climate change (since 1943) found that while air temperatures were warming and the break-up dates were earlier for lakes and ponds here, the evaporation season was not prolonged and evaporation rates did not increase owing to large variability from year-to-year. They did find that summer precipitation (rainfall) increased over the period diminishing soil moisture deficits, leading to wetter conditions. Their future modelling efforts suggested that conditions would continue to get wetter here and tundra ponds were more at risk of expanding than shrinking. This differed from Bouchard et al. (2013)'s study which suggested that low snowmelt runoff years could lead to widespread desiccation of shallow lakes existing in large landscapes such as the Hudson Bay lowlands (HBL) or the Peace-Athabasca Delta (PAD).

Climate warming has been tied to an increase in ground thaw, resulting in both the loss of lakes/ponds and expansion of ponds/lakes depending on permafrost conditions (Smith et al. 2005; Bouchard et al. 2013). At the global scale, Bouchard et al. (2013) estimate that due to degrading permafrost, the areal extent of wetlands will decline. Initially, there will be an increase in the number of days conducive to wetland formation owing to an increase in unfrozen soil moisture triggered from a lengthening of the thaw season. However, this will be followed by a dramatic decline in the days conducive to wetland formation, triggered by deeper ground thaw, leading to soil moisture draining further from the ground surface.

Thermokarst lakes on permafrost soils are expanding in size and number in certain parts of the Arctic, but in other locations they have been observed to suddenly drain as a result of thawing and erosion (Vincent et al. 2013). Thaw lakes have natural cycles of expansion, erosion, drainage and reformation, though this cycle appears to be accelerating under warmer climate conditions (Vincent et al. 2013) and other anthropogenic activities (Fedorov et al. 2014). A statistical forecast model by Arp et al. (2015) suggests that evaporation from bed-fast ice lakes will increase from 1.3 mm/d (2010–2019) to 2.0 mm/d (2090–2099) on the outer Arctic Coastal Plain, Alaska. The same model developed for floating ice lakes suggests an increase from 0.5 to 1.2 mm/d. Arp et al. (2015) surmise that there will be a "gradual convergence in hydrologic response between lakes of contrasting ice regimes as the climate warms, open-water duration lengthens, and lake evaporation increases".

Lake ice cover is a prominent feature of most arctic lakes during winter with an estimated area of up to 1.59×10^6 km^2 (Brooks et al. 2013). Ice cover has numerous effects on lake's physical, geochemical and biological characteristics affecting its ecosystem and socioeconomic services within the terrestrial arctic region (Wrona et al. 2016). Climatic variations have significant influence on the variability and change in lake ice characteristics (e.g., coverage, thickness and duration) that would have effects on evaporation, precipitation and their feedbacks on catchment hydrology (Rouse et al. 2008). There have been major reductions in the duration of lake ice coverage, particularly at more southerly latitudes, although the higher latitudes are also affected. Long-term (1846–2005) northern hemisphere

lake ice records indicated later freeze-up (+10.7 d/100 y), earlier breakup (–8.8 d/100 y) and an average reduction in ice cover duration (19.5 d/100 y) (AMAP 2011). When forced by a future climate under business as usual emission scenario (SRES A2), lake ice modelling over the northern hemisphere between 40° and 75° N projects that lake ice freeze-up will be delayed by 5–20 days and spring break-up will advance by 10–30 days, thereby resulting in an overall decrease in ice cover duration by about 15–50 days by 2040–2079, relative to the 1960–1999 baseline period (Dibike et al. 2011). These shifts are comparable to model results from Brown and Duguay (2011), using the same future climate scenario, focussing on the Canadian Arctic and Alaska (2041–2070 relative to 1961–1990). Here, the shifts were slightly reduced by including the far northern regions, with a projected mean freeze-up delay ranging from 0 to 15 days and a mean break-up advance ranging from 7 to 14 days for most of the region, with break-up in the far northern areas showing advances in the 10–25 days range. Furthermore, a shift from occasional persisting summer lake ice to seasonally ice free was projected through most of the Canadian Arctic Archipelago by the mid-century mean. These projected lake ice changes result in a reduction of maximum lake ice thickness by 10–50 cm for the northern hemisphere (Dibike et al. 2011) and 10–40 cm for the Canadian Arctic and Alaska (Brown and Duguay 2011).

The projected reductions in the duration and thickness of lake ice was also shown to result in an overall increase in lake water temperature, with summer stratification starting earlier and extending later into the year (Dibike et al. 2011). The greatest changes in water temperatures and the related vertical thermal structure are for summer and autumn with winter changes projected to be relatively small (Fig. 12.3). The range in projected changes to ice cover (and associated water changes) is due to regional variability, and the quality of temperature and snowfall projections, as well as lake-specific variables such as size and depth (Derksen et al. 2018). The loss of lake ice coverage, in terms of thickness and duration, is significant, and large reductions and associated enhanced heating of lake water have the potential to create a substantial new flux of moisture to the atmosphere and alter lake water budgets/levels. Changes in ice cover characteristics, such as changes in the proportion of white ice and the subsequent effects on light reflection and/or penetration through the ice, may also contribute to physical, chemical and biological changes within a lake.

12.3.2 Landscape Evolution

In the 1990s, Young and Woo (2000, 2003) and Woo et al. (2006) found that late-lying snowbeds were an important source of water to patchy wetlands, helping to maintain water levels and augment streamflow runoff past the end of the "normal" snowmelt season. By 2012, many of the late-lying snowbeds in the lee of slopes or existing in stream channels across the Canadian High Arctic had shrunk considerably or disappeared entirely off the landscape by summer's end. Ground thaw had increased, duration of flooding had declined and notable vegetation

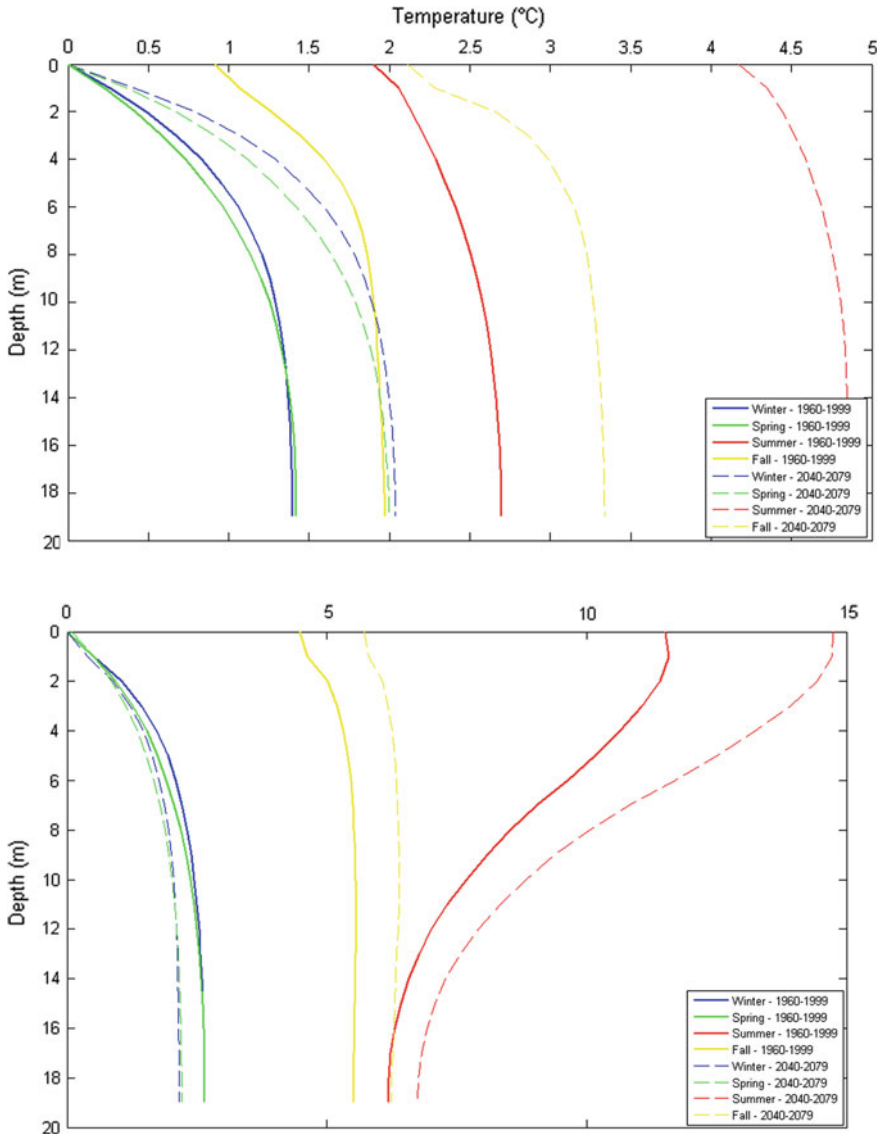

Fig. 12.3 Modelled seasonal mean lake-water temperature profiles during the 1960–1999 (solid lines) and 2040–2079 (dashed lines) time periods at **a** 60°N, and **b** 70°N latitudes located along 105°W longitude (blue: winter; green: spring; red: summer; and yellow: autumn) (modified after Dibike et al. 2011)

changes had occurred (% of plant cover, species type, and productivity) (Woo and Young 2014). It is likely that future landscape changes in upland areas due to climate warming (deepened thaw depths, vegetation cover) will also impact runoff into low-lying wetland areas. Miller and Young (2016) were able to show using a *fill-and-spill* analogy that the irregular surface topography of a mossy-lined streambed could impede surface flow to an adjacent low-lying wetland by acting as a barrier to streamflow. Lying above the water table, moss was able to absorb upslope waters to offset moisture deficits, and enhanced depression storage and evaporation loss. Greening is now occurring in the High Arctic (Jia et al. 2009), and any future increases could potentially expand moss covers into other gravelly hillslope streams, thereby modifying flow regimes into adjacent wetlands, but most likely during the post-snowmelt season.

In the subarctic, Connon et al. (2014) were able to demonstrate the recent increases in streamflow from a series of arctic streams draining large wetland watersheds which could be attributed to land use changes rather than ground ice melt contributions and groundwater flow alone. Accelerated permafrost loss was altering landscapes, shifting ones notable for storage of water (Peat Plateaus) into ones better suited for discharge (Channel Fens). They showed that it was the greater connectivity between the expanding channel fens which was leading to higher streamflow discharges.

Rapid drainage of ponds, lakes and wetlands across arctic landscapes in response to recent warming continue to be an interesting area of investigation (see Fortier et al. 2007; Boike et al. 2008; Fedorov et al. 2014 and others). Such drainage can result from the overflowing of pond rims, occur along frost cracks, subsurface piping (Woo and Dicenzo 1988) and near shorelines as a result of thermokarsting. Fedorov et al. (2014) found that increased water volumes in young thermokarst lakes often enhanced thermal erosion, and at the Yukechi site they observed the formation of thermal erosion gullies and lake drainage into a larger alas. In the short term, it appears that such rapid drainage can lead to the encroachment of vegetation grasses as the soil surface dries. Godin et al. (2014) note that the gullying processes on Bylot Island, an area of continuous permafrost where ice-wedge polygons are widespread, have resulted in increased drainage of wetlands while lowering the residence time of water near gullied areas. The gullying of the terrace in the valley has fragmented the terrace, changed the local hydrology and caused a shift in plant types (from moist to mesic) (see Perreault et al. 2015), and enabled permafrost thawing. Researchers have seen a shift in runoff type from water tracks and sheet flow to channelized flow out of the dissected ice-wedge polygons (Godin et al. 2014).

The linkages between climate warming and anthropogenic activity (e.g., agriculture, construction, water reservoirs) and their impact on the permafrost landscape are striking in Central Yakutia. Ulrich et al. (2017) indicate that disturbed surfaces, where the forest was destroyed for cultivation, are most vulnerable to permafrost degradation and thaw-lake initiation. A small active-layer deepening could initiate thermokarst processes within just a few years if ice-rich deposits are located near the surface. Yedoma lakes have grown fast in such disturbed areas over a period of

about 15 years up to 2008, with surface subsidence rates of 17–24 cm/yr. They have also increased in area and are expanding into formerly dry places. In the Nadym River Basin area, NW Siberia, Karlsson et al. (2015) report that there are some drained lakes appearing alongside stable ones. The researchers attribute this to local changes in permafrost and talik development in response to enhanced oil/gas infrastructure development in the area. If the changes were due to temporal changes in precipitation and evapotranspiration, then they would be seeing more homogenous lake-change patterns rather than a heterogeneous pattern.

12.4 Future Research Needs

As a result of climate change, it is clear that the northern landscapes are now entering a state of rapid transition (Vincent et al. 2013). Across diverse Arctic landscapes, wetlands, ponds and lakes are showing varying physical properties (expansion/contraction) along with ecosystem change (pond to wet meadow) as regional precipitation–evaporation regimes shift along with prevailing hydrologic pathways (e.g., deepening of active layer storage or enhanced talik development). There is still much debate about the causes for these changes and the rate of change. For example, Chen et al. (2014) indicate that terrestrialization/evapotranspiration is the primary mechanism for lake area reduction, and thermokarst is the primary mechanism for non-decreasing lakes (lakes that either expand or do not change). Studies by Arp et al. (2015) have shown the importance of considering the lake ice regime (bed-fast vs. floating ice) in quantifying vertical water losses and changes in hydrologic pathways. Clearly, continued investigation of both inter-lake and wetland variations in an area, not only to investigate areal change, may help provide a better understanding of the rapid hydrologic and geomorphic processes occurring within a region (Chen et al. 2014). Excellent studies of yedoma and alas landscapes in central Yakutia signal the importance of considering anthropogenic activity and its role in accelerating landscape changes in ice-rich environments and warmer climates (see Fedorov et al. 2013, 2014; Ulrich et al. 2017).

In terms of lake ice characteristics, research should continue to quantify the magnitude and spatial patterns of historical and projected changes in lake ice phenology, thickness and composition over the terrestrial Arctic region and identify the major atmospheric patterns that have produced such changes. The wider availability of satellite imagery available in recent years facilitates ice phenology monitoring through the logistically challenging northern regions, and work should continue towards developing satellite-based methods for ice thickness estimations. Research should also address the effects of ice cover changes on the regional climate, lake water-budgets, levels and local inflow regimes, including the associated physical, chemical and biological conditions.

The water budget still remains a useful framework to better improve our understanding of water dynamics in Arctic wetlands, though Arp et al. (2015) are correct in saying that measuring these components can be challenging, especially

evaporation from lakes during the open-water season. Nevertheless, we recommend continued efforts for detailed field measurements, so as to not only improve process understanding but to continue to provide reliable data for modelling efforts. This is especially needed for discontinuous landscapes that are experiencing an enhancement of talik pathways across diverse terrestrial landscapes (e.g., Connon et al. 2014).

Acknowledgments Some of the wetland information presented here is adapted and updated from a section titled "Hydrological Processes" by Woo, M. K. and K. L. Young, in a chapter titled *Arctic Wetlands and Natural Processes, Olivia, B.* et al. (2011). In: Oil and Gas Industry Impact on Arctic Wetlands, Mitigation, Recovery and Restoration Options. Peter Kershaw, A. Sirin, O. Bragg (Eds). Wetlands International Ede 2011. 184 pp. Final Report (unpublished). The authors of this chapter wish to thank Drs Daqing Yang and Doug Kane for their encouragement and editorial feedback on this chapter.

References

Abnizova A, Young KL (2008) Hillslope hydrological linkages: Importance to ponds within a polar desert High Arctic wetland. Hydrol Res 39:309–321

Abnizova A, Young KL (2010) Sustainability of High Arctic ponds in a polar desert environment. Arctic 63:67–84

Abnizova A, Young KL, Lafrenière M (2014) Pond hydrology and dissolved carbon dynamics at Polar Bear Pass wetland, Bathurst Island, Nunavut. Ecohydrology 7:73–90

Adams WP (1976) Diversity of lake cover and its implications. Musk-Ox 181:86–98

AMAP (2011) Snow, water, ice and permafrost in the Arctic (SWIPA): climate change and the cryosphere. Arctic Monitoring and Assessment Programme (AMAP), Oslo, Norway, xii + 538 pp

Arnalds O, Gudmundsson J, Oskarsson H et al (2016) Icelandic inland wetlands: characteristics and extent of draining. Wetlands 36:759–769

Arp CD, Jones BM, Lu Z et al (2012) Shifting balance of thermokarst lake ice regimes across the Arctic coastal plain of northern Alaska. Geophys Res Lett 39:L16503. https://doi.org/10.1029/2012gl052518

Arp CD, Jones BM, Liljedahl et al (2015) Depth, ice thickness, and ice-out timing cause divergent hydrologic responses among Arctic lakes. Water Resour Res 51:9379–9401

Assini J, Young KL (2012) Snowcover and snowmelt of an extensive High Arctic wetland: spatial and temporal seasonal patterns. Hydrol Sci J 57:738–755

Avis CA, Weaver AJ, Meissner KJ (2011) Reduction in areal extent of high-latitude wetlands in response to permafrost thaw. Lett Nat Geosci. https://doi.org/10.1038/ngeo1160

Bello R, Smith JD (1990) The effect of weather variability on the energy balance of a lake in the Hudson Bay Lowlands, Canada. Arctic Alpine Res 22:98–107

Bintanja R, Andry O (2017) Towards a rain-dominated Arctic. Nat Clim Chang. https://doi.org/10.1038/nclimate3240

Björnsson H (2010) Understanding jokulhlaups: from tale to theory. J Glaciol 56:1002–1010

Boike J, Wille C, Abnizova A (2008) The meteorology and energy and water balances of polygonal tundra in the Lena Delta, Siberia, during wet and dry years. J Geophys Res 113: G03025. https://doi.org/10.1029/2007/jg000540

Bouchard F, Turner KW, MacDonald LA et al (2013) Vulnerability of shallow subarctic lakes to evaporate and desiccate when snowmelt runoff is low. Geophys Res Lett 40:6112–6114

Bowling LC, Kane LD, Gieck RE et al (2003) The role of surface storage in a low-gradient Arctic watershed. Water Resour Res 39:1087. https://doi.org/10.1029/2002wr001466

Brooks RN, Prowse TD, O'Connell IJ (2013) Quantifying northern hemisphere freshwater ice. Geophys Res Lett 40(6):1128–1131
Brown LC, Duguay CR (2010) The response and role of ice cover in lake-climate interactions. Prog Phys Geogr 34:671–704
Brown LC, Duguay CR (2011) The fate of lake ice in the North American Arctic. The Cryosphere 5:869–892
Bullock A, Acreman M (2003) The role of wetlands in the hydrological cycle. Hydrol Earth Syst Sci Discuss EGU 7:358–389
Carey KL (1973) Icings developed from surface water and ground water. U.S. Army CRREL cold regions sciences and engineering monograph III-D3, p 65
Carey SK, Woo MK (1998) A case study of active layer thaw and its controlling factors. In: Proceedings of the 7th international conference on permafrost, yellowknife, NWT, pp 127–132
Chen M, Rowland JC, Wilson CJ et al (2014) Temporal and spatial pattern of thermokarst lake area changes at Yukon Flats, Alaska. Hydrol Process 28:837–852
Connon RF, Quinton WL, Craig JR et al (2014) Changing hydrologic connectivity due to permafrost thaw in the lower Liard River Valley, NWT. Hydrol Process 28:4163–4178
Derksen C, Burgess D, Duguay C et al (2018) Changes in snow, ice, and permafrost across Canada; chapter 5 in Canada's changing climate report. In Bush E and Lemmen DS (eds), Government of Canada, Ottawa, Ontario, pp 194–260
Dibike Y, Prowse T, Saloranta T et al (2011) Response of Northern Hemisphere lake-ice cover and lake-water thermal structure patterns to a changing climate. Hydrol Process 25(19):2942–2953
Eisner R, Cuomo CJ, Hinkel KM et al (2009) Advancing landscape change research through the incorporation of Inupiaq knowledge. Arctic 62:429–442
Fedorov AN, Gavrilev PP, Konstantinov PY et al (2014) Estimating the water balance of a thermokarst lake in the middle of the Lena River basin, eastern Siberia. Ecohydrology 7:188–196
Fedorva I, Chetverova A, Boishiyanov D et al (2013) Lena Delta hydrology and geochemistry. Biogeosci Discuss 10:20179–20237
FitzGibbon JE, Dunne T (1981) Land surface and lake storage during snowmelt runoff in a subarctic drainage system. Arctic Alp Res 13:277–285
Fortier D, Allard M, Shur Y (2007) Observation of rapid drainage system development by thermal erosion of ice wedges on Bylot Island, Canadian Arctic Archipelago. Permfr Periglac Process 18:229–243
Glenn MS, Woo MK (1997) Spring and summer hydrology of a valley-bottom wetland, Ellesmere Island, Northwest Territories, Canada. Wetlands 17:321–329
Godin E, Fortier D, Coulombe S (2014) Effects of thermo-erosion gullying on hydrologic flow networks, discharge and soil loss. Environ Res Lett 9:1051010
Godin E, Fortier D, Levesque E (2015) Nonlinear thermal and moisture dynamics of High Arctic wetland polygons following permafrost disturbance. Biogeosci Discuss 12:11797–11831
Gunn GE, Duguay CR, Brown LC et al (2015) Freshwater lake ice thickness derived using surface-based X- and Ku-band FMCW scattermeters. Cold Reg Sci Technol 120:115–126
Hayashi M, Quinton WL, Pietroniro A et al (2004) Hydrologic functions of wetlands in a discontinuous permafrost basin indicated by isotopic and chemical signatures. J Hydrol 296:81–97
IPCC (2014) Climate change 2014: synthesis report. Contribution of working groups I, II and III to the fifth assessment report of the intergovernmental panel on climate change. In Pachauri RK, Meyer LA (eds, core writing team) IPCC, Geneva, Switzerland, 151pp
Jia GJ, Epstein HE, Walker DA (2009) Vegetation greening in the Canadian arctic related to decadal warming. J Environ Monit 11:2231–2238
Jones BM, Arp CD (2015) Observing a catastrophic thermokarst lake drainage in Northern Alaska. Perm Perigl Process 26:119–128. https://doi.org/10.1002/ppp.1842
Kane DL, Yang D (eds) (2004) Northern research basins water balance. IAHS Publication, vol 290, 271pp

Karlsson JM, Jaramillo F, Destouni G (2015) Hydro-climatic and lake change patterns in Arctic permafrost and non-permafrost areas. J Hydrol 529:134–145

Kershaw KA, Rouse WR (1971) Studies on lichen dominated systems. I: the water relations of *Cladonia alpestries* in spruce lichen woodland in northern Ontario. Can. J of Botany 49:1389–1399

Lafleur PM (1990) Evapotranspiration from sedge-dominated wetland surfaces. Aquat Bot 37:41–353

Latifovic R, Pouliot D (2007) Analysis of climate change impacts on lake ice phenology in Canada using the historical satellite data record. Remote Sens Environ 106:492–507

Leppäranta M (2015) Freezing of lakes and the evolution of their ice cover. Springer, Berlin

Liljedahl AK, Hinzman LD, Harazono Y et al (2011) Nonlinear controls on evapotranspiration in arctic coastal wetlands. Biogeoscience 8:3375–3389

Macrae ML, Brown LC, Duguay CR et al (2014) Observed and projected climate change in the Churchill region of the Hudson Bay Lowlands and implications for pond sustainability. Arct Antarct Alp Res 46:272–285

Marsh P, Bigras SC (1988) Evaporation from Mackenzie Delta lakes, N.W.T., Canada. Arct Alp Res 20:220–229

Marsh P, Hey M (1989) The flooding hydrology of Mackenzie Delta lakes near Inuvik, N.W.T., Canada. Arctic 42:41–49

Marsh P, Schmidt T (1993) Influence of a Beaufort Sea storm surge on channel levels in the Mackenzie Delta. Arctic 46:35–41

Marsh P, Woo MK (1984a) Wetting front advance and freezing of meltwater within a snow cover. Observations in the Canadian Arctic. Water Resour Res 16:1853–1864

Marsh P, Woo MK (1984b) Wetting front advance and freezing of meltwater within a snow cover. 2. A simulation model. Water Resour Res 16:1865–1874

Marsh P, Russell M, Pohl S et al (2009) Changes in thaw lake drainage in the Western Canadian Arctic from 1950 to 2000. Hydrol Process 23:145–158

Mielko C, Woo MK (2006) Snowmelt runoff processes in a headwater lake and its catchment, subarctic Canadian Shield. Hydrol Process 20:987–1000

Miller EA, Young KL (2016) Evaluation of the presence of streambed vegetation on storage and runoff in hillslope streams in a High Arctic environment. Ecohydrol 9:719–737

Muster S, Langer M, Heim B et al (2012) Subpixel heterogeneity of ice-wedge polygonal tundra: a multi-scale analysis of land cover and evapotranspiration in the Lena River Delta, Siberia. Tellus 64:17301. https://doi.org/10.3402/tellusb.v64i0.17301

National Wetland Working Group (1988) Wetlands of Canada. Ecological land classification series no. 24, Environment Canada and Polysciences Publications Inc., Montreal, 452p

Oswald CJ, Rouse WR, Binyamin J (2008) Modeling energy fluxes in the Mackenzie River Basin using bulk aerodynamic mass transfer theory. In: Woo MK (ed) Cold region atmospheric and hydrologic studies, the Mackenzie GEWEX experience, vol 2, Hydrologic processes. Springer, Berlin, pp 161–180

Payette S, Delwaide A, Caccianiga M et al (2004) Accelerated thawing of subarctic peatland permafrost over the last 50 years. Geophys Res Lett 30:L18208. https://doi.org/10.1029/2004gl020358

Paquette M, Fortier D, Mueller DR, Sarrazin D, Vincent WF (2015) Rapid disappearance of perennial ice on Canada's most northern lake. Geophys Res Lett. https://doi.org/10.1002/2014GL062960

Perreault N, Levesque E, Fortier D et al (2015) Thermo-erosion gullies boost the transition from wet to mesic vegetation. Biogeosci Discuss 12:12191–12228

Peters DL, Prowse TD, Pietroniro A et al (2006) Flood hydrology of the Peace-Athabasca Delta, Northern Canada. Hydrol Process 20:4073–4096

Price JS, FitzGibbon JE (1987) Groundwater storage-streamflow relations during winter in a subarctic wetland, Saskatchewan. Can J Earth Sci 24:2074–2081

Prowse TD, Conly M (1998) Impacts of climatic variability and flow regulation on ice jam flooding of a northern Delta. Hydrol Process 12:1589–1610
Quinton WL, Roulet NT (1998) Spring and summer runoff hydrology of a subarctic patterned wetland. Arct Alpine Res 30:285–294
Quinton WL, Hayashi M, Pietroniro A (2003) Connectivity and storage functions of channel fens and flat bogs in northern basins. Hydrol Process 17:3665–3684
Quinton WL, Hayashi M, Carey SK (2008) Peat hydraulic conductivity in cold regions and its relation to pore size and geometry. Hydrol Process 22:2829–2837
Roulet NT, Woo MK (1986a) Low Arctic wetland hydrology. Can Water Resour J 11:69–75
Roulet NT, Woo MK (1986b) Wetland and lake evaporation in the Low Arctic. Arct Alp Res 18:195–200
Rouse WR, Blanken PD, Duguay CR, Oswald CJ, Schertzer WM (2008) Climate-lake interactions, in Cold Region atmospheric and hydrologic studies. The Mackenzie GEWEX experience. Springer, Heidelberg, pp 139–160
Rovansek RJ, Hinzman LD, Kane DL (1996) Hydrology of a tundra wetland complex on the Alaskan Arctic coastal plain. Arct Alp Res 28:311–317
Rydén BE (1977) Hydrology of truelove lowland. In: Bliss LC (ed) Truelove Lowland, Devon Island, Canada: A High Arctic ecosystem. University of Alberta Press, Edmonton, pp 107–236
Scheffel H-A (2018) Hydrology of a Sandur-Wetland in a Volcanic Environment, Southeast Iceland. Master's thesis, Department of Geography, York University, Toronto, Ontario, Canada (unpublished)
Seppälä M (1997) Piping causes thermokarst in permafrost, Ungava Peninsula. Quebec, Canada. Geomorphology 20:313–319
Smith LC, Sheng Y, MacDonald GM et al (2005) Disappearing Arctic lakes. Science 308:1429
Sturm M, Liston GE (2003) The snowcover on lakes of the Arctic Coastal Plain of Alaska, U.S.A. J Glaciol 49:370–380
Thompson DK, Woo MK (2009) Seasonal hydrochemistry of a High Arctic wetland complex. Hydrol Process 23:1397–1407
Ulrich M, Mattes H, Schirrmeister L et al (2017) Differences in behavior and distribution of permafrost-related lakes in Central Yakutia and their response to climatic drivers. Water Resour Res. https://doi.org/10.1002/2016wr019267
Vincent W, Laurion I, Pientz R et al (2013) Climate impacts on arctic lake ecosystems. In Goldman CR, Kumagai M, Robarts, RD (eds) Climatic change and global warming of inland waters: impacts and mitigation for ecosystems and societies. Wiley, London, pp 27–42
Walker HJ, Hudson PF (2003) Hydrologic and geomorphic processes in the Colville River delta, Alaska. Geomorphology 56:291–303
Winters TC (1988) A conceptual framework for assessing cumulative impacts on the hydrology of nontidal wetlands. Environ Man 12:605–620
Woo MK (1988) Wetland runoff regime in northern Canada. In: Proceedings of the 5th international conference on permafrost, Trondheim, Norway, vol 1, pp 644–649
Woo MK (2012) Permafrost hydrology. Springer, Berlin
Woo MK, diCenzo PD (1988) Pipeflow in James Bay coastal wetlands. Can J Earth Sci 25:625–629
Woo MK, Guan XJ (2006) Hydrological connectivity and seasonal storage change of tundra ponds in a polar oasis environment, Canadian High Arctic. Permafr Periglac Process 17:309–323
Woo MK, Heron R (1987) Breakup of small rivers in the subarctic. Can J Earth Sci 24:784–795
Woo MK, DiCenzo PD (1989) Hydrology of small tributary streams in a subarctic wetland. Can J Earth Sci 26:1557–1566
Woo MK, Young KL (1997) Hydrology of a small drainage basin with polar oasis environment, Fosheim Peninsula, Ellesmere Island. Permafr Periglac Process 8:257–277
Woo MK, Young KL (2003) Hydrogeomorphology of patchy wetlands in the High Arctic, polar desert environment. Wetlands 23:291–309

Woo MK, Young KL (2006) High Arctic wetlands: their occurrence, hydrological and sustainability. J Hydrol 320:432–450
Woo MK, Young KL (2012) Canadian Arctic wetlands. In: Bengtsson L, Herchy RW, Fairbridge RW (eds) Encyclopedia of lakes and reservoirs, pp 902–914. https://doi.org/10.1007/978-1-4020-4410-6
Woo MK, Young KL (2014) Disappearing semi-permanent snow in the High Arctic and its consequences. J Glaciol 44:2–20
Woo MK, Heron R, Steer P (1981) Catchment hydrology of a High Arctic lake. Cold Reg Sci Technol 5:29–41
Woo MK, Young KL, Brown L (2006) High arctic patchy wetlands: hydrologic variability and their sustainability. Phys Geograph 27:297–307
Woo MK, Thorne R, Brown LC (2018) Comparison of runoff and river flow in two large northern basins. Hydrol Res. https://doi.org/10.2166/nh.2018.199
Wright N, Quinton WL, Hayashi M (2008) Hillslope runoff from an ice-cored peat plateau in a discontinuous permafrost basin, Northwest Territories, Canada. Hydrol Process 22:2816–2828
Wright NW, Hayashi M, Quinton WL (2009) Spatial and temporal variations in active layer thawing and their implication on runoff generation in peat-covered permafrost terrain. Water Resour Res 45:W05414. https://doi.org/10.1029/2008WR006880
Wrona FJ, Johansson M, Culp JM et al (2016) Transitions in Arctic ecosystems: Ecological implications of a changing hydrological regime. J Geophys Res: Biogeosci 121(3):650–674
Young KL (2008) Role of snow in the hydrology of a High Arctic riparian wetland. Hydrol Res 39:277–286
Young KL (2019) Swings in runoff at Polar Bear Pass: An extensive low-gradient wetland, Bathurst Island, Nunavut. Hydrol Res 50(2):778–792
Young KL, Abnizova A (2011) Hydrologic thresholds of ponds in a polar desert wetland environment, Somerset Island, Nunavut, Canada. Wetlands 31:535–549
Young KL, Labine C (2010) Summer hydroclimatology of an extensive low-gradient wetland: Polar Bear Pass, Bathurst Island, Nunavut, Canada. Hydrol Res 41:492–502
Young KL, Lewkowicz AG (1988) Measurement of outflow from a snowbank with basal ice. J Glaciol 34:358–362
Young KL, Woo MK (2000) Hydrological response of a patchy high arctic wetland. Nord Hydrol 31:317–328
Young KL, Woo MK (2003) Thermo-hydrological responses to an exceptionally warm, dry summer in a High Arctic environment. Nord Hydrol 34:41–70
Young KL, Bolton WR, Killingtveit A et al (2006) Assessment of precipitation, snowcover in northern circumpolar basins. Nord Hydrol 37:377–391
Young KL, Assini J, Abnizova A et al (2013) Snowcover and melt characteristics of upland/lowland terrain: Polar Bear Pass, Bathurst Island, Nunavut, Canada. Hydrol Res 44:2–20
Young KL, Scheffel H-A, Abnizova A et al (2017) Spatial and temporal dynamics of groundwater flow across a wet meadow, Polar Bear Pass, Bathurst Island, Nunavut. Permafr Periglac Process 28:405–419
Young KL, Brown L, Labine C (2018) Snow cover variability at Polar Bear Pass, Nunavut. Arctic Sci 4:669–690
Young KL, Assini J, Abnizova A, De Miranda N (2010) Hydrology of hillslope-wetland streams, Polar Bear Pass, Nunavut, Canada. Hydrol Process 24:3345–3358

Dr. Kathy L. Young is a Professor in the Geography Department at York University starting here in July 1994. She completed both her undergraduate and M.Sc. degrees at the University of Toronto, and she attained her Ph.D. degree from McMaster University in 1995. She has spent about 30 years in the Canadian High Arctic. Her research continues to focus on snow cover and melt processes, and both hillslope and wetland hydrology in relation to landscape and climate variability. In 2008, she was made a Fellow of the Arctic Institute of North America in recognition of her contributions to hydrology research in the Canadian High Arctic. In 2012, she was awarded the Meritorious Service Award from the Canadian Geophysical Union. Since 2014, she has been studying hillslope and wetland hydrological processes in Iceland.

Dr. Laura Brown is currently an Associate Professor in the Department of Geography at the University of Toronto Mississauga, joining the department in 2014. She attained a Hon. B.Sc. and M.Sc. from York University, before completing her Ph.D. at the University of Waterloo. She has been active in Arctic hydrology research since 2000 and focusses primarily on snow and ice, using numerical modeling, remote sensing, and ground-based field studies to improve the understanding of the linkages between climate and the cryosphere. The bulk of her recent work has focused on improving the detection and modeling of freshwater ice to better understand the response of ice cover to climatic forcing, with a particular emphasis on comparing Arctic and mid-latitude ice covers. She is presently treasurer of the Canadian Geophysical Union.

Dr. Yonas Dibike is a Research Scientist at Environment and Climate Change Canada, Watershed Hydrology and Ecology Research Division at the University of Victoria. His research interests include hydrological, hydrodynamic, and transport modeling as well as hydro-climate analysis and climate change impact studies in cold region watersheds. He also holds adjunct faculty appointment at McMaster University, and the University of Victoria in Canada. He is the author/co-author of numerous (70) scientific articles that have appeared in a variety of peer-reviewed journals and conference proceedings. He is actively involved in Departmental and University-based researches and has co-supervised several graduate students and postdoctoral fellows.

River Ice Processes and Changes Across the Northern Regions

13

Daqing Yang, Hotaek Park, Terry Prowse, Alexander Shiklomanov, and Ellie McLeod

Abstract

River ice is critical for northern hydrology and ecosystems, such as the magnitude and timing of hydrologic extremes, i.e., low flows and floods. Historical data analyses and model studies clearly show widespread decreases in river ice thinness and duration due to climate warming across the northern regions. Reductions in river ice jam flooding may have major positive benefits for communities and infrastructure along the river margins, but could also alter the ecology of deltaic riparian and coastal marine ecosystems. The reduction in river and lake ice will influence transportation opportunities in remote regions. In situ observations are important to monitor the ongoing changes in river and lake ice features across the northern regions. Modeling and remote sensing tools are very useful to the understanding of ice processes, attributions of past changes,

D. Yang (✉) · T. Prowse · E. McLeod
Environment and Climate Change Canada, Watershed Hydrology and Ecology Division, Victoria, BC, Canada
e-mail: daqing.yang@canada.ca; daqing.yang@gmail.com

T. Prowse
e-mail: terry.prowse@canada.ca

E. McLeod
e-mail: ejmcleod839@gmail.com

H. Park
Japan Agency for Marine-Earth Science and Technology, Research Institute for Global Change, Yokohama, Kanagawa, Japan
e-mail: park@jamstec.go.jp

A. Shiklomanov
Earth Systems Research Center, University of New Hampshire, Durham, NH, USA
e-mail: sasha@eos.sr.unh.edu

D. Yang and D. L. Kane (eds.), *Arctic Hydrology, Permafrost and Ecosystems*,
https://doi.org/10.1007/978-3-030-50930-9_13

and projection of future ice conditions in a warming Arctic. More effort is necessary to combine observations, models, and remote sensing technology to investigate ice hydrology over the broader northern regions.

13.1 Introduction

River and lake ice creates critical processes for the northern regions and basin hydrology. For example, the magnitude and timing of hydrologic extremes, such as low flows and floods, are mostly controlled by the dynamics of river ice freeze-up and break-up (Beltaos and Prowse 2009). The process of river ice break-up is important not only within the basin but also on the spring climate of large river deltas (Prowse et al. 2011a, b). River ice is a key seasonal storage component affecting flow. Prowse and Carter (2002) examined the influence of ice storage on spring discharge of the Mackenzie River and found that over a 60-day period during river freeze-up, 27% of water flow that would have normally occurred during a non-freeze-up period was diverted to hydraulic and ice growth storage. During spring snowmelt, 15–19% of the total spring discharge volume could be accounted for by this "ice induced hydraulic storage." If ice growth during the fall flow depression is included, this value increases to 25%. It is therefore important that ice storage is accounted for in the measurement and analysis of spring discharge data; otherwise, the contribution of snowmelt and precipitation would be overestimated. The effects of ice on evapotranspiration, precipitation, and their feedbacks on hydrology may act on much larger scales, even influencing the water balance of large Arctic basins (Rouse et al. 2007). By contrast, meteorological and climatological effects of variations in freshwater ice (e.g., coverage and duration) are confined primarily to the local or regional scale (e.g., radiation and convective fluxes), with the greatest effects produced by ice cover on large lakes (Rouse et al. 2005).

Discharge regime during winter period is also strongly related to river ice condition. In some regions of the Russian Arctic, winter flow has increased over 40% when compared to the long-term mean (Georgievsky et al. 2013). Increase in air temperature and corresponding decrease in river ice could be partly responsible for greater winter flow. Decreasing river ice improves the exchange between ground and surface water, leading to higher runoff rates. On larger rivers, where floating ice cover can move vertically like a membrane in response to changing river flow (Prowse and Gridley 1993), this process does not occur. The effect of river ice on runoff is more important for small streams where ice thickness is comparable with winter river depth. Changes in runoff from many small streams, however, will influence the lower reaches (i.e., the large rivers) (Markov 2003). Thus, the relative flow contribution from small rivers to the medium and large rivers decreases in cold winters but increases during warmer winters for all rivers. For rivers with stable discharge recession during winter, this phenomenon is mainly seen in hydrographs

as a faster or slower depletion throughout winter. Gurevich (2009) analyzed changes in air temperature, ice thickness, and river discharge for 16 monitoring stations in the Aldan River basin (a tributary of the Lena river), and found winter air temperature was positively correlated with winter discharge. When deviations of winter air temperature from the long-term mean were 2−3 C, the deviation of Aldan river winter flow from long-term mean was 20–30%. This study shows that lower winter temperatures yielded faster winter runoff depletion, and warmer temperatures weaken the influence of ice cover on discharge, causing discharge to increase (Gurevich 2009).

Lakes with a seasonal ice cover are an important component of the northern landscape. They cover approximately 3.3% of the land area north of 58°N, and when ice-free, have the highest evaporation rates of the high-latitude terrestrial surface. The duration of lake ice determines the magnitude and timing of evaporation and controls the seasonal heat budget of lake systems. The presence (or absence) of ice cover on lakes during the winter months also affects both regional climate and weather events, for example, by thermal moderation and producing lake-effect snow events (Pour et al. 2017). Lake ice also is important to society, such as by providing transportation routes, and in fishing, recreation, and local cultural identity. For example, Indigenous communities use and rely on winter lake ice roads in northern regions for food, supplies, and social interactions. Warming winters have reduced the duration and quality of ice roads, limiting access to remote communities. The quality and duration of winter recreational activities have also declined with warming winters. Skating seasons in the largest outdoor skating rinks have become shorter, with a risk of no outdoor skating opportunities by the late twenty-first century.

Brooks et al. (2013) used a degree-day ice growth model and ice thickness data from five national archives to determine the areal extent and volume of freshwater (lake and river) ice in the Northern Hemisphere for the period from 1957 to 2002. An area of 1.71×10^6 km^2 was computed using freshwater ice north of the January 0 °C isotherm and excluding the Greenland Ice Sheet. This area of ice is approximately equivalent to the surface area of the Greenland Ice Sheet. The volume of ice was found to be 1.56×10^3 km^3. The values from Brooks et al. (2013) indicate the significance of freshwater ice in the cryosphere system. It should be noted that the values computed are considered to be very conservative estimates, given that very small lakes and rivers were not considered. This indicates that lake and river ice could account for an even larger portion of the Northern Hemisphere cryospheric system.

Magnuson et al. (2000) examined river and lake ice data for a 150-year period (1846–1995) across the Northern Hemisphere and found significant changes in ice regime and timing of ice events throughout the Northern Hemisphere. The major findings indicate changes in freeze-up date of 5.8 days later per 100 years and trends in break-up dates of 6.5 days later per 100 years. These results provide evidence of changes in freshwater ecosystems in response to warming and correlate to temperature changes of 1.2 °C warming per 100 years (Fig. 13.1).

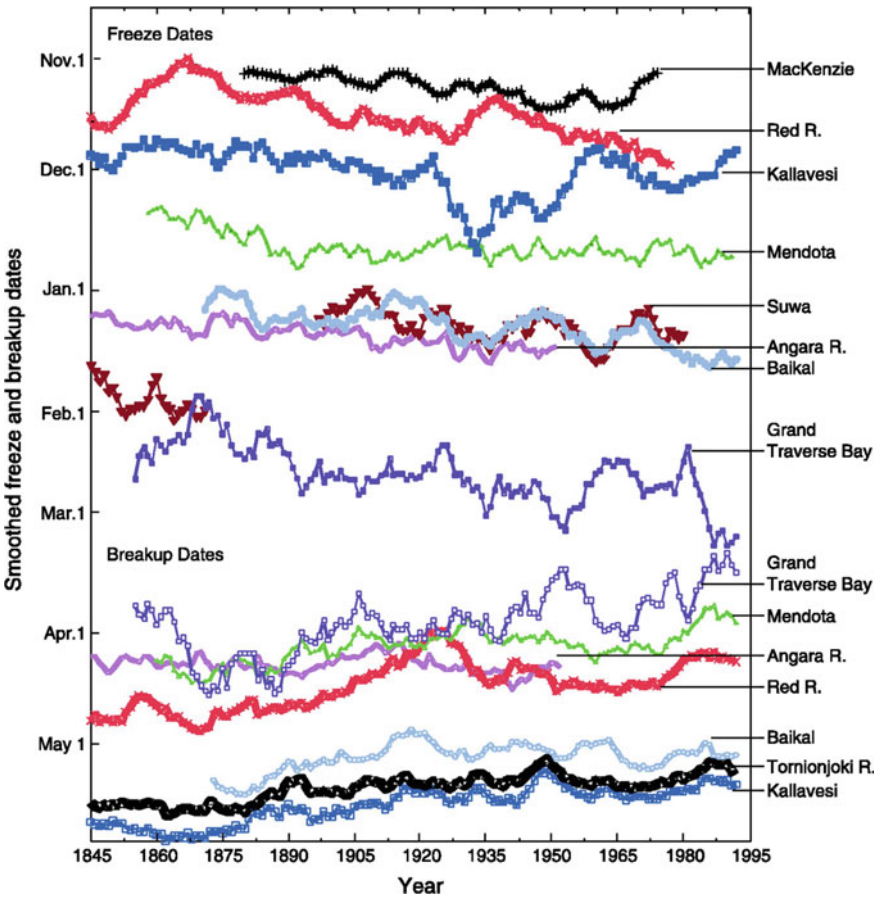

Fig. 13.1 Time series of freeze-up and break-up dates for selected lakes and rivers in the Northern Hemisphere for the period 1846–1995. Data are smoothed with a 10-year moving average (Magnuson et al. 2000, reprinted with permission from AAAS)

Beltaos and Prowse (2009) conducted a survey of numerous studies of river ice phenology in the Northern Hemisphere. They noted that fewer studies had been conducted for river ice thickness and strength than for ice timing and seasonality. This is partly due to lack of observations and data, the complexity of river ice formation, and the number of variables affecting ice formation. Beltaos and Prowse (2009) noted an almost universal trend toward earlier break-up dates, but considerable spatial variability in those for freeze-up. Changes are often more pronounced during the last few decades of the twentieth century. Overall, twentieth-century warming has led to a 10- to 15-day advance in break-up and delay in freeze-up, respectively (Lique et al. 2016). This pattern is consistent with warming trends and in agreement with earlier estimates (Magnuson et al. 2000), although the

relationship is complicated by changes in snow accumulation and spring runoff (Beltaos and Prowse 2009).

Similarly, the ice cover observations for Northern Hemisphere lakes indicate a shortening duration, with the time of break-up generally changing more rapidly than the freeze-up (Benson et al. 2012). Trends over 1855–2004 were steeper than those over 1905–2004, but the most rapid changes occurred in the most recent 30-year period, with freeze-up 1.6 days/decade later, break-up 1.9 days/decade earlier, and ice duration 4.3 days/decade shorter. Although ice cover tends to be more sensitive to air temperature variations at lower than at higher latitudes (Livingstone et al. 2010), remote sensing observations indicate that ice cover loss seems to be more rapid in very high-latitude lakes (Latifovic and Pouliot 2007). High-latitude lakes lost ice cover at 1.75 days/year during the 1970–2004 period of most rapid depletion, which is more than 4.5 times the rate of lakes in southern Canada. It is unclear whether this reflects the more recent and greater high-latitude warming or potential differences in observational techniques (Prowse and Brown 2010). Sharma et al. (2019), using observations from 513 lakes around the Northern Hemisphere, carried out a comprehensive large-scale assessment of lake ice loss, and identified lakes vulnerable to ice-free winters. Their analyses reveal the importance of air temperature, lake depth, elevation, and shoreline complexity in governing ice cover. They estimate that 14,800 lakes currently experience intermittent winter ice cover, increasing to 35,300 and 230,400 at 2 and 8 °C, respectively, and affecting up to 394 and 656 million people. These results illustrate that an extensive loss of lake ice will occur in the future, stressing the importance of climate mitigation strategies to preserve ecosystem structure and function, and winter cultural heritage.

This chapter provides a review of the recent work mainly on river ice for the Siberian and North America arctic regions, including ice observation networks and available datasets, regional/basin ice regimes, and changes due to climate impacts. It also synthesizes river ice models and remote sensing applications in the northern regions, and discusses the research gaps and future directions.

13.2 Russian Arctic River Ice Hydrology

Despite the importance of river ice to Arctic hydrology/ecosystem and northern communities, there are surprisingly few comprehensive observational records of river ice conditions. In most Arctic countries, including Canada and the USA, there are few complete records of ice observations. Since the late 1930s, hydrological observations in the Siberian regions, such as discharge, stream water temperature, river ice thickness, dates of river freeze-up and break-up, have been carried out by the Russian Hydrometeorological Services, and the observational records have been quality-controlled and archived by the same agency (Shiklomanov et al. 2007). These data are now available from the R-ArcticNET, a digital archive (CDROM) for the Arctic drainage (Lammers et al. 2001). There is also the Russian River Ice

Thickness and duration data set, from the National Snow and Ice Data Center, containing data during 1917–1992 with variable record lengths for 50 stations in the Northern Russia (Vuglinsky 2000). More recent river ice data for Russian pan-Arctic up to 2012 can be found at the NSF Arctic Data Center (Shiklomanov 2016) or obtained from the Russian Hydrometeorological Agency, Roshydromet, and the Arctic and Antarctic Research Institute (AARI) data server. Eight of the nine largest Arctic Rivers and approximately 85% of terrestrial runoff into the Arctic Ocean are located in Russia (Aagard and Carmack 1989). The availability of long-term data for Northern Russian river ice has led to many studies of the river ice regimes and changes across the Russian Arctic.

13.2.1 Ice Thickness and Change

Significant Arctic warming has been observed in recent decades (Overland et al. 2017). The Russian Arctic is no exception, with the observed warming trends of 0.25–0.75 °C per decade during 1961–1990 (Chapman and Walsh 1993). This warming has implications for basin hydrology features, inducing ice conditions. Yang et al. (2002) analyzed the long-term ice thinness data and defined the ice regime at the Lena basin outlet, i.e., the Kusur station, 70.70 N/127.65 E. River ice forms in October (with the mean of 5 cm), grows over the winter season, reaches the maximum (about 180–190 cm in April/May), and breaks up in June. The duration of ice cover is about 8 months or 240 days in northern Siberia. Snow observations over the river ice indicate a depth range from 10 to 25 cm from October to May (Fig. 13.2a). There is significant thinning of river ice during 1951–1992 as a result of climate warming; the ice pack was 20–35 cm thinner during 1970s–1980s when compared with the data over the 1950s–1960s. A recent update of the ice data analysis also shows a significant decrease in thickness at the Kusur station during 1954–2012 (Shiklomanov and Lammers 2014). Yang et al. (2002) found a negative relation ($R = 0.73$) between streamflow and river ice thickness at the Kusur station from November to April (Fig. 13.2b). This relationship suggests that winter climate warming produces more runoff and less river ice.

Along the Siberian coast, there have been changes in seasonal river ice thickness over the past several decades. Shiklomanov and Lammers (2014) examined the responses of river ice regimes of six major Arctic Russian rivers to warming climate, i.e., the Severnaya Dvina, Ob, Yenisey, Lena, Yana, and Kolyma (Fig. 13.3). They report a significant decreasing trend during 1950–2012 in maximum ice thickness for all major Russian Arctic Rivers except the Severnaya Dvina. The largest decrease in ice thickness was observed for the Lena River, by 73 cm over 1955–2012. All other major rivers have a significant decrease in ice thickness over the same period, including the Ob, Yana, Yenisey, and Kolyma rivers (Fig. 13.3). In a similar study, Vuglinsky and Gronskay (2006) compared changes in ice thickness over 1980–2000 on Russian Rivers to a baseline period of relative climatic norm during 1950–1979. They found that almost all large rivers in Russia

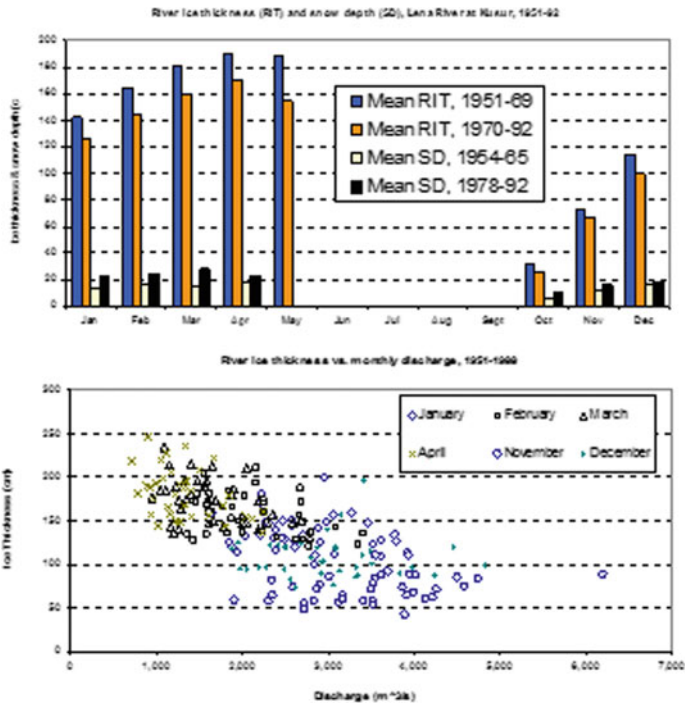

Fig. 13.2 Mean river ice thickness and snow depth (**a**), and monthly discharge vs. ice thickness (**b**), at the Kusur station for the Lena River over the period 1951–1992 (modified from Yang et al. 2002)

experienced a decrease in the maximum ice thickness by 2–14 cm in the last two decades of the twentieth century relative to the three preceding decades.

Russian river ice thickness forecasting has usually been based on air temperature. Shiklomanov and Lammers (2014), however, found little correlation between the maximum ice thickness and mean winter air temperature. While average temperature is the common indicator for seasonal climate conditions, it might be useful to consider using a cumulative of negative temperature values leading up to the date of maximum ice thickness, or alternatively, the coldest temperature of the months. Lake and reservoir ice formation is mainly dependent on air temperature. River ice formation, primarily dependent on air temperature, is affected by other factors, including flow rate, water temperature, snow thickness, and hydraulic conditions of the river reach (Beltaos 1997). The functioning of the relationship between river ice thickness, air temperature, and river discharge is not well understood (Shiklomanov and Lammers 2014).

Yang et al. (2002) found that, on a monthly time scale, higher air temperature was strongly correlated with decreased river ice thickness for the lower Lena watershed. Thinning of river ice was also associated with increasing river discharge,

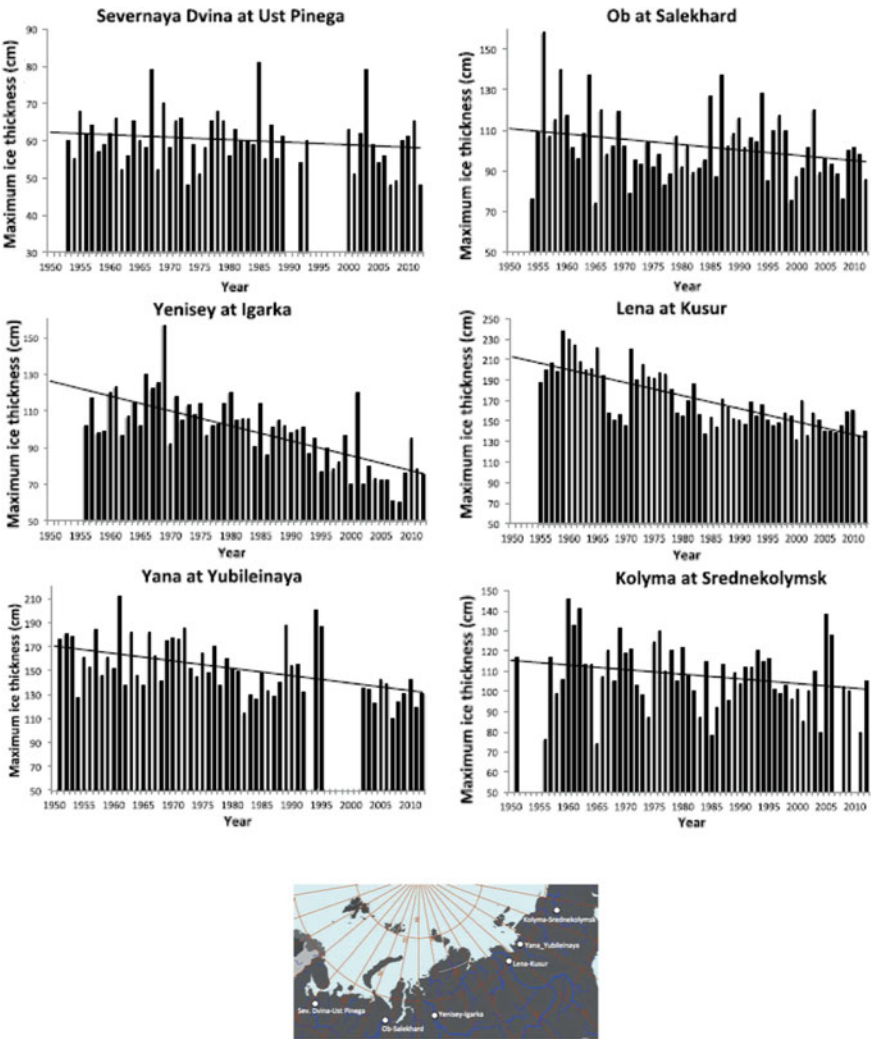

Fig. 13.3 Maximum winter ice thickness for six major Arctic Russian rivers during 1955–2012. Linear trend in ice thickness is shown as a solid line (modified from Shiklomanov and Lammers 2014)

suggesting that winter warming leads to greater runoff and subsequently thinner river ice. Increased discharge and thinner ice downstream of Lena River may also be related to reservoir regulation within the basin (Ye et al. 2009), i.e., enhanced winter flows at the expense of the summer discharge, thus leading to the formation of thinner ice. Another factor leading to thinning river ice could be higher snow depth and its insulation effect during the winter season. In a 2005 Arctic Climate

Impact Assessment, it was found that 60–70% of variability in the timings of ice break-up and freeze-up on lakes and rivers could be explained by air temperature (Walsh et al. 2005). Magnuson et al. (2000) estimated that variance in timing of freshwater freeze-up and break-up dates relative to changes in air temperature for the Northern Hemisphere to be approximately 5 days/°C. These findings support the evaluation by Shiklomanov and Lammers (2014) that a relationship should exist among river ice thickness, temperature, and discharge. Further research and examination of more detailed data will be required to better understand the dynamics of Arctic river ice and its response to climatic and environmental changes.

13.2.2 Timing of Ice Events and Changes

Based on long-term river ice observations across Northern Russia, Shiklomanov and Lammers (2014) assessed the patterns in ice formation. As a result of a strong air temperature gradient (warm in the west vs. cold in the east), river ice forms around late September to mid-October over the eastern sections, and ice appears around later in October to November in the west. There are significant trends for ice formation in the later fall (Fig. 13.4). This was true for all rivers except the Severnaya Dvina and Yenisey.

By contrast, river ice breaks up earlier (late May–early June) in the western region and later (early June to late June) in the eastern region along the arctic coast. There was a general trend of earlier break-up and earlier ice disappearance with significant trends for the three largest Siberian Rivers, the Ob, Yenisey, and Lena. The recent last dates for all ice events of the six rivers are 4–5 days earlier than they were in the 1950s. This correlates to observed shifts in timing of maximum spring discharge, i.e., an average of 4 days across Russia during 1960–2002 (Shiklomanov et al. 2007). The Severnaya Dvina is the only river with statistically insignificant shifts in timing for all ice events. This is consistent with the conclusions of an earlier study by Smith (2000) that changes in ice regime have been less drastic in Northern European Russia, where the Severnaya Dvina River is located.

For the six rivers, the latest dates of ice formation and the earliest dates of ice break-up have been observed since 1990. The data show a pattern of decreasing ice season from about 230–260 days in the east to approximately 170–190 days in the west across northern Siberia. From 1955 to 2012, there was an appreciable decrease in the duration of ice season by 7 and 20 days, resulting from later ice formation and earlier ice disappearance dates (Shiklomanov and Lammers 2014). For all rivers studied, an accelerating trend toward later ice formation and earlier ice disappearance was found for the last 15–20 years. This corresponds to the period of greatest temperature warming in the Arctic.

Smith (2000) also found a trend in earlier melt onset over 1917–1994 for central and eastern Siberian rivers, although there was no indication of earlier break-up during this period. Smith (2000) suggests that this change indicates a shift from a mechanically driven river ice break-up regime to a dominantly thermally driven

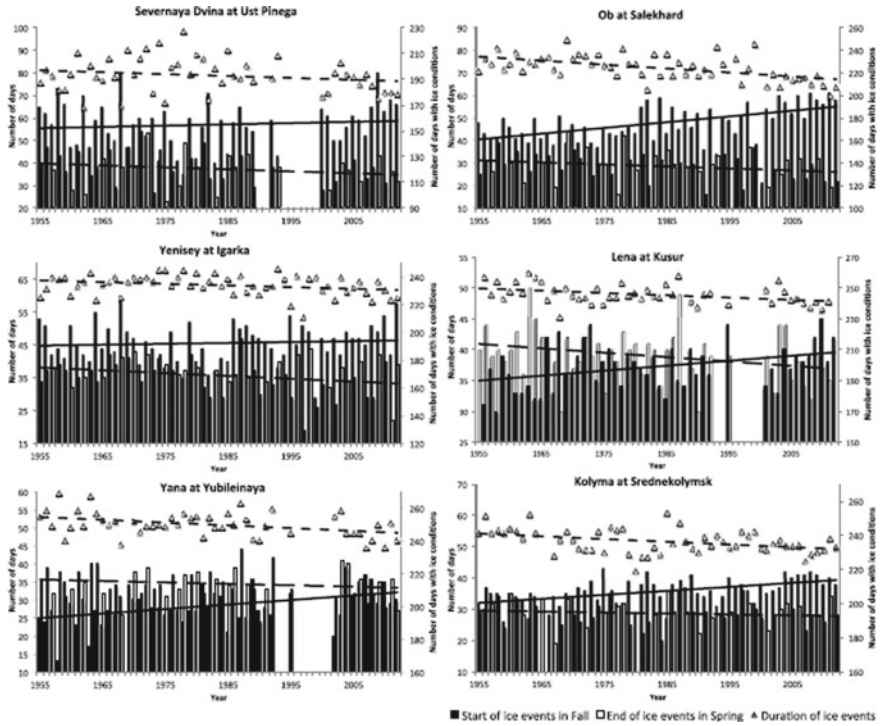

Fig. 13.4 Long-term variation in ice events for six rivers in Arctic Russia. The solid line is the linear trend of date of first ice appearance in the fall given as number of days from September 1 on the left vertical axis. The short dashed line shows the end date of ice conditions in the spring, given as the number of days from April 1 for all rivers except the Severnaya Dvina, which is given as the number of days from March 1 on the left vertical axis. The long dashed line is the linear trend of the number of days of total ice condition duration over the hydrological year on the right vertical axis (modified from Shiklomanov and Lammers 2014)

break-up regime in the Russian Arctic. This is characterized by an increase in the number of melt days prior to break-up, allowing ice to thin and weaken and resulting in less physical breakage events taking place. Smith's results for the 1917–1994 period are inconsistent with the observations of Shiklomanov and Lammers (2014), who observed earlier break-up events resulting in shorter overall duration of ice events. The time period examined by Shiklomanov and Lammers (2014), 1955–2012, encompasses the more recent period of accelerating warming in the Arctic, and Smith's (2000) covers the time frame 1917–1994. The different periods between these two studies may contribute to the differing results.

Change in Arctic air temperature is the most obvious potential driver of changes in timing of Arctic river ice regimes. Arctic air temperatures are increasing at double the rate of global mean temperature increase (Overland et al. 2017). Central Arctic winter (October–December) temperature anomalies exceeded +5 °C in 2017.

The air temperature of all six rivers in Shiklomanov and Lammers' (2014) study increased in the winter periods from 0.8 to 4.0 °C during 1955–2012 (Shiklomanov and Lammers 2014). Despite some uncertainty around a lesser effect of air temperature on some rivers, there is a good correlation between air temperature and timing of ice events for most rivers in the northern regions. The relationship between air temperature and timing of ice events appears to be weaker in Northern European Russia but the correlation strengthens moving east across Siberia.

13.3 North American Arctic River Ice Hydrology

Air temperatures over Canada have increased an average of 0.9 °C, and as much as 3.0 °C in some regions during the period 1900–1988 (Zhang et al. 2000), with the greatest warming in Western Canada. Bonsal and Prowse (2003) examined shifting seasonal 0 °C isotherms over Canada. Similar to Zhang et al. (2000), they found significant variability from west to east. In the western regions of Canada, there is a significant trend toward earlier springs, with dramatic changes in the last 20–30 years. In Eastern Canada, there is a shift toward later springs. These shifts are reflected in changes in hydrologic characteristics, such as snowmelt and river/lake ice break-up, and streamflow.

Although there are few long-term records of river ice regimes in Arctic Canada and Alaska, numerous studies have been undertaken to quantify and understand the ice regimes in these regions and the impact of climate change on ice events, such as timing and ice thickness. The United States National Snow and Ice Data Center database contain a number of river ice datasets for research conducted across Arctic Canada and Alaska. These data sets cover various time periods and regions around the world. Environment and Climate Change Canada also assemble records of river ice cover and break-up. These data sets cover highly variable periods depending on regions, and many are incomplete and/or discontinued.

de Rham et al. (2020) report on the progress of Environment and Climate Change Canada (ECCC) effort to develop an open Canadian River Ice Database using the Water Survey of Canada (WSC) archive. There is only limited work on the annual and seasonal variability in ice conditions across Canada, as the main purpose of most hydrometric measurements is to provide information about water availability and discharge, while the original water level data are generally less available to the research community and public. In addition, significant effort is required (and still lacking) to compile, archive, and extract river ice information from water level records. In this ongoing project (de Rham et al. 2020), ice records were extracted based on the process outlined by the Working Group on River Ice Jams, i.e., Guidelines from Extraction on Ice Break-Up from Hydrometric Station Records (Beltaos 1990). The records obtained and examined in this study cover the period 1894–2015 and evaluated the entire ice season rather than solely break-up regimes as is more commonly undertaken. As of May 2020, data from 130 of the 196 stations with records to 2015 have been extracted. Preliminary data analyses

suggest a general trend toward a delay in average freeze-up peak water level timing for regions affected by maritime climate. Trends also indicate an overall delay in ice occurrence over the entire study area. There are also increasing trends in mid-winter break-up on both naturally flowing and regulated rivers. Once completed, this database will provide an improved database, which will allow Canada to continue producing novel research in the field of river ice hydrology.

13.3.1 Ice Thickness and Change

Evans et al. (2015) monitored ice thickness on the Slave River in the Northwest Territories over the 2014 ice season. Ice thicknesses were measured across the delta's main channel in early February 2014. It was found that ice thickness across the channel was highly variable, ranging from 0.44 m to 0.75 m. In regions with greater snow depth, thinner ice was observed. This is likely due to the insulating effect of the snow. Later in the season, in April, another survey was undertaken and found decreased ice thickness in the central delta, although in some channels, ice thickness had increased. Thinner ice could be attributed to the onset of thermal break-up. It was also observed that an increase in stream discharge in February and March 2014 initiated cracking and break-up of ice. This suggests that if spring discharge were to increase or occur earlier in the season due to climate change, the break-up may also occur earlier.

Goulding et al. (2009) examined hydrometric controls of river ice break-up on the Mackenzie River Delta, NWT for the period 1974–2006. Data were obtained from the Arctic Red River Hydrometric Station. They found generally lower ice thickness from the 1990s onward when compared to thicknesses in the 70s and 80s. The average peak ice thickness during the 1990s is 1.26 m. It was observed that during the 1990s, peak river ice thickness never exceeded 1.30 m, while previously to the 1990s, maximums regularly exceeded 1.30 m (Fig. 13.5).

A study conducted in Ruby Village on the Yukon River used Indigenous knowledge to help understand changes in river ice regime on the Yukon and its tributaries (Wilson et al. 2015). Community experts noted that the length of time that the ice was taking to form was becoming much longer. They had observed that it took much longer for the ice to become thick enough to travel across than it had previously. It was also observed that when snow fell prior to complete ice formation, the ice for that season was much thinner. This is likely due to the insulating effect of snow. Overall, Community Experts in Ruby Village have observed a general trend in thinning ice throughout the season of ice cover.

13.3.2 Timing of Ice Events and Change

A comprehensive study by Lacroix et al. (2005) examined river ice data from the Canadian Ice Database and the Water Survey of Canada stations for regions across Canada. Analyses showed a general trend toward earlier break-up dates over the

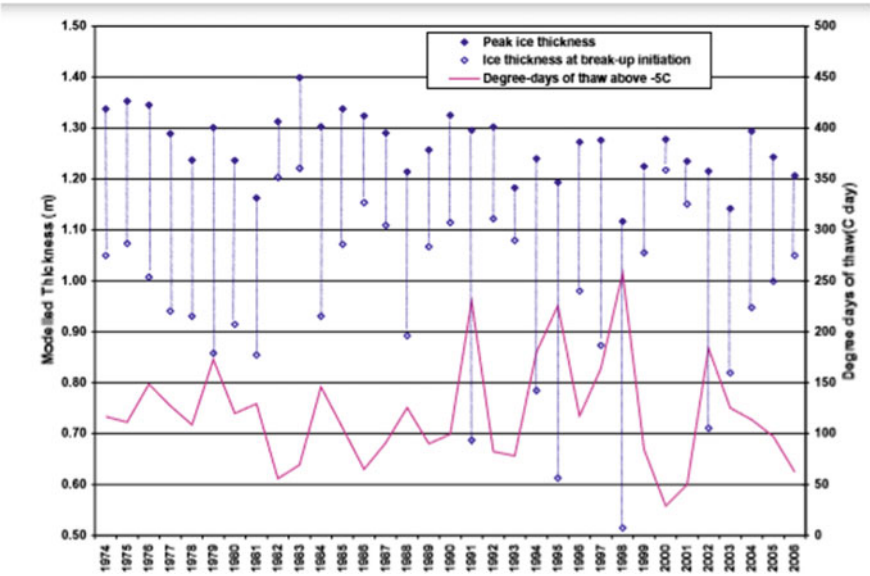

Fig. 13.5 Peak ice thickness, ice thickness at break-up initiation, and degree days of thaw above -5 °C for the Mackenzie River at Arctic Red River in the Northwest Territories during 1974–2006 (Goulding 2006)

whole country, especially during the recent period of 1961–1990. Freeze-up patterns were more spatially complex. Moderate-to-strong correlations were found between the river ice break-up dates and the spring 0 °C isotherm for 62–100% of sites. This relationship is less strong for the fall 0 °C isotherm, when only 20–75% of freeze-up dates correlate to the isotherm.

Marsh et al. (2002) observed earlier spring break-up dates over the Mackenzie River Delta during a period from the early 1960s to the late 1990s. The mean break-up date during the 1990s was 9 days earlier than that for the 1960s. Lesack et al. (2014) relate the earlier break-up on the Mackenzie River to changes in the timing of water level maximums in the central delta and break-up temperatures. Break-up temperatures were also strongly correlated to water level peaks at two other locations on the Mackenzie River delta, spanning 200 km north–south on the delta. Similar to Lacroix et al. (2005), Lesack et al. (2014) found that warming winter temperatures were only weakly correlated to changes in break-up dates (Fig. 13.6) and water level maximums. In addition to changes in break-up temperature, water level peaks, and break-up date, Lesack et al. (2014) also observed substantial decreases in snow cover during 1986–2012 relative to the period 1957–1985. This could also account for more rapid decay of river ice because of general declines in snow depth and therefore less insulation throughout the winter.

Wilson et al. (2015) applied Indigenous knowledge to study the changes in river ice regime on the Yukon River at Ruby Village. There was a general consensus

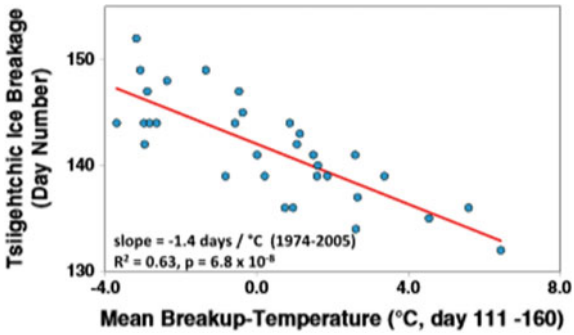

Fig. 13.6 Mean break-up temperature on the Mackenzie River at the point of river inflow into the delta (Tsiigehtchic) versus the day of initial ice breakage (Lesack et al. 2014)

among Community Experts that river ice freeze-up was occurring late and taking longer on the Yukon River main channel and its tributaries. Two community experts also noticed that if snowfalls before the ice have fully formed, the ice pack remains thin due to the insulation of the snow cover. The duration of ice cover was also observed to become shorter. Although there was no direct observation of the break-up date near the village, a number of Community Experts noted the change in the sound of the ice break-up. They observed that the break-up event was much quieter than it had been in the past. This could perhaps be indicative of a transition to more gradual thermal ice break-up. The observations of Community Experts in Ruby Village on the Yukon River are somewhat consistent with trends in river ice phenology in Interior Alaska reported by Bieniek et al. (2011). Trends were generally toward an earlier break-up due to warming spring air temperatures. It was also noted that break-up could occur later during cold ENSO events. This inter-annual variability as well as regional differences could account for the inconsistency between the observations in Ruby Village and overall in Interior Alaska.

A study of river ice phenology in the Western James Bay Region looked at river ice break-up and freeze-up records on the Albany, Attawapiskat, and Moose Rivers, and compared them to local knowledge of ice conditions (Ho et al. 2005). The Attawapiskat River showed statistically significant later break-up dates, while the Albany River showed statistically significant earlier break-up dates over the period 1950–2005. Some of this discrepancy could arise from the differing measurement of break-up on the two rivers. The Attawapiskat was measured using a marking stick, while the Albany was measured by observation of when the area between the mainland and a mid-river island washed away. Ho et al. (2005) also collected local Indigenous knowledge regarding river ice regimes. An interesting observation from the Mushkeogwuk was that ice break-up was becoming increasingly gradual.

Over the period 1999–2002, they did not record break-up dates because it was too gradual to pinpoint an exact date. This suggests a shift toward a less traditional break-up regime. In interviews with Cree Elders from Western James Bay, it was noted that there were observations of changes in the nature of break-up events. A number of Elders also had observed later freeze-up and indicated that freeze–thaw cycles had been much more unpredictable.

Sagarin and Micheli (2001) examined a community-based dataset (starting in 1917) of river ice break-up on the Nenana River in Alaska. A significant negative trend was observed, with river ice break-up occurring earlier, on average, 7 days/century during 1917–2018 (Fig. 13.7). In addition to this, Nenana residents observe that thermal break-up regimes, where the ice "rots" or melts away rather than dynamic, mechanical break-up regimes, are becoming increasingly common. This is consistent with the findings of Smith (2000) on Arctic Russian Rivers and the observations of community experts in the Ruby Village on the Yukon River (Wilson et al. 2015).

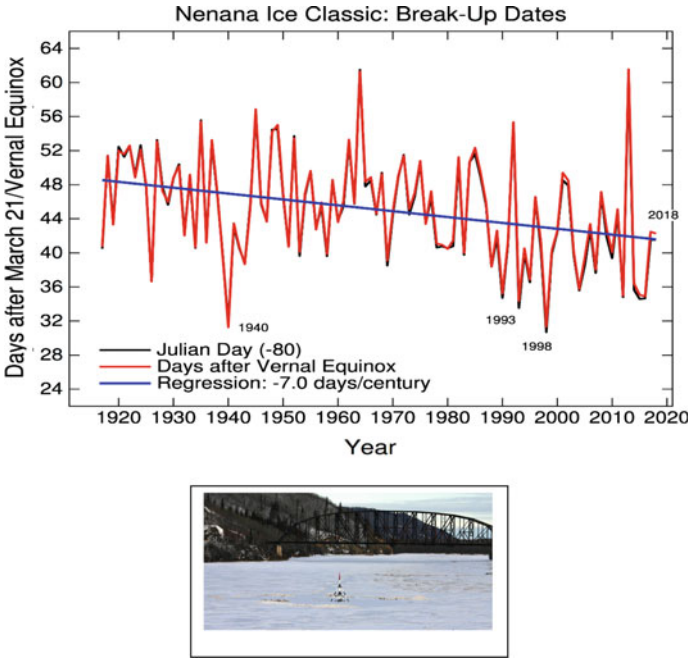

Fig. 13.7 Record of ice break-up date for the Nenana Ice Classic on the Tanana River in Nenana, Alaska over 1915–2018

13.4 River Ice Modeling and Remote Sensing

Models and remote sensing are useful tools to study river and lake ice in the northern regions. Andrishak and Hicks (2008) applied a one-dimensional hydrodynamic model that simulates river ice formation and melting processes to assess climate change impacts on the ice cover extent and duration over the Peace River in Alberta. Air temperatures predicted by the Canadian Coupled Global Climate Model (second generation) for the 2050s were used to assess changes in ice front progression dates relative to the base period, 1961–1990. At the Town of Peace River, the average total predicted reduction in ice cover duration is 28 days (13 days for later freeze-up and 15 days for earlier break-up) under the A2 scenario of population growth and cumulative CO_2 emissions. These findings are consistent with the general trends described by Beltaos and Prowse (2009).

To understand river ice impact to streamflow in the northern regions, Ma and Fukushima (2002) built a hydrologic model system for the Lena River (see Chap. 6 for basin hydrology) with four components, a one-dimensional soil–vegetation–atmosphere transfer (SVAT) model, a runoff-formation model, a river ice model, and a river routing model. Model runs produced reasonable hydrographs for 1986/1987, i.e., similar to flow observations in flood peak and sharpness of the peak, for most of the six stations in the upper part of the Lena basin. Comparisons of the simulations at the Tabaga station between the runs with and without ice show improved results, i.e., higher peaks with later timing due to the effects of ice melt and jamming. The model approach is expected to be useful in long-term flow simulations over the northern regions.

Park et al. (2016) improved the CHANGE model to simulate river ice processes during 1979–2009 for six major Arctic watersheds, the Ob, Yenisey, Lena, Kolyma, Yukon, and Mackenzie Rivers. Model outputs related to river ice process include freezing index during October–April, average snow depth for January–March, maximum river ice thickness, ice freeze-up and break-up and dates, and annual ice-free duration. The results revealed changes toward later fall freeze-up and earlier spring break-up, resulting in shorter overall seasonal ice duration. The dates of freeze-up and break-up were significantly related to surface air temperature warming (Fig. 13.8). Based on annual maximum ice thickness measurements, the river ice volume in the six pan-Arctic rivers decreased by 2.82 km^3 (0.5%) over the simulated period from 1979 to 2009. These findings are consistent with observations and analyses, i.e., a shorter ice duration and a general trend toward decrease in ice thickness across the Arctic.

The estimated ice volume also indicates a decreasing trend (20.091 km^3/yr 21, p, 0.061), but with large inter-annual variability (63.0 km^3 standard deviation) (Fig. 13.9). The average ice volume of the pan-Arctic rivers examined from 1979 to 2009 was 54.1 +/- 3.0 km^3 with estimated river ice extent of 0.048 $\times$ 10^6 km^2. The total decrease in estimated ice volume over the 1979–2009 study period was 2.8 km^3, which represented a 0.5% reduction from the long-term mean. Brooks et al. (2013) estimated 140 km^3 and 0.12 $\times$ 10^6 km^2 for peak river ice volume and

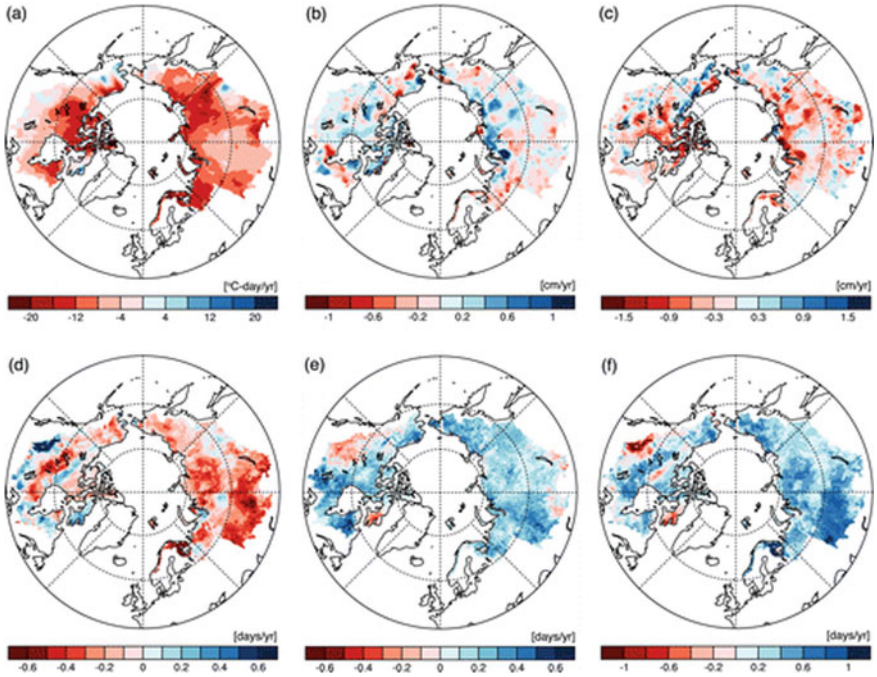

Fig. 13.8 Model-estimated trend maps for **a** freezing index during October–April, **b** average snow depth for January–March, **c** maximum river ice thickness, **d** ice break-up date, **e** ice freeze-up date, and **f** annual ice-free duration over the 1979–2009 simulation period (Park et al. 2016, © American Meteorological Society. Used with permission)

extent, respectively, over the Northern Hemisphere using a degree-day ice growth model based on the January freezing index. Both the CHANGE and degree-day model (Brooks et al. 2013) estimates indicate an average ice volume of 0.0012 km^3 for a given 1 km^2 ice area extent at annual maximum ice thickness.

River ice break-up process is very dynamic and difficult to observe in large watersheds with in situ technology. Remote sensing technology has shown great potential to investigate regional features of river ice processes. Pavelsky and Smith (2004) used daily time series imagery from moderate resolution imaging spectro-radiometer (MODIS) and advanced very high-resolution radiometer (AVHRR) to evaluate ice break-up regimes on the Ob, Lena, Yenisey, and Mackenzie Rivers. Recently, Cooley and Pavelsky (2016) examined the spatial and temporal patterns of Arctic river ice break-up with an automated ice detection from MODIS imagery. They determine dates of break-up for the Ob, Lena, Yenisey, and Mackenzie Rivers during the period 2000–2014, and show break-up dates and uncertainty associated with cloud contamination on the Lena for each year to illustrate large-scale break-up patterns and the variability in cloud uncertainty (Fig. 13.9). The mean break-up window is about ±1.3 days, with significant variability among rivers and

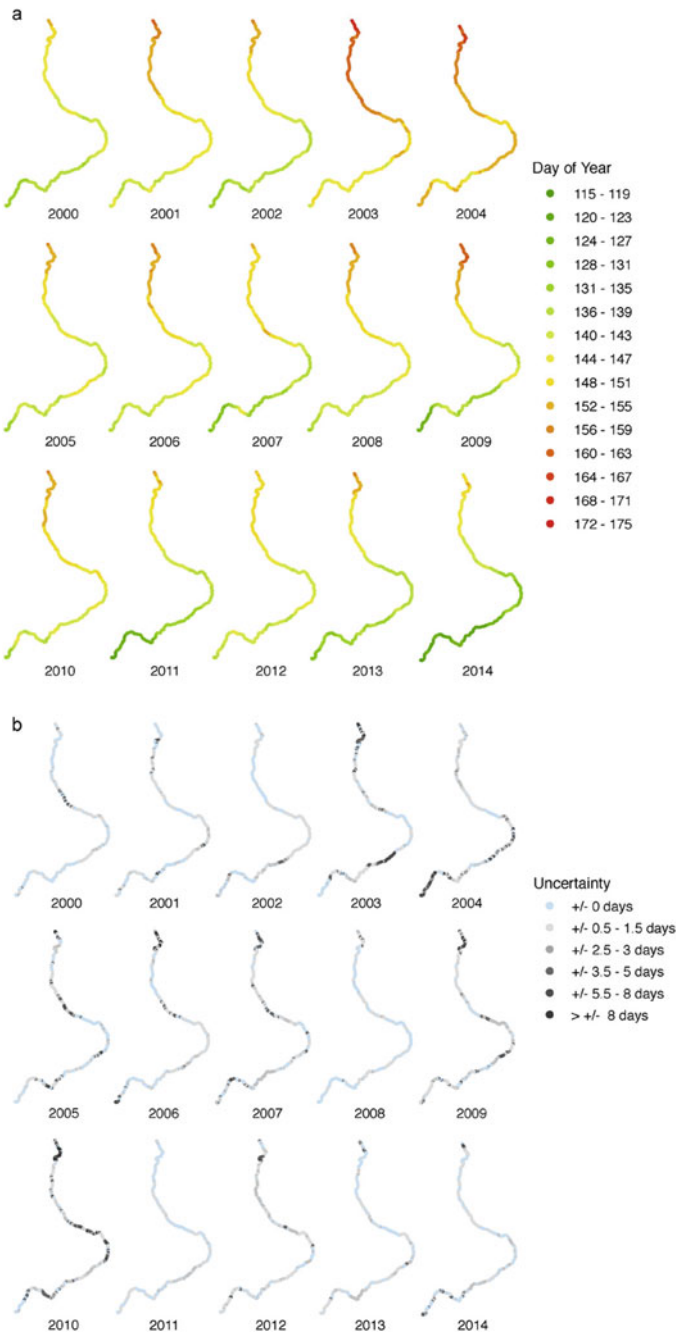

Fig. 13.9 Break-up dates (**a**) and uncertainty due to cloud-obscured imagery (**b**) for the Lena from 2000 to 2014. River reach shown is approximately 2800 km above the downstream Kusur Station near (Cooley and Pavelsky (2016)

years. Due to different climatic conditions governing western Canada versus central and eastern Siberia, the percent of river segments classified as clear (cloud by 50%) varies among the four rivers, ranging from 40.2% for the Yenisey to 50.8% for the Mackenzie. The average window of uncertainty for each break-up date also varies by river and by year. Despite the significant amount of cloud-obscured imagery, it is possible to detect break-up within a window of ±1 day for the majority of river segments.

The break-up dates plotted by distance from river mouth discern spatial patterns (Fig. 13.10). For each river, break-up primarily progresses monotonically northward and downstream. There is considerable variability from year to year in the timing and length of break-up, but the overall spatial patterns remain similar. All four rivers show evidence of discontinuous break-up, where a section may break-up several days or more after the surrounding river segments. These later break-up events are generally caused by tributaries and channel morphology; however, due to natural variability, these events are not always consistent from year to year. On the Mackenzie, break-up first occurs at the confluence with the Liard River, 300 km downstream from the initiation of the Mackenzie at Great Slave Lake. This pattern is likely due to warmer surface air temperatures in the Liard River basin and the influence of Great Slave Lake, which attenuates the impact of any flood wave generated by upstream melt and generally remains ice-covered until after the main stem of the Mackenzie has broken up. For the Lena, there is significant spatial and temporal variabilities in the upstream portions and relatively smooth progression of break-up downstream. The transition into a more temporally consistent break-up occurs near the confluence of the Lena and the Aldan Rivers, 1260 km from the mouth, suggesting that the addition of the Aldan moderates variability in break-up timing in the lower Lena. On the Ob', the northward and downstream progressions of break-up reverse slightly between approximately 1300 and 900 km from the mouth. This section of the river is associated with a change in the direction of the along-river temperature gradient (Prowse et al. 2010). As the river moves westward toward European Russia, the surface air temperatures actually increase downstream until the river again turns northward and eastward, likely explaining the observed reversal in break-up timing.

The mean date and length of break-up vary significantly among rivers and from year to year. While ice break-up does not progress downstream monotonically, break-up generally advances more rapidly on the Lena and the Ob', the longer, more braided rivers, at average rates of 79.8 km/day and 57.2 km/day, respectively. On the shorter and straighter Yenisey and Mackenzie rivers, break-up moves at average rates of 50.5 km/day and 41.7 km/day, respectively. The range of break-up rates observed also varies significantly by river and by year, with a maximum rate of 100 km/day on the Lena (in 2000, 2001, and 2012) and a minimum of 37.1 km/day on the Mackenzie (in 2000).

Cooley and Pavelsky (2016) demonstrated a successful approach to map ice break-up within a couple of days on large Arctic rivers. This capacity of remote sensing provides a solution to declining gauging and ground-based observations in the Arctic watersheds. Additionally, remote sensing enables observations along the

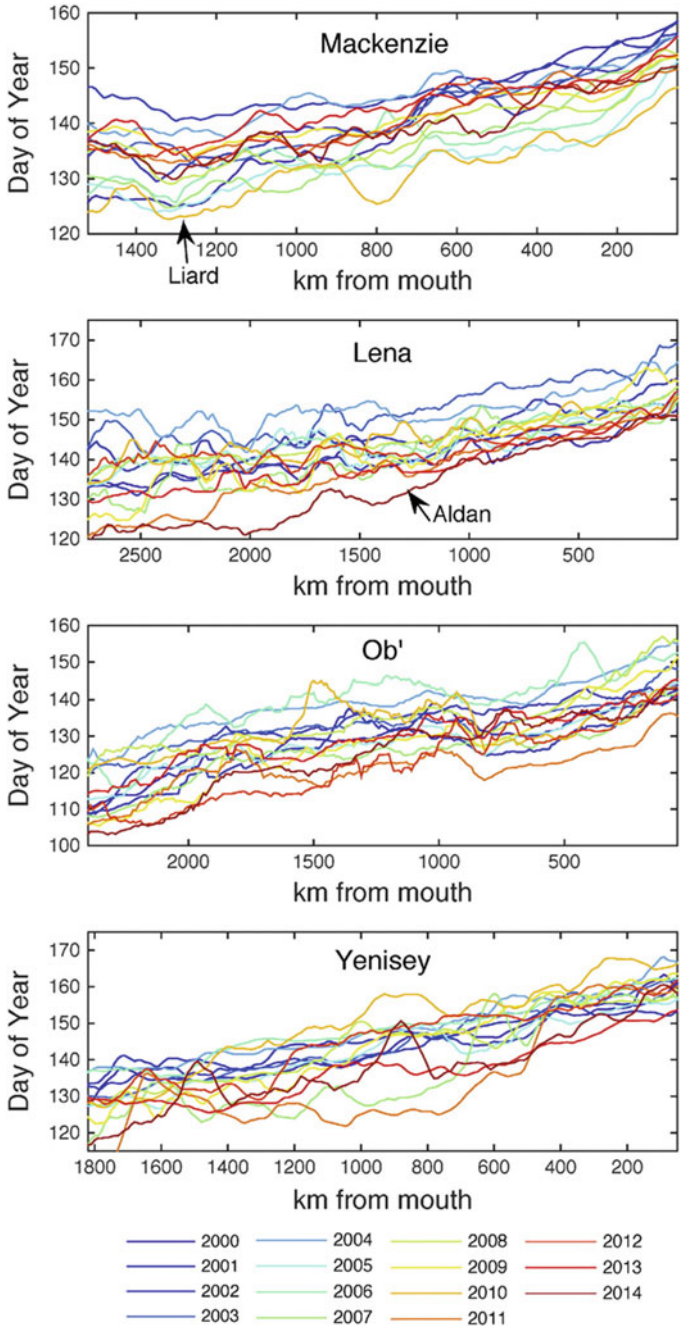

Fig. 13.10 Break-up dates plotted by kilometers from the mouth. Locations of major tributaries are noted for the Lena and Mackenzie (Cooley and Pavelsky (2016)

entire length of a river rather than only at discrete gauging or observation stations. This allows for more comprehensive records and predictions of river ice conditions as well as better opportunity for pattern recognition in data sets. A persistent problem in applying remote sensing data on these rivers is that break-up remains quite spatially variable over the length of some rivers. On the Mackenzie and Lena Rivers, there was considerable annual variation in river ice conditions over the length of the river. This variation was correlated with Pacific Decadal Oscillation trends, which will need to be accounted for in any predictive processing of remote sensing data for these rivers.

13.5 Conclusions and Discussions

Many studies clearly show decreases in river and lake ice thinness and duration due to climate warming across the northern regions. The reduction in river and lake ice will influence transportation opportunities in remote regions. A future reduction in thermal gradients along northward-flowing and ice-covered Arctic rivers may decrease spring flooding because of lessening in the severity of ice jamming (Prowse et al. 2010). Reductions in river ice jam flooding may have major positive benefits for communities and infrastructure along the river margins, but could also alter the ecology of deltaic riparian (Lesack and Marsh 2007) and coastal marine (Emmerton et al. 2008) ecosystems.

Lake ice cover will decrease in the future, according to a recent modeling study, in both thickness (10–50 cm) and duration (15–50 days) during 2040–2079 relative to 1960–1999 (Dibike et al. 2011a, b). The largest changes are projected for the Pacific coastal regions of North America, northeastern Canada, eastern Europe, Scandinavia, and northern Russia. Snow depth on lake ice surface is projected to change by −20 and +10 cm and the amount of white ice (i.e., ice forming from wet snow on top of ice) by −20 and +5 cm. In the high latitudes, white ice may form more easily in the future due to increasing snowfall and thinner ice cover. On the other hand, snow water equivalent in spring is projected to increase at high latitudes, particularly in areas with winter temperatures below −30 °C (Adam et al. 2009). The net result of these two factors (magnitude of spring snow water equivalent and severity of ice jams) remains to be quantified but will vary by river basin according to spatial and temporal variabilities in future precipitation and snowmelt regimes around the circumpolar north, including the headwaters of the large basins in more southerly latitudes (Prowse et al. 2011a, b).

One of the strongest ecological effects of the projected change in lake ice regimes is alterations to lake thermal structure (Bring et al. 2016). It has been reported that the high-latitude lakes along a 105°W transect (continental North America) exhibited less projected change in summer stratification than those along 90°E (continental Asia) (Dibike et al. 2011a, b); the differences are possibly due to regional contrasts in warming and/or differences in relative coldness. In a warming Arctic, shallower lakes that are not thermally stratified will have greater opportunity

for mixing surface waters with sediments, resulting in greater carbon recycling within the water column. In contrast, organic particles sinking below the thermocline in thermally stratified lakes may not return to surface water until fall turnover, decreasing the likelihood of carbon lost to sedimentation being recycled back into the water column. Alterations in the timing and duration of ice cover can also affect the distribution and fate of contaminants in freshwater systems. Greater methylation of mercury, for example, is likely to result from higher temperatures, particularly in shallow zones (Outridge et al. 2007). Moreover, higher water temperature is likely to increase pelagic production and thereby enhance algal scavenging of mercury, which is a pathway by which mercury can enter lentic food webs (Outridge et al. 2007). Higher surface water temperatures associated with a decrease in ice cover, and related changes in food and energy pathways and/or productivity (benthic to pelagic), will likely modify the movement of contaminants through such systems.

Ice-covered freshwater bodies comprise a significant portion of the high-latitude, sub-Arctic and tundra landscape, most climate and hydrological models, and however, do not consider ice processes in the northern regions. There is, thus, a need to improve hydrological models for better simulation of water cycle elements, including water temperature and ice, and to provide estimates of future changes as the result of climate warming in the cold regions (Prowse et al. 2011a, b; Lique et al. 2016; Vihma et al. 2016). Storage and its change are mostly unknown in northern regions (Yang et al. 2002). Basin storage capacity is a measure of the groundwater reservoir plus seasons changes of snow and ice. Typically, higher storage capacity leads to slower recession in streamflow, whereas lower storage volume leads to more rapid recession. Ye et al. (2009) pointed out very limited means through network observations to directly measure basin storage and amount in the northern regions, and thus the difficulty to quantify changes in basin storage and capacity over time. For river ice, it seems almost impossible to use local observations to determine the ice volume over large northern basins. For some lakes vulnerable to significant changes in ice conditions, it is useful to set up long-term research networks to better understand the influence of the changes, including the intermittent ice cover processes. However, recently developments in modeling and remote sensing provide opportunities to quantify river ice phenology and estimate river ice volume. It is important to have more effort on river/lake ice data and model integration, for example, to combine the ECCC river ice dataset (de Rham et al. 2020) with the CAHNGE model (Park et al. 2016) over northern Canada, so as to better test the model physics and performance in ice simulations over large arctic watersheds. Further research is also required to improve the models for ice processes (particularly where and when ice jams form and release), and for a better understanding how loss of lake ice impacts gas exchange between the lake and atmosphere, mixing of the water column, biogeochemical cycling, and ecosystem structure and function.

References

Aagard K, Carmack E (1989) The role of sea ice and other fresh water in Arctic circulation. J Geophys Res 94(C10). https://doi.org/10.1029/jc094ic10p14485

Adam J, Hamlet A, Lettenmaier D (2009) Implications of global climate change for snowmelt hydrology in the twenty-first century. Hydrol Process 23(7):962–972. https://doi.org/10.1002/hyp.7201

Andrishak R, Hicks F (2008) Simulating the effects of climate change on the ice regime of the Peace River. Can J Civ Eng 35(5):461–472. https://doi.org/10.1139/l07-129

Beltaos S (1990) Guidelines for extraction of ice break-up data from hydrometric station records in working group on river ice jams – field studies and research needs. NHRI science report. National Hydrology Research Institute, Environment Canada, Saskatoon, SK, pp 37–70

Beltaos S (1997) Onset of river ice breakup. Cold Reg Sci Technol 25(3):183–196. https://doi.org/10.1016/s0165-232x(96)00011-0

Beltaos S, Prowse T (2009) River-ice hydrology in a shrinking cryosphere. Hydrol Process 23 (1):122–144. https://doi.org/10.1002/hyp.7165

Benson BJ, Magnuson JJ, Jensen OP, Card VM, Hodgkins G, Korhonen J, Livingstone DM, Stewart KM, Weyhenmeyer GA, Granin NG (2012) Extreme events, trends, and variability in Northern Hemisphere lake-ice phenology (1855–2005). Clim Chang 112:299–323

Bieniek PA, Bhatt US, Rundquist LA, Lindsey SD, Zhang X, Thoman RL (2011) Large-scale climate controls of interior Alaska river ice breakup. J Clim 24(1):286–297. https://doi.org/10.1175/2010jcli3809.1

Bonsal BR, Prowse TD (2003) Trends and variability in spring and autumn 0°C-isotherm dates over Canada. Clim Chang 57(3):341–358. https://doi.org/10.1023/a:1022810531237

Bring A, Fedorova I, Dibike Y, Hinzman L, Karlsson JM, Mernild SH, Prowse T, Semenova O, Stuefer S, Woo M-K (2016) Arctic terrestrial hydrology: A synthesis of processes, regional effects and research challenges. J Geophys Res: Biogeosci (Special Issue) 121:621–649. https://doi.org/10.1002/2015jg003131

Brooks RN, Prowse TD, O'Connell IJ (2013) Quantifying Northern Hemisphere freshwater ice. Geophys Res Lett 40:1128–1131. https://doi.org/10.1002/grl.50238

Chapman WL, Walsh JE (1993) Recent variations of sea ice and air temperature in high latitudes. Bull Am Meteor Soc 74(1):33–47. https://doi.org/10.1175/1520-0477(1993)074%3c0033:RVOSIA%3e2.0.CO;2

Cooley SW, Pavelsky TM (2016) Spatial and temporal patterns in Arctic river ice breakup revealed by automated ice detection from MODIS imagery. Remote Sens Environ 175:310–322

de Rham L, Dibike Y, Beltaos S, Peters D, Bonsal B, Prowse T (2020) A Canadian river ice database from national hydrometric program archives, earth system science data. https://doi.org/10.5194/essd-2020-29

Dibike YB, Prowse T, Bonsal B, de Rham L, Saloranta T (2011a) Simulation of North American lake-ice cover characteristics under contemporary and future climate conditions. Int J Climatol. https://doi.org/10.1002/joc.2300

Dibike YB, Prowse T, Saloranta T, Ahmed R (2011b) Response of Northern Hemisphere lake-ice cover and lake-water thermal structure patterns to a changing climate. Hydrol Process. https://doi.org/10.1002/hyp.8068

Emmerton CA, Lesack LFW, Vincent WF (2008) Mackenzie river nutrient delivery to the arctic ocean and effects of the Mackenzie Delta during open water conditions. Glob Biogeochem Cycles 22(1):GB1024. https://doi.org/10.1029/2006gb002856

Evans E, McKay H, Sagin J, Das A, Lindenschmidt K, Van der Sanden J (2015) Monitoring the freeze-up and ice cover progression of the Slave River. Can J Civ Eng 42(9):609–621. https://doi.org/10.1139/cjce-2014-0286

Georgievsky V, Koronkevich N, Alexievsky N (2013) Water resources and hydrological regime of Russian rivers under the climate change conditions. In: Abstracts of plenary presentations, VII All-Russian hydrological symposium. SPB, Roshydromet, pp 26–32

Goulding HL (2006) Spatial and temporal patterns and hydroclimatic controls of river ice break-up in the Mackenzie Delta, NWT. MS thesis, Department of Geography, University of Victoria, 135pp

Goulding HL, Prowse TD, Bonsal B (2009) Hydroclimatic controls on the occurrence of break-up and ice-jam flooding in the Mackenzie delta, NWT, Canada. J Hydrol 379(3):251–267. https://doi.org/10.1016/j.jhydrol.2009.10.006

Gurevich E (2009) Influence of air temperature on the river runoff in winter (the Aldan river catchment case study). Russ Meteorol Hydrol 34(9):628–633. https://doi.org/10.3103/s1068373909090088

Ho E, Tsuji LJS, Gough WA (2005) Trends in river-ice break-up data for the western James Bay region of Canada. Polar Geogr 29(4):291–299. https://doi.org/10.1080/789610144

Lacroix MP, Prowse TD, Bonsal BR, Duguay CR, Menard P (2005) River ice trends in Canada. Committee on river ice processes and the environment. http://cripe.ca/docs/proceedings/13/Lacroix-et-al-2005.pdf

Lammers RB, Shiklomanov AI, Vörösmarty CJ, Fekete BM, Peterson BJ (2001) Assessment of contemporary arctic river runoff based on observational discharge records. J Geophys Res: Atmos 106(D4):3321–3334. https://doi.org/10.1029/2000JD900444

Latifovic R, Pouliot D (2007) Analysis of climate change impacts on lake ice phenology in Canada using the historical satellite data record. Remote Sens Environ 106(4):492–507. https://doi.org/10.1016/j.rse.2006.09.01

Lesack L, Marsh P (2007) Global Change in the Mackenzie River Delta. Geophys Res Lett 34: L23404. https://doi.org/10.1029/2007GL031656

Lesack LFW, Marsh P, Hicks FE, Forbes DL (2014) Local spring warming drives earlier river-ice breakup in a large Arctic delta. Geophys Res Lett 41(5):1560–1567. https://doi.org/10.1002/2013GL058761

Lique C, Holland MM, Dibike YB, Lawrence DM, Screen JA (2016) Modeling the arctic freshwater system and its integration in the global system: Lessons learned and future challenges. J Geophys Res: Biogeosci 121:540–566. https://doi.org/10.1002/2015JG003120

Livingstone DM, Adrian R, Blenckner T, George G, Weyhenmeyer GA (2010) Lake ice phenology. In: George DG (ed) The impact of climate change on European lakes. Springer, Berlin, pp 51–61

Ma X, Fukushima Y (2002) A numerical model of the river freezing process and its application to the Lena River. Hydrol Process 16(11):2131–2140. https://doi.org/10.1002/hyp.1146

Magnuson JJ, Robertson DM, Benson BJ, Wynne RH, Livingstone DM, Arai T et al (2000) Historical trends in lake and river ice cover in the Northern Hemisphere. Science 289 (5485):1743–1746. https://doi.org/10.1126/science.289.5485.1743

Markov ML (2003) Spatial-temporal dynamic of surface and ground water interaction. In: Proceedings of SHI, Hydrometeoizdat, vol 25, pp 90–104

Marsh P, Onclin C, Neumann N (2002) Water and energy fluxes in the Lower Mackenzie Valley, 1994/95. Atmos Ocean 40(2):245–256. https://doi.org/10.3137/ao.400211

Outridge P, Sanei H, Stern G, Hamilton P, Goodarzi F (2007) Evidence for control of mercury accumulation rates in Canadian high arctic lake sediments by variations of aquatic primary productivity. Environ Sci Technol 41(15):5259–5265. https://doi.org/10.1021/es070408x

Overland JE, Hanna E, Hanssen-Bauer I, Kim SJ, Walsh JE, Wang M, Bhatt US, Thoman RL (2017) Surface air temperature. In: Arctic report card 2017. National Oceanic and Atmospheric Administration. https://arctic.noaa.gov/Report-Card/Report-Card-2017/ArtMID/7798/ArticleID/700/Surface-Air-Temperature

Park H, Yoshikawa Y, Oshima K, Kim Y, Ngo-Duc T, Kimball JS, Yang D (2016) Quantification of warming climate-induced changes in terrestrial arctic river ice thickness and phenology. J Clim 29(5):1733–1754. https://doi.org/10.1175/JCLI-D-15-0569.1

Pavelsky TM, Smith LC (2004) Spatial and temporal patterns in arctic river ice breakup observed with MODIS and AVHRR time series. Remote Sens Environ 93(3):328–338. https://doi.org/10.1016/j.rse.2004.07.018

Pour HK, Duguay CR, Scott KA, Kang K (2017) Improvement of lake ice thickness retrieval from MODIS satellite data using a thermodynamic model. IEEE Trans Geosci Remote Sens 55 (10):5956–5965. https://doi.org/10.1109/TGRS.2017.2718533

Prowse TD, Gridley NC (1993) Summary. In: Prowse TD, Gridley NC (eds) Environmental aspects of river ice. NHRI science report no. 5, National Hydrology Research Institute, Environment Canada, pp 121–125

Prowse TD, Carter T (2002) Significance of ice-induced storage to spring runoff: a case study of the Mackenzie River. Hydrol Process 16:779–788. https://doi.org/10.1002/hyp.371

Prowse TD, Brown K (2010) Hydro-ecological effects of changing Arctic river and lake ice covers: a review. Hydrol Res 41(6):454–461. https://doi.org/10.2166/nh.2010.142

Prowse TD, Shrestha R, Bonsal B, Dibike Y (2010) Changing spring air temperature gradients along large northern rivers: implications for severity of river-ice floods. Geophys Res Lett 37: L19706. https://doi.org/10.1029/2010GL044878

Prowse T, Alfredsen K, Beltaos S, Bonsal B, Duguay C, Korhola A, McNamara J, Vincent W, Vuglinsky V, Weyhenmeyer G, Walter Anthony K, Bowden B, Buzin V, Dibike Y, Gantner N, Hinzman L, Lia L, Ouarda T, Pientiz R, Reist JD, Stickler M, Weckström J, Wrona F (2011a) Changing lake and river ice regimes: trends, effects, and implications. In: SWIPA, snow, water, ice permafrost in the Arctic. Scientific Assessment of the Arctic Monitoring and Assessment Program, Oslo, Norway, pp 6.1–6.52

Prowse T, Alfredsen K, Beltaos S, Bonsal BR, Bowden WB, Duguay CR, Korhola A, McNamara J, Vincent WF, Vuglinsky V, Walter Anthony KM, Weyhenmeyer GA (2011b) Effects of changes in arctic lake and river ice. Ambio 40:63–74. https://doi.org/10.1007/s13280-011-0217-6

Rouse WR, Oswald CJ, Binyamin J, Spence CR, Schertzer WM, Blanken PD, Bussieres N, Duguay CR (2005) The role of northern lakes in a regional energy balance. J Hydrometeorol 6:291–305

Rouse WR, Blanken PD, Duguay CR, Oswald CJ, Schertzer WM (2007) Climate–lake interactions. In: Woo MK (ed) Cold region atmospheric and hydrologic studies: the Mackenzie GEWEX experience. Springer, Berlin, pp 139–160

Sagarin R, Micheli F (2001) Climate change in non-traditional data sets. Science 294(5543):811. https://doi.org/10.1126/science.1064218

Sharma S, Blagrave K, Magnuson JJ, O'Reilly CM, Oliver S, Batt RD, Magee MR, Straile D, Weyhenmeyer GA, Winslow L, Woolway RL (2019) Widespread loss of lake ice around the Northern Hemisphere in a warming world. Nat Clim Chang 9:227–231. https://doi.org/10.1038/s41558-018-0393-5

Shiklomanov AI (2016) Data of river ice timing and thickness for selected river gauges in Russian pan-Arctic over 1970-2012. NSF Arctic Data Center. https://doi.org/10.18739/A2PW9R

Shiklomanov A, Lammers R (2014) River ice responses to a warming arctic - recent evidence from Russian rivers. Environ Res Lett 9(3). https://doi.org/10.1088/1748-9326/9/3/035008

Shiklomanov AI, Lammers R, Rawlins MA, Smith LC, Pavelsky TM (2007) Temporal and spatial variations in maximum river discharge from a new Russian data set. J Geophys Res-Biogeosci 112(G4). https://doi.org/10.1029/2006jg000352

Smith L (2000) Trends in Russian arctic river-ice formation and breakup, 1917 to 1994. Phys Geogr 21(1):46–56. https://doi.org/10.1080/02723646.2000.10642698

Vihma T, Screen J, Tjernström M, Newton B, Zhang X, Popova V, Deser C, Holland M, Prowse T (2016) The atmospheric role in the Arctic water cycle: A review on processes, past and future changes, and their impacts. J Geophys Res: Biogeosci 121:586–620. https://doi.org/10.1002/2015JG003132

Vuglinsky V (2000) Russian river ice thickness and duration, version 1. Boulder, Colorado USA. NSIDC: National Snow and Ice Data Center. https://doi.org/10.7265/N5J10129

Vuglinsky VS, Gronskay TP (2006) Changing of rivers and lakes ice regime within the Russian territory and their possible consequences for economy. In: Modern problems of hydrometeorology. St. Petersburg, Asterion, pp 229–245 (in Russian)

Walsh JE, Anisimov O, Hagen JOM, Jakobsson T, Oerlemans TD, Prowse TD, Romanovsky V, Savelieva N et al (2005) Cryosphere and hydrology. In: Arctic climate impact assessment. Arctic Monitoring and Assessment. https://www.amap.no/documents/doc/arctic-arctic-climate-impact-assessment/796

Wilson NJ, Walter MT, Waterhouse J (2015) Indigenous knowledge of hydrologic change in the Yukon river basin: a case study of Ruby, Alaska. Arctic 68(1):93–106. https://doi.org/10.14430/arctic4459

Yang D, Kane DL, Hinzman LD, Zhang X, Zhang T, Ye H (2002) Siberian Lena River hydrologic regime and recent change. J Geophys Res-Atmos 107(D23):4694-ACL 14-10. https://doi.org/10.1029/2002jd002542

Ye B, Yang D, Zhang Z, Kane DL (2009) Variation of hydrological regime with permafrost coverage over Lena Basin in Siberia. J Geophys Res-Atmos 114(D7):D07102. https://doi.org/10.1029/2008JD010537

Zhang X, Vincent LA, Hogg WD, Niitsoo A (2000) Temperature and precipitation trends in Canada during the 20th century. Atmos Ocean 38(3):395. https://doi.org/10.1080/07055900.2000.9649654

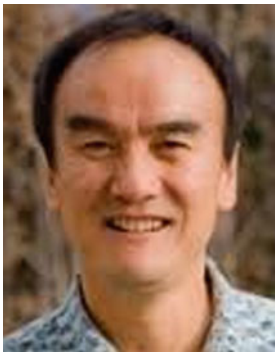

Dr. Daqing Yang is a Research Scientist at the Watershed Hydrology and Ecology Research Division, Environment and Climate Change Canada. He is also Affiliate Research Professor at the International Arctic Research Center, Univ. of Alaska Fairbanks. Over the past 25 years, he has conducted cryosphere system research in China, Canada, Japan, USA, and Norway. His primary research activities/interests include cold region hydrology and climate, particularly Arctic large river streamflow regime and change, snow cover and snowfall measurements, climate change and human impact to regional hydrology, and applications of remote sensing in cold regions. He has served as journal editor and subject editor for IAHS publications (cold region hydrology, northern research basin water balance, and cold/mountain region hydrological systems under climate change), and WMO technical reports (solid precipitation measurement intercomparison and integrated global observing strategy cryosphere theme). He also contributed as review and/or author to the IPCC Reports, and the Arctic Council's Snow, Water, Ice and Permafrost in the Arctic (SWIPA 2017 and follow up) assessment. His current research focuses on investigating the impacts of climate variability/change and human activities on hydrologic system across the broader northern regions.

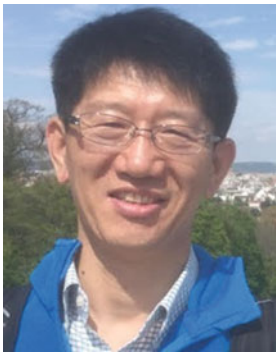

Dr. Hotaek Park is a Senior Scientist at JAMSTEC. He earned his Ph.D. at Graduate School of Bioagricultural Sciences, Nagoya University in 2000. Then, he worked at two Japanese Institutes as postdoctoral fellowship and joined the position of JAMSTEC research scientist in 2007. He is an expert on hydrology, biogeochemistry, and climate researches in cold regions, with interests in evaluating changes in land surface processes under climate changes and predicting future changes using land surface model, remote sensing data, reanalysis products, in site observations, and model outputs. He has the author/co-author of numerous scientific articles that have published on a variety of peer-reviewed journals, conference proceedings, and books. His recent research is focused on assessing impacts of changing snow and permafrost on hydrological processes in the context of climate variability and interactions between declining Arctic sea ice and terrestrial ecohydrologic processes coupling models of land–atmosphere–ocean processes.

Dr. Terry Prowse is (Emeritus) Senior Research Scientist at the Watershed Hydrology and Ecology Research Division, Environment and Climate Change Canada, and professor at Department of Geography, Univ. of Victoria. He research focused on the theme of climate impacts of water resources in the cold regions, including hydrologic, hydro-ecologic and hydro-climatic studies of alpine snow, permafrost, lake and river ice, northern rivers and wetland deltas, floods and disturbance ecology, Arctic freshwater budgets, water isotopes, reservoir supplies, and flow regulation. He chaired an international group formulating a research plan for the Arctic focussing on hydrology and the cryosphere (ICARPII for the International Arctic Science Council). He was also a member of the Scientific Steering Group for WCRP-CliC and led one of their four main science themes entitled "The Terrestrial Cryosphere and Hydroclimatology of Cold Regions. He was the lead and contributing author for the IPCC reports, the AMAP/Climate Change and the Cryosphere: Snow, Water, Ice, and Permafrost in the Arctic (SWIPA) assessment, and the Arctic Freshwater Synthesis".

Dr. Alexander Shiklomanov received M.Sc. (1983) and Ph.D. (1996) degrees from Russian Hydrometeorological State University, St. Petersburg. Since 1983, he has been working at the Arctic and Antarctic Research Institute (AARI), in Saint Petersburg, Russia; and in 1997 he joined the Earth Systems Research Center at the University of New Hampshire, USA. The focuses of his research are on cold region and Eurasian hydro-climatology, hydrological and water management modeling and analysis. Research interests include hydrological monitoring systems; water balance and streamflow routing models; human activity and its influence on hydrology; climate change and hydrological systems; and effect of land cover and land use change on hydrology. He has more than 60 publications including more than 45 in peer-reviewed journals. He is a co-developer of several regional hydrographic databases and a reviewer of multiple national and international scientific journals. He has been a Principal Investigator for many research projects sponsored by NASA and NSF.

Ms. Ellie McLeod is a student studying Environmental Geoscience and Indigenous Studies at the University of Victoria on Lekwungen and W̱SÁNEĆ territories. From July 2018 to September 2019, she worked with Daqing Yang at Environment and Climate Change Canada's Water and Climate Impacts Research Centre. During her time with Environment and Climate Canada, she also contributed to a project evaluating the efficacy of space-based measurements of sea surface salinity in Hudson Bay, resulting in a paper published in *Remote Sensing* in March 2020.

Part III
Permafrost and Frozen Ground

Permafrost Features and Talik Geometry in Hydrologic System

14

Kenji Yoshikawa and Douglas L. Kane

Abstract

Permafrost is widely distributed in the high latitudes. This chapter discusses frozen (permafrost) and unfrozen states of the hydrological geometry in the northern regions. The hydrological activities are very active and dynamic not only in discontinuous permafrost zone but also in cold continuous permafrost areas. Water carries significant amount of heat in aquifer and talik system. Water locates in the depth below the maximum ice formation can develop an unfrozen layer underneath the water body (i.e., talik and thaw bulb). Taliks could be open to connect to the sub-permafrost layer, while the hydrologic gradient makes flow in upward or downward directions. The heat balance of the super-, inter-, or sub-permafrost generates unique unfrozen geometry in the permafrost. This chapter also reviews various cellars developed and used in the arctic regions by indigenous people.

14.1 Introduction

Presence or absence of the permafrost have been discussed for years in the Arctic in regard to understanding the hydrological cycle in the cold environments. In general, permafrost acts as an impermeable substrate, that is why there are so many lakes, ponds, and wetlands in areas of permafrost regions despite the low amounts of

K. Yoshikawa (✉) · D. L. Kane
Water and Environment Research Center, University of Alaska Fairbanks, Fairbanks, AK, USA
e-mail: kyoshikawa@alaska.edu

D. L. Kane
e-mail: dlkane@alaska.edu

D. Yang and D. L. Kane (eds.), *Arctic Hydrology, Permafrost and Ecosystems*,
https://doi.org/10.1007/978-3-030-50930-9_14

annual precipitation. However, the property of hydraulic conductivity is not universally low; it can vary considerably depending upon soil/rock type, permafrost temperature, salinity, etc. Thin films of unfrozen water exist on the surface of the porous media and the greater the surface area of the substrate, the thicker the unfrozen film (greatest for warm clays). Generally, permafrost is considered as impermeable for hydrologic applications with sub-permafrost groundwater below the permafrost and suprapermafrost groundwater above.

In this chapter, we define terms of some permafrost terms and discuss the interaction between frozen soil and water. Permafrost is defined as any ground material (soil, rock, ice, water) staying below 0 °C for two or more consecutive years by today's scientific community and the western world, some of the former Soviet countries and Eastern countries define it as several years instead of two. However, these definitions prove to be problematic as not all water in permafrost freezes at 0 °C.

The current distribution of the permafrost is not only related to today's climate but also strongly linked to the late Pleistocene climate (e.g., glacier distributions) and somewhat by the Little Ice Age epic. The major permafrost forming period in the Arctic was slightly prior to the Last Glacial Maximum (LGM). That is why a majority of the ground ice (syngenetic ice wedges), also called "Yedoma" deposits, are present over most of the unglaciated regions. Also, permafrost is much more extensive in unglaciated areas, reaching depths exceeding 1 km in Eastern Siberia. Late Pleistocene glaciations covered considerable terrain in the North America, Scandinavia, and Greenland; these ice sheets blocked the severe climate from producing deeper permafrost (in some cases no permafrost). After retreat of the ice sheets, glacial isostatic rebounding took place in these areas and in one case producing newly developed coastal areas. This resulted in the development of young permafrost with complicated hydrogeological dynamics, including enrichments of the brines and the formation of unfrozen pockets (cryopegs).

Over the last fifty years, soil moisture measurement methods have been improved by the introduction of electromagnetic technology. Since the semiconductor industry has grown dramatically over the recent decades, many of the microchips (processing unit) and oscillators required for electromagnetic methods are now available at very low cost and small size. Cheaper, smaller, and more portable devices for measurement read-out (or datalogging) have also appeared on the commercial market. This has dramatically changed our understanding of active layer dynamics in Arctic regions. Smith and Tice (1988) compared nuclear magnetic resonance (NMR) and Time Domain Reflectometer (TDR) measurements of the unfrozen water content of frozen soils. The NMR technique is one of the most reliable methods for determining the unfrozen water content of soils (Tice et al. 1982), as it depends on the spatial density of hydrogen atoms in the sample. They concluded that very accurate readings were also possible using TDR for unfrozen water content determinations. Unfortunately, NMR's use is restricted to the laboratory. The water content of frozen materials strongly controls the freezing and thawing process (through latent heat exchange) of the active layer in arctic regions. The moisture content of the soil also affects the thermal properties (thermal offset)

of permafrost that is directly related to the thermal conductivity (Yoshikawa et al. 2002). Thus, periglacial processes are strongly influenced by the water content of the materials.

Talik is originally a Russian term about year around unfrozen soil structure of supra-, inter- or sub-permafrost layer. Taliks occur in many situations involving brackish and fresh water and are very common to find in the Arctic. Many arctic communities use fresh water taliks as drinking water sources. Cryopeg is another Russian term for the layer of unfrozen ground where phase change is prevented by freezing point depression due to the dissolved solids content of the pore water. The freezing point of the cryopeg is interestingly close to the zero annual amplitude permafrost temperature (Yoshikawa et al. 2004). Cryopegs are not as domestically useful as freshwater taliks, they present problems to design infrastructures, especially at marine deposit such as isostatic uplifting area or coastal active area. In northern Alaska and Chukotka, food in some of the native ice cellars located in easily excavated cryopeg layers was attributed to the self-maintained moisture from the cryopeg.

Freshwater taliks ("thaw bulb") are often located beneath the deeper water bodies (>2 m), including river channels. Brewer (1958a, b) reported that the talik zone beneath a deep lake at Barrow reached a depth of 60 m. Freshwater taliks are also present under many of the closed-system pingos and drained lakes in an area which extends from North Slope of Alaska to Mackenzie Delta in Canada e.g., Mackay 1997; Parameswaran and Mackay 1996). These freshwater taliks have a relatively short life, in contrast to brine layers in regions of thick continuous permafrost. Brown (1969) observed a high saline zone several meters below sea level at Utqiagvik (formerly Barrow) Alaska. Collett and Bird (1993) compiled drill logs from an oil field in the Prudhoe Bay/Kuparuk River area, where brine layers occur widely and extend offshore at depths of 50 m to more than 250 m. The rule governing the physical properties of freshwater taliks and brine layers is similar to liquid phase of H_2O, which has both the low resistivity and high dielectric constant. However, the thermal stability of a talik and a cryopeg layer has quite different regimes. A freshwater talik is only stable when the upper boundary temperature is above 0 °C or water is moving in the ground. On the other hand, the cryopeg layer is more stable for the long period of time without any conditions in the permafrost, because the cryopeg layer stays at similar temperature of surround permafrost.

There are many ways to develop a freshwater talik in the Arctic. Simply, a talik could establish by groundwater moving in an aquifer or in the bottom of a lake or, a river. Refreezing of the talik is an important process of pingo development. A pingo is a significant landform on the flat tundra of the Arctic. In this area of low vegetation and little elevation difference, a pingo is commonly the most prominent feature against an otherwise unbroken horizon. Pingos provide a target destination for polar travelers and a dry place in the surrounding wet tundra. Ancient hunters used pingos when hiding from animals. The artifacts and archeological sites found at pingos on the Alaska North Slope date to about 6000 years B.P. (Lobdell 1986). Porsild (1938) described and classified all mounds in North America numerous mounds from the Kotzebue Region to the Mackenzie Delta. As the first person to

use the term pingo, Porsild described what most likely are closed-system (hydrostatic) pingos. Pingos are ice-cored mounds, a definition used worldwide in permafrost regions. Each country or region with pingos has used its own name for this landform. Some studies before Porsild (1938) referred pingos as "heaved mounds" and "hydrolaccoliths" (e.g., de K Leffingwell 1919). The term pingo derives from the word pinga in the Inuit (Canadian Arctic) language or ping in the Inupiat (Alaskan Arctic) language. In Russia, the equivalent term for pingo, used by Yakuts, is bulgunniakh. Many pingos in Greenland were noted as mud volcanoes on maps, though actual mud volcanoes are rare, and possibly nonexistent in Greenland. Though pingos are still commonly referred as mud volcanoes in Greenland, maps published there since the 1980s use the word pingo. In Svalbard, pingo is a well-known and frequently used term. Orvin (1944) studied springs and mounds, calling them kildehaug, a term used only at that time.

Pingos have different origins, based on source of water and types of developed groundwater pressure. Classically, pingos are divided into two types, depending on the mechanism that pressurizes the groundwater, therefore pingos are either open-system (hydraulic) or closed-system (hydrostatic). Open-system pingos are formed by artesian pressure (Müller 1959; Holmes et al. 1968; French 1996). Water is supplied under pressure from surrounding higher terrains, it then flows beneath the surrounding impermeable permafrost, and finally discharges toward the ground surface through a talik at the base of a hill or in the valley bottom. In the discontinuous permafrost zone (e.g., warmer permafrost temperature), hydraulic conductivity is higher through taliks above, below, or within the permafrost. Thus, most open-system pingos occur mainly in the discontinuous permafrost zone near areas of marked relief, which supplies the hydraulic gradient (potential). Discontinuous permafrost provides the opportunity for upwelling (open talik environments). Artesian groundwater environments cause repeated injections of water into the weakest portion of the permafrost, leading to development of massive ice at the upper part of the permafrost and formation of the pingo's core. This type of pingo is commonly found in valleys near terminal moraines, at the toe of alluvial fans near river bottoms, in highly fractured or faulted uplands, and on rebounding marine terraces (Yoshikawa and Harada 1995).

In contrast to open-system (hydraulic) pingos, closed-system (hydrostatic) pingos occur in regions of continuous permafrost (Mackay 1979, 1998), where there is an impermeable layer at depth (closed talik environments). Most closed-system pingos form in drained thaw lakes or former streambeds, where the saturated lake basin sediments are exposed to the atmosphere. This exposure causes saturated sediments to freeze, forming new impermeable permafrost. However, residual ponds within the lakes retard permafrost growth, resulting in locally thinner permafrost and less resistance to deformation. As the permafrost aggrades, the pore water is expelled ahead of the freezing front. Blockage of this pore water flow by the continuous permafrost at depth redirects the flow inward from the basin edges. Injection of expelled water into the overlying permafrost, followed by freezing of the injected water, causes progressive doming. This doming, commonly situated

beneath the least permafrost aggradation, produces the massive ice that forms the core of the pingo.

For both types of pingos, the 9% expansion due to phase change from water to ice is insufficient to account for size; groundwater pressure is required to supply the volume of water to a pingo ice core. Both open- and closed-system pingos may undergo vertical pulsing (periods of uplift) because of the injection of groundwater to a sub-pingo water lens (Mackay 1998; Yoshikawa 2008). To summarize, closed-system pingos characteristically (1) contain a core of injection ice (frozen from bulk water), (2) occur on lake sediments but also on previously unfrozen sediments of abandoned stream channels, and (3) are caused by the expulsion of pore water when saturated coarse- or fine-grained lake sediments freeze (Mackay 1979).

There was a unique artesian sub-permafrost groundwater leakage problem in Fairbanks Alaska next to an open-system pingo. Leakage of groundwater on the outside of residential well casings is a common problem. An impermeable permafrost layer produces unique artesian conditions at base of a hill slope (permafrost acts as an aquitard). When a well is drilled through the permafrost, the water flowing in the well induces thawing outside the well casing. To stop the flow, the unfrozen soil around the casing must be refrozen or the hydraulic conductivity reduced (by grouting). Various techniques have been used for wells around Fairbanks, Alaska. In one case, liquid nitrogen was used to stop the flow around an artesian well (Fig. 14.1). In November 2005, liquid nitrogen was injected into the well. By February 2006 the area around the well was completely refrozen, stopping the groundwater discharge. We had the opportunity to monitor sub-permafrost groundwater pressures during and after this event. After the injection, well leakage was eventually stopped and the groundwater pressures to recover. Within a few weeks, the pressure returned to the original level (Fig. 14.1). In this setting, frozen silt layer is 27 m thick and overlies 15 m of creek gravel. The permafrost is 43 m thick. The hydraulic pressures of the nearby pingos and alluvial deposits are high (>68 kPa) measured by surrounding artesian well water from sub-permafrost aquifer, thus creating artesian conditions. Most of the homeowners have installed groundwater wells for domestic usage. One wants the water inside the well casing to remain unfrozen, but the soils around the casing to remain frozen, a challenging task. The discontinuous permafrost temperatures around Fairbanks are very warm (>−1 °C) and sub-permafrost groundwater is just a few degrees above the freezing point of water. In some cases, the ensuing discharge from the wells continues to flow through the winter, thus creating large masses of aufeis (icings), some of which have destroyed houses and covered roads.

Surface disturbances have also produced talik formations throughout time. A typical natural ground surface disturbances is wildfire. Wildfire effects on frozen ground include short-term increase in soil moisture content, followed by a long-term decrease in soil moisture content, warmer soils, and increased active layer depth. The short-term increase in soil moisture is caused by removal of vegetation, which causes decreased evapotranspiration. The thermal conductivity of the active layer soils is greatly increased by this increase in soil moisture content

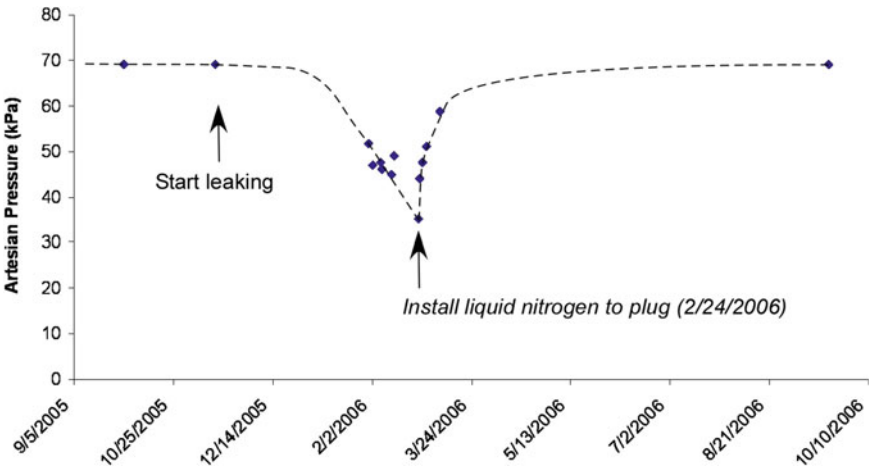

Fig. 14.1 Time series of an artesian pressure of groundwater. Liquid nitrogen was used to stop the flow leaking ground water around an artesian well

causing warmer soils than in adjacent unburned areas (also due to reduction in surface albedo and lack of surface organic material). However, the severity of the fire in part determines the amount of effectiveness of the increased soil thermal conductivity. There appears to be a threshold of the remaining organic material that determines the influence of wildfire on the frozen ground. This threshold is a function of the thickness of organic layer, thermal conductivity, and thawing index of the ground surface.

Similar disturbance to the permafrost can also occur because of urban development and agriculture. We have one of the longest disturbance studies at Fairbanks, Alaska. Comparing current results from this investigation with Linell (1973), it is apparent that in both of the plots where vegetation was removed, the permafrost retreated downward for 26 years, with the permafrost table eventually stabilizing at the partially disturbed site. This is likely due to the reestablishment of a boreal forest at the site within 25 years. At the site where all the surface vegetation and organic material were removed the permafrost table has continued to migrate downward for the past 35 years (Fig. 14.2). Vegetation at the site has continued to evolve and is currently migrating from a shrub-birch-willow forest to one with a higher density of spruce trees and moss (Douglas et al. 2012).

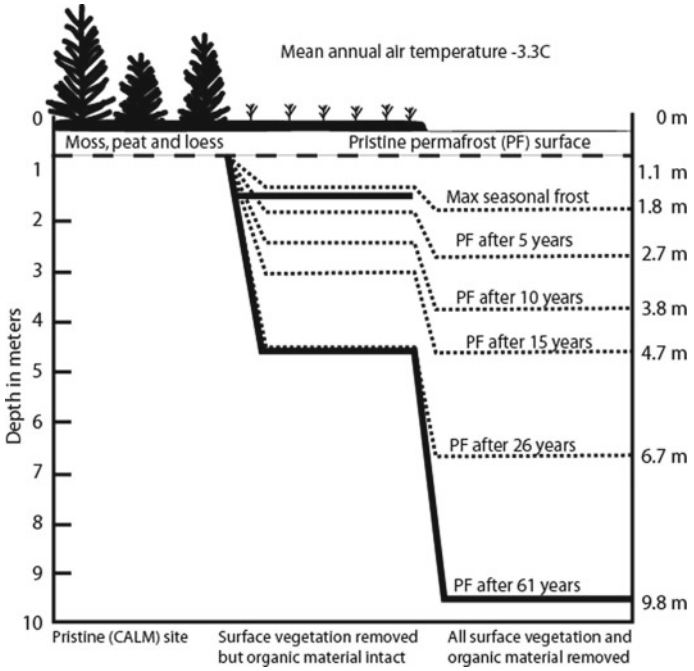

Fig. 14.2 61 years of surface vegetation and organic material removal and degradation of permafrost. A cross section based on Linell 1973. Vegetation removal from the two disturbed sites occurred in 1946. The bold line denotes the measurements collected in the fall of 2007 representing 61 years since disturbance (Douglas et al. 2012)

14.2 Historical Background

A majority of the world's permafrost is found in Eurasia including Siberia, Far Eastern Russia, Scandinavia, Arctic Islands, Mongolia, Tibet, Central Asia, Northeastern China, and Japan. Siberia is definitely the major location of permafrost with thickness from a few meters to over 1200 m. Also, Siberia has the oldest permafrost studies which originated in the nineteenth century. It means they collected temperature records since the Little Ice Age, which is very rare in the world. Permafrost temperature profile at the Shergin well (Fig. 14.3) shows little change since 1835 at a well in the middle of Yakutsk, after the town had an expanding the city limit during the last 180 years.

The main indicators of the geocryological conditions are the depth of active layer, permafrost temperature and the thickness of the frozen strata. For Siberia, the average annual temperature varies from +5 to –15 °C. The depth of active layer varies, depending on the conditions of heat exchange and climatic conditions, from 0.2 to 3.5 m, reaching 6.0 meters in mountain areas and foothills. Continuous

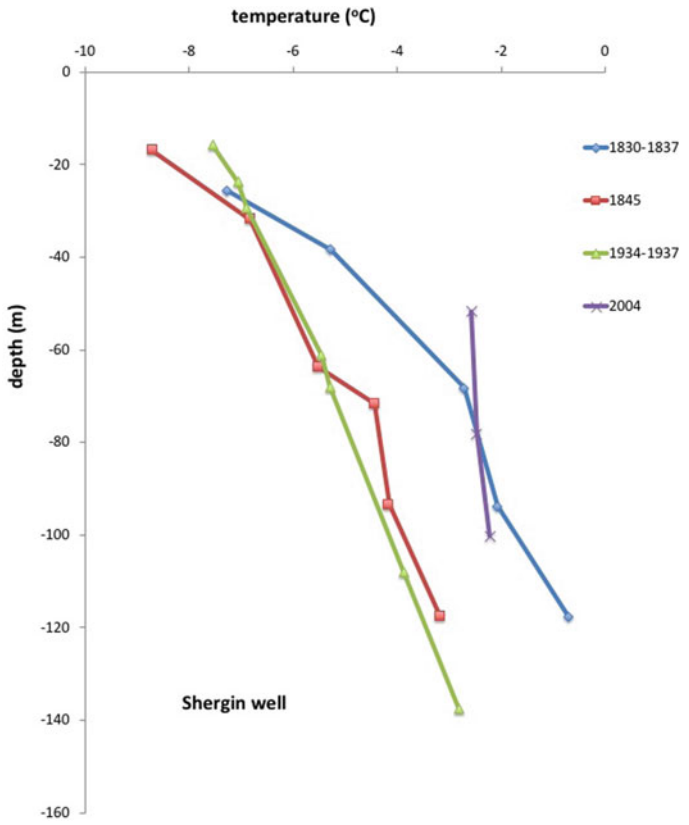

Fig. 14.3 Temperature profile in the Shergin mine, dug in Yakutsk in 1835. 1830–1837—measurements by Shergin; 1845—the measurement of Middendorf; 1934–1937—measurements of the Zatsepins; 2004—modern measurements

distribution of permafrost across the area is observed in the northern regions. But even there, under large rivers such as Lena, Yenisei, Kolyma, lakes, and in tectonic fractured zones with increased circulation of groundwater, there are zones that are absent of permafrost. Typically very complicated talik formations in such areas are difficult to predict. The dynamics of the interactions between permafrost and climate change are not easy to quantify and predict in different regions of the world. It depends on the features of atmospheric circulation processes, the conditions of heat exchange at the ground surface and the composition of soils. Over a 30-year-period in Siberia, the average annual air temperature everywhere tends to increase by 0.3 and 0.6 °C/10 years. The ice content of the permafrost is quite high in Siberia (called Yedoma deposits), including some in Alaska and Western Canada. The origin of the Yedoma deposit is syngenetic ice wedge network. These ice wedges grew upward following deposition of the eolian sediments. Most of the ice was

formed during late Pleistocene (30–40 k. y, BP). Huge outcrops are seen along the East Siberian Sea coastline and is experiencing rapidly erosion. In addition to northern Yakutia, some Yedoma deposits exist in central Yakutia. However, this high volume of the Yedoma ice does not significantly contribute to the local hydrology, even when it melts dramatically. There was a catastrophic Yedoma ice melting event in the early Holocene. During that epoch, most of the upper part of permafrost thawed and produced almost all of today's thermokarst lakes and alases. The volume of the annual thaw of ice-rich permafrost is very minimal; watershed hydrology is impacted more by the annual formation (from baseflow) and thaw of aufeis.

Other than the cold stable permafrost in Eastern Siberia, most of the permafrost areas have temperatures near the thawing point and are unstable. These warm permafrost areas generate more taliks, both inter-, subpermafrost. As a result, icings and/or open-system pingos are more common, especially in Mongolia and Tibet. These intra- permafrost aquifers can result in pingos and aufeis formations, but also connect to the groundwater system through taliks under rivers and lakes, as well as terrain at higher elevations. These hydrocryological structures (pingos, taliks, icings, etc.) developed mainly from early to middle Holocene. Also, it still happens that new springs and associated icings can develop after strong seismic activity in the southern fringes of permafrost, sporadic and/or isolated permafrost can be found (some as shallow as 10 m) beyond where continuous and discontinuous permafrost is found. These permafrost areas have a unique, thicker peat layer that shields the shallow permafrost from thawing, it is common to find this in places such as northern Scandinavia, Kola peninsula, western Siberia, Kamchatka, Sakhalin, Hokkaido, and Northeastern China. Typically, segregation ice developed in the peat layer during freezing process, thus forming palsas. Annual mean ground surface temperature can sometimes exceed +4 °C in these palsas, but the permafrost can have a stabilizing. Dried peat layer has very low thermal conductivity compared with wet frozen peat layer. These thermal property differences between the seasons makes for a strong thermal offset that results in stable permafrost in such relatively warm areas.

Permafrost is widely distributed in the high latitudes of North America (mostly Alaska in United States). However, geological and permafrost chronological distribution is quite different between eastern and western parts of North America. Much of Alaska and western Canada has thicker sediments with ice-rich permafrost; sometimes buried glacier ice also exist, mainly in Northwestern Alaska, Brooks Range, Yukon Territory, and Northwest Territory. These relict glacier ice bodies have produced some huge retrogressive thaw slumps in these areas and resulted in increased suspended sediment in river/coastal waters. It is not only buried glacier ice that is found in these areas, but also pingos and both types of ice wedges (syngenetic and epigenetic). Unlike Western North America, Eastern Canada and Greenland are covered by very old igneous and high grade metamorphic bedrocks. Also, this area was covered by an ice sheet during the last glacial maximum (LGM) that prevented permafrost expansion at depth. As results, most of the bedrock area had less ice contents, except in active fluvial terrain and wetlands.

Inter-permafrost hydrological activity is very active in most of the Alaska and Canada except the area covered by Canadian Shield. Many springs, icings, and open-, closed- system pingos are located in these areas. Glacial isostatic rebounding is another important process here. Very dynamic and formed/emerged beach lines established complicated permafrost hydrological interactions in Eastern Canada and Greenland. These areas have also considerable marine clay deposits that harbor cryopegs.

Most of the western Canada and interior Alaskan boreal forests are underlain by discontinuous permafrost. The discontinuous character of permafrost distribution creates a complex interrelationship between permafrost and vegetation in the boreal forest. Especially the type of forest floor varies from litters, lichens, feather mosses to Sphagnums. Permafrost thicknesses vary in this area from 0 to 150–200 m (Ferrians 1965; Brown et al. 1998). Permafrost temperatures are close to 0 °C, thus the permafrost is more susceptible to surface disturbances such as wildfire. Permafrost temperatures in the boreal forest are 0 to –4 °C and typically warmer than –2 °C. Other natural factors that influence permafrost temperature regime include the thickness, thermal properties, and duration of the snow cover (Brown and Pewe 1973; Romanovsky and Osterkamp 1995). The mean annual ground surface temperatures usually are 3–6 °C warmer than the mean annual air temperatures. As a result of relatively warm air temperatures and the effect of snow cover in reducing winter heat loss from soil, the mean annual ground surface temperatures in the boreal forest often exceed 0 °C and can be as high as 4 °C. Isolated permafrost was found to have a strong thermal offset in Bristol Bay area of Alaska, Anchorage Alaska and the Whitehorse area of Canada. Based on current borehole information, one of the coldest permafrost areas in the arctic and subarctic is the measured –27.6 °C near the summit of Denali (station elevation ca.5700 m). However, for low elevations, Alert (northern most end of the Canadian archipelago) was measured at –14 °C. All of Eurasian permafrost temperatures were warmer than Alert and Denali.

14.3 Research Highlights

14.3.1 Aufeis and Its Contribution to Base Flow

Significant amounts of aufeis are commonly observed in the permafrost regions of the northern hemisphere such as Alaska (Sloan et al. 1976; Slaughter 1982; Carey 1973), Arctic Canada (Pollard 2005), Yukon Canada (Harris et al. 1983), Svalbard (Liestøl 1977), Greenland (Yde and Knudsen 2005), Siberia (Alekseev and Tolstikhin 1973; Sokolov 1973), Mongolia (Froehlich and Slupik 1982), and Tibet (Zhou et al. 2000). The term “aufeis” is of German origin and roughly translates to “on or upon ice.” Icing (English) and naled (Russian) are also widely accepted terms in the scientific community. However, aufeis is the term more frequently used in Alaska, and is therefore used in this text. The history of aufeis research dates

back more than 150 years. Wrangel (1841) observed aufeis along the northern shore of Siberia. During the mid-nineteenth century, some Siberians explored and wrote about mounds and icing blisters (e.g., Middendorf 1861; Maydel 1896). Podyakonov collected detailed observations of river icing formations to develop the "Padyakonov formula" (Podyakonov 1903). This is an empirical equation that tries to identify those characteristics that enhance or reduce aufeis formation. Many researchers (e.g., Sumgin 1927) have examined this formula and modified several inherent limitations.

Sumgin was one of the first Russian scientists to study aufeis, and used the word "naled" to describe them. Parkhomenko (1932) studied ice formation from sub-permafrost and intrapermafrost groundwater in more detail. Tolstikhin pointed out that the river aufeis often developed in the areas where sub-permafrost water springs discharged into the river bottom. It is also common for the springs to be in the near vicinity of the stream. The volume of aufeis associated with the direct outflow of a source is determined by the following equation (Tolstikhin 1941):

$$V = Q * t * k * A$$

where:

V = aufeis volume (m^3),

Q = outflow of source (m^3/h),

t = time required for development of aufeis (hours),

k = coefficient of aufeis maturing, and

A = empirical coefficient depending on runoff conditions, evaporation, precipitation, and condensation at the ice body surface.

Tolstikhin (1963) empirically calculated aufeis runoff as a function of specific aufeis surface. The specific aufeis surface is based on following expression:

$$Fu\,F = Q$$

where Fu = specific aufeis surface, i.e., the gain in aufeis area per unit of outflow (m/s),

F = aufeis area (m^2), and Q = spring discharge (m^3/s).

Hall and Roswell (1981) tried to determine the coefficients and estimate groundwater discharge rates in the Brooks Range on the basis of Sokolov's formulation at five aufeis sites using 1972–1979 Landsat imagery and obtained:

$$V = 0.96\,F$$

Åkerman (1980) also added "glacier icing" and "pingo icing," which are located downstream of the glacier's terminal moraine and associated with open-system pingo formation, respectively. These are both common locations of groundwater emergence at the ground surface in permafrost regions. These aufeis categories are also mainly distinguished by having different sources of water. As expected, spring aufeis forms on or just downstream of a groundwater spring. An ice mound is

frequently observed at the spring in early or mid-summer. River aufeis is widely developed in valley bottoms, usually some distance downstream of a spring source. Ground aufeis forms when active layer water (suprapermafrost groundwater) seeps to the surface.

The chemical composition of the source water contrasts strongly between suprapermafrost, intrapermafrost, and sub-permafrost groundwater sources. Ground aufeis is highly concentrated in dissolved organic nitrogen (DON) and dissolved organic carbon (DOC). It is possible to determine the source of the water for each type of aufeis by measuring the dissolved inorganic carbon (DIC) and DOC ratio (DIC/DOC) (Yoshikawa et al. 1999). Spring aufeis has higher DIC and lower DOC as compared to other types of aufeis.

Ground aufeis also has a very high DOC content and commonly has a dark brown color due to the source water flowing through a layer of organic material. The characteristics of river aufeis lie between those of ground and spring aufeis. Romanovskii (1983) pointed out that the aufeis formation is not only affected by the sources of water, but also controlled by the permafrost conditions (e.g., continuous, discontinuous, or sporadic). Groundwater springs and associated aufeis are not uniformly distributed throughout the North Slope of Alaska. More than 30,000 l/s. of spring water discharge along the eastern part of the foothills of the Brooks Range (Kane et al. 2014; Childers et al. 1977). These springs with steady flow all year around result in large areas covered with aufeis every winter (Harden et al. 1977). Aufeis is second only to snow cover as the biggest temporary surface storage reservoir of fresh water during the winter period in unglaciated basins. Kane and Slaughter (1973a, b) and Slaughter (1982) suggested that up to 40% of winter streamflow (4% of the volume of annual runoff) may be stored as aufeis in a small watershed in interior Alaska. The reflection and emittance of electromagnetic radiation varies between frozen and unfrozen water. Many different remote sensing systems utilize this distinction to discriminate liquid water and ice. This is a common method for studying and characterizing aufeis deposition over wide areas (e.g., Landsat (Dean 1983; Harden et al. 1977; Hall and Roswell 1981) and SAR (Li et al. 1997)). Li et al. (1997) estimated aufeis formations using complex SAR data (interferometric SAR) at Ivishak River, Alaska. Accurate regional assessments of aufeis location and extent are now available because of new remote sensing techniques that have been recently developed using a combination of multiple wave bands as well as finer temporal resolution.

Seasonal characteristics of aufeis development and thawing were monitored at the aufeis field between 2004 and 2005 in the Kuparuk River basin north of Toolik Lake (Yoshikawa et al. 2007). The Kuparuk aufeis field is driven by a large spring that emerges about 2 km upstream of the aufeis. The discharge is around 800–1000 l/s. The water temperature is slightly below 0.0 °C. Analysis of SAR imagery from 1996 to 2006 indicated that 3–18% of the maximum aufeis accumulation remained at the end of the summer. The end-of-summer ice area seems to have increased between 1997 and 2005. The soil temperatures beneath the remnant aufeis after summer melt are never above 0 °C. Where remnant summer aufeis persists, stable or aggrading permafrost is found. This will have a positive feedback

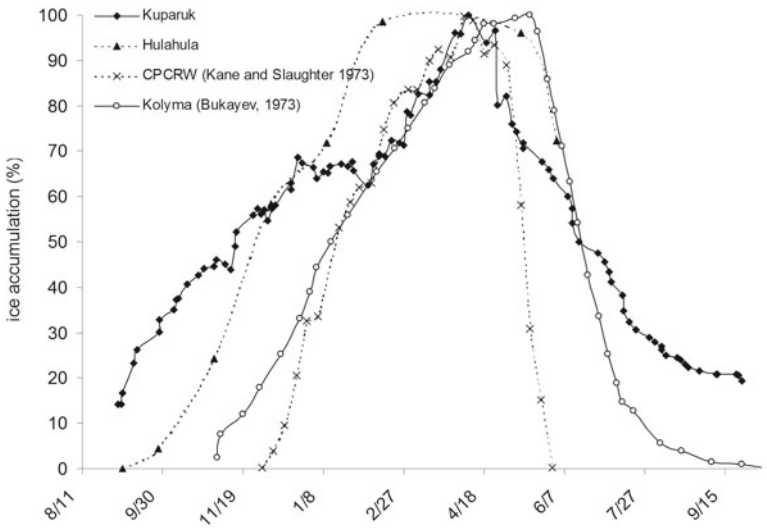

Fig. 14.4 indicates that aufeis in the Brooks Range starts to develop around October and continues to grow through early May; SAR image analysis for the Kuparuk River (2004–2005) and Hulahula River (2002–2003) throughout the winter were used for mapping

effect on the remaining summer aufeis and will also impact the geometry of the groundwater pathway above the permafrost.

Figure 14.4 Indicates that aufeis in the Brooks Range starts to develop around October and continues to grow through early May; SAR image analysis for the Kuparuk River (2004–2005) and Hulahula River (2002–2003) throughout the winter were used for mapping. Also Fig. 14.4 shows for comparison both the growth and decay of aufeis at Caribou-Poker Creeks Research Watershed (CPCRW) (Kane and Slaughter 1973a, b) representing warm discontinuous permafrost region and Kolyma River (Bukayev 1973) representing a Siberian continuous permafrost region. The North Slope of Alaska aufeis formations increase dramatically in late winter and the development of aufeis starts earlier in colder permafrost regions in response to earlier and longer winters than in the discontinuous permafrost regions.

Over the winter season about 50% of the aufeis has already formed on the North Slope of Alaska before December, more than 1 month ahead of time relative to the warmer discontinuous permafrost region to the south. The time series of the SAR images reveal the formation of the aufeis development. Aufeis fills the stream and river channels in early winter (stage 1). Aufeis develops a thicker and smoother surface during the middle of the winter (stage 2). Once a massive and smooth ice body has developed, aufeis starts to grow thicker and expand downstream in late winter (stage 3). Continued overflow water spreads widely into the floodplain and reaches farther downstream (often without freezing at the surface in late winter).

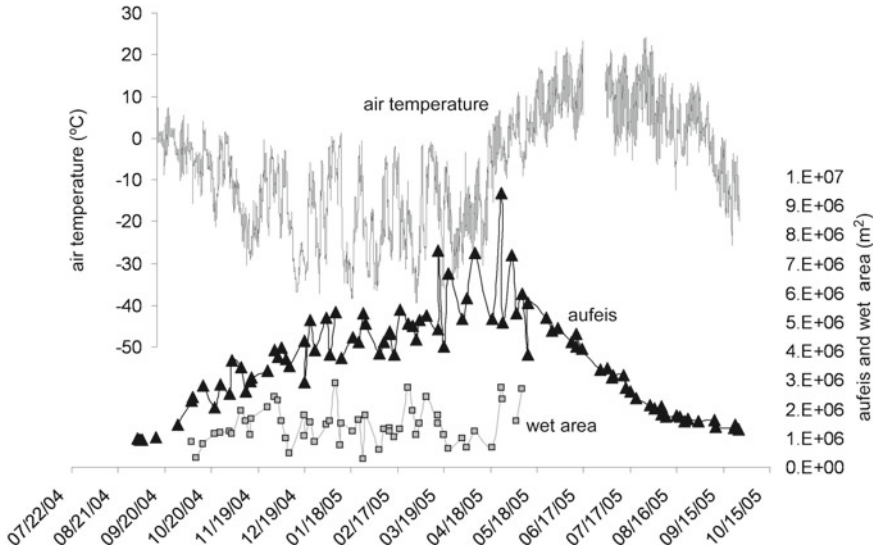

Fig. 14.5 Air temperature at the Upper Kuparuk River meteorological station near the Dalton Highway (about 30 km south of aufeis field) and overflow (wet surface) intensity during 2004–2005

Figure 14.5 shows the air temperature at the Upper Kuparuk River meteorological station near the Dalton Highway (about 30 km south of aufeis field) with overflow (wet surface) intensity during 2004–2005. The wet area was estimated using SAR imagery, which helps to understand aufeis formation processes and timing of growth. We cannot estimate the wet area during thawing season (before 20 October 2004 and after 18 May 2005). The timing of the aufeis formation corresponds with fluctuations of the air temperature. Overflow water on top of the aufeis principally occurred when large air temperature fluctuations occurred within a 2 day period.

Kane (1981) described a similar phenomenon in aufeis activity near Fairbanks, Alaska, through the use of piezometers. The cause of the overflow discharge is related to the increase of hydrostatic head during a warm period following a colder period. He observed maximum heads during the warmest periods during the winter and the lowest heads during extended cold periods. The thermal stability of the inner unfrozen channels in the aufeis appears to be an important parameter of aufeis development.

Lifshits et al. (1966) defined an aufeis melting coefficient (γ, mm/°C d) as follows:

$$\gamma = H/\Sigma t$$

where H = amount of melting (mm) and Σt = sum of average daily positive air temperature (thawing index). The average total amount of melting per year during

the period of 1996–2005 was 14,410,000 m^3/a, which requires a melting coefficient of 2.19 mm/°C d at the Kuparuk aufeis 1.90 mm/°C d in Sadlerochit spring aufeis and 3.62 mm/°C d in upper Lena River (Lifshits et al. 1966) aufeis. Thawing index is an important indicator of the rate of aufeis degradation. Colder regions have lower melting coefficients than the warmer discontinuous permafrost regions. The proportion of aufeis runoff (volume of aufeis) to total annual groundwater discharge is 27–30% for the Kuparuk River site. During the summer months, the Kuparuk aufeis releases water to the stream, especially in June and July. About 16 million m^3 of base flow from spring discharge went into storage as aufeis in the winter of 1999/2000. Approximately 1.1 million m^3 of aufeis carried over into the winter of 2000/2001 and approximately 15.9 million m^3 of new ice formed during the following winter. Aufeis activity is a sensitive indicator of winter base flow (spring discharge) and spring water temperatures. Analysis of periodic aerial photography collected over the past 50 years for the Hulahula, Sadlerochit, and Kongakat Rivers in Alaska indicate that the aufeis fields have not dramatically changed in either volume or extent. Throughout the Landsat era, the Kongakat River aufeis field has kept a constant volume as in the past (Harden et al. 1977). The Kongakat River aufeis has one of the longest records of observations by explorers (e.g., Franklin 1828) because it is one of the biggest ice fields and located close to the coast and therefore easy to observe from the Arctic Ocean. Norwegian explorer, Roald Amundsen described this aufeis field as a glacier in 1906 during his first voyage (Amundsen 1908).

14.3.2 Ground Ice Volume/Change and Its Impact on Regional Hydrology

Active ice wedge polygons may be observed near the southern boundary of the permafrost in areas such as Goldstream Creek valley in Fairbanks Alaska. In general, the frost contraction cracking process is inactive in the Fairbanks area under the contemporary climate. Many of these ice wedges developed 32,000–39,000 yBP (Marine Isotope Stages—3). However, Holocene (current) ice wedges are present in this area. Frost contraction cracking still occurs occasionally about every 10 years or so, particularly, during low-snow, severe winters in areas with substantial micro topography such as well-developed tussocks. Tussock tundra is a common vegetation in interior, western and northern Alaska. Tussocks develop as earth hummock type mounds (ca. 50 cm diameter) with relatively deep (20–50 cm) air-filled annular spaces around the tussock (sometimes filling with standing water). This micro topography produces conditions that are very difficult for people to traverse. Tussock tundra also experiences colder thermal conditions due to non-conductive heat transfer. Cooling is enhanced by convective heat transfer during winter months, evapotranspiration during the summer, and blocking of direct solar radiation by the rough surface tussock vegetation. This rough surface topography helps keep the ground cooling and is similar to the effects of rock glaciers or block fields.

Most areas in the southern boundary (Northern Hemisphere) of the mountain permafrost are occupied by rock glaciers or frozen block slopes. Rock glaciers or block slopes have the significant pore space available for convective heat transfer during winter periods. Woodcock (1974) reported 10 m of thickness of the permafrost at Mauna-Kea, Hawaii, despite a mean annual ground surface temperature at the summit of Mauna-Kea of +1.2 °C. Permafrost or massive ice body has been observed in many warm (positive ground surface temperature) locations due simply to the site-specific heat transfer process that is enhanced by convection during the winter but diminished during the warmer season. Goering and Kumar (1996) designed a road-bed that promotes winter-time convection in open graded embankments for cooling of the underlying, unstable permafrost. The road embankments are cooler than the surround ground during winter periods, driven by convective heat transfer as the cold, dense air circulates in the large pore spaces. During the summer, the surface is warmer and convective heat transfer is minimal as the warmer, less-dense air mass in the pore space does not sink. This type of structure is commonly seen in cold region engineering designs today such as the Tibetian-Qinghai railway. Non-conductive heat transfer is a very important process influencing the stability of permafrost in some unique settings. Also, these cooling processes increase the chance of secondary intrusive ground ice formations (such as ice wedges or rock glaciers) which are likely to remain because of topographical conditions in warm permafrost areas.

Permafrost stability in discontinuous permafrost regions is strongly controlled by soil type and the physical and thermal properties of the surface active layer. In general, the organic rich (peat or moss) layer increases the stability of permafrost, perhaps to the extent where the mean annual ground surface temperature may reach a positive temperature, due to the effect of the thermal offset (Gold et al. 1972). The thermal offset describes the process where more heat may escape from the active layer in the winter than enters the soil in the summer, because of the difference between frozen and unfrozen thermal conductivity of the surface soils.

14.3.3 Thermokarst and Open Talik Lake

It is important to understand the role that permafrost degradation plays in affecting the surface water balance and subsurface thermal dynamics. Soil moisture storage in the active layer is a key variable in understanding most ecological process interactions and atmospheric/terrestrial linkages in arctic regions (Boike et al. 1998; Romanovsky et al. 2002). The primary control on local hydrological processes in northern regions is dictated by the presence or absence of permafrost, but it is also influenced by the thickness of the active layer and the total thickness of the underlying permafrost. As permafrost becomes thinner or decreases in areal extent, the interaction of surface and sub-permafrost groundwater processes becomes more important (Woo 1986). The inability of soil moisture to infiltrate to deeper sub-permafrost groundwater zones due to ice-rich permafrost produces and maintains near surface wet soils in arctic regions. However, in the slightly warmer

regions of the subarctic, the permafrost is thinner and discontinuous. In permafrost-free areas, surface soils can be quite dry as infiltration is not restricted, thus impacting ecosystem dynamics, fire frequency, and latent and sensible heat fluxes. Other hydrologic processes impacted by degrading permafrost include increased winter stream flows (Yang et al. 2002), decreased summer peak flows (Bolton et al. 2000), changes in stream water chemistry (Petrone et al. 2000), and other fluvial geomorphological processes (McNamara et al. 1999). Hydrologic changes or changes that influence hydrologic processes documented among study sites include drying of thermokarst ponds, increased active layer thickness, increasing importance of groundwater in the local water balance and differences in the surface energy balance (Carr 2003).

In response to some imposed disturbance, such as a tundra fire or climatic warming, ice-rich permafrost may differentially thaw, creating irregular surface topography. Depressions forming on the surface soon form ponds, accelerating subsurface thaw through lower albedo and additional heat advected into the pond through runoff. In time, a thaw bulb or talik (a layer of unfrozen soil above the permafrost and below the pond) may form as the depth of water becomes greater than the amount that can refreeze during the winter. If the talik grows to a size that completely penetrates the underlying soil or connects to a subsurface layer that allows continued drainage, the pond may then begin to drain. Some ponds on the Seward Peninsula, Alaska are now exhibiting this behavior (Yoshikawa and Hinzman 2003). An ice wedge polygonal network exists outside of these ponds; both frost contraction and ice wedge cracking are unlikely to occur in the current warm climatic conditions (Lachenbruch 1962). This ice wedge terrain also has highly developed thermokarst in response to the recent warmer climate. Most of these ponds had drained previously (via bank rupture). Remaining ponds continue shrinking in surface area. The surrounding marsh areas are also draining with newly generated Palsas providing opportunities for spruce invasion.

Thermokarst topography forms as ice-rich permafrost thaws, either naturally or anthropogenically, and the ground surface subsides into the resulting thawed voids (Brown and Grave 1979a, b; Hinzman et al. 1997). The important processes involved in thermokarsting include thaw, ponding, surface and subsurface drainage, surface subsidence, and related erosion. These processes are capable of rapid and extensive modification of the landscape; predicting, preventing or controlling thermokarsting is a major challenge for northern development (Lawson 1986). Many thermokarst ponds and depressions have been observed across interior Alaska and Canada in regions of discontinuous permafrost (Jorgensen et al. 2001; Osterkamp et al. 2000; Burn and Smith 1990). Osterkamp and Romanovsky (1999) observed permafrost temperatures warming by 1.5 °C since the 1980s in interior Alaska. Permafrost temperatures in boreholes displayed a 2–4 °C increase over the last 50–100 years on the North Slope of Alaska (Lachenbruch and Marshall 1986). Thermokarst and permafrost degradation is not confined to Alaska and Canada. It is occurring worldwide, with thermokarst development particularly widespread at the southern limit of the discontinuous permafrost zone in countries such as Mongolia (Sharkuu 1998), China (Ding 1998), and Russia (Pavlov 1994; Czudek and Demek

1970). The dynamics of thermokarst lakes in areas of thick permafrost in the Arctic are probably associated with a changing surface water budget in response to some catastrophic event impacting near surface ice-rich materials (Sellmann et al. 1975). However, thermokarst processes are much more active in Subarctic regions of discontinuous permafrost. In the Subarctic, permafrost temperatures are frequently warmer than –1 °C and intra- or sub- permafrost water flow is often observed (Yoshikawa et al. 2002). The thermokarst water movement of the Subarctic is more complex than in the continuous permafrost regions. Ice-rich permafrost can be highly impermeable aquitard, frequently causing formation of artesian conditions (i.e., upward hydraulic gradients in low elevations). Kane and Slaughter (1973a, b) reported on the hydraulic processes associated with a lake recharged from a sub-permafrost aquifer near Fairbanks, Alaska. The thaw bulb below the pond had thawed completely through the permafrost thus enabling sub-permafrost groundwater to recharge the pond. In this case, the pond level was more stable as compared to ponds recharged only from surface runoff. Sub-permafrost groundwater is typically enriched in cations, resulting in higher electrical conductivity of pond water.

The water budget of the various pond types may be calculated as follows:

New thermokarst pond

$$Q_{\text{in}} + Q_{\text{thaw}} > Q_e + Q_{\text{out}}$$

New thermokarst depression

$$Q_{\text{in}} + Q_{\text{thaw}} < Q_e + Q_{\text{out}}$$

"Mature" shrinking pond

$$Q_{\text{in}} + Q_{\text{thaw}} < Q_e + Q_{\text{out}} + Q_g$$

where Q_{in} is input water from atmosphere, active layer or surface, Q_{thaw} is water from permafrost thawing, Q_e is evaporation and evapotranspiration, Q_{out} is outflow through the surface or active layer, Q_g is drainage to sub- or intra-permafrost groundwater through a talik.

The key phenomenon of the shrinking pond water budget is quantifying the magnitude of Q_g, which is primarily dependent upon the hydraulic gradient and hydraulic conductivity, both which can vary significantly. A drier climate and/or increasing water-holding capacity of the active layer will cause a lowering of the local groundwater levels, accelerating the shrinkage of pond surface areas.

The implications of this analysis are that in regions over shallow (<30 m), warm permafrost surface ponds (∼>10 m diameter) may shrink in size and newly developed small ponds may form. In addition, surface soils may become drier as the permafrost degrades. This depends upon regional hydraulic gradients (i.e., whether the region is a groundwater upwelling or down-welling zone). The same

mechanisms that allow drying of the ponds may also cause soil drying with significant impacts to latent and sensible heat fluxes.

Permafrost temperatures are strongly affected by the slope and aspect in this region. In Fairbanks area, south facing slopes, in general, are absent of permafrost while permafrost is usually present on north facing slopes and in the valley bottoms. One of the mature thaw lake features is a floating organic mat covering most of the lake surface. Where more than 1 m of floating organic material exist, the surface of the lake can usually be comfortably walked over all year round. Isabella Creek bog lake near Fairbanks, Alaska, is a 7 m deep water body surrounded be permafrost with an open talik underneath. 5 l/s. of discharge from the lake was measured in 2003. This area has permafrost with artesian conditions, which means the groundwater recharges the lake water all year round. Kane and Slaughter (1973a, b) studied this lake to estimate discharge and soil hydraulic conductivity using piezometric measurements at different depths in the middle of lake. They estimated the hydraulic conductivity and discharge using Darcy's Equation. The hydraulic gradients were measured at 0.2–0.5 m/m. The rate of discharge (Q) is calculated based on the talik area (A), hydraulic conductivity (k), and hydraulic groundwater gradient ($\mathrm{d}y/\mathrm{d}z$). The piezometric pressure was measured at four different depths. A positive vertical gradient was measured all year round (1969–1970), indicating this pond was recharged via the taliks throughout the year. As mentioned above, the discharge rate was calculated by Darcy's law:

$$Q = kA\,(\mathrm{d}y/\mathrm{d}z).$$

where Q is the vertical discharge, K is the hydraulic conductivity; A is the cross-sectional area of thaw, beneath the lake, and ($\mathrm{d}y/\mathrm{d}z$) is the hydraulic gradient. Hydraulic conductivities of the materials beneath the lakes were estimated based on unfrozen silt. Field observations in 2003 further support discharge rate of earlier work (Fig. 14.6).

Understanding 3-dimensional talik geometry or groundwater aquifer would be a significant contribution to permafrost hydrology. Especially needed is improved technology necessary for detecting permafrost cryopeg pockets and aquifers in the frozen layers of warm permafrost as well as usage of the ice cellar (storage) for local people. Drilling is one approach for understanding permafrost boundaries; however, it's not suitable for all applications because of the high cost and the time commitment. Geophysical investigations will be the best method to address this problem. In this section, we discuss resistivity and dielectric constant characteristics of the liquid content of frozen ground. Resistivity experiments in the cold chamber indicate that higher resistivity values occur at temperatures colder than the freezing point of bulk water. The liquid water content of the materials also has a strong influence on resistivity (Fig. 14.7).

Kawasaki and Osterkamp (1988) developed a temperature dependent conductivity model. The apparent conductivity of this model has a strong impact on the temperature regime. The electrical resistivity of soils, sediments, and rocks to the direct electrical current is a powerful and sensitive parameter for the detection of

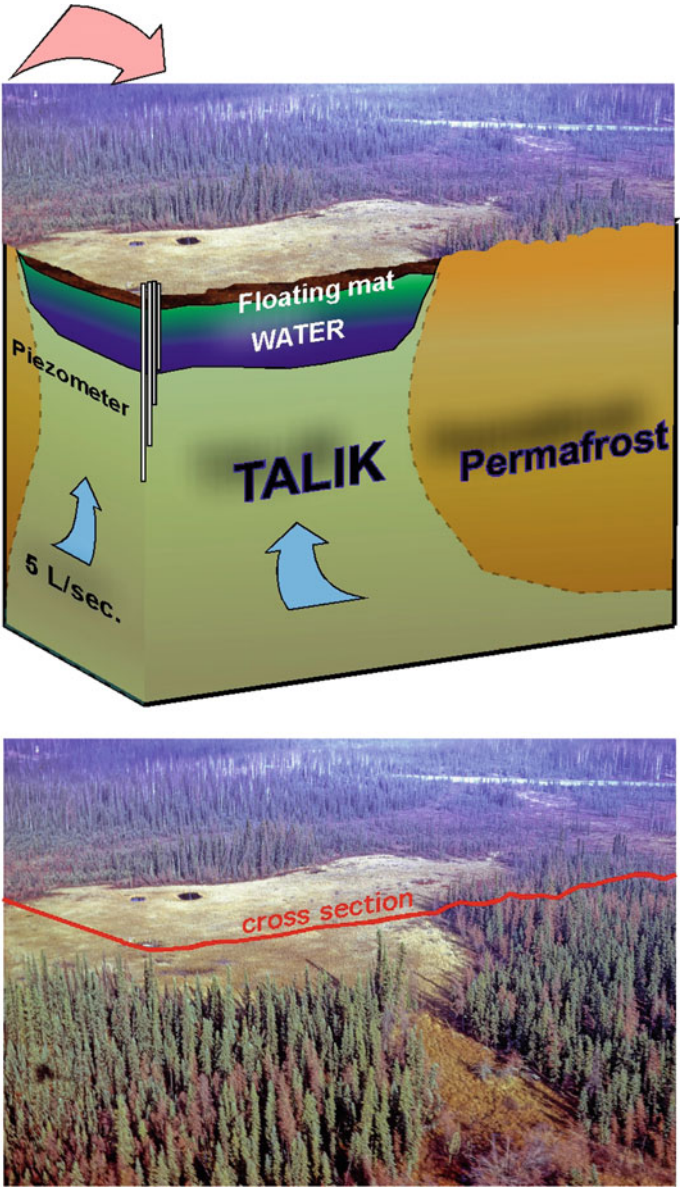

Fig. 14.6 Groundwater recharged lake. In general, bog lakes are connected through an open talik that allows recharge to the lakes. In this case, the lake water had much more minerals (higher electric conductivity) and ideal growth conditions for the floating vegetation

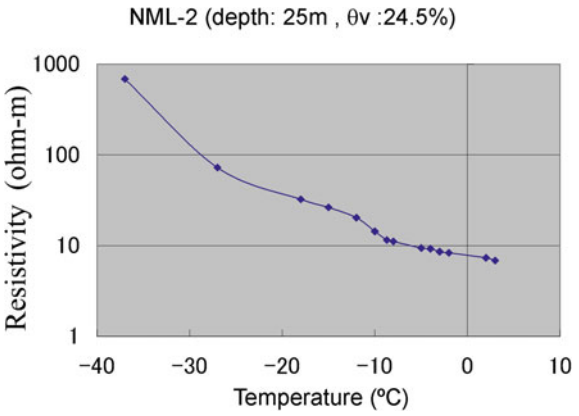

Fig. 14.7 Resistivity versus temperature regime from one of the brine samples from North Slop, Alaska. Ground temperature (–9.54 °C at 26 m depth) is the freezing point of this material in which the value increase immediately after the temperature is colder than –9.5 °C

brine layers (Duxbury et al. 2001, 2004). However, the resistivity is a less sensitive indicator of the soil type or water content under highly saline conditions. The higher frequency dielectric constant is an ideal parameter for the indication of the soil type, water content, and other physical properties. GPR surveys with the velocity analysis provide complex dielectric constants. Brine layers have an unusually high imaginary part of the dielectric constant. The imaginary part of the dielectric constant is strongly dependent on the freezing temperature. Thus, the ground temperature regime potentially controls the ionic concentration of brine waters. The annual temperature fluctuation zone in permafrost is especially important. The electric properties also change from season to season within this zone.

14.4 Permafrost Hydrology and Indigenous People

Arctic indigenous people live in the permafrost regions for many generations, their life style is well connected to the environment, including the usage of ice cellars. Ice cellars (Lednik in Russian, Bulus in Sakha, and Sigruaq in Inupiat) excavated into the permafrost layer, are a natural form of refrigeration for preserving block ice for drinking water, storing harvested food (fish, game meat, whale and livestock such as reindeer), and fermenting food. Ice cellars are traditionally used by indigenous Arctic people, such as Siberian Even, Evenk, Chukchi, Yukagir, Dolgan, and North American Inupiat, Yupik, and Inuit. Though ice cellars are widely used in permafrost regions, their structures and the purpose of their use, and the methods of maintenance are quite different among the communities due to the variations in permafrost setting. Monitoring ice cellar temperatures and recording

descriptions of ice cellars are important in climate change; it is also of interest in permafrost studies and archiving traditional techniques of living with permafrost.

In Siberia, over 90% of the land is underlain by permafrost, a region where most of the indigenous people of Siberia live; and the same is true for the North American Arctic people. In the Sakha Republic Russia, not only are subsistence foods stored in ice cellars, including caribou, ducks, fish, and marine mammals, which constitute a substantial proportion of the local diet, but also ice blocks for drinking water during the summer months, especially in Central Yakutia. These "ice houses" for temporary storage of ice cubes are not only common in arctic communities, but were also widely used in Europe, United State, Canada, and other countries in early times before the use of electric refridgeration. Ice cellar infrastructure has both cultural and practical significance. Concern has been expressed recently over the impact of climate change on ice cellars and future sustainability of this life style (Kintisch 2015). This section reports the results of an ongoing education and outreach project in permafrost regions to understand and accurately report the thermal state of ice cellar temperature regimes and the surrounding permafrost environments (Yoshikawa 2013). We visited over 500 communities including Mongolian, Even, Evenk, Chukchi, Yukagir, Dolgan, Inupiat, Yupik, and Inuit, where we discussed local ice cellars with residents.

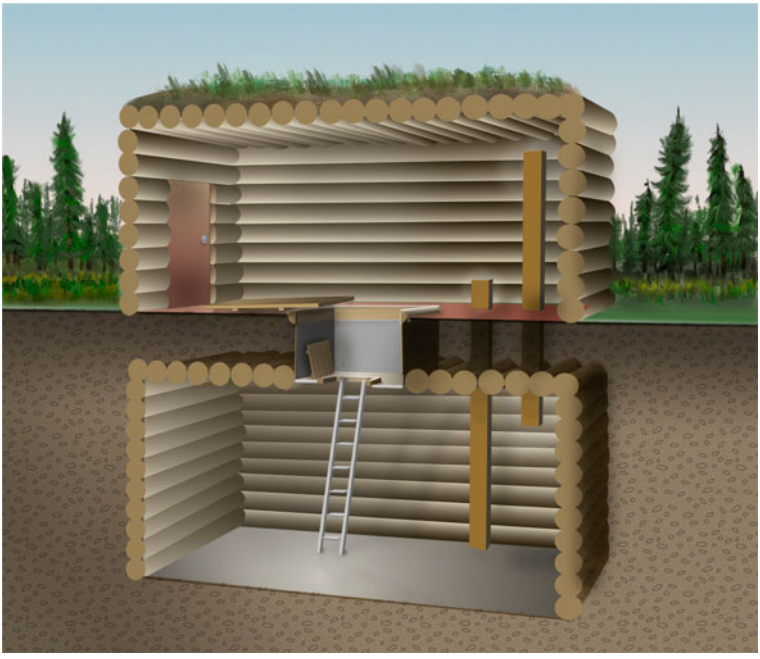

Fig. 14.8 Typical vertical cellar in central Yakutia (illustrated by M. Aoki)

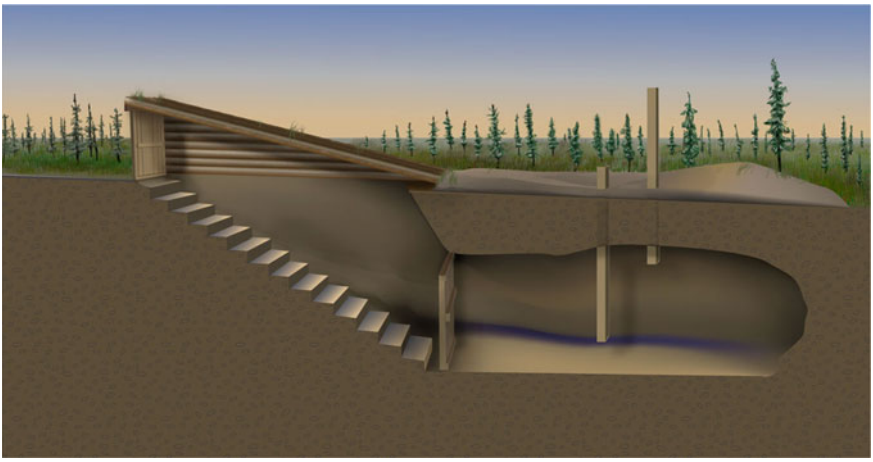

Fig. 14.9 Typical horizontal cellar in central Yakutia (illustrated by M. Aoki)

The long history of interest in permafrost and digging in frozen ground developed a variety of ice cellar types in Siberia. The Soviet Union era (about late 1950s), the Soviet government supported and encouraged the development of community-based or industrial ice cellars associated with mining activities, which resulted in unique ice cellar structures all over Siberia. Before the invention of modern day equipment, humans simply dug vertical shafts to store food in or buried food under sphagnum during summer months (M. Pogodaev, personal comm. 2016). Contemporary cellars in northern Sakha and North America regions are built primarily for personal use of one or several families (such as a fishing/whaling crews and their dependents), and typically consist of a vertical shaft that leads to a small chamber or horizontal tunnel excavated into permafrost (Fig. 14.8). These cellars vary in dimensions. The vertical shaft is 1 to 6 m deep and penetrates to a depth such that the ceiling of the chamber is below the permafrost table, which is usually less than 1 m in undisturbed areas but may be more than 2 m in villages. Older ice cellars or ones in southern permafrost areas are built primarily for personal use, and typically consist of a 15 to 20 degree declining tunnel entrance that leads to a small chamber excavated into permafrost or seasonally frozen soil (Fig. 14.9).

The depth of the chamber is 1–3 m from the ground surface. This type of cellar is similar in design to European wine and food cellars or icehouses, and provides easy access and maneuvering of what has been stored. In addition to private cellars, there are deeper, longer, and larger-capacity commercial/industrial cellars, most of which were built during the Soviet era for communities in many parts of Sakha and Chukotka regions. Many of these cellars were dug horizontally a few hundred meters, and even kilometers, into hillsides, and had railroads for managing frozen items. Though abundant, these large-capacity cellars today receive limited use;

Fig. 14.10 More than 100 years old cellar at Oymiakon, Sakha Republic where recent fall storm-flooding event and filling by ice

some have been reestablished as local museums. Recently, the media has referred to ice cellar "failures" (e.g., Kintisch 2015) or has reported that cellars no longer function reliably, because food has thawed while in storage or because an owner cannot safely access a cellar. In our visits to communities in Sakha Republic, we did not observe ice cellar failures; however, several cellars were closed due to a recent fall flooding event and filling by ice (e.g., Oymiakon, Verkhoyansk settlements, Sakha Republic Russia; see Fig. 14.10). Other than these closures, massive numbers of ice cellars were no longer manageable after the Soviet Union collapsed (e.g., Iengra, Tomtor).

Ice cellars are an efficient solution for storing large volumes of harvested ice, fish, and reindeer meat. Ice cellars require maintenance and annual cleaning; they are usually cleaned just before restocking. In northern communities, cleaning occurs in late fall for storage of marine mammals and fish during winter. In central Yakutia, ice cellars are used mostly for storage of block ice prepared in middle or late winter. Preparation involves removing all of the meat and fish from the previous year and thoroughly cleaning the cellar, including adding a layer of fresh snow.

Pond ice thickness is an important factor in the harvest and storage of block ice. The ice thickness must be 50–60 cm for cutting from a pond. Stored block ice is used mainly for drinking water during the summer months in many part of central Yakutia. Though ice storage in a permafrost cellar is ideal, the temperature inside the cellar does not have to be below zero year around; it just needs to stay cold enough to delay a rise in temperature during the warmer summer months. Underground storage this far north successfully functions because of a 4- to 5-month delayed response to rising surface temperatures. This method of cold storage is

similar to how icehouses were used in the nineteenth century before electric refrigeration.

Humidity is higher in cellars, and the potential for fungus growth is always present, even in constant negative temperatures. Some cellars used for fermentation purposes take advantage of temperature and relative humidity characteristics. Fermentation is more often practiced by the Chukchi in Chukotka and by North American indigenous cultures.

Every several years, water is sprayed on the walls of vertical cellars in northern regions and horizontal industrial cellars to develop an icy surface for preventing sublimation of the permafrost. These ice-coated cellar walls minimize sublimation, keep the cellar clean, and help stabilize the walls. The annual temperature cycle of most ice cellars indicates significant cooling during winter months due to opening of doors/entrances. The maximum daily temperature observed in the ice cellars ranged from −10.4 to +2.7 °C. The temperatures in some cellars in central Yakutia rise above 0 °C. The mean annual temperatures ranged from −14.4 to −3.6 °C. In contrast, the mean annual air temperature in Yakutsk is around −9 °C. The warmest cellar temperatures were observed in fall (September to October), and typically the doors/entrances are opened to introduce cold air after November. Thus, the coldest temperatures occur during the winter months, in direct response to air temperature. The average annual temperature amplitude, i.e., the difference between the warmest and coldest temperatures, range from 9.4 to 36 °C in the cellars. This difference results from the depth of the cellar chambers, the original permafrost seasonal amplitude range, and the structure of the cellars.

Based on public media reports and our own field observations, evidence indicates several major problems related to the maintenance and use of ice cellars in North America (Klene et al. 2012; Nyland et al. 2016). Factors other than climate warming could be negatively affecting cellars, including (1) local soils known to be ice-rich and high in salinity; (2) proximity to flooding rivers or the coast; (3) influence of urban development on local hydrology; and (4) a suite of potential influences related to proximity to other types of infrastructure (Nyland et al. 2016). However, in Yakutia, the same problems as in North American cellars were not observed. Descriptions of cellar failures in Yakutia most commonly involve flooding. For large rivers in the Arctic (Lena, Yana, Indigirka, and Kolyma, etc.), flooding occurs during spring breakup due to the snowmelt following the south-to-north stream flow. Springtime floodwater in a cellar would be relatively easy to remove during the warm summer months. Though fall flooding does occur occasionally, it has the potential to be a serious problem because there may not be enough time to remove the water before the air temperatures drop, or it may be too cold to operate draining equipment. If ice fills a cellar completely, it must be abandoned for use, such as with cellars in Oymiakon and Verkhoyansk due to recent fall flooding. During the Soviet era, Kolkhoz and Sovkhoz communities operated ice cellars that were well-maintained and managed, and overseen by responsible individuals. This kind of intense maintenance helps prevent cellar failure and flooding damage in a community, but has not been economically possible since the Soviet Union era.

Air convection system in a cellar is a unique design and typically seen in Even and Evenki communities, but not in North American indigenous cellars. During winter months, cellar temperature is typically –5 to –15 °C that is much warmer than outside air temperature in Siberia (–40 to –60 °C). Cold dense air goes into the bottom of the cellar through the lead pipe. Warmer cellar air escapes through the upper lead pipe to the atmosphere. This natural cooling system would be a great advancement. We observed this type of design in Siberian indigenous communities around Baikal and Chukotka. Air convection systems work efficiently during the winter months especially after cold snaps. During late winter, the temperature gradient in ice cellars is reversed and heat removal is terminated once outside air temperature getting warmer.

As mentioned earlier, ice cellars are an important cultural and economic resource for residents of Arctic communities. Changes in climate could significantly affect the ground thermal regime around ice cellars; in addition, processes of flooding and urban impact could further be detrimental to future ice cellars. The impact of a changing environment on ice cellars will require further site-specific investigations. Soil characteristics and ground ice conditions vary substantially over distances of only a few meters, necessitating detailed surveyings. In cases where ice cellar degradation is observed, many engineering options are available for maintenance; for example, thermo-siphons could be used to artificially maintain frozen conditions (Wendler 2011). Thermo-siphons, though having a long history of use in Sakha by Russian engineers, have never been used to maintain ice cellars except an oil company trying to test in Kaktovik, Alaska.

14.5 Summary and Conclusions

Permafrost is considered as impermeable layer in the ground. However, in real world, water moves in all seasons over permafrost regions. This chapter discussed and apprehend water geometry (unfrozen or brine) and the related indigenous people's life. Since Last Glacial Maximum, earth history indicated climate warming dramatically. Especially, big hydrological events happened in early Holocene (e.g., Climatic Optimum) formed many thermokarst lakes and permafrost degradating processes. After the Little Ice Age, there is a warm event on earth and that would be continuous with more warming in the future similar to the last interglacial period. Warming permafrost implies more dynamic hydrological process and necessary adaptation of human life in the North. Open talik formation will be more expanded in continuous permafrost regions that impact aufeis formations and/or lake geometries. Simply, surface water dynamics have to consider more factors and linkages, including underground water connections. In current state, we are not certain about relationship between aufeis formations (size) and climate variability. Aufeis has quite contribution of the winter baseflow and should including total annual discharge distribution.

For Ice cellar of northern people, there is some changing culture after electric freezer invented. The purpose of using cellar is not only for food storages depending on regions and tribes, although the cellar is used for seasonal storage meats, fishes, ice (drinking water for tea in summer), or fermentation purpose. Future permafrost temperature will be slightly changing the usage and strictures of the cellars. In case of permafrost warming, it could be more seeping out cryopeg's brine water into cellar as well as hazards to flooding events. However, in general, hydrological interactions are most impacted parameter such as weakening of the structure or collapsing of the ceiling.

References

Alekseev VR, Tolstikhin ON (1973) Questions of terminology in study of naleds. Siberian naleds. CRREL Draft Transl 399:187–191

Amundsen R (1908). The north west passage. Archibald Constable and Company Limited, London, p 397

Boike J, Roth K, Overduin PP (1998) Thermal and hydrological dynamics of the active layer at continuous permafrost site (Taymyr peninsula, Siberia). Water Resour Res 34:355–363

Bolton WR, Hinzman LD, Yoshikawa K. 2000. Stream flow studies in a watershed underlain by discontinuous permafrost. In: Kane DL (ed) Proceedings AWRA spring specialty conference, water resources in extreme environments, 1–3 May, 2000. American Water Resources Association, Anchorage, Alaska, pp 31–36

Brewer MC (1958a) The thermal regime of an arctic lake. Trans Am Geophys Union 39(1):278–284

Brewer MC (1958b) Some results of geothermal investigations of permafrost in northern Alaska. Trans Am Geophys Union 39(1):19–26

Brown J (1969) Ionic concentration gradients in permafrost, Barrow, Alaska. CRREL research report 272, 26p

Brown J, Grave NA (1979a). Physical and thermal disturbance and protection of permafrost. US Army CRREL special report no. 79-5, 42pp

Brown J, Grave NA (1979b) Physical and thermal disturbance and protection of permafrost. CRREL report 79-5, 42pp

Brown RJE, Pewe TL (1973) Distribution of permafrost in North America and its relationship to the environment, a review, 1963–1973. In: Proceedings of the second international conference on permafrost, Washington D.C., pp 71–100

Brown J, Ferrians OJ Jr, Heginbottom JA, Melnikov ES (1998) Revised February 2001. Circum-Arctic map of permafrost and ground-ice conditions. National Snow and Ice Data Center/World Data Center for Glaciology, Boulder, CO, Digital media

Bukayev NA (1973) Basic tendencies in regime of huge naleds in upper reaches of Kolyma River. In: Alekseyev VR et al (eds) Siberian naleds, Draft Translation 399, USACRREL, Hanover, NH, pp 92–117

Burn CR, Smith MW (1990) Development of thermokarst lakes during the Holocene at sites near Mayo, Yukon Territory. Permafr Periglac Process 1(2):161–176

Carey K (1973) Icings developed from surface and ground water. CRREL monograph III-D3, U. S. Army Cold Regions Research and Engineering Laboratory, Hanover, New Hampshire, 67p

Carr A (2003) Hydrologic comparisons and model simulation of subarctic watersheds containing continuous and discontinuous permafrost, Seward Peninsula, Alaska. M.S. thesis. University of Alaska Fairbanks

Childers JM, Sloan CE, Meckel JP, Nauman JW (1977) Hydrologic reconnaissance of the eastern North Slope, Alaska, 1975, U.S. geological survey open-file report 77–492, 65p

Collett TS, Bird KJ (1993) Unfrozen, high-salinity intervals within ice-bearing Permafrost, North Slope of Alaska. In: 6th international conference on permafrost, pp 1-7, South China Univ. of Technol. Press, Beijing

Czudek T, Demek J (1970) Thermokarst in Siberia and its influence on the development of lowland relief. Quat Res 1:103–120

de K Leffingwell E (1919) The canning river region, Northern Alaska. U.S. geological survey of professional paper 109, 251p

Dean, K.G., 1983. Stream Icing zones in Alaska, Final Report to Alaska Division of Geological and Geophysical Surveys, Fairbanks, AK, 1983

Ding Y (1998) Recent degradation of permafrost in China and Response to Climatic Warming. In: Lewkowicz AG, Allard M (eds) Proceedings of the international conference on Permafrost: seventh international conference, 2–5 August 1998, Yellowknife, Canada, Universite Laval, Quebec, Collection Nordicana 57, pp 225–231

Douglas TA, Torre Jorgenson M, Kanevskiy MZ, Romanovsky VR, Shur Y, Yoshikawa K (2012) Investigations into permafrost dynamics at the Fairbanks Permafrost Experimental Station near Fairbanks, Alaska. In: Ninth international conference on permafrost, Fairbanks, Alaska

Duxbury NS, Zotikov IA, Nealson KH, Romanovsky VE, Carsey FD (2001) A numerical model for an alternative origin of lake Vostok and its exobiological implications for Mars. J Geophys Res Planets 106:1453–1462

Duxbury NS, Abyzov S, Romanovsky V, Yoshikawa K (2004) A combination of radar and thermal approaches to search for methane clathrate in the Martian subsurface. Planet Sp Sci 52:109–115

Ferrians OJ (1965) Permafrost map of Alaska. U.S. geological survey miscellaneous geologic investigations map 1–445

Franklin J (1828) Narrative of a second expedition to the shores of the polar sea in the year 1825, 1826, and 1827, London, John Murray, 320p

French HM (1996) The periglacial environment, 2nd edn. Longman Group Limited, London, pp 5.1–5.7.4

Froehlich W, Slupik J (1982) River icings and fluvial activity in extreme continental climate: Khangai Mountains, Mongolia. In: Proceedings, Fourth Canadian permafrost conference. National Research Council of Canada, Ottawa, Ontario, pp 203–211

Goering DJ, Kumar P (1996) Winter-time convection in open-graded embankments. Cold Reg Sci Technol 24(1):57–74

Gold LW, Johnston GH, Slusarchuk WA, Goodrich LE (1972) Thermal effects in permafrost. In: Proceedings of the February 2–4, 1972, Canadian Northern pipeline conference: Ottawa, Ontario, Canada. National Research Council, Associate Committee for Geotechnical Research Technical Memorandum, vol 104, pp 25–36

Hall DK, Roswell C (1981) The origin of water feeding icings on the eastern North Slope of Alaska. Polar Record 20(0128):433–438

Harden D, Barnes P, Reimnitz E (1977) Distribution and character of naleds in northeast Alaska. Arctic 30(1):28–40

Harris SA, Van Everdingen RO, Pollard WH (1983) Guidebook to permafrost and related features. Nothern Yukon Territory and Mackenzie Delta, Canada. In: French HM, Heginbottom JA (eds) Fourth international conference on permafrost, Fairbanks, Alaska

Hinzman LD, Goering DJ, Li S, Kinney TC (1997) Numeric simulation of thermokarst formation during disturbance. In: Crawford RMM (ed) Disturbance and recovery in Arctic lands: an ecological perspective NATO Advanced Science Institutes series: (NATO ASI) partnership sub-series: 2 environment, vol 25. Kluwer Academic Publishers, Dordrecht, p 621. ISBN: 0-7923-4418-9

Holmes WG, Hopkins MD, Foster LH (1968) Pingos in central Alaska. US Geol Surv Bull 1241-H:34p

Jorgenson MT, Racine CH, Walters JC, Osterkamp TE (2001) Permafrost degradation and ecological changes associated with a warming climate in central Alaska. Clim Chang 48:551–579

Kane DL (1981) Physical mechanics of aufeis growth. Can J Civ Eng 8:186–195

Kane DL, Slaughter CW (1973a) Seasonal regime and hydrological significance of stream icings in central Alaska. In: Symposium of the role of snow and ice in hydrology, IAHS-UNESCO-WMO, Banff, Alberta, Canada, pp 528–540

Kane DL, Slaughter CW (1973b) Recharge of a central Alaska lake by subpermafrost groundwater. In: North American contribution, second international conference on permafrost, Yakutsk, U.S.S.R. National Academy of Sciences, Washington, DC, pp 458–462

Kane DL, Yoshikawa K, McNamara JP (2014) Regional groundwater flow in an area mapped as continuous permafrost, NE Alaska (USA). Hydrogeol J. https://doi.org/10.1007/s10040-012-0937-0, ISSN 1431-2174

Kawasaki K, Osterkamp TE (1988) Mapping shallow permafrost by electromagnetic induction—practical conditions. Cold Region Sci Technol 15:279–288

Kintisch E (2015) These ice cellars fed arctic people for generations. Now they're melting. National Geographic. http://news.nationalgeographic.com/2015/10/151030-ice-cellar-arctic-melting-climate-change/. Accessed 18 Dec 2015

Klene AE, Yoshikawa K, Streletskiy DA, Shiklomanov NI, Brown J, Nelson FE (2012) Temperature regimes in traditional Iñupiat ice cellars, Barrow, Alaska, USA. In: Proceedings of the tenth international conference on permafrost. Salekhard, Russia. Extended abstracts, vol 4, pp 268–269

Lachenbruch AH (1962) Mechanics of thermal contraction cracks and ice-wedgepolygons in permafrost. Geological Society of America special paper 70, 69p

Lachenbruch AH, Marshall BV (1986) Changing climate: geothermal evidence from permafrost in the Alaskan Arctic. Science 234:689–696

Lawson DE (1986) Response of permafrost terrain to disturbance: a synthesis of observations from northern Alaska. Arct Alp Res 18:1–17

Li S, Benson C, Shapiro L, Dean K (1997) Aufeis in the Ivishak River, Alaska, mapped from satellite radar interferometry. Remote Sensing of the Environment 60:131–139

Liestøl O (1977) Pingos, springs, and permafrost in Spitsbergen. Norsk Polarinstitutt Årbok 1977:7–29

Lifshits FA, Piguzova VM, Ustinova ZG (1966) Estimate of naled regulation of ground-water flow in the Chul'man River Basin (southern Yakutiya). Trans State Hydrol Inst (Trudy GGI) 133:82–89

Linell KA (1973) Long-term effects of vegetative cover on permafrost stability in an area of discontinuous permafrost. In: Proceedings of permafrost: North American contribution to the second international conference. National Academy of Sciences, National Research Council, pp 688–693

Lobdell J (1986) The Kuparuk Pingo Site: a Northern Archaic Hunting Camp of the Arctic Coastal Plain, North Alaska. Arctic 39(1):47–51

Mackay JR (1979) Pingos of the Tuktoyaktuk Peninsula, Northwest Territories. Geographie physique et Quaternaire 33:3–61

Mackay JR (1997) A full-scale field experiment (1978–1995) on the growth of permafrost by means of lake drainage, western Arctic coast: a discussion of the method and some results. 1997. Can J Earth Sci 34:17–33

Mackay JR (1998) Pingo growth and collapse, Tuktoyaktuk Peninsula area, western arctic coast, Canada: a long-term field study. Geographie physique et Quaternaire 52(3):271–323

Maydel G (ed) (1896) On Taryns in Yakutskaya Oblast. Travels through NE part of Yakutskaya Oblast from 1868–1870 2. Saint Petersburg

McNamara JP, Kane DL, Hinzman LD (1999) An analysis of an arctic channel network using a digital elevation model. Geomorphology 29:339–353

Middendorf AF (1861) Travels in the North and East of Siberia. Saint Petersburg

Müller F (1959) Beobachtungenber Pingos. Meddelelser om Grønland 153:1–127 (Trans. from the German. Ottawa, Nat. Res. Counc. Can. TT-1073, 1963, 117p)
Nyland KE, Klene AE, Brown J, Shiklomanov NI, Nelson FE, Streletskiy DA, Yoshikawa K (2016) Traditional Iñupiat ice cellars (SIĠḶUAQ) in barrow, Alaska: characteristics, temperature monitoring, and distribution. Geogr Rev. https://doi.org/10.1111/j.1931-0846.2016.12204.x
Orvin, A. K., 1944: Outline of the Geological History of Spitsbergen. *Skr. Svalbard og Ishavet,* Nr.78. 1–24
Osterkamp TE, Romanovsky VE (1999) Evidence for warming and thawing of discontinuous permafrost in Alaska. Permafr Periglac Process 10:17–37
Osterkamp TE, Viereck LA, Shur Y, Jorgenson MT, Racine C, Doyle A, Boone RD (2000) Observations of thermokarst and its impact on boreal forests in Alaska, USA. Arct Antarct Alp Res 32:303–315
Parameswaran VR, Mackay JR (1996) Electrical freezing potentials measured in a pingo growing in the western Canadian Arctic. Cold Reg Sci Technol 24:191–203
Parkhomenko SG (1932) Program for study of phenomena connected with soil permafrost and soil. Soviet Asia Press
Pavlov AV (1994) Current changes of climate and permafrost in the Arctic and sub-Arctic of Russia. Permafr Periglac Process 5:101–110
Petrone KC, Hinzman LD, Boone RD (2000) Nitrogen and carbon dynamics of storm runoff in three sub-arctic streams. In: Kane DL (ed) Proceedings of American water resources association on water resources in extreme environments, Anchorage, AK, 1–3 May 2000, pp 167–172
Podyakonov SA (1903) Naledi Vostochnoi Sibiri I prichiny ikh voznikneniia (icings of eastern Siberia and their origin). Izvestiia Vsesoyunogo Geograficheskogo Obshchestva 39:305–337
Pollard WH (2005) Icing processes associated with high Arctic perennial springs, Axel Heiberg Island, Nunavut, Canada. Permafr Periglac Process 16(1):51–68
Porsild AE (1938) Earth mounds in unglaciated arctic northwestern America. Geogr Rev 28:46–58
Romanovskii NN (1983) Taliks and icings of ground water. In: Ground water of cryolithozone. Moscow State University Publisher, pp 94–101
Romanovsky VE, Osterkamp TE (1995) Interannual variations of the thermal regime of the active layer and near surface permafrost in Northern Alaska. Permafr Periglac Process 6:313–335
Romanovsky VE, Burgess M, Smith S, Yoshikawa K, Brown J (2002) Permafrost temperature records: Indicators of climate change. Eos 83(50):586–594
Sellmann PV, Brown J, Lewellen RI, McKim H, Merry C (1975) The classification and geomorphic implication of thaw lakes on the Arctic Coastal Plain, Alaska. USA cold regions research and engineering laboratory, Research Report 344
Sharkuu N (1998) Trends of permafrost development in the Selenge River basin, Mongolia. In: Lewkowicz AG, Allard M (eds) Proceedings of the international conference on permafrost: seventh international conference, 2–5 August 1998, Yellowknife, Canada, Universite Laval, Quebec, Collection Nordicana 57, pp 979–985
Slaughter CW (1982) Occurrence of and recurrence of aufeis in an upland Taiga catchment. In: Canadian permafrost conference, 4th, Calgary, 1981, Proceedings. National Research Council of Canada, Ottawa, pp 182–188
Sloan CE, Zenone C, Mayo L (1976) Icings along the trans-Alaska pipeline route. U.S. geological survey professional paper 979, 31p
Smith MW, Tice AR (1988) Measurement of the unfrozen water content of soils – comparison of NMR and TDR methods. CRREL report, vol 88–18. US Army Cold Regions Research and Engineering Lab (CRREL)
Sokolov BL (1973) Certain features in structure and mechanical breakdown of naleds, their significance in estimates of naled runoff, Siberian naleds. CRREL Draft Transl 399:140–154
Sumgin MI (1927) Contribution to the study of permafrost in the peat mounds of the Kola Peninsula. Akademiya Nauk SSSR Komissiya izuch. vechnoi merzloty Trudy 3:107–115

Tice AR, Oliphant JL, Nakano Y, Jenkins TF (1982) Relationship between the ice and unfrozen water phases in frozen soil as determined by pulsed nuclear magnetic resonance and physical desorption data. US. Army. Cold Regions Research and Engineering Lab (CRREL), CRREL Report 82-15

Tolstikhin NI (1941) Underground water in frozen zone of lithosphere, gosgeolizdat, Moscow-Leningrad

Tolstikhin ON (1963) On possibility of utilizing naled area for rough evaluation of underground water resources, Materials on geology and minerals of Yakutsk ASSR, no. 11, Yakutsk

Wendler KD (2011) Numerical heat transfer model of a traditional ice cellar with passive cooling methods. M.S. thesis, University of Alaska Fairbanks, 164pp

Woo MK (1986) Permafrost hydrology in North America. Atmos Ocean 24(3):201–234

Woodcock AH (1974) Permafrost and climatology of a Hawaii volcano crater. Arct Alp Res 6 (1):49–62

Wrangel FP (1841) A journey to the northern shores of Siberia and along the Arctic Ocean made in 1820–1924. St. Petersburg

Yang D, Kane DL, Hinzman LD, Zhang X, Zhang T, Ye H (2002) Siberian Lena river hydrologic regime and recent charge. J Geophys Res—Atmos 107:4694. https://doi.org/10.1029/2002jd002542

Yde JC, Knudsen NT (2005) Observations of debris-rich naled associated with a major glacier surge event, Disko Island, West Greenland. Permafr Periglac Process 16(4):319–325

Yoshikawa K (2008) Stable isotope composition of ice in seasonally and perennially frozen mounds. In: Permafrost, ninth international conference on permafrost

Yoshikawa K (2013) Permafrost in our time. University of Alaska Fairbanks Permafrost Outreach Center. Fairbanks, AK, 300pp. http://issuu.com/permafrostbook/docs/piots

Yoshikawa K, Harada K (1995) Observations on nearshore pingo growth, Adventdalen, Spitsbergen. Permafr Periglac Process 6:361–372

Yoshikawa K, Petrone K, Hinzman LD, Bolton WR (1999) Aufeis development and stream baseflow hydrology in the discontinuous permafrost region, Caribou Poker Creeks Research Watershed, Interior Alaska. In: The 50th Arctic science conference. Denali National Park and Preserve, Alaska, 19–22 September 1999

Yoshikawa K, Bolton WR, Romanovsky VE, Fukuda M, Hinzman LD (2002) Impacts of wildfire on the permafrost in the boreal forests of Interior Alaska. J Geophys Res 107:8148. https://doi.org/10.1029/2001jd000438 (printed 108(D1), 2003)

Yoshikawa K, Overduin PP, Harden JW (2004) Moisture content measurements of moss (*Sphagnum spp*.) using recently developed commercial sensors. Permafr Periglac Process 15:1–11

Yoshikawa K, Hinzman LD (2003) Shrinking thermokarst ponds and groundwater dynamics in discontinuous permafrost. Permafr Periglac Process 14(2):151–160

Yoshikawa K, Hinzman LD, Kane DL (2007) Spring and aufeis (icing) hydrology in the Brooks Range, Alaska. J Geophys Res 112:G04S43. https://doi.org/10.1029/2006jg000294

Zhou Y, Guo D, Qiu G, Cheng G, Li S (2000) Geocryology in China. Cold and Arid Regions Environmental and Engineering Research Institute, Chinese Academy of Science, Beijing, 448p

Dr. Kenji Yoshikawa, a research professor, works at the Water and Environmental Research Center, University of Alaska Fairbanks, USA. His research areas are permafrost geomorphology, permafrost hydrology, and extraterrestrial permafrost. Pingos and icings are his primary interest, searching for them and drilling them to learn more, including two difficult quests by Yoshikawa—one into interior Antarctica and the other across the Sahara for ancient pingo scar, as described in his biography (Finding Mars) by Ned Rozell. His research locations have included Svalbard, Greenland, Alaska, Siberia, Tibet, Canadian Arctic, and Mongolia, where he found many pingos and examined their internal structures and hydrology. He organized and took part in many field investigations, including searching the permafrost in Kilimanjaro, Hawaii, Mexico, tropical Andes (Peru and Chile). He has published more than 50 peer-reviewed articles. He organized International Permafrost Association's summer schools for several years and served as chair of education and outreach committee in 2010–2018.

Dr. Douglas L. Kane is a Professor Emeritus at the Water and Environmental Research Center (WERC), University of Alaska Fairbanks (UAF). He served the UAF with distinction in teaching, research, and public service from 1971 to 2009. He is a world-renowned Arctic hydrologist who has played an important role in establishing the UAF as a global leader in Arctic water research. He is credited as the author, co-author, or editor of more than 100 refereed publications and more than 22 other publications; and was awarded the Can-Am Civil Engineering Amity Award by the American Society of Civil Engineers for exemplary professional activity. He is the Recipient of ASCE Harold R. Peyton award for Cold Regions Engineering and designated as a Fellow in the American Water Resources Association (AWRA). He has provided leadership in a variety of positions at the University, including as Director of the Water and Environmental Research Center for 20 years, as Director of the Institute of Northern Engineering for 6 years, and as a Full Professor of Water Resources and Civil Engineering for 30 years.

Ground Temperature and Active Layer Regimes and Changes

15

Lin Zhao, Cangwei Xie, Daqing Yang, and Tingjun Zhang

Abstract

Permafrost is degrading worldwide due to climate, leading to serious consequences for regional hydrology, climate, and ecosystems. Over the past decades, field observations in most permafrost regions of the Northern Hemisphere showed a warming trend in ground temperatures. The warming magnitude of low-temperature permafrost was significantly higher than that of high-temperature permafrost. Measurements from the CALM network revealed that in 2016, the increasing trend in the active layer thickness at all Arctic sites was about 1.2–1.9 cm/year across circum-Arctic regions. This change is at or near the long-term maximum for the past 18–21 years. This chapter discusses and reviews permafrost observation networks/programs and datasets, ground temperature variations, active layer changes, effect of snow cover on ground thermal regimes, ground ice distribution, carbon storage in frozen ground, and InSAR application in the northern regions. It is important to emphasize that

L. Zhao (✉)
School of Geographical Sciences, Nanjing University of Information Science & Technology, Nanjing, China
e-mail: lzhao@nuist.edu.cn; linzhao@lzb.ac.cn

C. Xie
Cryosphere Research Station on the Tibetan Plateau, Northwest Institute of Eco-Environment and Resources, Chinese Academy of Sciences, Lanzhou, China
e-mail: xiecw@lzb.ac.cn

D. Yang
Environment and Climate Change Canada, Watershed Hydrology and Ecology Division, Victoria, BC, Canada
e-mail: daqing.yang@canada.ca; daqing.yang@gmail.com

T. Zhang
College of Natural Resources, Lanzhou University, Lanzhou, China
e-mail: tzhang@lzu.edu.cn

D. Yang and D. L. Kane (eds.), *Arctic Hydrology, Permafrost and Ecosystems*,
https://doi.org/10.1007/978-3-030-50930-9_15

northern permafrost conditions have significantly changed and will continue to change in the future. In order to understand the past history and future of permafrost, we need to continue and expand the monitoring of the permafrost variables, particularly ground temperature and active layer thickness, via in situ and remote-sensing technologies.

15.1 Observation Networks and Datasets

Permafrost mainly distributes in the Northern Hemisphere, including more than half of Russia's and Canada's territory, about 22% of China's territory, 85% State of Alaska, USA, and 67% of Mongolia. Permafrost also exists in the mountainous regions of Central Asia and Europe, for example in the Tianshan Mountains and the Alps. In the Antarctica and Greenland, there is permafrost in the regions without ice cover and glaciers (Fig. 15.1). According to the circum-Arctic map of permafrost and ground ice conditions published by the International Permafrost Association, about 23.9% (22.79×10^6 km^2) of Northern Hemisphere's land area was occupied by permafrost regions (Zhang et al. 2008).

A series of international monitoring networks have been established to monitor the two key variables of permafrost and active layer: the thermal state of permafrost (TSP) and the active layer thickness (ALT). The Global Terrestrial Network for Permafrost (GTN-P) was developed in the 1990s by the International Permafrost Association (IPA) under the Global Climate Observing System (GCOS) and the Global Terrestrial Observing Network (GTOS), with the long-term goal of obtaining a comprehensive view of the spatial structure, trend, and variability in the active layer thickness and permafrost temperature (https://gtnp.arcticportal.org/). The GTN-P mainly consists of the Circumpolar Active Layer Monitoring (CALM), Permafrost and Climate in Europe: climate change, mountain permafrost degradation and geotechnical hazard (PACE), TSP, and other national networks.

The CALM program was established in the early 1990s, which was initially affiliated with the International Tundra Experiment (ITEX). The CALM's goals include monitoring the thickness of the active layer (Hinkel and Nelson 2003; Streletskiy et al. 2012), temperature in the near-surface layers of the permafrost regions (Hinkel et al. 2001), and surface movements attributable to frost heave and thaw settlement (Shiklomanov et al. 2013). The CALM program is among the international permafrost community's first large-scale efforts to construct a coordinated monitoring program capable of producing datasets suitable for evaluating the effects of climate change. The CALM network's history, organizational structure, site descriptions, and interim results were reported in Brown et al. (2000), Burgess et al. (2000), Nelson et al. (2004, 2008), and Shiklomanov et al. (2012). The CALM network currently consists of more than 240 field sites operated by research groups in Canada, China, Denmark/Greenland, Italy, Kazakhstan, Mongolia, New Zealand, Norway, Poland/Svalbard, Portugal, Russia, Spain, Sweden,

Fig. 15.1 Permafrost distribution in the circum-Arctic regions. Credit: Map by Philippe Rekacewicz, UNEP/GRID-Arendal; data from International Permafrost Association, 1998. Circumpolar Active-Layer Permafrost System (CAPS), version 1.0

Norway, Switzerland, and the USA. The CALM program includes four phases: CALM I (1997–2002), CALM II (2004–2009), CALM III (2009–2014), and CALM IV (2014–2019). The CALM is currently administered through the Department of Geography at George Washington University (https://www2.gwu.edu/~calm/). The CALM investigators measure the seasonal depth of thaw at plots of various dimensions using standardized protocols (Hinkel and Nelson 2003). Soil and air temperature, soil moisture content, and vertical movement are also measured at many sites. These measurements, combined with site-specific information about soils, landscape, and vegetation, can be used to "scale up" assessments of the stability and projected changes to regional and circumpolar scales (Nelson et al.

1997; Shiklomanov and Nelson 2002). They also have an important role in model validation (Shiklomanov et al. 2007).

The PACE program, a multinational effort, was established in December 1997 by the European Commission Environment and Climate Research Program. A major goal of the PACE program was to establish a continental scale north–south transect of permafrost monitoring stations across the higher mountains of Europe, from Svalbard to the Sierra Nevada (Harris et al. 2001, 2009). This monitoring network focused on the complementary investigations, including geophysical surveys, microclimatic investigations, numerical modeling of permafrost distribution, and physical modeling of permafrost-related slope instability. The program objective is to improve the understanding of dynamic processes, the validation of numerical models, and the assessment of potential permafrost hazards in the context of land-use planning and geotechnical engineering.

The GTN-P network consists of approximately 1074 boreholes in both hemispheres with more than 25 participating countries. Approximately 350 of the boreholes were drilled and instrumented during the International Polar Year (IPY) period under various nationally funded projects. The borehole metadata and inventory including mean annual ground temperatures (MAGT) for approximately 600 boreholes (snapshot) became available online as part of the IPY Data and Information Service (IPYDIS) in mid-2010 (Brown and Romanovsky 2008). The TSP project was the major IPA contribution to IPY during 2007–2009. TSP aimed at the development of spatially distributed observations of past and present permafrost thermal state and active layer thicknesses, with emphasis on permafrost temperatures. The ground temperature data serves as a baseline for the assessment of the change in permafrost conditions and provide input to climate models and engineering designs. The TSP is a field component of the GTN-P (Smith et al. 2009). Its accomplishments have been reported in a special issue of Permafrost and Periglacial Processes (Christiansen et al. 2010; Romanovsky et al. 2010a, b; Smith et al. 2010; Vieira et al. 2010; Zhao et al. 2010). The IPY also provided a unique opportunity to build on existing permafrost and periglacial research in the Antarctic with the development of new sites and mapping efforts. Argentina, Brazil, Bulgaria, Italy, New Zealand, Portugal, Russia, South Africa, Spain, Sweden, the UK, and the USA continued or expanded their Antarctic permafrost activities. IPA activities in the IPY period also took place outside the polar regions. Some European countries sponsored new activities or continued with their programs, such as Switzerland and its Permafrost Monitoring Switzerland (PERMOS) program (Vonder Mühll et al. 2008) and Thermal State of Permafrost in Norway and Svalbard (TSP NORWAY) project (Juliussen et al. 2010). Within the GTN-P, most of the boreholes and active layer monitoring sites are distributed in the Arctic region, for example, totally 1074 boreholes in the GTN-P database by the end of 2015 (Biskaborn et al. 2015), and 31 boreholes located in the mountain permafrost regions and 72 in Antarctica. The database is very useful to assess permafrost changes and its impacts on hydrology and ecosystem functions in the Arctic region.

15.2 Changes in Permafrost Temperature

Ground temperature is an important measure of permafrost condition. A large number of boreholes that are used to observe ground temperatures across northern hemisphere provide a database for feature extraction, spatial mapping, or change detection of permafrost characteristics. The long-term continuous observations of permafrost temperature are especially of great significance for climatic and ecological investigations (Romanovsky et al. 2002). In the Northern Hemisphere, permafrost temperatures vary from approximately −15 °C in continuous permafrost zones to around 0 °C near the southern boundary of discontinuous permafrost regions (Zhang 2012). This pattern reflects the influence of latitude on the thermal regime of permafrost. Altitude is another important factor affecting the ground temperature of permafrost. For example, the distribution of permafrost in the Alps of Europe is significantly affected by altitude (Boeckli et al. 2012). The spatial and temporal distributions of environmental elements, such as snow cover (Rödder and Kneisel 2012) and vegetation (Bakalin and Vetrova 2008; Kokelj et al. 2017), also affect the permafrost distribution and ground temperature at different spatial scales. Over the past 30 years, most of the permafrost regions in the Northern Hemisphere, except for a few individual areas, experienced warming according to field observations (Zhang 2012). The warming magnitude of low-temperature permafrost was significantly higher than that of high-temperature permafrost. For those high-temperature permafrost with high ice content, the increase of ground temperature is particularly slow (Romanovsky et al. 2010b; Zhang 2012) (Fig. 15.2).

Consistent with the warming trend in the past decades, permafrost in North America showed a warming trend in general. The warming in Alaska and Western Canada began in the 1970s, and the warming of permafrost in the western part of Canada started in the early 1990s (Smith et al. 2010). Permafrost with different thermal regimes has different responses to climate change and variation. The effect of latent heat makes the discontinuous permafrost to remain relatively stable and be close to 0 °C in the south of North America (Phillips et al. 2009). Thus, permafrost may remain in a relatively warmer environment in some cases.

Continuous ground temperatures monitoring from boreholes in Alaska (Smith et al. 2010; Zhang 2012) showed that permafrost temperature increased by 0.3 °C from the late 1970s to the early 1980s (Osterkamp 2007). There was a rapid warming period from the early 1980s to the end of 1990s, when permafrost temperature increased by approximately 1.5–2.5 °C (Smith et al. 2010). In the twenty-first century, permafrost temperatures increased slowly, and the maximum warming was about 0.6 °C (Osterkamp 2007). In the interior of Alaska, permafrost at some sites with relatively high temperatures had not warmed up or even cooled down slightly (Smith et al. 2010).

Since the 1970s, the annual mean ground surface temperature (MAGT) had increased by 2 °C in the undisturbed terrains of northwestern Canada due to climate warming (Kokelj et al. 2017). From the late 1970s to the early 2000s, annual mean ground temperature at 15 m depth had increased by 1.5 °C in the Arctic tundra

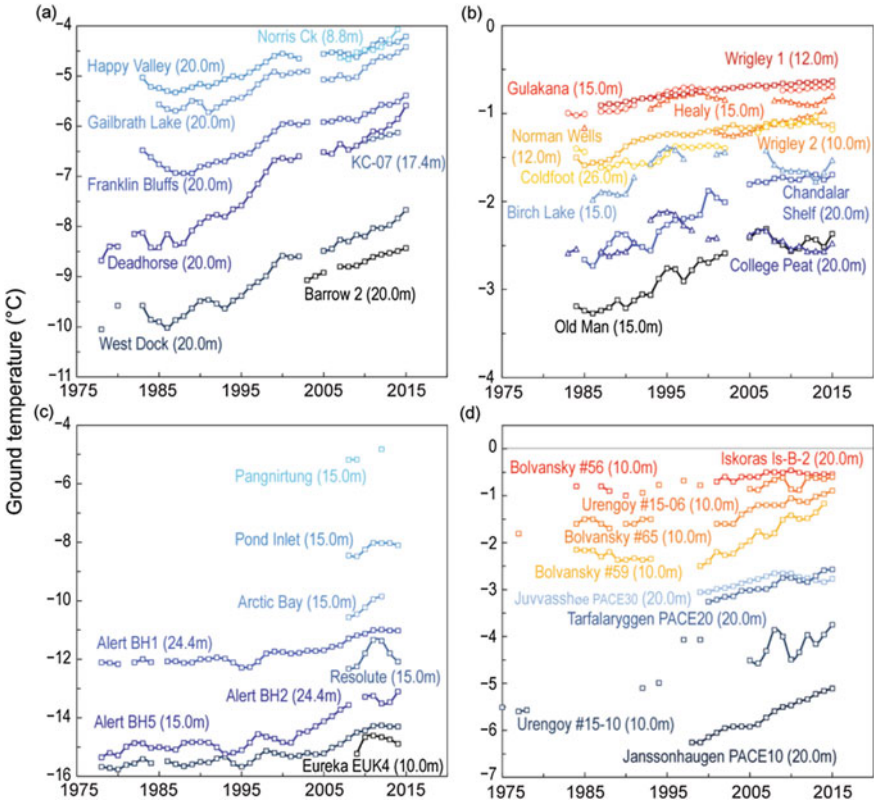

Fig. 15.2 Time series of mean annual ground temperature (MAGT) at depths of 9–26 m below the surface at selected measurement sites that fall roughly into the Adaptation Actions for a Changing Arctic Project (AMAP 2015) priority regions: **a** cold continuous permafrost of NW North America (Beaufort-Chukchi region); **b** discontinuous permafrost in Alaska and northwestern Canada; **c** cold continuous permafrost of eastern and high Arctic Canada (Baffin Davis Strait); **d** continuous to discontinuous permafrost in Scandinavia, Svalbard, and Russia/Siberia (Barents region). Temperatures are measured at or near the depth of penetration of the seasonal ground temperature variations. Data series are updated from Christiansen et al. (2010), Ednie and Smith (2015), Romanovsky et al. (2015), Smith et al. (2015). From the section "Terrestrial permafrost" of "State of the Climate in 2015" (Romanovsky et al. 2016). © American Meteorological Society. Used with permission

regions of eastern Canada (Fig. 15.2). In the Mackenzie Delta, the most substantial permafrost warming seemed to happen in the outer delta plain, where a temperature increment of 2 °C was recorded (Smith et al. 2010). Incenter of the delta, the monitored ground temperature at 15 m depth had only increased by 0.5 °C since the 1970s due to the influence of water bodies widely scattered all over the terrain (Kanigan et al. 2008).

In the Alert area of Ellesmere Island, the increasing rate of ground temperature at 15 m depth was about 0.1 °C/a over the last 30 years, mainly related to the rapid rising of air temperature (Smith et al. 2005b, 2010). In northern Quebec, permafrost temperature decreased slightly from the late 1980s to the middle 1990s, and then increased rapidly by 2 °C from 1993 to 2008 (Smith et al. 2010). The increase of winter temperature seems to be the main cause of permafrost warming after entering the twenty-first century, and the variation of snow depth also has a significant impact on the thermal regime of permafrost (Throop et al. 2010) (Fig. 15.2).

Woodbury et al. (2009) examined long-term surface air temperature and ground surface temperature changes at eight sites west of the Canadian Cordillera since the 1960s, concluding that ground surface temperature observations showed no apparent climate-induced perturbations, even though all sites showed significant increasing trends in surface air temperature. Their comparison of ground surface temperature and surface air temperature suggested that any trend in increased surface air temperature was masked by freeze-thaw and latent energy effects in the winter and spring.

In addition to the studies based on ground surface temperature observations from borehole measurements, Zhang et al. (2003) developed a process-based model of northern ecosystem soil temperature (NEST) to simulate the transient response of soil thermal regime to climate change in Canada. Their results show that, depending on the location, changes in annual mean soil temperature during the twentieth century differed from those in air temperature by −3 and +3 °C, and that the difference was more significant in winter and spring than in summer (Zhang et al. 2005). They found that on average, for the whole of Canada, the annual mean soil temperature at 20 cm depth increased by 0.6 °C while the annual mean air temperature increased by 1.0 °C.

Qian et al. (2011) analyzed soil temperature measured at 30 climate stations across Canada covering the period from 1958 to 2008; the data cover soil temperatures at six soil depths: 5, 10, 20, 50, 100, and 150 cm. They also analyzed air temperature, precipitation, and snow cover depth at the same locations and examined the relationships between the trends in soil temperature and other climate variables in Canada to better understand the effects of future climate change on soils and the associated biophysical and biochemical processes. They found that at about two-thirds of the stations, soil temperatures at depths below 5 cm showed a warming trend over the 50-year record. Many sites showed a significant positive trend in mean soil temperatures in spring and summer but not in winter (Fig. 15.3). Because snow insulates the ground, keeping the soil warm, the trend of declining snow depth explains why winter soil temperatures did not show a warming trend. The median warming rate in spring for soil at all depths was about 0.3 °C per decade. Their results show that rising soil temperatures were generally associated with rising air temperatures and decreasing snow cover depth, although there were variations across the sites.

The most obvious climate warming in Russia occurred between the 1970s and 1990s. Permafrost of most terrains had not suffered substantial warming before 2000, even with a slight cooling period from the late 1990s to the early 2000s at

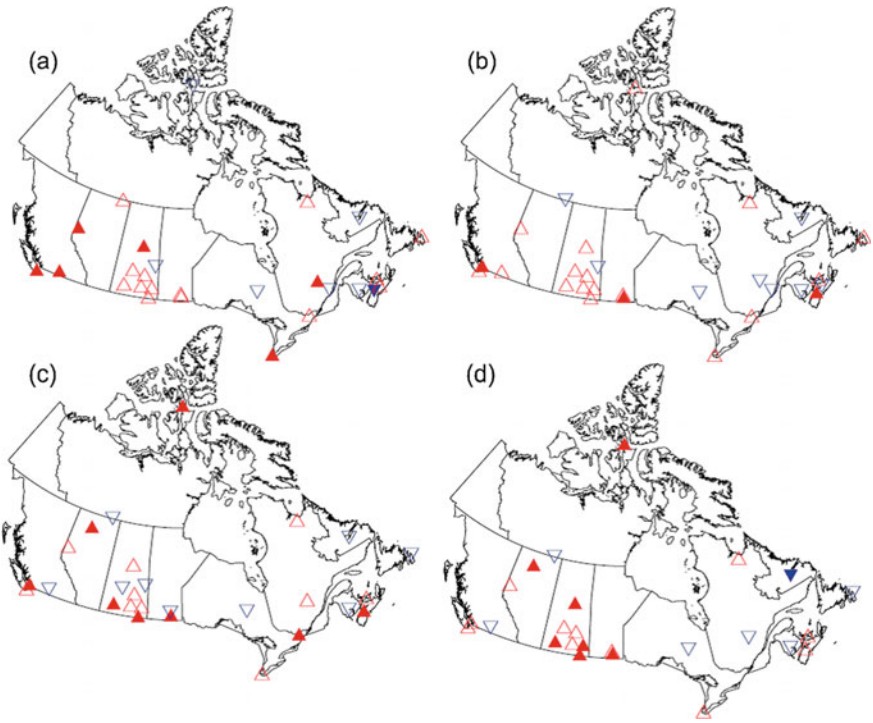

Fig. 15.3 Maps showing the trends of mean soil temperature across Canada in spring (March–April–May) at the depths of **a** 10 cm and **b** 100 cm and in summer (June–July–August) at the depths of **c** 100 cm and **d** 150 cm for the period 1958–2008. Upward and downward triangles show positive and negative trends, respectively. Solid triangles indicate trends significant at the 5% level (Qian et al. 2011)

some observation sites along the Arctic ocean coast (Romanovsky et al. 2008, 2010a). During the past two or three decades, substantial permafrost warming occurred, and the warming had great spatial heterogeneity. The variation of ground temperature at the depth of zero annual amplitude was in the range between 0.5 and 2 °C (Mishra and Riley 2014). In the Urengoy area of northwestern Siberia, the warming magnitude of low-temperature permafrost had been up to 2 °C from 1974 to 2007, while that of high-temperature permafrost was only 1 °C. Permafrost warming rates ranged from 0.003 °C/a to 0.02 °C/a in the Bolvansky Cape within the Pechora River Delta (Romanovsky et al. 2008, 2010b).

In the circumpolar region of central Siberia, such as Tiksi and Yakutsk, ground temperatures at 30 m depth showed a slight rising trend over the period between 1990 and 2005. In the 1980s and 1990s, the phenomenon of permafrost warming was barely observed in the northern or western Siberia. However, permafrost temperature had begun to increase rapidly since the late 2000s. The boreholes drilled in European Russia revealed that annual mean ground temperature of

permafrost in this region had increased by 0.3 and 1.0 °C over the period from 1983 to 2009 (Romanovsky et al. 2010a).

Permafrost in northern Europe tends to have a relatively higher temperature (generally 1 °C higher) than that in the regions with similar latitude in Siberia or North America, such as in Svalbard islands, Scandinavia Peninsula and north-eastern Greenland (Christiansen et al. 2010). During the period from 1999 to 2009, permafrost temperature in southern Norway had increased by 0.15 and 0.95 °C. The greatest rate of temperature increase was observed at sites having mean annual ground temperature slightly above 0 °C, and the lowest rate of increase was observed at marginal permafrost sites that are affected by latent heat exchange close to 0 °C (Isaksen et al. 2011). In Svalbard island and northern Scandinavia, permafrost warming at a depth of more than 60 m had been detected, and the increasing rate of mean annual ground temperature had reached 0.04 °C/a to 0.07 °C/a (Isaksen et al. 2007). In northern Sweden, the greatest rate of permafrost warming at 20 m depth had also reached 0.047 °C/a during the period from 2001 to 2011 (Jonsell et al. 2013).

15.3 Changes in Active Layer Thickness

In permafrost region, the active layer is the layer of ground that is subject to annual thawing and freezing in areas underlain by permafrost. The special variations of active layer thicknesses are influenced by many factors, including local climate, physical, and thermal properties of the surface soil, vegetation, soil moisture, and other factors. The special distribution of active layer depths has great influence, or controls on the hydrological processes in permafrost regions. The regional average of active layer thickness in Alaska is about 48–60 cm with large regional variations (Luo et al. 2016; Mishra and Riley 2014; Pastick et al. 2014). On the North Slope of Alaska (north of Brooks Range), the active layer thickness is generally less than 50 cm due to cold arctic climate, saturated soil water conditions, and relatively thick peat layers. In the Alaska Interior between the Brooks Range and the Alaska Range, the average active layer thickness is generally between 50 and 100 cm. In Canada, the active layer monitoring sites are mainly located in the Mackenzie River watershed and Yukon Territories. The average active layer thickness in these regions is about 93 cm, generally deeper than that in Alaska. In the Interior Yukon, active layer thickness is approximately 60 cm regionally averaged, slightly shallower than that in the Mackenzie River watershed and southern parts of Northwest Territories, which were between 75 and 150 cm (Luo et al. 2016). In Russia, the active layer monitoring sites are mainly located over Siberia. The active layer thickness is generally less than 1 m at the most northern locations above 72°N and increases to more than 3.5 m at the southern regions just above 50°N (Streletskiy et al. 2015). This spatial variation is mainly related to climatic continentality, snow, and soil conditions.

According to Peng et al. (2018), utilizing 347 active layer monitoring sites in the Northern Hemisphere, the lowest regional average active layer thickness is in Alaska, less than 40 cm in a continuous permafrost area, and 40–80 cm for the discontinuous permafrost. In the other part of North America continuous permafrost regions, the active layer thickness is between 80 and 200 cm and more than 240 cm in the sporadic and isolated permafrost regions in the Rocky Mountains. In Siberia, the active layer thickness ranges from 80 to 240 cm in the continuous permafrost regions. On the Mongolian Plateau, the active layer thickness is about 120 cm in continuous permafrost regions and more than 320 cm in sporadic and isolated permafrost regions.

Under the background of global warming, permafrost degradation is common in the Northern Hemisphere, that is, the rising temperatures in permafrost and the thickening of the active layer. Unlike the consistent temperature rising of permafrost, the variation of active layer thickness has a great regional difference. In addition to climate influence, the thickness of active layer is mainly controlled by local geographic factors, such as soil water condition, soil texture, vegetation, and soil organic matter.

In Russia, analysis of soil temperatures at 3.2 m depth shows an increase in temperature at almost all locations in the permafrost regions during the 1963–2013 period. The highest rates of the soil temperature rising, greater than 0.4 °C/decade, are occurred in the Central Siberian Plateau and southern mountainous regions, including Altay, Sayan Mountains and Stanovoy Range. In the Alaskan Arctic region (the North Slope), in situ measurements demonstrate that the surface air temperature has increased at a rate of 0.23 °C/decade during 1921–2015, at 0.53 °C/decade during 1951–2015, and at 0.71 °C/decade over 1998–2015 (Wang et al. 2017b). This demonstrates that in the Arctic permafrost region, air temperature warmed strongly in recent years.

In the past 50 years (up to 2013), the active layer thickness has generally increased in eastern Siberia and the Far East by about 1 cm/year; the changes were 3–4 cm/year at several locations, such as Isit, Sanaga, Norils'k, and Suntar (Streletskiy et al. 2015). Measurements from the Circumpolar Active Layer Monitoring network revealed that in 2016, the active layer thickness at all Arctic sites was at or near the long-term maximum for the past 18–21 years. At the West Siberian sites, active layer thickness reached an all-time high over the past 20 years (Blunden and Arndt 2017) (Fig. 15.4). In West Siberia and Russian European North, with the highest average active layer thickness of more than 1 m, the active layer thickness had the greatest change, with an average increase of about 1.2 and 1.9 cm/year during 1996–2016 across circum-Arctic regions. The lowest regional average active layer thickness appeared in the North Slope of Alaska, and this area had the least increase of about 0.2 cm/year during 1996–2016. The other regions, that is, Greenland, East Siberia, and Far East of Russia, the average active layer thicknesses and their increase are between the West Siberia and North Slope regions.

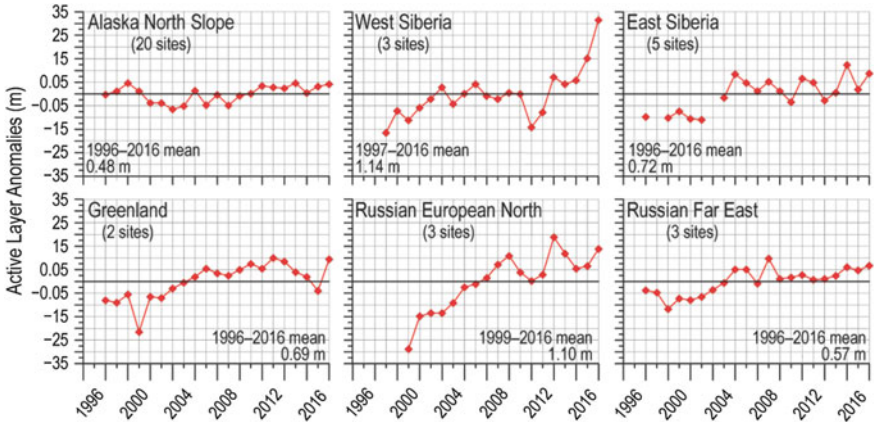

Fig. 15.4 Long-term ALT change (m, relative to the average value for the period of observations) in six different Arctic regions of CALM program. Thaw depth measurements are conducted at the end of the thawing season. Only sites having at least 15 years of observations are shown. From the section "Terrestrial permafrost" of "State of the Climate in 2016" (Romanovsky et al. 2017). © American Meteorological Society. Used with permission

Records from 25 sites in the Mackenzie Valley, northwestern Canada, show that active layer thickness in 2016 was on average 6 cm greater than the 2003–2012 mean, similar to the precious peak value of 0.78 m in 2012 (Blunden and Arndt 2017; Nelson et al. 2004). Smith et al. (2009) found that the soil water content and organic matter were the main control factors for the difference in active layer variation patterns in this region. Walker et al. (2003) pointed out that the insulation provided by more dense plant canopies and thicker soil organic horizons counters the active layer in an increasing trend.

15.4 Snow Cover Effect on Ground Temperature

The influence of snow cover on ground thermal regime depends on the occurrence time, duration, accumulation and melting process of snow cover, the thickness, density, and structure of seasonal snow cover, as well as the interaction of micro-meteorological conditions, local micro-topography, vegetation, and geographical location (Zhang 2005). The occurrence and duration of seasonal snow cover can cause changes in the magnitude and effect (cooling or warming) of the ground thermal condition. When snow accumulates in autumn, the snow cover was relatively thin, and when the temperature fluctuated around 0 °C, the snow cover played a cooling role on the ground. The reason for this cooling effect is that the solar altitude angle is still relatively high in autumn and albedo of new snow is higher. However, the duration of this cooling effect may be very short, so its impact

on the annual average surface temperature may be small. As the temperature decreases and the snow thickness increases, the thermal insulation of snow cover has become the main factor in preventing the ground from cooling. Assume that the temperature difference between the annual average surface temperature and the annual average air temperature is 1.1 °C (this is also the average temperature difference in summer snow-free period in northern Alaska), seasonal snow cover will increase the annual average surface temperature by 4 and 9 °C. However, snowfall in late winter or early spring may have a cooling effect on the ground thermal condition (Zhang 2005).

The snow thickness is another important factor that has a significant impact on the surface thermal condition. At a given time with the same air temperature, ground surface temperature varied by more than 10 °C within a short distance (Zhang 2005) (Fig. 15.5). Kudryavtsev (1992) reported that when the snow was thin and the albedo was high, the snow would cause the surface soil to cool. With the increase of snow cover thickness, the insulation of the snow is enhanced, leading to warming of surface soil. The insulation works best when the snow reaches the optimum thickness (about 40 cm). After that, the insulation decreases with the increasing of snow thickness. If the snow is thick enough to last until late

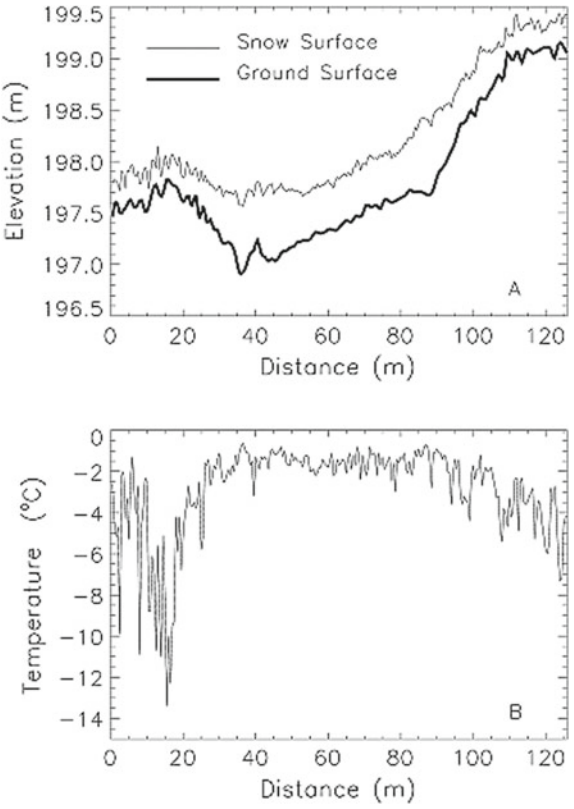

Fig. 15.5 Variations of **a** snow thickness and **b** snow-ground interface temperatures with local microrelief at Ivotuk, Alaska, taken on 17 November 1998 Figure modified from (Zhang 2005)

spring and early summer, the snow may be cooled by the albedo and the potential thermal effects. Generally, an increase in snow thickness of 5–15 cm will increase the average annual ground temperature by 1 °C (Yershov 2004). The annual average surface temperature can be positive when the average temperature is low but there is enough thick seasonal snow. Liang and Zhou (1993) believe that seasonal snow cover with a thickness of 21–36 cm causes the annual average ground temperature in Amur area to be about 2.8–5.0 °C higher than that in snow-free areas. Sensitivity analysis using the numerical model also shows that the annual average surface temperature increases with the increase of the maximum snow depth in the same temperature conditions and snow accumulation process (Zhang 1993), and the freezing period of the active layer will be delayed with the increase of the maximum snow depth.

The snow density varies from less than 100 kg m^{-3} (fresh snow and depth hoar) to the 600 kg m^{-3} (melting snow and wind slab), which has a significant impact on the thermal performance of snow, thus affecting the thermal condition of the ground. Zhong et al. (2014) used long-term ground observation data to study the snow density climatology and its spatiotemporal variations in the former Soviet Union (USSR) from 1966 to 2008. The results showed that the average monthly snow density in the study area was about 0.22 ± 0.05 g cm^{-3}. The areas with higher monthly snow density were mainly concentrated in the European regions of the former USSR, the Russian Arctic coast, and the Kamchatka Peninsula, while the area with lower density was mainly in central Siberia. From September to June, there was a significant increase in snow density, but the increase rate varies depending on the snow depth. The long-term average monthly and annual snow density has a significant downward trend from 1966 to 2008, especially in autumn. Zhang et al. (1996) used a model by Goodrich (1982) to study the influence of snow thermal conductivity on the ground thermal condition. The results show that the change of thermal conductivity of snow cover from 0.7 to 0.1 Wm^{-1} K^{-1} will lead to an increase in the annual average surface temperature from −6.5 to −1.0 °C, and the minimum surface temperature from −16.3 to −3.7 °C. The change of thermal conductivity will also reduce the annual amplitude of surface temperature from 10 to 3.6 °C and delays the freezing date of the active layer by more than 4 months. Benson and Sturm (1993) reported that tundra snow consists of a hard, high-density wind-packed layer at the top with coarse, and low-density depth hoar layer at the bottom. The density of the wind slab varies from 0.4 to 0.5 g cm^{-3} with a particle size of 0.5 to 1.0 mm. The density of the depth hoar layer varies from 0.1 to 0.25 g cm^{-3} with a particle size of 5.0 to 10.0 mm. The thermal conductivity varies from less than 0.01 Wm^{-1} K^{-1} to more than 1.0 Wm^{-1} K^{-1}. The depth hoar fraction can exceed 50% of the total snowpack (Sturm and Benson 1997). Sensitivity analysis shows that under the average snow cover and climate conditions along the Arctic coast of Alaska, the change of the depth hoar fraction from 0.0 (no depth hoar) to 0.6 would cause the surface temperature to rise by 12.8–5.5 °C (Zhang et al. 1996) (Fig. 15.6).

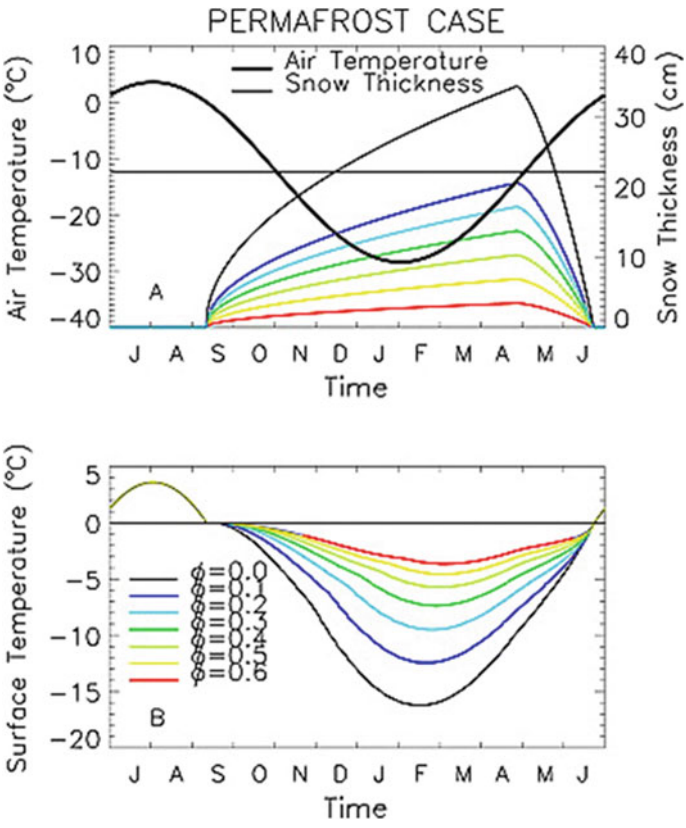

Fig. 15.6 Impact of changes in the depth hoar fraction of the seasonal snow cover on ground surface temperature (Zhang et al. 1996)

Geographically, the duration and thickness of seasonally frozen ground gradually increase from south to north in the Northern Hemisphere and from low to high altitude, and finally entered permafrost regions. According to the area of permafrost, it can be divided into four categories: continuous, discontinuous, sporadic, and isolated permafrost zones (Zhang et al. 1999). In the continuous permafrost zones, seasonal snow cover will increase the average annual temperature and the ground temperature of permafrost by several degrees. However, strong winds, relatively flat terrain, and undeveloped vegetation along the Arctic coast weaken the insulation of snow, resulting in lower permafrost temperatures (Zhang et al. 1996). Similar phenomenon also reported in Umujaq, east of Hudson Bay, Canada. Research shows that snow cover is the main factor controlling the distribution of discontinuous permafrost. Even if the annual average temperature in this area is around −4.5 °C, the thick snow will prevent the development of permafrost (Smith 1975). However, in isolated permafrost zones, thin snow cover or no seasonal snow

cover may be the key factor for the formation or existence of permafrost in high altitude areas at mid-low latitudes (Smith 1975). In the seasonally frozen ground zones, seasonal snow cover will cause the ground temperature to rise, reduce the ground frost depth, and increase the soil moisture. The daily variation of ground temperature at a depth of 5 cm is obviously reduced when the ground is covered with snow. The surface soil began to freeze in mid-late November when the temperature was below 0 °C. The albedo of fresh snow is high, and even the shallower snow (a few centimeters) will cool the ground, which makes the snow insulation relatively weak at this time. Zhang et al. (1999) believed that seasonally frozen soil would develop widely before the formation of snow on the regional scale. Once the snow is accumulated, its thickness increases with time and frozen soil may begin to thaw. Until the end of winter, there may be a thin frozen layer or no frozen soil under the snow, especially under the thicker snow layer. This is mainly because snow prevents the energy from the deep soil layer to the near surface from being released to the atmosphere, and this energy is eventually consumed by thawing frozen soil.

Interannual variations in seasonal snow conditions (occurrence time, duration, density, structure, and thickness) have a significant impact on long-term geothermal changes in cold season or cold regions. Reconstructing the history of surface temperature through the borehole temperature gradient is widely used as a method to study paleoclimate changes (Liu and Zhang 2014). The relationship between reconstructed ground temperature and air temperature has not been fully understood, and the change of the ground temperature alone cannot be explained by the change of the air temperature. Of course, the change in temperature alone cannot explain the change in ground temperature. Changes in snow cover conditions have dramatically changed the influence of temperature on ground thermal condition and may have contributed greatly to increase ground temperature over the past few centuries. Future work needs to better understand the influence of other parameters such as temperature, snow cover, precipitation, vegetation, and soil humidity on soil thermal condition. Both field and laboratory experiments have shown that winter heterotrophic activity increases with snowmelt and soil melting in spring due to the increase of activated carbon substrate (Schimel et al. 2001). During the winter months, the soil is isolated from the cold air temperature by snow cover. Thinner snow resulted in colder soil and more severe freezing. If the snow cover has been in a very thin state, the soil remains frozen throughout winter and microbial activity is suppressed. Conversely, if deep snow is formed later in winter, the previously frozen soil may melt, and microbial activity and heterotrophic respiration may be greatly enhanced. A similar degree of soil freezing may enhance the microbial activity and soil decomposition process in one area, while the other area will decrease. Therefore, the timing of snow accumulation seems to have an important impact on secondary biogeochemical activities and subsequent carbon and nitrogen fluxes. When the soil is frozen, there is a little exchange of carbon, methane, and other gases between the atmosphere and the surface, but this exchange becomes more obvious as the soil melts in the early spring. The release phenomenon is called "respiratory burst" by Skogland et al. (1988).

15.5 Ground Ice Distribution

Ground ice is the general term used for all types of ice formed in freezing and frozen ground. Ground ice occurs in the pores, cavities, voids, or other openings in soil or rock (ACGR 1988). Ground ice slowly forms over a long time period as a result of repetitive contraction and expansion associated with seasonal cycles of subsurface thawing and refreezing. Ground ice grows in forms of large ice lenses and ice wedges within the subsurface layers. It alters soil thermal properties, such as the overall thermal conductivity and heat capacity, as well as soil moisture conditions. As a result, ground ice may have a large impact on the rate of permafrost thaw due to the latent heat required to melt the extra ice. In addition, when ice-rich permafrost thaws, the land surface formerly sustained by ice wedges and lenses can collapse and create land surface subsidence. This land surface subsidence, also called thermokarst, alters local hydrology and can potentially influence the rate and the magnitude of permafrost carbon loss and subsequent greenhouse gas emissions, possibly accelerating future climate change.

Permafrost and ground-ice conditions are of major concern to scientists and engineers working on global change studies, resource development, foundation design, and protection of the environment in cold regions (Zhang et al. 1999). Based on the extent of permafrost and its ice content, the estimated volume of ground ice in the Northern Hemisphere is between 11.37 and 36.55 $\times$ 10^3 km^3, which corresponds to 3–10 cm sea-level equivalent. Ice content in the ice-rich permafrost is only 20–30% by volume in the calculation, while the actual ice content in Alaska and west Siberia could be 50–70% excluding ice wedges. Considering the generally low ice content value during the calculation, the result may underestimate the gross reserve of ground ice. Based on the average ice content of the boreholes along the Qinghai-Tibet Highway, Nan et al. (2003) estimate that the ground ice reserved in the permafrost region of the Qinghai-Tibet Plateau is between 10.9 $\times$ 10^3 and 17.4 $\times$ 10^3 km^3, which is 2–3 times of the ice volume in the glaciers over China. Zhao et al. (2010) estimate the ground ice reserved to be 9528 km^3 based on the horizontal and vertical distribution of ground ice within different geomorphic styles. Our latest results show that ground ice reserve could reach 12.7 $\times$ 10^3 km^3 based on new data and a map of permafrost distribution and thickness over the Qinghai-Tibet Plateau.

In the cold regions, the hydrological regime is closely related to permafrost conditions, such as permafrost extent and thermal characteristics. Ice-rich permafrost has a very low hydraulic conductivity and commonly acts as a barrier to deeper groundwater recharge or as a confining layer to deeper aquifers. Because it is a barrier to recharge, permafrost increases surface runoff and decreases subsurface flow. Permafrost extent over a region plays a key role in the distribution of surface–subsurface interaction. Permafrost and non-permafrost rivers have very different hydrologic regimes. Relative to non-permafrost basins, permafrost watersheds have higher peak flow and lower base flow. In the permafrost regions, watersheds with

higher permafrost coverage have lower subsurface storage capacity and thus a lower winter base flow and a higher summer peak flow (Woo et al. 2008; Ye et al. 2009).

Due to climate warming, ground ice in permafrost may melt. The released water may participate in the local hydrologic cycle. Synthesis of discharge data reveals that the average annual discharge of fresh water from the six largest Eurasian rivers to the Arctic Ocean increased by 7% from 1936 to 1999. The average annual rate of increase was 2.0 ± 0.7 cubic kilometers per year (Peterson et al. 2002). It is difficult to estimate the ground ice volume because of the soil heterogeneity in water retention capability. Observations from the Gravity Recovery and Climate Experiment (GRACE) mission provide a better understanding of changes in water storage in permafrost regions. Comparison of secular trends from GRACE to runoff suggests groundwater storage increased in the Lena and Yenisei watersheds, decreased in the Mackenzie watershed, and remained unchanged in the Ob' watershed. The groundwater storage changes are linked to the development of closed- and open-talik in the continuous permafrost zone and the decrease of permafrost extent in the discontinuous permafrost zone within the watersheds (Muskett and Romanovsky 2009). Analysis of 7-year GRACE data shows terrestrial water storage (TWS) increases twice as rapidly as in the rest of the Lena basin in an area of discontinuous permafrost near the center of the basin. Most of the TWS change is attributed to an increase in subsurface water storage. The estimated TWS increase in the Lena subregion implies an average increase in the groundwater table of 56 ± 9 cm or groundwater recharging through areas not underlain by permafrost, while changes in active layer thickness likely have little impact (Velicogna et al. 2012).

Thermokarst lakes are typically formed by the settlement of ground following the thawing of ice-rich permafrost or melting of massive ice (Van Everdingen 2005). Thermokarst lakes are typical features of the northern permafrost ecosystems and play an important role in the thermal exchange between atmosphere and subsurface. The process of soil thaw begins with subsidence at the flat bog with the formation of a soil depression, which is an "embryo" of the lake that continues growing until it achieves the kilometer-sized mature stage. At this stage, the lake may be drained after connecting to another water body or to a hydrological network, forming a drained lake or khasyrey. On the dry bottom of khasyreys, the frozen peat bogs begin to thaw, initiating a new thermokarst lake cycle. Remote sensing techniques demonstrate that in western Siberia the dominant processes are currently the increasing number of small thermokarst lakes in the north and the drainage of large lakes to the river network south of the cryolithozone (Manasypov et al. 2014). Smith et al. (2005a) compared Siberian satellite imagery taken in the early 1970s with satellite data during 1997–2004 and tracked the changes of more than 10,000 large lakes over three decades of rising soil and air temperatures in the region. The analysis reveals a widespread decline in lake abundance and area, despite a slight increase of precipitation.

Both regional and landscape-level analyses show inconsistent trends in surface water extent, with high seasonal, annual, and regional variability, due in part to differences in methods and spatial scales. The surface water analyses are revealing

complicated interactions involving water increases from permafrost degradation, lake initiation and shoreline erosion; decreases from lake drainage and shoreline planification; and multi-year bi-directional fluctuations due to water balance changes. Similarly, overall trends in high-resolution land cover in permafrost regions remain elusive due to differences in classification, imagery types, processing techniques, and the role of disturbance and succession in complicating long-term trends (Jorgenson and Grosse 2016). Bi-directional resizing of thermokarst lakes is observed in the boreal forests of Alaska. A significant reduction in the areas of lakes in the north and an increase in the areas of lakes in the southern regions were observed in Canada (Carroll et al. 2011), which is the reverse of that observed in western Siberia (Smith et al. 2005a). An increase in the total number of water bodies and a decrease in the total area of thermokarst lakes were reported for the southern extent of the continuous permafrost zone in Alaska (Jones et al. 2017).

15.6 Carbon Storage and Change

A cold condition in the permafrost region has hindered soil organic carbon (OC) from microbial decomposition and let long-term carbon accumulation in soil (Ping et al. 2015). As a result, the high-latitude and high-altitude permafrost regions, accounting for about 24% of the land area in the Northern Hemisphere (Zhang et al. 1999; Zhang et al. 2008), contains up to 1820 Pg OC (Tarnocai et al. 2009), which is more than two times the amount of current atmospheric carbon (C) (Schuur et al. 2015) or half of the estimated global soil OC pool (Tarnocai et al. 2009). The OC pool in the permafrost region is estimated to be 472 $\pm$ 27 Pg for the 0–1 m depth, 1,035 $\pm$ 150 Pg for the 0–3 m depth (Hugelius et al. 2014), and more than 800 Pg OC is stored in the permafrost and is not part of the active C cycle (Koven et al. 2015). Under present climate conditions, the Arctic permafrost region is estimated to be a carbon dioxide (CO_2) sink of 0.3–0.6 Pg C yr^{-1}, methane (CH4) source of 0.023–0.075 Pg C yr^{-1} (Van Huissteden and Dolman 2012; Vincent et al. 2013). Permafrost degradation caused by climate warming may cause the release of permafrost carbon to the atmosphere as CO_2 or CH_4, and further raise the carbon content of the atmosphere (Kittler et al. 2017).

Temperature is a key (crucial) factor regulating biogeochemical processes and C dynamics in the terrestrial ecosystems (Rustad et al. 2001). As permafrost ecosystem is strongly temperature limited, warming can potentially accelerate decomposition of permafrost organic matter stimulating greenhouse gas emissions (Sierra et al. 2015). Previous observations showed that permafrost temperature has increased by about 2–3 °C in Alaska, 0–2 °C in Canada, 0.3–2.8 °C in Siberian (Lemke et al. 2007). Arctic temperatures rise faster than the global average (Overland et al. 2014), and climate models also predict a strong high-latitude warming in the future (IPCC 2013). IPCC AR5 climate models project that global mean surface temperatures are likely to increase by 0.3 and 4.8 °C by the end of the twenty-first century relative to 1986–2005, with very high confidence that the

Arctic region will warm more rapidly. Projected temperature increases over the Arctic land region have a median/mean estimate of 1.9 °C (RCP2.6), 3.9 °C (RCP4.5), 4.5 °C (RCP6.0), and 7.5 °C (RCP8.5) (Christensen et al. 2013; Hartmann et al. 2013).

Estimates of the impact of climate change on permafrost carbon have typically been performed combining estimates of soil thermal changes with those of simplified soil carbon decomposition (Koven et al. 2015; Schneider von Deimling et al. 2015). Schuur et al. (2015) collated results from many of these studies and showed that the potential carbon release from today's permafrost zone would be between 37 and 174 Gt by the year 2100 under a "business-as-usual" scenario RCP8.5 (Meinshausen et al. 2011). This is comparable with the result of Koven et al. (2015), who estimated a permafrost carbon response of 28–113 Gt for the same time period and scenario based on a soil carbon decomposition model in which the response of soil carbon to warming was calibrated by the results of laboratory incubation experiments (Schädel et al. 2014). Climate models predict that permafrost C pool increases the land C emissions at stabilization by 0.09–0.19 Gt C yr^{-1} for stabilization target of 2 °C, reduced by 0.08–0.16 Gt C yr^{-1} when considering 1.5 °C stabilization targets. The simulations suggest that 225–345 and 60–100 Gt C are in thawed permafrost and may eventually be released to the atmosphere for stabilization target of 2 and 1.5 °C by 2500, respectively (Burke et al. 2018). These studies indicate that the northern permafrost region will lose huge OC under a warming climate.

15.7 InSAR Applications in the Northern Regions

The warming of the Arctic climate has resulted in massive degradation of permafrost in high latitudes. Interferometry Synthetic Aperture Radar (InSAR) is a remote-sensing technology that can detect ground deformation with accuracy of centimeter or even millimeter (Berardino et al. 2002; Gabriel et al. 1989). InSAR has been widely used in permafrost research in Canada, Alaska, Qinghai-Tibet Plateau, and Siberia, to reflect the development of permafrost due to its advantages of all weather, high precision, and wide range (Daout et al. 2018; Daout et al. 2017; Liu et al. 2010; Mironov and Muzalevskiy 2013; Rudy et al. 2018; Wang and Li 1999). Short et al. (2011) obtained permafrost deformation trend in the Herschel Island, Canada, through InSAR technology combined with SAR data of different wavelengths. The results show that the ground deformation rate of the island's northeast coast was 20–30 cm yr^{-1} from 2007 to 2010, and the maximum deformation rate was 5 cm yr^{-1} in the northern part of the island. Other studies with InSAR technology in Canada showed that glacial deposits, organic soil, and geological conditions as the main factors of ground subsidence in the permafrost region (LeBlanc et al. 2015; Wolfe et al. 2014).

Liu et al. (2010) used InSAR technology and ERS-1/ERS-2 SAR data to obtain the ground deformation over Alaska northern slope from 2002 to 2010. The results showed that the permafrost in the region tended to degrade at the beginning of the twenty-first century, with a settlement rate of 1–4 cm decade^{-1}. Subsequently, they used InSAR technology to estimate the change of active layer thickness in Prudhoe Bay from 1992 to 2002 and found a thickening trend by 30–80 cm over 10 years (Liu et al. 2012). Schaefer et al. (2015) using InSAR and field observation data examined the spatial distribution of active layer thickness near Barrow, Alaska. Antonova et al. (2018) found the land subsidence in the Lena River Delta permafrost region to be 9.3 ± 5.7 cm from 2013 to 2017, with the maximum subsidence to be 2 cm per year near a thermokarst lake. Chen et al. (2018), using InSAR data, studied the main reasons for the difference in the distribution of ground deformation in this region and speculated that it was mainly caused by the difference in soil moisture content. In addition, there are also application of InSAR data to detect deformation of periglacial landform in permafrost regions, such as the movement of the rock glacier, thawing slumping, changes of the thermokarst lakes, and frost mounds (Beck et al. 2015; Hosseini et al. 2018; Kenyi and Kaufmann 2003; Liu et al. 2014, 2015; Strozzi et al. 2013; Wang et al. 2017a).

15.8 Summary and Discussion

This chapter discussed and reviewed permafrost observation networks/programs and datasets, ground temperature variations, active layer changes, effect of snow cover on ground thermal regimes, ground ice distribution, carbon storage in frozen ground, and InSAR application in the northern regions. It is important to emphasize that northern permafrost conditions have significantly changed over recent decades and we have to continue the monitoring of the permafrost variables, particularly ground temperature and active layer thickness, via in situ and remote-sensing technologies.

The landscape freeze/thaw (FT) state plays a very important role in cold region hydrology and climate. Satellite observations of FT state are essential for monitoring and predicting the response of high-latitude environments to a changing climate. The Soil Moisture Active Passive (SMAP) satellite mission provides hemispheric estimates of landscape FT state at a spatial resolution of approximately 36 km^2. Validation studies of SMAP and other satellite FT products have compared satellite retrievals with point estimates obtained from in situ measurements of air and/or soil temperatures. Differences between the two are attributed to errors in the satellite retrieval. Significant differences can, however, occur between satellite and in situ estimates solely due to differences in scale between the measurements; these differences can be viewed as "representativeness errors" in the in situ product, caused by using a point estimate to represent a large-scale spatial average. Most validation efforts of landscape FT state have neglected representativeness errors entirely, resulting in conservative estimates of satellite retrieval skill. Lyu et al.

(2018) used a variant of triple collocation called "categorical triple collocation"—a technique that uses model, satellite, and in situ estimates to obtain relative performance rankings of all three products, without neglecting representativeness errors—to validate the SMAP landscape FT product. Performance rankings were obtained for nine sites at northern latitudes. They also investigated differences between using air or soil temperatures to estimate FT state, and between using morning (6 AM) or evening (6 PM) estimates. Overall, at most sites, the SMAP product or in situ FT measurement is ranked first, and the model FT product is ranked last (although rankings vary across sites). These results suggest that SMAP adds value to model simulations, providing higher-accuracy estimates of landscape FT states relative to models and, in some cases, even in situ estimates, when representativeness errors are properly accounted for in the validation analysis. They also suggest that comparing in situ FT estimates with SMAP FT retrievals (36 km^2) is more justified than comparisons with coarser-resolution satellite FT products (such as $\sim$100 km^2 Aquarius retrievals) used in other studies, since higher resolution FT products resolve more of the FT spatial variability. The FT state is difficult to monitor via in situ observations in the remote northern regions, and there is a need to carry out similar regional or grid-scale analyses of SMAP and other FT products in the high latitudes.

Models are useful tools to examine and understand permafrost process and its function in the arctic system. Compared with empirical and statistical models, physical-based numerical models can better describe and quantify the hydro-thermal process. With the advance in computing power and improved understanding of permafrost-climate linkage and interaction, some land surface process models consider ice-water phase transition and unfrozen water content in a relatively complete soil profile for the simulations of permafrost dynamics (Qin et al. 2017; Westermann et al. 2013). However, there are certain limitations in applying numerical models to simulate the permafrost distribution and changes because many input parameters and initial conditions have to be appropriately set up for model development and calibration. In recent years, with more attention to the changes in surface-to-air exchange due to climate change in large area of permafrost regions, the main development of permafrost models includes expanding permafrost thermal module from point heat transfer to geospatial distribution, such as the incorporation transient numerical thermal models within geospatial model and incorporation of permafrost into the global circulation model (GCM) surface process (Romanovsky et al. 2010a). The major challenge in the development of permafrost models is the lack of observation data. Because of the huge impact of latent heat, accurate simulation of the permafrost processes requires detailed information about the relationship between ice-water content and ground temperature. This information, however, is usually lacking in most permafrost monitoring network (Romanovsky et al. 2010b). For mountainous permafrost regions, it is especially challenging for permafrost modeling.

Because of the differences in elevation, snow cover, terrain features, orientation, and microclimate, all these factors cause great variations in surface and subsurface thermal conditions compared to plains and lowlands. Future research on permafrost

models will need to improve the monitoring networks, and obtain sufficient data and knowledge. These will allow us to establish a reasonable parameterization scheme for the sub-grid-scale land surface process and integration, leading to accurate simulation of the interaction between permafrost and climate across the broader northern regions. Furthermore, other relevant variables, such as vegetation distribution and evolution, should also be considered in the prediction of permafrost response to climate change.

Acknowledgments Xiaodong Wu, Qiangqiang Pang, Erji Du, Guangyue Liu, Yao Xiao, Defu Zou, Huayun Zhou and Lu Ma contributed to the preparation of this chapter. All of them are researchers at the Qinghai-Tibet Plateau Cryosphere Observation and Research Station, Chinese Academy of Sciences. Dr. Budong Qian also shared his ideas and time for this chapter.

References

ACGR (1988) Associate Committee on Geotechnical Research. Glossary of Permafrost Related Ground-Ice Terms National Research Council of Canada Technical Mem (142): p 156

Antonova S, Sudhaus H, Strozzi T, Zwieback S, Kääb A, Heim B, Langer M, Bornemann N, Boike J (2018) Thaw subsidence of a Yedoma landscape in Northern Siberia, measured in situ and estimated from TerraSAR-X interferometry. Remote Sens 10(4):494

Bakalin V, Vetrova V (2008) Vegetation-permafrost relationships in the zone of sporadic permafrost distribution in the Kamchatka Peninsula. Russ J Ecol 39(5):318–326

Beck I, Ludwig R, Bernier M, Strozzi T, Boike J (2015) Vertical movements of frost mounds in subarctic permafrost regions analyzed using geodetic survey and satellite interferometry. Earth Surf Dyn 3:409–421

Benson CS, Sturm M (1993) Structure and wind transport of seasonal snow on the Arctic slope of Alaska. Ann Glaciol 18:261–267

Berardino P, Fornaro G, Lanari R, Sansosti E (2002) A new algorithm for surface deformation monitoring based on small baseline differential SAR interferograms. IEEE Trans Geosci Remote Sens 40(11):2375–2383

Biskaborn BK, Lanckman J-P, Lantuit H, Elger K, Dmitry S, William C, Vladimir R (2015) The new database of the Global Terrestrial Network for Permafrost (GTN-P). Earth Syst Sci Data 7:245–259

Blunden J, Arndt DS (2017) State of the climate in 2016. Bull Am Meteorol Soc 98(8)

Boeckli L, Brenning A, Gruber S, Noetzli J (2012) Permafrost distribution in the European Alps: calculation and evaluation of an index map and summary statistics. The Cryosphere 6(4):807

Brown J, Romanovsky VE (2008) Report from the International Permafrost Association: state of permafrost in the first decade of the 21st century. Permafr Periglac Process 19(2):255–260

Brown J, Hinkel KM, Nelson F (2000) The circumpolar active layer monitoring (CALM) program: research designs and initial results. Polar Geogr 24(3):166–258

Burgess M, Smith S, Brown J, Romanovsky V, Hinkel K (2000) Global Terrestrial Network for Permafrost (GTNet-P): permafrost monitoring contributing to global climate observations

Burke EJ, Chadburn SE, Huntingford C, Jones CD (2018) CO2 loss by permafrost thawing implies additional emissions reductions to limit warming to 1.5 or 2°C. Environ Res Lett 13(2):024024

Carroll ML, Townshend J, DiMiceli C, Loboda T, Sohlberg R (2011) Shrinking lakes of the arctic: spatial relationships and trajectory of change. Geophys Res Lett 38(20)

Chen J, Günther F, Grosse G, Liu L, Lin H (2018) Sentinel-1 InSAR measurements of elevation changes over Yedoma Uplands on Sobo-Sise Island, Lena Delta. Remote Sens 10(7):1152

Christensen JH, Kanikicharla KK, Marshall G, Turner J (2013) Climate phenomena and their relevance for future regional climate change

Christiansen HH, Etzelmüller B, Isaksen K, Juliussen H, Farbrot H, Humlum O, Johansson M, Ingeman-Nielsen T, Kristensen L, Hjort J (2010) The thermal state of permafrost in the Nordic area during the International Polar Year 2007–2009. Permafr Periglac Process 21(2):156–181

Daout S, Doin MP, Peltzer G, Socquet A, Lasserre C (2017) Large-scale InSAR monitoring of permafrost freeze-thaw cycles on the Tibetan Plateau. Geophys Res Lett 44(2):901–909

Daout S, Doin MP, Peltzer G, Lasserre C, Socquet A, Volat M, Sudhaus H (2018) Strain partitioning and present-day fault kinematics in NW Tibet from Envisat SAR interferometry. J Geophys Res: Solid Earth 123(3):2462–2483

Ednie M, Smith S (2015) Permafrost temperature data 2008–2014 from community based monitoring sites in Nunavut. Geological Survey of Canada Open File 7784

Gabriel AK, Goldstein RM, Zebker HA (1989) Mapping small elevation changes over large areas: differential radar interferometry. J Geophys Res: Solid Earth 94(B7):9183–9191

Goodrich L (1982) The influence of snow cover on the ground thermal regime. Can Geotech J 19 (4):421–432

Harris C, Haeberli W, Vonder Mühll D, King L (2001) Permafrost monitoring in the high mountains of Europe: the PACE project in its global context. Permafr Periglac Process 12(1):3–11

Harris C, Arenson LU, Christiansen HH, Etzelmüller B, Frauenfelder R, Gruber S, Haeberli W, Hauck C, Hölzle M, Humlum O (2009) Permafrost and climate in Europe: Monitoring and modelling thermal, geomorphological and geotechnical responses. Earth-Sci Rev 92(3):117–171

Hartmann DL, Tank AMK, Rusticucci M, Alexander LV, Brönnimann S, Charabi YAR, Dentener FJ, Dlugokencky EJ, Easterling DR, Kaplan A (2013) Observations: atmosphere and surface climate change 2013 the physical science basis: working group I contribution to the fifth assessment report of the intergovernmental panel on climate change. Cambridge University Press

Hinkel KM, Nelson FE (2003) Spatial and temporal patterns of active layer thickness at Circumpolar Active Layer Monitoring (CALM) sites in northern Alaska, 1995–2000. J Geophys Res-Atmos 108(D2). Artn 8168. https://doi.org/10.1029/2001jd000927

Hinkel KM, Paetzold F, Nelson FE, Bockheim JG (2001) Patterns of soil temperature and moisture in the active layer and upper permafrost at Barrow, Alaska: 1993–1999. Glob Planet Chang 29 (3–4):293–309. https://doi.org/10.1016/S0921-8181(01)00096-0

Hosseini F, Pichierri M, Eppler J, Rabus B (2018) Staring spotlight TerraSAR-X SAR Interferometry for identification and monitoring of small-scale landslide deformation. Remote Sens 10(6):844

Hugelius G, Strauss J, Zubrzycki S, Harden JW, Schuur E, Ping C-L, Schirrmeister L, Grosse G, Michaelson GJ, Koven CD (2014) Estimated stocks of circumpolar permafrost carbon with quantified uncertainty ranges and identified data gaps. Biogeosci Discuss 11

IPCC (2013) Climate change 2013: the physical science basis. Contribution of working group I to the fifth assessment report of the intergovernmental panel on climate change. Cambridge University Press Cambridge, UK

Isaksen K, Sollid JL, Holmlund P, Harris C (2007) Recent warming of mountain permafrost in Svalbard and Scandinavia. J Geophys Res Earth Surf 112(F2)

Isaksen K, Ødegård RS, Etzelmüller B, Hilbich C, Hauck C, Farbrot H, Eiken T, Hygen HO, Hipp TF (2011) Degrading mountain permafrost in southern Norway: spatial and temporal variability of mean ground temperatures, 1999–2009. Permafr Periglac Process 22(4):361–377

Jones MC, Harden J, O'donnell J, Manies K, Treat C, Jorgenson T, Ewing S, O'donnell J (2017) Rapid carbon loss and slow recovery following permafrost thaw in boreal peatlands. Glob Chang Biol 23(3):1109–1127

Jonsell U, Hock R, Duguay M (2013) Recent air and ground temperature increases at Tarfala Research Station, Sweden. Polar Res 32(32):287–304

Jorgenson MT, Grosse G (2016) Remote sensing of landscape change in permafrost regions. Permafr Periglac Process 27(4):324–338

Juliussen H, Christiansen H, Strand G, Iversen S, Midttømme K, Rønning J (2010) NORPERM, the Norwegian permafrost database–a TSP NORWAY IPY legacy. Earth Syst Sci Data 2 (2):235–246

Kanigan J, Burn C, Kokelj S (2008) Permafrost response to climate warming south of treeline, Mackenzie Delta, Northwest Territories, Canada. In: Proceedings ninth international conference on permafrost, vol 1. Institute of Northern Engineering, University of Alaska: Fairbanks, pp 901–906

Kenyi LW, Kaufmann V (2003) Estimation of rock glacier surface deformation using SAR interferometry data. IEEE Trans Geosci Remote Sens 41(6):1512–1515

Kittler F, Heimann M, Kolle O, Zimov N, Zimov S, Göckede M (2017) Long-term drainage reduces CO2 uptake and CH4 emissions in a Siberian permafrost ecosystem. Glob Biogeochem Cycles 31(12):1704–1717

Kokelj S, Palmer M, Lantz T, Burn C (2017) Ground temperatures and permafrost warming from forest to tundra, Tuktoyaktuk Coastlands and Anderson Plain, NWT, Canada. Permafr Periglac 28(3):543–551

Koven CD, Lawrence DM, Riley WJ (2015) Permafrost carbon−climate feedback is sensitive to deep soil carbon decomposability but not deep soil nitrogen dynamics. Proc Natl Acad Sci 112 (12):3752–3757

Kudryavtsev V (1992) Principles of frozen ground forecasting during engineering and geocryological investigations (in Chinese) (Guodong C (ed), translated from Russian by Guo Dongxin et al.). Lanzhou University Press, Lanzhou

LeBlanc A-M, Short N, Mathon-Dufour V, Allard M, Tremblay T, Oldenborger GA, Chartrand J (2015) DInSAR seasonal surface displacement in built and natural permafrost environments, Iqaluit, Nunavut, Canada. In: 7th Canadian permafrost conference, Quebec

Lemke P, Ren J, Alley RB, Allison I, Carrasco J, Flato G, Fujii Y, Kaser G, Mote P, Thomas RH (2007) Observations: changes in snow, ice and frozen ground

Liang L, Zhou Y (1993) The characteristics of the distribution of snow cover and its effect on the temperature of permafrost, Amuer Region Da Hinggan Ling. In: Sixth international conference proceedings on permafrost, vol 1

Liu J, Zhang T (2014) Fundamental solution method for reconstructing past climate change from borehole temperature gradients. Cold Reg Sci Technol 102(11):32–40

Liu L, Zhang T, Wahr J (2010) InSAR measurements of surface deformation over permafrost on the North Slope of Alaska. J Geophys Res: Earth Surf 115(F3)

Liu L, Schaefer K, Zhang T, Wahr J (2012) Estimating 1992–2000 average active layer thickness on the Alaskan North Slope from remotely sensed surface subsidence. J Geophys Res: Earth Surf 117(F1)

Liu L, Schaefer K, Gusmeroli A, Grosse G, Jones BM, Zhang T, Parsekian AD, Zebker HA (2014) Seasonal thaw settlement at drained thermokarst lake basins, Arctic Alaska. Cryosphere 8:815–826

Liu L, Schaefer K, Chen A, Gusmeroli A, Zebker H, Zhang T (2015) Remote sensing measurements of thermokarst subsidence using InSAR. J Geophys Res: Earth Surf 120 (9):1935–1948

Luo D, Wu Q, Jin H, Marchenko SS, Lü L, Gao S (2016) Recent changes in the active layer thickness across the northern hemisphere. Environ Earth Sci 75(7):555

Manasypov R, Pokrovsky O, Kirpotin S, Shirokova L (2014) Thermokarst lake waters across the permafrost zones of western Siberia. Cryosphere 8(4):1177–1193

Meinshausen M, Smith SJ, Calvin K, Daniel JS, Kainuma M, Lamarque J-F, Matsumoto K, Montzka S, Raper S, Riahi K (2011) The RCP greenhouse gas concentrations and their extensions from 1765 to 2300. Clim Chang 109(1–2):213

Mironov V, Muzalevskiy K (2013) Impact of a freezing topsoil on determining the Arctic tundra surface deformation using InSAR. In: International Siberian conference on control and communications (SIBCON). IEEE, pp 1–3

Mishra U, Riley WJ (2014) Active-layer thickness across Alaska: comparing observation-based estimates with CMIP5 earth system model predictions. Soil Sci Soc Am J 78(3):894–902
Muskett RR, Romanovsky VE (2009) Groundwater storage changes in arctic permafrost watersheds from GRACE and in situ measurements. Environ Res Lett 4(4):045009
Nan Z, Gao Z, Li S, Wu T (2003) Permafrost changes in the northern limit of permafrost on the Qinghai-Tibet Plateau in the last 30 years. Acta Geogr Sin-Chin Ed 58(6):817–823
Nelson F, Shiklomanov N, Mueller G, Hinkel K, Walker D, Bockheim J (1997) Estimating active-layer thickness over a large region: Kuparuk River basin, Alaska, USA. Arct Alp Res 29 (4):367–378
Nelson F, Shiklomanov N, Hinkel K, Christiansen H (2004) The Circumpolar Active Layer Monitoring (CALM) workshop and the CALM II program. Polar Geogr 28(4):253–266
Nelson F, Shiklomanov N, Hinkel K, Brown J (2008) Decadal results from the Circumpolar Active Layer Monitoring (CALM) program. In: Proceedings of the ninth international conference on permafrost, vol 28. University of Alaska Press Fairbanks, Alaska, p 1273–1280
Osterkamp T (2007) Characteristics of the recent warming of permafrost in Alaska. J Geophys Res: Earth Surf 112(F2)
Overland JE, Wang M, Walsh JE, Stroeve JC (2014) Future Arctic climate changes: adaptation and mitigation time scales. Earth's Future 2(2):68–74
Pastick NJ, Jorgenson MT, Wylie BK, Rose JR, Rigge M, Walvoord MA (2014) Spatial variability and landscape controls of near-surface permafrost within the Alaskan Yukon River Basin. J Geophys Res Biogeosci 119(6):1244–1265
Peng X, Zhang T, Frauenfeld OW, Kang W, Luo D, Cao B, Hang S, Jin H, Wu Q (2018) Spatiotemporal changes in active layer thickness under contemporary and projected climate in the Northern Hemisphere. J Clim 31(1):JCLI-D-16-0721.1
Peterson TC, Taylor MA, Demeritte R, Duncombe DL, Burton S, Thompson F, Porter A, Mercedes M, Villegas E, Semexant Fils R (2002) Recent changes in climate extremes in the Caribbean region. J Geophys Res 107(21):ACL 16-1–ACL 16-9
Phillips M, Mutter EZ, Kern-Luetschg M, Lehning M (2009) Rapid degradation of ground ice in a ventilated talus slope: Flüela Pass, Swiss Alps. Permafr Periglac Process 20(1):1–14
Ping CL, Jastrow JD, Jorgenson MT, Michaelson GJ, Shur YL (2015) Permafrost soils and carbon cycling. Soil Discuss 1(1):147–171
Qian B, Gregorich EG, Gameda S, Hopkins DW, Wang XL (2011) Observed soil temperature trends associated with climate change in Canada. J Geophys Res Atmos 116(D2)
Qin Y, Wu T, Zhao L, Wu X, Li R, Xie C, Pang Q, Hu G, Qiao Y, Zhao G (2017) Numerical modeling of the active layer thickness and permafrost thermal state across Qinghai-Tibetan Plateau. J Geophys Res: Atmos 122(21)
Rödder T, Kneisel C (2012) Influence of snow cover and grain size on the ground thermal regime in the discontinuous permafrost zone, Swiss Alps. Geomorphology 175:176–189
Romanovsky V, Burgess M, Smith S, Yoshikawa K, Brown J (2002) Permafrost temperature records: indicators of climate change. EOS Trans Am Geophys Union 83(50):589–594
Romanovsky V, Kholodov A, Marchenko S, Oberman N, Drozdov D, Malkova G, Moskalenko N, Vasiliev A, Sergeev D, Zheleznyak M (2008) Thermal state and fate of permafrost in Russia: first results of IPY. In: Kane DL, Hinkel KM (eds) Proceedings of the 9th international conference on permafrost, vol 2. Institute of Northern Engineering, University of Alaska Fairbanks, Fairbanks, Alaska, USA, pp 1511–1518
Romanovsky V, Drozdov D, Oberman N, Malkova G, Kholodov A, Marchenko S, Moskalenko N, Sergeev D, Ukraintseva N, Abramov A (2010a) Thermal state of permafrost in Russia. Permafr Periglac Process 21(2):136–155
Romanovsky VE, Smith SL, Christiansen HH (2010b) Permafrost thermal state in the polar Northern Hemisphere during the international polar year 2007–2009: a synthesis. Permafr Periglac Process 21(2):106–116

Romanovsky V, Cable W, Kholodov A (2015) Changes in permafrost and active-layer temperatures along an Alaskan permafrost-ecological transect. In: Proceedings of 68th Canadian geotechnical conference and seventh canadian conference on permafrost (GEOQuébec 2015)

Romanovsky VE, Smith SL, Isaksen K, Shiklomanov NI, Streletskiy DA, Kholodov AL, Christiansen HH, Drozdov DS, Malkova GV, Marchenko SS (2016) Terrestrial permafrost [in "State of the Climate in 2015"]. Bull Amer Meteorol Soc 97(8):S149–S152

Romanovsky VE, Smith SL, Shiklomanov NI, Streletskiy DA, Isaksen K, Kholodov AL, Christiansen HH, Drozdov DS, Malkova GV, Marchenko SS (2017) Terrestrial permafrost [in "State of the Climate in 2016"]. Bull Am Meteorol Soc 98(8):S147–S149

Rudy AC, Lamoureux SF, Treitz P, Short N, Brisco B (2018) Seasonal and multi-year surface displacements measured by DInSAR in a High Arctic permafrost environment. Int J Appl Earth Obs Geoinf 64:51–61

Rustad L, Campbell J, Marion G, Norby R, Mitchell M, Hartley A, Cornelissen J, Gurevitch J (2001) A meta-analysis of the response of soil respiration, net nitrogen mineralization, and aboveground plant growth to experimental ecosystem warming. Oecologia 126(4):543–562

Schädel C, Schuur EA, Bracho R, Elberling B, Knoblauch C, Lee H, Luo Y, Shaver GR, Turetsky MR (2014) Circumpolar assessment of permafrost C quality and its vulnerability over time using long-term incubation data. Glob Chang Biol 20(2):641–652

Schaefer K, Liu L, Parsekian A, Jafarov E, Chen A, Zhang T, Gusmeroli A, Panda S, Zebker HA, Schaefer T (2015) Remotely sensed active layer thickness (ReSALT) at Barrow, Alaska using interferometric synthetic aperture radar. Remote Sens 7(4):3735–3759

Schimel DS, House JI, Hibbard KA, Bousquet P, Ciais P, Peylin P, Braswell BH, Apps MJ, Baker D, Bondeau A (2001) Recent patterns and mechanisms of carbon exchange by terrestrial ecosystems. Nature 414(6860):169

Schneider von Deimling T, Grosse G, Strauss J, Schirrmeister L, Morgenstern A, Schaphoff S, Meinshausen M, Boike J (2015) Observation-based modelling of permafrost carbon fluxes with accounting for deep carbon deposits and thermokarst activity. Biogeosciences 12(11):3469–3488

Schuur EA, McGuire AD, Schädel C, Grosse G, Harden J, Hayes DJ, Hugelius G, Koven C, Kuhry P, Lawrence DM (2015) Climate change and the permafrost carbon feedback. Nature 520(7546):171

Shiklomanov N, Nelson F (2002) Active-layer mapping at regional scales: a 13-year spatial time series for the Kuparuk region, north-central Alaska. Permafr Periglac Process 13(3):219–230

Shiklomanov NI, Zhang T, Nelson FE, Anisimov OA, Marchenko S, Oelke C (2007) Comparison of model-produced active layer fields: results for Northern Alaska. J Geophys Res Earth Surf 112(F2)

Shiklomanov NI, Streletskiy DA, Nelson FE (2012) Northern hemisphere component of the global circumpolar active layer monitoring (CALM) program. In: Proceedings of 10th international conference on permafrost, vol 1, pp 377–382

Shiklomanov NI, Streletskiy DA, Little JD, Nelson FE (2013) Isotropic thaw subsidence in undisturbed permafrost landscapes. Geophys Res Lett 40(24):6356–6361. https://doi.org/10.1002/2013gl058295

Short N, Brisco B, Couture N, Pollard W, Murnaghan K, Budkewitsch P (2011) A comparison of TerraSAR-X, RADARSAT-2 and ALOS-PALSAR interferometry for monitoring permafrost environments, case study from Herschel Island, Canada. Remote Sens Environ 115(12):3491–3506

Sierra CA, Trumbore SE, Davidson EA, Vicca S, Janssens I (2015) Sensitivity of decomposition rates of soil organic matter with respect to simultaneous changes in temperature and moisture. J Adv Model Earth Syst 7(1):335–356

Skogland T, Lomeland S, Goksøyr J (1988) Respiratory burst after freezing and thawing of soil: experiments with soil bacteria. Soil Biol Biochem 20(6):851–856

Smith MW (1975) Microclimatic influences on ground temperatures and permafrost distribution, Mackenzie Delta, Northwest Territories. Can J Earth Sci 12(8):1421–1438

Smith LC, Sheng Y, MacDonald G, Hinzman L (2005a) Disappearing arctic lakes. Science 308 (5727):1429

Smith SL, Burgess MM, Riseborough D, Mark Nixon F (2005b) Recent trends from Canadian permafrost thermal monitoring network sites. Permafr Periglac Process 16(1):19–30

Smith SL, Wolfe SA, Riseborough DW, Nixon FM (2009) Active-layer characteristics and summer climatic indices, Mackenzie Valley, Northwest Territories, Canada. Permafr Periglac Process 20(2):201–220

Smith S, Romanovsky V, Lewkowicz A, Burn C, Allard M, Clow G, Yoshikawa K, Throop J (2010) Thermal state of permafrost in North America: a contribution to the international polar year. Permafr Periglac Process 21(2):117–135

Smith S, Lewkowicz A, Duchesne C, Ednie M (2015) Variability and change in permafrost thermal state in Northern Canada. In: Proceedings of 68th Canadian geotechnical conference and seventh Canadian conference on permafrost (GEOQuébec 2015)

Streletskiy DA, Shiklomanov NI, Nelson FE (2012) Permafrost, infrastructure, and climate change: a GIS-based landscape approach to geotechnical modeling. Arct Antarct Alp Res 44 (3):368–380. https://doi.org/10.1657/1938-4246-44.3.368

Streletskiy DA, Tananaev NI, Opel T, Shiklomanov NI, Nyland KE, Streletskaya ID, Tokarev I, Shiklomanov AI (2015) Permafrost hydrology in changing climatic conditions: seasonal variability of stable isotope composition in rivers in discontinuous permafrost. Environ Res Lett 10(9):095003

Strozzi T, Ambrosi C, Raetzo H (2013) Interpretation of aerial photographs and satellite SAR interferometry for the inventory of landslides. Remote Sens 5(5):2554–2570

Sturm M, Benson CS (1997) Vapor transport, grain growth and depth-hoar development in the subarctic snow. J Glaciol 43(143):42–59

Tarnocai C, Canadell J, Schuur E, Kuhry P, Mazhitova G, Zimov S (2009) Soil organic carbon pools in the northern circumpolar permafrost region. Glob Biogeochem Cycles 23(2)

Throop J, Smith SL, Lewkowicz AG (2010) Observed recent changes in climate and permafrost temperatures at four sites in northern Canada. In: GEO2010, 63rd Canadian geotechnical conference and the 6th Canadian permafrost conference, calgary GEO2010 calgary organizing committee, pp 1265–1272

Van Everdingen R (2005) Multi-language glossary of permafrost and related ground-ice terms. National Snow and Ice Data Center/World Data Center for Glaciology, Boulder, CO. World Wide Web. http://www.nsidcorg/fgdc/glossary

Van Huissteden J, Dolman A (2012) Soil carbon in the Arctic and the permafrost carbon feedback. Curr Opin Environ Sustain 4(5):545–551

Velicogna I, Tong J, Zhang T, Kimball JS (2012) Increasing subsurface water storage in discontinuous permafrost areas of the Lena River basin, Eurasia, detected from GRACE. Geophys Res Lett 39(9)

Vieira G, Bockheim J, Guglielmin M, Balks M, Abramov AA, Boelhouwers J, Cannone N, Ganzert L, Gilichinsky DA, Goryachkin S (2010) Thermal state of permafrost and active-layer monitoring in the antarctic: advances during the international polar year 2007–2009. Permafr Periglac Process 21(2):182–197

Vincent WF, Laurion I, Pienitz R, Walter Anthony KM (2013) Climate impacts on Arctic lake ecosystems. In: Climatic change global warming of inland waters: impacts mitigation for ecosystems societies, pp 27–42

Vonder Mühll D, Noetzli J, Roer I (2008) PERMOS–a comprehensive monitoring network of mountain permafrost in the Swiss Alps. In: Proceedings, ninth international conference on permafrost, vol 29. Citeseer

Walker DA, Jia GJ, Epstein HE, Raynolds MK, Iii FSC, Copass C, Hinzman LD, Knudson JA, Maier HA, Michaelson GJ (2003) Vegetation-soil-thaw-depth relationships along a low-arctic bioclimate gradient, Alaska: synthesis of information from the ATLAS studies. Permafr Periglac Process 14(2):103–123

Wang Z, Li S (1999) Detection of winter frost heaving of the active layer of Arctic permafrost using SAR differential interferograms. In: IEEE 1999 international on geoscience and remote sensing symposium, IGARSS'99 Proceedings, vol 4. IEEE, pp 1946–1948

Wang C, Zhang Z, Zhang H, Wu Q, Zhang B, Tang Y (2017a) Seasonal deformation features on Qinghai-Tibet railway observed using time-series InSAR technique with high-resolution TerraSAR-X images. Remote Sens Lett 8(1):1–10

Wang K, Zhang T, Zhang X, Clow GD, Cao B (2017b) Continuously amplified warming in the Alaskan Arctic: implications for estimating global warming hiatus. Geophys Res Lett 44:9029–9038

Westermann S, Schuler T, Gisnås K, Etzelmuller B (2013) Transient thermal modeling of permafrost conditions in Southern Norway. Cryosphere 7(2):719–739

Wolfe SA, Short NH, Morse PD, Schwarz SH, Stevens CW (2014) Evaluation of RADARSAT-2 DInSAR seasonal surface displacement in discontinuous permafrost terrain, Yellowknife, Northwest Territories, Canada. Can J Remote Sens 40(6):406–422

Woo MK, Kane DL, Carey SK, Yang D (2008) Progress in permafrost hydrology in the new millennium. Permafr Periglac Process 19(2):237–254

Woodbury AD, Bhuiyan AKMH, Hanesiak J, Akinremi OO (2009) Observations of northern latitude ground-surface and surface-air temperatures. Geophys Res Lett 36(7):251–254

Ye B, Yang D, Zhang Z, Kane DL (2009) Variation of hydrological regime with permafrost coverage over Lena Basin in Siberia. J Geophys Res Atmos 114(D7)

Yershov ED (2004) General geocryology. Cambridge university press, Cambridge

Zhang T (1993) Climate, seasonal snow cover and permafrost temperatures in Alaska north of the Brooks Range. Ph.D, University of Alaska Fairbanks

Zhang TJ (2005) Influence of the seasonal snow cover on the ground thermal regime: an overview. Rev Geophys 43(4). https://doi.org/10.1029/2004rg000157

Zhang T (2012) Progress in global permafrost and climate change studies. Quat Sci 32:27–38

Zhang T, Osterkamp TE, Stamnes K (1996) Influence of the depth hoar layer of the seasonal snow cover on the ground thermal regime. Water Resour Res 32(7):2075–2086

Zhang T, Barry RG, Knowles K, Heginbottom J, Brown J (1999) Statistics and characteristics of permafrost and ground-ice distribution in the Northern Hemisphere. Polar Geogr 23(2):132–154

Zhang Y, Chen W, Cihlar J (2003) A process-based model for quantifying the impact of climate change on permafrost thermal regimes. J Geophys Res 108(D22)

Zhang Y, Chen W, Smith SL, Riseborough DW, Cihlar J (2005) Soil temperature in Canada during the twentieth century: Complex responses to atmospheric climate change. J Geophys Res 110(D3)

Zhang T, Barry RG, Knowles K, Heginbottom JA, Brown J (2008) Statistics and characteristics of permafrost and ground-ice distribution in the Northern Hemisphere. Polar Geogr 31(1–2):47–68. https://doi.org/10.1080/10889370802175895

Zhao L, Wu QB, Marchenko SS, Sharkhuu N (2010) Thermal state of permafrost and active layer in Central Asia during the international polar year. Permafr Periglac 21(2):198–207. https://doi.org/10.1002/ppp.688

Zhong X, Zhang T, Wang K (2014) Snow density climatology across the former USSR. Cryosphere 8(2):785

Dr. Lin Zhao is a Professor at the Nanjing University of Information Sciences & Technology, China. He used to be a Senior Research Scientist at the Northwest Institute of Eco-Environment and Resources, Chinese Academy of Sciences; a Professor at the University of Chinese Academy of Sciences; the manager of the Qinghai–Tibet Plateau (QTP Cryosphere Observation and Research Station, Chinese Academy of Sciences). He served as the representative of the International Permafrost Society, International Permafrost Land temperature monitoring network. His research included the distribution and characteristics of permafrost on the QTP, hydrothermal physical processes of permafrost, permafrost and global changes, and interaction between permafrost and ecology, soil in permafrost regions. He has more than 150 journal publications. E-mail: lzhao@nuist.edu.cn

Dr. Cangwei Xie is a Research Scientist at the Northwest Institute of Eco-Environment and Resources, Chinese Academy of Sciences; a Deputy Chief of the Qinghai–Tibet Plateau Cryosphere Observation and Research Station, Chinese Academy of Sciences. He is engaged in research on hydrology, glaciology, and permafrost in cold regions. As a team leader and member, he participated in many field trips in the permafrost and Tianshan glaciers in the Qinghai–Tibet Plateau. From October 2010 to August 2014, he conducted collaborative research at the University of Toronto and McMaster University in Canada, and participated in the development of the Cold Regions Hydrological Model. He has strong skills in using numerical methods to solve geoscience problems.

Dr. Daqing Yang is a Research Scientist at the Watershed Hydrology and Ecology Research Division, Environment and Climate Change Canada. He is also Affiliate Research Professor at the International Arctic Research Center, Univ. of Alaska Fairbanks. Over the past 25 years, he has conducted cryosphere system research in China, Canada, Japan, USA, and Norway. His primary research activities/interests include cold region hydrology and climate, particularly Arctic large river streamflow regime and change, snow cover and snowfall measurements, climate change and human impact to regional hydrology, and applications of remote sensing in cold regions. He has served as journal editor and subject editor for IAHS publications (cold region hydrology, northern research basin water balance, and cold/mountain region hydrological systems under climate change), and WMO technical reports (solid precipitation measurement intercomparison and integrated global observing strategy cryosphere theme). He also contributed as review and/or author to the IPCC Reports, and the Arctic Council's Snow, Water, Ice and Permafrost in the Arctic (SWIPA 2017 and follow up) assessment. His current research focuses on investigating the impacts of climate variability/change and human activities on hydrologic system across the broader northern regions.

Dr. Tingjun Zhang is Professor at the School of Earth and Environmental Sciences, Lanzhou University in China. He was a Senior Research Scientist and Fellow of the Cooperative Institute for Research in Environmental Sciences, University of Colorado at Boulder. Over the past 3 decades, he has published more than 150 peer-reviewed articles in the national and international scientific journals. His research interests include climate and climate change in cold regions, heat and mass transfer in porous media, interactions between changes in frozen ground/snow cover conditions and hydrological/carbon cycles, numerical modeling of geophysical phenomena and comparison with measurements, application of satellite remote sensing data to study snow, near-surface soil freeze/thaw status, and northern phenomena. He has organized numerous national and international scientific conferences and workshops. He is currently serving on several editorial boards of the international scientific journals and has also been invited to serve as Guest Editors. He was a lead author of the IPCC Fourth Assessment Report from 2003 through 2007, in charge of the assessment of changes in frozen ground worldwide.

Permafrost Hydrology: Linkages and Feedbacks

16

Tetsuya Hiyama, Daqing Yang, and Douglas L. Kane

Abstract

In the cold regions, hydrological regime is closely related with permafrost conditions, such as permafrost extent and thermal characteristics. Ice-rich permafrost has a very low hydraulic conductivity and commonly acts as a barrier to deeper groundwater recharge or as a confining layer to deeper aquifers. In regions underlain by permafrost, the active layer is the upper layer of the soil near the surface that undergoes thawing in the summer and freezing in the fall. The thawing starts from the surface in the spring, and the active layer reaches its maximum in late summer. The lower boundary of this layer is the top of the permafrost layer. The active layer is considered to produce base flow (or low flow) during the ice-free season. In this chapter, we discuss relationship between permafrost coverage and streamflow regime, detection of permafrost thawing trends from long-term streamflow data, determination of permafrost groundwater age, and water balance of northern permafrost basins.

Keywords

Permafrost coverage · Base flow (low flow) · Basin (terrestrial) water storage · Permafrost thawing trends · Groundwater age · Water balance

T. Hiyama (✉)
Institute for Space-Earth Environmental Research, Nagoya University, Nagoya Aichi, Japan
e-mail: hiyama@nagoya-u.jp

D. Yang
Environment and Climate Change Canada, Watershed Hydrology and Ecology Division, Victoria, British Columbia, Canada
e-mail: daqing.yang@canada.ca; daqing.yang@gmail.com

D. L. Kane
Water and Environment Research Center, University of Alaska Fairbanks, Fairbanks, AK, USA
e-mail: dlkane@alaska.edu

D. Yang and D. L. Kane (eds.), *Arctic Hydrology, Permafrost and Ecosystems*,
https://doi.org/10.1007/978-3-030-50930-9_16

16.1 Introduction

In the cold regions, hydrological regime is closely related with permafrost conditions, such as permafrost extent and thermal characteristics. Ice-rich permafrost has a very low hydraulic conductivity and commonly acts as a barrier to deeper groundwater recharge or as a confining layer to deeper aquifers (Ye et al. 2009). Because it is a barrier to recharge, permafrost increases the surface runoff and decreases subsurface flow. Permafrost extent over a region plays a key role in the distribution of surface–subsurface interaction (Carey and Woo 2001; Woo et al. 2008a). Permafrost and non-permafrost rivers have very different hydrologic regimes. Relative to non-permafrost basins, permafrost watersheds have higher peak flow and lower base flow (Woo 1986; Kane 1997). In the permafrost regions, watersheds with higher permafrost coverage have lower subsurface storage capacity and thus a lower winter base flow and a higher summer peak flow (Woo 1986; Kane 1997; Yang et al. 2003). It is a challenge to accurately determine changes in permafrost conditions. Our understanding of permafrost change and its effect on hydrological regime is incomplete. For instance, there are uncertainties regarding the impact of ground ice melt and its contribution to annual flow changes over large Siberian rivers (McClelland et al. 2004; Zhang et al. 2005a). Permafrost condition and streamflow characteristics vary within large watersheds in the northern regions. Examination and comparison of hydrological regimes between subbasins with various permafrost conditions can improve our understanding of impact of permafrost changes on cold region hydrology. Areas covered in this chapter are flow regimes in permafrost watersheds and the relationship with basin water storage (or terrestrial water storage) as well as permafrost coverage, base flow change and its indication for permafrost thawing, permafrost groundwater age, and basin water balance in the northern river basins.

16.2 Basin Permafrost Coverage and Flow Regime

Ye et al. (2009) examined the relationship between hydrological regime and permafrost coverage over nested subbasins within the Lena River in eastern Siberia. They analyzed monthly discharge data, with a focus on the ratio of the maximum to minimum discharge (Q_{max}/Q_{min}) and its relation with permafrost condition, because this ratio reflects the hydrological regime. The aim of their study is to quantify the impact of permafrost on streamflow regime and change, and to specifically define a relationship between basin permafrost extent and streamflow conditions over the Lena watershed. Ye et al. (2009) also examined relationship between basin air temperature and precipitation and their effects on permafrost extent and basin streamflow regimes. The results of their study enhance our knowledge of cold region hydrology and its change due to climate impact and human influence.

The Lena River originates from the Baikal Mountains in the southern part of central Siberian Plateau and flows northeast and north, entering into the Arctic Ocean via the Laptev Sea (Fig. 16.1). Its drainage area is about 2,430,000 km^2, mainly

covered by forest and underlain by permafrost. The Lena River contributes 524 km^3 of freshwater per year, or about 15% of the total freshwater flow into the Arctic Ocean (Yang et al. 2002; Ye et al. 2003). Relative to other large rivers, the Lena basin has less human activities and much less economic development (Dynesius and Nilsson 1994). There is only one large reservoir in the Vilui subbasin. A large dam (storage capacity 35.9 km^3) and a power plant were completed in 1967 near Chernyshevskyi (112.15 °E, 62.45 °N). This reservoir is used primarily for electric power generation: holding water in spring and summer seasons to reduce snowmelt and rainfall floods and releasing water to meet the higher demand for power in winter (Ye et al. 2003). Various type of permafrost exists in the Lena basin, including sporadic, or isolated permafrost in the source regions, and discontinuous and continuous permafrost in downstream regions (Fig. 16.1) (Brown et al. 1997). Approximately 78–93% of the Lena basin is underlain by permafrost (Zhang et al. 1999; McClelland et al. 2004). An overview of the geographical scope of the Lena River basin and the seasonal changes and long-term trends of the Lena River discharge are also described in detail by Hiyama et al. (2019).

Monthly discharge regimes vary over the Lena basin, although it is generally high in summer and low in winter. The ratio of Q_{max}/Q_{min} is a direct measure of hydrologic regime. They increase with drainage area from the headwaters to downstream within the Lena basin. This pattern is different from the non-permafrost watersheds. The ratios also change with basin permafrost coverage, suggesting that permafrost affects regional hydrological features. Regression analysis between the Q_{max}/Q_{min} ratio and basin Coverage of Permafrost (CP) reveals a significant relationship at 99% confidence. This relationship quantifies the effect of permafrost distribution on discharge process. It shows that permafrost conditions do not significantly affect streamflow regime over the low permafrost (less than 40%) regions, and it strongly

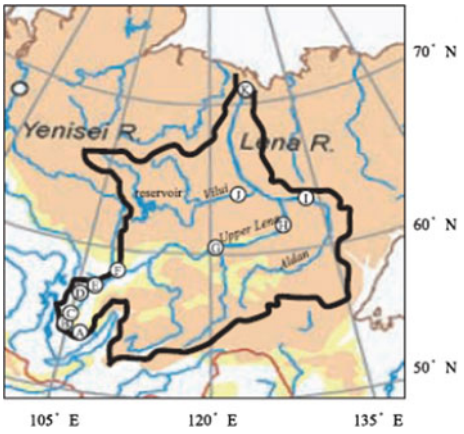

Fig. 16.1 The Lena River watershed permafrost distribution and hydrological stations (A through K) used in Ye et al. (2009)

affects discharge regime for regions with high (greater than 60%) permafrost coverage (Fig. 16.2). It is important to define this relation of permafrost impact to regional hydrology, as this knowledge is useful for further investigation into permafrost effect on basin hydrology over the large northern regions. On the other hand, temperature (T) and precipitation (P) have similar patterns among the subbasins. Basin precipitation has little association with permafrost conditions. There is a reasonable relationship between the freezing index and permafrost extent over the basin, indicating that cold climate leads to high coverage of permafrost. This relationship is useful to examine basin thermal condition with permafrost distribution. The combination of the relations between T–CP and CP–Q_{max}/Q_{min} links temperature, permafrost, and flow regime over the Lena basin. The variations in the Q_{max}/Q_{min} ratios reflect hydrologic regime changes. Trend analyses of the ratios show different results over the Lena basin. The ratios significantly decrease in the Vilui valley and at the Lena basin outlet due to dam regulation. In the unregulated upper Lena regions, the ratios do not show any trend during 1936–1998. This may imply that the permafrost changes in the region were not sufficient to affect hydrological processes. In the Aldan tributary without regulation, the ratios significantly decrease due to increase in base flow during 1942–1998. This change is consistent with significant group temperature warming (Fedorov et al. 2014a) and permafrost degradation over the eastern Siberia (Fedorov et al. 2014b). This consistency to some extent verifies permafrost influence on basin streamflow process and change (Ye et al. 2009).

Yang et al. (2014) recently used various statistical approaches for data analyses to calculate the mean, and standard deviation of the long-term daily discharge records of the Mackenzie River. Relative to other seasons, the minimum daily flows (usually in the winter season) range from 1680 to 4090 $m^3\ s^{-1}$ over the study period. The interannual variation is much smaller than that for the maximum daily flows. There is a weak tendency in the minimum daily flow increase during 1973 to

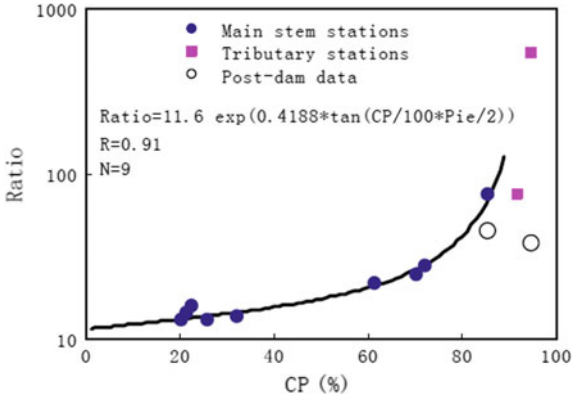

Fig. 16.2 The ratios of Q_{max}/Q_{min} versus Coverage of Permafrost (CP) at the nine stations from the upper Lena to basin outlet. Two additional stations (the Aldan and Vilui subbasins) are also shown Ye et al. (2009)

2011. This change in flow amount is very small and statistically insignificant; it is thus almost undetectable in terms of its contribution to the total flow, i.e., stable ratios of minimum daily flow/mean daily flow over the study period. It is important to mention that base flow increase has been reported for the northern regions and the Northwest Territories (NWT), Canada, due to recent climate warming (Woo et al. 2008a, b; Woo and Thorne 2014; St. Jacques and Sauchyn 2009). Yang et al. (2014) discovered Mackenzie basin monthly discharge increases during September to April. Basin water storage changes affect low-flow conditions and their changes. The Mackenzie basin has large seasonal storages due to many large lakes in the basin. The increases in the monthly and daily low flows may reflect changes in the basin storages, including lakes, groundwater, and permafrost and ground ice. Walvoord and Striegl (2007) also reported an increase in groundwater to stream discharge from permafrost thawing in the Yukon River basin. Suzuki et al. (2018) compared river discharge (R) and the GRACE (Gravity Recovery and Climate Experiment)-derived Terrestrial Water Storage (TWS) in the three largest pan-Arctic river basins from April 2002 to December 2016. They revealed strong positive correlations between R and TWS for the Lena River and Mackenzie River basins, but no significant correlation for the Yukon River basin, where TWS was sensitive to the changes in evapotranspiration. They also detected that the TWS among the three river basins was further controlled by the presence of continuous permafrost. Namely, the autumnal TWS in the Lena River basin, which exhibits continuous permafrost, persisted R through the spring of the following year. However, no such effect was observed in the Mackenzie River catchment, which is partially covered in both continuous permafrost and discontinuous permafrost. These results suggest regional to large scale change in permafrost characteristics. There is therefore a need to continue to explore the relationship among climate, river flow, and permafrost conditions over the high-latitude regions.

16.3 Detection of Permafrost Thawing Trends from Long-Term Streamflow Measurements

The low flows in a basin generally are fed by groundwater seepage from the upstream riparian aquifers in the basin. In the cold regions, permafrost thawing and permafrost growth directly affect the groundwater storage amount and mobility, which in turn control the seepage from these aquifers. Thus, long-term streamflow records are a useful but hitherto unexplored source of information on the past history of permafrost changes during the same period. On the basis of this principle and hydraulic groundwater theory, Brutsaert and Hiyama (2012) proposed three methods to relate low flows during the open water season with the rate of change of the active groundwater layer thickness resulting from permafrost thawing at the scale of the upstream river basin. They applied their methods to detect basin-scale permafrost thawing trends from long-term summertime base flow measurements.

16.3.1 Base Flow and Basin-Scale Groundwater Storage

The proposed approach is an extension of a method developed earlier (Brutsaert 2008, 2012; Brutsaert and Sugita 2008) to determine groundwater storage changes, as manifested in available streamflow records. Streamflow occurring in the absence of precipitation or upstream water inputs is referred to variously as base flow, fair weather flow, drought flow, or low flow; it can normally be assumed to consist of the cumulative outflow from all upstream phreatic aquifers along the banks. The lowest of the low-flow recessions, as small perturbations of the no-flow steady state, can simply be expressed as an exponential decay phenomenon and can be formulated as

$$y = y_0 \exp(-t/K) \tag{16.1}$$

where y is the rate of flow in the stream per unit of catchment area, y_0 is the value of y at the arbitrarily selected time origin t = 0, and K is the characteristic time scale of the catchment drainage process, also commonly referred to as the storage coefficient. Note that 0.693 K can be considered the storage half-life of the upstream riparian aquifers. The water stored in a river basin can be expressed as linear relationship between groundwater storage S = S(t) and base flow y = y(t), as

$$S = Ky. \tag{16.2}$$

The storage S can be visualized as the average thickness of a layer of water above the zero flow level. However, the thickness of this layer occupied inside the soil profile is larger than S. In the simplest approach, capillary effects above the water table are parameterized by means of the drainable porosity n_e, also known as the specific yield. This means that the water table is assumed to be a free surface and the fraction of the soil volume occupied by free and movable water is assumed to be n_e. The average thickness of the water layer stored in the soil profile, that is the active groundwater layer above permafrost, is given by

$$\eta_0 = S/n_e. \tag{16.3}$$

Before using (16.2) and (16.3) to relate changes in average layer thickness η_0 with observed changes in base flow y, it is necessary to determine how changes in η_0 might affect the drainage time scale parameter K.

16.3.2 Active Groundwater Layer Thickness Trend

If it can be assumed that n_e in the aquifer remains unaffected by changes in the underlying permafrost layer, the determination of the growth of the groundwater active layer can be expressed as follows:

$$\frac{\mathrm{d}\eta_0}{\mathrm{d}t} = \frac{K}{2n_e}\frac{\mathrm{d}y}{\mathrm{d}t}. \tag{16.4}$$

If a good estimate of the drainable porosity n_e and of the drainage time scale K is unavailable or impossible, but an estimate of a reference or typical value of the layer thickness, say η_{0r}, can be obtained, an alternative expression can be derived.

$$\frac{\mathrm{d}\eta_0}{\mathrm{d}t} = \frac{\eta_{0r}}{2y_r}\frac{\mathrm{d}y}{\mathrm{d}t} \tag{16.5}$$

where y_r is a typical or reference base flow around the time when η_{0r} was observed. The choice between (16.4) and (16.5) has to depend on the availability of estimates of K, n_e, and η_{0r}.

Whenever an estimate of a reference or typical value of the active groundwater layer thickness η_{0r} is available, and because the drainage time scale K is inversely proportional to η_0, the growth rate of the active groundwater layer can also be written as

$$\frac{\mathrm{d}\eta_0}{\mathrm{d}t} = \eta_{0r}K_r\frac{\mathrm{d}K^{-1}}{\mathrm{d}t} \tag{16.6}$$

where K_r is the value of the drainage time scale at the time of η_{0r}.

16.3.3 Application to the Lena River Basin

The three methods were tested with data from four gaging stations within the Lena River basin in eastern Siberia. The data were obtained from two sources. The daily discharge data for the period 1950–2003 were obtained through courtesy of the Japan Agency for Marine-Earth Science and Technology (JAMSTEC), whereas for the more recent period 2000–2009, they were obtained from R-ArcticNet (A Database of Pan-Arctic River Discharge developed by the Water Systems Analysis Group at the University of New Hampshire). The three methods were applied with the streamflow data of May through September for each decade from 1950 through August 2009 for the four subbasins (upper Lena, Olyokma, and two Aldan subbasins) in the Lena River watershed.

Because, sometimes, daily flow data are subject to measurement uncertainties, it was decided to use a running average of five days as a more reliable measure of y. These annual lowest 5-day flows were calculated for each of the four basins, and the resulting values were then used to calculate the changes in base flow dy/dt, which are needed for (16.4) and (16.5). Beside dy/dt, a knowledge is required for the characteristic drainage time scale K and of its long-term changes $\mathrm{d}K^{-1}/\mathrm{d}t$ or dK/dt. The procedure consists of determining the lower envelope of a logarithmic plot of appropriate −dy/dt data versus the corresponding y data; it also makes use of the observations for y = − K(dy/dt).

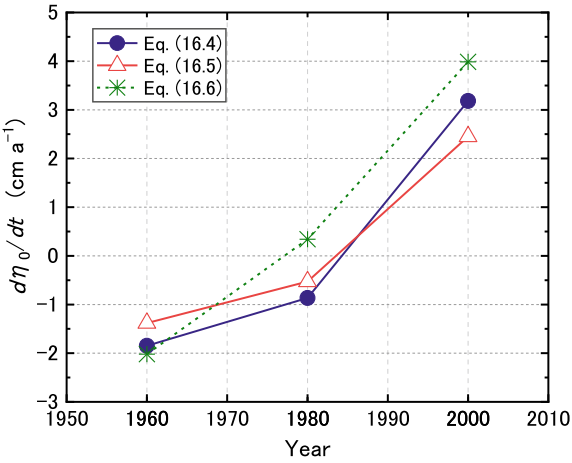

Fig. 16.3 Trends of the active groundwater layer thickness $d\eta_0/dt$ in cm a^{-1} over the periods 1950–1969, 1970–1989, and 1990–2008 in the Aldan subbasin (Aldan-2 (A2) of Brutsaert and Hiyama 2012). Needed values for the use of Eq. (16.4) were $n_e = 0.01$ and $K = 46.33$ as the station average. Those for Eq. (16.5) were $\eta_{0r} = 1.88$ m and y_r as average of the annual lowest 5-day flows during each period. Those for Eq. (16.6) were $\eta_{0r} = 1.88$ m and $K_r = 46.33$ as the station average

In the three expressions to calculate $d\eta_0/dt$, namely (16.4), (16.5), and (16.6), it would seem that (16.5) is the most parsimonious one because only required knowledge or input is the average active groundwater layer depth η_{0r} at the end of summer. Based on the ground temperature measurements during 1956–1990 at 17 stations over the Lena River basin, Zhang et al. (2005b) found the average active layer thickness to be 1.88 m, ranging from 1.2 m to 2.3 m. With the assumptions that $\eta_{0r} = 1.88$ m, and that y is the average of the annual lowest 5-day flows during each period, it is possible to implement (16.5). The results of this application for the Aldan subbasin are presented in Fig. 16.3.

Equation (16.4), similar to (16.5), can also be implemented by means of the values of dy/dt with the average of the annual lowest 5-day flows. In addition, however, values of K and of n_e are required. No information is available for the drainable porosity n_e in the Lena region. On the basis of several findings (e.g., Brutsaert 2008) and in the absence of more specific information of n_e, (16.4) was implemented with the values of $n_e = 0.01$, dy/dt using the average of the annual lowest 5-day flows during each period, and K averaged over each of the three periods. The results are presented and compared in Fig. 16.3 with that from (16.5) so as to check how realistic the adopted value n_e is. The results from (16.4) can match that from (16.5) by very slightly adjusting n_e from 0.01 to 0.0121. This is a very small change that supports the use of the present rough estimate of $n_e = 0.01$.

For the application of (16.6), the $d(K^{-1})/dt$ values were calculated as finite differences between the values of K^{-1} at different times. The required values of K_r

were taken as the average values for each basin, and the corresponding value of the active groundwater layer thickness was given as η_{0r} = 1.88 m. Relative to the results obtained with (16.4) and (16.5), (16.6) produced higher $d\eta_0/dt$ in general (Fig. 16.3). It is difficult to judge or assess which method had the best performance. Due to subjective determination of K and a fortiori its derivatives $d(K^{-1})/dt$ for (16.6), and the relatively straightforward way of determining dy/dt, it seems that (16.4) and (16.5) should be given preference over (16.6). Because (16.5) makes use of measured data, it should probably be given preference over (16.4).

Brutsaert and Hiyama (2012) also compare the values of $d\eta_0/dt$ with the recent field observations, which indicate acceleration in permafrost deterioration. At the study site of Spasskaya Pad, some 20 km north of Yakutsk, the annual maximum depth of the 0 °C isotherm was recorded (Ohta et al. 2008) to increase from around 1.27 m in 1998 to 2.0 m in 2006, i.e., an average rate of about 9.1 cm a^{-1}. On the other hand, in a parallel study at the same location (Iijima et al. 2010), manual observations of the annual maximal thaw depth by a frost tube indicated that between 2000 and 2007 it increased from around 1.37–1.67 m, i.e., at a rate of about 3.3 cm a^{-1}. Since manual measurements are considered more reliable, the latter rate of 3.3 cm a^{-1} is probably more representative. This change is in agreement with the results shown in Fig. 16.3.

16.4 Determination of Permafrost Groundwater Age

Understanding groundwater characteristics such as pathways and residence time (groundwater age) is the most important research issue in groundwater hydrology as well as for sustainable use of groundwater resources. This issue is also applicable for permafrost region. Transient tracers such as tritium (^{3}H), chlorofluorocarbons (CFCs), and sulfur hexafluoride (SF_6) have been widely used to determine groundwater age in humid and semi-arid regions (Busenberg and Plummer 1992, 2000; IAEA 2006). However, only a few studies have used such tracers in permafrost regions. Hiyama et al. (2013) is one of such researches, and they have applied transient tracers to detect groundwater age to several spring discharges in eastern Siberia. In this section, the paper of Hiyama et al. (2013) is introduced and revisited very briefly.

16.4.1 Groundwater Age Estimation Using ^{3}H

Tritium (^{3}H) concentration has previously been used for estimating groundwater age, especially in the Northern Hemisphere. The ^{3}H concentration of precipitation peaked around 1963 due to nuclear testing (Fig. 16.4a). The half-life of ^{3}H is relatively short (12.3 years), and therefore when nuclear testing was terminated the concentration declined. However, if the mean residence time of permafrost

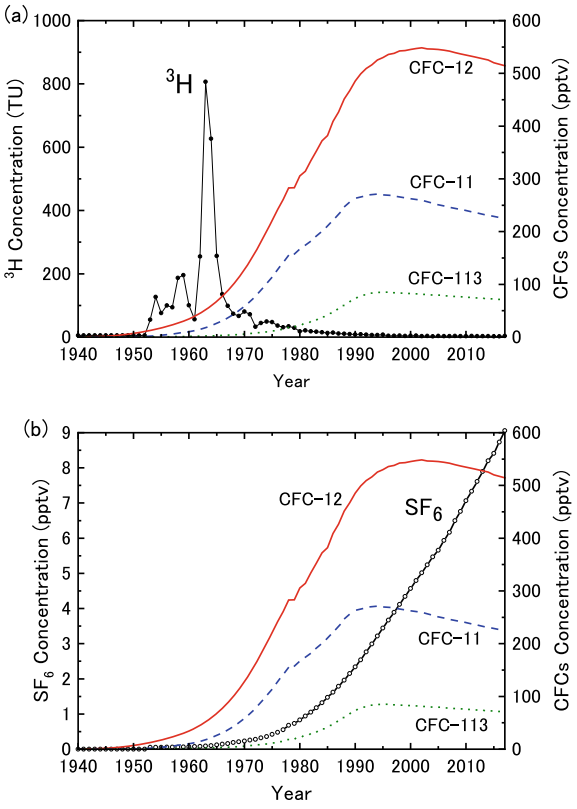

Fig. 16.4 Time series of the tritium (^{3}H) concentration (TU) in precipitation **a** obtained at Ottawa, Canada, observed by IAEA (International Atomic Energy Agency) (https://nucleus.iaea.org/wiser/index.aspx). Also shown are the atmospheric CFCs concentrations (**a**, **b**) and the atmospheric SF_6 concentration **b** observed by the Reston Groundwater Dating Laboratory of the USGS (US Geological Survey) (https://water.usgs.gov/lab/software/air_curve/index.html)

groundwater is around 50–60 years, ^{3}H may be a useful tracer to detect the extent to which the groundwater originated from precipitation after nuclear testing.

16.4.2 Groundwater Age Estimation Using CFCs and SF_6

CFCs and SF_6, as transient tracers, can also be used to estimate groundwater age (IAEA 2006). CFCs are anthropogenic gases that were emitted into the atmosphere from the 1930s to 1987. Atmospheric concentrations of the major CFCs such as dichlorodifluoromethane (CCl_2F_2; CFC-12), trichlorofluoromethane (CCl_3F; CFC-11), and trichlorotrifluoroethane ($C_2Cl_3F_3$; CFC-113) peaked in the 1990s (Fig. 16.4). SF_6 emissions began in the 1960s as it was used as an isolation gas, and its use continued through recent decades (Fig. 16.4b). Thus, CFCs can be used to estimate groundwater age recharged around 30–80 years ago. SF_6 can also be used for groundwater recharged around 1–50 years ago.

Three assumptions are needed when we apply CFCs and SF_6 concentrations to estimate groundwater age. First, the sampled water truly contained CFCs and SF_6 concentrations of the target groundwater in the aquifer. Second, the recharged water

reached full equilibrium in solubility with the soil gas (or the atmosphere), and the dissolved CFCs and SF_6 were preserved within the aquifer. Third, ground ice melting in permafrost contributes to decline the concentrations of CFCs and SF_6 of the aquifer. This is because the above-mentioned assumptions could be also applied to the permafrost groundwater layer.

Henry's solubility law (e.g., Warner and Weiss 1985) is used to estimate recharge year (when the sampled water entered the aquifer) from the dissolved CFCs and SF_6 in the sampled water. For accurate chemical analyses of dissolved CFCs and SF_6 concentrations in the sampled water, they should be kept isolated from the ambient atmosphere. Using analyzed concentrations of CFC-12, CFC-11, CFC-113, and SF_6 from the sampled spring water together with temperature and elevation data, it is possible to estimate the recharge year using Henry's solubility law.

16.4.3 Application to the Lena River Basin

Spring water samples were taken in July 2009, July 2010, August 2011, and August 2012, at four sites: Buluus (61°20'N, 129°04'E), Ulakhan-Taryn (61°34'N, 129°33'E), Eruu (61°42'N, 129°45'E), and Michita (61°23'N, 129°11'E) discharges. These four spring discharges are hydrological monitoring sites of the Melnikov Permafrost Institute of the Siberian Branch of the Russian Academy of Sciences.

^3H counting was conducted using a low-background liquid scintillation counter, Aloka model LB5, following electrolytic enrichment of ^3H by a factor of about 25 using Fe–Ni electrodes. Total analytical precision was better than ± 0.23 tritium unit (TU) ($\pm 1\sigma$). The ^3H measurements were conducted at the Geo-Science Laboratory Co. Ltd, Nagoya, Japan. CFC content in the samples was measured using a purge and trap Gas Chromatography procedure with an Electron Capture Detector (GC-ECD) at the Geo-Science Laboratory Co. Ltd, Nagoya, Japan. The procedure involved stripping 40 mL sample water of CFCs using ultra-pure nitrogen gas. The extracted CFCs were purified and concentrated using a cold trap, and finally injected into the GC-ECD. The precision and detection limit of the analysis were less than 2% and 1 pg L^{-1}, respectively. SF_6 content was measured using the same procedure and GC-ECD at the Geo-Science Laboratory. The only difference was that, after stripping 400 mL sample water, the extracted SF_6 was purified and concentrated using two cold traps. The precision and detection limit of the analysis were less than 3% and 0.05 fmol L^{-1}, respectively.

^3H was detected in all of the spring water. The concentration at Buluus and Eruu springs was higher (9–11 TU) than that at Ulakhan-Taryn spring (1–7 TU). ^3H concentration at Michita is the highest (15–17 TU). The clear difference among the springs indicates that the origin and mixing conditions of groundwater are different. There was no significant difference in ^3H concentration at Buluus and Michita in the sampling years (2009–2012). Buluus and Eruu springs may have mostly originated from precipitation that recharged the aquifer after the nuclear testing period of the 1960s. If we assume that groundwater pathways in talik zone have a piston-like

flow, the ages of the Buluus and Eruu spring water can be estimated to be about 1–40 years old. However, because the ^{3}H concentrations of both samples were not significantly higher than those of precipitation at Yakutsk, the water of Buluus and Eruu may contain older precipitation recharged before nuclear testing. Ulakhan-Taryn was the lowest value compared to Buluus, Eruu, and Michita. As ^{3}H concentration of the Ulakhan-Taryn samples was clearly lower than that of precipitation that fell after the 1960s, it may have been recharged mostly by precipitation before the 1960s. If we set the ^{3}H concentration of precipitation after the 1960s at 16 TU (the current value at Yakutsk), and that before the 1960s as 0.5 TU (the concentration of the 1950s), the percentages of precipitation recharge before the 1960s to the Ulakhan-Taryn spring water are 90–95%. If we assume that groundwater pathways have a piston-like flow, the recharge year of the spring water can be estimated as 1955, i.e., the age of the groundwater is 55 years. The Michita water seems to have been recharged by very recent precipitation.

CFC-12 was detected at all sites. However, CFC-113 was not detected at Ulakhan-Taryn and Eruu springs. This may have been caused by deoxidizing conditions at Ulakhan-Taryn and Eruu. Under deoxidizing conditions, methane-producing bacteria appear to remove dissolved CFC-11 and CFC-113 (Happell et al. 2003). In contrast, three kinds of CFCs (CFC-12, CFC-11, and CFC-113) were detected at Buluus and Michita. Thus, microbial degradation likely plays a smaller role at both springs. This means the groundwater age could be estimated more reliably at Buluus and Michita.

The concentration of SF_6 ranged from 1.71 to 5.67 fmol kg^{-1}, and was higher at Michita and Buluus than at Ulakhan-Taryn and Eruu. This result is similar to that of the CFCs analysis, suggesting that the groundwater age of the Buluus and Michita springs is younger than that of the Ulakhan-Taryn and Eruu springs.

The equivalent air concentration of the three CFCs and the SF_6 was calculated using Henry's solubility law (Warner and Weiss 1985) in which the solubility potentials of CFCs and SF_6 depend on the air temperature and air pressure when the precipitation fell. Because the water should be recharged above 0 °C, representative value of the temperature was assumed to be 0 °C. Mean surface elevation of the recharge area was assumed to be 150 m based on the topography map. The estimated recharge years using the CFCs method were from around 20 to 40 years. However, those using the SF_6 were quite younger. The SF_6 concentration might have increased mainly due to the mixture of SF_6 from basement rock with permafrost groundwater, which would cause a younger estimate of SF_6-based groundwater age. Another possible reason is due to excess air, redundant SF_6 may have dissolved into the recharging water, leading to overestimated SF_6 levels and thus younger groundwater ages. Although these differences were observed among three tracers (^{3}H, CFCs, and SF_6), the relative order of apparent ages was consistent with each other.

Finally, we should note that the ^{3}H-based ages and the CFC-12-based ages at Ulakhan-Taryn springs varied widely. This is because we applied a simple piston-like flow scheme to the groundwater system, although the samples were a mixture of supra-permafrost and intra-permafrost groundwater. It was not possible

to separate these two types of permafrost groundwater. Nevertheless, it should be noted that large variability in the concentrations of ^{3}H and CFC-12 at Ulakhan-Taryn indicates unstableness of groundwater pathways and its recharge sources. Because soil pore ice was found below the active layer, i.e., between the active layer and the upper boundary of the intra-permafrost groundwater aquifer in this area, melted pore ice could contribute to the source of the spring water at Ulakhan-Taryn.

16.5 Water Balance of Northern Permafrost Basins

Water balance analysis is a widely used tool for evaluating the availability and sustainability of water resources and supply (Healy et al. 2007). Carried out for a long enough period, the results of water balance calculation can be useful for quantifying natural variability, climate change, and man-induced alterations. Ice, snow, frozen soils, and large annual fluctuations in the surface energy balance are characteristics of the high-latitude watersheds. The hydrologic responses of northern watersheds differ from those in the temperate regions, and such differences should be reflected in the water balance results. The difficulty in quantifying these differences is mainly due to few water balance studies at high latitudes, often marginally supported and only for short study periods.

Most of the early studies concentrated on watersheds in areas of discontinuous permafrost because of logistical reasons. To carry out water balance computations, it is necessary to measure liquid and solid precipitation and runoff and to make estimates of evapotranspiration losses and any significant changes in storage. All these elements of the hydrologic cycle in the high latitudes are quite variable and often are not accurately measured.

Water balance data from 39 high-latitude watersheds (Fig. 16.5) over the past 50 or more years were presented and discussed in a synthesis workshop in 2004 at Victoria, BC, Canada (Kane and Yang 2004a). Less than one-third of these watersheds continue to be active. These studies ranged from one year in length to over 50 years (Seuna and Linjama 2004). Characteristically, these experimental watersheds are small, from less than 1 km^2 to 432 km^2.

The three main features of the water balance equation are the input (P), changes in various storage terms (DS), and outputs (ET and R):

$$P = ET + R \pm DS_{sur} \pm DS_{sub} \pm DS_{vad} \pm DS_{glac} \pm DS_{snow/ice} + \eta \qquad (16.7)$$

where P is precipitation, including both snowfall and rainfall (and possibly also condensation), ET is evapotranspiration (possibly also sublimation), R is discharge throughout the entire period of flow, DS_{sur} is change in surface storage (lakes, wetlands, reservoirs, channels, etc.), DS_{sub} is change in subsurface storage of groundwater, DS_{vad} is change in storage of unsaturated (vadose or active layer) zone, DS_{glac} is change in glacier storage, $DS_{snow/ice}$ is change in storage of

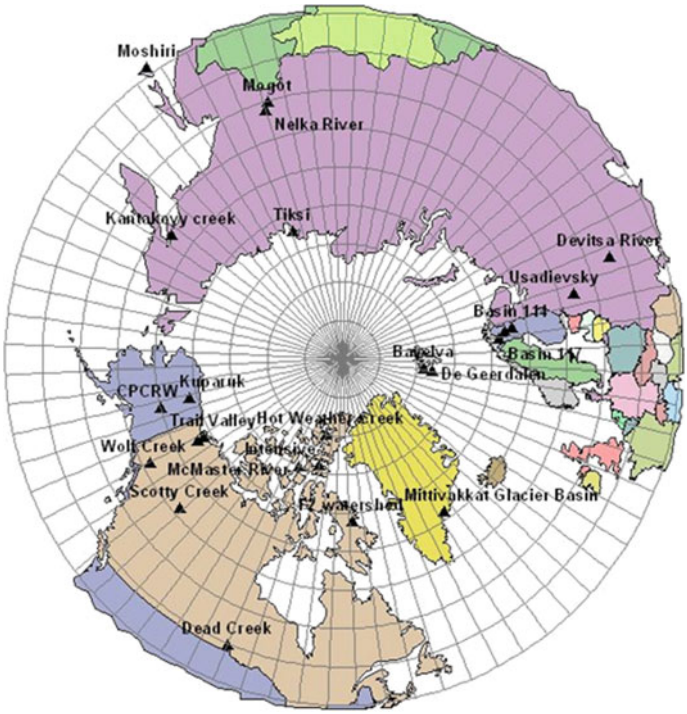

Fig. 16.5 Names and locations of 39 long-term water balance study watersheds in the northern regions. (map modified from Kane and Yang (2004a)

snowpack (including late-lying snowdrifts, aufeis, river and lake ice, etc.), and η is error term on closure. Typically, precipitation and discharge are measured by national hydrologic networks. However, in extreme environments, the error associated with these measurements can be considerable (e.g., the difficulties in measuring solid precipitation and streamflow in ice-choked drainages).

Except for experimental watersheds, all of the terms in this equation are seldom measured. ET is difficult to spatially and temporally quantify over a watershed through field measurements. Even for experimental watersheds, changes in the various storage terms are challenging to quantify; more often they are assumed to remain unchanged over a time period of a year (although this is seldom true). Theoretically, η should be zero, a condition seldom satisfied. For those watersheds where the error term was determined (Kane and Yang 2004b), the error ranged from zero to 27% of annual precipitation, with an average of about 8%. Assuming that the quality of measurements are the same in all research watersheds, this implies that overall researchers are doing a fair job of measuring the variables in the water balance equation, but it does not indicate the measurement error associated with each individual term. Although there are many limitations to these water balance

studies, they represent the best hydrologic data that we presently have for northern basins. Therefore, results from the IAHS Redbook papers (Kane and Yang 2004a) on the individual watersheds and the synthesis papers should be useful for verifying modeling results from meso- and global-scale climate models. For example, modeled fluxes should correspond reasonably close to measured fluxes from these individual watershed studies for a given region. This could be extended to estimate the latitudinal decrease in the precipitation rate based on the data obtained collectively from all watersheds, particularly for basins dominated by a continental climate. For the watersheds with a continental climate, there is a decreasing rate in annual precipitation of 16 mm/8 latitude (Kane and Yang 2004b). A similar decreasing trend is seen for more coastal watersheds, but their annual precipitation rates are higher.

On average, for all of the watersheds, about half of the annual precipitation leaves the basin as ET. Although there are some outliers, the decreasing trend in ET with latitude is numerically similar to that of precipitation. This trend is primarily driven by declining solar radiation at the surface (also reflected in the lower mean annual temperature) and in some cases by moisture limitation (e.g., in the Canadian High Arctic). Methods of measuring/estimating ET are quite variable, ranging from mass and energy balances to simple empirical methods (Kane et al. 1990; Mendez et al. 1998; Shutov et al. 2006). Owing to the wide variety of methods for obtaining ET and because of their disjointed measurement periods, it is difficult to elucidate its spatial and temporal variability. An area of pressing interest is to improve estimates of ET, particularly for larger areas.

In this context, newly produced reanalysis data are useful for detecting spatial and temporal variability of ET. Using multi-model ensemble of reanalyzed data from GLDAS1 and GLDAS2, Suzuki et al. (2018) revealed negative trend in the TWS throughout the Arctic Circumpolar Tundra Region (ACTR) and this was primarily driven by ET. Meanwhile, it was indicated that precipitation has a minor impact on the TWS.

The average percentage of annual precipitation is falling as snow increases with latitude from a low of about 10% to a high of about 80%. Again, there is considerable variation, particularly for coastal watersheds. It is apparent that the snow water equivalent of the annual snowpack for most watersheds, with the exceptions of some near the coast, is generally below 200 mm a^{-1} (Kane and Yang 2004b). Ideally, we should have several research watersheds in the circumpolar Arctic that have been in operation for several decades and are much larger than those described in Kane and Yang (2004b). This would allow us to capture the natural variability (both drought and flood conditions) and to look for trends in the fluxes and storage terms due to climate change. The present experimental watersheds are so small that when considered in the global context, they are no more than single points. It is also clear that we need to do a better job of actually measuring the various fluxes and storage reservoirs.

16.6 Summary and Future Directions

This chapter reviewed and discussed selected topics in permafrost hydrology of the northern regions, particularly the association of Lena river flow regime with permafrost coverage within nested watershed, base flow change and its implication to active layer variation, groundwater age, and water balance analyses in long-term experimental basins across the northern regions. Below are a brief summary of main discussions and some consideration for future research needs.

There are similarity and variation in streamflow regimes over the Lena watershed. The ratios of monthly maximum/minimum flows directly reflect discharge regimes. The ratios increase with drainage area from the headwaters to downstream within the Lena basin (Ye et al. 2009). It is important to point out that pattern is different from the non-permafrost watersheds, and it clearly reflects permafrost effect on regional hydrological regime. There is a significant positive relationship between the ratio and basin permafrost coverage. This relationship indicates that permafrost condition does not significantly affect streamflow regime over the low permafrost (less than 40%) regions, and it strongly influences discharge regime for regions with high permafrost (greater than 60%). This is consistent with the result of Suzuki et al. (2018). There is a need to refine this relationship for various climate and permafrost conditions in the high-latitude regions.

Three distinct procedures were developed by Brutsaert and Hiyama (2012) to relate summer low flows with the changes in the active groundwater layer thickness due to permafrost thawing in the upstream Lena river basin. Their methodology has distinct benefits: first, it provides a tool to upscale local measurements over the entire upstream river basin, possibly after calibration with such local measurements; second, it can produce historical information of permafrost conditions that predate most field observations since streamflow measurements started well before permafrost observations. Application of the methods in the Aldan subbasin of the Lena River show that, in the period 1950–1970, active layer thickness decreased without much thawing. However, from the 1990s onward, active layer growth rates were as high as 2 cm a^{-1} or more. These results agree with previously published active layer changes at many sites in eastern Siberia. However, accurate determination of the drainage time scale K and its temporal rate of change dK/dt or $d(K^{-1})/dt$ still poses challenges. Additionally, it should be noted that the four catchments in Brutsaert and Hiyama (2012) are too large to draw strong conclusions. It is thus recommended that the methods should be applied to smaller basins for validations. The loss of upper permafrost layer might be more serious than what Brutsaert and Hiyama (2012) estimated since they assumed that the entire catchment contributed to the base flow, whereas in reality the contributing area is limited to the immediate vicinity of the river channel.

The apparent ages of the mixture of supra-permafrost and intra-permafrost groundwater in the middle of the Lena River basin were estimated to be 1–55 years old. The spring water at Ulakhan-Taryn appeared to contain more than 90% recharge by precipitation before the 1960s nuclear testing era. Because soil pore ice

was found below the active layer around the site, melted ice could contribute to the source of the spring water. If recent global warming causes permafrost degradation in the region, it could drive changes of groundwater recharge source as well as the rates, especially increasing the contribution from thawing permafrost. It is important to note the insufficient data to characterize permafrost characteristics and groundwater conditions in cryohydrogeological point of view. Groundwater dating is one of the greatest challenges in permafrost regions.

There has been increased attention at the permafrost regions hydrology due to resource development and climate change over the northern regions. This chapter reflects some recent advances in permafrost hydrology. Much of the recent research has focused on surface water, less on springs and groundwater contribution to streamflow. It is very clear that data limitation and poor quality remain serious concerns for permafrost hydrology research and applications. A compendium of water balance research from 39 high-latitude catchments reveals the strengths and limitations of the available results, as most of the basins are restricted to only a few years of study at the small watershed scale. The response of discharge to climate receives increasing attention, including extreme hydrologic events to the changing flow regimes in large northern watersheds. The effect of climate change and the role of permafrost on the changing discharge of large pan-Arctic rivers are major interest for further investigation. Extended field and modeling research on physical processes will improve knowledge of permafrost hydrology and enhance its relevance to societal needs.

Acknowledgments Parts of this chapter (Sects. 16.3 and 16.4) were based on researches supported by Research Project No. C-07 of the Research Institute for Humanity and Nature (RIHN) entitled "Global Warming and the Human–Nature Dimension in Siberia: Social Adaptation to the Changes of the Terrestrial Ecosystem, with an Emphasis on Water Environments" (Principal Investigator: Tetsuya Hiyama). The editing work was partly supported by a grant from the Arctic Challenge for Sustainability (ArCS) Project of the Ministry of Education, Culture, Sports, Science and Technology (MEXT), Japan. We thank Prof. W. Brutsaert for his valuable comments.

References

Brown J, Ferrians OJ, Heginbottom JA, Melnikov ES (1997) Circum-Arctic map of permafrost and ground-ice conditions. Washington, DC: US Geological Survey in Cooperation with the Circum-Pacific Council for Energy and Mineral Resources

Brutsaert W (2008) Long-term groundwater storage trends estimated from streamflow records: climatic perspective. Water Resour Res 44:W02409. https://doi.org/10.1029/2007WR006518

Brutsaert W (2012) Are the North American deserts expanding? Some climate signals from groundwater storage conditions. Ecohydrol 5:541–549. https://doi.org/10.1002/eco.263

Brutsaert W, Hiyama T (2012) The determination of permafrost thawing trends from long-term streamflow measurements with an application in eastern Siberia. J Geophys Res 117:D22110. https://doi.org/10.1029/2012JD018344

Brutsaert W, Sugita M (2008) Is Mongolia's groundwater increasing or decreasing? The case of the Kherlen River Basin. Hydrol Sci J 53:1221–1229. https://doi.org/10.1623/hysj.53.6.1221

Busenberg E, Plummer LN (1992) Use of chlorofluorocarbons (CCl_3F and CCl_2F_2) as hydrologic tracers and age-dating tools: The alluvium and terrace system of central Oklahoma. Water Resour Res 28:2257–2283

Busenberg E, Plummer LN (2000) Dating young groundwater with sulfur hexafluoride: Natural and anthropogenic sources of sulfur hexafluoride. Water Resour Res 36:3011–3030

Carey SK, Woo M (2001) Slope runoff processes and flow generation in a subarctic, subalpine catchment. J Hydrol 253:110–129. https://doi.org/10.1016/S0022-1694(01)00478-4

Dynesius M, Nilsson C (1994) Fragmentation and flow regulation of river systems in the northern third of the world. Science 266:753–762

Fedorov AN, Ivanova RN, Park H, Hiyama T, Iijima Y (2014a) Recent air temperature changes in the permafrost landscapes of northeastern Eurasia. Polar Sci 8:114–128. https://doi.org/10.1016/j.polar.2014.02.001

Fedorov AN, Gavriliev PP, Konstantinov PY, Hiyama T, Iijima Y, Iwahana G (2014b) Estimating the water balance of a thermokarst lake in the middle of the Lena River basin, eastern Siberia. Ecohydrology 7:188–196. https://doi.org/10.1002/eco.1378

Happell JD, Price RM, Top Z, Swart PK (2003) Evidence for the removal of CFC-11, CFC-12, and CFC-113 at the groundwater–surface water interface in the Everglades. J Hydrol 279:94–105

Healy RW, Winter TC, LaBaugh JW, Franke OL (2007) Water budgets: foundations for effective water-resources and environmental management. US Geological Survey Circular 1308

Hiyama T et al (2013) Estimation of the residence time of permafrost groundwater in the middle of the Lena River basin, eastern Siberia. Environ Res Lett 8:035040. https://doi.org/10.1088/1748-9326/8/3/035040

Hiyama T, Hatta S, Park H (2019) River Discharge. In: Water-Carbon Dynamics in Eastern Siberia (Ohta T et al. eds). Ecol Stud 236/Springer, Singapore, pp 207–229. https://doi.org/10.1007/978-981-13-6317-7_9. ISBN:978-981-13-6317-7

IAEA (2006) Use of chlorofluorocarbons in hydrology–A Guidebook. International Atomic Energy Agency, Vienna

Iijima Y et al (2010) Abrupt increases in soil temperatures following increased precipitation in a permafrost region, central Lena river basin, Russia. Permafrost Periglacial Process 21:30–41. https://doi.org/10.1002/ppp.662

Kane DL (1997) The impact of Arctic hydrologic perturbations on Arctic ecosystems induced by climate change. In: Global change and Arctic terrestrial ecosystems. Ecol Stud 124/Springer, New York, pp 63–81

Kane DL, Gieck RE, Hinzman LD (1990) Evapotranspiration from a small Alaskan Arctic watershed. Nordic Hydrol 21:253–272

Kane DL, Yang D (eds) (2004a) Northern research basins water balance, vol 290. IAHS Publication, Wallingford, UK, p 271

Kane DL, Yang D (2004b) Overview of water balance determinations for high latitude watersheds. In: Kane DL, Yang D (eds) Northern research basins water balance, vol 290. IAHS Publication, Wallingford, UK, pp 1–12

McClelland JW, Holmes RM, Peterson BJ, Stieglitz M (2004) Increasing river discharge in the Eurasian Arctic: consideration of dams, permafrost thaw, and fires as potential agents of change. J Geophys Res 109:D18102. https://doi.org/10.1029/2004JD004583

Mendez J, Hinzman LD, Kane DL (1998) Evapotranspiration from a wetland complex on the Arctic coastal plain of Alaska. Nordic Hydrol 29:303–330

Ohta T et al (2008) Interannual variation of water balance and summer evapotranspiration in an eastern Siberian larch forest over a 7-year period (1998–2006). Agric Forest Meteorol 148:1941–1953. https://doi.org/10.1016/j.agrformet.2008.04.012

Seuna P, Linjama J (2004) Water balances of the northern catchments of Finland. In: Kane DL, Yang D (eds) Northern research basins water balance, vol 290. IAHS Publication, Wallingford UK, pp 111–119

Shutov V, Gieck RE, Hinzman LD, Kane DL (2006) Evaporation from land surface in high latitude areas: a review of methods and study results. Nordic Hydrol 37:393–411

St Jacques J-M, Sauchyn DJ (2009) Increasing winter baseflow and mean annual streamflow from possible permafrost thawing in the Northwest Territories. Canada. Geophys Res Lett 36: L01401. https://doi.org/10.1029/2008GL035822

Suzuki K, Matsuo K, Yamazaki D, Ichii K, Iijima Y, Papa F, Yanagi Y, Hiyama T (2018) Hydrological variability and changes in the Arctic circumpolar tundra and the three largest pan-Arctic river basins from 2002 to 2016. Remote Sens 10:402. https://doi.org/10.3390/rs10030402

Walvoord MA, Striegl RG (2007) Increased groundwater to stream discharge from permafrost thawing in the Yukon River basin: Potential impacts on lateral export of carbon and nitrogen. Geophys Res Lett 34:L12402. https://doi.org/10.1029/2007GL030216

Warner MJ, Weiss RF (1985) Solubilities of chlorofluorocarbons 11 and 12 in water and seawater. Deep-Sea Res 32:1485–1497

Woo M-K (1986) Permafrost hydrology in North America. Atmos Ocean 24:201–234

Woo M-K, Kane DL, Carey SK, Yang D (2008a) Progress in Permafrost Hydrology in the New Millennium. Permafrost Periglac Process 19:237–254. https://doi.org/10.1002/ppp.613

Woo MK, Thorne R, Szeto K, Yang D (2008b) Streamflow hydrology in the boreal region under the influences of climate and human interference. Philos Trans R Soc B:363

Woo MK, Thorne R (2014) Winter flows in the Mackenzie drainage system. Arctic 67:238–256

Yang D, Kane D, Hinzman L, Zhang X, Zhang T, Ye H (2002) Siberian Lena river hydrologic regime and recent change. J Geophys Res 107(D23):4694. https://doi.org/10.1029/2002JD002542

Yang D, Robinson D, Zhao Y, Estilow T, Ye B (2003) Streamflow response to seasonal snow cover extent changes in large Siberian watersheds. J Geophys Res 108(D18):4578. https://doi.org/10.1029/2002JD003149

Yang D, Shi X, Marsh P (2014) Variability and extreme of Mackenzie River daily discharge during 1973-2011. Quat Int. https://doi.org/10.1016/j.quaint.2014.09.023

Ye B, Yang D, Kane DL (2003) Changes in Lena River streamflow hydrology: Human impacts versus natural variations. Water Resour Res 39(7):1200. https://doi.org/10.1029/2003WR001991

Ye B, Yang D, Zhang Z, Kane DL (2009) Variation of hydrological regime with permafrost coverage over Lena Basin in Siberia. J Geophys Res 114:D07102. https://doi.org/10.1029/2008JD010537

Zhang T, Barry RG, Knowles K, Heginbottom JA, Brown J (1999) Statistics and characteristics of permafrost and ground-ice distribution in the Northern Hemisphere. Polar Geography 23:132–154

Zhang T, Frauenfeld OW, Barry RG, Etinger A, McCreight J, Gilichinksy D (2005a) Response of changes in active layer and permafrost conditions to hydrological cycle in the Russian Arctic. Eos Trans (AGU Fall Meeting Suppl Abstract) 86:C21C–1118

Zhang T et al (2005b) Spatial and temporal variability in active layer thickness over the Russian Arctic drainage basin. J Geophys Res 110:D16101. https://doi.org/10.1029/2004JD005642

Dr. Tetsuya Hiyama is a Professor at the Institute for Space-Earth Environmental Research (ISEE), Nagoya University, Japan. He received Ph.D. in 1995 at the University of Tsukuba, Japan, and has worked as an Assistant Professor at the Institute for Hydrospheric Atmospheric Sciences of Nagoya University, an Associate Professor at the Hydrospheric Atmospheric Research Center of Nagoya University (1995–2010) and at the Research Institute for Humanity and Nature (RIHN), Kyoto, Japan (2010–2014). He specializes in the fields of ecohydrology and hydroclimatology. His research interests include global warming and the human-nature dimension in Siberia, forest–permafrost–groundwater dynamics, and soil–vegetation–climate interactions in the Arctic circumpolar region. He has been a project leader of the research project (No. C-07) of RIHN, entitled "Global Warming and the Human–Nature Dimension in Siberia: Social Adaptation to the Changes of the Terrestrial Ecosystem, with an Emphasis on Water Environments". He has co-edited and published three books from Springer, focusing on climate change and social adaptation in northern Eurasia (ISBN:978-981-10-4648-3), groundwater characteristics under current climate condition in Japan (ISBN:978-4-431-54968-0), and water–carbon dynamics in eastern Siberia (ISBN:978-981-13-6317-7).

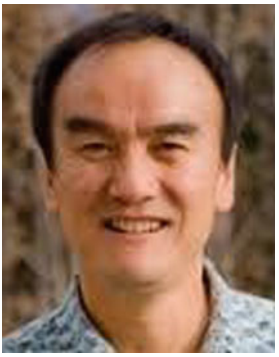

Dr. Daqing Yang is a Research Scientist at the Watershed Hydrology and Ecology Research Division, Environment and Climate Change Canada. He is also Affiliate Research Professor at the International Arctic Research Center, Univ. of Alaska Fairbanks. Over the past 25 years, he has conducted cryosphere system research in China, Canada, Japan, USA, and Norway. His primary research activities/interests include cold region hydrology and climate, particularly Arctic large river streamflow regime and change, snow cover and snowfall measurements, climate change and human impact to regional hydrology, and applications of remote sensing in cold regions. He has served as journal editor and subject editor for IAHS publications (cold region hydrology, northern research basin water balance, and cold/mountain region hydrological systems under climate change), and WMO technical reports (solid precipitation measurement intercomparison and integrated global observing strategy cryosphere theme). He also contributed as review and/or author to the IPCC Reports, and the Arctic Council's Snow, Water, Ice and Permafrost in the Arctic (SWIPA 2017 and follow up) assessment. His current research focuses on investigating the impacts of climate variability/change and human activities on hydrologic system across the broader northern regions.

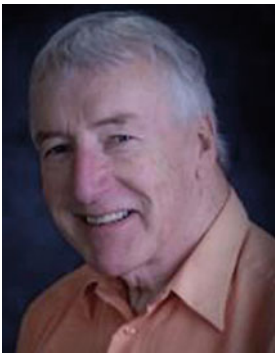

Dr. Douglas L. Kane is a Professor Emeritus at the Water and Environmental Research Center (WERC), University of Alaska Fairbanks (UAF). He served the UAF with distinction in teaching, research, and public service from 1971 to 2009. He is a world-renowned Arctic hydrologist who has played an important role in establishing the UAF as a global leader in Arctic water research. He is credited as the author, co-author, or editor of more than 100 refereed publications and more than 22 other publications; and was awarded the Can-Am Civil Engineering Amity Award by the American Society of Civil Engineers for exemplary professional activity. He is the Recipient of ASCE Harold R. Peyton award for Cold Regions Engineering and designated as a Fellow in the American Water Resources Association (AWRA). He has provided leadership in a variety of positions at the University, including as Director of the Water and Environmental Research Center for 20 years, as Director of the Institute of Northern Engineering for 6 years, and as a Full Professor of Water Resources and Civil Engineering for 30 years.

Permafrost Hydrogeology

17

Barret L. Kurylyk and Michelle A. Walvoord

Abstract

Groundwater processes are often overlooked in permafrost environments, but subsurface storage and routing can strongly influence water and biogeochemical cycling in northern catchments. Groundwater flow in permafrost regions is controlled by the temporal and spatial distribution of frozen ground, causing the hydrogeologic framework to be temperature-dependent. Most flow occurs in geologic units above the permafrost table (supra-permafrost aquifers) or below the permafrost base (sub-permafrost aquifers). In the context of climate change, thawing permafrost is altering groundwater flowpaths and thereby inducing positive trends in river baseflow in many discontinuous permafrost basins. Activated groundwater systems can provide new conduits for flushing Arctic basins and transporting nutrients to basin outlets. The thermal and hydraulic physics that govern groundwater flow in permafrost regions are strongly coupled and more complex than those in non-permafrost settings. Recent research activity in permafrost hydrogeological modeling has resulted in several mainstream groundwater models (e.g., SUTRA, FEFLOW, HYDRUS) offering users advanced capabilities for simulating processes in aquifers that experience dynamic freeze-thaw. This chapter relies on field examples to review key processes and conditions that control groundwater dynamics in permafrost settings and presents an up-to-date synthesis of the mathematical representation of heat transfer and groundwater flow in northern landscapes.

B. L. Kurylyk (✉)
Department of Civil, and Resource Engineering and Centre for Water Resources Studies, Dalhousie University, Halifax, Nova Scotia, Canada
e-mail: barret.kurylyk@dal.ca

M. A. Walvoord
Earth System Processes Division, U.S. Geological Survey, Denver, CO, USA
e-mail: walvoord@usgs.gov

D. Yang and D. L. Kane (eds.), *Arctic Hydrology, Permafrost and Ecosystems*,
https://doi.org/10.1007/978-3-030-50930-9_17

17.1 Overview

Permafrost hydrogeology has historically been the subject of very little research in comparison to permafrost surface hydrology (Woo et al. 2008). The underlying assumption of many surface hydrology studies is that permafrost is an impermeable layer that restricts catchment hydrologic processes to the surface or, in the summer, through the seasonally thawed active layer. However, hydrogeological processes are important for storing and conveying meteoric water in permafrost regions across a range of landscapes and climate conditions (Williams 1965), and are expected to become increasingly important with projected permafrost degradation (Bring et al. 2016; Walvoord and Kurylyk 2016). Groundwater is critical for maintaining river discharge in cold regions during the dry or winter seasons (St. Jacques and Sauchyn 2009) and for creating patches of cool (warm) water for habitat during the summer (winter) seasons. Groundwater also serves as an important drinking water resource for some northern communities and could function as a primary source of drinking water in other communities that presently rely on surface water (Lemieux et al. 2016).

Geologic deposits in discontinuous permafrost regions that were formerly frozen and functioned as aquitards or aquicludes (low hydraulic conductivity units) have been warming and thawing in recent decades, causing hydrologic regime shifts. These regime shifts are manifested by increases in baseflow and have been observed in watersheds across the Arctic (Duan et al. 2017; St. Jacques and Sauchyn 2009; Rennermalm et al. 2010; Smith et al. 2007; Walvoord and Striegl 2007). They can be phenomenologically explained by the 'replumbing' of the landscape due to permafrost thaw as more water is stored in and conveyed through subsurface pathways. Recent numerical modeling results support these causal explanations (Bense et al. 2009; Ge et al. 2011). In addition to changing baseflow and streamflow dynamics, northern landscapes are often also characterized by complex drying and wetting patterns that cause decreases (Smith et al. 2005; Lebreque et al. 2009; Carroll et al. 2011) or increases (Sannikov 2012; Korosi et al. 2017) in the size and density of wetlands and lakes. Streamflow and surface water distribution changes in permafrost regions represent a holistic watershed response to changing meteorological forcing (precipitation and evapotranspiration) as well as a the hydrogeologic response influenced by permafrost thaw and landscape change. Alterations to the temporal and spatial distribution of water storage and release in permafrost regions have implications for future water security, economics, wildlife habitat, and greenhouse gas emissions in northern regions and provide the impetus for further field- and modeling-based studies of permafrost hydrogeology.

Hydrogeologic processes in permafrost systems are complicated by many feedbacks and interconnected processes. For example, groundwater flow induces advective heat transfer, which can accelerate permafrost thaw and increase hydraulic conductivity, and thereby further enhance groundwater flow. Also, groundwater flow is an important solute transport mechanism, especially in the

context of the mobilization of previously sequestered carbon (Schuur et al. 2008), mercury (Schuster et al. 2018), or industrial contaminants (Pearce et al. 2011) released by permafrost thaw. This chapter provides an overview of the physical processes controlling groundwater flow in permafrost settings and highlights the global environmental implications of these processes.

17.2 Groundwater in Permafrost Landscapes

17.2.1 Zones of Groundwater Flow

As a hydrogeologic unit, permafrost acts as an aquitard (Fig. 17.1a) due to the substantial reduction in hydraulic conductivity when porewater exists predominately as ice vs. liquid water (see Sect. 4.2). Permafrost is thus generally considered impermeable, except where a dense network of macropores can enable short

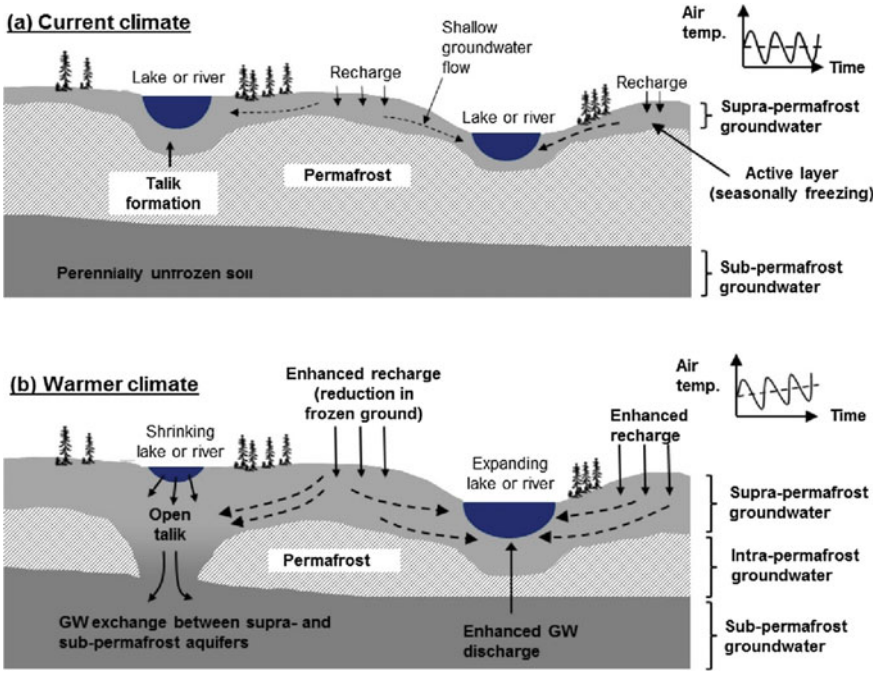

Fig. 17.1 **a** Profile view of a permafrost landscape with shallow (supra-permafrost) and deep (sub-permafrost) groundwater (GW) flow. **b** Warming atmospheric conditions lead to permafrost thaw and increased hydrologic and hydrogeologic connections between lakes, rivers, and shallow and deep aquifers and can result in some landscapes becoming dryer while others become wetter. (from Walvoord and Kurylyk 2016)

circuiting of water flow through permafrost. Seasonally or perennially unfrozen zones in systems with permafrost serve as potential conduits of focused groundwater flow that can hydraulically connect water bodies that are otherwise vertically or laterally disconnected by the presence of permafrost (Connon et al. 2018). Groundwater in permafrost systems occurs in three primary zones: supra-permafrost, intra-permafrost, and sub-permafrost (Fig. 17.1). The degree of hydraulic connectivity between these zones depends strongly on the configuration of permafrost and underlying hydrogeologic framework. Reduced coverage of permafrost favors circulation of groundwater between the three zones and enhances hydraulic connection of groundwater to surface water bodies such as rivers and lakes.

17.2.1.1 Supra-Permafrost Groundwater

Groundwater in the zone between the land surface and the top of permafrost is referred to as supra-permafrost groundwater. Supra-permafrost groundwater undergoes complete freezing (except for residual liquid water) for cases in which the seasonal frost boundary moves downward through the winter season and meets the permafrost table. In these cases, all supra-permafrost groundwater exists in the active layer that seasonally freezes and thaws. This scenario is typical of cold, continuous permafrost settings. In warmer, less continuous permafrost settings, as well as areas that have undergone disturbance (e.g., fire, built infrastructure, flooding), supra-permafrost groundwater may include both (1) water in the active layer, and (2) water in a lateral perennially thawed zone, also referred to as a supra-permafrost talik, below the maximum depth of the frost layer and above permafrost (e.g., Sloan and van Everdingen 1988).

Because the supra-permafrost zone is subject to seasonal freeze-thaw cycles, supra-permafrost groundwater flowpath depths are seasonally dependent. The active layer thaws from the top down in the spring and predominantly freezes from the top down in the fall. These seasonal dynamics promote shallow supra-permafrost groundwater flow early in the thaw season and progressively allow for deeper flow in the active layer later in the thaw season. In settings with perennially thawed zones, deeper flowpaths may be able to be activated earlier in the thaw season. The magnitude of supra-permafrost groundwater flow also has a strong temporal component controlled by seasonally frozen ground dynamics. Assuming a constant water table elevation, the transmissivity of the supra-permafrost zone increases through the thaw season. In this case, maximum supra-permafrost groundwater flow is expected to occur late in the thaw season. However, the assumption of a constant water table elevation is most applicable to areas that are not water limited and has limited applicability to areas that experience substantial summer drying of active layer soils. For the latter case, a water-table decline through the thaw season could result in a reduction in supra-permafrost transmissivity, particularly with a concomitant reduction in soil hydraulic conductivity with depth (Walvoord and Kurylyk 2016).

17.2.1.2 Intra-permafrost Groundwater

Intra-permafrost groundwater exists within perennially unfrozen zones (taliks) that may be hydrologically isolated (closed) or hydrologically connective (open), the latter serving as conduits between flow systems (Fig. 17.1b). The hydrogeologic function of permafrost as a confining unit can lead to over-pressuring at depth, thereby promoting strong hydraulic gradients through permafrost, which in turn support the development of taliks and enhancement of flow through these taliks. Thus, the closed vs. open distinction is an important one in determining the role of intra-permafrost taliks in influencing groundwater circulation. Intra-permafrost groundwater in closed taliks is relatively stagnant, having only a localized sphere of influence and limited flow potential. In contrast, intra-permafrost groundwater flow in open taliks may be quite active even in regions with low topographic gradients (Rowland et al. 2011). In upland regions, intra-permafrost taliks may serve as primary conduits of recharge to the deeper groundwater flow system. In down-gradient regions, taliks may serve as conduits for groundwater discharge.

17.2.1.3 Sub-permafrost Groundwater

Groundwater that exists below permafrost is referred to as sub-permafrost groundwater (Haldorsen et al. 1996). In regions of thick, cold permafrost, the top of this zone may be hundreds of meters deep. In permafrost regions on the warm end of the spectrum, the top of the sub-permafrost zone may be a few meters to tens of meters deep. The bottom of the sub-permafrost zone, with respect to hydrogeological relevance, is typically defined by the contact with crystalline bedrock or another lithologic unit with very low hydraulic conductivity. Here again, the boundary is highly site-specific as are the hydraulic properties of the sub-permafrost groundwater zone. Favorable/productive aquifer conditions for the sub-permafrost zone are comparable to those for porous media in non-permafrost regions. High hydraulic conductivity and hydraulic gradients favor enhanced sub-permafrost groundwater circulation. Sub-permafrost groundwater may be strongly over-pressured resulting from confining properties of permafrost creating artesian-like conditions in some areas.

17.2.2 Groundwater Circulation and Connectivity

The circulation of water between primary zones of groundwater flow strongly relates to the relative spatial coverage of permafrost, and is thus discussed separately for continuous, discontinuous, and sporadic to isolated permafrost regions.

17.2.2.1 Continuous Permafrost

Active groundwater flow in regions with continuous permafrost tends to be dominated by seasonal supra-permafrost flow with localized intra-permafrost circulation. Sub-permafrost groundwater with long residences times may be present in continuous permafrost, particularly those associated with deep sedimentary basins, but here sub-permafrost groundwater flow tends to be slow-moving and isolated

from active shallower groundwater flow systems and surface water. The component of streamflow derived from groundwater in continuous permafrost environments tends to be dominated by supra-permafrost flow, and therefore is sensitive to changes in active layer thickness and seasonal freeze-thaw dynamics. Hydraulic connections (i.e., open taliks) between local flow systems are limited in continuous permafrost. Some exceptions include large river corridors and deep lakes that do not freeze to their beds in the winter, thus supplying sufficient thermal energy to maintain unfrozen conduits beneath these surface water bodies. Although local groundwater flow systems in continuous permafrost tend to be dominated by supra-permafrost groundwater flow, deeper, regional groundwater flow systems may be active in continuous permafrost zones (Kane et al. 2013) and connect recharge and discharge zones separated by hundreds of kilometers.

17.2.2.2 Discontinuous Permafrost

In discontinuous permafrost, the three-dimensional configuration of permafrost strongly controls local and regional groundwater fluxes and flow patterns. Taliks focus groundwater flow, and in turn, groundwater flow transmits thermal energy to enhance talik development, creating a positive feedback. Due to the restriction of water flow through permafrost coupled with the confining properties of permafrost, regional groundwater flow systems that develop in discontinuous permafrost may be much more complex than the topography and an assumption of a homogenous subsurface would predict. The dearth of cold regions hydrogeologic and deep groundwater chemistry data typically used to define groundwater flowpaths and residence times requires a certain reliance on numerical modeling to evaluate deep groundwater flow in permafrost systems and assess potential response to perturbations, such as permafrost thaw (Bense et al. 2009; Walvoord et al. 2012; McKenzie and Voss 2013).

17.2.2.3 Sporadic to Isolated Permafrost

Systems with increasingly less permafrost coverage tend to become more hydraulically connected, promoting deeper and enhanced groundwater circulation as supported by the underlying hydrogeologic framework. Groundwater flow patterns in sporadic permafrost tend to be influenced by the presence of isolated permafrost bodies only at local scales (Kurylyk et al. 2016). Widespread over-pressuring from permafrost is not a factor, and therefore the underlying (unfrozen) hydrogeologic framework exerts dominant control at regional scales.

17.2.3 Groundwater Contribution to Surface Water Bodies

Groundwater discharge in permafrost regions occurs in areas of relatively low hydraulic head, following local to regional hydraulic gradients, similar to non-permafrost systems. A distinguishing aspect of groundwater discharge in northern latitudes, however, is that both the magnitude and pattern are strongly influenced by the three-dimensional configuration of permafrost, a hydrogeologic

confining feature that is subject to change over time. Groundwater may be issued to both lotic (flowing surface water systems such as streams and rivers) and lentic (still bodies of water, including lakes and pond) inland water systems. Sufficiently large contributions of groundwater to inland waters can affect not only the water budget, but also impact temperature, pH, nutrient delivery, and chemical inputs to surface water systems (Vonk et al. 2015). The contribution and importance of groundwater to the high-latitude coastal ocean via direct subsurface flowpaths is the subject of current research.

17.2.3.1 Groundwater Discharge to Stream and Rivers

Groundwater discharge to streams and rivers in permafrost-impacted systems may be derived from both lateral and vertical subsurface flowpaths and is considered to be the principal component of *baseflow*. Groundwater is discharged through diffuse seepage and more focused springs directly to the stream bed. In addition, groundwater is issued as seeps and springs along the stream corridor that feed into the main channel.

Supra-permafrost groundwater discharge to streams and rivers occurs primarily during the active layer thaw season and tends to have a strong lateral component as water moves downgradient to the stream along the permafrost table. Baseflow in streams fed by supra-permafrost flow alone is substantially or entirely diminished in the winter season when the supra-permafrost aquifer is (partially) frozen, hydraulically non-conductive, and lacking a continuous source of liquid water. These types of streams, which may completely freeze solid during the winter, are typical of those found in continuous permafrost and are generally characterized as having closed taliks.

Intra-permafrost and sub-permafrost groundwater contribution to streams and rivers occurs in regions with intra-permafrost taliks and open taliks beneath streams and rivers. Here, hydraulic gradients promote groundwater upwelling and maintain talik development. Streams with substantial baseflow from deep flowpaths and connection to the sub-permafrost aquifer are likely to sustain perennial flow, even during the winter when surficial sources of liquid water are sparse to absent. These streams do not freeze to their beds and maintain baseflow under a sheet of river ice that may be continuous or in other cases may contain openings (open leads) that coincide with locations of focused upwelling of warm groundwater from depth (Fig. 17.2, left). Open leads in large rivers used for winter transportation via snow machines are important safety concerns. Historically thinning river ice in Alaska, perhaps due in part to increases in groundwater discharge (Jones et al. 2015), has been documented and remains a hazard concern among indigenous communities for winter transportation that supports social and subsistence activities (Herman-Mercer et al. 2011). In rare cases, warm groundwater discharge to streams can eliminate the formation of winter stream ice (Clearwater Creek, near Delta Junction, Alaska, USA, for example). In other cases, substantial groundwater upwelling to streams or small rivers may result in the progressive upward piling of ice along the surface water corridor. These expressions are called *aufeis* or *icings* (Fig. 17.2, right).

Fig. 17.2 (Left) Photo of Beaver Creek (near Victoria Creek junction, Yukon Flats, Alaska) with an open lead, presumably due to groundwater discharge. Photo date: late March 2011. Image courtesy of Heather Best, U.S. Geological Survey. (Right) Photo of an *aufeis* feature east of Gordlan Lake, Slave Geological Province, Northwest Territories, Canada. Photo date: March 10, 2015. Image courtesy of Dr. Peter Morse, Geological Survey of Canada

The relative contribution of groundwater to total stream discharge in permafrost settings varies widely. Discontinuous permafrost with open taliks, coarse-grained permeable substrate, and strong driving hydraulic gradients favor a high proportion of groundwater to total streamflow. Likewise, continuous permafrost with closed taliks, fine-grained impermeable substrate, and low hydraulic gradients favor a low proportion of groundwater to total streamflow. A study of major rivers in the Yukon River Basin of Alaska and western Canada estimated groundwater contribution to annual streamflow ranging from 4.7 to 47.4% and attributed the variability to sub-basin specific geology and permafrost coverage (Walvoord and Striegl 2007). River systems with a proportionally large contribution of groundwater to annual streamflow exhibit reduced seasonal variability in streamflow magnitude, streamflow temperature, and chemical concentrations (O'Donnell et al. 2012), because groundwater via deep flowpaths supplies a relatively constant source of water, heat, and chemical composition to the stream.

17.2.3.2 Groundwater–Lake Exchange

Groundwater flow into and out of lakes surrounded by permafrost may occur via shallow supra-permafrost flowpaths and via exchange in open taliks that connect the lake to the deep sub-permafrost aquifer (Wellman et al. 2013). Supra-permafrost flow is generally seasonally dependent, though a supra-permafrost talik could support perennial flow if a constant source of liquid water is available (e.g., between two adjacent lakes). In contrast, groundwater exchange through open taliks occurs year-round below lakes that do not freeze to their bottoms. The magnitude and direction of groundwater exchange in these systems are determined by hydraulic gradients and the hydraulic properties along subsurface flowpaths. In general, lowland lakes surrounded by higher terrain tend to be subjected to upward gradients and therefore are considered as gaining lakes if groundwater contribution is appreciable. Likewise, upland lakes have a greater proclivity toward downward

gradients that could support losing lake systems. Numerical modeling work has demonstrated that relative to hydrostatic conditions, the presence of vertical hydraulic gradients (upward or downward) substantially accelerates the development of open taliks beneath lakes due to the added advective heat transfer (Rowland et al. 2011; Wellman et al. 2013). Furthermore, deep groundwater–lake exchange via open taliks can greatly exceed the magnitude of supra-permafrost groundwater–lake exchange if deep sediments are relatively permeable and fine-grained lake-bed sediments are thin or absent (Wellman et al. 2013).

17.2.3.3 Submarine Groundwater Discharge to the Coastal Ocean

Submarine groundwater discharge is distinguished from groundwater conveyed via river baseflow to the coastal ocean. The former discharges directly to the marine environment via subsurface flowpaths and may be both volumetrically and chemically important to coastal systems. Submarine groundwater discharge is influenced not only by typical hydrogeologic controls imposed on freshwater systems, but also by wave and tidal pumping and buoyancy differences from salinity contrasts. The magnitude of circum-Arctic submarine groundwater contribution is not well constrained at present. The handful of studies that have attempted to quantify submarine groundwater discharge from permafrost basins together with global comparison of submarine groundwater discharge studies suggest that volumetric contributions from arctic regions are low compared with temperate regions, though large uncertainties remain (Taniguichi et al. 2002; Dimova et al. 2015; Lecher 2017). One study provides direct observation and quantification of submarine groundwater discharge along the Siberian Arctic coast (Charkin et al. 2017), and it represents just a small fraction of the total Eastern Siberian Arctic Shelf zone. Continued motivation to better quantify circum-Arctic submarine groundwater discharge is provided by work indicating that submarine groundwater discharge may play an important role in gas hydrate formation along the Arctic continental shelf (Frederick and Buffett 2016). Another recent study analyzed radium isotope data to infer an increase of shelf-derived material inputs to the Arctic Ocean that could be partially attributed to increased submarine groundwater discharge resulting from permafrost thaw (Kipp et al. 2018). Submarine groundwater discharge may be derived from a combination of supra-permafrost, intra, and sub-permafrost flowpaths, and potentially impact the local temperature field, sediment salinity, nutrient conditions, and methane availability. Further work is needed to adequately assess the importance of submarine groundwater discharge from permafrost regions.

17.2.4 Effects of Permafrost Thaw on Groundwater

Permafrost exerts a strong influence on groundwater flow, flowpaths, and storage (Fig. 17.1). Permafrost degradation impacts these characteristics of groundwater in northern environments and is expected to continue into the future. The effects of

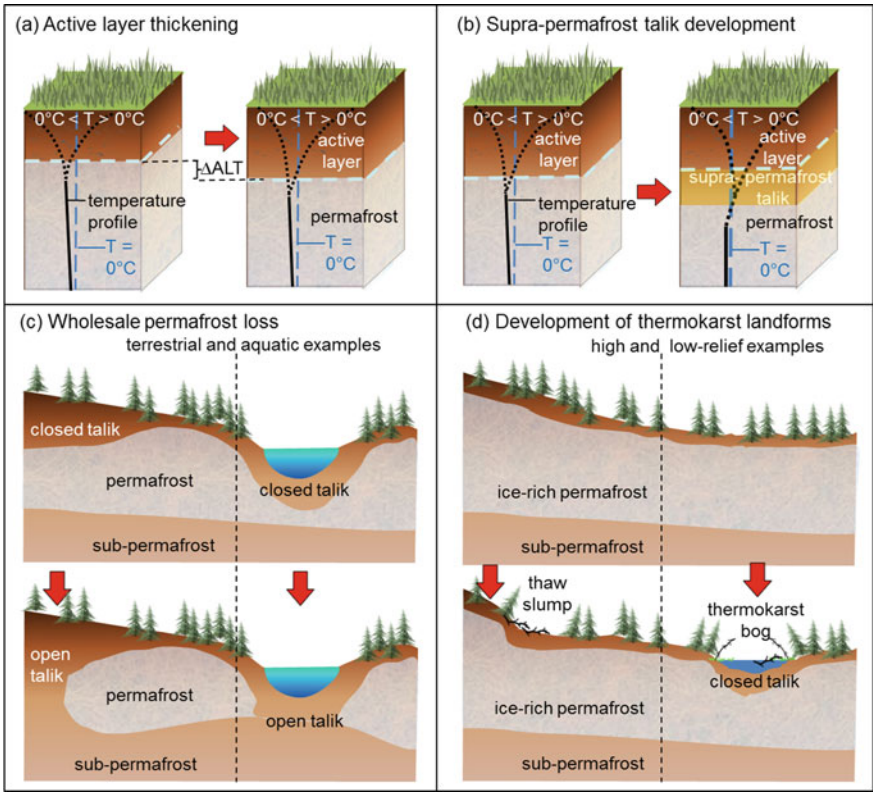

Fig. 17.3 Modes of permafrost thaw (see Sect. 17.2.4). Red arrows indicate the progression from an initial state toward an enhanced thawed state representative of **a** active layer thickening, **b** supra-permafrost talik development, **c** wholesale permafrost loss, and **d** development of thermokarst landforms

permafrost thaw on groundwater strongly depend on the mode of permafrost thaw and the hydrologic susceptibility of the region over which the thaw occurs. It is therefore important to make distinctions between modes of permafrost thaw and expected groundwater responses. Figure 17.3 presents the various modes of permafrost thaw, which are discussed below.

17.2.4.1 Active Layer Thickening

Active layer thicknesses typically range from tens of centimeters to a few meters depending on climatic conditions, landscape factors affecting the surface energy balance, soil moisture conditions, and thermal properties of the subsurface. Long-term thaw occurring at the top of permafrost typically results in a deepening and thickening of the active layer that also seasonally varies in temperature above and below 0 °C (Fig. 17.3a). A counter example is the special case in which the

added active layer thickness resulting from permafrost thaw is equally balanced by ground subsidence culminating in the net zero response in active layer thickness (Shiklomanov et al. 2013).

Active layer thickening is a shallow and typically gradual response to ground temperature warming. Active layer thickening increases potential shallow groundwater storage by allowing for a greater thawed volume above permafrost to store water. It also tends to increase shallow lateral groundwater flow unless the active layer thickening is accompanied by a decline of the water table, due to limited water availability, such that more water is transmitted through a newly thawed zone that has a reduced hydraulic conductivity relative to the shallower active layer. Active layer thickening will have a proportionally greater impact on groundwater flow in regions that are dominated by supra-permafrost flow, such as in continuous permafrost and watersheds with shallow bedrock. Likewise, it will have the greatest effect on baseflow in streams that are dominated by contributions from supra-permafrost flow. Historical increases in baseflow in headwater catchments have been observed and attributed to active layer thickening (Sjöberg et al. 2013). Numerical modeling studies support the linkage between increased groundwater discharge to streams and a thicker active layer (Bense et al. 2009; Ge et al. 2011; Frampton et al. 2013). Methods for estimating rates of permafrost thaw via active layer thickening using recession flow analysis are described in Lyon et al. (2009) and Brutsaert and Hiyama (2012).

17.2.4.2 Supra-Permafrost Talik Development

When the depth to permafrost exceeds the depth of the seasonal frost layer, a supra-permafrost talik develops (Fig. 17.3b). This zone, above permafrost and below the seasonally active layer, remains above 0 °C all year with liquid water present. Supra-permafrost talik development is the progressive thaw stage that follows active layer thickening and precedes wholesale permafrost loss (described in next sub-section). Supra-permafrost talik development may be localized and can also represent a transient, and in some cases reversible, response to landscape perturbations and prolonged temperature anomalies as described in Shur et al. (2005). Groundwater flow through supra-permafrost taliks is difficult to measure and monitor given current characterization technology, but Connon et al. (2018) have recently demonstrated the importance of supra-permafrost taliks for water routing using field data from a discontinuous permafrost zone in the Northwest Territories, Canada. Observed trends in lake area patterns have been attributed to supra-permafrost talik development as a means of enhancing shallow subsurface connectivity and groundwater exchange (Jepsen et al. 2013).

17.2.4.3 Wholesale Permafrost Loss

Wholesale permafrost loss refers to complete permafrost degradation at depth resulting in wholly unfrozen connection between the shallow and deep subsurface. It represents the final stage in the progression following active layer thickening to supra-permafrost talik development. Whole sale permafrost loss may occur in terrestrial settings or underlying a stream, river, or lake (Fig. 17.3c). Vertical permafrost

thaw is bi-directional (i.e., from above and below the permafrost), but top-down thaw tends to dominate, especially under high surface warming rates (McKenzie and Voss 2013). Wholesale permafrost loss opens potential pathways for groundwater flow, enhances recharge and discharge, and promotes deep groundwater circulation given a favorable hydrologic framework. Areas of warm, thin, discontinuous permafrost are most likely to experience and be impacted by complete loss of permafrost at depth. Wholesale permafrost thaw has the potential to influence groundwater fluxes and flowpaths at intermediate to basin-wide scales by altering the hydrogeologic framework that controls flow, storage, and hydrologic connectivity among inland waters, shallow groundwater, and deep sub-permafrost groundwater.

Observations of increased streamflow minimums and baseflow and/or altered streamflow recession curves have been observed for major rivers in Canada (St Jacques and Sauchyn 2009), Siberia (Ye et al. 2003, 2009; Smith et al. 2007), Alaska (Walvoord and Striegl 2007; Ge et al. 2013), and China (Duan et al. 2017). These changes have been at least partially attributed to wholesale permafrost thaw (Fig. 17.4). These widespread, consistent observations reinforce the paradigm that proportionally more water can be recharged, stored, and circulated through deep subsurface pathways opened by extensive permafrost loss and discharged to river corridors (Walvoord et al. 2012). Determination of the hydrologic impacts of wholesale permafrost loss requires site-specific consideration due to the strong influence of the underlying (unfrozen) hydrogeologic structure. For example, transitions from frozen to unfrozen coarse-grained sediment with high thawed permeability will invoke greater hydrogeologic changes than transitions from frozen to unfrozen bedrock with low thawed permeability.

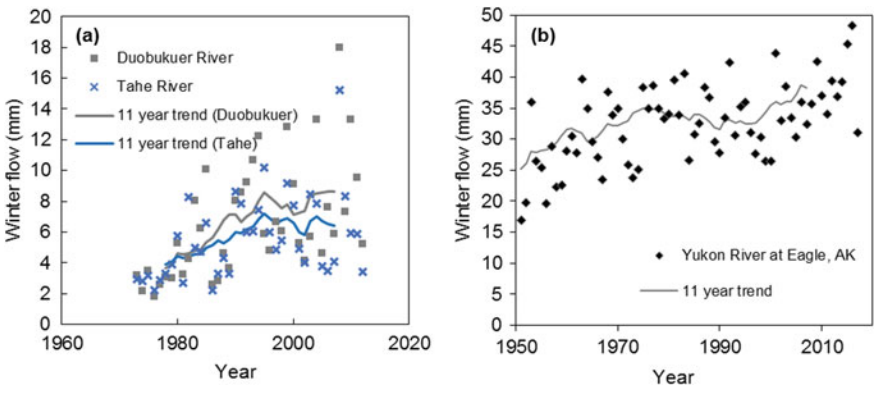

Fig. 17.4 **a** Trends in winter flow (interpreted as baseflow from groundwater discharge) in the Duobukkuer River (3094 km^2 drainage basin) and the Tahe River (6851 km^2) in discontinuous permafrost environments in northeastern China (data from Duan et al. 2017, figure updated) and **b** the Yukon River, Alaska (data from the U.S. Geological Survey's National Water Information System; waterdata.usgs.gov/nwis; site 15356000). Trends are represented by 11-year moving averages. Winter flow is calculated as the cumulative volume of November to March river discharge divided by the drainage area

17.2.4.4 Development of Thermokarst Landforms

When ice-rich permafrost thaws, reduction of pore space associated with ice melt can cause deformation of the ground surface via subsidence and/or erosion. Thaw-driven subsidence produces distinct thermokarst thaw lakes, drained basins, water tracks, and bogs and gullies in low relief settings (e.g., Yoshikawa and Hinzman 2003) as described in more detail in Chap. 14. In settings with moderate to high topographic relief, thaw slumps and active layer detachment slides commonly occur (Fig. 17.3d). In addition to causing changes in landscape topography, a primary driver of groundwater flow, thermokarst processes also influence the hydraulic properties of the thawed and collapsed substrate. Reduction in porosity is a common trajectory associated with the melting of excess ground ice in ice-rich permafrost. On a landscape scale, preferential subsidence and erosion can cause patterns conducive to ponding in some areas leading to increases in surface water area (bog, pond, and lake development) (Fig. 17.3d), or increases in surface water drainage as thermokarst development evolves and the surface water connectivity increases (Connon et al. 2014). Changes in surface water storage and routing may impact groundwater flow through the redistribution of water and energy. For example, ponding favors talik formation, potentially leading to increases in subsurface hydraulic connectivity.

17.3 Groundwater Resources in Permafrost Environments

Groundwater offers at least two key advantages over surface water as a freshwater resource. First, the global volume of groundwater is approximately 70 times the volume of liquid freshwater stored in rivers, streams, ponds, and lakes (Hiscock and Bense 2014). The large storage capacity of aquifers provides a significant buffer to resist the impacts of short-term droughts on water supply. Secondly, groundwater resources are at least somewhat protected from surface contamination due to natural filtration and attenuation processes. In cold regions, groundwater offers a third significant advantage. Surface water resources in shallow water bodies are prone to freezing to the bottom of the water column, whereas groundwater resources below permafrost remain unfrozen year-round.

Permafrost functions as an aquitard or aquiclude, so the potential for development of groundwater resources must be sought above or below permafrost or within taliks. Supra-permafrost zones in continuous permafrost are often not considered to be productive groundwater supply reservoirs, as they are typically thin. Also, in these settings, the active layer portion of the supra-permafrost zone is frozen during the winter months. The one exception to this general rule is when large taliks are found beneath rivers and lakes as these may yield a perennial source of supra-permafrost groundwater (Williams 1970). In general, sub-permafrost aquifers can provide domestic and industrial groundwater supply in environments where the permafrost zone is thin and drilling beneath the permafrost is not cost-prohibitive. Such wells can freeze throughout the vertical extent of surrounding permafrost and

may need to be heated or continuously pumped. Like in groundwater systems at lower latitudes, sub-permafrost aquifers can be found in fractured rock, karst formations, and unconsolidated sediment. Unconsolidated stream sediment (alluvium) and coarse, unconsolidated glacial deposits typically yield the most productive sub-permafrost aquifers (Cederstrom et al. 1953). In Alaska, alluvial deposits in river valleys provide the most economically viable groundwater supplies. The potential yield of these aquifers in discontinuous permafrost zones can decrease substantially during the winter if they extend into the seasonal frost zone (Williams and Smith 1989). These effects can be mitigated by screening the well at appropriate intervals below the seasonal frost zone.

The capacity of an aquifer to yield groundwater is typically reflected by the magnitude of its transmissivity, that is, the product of vertical aquifer thickness and hydraulic conductivity. In locations where the permafrost zone extends down into the alluvium, the permafrost acts as a confining unit and the transmissivity of the sub-permafrost aquifer is controlled by the difference in the elevation of the permafrost base and the bottom of the alluvium. Thus, the permafrost geometry can exert control on sub-permafrost aquifer properties. Conversely, if the top surface of a confined aquifer is located below the base of permafrost, then the presence of permafrost has no direct influence on the hydrogeologic response to pumping, except perhaps over long periods by limiting recharge. One limitation from a groundwater quality perspective is that sub-permafrost groundwater is generally characterized by long residence times with extended exposure to deep weathering products, thus resulting in high dissolved solids concentrations (Michel et al. 2014).

Hydrogeological investigations in permafrost require more intensive engineering than similar studies further south. For example, boreholes are typically instrumented with thermistors to record the extent of permafrost and to monitor any changes. Geophysical methods are often applied to map permafrost conditions across a study site. Drilling can be complicated by the difference in the properties of frozen and unfrozen ground. Furthermore, site access is often difficult and expensive. All of these logistical and financial impediments have resulted in a paucity of hydrogeological field data in northern regions. Early studies of groundwater resource mapping in permafrost settings were conducted for Alaska (Williams 1970), Canada (van Everdingen 1974), and Russia (Tolstikhin and Tolstikhin 1974). These early studies provided a detailed compendium of hydrogeologic units in permafrost environments and highlighted the potential for continuing or initiating groundwater resource extraction across much of the Arctic. In some cases, recent updates can be found (e.g., Callegary et al. 2013). The present rate of groundwater extraction in northern communities varies widely. In Alaska, 83% of the approximately 1600 public drinking water systems are fully or partially groundwater-sourced (Alaska Department of Environmental Conservation 2008). Over 99% of residents in the Yukon Territory, Canada, rely at least partially on groundwater for residential water supply (Michel et al. 2014). On the other hand, groundwater development in Canada's other northern territories (Nunavut and Northwest Territories) is more limited, as only 28% of the residents rely on aquifers for their water supply. Lemieux et al. (2016) investigated the hydrogeological

potential of deposits in permafrost regions of northern Québec, Canada and concluded that groundwater could service northern communities looking to enhance their water supply. They also postulated that aquifers could provide an increasingly viable drinking water supply in the coming decades due to the impacts of climate warming and permafrost thaw on previously dormant aquifers.

The influence of permafrost thaw on groundwater resources is not all positive however. Contaminants that were previously contained in impermeable geologic units may be released and transported by an activated groundwater system. One such example is the Giant Mine in the Northwest Territories, which is known to have high levels of arsenic (Banfield and Jardine 2013) and is experiencing rapid permafrost thaw. Another example is sewage contamination from thawing permafrost in villages on the northwest coast of Alaska. These contaminated sites can be managed by active ground freezing to prevent migration, but this type of strategy incurs costs and energy resources that may be prohibitive for indigenous communities to support. In general, groundwater resource development in permafrost environments has been characterized by logistical and economic challenges. Climate change adds another layer of complexity to these issues due to the influence of ground thaw on aquifer transmissivity and contaminant transport. Northern governments and communities will likely begin to increasingly consider aquifers for future domestic and industrial water supply.

17.4 Permafrost Hydrogeology Theory

17.4.1 Darcy's Law

The most well-known hydrogeological equation is Darcy's (1856) law, which expresses the groundwater flux in all directions as the product of the hydraulic gradient and a proportionality constant:

$$\underline{q} = -\underline{\underline{K}}\underline{\nabla} h \tag{17.1}$$

where $\underline{q}$ is the three-dimensional Darcy flux vector (m s^{-1}), $\underline{\nabla} h$ is the hydraulic head gradient (m m^{-1}), and $\underline{\underline{K}}$ is the hydraulic conductivity tensor (m s^{-1}) that functions as the coefficient of proportionality between the flux and the gradient. In one dimension, this reduces to the following form:

$$q = -K\frac{\partial h}{\partial l} \tag{17.2}$$

where q is the Darcy flux (m s^{-1}), K is the hydraulic conductivity in the flux direction (m s^{-1}), and $\frac{\partial h}{\partial l}$ is the hydraulic gradient in the same direction.

This law is physically and mathematically analogous to Fick's law in solute diffusion, Fourier's law in heat transport, and Ohm's law in electricity. Unlike in

fluid mechanics, hydraulic head calculations in hydrogeology do not include velocity head due to the very low velocities experienced in groundwater flow systems (Fetter 2001). Thus, hydraulic head h is composed of just the pressure head and the elevation head. The hydraulic head is a scalar field, but its gradient is a vector. As the negative sign indicates in Eqs. (17.1) and (17.2), groundwater flow always occurs in the direction of decreasing head or hydraulic energy.

The Darcy flux is the groundwater flow rate per unit area of porous media, with both the pore space and the medium solids (soil grains) used to calculate the area. Since water flow only occurs thorough the pore space, the Darcy flux is not equivalent in magnitude to the groundwater velocity. The average linear porewater velocity (v, m s^{-1}) can be obtained from the Darcy flux by dividing through by the product of the effective porosity (ε) and the volumetric liquid water saturation (S_L, volume of liquid water divided by volume of pores). Thus, the groundwater velocity always exceeds the Darcy flux, and for very low water saturations (e.g., in partially frozen ground where the pore space predominantly consists of ice), the groundwater velocity can be orders of magnitude higher than the Darcy flux.

$$v = \frac{q}{S_L \varepsilon} \tag{17.3}$$

17.4.2 Relative Hydraulic Conductivity

Equations (17.1)–(17.3) are fundamental equations in physical hydrogeology and are applicable in all environments. The primary complicating factor for groundwater flow in permafrost settings is that the hydraulic conductivity is dependent on the cryotic state (frozen or unfrozen pore water) and thus strongly on temperatures near 0 °C. An analog to this can be found in unsaturated zone hydrology, where the hydraulic conductivity depends on the moisture content, which in turn depends on the matric potential. Saturated zone hydrogeology studies are usually predicated on the assumption that the hydrogeologic framework and properties are constant in time. This assumption is clearly not valid in permafrost environments experiencing subsurface temperature change, and thus the physics of groundwater flow in permafrost are highly nonlinear and require additional equations.

The hydraulic conductivity of porous media in partially frozen ground is typically represented as the product of the hydraulic conductivity in saturated, unfrozen conditions K_u (m s^{-1}) and a dimensionless 'relative hydraulic conductivity' K_r that is less than 1 and a function of the liquid water saturation S_L.

$$K = K_u K_r(S_L) \tag{17.4}$$

The magnitude of K_r can become very low (e.g., 1×10^{-6}) as temperatures decrease and the pore water freezes. There are several approaches for representing the relationship between relative hydraulic conductivity and liquid water saturation (i.e., $K_r(S_L)$). These are often based on classic relative hydraulic conductivity

functions derived for unfrozen, drying soils (e.g., Mualem 1976) with pore water pressure or water saturation as the independent variable. These relative hydraulic conductivity functions for drying soils, when expressed with water saturation as the independent variable, are transferrable for saturated freezing soils with liquid water saturation as the independent variable.

Early modeling studies employing this approach of using drying soil K_r functions for frozen soil applications yielded calculated K values that were too high in comparison to those inferred from laboratory experiments on the same frozen soils (Harlan 1973). Several researchers (e.g., Jame and Norum 1980; Lundin 1990) attributed this apparent discrepancy to the fact that unsaturated zone relative hydraulic conductivity functions were developed with air and liquid water as the two pore phases, whereas in saturated zone permafrost hydrogeology, the two pore phases are liquid water and ice. Pore ice is thought to exhibit more of a hydraulic 'no slip' interface compared to pore air. Thus, multiple studies have proposed employing an additional, empirical hydraulic impedance term (Ω) that is a function of the pore ice saturation (S_i). This results in a modified form of Eq. (17.4).

$$K = K_u K_r(S_L)\Omega(S_i) \tag{17.5}$$

Various forms of the impedance factor have been proposed and are reviewed by Kurylyk and Watanabe (2013). This impedance approach has been heavily criticized due to its arbitrary and empirical nature and the lack of a physical basis for its inclusion (Newman and Wilson 1997). Recent work has shown that the impedance factor is not required (Newman 1995; Painter 2011), although the vast majority of permafrost hydrogeology studies still employ this approach. Bi-modal porosity-hydraulic conductivity functions (e.g., Priesack and Durner 2006) typically perform better for frozen soils as suctions can be much higher than in drying soils (Kurylyk and Watanabe 2013). Figure 17.5a presents laboratory data that indicate that the hydraulic conductivity of frozen and unfrozen soils at the same liquid water content are reasonably similar over a large range of water contents. However, there are discernible differences for the Andisol soil at moisture contents around 0.35 and the silt loam at moisture contents below 0.25.

17.4.3 Soil Freezing Characteristic Curves

Relative hydraulic conductivity functions for frozen soils depend on the liquid water content, and thus a mathematical function is required to calculate the liquid water content for sub-zero temperatures in °C. This function, known as the soil freezing curve (SFC), can be estimated from soil water characteristic curves (SWCs) used in unfrozen, drying soils to relate the water content to the matric potential (e.g., Brooks and Corey 1964; van Genuchten 1980). In drying soils, complete desaturation does not immediately occur as the pore water pressure drops below atmospheric pressure, but rather it occurs over a range of matric potential (negative pressures). This range is dependent on the soil structure, with

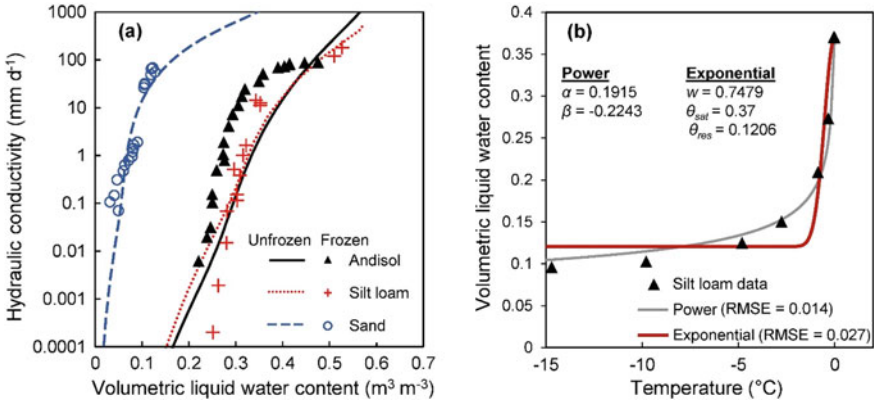

Fig. 17.5 **a** Hydraulic conductivity versus volumetric liquid water content for unfrozen (lines) and frozen (symbols) conditions for three types of soils (colors). Data are from Watanabe and Osada (2016, figure updated), and further experimental details are presented in that study. **b** Volumetric liquid water content versus temperature (i.e., soil freezing curves) from a laboratory experiment for silt loam (data from Watanabe and Wake 2009; Kurylyk and Watanabe 2013, figure updated) and the best fit power (Eq. 17.6) and exponential (Eq. 17.7) curves obtained by adjusting the parameters to minimize the root-mean-square-error (RMSE). Optimized parameters are indicated. The parameters α, β, w, θ_{sat}, and θ_{res} are defined below Eqs. 17.6 and 17.7

coarse-grained soils drying over a narrow potential range, and fine-grained soils desaturating over a much wider potential range. This phenomenon occurs because fine-grained soils retain water on the soil grains through capillary and sorptive forces. These drying processes are analogous to the transition of liquid pore water to pore ice during soil freezing. Pore water freezing occurs over a range of negative temperatures, and this range is primarily controlled by the soil structure. Fine-grained soils retain liquid water at lower temperatures than coarse-grained soils due to capillary and sorptive forces (Kurylyk and Watanabe 2013). Like soil drying and wetting, soil freezing and thawing exhibits hysteresis (Koopmans and Miller 1966; Parkin et al. 2013; Smerdon and Mendoza 2010); in other words, the soil characteristic curves differ depending on the directionality of freezing/drying and thawing/wetting. This has led a number of researchers to note the similarity between soil freezing and soil drying and to exploit this similarity to obtain SFCs based on previously determined SWCs (Koopmans and Miller 1966; Spaans and Baker 1996).

The primary independent variable of the SWC is pressure, and the primary variable of the SFC is temperature. Thus, the Clapeyron equation, which relates pressure and temperature during equilibrium phase change, is applied to directly transfer between the SWC and SFC. Kurylyk and Watanabe (2013) provide an overview of different forms of the Clapeyron equation and the tacit assumptions underlying each form. This approach of obtaining the SFC from the SWC is

powerful as SWC parameters have already been obtained for many types of soils, and thus further laboratory analyses are not required.

Other researchers have developed SFCs independently of any SWC. In such approaches, simple mathematical functions that are continuously differentiable are employed, and the parameters are adjusted to fit laboratory or field data. The power curve SFC is commonly applied in the permafrost geotechnical engineering field:

$$\theta_L = \alpha(-T)^{\beta} \tag{17.6}$$

where θ_L is the liquid water content (liquid saturation times porosity), T is the sub-zero temperature in °C, and α and β are empirical fitting parameters. Andersland and Ladanyi (1994, p. 40) tabulated values for α and β for 34 different soil types. Caution should be employed when obtaining these fitting parameters from geotechnical engineering books as this discipline expresses water content as a percent of dry unit weight rather than the volumetric ratios used in hydrology. However, a simple conversion can be used to apply the power curve parameters used in geotechnical studies for a volumetric saturation-based SFC (Eq. 22 of Kurylyk and Watnabe 2013). Recent permafrost hydrogeology models also often employ an exponential SFC (Mottaghy and Rath 2006):

$$\theta_L = \theta_{\text{res}} + (\theta_{sat} - \theta_{\text{res}}) \exp\left(-\left(\frac{T}{w}\right)^2\right) \tag{17.7}$$

where θ_{res} is the residual water content that exists even at very low temperatures, θ_{sat} is the saturated liquid water content and w is an empirical fitting parameter. Figure 17.5b presents experimental data for the SFC of a silt loam sample as well as the power and exponential fits obtained by minimizing the error between the laboratory data and functions.

17.4.4 Permafrost Hydrogeology and Heat Transfer

Given the influence of temperature on pore ice and hydraulic conductivity, hydrogeological processes are highly temperature-dependent in permafrost regions. Conversely, hydrogeological processes influence the ground thermal regime and permafrost distribution because groundwater flow induces heat advection (McKenzie and Voss 2013) and water contents influence ground thermal properties. Thus, heat transfer and water flow must be treated as fully coupled processes with interrelated physics. Chapter 28 of this book discusses heat transfer processes in more detail, and they are only briefly introduced here with nomenclature consistent with hydrogeological literature. In one dimension (z), the conductive heat flux (f_{cond}, W m^{-2}) is dependent on the thermal gradient $\frac{\partial h}{\partial l}$, °C m^{-1}) and the bulk medium thermal conductivity (λ, W m^{-1} °C^{-1}) in accordance with Fourier's law:

$$f_{\text{cond}} = -\lambda \frac{\partial T}{\partial z} \tag{17.8}$$

In one dimension, the advective heat flux due to mobile pore water (f_{adv}, W m^{-2}) is a function of the Darcy flux (q, m s^{-1}), the liquid water density (ρ_w, kg m^{-3}), the difference between the temperature T (°C) and a thermal datum (T_0, °C), and the liquid water specific heat c_w (J kg^{-1} °C^{-1}) (Lee 1998):

$$f_{\text{adv}} = q c_w \rho_w (T - T_0) \tag{17.9}$$

The effective heat capacity (C_{eff}, J m^{-3} °C^{-1}) is a measure of the medium's resistance to temperature change and includes heat storage due to both sensible and latent heat effects. In its simplest form, this is often presented as (Hansson et al. 2004):

$$C_{\text{eff}} = \left(C + L_f \rho_w \frac{\partial \theta_L}{\partial T} \right) \tag{17.10}$$

where C is the bulk medium sensible heat capacity (J m^{-3} °C^{-1}) and L_f is the latent heat of fusion for water (334,000 J kg^{-1}). The derivative in Eq. (17.10) is the rate of change of the liquid water content with respect to temperature. The appearance of this derivative in the effective heat capacity term implies that SFCs used in models must be continuously differentiable with respect to temperature over the thermal interval of phase change. Since liquid water content increases with increasing temperature, this derivative is always positive and adds to the magnitude of the effective heat capacity term. The first term on the right-hand side of Eq. (17.10) represents sensible heat storage, and the second term on the right-hand side represents latent heat storage. During phase change, the latent heat term strongly dominates C_{eff}. However, at temperature above 0 °C or below the freezing interval, this water content derivative is 0 and latent heat has no influence on C_{eff}.

Groundwater models for cold regions must represent both energy transport and water flow, and thus fully coupled partial differential equations are required for both processes. In essence, the governing equation for energy transport is formulated by equating the spatial derivatives (negative divergences) of the advective and conductive heat fluxes to the rate of change of energy stored in the form of sensible and latent heat. In one dimension (z), this can be readily shown to be the following from Eqs. (17.8)–(17.10) (Kurylyk et al. 2014a):

$$\frac{\partial}{\partial z}\left(\lambda \frac{\partial T}{\partial z} \right) - \frac{\partial}{\partial z}(q_z c_w \rho_w T) = \left(C + L_f \rho_w \frac{\partial \theta_L}{\partial T} \right) \frac{\partial T}{\partial t} \tag{17.11}$$

Note that the selection of the thermal datum T_0 is of no consequence once the spatial derivative of the advective heat flux is taken. Equation (17.11) is a simplified form of the heat transfer equation employed in most permafrost

hydrogeology models (Bense et al. 2009; McKenzie et al. 2007), and the inclusion of the Darcy flux indicates that groundwater flow influences the distribution of ground temperature and permafrost.

17.5 Permafrost Hydrogeology Model Development

Early, one-dimensional permafrost hydrogeology models emerged in the 1970s as resource development expanded rapidly into northern regions (e.g., Guymon and Luthin 1974; Harlan 1973; Jame 1977), but such models were mostly confined to research projects and not widely applied in practice. There has been renewed interest in permafrost hydrogeological modeling in recent years due to questions surrounding the impacts of intensified climate change on water, solute, and heat transport in permafrost environments as well as the increased demand for potable water supply in northern regions. Such studies have examined both the impacts of permafrost thaw on groundwater flow systems (Bense et al. 2009; Ge et al. 2011) as well as the impacts of groundwater flow systems on permafrost thaw rates (Kurylyk et al. 2016; McKenzie and Voss 2013; Sjöberg et al. 2016).

Established and widely applied subsurface flow models, including HYDRUS-1D (Hansson et al. 2004), SUTRA (McKenzie et al. 2007), and FEFLOW (Rühaak et al. 2015), have been enhanced to accommodate permafrost conditions. The inclusion of permafrost physics into groundwater models that hydrogeological practitioners are already familiar with should encourage the adoption of these models in industry. Assuming a groundwater model already has the capability to simulate groundwater flow and coupled thermal energy transfer, the four essential aspects of the code that must be modified to allow for ground freeze-thaw are: (1) latent heat effects in the effective heat capacity term and energy balance equation, (2) a relative hydraulic conductivity function that decreases the medium conductivity as pore ice forms, (3) a soil freezing curve that interacts with the heat capacity term as well as the relative hydraulic conductivity function, and (4) bulk thermal property functions that include the influence of pore ice on the medium thermal conductivity and volumetric heat capacity. State-of-the-art models include capabilities like deformable meshes (due to ground ice melt and ground subsidence) and capacity for massively parallel computing (Karra et al. 2014). Kurylyk and Watanabe (2013) provide a review of several of these codes and their different parameterizations, particularly in the choice of the SFC and K_r functions. These models have been applied to investigate a wide range of topics, including groundwater resource development in northern regions, contaminant transport issues arising from permafrost thaw, nuclear waste storage facility design, and groundwater flow effects on permafrost thaw and infrastructure stability.

In the past, development of these 'cryohydrogeology' models has predominantly occurred in relatively isolated modeling teams. However, the groundwater modeling consortium InterFrost was established in 2014 to facilitate international cooperation and to assess the performance of codes via standardized benchmarks

(https://wiki.lsce.ipsl.fr/interfrost/doku.php; Grenier et al. 2018). All InterFrost models have been favorably tested against analytical solutions to one-dimensional heat transfer equations that include conduction, advection, and freezing (Kurylyk et al. 2014b; McKenzie et al. 2007) and more rigorously tested using multi-dimensional numerical solution benchmarks (Rühaak et al. 2015; Grenier et al. 2018).

Table 17.1 presents recent numerical modeling studies of groundwater flow in permafrost settings that consider the influence of climate change. The majority of these are theoretical in nature and not fully grounded in hydrogeological field data. However, the past gap between field- and modeling-based permafrost hydrogeologists is slowly being bridged, and integrated projects that combine rigorous numerical modeling with intensive data collection are presently underway.

17.6 Summary and Future Directions

Groundwater storage and transmission processes strongly influence the distribution of both surface and subsurface water and ground temperatures (i.e., permafrost) in northern landscapes. The physics of groundwater flow in permafrost environments is complicated by the strong dependence of hydraulic conductivity on pore ice and thus temperature. Consequently, changing permafrost conditions arising from climate warming and infrastructure development are impacting the framework and functioning of hydrogeologic units. Hydrogeologic shifts in permafrost settings have been revealed by significant positive trends in river baseflow, and the postulated causal explanations for these trends (i.e., permafrost thaw leading to increased groundwater flow) have been supported through numerical simulations.

Although permafrost hydrogeology is a not a new research discipline, the field has been characterized by renewed interest and intensified research activity in recent years. Much of this research has been focused on the development of numerical models, but there are also now a larger number of permafrost-groundwater monitoring sites being established across the Arctic. There are still many opportunities for further cryohydrogeological model development. For example, few of the studies in Table 17.1 consider coupled solute transport dynamics. Such multi-physics capabilities would enable modelers to investigate the role of coupled heat, water, and solute transport in permafrost environments. Potential topics include carbon and other nutrient transport as well as contaminant mobilization following permafrost thaw. Also, the application of fully 3D groundwater models to study transient permafrost and groundwater conditions is challenging due to the computational requirements. It is expected that more codes will adapt by implementing massive parallel routines.

The greatest challenge facing researchers or practitioners who develop and/or apply cryohydrogeological models is the lack of data characterizing both permafrost and groundwater conditions. Likewise, a primary challenge to infer groundwater input and flowpaths in permafrost catchment from field techniques that use stream

Table 17.1 Modeling studies investigating the influence of climate change on permafrost thaw and groundwater flow. ALT = active layer thickness; PF = permafrost; GW = groundwater. Updated from Walvoord and Kurylyk (2016)

Model attribute	Trajectory (comment)	Model dimension	Scale (m) (Vertical × horizontal)	Location (model basis)	Model name	References
GW discharge	Increase (due to PF thaw)	2D	200 × 1000	Hypothetical scenario	Modified FlexPDE	Bense et al. (2009)
ALT (1) and supra-permafrost flow (2)	Increase (up to 3-fold) for (1) and (2)	2D	200 × 250	Tibet Plateau, China	SUTRA	Ge et al. (2011)
ALT (1) and seasonal variability of GW discharge (2)	Increase (1) and decrease due to permafrost thinning (2)	2D	30 × 100	Hypothetical scenario	MarsFlo	Frampton et al. (2011)
ALT	Increase (to 3 m)	1D	50 (vertical)	Alaska, USA	Hydrus	Jiang et al. (2012)
Baseflow and sub-permafrost flow	Increase	2D	600 × 10,000	Hypothetical scenario	Modified FlexPDE	Bense et al. (2012)
Glaciation cycles and sub-river talik closure	Talik closure post glaciation	2D	200 × 500	Paris Basin, France	Cast3M	Grenier et al. (2013)
PF distribution, GW flow	Enhanced PF thaw, GW flux, open talik formation	2D	2000 × 5000	Hypothetical scenario	SUTRA	McKenzie and Voss (2013)
PF thaw and GW flow	Decrease in intra-annual flow variability	2D	30 × 100	Hypothetical scenario	MarsFlo	Frampton et al. (2013)
ALT, supra-PF flux, lake/GW exchange	Enhanced ALT, supra-PF flux, lake/GW exchange, and lake talik evolution time	2D	500 × 1800	Alaska, USA	SUTRA	Wellman et al. (2013)
		1D	20	Alaska, USA	SUTRA	

(continued)

Table 17.1 (continued)

Model attribute	Trajectory (comment)	Model dimension	Scale (m) (Vertical × horizontal)	Location (model basis)	Model name	References
PF distribution and dynamics after lake recession	Decreased likelihood of reforming PF following lake recession					Briggs et al. (2014)
ALT, solute travel time	Increase in ALT, minimum and mean solute travel times through the subsurface	2D	30 × 100	Hypothetical scenario	MarsFlo	Frampton and Destouni (2015)
Alpine GW flow following PF thaw	3-fold increase in GW discharge	3D	2000 (deep) and 25 × 10^6 (area)	Qinghai-Tibet Plateau, China	SUTRA (but no coupled heat transfer)	Evans et al. (2015)
PF thaw, landscape change, and GW flow	Decreased plateaus, increased wetlands, rapid PF thaw, enhanced GW flow	3D	50 × 120 × 60	Scotty Creek, NWT	SUTRA	Kurylyk et al. (2016)
PF thaw and integrated surface/subsurface hydrology	ALT increase and changes to surface hydrological conditions	2D	Somewhat unspecified	Barrow, Alaska	Arctic Terrestrial Simulator	Painter et al. (2016)
PF thaw, GW flow, thaw settlement	Surface warming, GW flow and snow accumulation result in PF thaw and settlement	2D	50 × 100	Iqaluit, Nunavut	Heatflow/Smoker	Ghias et al. (2017)
GW flow in seasonally frozen and PF environments	Surface warming increases GW discharge more in PF than in seasonally frozen hillslopes	2D	Varying domains	Based loosely on the Tibet Plateau, China, and Yukon Flats, Alaska	SUTRA	Evans and Ge (2017)

hydrograph, chemistry, isotope, and/or temperature data (i.e., Koch et al. 2014) is lack of complementary subsurface characterization. Improved subsurface characterization through classic hydrogeological investigation techniques (e.g., borehole installation and pumping tests or single well tests; groundwater dating and geochemical analysis) and through the development and application of improved geophysical techniques and instruments is needed. Detailed hydrogeological data in permafrost settings are often possessed by companies interested in the extraction of natural resources and are considered proprietary. This hydrogeological information is critical, for example, for predicting dewatering rates during mining operations. Thus, stronger connections between academics and industry may be beneficial for advancing this discipline. Substantial research grants recently funded by the federal governments of Canada and the United States may also enable the development of publicly available datasets in permafrost settings. In general, amplified warming in northern environments (Serreze and Barry 2011) and the potential for groundwater resource development in northern communities should provide the interest and financial impetus for further research and new discoveries in permafrost hydrogeology in the coming years.

Acknowledgments Dr. Liangliang Duan (Northeast Forest University) is thanked for sharing the winter baseflow data from Fig. 17.4a; Dr. Joshua Koch (USGS) and Dr. Daqing Yang (Environment and Climate Change Canada) are thanked for reviewing the chapter and providing helpful comments. Dr. Peter Morse (Natural Resources Canada) graciously provided the photograph of the aufeis (Fig. 17.2, right). Kunio Watanabe (Mie University) kindly shared the data shown in Fig. 17.5.

References

Alaska Department of Environmental Conservation (2008) Groundwater in Alaska. Fact sheet available at: https://dec.alaska.gov/eh/pdf/dw/dwp-groundwater-fact-sheet-2008.pdf

Andersland OB, Ladanyi B (1994) An introduction to frozen ground engineering. Chapman & Hall, New York

Banfield L, Jardine CG (2013) Consultation and remediation in the north: meeting international commitments to safeguard health and well-being. Int J Circumpolar Health 72(1). https://doi.org/10.3402/ijch.v72i0.21231

Bense VF, Ferguson G, Kooi H (2009) Evolution of shallow groundwater flow systems in areas of degrading permafrost. Geophys Res Lett 36(22):L22401. https://doi.org/10.1029/2009GL039225

Bense VF, Kooi H, Ferguson G, Read T (2012) Permafrost degradation as a control on hydrogeological regime shifts in a warming climate. J Geophys Res-Earth Surf 117(F3): F030363. https://doi.org/10.1029/2011JF002143

Briggs MA, Walvoord MA, McKenzie JM et al (2014) New permafrost is forming around shrinking Arctic lakes, but will it last? Geophys Res Lett 41(5):1585–1592. https://doi.org/10.1002/2014GL059251

Bring A, Fedorova I, Dibike Y, Hinzman L, Mård J, Mernild SH, Prowse T, Semenova O, Stuefer SL, Woo M-K (2016) Arctic terrestrial hydrology: A synthesis of processes, regional effects, and research challenges. J Geophys Res Biogeosci 121:621–649. https://doi.org/10.1002/2015JG003131

Brooks RH, Cory AT (1964) Hydraulic properties of porous media. Hydrology Papers, vol 3. Colorado State University, Fort Collins, CO

Brutsaert W, Hiyama T (2012) The determination of permafrost thawing trends from long-term streamflow measurements with an application in eastern Siberia. J Geophys Res 117(D22110). https://doi.org/10.1029/2012jd018344

Callegary JB, Kikuchi CP, Koch JC, Lilly MR, Leake SA (2013) Review: groundwater in Alaska. Hydrogeo J 21(1):25–39. https://doi.org/10.1007/s10040-012-0940-5

Carroll ML, Townshend JRG, DiMiceli CM, Loboda T, Sohlberg RA (2011) Shrinking lakes of the Arctic: spatial relationships and trajectory of change. Geophys Res Lett 38:L20406. https://doi.org/10.1029/2011GL049427

Cederstrom DG, Johnston PM, and Subitzky S (1953) Occurrences and development of ground water in permafrost regions. U.S. Geological Survey Circular 275, Washington DC

Charkin AN, Rutgers van der Loeff M, Shakhova NE, Gustafsson Ö, Dudarev OV, Cherepnev MS, Salyuk AN, Koshurnikov AV, Spivak EA, Gunar AY, Ruban AS, Semiletov IP (2017) Discovery and characterization of submarine groundwater discharge in the Siberian Arctic seas: a case study in the Buor-Khaya Gulf, Laptev Sea. Cryosphere 11:2305–2327. https://doi.org/10.5194/tc-11-2305-2017

Connon RF, Quinton WL, Craig JR, Hayashi M (2014) Changing hydrologic connectivity due to permafrost thaw in the lower Liard River valley, NWT, Canada. Hydrol Process 28:4163–4178. https://doi.org/10.1002/hyp.10206

Connon R, Devoie E, Hayashi M et al (2018) The influence of shallow taliks on permafrost thaw and active layer dynamics in subarctic Canada. J Geophys Res—Earth Surf, 123(2): 281–297. https://doi.org/10.1002/2017jf004469

Darcy H (1856) Les Fontaines Publiques de la Ville de Dijon. Dalmont, Paris

Dimova NT, Paytan A, Kessler JD, Sparrow KJ, Kodovska FG-T, Lecher A, Murray J, Tulaczyk SM (2015) Current magnitude and mechanisms of groundwater discharge in the Arctic: case study from Alaska. Environ Sci Tech 49(20):12036–12043

Duan L, Man X, Kurylyk, BL, Cai T (2017) Increasing winter baseflow in response to permafrost thaw and precipitation regime shifts in northeastern China. Water 9(1). https://doi.org/10.3390/w9010025

Evans SG, Ge S (2017) Contrasting hydrogeologic responses to warming in permafrost and seasonally frozen ground hillslopes. Geophys Res Lett 44(4):1803–1813. https://doi.org/10.1002/2016GL072009

Evans SG, Ge S, Liang S (2015) Analysis of groundwater flow in mountainous, headwater catchments with permafrost. Water Resour Res 51:9564–9576. https://doi.org/10.1002/2015WR017732

Fetter CW (2001) Applied hydrogeology, vol 4. Prentice-Hall, Inc., New Jersey

Frampton A, Destouni G (2015) Impact of degrading permafrost on subsurface solute transport pathways and travel times. Wat Resour Res 51(9):7680–7701. https://doi.org/10.1002/2014WR016689

Frampton A, Painter SL, Destouni G (2013) Permafrost degradation and subsurface-flow changes caused by surface warming trends. Hydrogeo J 21(1):271–280. https://doi.org/10.1007/s10040-012-0938-z

Frampton A, Painter S, Lyon SW, Destouni G (2011) Non-isothermal, three-phase simulations of near-surface flows in a model permafrost system under seasonal variability and climate change. J Hydrol 403(3–4):352–359. https://doi.org/10.1016/j.jhydrol.2011.04.010

Frederick JM, Buffett BA (2016) Submarine groundwater discharge as a possible formation mechanism for permafrost-associated gas hydrate on the circum-Arctic continental shelf. J Geophys Res Solid Earth 121:1383–1404. https://doi.org/10.1002/2015JB012627

Ge S, McKenzie JM, Voss CI, Wu Q (2011) Exchange of groundwater and surface-water mediated by permafrost response to seasonal and long term air temperature variation. Geophys Res Lett 38(14):L14402. https://doi.org/10.1029/2011GL047911

Ge S, Yang D, Kane DL (2013) Yukon River Basin long term (1977–2006) hydrologic and climatic analysis. Hydrol Process 27(17):2475–2484. https://doi.org/10.1002/hyp.9282

van Genuchten MT (1980) A closed-form equation for predicting the hydraulic conductivity of unsaturated soils. Soil Sci Soc Am J 44(5):892–898. https://doi.org/10.2136/sssaj1980.03615995004400050002x

Ghias MS, Therrien R, Molson J, Lemieux J-M (2017) Controls on permafrost thaw in a coupled groundwater-flow and heat-transport system: Iqaluit Airport, Nunavut, Canada. Hydrogeol J 25 (3):657–673. https://doi.org/10.1007/s10040-016-1515-7

Grenier C, Regnier D, Mouche E et al (2013) Impact of permafrost development on groundwater flow patterns: a numerical study considering freezing cycles on a two-dimensional vertical cut through a generic river-plain system. Hydrogeol J 22(1):257–270. https://doi.org/10.1007/s10040-012-0909-4

Grenier C, Anbergen H, Bense V et al (2018). Groundwater flow and heat transport for systems undergoing freeze-thaw: Inter-comparison of numerical simulators for 2D test cases. Adv Wat Res. 114:196–218. https://doi.org/10.1016/j.advwatres.2018.02.001

Guymon GL, Luthin JN (1974) A coupled heat and moisture transport model for Arctic soils. Wat Resour Res 10(5):995–1001. https://doi.org/10.1029/WR010i005p00995

Haldorsen S, Heim M, Lauritzen S-E (1996) Subpermafrost groundwater, western Svalbard. Hydro Res 27(2):57–68

Hansson K, Simunek J, Mizoguchi M et al (2004) Water flow and heat transport in frozen soil: Numerical solution and freeze-thaw applications. Vad Zone J 3(2):693–704. https://doi.org/10.2113/3.2.693

Harlan RL (1973) Analysis of coupled heat-fluid transport in partially frozen soil. Water Resour Res 9(5):1314–1323. https://doi.org/10.1029/WR009i005p01314

Herman-Mercer N, Schuster PF, Maracle KB (2011) Indigeneous observations of climate change in the lower Yukon River basin, Alaska. Hum Organ 70:244–252

Hiscock KM, Bense VF (2014) Hydrogeology: Principles and practice, 2nd edn. John Wiley and Sons Ltd, Sussex, UK

Jame YW, Norum DI (1980) Heat and mass-transfer in a freezing unsaturated porous-medium. Wat Resour Res 16(4):811–819. https://doi.org/10.1029/WR016i004p00811

Jame YW (1977). Heat and mass transfer in freezing unsaturated soil. PhD thesis, University of Saskatchewan, Saskatoon, Saskatchewan

Jepsen SM, Voss CI, Walvoord MA, Minsley BJ, Rover J (2013) Linkages between lake shrinkage/expansion and sublacustrine permafrost distribution determined from remote sensing of interior Alaska, USA. Geophy Res Lett 40:882–887. https://doi.org/10.1002/grl.50187

Jiang Y, Zhuang Q, O'Donnell JA (2012) Modeling thermal dynamics of active layer soils and near-surface permafrost using a fully coupled water and heat transport model. J Geophys Res-Atmos 117(D11110). https://doi.org/10.1029/2012jd017512

Jones CE, Kielland K, Hinzman LD (2015) Modeling groundwater upwelling as a control on river ice thickness. Hydrol Res 46(4):566–577

Kane DL, Yoshikawa K, McNamara J (2013) Regional groundwater flow in an area mapped as continuous permafrost. Hydrogeo J 21(1):41–51. https://doi.org/10.1007/s10040-012-0937-0

Karra S, Painter SL, Lichtner PC (2014) Three-phase numerical model for subsurface hydrology in permafrost-affected regions (PFLOTRAN-ICE v1.0). Cryosphere 8:1935–1950. https://doi.org/10.5194/tc-8-1935-2014

Kipp LE, Charette MA, Moore WS, Henderson PB, Rigor IG (2018) Increased fluxes of shelf-derived material to the central Arctic Ocean. Sci Adv 4(1). https://doi.org/10.1126/sciadv.aao1302

Koch J, Kikuchi CP, Wickland K, Schuster P (2014) Runoff sources and flowpaths in a partially burned, upland boreal catchment underlain by permafrost. Water Resour Res 50:8141–8158. https://doi.org/10.1002/2014WR015586

Koopmans RWR, Miller RD (1966) Soil freezing and soil water characteristic curves. Soil Sci Soc Am Proc 30(6):680–685. https://doi.org/10.2136/sssaj1966.03615995003000060011x

Korosi JB, Thienpont JR et al (2017) Broad-scale lake expansion and flooding inundates essential wood bison habitat. Nat Commun 8:1–8. https://doi.org/10.1038/ncomms14510

Kurylyk BL, Hayashi M, Quinton WL et al (2016) Influence of vertical and lateral heat transfer on permafrost thaw, peatland landscape transition, and groundwater flow. Wat Resour Res 52 (2):1286–1305. https://doi.org/10.1002/2015WR018057

Kurylyk BL, MacQuarrie KTB, McKenzie JM (2014a) Climate change impacts on groundwater and soil temperatures in cold and temperate regions: implications, mathematical theory, and emerging simulation tools. Earth-Sci Rev 138:313–334. https://doi.org/10.1016/j.earscirev.2014.06.006

Kurylyk BL, McKenzie JM, MacQuarrie KTB, Voss CI (2014b) Analytical solutions for benchmarking cold regions subsurface water flow and energy transport models: one-dimensional soil thaw with conduction and advection. Adv Wat Resour 70:172–184. https://doi.org/10.1016/j.advwatres.2014.05.005

Kurylyk BL, Watanabe K (2013) The mathematical representation of freezing and thawing processes in variably-saturated, non-deformable soils. Adv Wat Resour 60:160–177. https://doi.org/10.1016/j.advwatres.2013.07.016

Lebreque S, Lacelle D, Duguay CR, Lauriol B, Hawkings JIM (2009) Contemporary (1951–2001) evolution of lakes in the Old Crow Basin, northern Yukon, Canada: Remote sensing, numerical modeling, and stable istope analysis. Arctic 62(2): 119–225.

Lecher A (2017) Groundwater discharge in the Arctic: a review of studies and implications for biogeochemistry. Hydrol 4(41). https://doi.org/10.3390/hydrology40300041

Lee T-C (1998) Applied mathematics in hydrogoelogy. CRC Press, Boca Raton, Florida

Lemieux J-M, Fortier R, Talbot-Poulin M-C et al (2016) Groundwater occurrence in cold environments: examples from Nunavik, Canada. Hydrogeo J 24(6):1497–1513. https://doi.org/10.1007/s10040-016-1411-1

Lundin L-C (1990) Hydraulic properties in an operational model of frozen soil. J Hydrol 118(1–4):289–310. https://doi.org/10.1016/0022-1694(90)90264-X

Lyon SW, Destouni G, Giesler R et al (2009) Estimation of permafrost thawing rates in a sub-arctic catchment using recession flow analysis. Hydrol Earth Syst Sci 13:595–604. https://doi.org/10.5194/hess-13-595-2009

McKenzie JM, Voss CI (2013) Permafrost thaw in a nested groundwater-flow system. Hydrogeo J 21(1):299–316. https://doi.org/10.1007/s10040-012-0942-3

McKenzie JM, Voss CI, Siegel DI (2007) Groundwater flow with energy transport and water–ice phase change: numerical simulations, benchmarks, and application to freezing in peat bogs. Adv Water Resour 30(4):966–983. https://doi.org/10.1016/j.advwatres.2006.08.008

Michel FA, van Everdingen RO, Woo M-K, Dyke L (2014) Permafrost groundwater region. In: Rivera A (ed) Canada's groundwater resources. Fitzhenry and Whiteside, Markham, Canada, pp 598–636

Mottaghy D, Rath V (2006) Latent heat effects in subsurface heat transport modelling and their impact on palaeotemperature reconstructions. Geophys J Int 164(1):236–245. https://doi.org/10.1111/j.1365-246X.2005.02843.X

Mualem Y (1976) New model for predicting hydraulic conductivity of unsaturated porous-media. Wat Resour Res 12(3):513–522. https://doi.org/10.1029/WR012i003p00513

Newman GP (1995) Heat and mass transfer in unsaturated soils during freezing. University of Saskatchewan, Saskatoon, Saskatchewan, Thesis

Newman GP, Wilson GW (1997) Heat and mass transfer in unsaturated soils during freezing. Can Geotech J 34(1):63–70. https://doi.org/10.1139/cgj-34-1-63

O'Donnell JA, Aiken GR, Walvoord MA, Butler KD (2012) Dissolved organic matter composition of winter flow in the Yukon River basin: Implications of permafrost thaw and increased groundwater discharge. Glob Biogeochem Cycles 26:GB0E06. https://doi.org/10.1029/2012gb004341

Painter SL (2011) Three-phase numerical model of water migration in partially frozen geological media: model formulation, validation, and applications. Comp Geosci 15(1):69–85. https://doi.org/10.1007/s10596-010-9197-z

Painter SL, Coon ET, Atchley AL et al (2016) Integrated surface/subsurface permafrost thermal hydrology: model formulation and proof-of-concept simulations. Wat Resour Res 52(8):6062–6077. https://doi.org/10.1002/2015WR018427

Parkin G, von Bertoldi A, McCoy AJ (2013) Effect of tillage on soil water content and temperature under freeze-thaw conditions. Vadose Zone J 12(1). https://doi.org/10.2136/vzj2012.0075

Pearce TD, Ford JD, Prno J, Duerden F, Pittman J, Beumier M, Berrang-Ford L, Smit B (2011) Climate change and mining in Canada. Mitig Adapt Strat Glob Change 16(3):347–368. https://doi.org/10.1007/s11027-010-9269-3

Priesack E, Durner W (2006) Closed-form expression for the multi-modal unsaturated conductivity function. Vadose Zone J 5(1):121–124. https://doi.org/10.2136/vzj2005.0066

Rennermalm AK, Wood EF, Troy TJ (2010) Observed changes in pan-arctic cold-season minimum monthly river discharge. Clim Dyn 35(6):923–939. https://doi.org/10.1007/s00382-009-0730-5

Rowland JC, Travis BJ, Wilson CJ (2011) The role of advective heat transport in talik development beneath lakes and ponds in discontinuous permafrost. Geophys Res Lett 38: L17504. https://doi.org/10.1029/2011GL048497

Rühaak W, Anbergen H, Grenier C et al (2015) Benchmarking numerical freeze/thaw models. Energy Procedia 76:301–310. https://doi.org/10.1016/j.egypro.2015.07.866

Sannikov G (2012) Mapping-based research into the thermokarst lakes within Bova gas field territory Yamal peninsula. (*in Russian*). Kriosphera Zemli 2:30–37

Schuster PF, Schaefer KM, Aiken GR et al. (2018) Permafrost stores a globally significant amount of mercury. Geophys Res Lett 45. https://doi.org/10.1002/2017GL075571

Schuur EAG, Bockheim J, Canadell JG, Euskirchen E, Field CB et al (2008) Vulnerability of permafrost carbon to climate change: implications for the global carbon cycle. Bioscience 58:701–714

Serreze MC, Barry RC (2011) Processes and impacts of Arctic amplification: a research synthesis. Glob Planet Change 77:85–96

Shiklomanov N, Streletskiy DA, Little JD, Nelson FE (2013) Isotropic thaw subsidence in undisturbed permafrost landscapes. Geophys Res Lett 40:6331–6356. https://doi.org/10.1002/2013GL058295

Shur Y, Hinkel K, Nelson FE (2005) The transient layer: Implications for geocryology and climate-change science. Perma Periglac Process 16:5–17. https://doi.org/10.1002/ppp.518

Sjöberg Y, Coon E, Sannel K et al (2016) Thermal effects of groundwater flow through subarctic fens: a case study based on field observations and numerical modeling. Water Resour Res 52 (3):1591–1606. https://doi.org/10.1002/2015WR017571

Sjöberg Y, Frampton A, Lyon S (2013) Using streamflow characteristics to explore permafrost thawing in northern Sweden. Hydrogeol J 21(1):121–131. https://doi.org/10.1007/s10040-012-0932-5

Sloan CE, van Everdingen RO (1988) Region 28, permafrost region. In: Back W, Rosenshein JS, Seaber PR (eds) Hydrogeology. Geological Society of America, USA, pp 263–270

Smerdon BD, Mendoza CA (2010) Hysteretic freezing characteristics of riparian peatlands in the Western Boreal Forest of Canada. Hydrol Proc 24(8):1027–1038. https://doi.org/10.1002/hyp.7544

Smith LC, Sheng Y, MacDonald GM, Hinzman LD (2005) Disappearing Arctic lakes. Science 308 (5727)

Smith LC, Pavelsky TM, MacDonald GM et al (2007) Rising minimum daily flows in northern Eurasian rivers: a growing influence of groundwater in the high-latitude hydrologic cycle. J Geophys Res-Biogeosci 112(G4):G04S47. https://doi.org/10.1029/2006JG000327

Spaans EJA, Baker JM (1996) The soil freezing characteristic: Its measurement and similarity to the soil moisture characteristic. Soil Sci Soc Am J 60:13–19. https://doi.org/10.2136/sssaj1996.03615995006000010005x

St. Jacques J-M, Sauchyn DJ (2009) Increasing winter baseflow and mean annual streamflow from possible permafrost thawing in the Northwest Territories, Canada. Geophys Res Lett 36(1): L01401. https://doi.org/10.1029/2008GL035822

Taniguchi M, Burnett WC, Cable JE, Turner JV (2002) Investigation of submarine groundwater discharge. Hydrol Proc 16:2115–2129. https://doi.org/10.1002/hyp.1145

Tolstikhin NI, Tolstikhin ON (1974) Groundwater and surface water in the permafrost region. In: Melnikov PI, Tolstikhin ON (eds) Chap. 9, General permafrost studies USSR Academy of Sciences (Trans. by Environment Canada, Technical Bulletin 97)

Vonk JE, Tank SE, Bowden WB et al (2015) Reviews and syntheses: effects of permafrost thaw on Arctic aquatic ecosystems. Biogeosci 12:7129–7167

Walvoord MA, Striegl RG (2007) Increased groundwater to stream discharge from permafrost thawing in the Yukon River basin: Potential impacts on lateral export of carbon and nitrogen. Geophys Res Lett 34(12):1–6. https://doi.org/10.1029/2007GL030216

Walvoord MA, Voss CI, Wellman TP (2012) Influence of permafrost distribution on groundwater flow in the context of climate-driven permafrost thaw: Example from Yukon Flats Basin, Alaska, United States. Water Resour Res 48(W07524). https://doi.org/10.1029/2011wr011595

Walvoord MA, Kurylyk BL (2016) Hydrologic impacts of thawing permafrost- A review. Vadose Zone J 15(6)

Watanabe K, Wake T (2009) Measurement of unfrozen water content and relative permittivity of frozen unsaturated soil using NMR and TDR. Cold Reg Sci Technol 59(1):34–41. https://doi.org/10.1016/j.coldregions.2009.05.011

Watanabe K, Osada Y (2016). Comparison of hydraulic conductivity in frozen saturated and unfrozen unsaturated soils. Vadose Zone J 15(5). https://doi.org/10.2136/vzj2015.11.0154

Wellman TC, Voss CI, Walvoord MA (2013) Impacts of climate lake size, and supra- and sub-permafrost groundwater flow on lake-talik evolution, Yukon Flats, Alaska (USA). Hydrogeol J 21(1):281–298. https://doi.org/10.1007/s10040-012-0941-4

Williams PJ, Smith MW (1989) The frozen earth: fundamentals of geocryology. Cambridge University Press, Cambridge, UK

Williams JR (1970) Ground water in the permafrost regions of Alaska. Professional Paper 696, U. S. Geological Survey, Washington DC

Williams JR (1965) Ground water in permafrost regions—An annotated bibliography. U.S. Geological Survey Water-Supply Paper 1792, Washington DC

Woo M-K, Kane DL, Carey SK, Yang D (2008) Progress in permafrost hydrology in the new millennium. Perma Periglac Process 19(2):237–254. https://doi.org/10.1002/ppp.613

Ye B, Yang D, Kane DL (2003) Changes in Lena river streamflow hydrology: Human impacts vs. natural variations. Wat Resour Res 39(8). https://doi.org/10.1029/2003wr001991

Ye B, Yang D, Zhang Z, Kane DL (2009) Variation of hydrological regime with permafrost coverage over Lena Basin in Siberia. J Geophys Res 114(D7). https://doi.org/10.1029/2008jd010537

Yoshikawa K, Hinzman LD (2003) Shrinking thermokarst ponds and groundwater dynamics in discontinuous permafrost near council, Alaska. Perma Periglac Process 14:151–160. https://doi.org/10.1002/ppp.451

van Everdingen RO (1974) Ground water in permafrost regions of Canada. In: Proceedings, workshop seminars on permafrost hydrology, Canadian National Committee, International Hydrology Decade, Environment Canada, Ottawa, pp 83–93

Dr. Barret L. Kurylyk is an Assistant Professor and Canada Research Chair in the Department of Civil and Resource Engineering and the Centre for Water Resources Studies at Dalhousie University in Halifax, Nova Scotia, Canada. His research interest and activities along permafrost themes include phase change physics in porous media, permafrost hydrology and hydrogeology, numerical model development, climate change impacts, and subsurface coastal zone processes. He received his Doctoral degree in Civil Engineering at the University of New Brunswick (Canada) and was a Killam and NSERC Postdoctoral Fellow at the University of Calgary.

Dr. Michelle A. Walvoord is Research Hydrologist in the Earth System Processes Division of the U.S. Geological Survey in Denver, Colorado (USA) and serves as an adjunct faculty member at the Colorado School of Mines. Her cold regions research activities focus on understanding climate change impacts on hydrologic processes in permafrost regions of the Yukon River Basin of Alaska and western Canada. Her work relies on integrated multi-scale field and modeling approaches from various disciplines including hydrology, hydrogeology, biogeochemistry, hydrogeophysics, and remote sensing. She received her Master's and Doctoral degrees in Hydrology and Earth & Environmental Science, respectfully, at the New Mexico Institute of Mining and Technology, in Socorro, New Mexico (USA).

Part IV
Ecosystem Change and Impact

Greenhouse Gases and Energy Fluxes at Permafrost Zone

18

Masahito Ueyama, Hiroki Iwata, Hideki Kobayashi, Eugénie Euskirchen, Lutz Merbold, Takeshi Ohta, Takashi Machimura, Donatella Zona, Walter C. Oechel, and Edward A. G. Schuur

Abstract

Energy, water, and greenhouse gas exchange in the permafrost zone play an important role in the regional and global climate system at multiple temporal and spatial scales. High-latitude warming in recent years has substantially altered ecosystem function, including biosphere–atmosphere interaction, which may amplify or dampen future high-latitude warming through a variety of feedback

M. Ueyama (✉)
Graduate School of Life and Environmental Sciences, Osaka Prefecture University, Osaka, Japan
e-mail: ueyama@envi.osakafu-u.ac.jp

H. Iwata
Department of Environmental Science, Faculty of Science, Shinshu University, Matsumoto, Japan
e-mail: hiwata@shinshu-u.ac.jp

H. Kobayashi
Japan Agency for Marine-Earth Science and Technology, Research Institute for Global Change, Institute of Arctic Climate and Environment Change Research, Yokohama, Japan
e-mail: hkoba@jamstec.go.jp

E. Euskirchen
University of Alaska Fairbanks, Institute of Arctic Biology, Fairbanks, AK, USA
e-mail: seeuskirchen@alaska.edu

L. Merbold
International Livestock Research Institute (ILRI), Mazingira Centre, Nairobi, Kenya
e-mail: lutz.merbold@gmail.com

T. Ohta
School of Agriculture, Nagoya University, Nogoya, Japan
e-mail: takeshi_1956@grace.ocn.ne.jp

D. Yang and D. L. Kane (eds.), *Arctic Hydrology, Permafrost and Ecosystems*,
https://doi.org/10.1007/978-3-030-50930-9_18

processes. In this chapter, we have reviewed the current state of energy, water, CO_2, and CH_4 exchange at the northern high-latitude permafrost zone, with synthesizing observed micrometeorological fluxes. Tundra has a higher summer and winter albedo with a longer snow period than boreal forests, resulting in that tundra less transfers sensible and latent energy to the atmosphere. Growing season length determines the spatial variability of the annual gross primary productivity and net growing season CO_2 sink. In contrast, interannual variabilities of the annual CO_2 budget at boreal forests are determined by ecosystem respiration, indicating an importance of ecosystem respiration in the boreal forests. The CO_2 fertilization effect could be an important determinant of the long-term greenhouse gas budget at sites with a near neutral CO_2 budget. In terms of annual greenhouse gas budget, CH_4 emission is more important than CO_2 budget for both boreal forest and Arctic wet tundra. Based on this synthesis, finally, we discuss future possible directions of study to reach a better understanding of changing high-latitude ecosystems, by synthesizing tower flux measurements in Alaska and Siberia and combining these in situ measurements with remote sensing data.

18.1 Introduction

The Arctic and boreal permafrost zone is experiencing substantial warming. This warming happens more than twice as rapid as the global warming trend (AMAP 2017). The predicted increase in northern high-latitude temperature is 5–9 °C later in this century (IPCC 2013). This high-latitude warming changes the terrestrial ecosystems' processes and conditions (Hinzman et al. 2005), such as permafrost integrity, plant community structure, biomass, growth and decomposition, disturbance regime, ecophysiology, hydrology, and biogeochemical cycle. The changes

T. Machimura
Graduate School of Engineering, Osaka University, Osaka, Japan
e-mail: mach@see.eng.osaka-u.ac.jp

D. Zona · W. C. Oechel
Biology Department, San Diego State University, San Diego, CA, USA
e-mail: dzona@sdsu.edu

W. C. Oechel
e-mail: woechel@sdsu.edu

E. A. G. Schuur
Department of Biological Sciences, Northern Arizona University, Center for Ecosystem Science and Society, Flagstaff, AZ, USA
e-mail: Ted.Schuur@nau.edu

induce positive and/or negative feedbacks to the earth's climate system predominantly through changes in the surface energy balance and carbon cycle.

In the northern high-latitude permafrost zone, most of the carbon is stored within the active layer and permafrost of the permanently frozen soils, whereas comparatively little is stored within the vegetation (Chapin et al. 2011; Hugelius et al. 2014; Schuur et al. 2015; Tarnocai et al. 2009). This is because severe climate restricts vegetation productivity, whereas historically cold temperatures and poorly wet, drained soils have inhibited soil decomposition and heterotrophic respiration. High-latitude warming changes thermal and hydrological conditions, increasing the active layer depth and microbial activity, resulting in enhanced greenhouse gas emissions (Commane et al. 2017; Piao et al. 2008). This warming simultaneously stimulates plant productivity by prolonged growing seasons (Euskirchen et al. 2006; Forkel et al. 2016), which may promote greater carbon storage in the vegetation biomass. Consequently, high-latitude warming accelerates the carbon cycling (Graven et al. 2013), but it is still highly uncertain which of the two opposite feedbacks will be more dominated under the high-latitude warming (Belshe et al. 2013; McGuire et al. 2012).

Methane (CH_4) is important greenhouse gas originating in the Arctic and boreal zone. CH_4 occurs due to stagnant water table above permafrost leading to anoxic soil conditions. Extratropical wetlands comprise approximately 30% of the global wetland CH_4 emission (Melton et al. 2013). CH_4 is produced in anoxic soils by methanogenic archaea, and is emitted to the atmosphere primarily via three dominant pathways: molecular diffusion, plant-mediated transport through aerenchyma, and ebullition (McEwing et al. 2015; Tokida et al. 2007; Walter et al. 2006). During the transport processes, methanotrophic bacteria oxidize some of the CH_4 before it can escape to the atmosphere if aerobic surface soils and/or water exist. CH_4 production, oxidation, and its dominant emission pathway differ by wetland type and differ over space and time (Turetsky et al. 2014). Thus, CH_4 fluxes between ecosystems and the atmosphere show a nonlinear response to various environmental variables, such as water table depth (Olefeldt et al. 2013), soil temperature (Yvon-Durocher et al. 2014), active layer depth (Iwata et al. 2015), atmospheric pressure (Tokida et al. 2007), redox potentials, soil pH, and available organic carbon. Wetland plants provide substrates for CH_4 and effectively transport CH_4 to the atmosphere, resulting in which plant type, phenology, and microtopography determine magnitude of CH_4 flux (McEwing et al. 2015; Olefeldt et al. 2013; Sturtevant and Oechel 2013; Sachs et al. 2010). Microbial community differed over space and time, which also affects CH_4 flux (Wagner et al. 2017). Consequently, CH_4 fluxes are highly heterogeneous across temporal and spatial scales, hindering an accurate estimation of global CH_4 emission (Kirschke et al. 2013).

The surface energy balance also changes with the high-latitude warming (Chapin et al. 2000; Ueyama et al. 2014a). The warming alters surface albedo through an increase in wild fires (Randerson et al. 2006), vegetation greening (Pearson et al. 2013), northward migration of tree line (Hinzman et al. 2005), and a decrease in snow-covered periods (Euskirchen et al. 2007, 2010, 2016). From 2000 to 2011, a decrease in spring albedo was observed due to an earlier snowmelt that increased

the regional net radiation by 0.56 W m^{-2} $decade^{-1}$ (Ueyama et al. 2014a). The heating effect was comparable to cooling effect (0.59 W m^{-2} $decade^{-1}$) with increase in albedo by replacement of spruce forests with broadleaf forests after wild fires (Ueyama et al. 2014a). In addition to albedo, surface characteristics, such as roughness length, canopy conductance, and Bowen ratio, differ among high-latitude ecosystems (Beringer et al. 2005; McFadden et al. 2003), which, in turn, determines energy redistribution and water balance.

In the permafrost zone, micrometeorological flux measurements for greenhouse gases were first applied in the early 1990s during a summer field campaign (e.g., Oechel et al. 2000; Harazono et al. 1998; Hollinger et al. 1998; Vourlitis et al. 2000), and continuous monitoring only started in the late 1990s (e.g., Harazono et al. 2003; Kwon et al. 2006). Monitoring sites increased in 2000s for evaluating interactions between permafrost and energy fluxes (Iwata et al. 2012; Ohta et al. 2008), disturbance effects after fires (Chambers and Chapin 2003; Liu et al. 2005; Rocha and Shaver 2011; Randerson et al. 2006), permafrost degradation (Euskirchen et al. 2014, 2017b; Helbig et al. 2016a, 2017), contributions of understory in boreal forests (Ikawa et al. 2015), long-term CO_2 budgets (Euskirchen et al. 2017a; Ueyama et al. 2014b; Ohta et al. 2014), and CH_4 fluxes (Iwata et al. 2015; Harazono et al. 2006; Zona et al. 2009; 2016). Currently, a number of sites are operated in the permafrost zone as a part of the global network, FLUXNET. These measurements are providing valuable data for understanding the response of greenhouse gases and energy exchanges to climatic change.

In this chapter, we provide an overview of the current state of greenhouse gases and energy exchanges within the permafrost zone, and how this knowledge relates to a need for both continuing and expanding flux measurements and modeling in northern high latitudes. First, we present the basics of the tower flux measurements. We then show seasonal and spatial variation of the energy and greenhouse gas fluxes through a synthesis of flux tower measurements and remote sensing data. Finally, we discuss future possible directions of study to reach a better understanding of changes in the ecosystem function under a warming climate.

18.2 Theory

18.2.1 Micrometeorological Measurements

The micrometeorological eddy covariance method can quasi-continuously measure spatially representative fluxes between the biosphere and the atmosphere at the half-hourly or hourly timescale (Baldocchi 2008). Installing a sonic anemometer and gas analyzer that can measure all eddies contributing to the transfer over a vegetative canopy; the eddy covariance method provides areal mean flux (F) as a covariance between vertical wind velocity (w) and mixing ratio (m):

$$F = \rho \overline{w'm'} \tag{18.1}$$

where ρ represents air density, and overbar and prime represent time mean and fluctuation, respectively. The typical footprint of the eddy covariance flux stretches dozens of times of the measurement height to the upwind direction in unstable atmospheric conditions, but expands to more than 100 times during stable nighttime conditions.

18.2.2 Basic Equations of Surface Energy Exchange

The surface energy balance of terrestrial ecosystems is commonly determined as the difference between incoming and outgoing shortwave and longwave radiation:

$$\begin{aligned} Rn &= Rsd - Rsu + Rld - Rlu \\ &= Rsd(1-\alpha) + Rld - Rlu \end{aligned} \tag{18.2}$$

where Rn is net radiation, Rsd is incoming shortwave radiation, Rsu is outgoing shortwave radiation, Rld is incoming longwave radiation, Rlu is outgoing shortwave radiation, and α is albedo. Net radiation is redistributed to the heat fluxes including sensible heat (H), latent heat (LE), ground heat (G), and heat storage change in vegetation and air within a canopy (J):

$$Rn = H + LE + G + J. \tag{18.3}$$

In high-latitude ecosystems, ground heat flux often contains large uncertainties, because of heat storage of water and tussocks above installing heat plate depth and/or a different thermal conductivity of the plate compared with surrounding soil or mosses (Iwata et al. 2012; Nakai et al. 2013). In spring, the latent heat to melt snow and ice is also important term of radiation balance (Zhang 2005), which often consists of more than 30% of net radiation (Nakai et al. 2013).

Component of net radiation determines the available energy for atmospheric heating directly (sensible heat flux) and for evaporating water (latent heat flux) which determines atmospheric water vapor. The component of the energy budget involved in heating the soils is ground heat flux. Changes of net radiation and its partitioning thus alter atmospheric temperature and water vapor concentration, the freeze/thaw cycle of soil active layer, permafrost integrity, the height of planetary boundary layer, and biogeochemical and hydrological cycles, resulting in modifying the regional and global climate directly or indirectly (Chapin et al. 2000, 2005; Euskirchen et al. 2010; Helbig et al. 2016a).

18.2.3 Basic Equations of Greenhouse Gas Exchange

CO_2 exchange between the biosphere and the atmosphere is determined by the balance of two large gross fluxes: photosynthetic assimilation and autotrophic (Ra) and heterotrophic (Rh) respiration (Chapin et al. 2011). Net Ecosystem

Exchange of CO_2 (NEE) is defined as a difference between Ecosystem Respiration (RE) and Gross Primary Productivity (GPP).

$$\begin{aligned} NEE &= RE - GPP \\ &= Ra + Rh - GPP \\ &= Rh - NPP \\ &= -NEP \end{aligned} \tag{18.4}$$

Ecosystem respiration is sum of autotrophic and heterotrophic respiration. Net Primary Productivity (NPP) is net assimilation by autotrophs, and thus NEE is reformulated as a difference between Rh and NPP. Finally, Net Ecosystem Productivity (NEP) is opposite in sign to NEE; ecologists use NEP and define the flux as positive when carbon is gained into an ecosystem. CO_2 flux measured by the micrometeorological methods needs to account CO_2 storage within air space in the canopy; the term NEE is referred as a sum of measured CO_2 flux and the storage flux in micrometeorology.

Vegetation and soil play an important role in the CO_2 and CH_4 exchange in the permafrost zone. Plants uptake CO_2 by photosynthesis during the growing season while a part of the fixed carbon is respired through autotrophic respiration. Soil microbes decompose organic carbon, resulting in CO_2 emission as heterotrophic respiration under aerobic conditions and CH_4 under anaerobic conditions. Various types of soil organic carbon (e.g., plant litter, coarse woody debris, stored carbon within active layer, and permafrost) have different turnover rates and their decomposition rate, which has different responses to environmental factors. Contributions of autotrophic and heterotrophic respirations to ecosystem respiration differed among vegetation type (Hicks Pries et al. 2015). Consequently, the CO_2 balance is determined by leaf area index (McFadden et al. 2003; Ueyama et al. 2013b), disturbance history (Amiro et al. 2010; Goulden et al. 2010), growing season length (Ueyama et al. 2013b), soil organic carbon content, and changes in basic environmental factors (Hicks Pries et al. 2015). Since CH_4 is produced only under anaerobic conditions, hydrological conditions are the critical factors controlling ecosystem CH_4 exchange.

18.3 Synthesis of Flux Tower Data in Permafrost Zone

18.3.1 Study Sites

We review energy and greenhouse gas fluxes in Alaska and Siberia based on a synthesis of 28 flux tower sites (Table 18.1). The available data covers major ecosystems within the permafrost zone, including wet sedge tundra, moist tussock tundra, heath tundra, larch forests, and pine forest on the continuous permafrost

Table 18.1 Site characteristics including location, vegetation type, permafrost, mean annual temperature, annual sum of precipitation, years contained in the analysis, and references

Site name (code)	FLUXNET code	Latitude	Longitude	Region	Vegetation	Permafrost	Air temperature	Precipitation	Years	References
Barrow (BRW)	US-Brw	71.32	−156.63	Alaska	Wet sedge tundra	Continuous	−12.6	274[a]	1998 −2006 2013 −2016	Kwon et al. (2006)
Central Marsh (CMS)	US-CMS	71.32	−156.62	Alaska	Wet sedge tundra	Continuous	−12.6	274[a]	1999 −2005	Harazono et al. (2003)
Barrow Environmental Observatory (BEC)		71.28	−156.60	Alaska	Wet sedge tundra	Continuous	−12.6	274[a]	2005 −2008	Zona et al. (2009)
Barrow Environmental Observatory (BES)	US-Bes	71.28	−156.60	Alaska	Wet sedge tundra	Continuous	−12.6	274[a]	2013 −2016	Zona et al. (2009)
Barrow Environmental Observatory (BEO)		71.28	−156.61	Alaska	Wet sedge tundra	Continuous	−12.6	274[a]	2015 −2016	Zona et al. (2009)
Atqasuk (ATQ)	US-Atq	70.47	−157.41	Alaska	Moist tussock tundra	Continuous	−9.7	178	1999 −2006 2013 −2016	Oechel et al. (2014)
Sag River side (SAG)	US-SAG	69.51	−148.23	Alaska	Moist tussock tundra	Continuous	−8.0	121	1996	Harazono et al. (2006)
Happy Valley (HVA)	US-Hvs	69.14	−148.84	Alaska	Wet sedge tundra	Continuous	−10.29	217	1995	Harazono et al. (2006)
Anaktuvuk River Unburned (ARC)	US-An3	68.93	−150.27	Alaska	Moist tussock tundra	Continuous	−8.5	174	2008 −2010	Rocha and Shaver (2011)
	US-ICh	68.61	−149.30	Alaska	Heath tundra	Continuous	−7.4	318		

(continued)

Table 18.1 (continued)

Site name (code)	FLUXNET code	Latitude	Longitude	Region	Vegetation	Permafrost	Air temperature	Precipitation	Years	References
Imnavait Creek (IMH)									2007	Euskirchen et al. (2012, 2017a)
Imnavait Creek (IMT)	US-ICt	68.61	−149.30	Alaska	Moist tussock tundra	Continuous	−7.4	318	2007 −2011	Euskirchen et al. (2012, 2017a)
Imnavait Creek (IMW)	US-ICs	68.61	−149.31	Alaska	Wet sedge tundra	Continuous	−7.4	318	2007 −2017	Euskirchen et al. (2012, 2017a)
Ivotuk (IVO)	US-Ivo	68.49	−155.75	Alaska	Moist tussock tundra	Continuous	−8.28	304	2003 −2007 2013 −2016	McEwing et al. (2015)
Poker Flat Research Range (PRR)	US-Prr	65.12	−147.49	Alaska	Black spruce forest	Discontinuous	−2	275	2011 −2016	Ikawa et al. (2015)
Council spruce forest (COS)		64.91	−163.67	Alaska	White spruce forest	No prresence	−3.0	406	2000	Beringer et al. (2003, 2005)
Univeristy of Alaska, Fairbanks (UAF)	US-Uaf	64.87	−147.86	Alaska	Black spruce forest	Discontinuous	−2.9	263	2003 −2016	Ueyama et al. (2014b)
Council tundra (COT)		64.84	−163.69	Alaska	Moist tussock tundra	No prresence	−3.0	406	2000	Beringer et al. (2003, 2005)
Bonanza Creek Long term Experimental Forest (BNZ)		64.70	−148.32	Alaska	Black spruce forest	Discontinuous	−2.2	263	2010 −2017	Euskirchen et al. (2014)

(continued)

Table 18.1 (continued)

Site name (code)	FLUXNET code	Latitude	Longitude	Region	Vegetation	Permafrost	Air temperature	Precipitation	Years	References
Delta Junction spruce forest (DLS)		63.92	−145.75	Alaska	Black spruce forest	No prresence	−1.9	303	2002 −2004	Welp et al. (2007)
Delta Junction aspen forest (DLA)		63.92	−145.37	Alaska	Aspen forest	No prresence	−1.9	303	2002 −2004	Welp et al. (2007)
Eight Mile Lake (EML)	US-EML	63.88	−149.25	Alaska	Shrub tundra	Degrading	−1	378	2008 −2015	Trucco et al. (2012)
Chokurdkh (Cok)	RU-Cok	70.83	147.49	Siberia	Wet sedge/floodplain taundra	Continuous	−14.3	232	2003 −2013	van der Molen et al. 2007)
Cherski (Che)	RU-Che	68.61	161.34	Siberia	Drained moist tussock tundra	Continuous	−12.5	200	2002 −2005	Merbold et al. (2009)
Pleistocene Park (AON)		68.51	161.53	Siberia	Larch/mixed forest ecotone	Continuous	−12.5	200	2009, 2012 −2014	Euskirchen et al. (2017b)
Tura (TUR)		64.21	100.46	Siberia	Larch forest	Continuous	−9.2	317	2004	Nakai et al. (2008)
Nelegel (NEL)		62.32	129.50	Siberia	Larch forest	Continuous	−9.5	238	2000 −2006	Machimura et al. (2005)
Yakutsk Larch Forest (Spasskaya Pad) (YLF)	RU-SkP	62.25	129.62	Siberia	Larch forest	Continuous	−9.5	238	1998 −2010	Ohta et al. (2008, 2014)
Yakutsk Pine Forest (Spasskaya Pad) (YPF)		62.24	129.65	Siberia	Pine forest	Continuous	−9.5	238	2004 −2008	Matsumoto et al. (2008) Hamada et al. (2004)

[a]Climatorogical precipitation corrected for underestimation of snow precipitation (Liljedahl et al. 2017)

zone as well as shrub tundra; spruce forests on the discontinuous permafrost zone; and spruce forests and aspen forest on non-permafrost soil.

18.3.2 Synthesized Data

Energy, water, and CO_2 fluxes were measured using the eddy covariance method at all sites, whereas CH_4 fluxes were measured using the eddy covariance or flux-gradient methods. We used two datasets that were prepared in previous syntheses for Alaska (Ueyama et al. 2013a, b) and Siberia (Ichii et al. 2017). Half-hourly fluxes were post-processed in a standardized methodology, including flux partitioning into Gross Primary Productivity (GPP) and Ecosystem Respiration (RE) using nighttime data, and gap filling. Following these steps, we calculated daily and growing season fluxes. The only difference between the two datasets is a different temperature response function to estimate RE. A Q_{10} model was used for the Alaska dataset (Ueyama et al. 2013b), whereas so-called the Lloyd and Taylor equation (Lloyd and Taylor 1994) was used for the Siberia dataset.

Albedo data were collected from published literature for the Arctic and boreal regions (113 studies) in addition to the data from the synthesis papers before. Albedo data were divided into snow-free season and winter data based on a threshold of 0.2 albedo, and averaged separately for evergreen needleleaf forest, deciduous needleleaf forest, deciduous broadleaf forest, and tundra.

18.3.3 Radiation and Energy Fluxes

Net radiation showed a clear seasonal variation (Fig. 18.1). During the winter period, net radiation was negative since incoming shortwave radiation is limited and smaller than radiation lost as longwave radiation. The negative net radiation is greater in tundra ecosystems (-12.2 ± 7.7 W m^{-2}, n = 12) than in boreal forests (-1.0 ± 5.4 W m^{-2}, n = 7) during winter from November to March ($p < 0.01$; Welch t test). This is because boreal regions experience greater incoming shortwave radiation in winter than tundra region (in this analysis, 10 W m^{-2}; $p < 0.1$ by Welch t test) since boreal forests are located further south than tundra. Boreal forests have a complex and tall canopy compared with tundra, and snow does not remain long on the trees. Those factors lead to generally lower albedo in boreal forest than in tundra (Fig. 18.2), with the result that boreal forests are effectively capturing incoming shortwave radiation even in winter. Due to long snow periods in tundra, the time period of positive net radiation is more than two months shorter in tundra (170 ± 30 days, n = 12) than in boreal forests (229 ± 23 days, n = 8). Together with shorter snow periods in boreal forests, tundra less transfers sensible and latent energy to the atmosphere ($p = 0.1$): annual mean sensible heat flux of tundra (5.9 ± 4.0 W m^{-2}, n = 9) and boreal forests (12.4 ± 4.1 W m^{-2}, n = 4), and annual mean latent heat flux of tundra (11.0 ± 5.2 W m^{-2}, n = 8) and boreal forests (17.1 ± 2.1 W m^{-2}, n = 4).

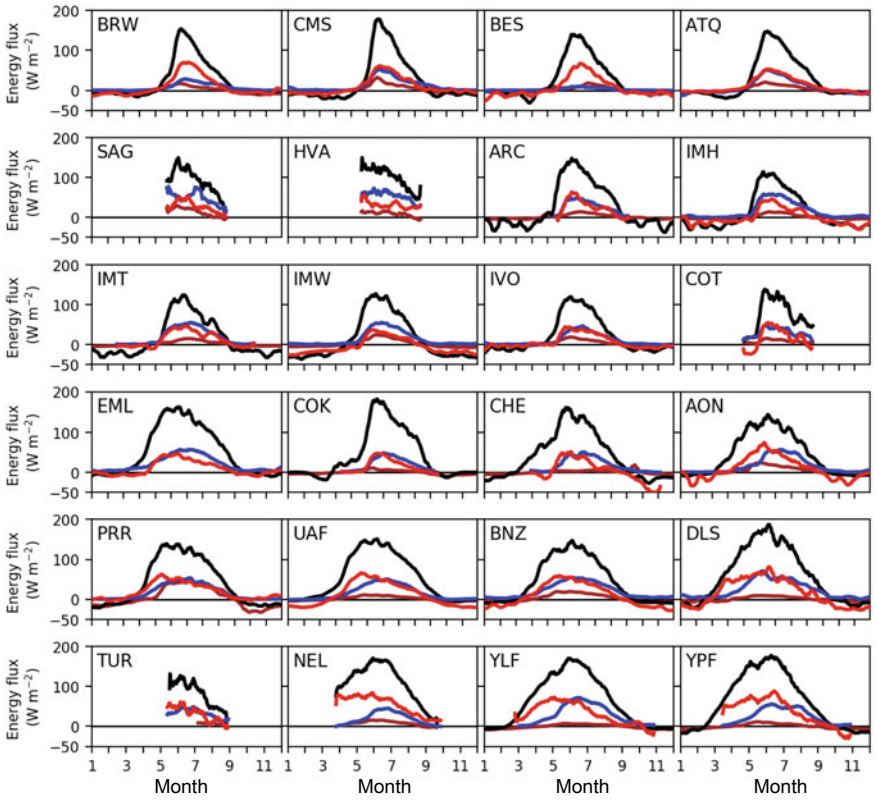

Fig. 18.1 Mean annual cycle of energy fluxes of net radiation (black), sensible heat flux (red), latent heat flux (blue), and ground heat flux (brown). The lines are 14-day moving mean

In northern high-latitude regions, winter albedo differs in vegetation types (Fig. 18.2). Winter albedo is higher in tundra (0.64 ± 0.19, $n = 15$) than in boreal forests (0.25 ± 0.12, $n = 27$) ($p < 0.01$) because snow effectively covers low vegetation. Albedo is higher during the winter when snow covers the ground compared to the albedo during the growing season when the vegetation is exposed (Fig. 18.2) due to a high reflectance of snow. Consequently, the length of the snow period is important in determining radiation balance. Spring snow cover is particularly important because incoming shortwave radiation is high near the summer solstice. This is why earlier snowmelt due to recent warming spring induces positive feedback, known as snow albedo feedback, because the earlier snowmelt induces atmospheric heating (Derksen and Brown 2012; Euskirchen et al. 2007; Ueyama et al. 2014a).

Growing season albedo is lower than those in winter periods (Fig. 18.2). During the growing season, tundra (0.15 ± 0.03, $n = 55$) has a higher albedo than

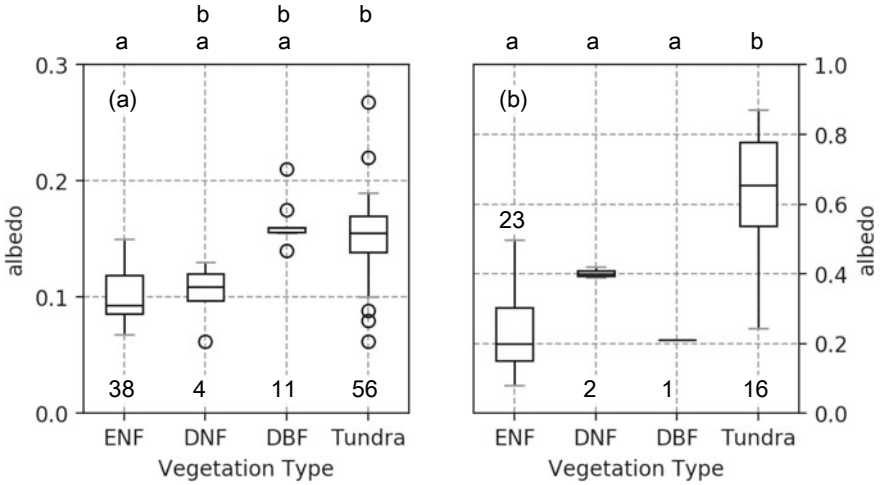

Fig. 18.2 Box plot of snow-free season **a** and winter **b** albedo for Evergreen Needleleaf Forest (ENF), Deciduous Needleleaf Forest (DNF), Deciduous Broadleaf Forest (DBF), and tundra. The number in the figure represents sample number for each plant functional type. The albedo is based on the eddy covariance tower synthesis and 113 papers identified in a literature for the Arctic and boreal zone. The mean of the category with the same letter is not significantly different (Tukey–Kramer test; $p < 0.1$)

evergreen needleleaf forests (0.12 ± 0.11, $n = 38$) ($p < 0.1$) because boreal forests have a complex stand structure. A higher reflectance of leaves of shrub and grasses than needle-leaved boreal forests further contributes to the high albedo in tundra. Low vegetation cover in tundra causes exposure of litter and bare soils, which have a high reflectance. Owing to the difference in albedo, migration of the tree line toward north increases net radiation, resulting in additional regional warming. In boreal forests, forest fires reduce regional albedo over an 80-year fire cycle by canopy replacement from spruce forests to young deciduous forests, resulting in a net surface cooling (Randerson et al. 2006).

Energy fluxes differ across seasons and among ecosystems (Fig. 18.1). Due to small net radiation in winter, sensible and latent heat fluxes are small and/or often show negative values. Ground heat flux is also low in winter due to the insulating effect of snow cover, whose effects depend on snow depth, density, and structure (Sturm et al. 1997; Zhang et al. 2005). During the winter and the period just after the snowmelt, net radiation in boreal forests tends to be mostly redistributed into sensible heat flux due to limited transpiration. With the start of the growing season, latent heat flux increases. The Bowen ratio, defined as ratio between sensible heat flux and latent heat flux, is highly variable within and among vegetation types due to different water use efficiencies in a given vegetation type (Fig. 18.3a). In summary, the Bowen ratio tends to be higher in boreal forests (1.36 ± 0.45, $n = 10$) than in evergreen needleleaf forest (1.35 ± 1.34, $n = 6$) when sum of sensible and

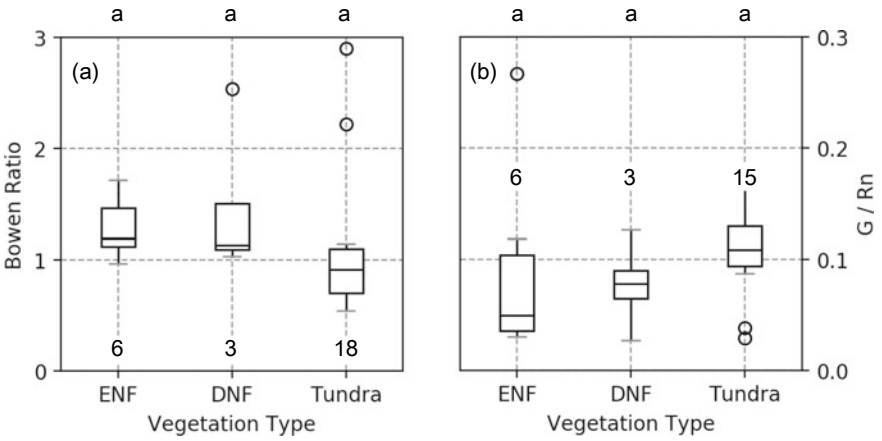

Fig. 18.3 Box plot of Bowen ratio **a** and ground heat flux (G) per net radiation (Rn) **b** during a period when sum of sensible and latent heat fluxes were greater than 20 W m^{-2}. The number in the figure represents sample number for each plant functional type. The mean of the category with the same letter is not significantly different (Tukey–Kramer test; $p < 0.1$)

latent heat fluxes is greater than 20 W m^{-2}. The growing season Bowen ratio shows large spatial variability within vegetation type, resulting in statistically insignificant differences among the vegetation types. Ground heat flux per net radiation tends to be smaller in boreal forests (9 ± 7%, n = 10) than in tundra (11 ± 3%, n = 14) during the growing season (Fig. 18.3b) because higher leaf area in boreal forests prevents radiative transfer to the ground while additionally ground-covered mosses function as a soil insulator (Zhuang et al. 2003).

In terms of the water budget, the annual sum of evapotranspiration and sublimation is on average 139 ± 66 mm yr^{-1} (n = 8) in tundra and 217 ± 27 mm yr^{-1} in boreal forests (n = 4) (Fig. 18.4a). The smaller amount of evapotranspiration in tundra is caused by higher surface and aerodynamic resistance when compared with boreal forests (Beringer et al. 2005; Kasurinen et al. 2014; McFadden et al. 2003). Consequently, evapotranspiration in tundra is known to be less sensitive to increases in vapor pressure deficit (Kasurinen et al. 2014). Smaller net radiation by longer snow periods also contributed smaller evapotranspiration in tundra than in boreal forests (Fig. 18.1). Interannual variations in evapotranspiration are less than in precipitation (Iwata et al. 2012; Ohta et al. 2008). The small interannual variation in the annual evapotranspiration is associated with a buffer effect of the stored water in frozen soils (Iwata et al. 2012; Ohta et al. 2008).

On average, the annual evapotranspiration is less than the annual precipitation. The ratio of the annual evapotranspiration to the annual precipitation showed an approximate 0.88 for boreal forests (PFF, UAF, BNZ, and AON) and 0.47 for tundra (BRW, CMS, BES, ATQ, IMH, IMW, IVO, and EML) (Fig. 18.4b). The value of boreal forests is higher than those for other estimates in high latitudes

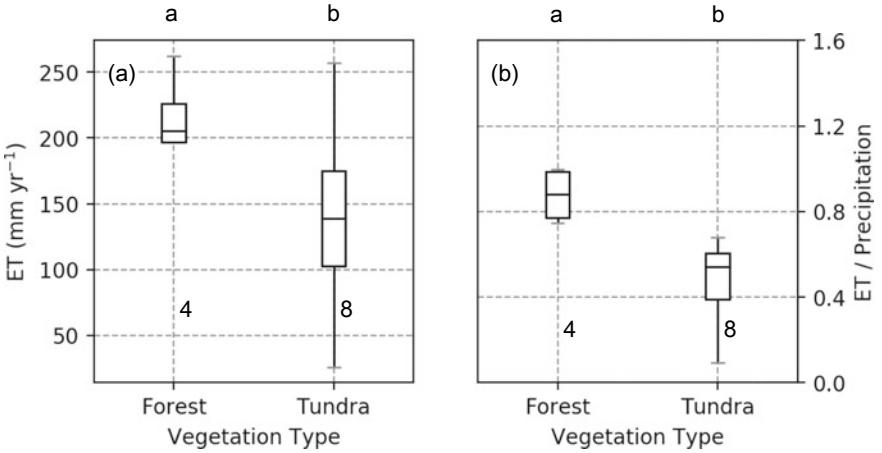

Fig. 18.4 Box plot of annual Evapotranspiration (ET) **a** and the ratio of annual ET to annual precipitation **b**. The number in the figure represents sample number for each plant functional type. Analysis was done for sites that have both winter and growing season ET, and thus only four lowland forests were available for the forest type. The mean of the category with the same letter are not significantly different (Tukey–Kramer test; $p < 0.1$)

ranging from 0.5 to 0.7 (Troy et al. 2011: Shutov et al. 2006). The high values for the boreal forests are probably because the four boreal forests are located at lowland gaining extra water from inflow from the surrounding area. The high ratio of evapotranspiration to precipitation represents the boreal ecosystems, which are potentially susceptible to drought stress (Euskirchen et al. 2017b; Welp et al. 2007), although precipitation measurements at high latitudes are known to be underestimated (Engstrom et al. 2006; Liljedahl et al. 2017), biasing the ratio.

18.3.4 Greenhouse Gas Fluxes

Tundra and boreal forests have a different seasonality in CO_2 fluxes in terms of magnitude of the gross fluxes and the growing season length (Fig. 18.5). In high-latitude ecosystems, the greater magnitudes of net photosynthesis link to higher water availability by the soil thaw (Jarvis and Linder 2000), although net photosynthesis of coniferous trees occurs at near zero air temperatures on frozen soils using stem water and melt water (Sevanto et al. 2006). Consequently, rising air temperature triggers the start of growing season (Suni et al. 2003). The growing season length, defined as days when daily GPP is continuously greater than 20% of annual maximum GPP, is approximately 40 days longer in boreal forests (125 ± 23 days) than in tundra (92 ± 15 days). On average, the magnitude of the annual GPP is more than two times greater in boreal forests (547 ± 230 g C m^{-2} yr^{-1}) than in tundra (212 ± 76 g C m^{-2} yr^{-1}). This is because warmer air

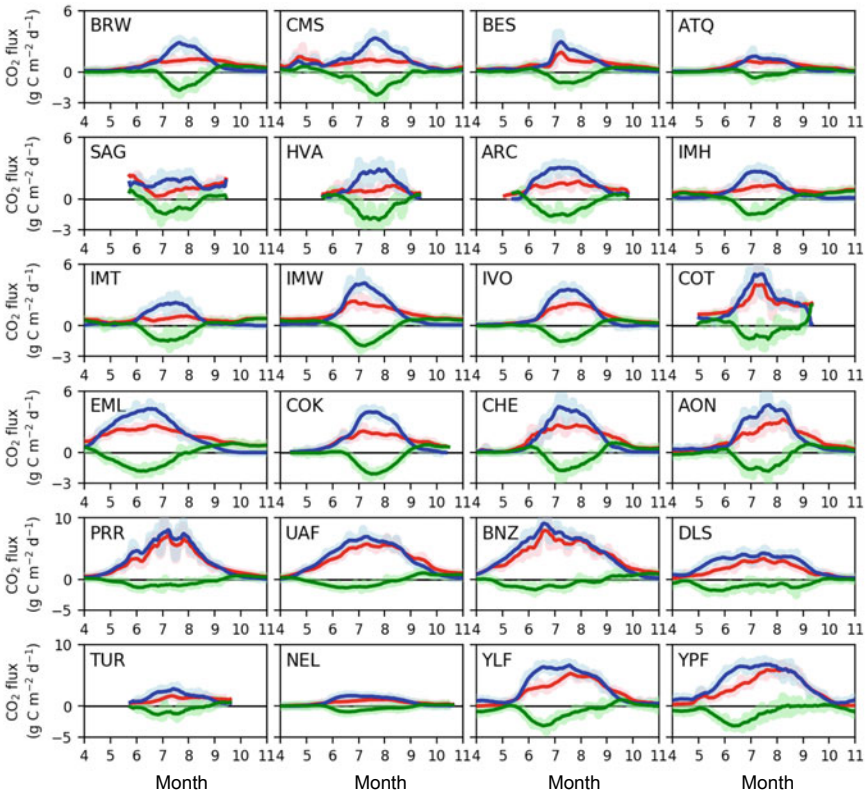

Fig. 18.5 Mean annual cycle of CO_2 fluxes of net ecosystem exchange of CO_2 (green), gross primary productivity (blue), and ecosystem respiration (red). The lines and shadows are 14-day moving mean and standard deviation, respectively. The scale for boreal forests (lower four lines) was different to those for tundra (upper four lines)

temperatures and a longer growing season support greater leaf area on boreal forests than in tundra, resulting in greater accumulation of CO_2 in boreal forests (McFadden et al. 2003; Ueyama et al. 2013b).

Across the boreal forests and tundra, spatial variations of the annual GPP can be explained by the growing season length ($R^2 = 0.64$, $p < 0.01$) (Fig. 18.6). The explanatory power of the growing season length is larger among boreal forests ($R^2 = 0.45$, $p = 0.02$, $n = 11$) than tundra ($R^2 = 0.38$, $p < 0.01$, $n = 17$). GPP standardized by the growing season length (namely, growing season GPP divided by the growing season) is greater in boreal forests (4.29 ± 1.52 g C m^{-2} d^{-1}) than in tundra (2.28 ± 0.65 g C m^{-2} d^{-1}). This indicates that daily GPP is approximately 1.8 times greater in boreal forest than in tundra because boreal forests have a higher peak on GPP due to higher leaf area (Ueyama et al. 2013b). Consequently, the differences in the growing season length and daily GPP are equally important

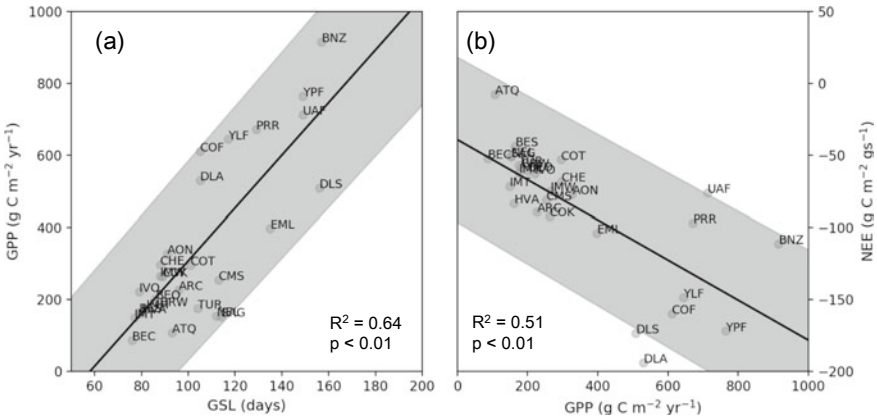

Fig. 18.6 Relationship between Growing Season Length (GSL) and Gross Primary Productivity (GPP) **a**, and relationship between GPP and growing season Net Ecosystem Exchange of CO_2 (NEE) **b**. Linear regression lines and its 90% confidence interval are also shown

for explaining the differences in the annual GPP among boreal forests and tundra. Among the four larch forests (YLF, NEL, TUR, and AON), the magnitude of the carbon fluxes differed greatly. The productive site (YLF) is located on a sandy soil (Ohta et al. 2008), whereas the other unproductive sites are on poorly drained soils (NEL and TUR; Machimura et al. 2005; Nakai et al. 2008) and on tundra-forest ecotone (AON; Euskirchen et al. 2017b). In contrast to the Siberian larch forests, three open black spruce forests on poorly drained soils (UAF, PFF, and BNZ) show a similar magnitude and seasonality in CO_2 fluxes. The closed black spruce forest on a well-drained non-permafrost soil (DLS) showed smaller gross fluxes than the open black spruce forests.

The boreal and tundra ecosystems act as a net growing season CO_2 sink (Fig. 18.6b; Ueyama et al. 2013b). The growing season CO_2 sink is approximately twice as large as the sink in boreal forests (-120 ± 49 g C m^{-2} season^{-1}) than in tundra (-66 ± 22 g C m^{-2} season^{-1}) (Fig. 18.6b). The largest CO_2 sink was observed at the deciduous broadleaf forest in Alaska (DLA). Ecosystems with higher annual GPP act as a greater growing season CO_2 sinks ($R^2 = 0.51$, $p < 0.01$, $n = 11$) (Fig. 18.6b). The relationship was significant within the tundra ($R^2 = 0.41$, $p < 0.01$, $n = 17$), but not within the boreal forests ($R^2 = 0.23$, $p = 0.13$, $n = 11$). Growing season length also weakly explains the spatial variation of NEE ($R^2 = 0.29$, $p < 0.01$, $n = 28$). NEE standardized by the growing season length was -0.72 ± 0.22 g C m^{-2} d^{-1} for tundra and -0.97 ± 0.43 g C m^{-2} d^{-1} for boreal forests. This indicates that carbon sink capacity standardized by the growing season length is approximately 30–40% greater in boreal forests than in tundra. This is modest compared with the 1.8 times greater daily GPP in boreal forest than tundra (discussed in above paragraph). Higher variability between GPP and NEE is shown in boreal forests than in tundra ecosystems (Fig. 18.6b), suggesting that a greater

contribution of ecosystem respiration in the growing season CO_2 budget of boreal forests than in tundra.

The annual NEE fluctuated from net sink to source, showing large interannual variability (Fig. 18.7). This is because the annual NEE is a small difference between large two opposite gross fluxes in high-latitude ecosystems (Lindroth et al. 1998; Ueyama et al. 2006). Similar-aged two open black spruce forests located within approximately 80 km (UAF and PFF) showed similar anomalies in some years (2012, 2103, and 2016), but inconsistent anomalies in other years (2011, 2014, and 2015). This indicates that similar ecosystems can show different responses to the same climate. The interannual variations in the annual NEE were mostly determined by those in RE for both forests. High sensitivity in RE to autumn temperatures was found to be the major driver of the annual CO_2 budget for UAF (Ueyama et al. 2014b), although summer high VPD and cold spring also limited GPP in anomalous years (Nagano et al. 2017). The importance in autumn and early winter temperatures to the annual CO_2 budget was also reported at Arctic tundra ecosystems in Alaska (Commane et al. 2017; Euskirchen et al. 2017a, b).

Rising atmospheric CO_2 concentrations potentially stimulate GPP, and thus may lead to an enhanced CO_2 sink. This effect is known as the CO_2 fertilization effect. Long-term measurements can constrain the determinant parameters for estimating the CO_2 fertilization effects (Ueyama et al. 2016): stomatal response to atmospheric CO_2 concentration (Ball et al. 1987) and photosynthetic response to intercellular CO_2 concentration (Farquhar et al. 1980). Model inversion using the eddy covariance data suggested that an increase of 23 g C m^{-2} $decade^{-1}$ was explained by the CO_2 fertilization effect associated with 20 ppm rising atmospheric CO_2 concentration (Fig. 18.8). In total number, from 2003 to 2014, an additional 150 g C was fixed due to the CO_2 fertilization effect. This result suggests that approximately half of the decadal increase in GPP could be explained by the CO_2 fertilization effect. This was greater than the long-term carbon sink of 61 g C m^{-2} yr^{-1} at

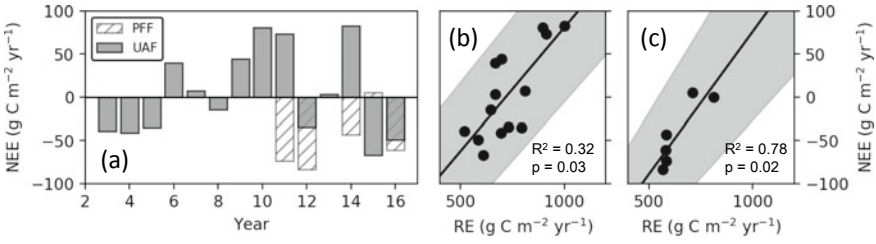

Fig. 18.7 Interannual variations in the annual Net Ecosystem Exchange of CO_2 (NEE) of two mature black spruce forests on permafrost in interior Alaska between 2003 and 2016 **a**. Relationships between the annual NEE and ecosystem respiration for University of Alaska, Fairbanks site (UAF) **b**, and Poker Flat Research Range site (PRR) **c**. Lines and shadows represent a linear regression and its 90% confidence interval, respectively

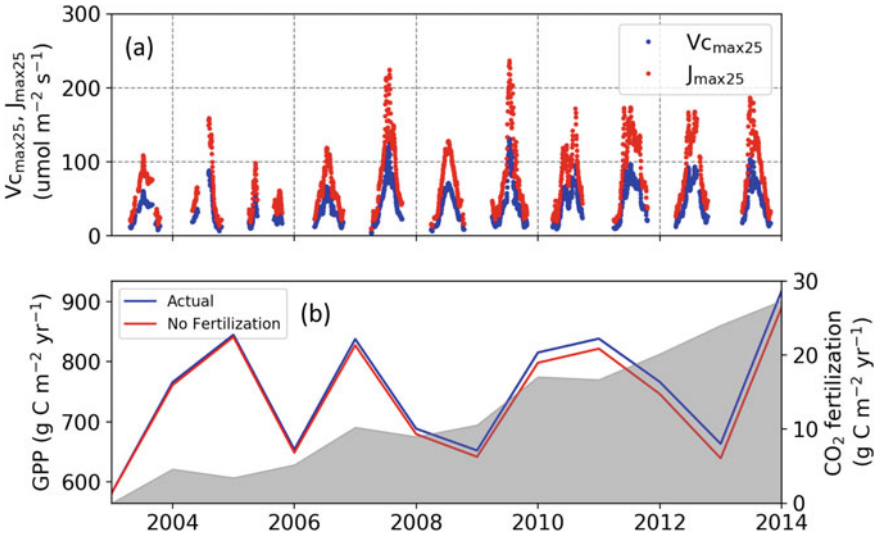

Fig. 18.8 Ecophysiological parameters, maximum canopy-integrated carboxylation and electron transport rate at 25 °C (Vcmax25 and Jmax25, respectively), optimized using eddy-covariance-based GPP and evapotranspiration at a boreal black spruce forest (UAF) **a**, and interannual variation of GPP **b**. GPP in (**b**) is shown for GPP including the CO_2 fertilization effect (eddy-covariance-based GPP; blue line) and not including the effect (eddy-covariance-based GPP subtracted the CO_2 fertilization effect; red line). The CO_2 fertilization effect was calculated as a partial difference of GPP in terms of change in the atmospheric CO_2 concentration using the optimized canopy photosynthesis model (Ueyama et al. 2016), and shown as gray shadow in (**b**). Here, the CO_2 fertilization effect is shown as a change in GPP after the baseline year—in this study 2003

the UAF black spruce site from 2003 to 2016. The CO_2 fertilization effect could be an important determinant of the long-term CO_2 budget at sites with a near neutral CO_2 budget.

The CH_4 budget plays a substantial role in the overall greenhouse gas budget (Fig. 18.9) because Global Warming Potential (GWP) of CH_4 is 34 times greater than that of CO_2 at a 100-year horizon (IPCC 2013) on a mass basis. GWP budget for a wet sedge tundra (CMS) and open black spruce forest (UAF) indicates that contributions of CH_4 budget were more important than CO_2 budget at the annual timescale. For the black spruce forest, the long-term CO_2 budget was almost neutral (Ueyama et al. 2014b), and thus even small CH_4 emissions (Iwata et al. 2015) greatly contributed to the GWP potential. For the wet sedge tundra, the magnitude of the CH_4 emission was an order of magnitude than the black spruce forest (Harazono et al. 2006), and thus the contribution of the CH_4 emission into the GWP budget and net radiative forcing was large (Helbig et al. 2017).

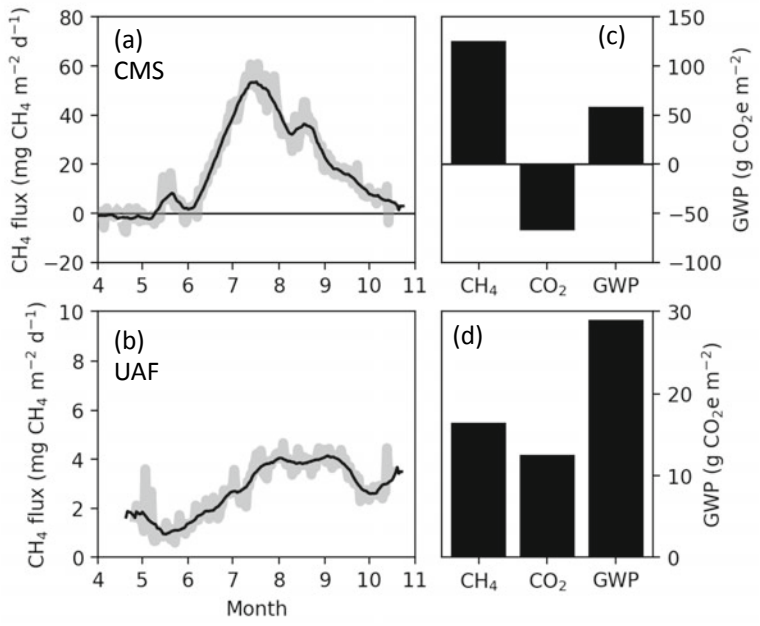

Fig. 18.9 Seasonal variation of CH_4 fluxes and annual Global Warming Potential (GWP) at a coastal wet sedge tundra (CMS) (**a**, **c**) and boreal black spruce forest (UAF) (**b**, **d**). For calculating GWP, CH_4 flux at winter months were neglected due to limited observations, and GWP of CH_4 was 34 times greater than that of CO_2 on a mass basis (IPCC 2013)

18.3.5 Regional Fluxes

Synthesizing the network of the eddy covariance measurements with remote sensing data, spatial distributions of fluxes can be estimated. The eddy covariance energy and CO_2 fluxes were upscaled at an 8-day timescale using a Support Vector Regression (SVR) with satellite remote sensing data (Ueyama et al. 2013a, 2014a; Ichii et al. 2017). SVR is a machine-learning-based regression (Cristianini and Shawe-Taylor 2000), which is applicable for a nonlinear problem using kernel functions, and is robust to overfitting due to insensitive bands and minimizing regression coefficients. Machine learning techniques, including SVR (Yang et al. 2006), were effectively used for upscaling flux tower data from continental to global scales (e.g., Jung et al. 2017).

Upscaled CO_2 fluxes based on SVR showed distinct differences between tundra and boreal forests (Fig. 18.10). High GPP and RE with net annual sink of CO_2 were estimated for boreal forests. Low gross fluxes and a net annual source of CO_2 were estimated for Alaskan tundra. This was consistent with field observations, which showed a net annual CO_2 source in Alaskan tundra (Commane et al. 2017; Euskirchen et al. 2012, 2017a; Oechel et al. 2014). In contrast, a net annual CO_2

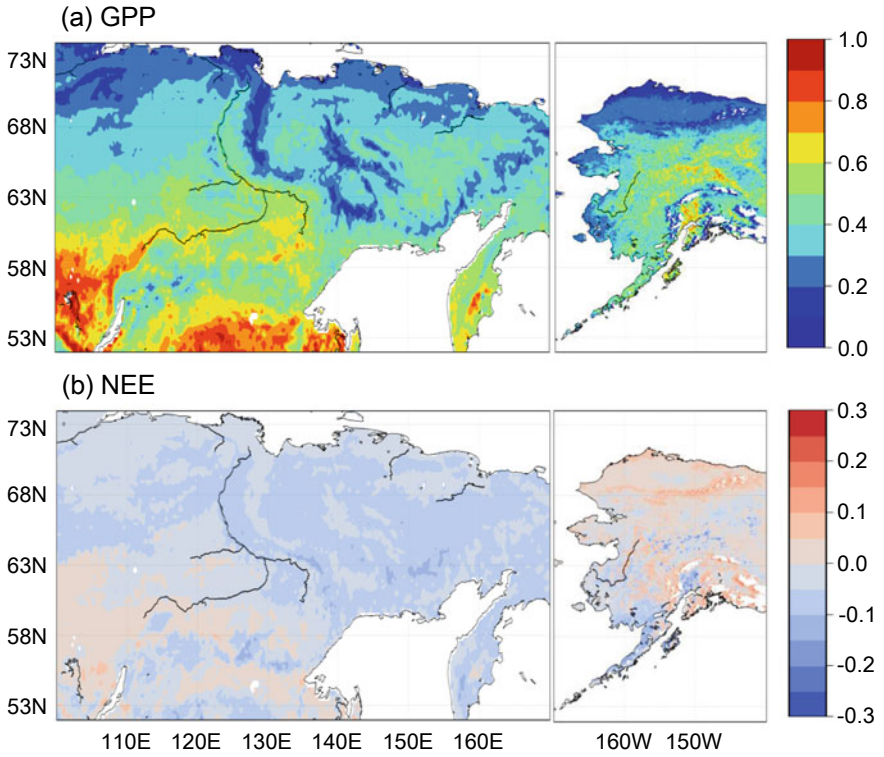

Fig. 18.10 Spatial distributions of Gross Primary Productivity (GPP), and Net Ecosystem Exchange of CO_2 (NEE) between 2000 and 2015 based on upscaling eddy covariance fluxes with satellite remote sensing data (kg C m^{-2} yr^{-1}). The maps are the reprocessed data with up-to-date satellite data using methods based on Ichii et al. (2017) for Siberia, and Ueyama et al. (2013a) for Alaska, respectively

sink was estimated for tundra in Siberia, which was inconsistent to annual CO_2 sources in tundra based on observations (Belshe et al. 2013; Merbold et al. 2009). The spatial variation of the CO_2 budget was influenced by vegetation recovery after fires in Alaska (Ueyama et al. 2013a), indicating fire disturbance was the major driver of the spatial variation in CO_2 budget at boreal forests at the regional scale. Interannual variation in the regional CO_2 budget correlated summer temperatures over Alaska, with warmer summers increasing the regional CO_2 sink (Ueyama et al. 2013a). The interannual variation was consistent with those by a top-down estimate (CarbonTracker; Peters et al. 2007), although its magnitudes were smaller in the upscaled CO_2 fluxes.

The current available machine-learning-based upscaled products could contain uncertainties because of limited data availability for tuning regression models in high latitudes. The different carbon budgets in tundra among Siberia and Alaska

(Fig. 18.10) were possibly caused by different input satellite data, processing, and/or data for tuning the machine learning model. The comparison to the top-down-based CO_2 budgets showed that interannual variability in the machine-learning-based regional CO_2 budget was underestimated in Alaska (Ueyama et al. 2013a) and Siberia (Takata et al. 2017), although mean seasonality was plausible (Ueyama et al. 2013a: Ichii et al. 2017; Takata et al. 2017). An important challenge for accurately estimating CO_2 budget in high latitudes is upscaling CO_2 emissions during snow periods because recent tower and aircraft observations show that autumn to early winter CO_2 emission is very important to estimate annual CO_2 budget (Commane et al. 2017; Euskirchen et al. 2017a, b; Ueyama et al. 2014b).

Upscaled energy fluxes highlight two important processes for the regional energy balance (Ueyama et al. 2014a). From 2000 to 2011, decreases in spring snow cover induced a net heating effect (0.56 W m^{-2} $decade^{-1}$) due to increases in the regional net radiation. The heating effect was comparable to the net cooling effect due to increased albedo after fire disturbance (up to 0.59 W m^{-2} $decade^{-1}$). Upscaled energy fluxes suggest the importance of a positive feedback by spring snow albedo and a negative feedback by fire-induced albedo changes under the expected warming climate in the high latitudes (Ueyama et al. 2014a). The upscaling also indicates that precise information of fire history improves regional energy flux estimate.

18.4 Future Directions

Ecosystem processes and functions can be inferred by synthesizing observed data and models. Previously, observed data were mostly used for model parameterization, validation, and tuning, but further sophisticated syntheses, such as model–data fusion, are available in current data-rich environments. One such example is shown in this review for constraining the CO_2 fertilization effect by optimizing the coupled stomatal conductance and canopy photosynthesis model (Ueyama et al. 2016). Further, constraining processes, such as respiration, radiative transfer, snow sublimation, and CH_4 flux, could be inferred using optimization or data assimilation techniques. Long-term monitoring of various environmental factors and fluxes could be useful for understanding ecosystem processes and functions.

Precise measurements during winter are among the major challenges in permafrost regions. This is the case for both gases CO_2 and CH_4. Winter CO_2 fluxes contribute largely to the annual budget due to long-winter periods (Belshe et al. 2013; Oechel et al. 2014; Euskirchen et al. 2017a). This study synthesized the growing season CO_2 fluxes only, due to limited availability in winter data. Although the growing season CO_2 budget is mostly a sink for the Arctic and boreal ecosystems (Fig. 18.6), annual CO_2 fluxes were reported to be a net CO_2 source in the Arctic tundra (Belshe et al. 2013; Euskirchen et al. 2012, 2017a; Oechel et al. 2014), and a CO_2 neutral to small sink at the boreal forests (Euskirchen et al. 2014,

2017b; Ueyama et al. 2014b). Gas analyzers, often used in early 2000s, were influenced by a known bias during cold periods (Burba et al. 2008), while more sophisticated analyzers became only available recently (Helbig et al. 2016b; Nakai et al. 2011). Quantifications and responses to environmental variations of winter CO_2 fluxes are possible using newly available winter data.

Our results indicate that understanding CH_4 flux is necessary for predicting the high-latitude greenhouse gas budget and climate change. Currently, the number of CH_4 flux measurement sites using micrometeorological methods is increasing in the permafrost zone (Zona et al. 2009; Iwata et al. 2015; Euskirchen et al. 2014), but measurements remain limited to few years of data or growing season data only. Since Zona et al. (2016) reported that contributions of winter CH_4 fluxes were important in the Arctic, further measurements including winter seasons are critically needed in future. Current measurements of CH_4 flux are located in areas of high CH_4 emission, such as wetland, and thus CH_4 flux at other ecosystems, such as upland forests (Sundqvist et al. 2015; Ueyama et al. 2018), is understudied (Chang et al. 2014). It is important to continue to synthesize CH_4 flux data since regional assessments of CH_4 flux are key in estimating the current state of the regional CH_4 budget. Only limited studies for regional CH_4 budgets are available using satellite remote sensing (Watts et al. 2014), aircraft measurements (Chang et al. 2014), or process-based modeling (Melton et al. 2013; Xu et al. 2016). Furthermore, more precise inputs for the regional studies, such as an inundated wetland map and water table depth, essential to be developed.

Disturbance changes the energy, water, and greenhouse gas fluxes at multiple temporal and spatial scales. Various disturbances currently influence biosphere–atmosphere interactions in the permafrost zone. These include forest and tundra fires (Amiro et al. 2006, 2010; Goulden et al. 2010; Randerson et al. 2006; Rocha and Shaver 2011), permafrost degradation (Euskirchen et al. 2014, 2017b; Helbig et al. 2016a, 2017), drought (Welp et al. 2007; Zona et al. 2014), and water stress (Ohta et al. 2014). Fluxes in disturbed ecosystems are understudied compared to non-disturbed ecosystems. The influence of fire disturbance is often measured using a chronosequence approach (Goulden et al. 2010; Randerson et al. 2006; Ueyama et al. 2019), but studies within the permafrost zone remain limited. Furthermore, disturbance effects caused by dry and wet spells are only measureable with continuous long-term monitoring (Ohta et al. 2014).

Finally, the continuation of long-term measurements is important for detecting long-term trends associated with climate change and rising atmospheric CO_2 concentration. Since the high-latitude climate oscillates at one to several decades (e.g., Arctic oscillation, pacific decadal oscillation, and El Nino-Southern oscillation), long-term measurements covering one to two cycles of the oscillation must be required for detecting known environmental trends and quantifying carbon balance (Ueyama et al. 2014b). Maintaining measurements under harsh environments is labor intensive, and large data gaps are difficult to be avoided. Duplicated measurements within a similar climate region could be helpful to check data quality and heterogeneity of each measurement site or ecosystem type as reviewed in this study (Fig. 18.7). The continuation of long-term measurements at various locations finds

vulnerable ecosystems, such as wet sedge tundra among various tundra type, to high-latitude warming (Euskirchen et al. 2017a), and it is therefore critical to understand the ecosystem functioning of these high-latitude systems (Zona 2016).

Acknowledgments We thank Dr. K Ichii of Chiba University for providing the upscaled flux products, and Dr. T Hiyama of Nagoya University for discussion about water budget. We thank Dr. Y Harazono of Osaka Prefecture University, Dr. AV Rocha of University of Notre Dame, Dr. J Randerson of University of California, Irvine, for providing eddy covariance data at Alaska. We thank Dr. Y Matsuura of Forestry and Forest Products Research Institute, and Dr. H Dolman of Vrije Universiteit Amsterdam, for providing eddy covariance data at Siberia. Eddy flux data at Council were observed by Dr. J Beringer of University of Western Australia, FS Chapin III and C Copass-Thompson of the University of Alaska Fairbanks, and provided through the NCAR Earth Observing Laboratory. Databases of eddy covariance measurements (AsiaFlux, European Fluxes Database Cluster, the NSF Arctic Observatory Network, and NSF Arctic Data Center) facilitated this study. The US-Uaf site were supported by the Arctic Challenge for Sustainability (ArCS) project awarded to MU. The Barrow, and Atqasuk eddy covariance towers were supported by Office of Polar Programs of the National Science Foundation (NSF) awarded to DZ, and WCO (award number 1204263, and 1702797) with additional logistical support funded by the NSF Office of Polar Programs, and by the Carbon in Arctic Reservoirs Vulnerability Experiment (CARVE), an Earth Ventures (EV-1) investigation, under contract with the National Aeronautics and Space Administration, and by the ABoVE (NNX15AT74A; NNX16AF94A).

References

AMAP (2017) Snow, water, ice and permafrost in the Arctic Summary for Policy-makers. Arctic Council, Oslo, p 19

Amiro BD et al (2006) The effects of post-fire stand age on the boreal forest energy balance. Agric For Meteorl 140:41–50

Amiro BD et al (2010) Ecosystem carbon dioxide fluxes after disturbance in forests of North America. J Geophys Res 115:G00K92. https://doi.org/10.1029/2010jg001390

Baldocchi D (2008) 'Breathing' of the terrestrial biosphere: lessons learned from a global network of carbon dioxide flux measurement systems. Australian J Bot 56:1–26

Ball J, Woodrow I, Berry J (1987) A model predicting stomatal conductance and its contribution to the control of photosynthesis under different environmental conditions. In: Biggins J (ed) Progress in photosynthesis research. Martinus Nijhoff Publishers, Dordrecht, pp 221–224

Belshe EF, Schuur EAG, Bolker BM (2013) Tundra ecosystems observed to be CO_2 sources due to differential amplification of the carbon cycle. Ecol Lett 16:1307–1315

Beringer J, Chapin FS III, Copass C (2003) Climate and flux data from alaska sites, 1998–2000, ARCSS Data Archive. Natl Cent Atmos Res Boulder Colo

Beringer J, Chapin FS III, Thompson CC, McGuire AD (2005) Surface energy exchanges along a tundra-forest transition and feedbacks to climate. Agric For Meteorol 131:143–161

Burba GG, McDermitt DK, Grelle A, Anderson DJ, Xu L (2008) Addressing the influence of instrument surface heat exchange on the measurements of CO_2 flux from open-path gas analyzers. Glob Change Biol 14:1854–1876. https://doi.org/10.1111/j.1365-2486.2008.01606.x

Chambers SD, Chapin FS III (2003) Fire effects on surface-atmosphere energy exchange in Alaskan black spruce ecosystems: implications for feedbacks to regional climate. J Geophys Res 108:8145. https://doi.org/10.1029/2001JD000530

Chang RY-W et al (2014) Methane emissions from Alaska in 2012 from CARVE airborn observations. Proc Natl Acad Sci USA 111:16694–16699. https://doi.org/10.1073/pnas.1412953111

Chapin FS III et al (2005) Role of land-surface changes in arctic summer warming. Science 310:657–660

Chapin FS III, Eugster W, McFadden JP, Lynch AH, Walker DA (2000) Summer differences among arctic ecosystems in regional climate forcing. J Climate 13:2002–2010

Chapin FS III, Matson PA, Vitousek PM (2011) Principles of terrestrial ecosystem ecology, 2nd edn. Springer, New York

Commane R et al (2017) Carbon dioxide sources from Alaska driven by increasing early winter respiration from Arctic tundra. Proc Natl Acad Sci 114:5361–5366

Cristianini N, Shawe-Taylor J (2000) An introduction to support vector machines and other kernel-based learning methods. Cambridge University Press, Cambridge, UK, p 189

Derksen C, Brown R (2012) Spring snow cover extent reductions in the 2008–2012 period exceeding climate model projections. Geophys Res Lett 29:L19504. https://doi.org/10.1029/2012GL052287

Engstrom R, Hope A, Kwon H, Harazono Y, Mano M, Oechel W (2006) Modeling evapotranspiration in Arctic coastal plain ecosystems using a modified BIOME-BGC model. J Geophys Res Biogeosci 111:G02021. https://doi.org/10.1029/2005JG000102

Euskirchen ES, Bennett AL, Breen AL, Genet H, Lindgren T, Kukowski AD, McGuire AD, Tupp TS (2016) Consequences of changes in vegetation and snow cover for climate feedbacks in Alaska and northwest Canada. Environ Res Lett 11:105003. https://doi.org/10.1088/1748-9326/11/10/105003

Euskirchen ES, Bret-Harte MS, Scorr GJ, Edgar C, Shaver GR (2012) Seasonal patterns of carbon dioxide and water fluxes in three representative tundra ecosystems in northern Alaska. Ecosphere 3(1):1–19. https://doi.org/10.1890/ES11-00202.1

Euskirchen ES, Bret-Harte MS, Shaver GR, Edgar CW, Romanovsky VE (2017a) Long-term release of carbon dioxide from Arctic tundra ecosystems in Alaska. Ecosystems 20:960–974. https://doi.org/10.1007/s10021-016-0085-9

Euskirchen ES, Edgar CW, Bret-Harte MS, Kade A, Zimov N, Zimov S (2017b) Interannual and seasonal patterns of carbon dioxide, water and energy fluxes from ecotonal and thermokarst-impacted ecosystems on carbon-rich permafrost soils in northeastern Siberia. J Geophys Res Biogeosci 122:2651–2668. https://doi.org/10.1002/2017JG004070

Euskirchen ES, McGuire AD, Chapin FS III (2007) Energy feedbacks of northern high-latitude ecosystems to the climate system due to reduced snow cover during 20th century warming. Glob Change Biol 13:2425–2438. https://doi.org/10.1111/j.1365-2486.2006.01113.x

Euskirchen ES, McGuire AD, Chapin FS III, Rupp TS (2010) The changing effects of Alaska's boreal forests on the climate system. Can J For Res 40:1336–1346

Euskirchen ES, McGuire AD, Kicklighter DW, Zhuang Q, Clein JS, Dargaville RJ, Dye DG, Kimball JS, McDonald KC, Melillo JM, Romanovsky VE, Smith NV (2006) Importance of recent shifts in soil thermal dynamics on growing season length, productivity, and carbon sequestration in terrestrial high-latitude ecosystems. Glob Change Biol 12:731–750. https://doi.org/10.1111/gcb.12071

Euskirchen ES, Edgar CW, Turetsky MR, Waldrop MP, Harden JW (2014) Differential response of carbon fluxes to climate in three peatland ecosystems that vary in the presence and stability of permafrost. J Geophys Res Biogeosci 119. https://doi.org/10.1002/2014jg002683

Farquhar GD, von Caemmerer S, Berry JA (1980) A biochemical model of photosynthesis CO_2 assimilation in leavers of C3 species. Planta 149:78–90

Forkel M, Carvalhais N, Rödenbeck C, Keeling R, Heimann M, Thonicke K, Zaehle S, Reichstein M (2016) Enhanced seasonal CO_2 exchange caused by amplified plant productivity in northern ecosystems. Science 351:696–699

Goulden ML, McMillan AMS, Winston GC, Rocha AV, Manies KL, Harden JW, Bond-Lamberty BP (2010) Patterns of NPP, GPP, respiration, and NEP during boreal forest succession. Global Change Biol 17:855–871. https://doi.org/10.1111/j.1365-2486.2010.02274.x

Graven HD et al (2013) Enhanced seasonal exchange of CO_2 by northern ecosystems since 1960. Science 341(6150):1085–1089

Hamada S, Ohta T, Hiyama T, Kuwada T, Takahashi A, Maximov TC (2004) Hydrometeorological behavior of pine and larch forests in eastern Siberia. Hydrol Process 18:23–39

Harazono Y, Mano M, Miyata A, Yoshimoto M, Zulueta RC, Vourlitis V, Kwon H, Oechel W (2006) Temporal and spatial differences of methane flux at arctic tundra in Alaska. Mem Natl Inst Polar Res Spec Issue 59:79–95

Harazono Y, Mano M, Miyata A, Zulueta RC, Oechel WC (2003) Inter-annual carbon dioxide uptake of a wet sedge tundra ecosystem in the Arctic. Tellus 55B:215–231

Harazono Y, Yoshimoto M, Mano M Vourlitis V, Oechel W (1998) Characteristics of energy and water budgets over wet sedge and tussock tundra ecosystems at North Slope in Alaska. Hydrol Proc 12:2163–2183

Helbig M et al (2016b) Addressing a systematic bias in carbon dioxide flux measurements with the EC150 and the IRGASON open-path gas analyzers. Agric For Meteorol 228–229:349–359

Helbig M, Chasmer LE, Kljun N, Quinton WL, Treat CC, Sonnentag O (2017) The positive net radiative greenhouse gas forcing of increasing methane emissions from a thawing boreal forest-wetland landscape. Glob Change Biol 23:2413–2427. https://doi.org/10.1111/gcb.13520

Helbig M, Wischnewski K, Kljun N, Chasmer LE, Quinton WL, Detto M, Sonnentag O (2016a) Regional atmospheric cooling and wetting effect of permafrost thaw-induced boreal forest loss. Glob Change Biol 22:4048–4066. https://doi.org/10.1111/gcb.13348

Hicks Pries CE, van Logtestijn RSP, Schuur EAG, Natali SM, Cornelissen JHC, Aerts R, Dorrepaal E (2015) Decadal warming causes a consistent and persistent shift from heterotrophic to autotrophic respiration in contrasting permafrost ecosystems. Global Change Biol 21:4508–4519

Hinzman LD et al (2005) Evidence and implications of recent climate change in northern Alaska and other Arctic regions. Clim Change 72:251–298. https://doi.org/10.1007/s10584-005-5352-2

Hollinger DY et al (1998) Forest-atmosphere carbon dioxide exchange in eastern Siberia. Agric For Meteorol 90:291–306

Hugelius G et al (2014) Estimated stocks of circumpolar permafrost carbon with quantified uncertainty ranges and identified data gaps. Biogeosciences 11:6573–6593

Ichii K et al (2017) New data-driven estimation of terrestrial CO_2 flux in Asia using a standardized database of eddy covariance measurements, remote sensing data, and support vector regression. J Geophys Res Biogeosci 122. https://doi.org/10.1002/2016jg003640

Ikawa H et al (2015) Understory CO_2, sensible heat, and latent heat fluxes in a black spruce forest in interior Alaska. Agric For Meteorol 214–215:80–90

Intergovernmental Panel on Climate Change (2013) Climate Change 2013: The Physical Science Basis. Contribution of Working Group I to the Fifth Assessment Report of the Intergovernmental Panel on Climate Change [Stocker TF, Qin D, Plattner G-K, Tignor M, Allen SK, Boschung J, Nauels A, Xia Y, Bex V, Midgley PM (eds)]. Cambridge University Press, Cambridge, United Kingdom and New York, NY, USA, p 1535. https://doi.org/10.1017/cbo9781107415324

Iwata H, Harazono Y, Ueyama M (2012) The role of permafrost in water exchange of a black spruce forest in interior Alaska. Agric For Meteorol 161:107–115

Iwata H, Harazono Y, Ueyama M, Sakabe A, Nagano H, Kosugi Y, Takahashi K, Kim Y (2015) Methane exchange in a poorly-drained black spruce forest over permafrost observed using the eddy covariance technique. Agric For Meteorol 214–215:157–168

Jarvis P, Linder S (2000) Constraints to growth of boreal forests. Nature 405:904–905

Jung M et al (2017) Compensatory water effects link yearly global land CO_2 sink changes to temperature. Nature 541:516–520. https://doi.org/10.1038/nature20780

Kasurinen V et al (2014) Latent heat exchange in the boreal and arctic biomes. Global Change Biol 20:3439–3456

Kirschke S (2013) Three decades of global methane sources and sinks. Nat Goesci 6:813–823

Kwon HJ, Oechel WC, Zulueta RC, Hastings SJ (2006) Effects of climate variability on carbon sequestration among adjacent wet sedge tundra and moist tussock tundra ecosystems. J Geophys Res Biogeosci 111. https://doi.org/10.5194/bg-10-753-2013

Liljedahl AK, Hinzman LD, Kane DL, Oechel WC, Tweedie CE, Zona D (2017) Tundra water budget and implications of precipitation underestimation. Water Resour Res 53. https://doi.org/10.1002/2016wr020001

Lindroth A, Grelle A, Morén A-S (1998) Long-term measurements of boreal forest carbon balance reveal large temperature sensitivity. Global Change Biol 4:443–450

Liu HP, Randerson JT, Lindfors J, Chapin FS III (2005) Changes in the surface energy budget after fire in boreal ecosystems of interior Alaska: An annual perspective. J Geophys Res 110: D13101. https://doi.org/10.1029/2004JD005158

Lloyd J, Taylor JA (1994) On the temperature dependence of soil respiration. Funct Ecol 8:315–323

Machimura T, Kobayashi Y, Iwahana G, Hirano T, Lopez L, Fukuda M, Fedorov AN (2005) Change of carbon dioxide budget during three years after deforestation in eastern Siberian larch forest. J Agric Meteorol 60:653–656

Matsumoto K, Ohta T, Nakai T, Kuwada T, Daikoku K, Iida S, Yabuki H, Kononov AV, van der Molen MK, Kodama Y, Maximov TC, Dolman AJ, Hattori S (2008) Responses of surface conductance to forest environments in the Far East. Agric For Meteorol 148:1926–1940

McEwing KR, Fisher JP, Zona D (2015) Environmental and vegetation controls on the spatial variability of CH_4 emission from wet-sedge and tussock tundra ecosystems in the Arctic. Plant Soil 388:37–52. https://doi.org/10.1007/s11104-014-2377-1

McFadden JP, Eugster W, Chapin FS III (2003) A regional study of the controls on water vapor and CO_2 exchange in arctic tundra. Ecology 84(10):2762–2776

McGuire AD, Christensen TR, Hayes D, Heroult A, Euskirchen E, Kimball JS, Koven C, Lafleur P, Miller PA, Oechel W, Peylin P, Williams M, Yi Y (2012) An assessment of the carbon balance of Arctic tundra: comparisons among observations, process models, and atmospheric inversions. Biogeosci 9:3185–3204

Melton JR et al (2013) Present state of global wetland extent and wetland methane modelling: conclusions from a model inter-comparison project (WETCHIMP). Biogeosciences 10:753–788. https://doi.org/10.5194/bg-13-5043-2016

Merbold L, Kutsch WL, Corradi C, Kolle O, Rebmann C, Stoy PC, Zimov ZA, Schulze E-D (2009) Artificial drainage and associated carbon fluxes (CO_2/CH_4) in a tundra ecosystem. Glob Change Biol 15:2599–2614

van der Molen MK, van Huissteden J, Parmentier FJW, Petrescu AMR, Dolman AJ, Maximov TC, Kononov AV, Karsanaev SV, Suzdalov DA (2007) The growing season greenhouse gas balance of a continental tundra site in the Indigirka lowlands, NE Siberia. Biogeosciences 4:985–1003

Nagano et al (2017) Extremely dry environment down-regulates nighttime respiration of a black spruce forest in Interior Alaska. Agric For Meteorol 249(15):297–309

Nakai T et al (2013) Characteristics of evapotranspiration from a permafrost black spruce forest in interior Alaska. Polar Sci 7:136–148

Nakai T, Iwata H, Harazono Y (2011) Importance of mixing ratio for a long-term CO_2 flux measurement with a closed-path system. Tellus 63B:302–308

Nakai Y, Matsuura Y, Kajimoto T, Abaimov AP, Yamamoto S, Zyryanova OA (2008) Eddy covariance CO_2 flux above a Gmelin larch forest on continuous permafrost of central Siberia during a growing season. Theor Appl Climatol 93:133–147

Oechel WC, Laskowski CA, Burba G, Gioli B, Kalhori AAM (2014) Annual patterns and budget of CO_2 flus in an Arctic tussock tundra ecosystem. J Geophys Res Biogeosci 119:323–339. https://doi.org/10.1002/2013JG002431

Oechel WC, Vourlitis GL, Hastings SJ, Zulueta RC, Hinzman L, Kane D (2000) Acclimation of ecosystem CO_2 exchange in the Alaskan Arctic in response to decadal climate warming. Nature 406:978–981

Ohta T et al (2008) Interannual variation of water balance and summer evapotranspiration in an eastern Siberian larch forest over a 7-year period (1998–2006). Agric For Meteorol 148:1941–1953

Ohta T et al (2014) Effects of waterlogging on water and carbon dioxide fluxes and environmental variables in a Siberian larch forest, 1998-2011. Agric For Meteorol 188:64–775

Olefeldt D, Turetsky MR, Crill PM, McGuire D (2013) Environmental and physical controls on northern terrestrial methane emissions across permafrost zones. Glob Change Biol 19:589–603. https://doi.org/10.1111/gcb.12071

Pearson RG, Philips SJ, Loranty MM, Beck PSA, Damoulas T, Knight SJ, Goetz SJ (2013) Shifts in arctic vegetation and associated feedbacks under climate change. Nat Clim Change 3:673–677. https://doi.org/10.1038/nclimate1858

Peters W et al (2007) An atmospheric perspective on North American carbon dioxide exchange: CarbonTraker. Proc Natl Acad Sci 104:925–930

Piao S et al (2008) Net carbon dioxide losses of northern ecosystems in response to autumn warming. Nature 451:49–52. https://doi.org/10.1038/nature06444

Randerson JT et al (2006) The impact of boreal forest fire on climate warming. Science 314:1130–1132

Rocha AV, Shaver GR (2011) Burn severity influences postfire CO_2 exchange in arctic tundra. Ecol Appl 21(2):477–489

Sachs T, Giebels M, Boike J, Kutzbach L (2010) Environmental controls on CH_4 emission from polygonal tundra on the microsite scale in the Lena river delta, Siberia. Global Change Biol 16:3096–3110. https://doi.org/10.1111/j.1365-2486.2010.02232.x

Schuur EAG, McGuire AD, Schädel C, Grosse G, Harden JW, Hayes DJ, Hugelius G, Koven CD, Kuhry P, Lawrence DM, Natali SM, Olefeldt D, Romanovsky VE, Schaefer K, Turestsky MR, Treat CC, Conk JE (2015) Climate change and the permafrost carbon feedback. Nature 520:171–179

Sevanto S et al (2006) Wintertime photosynthesis and water uptake in a boreal forest. Tree Physiol 26:749–757

Shutov V, Gieck RE, Hinzman LD, Kane DL (2006) Evaporation from land surface in high latitude areas: a review of methods and study results. Nordic Hydrol 37:393–411. https://doi.org/10.2166/nh.2006.022

Sturm MJ, Holmgren J, König M, Morris K (1997) The thermal conductivity of seasonal snow. J Glaciol 43:26–40

Sturtevant CS, Oechel WC (2013) Spatial variation in landscape-level CO_2 and CH_4 fluxes from arctic coastal tundra: influence from vegetation, wetness, and the thaw lake cycle. Glob Change Biol 19:2853–2866. https://doi.org/10.1111/gcb.12247

Sundqvist E, Mölder M, Crill P, Kljun N (2015) Methane exchange in a boreal forest estimated by gradient method. Tellus B 67:26688

Suni T et al (2003) Air temperature triggers the recovery of evergreen boreal forest photosynthesis in spring. Glob Change Biol 9:1410–1426

Takata K et al (2017) Reconciliation of top-down and bottom-up CO_2 fluxes in Siberian larch forest. Environ Res Lett 12:125012

Tarnocai C, Canadell JG, Schuur EGA, Kuhry P, Mazhitova G, Zimov S (2009) Soil organic carbon pools in the northern circumpolar permafrost region. Glob Biogeochem Cycles 23: GB2023. https://doi.org/10.1029/2008gb003327

Tokida T, Miyazaki T, Mizoguchi M, Nagata O, Takakai F, Kagemoto A, Hatano R (2007) Falling atmospheric pressure as a trigger for methane ebullition from peatland. Glob Biogeochem Cycl 21:GB2003. https://doi.org/10.1029/2006gb002790

Troy TJ, Sheffield J, Wood EF (2011) Estimation of the terrestrial water budget over northern Eurasia through the use of multiple data source. J Climate 24:3272–3293

Trucco C, Schuur AG, Natali SM, Belshe EF, Bracho R, Vogel J (2012) Seven-year trends of CO_2 exchange in a tundra ecosystem affected by long-term permafrost thaw. J Geophys Res Biogeosci 117:G02031. https://doi.org/10.1029/2011JG001907

Turetsky MR et al (2014) A synthesis of methane emissions from 71 northern, temperate, and subtropical wetlands. Glob Change Biol 20(7). https://doi.org/10.1111/gcb.12580

Ueyama M et al (2013a) Upscaling terrestrial carbon dioxide fluxes in Alaska with satellite remote sensing and support vector regression. J Geophys Res Biogeosci 118:1–16. https://doi.org/10.1002/jgrg.20095

Ueyama M et al (2014a) Change in surface energy balance in Alaska due to fire and spring warming, based on upscaling eddy covariance measurements. J Geophys Res Biogeosci 119:1947–1969. https://doi.org/10.1002/2014JG002717

Ueyama M et al (2016) Optimization of a biochemical model with eddy covariance measurements in black spruce forests of Alaska for estimating CO_2 fertilization effects. Agric For Meteorol 222:98–111

Ueyama M, Harazono Y, Ohtaki E, Miyata A (2006) Controlling factors on the interannual CO_2 budget at a subarctic black spruce forest in interior Alaska. Tellus 58B:491–501

Ueyama M, Iwata H, Harazono Y (2014b) Autumn warming reduces the CO_2 sink of a black spruce forest in interior Alaska based on a nine-year eddy covariance measurement. Global Change Biol 20(4):1161–1173. https://doi.org/10.1111/gcb.12434

Ueyama M, Iwata H, Harazono Y, Euskirchen ES, Oechel WC, Zona D (2013b) Growing season and spatial variations of variations of carbon fluxes of Arctic and boreal ecosystems in Alaska (USA). Ecol Appl 22(8):1798–1816

Ueyama M, Iwata H, Nagano H, Tahara N, Iwama C (2019) Carbon dioxide balance in early-successional forests after fires in interior Alaska. Agric For Meteorol 275:196–207

Ueyama M, Yoshikawa K, Takagi K (2018) A cool-temperate young larch plantation as a net methane source- a 4-year continuous hyperbolic relaxed eddy accumulation and chamber measurements. Atm Environ 184:110–120. https://doi.org/10.1016/j.atmosenv.2018.04.025

Vourlitis GL, Harazono Y, Oechel WC, Yoshimoto M, Mano M (2000) Spatial and temporal variations in hectare-scale net CO_2 flux, respiration and gross primary production of Arctic tundra ecosystems. Func Ecol 14:203–214

Wagner R, Zona D, Oechel W, Lipson D (2017) Microbial community structure and soil pH correspond to methane production in Arctic Alaska soils. Environ Microbiol 19(8):3398–3410. https://doi.org/10.1111/1462-2920.13854

Walter KM, Zimov SA, Chanton JP, Verbyla DV, Chapin FS III (2006) Methane bubbling from Siberian thaw lakes as a positive feedback to climate warming. Nature 443:71–75. https://doi.org/10.1038/nature05040

Watts JD, Kimball JS, Bartsch A, McDonald KC (2014) Surface water inundation in the boreal-Arctic: potential impacts on regional methane emissions. Environ Res Lett 9:075001. https://doi.org/10.1088/1748-9326/9/7/075001

Welp LR, Randerson JT, Liu HP (2007) The sensitivity of carbon fluxes to spring warming and summer drought depends on plant functional type in boreal forest ecosystems. Agric For Meteorol 147:172–185

Xu et al (2016) A multi-scale comparison of modeled and observed seasonal methane emissions in northern wetlands. Biogeosciences 13:5043–5056. https://doi.org/10.5194/bg-13-5043-2016

Yang F et al (2006) Prediction of continental-scale evapotranspiration by combining MODIS and AmeriFlux data through support vector machine. IEEE Trans Geosci Remote Sens 44 (3452):3561

Yvon-Durocher G, Allen AP, Bastviken D, Conrad R, Gudasz C, St-Pierre A, Thnh-Duc N, del Giorgio PA (2014) Methane fluxes show consistent temperature dependence across microbial to ecosystem scales. Nature 507:489–491. https://doi.org/10.1038/nature13164

Zhang T (2005) Influence of the seasonal snow cover on the ground thermal regime: an overview. Rev Geophys 43:RG4002

Zhuang Q, McGuire AD, O'Neill KP, Harden JW, Romanovsky VE, Yarie J (2003) Modeling soil thermal and carbon dynamics of a fire chronosequence in interior Alaska. J Geophys Res Biogeosci 108:8147. https://doi.org/10.1029/2001JD001244

Zona D et al (2014) Delayed responses of an Arctic ecosystem to an extreme summer: impacts on net ecosystem exchange and vegetation functioning. Biogeosciences 11:5877–5888. https://doi.org/10.5194/bg-11-5877-2014

Zona D (2016) Long-term effects of permafrost thaw. Nature 537:625–626 https://doi.org/10.1038/537625a

Zona D et al (2016) Cold season emissions dominate the Arctic tundra methane budget. Proc Natl Acad Sci USA 113(1):40–45

Zona D et al (2009) Methane fluxes during the initiation of a large-scale water table manipulation experiment in the Alaskan Arctic tundra. Global Biogeochem Cycl 23:GB2013. https://doi.org/10.1029/2009gb003487

Dr. Masahito Ueyama is an Associate Professor in the Graduate School of Life and Environmental Sciences of Osaka Prefecture University in Sakai, Japan. His research interest is the land–atmosphere interaction of energy, water, and trace gases. His approach relies on integration and synthesis of field observations, numerical models, and remote sensing data. He received his Doctoral degree in Science at the Graduate School of Natural and Technology, Okayama University, and worked at International Arctic Research Center, University of Alaska, Fairbanks, USA as a visiting research scholar.

Dr. Hiroki Iwata is an Assistant Professor in the Department of Environmental Sciences, Shinshu University in Matsumoto, Japan. His research interests include turbulent transport of gases in the atmospheric boundary layer and its application to surface flux observations. He received his Doctoral degree in Science at Tsukuba University, and worked at Terrestrial Environment Research Center, Tsukuba University, Tsukuba, Japan, International Arctic Research Center, University of Alaska, Fairbanks, USA, and Graduate School of Agriculture, Kyoto University, Kyoto, Japan.

Dr. Hideki Kobayashi received the Ph.D. degree in Environmental Science and Technology from Tokyo Institute of Technology, Tokyo, Japan in 2004. He was a Postdoctoral Fellow in Japan Agency for Marine-Earth Science and Technology (JAMSTEC) and University of California, Berkeley. He is currently a Deputy Research Unit Leader in Institute of Arctic Climate and Environmental Research, JAMSTEC and also serves as Adjunct Associate Professor at Tokyo Institute of Technology and Visiting Associate Professor at Chiba University. His recent research interests are in plant canopy radiative transfer and integration of the near-surface, airborne, and satellite remote sensing of plant canopies with particular focus on northern high latitudes.

Dr. Eugénie Euskirchen is a Research Associate Professor of Terrestrial Ecology in the Institute of Arctic Biology at the University of Alaska Fairbanks, USA. Her research focuses on applying field-based micrometeorological measurements and process-based ecological modeling to reach a better understanding of high-latitude climate change. She received her doctoral degree in forest ecology at Michigan Technological University in Houghton, Michigan, USA and her master's degree in mathematical sciences at Johns Hopkins University in Baltimore, Maryland, USA.

Dr. Lutz Merbold is a Senior Scientist heading the Mazingira Centre (environmental and educational laboratory) within the International Livestock Research Institute (ILRI) in Nairobi, Kenya. His recent research focuses on environmental footprints of agricultural production systems in developing countries, predominantly in Africa. Before joining ILRI, he was a Senior Scientist/Lecturer and a Postdoctoral Researcher at ETH Zurich, Switzerland investigating greenhouse gas exchange and the underlying processes from a variety of ecosystem in Central Europe. His Ph.D. work involved a comparison of carbon dioxide and methane exchange in highly seasonal environments, including Arctic tundra ecosystem as well as tropical woodlands.

Dr. Takeshi Ohta is a Professor of Graduate School of Bioagricultural Sciences of Nagoya University in Aichi prefecture, Japan. His research interest is the forest hydrology, especially the dynamics of water, energy, and carbon dioxide exchanges. His main field is the Yakutsk region of eastern Siberia, Russia, and is working with the staffs of the Institute of Biological Problems of Cryolithzone, Siberian Division of Russian Academy of Sciences, since 1994.

Dr. Takashi Machimura is an Associate Professor at Graduate School of Engineering, Osaka University, Suita, Osaka, Japan. His research targets range widely over natural and social ecosystems including vegetation, wildlife, water and mass cycles, land use, rural communities, energy systems, etc. which are to be integrated for designing the sustainable future of human being. He received the Ph.D. degree in Agriculture from Hokkaido University, Japan.

Dr. Donatella Zona is an Associate Professor at San Diego State University, USA and a Senior Research Fellow at the University of Sheffield, UK. Her research integrates the study of the functioning of a variety of ecosystems, natural (Arctic tundra) and managed (oak forest, agro-ecosystems), and emphasizes the impact of climate change on biodiversity, ecosystem functioning, and greenhouse gas emission (CO_2 and CH_4) in the Arctic.

Dr. Walter C. Oechel is Distinguished Professor at Department of Biology and the Director for the Global Change Research Group, San Diego State University. His research focuses on developing and understanding the predictive capability of the interconnections of terrestrial, atmospheric, and marine systems on global change. He focuses primarily on the Arctic (Alaska, Russia), the Pacific Basin (Baja California Sur, Mexico, Indonesia), and the semi-arid ecosystems of Italy and San Diego. He incorporates a small research aircraft, eddy covariance towers, soil measurements, remote sensing, and modeling in his research programs. He leads a highly active research group and advises many Ph.D. students, and several master's and undergraduate students.

Dr. Edward A.G. Schuur is a Professor in the Center for Ecosystem Science and Society at Northern Arizona University. He is an ecologist who has studied links between ecosystems and climate in locations across Alaska and the Arctic. He is also the lead investigator for the Permafrost Carbon Network, an international consortium of researchers aimed at synthesizing new knowledge on permafrost carbon and climate. He graduated Magna Cum Laude with a BS from the University of Michigan, and he received a Ph.D. from the University of California-Berkeley.

Spring Phenology of the Boreal Ecosystems

19

Nicolas Delbart

Abstract

Ecosystem phenology, i.e., the timing of key biological events, is often considered as both a witness and an actor of climate change. Phenological interannual variations and decadal changes reflect climate variability and trends. Deciduous plant phenology also directly influences the carbon, water, and energy exchanges of the ecosystem with the atmosphere. In the northern forests, a trend to earlier spring has been widely reported, often based on remote sensing methods. This trend is suggested to explain a part of the residual carbon sink. However methodological issues, especially related to the combined effects of the vegetation and of the snow cover seasonal changes on the remote sensing signal, were found to affect the results. This chapter describes a remote sensing green-up retrieval method designed to avoid signal contamination by snow. The result validation with ground observations showed that the method catches the interannual variations in phenology of the plant community. Changes in the 1998–2017 period are analyzed and positioned in a longer term. This shows that the most persistent feature over the last decades is a large-scale shift in the green-up date at the end of the 1980s, and that the green-up date has not recovered yet to its status prior to 1987. Finally the green-up date maps were used to represent phenology in the northern ecosystem carbon budget simulations. No unidirectional effect of phenological changes in the annual carbon balance could be identified because of a complex interplay between vegetation, water resources and climate.

This chapter is dedicated to the memory of Rikie Suzuki.

N. Delbart (✉)
Laboratoire des Energies de Demain / UMR8586 PRODIG, Université de Paris, UMR CNRS 8236, 75013 Paris, France
e-mail: nicolas.delbart@univ-paris-diderot.fr

D. Yang and D. L. Kane (eds.), *Arctic Hydrology, Permafrost and Ecosystems*,
https://doi.org/10.1007/978-3-030-50930-9_19

19.1 Introduction

Phenological shifts, i.e., changes in the timing of key biological events within the year, are often reported among the most obvious impacts of climate changes and climate variability on ecosystems (Walther et al. 2002; Parmesan and Yohe 2003; Root et al. 2003; Walther 2010; Bellard et al. 2012). Especially spring phenology has advanced during the last decades with a number of days that vary according to the organisms. Phenological changes also display feedbacks to the atmosphere through several processes, including changes in the seasonal courses and the annual balances of energy, water and carbon exchanges (Richardson 2013). Therefore research on phenology addresses questions regarding the observation strategies from the plant scale to the biome scale, changes in phenology in relationship with climate changes, or the consequences of these changes. Answering these questions is crucial in the boreal ecosystems where the observed warming is especially strong (Solomon 2007) with multiple consequences on physical and biological functions (Hinzman et al. 2005; Post et al. 2009) and where the warming is predicted to be enhanced in the future (IPCC 2013).

This chapter summarizes the research in the boreal ecosystem phenology using remote sensing-based methods. It describes the methodologies that were developed to map the date of green-up at the scale of the circumpolar forests and low-arctic tundra with reduced influence of snowmelt on the radiometric signal. It also documents the variations in phenology in boreal North America and Eurasia boreal forests over the last decades. Finally, it reports how the remote sensing green-up maps were used to improve the modeling of the carbon budget of northern ecosystems.

19.2 Mapping the Date of the Beginning of the Boreal Spring with Remote Sensing

The diversity of impacts of phenological changes has resulted in a diversity of methods of observation and analyses, such as the networks of field observations by scientists (Menzel 2000) or by citizens (Beaubien and Hamann 2011b), the modeling (Schwartz et al. 2006) or remote sensing. Observing phenology using repetitive optical remote sensing has been experimented since the 1970s (Dethier et al. 1973; Rea and Ashley 1976; Vinogradov 1977). These studies, based on Landsat-1 data, introduced key concepts on which recent works about land surface phenology still rely, such as the radiometric data preprocessing, use of spectral indices combining radiometric measurements in the visible and near-infrared spectral domains, or the validation via ground observations. These concepts were further applied to large swath optical remote sensing which allows high frequency of radiometric measurement at the global scale (Justice et al. 1985, 1986; Townshend and Justice 1986), revealing an increase in the greenness of ecosystems at 45–75°N latitudes, especially in the spring interpreted as an advance of the beginning of the growing

season during 1982–1991 (Myneni et al. 1997, 1998). This advance matched a similar trend in ground phenology observations (Schwartz 1998) and explained the changes in the seasonal variations of atmospheric carbon dioxide concentrations as increased greenness is associated with an increase in carbon uptake (Keeling et al. 1996). Remote sensing has also been used to study phenology of specific ecosystems, in mountainous areas (Colombo 2011; Guyon 2011), temperate forests (Duchemin et al. 1999; Soudani 2008), semi-arid areas like Sahel (Guan 2014; Meroni et al. 2014), boreal regions (Suzuki et al. 2003; Zeng 2013), or even tropical forests (Pennec et al. 2011). Nevertheless the exact meaning of the land surface phenology (LSP) metrics, i.e., the recorded timing of the radiometric transition, is still questioned for various reasons (Helman 2018). The LSP metrics differ strongly with both the data preprocessing and extraction methods (Schwartz et al. 2002; Morisette et al. 2009; White et al. 2009; Helman 2018) so that validation, for example, using ground phenology observations and photosynthesis measurements remains a key issue (Badeck et al. 2004; Liang et al. 2011; Pouliot 2011; Gonsamo 2013; Misra et al. 2016).

One source of uncertainty is specific to the boreal regions and to the mountainous areas when observing the start of the growing season: snowmelt at spring strongly influences the radiometric changes (Moulin et al. 1997; Shabanov et al. 2002; Dye and Tucker 2003). The widely used Normalized Difference Vegetation Index (NDVI), defined as the normalized difference of reflectance in the red and the near-infrared spectral bands, increases when the snow cover fraction in the pixel decreases (Fig. 19.1), even without any change in the vegetation, because its denominator decreases (Suzuki et al. 2011). The initial increase in NDVI must therefore not be interpreted as related to foliage expansion. Thus some proposed methods have been consisted in catching the time at which NDVI exceeds a relatively high threshold (Suzuki et al. 2003). In other methods snow affected values are replaced by snow-free values (Beck et al. 2006; Park et al. 2016). Other indices based on the same spectral bands were also developed using radiative transfer simulations to reduce the impact of snow cover variations (Jin et al. 2017). Alternatively, a method based on the Normalized Difference Water Index (NDWI), which is the normalized difference of near-infrared (NIR) and short-wave infrared reflectance (SWIR) was proposed (Delbart et al. 2005). NDWI decreases with the progressive disappearance of the snow cover, and increases during the foliage development (Fig. 19.1). The green-up date is recorded as the time when the NDWI starts increasing. Precisely it is taken as the last date within the March–July period when NDWI has increased by less than 20% of its total increase in this period. This method was applied to SPOT-VEGETATION S10 data. SPOT-VEGETATION is a push-broom sensor, which ensures that the spatial resolution is much more constant with the incidence angle than with the commonly used whisk-broom sensors MODIS and AVHRR (Helman 2018). The S10 data give a reflectance value for four spectral bands once every ten days, selected among all the measurements acquired at least once daily. The selected value is the "best" measurement that has been made during the 10-day period, following the "maximum value composite" method (Holben 1986). This preprocessing aims at minimizing the signal

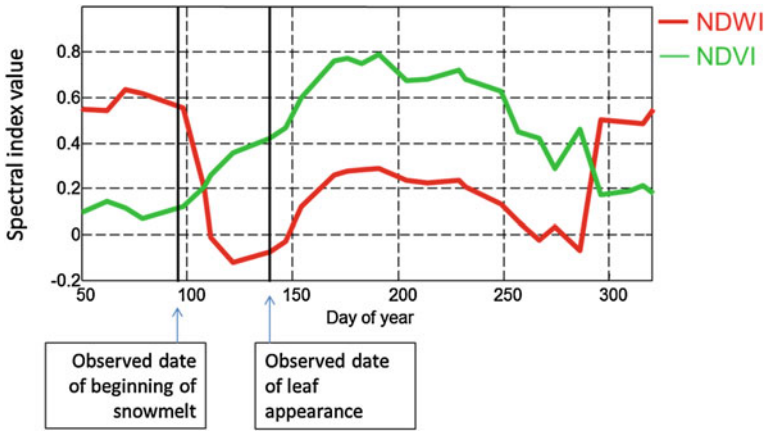

Fig. 19.1 Pixel scale intra-annual variations in two spectral indices (NDVI: Normalized Difference Vegetation Index; NDWI: Normalized Difference Water Index). Vertical bars represent the dates of the beginning of snowmelt and of leaf appearance that were observed within the pixel

contamination by aerosols and clouds. The exact date of the selected measurement is given individually for each pixel.

The green-up maps were compared to ground measurements of deciduous tree leaf appearance date for ten taiga sites in Siberia, showing a root mean square error (RMSE) of 8.7 days, with no bias (Delbart et al. 2005). The method was further tested at a few more sites in other parts of boreal Eurasia (2008) and at one site in Alaskan tundra (Delbart and Picard 2007), showing similar agreements. The green-up date averaged at the regional scale reproduces a large part of the interannual variations in the leafing date observations at several locations within the region (Delbart et al. 2008). It was also compared to phenological observations by citizens in Canada (Delbart et al. 2015): a lower agreement was then found at the site scale, likely because of the landscape heterogenity around the observation sites and within the pixel. This lower agreement consisted in a higher non-systematic error only, as the green-up date remained unbiased with ground observations. Moreover, this comparison allowed to determine that the green-up date is related to deciduous tree leaf appearance even in urban lansdscapes and evergreen dominated forests. This is true only if the NDWI increase is large enough to be significant, which occurs only if the deciduous vegetation is largely present in the pixel (Delbart et al. 2005). The agreement between the green-up date and the deciduous tree leaf appearance indirectly confirms that our metrics are not related to the needle appearance in the evergreen forests. The retrieval is inefficient for pixels dominated by water or agriculture (Delbart et al. 2015), which must be excluded from the produced dataset (see next section). However, when averaged over larger regions the remote sensing green-up date time series was shown to reproduce interannual variability in phenology not only in the timing of leafing-out but also in the flowering time (Delbart et al. 2015), because various spring phenophase interannual variations are generally related to spring air temperature variations

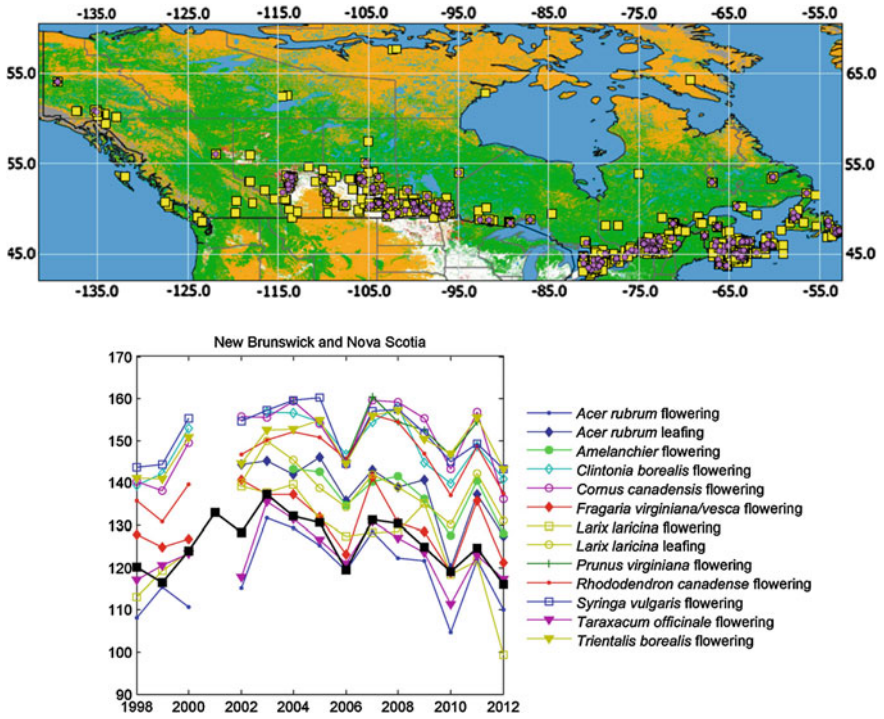

Fig. 19.2 Time series of phenological events (first flowering and leaf-out) resulting from the aggregation at the scale of New Brunswick–Nova Scotia region (delimited in the top panel) of the individual site observations by citizen scientists, and time series of the remote sensing green-up dates using the NDWI-VGT method (Delbart et al. 2005) (black squares). Site observations were collected in the framework of the PlantWatch project (Beaubien and Hamann 2011a). The spatial aggregation of the in situ observations is derived from Hakkinen et al. (1995). *Source* Delbart et al. (2015)

(Fig. 19.2). Furthermore, the evaluation of the method in mountainous areas shows that it was more efficient than the NDVI-based methods at lower elevations but less efficient at higher altitudes (Dunn and de Beurs 2011). The NDWI was also combined with the NDVI to evaluate phenology in the eucalyptus forests of the Australian Alps (Thompson 2015; Thompson and Paull 2017).

The method could be applied to SPOT-VEGETATION dataset starting in 1998. In order to extend the study period back to 1982, the results were used to improve the AVHRR NDVI-based threshold method (Suzuki et al. 2003) by adjusting the threshold value for each pixel individually (Delbart et al. 2006). This was possible using the overlap between the SPOT-VEGETATION dataset and the AVHRR Pathfinder 10-day composite dataset (James and Kalluri 1994): for each common year between the two datasets, the AVHRR NDVI value at the green-up date given by our algorithm applied to SPOT-VEGETATION data was recorded. For this purpose, both AVHRR Pathfinder NDVI and SPOT-VEGETATION reflectance was first resampled to a common 0.1° spatial resolution. The threshold map was

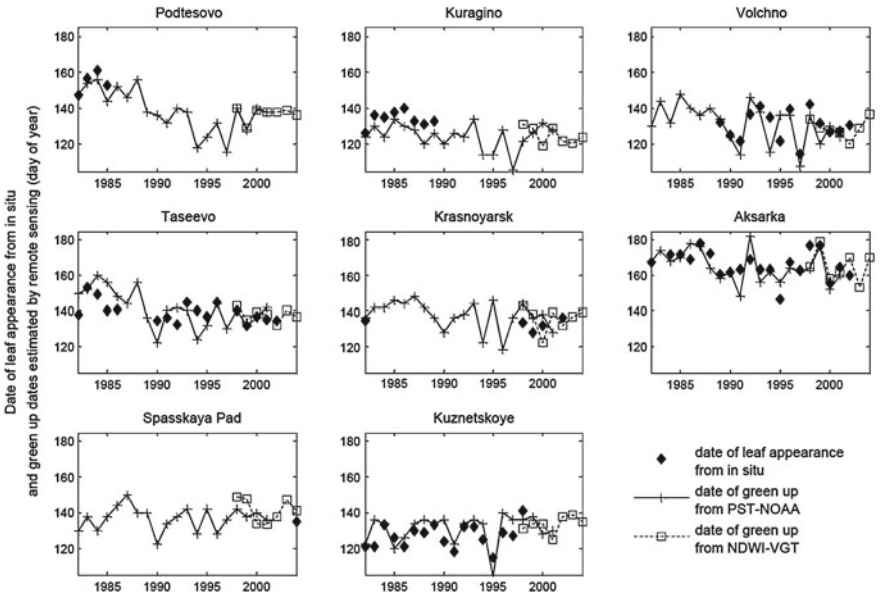

Fig. 19.3 Dates of onset of greening retrieved with the PST-NOAA method (plus signs) and with the NDWI-VGT method (squares), and in situ dates of leaf appearance (filled diamonds) at the eight validation sites in Siberia. *Source* Delbart et al. 2006)

obtained as the multiyear average value of these NDVI. Then, for all years from 1982, the green-up date was recorded as the date when the seasonal course of AVHRR NDVI reached the pixel-specific threshold (PST). The method was named as PST-NOAA. The produced results showed negligible bias and an RMSE equal to 8 days when validated in Siberia. Associated with the SPOT-VEGETATION based method applied at the 0.1° spatial resolution, it could track the interannual variations of the observed tree leaf appearance date in boreal forests (Fig. 19.3) and tundra shrublands that have occurred since 1982 (Delbart and Picard 2007; Delbart et al. 2008) (see Fig. 19.3).

19.3 Phenology: Witness of Climate Change and Variability in the Boreal Regions

19.3.1 Phenology Trend and Interannual Changes During 1982–2005

The dataset of green-up date maps resulting from our two remote sensing methods (Delbart et al. 2005, 2006) was used to analyze the interannual variations in phenology in boreal Eurasia (Delbart et al. 2008) and in circumpolar tundra

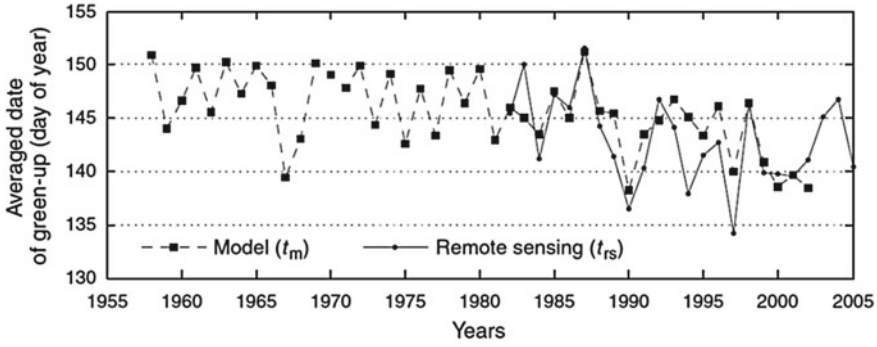

Fig. 19.4 Green-up date from remote sensing (trs) and modeling (tm) averaged over Eurasian deciduous forests (see study area in Fig. 19.5). The remote sensing dataset comes from the NDWI-VGT and the PST-NOAA methods applied at the 0.1° spatial resolution (Delbart et al. 2005, 2006). The modeled green-up date maps come from a degree-day model applied to ERA40 reanalysis temperature and calibrated using remote sensing green-up maps (Picard et al. 2005). *Source* Delbart et al. (2008)

(Delbart and Picard 2007) during 1982–2005. These times series were complemented by those from a phenology model based on air temperature only (Picard et al. 2005), to relate the observed changes to climate and to elongate the study period. Model calibration procedure is described in the next section. These studies also benefited from a few long-term time series of ground observations of leaf appearance date.

On average, over the whole Eurasian taiga area, a five-day shift in phenology between 1987 and 1990 was found (Delbart et al. 2008), directly explained by climate as it was reproduced by the modeling based on air temperature (Fig. 19.4). This change was confirmed by other methods and was shown to be directly related to the shift in the North Atlantic Oscillation (NAO), thus a witness to changes of the global climate, and interpreted as the main mechanism behind the Siberian carbon sink (Buermann 2016). This biome scale average hides contrasted regional variations (Fig. 19.5). During the study period (1982–2005) some regions like Yakoutia in eastern Siberia showed almost no trend, and others displayed an advance (Fig. 19.5). The largest trend was found for Central Siberia with a 20-day advance. However, long-term ground observations and the model applied to temperatures at meteorological stations within the subregion have revealed that half of this large advance was explained by exceptionally late spring in 1983 and 1984. This is associated with cold temperatures in this region at the beginning of the period that is accessible through remote sensing, and thus must be attributed to climate variability and not to climate change. The model also revealed some fluctuations in phenology in the longer term, such as a trend to later spring in 1936–1960 for the whole Siberia from the east of the Ob River. On the contrary, several successive periods of advances have occurred since 1936 in the western part of the study area, with no period showing a trend to later spring. It was also found that the interannual variations in spring phenology in central Siberia were correlated with the south

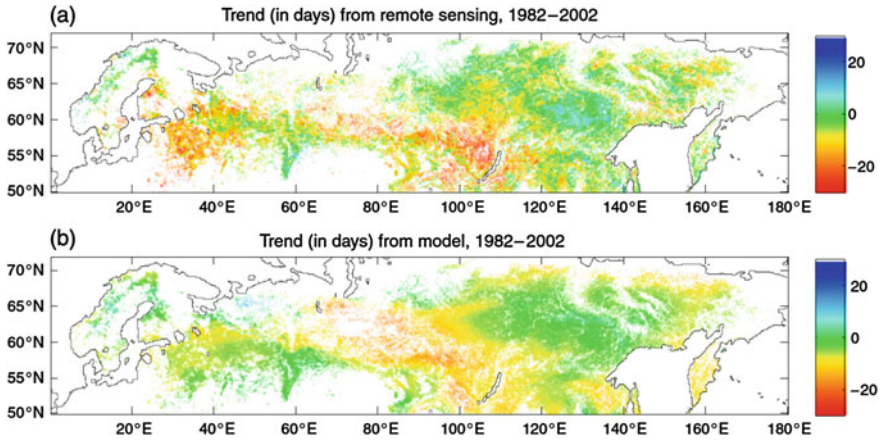

Fig. 19.5 Linear regression of the green-up date from remote sensing (top) and modeling (bottom). Each map gives the change (in days) computed as the rate of change from the linear regression (least squares) multiplied by the number of years. **a** 1982–2002, from remote sensing, **b** same period 1982–2002 from modeling. Same source of data than Fig. 19.4. *Source* Delbart et al. (2008)

oscillation index, with late springs during El Niño years and early springs during La Niña years, linking with the dominant wind directions, very different between the two types of years (Vicente-Serrano et al. 2006). In the sub-Arctic tundra, advances in spring over the last decades were found in north Alaska and in north-west Siberia (Delbart and Picard 2007).

19.3.2 Phenological Changes in 1998–2017

The following part aims at completing the previous studies by documenting the interannual variability in forest phenology over the whole circumpolar region during the last twenty years (1998–2017), with the objective of showing the variability and the trends.

19.3.2.1 Dataset and Study Region

The phenological algorithm (Delbart et al. 2005) is applied to the SPOT-VEGETATION (VGT) data for the years 1998–2013 and to the successor satellite PROBA-V data for the years 2014–2017, in order to provide a full 20-year spring phenology time series. Both datasets are provided by VITO (https://www.vito-eodata.be). The PROBA-V data full resolution is 300 m, but here the 1 km resolution product is used to match the resolution of if predecessor and to follow the same compositing rules. Here, the algorithm is applied at the full SPOT-VGT spatial resolution (0.0089°). The algorithm is run for the years 1998 to 2013 on SPOT-VGT data and on PROBA-V over the years 2014–2017, to obtain one

green-up day map each year at the 1 km. This differs from previous time series studies (Delbart and Picard 2007; Delbart et al. 2008) for which the SPOT-VGT reflectance data were first averaged at 0.1°. It is important to notice that the PST-NOAA algorithm was calibrated using the results from this 0.1° aggregated SPOT-VGT dataset. Thus the results from the full resolution SPOT-VGT data did not combine with the PST-NOAA dataset, so that the following analysis will be restricted to 1998–2017.

The full resolution dataset reveals spatial details that were not visible in the previous version. Moreover, the comparison of the 1 km resolution green-up dataset with a massive number of phenology ground observations by citizens has revealed that the reliability of the green-up date differs strongly with the dominant landcover types within the remote sensing pixel (Delbart et al. 2015). Especially it was found that pixels of purely agricultural land or as water body by the Global Land Cover 2000 (GLC2000) dataset (Bartholomé and Belward 2005) should be excluded from the green-up date maps. We then aggregate through local averaging the not-excluded pixels to a spatial resolution ten times lower of the original one. This allows to reduce both the fraction of territory with missing data and the dataset size. Moreover, previous studies have shown that this dataset better matches interannual variability when spatially averaged (Delbart et al. 2008, 2015).

The map of the Köppen-Geiger climate classification (Peel et al. 2007) and the landcover map GLC2000 (Bartholomé and Belward 2005) are used to restrict the study area to the circumpolar forests and shrublands (CLC2000 classes 1 to 12) located in a cold or polar climate (Köppen-Geiger zones D and E). The GLC2000 dataset reports a pixel as forest if the tree cover fraction is more than 15%, the used criteria allows to define the current study area as the taiga and the sub-Arctic tundra regions, for which ligneous vegetation is settled but not necessarily dominant. Green-up date reported for evergreen forests is related to the leaf phenology of the sparse deciduous trees.

19.3.2.2 Delineating Phenoregions

At large scale the time variations in phenology are often represented through a trend analysis at the pixel level complemented by a spatial average over large regions (e.g., (Schwartz et al. 2006; Delbart et al. 2008; Gonsamo and Chen 2016). Both methods have drawbacks: trend analysis results are very much dependant on the time range of the dataset; spatial averaging over arbitrary regions, like hemisphere (Schwartz et al. 2006; Gonsamo and Chen 2016) or rectangles (Delbart et al. 2008, 2015), results in hiding spatial differences within the considered region and necessarily combines subregions of different variability. Recent studies extending the study of the variations in phenology (Gonsamo and Chen 2016; Park et al. 2016) provide maps of the trend that cannot be compared because of different period limits. There is a need to, in addition to the maps of trend, to delineate regions, the so-called "phenoregions," that are homogeneous in terms of interannual variability in phenology, with no hypothesis on the region shape or size. For these regions the interannual variability in phenology will be displayed, with the aim to visualize the variations in phenology for some key regions of interest in the study area, i.e., regions displaying strong trends.

The term "phenoregion" differs from the previous occurrence for which the whole annual cycle of spectral indices was used (White et al. 2005). Here, phenoregions are the regions for which the interannual variability of the green-up date is homogeneous. They are delineated from the annual anomalies in the green-up date. The first step consists of subtracting the 20-year average green-up date from each annual map to provide a time series of maps of temporal anomaly in phenology, free of spatial gradients. In this time series a k-means classification is conducted with a large and arbitrary number of classes (here, 300 classes). Closely related classes are merged using an ascending hierarchical clustering based on a dissimilarity measure that is 1 *minus* the correlation between each of the 300 above classes. The classes are then aggregated if their dissimilarity is less than a chosen threshold, here 0.439, i.e., if their correlation is positive and significant at 0.01 level.

19.3.2.3 Spatial and Temporal Variability

The twenty-year average green-up date follows a south to north gradient in Eurasia and a south-west to north-east gradient in North America, with no difference in averages and distributions between the two continents (Fig. 19.6). The interannual variability in the green-up date is highly spatially variable, and can take some large values: the temporal amplitude, i.e., the difference between the earliest and latest dates recorded at one pixel, ranges from 20 to 50 days (Fig. 19.6). The overall direction of changes is summarized through the slope of the linear regression of the green-up date over time. Slope ranges from-0.68 to 0.5 days/year, with a mean value of-0.11 days/year, indicating a moderate trend to an earlier green-up on average over the circumpolar forests during the last twenty years. Using different sensors, metrics and study periods, slightly different trends were found at the circumpolar scale: a small delay of +0.085 days/year over 2000–2014 (Park et al. 2016), or a small advance of-0.23 days/year in 1999–2013 (Gonsamo and Chen 2016).

The spatial distribution of the slope values reveal that the strongest trends are not necessarily found for pixels displaying the strongest variability. However, a relatively clear pattern emerges: several large regions display a delay (e.g., Western boreal Eurasia, most of Canada) while others show an advance (Ural region, a large region including Alaska, Yukon, and Canadian north-west territories, Yakoutia, Fennoscandia).

19.3.2.4 Interannual Variability at the Phenoregion Level

The slope of the linear regression is highly variable spatially. It is also well known that the time limits of the study period have a strong influence on the regression slope of a time series. The green-up date time series for several phenoregions are displayed in Figs. 19.7, 19.8 and 19.9, in order to better understand the slope values, for North America (Fig. 19.7), western boreal Europe (Fig. 19.8), and boreal Asia (Fig. 19.9). The selected phenoregions are corresponding to the regions with strong trends. This is possible to identify them since the location of most phenoregions corresponds to an area of rather homogeneous slope. This is not true

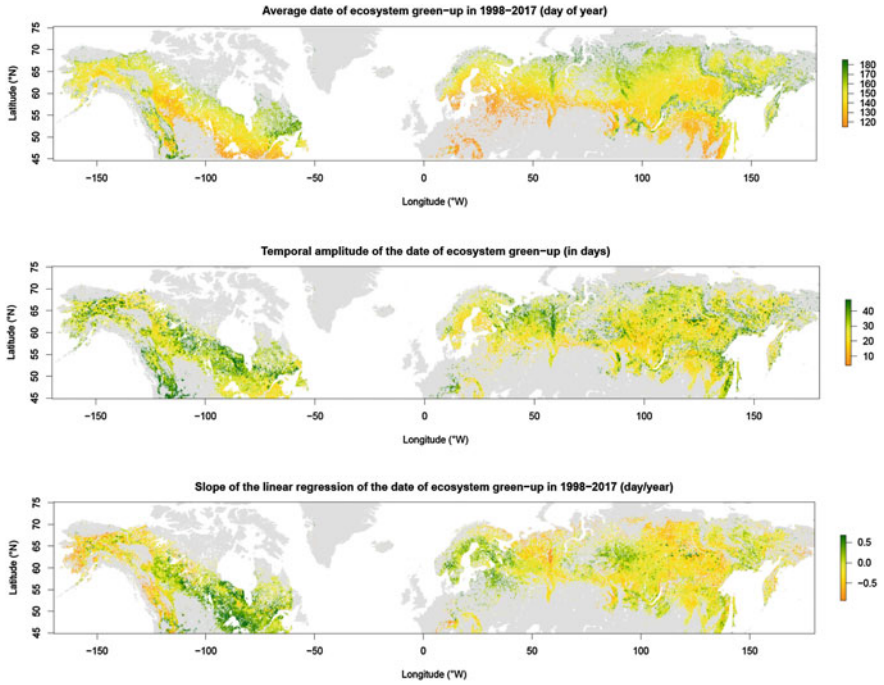

Fig. 19.6 Summary of spatial and temporal variations in phenology in 1998–2017 as estimated from the SPOT-VEGETATION and PROBA-V using the NDWI algorithm (Delbart et al. 2005) at the full resolution before data exclusion based on validation (Delbart et al. 2015). Top: 20-year average date of green-up (day of year). Middle: amplitude of the interannual variations (in days). Bottom: slope of the linear regression on chronological time series of the green-up date (days. year^{-1})

for one of the selected phenoregions located in central boreal Eurasia, which groups pixels with positive and negative slopes despite correlated interannual variations. The central Eurasia area with positive slope (Fig. 19.6) is in fact distributed to at least two phenoregions and thus corresponds to at least two modes of variations (Fig. 19.9).

Very clearly, it appears that a viewal examination of the time series contradicts the regression analysis, and that for almost none of the regions a clear trend can be identified. This of course matches the interpretation of the associated p-value of the regression slope. p-values were lower than 0.01 for only 1.9% of pixels moreover scattered in the study area; p-values were lower than 0.05 for only 8.4% of pixels, meaning that the interannual variability exceeds the trend. This is true for phenoregions displaying progressive delay and for the ones showing an advance in green-up dates. The only exception stands for Alaska and north-west Canada

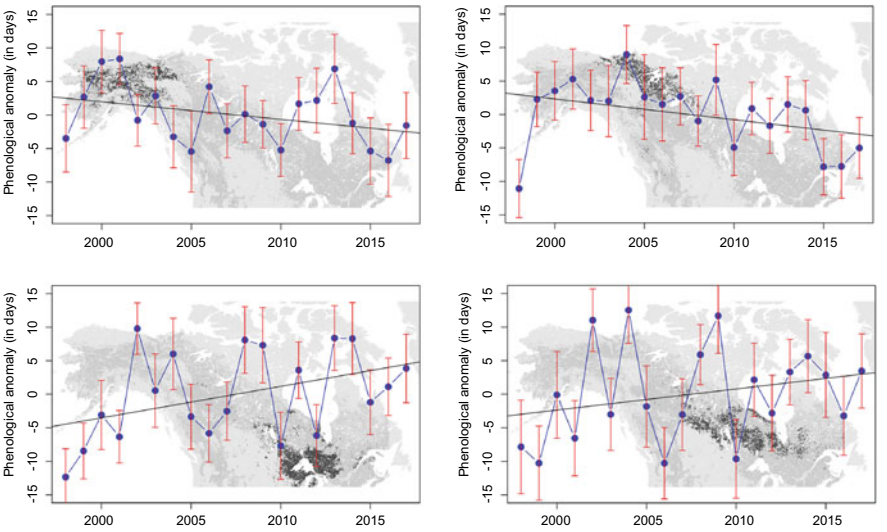

Fig. 19.7 Time series of the green-up date averaged at the scale of a selected set of phenoregions in North America (in day of year). Same source of data as for Fig. 19.6

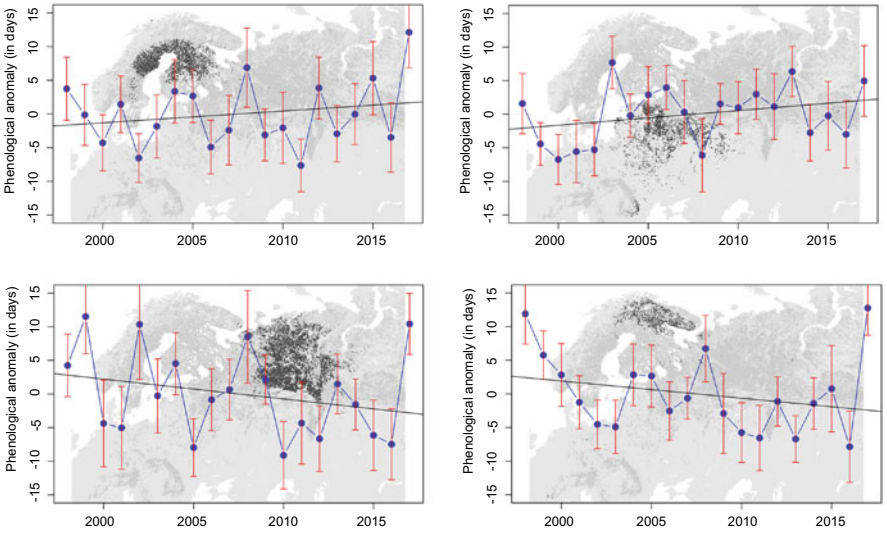

Fig. 19.8 Time series of the green-up date averaged at the scale of a selected set of phenoregions in boreal Europe (in day of year). Same source of data as for Fig. 19.6

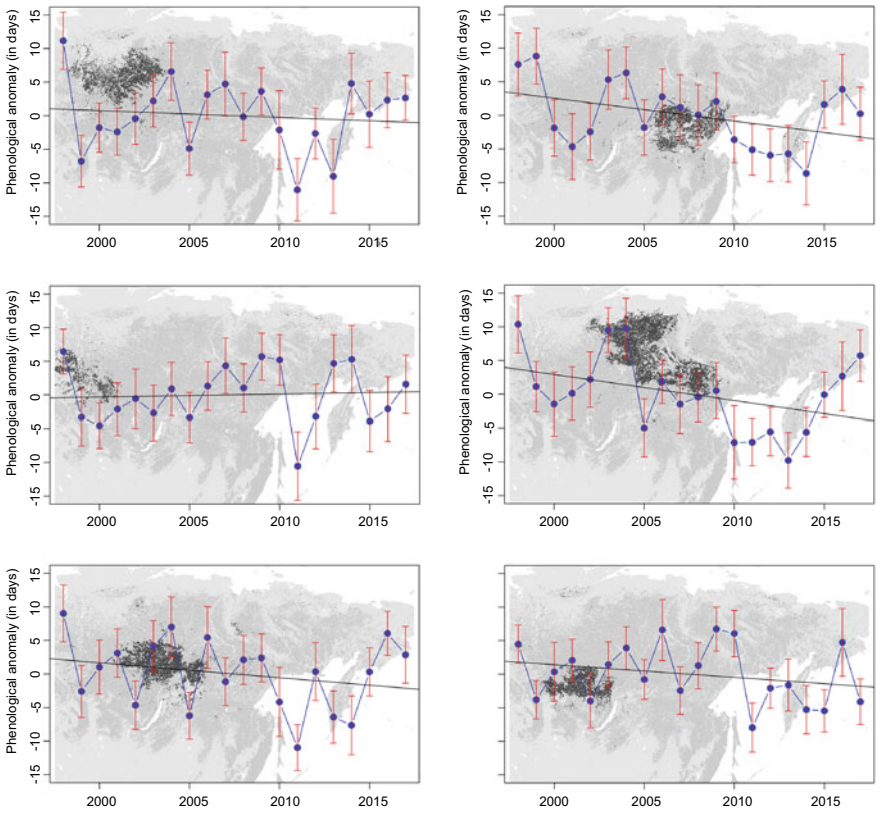

Fig. 19.9 Time series of the green-up date averaged at the scale of a selected set of phenoregions in boreal Asia (in day of year). Same source of data as for Fig. 19.6

(Yukon and north-west territories) where the trend to earlier green-up is more robust (Fig. 19.7).

19.3.3 Summary

In the northern regions, the last twenty years do not display a clear and significant trend in the spring green-up date, relative to the interannual variability in green-up date, except for the north-west North America. Contrarily, the previous period (1982–1999) has shown a strong trend to earlier spring (Park et al. 2016), i.e., a 5-day shift when averaged at a continental scale. This change corresponded to a climate shift (Buermann 2016), and linked to temperature warming as it can be reproduced by a temperature-based model (Delbart et al. 2008). Other trends to earlier spring were found locally (Delbart et al. 2008). This 5-day shift is the most persistent feature in the phenology time series. The lack of trend since then also

indicates the date of green-up has not recovered to the values prior to 1987. In addition to this shift in green-up date, the key point is the interannual variability. The section below discusses its effect over the annual carbon budget in the boreal ecosystems.

19.4 Phenology and Ecosystem Carbon Budget

Phenology is considered as one of the essential biodiversity variables (Pereira et al. 2013) while leaf area index and its seasonal variations are listed as one of the essential climate variables (Bojinski et al. 2014). Phenology is widely studied because of its impacts on both ecological and climatic processes. For example, phenological interannual variability that differs among species affects several ecosystems functions, like the plant–pollinators relationships (Kiers et al. 2010) or the trophic networks (Both et al. 2009). In the northern environments, trophic mismatch due to differentiated phenological changes between forage plants and herbivores lead to decrease the reproduction success rates of caribous and reindeers (Post et al. 2008; Post and Forchhammer 2008) which is further accented by changes in phenology of harassing insects (Vors and Boyce 2009). Phenology is also one essential trait for understanding and modeling the species spatial current and future spatial distribution (Morin et al. 2008; Chuine 2010).

As mentioned above, the large-scale lengthening of the growing season revealed by remote sensing (Myneni et al. 1997) matched the change in the atmospheric carbon dioxide seasonality changes (Keeling et al. 1996). About half of the carbon dioxide anthropogenic emission accumulates in the atmospheric, while about one quarter is absorbed by the ocean and the last quarter by the continental ecosystems (Le Quéré et al. 2014), northern ecosystems being one of the carbon sinks that mitigates the rise of atmospheric CO_2 concentration (Forkel et al. 2016). In addition to the structural and functional changes affecting vegetation, the lengthening of the growing season in the northern ecosystems is considered among the main processes explaining the continental carbon sink (Graven et al. 2013; Le Quéré et al. 2014; Buermann 2016; Forkel et al. 2016), as the increase in the annual gross carbon uptake by ecosystems due to a lengthening growing season is only partially offset by the increase in respiration at autumn (Richardson et al. 2010), so that the net carbon uptake increases with the length of the growing season (Baldocchi et al. 2001; Zhou et al. 2016).

However some contradictory results exist (Buermann 2013) as the growing season lengthening does not necessarily transfer into an increased annual net productivity because of water stress (White and Nemani 2003) or increased soil respiration (Goulden et al. 1998). Spring advance was even found associated with a decrease in annual carbon uptake measured at the Kitalik station in the Siberian arctic (Parmentier et al. 2011). Remote sensing has revealed complex geographical patterns of the correlation between the respective dates of spring and autumn: for large regions of Canada and Siberia, early autumn was associated with early spring

which reduced the influence of the date of the beginning of spring on the growing season length (Liu et al. 2016). This result was also found in some temperate forests (Keenan 2015). However, the inverse relationship was found for other regions in Canada and Siberia (Liu et al. 2016). Combining passive microwave and optical remote sensing also revealed that early spring (and early snowmelt) leads to decreased ecosystem greenness in summer in parts of Siberia (Grippa et al. 2005). Overall these results indicate a complex relationship between phenology and annual carbon uptake, which cannot be separated from other processes affecting the vegetation functioning or the water balance. Therefore our efforts have mainly concentrated on improving dynamic vegetation models (DVM) that simulate a cascade of processes involved in carbon uptake and release, energy and water exchanges, and plant growth.

The maps of green-up dates have been used to calibrate the modeling of phenology in the Sheffield Dynamic Vegetation Model (Woodward et al. 1995) aiming to simulate the carbon budget of Siberia ecosystems (Picard et al. 2005). Phenological models aim at predicting the date of budburst from daily air temperature time series. The model that was used is the degree-day model to predict the date of budburst as the date when the cumulative (from the 1st of January) difference between the daily temperature and a fixed base-temperature reaches a threshold value. Both the base-temperature and the threshold were calibrated (Picard et al. 2005). Other three models including the chilling requirement, i.e., the need for a cold period to release the dormancy, did not display better agreement with remote sensing than the simpler degree-day model, probably because the need for cold was always fulfilled in the central Siberia. The calibration has consisted in determining the set of model parameters that maximized the agreement with the remote sensing maps (Picard et al. 2005). The modeled budburst date was compared to ground observations at various sites in boreal Eurasia located inside or outside the calibration area (Fig. 19.10) (Delbart et al. 2008). Remarkably the RMSE was 7.3 days, with no bias, which is one day better that the agreement between the remote sensing green-up date and the ground observations. The model was also shown to perform as well for tundra shrubs than for taiga trees, and as well as phenology models designed specifically for tundra (Fig. 19.11) (Delbart and Picard 2007). This model can be used across the taiga-tundra ecotone even for simulations under future climate if the ecotone is simulated to move.

Sensitivity study showed that a one day bias in the modeled green-up date would translate to a 2.2% error on the annual net primary productivity for the central Siberia study area (Picard et al. 2005). Removing the radiometric effect of the snowmelt on the green-up date detection had therefore led to a decrease in the annual NPP uncertainty. The same phenology model was introduced in a second DVM, SEIB-DVM (Sato et al. 2007, 2010), that differs from the first model by simulating the growth of individuals. Simulations under increasing temperature have revealed that for Eastern Siberian larch forests the lengthening of the growing season was accompanied by an increase in water stress in summer and in the carbon release through respiration, resulting altogether in a decrease of the annual NPP,

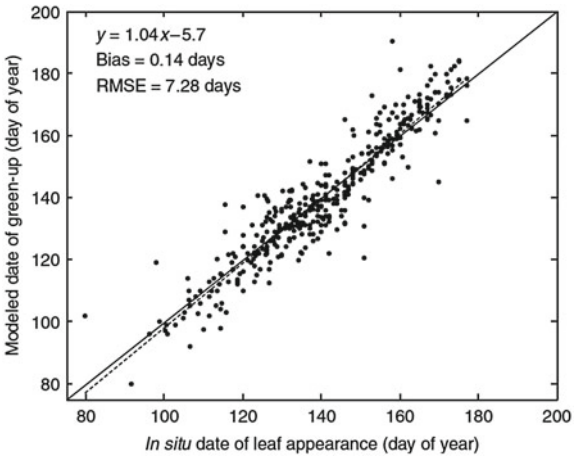

Fig. 19.10 Modeled leaf-out dates versus in situ leaf appearance dates observed at ten locations in boreal Eurasia. The model is a degree-day model applied to temperature time series from the ERA40 reanalysis dataset (Picard et al. 2005). *Source* Delbart et al. (2008)

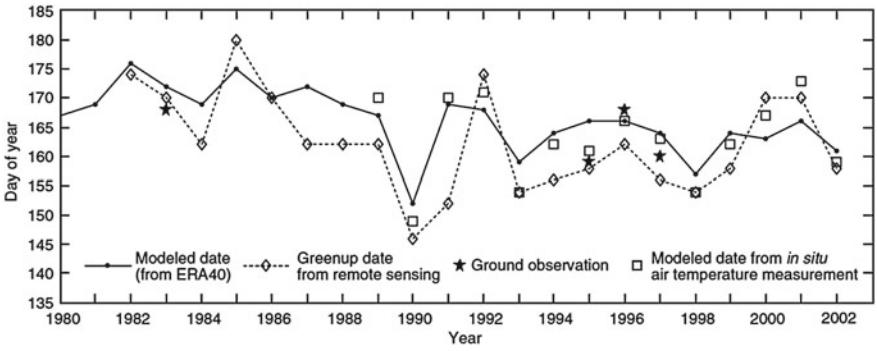

Fig. 19.11 In situ dates of leaf appearance, simulated green-up dates (Picard et al. 2005), and remote sensing green-up dates from the NDWI-VGT and PST-NOAA methods (Delbart et al. 2005, 2006) at the Toolik Station *Source* Delbart and Picard (2007)

which was also reported in the abovementioned studies (Goulden et al. 1998; Parmentier et al. 2011; Liu et al. 2016).

In conclusion, the impact of phenological responses to temperature variations on the annual productivity of boreal ecosystems is still unclear and strongly depends on regional and local conditions, and especially depends on all processes affecting the water availability. It does not seem that a specific homogeneous effect of phenology can be clearly identified. Phenology is a temperature-driven process, among other climate-driven processes that must all be modeled taking into account

the regional specificities of the interplay between soil, water, and carbon cycles. To this end, an arctic-specific version of a third land surface model (LSM), ORCHIDEE (Krinner et al. 2005; Guimberteau et al. 2018), was recently designed by incorporating specific developments of the processes related to permafrost, snow, plant functional type distribution (Ottlé et al. 2013), and through a rational selection of key parameters to be calibrated (Dantec-Nédélec et al. 2017). This version was evaluated through a comparison to a large set of ground observations, fluxes time series, and satellite-derived parameters including phenology and leaf area index (Dantec-Nédélec 2017), and will be used to explore the future of the carbon balance. Besides, it must be noticed that actual plant productivity, and not only greenness, may be monitored by other types of remote sensing like solar-induced fluorescence, leading to new insight into boreal ecosystem carbon budget (Walther et al. 2016).

19.5 Conclusion

This chapter has summarized the results obtained in three directions. The first one concerns the methods to measure and map the green-up date of boreal ecosystems without signal disturbance by snowmelt, and has established its link to the actual tree leaf appearance date. It was also shown that the interannual variations in the green-up date correspond to the phenology of a whole community of plants. The second one is the analysis of the time variations in green-up date, which has revealed a 5-day shift to earlier spring between 1987 and 1990. Before 1987 and after 1990, trends can be found locally but not at large scale, as interannual variability in the green-up date exceeds its trend. The third study direction is the integration of phenology in ecosystem models designed to simulate the carbon, energy, and water exchanges between the ecosystem and the atmosphere. Remote sensing green-up date maps were successfully used to calibrate a phenology model that was unbiased and able to reproduce spatial and temporal variations in phenology from the daily temperature time series. The integration of such a model was crucial as it avoids bias in the simulated productivity, as the green-up date may influence the growing season length and thus the annual carbon budget. However, because the annual carbon budget depends only partly on phenology, and because earlier spring may induce an early depletion of water resources, there is no consensus on the effect of phenology on the annual carbon budget for the boreal ecosystems. Improving all processes involved in carbon and water cycles, in soils and vegetation, and in ecosystem models is crucial. Besides, improvements in the remote sensing of other variables are necessary. Among the variables directly related to vegetation can be listed as the leaf area index (Kobayashi et al. 2010), vegetation stress and actual productivity (Walther et al. 2016), or the date of senescence. The attempts to derive a date of senescence from spectral indices failed (Delbart et al. 2005). Results reported in the Chap. 21 by Yongwon Kim show that the snow also disturbs the retrieval of the senescence date. Other teams display

better agreement of the senescence date with ground measurements (e.g., Jin and Eklundh 2014). However, it is difficult to select a single date from the remote sensing time series to represent senescence because it is a gradual process at all scales from the leaf, the tree to the community that is observable in the medium resolution remote sensing pixel. Dense time series of high spatial resolution optical remote sensing images that are now available may partly solve this issue by zooming the phenology studies nearly up to the individuals trees.

Acknowledgments Many thanks to the authors and coauthors of the published results that are summarized in this chapter, and in particular Elisabeth Beaubien, Sarah Dantec-Nédélec, Dennis Dye, Manuela Grippa, Laurent Kergoat, Hideki Kobayashi, Thuy Le Toan, Fabienne Maignan, Catherine Ottlé, Ghislain Picard, Hisashi Sato, and Sergio Vicente-Serrano. Thanks to VITO for providing SPOT-VEGETATION and PROBA-V data. The algorithm for green-up date extraction from PROBA-V data was implemented on the VITO MEP.

References

Badeck F-W, Bondeau A, Böttcher K, Doktor D, Lucht W, Schaber J, Sitch S (2004) Responses of spring phenology to climate change. New Phytol 162:295–309

Baldocchi D, Falge E, Gu L et al (2001) FLUXNET: a new tool to study the temporal and spatial variability of ecosystem-scale carbon dioxide, water vapor, and energy flux densities. Bull Am Meteor Soc 82:2415–2434

Bartholomé E, Belward AS (2005) GLC2000: A new approach to global land cover mapping from earth observation data. Int J Remote Sens 26:1959–1977

Beaubien EG, Hamann A (2011a) Plant phenology networks of citizen scientists: recommendations from two decades of experience in Canada. Int J Biometeorol 55:833–841

Beaubien E, Hamann A (2011b) Spring flowering response to climate change between 1936 and 2006 in Alberta, Canada. Bioscience 61:514–524

Beck PSA, Atzberger C, Høgda KA, Johansen B, Skidmore AK (2006) Improved monitoring of vegetation dynamics at very high latitudes: a new method using MODIS NDVI. Remote Sens Environ 100:321–334

Bellard C, Bertelsmeier C, Leadley P, Thuiller W, Courchamp F (2012) Impacts of climate change on the future of biodiversity. Ecol Lett 15:365–377

Bojinski S, Verstraete M, Peterson TC, Richter C, Simmons A, Zemp M (2014) the concept of essential climate variables in support of climate research, applications, and policy. Bull Am Meteor Soc 95:1431–1443

Both C, Van Asch M, Bijlsma RG, Van Den Burg AB, Visser ME (2009) Climate change and unequal phenological changes across four trophic levels: constraints or adaptations? J Anim Ecol 78:73–83

Buermann JL (2016) Climate-driven shifts in continental net primary production implicated as a driver of a recent abrupt increase in the land carbon sink. Biogeosciences 13:1597–1607

Buermann M (2013) Earlier springs decrease peak summer productivity in North American boreal forests. Environ Res Lett 8

Chuine I (2010) Why does phenology drive species distribution? Philosophical Transactions of the Royal Society B: Biological Sciences 365:3149–3160

Colombo UM (2011) Phenological monitoring of grassland and larch in the Alps from Terra and Aqua MODIS images. Italian J Remote Sens/Rivista Italiana di Telerilevamento 43:83–96

Dantec-Nédélec S (2017) Evaluation multi-échelle des bilans d'énergie et d'eau du modèle ORCHIDEE sur la Sibérie et leur réponse à l'évolution du climat. Paris Saclay

Delbart N, Beaubien E, Kergoat L, Le Toan T (2015) Comparing land surface phenology with leafing and flowering observations from the PlantWatch citizen network. Remote Sens Environ 160:273–280

Delbart N, Kergoat L, Le Toan T, Lhermitte J, Picard G (2005) Determination of phenological dates in boreal regions using normalized difference water index. Remote Sens Environ 97:26–38

Delbart N, Le Toan T, Kergoat L, Fedotova V (2006) Remote sensing of spring phenology in boreal regions: a free of snow-effect method using NOAA-AVHRR and SPOT-VGT data (1982–2004). Remote Sens Environ 101:52–62

Delbart N, Picard G (2007) Modeling the date of leaf appearance in low-arctic tundra. Glob Change Biol 13:2551–2562

Delbart N, Picard G, Le Toan T, Kergoat L, Quegan S, Woodward I, Dye D, Fedotova V (2008) Spring phenology in boreal Eurasia over a nearly century time scale. Glob Change Biol 14:603–614

Dethier BE, Ashley MD, Blair BO, Caprio JM, Hopp RJ, Rouse Jr, J (1973) Phenology satellite experiment.[detection of brown wave and green wave in north-south corridors of United States]

Duchemin B, Goubier J, Courrier G (1999) Monitoring phenological key stages and cycle duration of temperate deciduous forest ecosystems with NOAA/AVHRR data. Remote Sens Environ 67:68–82

Dunn AH, de Beurs KM (2011) Land surface phenology of North American mountain environments using moderate resolution imaging spectroradiometer data. Remote Sens Environ 115:1220–1233

Dye DG, Tucker CJ (2003) Seasonality and trends of snow-cover, vegetation index, and temperature in northern Eurasia. Geophys Res Lett 30:1–58

Forkel M, Carvalhais N, Rödenbeck C, Keeling R, Heimann M, Thonicke K, Zaehle S, Reichstein M (2016) Enhanced seasonal CO_2 exchange caused by amplified plant productivity in northern ecosystems. Science 351:696–699

Gonsamo A, Chen JM (2016) Circumpolar vegetation dynamics product for global change study. Remote Sens Environ 182:13–26

Gonsamo C (2013) Citizen science: linking the recent rapid advances of plant flowering in Canada with climate variability. Sci Rep 3

Goulden ML, Wofsy SC, Harden JW, Trumbore SE, Crill PM, Gower ST, Fries T, Daube BC, Fan S-M, Sutton DJ, Bazzaz A, Munger JW (1998) Sensitivity of boreal forest carbon balance to soil thaw. Science 279:214–217

Graven HD, Keeling RF, Piper SC, Patra PK, Stephens BB, Wofsy SC, Welp LR, Sweeney C, Tans PP, Kelley JJ, Daube BC, Kort EA, Santoni GW, Bent JD (2013) Enhanced Seasonal Exchange of CO_2 by Northern Ecosystems Since 1960. Science 341:1085–1089

Grippa M, Mognard N, Le Toan T (2005) Comparison between the interannual variability of snow parameters derived from SSM/I and the Ob river discharge. Remote Sens Environ 98:35–44

Guan S-J (2014) Deriving vegetation phenological time and trajectory information over africa using seviri daily LAI. IEEE Trans Geosci Remote Sens 52:1113–1130

Guimberteau M, Zhu D, Maignan F, Huang Y, Chao Y, Dantec-Nédélec S, Ottlé C, Jornet-Puig A, Bastos A, Laurent P (2018) ORCHIDEE-MICT (v8. 4.1), a land surface model for the high latitudes: model description and validation. Geosci Model Develop 11:121

Guyon J-P (2011) Monitoring elevation variations in leaf phenology of deciduous broadleaf forests from SPOT/VEGETATION time-series. Remote Sens Environ 115:615–627

Hakkinen R, Linkosalo T, Hari P (1995) Methods for combination phenological time series: Application to bud burst in birch (Betula pendula) in central Finland for the period 1896–1955. Tree Physiol 15:721–726

Helman D (2018) Land surface phenology: What do we really "see" from space? Sci Total Environ 618:665–673

Hinzman LD, Bettez ND, Bolton WR et al (2005) Evidence and implications of recent climate change in Northern Alaska and other Arctic regions. Clim Change 72:251–298

Holben BN (1986) Characteristics of maximum-value composite images from temporal AVHRR data. Int J Remote Sens 7:1417–1434
IPCC (2013) Climate change 2013: The physical science basis. contribution of working group i to the fifth assessment report of the intergovernmental panel on climate change. Cambridge University Press, Cambridge, United Kingdom and New York, NY, USA
James ME, Kalluri SNV (1994) The pathfinder AVHRR land data set: an improved coarse resolution data set for terrestrial monitoring. Int J Remote Sens 15:3347–3363
Jin H, Eklundh L (2014) A physically based vegetation index for improved monitoring of plant phenology. Remote Sens Environ 152:512–525
Jin H, Jönsson AM, Bolmgren K, Langvall O, Eklundh L (2017) Disentangling remotely-sensed plant phenology and snow seasonality at northern Europe using MODIS and the plant phenology index. Remote Sens Environ 198:203–212
Justice BO, Holben BN, Gwynne MD (1986) Monitoring east african vegetation using AVHRR data. Int J Remote Sens 7:1453–1474
Justice CO, Townshend JRG, Holben AN, Tucker CJ (1985) Analysis of the phenology of global vegetation using meteorological satellite data. Int J Remote Sens 6:1271–1318
Keeling CD, Chin JFS, Whorf TP (1996) Increased activity of northern vegetation inferred from atmospheric CO_2 measurements. Nature 382:146–149
Keenan AD (2015) The timing of autumn senescence is affected by the timing of spring phenology: Implications for predictive models. Glob Change Biol 21:2634–2641
Kiers ET, Palmer TM, Ives AR, Bruno JF, Bronstein JL (2010) Mutualisms in a changing world: an evolutionary perspective. Ecol Lett 13:1459–1474
Krinner G, Viovy N, de Noblet-Ducoudré N, Ogée J, Polcher J, Friedlingstein P, Ciais P, Sitch S, Prentice IC (2005) A dynamic global vegetation model for studies of the coupled atmosphere-biosphere system. Global Biogeochem Cycles 19:1–33
Le Quéré C, Peters GP, Andres RJ et al (2014) Global carbon budget 2013. Earth Syst Sci Data 6:235–263
Liang L, Schwartz MD, Fei S (2011) Validating satellite phenology through intensive ground observation and landscape scaling in a mixed seasonal forest. Remote Sens Environ 115:143–157
Liu Q, Fu YH, Zhu Z, Liu Y, Liu Z, Huang M, Janssens IA, Piao S (2016) Delayed autumn phenology in the Northern Hemisphere is related to change in both climate and spring phenology. Glob Change Biol 22:3702–3711
Menzel A (2000) Trends in phenological phases in Europe between 1951 and 1996. Int J Biometeorol 44:76–81
Meroni M, Verstraete MM, Rembold F, Urbano F, Kayitakire F (2014) A phenology-based method to derive biomass production anomalies for food security monitoring in the Horn of Africa. Int J Remote Sens 35:2472–2492
Misra G, Buras A, Menzel A (2016) Effects of different methods on the comparison between land surface and ground phenology—a methodological case study from South-Western Germany. Remote Sen 8
Morin X, Viner D, Chuine I (2008) Tree species range shifts at a continental scale: new predictive insights from a process-based model. J Ecol 96:784–794
Morisette JT, Richardson AD, Knapp AK, Fisher JI, Graham EA, Abatzoglou J, Wilson BE, Breshears DD, Henebry GM, Hanes JM, Liang L (2009) Tracking the rhythm of the seasons in the face of global change: Phenological research in the 21st century. Front Ecol Environ 7:253–260
Moulin S, Kergoat L, Viovy N, Dedieu G (1997) Global-scale assessment of vegetation phenology using NOAA/AVHRR satellite measurements. J Clim 10:1154–1170
Myneni RB, Keeling CD, Tucker CJ, Asrar G, Nemani RR (1997) Increased plant growth in the northern high latitudes from 1981 to 1991. Nature 386:698–702
Myneni RB, Tucker CJ, Asrar G, Keeling CD (1998) Interannual variations in satellite-sensed vegetation index data from 1981-1991. J Geophys Res D: Atmos 103:6145–6160

Ottlé C, Lescure J, Maignan F, Poulter B, Wang T, Delbart N (2013) Use of various remote sensing land cover products for plant functional type mapping over Siberia. Earth Syst Sci Data 5:331–348

Park T, Ganguly S, Tømmervik H, Euskirchen ES, Høgda K-A, Karlsen SR, Brovkin V, Nemani RR, Myneni RB (2016) Changes in growing season duration and productivity of northern vegetation inferred from long-term remote sensing data. Environ Res Lett 11:084001

Parmentier FJW, Van Der Molen MK, Van Huissteden J, Karsanaev SA, Kononov AV, Suzdalov DA, Maximov TC, Dolman AJ (2011) Longer growing seasons do not increase net carbon uptake in the northeastern Siberian tundra. J Geophys Res: Biogeosci 116

Parmesan C, Yohe G (2003) A globally coherent fingerprint of climate change impacts across natural systems. Nature 421:37–42

Peel MC, Finlayson BL, McMahon TA (2007) Updated world map of the Köppen-Geiger climate classification. Hydrol Earth Syst Sci 11:1633–1644

Pennec A, Gond V, Sabatier D (2011) Tropical forest phenology in French Guiana from MODIS time series. Remote Sens Lett 2:337–345

Pereira HM, Ferrier S, Walters M et al (2013) Essential biodiversity variables. Science 339:277–278

Picard G, Quegan S, Delbart N, Lomas MR, Le Toan T, Woodward FI (2005) Bud-burst modelling in Siberia and its impact on quantifying the carbon budget. Glob Change Biol 11:2164–2176

Post E, Forchhammer MC (2008) Climate change reduces reproductive success of an Arctic herbivore through trophic mismatch. Philos Trans R Soc Lond B: Biol Sci 363:2367–2373

Post E, Forchhammer MC, Bret-Harte MS, Callaghan TV, Christensen TR, Elberling B, Fox AD, Gilg O, Hik DS, Høye TT (2009) Ecological dynamics across the Arctic associated with recent climate change. Science 325:1355–1358

Post E, Pedersen C, Wilmers CC, Forchhammer MC (2008) Warming, plant phenology and the spatial dimension of trophic mismatch for large herbivores. Proc R Soc Lond B: Biol Sci 275:2005–2013

Pouliot I (2011) Evaluation of compositing period and AVHRR and MERIS combination for improvement of spring phenology detection in deciduous forests. Remote Sens Environ 115:158–166

Rea J, Ashley M (1976) Phenological evaluations using Landsat—1 sensors. Int J Biometeorol 20:240–248

Richardson AD, Black TA, Ciais P et al (2010) Influence of spring and autumn phenological transitions on forest ecosystem productivity. Philos Trans R Soc B: Biol Sci 365:3227–3246

Richardson M (2013) Climate change, phenology, and phenological control of vegetation feedbacks to the climate system. Agric For Meteorol 169:156–173

Root TL, Price JT, Hall KR, Schneider SH, Rosenzweig C, Pounds JA (2003) Fingerprints of global warming on wild animals and plants. Nature 421:57–60

Sato H, Itoh A, Kohyama T (2007) SEIB-DGVM: a new Dynamic Global Vegetation Model using a spatially explicit individual-based approach. Ecol Model 200:279–307

Sato H, Kobayashi H, Delbart N (2010) Simulation study of the vegetation structure and function in eastern Siberian larch forests using the individual-based vegetation model SEIB-DGVM. For Ecol Manage 259:301–311

Schwartz MD (1998) Green-wave phenology [4]. Nature 394:839–840

Schwartz MD, Ahas R, Aasa A (2006) Onset of spring starting earlier across the Northern Hemisphere. Glob Change Biol 12:343–351

Schwartz MD, Reed BC, White MA (2002) Assesing satellite-derived start-of-season measures in the conterminous USA. Int J Climatol 22:1793–1805

Shabanov NV, Zhou L, Knyazikhin Y, Myneni RB, Tucker CJ (2002) Analysis of interannual changes in northern vegetation activity observed in AVHRR data from 1981 to 1994. IEEE Trans Geosci Remote Sens 40:115–130

Solomon S (2007) Climate change 2007-the physical science basis: working group I contribution to the fourth assessment report of the IPCC. Cambridge University Press
Soudani S (2008) Evaluation of the onset of green-up in temperate deciduous broadleaf forests derived from Moderate Resolution Imaging Spectroradiometer (MODIS) data. Remote Sens Environ 112:2643–2655
Suzuki R, Kobayashi H, Delbart N, Asanuma J, Hiyama T (2011) NDVI responses to the forest canopy and floor from spring to summer observed by airborne spectrometer in eastern Siberia. Remote Sens Environ 115:3615–3624
Suzuki R, Nomaki T, Yasunari T (2003) West-east contrast of phenology and climate in northern Asia revealed using a remotely sensed vegetation index. Int J Biometeorol 47:126–138
Thompson BG (2015) Using phase-spaces to characterize land surface phenology in a seasonally snow-covered landscape. Remote Sens Environ 166:178–190
Thompson JA, Paull DJ (2017) Assessing spatial and temporal patterns in land surface phenology for the Australian Alps (2000–2014). Remote Sens Environ 199:1–13
Townshend JRG, Justice CO (1986) Analysis of the dynamics of african vegetation using the normalized difference vegetation index. Int J Remote Sens 7:1435–1445
Vicente-Serrano SM, Delbart N, Le Toan T, Grippa M (2006) El Niño-Southern Oscillation influences on the interannual variability of leaf appearance dates in central Siberia. Geophys Res Lett 33
Vinogradov BV (1977) Remote sensing in ecological botany. Remote Sens Environ 6:83–94
Vors LS, Boyce MS (2009) Global declines of caribou and reindeer. Glob Change Biol 15:2626–2633
Walther G-R (2010) Community and ecosystem responses to recent climate change. Philos Trans R Soc B: Biol Sci 365:2019–2024
Walther G-R, Post E, Convey P, Menzel A, Parmesan C, Beebee TJC, Fromentin J-M, Hoegh-Guldberg O, Bairlein F (2002) Ecological responses to recent climate change. Nature 416:389–395
Walther S, Voigt M, Thum T, Gonsamo A, Zhang Y, Köhler P, Jung M, Varlagin A, Guanter L (2016) Satellite chlorophyll fluorescence measurements reveal large-scale decoupling of photosynthesis and greenness dynamics in boreal evergreen forests. Glob Change Biol 22:2979–2996
White MA, de Beurs KM, Didan K et al (2009) Intercomparison, interpretation, and assessment of spring phenology in North America estimated from remote sensing for 1982–2006. Glob Change Biol 15:2335–2359
White MA, Hoffman F, Hargrove WW, Nemani RR (2005) A global framework for monitoring phenological responses to climate change. Geophys Res Lett 32:1–4
White MA, Nemani RR (2003) Canopy duration has little influence on annual carbon storage in the deciduous broad leaf forest. Glob Change Biol 9:967–972
Woodward FI, Smith TM, Emanuel WR (1995) A global land primary productivity and phytogeography model. Global Biogeochem Cycles 9:471–490
Zeng BC (2013) Shifts in Arctic phenology in response to climate and anthropogenic factors as detected from multiple satellite time series. Environ Res Lett 8
Zhang X, Friedl MA, Schaaf CB, Strahler AH, Hodges JCF, Gao F, Reed BC, Huete A (2003) Monitoring vegetation phenology using MODIS. Remote Sens Environ 84:471–475
Zhou G (2016) Explaining inter-annual variability of gross primary productivity from plant phenology and physiology. Agric For Meteorol 226–227:246–256

Nicolas Delbart Nicolas Delbart is a professor in the geography department at Université de Paris, and is affiliated to the Paris Interdisciplinary Energy Research Institute. He was until recently involved at the PRODIG research unit, and previously at the Centre d'Etudes Spatiales de la Biosphère (CESBIO, (Toulouse, France), the Laboratoire des Sciences du Climat et de l'Environnement (LSCE, Gif-sur-Yvette, France) and at the Frontier Research Center for Global Change (FRCGC, Yokohama, Japan). He is responsible for the master degree Remote Sensing and Geomatics Applied to Environmental Studies (in French, "Télédétection et Géomatique Appliquées à l'Environnement") and teaches remote sensing in the bachelor and master geography cursus. His research focuses on the remote sensing of vegetation seasonal variations. In addition to his phenological studies in the northern ecosystems, his research addresses the phenology of crops in mixed pixels in France and the monitoring of forest density via the seasonal variations in the remote sensing signal, in particular in Nepal. His research has also involved the use and validation of several dynamic vegetation models, and has extended to the remote sensing of water resources seasonal variations in semi-arid environments.

Diagnosing Environmental Controls on Vegetation Greening and Browning Trends Over Alaska and Northwest Canada Using Complementary Satellite Observations

20

Youngwook Kim, John S. Kimball, Nicholas Parazoo, and Peter Kirchner

Abstract

Tundra and boreal forest regions have undergone extreme environmental changes in recent decades. Many studies have documented these changes and associated ecosystem impacts using a variety of methods including field measurements, remote sensing and biophysical modeling. Combined observations from satellite optical-infrared and microwave remote sensing have also been used for regional assessment and monitoring of environmental change, ecosystem processes and biogeochemical cycles in the Arctic. Remote sensing derived vegetation parameters range from relatively direct observations of vegetation greenness and chlorophyll fluorescence to higher-level vegetation productivity estimates. However, satellite remote sensing of land surface conditions is particularly challenging at high latitudes due to seasonal variations in solar illumination, snow cover, persistent cloud cover and atmospheric aerosol contamination. Here, we used satellite-derived observations of vegetation

A Chapter in Arctic hydrology, permafrost, and ecosystem: linkages and interactions.

Y. Kim (✉)
Biology Department, United Arab Emirates University, Al Ain, UAE
e-mail: youngwook.kim@uaeu.ac.ae

J. S. Kimball
NTSG, University of Montana, Missoula, MT, USA
e-mail: johnk@ntsg.umt.edu

N. Parazoo
Jet Propulsion Laboratory, Carbon Cycle and Ecosystems, Sierra Madre, CA, USA
e-mail: nicholas.c.parazoo@jpl.nasa.gov

P. Kirchner
National Park Service, Southwest Alaska Network, Anchorage, AK, USA
e-mail: peter_kirchner@nps.gov

D. Yang and D. L. Kane (eds.), *Arctic Hydrology, Permafrost and Ecosystems*,
https://doi.org/10.1007/978-3-030-50930-9_20

greenness (EVI), sun-induced chlorophyll fluorescence (SIF) and gross primary productivity (GPP) to clarify regional patterns and recent variations in vegetation growth over the Arctic Boreal Vulnerability Experiment (ABoVE) domain. The annual non-frozen (NF) period and volumetric soil moisture (VSM) retrieved from satellite microwave remote sensing were used as proxies for growing season length and water supply controls to investigate the impacts of climate on vegetation growth. Positive trends in regional productivity generally coincide with a longer NF season. However, the benefit of a longer NF season to vegetation growth is reduced in soil moisture constrained regions, which have become more widespread in the recent decade over almost half (48.9%) of the domain. Our results document the influence of a changing environment on regional vegetation growth and the northern terrestrial carbon sink for atmospheric CO_2.

20.1 Introduction

The potential growing season in boreal forest and tundra ecosystems at high northern latitudes (HNL) is strongly limited by the annual non-frozen period (Kim et al. 2012; Vickers et al. 2016; Xu et al. 2013) and snow-free season length (Malnes et al. 2016). The non-frozen period bounds the number of days each year when land surface temperatures are above freezing and solar energy and liquid water are more readily available to support hydrological and ecological processes, including vegetation growth and evapotranspiration (Kim et al. 2012; Zhang et al. 2011). The timing and magnitude of seasonal snowmelt closely follows the spring freeze/thaw transition and influences the availability of soil moisture for annual productivity (Barnett et al. 2005; Parazoo et al. 2018; Yi et al. 2015). The non-frozen period generally represents less than half (47.7%) of the HNL annual cycle due to a lengthy cold season in which ecological processes are largely dormant. However, the HNL domain is currently warming at roughly twice the global rate due to the Arctic amplification of global warming (Cowtan and Way 2014; Screen 2017). Recent HNL impacts from climate warming include earlier spring thawing and a longer non-frozen period (Parazoo et al. 2018; Verbyla 2015). However, the impacts of warmer temperatures and a longer non-frozen season on vegetation growth are uncertain due to concomitant changes in fire disturbance and drought restrictions on ecosystem productivity (Hoy et al. 2016; Sulla-Menashe et al. 2018; Walker and Johnstone 2014).

Ecosystem gross primary productivity (GPP) can be defined as the accumulation of atmospheric carbon dioxide (CO_2) in vegetation by photosynthesis. Spatial and temporal variability in terrestrial GPP over the HNL domain is closely linked to spring thaw timing and the duration of the non-frozen period (Emmerton et al. 2016; Beck and Goetz 2011; Gamon et al. 2013). Thus, increased boreal-Arctic GPP from earlier vegetation growth may provide a major carbon sink offsetting radiative forcing and climate warming potential from fossil fuel burning and anthropogenic CO_2

emissions (Kasischke et al. 2010a). Regional trends toward a longer non-frozen period, that starts earlier, are congruent with recent warming trends and provide a physical explanation for vegetation greening and increases in annual integrated GPP through a longer growing season with temperatures conducive to photosynthesis (Hellmann et al. 2016; Kolk et al. 2016). In contrast, other studies have reported vegetation browning trends and reduced productivity due to increased summer drought stress under warmer temperatures and an extended non-frozen period (Buermann et al. 2013; Bjorkman et al. 2017; Girardin et al. 2016; McGuire et al. 2010). The HNL vegetation growth reduction due to the increasing frequency and intensity of wildfire has also been documented, while the longer-term effects of these changes on forest succession and productivity are more uncertain (Kasischke et al. 2010a; Loranty et al. 2016; Rogers et al. 2015). A longer non-frozen season is contributing to carbon emissions from permafrost thawing as factors offsetting potential carbon gains from enhanced vegetation growth (Loranty et al. 2016).

Better understanding of vegetation productivity trends and their underlying drivers has been impeded by the remote, regionally extensive and varied geography of the HNL domain, as well as the extreme regional weather conditions and sparse environmental monitoring network. In addition to having sparse in situ observations, the region also has limitations with satellite remote sensing due to a lengthy season of polar darkness, frequent cloud cover, smoke and other atmospheric aerosols that can degrade land surface remote sensing, particularly in the visible and infrared wavelengths. However, some of these limitations are offset by the global coverage, frequent sampling and extended continuity of some polar-orbiting satellite records. Some examples of successful HNL satellite remote sensing research include: assessments of Arctic browning trends (Baird et al. 2012; Phoenix and Bjerke 2016), diverse HNL vegetation growth trends (Kim et al. 2014; Miles and Esau 2016) and regional variation in vegetation productivity in response to warming (Bastos et al. 2017; Pearson et al. 2013; Rogers et al. 2018). The availability of complimentary data records from overlapping satellites also allows for enhanced regional assessments involving multiple environmental parameters that can better distinguish vegetation conditions and environmental controls (Beck and Goetz 2011; Jia et al. 2009; Kim et al. 2014; Walther et al. 2018).

Complimentary satellite observations that have been widely used for ecosystem productivity assessments include vegetation indices (VIs) that exploit differences in red and near-infrared spectral wavelengths sensitive to changes in vegetation greenness. The Enhanced Vegetation Index (EVI) has been used to assess regional HNL growth patterns and has relatively robust vegetation sensitivity at higher forest biomass levels, and with reduced sensitivity to snow and atmosphere aerosol contamination relative to other optical-infrared VIs (Huete et al. 2002; Shabanov et al. 2015, Shi et al. 2017). The MODerate resolution Imaging Spectroradiometer (MODIS) sensors on the NASA EOS Terra and Aqua satellites provide a well-calibrated and validated global operational EVI record spanning almost two decades, and with relatively fine (250 m) spatial resolution and 16-day temporal compositing suitable for distinguishing seasonal canopy changes at the level of individual vegetation community patches. Global satellite observations of

solar-induced chlorophyll fluorescence (SIF) are also available over the HNL domain and provide a close observational surrogate for GPP (Parazoo et al. 2015; Madani et al. 2017); however, coarse ($\geq 0.5°$) spatial gridding and monthly compositing of the SIF data is generally required to provide adequate signal-to-noise. Satellite data-driven models have also been used to acquire landscape-level GPP estimates over the HNL (Madani et al. 2017; Luus et al. 2017). These models combine synergistic satellite observations, including VIs, with other ancillary information in a light use efficiency (LUE) model framework that allows for spatially and temporally continuous GPP estimates despite potential gaps in the satellite record. The model products also provide relatively comprehensive estimates of GPP and underlying environmental controls that are comparable with in situ measurements of these processes (i.e. 500 m–1 km resolution), and with daily to weekly temporal fidelity (Baldocchi 2008).

In this chapter, we examine recent changes and spatiotemporal patterns in vegetation productivity, non-frozen season and surface soil moisture across Alaska and Northern Canada using some of the latest satellite remote sensing data records. The Alaska and Canada study region represents ~22% (~6.4 million km^2) of the HNL Arctic and boreal land area, and encompasses the Arctic Boreal Vulnerability Experiment (ABoVE) extended domain. ABoVE is a NASA-led multi-year field campaign designed to assess the role and complexity of land–atmosphere interactions in HNL ecosystems by combining field observations, modeling and satellite remote sensing (Kasischke et al. 2010b). Here, we evaluate and compare complimentary satellite-based ecosystem productivity data records including GPP, EVI and SIF, over a 10-year study period (2007–2016). We analyze the productivity records along with other satellite environmental data on wildfire disturbance, landscape freeze/thaw (FT) and volumetric soil moisture (VSM) to clarify disturbance-related impacts and non-frozen season, and surface moisture constraints to productivity. Our results document the influence of a changing environment on vegetation growth and the northern terrestrial carbon sink for atmospheric CO_2.

20.2 Study Domain

The HNL Arctic tundra and boreal forests are experiencing rapid environmental changes and disturbances from global warming (Barichivich et al. 2014; Berner et al. 2011). This region encompasses a large percentage (~49.2 million km^2 or 25%) of the global land area (McGuire et al. 2009) and terrestrial carbon storage (Schimel et al. 2015), and thus is likely to contribute significantly to carbon-climate feedbacks. The study area encompasses the ABoVE extended domain (Goetz et al. 2011; Kasischke et al. 2010b), a subset of the HNL region, consisting of tundra (~13%) and boreal forest (~85%) biomes representative of the larger HNL domain, which is a substantial (~9.9 Pg C yr^{-1}) contributor to the global terrestrial carbon sink (Beer et al. 2010). Recent impacts from climate warming, indicated from the satellite record, include earlier and longer non-frozen seasons, a decline in

permafrost extent and stability (Kim et al. 2014; Park et al. 2016a; Liljedahl et al. 2016), tundra greening and woody shrub cover increases contrasting with boreal forest browning and drought-induced productivity declines (Tape et al. 2006; Beck and Goetz 2011), and increased frequency and severity of wildfire disturbance (Morton et al. 2013). While considerable research has focused on the effects of climate and environmental changes in Arctic tundra and boreal forest biomes, significant gaps remain in rectifying the interannual vegetation growth variations from different satellite records, and clarifying the role of changing temperature and moisture constraints, and disturbances influencing these variations. We address these knowledge gaps in the current chapter through a focused regional study in the ABoVE domain using a set of complimentary satellite observational records.

20.3 Data

The ability of satellite remote sensing methods to estimate vegetation productivity has significantly improved in recent years through: extension of existing sensors, recognition of novel vegetation metrics in existing sensors, deployment of new complimentary sensors and ongoing calibration refinements that have improved existing data records and land parameter retrieval algorithms. In this study, selected complimentary global satellite observational data were used to evaluate the pattern of seasonal vegetation growth and climate constraints within the ABoVE study domain. Satellite-based observations representing vegetation growth included EVI, SIF and GPP. The EVI and SIF records were obtained from direct satellite observations, while GPP was derived using satellite data-driven LUE models combining satellite VI-based inputs for land cover type and canopy leaf area with daily surface meteorological inputs from global model re-analysis data. Other satellite remote sensing records used in this study included daily landscape FT status and surface VSM derived from passive microwave sensor retrievals that were used to represent respective non-frozen season and soil moisture-related constraints to vegetation growth. Satellite-derived burned area data records were also used to assess wildfire impacts on vegetation productivity within the domain.

20.3.1 Vegetation Indices

The satellite VI data selected for this study included MODIS normalized difference vegetation index (NDVI) and enhanced vegetation index (EVI) records, which are sensitive to photosynthetic vegetation cover and have been widely used to analyze regional patterns and temporal trends in vegetation greenness, phenology and productivity (Guay et al. 2014; Luus et al. 2017; Yi et al. 2013). We used 16-day, 0.05° resolution MODIS NDVI and EVI records (MOD13C1 VI version 6) extending over the 2007–2016 study period. The MODIS products provide robust atmospheric correction and cloud screening criteria, which benefit product accuracy

and performance relative to other available satellite global VI records (Didan et al. 2015). MODIS NDVI was used to estimate the fraction of canopy-absorbed photosynthetically active radiation (FPAR) inputs required for the LUE model-based GPP calculations described in Sect. 20.3.3, where a HNL biome-specific NDVI to FPAR conversion was used following previous studies (Yi et al. 2013). The EVI was used as a more direct observational proxy of vegetation greenness and productivity over the domain (Gamon et al. 2013; John et al. 2016; Potter 2014). The NDVI and EVI are both sensitive to photosynthetic canopy cover by exploiting reflectance differences between red and near-infrared spectral bands, while the EVI incorporates additional spectral information in the blue reflectance channel (Huete et al. 2002; Kim et al. 2010). The EVI also provides a relatively robust measure of vegetation conditions over a greater range of canopy biomass cover and is less sensitive to potential noise from variations in sun-sensor geometry, understory effects, and atmosphere aerosol contamination (Huete et al. 2002; Shabanov et al. 2015; Shi et al. 2017). However, several studies have reported VI contamination from snow cover, surface wetness and atmosphere effects at high latitudes, which can degrade the vegetation signal (de Beurs and Henebry 2010; Karkauskaite et al. 2017; Luus et al. 2017). To reduce potential contamination effects, we used only best-quality NDVI and EVI pixels identified from the MODIS VI quality assurance field (Didan et al. 2015; Shi et al. 2017; Vermote et al. 2002).

20.3.2 Sun-Induced Chlorophyll Fluorescence

Sunlight absorbed by chlorophyll in vegetation is mainly used for photosynthesis, but some radiation can also be dissipated as heat or reradiated at a longer wavelength (650–850 nm), through chlorophyll fluorescence (Baker 2008; Flexas et al. 2002; Meroni et al. 2009). Satellites can detect sun-induced chlorophyll fluorescence (SIF) from spatially aggregated photosynthesis occurring within the sensor footprint at the time of the satellite overpass. The SIF retrieval provides a close proxy for photosynthesis, APAR and LUE (Guanter et al. 2014; Yang et al. 2015), while the satellite-derived SIF retrievals are directly proportional to GPP (Parazoo et al. 2015; Madani et al. 2017) and vegetation photosynthetic activity (Luus et al. 2017). Although SIF energy represents only small portion ($\sim$1–4%) of canopy-absorbed PAR, aggregating to coarser spatial (e.g. 0.5°) and temporal (monthly) scales can substantially improve the signal-to-noise (Joiner et al. 2014). For this study, we used the longest existing global record of satellite SIF (in radiance units), derived from the GOME-2 (Global Ozone Mapping Experiment 2) instrument onboard the Eumetsat MetOp-A platform launched in October 2006 (Joiner et al. 2013). The GOME-2 sensor measures solar irradiance in the 240–790 nm spectral range with 0.2–0.5 nm resolution, and a nominal spatial footprint of 40 $\times$ 80 km^2 at 9:30 a.m. local sampling time (Yang et al. 2015). The SIF retrievals are based on the inversion of top-of-atmosphere measurements in the near-infrared (715–758 nm) spectral window overlapping the second peak of the SIF emission distribution. We used the bias-corrected level 3 monthly half-degree

retrievals from the GOME-2 version 27 SIF record extending from 2007 to 2016. Previous studies have used the GOME-2 monthly SIF record for analyzing global vegetation phenology and productivity patterns, and underlying environmental controls with favorable results (Joiner et al. 2014; Madani et al. 2017), including the North American boreal-Arctic domain (Commane et al. 2017; Luus et al. 2017; Parazoo et al. 2018).

20.3.3 Gross Primary Production

GPP represents the rate at which atmospheric CO_2 is sequestered by canopy net photosynthesis. We used a satellite data-driven modeling approach to derive GPP over the study domain. To first order, GPP varies as a function of plant functional type, plant structure including canopy cover and environmental conditions including solar radiation, temperature and available moisture. GPP was estimated using a LUE model, where the term LUE defines the rate at which canopy-absorbed photosynthetically active solar radiation (APAR) is converted to vegetation biomass carbon during photosynthesis. The LUE model and GPP record used in this study were previously developed to evaluate GPP dynamics over HNL boreal and Arctic biomes (Zhang et al. 2008; Yi et al. 2013; Dass et al. 2016). This model is similar to the model used by NASA to produce the MODIS MOD17 global operational GPP product (Zhao et al. 2011), but includes several regional refinements, including different meteorological and canopy inputs, and calibration refinements to better represent Arctic and boreal ecosystems. Here, LUE is reduced from potential (LUE_{max}) rates prescribed for different land cover types under suboptimal environmental conditions determined as the product of daily environmental constraints defined from surface meteorological inputs (Dee et al. 2011). The daily meteorological inputs to the model are derived from the ERA-Interim global re-analysis at 0.25° (~25 km) spatial resolution (Dee et al. 2011), while the land cover inputs are derived from the MODIS MCD12Q1 IGBP land cover product (Friedl et al. 2002). Daily surface meteorological inputs to the model include incident solar radiation (SW_{rad} [MJ m^{-2}]), minimum and average daily air temperature (T_{min} and T_{avg} [° C]), and atmospheric vapor pressure deficit (VPD [Pa]). GPP is derived on a daily basis as (Zhang et al. 2008):

$$\mathrm{GPP} = \varepsilon \times 0.45 \times SW_{\mathrm{rad}} \times \mathrm{FPAR}. \tag{20.1}$$

$$\varepsilon = \varepsilon_{\max} \times T_f \times VPD_f \tag{20.2}$$

where ε is a LUE parameter (g C MJ^{-1}) for the conversion of photosynthetically active radiation (PAR, MJ m^{-2}) to GPP (g C m^{-2}); ε_{max} is the maximum LUE obtained from a biome-properties look-up table (BPLUT) developed from previous HNL studies (Dass et al. 2016; Yi et al. 2013). FPAR is estimated from the NDVI using biome-specific empirical relationships emphasizing northern ecosystems (Yi et al. 2013). T_f and VPD_f are air temperature and vapor pressure deficit reduction

scalars for the biome-specific ε_{max} values. T_f and VPD_f are defined using linear ramp functions calibrated for boreal and Arctic ecosystems (Yi et al. 2013). The 16-day MODIS NDVI records were temporally interpolated to a daily time step to estimate daily FPAR following the previously established methods (Dass et al. 2016; Mu et al. 2007; Yi et al. 2013). The resulting daily GPP record was then aggregated to a monthly time step for this study. The model simulations were derived at 25-km spatial resolution consistent with the ERA-Interim re-analysis inputs and similar in scale to the satellite passive microwave remote sensing-based VSM and FT retrievals used as proxies for non-frozen season and soil moisture-related controls on regional productivity. The model simulations extended over all vegetated land areas within the HNL (>45 °N) polar EASE-grid domain (Brodzik and Knowles 2002). The model simulations were conducted by assuming homogeneous vegetation and climate conditions within each 25 km resolution grid cell. Land cover and vegetation conditions were obtained from spatially averaged MODIS 250 m FPAR inputs and the dominant vegetation class within each grid cell defined from the ancillary 1 km IGBP land cover map. For this study, the model GPP simulations extended over a 10-year record (2007–2016).

Another satellite-based GPP record was used for comparison purposes and was obtained from the soil moisture active passive (SMAP) mission level 4 carbon (L4C V3) product (Kimball et al. 2017), which represents the latest generation of NASA global operational GPP data products. The L4C product combines MODIS land cover and FPAR information with SMAP and data assimilation enhanced surface to root zone soil moisture (RZSM) inputs to estimate net ecosystem CO_2 exchange and component carbon fluxes, including GPP, on a daily basis. The L4C product uses a similar LUE modeling approach to estimate GPP, except that the model includes additional environmental constraints for frozen conditions and low soil moisture (Jones et al. 2017; Kimball et al. 2016). Here, RZSM is used with VPD to represent both soil water supply and atmospheric moisture demand controls on GPP, whereas in the baseline GPP record described above (Eqs. 20.1 and 20.2), VPD represents the sole moisture constraint to productivity. The BPLUT used to define the SMAP L4C model response characteristics is calibrated for different plant functional types from a global network of in situ tower eddy covariance CO_2 flux measurement records, including HNL boreal forest and Arctic tundra sites. The L4C GPP product provides favorable accuracy and performance over global, HNL and ABoVE domains relative to a diverse set of independent observations, including other satellite-based productivity (SIF, GPP) records, atmospheric carbon model inversions and tower CO_2 flux measurements (Jones et al. 2017). The daily inputs to the L4C LUE algorithm include MODIS 8-day, 500 m FPAR (v0006); SMAP daily, 9 km level 4 RZSM (L4SM, Reichle et al. 2018) inputs; and GMAO 0.25° daily surface meteorology inputs. The L4C GPP simulations are derived at 1 km resolution similar to the MODIS vegetation inputs, while the model outputs are spatially aggregated and posted to a 9 km global EASE-grid 2.0 projection (Brodzik et al. 2014) consistent with the RZSM inputs and other SMAP L4 products. The L4C (V3) data available at the time of this study extended over the initial SMAP operational record from March 2015 to December 2017.

20.3.4 Freeze/Thaw and Non-frozen Period

We used a consistent global record of daily landscape freeze/thaw (FT) dynamics derived from satellite passive microwave remote sensing retrievals to define spatial and temporal variations in the annual non-frozen season over the HNL domain (Kim et al. 2017a). The FT Earth System Data Record (FT-ESDR V4) used for this study was derived from calibrated 37 GHz, vertically polarized microwave brightness temperature (Tb) retrievals from Defense Meteorological Satellite Program SSM/I(S) (Special Sensor Microwave Imager (sounder)) sensor records (Kim et al. 2017b). The FT-ESDR is derived using a temporal change classification of daily Tb retrievals that are strongly sensitive to the large changes in landscape dielectric properties that occur during FT transitions, and insensitive to atmosphere contamination and solar illumination effects (Derksen et al. 2017; Kim et al. 2017a). The FT retrievals are processed separately for satellite ascending and descending orbits, enabling twice-daily sampling of FT conditions from morning (a.m.) and afternoon (p.m.) overpasses. The FT-ESDR is composited into a daily record that defines four discrete FT classification levels, including frozen (a.m. and p.m.), non-frozen (a.m. and p.m.), transitional (a.m. frozen, p.m. non-frozen) and inverse-transitional (a.m. non-frozen, p.m. frozen) categories. For this study, FT-ESDR daily non-frozen conditions were summed from January 1 to August 31 (NF_{JaAu}) for each calendar year and grid cell to define the non-frozen season influencing summer vegetation growth over the 2007–2016 study period.

The landscape FT signal defined from the satellite record represents the predominant frozen (FR) or non-frozen (NF) status of the landscape within the sensor footprint and doesn't distinguish soil, snow or vegetation elements within a grid cell. The Tb retrieval at 37 GHz frequency is also more directly sensitive to FT conditions at the land surface rather than deeper soil, snow and vegetation layers (Kim et al. 2011, 2012) and has been closely linked to cold temperature constraints affecting HNL vegetation phenology and productivity, landscape water mobility and land–atmosphere carbon exchange (Zhang et al. 2011; Kim et al. 2014; Park et al. 2016b).

20.3.5 Volumetric Soil Moisture

We selected volumetric soil moisture (VSM) retrievals from a global satellite passive microwave remote sensing-based land parameter data record to represent growing season soil moisture variations influencing ecosystem productivity over the HNL domain. The VSM retrievals were derived under classified non-frozen conditions from similar calibrated Tb records from AMSR-E (Advanced Microwave Scanning Radiometer for EOS) and AMSR2 (AMSR follow-on instrument onboard the JAXA GCOM-W1 satellite) (Du et al. 2017a). The AMSR VSM data records have global coverage and 1–3-day temporal resolution as derived from p.m. orbit Tb observations, while an iterative retrieval algorithm is used with multiple Tb frequencies and polarizations to account for potential negative impacts on the soil

moisture retrievals from atmospheric precipitable water vapor, open water inundation, vegetation biomass cover and surface temperature variations (Du et al. 2017a; Jones et al. 2010). The VSM algorithm minimizes the influence of standing water on the soil moisture retrievals, which is particularly important in HNL landscapes that are frequently inundated. The resulting AMSR 10.7 GHz VSM retrievals are primarily sensitive to moisture conditions within the surface ($\sim$ 0–2 cm depth) soil layer under low to moderate vegetation biomass cover characteristic of grassland and shrubland vegetation, while also showing favorable accuracy in HNL boreal-Arctic ecosystems (Kimball et al. 2009, Du et al. 2016). The AMSR VSM data records were previously used for evaluating soil moisture-related impacts on vegetation productivity (Kimball et al. 2009; Geruo et al. 2017; Yi et al. 2014), while the latest (version 2) AMSR global VSM product was used for the current study (Du et al. 2017b). The AMSR VSM record used extends from 2007 to 2016, but includes a 10-month gap between the end of AMSR-E operations in September 2011 and the beginning of the AMSR-2 record in May 2012 (Du et al. 2014).

20.3.6 Wildfire Disturbance

The global fire emissions database version 4 (GFED4) product is derived from an ensemble of satellite observations and was used to define monthly mean burned area dynamics over the 2007–2016 record and ABoVE study domain. The GFED4 monthly burned area data is derived from the 500 m MODIS direct broadcast burned area product (MCD64A1) aggregated to 0.25° spatial resolution (Giglio et al. 2013). The GFED4 monthly burned area record was used as a proxy for regional wildfire disturbance extent and recovery status potentially affecting vegetation greening and productivity within the domain. However, the burned area metric may be a poor indicator of wildfire severity, which strongly impacts post-fire recovery and vegetation succession in the boreal-Arctic (Chu and Guo 2014; Kasischke et al. 2010a; Rogers et al. 2015).

20.3.7 Data Processing

We computed monthly values of all data records used in this study over a consistent 10-year record (2007–2016) corresponding to the GOME-2 SIF data period. The satellite VI signal is more susceptible to degradation from artifacts, including snow cover and cloud effects independent of canopy changes during the shoulder seasons (Delbart et al. 2006; Jeganathan et al. 2014; Wang et al. 2017), while the satellite microwave VSM retrievals are also influenced by snow cover effects during the spring and autumn FT transition periods (Du et al. 2017a). To reduce these effects, we only used summer mean values of the remote sensing metrics as growing season environmental indicators. The summer values of GPP, EVI and SIF for each grid-cell within the study domain were calculated by averaging the June, July and

August (JJA) values for each year of record. The non-frozen period from January to August for each year of record was defined from the FT-ESDR daily time series (Kim et al. 2012, 2014) and compared with the vegetation productivity metrics (GPP_{JJA}, SFI_{JJA} and EVI_{JJA}). The AMSR VSM_{JJA} record was used to assess the relationship between vegetation growth and regional soil moisture variations. The GFED burned area record was used to define annual wildfire disturbance extent over the study period. The study domain includes all vegetated land areas within the ABoVE extended domain; excluding grid cells with >20% open water fraction, permanent wetland, snow/ice, urban and barren areas as defined from the static land cover map. This screening process was used to emphasize the vegetation signal and minimize surface water contamination effects on the microwave FT and VSM records over land. Here, land cover type was determined from the 1 km MODIS IGBP global land cover product (MOD12Q1; Friedl et al. 2002). An ancillary map of principal climate zones (SNAP 2012) was used to define the extent of Arctic tundra and boreal forest biomes within the domain. All geospatial data used in this investigation were re-projected from their native formats to a consistent 25 km resolution polar EASE-grid projection using nearest-neighbor re-sampling of coarser resolution grid cells or drop-in-bucket averaging of finer resolution pixels.

20.3.8 Terrain Data

A 30 m resolution elevation map derived from the Advanced Spaceborne Thermal Emission and Reflection Radiometer (ASTER) global digital elevation model version 2 product (GDEM V2; Tachikawa et al. 2011) was used to characterize terrain heterogeneity within each 25 km EASE-grid cell. The ENVI topographic modeling module was also applied to create an aspect (degree) map from the 25 km EASE-grid ASTER GDEM data. The resulting elevation and aspect information was used as a relative indicator of terrain conditions influencing regional vegetation and climate. Aspect intensity (the sine of the slope multiplied by cosine of the DEM aspect) was used as a proxy of seasonality in the incoming solar radiation (Piedallu and Gégout 2008).

20.3.9 Data Analysis

To investigate interannual variations in the satellite environmental metrics, we computed temporal anomalies relative to the trend line defined from each satellite record where a significant trend ($p < 0.05$) was indicated; the trend lines and anomalies were derived over a 10-year (2007–2016) study period for all metrics except VSM, where the 2012 portion of record was excluded due to the gap between AMSR-E and AMSR2 operations. Where no significant trend was indicated, the normalized anomalies were derived as the difference between the observation and temporal mean divided by the standard deviation. The interannual

anomalies were computed for aggregated regions representing tundra and boreal forest biomes within the ABoVE domain as defined from the land cover map.

The correlation coefficient (r-value) from multiple regression was used to assess the sign and strength of the relationships between the individual productivity metrics (GPP_{JJA}, SIF_{JJA}, EVI_{JJA}) and the environmental parameters (NF_{JaAu} and VSM_{JJA}). For computing the grid-cell-wise multi-variate correlation coefficients, temporal anomalies of the parameter series were initially computed as annual differences from 9-year average conditions (excluding 2012 due to unavailability of the AMSR VSM record); where a significant trend was identified (p-value < 0.05), the temporal anomalies were determined as differences from the detrended mean (Barichivich et al. 2014; Kim et al. 2014).

20.4 Results

The spatial distribution of summer values derived from the different remote sensing records are shown for selected year 2016 (Fig. 20.1). These results show characteristically lower vegetation growth in the tundra biome, relative to boreal forest. The two GPP_{JJA} data products show similar spatial patterns, with a more productive bias in SMAP L4C at higher latitudes, which may be due to the shorter data record. The EVI_{JJA} and SIF_{JJA} records are more similar in regional patterns of vegetation growth than the GPP_{JJA} records, with the exception that both EVI and SMAP L4 GPP_{JJA} records show similar positive productivity bias in northern tundra. The FT record shows a strong latitudinal gradient that captures the characteristic NF_{JaAu} decline at higher latitudes.

The mean summer environmental conditions defined from the recent satellite record for the ABoVE domain and the two major regional biomes are summarized in Table 20.1. All records extend from 2007 to 2016 with the exception of the L4C GPP_{JJA} metric, which is summarized for 2015–2016 because the SMAP operational record only extends from mid-2015 to present. The GPP_{JJA} results show a mean value of 123.8 ± 4.2 gC/m^2 over the entire domain, while the estimated total mean annual GPP was 2.79 Pg C/yr. The mean GPP_{JJA} was also higher for boreal forest (135.4 ± 4.6 gC/m^2) than tundra (90.5 ± 4.6 gC/m^2) portions of the domain. The resulting GPP magnitudes are consistent with previous reports from regional tower eddy covariance CO_2 flux measurements, carbon modeling and satellite-based GPP observations (Ueyama et al. 2013; Yi et al. 2013; Zhang et al. 2017). The GPP_{JJA} results are similar to the SMAP L4C record in the boreal forest biome, but with a larger positive L4C productivity bias in the tundra biome. The mean NF_{JaAu} period is 114.7 ± 4.9 days while the mean VSM_{JJA} is 0.23 ± 0.004 m^3/m^3 over the entire ABoVE domain. The FT results show a 3–4-week longer NF period in boreal forest (120.4 ± 5.5 days) than tundra (97.4 ± 4.1 days), whereas VSM_{JJA} is similar across the two biomes (Table 20.1). The GPP_{JJA}, SIF_{JJA} and EVI_{JJA} results are all generally larger in boreal forest than in tundra, consistent with a general productivity and NF_{JaAu} decline at higher latitudes.

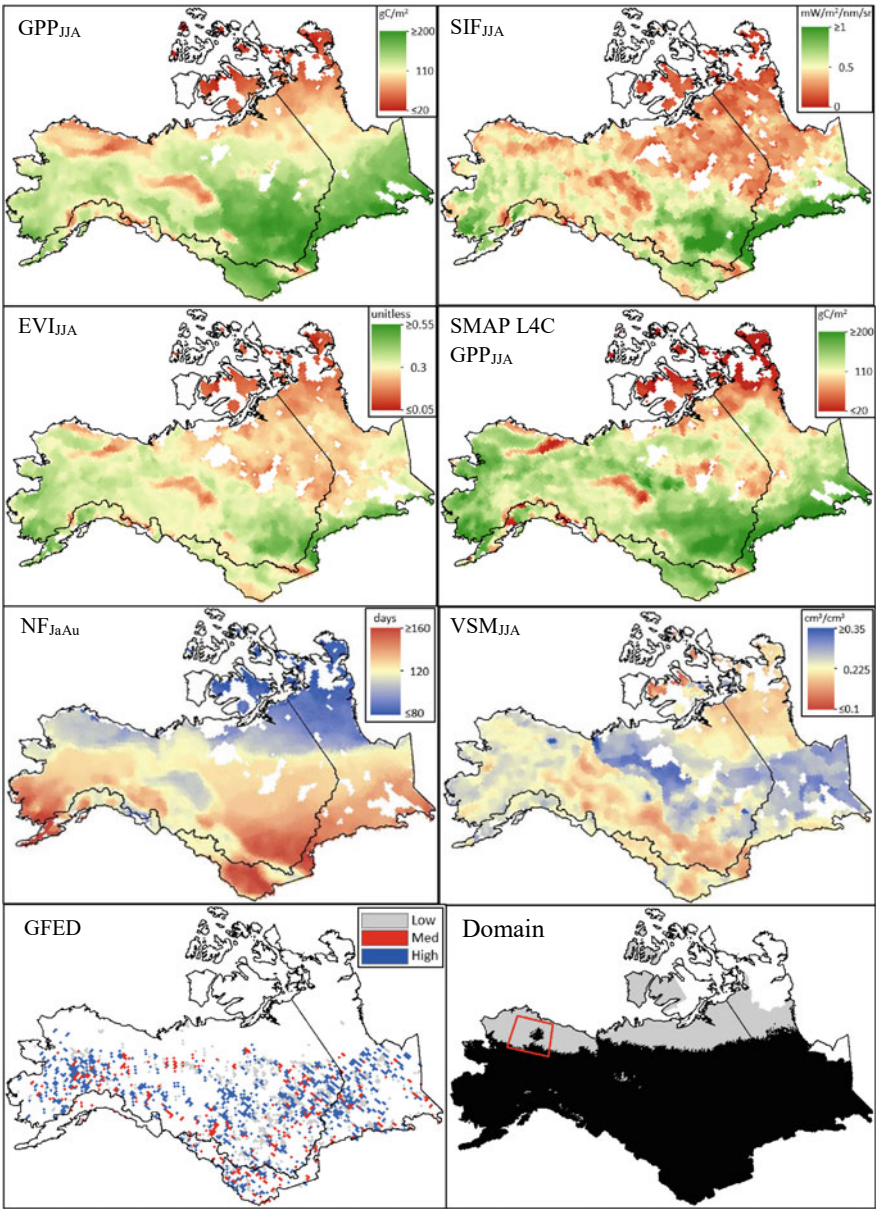

Fig. 20.1 Regional patterns of grid-cell-wise values of GPP_{JJA} [gC/m^2], SIF_{JJA} [$mW/m^2/nm/sr$], EVI_{JJA} [unitless], SMAP L4C GPP_{JJA} [gC/m^2], NF_{JaAu} [days], and VSM_{JJA} [cm^3/cm^3] for selected year 2016, and GFED burn areas for 2007–2016. Large open water fraction (>20 %), permanent wetland, urban, snow/ice and barren areas were masked from the analysis. Domain denotes Arctic Tundra (grey) and Boreal Forest (black) areas. Black lines denote the ABoVE core and extended domain used for this study. Red polygon delineates the Brooks Range, Alaska sub-region used for the topographic analysis. Spatial convolution of a median filter was applied to these maps, except for GFED and Domain maps

Table 20.1 2007-2016 average of satellite measured summer (JJA) vegetation growth and bioclimatic variables for boreal forest and tundra in the NASA ABoVE domain

	Statistics	ABoVE	Tundra	Boreal Forest
GPP_{JJA} [gC/m^2]	Mean	123.8	90.5	135.4
	Temporal-SD	4.2	4.6	4.6
*SMAP L4C GPP_{JJA} [gC/m^2]	Mean	125.5	105.0	135.6
	Temporal-SD	6.0	8.8	5.7
SIF_{JJA} [$mW/m^2/nm/sr$]	Mean	0.49	0.36	0.55
	Temporal-SD	0.02	0.01	0.03
EVI_{JJA} [unitless]	Mean	0.30	0.27	0.32
	Temporal-SD	0.005	0.005	0.005
NF_{JaAu} [days]	Mean	114.7	97.4	120.4
	Temporal-SD	4.9	4.1	5.5
VSM_{JJA} [cm^3/cm^3]	Mean	0.23	0.22	0.24
	Temporal-SD	0.004	0.005	0.004

*only 2015 and 2016 SMAP data were used in this analysis

While several major mountain ranges are in the ABoVE domain, including the Brooks Range which separates polar tundra on the Arctic coastal plain from warmer boreal forest areas of central Alaska and Canada, their orographic impact on climate and vegetation growth is largely unresolved by the relatively coarse global satellite observations. To investigate the regional impacts of topographic elevation and aspect variability on NF season, VSM and vegetation productivity we selected a sub-region extending across the Alaskan Brooks Range (red polygon defined in Fig. 20.1 map). Despite the relatively coarse spatial scale of this investigation, our results show a general decrease in both the NF_{JaAu} period and vegetation growth at higher elevations (Fig. 20.2). The SIF record shows less elevation-dependent distribution attributed to the large GOME-2 sensor footprint relative to underlying topographic heterogeneity. A longer NF_{JaAu} period and higher productivity from GPP and SIF generally occur on south-facing slopes and lower latitudes, while there are less latitude and aspect apparent patterns in the EVI record (Fig. 20.3). South-facing slopes are associated with relatively dry VSM conditions, consistent with enhanced radiation loading and evaporation compared to wetter north-facing slopes.

Annual variability in the satellite-based summer productivity (GPP_{JJA}, SIF_{JJA}, EVI_{JJA}), climate (NF_{JaAu}, VSM_{JJA}) and disturbance (GFED) metrics over the study domain and 10-year record is presented in Fig. 20.4. Positive (negative) anomalies indicate that the values are above (below) the long-term average (or trend). The annual variations in GPP_{JJA}, EVI_{JJA} and SFI_{JJA} are generally similar, indicating relatively lower productivity (negative anomalies) from 2009 to 2011 and higher productivity (positive anomalies) for 2012, 2013 and 2016. Lower productivity from 2009 to 2011 coincides with documented drought conditions in 2009 linked to the multi-variate El Niño Southern Oscillation (ENSO) index, which also coincides with reduced VSM_{JJA} (2009–2011) and enhanced wildfire activity (2010–2011).

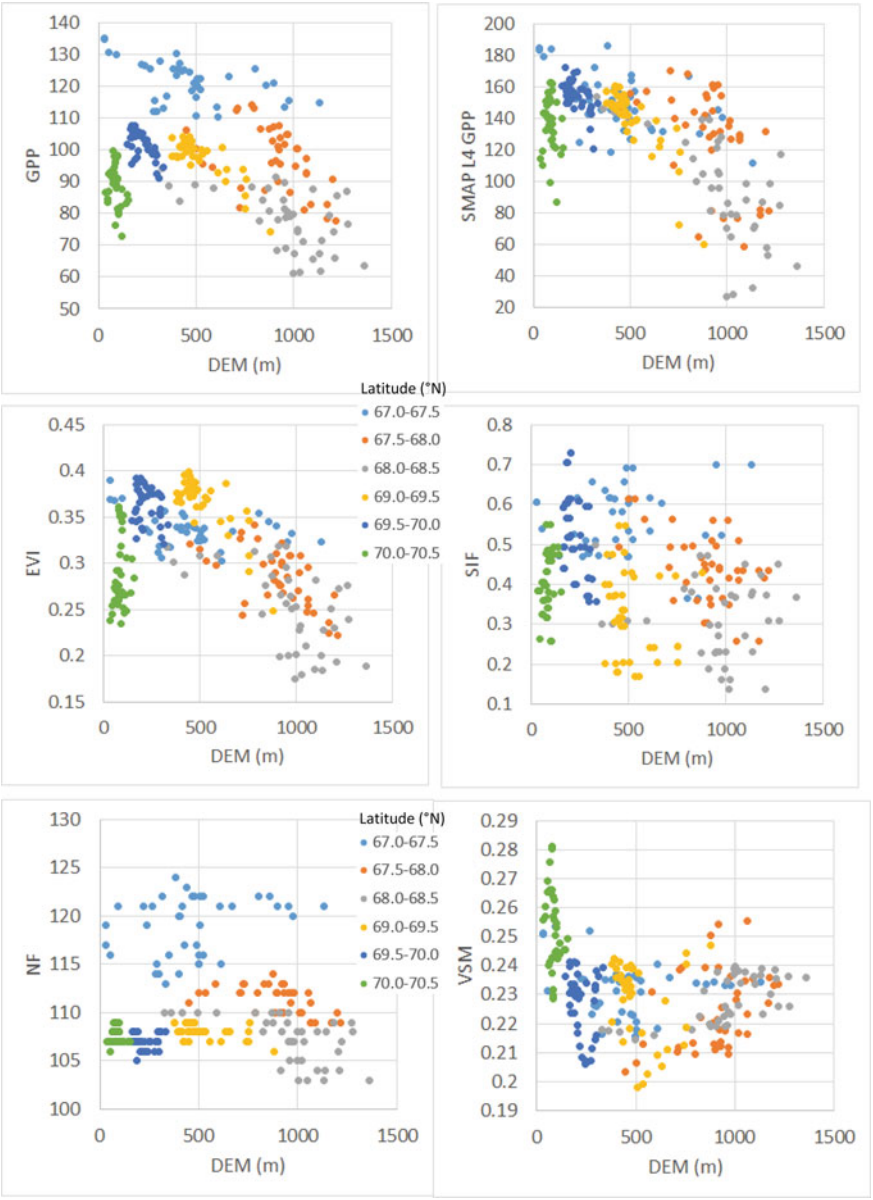

Fig. 20.2 Elevational (DEM) distribution of GPP_{JJA} [gC/m^2], SMAP L4C GPP_{JJA} [gC/m^2], EVI_{JJA} [unitless], SIF_{JJA} [mW/m^2/nm/sr], NF_{JaAu} [days], and VSM_{JJA} [cm^3/cm^3] within a sub-region extending across the Brooks Range of Alaska (red polygon in Fig. 1 map), and binned by latitude (°N)

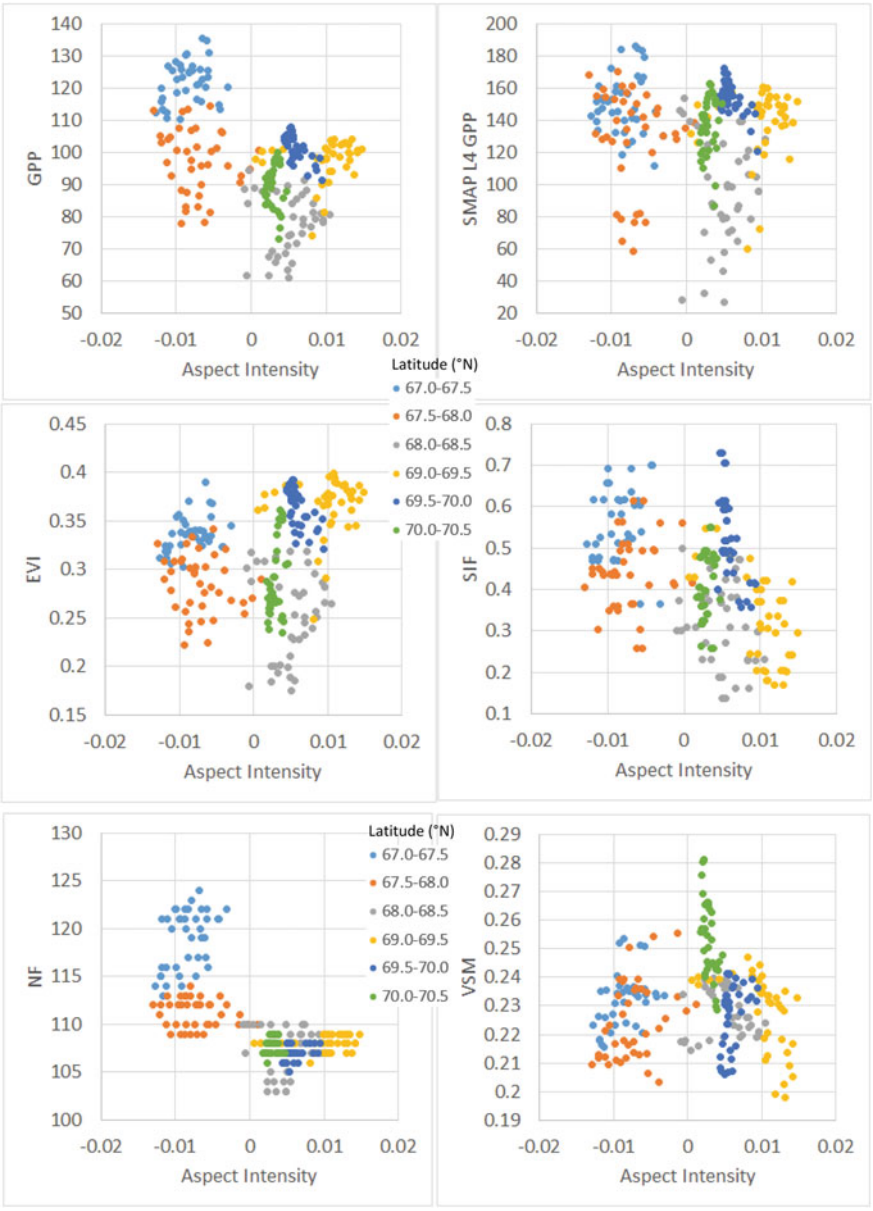

Fig. 20.3 Distribution of GPP_{JJA} [gC/m^2], SMAP L4C GPP_{JJA} [gC/m^2], EVI_{JJA} [unitless], SIF_{JJA} [mW/m^2/nm/sr], NF_{JaAu} [days], and VSM_{JJA} [cm^3/cm^3] by terrain aspect; aspect intensity (in degrees where positive sign denotes north facing) derived from the sine of the slope multiplied by cosine of the DEM aspect within a sub-region extending across the Brooks Range of Alaska (red polygon in Fig. 1 map), and binned by latitude (°N)

Consistency among the different productivity metrics is lower in 2007, 2008, 2014 and 2015. The negative anomalies in EVI_{JJA} and SFI_{JJA} in 2015 are congruent with a large positive ENSO (El Niño) phase, but the associated drought impact is less apparent for GPP_{JJA}. There are generally opposite anomaly patterns between GFED and VSM_{JJA}, whereby wetter (drier) soil moisture conditions are associated with less (greater) fire activity. The longer NF_{JaAu} period and reduced VSM_{JJA} in 2015 correspond with a strong El Niño that extended from approximately May 2015 to May 2016, which also coincides with enhanced GFED fire activity and much lower productivity indicated from the SIF_{JJA} and EVI_{JJA} records.

We extracted anomaly values of EVI_{JJA}, SIF_{JJA} and GPP_{JJA} within the major wildfire burn areas identified from GFED over the 2007–2016 study period (e.g. see GFED polygons in Fig. 20.1). The mean EVI_{JJA} and SIF_{JJA} anomalies within these burned areas showed a small ($\sim$ 5.5%) reduction in productivity of -0.07 ± 1.0 (unitness) and -0.04 ± 0.9 (mW m^{-2} nm^{-1} sr^{-1}), respectively, whereas the GPP_{JJA} anomalies showed a small (2%) productivity increase ($+0.2 \pm 0.9$ gCm^{-2}) relative

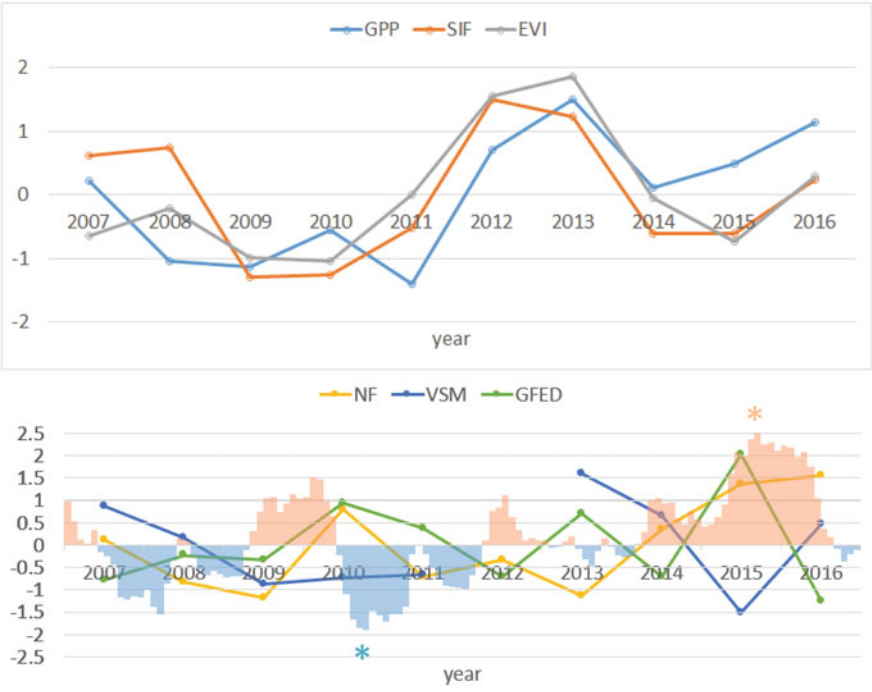

Fig. 20.4 Annual variations in mean GPP_{JJA} [gC/m^2], SIF_{JJA} [$mW/m^2/nm/sr$], EVI_{JJA} [unitless], GFED [ha], NF_{JaAu} [days], and VSM_{JJA} [cm^3/cm^3] anomalies over the ABoVE domain from 2007–2016. The monthly multivariate ENSO index (MEI) is shown in the shaded bar graph denoting positive (El Niño) and negative (La Niña) MEI values; red and blue * symbols denote the respective major El Niño and La Niña phases during the study period. The 2012 VSM data were excluded due to insufficient AMSR data availability

to other years of record prior to and following the burn years. The positive GPP_{JJA} anomalies may reflect higher productivity in boreal forest following large wildfire events (Loranty et al. 2016). However, the combined observations indicate relatively low sensitivity to wildfire events, which is attributed to wildfire severity rather than burned areas being a more direct measure of fire-related impacts on vegetation productivity (Rogers et al. 2018).

The regional pattern (Fig. 20.5) of correlations between the GPP_{JJA} and NF_{JaAu} anomalies indicates that years with a relatively longer non-frozen period are less productive in interior Alaska, while a widespread positive correlation occurs in other areas. There is a more heterogeneous pattern of positive and negative correlation areas in the SIF_{JJA} results, while the EVI_{JJA} results show a larger extent of negative correlation areas (Fig. 20.5). The different EVI and SIF response patterns may reflect lower signal-to-noise in the satellite observations at higher latitudes and the resulting coarse (16-day to monthly) temporal compositing of the data (Joiner et al. 2014; Luus et al. 2017). The unanimous productivity response to NF_{JaAu}

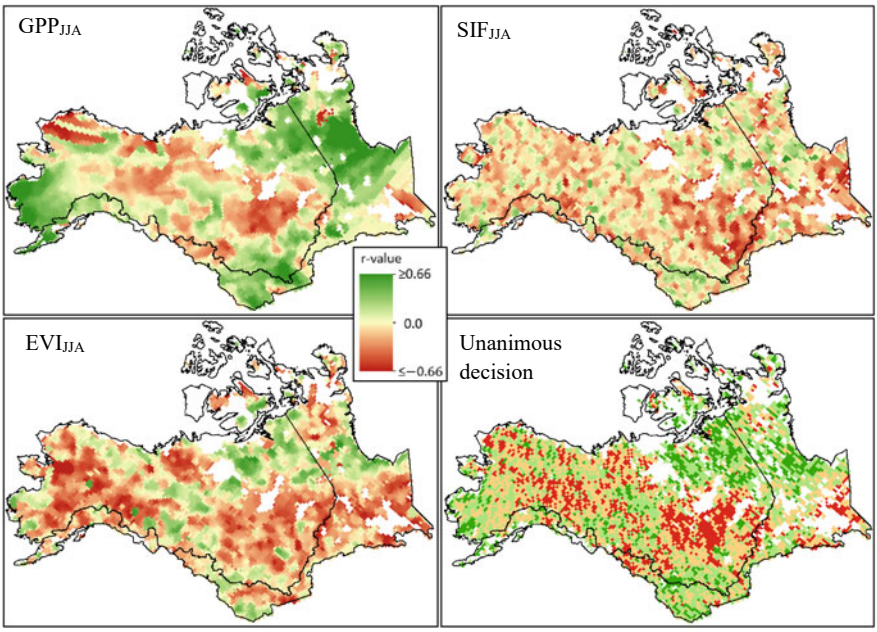

Fig. 20.5 Regional patterns of per grid cell correlations (r-values) between NF_{JaAu} and the vegetation growth metrics (GPP_{JJA}, SIF_{JJA}, EVI_{JJA}) for 2007–2016. The regional unanimous decision method was applied to the three productivity datasets, where green (red) cells indicate unanimously positive (negative) relationships for all three datasets. Light green (orange) pixels denote areas where a smaller majority (67%) of datasets are positive (negative). Large open water fraction (>20 %), permanent wetland, urban, snow/ice and barren areas were masked from the analysis. Spatial convolution of a median filter was applied to these maps, except for the unanimous decision map

variability from the three vegetation metrics (Fig. 20.5) shows areas of consistent positive (green) and negative (red) correlations. The unanimous decision shows approximately 14.7 and 17.8% of the domain with respective positive (green) and negative (red) productivity response to NF_{JaAu}. Lighter colors denote areas where a smaller majority (67%) of the productivity metrics show a positive (green) or negative (orange) response to NF_{JaAu}. Positive correlation (green and light green) areas indicate where productivity is directly proportional to NF_{JaAu} and a longer non-frozen season, which promotes greater vegetation growth. The larger area (53.6%) of red and orange pixels indicate where the potential benefit of a longer NF season to vegetation growth is reduced or reversed.

The regional pattern (Fig. 20.6) of correlations between the vegetation growth and VSM_{JJA} anomalies shows generally the opposite pattern from the NF_{JaAu} correlation (Fig. 20.5). Green areas indicate where vegetation growth sensitivity to climate warming may depend on regional summer moisture availability (Fig. 20.6). The unanimous decision shows approximately 19.1 and 18.6% of the domain with respective positive (green) and negative (red) productivity response to VSM_{JJA}. Summer moisture-limited vegetation growth is more apparent over much of the interior study domain, indicating a stronger summer soil moisture constraint on boreal forest productivity. Areal proportions of positive and negative correlations

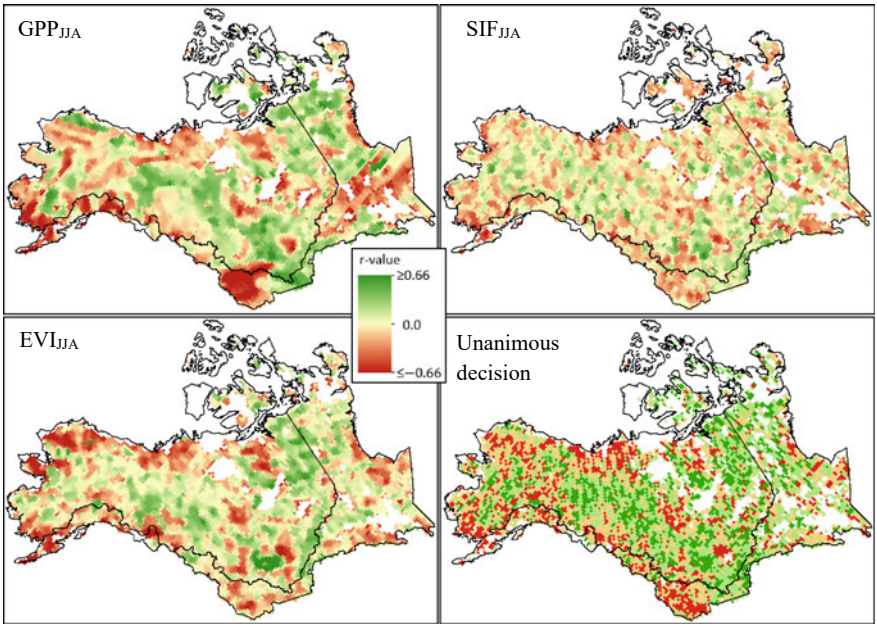

Fig. 20.6 Regional patterns of grid-cell-wise correlations (r-values) between VSM_{JJA} and the vegetation growth metrics (GPP_{JJA}, SIF_{JJA}, EVI_{JJA}) for 2007–2016. The 2012 data were excluded due to insufficient AMSR VSM data availability. Format here is the same as in Fig. 5

Table 20.2 Spatial extent of multivariate correlations between summer vegetation growth (GPP_{JJA} [gC/m^2], EVI_{JJA} [unitless], SFI_{JJA} [$mW/m^2/nm/sr$]) and bioclimatic metrics (NF_{JaAu} [days] and VSM_{JJA} [cm^3/cm^3]) expressed as percent of tundra and boreal forest biomes. 'Positive' represents unanimous positive correlation in all three regression values, while 'negative' denotes a unanimous negative correlation. 'Likely positive' and 'likely negative' indicate where a smaller majority of regression values are positive and negative, respectively

	Biome	Positive (Green)	Likely positive (Light green)	Likely negative (Orange)	Negative (Red)
NF_{JaAu}	ABoVE	14.7	31.7	35.8	17.8
	Tundra	20.9	34.4	32.0	12.7
	Boreal Forest	13.5	31.1	36.6	18.8
VSM_{JJA}	ABoVE	19.1	32.0	30.3	18.6
	Tundra	17.4	29.8	32.1	20.8
	Boreal Forest	19.5	32.4	29.9	18.2

between climate constraints and vegetation growth anomalies are summarized over the study domain and for the two major biomes in Table 20.2. Tundra areas show more widespread (55.3%) positive correspondence between NF_{JaAu} and summer vegetation growth, whereas a greater extent of negative correlations is found in boreal forest. Boreal biomes also show greater areal proportion of positive correlations (51.9%) between VSM_{JJA} and summer vegetation growth than tundra (47.2%). These contrasting productivity correlations with NF_{JaAu} and VSM_{JJA} are consistent with relatively greater moisture limitations to growth in boreal forest and greater energy limitations to growth in tundra (Guo et al. 2018; Kim et al. 2014).

20.5 Discussion and Conclusion

Understanding the vulnerability and resilience of tundra and boreal forest biomes in response to warming requires the analysis of relationships between climate constraints, disturbance and vegetation productivity. Satellite remote sensing results from this study document the variable response of boreal forest and tundra productivity in the ABoVE domain to key climate constraints, including non-frozen season duration and summer soil moisture supply available to support vegetation growth. We also examined the relative impact of large regional wildfire disturbances on productivity represented by ensemble satellite observations of annual burned area. However, satellite remote sensing is limited at higher latitudes by low signal-to-noise and data loss from variable lighting and polar darkness, persistent cloud cover, smoke and associated atmospheric contamination effects. We therefore employed an ensemble of vegetation productivity metrics derived from different satellite sensors and algorithms, including SIF from GOME-2, EVI from MODIS,

and GPP from MODIS and SMAP sensor records to overcome these limitations. We also constrained our analysis to the summer months to further reduce the potential impacts of larger satellite observational error during the shoulder seasons. We then conducted an analysis of the majority response of the summer productivity metrics to variations in non-frozen season (NF_{JaAu}) and soil moisture (VSM_{JJA}) derived from the daily AMSR record, as surrogates for potential growing season and water supply constraints to vegetation growth. Finally, we examined the variable response in the productivity patterns between recently burned and unburned areas defined from the GFED record.

The correlation analysis of the vegetation productivity metrics (GPP_{JJA}, SIF_{JJA} and EVI_{JJA}) with NF_{JaAu} and VSM_{JJA} supports previous reports documenting a widespread negative boreal forest growth response to warmer temperatures in Alaska and Canada (Walker and Johnstone 2014; Sulla-Menashe et al. 2018). Plant-available moisture limitations on vegetation growth are increasing while non-frozen season constraints to productivity are reduced in a warming climate and both should be considered in future projections of HNL ecosystem productivity and carbon sink activity. However, we found significant differences in environmental sensitivity among the three satellite productivity metrics. The EVI and SIF variations with topographic aspect were different from the GPP metrics, and the GPP sensitivity to wildfire events was less apparent than the EVI and SIF metrics. Although the NF correlation analysis shows less energy constraint in the boreal biome, there was relatively weak correspondence between summer soil moisture and boreal forest growth (Table 20.1), which may reflect larger AMSR VSM retrieval uncertainties in more densely forested areas (Du et al. 2017a). Our results showed a lower than anticipated productivity response to wildfire disturbance indicated from the GFED burned area record. Fire severity, rather than burned area, is a more appropriate indicator of fire-related impacts on vegetation owing to the large characteristic heterogeneity in fire combustion and intensity in boreal forest and tundra (Kasischke et al. 2010a; Rogers et al. 2018). However, consistent spatial records documenting fire severity for the entire domain are lacking and should be prioritized for further development given the important and changing role of fire disturbance in boreal ecosystems (Giglio et al. 2013; Kasischke et al. 2010a).

The variable patterns and response characteristics among the different vegetation productivity metrics may reflect one or more factors. The GPP records used in this study are sensitive to various uncertainties contributed from the underlying model assumptions and parameterizations, MODIS vegetation inputs and the coarse daily meteorological inputs derived from global re-analysis data (Alexeev et al. 2012; Jones et al. 2013; Kimball et al. 2016). These coarse model-based assessments likely do not adequately represent the more heterogeneous vegetation response to complex environmental conditions and surface hydrology in permafrost landscapes (Keane et al. 2015; Keith et al. 2010; Sitch et al. 2007). Differences in the EVI and SIF observations and metrics are attributed to the large differences in sampling footprint between these sensors, the variable sensitivity of the retrievals to environmental conditions, and the different spatial and temporal compositing of the data (Joiner et al. 2014; Luus et al. 2017; Wagle et al. 2016). Differences in the SIF_{JJA},

GPP_{JJA} and EVI_{JJA} response characteristics may also be associated with the relatively coarse resolution of the model grid used in this study, which is similar to the SIF spatial grid from GOME-2, but reduces sub-grid spatial heterogeneity depicted in the finer scale EVI and GPP records. The GPP records combine synergistic information from direct satellite observations and daily surface meteorology within a LUE model for estimating GPP; the resulting model calculations are less sensitive to remote sensing uncertainty, but include other uncertainties contributed from the model assumptions and parameterizations, and other ancillary inputs (Heinsch et al. 2006; Jones et al. 2017). All of the productivity metrics employ different retrieval algorithms and mechanisms for inferring vegetation growth that can contribute to different response characteristics. Our majority analysis reduced the dependence on any single vegetation metric, and makes it possible to identify areas where productivity trends and underlying controls are identified with greater confidence, while also identifying areas with greater uncertainty that may warrant further study. Further clarification of climate and disturbance-related impacts on vegetation productivity will likely result from analyzing a longer satellite data record with detailed ground truth measurements, while also combining multiple remote sensing observations using appropriate data assimilation techniques.

Acknowledgments This work was conducted at the University of Montana under contract to NASA (NNX14AB20A, NNX15AT74A, NNX14AI50G). The GOME-2 SIF data used in this study are available at (https://acd-ext.gsfc.nasa.gov/People/Joiner/my_gifs/GOME_F/GOME-F.htm), while the GFED4 data record is available at (http://www.globalfiredata.org/). The SMAP L4C, AMSR VSM and FT-ESDR data were obtained from the National Snow and Ice Data Center (NSIDC), while the MODIS VI records were obtained from the NASA LP DAAC (https://modis.gsfc.nasa.gov/data/dataprod/mod13.php).

Appendix A

Acronyms and Abbreviations

ABoVE	Arctic-Boreal Vulnerability Experiment
AMSR-E	Advanced Microwave Scanning Radiometer for EOS
AMSR2	AMSR follow-on instrument onboard the JAXA GCOM-W1 satellite
APAR	Absorbed Photosynthetically Active solar Radiation
ASTER	Advanced Spaceborne Thermal Emission and Reflection sensor
BPLUT	Biome-Properties Look-Up Table
DEM	Digital Elevation Model
ENSO	El Niño Southern Oscillation
EVI	Enhanced Vegetation Index
FPAR	Fraction of canopy-absorbed Photosynthetically Active Radiation
FR	Frozen
FT	Freeze/Thaw
FT-ESDR	Freeze/Thaw Earth System Data Record
GDEM	Global Digital Elevation Map
GFED	Global Fire Emissions Database
GOME-2	Global Ozone Mapping Experiment 2

GPP	Gross Primary Productivity
HNL	High Northern Latitudes
L4C	Level 4 Carbon
LUE	Light Use Efficiency
MODIS	MODerate resolution Imaging Spectroradiometer
NASA	National Aeronautics and Space Administration
NDVI	Normalized Difference Vegetation Index
NF	Non-frozen
PAR	Photosynthetically Active Radiation
RZSM	Root Zone Soil Moisture
SIF	Solar-Induced chlorophyll Fluorescence
SMAP	Soil Moisture Active Passive
SSM/I(S)	Special Sensor Microwave Imager (sounder)
Tb	Brightness Temperature
VI	Vegetation Index
VPD	Vapor Pressure Deficit
VSM	Volumetric Soil Moisture

References

Geruo A, Velicogna I, Kimball JS, Du J, Kim Y, Colliander A, Njoku E (2017) Satellite-observed changes in vegetation sensitivities to surface soil moisture and total water storage variations since the 2011 Texas drought. Environ Res Lett 12:054006

Alexeev VA, Esau I, Polyakov IV, Byam SJ, Sorokina S (2012) Vertical structure of recent arctic warming from observed data and re-analysis products. Clim Change 111:215–239

Baird AB, Verbyla D, Hollingsworth TN (2012) Browning of the landscape of interior Alaska based on 1986–2009 Landsat sensor NDVI. Can J For Res 42:1371–1382

Baker NR (2008) Chlorophyll Fluorescence: a probe of photosynthesis in vito. Annu Rev Plant Biol 59(1):89–113

Baldocchi D (2008) Breathing of the terrestrial biosphere: Lessons learned from a global network of carbon dioxide flux measurement systems. Aust J Bot 56(1):1–26

Barichivich J, Briffa KR, Myneni R, Schrier G, Dorigo W, Tucker CJ, Osborn TJ, Melvin TM (2014) Temperature and snow-mediated moisture controls of summer photosynthetic activity in northern terrestrial ecosystems between 1982 and 2011. Remote Sens 6:1390–1431

Barnett TP, Adam JC, Lettenmainer DP (2005) Potential impacts of a warming climate water availability in snow-dominated regions. Nature 438:303–309

Bastos A, Ciais P, Park T, Zscheischler J, Yue C, Barichivich J, Myneni RB, Peng S, Piao S, Zhu Z (2017) Was the extreme Northern Hemisphere greening in 2015 predictable? Environ Res Lett 12:044016

Beck PSA, Goetz SJ (2011) Satellite observations of high northern latitude vegetation productivity changes between 1982 and 2008: ecological variability and regional differences. Environ Res Lett 6:045501

Beer C, Reichstein M, Tomelleri E et al (2010) Terrestrial gross carbon dioxide update: global distribution and covariation with climate. Science 329:834–838

Berner LT, Beck PSA, Gunn AG, Lloyd AH, Goetz SJ (2011) High-latitude tree growth and satellite vegetation indices: Correlations and trends in Russia and Canada (1982-2008). J Geophys Res-Biogeosci 116:G01015

Bjorkman AD, Vellend M, Frei ER, Henry GHR (2017) Climate adaptation is not enough: warming does not facilitate success of southern tundra plant populations in the high Arctic. Glob Change Biol 23:1540–1551

Brodzik MJ, Knowles KW (2002) EASE-grid: a versatile set of equal area projections and grids in discrete global grids, Goodchild M (ed) Santa Barbara, CA: Nat. Center Geographic Inf. Anal.

Brodzik MJ, Billingsley B, Haran T, Raup B, Savoie MH (2014) Correction: Brodzik MJ et al (2012) EASE-Grid 2.0: Incremental but significant improvements for Earth-Gridded Data Sets. ISPRS Int J Geo-Inf 1:32–45; ISPRS Int J Geo-Inf 3(3):1154–1156. https://doi.org/10.3390/ijgi3031154

Buermann W, Bikash PR, Jung M, Burn DH, Reichstein M (2013) Earlier Springs Decrease Peak Summer Productivity in North American Boreal Forests. Environ Res Letters 8(2):024027. https://doi.org/10.1088/1748–9326/8/2/024027

Chu T, Guo X (2014) Remote sensing techniques in monitoring post-fire effects and patterns of forest recovery in boreal forest regions: a review. Remote Sens 6(1):470–520

Commane R, Lindaas J, Benmergui J, Luus KA, Chang RYW, Daube BC, Euskirchen ES, Henderson JM, Karion A, Miller JB, Miller SM, Parazoo NC, Randerson JT, Sweeney C, Tans P, Thoning K, Veraverbeke S, Miller CE, Wofsy SC (2017) Carbon dioxide sources from Alaska driven by increasing early winter respiration from Arctic tundra. Proc Natl Acad Sci USA 114(21):5361–5366

Cowtan K, Way RG (2014) Coverage bias in the HadCRUT4 temperature series and its impact on recent temperature trends. Q J R Meteorol Soc Wiley. http://dx.doi.org/10.1002/qj.2297

Dass P, Rawlins MA, Kimball JS, Kim Y (2016) Environmental controls on the increasing GPP of terrestrial vegetation across northern Eurasia. Biogeosciences 13:45–62

de Beurs KM, Henebry GM (2010) A land surface phenology assessment of the northern polar regions using MODIS reflectance time series. Can J Remote Sens 36(Suppl 1):S87–S110

Dee DP, Uppala SM, Simmons AJ, Berrisford P, Poli P, Kobayashi S, Andrae U, Balmaseda MA, Balsamo G, Bauer P, Bechtold P, Beljaars ACM, van de Berg I, Biblot J, Bormann N, Delsol C, Dragani R, Fuentes M, Greer AJ, Haimberger L, Healy SB, Hersbach H, Holm EV, Isaksen L, Kallberg P, Kohler M, Matricardi M, McNally AP, Mong-Sanz BM, Morcette JJ, Park BK, Peubey C, de Rosnay P, Tavolato C, Thepaut JN, Vitart F (2011) The ERAInterim reanalysis: configuration and performance of the data assimilation system. Q J R Meteorol Soc 137:553–597

Delbart N, Toan T, Kergoat L, Fedotova V (2006) Remote sensing of spring phenology in boreal regions: a free of snow-effect method using NOAA-AVHRR and SPOT-VGT data (1982-2004). Remote Sens Environ 101(1):52–62

Derksen C, Xu X, Dunbar RS, Colliander A, Kim Y, Kimball JS, Black TA, Euskirchen E, Langlois A, Loranty MM, Marsh P, Rautiainen K, Roy A, Royer A Stephens J (2017) Retrieving landscape freeze/thaw state from soil moisture active passive (SMAP) radar and radiometer measurements. Remote Sens Environ 194:48–62

Didan K, Munoz AB, Solano R, Huete A (2015) MODIS Vegetation Index User's Guide (MOD13 Series) Version 3.0 June 2015 Collection 6. https://vip.arizona.edu/documents/MODIS/MODIS_VI_UsersGuide_June_2015_C6.pdf

Du J, Kimball JS, Jones LA, Kim Y, Glassy J, Watts JD (2017a) A global satellite environmental data record derived from AMSR-E and AMSR2 microwave earth observations. Earth Syst Sci Data 9:791–808

Du J, Jones LA, Kimball JS (2017b) Daily global land parameters derived from AMSR-E and AMSR2, Version 2. [Indicate subset used]. Boulder, Colorado USA. NASA National Snow and Ice Data Center Distributed Active Archive Center. doi:https://doi.org/10.5067/RF8WPYOPJKL2. [Date Accessed]

Du J, Kimball JS, Jones LA (2016) Passive microwave remote sensing of soil moisture based on dynamic vegetation scattering properties for AMSR-E. IEEE Trans Geosci Remote Sens 54:597–608

Du J, Kimball JS, Shi J, Jones LA, Wu S, Sun R, Yang H (2014) Inter-calibration of satellite passive microwave land observations from AMSR-E and AMSR2 using overlapping FY3B-MWRI sensor measurements. Remote Sens 6:8594–8616

Emmerton CA, Louis VL, Humphreys ER, Gamon JA, Barker JD, Pastorello GZ (2016) Net ecosystem exchange of CO2 with rapidly changing high Arctic landscapes. Glob Change Biol 22:1185–1200

Flexas J, Escalona J, Evain S, Gulias J, Moya I, Osmond C, Medrano H (2002) Steafy-state chlorophyll fluorescence (Fs) measurements as a tool to follow variations of net CO2 assimilation and stomatal conductance during water-stress in C3 plant. Physiol Plant 114:231–240

Friedl MA, McIver DK, Hodges JCF, Zhang XY, Muchoney D, Strahler AH, Woodcock CE, Gopal S, Schneider A, Cooper A, Baccini A, Gao F, Schaaf C (2002) Global land cover mapping from MODIS: algorithms and early results. Remote Sens Environ 83:287–302

Gamon JA, Huemmrich KF, Stone RS, Tweedie CE (2013) Spatial and temporal variation in primary productivity (NDVI) of coastal Alaska tundra: Decreased vegetation growth following earlier snowmelt. Remote Sens Environ 129:144–153

Giglio L, Randerson JT, van der Werd GR (2013) Analysis of daily, monthly, and annual burned area using the fourth-generation global fire emissions database (GFED4). J Geophys Res 118:317–328

Girardin MP, Hogg EH, Bernier PY, Kurz WA, Guo Z, Cyr G (2016) Negative impacts of high temperatures on growth of black spruce forests intensify with the anticipated climate warming. Glob Change Biol 22(2):627–643

Goetz S, Kimball JS, Mack M, Kasischke E (2011) Scoping completed for an experiment to assess vulnerability of Arctic and Boreal ecosystems. EOS 92(18)

Guanter L et al (2014) Global and time-resolved monitoring of crop photosynthesis with chlorophyll fluorescence. Proc Natl Acad Sci USA 111(14):E1327–E1333

Guay KC, Beck PSA, Berner LT, Goetz SJ, Baccini AL, Buermann W (2014) Vegetation productivity patterns at high northern latitudes: a multi-sensor satellite data assessment. Glob Change Biol 20:3147–3158

Guo W, Liu H, Wu X (2018) Vegetation greening despite weakening coupling between vegetation growth and temperature over the boreal region. J Geophys Res. https://doi.org/10.1029/2018JG004486

Heinsch FA, Zhao M, Running SW, Kimball JS, Nemani RR, Davis KJ, Bolstad PV, Cook BD, Desai AR, Ricciuto DM, Oechel WC, Kwon HJ, Luo H, Wofsy S, Dunn AL, Munger W, Baldocchi D, Xu L, Hollinger DY, Richardson AD, Stoy PC, Siqueira MBS, Monson R, Burns SP, Flanagan LB (2006) Evaluation of remote sensing based terrestrial productivity from MODIS using regional tower eddy flux network observations. IEEE Trans Geosci Remote Sens 44(7):1908–1925

Hellmann L, Agafonov L, Ljungqvist FC, Churakova O, Duthorn E, Esper J, Hulsmann L, Kirdyanov AV, Moiseev P, Myglan VS, Nikolaev AN, Reinig F, Schweingruber FH, Solomina O, Tegel W, Buntgen U (2016) Diverse growth trends and climate responses across Eurasia's boreal forest. Environ Res Lett 11:074021

Hoy EE, Turetsky MR, Kasischke ES (2016) More frequent burning increases vulnerability of Alaska boreal black spruce forests. Environ Res Lett 11:095001

Huete A, Dinan K, Miura T, Rodriguez EP, Gao X, Ferreira LG (2002) Overview of the radiometric and biophysical performance of the MODIS vegetation indices. Remote Sens Environ 83:195–213

Jeganathan C, Dash J, Atkinson PM (2014) Remotely sensed trends in the phenology of northern high latitude terrestrial vegetation, controlling for land cover change and vegetation type. Remote Sens Environ 143:154–170

Jia GJ, Epstein HE, Walker DA (2009) Vegetation greening in the Canadian arctic related to decadal warming. J Environ Monit 11:2231–2238

John R, Chen J, Kim Y, Ou-yang Z, Xiao J, Park H, Shao C, Zhang Y, Amarjargal A, Batkhshig O, Qi J (2016) Differentiating anthropogenic modification and precipitation-driven change on vegetation productivity on the Mongolian Plateau. Landscape Ecol 31:547–566

Joiner JL et al (2014) The seasonal cycle of satellite chlorophyll fluorescence observations and its relationship to vegetation phenology and ecosystem atmosphere carbon exchange. Remote Sens Environ 152:375–391

Joiner J, Guanter L, Lindstrot R, Voigt M, Vasilkov AP, Middleton EM, Huemmrich KF, Yoshida Y, Frankenberg C (2013) Global monitoring of terrestrial chlorophyll fluorescence from moderate spectral resolution near-infrared satellite measurements: methodology, simulation, and application to GOME-2. Atmos Meas Tech 5:809–829

Jones LA, Kimball JS, Reichle RH, Madani N, Glassy J, Ardizzone JV, Colliander A, Cleverly J, Desai AR, Eamus D, Euskirchen E, Hutley L, Macfarlane C, Scott RL (2017) The SMAP Level 4 carbon product for monitoring ecosystem land-atmosphere CO_2 exchange. IEEE Trans Geosci Remote Sens 55(11):6517–6532

Jones MO, Kimball JS, Jones LA (2013) Satellite microwave detection of boreal forest recovery from the extreme 2004 wildfires in Alaska and Canada. Glob Change Biol 19:3113–3122

Jones LA, Ferguson CR, Kimball JS, Zhang K, Chan STK, McDonald KC, Njoku EG, Wood EF (2010) Satellite microwave remote sensing of daily land surface air temperature minima and maxima from AMSR-E. IEEE J Sel Top Appl Earth Obs Remote Sens 3(1):111–123

Karkauskaite P, Tagesson T, Fensholt R (2017) Evaluation of the plant phenology index (PPI), NDVI and EVI for start-of-season trend analysis of the northern hemisphere boreal zone. Remote Sens 9(5):485

Kasischke ES, Verbyla DL, Rupp TS, McGuire AD, Murphy KA, Chapin FS III, Calef M, Allen JL, Duffy PA, Hoy EE, Jandt R, Turetsky MR (2010a) Alaska's changing fire regime: implications for the vulnerability of its boreal forest. Canadian J Forest Res 40:1313–1324

Kasischke ES, Goetz SJ, Kimball JS, Mack MM (2010b) The Arctic-Boreal Vulnerability Experiment (ABoVE): A Concise plan for a NASA-Sponsored Field Campaign Available online: http://cce.nasa.gov/terrestrial_ecology/pdfs/ABoVE%20Final%20Report.pdf. (Accessed 16 July 2018)

Keane RE, McKenzie D, Falk DA, Smithwick EAH, Miller C, Kellogg LB (2015) Representing climate, disturbance, and vegetation interactions in landscape models. Ecol Model 309–310:33–47

Keith H, Mackey B, Berry S, Lindenmayer Gibbons P (2010) Estimating carbon carrying capacity in natural forest ecosystems across heterogeneous landscapes: addressing sources of error. Glob Change Biol 16:2971–2989

Kim Y, Kimball JS, Glassy J, Du J (2017a) An extended global earth system data record on daily landscape freeze-thaw status determined from satellite passive microwave remote sensing. Earth Syst Sci Data 9:133–147

Kim Y, Kimball JS, Glassy J, McDonald K C (2017b) Measures global record of daily landscape freeze/thaw status, Version 4. [Indicate subset used]. Boulder, Colorado USA. NASA National Snow and Ice Data Center Distributed Active Archive Center. doi:https://doi.org/10.5067/MEASURES/CRYOSPHERE/nsidc-0477.004. [Date Accessed]

Kim Y, Kimball JS, Zhang K, Didan K, Velicogna I, McDonald KC (2014) Attribution of divergent northern vegetation growth responses to lengthening non-frozen seasons using satellite optical-NIR and microwave remote sensing. Int J Remote Sens 35(10):3700–3721

Kim Y, Kimball JS, Zhang K, McDonald KC (2012) Satellite detection of increasing northern hemisphere non-frozen seasons from 1979 to 2008: Implications for regional vegetation growth. Remote Sens Environ 121:472–487

Kim Y, Kimball JS, McDonald KC, Glassy J (2011) Developing a global data record of daily landscape freeze/thaw status using satellite passive microwave remote sensing. IEEE Trans Geosci Remote Sens 49(3):949–960

Kim Y, Huete AR, Miura T, Jiang Z (2010) Spectral compatibility of vegetation indices across sensors: band decomposition analysis with Hyperion data. J Appl Remote Sens 4:043520

Kimball J S, Jones L A, Glassy J, Reichle R (2017) SMAP L4 Global Daily 9 km Carbon Net Ecosystem Exchange, Version 3. [Indicate subset used]. Boulder, Colorado USA. NASA National Snow and Ice Data Center Distributed Active Archive Center. doi:https://doi.org/10.5067/O4HAQJEWWUU8. [Date Accessed]

Kimball JS, Jones LA, Glassy J, Stavros EN, Madani N, Reichle RH, Jackson T, Colliander A (2016) Soil moisture active passive mission L4_C data product asssessment (version 2 validated release), Greenbelt, MD, NASA Goddard Space Flight Center, USA. [online] Available: https://ntrs.nasa.gov/archive/nasa/casi.ntrs.nasa.gov/20160008108.pdf

Kimball JS, Jones LA, Zhang K, Heinsch FA, McDonald KC, Oechel WC (2009) A satellite approach to estimate land-atmosphere CO2 exchange for boreal and arctic biomes using MODIS and AMSR-E. IEEE Trans Geosci Remote Sens 47(2):569–587

Kolk H, Heijmans MMPD, Huissteden J, Pullens JWM, Berendse F (2016) Potential arctic tundra vegetation shifts in response to changing temperature, precipitation and permafrost thaw. Biogeosciences 13:6229–6245

Liljedahl AK, Boike J, Daanen RP, Fedorov AN, Frost GV, Grosse G, Hinzman LD, Iijma Y, Jorgenson JC, Matveyeva N, Necsoiu M, Raynolds MK, Romanovsky VE, Schulla J, Tape KD, Walker DA, Wilson CJ, Yabuki H, Zona D (2016) Pan-Arctic ice-wedge degradation in warming permafrost and its influence on tundra hydrology. Nat Geosci 9:312–318

Loranty MM, Lieberman-Cribbin W, Berner LT, Natali SM, Goetz SJ, Alexander HD, Kholodov AL (2016) Spatial variation in vegetation productivity trends, fire disturbance, and soil carbon across arctic-boreal permafrost ecosystems. Environ Res Lett 11(9):095008

Luus KA, Commane R, Parazoo NC, Benmergui J, Euskirchen ES, Frankenberg C, Joiner J, Lindaas J, Miller CE, Oechel WC, Zona D, Wofsy S, Lin JC (2017) Tundra photosynthesis captured by satellite-observed solar-induced chlorophyll fluorescence. Geophys Res Lett 44:1564–1573

Madani N, Kimball JS, Jones LA, Parazoo NC, Guan K (2017) Global analysis of bioclimate controls on ecosystem productivity using satellite observations of solar-induced chlorophyll fluorescence. Remote Sens 9:530

Malnes E, Karlsen SR, Johansen B, Bjerke J, Tommervik H (2016) Snow season variability in a boreal-Arctic transition area monitored by MODIS data. Environ Res Lett 11:125005

McGuire AD, Chapin FSIII, Ruess R (2010) The dynamics of change in Alaska's boreal forests: resilience and vulnerability in response to climate warming. Can J For Res 40(7):1195–1196

McGuire AD, Anderson LG, Christensen TR, Dallimore S, Guo L, Hayes DJ, Heimann M, Lorenson TD, Macdonald RW, Roulet N (2009) Sensitivity of the carbon cycle in the Arctic to climate change. Ecol Monogr 79(4):523–555

Meroni M, Rossini M, Guanter L, Alonso L, Rascher U, Colombo R, Moreno J (2009) Remote sensing of solar-induced chlorophyll fluorescence: review of methods and applications. Remote Sens Environ 113:2037–2051

Miles VV, Esau I (2016) Spatial heterogeneity of green and browning between and within bioclimatic zones in northern West Siberia. Environ Res Lett 11:115002

Morton DC, Le Page Y, DeFries R, Collatz GJ, Hurtt GC (2013) Understorey fire frequency and the fate of burned forests in southern Amazonia. Phil Trans R Soc B 368: 20120163. http://dx.doi.org/10.1098/rstb.2012.0163

Mu Q, Heinsch FA, Zhao M, Running SW (2007) Development of a global evapotranspiration algorithm based on MODIS and global meteorology data. Remote Sens Environ 111:519–536

Parazoo NC, Arneth A, Pugh TAM, Smith B, Steiner N, Luus K, Commane R, Benmergui J, Stofferahn E, Liu J, Rodenbeck C, Kawa R, Euskirchen E, Zona D, Arndt K, Oechel W, Miller C (2018) Spring photosynthetic onset and net CO_2 uptake in Alaska triggered by landscape thawing. Glob Change Biol 24:3416–3435

Parazoo CN, Bowman K, Fisher JB, Frankenberg C, Jones DBA, Cescatti A, Perez-Priego O, Wohlfahrt G, Montagnani L (2015) Terrestrial gross primary production inferred from satellite fluorescence and vegetation models. Glob Change Biol 20:3103–3121

Park H, Kim Y, Kimball JS (2016a) Widespread permafrost vulnerability and soil active layer increases over the high northern latitudes inferred from satellite remote sensing and process model assessments. Remote Sens Environ 175:349–358

Park H, Yoshikawa Y, Oshima K, Kim Y, Ngo-duc T, Kimball JS, Yang D (2016b) Quantification of warming climate-induced changes in terrestrial arctic river ice thickness and phenology. J Clim 29:1733–1754

Pearson RG, Phillips SJ, Loranty MM, Beck Beck P S A, Damoulad T, Knight SJ, Goetz SJ (2013) Shifts in Arctic vegetation and associated feedbacks under climate change. Nat Clim Change 3:673–677

Phoenix GK, Bjerke JW (2016) Arctic browning: extreme events and trends reversing arctic greening. Glob Change Biol 22:2960–2962

Piedallu C, Gégout J (2008) Efficient assessment of topographic solar radiation to improve plant distribution models. Agric For Meteorol 148(11):1696–1706

Potter C (2014) Regional analysis of NASA satellite greenness trends for ecosystems of Arctic Alaska. Int J Geosci 5:997–1006

Reichle R, De Lannoy G, Koster RD, Crow WT, Kimball JS, Liu Q (2018) SMAP L4 Global 3-hourly 9 km EASE-Grid Surface and Root Zone Soil Moisture Geophysical Data, Version 4. [Indicate subset used]. Boulder, Colorado USA. NASA National Snow and Ice Data Center Distributed Active Archive Center. https://doi.org/10.5067/KPJNN2GI1DQR

Rogers BM, Solvik K, Hogg EH, Ju J, Masek JG, Michaelian M, Berner LT, Goetz SJ (2018) Detecting early warning signals of tree mortality in boreal North America using multiscale satellite data. Glob Change Biol 24:2284–2304

Rogers BM, Soya AJ, Goulden ML, Randerson JT (2015) Influence of tree species on continental differences in boreal fires and climate feedbacks. Nat Geosci 8:228–234

Schimel D, Pavlick R, Fisher JB, Asner GP, Saatchi S, Townsend P, Miller C, Frankenberg C, Hibbard K, Cox P (2015) Observing terrestrial ecosystems and the carbon cycle from space. Glob Change Biol 21(5):1762–1776. https://doi.org/10.1111/gcb.12822

Screen JA (2017) Far-flung effects of Arctic warming. Nat Geosci 10:253–254

Shabanov N, Vargas M, Miura T, Sei A, Danial A (2015) Evaluation of the performance of Suomi NPP VIIRS top of canopy vegetation indices over AERONET sites. Remote Sens Environ 162:29–44

Shi H, Li L, Eamus D, Huete A, Cleverly J, Tian X, Yu Q, Wang S, Montagnani L, Magliulo V, Rotenberg E, Pavelka M, Carrara A (2017) Assessing the ability of MODIS EVI to estimate terrestrial ecosystem gross primary production of multiple land cover types. Ecol Ind 72:153–164

Sitch S, McGuire AD, Kimball J, Gedney N, Gamon J, Engstrom R, Wolf A, Zhuang Q, Clein J, McDonald KC (2007) Assessing the carbon balance of circumpolar arctic tundra using remote sensing and process modeling. Ecol Appl 17(1):213–234

SNAP (2012) Predicting Future Potential Climate-Biomes for the Yukon, Northwest Territories, and Alaska (https://www.snap.uaf.edu/attachments/Cliomes-FINAL.pdf)

Sulla-Menashe D, Woodcock CE, Friedl MA (2018) Canadian boreal forest greening and browning trends: an analysis of biogeographic patterns and the relative roles of disturbance versus climate drivers. Environ Res Lett 13:014007

Tachikawa T, Hato M, Kaku M, Iwasaki A (2011) The characteristics of ASTER GDEM version 2, IGARSS

Tape K, Sturm M, Racine C (2006) The evidence for shrub expansion in Northern Alaska and the Pan-Arctic. Glob Change Biol 12:686–702. https://doi.org/10.1111/j.1365-2486.2006.01128.x

Ueyama M, Iwata H, Harazono Y, Euskirchen ES, Oechel WC, Zona D (2013) Growing season and spatial variations of carbon fluxes of Arctic and boreal ecosystems in Alaska (USA). Ecol Appl 23(8):1798–1816

Verbyla D (2015) Remote sensing of interannual boreal forest NDVI in relation to climatic conditions in interior Alaska. Environ Res Lett 10:125016

Vermote EF, El Saleous NZ, Justice CO (2002) Atmospheric correction of MODIS data in the visible to middle infrared: first results. Remote Sens Environ 83:97–111

Vickers H, Hogda KA, Solbo S, Karlsen SR, Tommervik H, Aanes R, Hansen BB (2016) Changes in green in the high Arctic: insights from a 30 year AVHRR max NDVI dataset for Svalbard. Environ Res Lett 11:105004

Wagle P, Zhang Y, Jin C, Xiao X (2016) Comparison of solar-induced chlorophyll fluorescence, light-use efficiency, and process-based GPP models in maize. Ecol Appl 26(4):1211–1222

Walker X, Johnstone JF (2014) Widespread negative correlations between black spruce growth and temperature across topographic moisture gradients in the boreal forest

Walther S, Guanter L, Heim B, Jung M, Duveiller G, Wolanin A, Sachs T (2018) Assessing the dynamics of vegetation productivity in circumpolar regions with different satellite indicators of greenness and photosynthesis. Biogeosciences https://doi.org/10.5194/bg-2018-196

Wang C, Chen J, Wu J, Tang Y, Shi P, Black TA, Zhu K (2017) A now-free vegetation index for improved monitoring of vegetation spring green-up date in deciduous ecosystems. Remote Sens Environ 196:1–12

Xu L, Myneni RB, Chapin FS III, Callaghan TV, Pinzon JE, Tucker CJ, Zhu Z, Bi J, Ciais P, Tommervik H, Euskirchen ES, Forbes BC, Piao SL, Anderson BT, Ganguly S, Nemani RR, Goetz SJ, Beck PSA, Bunn AG, Cao C, Stroeve JC (2013) Temperature and vegetation seasonality diminishment over northern lands. Nat Clim Change 3:581–586

Yang X, Tang J, Mustard JF, Lee JE, Rossini M, Joiner J, Munger JW, Kornfeld A, Richardson AD (2015) Solar-induced chlorophyll fluorescence that correlates with canopy photosynthesis on diurnal and seasonal scales in a temperate deciduous forest. Geophys Res Lett 42:2977–2987

Yi Y, Kimball JS, Rawlins MA, Moghaddam M, Euskirchen ES (2015) The role of snow cover affecting boreal-arctic soil freeze-thaw and carbon dynamics. Biogeosciences 12:5811–5829

Yi Y, Kimball JS, Reichle RH (2014) Spring hydrology determines summer net carbon uptake in northern ecosystems. Environ Res Lett 9:046003

Yi Y, Kimball JS, Jones LA, Reichle RH, Nemani R, Margolis HA (2013) Recent climate and fire disturbance impacts on boreal and arctic ecosystem productivity estimated using a satellite-based terrestrial carbon flux model. J Geophys Res-Biogeosci 118:606–622

Zhang K, Kimball JS, Kim Y, McDonald KC (2011) Changing freeze-thaw seasons in northern high latitudes and associated influences on evapotranspiration. Hydrol Process 25(26):4142–4151

Zhang K, Kimball JS, Hogg EH, Zhao M, Oechel WC, Cassano JJ, Running SW (2008) Satellite-based model detection of recent climate-driven changes in northern high-latitude vegetation productivity. J Geophys Res-Biogeosci 113:G03033

Zhang Y, Xiao X, Wu X, Zhang G, Qin Y, Dong J (2017) Data descriptor: a global moderate resolution dataset of gross primary production of vegetation for 2000–2016. Sci Data 4:170165

Zhao M, Running SW, Heinsch FA, Nemani RR (2011) MODIS derived terrestrial primary production. In: Land remote sensing and global environmental change. Springer, New York, pp 635–660. http://dx.doi.org/10.1007/978-1-4419-6749-7_28

Dr. Youngwook Kim is a Research Scientist in the Numerical Terradynamic Simulation Group at the University of Montana. He received the Ph.D. in soil, water, and environmental science with remote sensing and spatial analysis focus. His research focuses on the development of biophysical and geophysical data records with the integration of optical and microwave remote sensing. He has contributed to assess climate and environmental change impacts on global terrestrial carbon, water, and energy cycles. He has served on the NASA Soil Moisture Active Passive (SMAP) freeze/thaw algorithm development team.

Dr. John S. Kimball is a Professor of Systems Ecology in the College of Forestry and Conservation at the University of Montana (UM). He is also Director of the Numerical Terradynamic Simulation Group (NTSG), a UM research center pioneering the use of remote sensing and computational ecology for quantifying and understanding environmental change. He received the Ph.D. in Bioresource Engineering from Oregon State University in 1995, working to improve physical process modeling of vegetation, snow, and soil moisture-related impacts on land–atmosphere water–carbon–energy exchanges. He has contributed to more than 150 peer-reviewed scientific publications documenting and improving understanding of climate change-related environmental impacts, emphasizing boreal and Arctic ecosystems. He is an IEEE Senior Member and has served on several NASA mission Science Teams developing new satellite retrievals, operational land products, and applications to meet NASA Earth Science objectives.

Dr. Nicholas Parazoo received a Bachelor's in Environmental Science at Oregon State University (2004) and Ph.D. in Atmospheric Science at Colorado State University (2011). His research focuses on the interaction of terrestrial ecosystems with the planet's climate through breathing in and out of CO2 by photosynthesis and respiration. He specializes in using remote sensing observations with carbon models to quantify CO2 exchanges toward improved understanding of their sensitivity to climate, with emphasis on northern boreal and tundra ecosystems where carbon–climate feedbacks are large, observations are sparse, and process understanding is limited.

Peter Kirchner is the Physical Scientist for the Southwest Alaska Inventory and Monitoring Network of the National Park Service and affiliate faculty at the University of Montana. He has over 25 years of experience researching and communicating the relationships between the climate and ecologic, hydrologic, and biogeochemical processes through the integration of ground-based and remote sensing observations.

Boreal Forest and Forest Fires

21

Yongwon Kim, Hideki Kobayashi, Shin Nagai, Masahito Ueyama, Bang-Yong Lee, and Rikie Suzuki

Abstract

Boreal forest has played a role as sink of atmospheric CO_2 due to the slow growth of black spruce; however, changes in source of atmospheric CO_2 by forest fires and recent warming have significantly triggered modulation in physiological ecology and biogeochemistry over the boreal forest of Alaska. This chapter describes recent research findings in boreal forest ecosystem of

Y. Kim (✉)
International Arctic Research Center, University of Alaska Fairbanks, Alaska, AK, USA
e-mail: kimywjp@gmail.com

H. Kobayashi · S. Nagai · R. Suzuki
Japan Agency for Marine-Earth Science and Technology, Research Institute for Global Change, Institute of Arctic Climate and Environment Change Research, Yokohama, Japan
e-mail: hkoba@jamstec.go.jp

S. Nagai
e-mail: nagais@jamstec.go.jp

S. Nagai
Japan Agency for Marine-Earth Science and Technology, Research Institute for Global Change, Yokohama, Kanagawa, Japan

M. Ueyama
Graduate School of Life and Environmental Sciences, Osaka Prefecture University, Osaka, Japan
e-mail: ueyama@envi.osakafu-u.ac.jp

B.-Y. Lee
Division of Polar Climate Sciences, Korea Polar Research Institute (KOPRI), Incheon, South Korea
e-mail: bylee@kopri.re.kr

D. Yang and D. L. Kane (eds.), *Arctic Hydrology, Permafrost and Ecosystems*,
https://doi.org/10.1007/978-3-030-50930-9_21

Alaska: (1) the forest aboveground biomass (AGB) with field survey data and satellite data, (2) latitudinal gradients of phenology with time-lapsed camera and satellite data, (3) spatio-temporal variation of leaf area index (LAI) with the analysis of satellite data, (4) latitudinal distribution of winter and spring season soil CO_2 emission, and (5) successional changes in CO_2 and energy balance after forest fires. As a result, mapping of forest AGB is useful for the evaluation of vegetation models and carbon stock in the biogeochemical cycle. Latitudinal distribution of phenology understands the recent and future phenological changes including post-fire recovery forests. Interannual variation of LAI shows the leaf dynamics and near-surface remote-sensing approaches with the analyses of time-lapsed digital camera and satellite data. Spring carbon contributions are sensitive to subtle changes in the onset of spring. Vegetation recovery after forest fire is the major driver of the carbon balance in the stage of early succession. Increasing soil carbon emission in response to abrupt climate warming in Alaska is a significant driver of carbon balance.

21.1 Introduction

Boreal forest, also called taiga that represents "a marshy forest in Siberia" in Russia, is the largest terrestrial ecosystem on Earth, covering 17% of the planet's land surface area in a circumpolar belt of far Northern Hemisphere (Apps and Prices 1996; Kasischke and Stocks 2000). Boreal forest contains approximately 66% of the world's forest soil carbon pools (Van Cleve et al. 1983; Billings 1997; Oechel and Vourlitis 1997; Kasischke and Stocks 2000). Because boreal forests absorb atmospheric carbon dioxide and slowly decompose the litter, fibric, and humic substances, the ecosystems are known as carbon sinks (Schlesinger 1997; Fan et al. 1998). Boreal forest is found throughout the high northern latitudes, between the tundra and the temperate forest, from about 50°N to 70°N, stretching across the interiors of Siberia, northern Asia, and northern Europe, and occupying millions of acres of North America. Also, boreal forest is characterized by the dominantly coniferous species like pine (*Pinus*), spruce (*Pices*), larch (*Larix*), and fir (*Abies*), and deciduous species such as birch (*Betula*), poplar/aspen (*Poplus*), and alder (*Alnus*). Understory plants of boreal forest are inhabited different kinds of shrubs, mosses, lichens, and ferns (Vitt et al. 1988; Johnson et al. 1995). These species have adapted to short growing seasons with long days and very cold winters with short days and persistent snowpack. Further, discontinuous permafrost, dominating 50–90% of boreal forest, distributes under the boreal coniferous forests that are situated in the north slope of forests (AMAP 2017).

In Alaska, boreal forest exists in the Interior Alaska lands between the Brooks Ranges in the north and the Alaska Ranges in the south. At higher elevations within the broad range of the boreal forest ecosystem are pockets of alpine tundra vegetation, and along the margins of the ranges, it intergrades with lowland or arctic

tundra. Black spruce communities are widely distributed in boreal Alaska. Around 30–40% of Alaska's landscape is boreal black spruce forest (Barney and Stocks 1983), which is the most common boreal forest type in Interior Alaska (Viereck et al. 1992; Cronan et al. 2012). Alaskan black spruce communities typically occur on cold, poorly drained, nutrient-poor sites with a shallow permafrost layer; hence, the productivity is usually low (Viereck et al. 1992). The most common black spruce types are broadly divided into upland and lowland types. Typically, upland types occupy low gradient or north slopes, while lowland types occupy broad valleys or old river terraces. Less common types are productive black spruce forests on south slopes and black spruce-lichen woodlands.

Forest fire, which is largely controlled by local weather and vegetation, is a major disturbance in boreal forests with its occurrence closely coupled to climate patterns. Therefore, changes in climate will result in change in the fire regimes. Although boreal forests are presently one of the major terrestrial carbon pools, shifts in the fire regime and ecosystem distribution in high latitudes associated with climate change are likely to result in significant increases in atmospheric concentrations of carbon dioxide and other greenhouse gases (Kasischke et al. 1995, 2000a, b; Kasischke 2000; Richter et al. 2000; Kim and Tanaka 2003; Himzman et al. 2003). As boreal forests emit higher concentrations of carbon to the atmosphere immediately after the fire, forest fires in the northern stands are well known as carbon sources (Seiler and Crutzen 1980; Crutzen and Andreae 1990; Levine 1991; Kasischke et al. 2000b, c). Hansen et al. (1996) showed that, based on the average temperature over the past 30 years, the most significant areas of warming coincide with the region occupied by the boreal forest. Given the close linkage between fire occurrence and climate, there should be little surprise that over the past two decades, there has been a significant increase (almost threefold) in the annual area burned in the North American boreal forest (Kasischke and Stocks 2000). Interestingly, boreal black spruce communities need the fire by alternatively lightening and/or human-cause for the next generation. The survival strategy of black spruce forest is to (1) dangle the cones in the top of stem, (2) ignite the dead branches as a fuel in the bottom stem by the fire, (3) move a fire from bottom to top of stem, (4) activate the cones by a fire, (5) open physiologically the cones after the extinguishment, and (6) scatter the seeds by wind and settle down the seeds on the burned soil surface for seeding. The forest fire is called "crown fire" in boreal black spruce communities. On the other hand, the fire in larch forest of Siberia is "ground fire". Fire return time ranges from 50 to 500 years (Yarie 1981; Dyrness et al. 1986; Kasische et al. 1995; Kasischke and Stocks 2000; Lynch et al. 2003). This fire regime is highly variable because of its sensitivity to vegetation, topography, climate (especially short-term extreme fire-weather events), and human activities (as both a source of ignition and an agent of fire control) (Kasischke et al. 1995; Stocks et al. 2003; Dissing and Verbyla 2003).

Alaska fire history since 1940 is concentrated in boreal forest, Interior Alaska between Alaska Ranges and Brooks Ranges (Fig. 21.1). It is clear that boreal forest of Alaska has ever damaged by the forest fire. Hence, recent boreal forests are mostly the secondary forest regenerated through the ecologically successional stages after the forest fires.

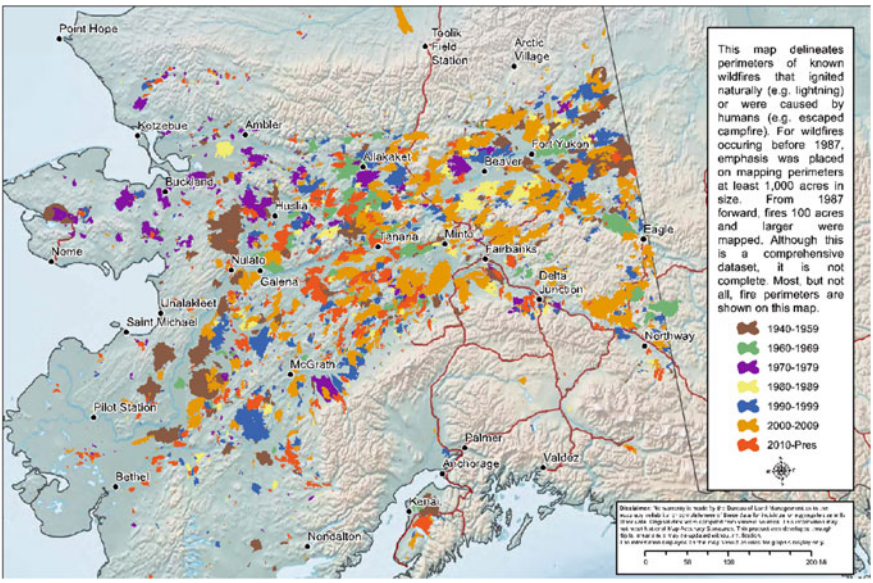

Fig. 21.1 Alaska fire history from 1940 to present Alaska Interagency Coordination Center (2018)

In this chapter, we describe recent research and understanding of: (1) the change in aboveground biomass with the analysis of field data and remote-sensing satellite data, (2) the latitudinal gradients of snow-on and snow-off dates with time-lapsed camera and remote-sensing data, (3) the spatio-temporal variations of normalized deviation vegetation index (NDVI) and leaf area index (LAI), (4) spatial distribution of winter and spring soil CO_2 emissions along the trans-Alaska pipeline, and finally (5) changes in carbon with soil chamber and eddy covariance tower methods in Interior Alaska after forest fire.

21.2 Recent Research and Results

21.2.1 Changes in Aboveground Biomass (AGB)

The carbon assimilation in woody components in boreal forests contributes to mitigate the global carbon cycles (IPCC 2014). Assimilated carbon in woody (forest biomass) represents the available biological resources. Wildfires alter boreal forest landscapes in Interior Alaska, thus causes the long-term changes in forest biomass distribution. Remote-sensing technologies are expected to provide the geographical patterns in forest biomass distribution from space. In remote-sensing observation, forest biomass specifically indicates the dry weight of biomass. As the remote-sensing techniques are only able to apply for the targets seen from satellite,

aboveground biomass (AGB) is often used as the representative term. AGB is further divided into trunk, branch, and leaf biomasses and their allometries depend on the tree species.

Microwave synthetic aperture radar (SAR) is one of the promising remote-sensing information for AGB estimation. SAR is an active microwave sensor. The emitted microwave pulses from the orbital satellite antennas reach to the Earth's surface and is backscattered. The intensity of the backscattered signal contains the land surface structure such as forest characteristics including AGB (e.g., Ulaby et al. 1986; Belchansky 2004). Because microwaves are less affected by cloud cover, SAR technology provides the all-weather signals in regions where cloud cover is high, such as boreal forest regions. The SAR backscatter is characterized by the polarized (horizontal or vertical) combinations of the transmitted and received signals. The "HH" mode indicates the combination of a horizontally (H) polarized transmitted signal and a horizontally (H) polarized received signal. "HV" stands for the combination of a horizontally polarized (H) transmitted signal and a vertically polarized (V) received signal. Generally, the sensitivity of the backscatter intensity to the biophysical parameters of land surface vegetation is examined in different combinations of polarized modes. The L-band SAR data have been used for the AGB estimation from tropical to boreal forest ecosystems (Suzuki et al. 2013). The forest regrowth monitoring after the fire disturbance was also explored (Kasischke et al. 2011). However, current SAR-based AGB estimation methods rely on the regression between SAR signals and ground-based AGB samples. Therefore, the ground-based AGB surveys with diverse forest growth stage are of particular importance.

Tree census survey is the most common approach to obtain canopy height, diameter of breast height (DBH), and other ancillary information and thus is the best method to obtain reliable AGB at site scale. However, tree census survey is very labor-intensive, which impede to conduct the data acquisition from multiple sites, such as post-fire regrowth to mature stage forests. The Bitterlich angle-count sampling method is a sampling method of the total basal area within the forest plot. By combining the Bitterlich method with allometry equation, AGB is also estimated. Details of this method are summarized in Osumi (1987) and Nagumo and Minowa (1990). The Bitterlich survey only takes approximately 30 min for one forest plot, thus it enables to obtain the AGB from various forest stands. Figure 21.2 shows the geographical distribution of Bitterlich sampling locations in Interior Alaska, along the Dalton Highway from Fairbanks (64° 51′N, 147° 51′W) to the foothill of Brooks Ranges (67° 59′N, 149° 45′W).

The AGBs listed in Table 21.1 are the summary of the Bitterlich survey for the 29 locations. Allometric equations derived by Yarie et al. (2007) were used for the AGB calculation of the dominant tree species in Interior Alaska. In addition to the Bitterlich surveys, conventional census survey (the fixed plot method) is performed at the site #8. Thus, DBH and tree height measurements of all trees (284 tree stands) in the 25 m by 25 m plot were performed. From the comparison of two approaches, it is found that the AGB estimation by the Bitterlich method was slightly higher than that of the fixed plot method (4–22%). However, the difference was fairly

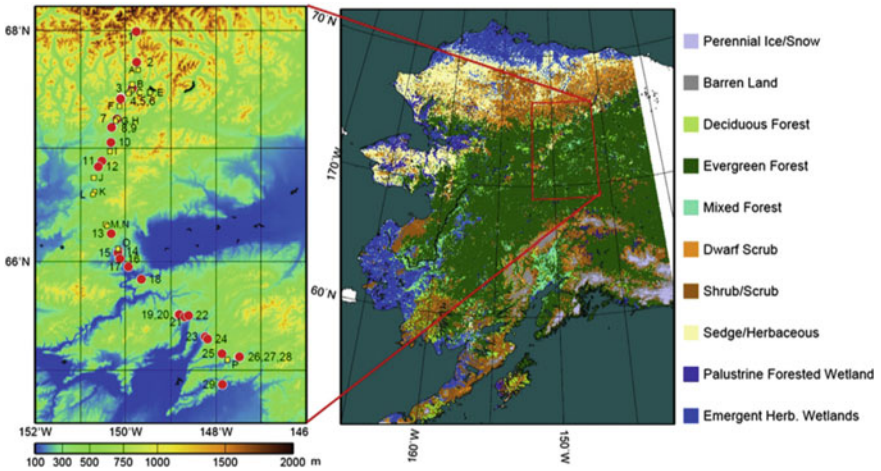

Fig. 21.2 The 29 sampling forest locations (red circles) and the 16 non-forest sites for the background information (yellow dots) in Interior Alaska (left). The land cover is classified according to the U.S. National Land Cover Database 2001 (right) (after Suzuki et al. 2013)

small, suggesting the multi-site Bitterlich surveys are reliable around the site #8. Due to severe climate situations, AGBs from the spruce forest sites were generally small. The range of AGBs and tree densities were from 2.2 Mg ha^{-1}, to 1266 trees ha^{-1} (site #5) and 116.2 Mg ha^{-1} to 814 trees ha^{-1} (#16). The fire history affects the spruce forest structures. The forest site #17 was a relatively young forest after wildfires and was the densest (11263 trees ha^{-1}), medium AGB (81.7 Mg ha^{-1}), and low tree height (average = 5.9 m).

The phased array type L-band synthetic aperture radar (PALSAR) onboard the advanced land observing satellite (ALOS) is one of L-band microwave SAR sensor. The sampling footprint is 20 m by 10 m (Rosenqvist et al. 2007). The digital number (DN) values (arbitrary backscattering intensity) from two polarization modes (HV and HH) were converted to a normalized radar cross-section (NRCS), that is, σ^0_{HV} and σ^0_{HH}. Details for the NRCS calculation were provided in Suzuki et al. (2013) and Shimada et al. (2009). The 20 scenes were merged into one continuous image, then manually identified the forest locations of the 29 forest and 16 non-forest (background) sites on the PALSAR images by visual interpretation. The relationship between σ^0_{HV} and AGB was regressed by logarithmic function. Figure 21.3 shows regression curvature for two polarization data sets (HV and HH). When regressing, the saturation level of the forest AGB has to be determined. The saturation level was defined as the value of AGB when the slope of the logarithmic regression curve decreased to 0.02 dB against 1% of the range (minimum to maximum) of the AGB obtained by the field survey.

The scatter-diagrams and logarithmic regression equations in Fig. 21.2 demonstrate the fitness of the relationships between the in situ forest AGB and satellite

Table 21.1 Location (latitude and longitude) of the forest sites, dominant tree species, and forest aboveground biomass (AGB)

Site ID	Latitude (N)	Longitude (W)	Dominant tree species	Forest AGB (Mg ha^{-1})	Tree density (ha^{-1})
1	67° 59′	149° 45′	White spruce	4.8	795
2	67° 44′	149° 45′	White spruce	31.9	740
3	67° 30′	149° 50′	White spruce	27.5	1228
4	67° 26′	150° 05′	White spruce	25.4	2063
5	67° 25′	150° 06′	White spruce	2.2	266
6	67° 25′	150° 06′	White spruce	20.8	1519
7	67° 15′	150° 11′	Black & white spruce	5.8	974
8	67° 10′	150° 17′	Black spruce	22.4	4740
9	67° 10′	150° 18′	Black spruce	35.0	2960
10	67° 02′	150° 19′	Black & white spruce	12.3	1475
11	66° 53′	150° 31′	Black spruce	4.3	1261
12	66° 50′	150° 36′	White spruce	69.8	916
13	66° 14′	150° 18′	Black & white spruce	24.8	2561
14	66° 05′	150° 09′	Black spruce	7.3	3035
15	66° 04′	150° 09′	Black spruce	12.6	2895
16	66° 01′	150° 07′	White spruce	116.2	814
17	65° 57′	149° 56′	Black spruce	81.7	11263
18	65° 50′	149° 38′	Black spruce	30.8	3848
19	65° 31′	148° 49′	Black spruce	66.9	7430
20	65° 31′	148° 48′	Black spruce	36.0	4269
21	65° 29′	148° 41′	Black spruce	40.1	5342
22	65° 30′	148° 36′	Black spruce	16.3	1403
23	65° 18′	148° 14′	Birch	100.2	946
24	65° 17′	148° 10′	Birch & white spruce	92.7	3292
25	65° 09′	147° 52′	Black spruce	15.3	1546
26	65° 07′	147° 29′	Black spruce	50.7	6013
27	65° 07′	147° 28′	Black spruce	6.6	1665
28	65° 07′	147° 28′	Black spruce	12.7	873
29	64° 51′	147° 51′	Black spruce	12.8	3432

signals $\left(\sigma^0_{\mathrm{HV}} \text{ and } \sigma^0_{\mathrm{HH}}\right)$. Because the in situ forest AGB values are weighted in a small size AGB range within 0 to 40 Mg ha^{-1}, the regression curvatures are highly skewed due to this clumped data. In order to overcome this issue, the regressions were performed with average AGB for each 5 Mg ha^{-1} AGB class denoted as open

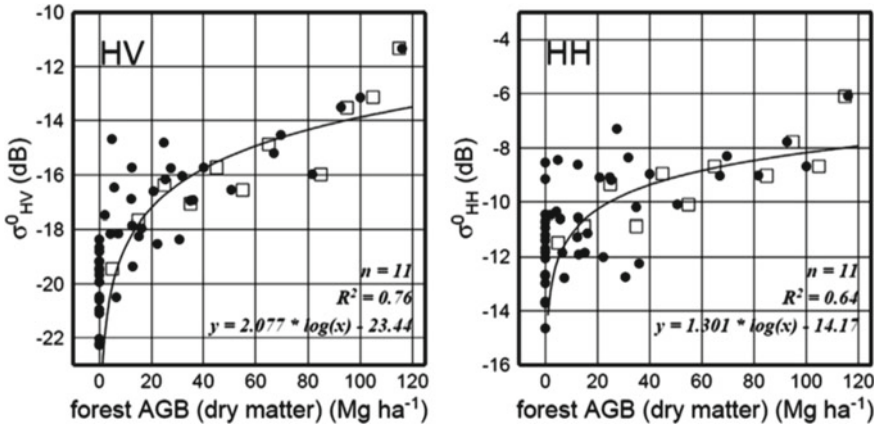

Fig. 21.3 Relationship between the in situ forest AGB and σ^0_{HV} (left) and σ^0_{HH} (right) of ALOS/PALSAR. Closed circles are the original values of the 45 sites. Open squares denote the mean σ^0 value for each forest AGB class (5 Mg ha^{-1} interval) (after Suzuki et al. 2013)

squares in Fig. 21.2. This demonstrates that the saturation level of σ^0_{HV} is higher than that of σ^0.

The spatial distribution of forest AGB was estimated from ALOS/PALSAR data and the regression equations (Fig. 21.3). The geographical and latitudinal distribution of the forest AGB (Fig. 21.4) are presented well in the AGB map, but some erroneous values due to "foreshortening" cannot be avoided in the slope surfaces (e.g., Shimada 2010). Although the accurate correction of the slope effect is challenging, the slope correction improves the spatial representativeness of the AGB in Interior Alaska. Maps of forest AGB can be useful for the evaluation of forest ecosystem and vegetation models (Le Toan et al. 2004). AGB maps are also useful to evaluate the carbon stock in the context of the global biogeochemical cycle in pre- and post-fire landscapes.

21.2.2 Multi-scale Phenology Observation in Boreal Forest Ecosystems

Phenology is defined as recursive events of plants. Leaf, flower, and other activities have their own phenological patterns. Seasonal leaf area changes are useful information in the context of terrestrial carbon cycles and climate change. Reliable evaluation of start of growing season (SOS), end of growing season (EOS), and growing season length is essential to understand how terrestrial vegetation responds to climate changes (Buermann et al. 2014; Keenan et al. 2014; Nagai et al. 2013; Piao et al. 2011; Richardson et al. 2013a; Schwartz et al. 2013; Verbyla 2008; Xu et al. 2013). It is also important to understand how forest fires alter the plant species

compositions, their recovery, and phenology timings (Tsuyuzaki et al. 2009, 2013; Kobayashi et al. 2016). In boreal forests and tundra regions, there are several evidences that the SOS timings were advanced (Buermann et al. 2014; Delbart et al. 2008; Hogda et al. 2013; Myneni et al. 1997; Piao et al. 2011). On the other hand, trends in EOS are less studied due to very limited ground-based information (Jeong and Medvigy 2014). Some recent studies showed a trend for later EOS in Europe (Garonna et al. 2014), North America (Zhu et al. 2012), and for temperate vegetation over the northern hemisphere (Jeong et al. 2011). However, it is not clear whether the environmental factors (e.g., photoperiods and temperature changes) actually influence the changes in EOS (Delpierre et al. 2009; Jeong and Medvigy 2014; Richardson et al. 2013b).

Satellite observation is necessary to quantify the actual plant phenology over large area. The satellite estimation utilizes the vegetation indices such as normalized difference vegetation index (NDVI = (NIR – Red)/(NIR + Red)), where NIR and Red are reflectances in near-infrared and red spectral regions. Satellite method provides the continental scale geographical patterns in phenology. However, several issues remained. First, SOS and EOS estimated to quantify how much spring snowmelt and autumn snow condition affects the satellite signal and phenology retrievals. Second, frequent cloud appearance prevents from retrieving the sufficient number of surface reflectances, making it difficult to determine phenology timings.

Boreal forests in Alaska are extremely sparse. Large amount of sunlight reaches the understory layer, making the understory layer bright. In other words, understory plants greatly affect the phenology and seasonality obtained by satellite (Pisek and Chen 2009; Rautiainen and Heiskanen 2013; Yang et al. 2014). In Interior Alaska, evergreen needles such as black and white spruce are the dominant species. Satellite phenology observation is greatly influenced by understory plant phenology. However, the effect of overstory and understory on satellite-based phenology is less investigated. Recent time-lapse camera networks enable to obtain the ground-truth of the phenology timings in various forest and tundra conditions including post-fire locations.

Alaskan boreal forest and tundra are located from a latitudinal range of 61°N–71°N (Fig. 21.5). This region is divided into two distinct ecosystems. Lower latitude zone (61°N–68°N) is covered by the evergreen coniferous and deciduous forests. The dominant tree species in the boreal zone is black spruce (*Picea mariana*). White spruce (*Picea glauca*) and aspen (*Populus tremuloides*) are also common (Chapin III et al. 2006). The understory layer is covered with rusty peat moss (*Sphagnum* spp.) and splendid feather moss (*Hylocomium splendens*). These species show highly variable colors (brown to green) spatially and seasonally. The understory layer is also partly covered with "tussocks". It consists of herbaceous perennial cotton grass (*Eriophorum vaginatum*) (Kim et al. 2013). The low shrubs and herbs such as Labrador tea (*Ledum groenlandicum*), bog bilberry (*Vaccinium uliginosum*), dwarf birch (*Betula nana*), and cloudberry (*Rubus chamaemorus*) are dominant deciduous vascular plants. Tundra is further divided into heath tundra and moist acidic tundra areas. The moist acidic tussock tundra is dominated by tussock

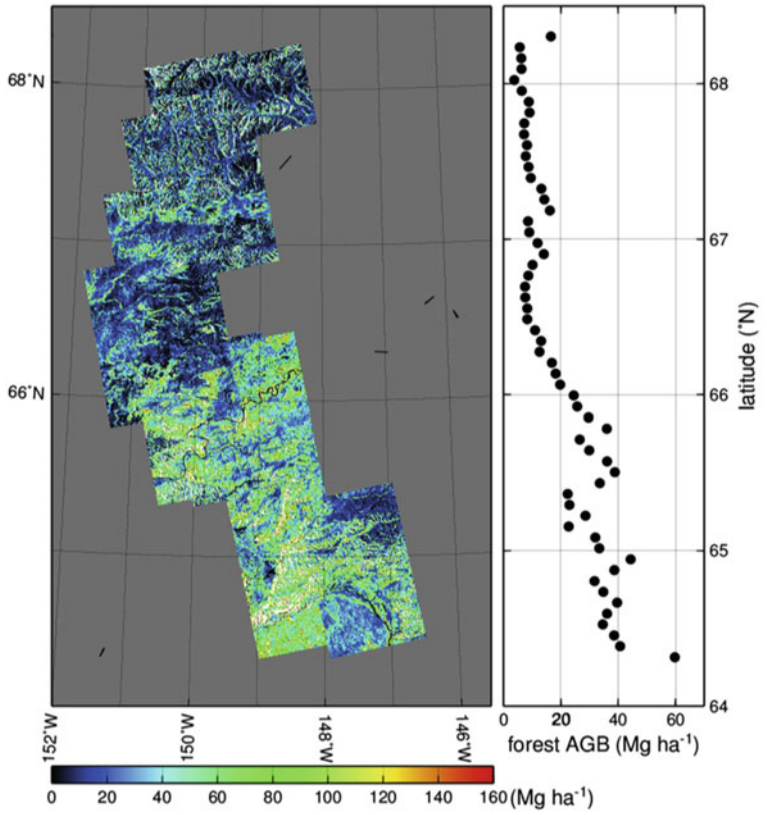

Fig. 21.4 Forest AGB distribution in Interior Alaska as estimated by ALOS/PALSAR backscatter intensity (HV) in summer of 2007 (Left). The latitudinal gradient of forest AGB (right) (after Suzuki et al. 2013)

sedge (*Eriophorum vaginatum*) and dwarf shrubs (*Betura nana, Carex bigelowii, Vaccinium vitis-idaea, and Ledum palustre*) (Euskirchen et al. 2012; Kim et al. 2014; Oechel et al. 2014). The dry heath tundra is dominated by *Dryas* spp., lichen, and dwarf shrubs (Euskirchen et al. 2012).

Time-lapse camera is a useful tool to track the seasonality of surface conditions. It has been widely used for the determination of phenological timings (Richardson et al. 2007; Woebbecke et al. 1995). The time-lapse camera system was used to quantify the phenology at 17 sites across Alaska (Fig. 21.5). The six northern sites are located in tundra and the other 11 sites are in boreal forests. In boreal forest sites, there is a site that was experienced by the large forest fire events in 2004 (Iwata et al. 2011, 2013). At these sites, there are three different time-lapse camera systems: GardenWatchCams (Brinno Inc., Taiwan), webcams, and a fish-eye camera (Nikon Coolpix 4500 with an FC-E8 fisheye lens). These camera systems

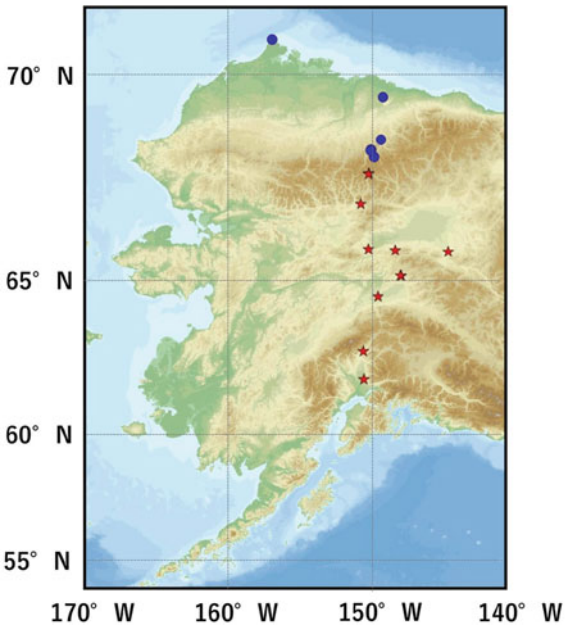

Fig. 21.5 Ground-based time-lapse camera locations in Interior Alaska and tundra zones

viewed the tundra and forest understory vegetation at a nadir or horizontal view with a sampling interval from 15 min to 6 h.

There are several global environmental satellites such as NOAA's Advanced Very High Resolution Radiometer (AVHRR), Moderate resolution imaging spectroradiometer (MODIS) on Terra and Aqua, SPOT-VEGETATION, Prova-V, and more recently Suomi-NPP's Visible Infrared Imaging Radiometer Suite (VIIRS), European Sentinel series (Sentinel-2 & 3), and Japanese Global Climate Observation Mission (GCOM-C). These satellites measure and produce a global terrestrial coverage every two- to three-day interval. To screen out the cloud-contaminated measurements in the surface reflectance data, 8–10 days composing is common, which is the method to extract the best quality of a sampling within a compositing period. The NDVI and normalized difference infrared index (NDII) were widely used for the phenology estimations, where NDII = (NIR − SWIR)/(NIR + SWIR) and SWIR is a shortwave infrared (wavelength of ∼1.6 μm). There are several satellite algorithms to determine SOS and EOS, for example, local NDVI threshold method (White et al. 1997), the NDII method (Delbart et al. 2005), and the sigmoid method (Zhang et al. 2003).

The phenology and snow cover conditions can be estimated by both satellites and time-lapse images. Figure 21.6 is the estimated phenology (SOS and EOS) and snow timings (snowmelt and continuous snow cover dates) in 2011. Phenology in boreal evergreen forest indicates the spring leaf emergence and autumn senescence timing of understory plants. The snowmelt in spring comes 16–19 days earlier than SOS estimated by the time-lapse camera and the satellite method. In autumn, the

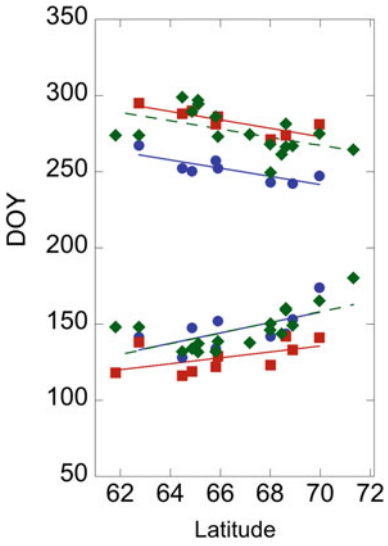

Fig. 21.6 Latitudinal gradients of SOS and EOS derived from satellite (green closed diamond) and time-lapse camera (blue open circle). The snowmelt and autumn snow coverage are also depicted (red closed square). The satellite SOS and EOS are derived by the average of three methods (the local threshold method, the NDII minimum method, and the sigmoid fitting method) from two satellites (Terra-MODIS and SPOT-VEGETATION). Details are provided in Kobayashi et al. (2016)

satellite EOS comes almost in the same timing with autumn snow coverage. However, the satellite EOS was 19–26 days later than the EOS by time-lapse camera. This result suggests that satellite EOS is mostly affected by the autumn snow events rather than the plant phenology (Fig. 21.6).

In spring phenology, satellite-based SOS is known to be partially affected by the snowmelt in boreal forests and tundra zones. Despite this issue, the satellite-based SOS may be related to leaf emergence in spring because leaf emergence (SOS) occurs soon after the snowmelt. The SOS accuracy depends on the degree of synchronism in snowmelt and leaf emergence timings.

For the EOS timings, camera-based EOS is not correlated well with the satellite-based EOS. The satellite-based EOS was more related to the timings of autumn snow coverage whereas the camera-based EOS was not entirely correlated with autumn snow coverage (Fig. 21.7). These results show the potential utility and limitation of the satellite-based phenology observation and also a usefulness of time-lapse camera networks. The rising temperature in the northern high latitudes is abrupt and strong. Regarding the key issues of boreal ecosystems in the context of climate change, plant phenology, spring green-up, and autumn senescence are essential information for regional and global carbon cycle. The satellite and

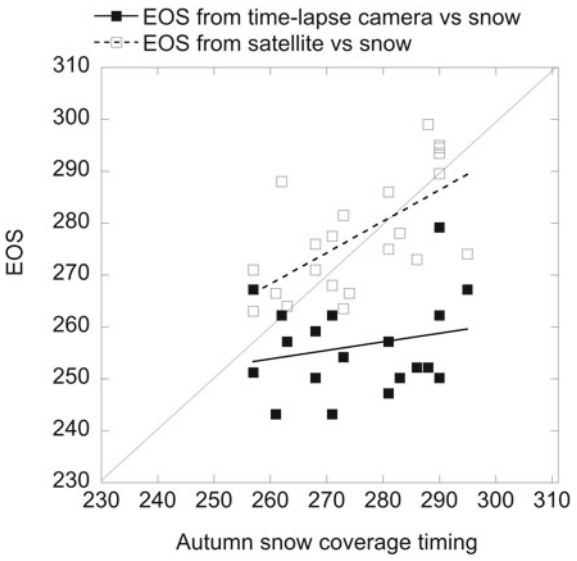

Fig. 21.7 The relationship between the autumn snow coverage timing and EOS. The correlation coefficients for the EOS from satellite and EOS from time-lapse camera are $R = 0.63$ ($p = 0.017$) and $R = 0.19$ ($p = 0.88$), respectively

ground-observation networks are thus very important in order to understand the future phenological changes including post-fire recovery forests.

21.2.3 Interannual Variations of Northern LAI

Leaf area index (LAI) is defined as one half of the total leaf area per unit of horizontal ground area ($m^2\ m^{-2}$). The annual maximum LAI in open-canopy forests in Alaska (with low aboveground biomass) is smaller than that in closed-canopy tropical forests (with high AGB) (Myneni et al. 2002; Zhu et al. 2013; Iio et al. 2014). In association with the characteristics of the timings and patterns of plant phenology, such as leaf-flush and leaf-fall among ecosystems and tree species, LAI shows interannual and seasonal variations (Nasahara et al. 2008; Muraoka et al. 2013; Nagai et al. 2017). Plant phenology affects carbon, water, and energy cycles through the CO_2 uptake by photosynthesis, latent and sensible heat by evapotranspiration, surface albedo, and aerodynamic roughness of land surface (Richardson et al. 2013a). To better understand the interaction between ecosystems and climate change in Alaska, accurate detection of spatio-temporal LAI variability is an important but challenging task.

LAI in forest ecosystems can be estimated by the direct method (e.g., counting leaves and leaf litter collection approaches; Eschenbach and Kappen 1996; Nasahara et al. 2008; Potithep et al. 2013; Iio et al. 2014; Nagai et al. 2017) and indirect method (i.e., near-surface and satellite remote-sensing approaches; Eschenbach and Kappen 1996; Myneni et al. 1997, 2002; Ueyama et al. 2006, Kobayashi and

Iwabuchi 2008; Nasahara et al. 2008; Ryu et al. 2010; Richardson et al. 2011; Muraoka et al. 2013; Potithep et al. 2013; Zhu et al. 2013).

Direct method is the "counting leave" approach, that is, to count the number of leaves within a target area from the canopy-access tower and measure the mean area of sampling leaves by using a leaf area meter. The LAI is then estimated by mean leaf area and number of leaves for a target area (Eschenbach and Kappen 1996). In the "leaf litter collection" approach, we divide the dry weighted leaf litter, which was sorted into each tree species, by the leaf mass per area (LMA) of each tree species. Seasonal variation in LAI for each tree species can be estimated by collecting and sorting leaf litter four or five times in autumn (Nasahara et al. 2008; Potithep et al. 2013; Nagai et al. 2017). On the other hand, we can evaluate LAI in spring by examining the relationship between LAI in autumn and seasonality of leaf phenology data, such as number of leaves per shoot and a leaf size for each tree species, which were periodically observed during a leafy period (Nasahara et al. 2008; Potithep et al. 2013; Nagai et al. 2017). The total LAI of overstory and understory tree species can be estimated by adding LAI for each tree species. Direct method allows obtaining nearly true value, but we require the canopy-access tower for counting the number of leaves and measuring leaf size, and field surveys are also not labor-intensive. For these reasons, it's not so easy to apply direct methods to multiple points.

The non-destructive "near-surface and satellite-remote sensing" approach is useful to evaluate LAI over a wide area. In the "near-surface remote-sensing" approach, LAI was estimated by measurement of the incident photosynthetically active photon flux density (PPFD) above the forest canopy and on the forest floor (Muraoka et al. 2013), analysis of digital hemispherical photography images (Ryu et al. 2010; Richardson et al. 2011), and measurement of the LAI-2000/2200C Plant Canopy Analyzer (Li-Cor Inc., USA; Ueyama et al. 2006; Nasahara et al. 2008; Ryu et al. 2010; Richardson et al. 2011). These methods are theoretically based on the "Monsi-Saeki theory" (Hirose 2005), which consists of the exponential relationship between the attenuation of light transmittance and stratification of plant biomass (leaves, stem, and branch). The estimated LAI in a leafy period is equal to plant area index (PAI), which includes leaves, stems, and branches. To estimate accurate LAI in forests, we should subtract the estimated LAI in a leaf-less period from the estimated LAI in a leafy period (i.e., PAI). However, non-destructive "near-surface remote sensing" approach allows estimating the interannual and seasonal variations in LAI at multiple points, where there are no canopy-access towers.

In an open-canopy black spruce (*Picea mariana*, evergreen coniferous) forest in Alaska, LAI above ground measured by the LAI-2000 Plant Canopy Analyzer was 2.4, while LAI above 1.0 m (i.e., measurement of only overstory vegetation) was 0.1–0.5 without a clear seasonality (Ueyama et al. 2006). The forest floor (i.e., understory vegetation) is covered by mosses and lichens (Ueyama et al. 2006). Accurate LAI in a forest ecosystem is the sum of understory (shrub and herb) and overstory vegetation (canopy trees). For this reason, the light transmittance above 1.0 m, which is a general measurement height of the LAI-2000/2200C Plant

Canopy Analyzer, causes underestimation of LAI in open-canopy forests. To estimate accurate LAI in open-canopy forests, at least we should measure the light transmittance above ground rather than above 1.0 m. We should also concern about the heterogeneity of understory and/or overstory vegetation at each measurement point.

In the "satellite remote-sensing" approach, LAI was estimated by the radiative-transfer model inputting the surface reflectance data (Kobayashi and Iwabuchi 2008) and by the empirical regression model based on the relationship between LAI and normalized difference vegetation index (NDVI) (Myneni et al. 1997; Potithep et al. 2013). In the former, we examine the relationship among azimuth angle of satellite sensor, solar zenith and azimuth angles, characteristic of canopy structure, and surface reflectance data observed by satellite remote sensing. We then theoretically estimate the LAI through its relationship. In the latter, we estimate the LAI by applying the NDVI–LAI relationship to satellite-observed NDVI. To develop the accuracy of both methods, we require abundant ground-truth in multiple points in various forest ecosystems for input, calibration, and validation parameters.

We can use long-term global LAI data sets estimated by the satellite remote sensing such as "LAI3g" (http://cliveg.bu.edu/modismisr/lai3g-fpar3g.html, 15-day temporal frequency, 1/12 degree spatial resolution, temporal span of July 1981 to December 2011, Zhu et al. 2013) and "MOD/MYD15 Leaf Area Index" (https://modis.gsfc.nasa.gov/data/dataprod/dataproducts.php?MOD_NUMBER=15, 8-day temporal frequency, 1 km spatial resolution, temporal span of February to current, Myneni et al. 2002). The "LAI3g" and "MOD/MYD15" data sets were used in canopy surface reflectance data observed by AVHRR sensors mounted on NOAA satellite series and MODIS sensors mounted on Terra and Aqua satellites, respectively. However, the canopy surface reflectance data in open-canopy forests in Alaska detect both understory and overstory vegetation, while that in closed-canopy forests in tropics detect only canopy-surface overstory vegetation. This fact indicates an importance that discrimination between LAI of understory vegetation (LAIu) and that of overstory vegetation is required to estimate accurate LAI in forest ecosystems on a global scale.

In an open-canopy evergreen coniferous forest in Alaska, seasonal variation in LAI is affected by plant phenology in understory vegetation, which showed clear interannual and seasonal variations (Fig. 21.8). Leaf-flush and leaf-fall in understory vegetation occurred late May (around day of year (DOY) 145) and middle September (around DOY 260), respectively. For instance, the timing of leaf-flush in understory vegetation in 2013 was later than other years, while the year-to-year variability of the timing of leaf-fall in understory vegetation was not so clear. In the high-altitude regions, satellite view angle and snow cover affected the seasonal variation in canopy surface reflectance data (Kobayashi et al. 2016). These facts suggest a possibility that canopy surface reflectance data including non-phenological elements mislead seasonal variation in LAI. To estimate the LAIu, the understory NDVI (NDVIu) was first retrieved in boreal forests using satellite-observed bidirectional reflectance distribution function data (Yang et al.

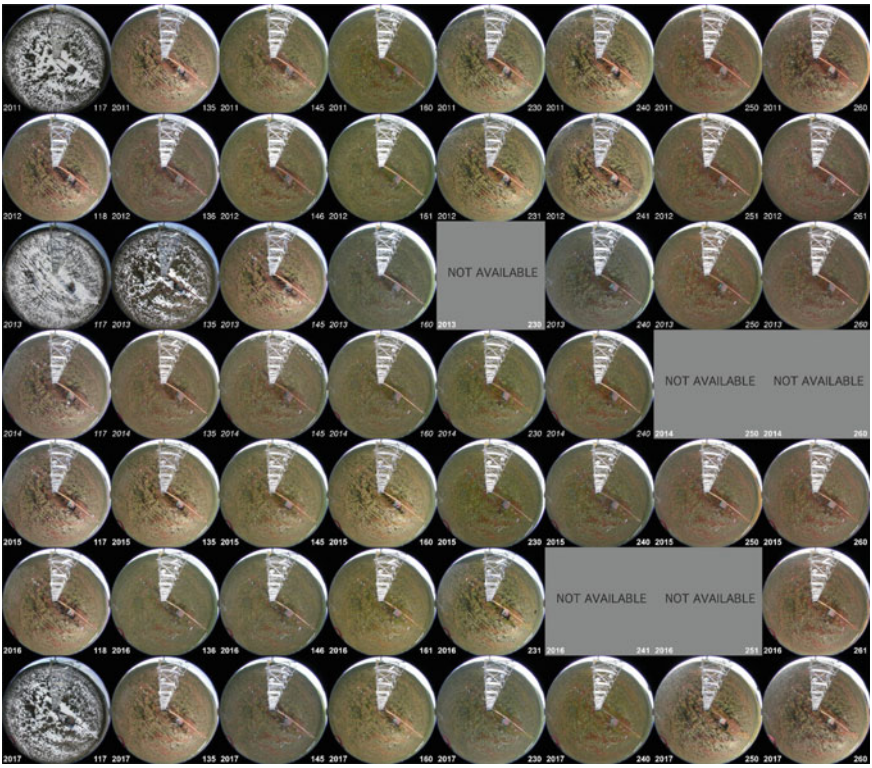

Fig. 21.8 Year-to-year variability of typical canopy surface images from April 2009 to September 2017 in an open-canopy evergreen coniferous forest in Alaska: Poker Flat Research Range site (65°7′24″N, 147°29′15″W, 210 masl; Nagai et al. 2018, http://pen.jamstec.go.jp/). Year and day of year were shown in the left bottom and right bottom in each canopy surface image, respectively

2014), then the LAIu was estimated from NDVIu through a look-up table generated by the radiative-transfer model (Yang and Kobayashi 2018). Figure 21.9 shows an example of the estimated monthly average LAIu for boreal forests in July 2010.

To develop estimation of spatio-temporal variability of LAI in various ecosystems in Alaska, the following two tasks should be considered: (1) accurate detection of spatio-temporal variability in the timing of snowmelt, leaf-flush, leaf-fall, and snow on date, and (2) collection of ground-truth of LAI, plant phenology, and stratification of forest structure in multiple points. The timing of snowmelt is important for plant phenology in understory vegetation in Alaska although the consistency between the year-to-year variability in snowmelt dates and time of leaf-flush may not be assured. The timing of leaf-flush and leaf-fall also affects estimation of the interannual and seasonal variations in LAI.

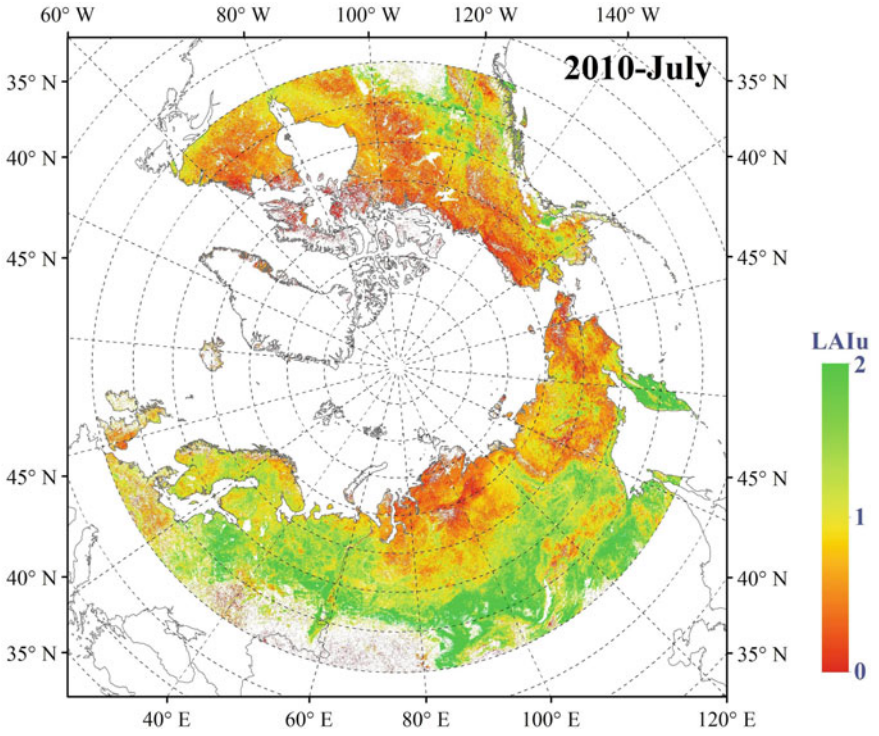

Fig. 21.9 Spatial distribution of understory LAI (LAIu) in July 2010 in Pan-Arctic ecosystems (Yang et al. unpublished data)

To detect the spatio-temporal variability in leaf-flush and leaf-fall timing in Alaska, analysis of the time-series in daily satellite-observed vegetation index is useful. Although the definition of the timing of leaf-flush and leaf-fall by satellite-based analysis was not consistent with that by in situ observations, we can evaluate the spatio-temporal variability of the timing of start and end of growing season (Fig. 21.10), as the timing of start and end of growing season is proxy for the leaf-flush and leaf-fall, respectively. The results of satellite-based analysis include uncertainty due to heterogeneity of vegetation within an area per pixel in satellite remote-sensing data, and cloud contamination and atmospheric noise. The timing of snowmelting, leaf-flush, leaf-fall, and snow covering was affected by the latitudinal gradient in Alaska (Fig. 21.10, Sugiura et al. 2013; Kobayashi et al. 2016). To obtain ground-truth of this characteristic, phenological observations using time-lapse digital cameras installed along the Alaskan highway are useful (Sugiura et al. 2013; Kobayashi et al. 2016). Further field studies at multiple points where time-lapse digital cameras have been installed should be conducted to obtain ground-truth of LAI estimation. In this case, we should pay heed to the relationship among canopy-openness, LAIu, and LAIo in each study site.

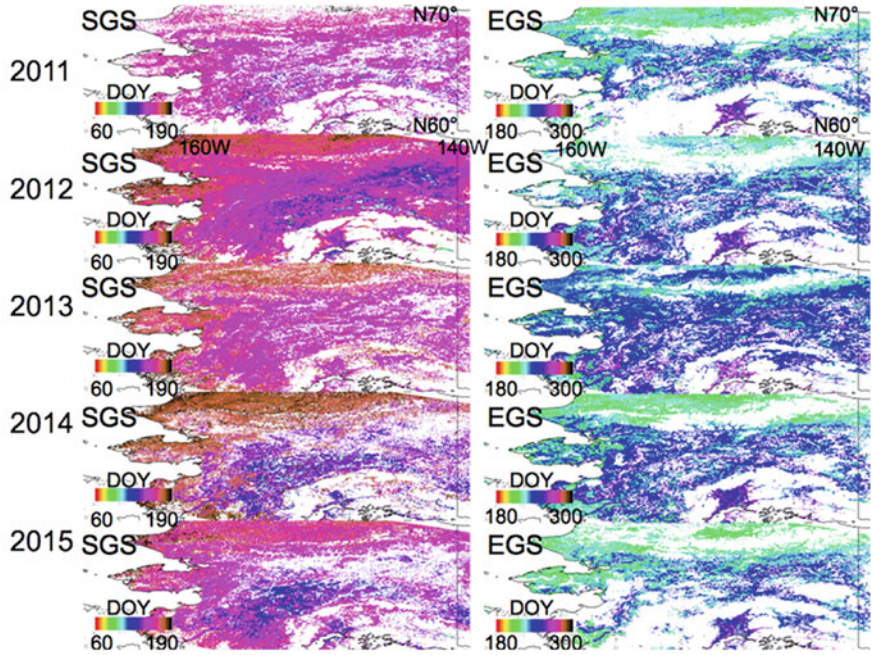

Fig. 21.10 Spatio-temporal distribution of the timing of start (SGS) and end of growing season (EGS) from 2011 to 2015 in Alaska analyzed by time-series in daily MODIS Terra/Aqua satellites-observed green-red vegetation index (GRVI). The timing of SGS and EGS was defined as the first day on which GRVI was more than or equal to zero in spring and the first day on which it was less than zero in autumn, respectively (Nagai et al. 2015). White shows pixels where we could not evaluate the timing of SGS and EGS or evergreen forests

21.2.4 Spatial Distribution of Winter and Spring Soil CO_2 Emission

Soil CO_2 efflux, produced by decomposition of soil organic carbon and roots, signifies the second largest terrestrial carbon source on both time and space scales (Schlesinger and Andrews 2000). The magnitude of soil CO_2 efflux may depend on the timing of snow disappearance and the snow cover duration (Sturm et al. 2005). During the seasonally snow-covered period, winter CO_2 measurements in boreal forests (Winston et al. 1997; Kim et al. 2007, 2013; Kim 2014), account for 10–30% of the variability in annual carbon emissions. On the other hand, it is difficult to determine the timing of snow disappearance in the early spring season, due to fast snowmelt, including change of −0.94 day $year^{-1}$ over 14 years in terrestrial Pan-Arctic drainage basin and Alaska, according to microwave remote sensing (McDonald et al. 2004). Such shifts may cause decrease in subarctic CO_2 efflux in both winter and the growth season (Sturm et al. 2005), resulting from changes in solar radiation (e.g., energy exchange) (Eugster et al. 2000). It is important,

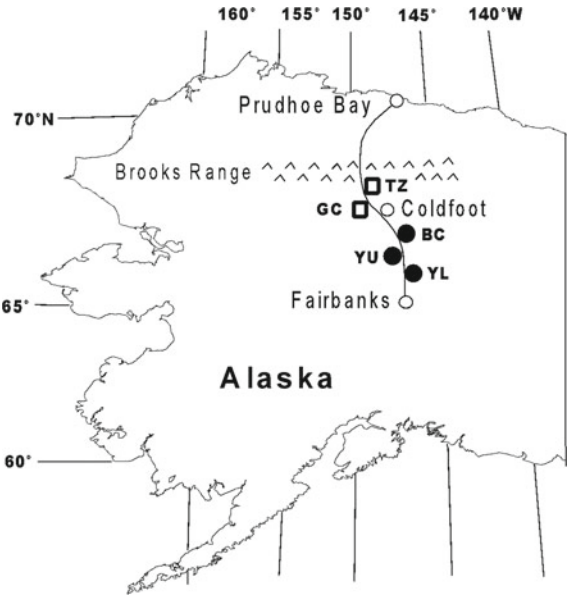

Fig. 21.11 Site locations along the trans-Alaska pipeline, during winter and spring seasons of 2010–2012. Solid circles are black spruce forest sites and open squares are white spruce forest sites (revised by Kim 2014)

therefore, to understand and qualify soil carbon balance—whether it shows the acceleration of photosynthesis and respiration or their decline—as it controls the terrestrial carbon budget in response to a changing climate in northern high latitudes.

Quantification of winter carbon emission is extremely significant in determining annual carbon budget. Using a dynamic chamber system, soil CO_2 efflux was measured at five boreal forest sites, two in white spruce and three in black spruce forest along the Dalton Highway, over a distance of 700 km, during the winter and spring seasons of 2010–2012 (Fig. 21.11).

Sites were classified as two ecotypes in interior Alaska: white spruce forest (TZ and GC) and black spruce forest (BC, YU, and YL), depending on dominant vegetation, local weather, and permafrost. The boreal forest extends across the lowlands and uplands of the Tanana-Yukon flats, comprising white and black spruce and deciduous forests (Raynolds et al. 2006; Kim et al. 2013; Kim 2014).

Snowpack began to melt in areas surrounding boreal forest trees during early May (Fig. 21.12). The melt process around trees proceeds as follows (Kojima 2001): (1) tree trunks directly absorb strong solar energy (e.g., short wavelength) from the sun, due to lower reflectance of trees; (2) temperatures of tree stems increase; (3) warmed stems emit radiation as long wavelengths during nighttime; (4) snow surrounding tree trunks melts in concentric circles (e.g., ablation rings) around stems (Winston et al. 1997); (5) dents surrounding stems and tussock open in round and oval shapes; (6) dents extend to the ground; (7) soil around stems expose; (8) ground is exposed as the temperature rises; and finally (9) larger dents from melting snow are completed down to the bases of stems. For the Canadian

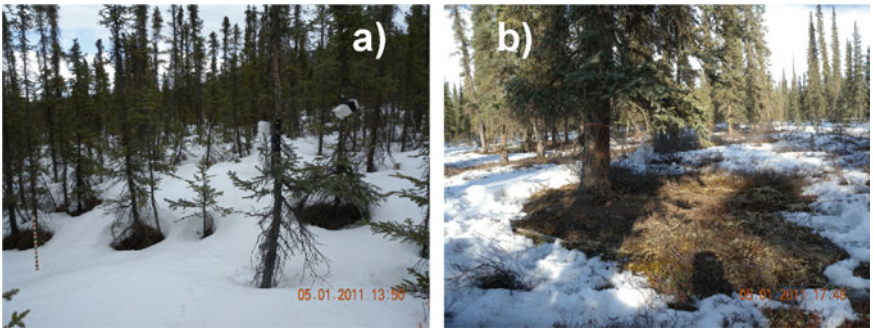

Fig. 21.12 Site views in **a** black spruce forest site (BC, YU, and YL), **b** white spruce sites (GC and TZ) during spring of 2011. Exposed soils were found in surrounding truck well due to fast snowmelt by shortwave radiation for nighttime (Photos by Y. Kim)

boreal forest, Winston et al. 1997 and Kim 2014 explained that an important mechanism of CO_2 transport through the forest snowpack was by macro-channels along trunks and stems, as previously described regarding snow-melting mechanisms near the tree stem. Soil CO_2 efflux was measured in the exposed and snow-covered soils of boreal forests during spring.

Using a portable chamber, soil CO_2 efflux measurements were conducted during snow-covered and snow-melting periods to minimize artificial effects, as described in Kim et al. (2013). Nine chamber bases were inserted into the soils of boreal forest sites during spring. To prevent contamination and disturbance, chamber bases were not used at boreal sites during snow-covered periods, due to soft snow surface (Kim et al. 2007, 2013; Kim 2014).

Flux measurement times were at 5–10 min intervals, depending on local weather and soil surface conditions, and efflux was calculated using the following equation, as described by Kim et al. (2007, 2013):

$$F_{CO_2} = \rho_a \times (\Delta C/\Delta t) \times (V/A) \tag{21.1}$$

where ρ_a is the molar density of dry air (mol m^{-3}), ΔC (ppmv) is the change in CO_2 concentration during the measurement period (Δt, 5–10 min), V is chamber volume, and A is surface area (cross section = 0.28 m^2). The pump was maintained at a flow rate of 1.0 L min^{-1} to avoid underestimation or overestimation of carbon flux from the occurrence of under- and over-pressurization between the inside and outside of the chambers (Savage and Davidson 2003). The height of each chamber was also measured alongside the chamber to allow efflux calculation.

To estimate the response from temperature dependence on soil CO_2 efflux, the relationship was plotted, showing exponential curves on soil temperature at 5 cm depth from the equation:

$$\mathrm{CO_2\,efflux} = \beta_0 \times e^{\beta 1 \times T} \tag{21.2}$$

where CO_2 *efflux* is the measured *soil* CO_2 *efflux* (g C m^{-2} day^{-1}), T is soil temperature (°C), and β_0 and β_1 are constants. This exponential relationship is commonly used to represent soil carbon flux as a function of temperature (Davidson et al. 1998; Xu and Qi 2001; Davidson and Janssens 2006; Rayment and Jarvis 2000; Kim et al. 2007, 2013; Kim 2014). Q_{10} temperature coefficient values were calculated as in Davidson et al. (1998), Kim et al. (2013), and Kim (2014):

$$Q_{10} = e^{\beta 1 \times 10} \tag{21.3}$$

where Q_{10} is a measure of the change in reaction rate at intervals of 10 °C and is based on Van't Hoff's empirical rule that a rate increase of two to three times occurs for every 10 °C rise in temperature (Lloyd and Taylor 1994).

During the winter season, CO_2 concentration gradients in snowpack between trees and near tree wells were 2.52–4.78 and 0.93–1.20 ppm cm^{-1}, measured using a stainless steel-made probe (0.4 cm OD; 0.2 cm ID; 80 cm long) with connecting tubing, tri-way stopcock, and syringe at sub-surface and bottom snowpack depths, respectively. This suggests that a lower CO_2 gradient near the tree trunk results in faster CO_2 transport from the soil through snowpack to the atmosphere than through snowpack between trees. This demonstrates that the air–snow–soil interface surrounding the tree trunk is much thinner than in forest opening areas.

During spring, average CO_2 effluxes are much higher in exposed than snow-covered soils. Because the snow-disappearance date in 2011 was approximately 10–17 days earlier than in both 2010 and 2012, based on four-hour time-lapse camera measurements, and spring CO_2 efflux in exposed soils in 2011 was at least tenfold higher than in snow-covered soils.

Three-year average spring CO_2 effluxes are completely different in four directions within the white spruce forest (Fig. 21.13a and b). The magnitude of snow disappearance depends on solar radiation and the strength of long wavelengths from the tree trunk at nighttime during the spring. The much wider exposed area showed south > east $\geqq$ west $\gg$ north, in turn, from trunks in the white spruce forest. Average diameter at breast height (DBH; 18 ± 4.5 cm) for white spruce is much thicker than black spruce (DBH 5.8 ± 3.2 cm), suggesting that the difference in radiation uptake and heat emission capacity between both forests resulted in that of dent size, as shown in Fig. 21.13a and b. This feature is related to the differences in exposed extent and soil CO_2 production within boreal forest sites.

Higher Q_{10} values for the winter and spring seasons were found within boreal white and black spruce forests, and tundra sites across the Dalton Highway, relative to Q_{10} values of 2.1–18 in the growing season (Kim et al. 2013). This result suggests the exponential growth of microbes (e.g., snow molds) results from warming of soils below snowpack from −3 to 0 °C produced higher CO_2 in a subalpine forest in the Colorado Front Range (Monson et al., Monson et al. 2006a, b; Schmidt et al. 2007). Monson et al. (2006a, b) demonstrated that soil microbes'

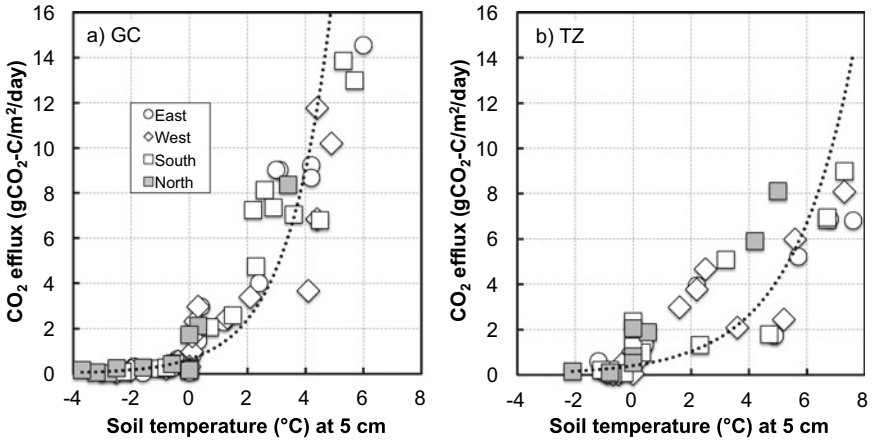

Fig. 21.13 Responses of spring CO_2 efflux on soil temperature at 5 cm below the surface measured in four-direction from the stem of white spruce in **a** GC and **b** TZ sites during the spring. The dotted curves denote the 3-year exponential relationship between spring CO_2 efflux and soil temperature

beneath-snow CO_2 efflux response (e.g., Q_{10} value: 105 to 1.25 × 10^6) corresponded to a narrower range of soil temperature (−1.0 to 0.0 °C). Further, the drastic increase in CO_2 efflux was induced by a strong response from beneath-snow microbes, with a much higher dependence from microbial biomass upon an increase in soil temperature in the late winter and early spring seasons (Schmidt et al. 2007).

The response of spring CO_2 efflux to soil temperature at 5 cm below the soil surface at all sites during the spring seasons of 2010–2012 is shown in Fig. 21.14. Three-year spring CO_2 efflux shows spatial distribution across 66–70°N, along the Dalton Highway, with latitudinal distribution of soil temperature at 5 cm. Higher efflux was seen in white spruce forest sites, at >5 g C m^{-2} day^{-1}, reflecting an ablation ring effect. Winston et al. (1997) further suggested that soil CO_2 efflux from a tree well was tenfold higher than that for forest openings. There is thus a clear difference in spring CO_2 efflux between a tree trunk in exposed soils and a forest opening in seasonally snow-covered soils.

Growing season CO_2 efflux measurements were conducted at each site from August to September of 2010. However, as efflux could not be measured during 2011 and 2012, due to rainy and cold weather conditions in the late fall season (i.e., late September to early October), calculation of seasonal emissions has used data observed in 2010 and by Kim et al. (2013). Further, the contribution of average three-year winter and spring CO_2 emissions to the atmosphere corresponds to roughly 14–22% for tundra and 9–24% for boreal forest sites, of the total annual carbon respired. Winter CO_2 contributions to annual carbon emissions within tundra, alpine, and boreal forest ecosystems represent from 17% for Alaskan tundra (Fahnestock et al. 1998) to >25% for alpine and subalpine regions (Sommerfeld

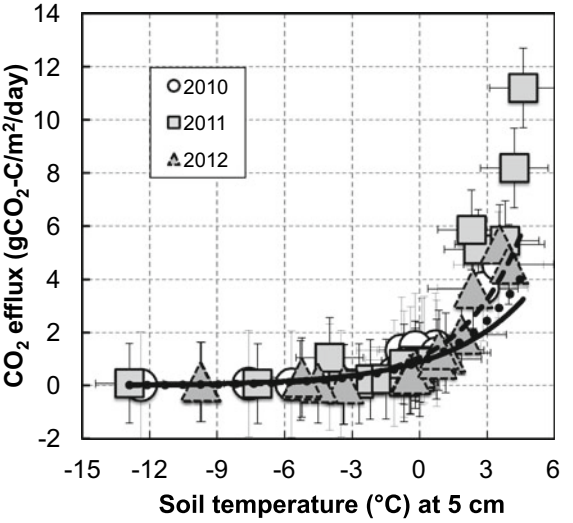

Fig. 21.14 Responses of spring CO_2 efflux on soil temperature at 5 cm below the surface in whole sites during the spring seasons of 2010 and 2012. The dashed, dotted, and solid curves denote 2010, 2011, and 2012, respectively

et al. 1993), suggesting that the results of this study are comparable with others. However, spring CO_2 contributions from the boreal forest reached to almost 50% of growing season carbon emissions, demonstrating the strong tree-well effect (Winston et al. 1997) of the boreal forest (Kim et al. 2007, 2013; Kim 2014). Spring carbon contributions, like growing season CO_2 emissions, were sensitive to subtle changes in the onset of spring and snowpack covering duration.

21.2.5 Successional Changes in CO_2 and Energy Balance After Forest Fires

Vegetation in boreal forest ecosystems is a net carbon sink of 0.54 Gt $year^{-1}$ and that the soil of boreal forest and peatlands represent a net carbon sink of 0.70 Gt $year^{-1}$ (Apps et al. 1993). Further, boreal forest ecosystems are particularly subject to cyclic disturbance by forest fire (e.g., wildfire). The shift of the boreal forest from a net sink to a net source of atmospheric carbon, then, will likely originate from two sources, both anthropogenic in their origin: (1) likely increases in deforestation activities in the boreal forest; and (2) increases in disturbances in the region due to climate change, such as fire, insect outbreak, and pathogens (Kasischke and Stocks 2000). Recent studies in the boreal black spruce forest biomes of Alaska have shown that changes in the local energy balance may result in post-fire biogenic emissions of carbon that equal or exceed the amount of carbon dioxide (CO_2) released during forest fire (Richter et al. 2000; Hicke et al. 2003; Kim and Tanaka 2003; O'Neill et al. 2003, 2006), potentially shifting large areas of the landscape from net CO_2 sinks to net CO_2 sources. This is to say that, immediately following forest fire, the fixation of CO_2 by vegetation such as juniper haircap moss is

minimal to non-existent, while rates of decomposition may be stimulated as a result of warmer soil temperature and changes in soil drainage (Richter et al. 2000; Kim and Tanaka 2003; O'Neill et al. 2003).

Juniper haircap moss (*Polytrichum juniperinum)* is typically a pioneer species—the first groundlayer species to establish after fire—and is characteristically found on burned mineral soils and other charred substrates (Fryer 2008). Also, juniper haircap moss, as a fire-follower, may actually survive fire, and it shows a strong ability to colonize newly burned areas, due to the penetration of its rhizoids into mineral soil (Skutch 1929; Schimmel and Granstrom 1996; Ruokolainen and Salo 2006). This adaptation allows juniper haircap moss to survive some surface fires. The species is well adapted to large fluctuations in summer temperature, higher light levels, and the low humidity levels typical of recently burned soils (O'Neill et al. 2006). Under optimal moisture conditions, mosses contributed between 10 and 55% of total soil respiration after forest fire, with highest contributions from early successional moss species (*Ceratodon purpureus* and *P. juniperinum*) (O'Neill et al. 2006). Just after fire, soil respiration decreased by, at most, 50%; however, microbial respiration estimated after the fire was almost three times as high as calculated respiration before the fire (Kim and Tanaka 2003). This indicates that the post-fire condition may stimulate microbial respiration, on account of higher nutrients and substrates in remnant soils and enhanced soil temperature (Kim and Tanaka 2003). It is important, then, to understand carbon dynamics in juniper haircap moss regimes after forest fire.

Our study site began as a mature black spruce (*Picea mariana*) forest before the fire of 2004, located within the Poker Flat Research Range (PFRR) of the University of Alaska Fairbanks (UAF) in interior Alaska. The forest fire ignited due to lightning in mid-June of 2004 and continued until early August 2004. We subsequently measured CO_2 exchange rates and microbial respiration using an automated chamber system over August–October 2009 at this severely burned site (65° 08′N, 147° 26′W, 491 masl). The site was selected according to the criterion that no vegetation other than juniper haircap moss regimes occurs within a 10-m radius. A single chamber system set, consisting of transparent and opaque chambers, was installed on the moss regime for the estimation of CO_2 exchange rates. Two sets were prepared over a no-plants regime for microbial respiration rate (MR). The remaining soil organic layer was 2 cm deep, underlain by sandy silt with gravel (Iwata et al. 2011). We assumed that the dead roots of the severely burned black spruce were not yet decomposed and contributed to soil respiration, due to their completely charred roots. This suggests that the microbial respiration rates produced in burned black spruce forest soil are presumably constant. Most of the burned black spruce trees remained snag, and some were logged due to snowfall after winter. The fractional area covered by vegetation at a nearby area with similar burn conditions was 26% in August 2005; this increased to 85% in August 2008, four years after the fire (Tsuyuzaki et al. 2009). Major vegetation consisted of paper birch (*Betula paperifera*), quaking aspen (*Populus tremuloides*), Labrador tea (*Ledum palustre*), bog blueberry (*Vaccinium uliginosum*), sedge (*Eriphorum scheuchzeri*), fireweed (*Epilobium angustifolium*), and juniper haircap moss

(*Polytrichum juniperinum*). As juniper haircap moss is typically among the first ground-layer species to establish after fire (Foster 1985), our study focuses on the carbon dynamics of juniper haircap moss during the fall season.

CO_2 exchange rates (i.e., NPP: net primary productivity, Re: ecosystem respiration, and GPP: gross primary productivity) were measured in this instance of burned black spruce forest moss. NPP and Re were measured using light and dark chambers; NPP may be calculated using the following equation and NEP (net ecosystem productivity) using Eq. (21.5).

$$NPP = Re - GPP \tag{21.4}$$

$$NEP = NPP - MR \tag{21.5}$$

where *MR* is microbial respiration (g CO_2 m^{-2} h^{-1}) measured in a no-vegetation condition of the burned black spruce forest.

A reference value of R_{10} (MR normalized to a temperature of 10 °C) was then calculated as:

$$R_{10} = R_i \cdot Q_{10}^{[(10-T)/10]}, \tag{21.6}$$

where R_i is the measured MR (g CO_2 m^{-2} h^{-1}) at T temperatures in air (°C). Using the calculated values of Q_{10} and R_{10}, MR was simulated on the basis of the measured air temperature. Simulated MR values, R_i (g CO_2 m^{-2} h^{-1}), were calculated as:

$$R_i = R_{10} \Big/ Q_{10}^{[(10-T)/10]}, \tag{21.7}$$

Using the automated chamber system, we measured CO_2 exchange rates of juniper haircap moss and soil—primarily microbial (e.g., heterotrophic)—respiration, within the burned black spruce forest. Microbial respiration can only be estimated in the burned forest, as root activity ceased after the wildfire. Two kinds (transparent and opaque) of chambers were assembled in *P. juniperinum* moss in order to measure CO_2 exchange rates, the rest were placed in no-vegetation ground of the burned black spruce forest to capture microbial respiration.

21.2.6 Seasonal Variation in CO_2 Exchange Rate in Juniper Haircap Moss

CO_2 exchange rates, such as NPP by light chamber and Re by dark chamber, were measured in juniper haircap moss of burned black spruce forest during the fall season of 2009. Mean NPP and Re were -0.01 ± 0.33 and 0.31 ± 0.19 g CO_2 m^{-2} h^{-1}, respectively. Mean GPP was calculated using Eq. (21.1), yielding 0.31 ± 0.41 g CO_2 m^{-2} h^{-1}. In no-vegetation soil of the burned black spruce

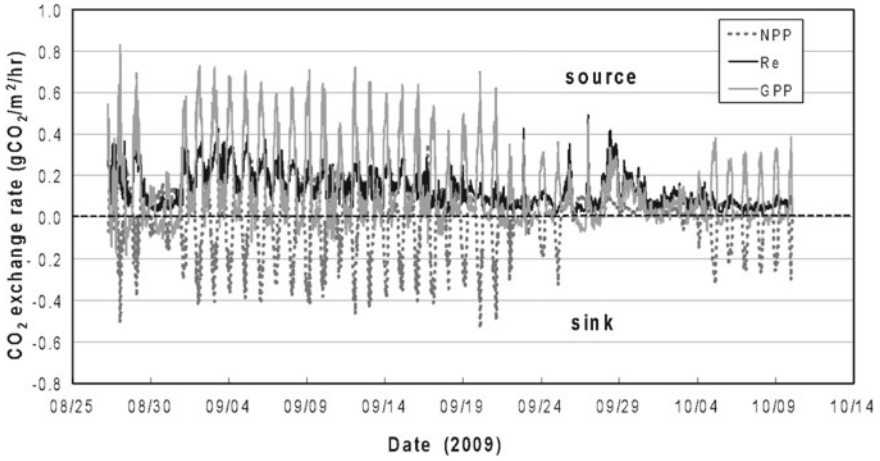

Fig. 21.15 Seasonal variations of NPP (dashed line), Re (solid line), and GPP (thin solid line) in the haircap moss of burned black spruce forest Source, that carbon dioxide emits to the atmosphere, denotes over the zero as Re and GPP, and sink, that the moss photosynthesizes, shows below the zero, as NPP (Kim et al. 2014)

forest, mean microbial respiration from light and dark chambers showed 0.21 ± 0.10 g CO_2 m^{-2} h^{-1}, and 0.29 ± 0.11 g CO_2 m^{-2} h^{-1}, respectively—not a significant difference at a 95% confidence level. This suggests that the microbial respiration of the burned plot can be considered constant within 50% of CV. Mean NEP was calculated using Eq. (21.5), yielding -0.28 ± 0.38 g CO_2 m^{-2} h^{-1} and a range of -1.65 to 0.44 g CO_2 m^{-2} h^{-1}, indicating juniper haircap moss as a net sink in the five-year-old burned black spruce forest (Fig. 21.15).

Simulated microbial respiration was calculated using Eq. (21.7), yielding mean simulated MR (L and D) of 0.23 ± 0.14 (CV: 57%) and 0.32 ± 0.16 (CV: 48%) g CO_2 m^{-2} h^{-1}, respectively. Based on a one-way ANOVA at a 95% confidence level, these values show no significant differences in measured MR (L and D). Litvak et al. (2003) and O'Neill et al. (2003) estimated NEP and C source-sink dynamics for various stands using a modified mass balance model of C storage that allowed both decomposition and NPP to vary over the fire cycle. Mean daily NEP calculated in our study was 0.28 ± 0.16 (CV: 58%) g CO_2 m^{-2} h^{-1} in the juniper haircap moss of burned black spruce forest. NPP of *P. juniperinum* moss ranged from 0.25 Mg C ha^{-1}, as a source of atmospheric CO_2, to 0.56 MgC ha^{-1}, as a net sink during the 45-day fall period. Using Eq. (21.5), mean NEP of *P. juniperinum* moss was 0.49 ± 0.28 Mg C ha^{-1}, after 5-year-old forest fire. O'Neill et al. (2006) reported that total inputs to the soil system (NPP) were estimated to increase from 0.0 to 0.8–1.5 Mg C ha^{-1} during the first 100 years after fire. The difference between modeled NPP and decomposition suggested that these soils were a net C source for 7–14.5 years after fire and a net sink of 0.3–0.6 Mg C ha^{-1} over the remaining (140) years (O'Neill et al. 2006). These trends are generally consistent

with those of Bond-Lamberty et al. (2004) for a black spruce fire chronosequence in Manitoba, Canada, in which NEP showed a small post-fire net C loss followed by a long period of positive accumulation with a maximum NEP of 1.1 Mg C ha^{-1} (71 years post-fire). However, our NEP finding suggests that *P. juniperinum* moss plays a net sink role within a 5-year burned black spruce forest during fall season. To estimate ecosystem NEP after a fire during the growing season, additional study is required to monitor CO_2 exchange rates in other ground plants such as shrubs and bryophyte within the same site.

Based on the relationship between measured microbial respiration and simulated microbial respiration, normalized to a temperature of 10 °C by Eq. (21.7) using light and dark chambers in black spruce forest after fire, we calculated seasonal simulated MR using Eq. (21.7), based on daily air temperature during the growing season (May to October) of 2009 (Fig. 21.16). During the 45-day observation period, the cumulative measured MR of 11.2 g CO_2 m^{-2} is similar to 10.8 g CO_2 m^{-2} of simulated MR, suggesting no significant difference between both at a 95% confidence level, and that air temperature as a significant factor in regulating microbial respiration in the burned black spruce forest of interior Alaska, five years after forest fire.

Forest fires return old-growth forests to young productive ecosystems. In boreal Alaska and Canada, chronosequence studies showed the successional trajectory of CO_2 budget after forest fires (Amiro et al. 2010; Goulden et al. 2010). Just after the fire, fire scars acted as net annual CO_2 source of approximately 200 g C m^{-2} $year^{-1}$ (Goulden et al. 2010). Due to vegetation recovery, carbon source decreased quickly in second year after the fire, but still acted as small CO_2 source for 10–20 years. This early successional stage is mostly dominated by grasses, shrubs, and young tree saplings. Then, deciduous trees (e.g., *Populus tremuloides* and *Betula papyrifera*) become dominant and the ecosystem turn to strong CO_2 sink. Through this

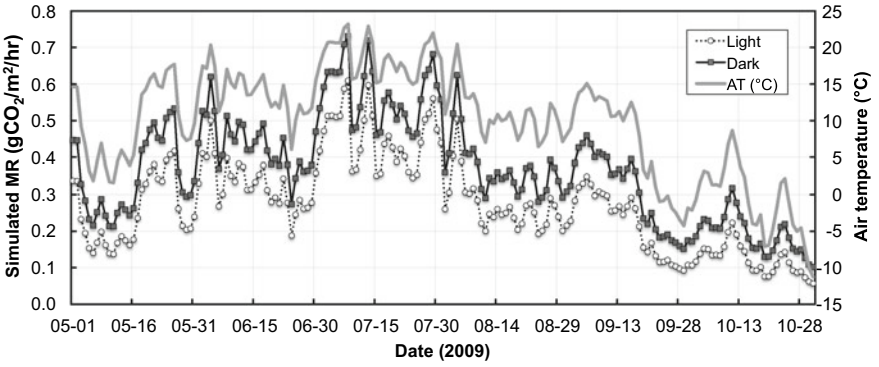

Fig. 21.16 Temporal variations of microbial respiration from light (dotted line) and dark (solid line) chambers, and air temperature at 2.3 m (grey line) during the growing season (May to October) of 2009, based on the estimation of the Eq. (21.7)

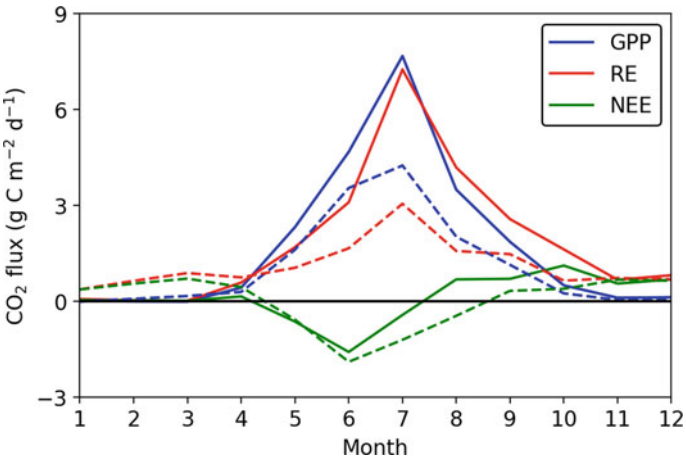

Fig. 21.17 Seasonal variations of CO_2 fluxes at a mature black spruce forest (solid line) and a burned forest five years after the fire (dashed line) at interior Alaska (after Iwata et al. 2011)

productive stage, ecosystems accumulate carbon in vegetation, litter, and soils, resulting in slowly succession to mature stage where evergreen needle leaf tress (e.g., *Picea mariana*) dominates. In the mature to old growth stage, CO_2 sink of the ecosystems slowly dampened due to increases in autotrophic and heterotrophic respiration. Since mature and old growth forests are susceptible to fires due to much of fuel loads, fires return these forests to young forest, and emit almost all carbon accumulated in the succession into the atmosphere. Consequently, boreal forests are presumed to be a net CO_2 neutral throughout this fire cycle.

Eddy covariance measurements in interior Alaska showed the different carbon budget among early succession after a forest fire and a mature black spruce forest, in terms of magnitude of fluxes, and the annual budget (Fig. 21.17). Magnitude of the annual GPP was approximately 40% smaller in early succession (five years after a forest fire) than a mature forest. Despite of the smaller GPP, CO_2 sink during May to August was greater in the early succession (approximately 500 g C m^{-2} $year^{-1}$) than the mature forest (approximately 240 g C m^{-2} $year^{-1}$). This was because the heterotrophic respiration was smaller in the early succession than the mature forest (Iwata et al. 2011). In the early succession, soil and litter carbon were burned in the fire, and were not accumulated. Thus, vegetation recovery was the major driver of the carbon balance in the stage of early succession. In contrast, carbon accumulation and associated increase in respiration was the driver of the carbon balance in the mature stage (Amiro et al. 2010; Goulden et al. 2010).

Effects of forest fires were also seen in satellite remote sensing at the regional scale. An upscaled CO_2 fluxes using satellite remote sensing showed patchy increase or decrease trends in recently burned areas over Alaska (Ueyama et al. 2013). The disturbance effects were seen early successions until approximately

20 years after fires by the satellite remote sensing. Areas suffered from recent fires showed negative trends of GPP, and RE, and positive trends of NEE during the period from 2000 to 2011, due to a sudden decline of productivity. In contrast, areas that suffered from fires more than 10–20 years ago showed positive trends of GPP, and RE, and negative trends of NEE due to a vegetation recovery. Increasing trends in GPP were generally seen until approximately 60 years after fires, and then showed negative or insignificant trends. Consequently, forest fires strongly affect spatial distributions in CO_2 balance of boreal forests in interior Alaska.

Boreal forest fire changes the surface albedo. Just after forest fires, summer albedo decreases due to an exposure of black charcoal (Chambers and Chapin 2003). But, this is not necessarily the case, where summer albedo just after the fire was reported to be greater in fire scar than coniferous forest (Liu and Randerson 2008). Based on a satellite observation of surface albedo, summer albedo increased 0.135 ± 0.006 by dominating shrubs and young trees in stands 20–35 years, which was greater than deciduous or coniferous forests (Lyons et al. 2008). Even summer albedo slowly decreased at stands 40–50 years after fires, the albedo was still higher than coniferous forests (Lyons et al. 2008). Winter albedo in fires scars was higher than the coniferous forest until near 50 years after fire (Lyons et al. 2008).

Change in surface energy balance associated with the albedo change cools the regional climate (Randerson et al. 2006). The increases in albedo increase net shortwave radiation, and thus decrease net radiation (Euskirchen et al. 2010; Ueyama et al. 2014). Albedo-induced change in radiative forcing was estimated as -4.2 W m^{-2}, which was greater than changes by other fire-induced radiative forcing, such as greenhouse gas budget, ozone, black carbon deposition, and aerosols (Randerson et al. 2006). Consequently, boreal forest fires were estimated to act as a net surface cooling due to decreasing net radiative forcing by -2.3 W m^{-2} over an 80-year fire cycle (Randerson et al. 2006).

Forest fire significantly decreased soil CO_2 efflux by a range of 22–50% compared to before fire in the black spruce forest (Kim and Tanaka 2003). Kasischke (2000) and Richter et al. (2000) found that the fire decreased total soil respiration rate by 33–59 and 44–58%, respectively. The differences in rate decreased depend on fire severity, indicating that fire typically consumes between 20 and 90% of the organic soil layer, including any living roots present in this layer (Kasischke et al. 2000a, b). Forest fire in the study site was extremely severe (Iwata et al. 2011). We used mean soil respiration (0.22 ± 0.09 (CV: 40%) g CO_2 m^{-2} h^{-1}, unpublished data) for the partition of root and heterotrophic respiration rates, which is the sum of plant root respiration and microbial respiration, in mature black spruce forest during the fall season of August 27 to October 5, 2009. Schlentner and Can Cleve (1985) estimated that approximately 20% of soil respiration in mature black spruce forest was derived from microbial respiration, and the remainder was from plant root respiration. Using the partition and mean soil respiration measured in mature black spruce forest, microbial respiration can be calculated as 0.043 ± 0.017 g CO_2 m^{-2} h^{-1}, possibly solely from microbial respiration from the soil. This is almost six-fold higher than the mean microbial respiration estimated by this study, using the factor of Schlentner and Van Cleve (1985). This finding

indicates that the post-fire condition may greatly stimulate microbial respiration, due to higher nutrients and substrates in remnant soil after forest fire. Furthermore, Kashischke (2000) and Van Cleve et al. (1983) demonstrated that the forest floor temperature for boreal black spruce forests underlain by permafrost remains warmer than in unburned black spruce forests for at least 20–30 years after fire.

According to the proportionality of Schlentner and Van Cleve (1985), mean microbial respiration in 5-year-old burned black spruce forest is estimated to be 0.27 g CO_2 m^{-2} h^{-1}. Of this, 0.23 g CO_2 m^{-2} h^{-1} is attributed to post-fire stimulation of microbial decomposition after the fire. For the 45-day fall season observation period of 2009, microbial respiration may be stimulated by as much as 0.40 ± 0.23 Mg C ha^{-1} in burned black spruce forest, compared with 0.15 Mg C ha^{-1} in one year, 0.38 Mg C ha^{-1} in seven years, and 0.40 Mg C ha^{-1} in ten years after severe forest fire during the fall season (Richter et al. 2000), and with 0.33 Mg C ha^{-1} in one year, 0.58 Mg C ha^{-1} in seven years, and 0.45 Mg C ha^{-1} in ten years after forest fire during the fall season (O'Neill et al. 2006). With the successional vegetation stage, atmospheric CO_2 is steadily taken up to ground vegetation (e.g., post-fire frontier species—juniper haircap moss and fireweed, sedge, Labrador, bog blueberry, paper birch, quaking aspen) after a fire. However, soil-originated CO_2 emission to the atmosphere (e.g., primarily microbial respiration and plant respiration) is much more than atmospheric carbon fixation by vegetation in burned black spruce forest. This suggests that the post-fire black spruce forest plays a prolonged, crucial role as a source of atmospheric CO_2 after forest fire, and that fire severity also yields long-term patterns of post-fire floor temperature and moisture in boreal forest by way of drastic changes in albedo (Richter et al. 2000; O'Neill et al. 2006). Occasionally, we found greater differences in the magnitude of post-fire carbon emission according to research sites, at which the difference in emissions results from a magnitude of fire severity that is closely related to successional chronosequence, soil temperature, and soil moisture (Van Cleve et al. 1983; Kasischke 2000; Kasischke et al. 2000a, b).

In order to understand floor-level carbon dynamics in dominant ground plants of burned black spruce forest, additional study was conducted in order to monitor CO_2 exchange rates and microbial respiration, using an improved automated chamber system during the growing season, and an FD (forced diffusion) soil CO_2 efflux method during the winter season (Risk et al. 2011). Figure 21.18 showed temporal variations of microbial respiration, air temperature, and soil temperature in burned black spruce forest soil of the Poker Flat Research Range (PFRR), from August 2015 to October 2016. Their data provide the estimation of carbon exchange rates on juniper haircap moss and young black spruce through the ecologically successional stages after 2004 forest fire.

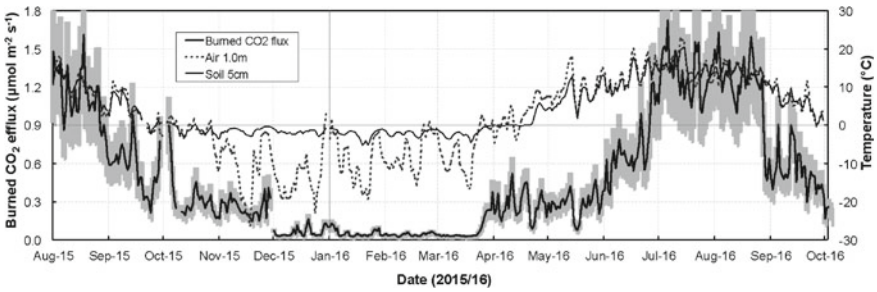

Fig. 21.18 Temporal variations of microbial respiration with FD chamber (thick solid line), air temperature at 1.0 m above soil surface (dotted line), and soil temperature at 5 cm depth under the surface in 2004 burned black spruce forest soil of the Poker Flat Research Range (PFRR) from August 2015 to October 2015 (unpublished data)

21.3 Summary

Boreal forest is a significantly net carbon sink reservoir of 0.54 Gt C $year^{-1}$, whereas tundra ecosystems are currently a net carbon source of 0.17 Gt C $year^{-1}$ (Apps et al. 1993). However, boreal forest may become a net source of carbon, resulting from deforestation activity and increase in the disturbances (e.g., forest fire, insects and pathogens) in response to the warming of Sub-Arctic and Arctic regions. In turn, boreal forest will cause a net release of carbon by anthropogenic and naturally lighting-caused forest fires.

Our main research findings are as follows. First, the aboveground biomass (AGB) mapping in boreal forest is beneficial to evaluate the plant biomass carbon stock, based on in situ field survey and remote-sensing satellite data, in the context of the global biogeochemical cycle in pre- and post-fire landscapes. Second, the responses of climate change, plant phenology, spring green-up, and autumn senescence, as well as timing of snow cover and disappearance in the boreal forest, can be sufficiently investigated with satellite and ground-based observation networks, providing better understanding of the future phonological changes in the successional recovery of disturbed forests after the wildfires. Third, the analysis of time-series of daily satellite-observed vegetation index is useful to detect the spatiotemporal variability of leaf area index (LAI) in the Pan-Arctic terrestrial ecosystems, based on (1) accurate detection of spatiotemporal variability in the timing of snowmelt, leaf-flush, leaf-fall, and snow on date, and (2) collection of ground-truth of LAI, plant phenology, and stratification of forest structure at multiple research stations. Fourth, spring carbon contributions, corresponding to almost 50% of growing season CO_2 emissions, are sensitive to subtle changes at the onset of snowmelt and snow-cover duration in northern high latitudes along the trans-Alaska pipeline, in response to recent Sub-Arctic and Arctic climate change. Lastly, the under- and overstory vegetation recovery with the successional stages

after wildfires affects the carbon and energy balance in burned boreal forests. Additional study needs to monitor yearlong soil carbon emission in disturbed boreal forest soils for the understanding of floor- and canopy-level carbon dynamics in pre- and post-fire landscapes with eddy covariance tower methods.

Acknowledgments This research was supported by a National Research Foundation of Korea Grant from the Korean Government (MSIT; the Ministry of Science and ICT) (NRF-2016M1A5A1901769) (KOPRI-PN20081) (Title: Circum-Arctic Permafrost Environment Change Monitoring, Future Prediction and development Techniques of useful biomaterials (CAPEC Project)). Also, this research was conducted under the JAMSTEC-IARC Collaboration Study (JICS) Project, with funding provided by the Japan Agency for Marine-Earth Science and Technology (JAMSTEC). We are grateful to Dr. Yang Wei (Chiba University) for his valuable comment and for providing a figure. Finally, this manuscript is dedicated to the late Dr. Rikie Suzuki of the JMASTEC, our most treasured colleague.

References

Alaska Interagency Coordination Center (2018) Alaska fire history from 1940 to present. https://fire.ak.blm.gov/aicc.php

AMAP (2017) Snow, Water, Ice and Permafrost. Summary for Policy-makers. Arctic Monitoring and Assessment Programme (AMAP), Oslo, Norway

Amiro BD et al (2010) Ecosystem carbon dioxide fluxes after disturbance in forests of North America. J Geophys Res 115:G00K92. https://doi.org/10.1029/2010jg001390

Apps MJ, Kurz WA, Luxmoore RJ, Nilsson LO, Sedjo RA, Schmidt R, Simpson LG, Vinson TS (1993) Boreal forests and tundra. Water Air Soil Pollut 70:39–53

Apps MJ, Pries DT (1996) Forest Management and the Global Carbon Cycle, NATO ASI Series, subseries 1, vol. 40, Global Environment Change. Springer-Verlag, Berlin

Barney RJ, Stocks BJ (1983) Fire frequencies during the suppression period. In: Wein RW, MacLean DA (eds) The role of fire in northern circumpolar ecosystems. Wiley, New York, pp 45–61

Belchansky GI (2004) Arctic ecological research from microwave satellite observations. CRC Press, Boca Raton, FL, USA, p 248

Billings WD (1997) Challenges for the future: Arctic and alpine ecosystems in a changing world. In: Oechel WC, Callagham T, Gilmanov T, Holten JI, Maxwell B, Molau U, Svebjörnsson B (eds) Global change and Arctic terrestrial ecosystems. Springer, New York, pp 1–18

Bond-Lamberty B, Wang C, Gower ST (2004) Contribution of root respiration to soil surface CO_2 flux in a boreal black spruce chronosequence. Tree Physiol 24:1387–1395

Buermann W, Parida B, Jung M, MacDonald GM, Tucker CJ, Reichstein M (2014) Recent shift in Eurasian boreal forest greening response may be associated with warmer and drier summers. Geophys Res Let 41:1995–2002

Chambers SD, Chapin FS III (2003) Fire effects on surface-atmosphere energy exchange in Alaskan black spruce ecosystems: implications for feedbacks to regional climate. J Geophys Res 108:8145. https://doi.org/10.1029/2001JD000530

Chapin FS III, Hollingsworth T, Murray DF, Viereck LA, Walker MD (2006) Floristic diversity and vegetation distribution in the Alaskan boreal forest. Oxford University Press, New York

Cronan J, McKenzie D, Olson D (2012) Fire regimes of the Alaskan boreal forest. Gen. Tech. Rep. PNW-GTR-XXX. Portland, OR: U.S. Department of Agriculture, Forest Service, Pacific Northwest Research Station

Crutzen PJ, Andreae MO (1990) Biomass burning in the tropics: impact on atmospheric chemistry and biogeochemical cycles. Science 250:1669–1678

Davidson EA, Belk E, Boone RD (1998) Soil water content and temperature as independent or confounded factors controlling soil respiration in a temperate mixed hardwood forest. Global Change Biol 4:217–227

Davidson EA, Jassens IA (2006) Temperature sensitivity of soil carbon decomposition and feedback to climate change. Nature 440:165–173

Delbart N, Kergoat L, Le Toan T, Lhermitte J, Picard G (2005) Determination of phenological dates in boreal regions using normalized difference water index. Remote Sens Environ 97:26–38

Delbart N, Picard G, Le Toans T, Kergoat L, Quegan S, Woodward I, ... Fedotova V (2008) Spring phenology in boreal Eurasia over a nearly century time scale. Glob Change Biol 14:603–614

Delpierre N, Dufrene E, Soudani K, Ulrich E, Cecchini S, Boe J, Francois C (2009) Modelling interannual and spatial variability of leaf senescence for three deciduous tree species in France. Agric For Meteorol 149:938–948

Dissing D, Verbyla DL (2003) Spatial patterns of lightning strikes in interior Alaska and their relations to elevation and vegetation. Can J For Res 33:770–782

Dyrness CT, Viereck LA, Van Cleve K (1986) Fire in taiga communities of interior Alaska. In: Van Cleve K, Chapin FS, Flanagan PW, Viereck LA. Forest ecosystems in the Alaskan Taiga. Springer-Verlag, New York, pp 74–86

Eschenbach C, Kappen L (1996) Leaf area index determination in an alder forest: a comparison of three methods. J Exp Bot 47(302):1457–1462

Eugster W, Rouse W, Pielke RA, McFadden JP, Baldocchi D, Kittel TF, Chapin FS, Liston GE, Vidale PL, Vaganov E, Chambers S (2000) Land-atmosphere energy exchange in Arctic tundra and boreal forest: available data and feedbacks to climate. Global Change Biol 6:84–115

Euskirchen ES, McGuire AD, Chapin FS III, Rupp TS (2010) The changing efforts of Alaska's boreal forests on the climate system. Can J For Res 40:1336–1346

Euskirchen ES, Bret-Harte MS, Scott GJ, Edgar C, Shaver GR (2012) Seasonal patterns of carbon dioxide and water fluxes in three representative tundra ecosystems in northern Alaska. Ecosphere 3(1)

Fahnestock JT, Jones MH, Brooks PD, Walker DA, Welker JM (1998) Winter and early spring CO_2 efflux from tundra communities of northern Alaska. J Geophys Res 103:29023–29027

Fan S, Gloor M, Mahlman J, Pacala S, Sarmiento J, Takahashi T, Peng T (1998) A large terrestrial carbon sink in North America implied by atmospheric and oceanic carbon dioxide data and models. Science 282:442–446

Foster DR (1985) Vegetation development following fire in *Picea mariana* (black spruce)-Pleurozium forests of southeastern Labrador, Canada. J Ecology 73:517–534

Fryer JL (2008) Polytrichum juniperinum, in Fire Effect Information System, U.S. Department of Agriculture, Forest Service, Rocky Mountain Research Station, Fire Sciences Laboratory. http://www.fs.fed.us/database/feis

Garonna I, De Jong R, De Wit AJW, Mucher CA, Schmid B, Schaepman ME (2014) Strong contribution of autumn phenology to changes in satellite-derived growing season length estimates across Europe (1982–2011). Glob Change Biol 20:3457–3470

Goulden ML, McMillan AMS, Winston GC, Rocha AV, Manies KL, Harden JW, Bond-Lamberty BP (2010) Patterns of NPP, GPP, respiration, and NEP during boreal forest succession. Global Change Biol 17:855–871. https://doi.org/10.1111/j.1365-2486.2010.02274.x

Hansen J, Ruedy R, Sato M, Reynolds R (1996) Global surface air temperature in 1995: return to ore-Pinatubo level. Geophys Res Lett 23:1665–1668

Hicke JA, Asner GP, Kasischke ES, French NHF, Randerson JT, Stocks BJ, Tucker CJ, Los SO, Field CB (2003) Post fire response of North American net primary productivity measured by satellite imagery. In: Johnson D, Kershaw L, MacKinnon A, Pojar J (eds) Plants of the Western forest. Boreal and Aspen Parkland, Alberta, pp 1145–1157

Himzman LD, Fukuda M, Sandberg DV, Chapin FS, Dash D (2003) FORSTFIRE: An experimental approach to predicting the climate feedbacks from the changing boreal fires regime. H Geophys Res 108(D1):8154. https://doi.org/10.1029/2001JD000415

Hirose T (2005) Development of the Monsi-Saeki theory on canopy structure and function. Ann Bot 95:483–494

Hogda KA, Tommervik H, Karlsen SR (2013) Trends in the start of the growing season in Fennoscandia 1982–2011. Remote Sens 5:4304–4318

Iio A, Hikosaka K, Anten NPR, Nakagawa Y, Ito A (2014) Global dependence of field-observed leaf area index in woody species on climate: a systematic review. Glob Ecol Biogeogr 23:274–285

IPCC (2014) Climate change 2014: synthesis report. In: Core Writing Team, Pachauri RK and Meyer LA (eds.) Contribution of working groups I, II and III to the fifth assessment report of the intergovernmental panel on climate change, IPCC, Geneva, Switzerland, p 151

Iwata H, Ueyama M, Harazono Y, Tsuyuzaki S, Kondo M, Uchida M (2011) Quick recovery of carbon dioxide exchanges in a burned black spruce forest in interior Alaska. SOLA 7(7):105–108. https://doi.org/10.2151/sola.2011-027

Iwata H, Ueyama M, Harazono Y, Tsuyuzaki S, Kondo M, Uchida M (2011b) Quick recovery of carbon dioxide exchanges in a burned black spruce forest in interior Alaska. SOLA 7:105–108

Iwata H, Ueyama M, Iwama C, Harazono Y (2013) A variation in the fraction of absorbed photosynthetically active radiation and a comparison with MODIS data in burned black spruce forests of interior Alaska. Polar Sci 7:113–124

Jeong S-J, Ho C-H, Gim H-J, Brown ME (2011) Phenology shifts at start vs. end of growing season in temperate vegetation over the Northern Hemisphere for the period 1982–2008. Glob Change Biol 17:2385–2399

Jeong S-J, Medvigy D (2014) Macroscale prediction of autumn leaf coloration throughout the continental United States. Glob Ecol Biogeogr 23:1245–1254

Johnson D, Kershaw L, MacKinnon A, Pojar J (eds) (1995) Plants of western forest: alaska to Minnesota boreal and aspen parkland, Lone Pine Publishing, Edmonton

Kasische ES, Christensen NL, Stocks BR (1995) Fire, global warming, and the carbon balance of boreal forests. Ecol Appl 5:437–451

Kasischke ES (2000) Boreal ecosystems in the global carbon cycle. In: Kasische ES, Stocks BR (eds) Fire, climate change, and carbon cycling in the Boreal Forest. Springer, New York, pp 19–30

Kasische ES, Stocks BR (eds) (2000) Fire, climate change, and carbon cycling in the boreal forest, Ecological Studies, vol 138. Spriger-Verlag, New York

Kasischke ES, Stocks BJ, O'Neill K, French NHF, Bourgeau-Chavez LL (2000a) Direct effects of fire on the boreal forest carbon budget. In: Innes JL, Beniston M, Verstraete MM (eds) Biomass burning and its inter-relationships with the climate system. Kluwer Academic, Dordrecht, pp 51–68

Kasischke ES, O'Neill K, Bourgeau-Chavez LL, French NHF (2000b) Indirect and long-term effects of fire on the boreal forest carbon budget. In: Innes JL, Beniston M, Verstraete MM (eds) Biomass burning and its inter-relationships with the climate system. Kluwer Academic, Dordrecht, pp 263–280

Kasischke ES, O'Neill K, French NHF, Bourgeau-Chavez LL (2000c) Controls on patterns of biomass burning in Alaskan boreal forest. In: Innes JL, Beniston M, Verstraete MM (eds) Biomass burning and its inter-relationships with the climate system. Kluwer Academic, Dordrecht, pp 173–196

Kasischke ES, Tanase MA, Bourgeau-Chavez LL, Borr M (2011) Soil moisture limitations on monitoring boreal forest regrowth using spaceborne L-band SAR data. Remote Sens Environ 115:227–232

Keenan TF, Gray J, Friedl MA, Toomey M, Bohrer G, Hollinger DY, Munger W, O'Keefe J, Schmid HP, Wing IA, Yang B, Richardson AD (2014) Net carbon uptake has increased through warming-induced changes in temperate forest phenology. Nat Clim Change 4:598–604

Kim Y, Tanaka N (2003) Effect of forest fire on the fluxes of CO_2, CH_4, and N_2O in boreal forest soils, interior Alaska. J Geophys Res 108(D1):8154. https://doi.org/10.1029/2001JD000663

Kim Y, Ueyama M, Nakagawa F, Tsunogai U, Tanaka N, Harazono Y (2007) Assessment of winter fluxes of CO_2 and CH_4 in boreal forest soils of central Alaska estimated by the profile method and the chamber method: a diagnosis of methane emission and implications for the regional carbon budget. Tellus 59B:223–233

Kim Y, Kim SD, Enomoto H, Kushida K, Kondoh M, Uchida M (2013) Latitudinal distribution of soil CO_2 efflux and temperature along the Dalton Highway, Alaska. Polar Sci 7:162–173

Kim Y (2014) Effect of ablation rings and soil temperature on 3-year sprung CO2 efflux along the Dalton Highway, Alaska. Biogeosciences 11:6539–6552. https://doi.org/10.5194/bg-11-6539-2014

Kim Y, Kodama Y, Shim C, Kushida K (2014) Carbon exchange rates in *Polyytrichim jiniperinum* moss of burned black spruce forest in interior Alaska. Polar Sci 8:146–155

Kobayashi H, Iwabuchi H (2008) A coupled 1-D atmosphere and 3-D canopy radiative transfer model for canopy reflectance, light environment, and photosynthesis simulation in a heterogeneous landscape. Remote Sens Environ 112:173–185

Kobayashi H, Yunus AP, Nagai S, Sugiura K, Kim Y, Van Dam B, Nagano H, Zona D, Harazono Y, Bret-Harte MS, Ichii K, Ikawa H, Iwata H, Oechel W, Ueyama M, Suzuki R (2016) Latitudinal gradient of spruce forest understory and tundra phenology in Alaska as observed from satellite and ground-based data. Remote Sens Environ 177:160–170

Kojima K (2001) Contribution of snow dent around stem on the snowmelt rate in larch forest Japan. Snow Ice Hokkaido 20:9–12 (in Japanese)

Levine JS (1991) Global biomass burning: atmospheric, climate, and biospheric implications. MIT Press, Cambridge

Le Toan T, Quegan S, Woodward I, Lomas M, Delbart N, Picard G (2004) Relating radar remote sensing of biomass to modelling of forest carbon budgets. Clim Change 67:379–402

Litvak M, Miller S, Wofsy SC, Goulden M (2003) Effect of stand age on whole ecosystem CO_2 exchange in the Canadian boreal forest. J Geophys Res 108(3):8225. https://doi.org/10.1029/2001JD000854

Liu H, Randerson JT (2008) Interannual variability of surface energy exchange depends on stand age in a boreal forest fire chronosequence. J Geophys Res 113:G01006. https://doi.org/10.1029/2007JG000483

Lloyd J, Taylor JA (1994) On the temperature dependence of soil respiration. Funct Ecol 8:315–323

Lynch JA, Clark JS, Bigelow NH, Edwards ME, Finney BP (2003) Geographic and temporal variations in fire history in boreal ecosystems of Alaska. J Geophys Res. https://doi.org/10.1029/2001JD000332

Lyons EA, Jin Y, Randerson JT (2008) Changes in surface albedo after fire in boreal forest ecosystems of interior Alaska assessed using MODIS satellite observations. J Geophys Res 113:G02012. https://doi.org/10.1029/2007JG000606

McDonald KC, Kimball JS, Njoke E, Zimmermann R, Zhao M (2004) Variability in springtime thaw in the terrestrial high latitudes: monitoring a major control on the biospheric assimilation of atmospheric CO_2 with spaceborne microwave remote sensing. Earth Interact 8:1–23

Monson RK, Lipson DL, Burns SP, Turnipseed AA, Delany AC, Williams MW, Schmidt SK (2006a) Winter forest soil respiration controlled by climate and microbial community composition. Nature 439. https://doi.org/10.1038/nature04555

Monson RK, Burns SP, Williams MW, Delany AC, Weintraub M, Lipson DL (2006b) The contribution of beneath-snow soil respiration to total ecosystem respiration in a high-elevation, subalpine forest. Global Biogeochem Cycles 20, GB3030, https://doi.org/10.1029/2005gb002684

Muraoka H, Noda HM, Nagai S, Motohka T, Saitoh TM, Nasahara KN, Saigusa N (2013) Spectral vegetation indices as the indicator of canopy photosynthetic productivity in a deciduous broadleaf forest. J Plant Ecol 6:393–407

Myneni RB, Keeling CD, Tucker CJ, Asrar G, Nemani RR (1997) Increased plant growth in the northern high latitudes from 1981 to 1991. Nature 386:698–702

Myneni RB, Hoffman S, Knyazikhin Y et al (2002) Global products of vegetation leaf area and fraction absorbed PAR from year one of MODIS data. Remote Sens Environ 83:214–231
Nagai S, Saitoh TM, Kurumado K, Tamagawa I, Kobayashi H, Inoue T, Suzuki R, Gamo M, Muraoka H, Nasahara KN (2013) Detection of bio-meteorological year-to-year variation by using digital canopy surface images of a deciduous broad-leaved forest. Sola 9:106–110
Nagai S, Saitoh TM, Nasahara KN, Suzuki R (2015) Spatio-temporal distribution of the timing of start and end of growing season along vertical and horizontal gradients in Japan. Int J Biometeorol 59:47–54
Nagai S, Nasahara KN, Yoshitake S, Saitoh TM (2017) Seasonality of leaf litter and leaf area index data for various tree species in a cool-temperate deciduous broad-leaved forest, Japan, 2005–2014. Ecol Res 32:297–297
Nagai S, Akitsu T, Saitoh TM et al (2018) 8 million phenological and sky images from 29 ecosystems from the Arctic to the tropics: the phenological eyes network. Ecol Res 33:1091–1092
Nagumo H, Minowa M (1990) Sokujugaku (Dendrometry). Chikyusha, Tokyo, Japan, p 243
Nasahara KN, Muraoka H, Nagai S, Mikami H (2008) Vertical integration of leaf area index in a Japanese deciduous broad-leaved forest. Agric For Meteorol 148:1136–1146
Oechel WC, Vourlitis GL (1997) Climate change in northern latitudes: alterations in ecosystem structure and function and effects on carbon sequestration. In: Oechel WC, Callagham T, Gilmanov T, Holten JI, Maxwell B, Molau U, Svebjörnsson B (eds) Global change and Arctic terrestrial ecosystems. Springer, New York, pp 381–401
Oechel WC, Laskowski CA, Burba G, Gioli B, Kalhori AAM (2014) Annual patterns and budget of CO_2 flux in an Arctic tussock tundra ecosystem. J Geophysl Res Biogeosci 119:323–339
O'Neill KP, Kasischke ES, Richter DD (2003) Seasonal and decadal patterns of soil carbon uptake and emission along an age-sequence of burned black spruce forest stands in interior Alaska. J Geophys Res 108(D1):8155. https://doi.org/10.1029/2001JD000443
O'Neill KP, Richter DD, Kasischke ES (2006) Succession-driven changes in soil respiration following fire in black spruce stands of interior Alaska. Biogeochemistry 80:1–20
Osumi S (1987) Shinrin keisoku-gaku kogi (Lecture on forest dendrometry). Yokendo, Tokyo, Japan, p 287
Piao S, Wang X, Ciais P, Zhu B, Wang T, Liu J (2011) Changes in satellite-derived vegetation growth trend in temperate and boreal Eurasia from 1982 to 2006. Glob Change Biol 17:3228–3239
Pisek J, Chen JM (2009) Mapping forest background reflectivity over North America with Multi-angle Imaging SpectroRadiometer (MISR) data. Remote Sens Environ 113:2412–2423
Potithep S, Nagai S, Nasahara KN, Muraoka H, Suzuki R (2013) Two separate periods of the LAI–VIs relationships using in situ measurements in a deciduous broadleaf forest. Agric For Meteorol 169:148–155
Randerson JT et al (2006) The impact of boreal forest fire on climate warming. Science 314:1130–1132
Rautiainen M, Heiskanen J (2013) Seasonal contribution of understory vegetation to the reflectance of a boreal landscape at different spatial Scales. IEEE Geosci Remote Sens Lett 10:923–927
Raynolds MK, Walker DA, Maier HA (2006) Alaska arctic tundra vegetation map. Scale 1:4,000,000. Conservation of Arctic Flora and Fauna (CAFF) Map No. 2. U.S. Fish and Wildlife Service, Anchorage, Alaska
Rayment MB, Jarvis PG (2000) Temporal and spatial variation of soil CO_2 efflux in a Canadian boreal forest. Soil Biol Biochem 32:35–45
Richardson AD, Dail DB, Hollinger DY (2011) Leaf area index uncertainty estimates for model–data fusion applications. Agric For Meteorol 151:1287–1292
Richardson AD, Jenkins JP, Braswell BH, Hollinger DY, Ollinger SV, Smith ML (2007) Use of digital webcam images to track spring green-up in a deciduous broadleaf forest. Oecologia 152:323–334

Richardson AD, Keenan TF, Migliavacca M, Ryu Y, Sonnentag O, Toomey M (2013a) Climate change, phenology, and phenological control of vegetation feed- backs to the climate system. Agric For Meteorol 169:156–173

Richardson AD, Carbone MS, Keenan TF, Czimczik CI, Hollinger DY, Murakami P, Schaberg PG, Xu X (2013b) Seasonal dynamics and age of stemwood nonstructural carbohydrates in temperate forest trees. New Phytol 197:850–861

Richter DD, O'Neill KP, Kasischke ES (2000) Postfire stimulation of microbial decomposition in black spruce (*Picea mariana* L.) forest soils: a hypothesis. In: Kasische ES, Stocks BR (eds) Fire, climate change, and carbon cycling in the Boreal Forest. Springer, New York, pp 173–196

Risk D, Nickerson N, Creelman C, McArthur G, Owens J (2011) Forced diffusion soil flux: A new technique for continuous monitoring of soil gas efflux. Agr For Meteorol 151:1622–1631

Rosenqvist A, Shimada M, Ito N, Watanabe M (2007) ALOS PALSAR: a pathfinder mission for global-scale monitoring of the environment. IEEE Trans Geosci Remote Sens 45:3307–3316

Ruokolainen L, Salo K (2006) The succession of boreal forest vegetation during ten years after slash-burning in Koli National Park, eastern Finland. Ann Bot Fennici 43:363–378

Ryu Y, Sonnentag O, Nilson T, Vargas R, Kobayashi H, Wenk R, Baldocchi DD (2010) How to quantify tree leaf area index in an open savanna ecosystem: a multi-instrument and multi-model approach. Agric For Meteorol 150:63–76

Savage KE, Davidson EA (2003) A comparison of manual and automated systems for soil CO_2 flux measurements: trade-offs between spatial and temporal resolution. J Exper Botany 54:891–899

Schlentner RE, Van Cleve K (1985) Relationships between CO_2 evolution from soil, substrate temperature, and substrate moisture in four mature forest types in interior Alaska. Can J For Res 15:97–106

Schlesinger WH (1997) Biogeochemistry: an analysis of global change. Academic, San Diego, California

Schlesinger WH, Andrews JA (2000) Soil respiration and the global carbon cycle. Biogeochemistry 48:7–20

Schmidt SK, Costello EK, Nemergut DR, Cleveland CC, Reed SC, Weitraub MN, Meyer AF, Martin AM (2007) Biogeochemical consequences of rapid microbial turnover and seasonal succession in soil. Ecology 88:1379–1385

Schimmel J, Granstrom A (1996) Fire severity and vegetation response in the boreal Swedish forest. Ecology 77:1436–1450

Schwartz MD, Ault TR, Betancourt JL (2013) Spring onset variations and trends in the continental United States: past and regional assessment using temperature-based indices. Int J Climatol 33:2917–2922

Seiler W, Crutzen PJ (1980) Estimates of gross and net fluxes of carbon between the biosphere and atmosphere from biomass burning. Clim Change 2:207–247

Shimada M (2010) Ortho-rectification and slope correction of SAR data using DEM and its accuracy evaluation. IEEE J Sel Topics Appl Earth Observ Remote Sens 3:657–671

Shimada M, Isoguchi O, Tadono T, Isono K (2009) PALSAR radiometric and geometric calibration. IEEE Trans Geosci Remote Sens 47:3915–3932

Skutch AF (1929) Early stages of plant succession following forest fires. Ecology 10:177–190

Sommerfeld RA, Mosier AR, Musselman RC (1993) CO_2, CH_4 and N_2O flux through a Wyoming snowpack and implications for global budgets. Nature 361:140–142

Stocks BJ, Mason JA, Todd JB, Bosch EM, Wotton BM, Amiro BD, Flannigan MD, Hirsch KG, Logan KA, Martell DL, Skinner WR (2003) Large forest fires in Canada, 1959–1997. J Geophys Res. https://doi.org/10.1029/2001JD000484

Sturm M, Schimel J, Michaelson G, Welker JM, Oberbauer SF, Liston GE, Fahnestock J, Romanovsky V (2005) Winter biological processes could help convert Arctic tundra to shrubland. Biosci 55:17–26

Sugiura K, Nagai S, Nakai T, Suzuki R (2013) Application of time-lapse digital imagery for ground-truth verification of satellite indices in the boreal forests of Alaska. Polar Sci 7:149–161

Suzuki R, Kim Y, Ishii R (2013) Sensitivity of the backscatter intensity of ALOS/PALSAR to the above-ground biomass and other biophysical parameters of boreal forest in Alaska. Polar Sci 7 (2):100–112

Tsuyuzaki S, Kushida K, Kodama Y (2009) Recovery of surface albedo and platn cover after wildfire in a Picea mariana forest in interior Alaska. Clima Change 93:517–525

Tsuyuzaki S, Narita K, Sawada Y, Harada K (2013) Recovery of forest-floor vegetation after a wildfire in a Picea mariana forest. Ecol Res 28:1061–1068

Ueyama M, Harazono Y, Ohtaki E, Miyata A (2006) Controlling factors on the interannual CO_2 budget at a subarctic black spruce forest in interior Alaska. Tellus B Chem Phys Meteorol 58 (5):491–501

Ueyama M et al (2013) Upscaling terrestrial carbon dioxide fluxes in Alaska with satellite remote sensing and support vector regression. J Geophys Res Biogeosci 118:1–16. https://doi.org/10.1002/jgrg.20095

Ueyama M et al (2014) Change in surface energy balance in Alaska due to fire and spring warming, based on upscaling eddy covariance measurements. J Geophys Res Biogeosci 119:1947–1969. https://doi.org/10.1002/2014JG002717

Ulaby FT, Moore RK, Fung AK (1986) Microwave remote sensing: active and passive, volume III: from the theory to applications. Artech House, Norwood, MA, USA, p 2162

Van Cleve K, Dryness CT, Viereck LA, Fox J, Chapin FS, Oechel W (1983) Taiga ecosystems in interior Alaska. Bioscience 33:39–44

Verbyla D (2008) The greening and browning of Alaska based on 1982–2003 satellite data. Glob Ecol Biogeogr 17:547–555

Viereck LA, Dyrness CT, Batten AR, Wenzlick KJ (1992) The Alaska vegetation classification. Gen. Tech. Rep. PNW-GTR-286. Portland, OR: U.S. Department of Agriculture, Forest Service, Pacific Northwest Research Station

Vitt DH, Marsh JE, Bovey RB (eds) (1988) Mosses, Lichens and Ferns of Northwest North America. Alberta, Canada

White MA, Thornton PE, Running SW (1997) A continental phenology model for monitoring vegetation responses to interannual climatic variability. Global Biogeochem Cycles 11:217–234

Winston GC, Sundquist ET, Stephens BB, Trumbore SE (1997) Winter CO_2 fluxes in a boreal forest. J Geophys Res 102:28795–2880

Woebbecke DM, Meyer GE, Vonbargen K, Mortensen DA (1995) Color indexes for weed identification under various soil, residue, and lighting conditions. Trans Asae 38:259–269

Xu L, Myneni RB, Chapin FS III, Callaghan TV, Pinzon JE, Tucker CJ, Zhu J, Bi J, Ciais P, Tommervik H, Euskirchen ES, Forbes BC, Piao SL, Anderson BT, Ganguly S, Nemani RR, Goetz SJ, Beck PSA, Bunn AG, Cao C, Stroeve JC (2013) Temperature and vegetation seasonality diminishment over northern lands. Nat Clim Change 3:581–586

Xu M, Qi Y (2001) Soil-surface CO_2 efflux and its spatial and temporal variations in a young ponderosa pine plantation in northern California. Global Change Biol 7:667–677

Yarie J (1981) Forest fire cycles and life tables: a case study from interior Alaska. Can J For Res 11:554–562

Yarie Y, Kane E, Mack M (2007) Aboveground biomass equations for the trees of interior Alaska. Agricult For Exper Station Bull 115:1–16

Yang W, Kobayashi H, Suzuki R, Nasahara KN (2014) A simple method for retrieving understory NDVI in sparse needleleaf forests in Alaska using MODIS BRDF data. Remote Sens 6:11936–11955

Yang W, Kobayashi H (2018) Satellite estimation of overstory and understory LAI in boreal forests: a research land product of JAXA GCOM-C project. In: Proceedings of the 64th spring conference of the remote sensing society of Japan, Kashiwa Campus of the University of Tokyo, pp 95–96

Zhang XY, Friedl MA, Schaaf CB, Strahler AH, Hodges JCF, Gao F, Reed B, Huete A (2003) Monitoring vegetation phenology using MODIS. Remote Sens Environ 84:471–475

Zhu WQ, Tian HQ, Xu XF, Pan YZ, Chen GS, Lin WP (2012) Extension of the growing season due to delayed autumn over mid and high latitudes in North America during 1982–2006. Glob Ecol Biogeogr 21:260–271

Zhu Z, Bi J, Pan Y, Ganguly S, Anav A, Xu L, Samanta A, Piao S, Nemani RR, Myneni RB (2013) Global data sets of vegetation leaf area index (LAI)3 g and fraction of photosynthetically active radiation (FPAR)3g derived from global inventory modeling and mapping studies (GIMMS) normalized difference vegetation index (NDVI3g) for the period 1981 to 2011. Remote Sens 5:927–948

Dr. Yongwon Kim received the Ph.D. degree in the Graduate School of Environmental Earth Science from the Hokkaido University, Sapporo, Japan in 1998. He was a Postdoctoral Fellow in the Japan Aerospace Exploration Agency (JAXA), the Japan Agency for Marine-Earth Science and Technology (JAMSTEC), Japan, and the International Arctic Research Center (IARC) of the University of Alaska Fairbanks (UAF), USA. He is currently a Research Associate Professor in the IARC of UAF. His main research concerns are to quantify soil carbon emission in response to changes in climate and environment in the Sub-Arctic and Arctic terrestrial ecosystems.

Dr. Hideki Kobayashi received the Ph.D. degree in Environmental Science and Technology from Tokyo Institute of Technology, Tokyo, Japan in 2004. He was a Postdoctoral Fellow in Japan Agency for Marine-Earth Science and Technology (JAMSTEC) and University of California, Berkeley. He is currently a Deputy Research Unit Leader in Institute of Arctic Climate and Environmental Research, JAMSTEC, and also serves as Adjunct Associate Professor at Tokyo Institute of Technology and Visiting Associate Professor at Chiba University. His recent research interests are in plant canopy radiative transfer and integration of the near-surface, airborne and satellite remote sensing of plant canopies with particular focus on northern high latitudes.

Dr. Shin Nagai defensed the Ph.D. degree in the Graduate School of Environmental Studies from the Nagoya University, Nagoya, Japan in 2007. He was a Postdoctoral Fellow in the Gifu University, Gifu, Japan. Currently, he is a Senior Scientist in the Research Institute for Global Change of Japan Agency for Marine-Earth Science and Technology (JAMSTEC), Yokohama, Japan. His main research concerns are to evaluate the spatio-temporal variability of plant phenology in response to changes in climate and environment in the Arctic, temperate, and tropical ecosystems by remote sensing observations.

Dr. Masahito Ueyama is an Associate Professor of Graduate School of Life and Environmental Sciences of Osaka Prefecture University in Sakai, Japan. His research interest is the land-atmosphere interaction of energy, water, and trace gases. His approach relies on integration and synthesis of field observations, numerical model, and remote sensing data. Dr. Ueyama received his Doctoral degree in Science at Graduate School of Natural and Technology, Okayama University, and worked at International Arctic Research Center, University of Alaska, Fairbanks, USA as a visiting research scholar.

Dr. Bang Yong Lee Lee received the Ph.D. degree in the Graduate School of Atmospheric Sciences from the Yonsei University, Seoul, Korea in 2000. He is currently a Senior Research Scientist in the Korea Polar Research Institute (KOPRI). His main research concerns are to understand the process of greenhouse gas exchange between climate, ecosystem, and frozen soil, and combined with satellite exploration to improve the accuracy of environmental change forecast across the entire scale of the Pan-Arctic permafrost regions.

Dr. Rikie Suzuki (the deceased) received the Ph.D. degree in the Climate and Meteorology from the University of Tsukuba in 1989. From 1989 to 1998, he was a Postdoctoral Fellow, Research Associate, and Assistant Professor in University of Tsukuba. In 1998, he joined the Frontier Research System for Global Change. In 2004, he joined the Japan Agency for Marine-Earth Science and Technology (JAMSTEC) and served as a Senior Researcher, Team Leader, and Director until 2017. He also served as an associated editor in Polar Science Journal, Chigaku Zasshi (In Japanese) and a committee member in Earth and Planetary Science Division of Science Council of Japan. His past research interests were in geographical analysis of climate and plant interactions using remote sensing and climate data sets. His research target was on the Eastern Siberia and Alaska. He experienced and led several field-work projects in China, Mongolia, Siberia, and Alaska.

Northern Ecohydrology of Interior Alaska Subarctic

22

Jessica M. Young-Robertson, W. Robert Bolton, and Ryan Toohey

Abstract

Ecohydrology—as an interdisciplinary field—developed in and explores processes in warm semi-arid and arid ecosystems. This field is in its infancy with respect to arctic and subarctic systems in Alaska. However, similar to warm and dry regions, soil moisture storage is a driver of ecohydrological processes in these northern regions. The presence or absence of permafrost impacts soil moisture storage and determines whether ecological or hydrological processes drive water cycling. The arctic is in the zone of continuous permafrost distribution, and the subarctic is in the zone of discontinuous permafrost distribution. In the subarctic, hydrological processes are dominated by soil moisture storage in areas with permafrost and by ecological processes in areas without permafrost. Given the infancy of the ecohydrology discipline in arctic and subarctic systems, there are a number of knowledge gaps outlined at the end of this chapter.

Keywords

Boreal forest · Alaska · Birch · Black spruce · Soil storage · Active layer · Permafrost

J. M. Young-Robertson (✉)
Agricultural and Forestry Experiment Station, Institute of Agriculture, Natural Resources and Extension, University of Alaska Fairbanks, Fairbanks, AK, USA
e-mail: jmrobertson3@alaska.edu

W. R. Bolton
International Arctic Research Center, University of Alaska Fairbanks, Fairbanks, AK, USA
e-mail: wrbolton@alaska.edu

R. Toohey
Alaska Climate Adaptation Science Center, Anchorage, AK, USA
e-mail: rtoohey@usgs.gov

D. Yang and D. L. Kane (eds.), *Arctic Hydrology, Permafrost and Ecosystems*,
https://doi.org/10.1007/978-3-030-50930-9_22

22.1 Introduction

Ecohydrology is an interdisciplinary field that examines the soil–plant–atmosphere continuum, and specifically focuses on the hydrological processes that drive ecological processes. The field of ecohydrology has largely developed based on the water balance processes in desert regions, which experience high evaporation rates and potential evapotranspiration (PET), high competition for water among plants, strong wet–dry soil moisture dynamics, and high water stress. According to an ecohydrology review by Rodriguez-Iturbe (2000), soil moisture is the link for the plant-atmosphere continuum and for integrating the spatiotemporal dynamics of ecological and hydrological processes. Soil moisture storage can act as a reservoir for plants to utilize and support them during periods of low rainfall. This is true for desert and non-desert regions, such as Alaskan arctic and subarctic systems that will be discussed herein.

Permafrost is defined as ground (soil, rock, sediment) that is frozen (<0 °C) for two or more consecutive years. Near-surface permafrost resides below a thin (typically <1 m thick) seasonally frozen and thawed soil layer (the "active layer") (Pastick et al. 2015). In the zone of discontinuous permafrost (mostly subarctic), permafrost is found primarily on north facing slopes and valley bottoms (Jorgenson et al. 2010). Within Alaskan arctic and subarctic systems, which are located in the zone of continuous and discontinuous permafrost, storage dynamics—such as seasonal soil freeze–thaw, the presence or absence of permafrost, snow accumulation and ablation, and tree water dynamics—dominate hydrological processes. However, these mechanisms and processes of storage dynamics are an active and expanding research area. Some of the knowledge gaps in these areas limit accurate modeling and predicting of changes in hydrology (Bring et al. 2016). Storage is defined as water detained within a watershed. Storage mechanisms include soil moisture, groundwater, lake and ponds, and snow/glaciers, etc. It is critical to determine the storage capacity of soils and vegetation in Arctic and subarctic systems. In some hydrological models, storage can be included in a vaguely defined error term, which can include uncertainties associated with other aspects of the water balance (precipitation, evapotranspiration, plant storage, and discharge). It can be challenging to predict changes in water balance if vague error terms (that lack mechanistic functions) describe storage in a storage-dominated system. Further, error propagation into model estimates can be large when scaling water balance to the landscape level because the storage terms are not well quantified or mechanistically understood. Permafrost, hydrology, ecosystem water use, and climate are tightly interconnected and impact storage processes. However, understanding their interconnectedness has rarely been approached in a holistic manner in field or modeling research. The largely disciplinary approach taken thus far further hinders modeling efforts aimed at capturing the impact of climate change and permafrost thaw on ecosystems. Changes in storage—due to thawing permafrost, change in vegetation communities, snow accumulation and ablation, and deepening of the active layer—has implications for stream flow and ultimately freshwater

export from the boreal forest (McGuire et al. 2006; McGuire and Chapin 2006). Implications of storage change also exist for tree resistance to drought, snowmelt water pathways, groundwater recharge in permafrost-free areas, fish population, atmospheric moisture, and climate. The presence or absence of ice-rich permafrost is *the* primary control on the processes impacting hydrology and ecology in subarctic systems (Kane et al. 2008; Hinzman et al. 2005, 2006a, b; Jorgenson et al. 2013). See Fig. 22.1.

22.2 Permafrost and Ecohydrology

The presence or absence of permafrost impacts the ecosystem and its components. Areas underlain with ice-rich permafrost have relatively cold, wet soils and thick organic layers that support an extensive non-vascular plant community (mosses) and, in the subarctic, small-statured black spruce trees (*Picea mariana*). Permafrost-free areas (in the subarctic), with relatively dry, warm soils and thin organic layers, support large deciduous trees (primarily *Betula neoalaskana* and *Populus tremuloides*), along with some understory shrubs, herbaceous plants, and white spruce (*Picea glauca*). Each of these ecosystems has different water use strategies and, thus, different water pathways (i.e., vertical vs. horizontal). Hydrological, rather than ecological, processes appear to dominate the ecohydrology of areas with ice-rich permafrost, wherein the understory species and black spruce have low water use rates and water storage, with transpiration rates around 10–50 mL water day^{-1} (black spruce, Young-Robertson pers obs) and stem water contents around 25–50% (Young-Robertson et al. 2016, Fig. 22.2). The dominant water pathway is lateral, or horizontal, through the soil as ice-rich permafrost effectively creates an aquitard due to its reduced permeability (Dingman 1975; Woo and Marsh 1990; Woo 2012). This prevents near-surface waters from percolating into deeper soils, thereby forcing near-surface water to move laterally over the ice-rich soils and into the streams in the valley bottoms.

Conversely, ecological rather than hydrological, processes dominate the ecohydrology of permafrost-free areas. Deciduous trees have very high water use rates and water storage, with transpiration rates nearly an order of magnitude greater than the black spruce and water contents around 75–100% (Young-Robertson et al. 2016, Fig. 22.2). The dominant water pathway is vertical, wherein water either moves into the trees or down through the soil as it percolates into groundwater (Fig. 22.3). Evapotranspiration is discussed with respect to partitioning in the next section and with more discussion on storage in Sect. 22.2.

22.2.1 Evapotranspiration Process and Its Impact

In northern environments, growing season and snow cover duration often provide the initiation and termination bounds of the evapotranspiration (ET) flux with soil

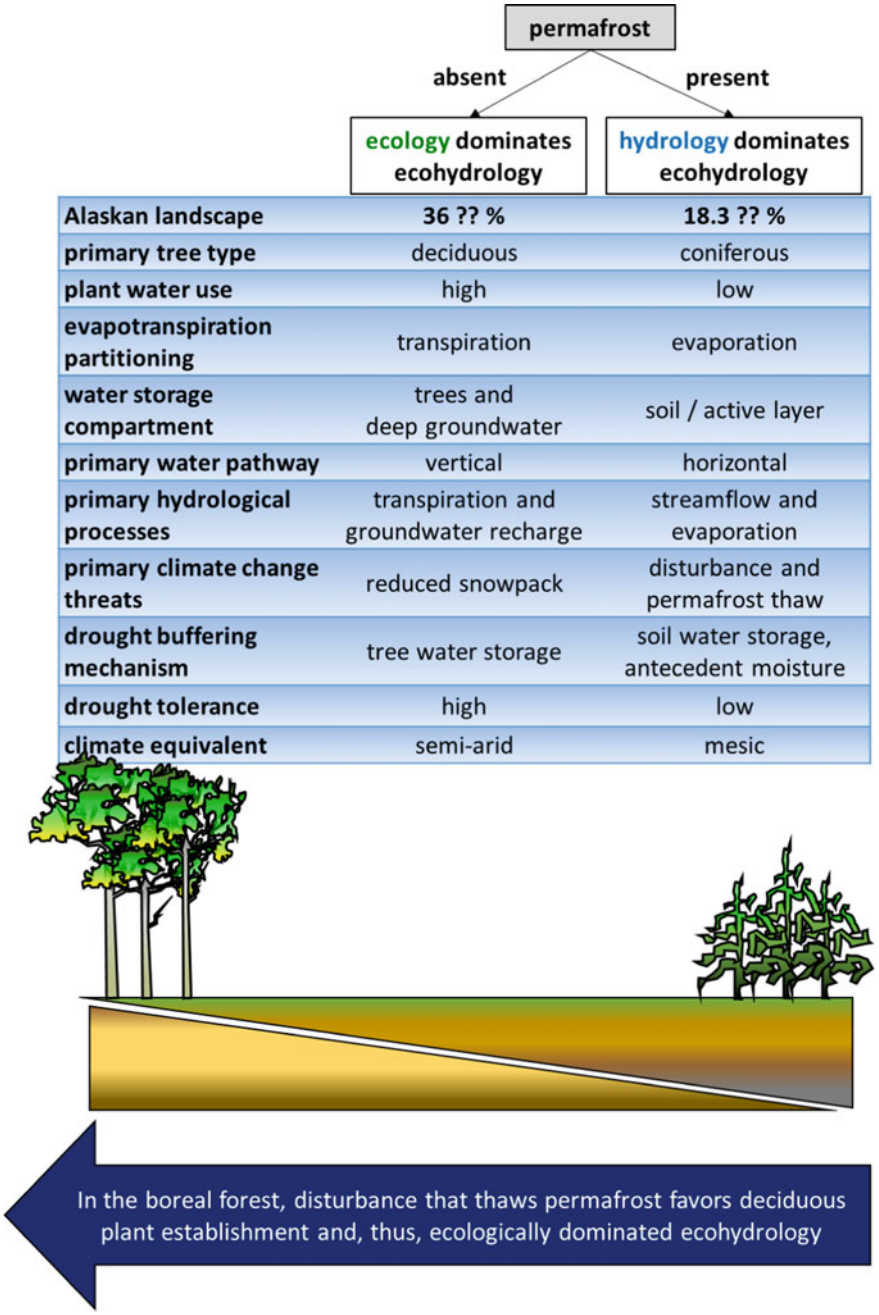

Alaskan landscape	**36 ?? %**	**18.3 ?? %**
primary tree type	deciduous	coniferous
plant water use	high	low
evapotranspiration partitioning	transpiration	evaporation
water storage compartment	trees and deep groundwater	soil / active layer
primary water pathway	vertical	horizontal
primary hydrological processes	transpiration and groundwater recharge	streamflow and evaporation
primary climate change threats	reduced snowpack	disturbance and permafrost thaw
drought buffering mechanism	tree water storage	soil water storage, antecedent moisture
drought tolerance	high	low
climate equivalent	semi-arid	mesic

◀ **Fig. 22.1** Conceptual figure of the ecohydrology of Interior Alaskan subarctic systems, focusing on upland areas during the growing season. The primary tree type of permafrost-free areas are deciduous species such as birch and aspen (*Betula neoalaskana* and *Populus tremuloides*, respectively) with some white spruce (*Picea glauca*), and coniferous species (black spruce, *Picea mariana*) dominates the permafrost areas. Tree water use is high and dominates the evapotranspiration partitioning in the permafrost-free areas but low tree water use and evaporation occur in the areas with permafrost. The primary water storage compartments in the permafrost-free areas are trees and deep groundwater, but the active layer is the dominant compartment in areas with permafrost. The primary water pathway and hydrological processes in areas without permafrost are vertical, wherein transpiration and groundwater recharge dominate the water pathways. However, in areas with permafrost, the primary water pathway is horizontal and the dominant hydrological processes are stream flow and evaporation. We suspect that the primary climate change threats in the permafrost-free areas are reduced snowpack that may reduce tree water storage, but disturbance (such as fire) and permafrost thaw are the primary threats in areas with permafrost. We suspect that the drought tolerance of permafrost-free ecosystems is high, with tree water storage as the primary drought buffering mechanism. However, we suspect the drought tolerance in permafrost areas is low and soil water storage of antecedent water is the primary drought buffering mechanism. The climate equivalent (based upon the hydrological definitions of drought) is semi-arid in the permafrost-free area but mesic in the permafrost area

temperature being a primary control on ET variability (Cable et al. 2014; Bring et al. 2016; Young-Robertson et al. 2017). Throughout the Arctic, the spatial and temporal extent of snow cover has generally decreased over the last century even though winter precipitation and snow depth have increased in many areas (Saito et al. 2013; Bring et al. 2016). At least partially due to this increased insulation of snow cover within permafrost regions, soil temperatures and active layer depths have increased throughout the Arctic (Saito et al. 2013).

Evapotranspiration (ET) is a critical part of the water cycle in the Arctic and semi-arid Interior Alaskan subarctic climate. During the snow-free season of the Arctic Coastal Plain, ET can be the dominant hydrological loss pathway (Fig. 22.5, Liljedahl et al. 2017; Young-Robertson et al. 2018). Within many low-gradient arctic river basins, ET flux can be greater than runoff as a percentage of precipitation (Bring et al. 2016; Liljedahl et al. 2017). While generally less than precipitation, summer ET can exceed summer or annual precipitation in limited locales such as southern interiors (Serreze et al. 2006), lakes, and wetlands (Bowling et al. 2003; Bring et al. 2016). While ET is notoriously difficult to estimate, field-based observations and remote sensing data provide a wide range of ET flux from approximately 150–280 mm yr^{-1} over the northern environments (Fig. 22.4, Liljedahl et al. 2017; Nakai et al. 2013; Zhang et al. 2009; Bring et al. 2016). Atmospheric demand is often correlated with the amount of ET in tundra; in boreal forest, soil moisture, permafrost, and forest type often regulate the amount of ET (Ohta et al. 2008; Saito et al. 2013).

ET can affect soil moisture and surface water processes (Riordan et al. 2006), while providing a source of local moisture for the atmosphere (Molders 2012). Increasing groundwater and surface water connectivity due to permafrost thaw can also influence soil moisture and lake dynamics, which may influence moisture

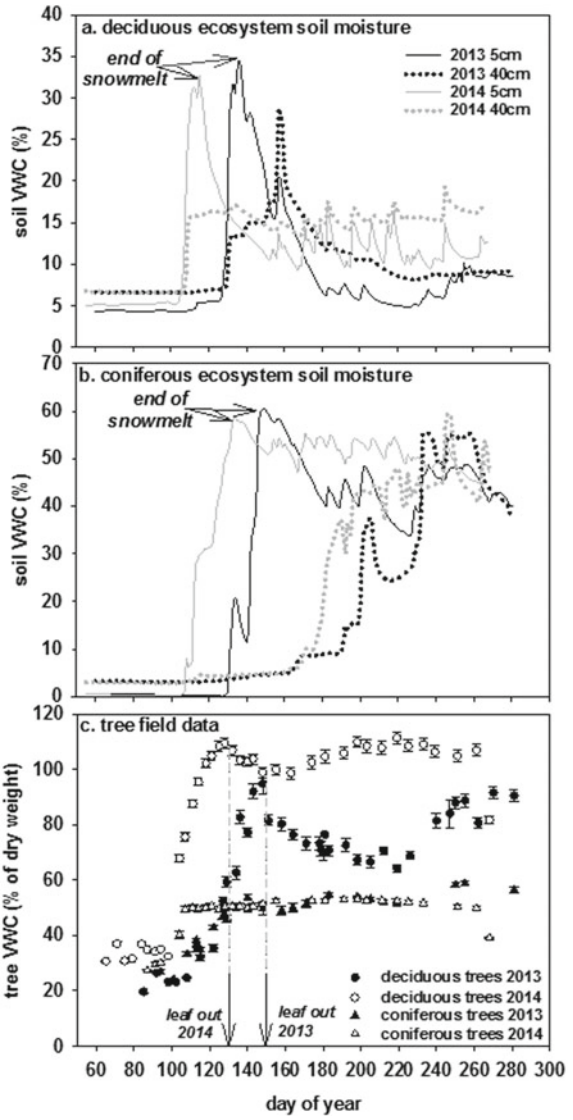

Fig. 22.2 Field data collected from CPCRW research sites in 2013 and 2014. Soil moisture (volumetric water content, VWC, %) at 5 and 40 cm in the **a** deciduous ecosystems, **b** coniferous ecosystems, and **c** tree volumetric water content (VWC, % dry weight) measured on deciduous and coniferous trees. Arrows indicate the conclusion of snowmelt (when there is no snow remaining on the ground) and the approximate leaf-out days (Young-Robertson et al. 2016)

exchange with the atmosphere (Bring et al. 2016). Vegetation plays an additional role by intercepting snow and rain and sublimating or evaporating the precipitation before it reaches the soil (Liston and Heimstra 2011). Convective storms derived from local moisture (ET) are a significant aspect of summertime precipitation, particularly in Interior Alaska (Slaughter and Viereck 1986). More research is needed on the processes and mechanisms of how forests influence water vapor within interior ecosystems (Saito et al. 2013).

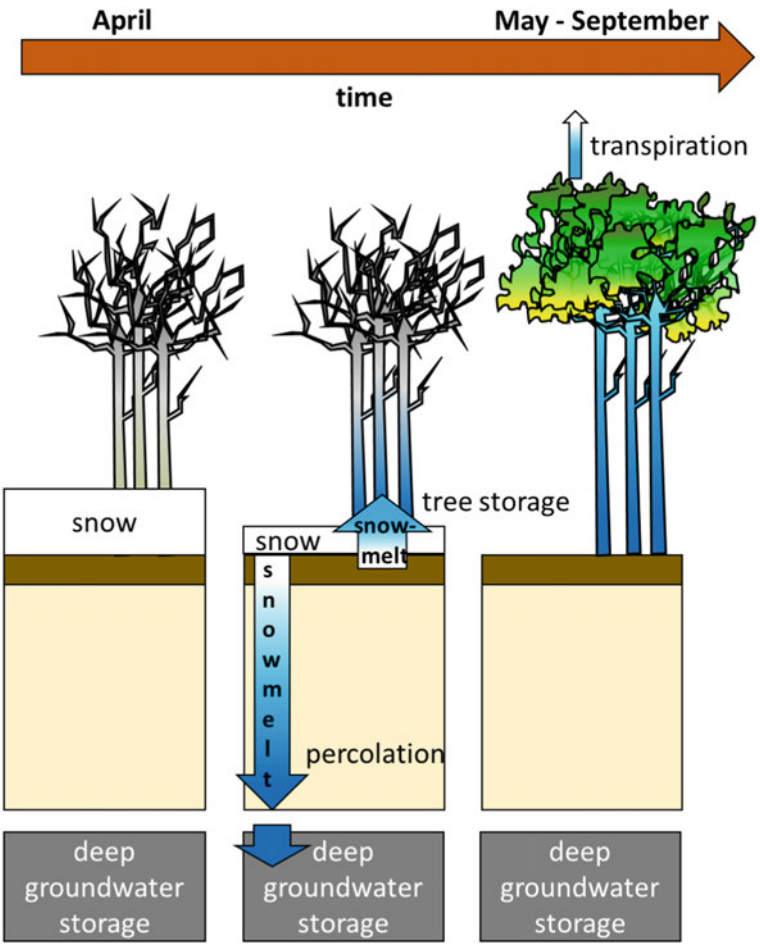

Fig. 22.3 The soil/active layer storage dynamics in areas with permafrost throughout the summer (from snowmelt in April to when the ground starts freezing in September). Early in the summer, storage capacity is low due to shallow thaw depths, but as the summer progresses, the thaw depth increases and reveals the different organic layers with differing water retention properties. Organic layer 1 is the least dense and least decomposed down to organic layer 3 which is the most dense and decomposed. The mineral soil is a fine textured silt located atop the permafrost

One of the major gaps in our understanding and quantification of ET investigates the degree to which plants control ET in subarctic ecosystems (e.g., the partitioning into evaporation [E] and transpiration [T]). The partitioning of ET is important for understanding the sources of soil moisture that are lost to the atmosphere (E = daily rainfall or T = seasonally integrated rainfall), soil–atmosphere connectivity (E = surface soil moisture or T = moisture from the rooting depth of the soil profile), the primary controls on ecosystem water vapor flux (E = physically

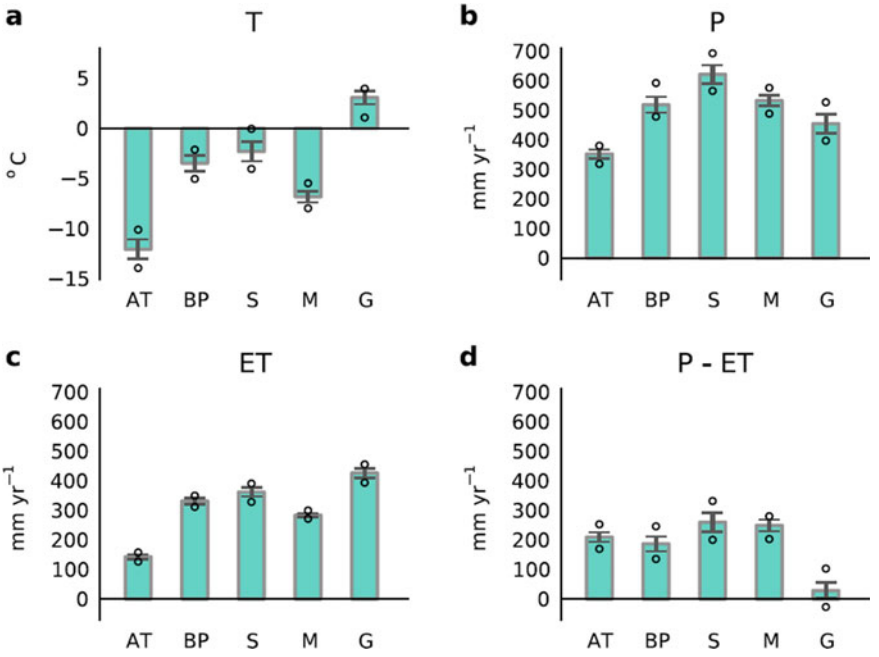

Fig. 22.4 From Bring et al. (2016): "Climatology of Arctic hydrophysiographical regions. Annual averages of grid-based **a** temperature, **b** precipitation, **c** evapotranspiration, and, as a proxy for runoff, **d** precipitation minus evapotranspiration values, over the regions defined in Fig. 22.1 for the period 1979–2013. Regions are abbreviated as AT: Arctic tundra, BP: Boreal plains, S: Shields, M: Mountains, and G: Grasslands. Error bars denote one standard deviation of annual means, and open circles denote maximum and minimum annual means during the period. All data are from the ERA-Interim reanalysis product and are available at http://apps.ecmwf.int/datasets/data/interim-full-daily. Glaciers and ice sheets are not included here due to low density of observations in these ecoregions."

controlled or T = physiological controlled), and the potential for changes in ecosystem structure or climate change to impact vapor fluxes (shift from E to T dominated fluxes or vice versa) (Jasechko et al. 2013). In general, E appears to drive ET throughout permafrost areas, while T increases with increasing soil temperatures and/or deciduous vegetation (Figs. 22.5, 22.6 and 22.9, Cable et al. 2014; Young-Robertson et al. 2018). We suspect that evaporation dominates ET in permafrost areas with black spruce, given low tree transpiration fluxes (Fig. 22.9, Cable et al. 2014). Further, we suspect transpiration dominates ET in subarctic, deciduous, permafrost-free areas, given the high tree transpiration rates and limited energy due to a closed canopy that blocks incoming solar radiation at the litter surface to drive evaporation (Fig. 22.6). However, rigorous quantification of ET partitioning has not been done in either of the previously discussed ecosystem types. Changes in ecosystem structure—due to wildfire, permafrost thaw, and

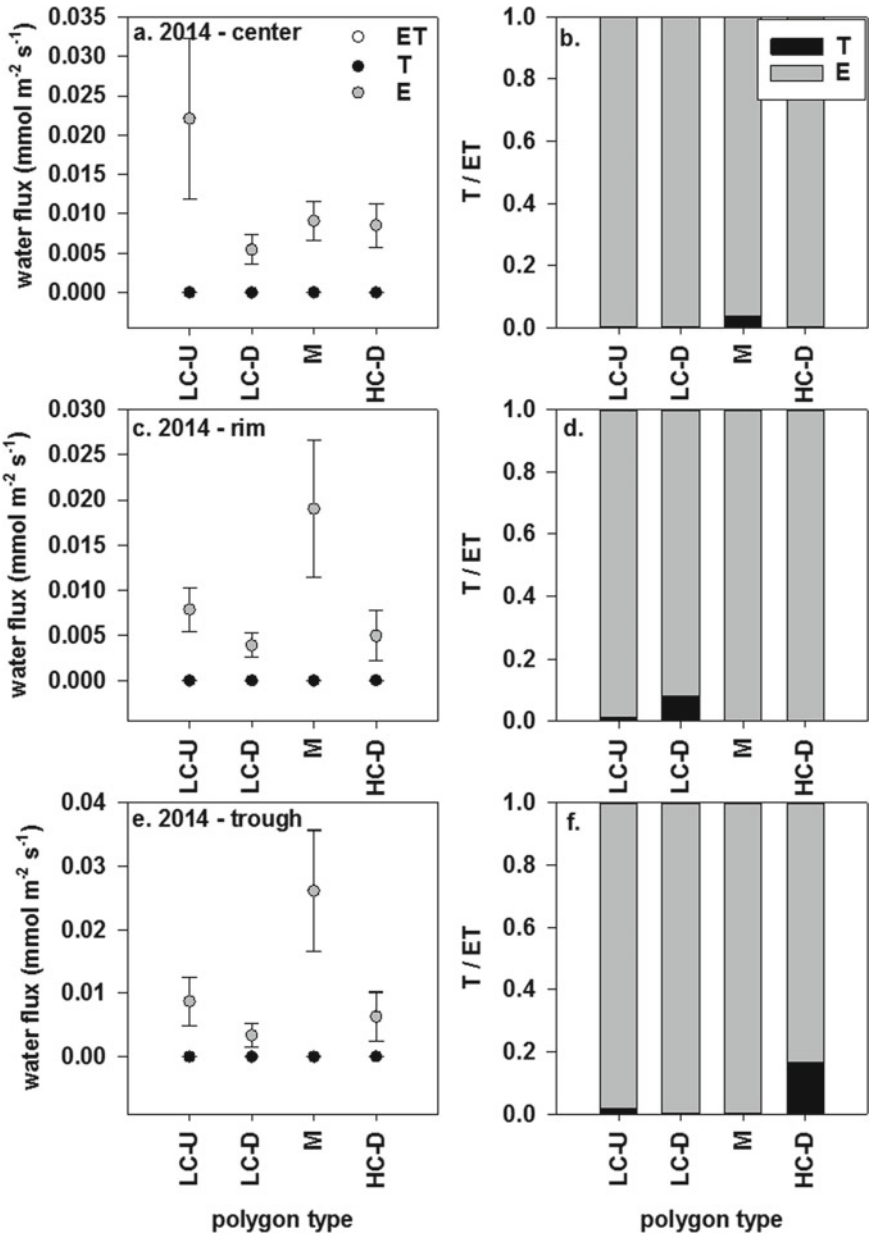

Fig. 22.5 Means and standard errors for the water flux rates and means for the evapotranspiration (ET) partitioning into evaporation (E) and transpiration (T) for 2014 in the different polygon features (polygon center in panels A and B, polygon edge in panels C and D, and polygon trough in panels E and F) across the polygon degradation gradient (D = least degraded, disturbed = most degraded). Data are from measurement days 205–207 (2013) and 189–193 (2014). The different polygon types are low-centered undegraded (LC-U), low-centered degraded (LC-D), mix of high- and low-center polygons (M), high-centered degraded (HC-D), and disturbed (Young-Robertson et al. 2018)

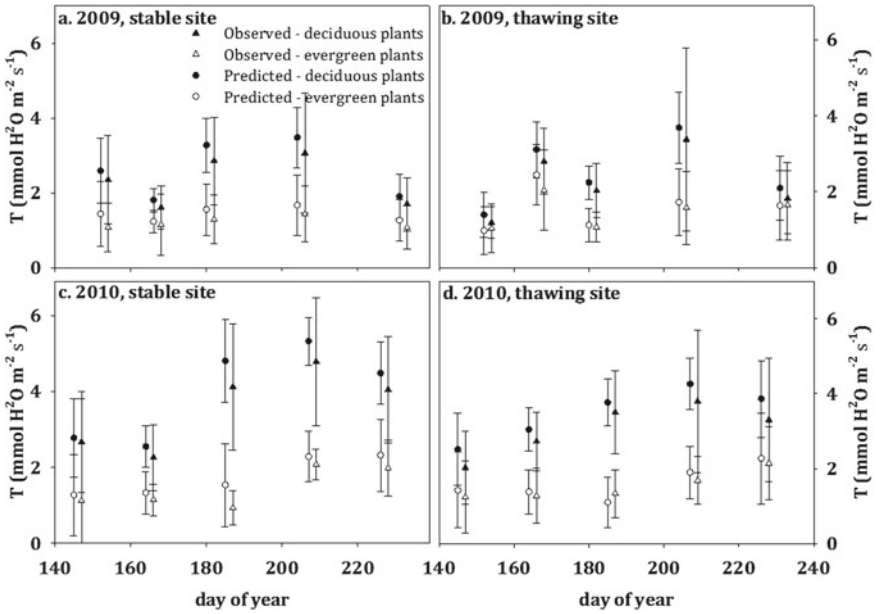

Fig. 22.6 The observed versus predicted transpiration rates plotted for each measurement day and plant functional type in 2009 (**a**, **b**) and 2010 (**c**, **d**) for the stable permafrost site (**a**, **c**) and thawing permafrost site (**b**, **d**). The observed values are the mean and standard errors, and the predicted values are posterior means and 95% credible intervals

deciduous shrub encroachment—will likely result in a shift between evaporation and transpiration-dominated ET fluxes, with consequences for soil moisture, atmospheric moisture, soil carbon storage and flux, and stream flow dynamics (Yoshikawa et al. 2002; Hinzman et al. 2005; Prowse et al. 2006). For example, a shift to deciduous dominated landscapes after intense wildfire may result in soil drying and atmospheric wetting as the plants transpire a large amount of water to the atmosphere (e.g., Riordan et al. 2006; Jasechko et al. 2013).

22.2.2 Storage Processes in Permafrost and Non-permafrost Systems

The heterogeneous subarctic landscape, with its two primary ecosystem types and differing permafrost conditions, has several major water storage compartments. We focus on the three compartments that relate to subarctic uplands, rather than ponds, lakes, and glaciers. During the growing season, the primary water storage compartment in permafrost areas is the seasonally thawed soil (the active layer) (Fig. 22.7). Deep groundwater may also be important in permafrost areas, although it is likely disconnected from vegetation. Vegetation and deep groundwater are the

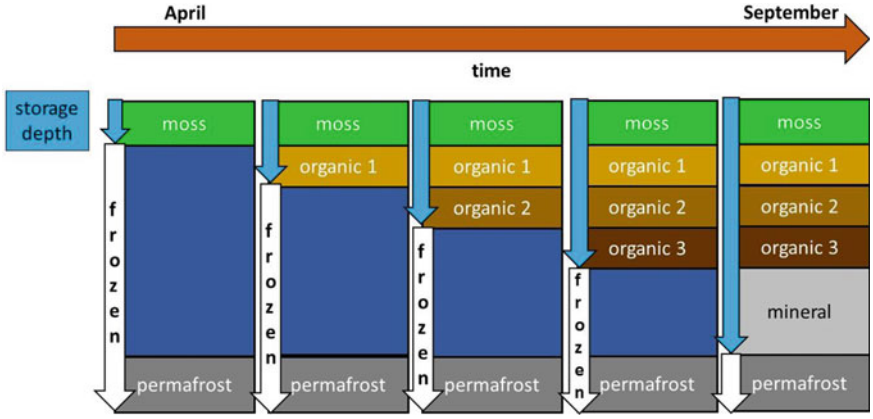

Fig. 22.7 The storage dynamics in permafrost-free areas, wherein snowmelt water either infiltrates into the soil and percolates into deep groundwater or is taken up by the deciduous trees prior to leaf-out. The water remains in and is utilized by the trees throughout the summer

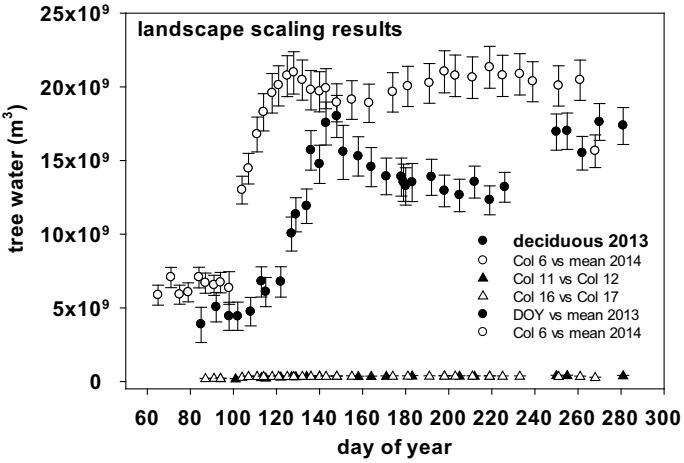

Fig. 22.8 Mean and 95% credible intervals for tree water content scaled to the landscape level (m^3 water) for 2013 and 2014 for deciduous tree and coniferous tree dominated ecosystems (Young-Robertson et al. 2016)

primary compartments in permafrost-free areas. While we can identify these storage compartments, we will describe the characteristics that make their dynamics difficult to quantify and, thus, result in knowledge gaps (Figs. 22.8, 22.9, 22.10).

Within permafrost areas (See Fig. 22.2), the active layer essentially defines the spatial distribution of the rooting zone, water storage, and lateral flow (Chapin et al.

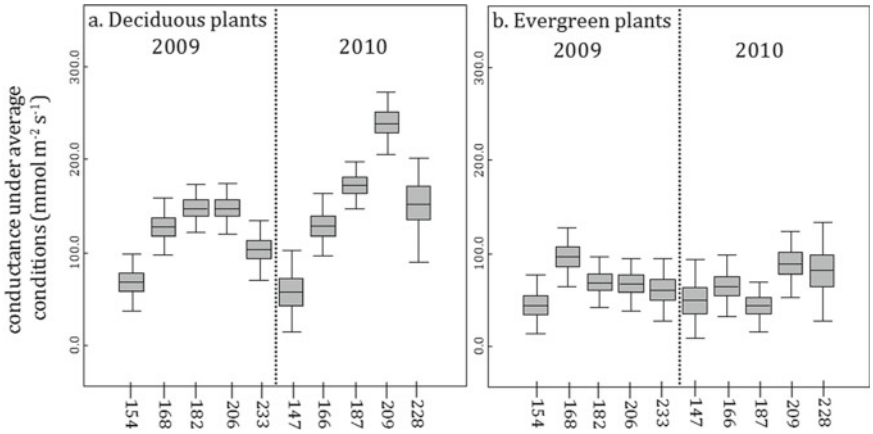

Fig. 22.9 Posterior means and 95% credible intervals for the reference stomatal conductance under average *S*, *T*, and *D* conditions for each measurement day in 2009 (left subpanels) and 2010 (right subpanels) for the **a** deciduous and **b** evergreen plants (Cable et al. 2014)

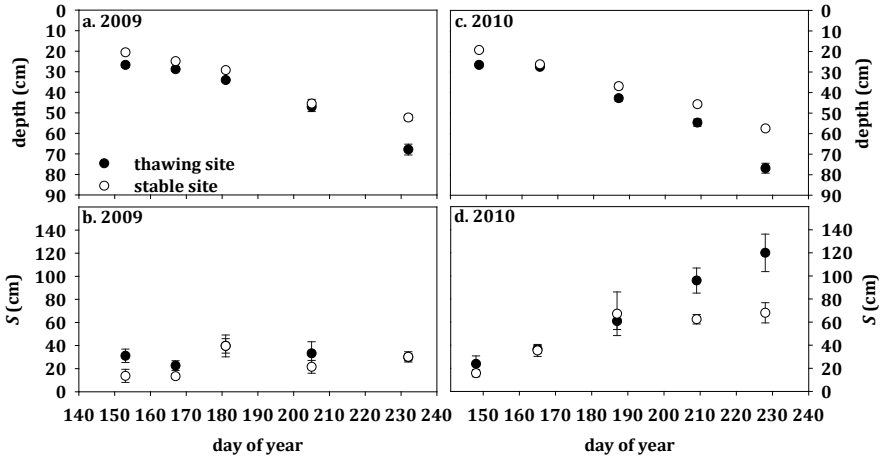

Fig. 22.10 Means and standard errors for observed thaw depths (**a**, **c**) and soil column water contents (*S*) (**b**, **d**) for 2009 (**a**, **b**) and 2010 (**c**, **d**) at the two sites (thawing permafrost, stable permafrost) (Cable et al. 2014)

1992; Saito et al. 2013). Active layer depth varies due to latitude, altitude, and ecosystem with a depth of 30–60 cm in tundra and over 2 m in boreal forest (Brown et al. 2000; Akerman and Johansson 2008; Saito et al. 2013). Thaw depth as a storage compartment is dynamic over the year, particularly the summer, wherein it is shallow early in the summer resulting in low soil water availability

(Cable et al. 2014). As the summer progresses, the seasonal thaw depth increases [deepens], increasing both soil water availability and the liquid water storage capacity of the soils (Bolton et al. 2004; Prowse et al. 2006; Cable et al. 2014) (Figs. 22.7, 22.9). The dynamic nature of the size of this storage compartment is complicated by the vastly different soil textures within the soil profile (Ping et al. 1997). A thick mossy layer (~10 cm) overlays a thick organic layer (~25 cm) that decreases in porosity from the surface to deeper layers (Slaughter and Kane 1979; Haugen et al. 1982). Note the depths of the layers are approximate and can be spatially heterogeneous. In general, both of these layers reside on top of a more finely textured mineral soil. A stark hydrological boundary occurs between the organic and dense, fine textured mineral soils that create a two-layer flow system, wherein most water flows through the organic soils or along the organic/mineral boundary through soil pipes (Carey and Woo 2001). The different soil layers vastly differ in their hydraulic properties and thus, their ability to store and release water (Carey and Woo 2001; Quinton and Marsh 1999; Koch et al. 2014). With relatively high permeability and hydraulic conductivities, the organic soils release water more readily for plant uptake and/or lateral flow. Figure 22.12 shows deciduous and evergreen plant water uptake from the different organic soil layers and the mineral soil at a stable and a thawing permafrost location in two years with contrasting precipitation amounts (dry—2009, average—2010). The organic soil layers that primarily contain rainwater are the primary water source for subarctic plants until late in the summer when they access the mineral soil (Figs. 22.11, 22.12, Young-Robertson et al. 2017).

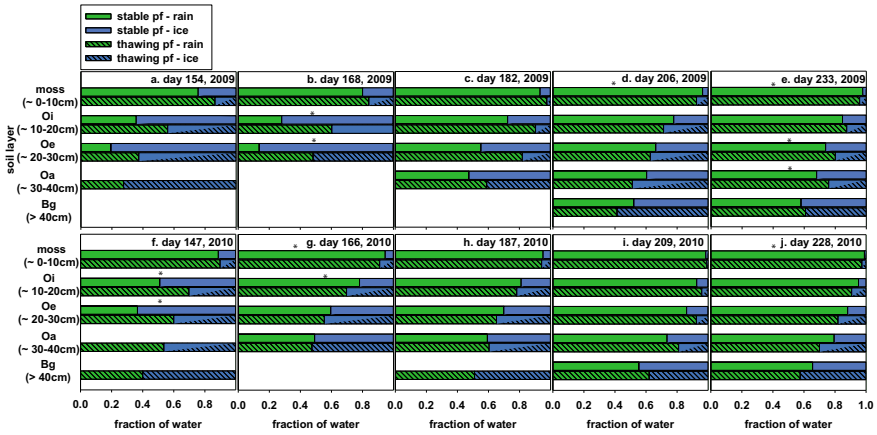

Fig. 22.11 Posterior means and 95% credible intervals of the relative fraction of water derived from rain (green bars) versus thawing seasonal ground ice (blue bars) in each soil layer (moss, Oi, Oe, Oa, Bg) for each measurement day in both years at the stable permafrost site (stable pf, non-hatched bars) and at the thawing permafrost site (thawing pf, hatched bars). Statistically significant differences (at the 5% level) between sites are denoted with an asterisk located above the bars (Young-Robertson et al. 2017)

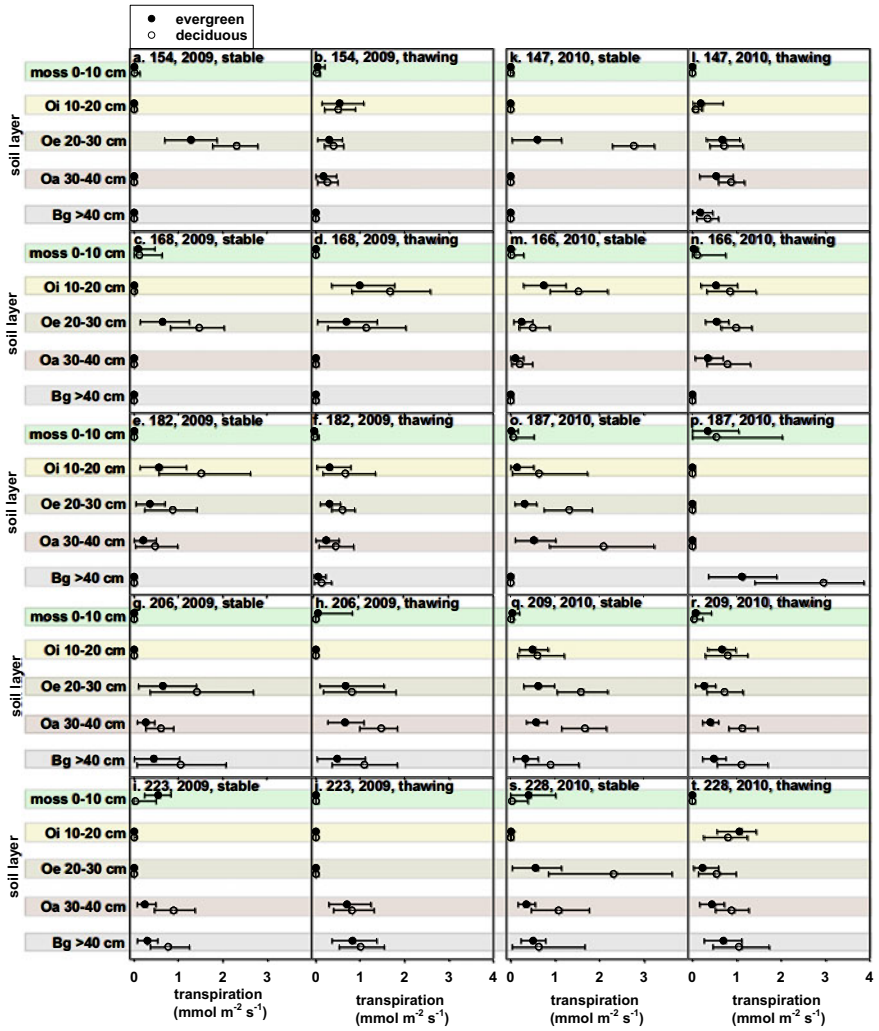

Fig. 22.12 Posterior means and 95% credible intervals for transpiration rates (mmol m^{-2} s^{-1}) partitioned among the five different soil layers (moss, Oi, Oe, Oa, Bg, approximate depths given) for the two plant functional types (evergreen, deciduous) on each measurement day at the thawing and stable permafrost sites in 2009 (**a**–**j**) and 2010 (**k**–**t**) (Young-Robertson et al. 2017)

Each of these factors (permeability, plant water use, lateral flow) can lead to extremely dry soils. The mineralogy of the clay soils results in tightly bound water that is far less available for plant uptake. Due to the mineralogy, the relatively low hydraulic conductivities of these soils also reduces lateral transport, when compared to the organic soils, often resulting in fairly high moisture contents (Slaughter and Kane 1979; Carey and Woo 2001). Based upon porosity (Φ), the organic soils have

a higher storage capacity ($\Phi \sim 0.7 - 0.95$) but based upon total volume at peak thaw ($\sim$ late September), mineral soils have higher total storage capacity ($\Phi \sim 0.43 - 0.48$, Beringer et al. 2001). Thus, as the thaw depth progresses from the organic to the mineral soil layers, soil water availability for plant uptake and lateral transport is reduced (Fig. 22.12, Young-Robertson et al. 2017). When trying to unravel the complexity of watershed-level storage in these systems, it is critical to understand the implications of variable active layer depths and contrasting soil textures that are highly spatially heterogeneous (Koch et al. 2017). Further, it is critical to understand the potential changes in soil storage capacity associated with climate change. These changes include extreme wildfire that burns the organic soil and encourages establishment of shrubs and leads to fundamental changes in soil permeability as soil pipes form, permafrost thaw leading to subsidence, and how extreme precipitation events may influence soil moisture, runoff, and stream flow as the result of these changes.

Previously, in permafrost-free areas, it had been assumed that deep groundwater was the only storage compartment (Kane and Stein 1985). However, recent work by Young-Robertson et al. (2016) show that deciduous trees are also a significant and under-explored storage compartment. Snowmelt is the hydrologic event of the year in subarctic Interior Alaskan systems, with $\sim$30% of the annual water budget released over a 2–3 week period of time (Bolton et al. 2004). Between the onset of snowmelt and the beginning of leaf-out ($\sim$2–3 week period), deciduous trees (birch, aspen) take up 21–25% of snowmelt water (from their respective ecosystems) (Table 22.1, Young-Robertson et al. 2016). In contrast, black spruce trees in the areas with permafrost take up <1% of the snowmelt water. The deciduous trees expand in girth as they fill with water to the point of saturation (Fig. 22.2). Young-Robertson et al. (2016) estimated that the deciduous tree water uptake accounts for about 17.8–20.9 billion m^3 of water in Alaska, which is equivalent to 8.7–10.2% of the Yukon River's annual discharge. In contrast, the coniferous trees only remove about 0.4–2.2 billion m^3 of water in Alaska (Fig. 22.8). Thus, while the greater proportion of snowmelt goes into groundwater recharge in permafrost-free areas (maximum of 75%), a large fraction is also stored in trees and utilized over the summer to support transpiration (Fig. 22.3, Young-Robertson et al. 2016). This is an area of evolving research but it is clear that this major storage compartment is also dynamic in the sense that disturbance, such as wildfire, promotes the establishment of deciduous vegetation (Barrett et al. 2011) with potentially large impacts for snowmelt water and groundwater recharge (Young-Robertson et al. 2016). The trees start the spring with very low ($\sim$25–45%) water contents and end in fall with high (80–100%) water contents (Fig. 22.2). Research is needed on wintertime dry-down dynamics.

22.2.3 Changing ET and Subarctic Alaska Drought

With rising temperatures, decreasing snow cover extent and duration, ET has the potential to increase throughout the Arctic and subarctic (Bring et al. 2016).

Table 22.1 Landscape area for each ecosystem type in Alaska and the shared watersheds in western Canada, including the Yukon River watershed, fraction of snowmelt water taken up prior to leaf-out, snowmelt water uptake during the period of maximum tree water content (between snowmelt and leaf-out), and projected snowmelt water uptake with an increase in deciduous cover

		Ecosystem type	
		Deciduous tree dominated	Coniferous tree dominated
Landscape area (km^2; %)		579,568; 61.6%	360,980; 38.4%
Fraction of snowmelt uptake (%)	2013	21.3% [18.9%, 24.1%]	0.65% [0.55%, 0.75%]
	2014	25.0% [22.4%, 28.0%]	0.62% [0.53%, 0.73%]
Snowmelt water uptake (m^3) at maximum water content (prior to leaf-out)	2013	17.79×10^9 [16.45×10^9, 19.15×10^9]	33.84×10^7 [29.79×10^7, 38.42×10^7]
	2014	20.88×10^9 [19.57×10^9, 22.22×10^9]	32.70×10^7 [28.68×10^7·37.30×10^7]
Snowmelt water uptake (m^3) with an increase in deciduous tree cover by 1, 5,10, or 15%:	1%	19.6×10^9 [18.3×10^9, 21.0×10^9]	—
	5%	20.4×10^9 [19.0×10^9, 21.9×10^9]	—
	10%	21.4×10^9 [19.9×10^9, 22.9×10^9]	—
	15%	22.3×10^9 [20.8×10^9, 23.9×10^9]	—

However, due to its association with landscape diversity, regional and temporal uncertainty remain high. Both tundra and boreal forest are projected to have increased annual ET that may decrease summer soil moisture (Bring et al. 2016).

Vegetation change is another factor driving these ET projections. Increased summer temperatures have led to increasing circumpolar aboveground biomass (Jia et al. 2009; Forbes et al. 2010; Saito et al. 2013). Increasing temperatures, precipitation, and snowpack are also thought to have contributed to shrub expansion over the past several decades as one of the key components of this biomass (Wrona et al. 2016; Sturm et al. 2005; Tape et al. 2012). Boreal forest expansion into the arctic and alpine ecosystems also appears to be the result of increased warming (Chapin et al. 2000). While browning trends across the interior associated with wildfire have occurred at significant scales, recovery from wildfire, insect damage, and timber harvest appears to have promoted photosynthetic activity (Pastick et al. 2018). In particular, wildfire and thermokarst may promote shrubification through

the creation of mineral-rich seedbeds (Lantz et al. 2009). Increasing shrub and tree extent can enhance the ET-mediated decline in surface/organic soil moisture (Wrona et al. 2016).

Permafrost thaw (i.e., thermokarst and lake dynamics) have also led to increased photosynthetic activity (Pastick et al. 2018). Throughout the pan-Arctic, permafrost temperatures have significantly increased (Romanovsky et al. 2010) along with increasing air temperatures, thawing index, and decreasing freezing index (Burn and Kokelj 2009; Thisbual and Payeete 2009; Osterkampt et al. 2009; Saito et al. 2013). As a result of these dynamics, warming regions may experience drought stress leading to declines in plant productivity and higher likelihood of exposure to fire, disease, and ultimately mortality (Rogers et al. 2018; Trugman et al. 2018; Pastick et al. 2018) that may favor conversion to deciduous vegetation.

Drought has many definitions depending upon the topic of interest (e.g., agricultural, hydrological, meteorological, socioeconomic) but all have some relationship to highly reduced water availability for human or natural systems (e.g., drought.unl.edu/DroughtBasics/TypesofDrought.aspx). Much of Interior Alaska is climatically defined as semi-arid with the average annual (1971–2000) precipitation ranging between 20 and 30 cm (Wendler et al. 2017). Yet, only recently (i.e., early 2000s), have studies indicated that Alaskan ecosystems can experience drought even with extensive surface water bodies, high soil moisture in some areas, and an average greenness index that rivals mesic ecosystems (Beck and Goetz 2011; Barber et al. 2000; Juday and Alix 2012). Further, it is also critical to understand the different buffering mechanisms in each system—particularly those that relate to storage—that can limit the impacts of drought in the near term.

In permafrost-free areas, soil moisture is generally extremely low at shallow/rooting depths after the conclusion of snowmelt, and the remaining water present is tightly bound in the deeper, fine textured mineral soils (Fig. 22.2, Young-Robertson et al. 2016) (thus, soils have to be fairly wet and within the rooting depth for plants to be able to utilize the moisture). Despite low rainfall, the deciduous trees that dominate the landscape can limit their water stress over the growing season as they store water in their trunks to utilize over the growing season (Young-Robertson et al. 2016). During very dry periods (e.g., multi-week periods without rain), it appears the trees draw on their stored water supply to limit severe water stress and maintain transpiration rates (Young-Robertson unpublished data). Similar water stress levels are observed in wet and dry years (~ -0.2 to -2 MPa, Young-Robertson unpublished data). The trees replenish their internal stores with new precipitation derived from summer rainfall when observed increases in water content associated with increases in soil moisture from rainfall. The minimum water content threshold is unclear for the trees before drought stress has detrimental effects, like reduced productivity (Yarie 2008). Given the reliance of the trees on stored water, it is clear that drought-related climatic conditions that limit the amount of water stored in deciduous trees (i.e., reduced snowpack or prolonged periods of low rainfall) will negatively impact these ecosystems. Thus, permafrost-free areas of the subarctic are drought-prone and appear more as a semi-arid system. However, we suspect that at least the deciduous trees are more drought tolerant than

areas with permafrost because of the buffering effect of tree water storage, allowing them to cope with low rainfall periods (Young-Roberson et al. 2016).

It is in areas of near-surface ice-rich permafrost that creates the illusion of a mesic subarctic, with lush mossy ground cover, wet soils, and numerous surface water bodies in lowland areas. However, these ecosystems can experience very dry soil conditions in the primary plant rooting zone (top 25–30 cm) during low rainfall periods when the seasonal thaw depth is deeper than the rooting zone (e.g., mid-July–September) (Walker and Johnstone 2014; Walker et al. 2015). It is hypothesized that the shallowly rooted black spruce experience water stress more than previously thought and, in addition to the warmer temperatures, are at the limit of their climatic envelope (Walker and Johnstone 2014; Walker et al. 2015; Wolken et al. 2016). Climate warming that results in direct or indirect permafrost thaw (e.g., via wildfire) causes drier soils due largely to enhanced soil drainage (Prowse et al. 2006; Hinzman et al. 2006a, b) and establishment of deciduous vegetation with high water use rates. However, this latter mechanism has not been rigorously explored. Thus, permafrost thaw may essentially shift these mesic-looking portions of the landscape to one that is ecohydrologically similar to their permafrost-free semi-arid counterparts. Additionally, the role of antecedent moisture in limiting drought stress has not been rigorously quantified, wherein rainfall primarily from the prior summer and fall is frozen and stored in the seasonally frozen soil over the winter (Slaughter and Kane 1979; Kane and Stein 1985). Upon snowmelt and seasonal thaw, this moisture is released to the soil and available for plant use. This suggests that drought in the prior year or years may impact vegetation in a given summer because of this carry-over or antecedent effect. In the current state, with permafrost, black spruce and mosses, we suspect these systems are not drought tolerant because the plants (vascular and non-vascular) have not evolved drought coping strategies. However, soil water storage can act as a buffer against drought in the near term, as long as the moisture front does not get below the primary rooting zone.

22.3 Knowledge Gaps

Here we summarize several knowledge gaps that limit our understanding of subarctic ecohydrology and thus, our ability to model and predict change with climate warming. One of the first knowledge gaps that has recently changed is the revelation that tree water storage can be a significant part of the water balance (Young-Robertson et al. 2016). The current state of knowledge is that tree water storage plays a big role in the subarctic hydrologic cycle of non-permafrost areas, wherein deciduous trees use and store a large amount of water. Nearly 25% of snowmelt water is diverted from groundwater recharge into deciduous trees. However, there is little data on tree water storage from fall to spring (senescence to snowmelt), on the diurnal water storage dynamics during the growing season, and on the mechanisms of snowmelt water uptake prior to leaf-out.

The second knowledge gap deals with ET partitioning. The current state of knowledge supports that evaporation dominates permafrost areas and transpiration dominates non-permafrost areas, as transpiration rates in permafrost areas (from black spruce) are very low but evaporation rates are high. Transpiration rates in permafrost-free areas (from deciduous trees) are very high but evaporation rates are low. However, another knowledge gap exists for the actual quantification of ET partitioning throughout the summer with respect to variability in rainfall, active layer depths, and vegetation community.

The third knowledge gap pertains to areas underlain by permafrost. The potential soil water storage capacity is dynamic with a very low capacity immediately following snowmelt and reaching its maximum at the end of the summer when the seasonal soil thaw reaches its maximum depth. The current state of knowledge theorizes that ice-rich soils at the top of permafrost severely limit vertical movement of water into deeper soil layers, but there are large information gaps on our understanding of how storage will change with disturbance. Additional information is needed on how soil storage capacity responds to permafrost thaw (via subsidence, altered soil thermal properties, and moisture), vegetation change (shrub encroachment), fire (loss of or reduction in organic soil layer), and extreme events (large and intense rainstorms).

The fourth knowledge gap involves recognizing that subarctic Alaska experiences water-limited conditions. The current state of knowledge is that extremely dry conditions can occur, and the permafrost-free part of the landscape experiences and copes with dry conditions (as long as moisture for tree water storage is available). The ecology in areas with permafrost can cope with dry conditions only so far as soil moisture can remain reasonably high due to the presence of permafrost. Loss of permafrost, due to warming or fire, will likely make this ecosystem type appear more semi-arid as plants that can cope with drought replace those that cannot. Also, the impact of drought during the prior year or years may impact ecosystems in the current year in areas with permafrost by limiting the amount of stored water in the active layer. More information is needed to quantify drought thresholds (e.g., lower limit of rainfall and snowfall) of vegetation in ecosystems with and without permafrost. Quantification of the importance of the antecedent moisture effect, particularly in areas with permafrost is also needed. More information on the buffering mechanisms within the different subarctic ecosystems that impart resilience to drought is needed.

22.4 Summary

Storage processes dominate the ecohydrology of subarctic systems in Alaska. Yet, we do not understand enough about these processes to build a mechanistic framework in water balance models, limiting the predictability of changes associated with climate warming. The presence or absence of permafrost determines whether ecological or hydrological processes drive water cycling. Some basic

assumptions about Interior Alaskan subarctic ecohydrology have left large knowledge gaps about the role of tree water storage in permafrost-free areas, the degree that plants control evapotranspiration, potential changes in soil storage capacity, and the degree to which the subarctic experiences drought. Filling these knowledge gaps will help us predict how subarctic water balance will change in the face of warmer temperatures, increased wildfire frequency, and intensity, vegetation shifts to deciduous species, and permafrost thaw. Further, filling the knowledge gaps will help us understand the consequences of shifting the ecohydrology of subarctic Alaskan systems to more ecologically-driven.

References

Åkerman HJ, Johansson. M (2008) Thawing permafrost and thicker active layers in sub-arctic Sweden. Permafrost Periglac Process 19:279–292

Barrett K, McGuire AD, Hoy EE, Kasischke ES (2011) Potential shifts in dominant forest cover in interior Alaska driven by variations in fire severity. Ecol Appl 21:2380–2396

Barber VA, Juday GP, Finney BP (2000) Reduced growth of Alaskan white spruce in the twentieth century from temperature-induced drought stress. Nature 405:668–672

Beck PSA, Goetz SJ (2011) Satellite observations of high northern latitude vegetation productivity changes between 1982 and 2008: ecological variability and regional differences. Environ Res Lett 6:045501

Beringer J, Lynch AH, Chapin III FS, Mack M, Bonan GB (2001) The representation of arctic soils in the land surface model: the importance of mosses. J Clim 14(15):3324–3335

Bolton WR, Hinzman L, Yoshikawa K (2004) Stream flow studies in a watershed underlain by discontinuous permafrost. In: Kane DL, Yang D (eds) Northern research basins water balance. IAHS Series of Proceedings and Reports, Victoria, Canada

Bowling LC, Kane DL, Gieck RE, Hinzman LD, Lettenmaier DP (2003) The role of surface storage in a low-gradient arctic watershed. Water Resour Res 39(4):1087. https://doi.org/10.1029/2002WR001466

Bring A, Fedorova I, Dibike Y, Hinzman L, Mård J, Mernild SH, Prowse T, Semenova O, Stuefer SL, Woo MK (2016) Arctic terrestrial hydrology: a synthesis of processes, regional effects, and research challenges. J Geophys Res Biogeosci 121:621–649. https://doi.org/10.1002/2015JG003131

Brown RD (2000) Northern hemisphere snow cover variability and change, 1915–97. J Clim 13:2339–2355

Burn CR, Kokelj SV (2009) The environment and permafrost of the Mackenzie Delta area. Permafrost Periglac Process 20:83–105

Cable JM, Ogle K, Bolton WR, Bentley LP, Romanovsky V, Iwata H, Harazono Y, Welker J (2014) Permafrost thaw affects boreal deciduous plant transpiration through increased soil water, deeper thaw, and warmer soils. Ecohydrology 7(3):982–997

Carey SK, Woo MK (2001) Slope runoff processes and flow generation in a subarctic, subalpine catchment. J Hydrol 253:110–129. https://doi.org/10.1016/S0022-1694(01)00478-4

Chapin FS III, Eugster W, McFadden JP, Lynch AH, Walker DA (2000) Summer differences among arctic ecosystems in regional climate forcing. J Clim 13(12):2002–2010. https://doi.org/10.1175/15200442(2000)013%3c2002:SDAAEI%3e2.0.CO;2

Chapin FS III, Jefferies RL, Reynolds JF, Shaver GR, Svoboda J (1992) Arctic ecosystems in a changing climate: an ecophysiological perspective. Academic Press, San Diego, California, USA

Dingman SL (1975) Hydrologic effects of frozen ground. CRREL Publication, p 218

Forbes BC, Fauria MM, Zetterberg P (2010) Russian Arctic warming and "greening" are closely tracked by tundra shrub willows. Glob Change Biol 16:1542–1554

Haugen R, Slaughter CW, Howe K, Dingman SL (1982) Hydrology and climatology of the Caribou-Poker creeks research watershed, Alaska. CRREL Publication, pp 82–86

Hinzman L, Bolton WR, Petrone KC, Jones JB, Adams PC (2006a) Watershed hydrology and chemistry in the Alaskan boreal forest: the central role of permafrost. In: Chapin FS, Oswood MW, Van Cleve K, Viereck L, Verbyla D (eds) Alaska's changing boreal forest. Oxford University Press, pp 269–284

Hinzman L, Viereck L, Adams PC, Romanovsky V, Yoshikawa K (2006b) Climate and permafrost dynamics of the Alaskan boreal forest. In: Chapin FS, Oswood MW, van Cleve K, Viereck L, Verbyla D (eds) Alaska's changing boreal forest. Oxford University Press, pp 39–61

Hinzman LD, Bettez ND, Bolton WR, Chapin FS, Dyurgerov MB, Fastie CL, Griffith B, Hollister RD, Hope A, Huntington HP, Jensen AM, Jia GJ, Jorgenson T, Kane DL, Klein DR, Kofinas G, Lynch AH, Lloyd AH, McGuire AD, Nelson FE, Oechel WC, Osterkamp TE, Racine CH, Romanovsky VE, Stone RS, Stow DA, Sturm M, Tweedie CE, Vourlitis GL, Walker MD, Walker DA, Webber PJ, Welker JM, Winker K, Yoshikawa K (2005) Evidence and implications of recent climate change in northern Alaska and other arctic regions. Clim Change 72:251–298. https://doi.org/10.1007/s10584-005-5352-2

Jasechko S, Sharp ZD, Gibson JJ, Birks SJ, Yi Y, Fawcett PJ (2013) Terrestrial water fluxes dominated by transpiration. Nature 496:347–350. https://doi.org/10.1038/Nature11983

Jia GJ, Epstein HE, Walker DA (2009) Vegetation greening in the Canadian Arctic related to decadal warming. J Environ Monit 11:2231–2238

Jorgenson MT, Romanovsky V, Harden J, Shur Y, O'Donnell J, Schuur EAG et al (2010) Resilience and vulnerability of permafrost to climate change. Can J Forest Res 40(7)

Jorgenson MT, Harden J, Kanevskiy M, O'Donnell J, Wickland K, Ewing S, Manies K, Zhuang Q, Shur Y, Striegl R, Koch J (2013) Reorganization of vegetation, hydrology and soil carbon after permafrost degradation across heterogeneous boreal landscapes. Environ Res Lett 8(3):035017, 13pp

Juday GP, Alix C (2012) Consistent negative temperature sensitivity and positive influence of precipitation on growth of floodplain of Picea glauca in Interior Alaska. Can J For Res 42:561–573

Kane DL, Hinzman LD, Gieck RE, McNamara JP, Youcha EK, Oatley JA (2008) Contrasting extreme runoff events in areas of continuous permafrost, Arctic Alaska. Hydrol Res 39:287–298. https://doi.org/10.2166/Nh.2008.005

Kane DL, Stein J (1985) Water-movement into seasonally frozen soils—reply. Water Resour Res 21:1053–1054. https://doi.org/10.1029/Wr021i007p01053

Koch JC, Toohey RC, Reeves DM (2017) Tracer-based evidence of subsurface flow and storage heterogeneity within a boreal hillslope. Hydrol Process 31(13):2453–2463

Koch JC, Kikuch CP, Wickland KP, Schuster P (2014) Runoff sources and flow paths in partially burned, upland boreal catchment underlain by permafrost. Water Resour Res 50(10):8141–8158

Lantz TC, Kokelj SV, Gergel SE, Henry GHR (2009) Relative impacts of disturbance and temperature: Persistent changes in microenvironment and vegetation in retrogressive thaw slumps. Glob Change Biol 15(7):1664–1675. https://doi.org/10.1111/j.1365-2486.2009.01917

Liljedahl AK, Hinzman LD, Kane DL, Oechel WC, Tweedie CE, Zona D (2017) Tundra water budget and implications of precipitation underestimation. Water Resour Res 53:6472–6486. https://doi.org/10.1002/2016WR020001

Liston GE, Hiemstra CA (2011) The changing cryosphere: pan-arctic snow trends (1979–2009). J Clim 24:5691–5712

McGuire AD, Chapin FS (2006) Climate feedbacks in the Alaskan boreal forest. In: Chapin FS, Oswood MW, van Cleve K, Viereck L, Verbyla D (eds) Alaska's changing boreal forests. Oxford University Press, pp 309–322

McGuire AD, Chapin FS, Walsh JE, Wirth C (2006) Integrated regional changes in arctic climate feedbacks: implications for the global climate system. Annu Rev Env Resour 31:61–91. https://doi.org/10.1146/annurev.energy.31.020105.100253

Molders N (2012) Land-use and land-cover changes. Springer-Science

Nakai T, Kim Y, Busey RC, Suzuki R, Nagai S, Kobayashio H, Park H, Sugiura K, Ito A (2013) Characteristics of evapotranspiration from a permafrost black spruce forest in interior Alaska. Polar Sci 7:136–148

Ohta T et al (2008) Interannual variation of water balance and summer evapotranspiration in an eastern Siberian larch forest over a 7-year period 1998–2006. Agric For Meteorol 148:1941–1953

Osterkamp T, Jorgenson MT, Schuur EAG, Shur YL, Kanevskiy MZ, Vogel JG, Tumskoy VE (2009) Physical and ecological changes associated with warming permafrost and thermokarst in interior Alaska. Permafrost Periglac Process 20:235–256

Pastick NJ, Jorgenson MT, Wylie BK, Nield SJ, Johnson KD, Finley AO (2015) Distribution of near-surface permafrost in Alaska: estimates of present and future conditions. Remote Sens Environ 168:301–315

Pastick NJ, Jorgenson MT, Goetz SJ, Jones BM, Wylie BK, Minsley BJ, Genet H, Knight JF, Swanson DK, Jorgenson JC (2018) Spatiotemporal remote sensing of ecosystem change and causation across Alaska. Global Change Biol 1–19. https://doi.org/10.1111/gcb.14279

Ping CL, Michaelson GJ, Kimble JM (1997) Carbon storage along a latitudinal transect in Alaska. Nutr Cycl Agroecosys 49:235–242. https://doi.org/10.1023/A:1009731808445

Prowse TD, Wrona FJ, Reist JD, Gibson JJ, Hobbie JE, Levesque LMJ, Vincent WF (2006) Historical changes in Arctic freshwater ecosystems. Ambio 35:339–346

Quinton WL, Marsh P (1999) A conceptual framework for runoff generation in a permafrost environment. Hydrol Process 13 (16):2563–2581

Romanovsky VE, Smith SL, Christiansen HH (2010) Permafrost thermal state in the polar Northern Hemisphere during the international polar year 2007–2009: a synthesis. Permafrost Periglac Process 21(2):106–116

Rodriguez-Iturbe I (2000) Ecohydrology: a hydrologic perspective of climate-soil-vegetation dynamics. Water Resour Res 36(1):3–9

Rogers BM, Solvik K, Hogg EH, Ju J, Masek JG, Michaelian M,… Goetz SJ (2018) Detecting early warning signals of tree mortality in boreal North America using multi-scale satellite data. Global Change Biol 1–21. https://doi.org/10.1111/gcb.14107

Riordan B, Verbyla D, McGuire AD (2006) Shrinking ponds in subarctic Alaska based on 1950–2002 remotely sensed images. J Geophys Res-Biogeo 111. https://doi.org/10.1029/2005jg000150. G04002

Saito K, Zhang T, Yang D, Marchenko S, Barry RG, Romanovsky V, Hinzman L (2013) Influence of the physical terrestrial Arctic in the eco-climate system. Ecol Appl 23(8):1778–1797

Serreze MC, Barrett AP, Slater AG, Woodgate RA, Aagaard K, Lammers RB, Steele M, Moritz R, Meredith M, Lee CM (2006) The large-scale freshwater cycle of the Arctic. J Geophys Res 111:C11010. https://doi.org/10.1029/2005JC003424

Slaughter CW, Kane DL (1979) Hydrologic role of shallow organic soils in cold climates. In: Proceedings of the Canadian hyrdrology symposium. Cold Climate Hydrology, National Research Council of Canada, Ottowa, pp 380–389

Slaughter CW, Viereck L (1986) Climatic characteristics of the taiga in Interior Alaska. In: Van Cleve K, Chapin FS, Flanagan PW, Viereck L, Dyrness CT (eds) Forest ecosystems in the Alaskan Taiga. Springer, New York, pp 9–21

Sturm M, Schimel J, Michaelson G, Welker JM, Oberbauer SF, Liston GE, Fahnestock J, Romanovsky VE (2005) Winter biological processes could help convert Arctic tundra to shrubland. Bioscience 55(1):17–26

Tape KD, Hallinger M, Welker JM, Ruess RW (2012) Landscape heterogeneity of shrub expansion in Arctic Alaska. Ecosystems 15(5):711–724

Thibault S, Payette S (2009) Recent permafrost degradation in bogs of the James Bay Area, Northern Quebec, Canada. Permafrost Periglac Process 20:383–389

Trugman AT, Medvigy D, Anderegg WRL, Pacala SW (2018) Differential declines in Alaskan boreal forest vitality related to climate and competition. Glob Change Biol 24:1097–1107. https://doi.org/10.1111/gcb.13952

Walker X, Johnstone JF (2014) Widespread negative correlations between black spruce growth and temperature across topographic moisture gradients in the boreal forest. Environ Res Lett 9. https://doi.org/10.1088/1748-9326/9/6/064016

Walker XJ, Mack MC, Johnstone JF (2015) Stable carbon isotope analysis reveals widespread drought stress in boreal black spruce forests. Global Change Biol 21:3102–3113. https://doi.org/10.1111/gcb.12893

Woo M (2012) Permafrost hydrology. Springer-Verlag

Woo MK, Marsh P (1990) Response of soil-moisture change to hydrological processes in a continuous permafrost environment. Nord Hydrol 21:235–252

Yarie J (2008) Effects of moisture limitation on tree growth in upland and floodplain forest ecosystems in interior Alaska. Forest Ecol Manag 256:1055–1063. https://doi.org/10.1016/j.foreco.2008.06.022

Wendler G, Gordon T, Stuefer M (2017) On the precipitation and precipitation change in Alaska. Atmosphere 8(12):253–263

Wolken JM, Mann DH, Grant TA, Lloyd AH, Rupp TS, Hollingsworth TN (2016) Climate-growth relationships along a blackspruce toposequence in interior Alaska. Arct Antarct Alp Res 48 (4):637–652

Wrona FJ, Johansson M, Culp JM, Jenkins A, Mård J, Myers-Smith IH, Prowse TD, Vincent WF, Wookey PA (2016) Transitions in Arctic ecosystems: ecological implications of a changing hydrological regime. J Geophys Res Biogeosci 121:650–674. https://doi.org/10.1002/2015JG003133

Yoshikawa K, Bolton WR, Romanovsky VE, Fukuda M, Hinzman LD (2002) Impacts of wildfire on the permafrost in the boreal forests of Interior Alaska. J Geophys Res-Atmos 108. https://doi.org/10.1029/2001jd000438. 8148

Young-Robertson JM, Bolton WR, Bhatt U, Cristobal J, Thoman R (2016) Deciduous trees are an enormous and overlooked sink for snowmelt water in Alaska. Sci Rep 6, Article number 29504

Young-Robertson JM, Ogle K, Welker JM (2017) Thawing seasonal ground ice: an important water source for boreal forest plants in Interior Alaska. Ecohydrology 10(3):e1796

Young-Robertson JM, Raz-Yaseef N, Cohen LR, Newman B, Rahn T, Sloan V, Wilson C, Wullschleger SD (2018) Evaporation dominates evapotranspiration on Alaska's Arctic Coastal Plain. Arct Antarct Alp Res 50(1):e1435931

Zhang K, Kimball JS, Mu Q, Jones LA, Goetz SJ, Running SW (2009) Satellite based analysis of northern ET trends and associated changes in the regional water balance from 1983 to 2005. J Hydrol 379(1):92–110

Dr. Jessie Young-Robertson is a Research Assistant Professor in the Agricultural and Forestry Experiment Station at the University of Alaska Fairbanks. She has over 10 years of experience as a boreal forest researcher studying the interaction between ecological and hydrological processes in permafrost and permafrost-free systems. Her work focuses on field measurements and model development of tree water use and storage in response to environmental drivers. She was an NSF Office of Polar Programs postdoctoral fellow studying the response of boreal plant water uptake to permafrost thaw. Prior to that, she was a postdoctoral researcher at the University of Wyoming developing Bayesian statistical modeling skills and analyzing datasets from her graduate studies on desert soil respiration responses to vegetation and climate variability. She got her Ph.D. and M.S. in Ecology and Evolutionary Biology with a minor in Global Change at the University of Arizona in Tucson, Arizona, and her BS in Biology at Fort Lewis College in Durango, CO.

Dr. Bolton is a Research Associate Professor at the International Arctic Research Center, University of Alaska Fairbanks. He is an expert in permafrost hydrology, hydrologic modeling, and thermokarst. He specializes in quantifying the timing and pathways of streamflow in a both the Arctic and sub-Arctic environments through a combination of numerical modeling and field observation. He received a B.A. in Geology from California Lutheran University, a M.S. in Geological Engineering from the University of Alaska Fairbanks and a Ph.D. in Hydrologic Engineering from the University of Alaska Fairbanks.

Dr. Ryan Toohey has worked for over 20 years in water resources specializing in interdisciplinary applications of hydrology, water quality, ecosystem services, and governance from the tropics to Alaska. His current position with the US Geological Survey, Alaska Climate Adaptation Science Center includes research that involves investigating environmental change, hydrological modeling, and community-based research that integrates Indigenous Knowledge, social, water and soils science. Over the past 10 years, Ryan has been investigating permafrost dynamics and their relationships to changes in water biogeochemistry of small and large rivers within the Alaskan and Yukon Boreal forest. Ryan has received the USGS Balsey Award for Technology Transfer, EPA STAR and NSF IGERT fellowships for his work throughout the years. He received his Ph.D. in Environmental Science (Hydrology) from University of Idaho and his B.Sc. in Environmental Science (Water Quality) from Western Washington University.

Yukon River Discharge-NDVI Relationship

23

Weixin Xu and Daqing Yang

Abstract

Similar to the Mackenzie River, a strong seasonal consistency between NDVI and discharge exists for Yukon River. The flow-NDVI association is particularly strong before June, discharge rapidly rises and reaches the peak the 1st half of June, while the NDVI in the period of April to June increases fastest and reaches the maximum in July. In the mid and late summer, both discharge and NDVI decline gradually. Similarly, two sensitive periods while NDVI significantly correlates to discharge variations were also found in this region. May to June is key time of vegetation relates to discharge, the NDVI on 2nd half of May and 1st half of June is significantly correlated to the 1st half of May discharge mainly in midstream zone. August is another sensitive period, the 2nd half of August NDVI closely related to the synchronous and previous half-month discharge. River discharge decreased during growing season except in May from 1982 to 2013 in Yukon Basin. The significant decrease about 8–15% of the average flow, but a significant increase with a trend above 34.2% occurred in May. The NDVI trends during the growing season from May to September almost inversely correspond to discharge changes with a weak increments about 5% of the mean NDVI. In addition, examination of extreme flow years and corresponding NDVI conditions also reveals that low runoff year was associated

W. Xu (✉)
College of Resources and Environment, Chengdu University of Information Technology, Chengdu, Sichuan, China
e-mail: weixin.xu@163.com

D. Yang
Watershed Hydrology and Ecology Research Division, Environment and Climate Change Canada, Victoria, BC, Canada
e-mail: daqing.yang@canada.ca

D. Yang and D. L. Kane (eds.), *Arctic Hydrology, Permafrost and Ecosystems*,
https://doi.org/10.1007/978-3-030-50930-9_23

with a lower basin NDVI with an earlier maximum, while the higher flow year was linked with a higher NDVI and a longer growth season. It may imply the better water supply with higher flow in the spring will induce a higher vegetation production.

23.1 Introduction

Climate in the high latitudes has experienced significant changes over the past several decades. These changes affect northern environment, including ecosystem, hydrology, and permafrost (Saito et al. 2012). Many studies investigate and report ecosystem changes associated with strong climate warming in the northern regions, such as earlier and longer growing seasons (Kim et al. 2012; McManus et al. 2012; Tape et al. 2012; Beck and Goetz 2011; Zhang et al. 2008). Other studies show that vegetation growth process over the northern regions is mainly constrained by seasonal temperatures and the exchange of heat and moisture (Qian et al. 2010; Friedlingstein et al. 2006; Nemani et al. 2003). Several investigations indicate that widespread drought and wildfire enhanced by climate warming have led to frequent tree mortality and declines in the boreal productivity across the northern lands (Girardin et al. 2014). Kim et al. (2014), however, pointed that cold temperature constraints to northern growing seasons are relaxing, while the potential benefits for productivity and carbon sink activity become more dependent on terrestrial water balance and supply of plant-available moisture. Other studies also clearly demonstrate, in a warming climate, the increasing importance of water availability to the northern ecosystem (Bi et al. 2013; Bertoldi et al. 2011; Olthof and Latifovic 2007).

River flows integrate basin processes, including surface water mobility, recharge of soil moisture, and subsurface storage variation over space and time. River discharge is the direct measure of water storage and availability over large regions and in the northern watersheds. In the high latitudes, spring snowmelt runoff and its peak flow reflect the amount of winter snow accumulation and the melting process (Yang et al. 2002, 2014b); summer discharge and high floods respond to heavy rainfall activities; while fall-winter base flows indicate basin storage capacity and recession process. River discharge has been systematically reported through water level and flow relationships in the northern basins, although it is very difficult to measure soil moisture and recharge rate over large regions. Climate variables have been often used to infer soil moisture conditions. For example, climatic moisture index (CMI), i.e., mean annual precipitation (P) minus mean annual potential evapotranspiration (P-ET), has been defined and related with vegetation and forest processes (Hogg 1994, 1997), including the impacts of regional droughts and climate change on forest growth and dieback. It is important to note that, in terms of basin water balance, the index (P-ET = R + storage change) reveal river runoff and basin storage, or in other words, basin water availability.

River discharge reflects basin water supply and storage. It is important to understand the fundamental characteristics, including temporal variations and changes of streamflow over the basins. A study by Yi et al. (2014) found that spring hydrology affects soil respiration in relatively wet boreal and arctic ecosystems, and plays an important role in determining summer net carbon uptake. Late spring and early summer flows are the highest contributors to the annual flow in northern basins. Higher spring flows usually lead to high summer flows, thus providing necessary water to support vegetation activities from spring to the later season. It is likely that river flow in the earlier season may affect vegetation in the later season. For example, there is a close correlation between NDVI and streamflow during the entire growing season over the Yellow River Delta, China; and the positive correlation has a time lag about a month (Jiang et al. 2013).

Over most northern basins, river runoff is much higher in magnitude than the storage term and its change. Many studies report remarkable changes in the northern hydrology system, such as increases in large Arctic river discharge (McClell et al. 2006; Peterson et al. 2002), discharge increases in winter and decreases in summer for the Yenisei, Lena, Ob watersheds in Siberia (Girardin et al. 2014; Yang et al. 2014b; Saito et al. 2012), the earlier melt of snow cover (Fretwell et al. 2010; Hogg 1997; Myneni et al. 1995); and river ice breakup (Bonsal et al. 2006; Yang et al. 2002; Hogg 1994), shift of peak flows in spring season for the Yukon and Mackenzie rivers (Yang et al. 2004a, b; Hogg 1997). These changes in streamflow hydrology conditions are due to climate variations and human impacts (Girardin et al. 2014; Yang et al. 2014b; Saito et al. 2012).

The Normalized Difference Vegetation Index (NDVI) has been widely used to investigate vegetation changes and its relationship with regional climate. Several studies reveal an increasing NDVI trend over the northern regions (Pouliot et al. 2009). The positive NDVI trends in southern regions of Canada were mostly influenced by land cover change (Olthof and Latifovic 2007). In northern regions, such as Canada, the principal factor for vegetation process seems to be energy, although soil water is also important (Bi et al. 2013; He et al. 2012; Wang et al. 2011; Bhatt et al. 2010). Our knowledge of vegetation–hydrology linkage over the broader northern regions is incomplete. Long-term discharge and Vegetation index records are available on a global scale. Most vegetation change analyses have been done on regional scales, however, there is little effort to systematically examine their interactions over the large northern rivers with significant past and ongoing environmental changes. It is clear both hydrology and ecology are changing in the high latitudes. There are many major questions for eco-hydrology research, for instance, what are the characteristics of basin hydrology, ecology, and their changes? What is the impact of basin hydrology change on ecosystem function? Is there (in)consistency in river flow and vegetation trends over the northern basins? In order to fill these knowledge gaps, basin-scale analyses of eco-hydrology are necessary.

In this chapter, the Yukon River was chosen as a demonstration, long-term discharge, and NDVI (Normalized Difference Vegetation Index) data over the river basins were compiled and analyzed. It focuses on the basin scale to investigate the main features of watershed hydrology, ecology, and their linkages. It quantifies the

seasonal cycles of basin vegetation and discharge, and examines their space–time consistency and changes over the summer growing season. The main objective of this investigation is to explore and establish a relationship between streamflow and NDVI over a large northern watershed. The methods and results of this work will improve our understanding of hydrology and ecosystem interactions over the broader northern regions.

23.2 Basin and Data

The Yukon River, located in northwestern Canada and central Alaska, drains an area of more than 528 km^2, making it the fourth largest drainage basin in North America (Brabets et al. 2000). Yukon River Basin, which indicates the large diversity of natural features of the watershed, such as climate, soils, permafrost, and geology. Annual mean discharge of the Yukon River near its mouth is more than 5600 m^3/s, most of the flow occurs in the summer months from snowmelt, rainfall, and glacial melt. Eight major rivers flow into the Yukon River. Two of these rivers, the Tanana River and the White River, are glacier-fed rivers and together account for 29% of the total water flow of the Yukon. Two others, the Porcupine River and the Koyukuk River, are underlain by continuous permafrost and drain larger areas than the Tanana and the White, but together contribute only 22% of the total water flow in the Yukon. Yukon climate is typified by long, cold winters and short, warm summers. The Yukon has the most variable climate in North America, and across the Territory, nine distinct climatic regions can be recognized. The dominant vegetation types in Yukon Basin are arctic tundra, alpine tundra, taiga or subarctic forest, boreal forest, and subalpine-shrub forest. The forest covers over 70% area in Yukon, and the growing days for four eco-regions in Alaska ranged from 130 to 194 days (Fretwell et al. 2010).

Streamflow records observed at the watershed outlet reflects basin integration of both natural variations and human-induced changes, such as changes of land cover/land use and regulations of large dams within the watersheds (Girardin et al. 2014; Saito et al. 2012). Discharge data collected at the river mouth are particularly important as they represent freshwater input to the ocean and are often used for basin-scale water balance calculations, climate change analysis, and validations of land surface schemes and GCMs over large spatial scales (Yang et al. 2014a, b; Wang et al. 2014). The daily discharge data of the Yukon River were downloaded from USGS website (https://www.usgs.gov/mission-areas/water-resources/data-tools).

The Normalized Difference Vegetation Index (NDVI) derived from the Advanced Very-High-Resolution Radiometer (AVHRR) is available at http://daac.gsfc.nasa.gov/. These data have been used extensively to examine the vegetation patterns and changes over the northern regions (Kim et al. 2014; Peng et al. 2012; Wang et al. 2011; Bhatt et al. 2010). The dataset has been organized at 8-km-resolution with a half-month maximum NDVI value from 1982 to 2013. This dataset has been processed to minimize corruption of vegetation signals from

atmospheric effects, scan angle effects, cloud contamination, volcanic eruption, and effects of varying solar zenith angle. The NDVI is generally expressed on a scale range from 0.0 to 0.7, and the higher value indicates the denser vegetation (Yang et al. 2014a; Prowse et al. 2010; Bonsal et al. 2006). Lower values generally contain more spurious signals (e.g., from the snow, lakes, soil background, etc.), which were not related to photosynthetically active vegetation. Previous studies show the NDVI values greater than 0.05 can more accurately extract the vegetation information (Fretwell et al. 2010; Myneni et al. 1995). Therefore, in this study, the NDVI values above 0.05 are considered useful to represent vegetation activities over the Mackenzie Basin.

Daily data were used to generate half-month discharge time series to compare with the NDVI records. The long-term means and standard deviation for the NDVI and discharge data were calculated and the trend analysis and statistical significance test to identify long-term changes in streamflow and vegetation. Linear regression to the records to determine its changes as a function of time (year). The total trend is defined by the difference of flows or NDVI shown on the regression line between the first year and the last year. The standard Student t-test is used to determine the statistical significance of the trends. Then, it was compared the results of trend and spatial difference between river discharge and NDVI via regression and correlation analyses, as well as the extreme high/low flow years and the associated NDVI conditions.

23.3 Relationship Between Basin NDVI and Discharge

23.3.1 Seasonality of NDVI and Discharge

Figure 23.1 shows the basin mean half-month NDVI and discharge in Yukon Basin for the period 1982–2013. The NDVI values range from 0.22 in early spring to near 0.80 in summer. During the period of January to the March and 2nd half of October

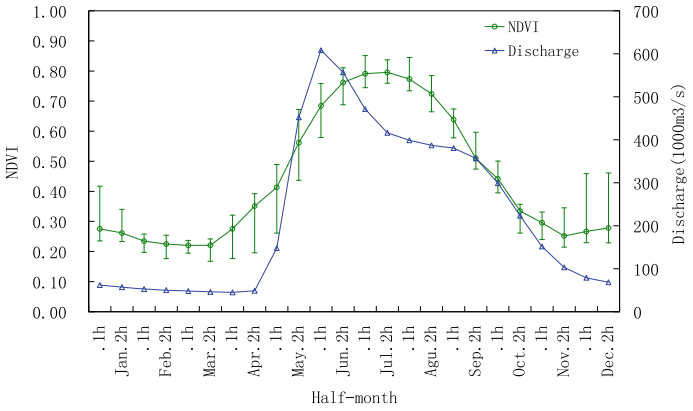

Fig. 23.1 Basin mean NDVI and discharge for the period 1982 to 2013

to December, the NDVI is below 0.30. These times are the cold seasons with a stable snow cover and basin temperature usually below −20 °C. There is little vegetation activity in the cold season with snow cover. During May to early October, the NDVI values are usually above 0.40, when air temperatures are above 0 °C and vegetation is active (Olthof and Latifovic 2007). For instance, the NDVI increases rapidly after the 1st half of May and reaches the maximum value (0.80) at the 2nd half of July. This value of NDVI is greater than other areas in high latitudes, maybe due to a wider forest cover in the basin. It then declines gradually until October. In the rising stage from the early May to late July, NDVI changes significantly. The fast increase in May indicates the onset of vegetation growth over most parts of Yukon Basin. In the summer (June to August), the NDVI remains high, around 0.68–0.80. However, the NDVI in September has the largest drop, suggesting vegetation gradually wilts after the 2nd half of September over the Yukon Basin. According to the report by U.S. GEOLOGICAL SURVEY that the growing days for four ecoregions in Alaska ranged from 130 to 194 days (Fretwell et al. 2010). Therefore, the period from May to September can be regarded as the growing season in the Yukon region.

To reveal the spatial pattern of vegetation change in the growing season over the Yukon Basin, average NDVI from 1982 to 2013 was calculated for each grid cell during May to September (Fig. 23.1). Over most areas of the basin, the NDVI increases from May to July and reaches the maximum at the 2nd half of July, and then it gradually reduces until the 2nd half of September. There are significant spatial variations in the NDVI values over the basin (Fig. 23.2). In the Yukon River valley and lowland areas around the main river, the vegetation type is dominated by needleleaf forest and broadleaf forest (Fig. 23.2). These are areas with the maximum NDVI value above 0.80 in July. Moreover, the vegetation in these areas and the surrounding regions begin to turn green earlier than other regions in the basin. Edge zone of the Basin spatially in area of Alaska Range and Central and Eastern Brooks Range, vegetation cover is relatively poor, with the maximum NDVI being less than 0.50 in the mid-summer. Due to the dominated vegetation type of forests and shrubs; vegetation generally turn brown in a relatively long term even if the growth activity is near to stop. Therefore, the NDVI value is around 0.50 at the 2nd half of September, it still has a relatively high level.

The half-month mean discharge of the Yukon River is very low and generally lower than 62,000 m^3/s during January to April (Fig. 23.3). Discharge increases at the 1st half of May; the rate of change is sharp at the 2nd half of May, and flow reaches the highest amount (608,500 m^3/s) at the 1st half of June. The process of discharge increasing is quick, reaching the highest peak within 3 half months. High flow period runs from May to September as the results of spring snowmelt and summer rainfall contributions. Discharge decreases slowly from the peak value in June to September, but it enters into second declined period after in September.

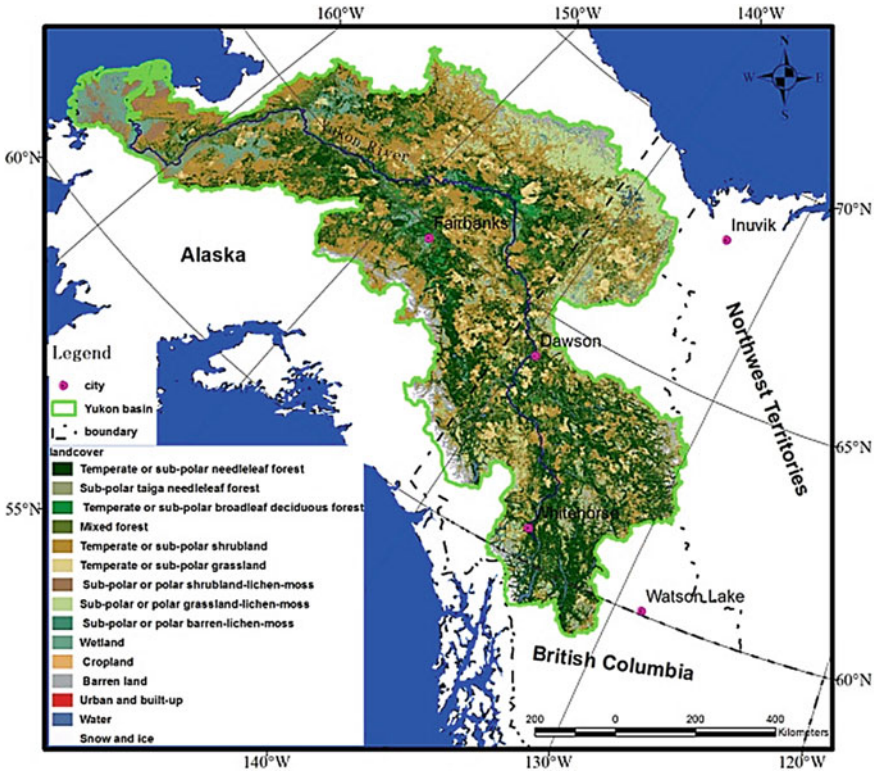

Fig. 23.2 Land cover types and rivers over the Yukon Basin

The patterns of NDVI and discharge are similar in the cold season, because they are both low and change little over the winter. At the beginning of the growing season (after the 1st half of May), along with a dramatic increase of the discharge from the 1st half of May to 1st half of June, the NDVI rises rapidly. The timing of NDVI rises closely couples with the process of rapid discharge increase during this period. The discharge reached the peak at 1st half of June, but NDVI is the highest at the 2nd half of July; there is a lag of 1.5 months between flow and NDVI peaks. Discharge declines rapidly after the 1st half of June, but the decreasing trend was hold and becomes steady after the 2nd half of July. It is worth noting that the discharge remains above 350,000 m^3/s during the declined stage of June to September. This suggests sufficient water and soil moisture supply for vegetation growth, even though discharge has decreased significantly since the 1st half of June. After the 2nd half of September, both NDVI and discharge gradually declined with a similar pace.

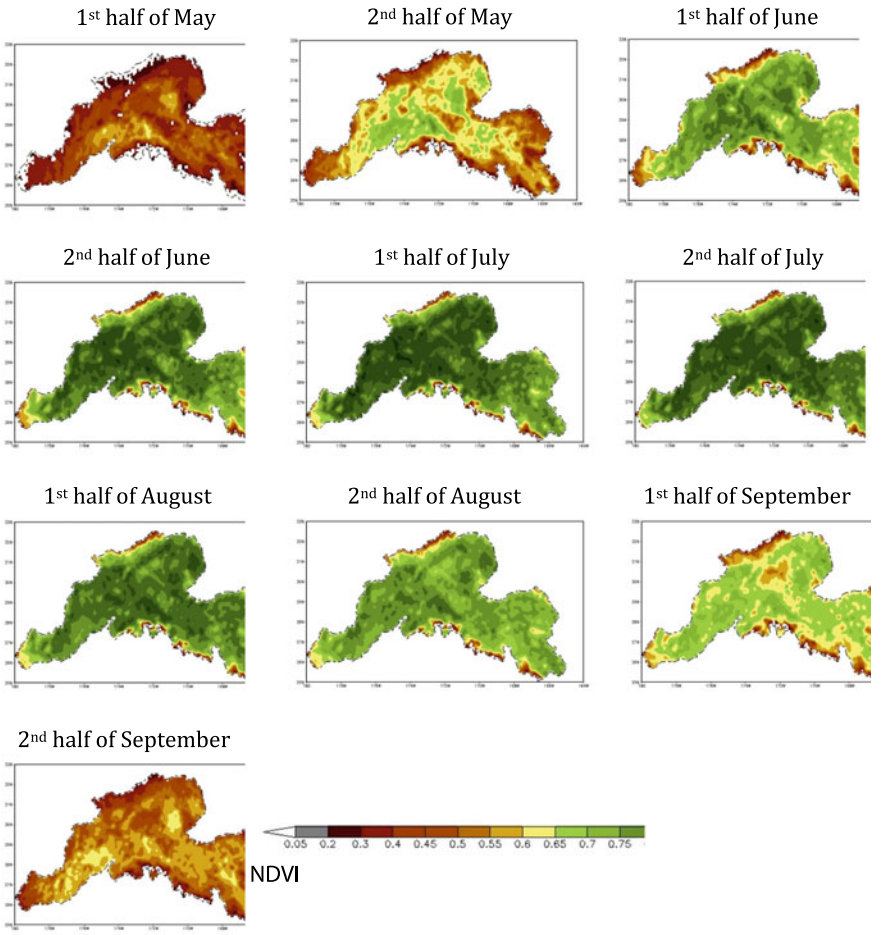

Fig. 23.3 The 9th to 18th biweekly mean NDVI during 1982 to 2013 over the Yukon Basin

23.3.2 Trends of NDVI and Discharge

Trend analyses for growing season NDVI during 1982 to 2013 indicate an increasing tendency for most months in growing season, except the 1st half of September (Fig. 23.4). The significant increases mainly occurred in June, the 1st half of July, and the 2nd half of September. In this period, the total NDVI increments over the 32 years were greater than 0.04 (about 5% of the mean NDVI). A weak decrease was found at the 1st half of September with the cumulative change of 0.01 ($P < 0.544$), and 1.5% relative to the mean NDVI.

River discharge decreased in most time of the year except in May and the period from the 2nd half of October to December. Discharge at the 1st half of June to the

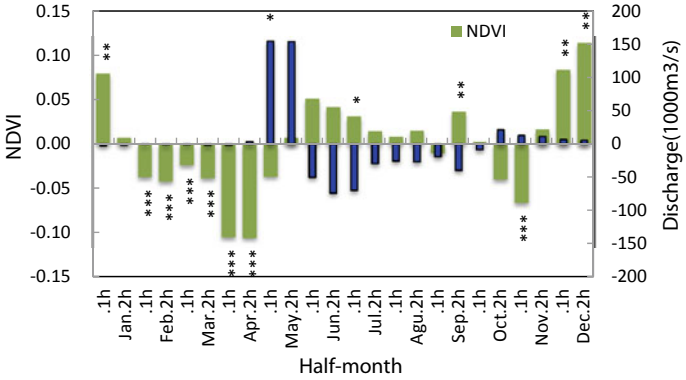

Fig. 23.4 Trends of discharge and mean NDVI over the Yukon Basin during 1982 to 2013. The stars indicate trend significant at different levels. *for significance at 0.05 level, **for at 0.01 level, and ***for significance at 0.001 level

1st half of July shows significant decrease by approximately 1554 m^3/s/a ($P < 0.523$), 2301 m^3/s/a ($P < 0.308$), and 2170 m^3/s/a ($P < 0.174$) as sequence, or about 8, 13, and 15% of the average flow. The most significant increase occurred in May, with the total trend of 4,852 m^3/s/a ($P < 0.053$) in the 1st half of May and 4,833 m^3/s/a ($P < 0.143$) in the 2nd half of May, or 104.8% and 34.2% of the mean discharge, respectively.

The trends of NDVI and discharge from 1982 to 2013 are similar or different depending on the time of the year. It is worth to noting that, the tendency of NDVI and discharge almost is unversed during the growing season (May to September). As we can see, the NDVI increased from the 1st half of June to 2nd half of September (only except for 1st half of September), and all the discharge trends showed negative changes for the same time periods. The tendency of NDVI at the 1st half of May is decrease while the trend of discharge shows a significant increase. It may imply that vegetation change is closely related to discharge variation over the growing season in the study area. This result suggests that a lower flow in the warm season may lead to a better vegetation production over the basin.

23.4 NDVI-Discharge Correlation

Table 23.1 presents the results of correlations analysis between NDVI and discharge during the growing season. The results show a sensitive period for NDVI to respond or associate to discharge during May to June. This period is the time of NDVI rapid rise, the NDVI increase rapidly from the 1st half of May to 2nd half of June, with the most significant increase during the 2nd half of May to the 1st half of June after vegetation onset. There is a strong correlation between the 2nd half of

Table 23.1 Lag correlation coefficients between biweekly NDVI and discharge during the growing season

Month lag	Half									
	May		Jun		Jul		Aug		Sep	
	1 h	2 h	1 h	2 h	1 h	2 h	1 h	2 h	1 h	2 h
0	0.2896	0.5745	−0.1961	−0.1858	−0.0113	−0.0153	0.1724	0.1318	0.4316	0.0708
−1	0.1011	0.3486	0.4669	−0.1035	−0.1009	0.2328	0.0894	0.1292	0.3978	0.1548
−2	−0.1545	0.2278	0.4502	0.3853	0.0461	0.2643	0.1049	0.1475	0.2240	0.0316
−3	−0.1939	0.0582	0.4350	0.3746	0.0116	0.1411	0.3477	0.2444	0.1059	−0.0527
−4	−0.2326	−0.0105	0.2409	0.3155	−0.0241	0.0242	−0.0970	0.2807	0.0247	−0.0712
−5	−0.1830	−0.0892	0.1912	0.2489	0.0159	**−0.3127**	−0.0121	**−0.3274**	−0.0841	−0.1965
−6	−0.1955	−0.1113	0.0691	0.2197	0.2805	**−0.3729**	−0.1350	−0.0973	**−0.3792**	−0.1034

May NDVI and discharge (with 0 lag). NDVI at the 1st half of June and 2nd half of June also correlates closely with discharge at the 2nd half of May. Discharge at the 1st half of May also relates to the NDVI at the 2nd half of May to the 2nd half of June. This result suggests that the discharge in May is a key factor to affect vegetation growth in May and June. Spring flow reflects basin water storage and soil moisture condition that may influence vegetation processes over the whole summer. It is an interesting phenomenon that NDVI at the 2nd half of August also related closely to the contemporary and previous discharge. However, the NDVI at this time has a positive correlation with 1st and 2nd half of August and with a negative relation to 2nd half of May. The results suggest that, vegetation growth during the 2nd half of August positively responses to river flow at the 1st and 2nd half of August, and higher discharge in late May would reduce vegetation growth in August. The coefficients between the 2nd half of May discharge and the 2nd half of May and the 1st half of June NDVI have the highest values of 0.5745 ($P < 0.01$) and 0.4669 ($P < 0.01$). The correlation of August NDVI to discharge at the 1st and 2nd half of August and the 2nd half of May are all significant at 0.05 level. There is a long lag of NDVI behind flow; this seems to suggest the cumulative effect of river flow to basin water storage and maybe soil moisture variation over the growing season.

As a critical period, May discharge has a strong effect on the NDVI from the 2nd half of May to the 2nd half of June. To understand the spatial pattern of the relationship, we calculated the correlation coefficients between the 2nd half of May discharge and NDVI at the 2nd half of May, the 1st half of June, and the 2nd half of June over the Yukon Basin.

Figure 23.5 shows the grids with correlations significant at 0.10, 0.05, and 0.01 level. As seen in Figure 23.5a, NDVI is related closely to discharge variation in most areas except the regions of downstream and headwater and the region of Central and Eastern Brooks Range. Moreover, nearly 70% of the basin has close correlation relationship and around 40% significant at above 0.01 level.

Figure 23.5b, c shows that the 2nd half of May discharge also relates to June NDVI over the basin, although the correlations are obviously weaker than the 2nd half of May and shrink markedly in size. This result is consistent with the basin mean correlations in Table 23.1. Specifically, the correlation patterns between the 2nd half of May discharge and the 1st half of June NDVI are overlapped to that of the 2nd half of May NDVI. The high correlation zones are mainly located in the northern edge of the basin with higher elevation, and it seemly mainly relate to the change in tall and low shrublands. To the 2nd half of June, the significant influence of the 2nd half of May discharge on vegetation still can be seen (Fig. 23.5c), although both the area and significance decline sharply.

Figure 23.5d presents the 2nd half of May discharge and mean NDVI records during 1982 to 2013. These data suggest a clear increasing trend by 4830 $m^3/s/yr$, while the NDVI shows a very weak upward trend. Despite the weak trend, there are consistent interannual fluctuations between discharge and NDVI data. Over the study period, when the discharge was higher (or lower), the NDVI was correspondingly higher (or lower). This association was especially clear in early 1990s

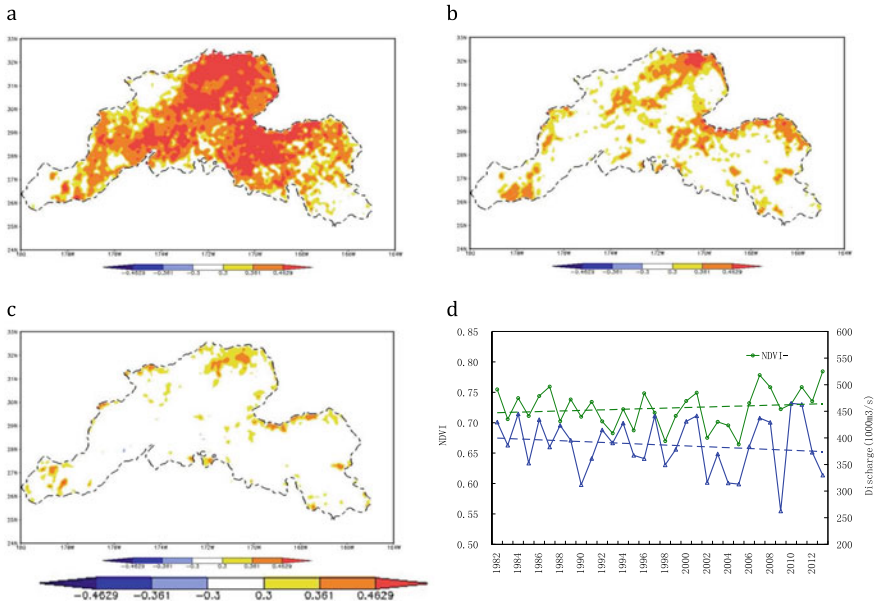

Fig. 23.5 Correlation coefficients between the 2nd half of May discharge and NDVI at the 2nd half of May (**a**), 1st half of June (**b**) and 2nd half of June (**c**) over Yukon Basin, and the 2nd half of May discharge and basin mean NDVI during 1982 to 2013 (**d**)

and 2000s. In these years, both discharge and NDVI were high in 1990, 1995, and 2002, significantly lower in 1992. Synchronous variation in both records further confirms a direct relationship between discharge fluctuation and vegetation growth over the basin. However, for 1990 and 2013, the flows were lower with above normal NDVI values over the basin.

The 2nd half of August is the time when the NDVI sensitively responds to discharge from May to August (Table 23.1). Similar to the 2nd half of May, we calculated the correlations between NDVI and discharge for all the cells within the basin.

Figure 23.6 shows the maps of correlations between the 2nd half of August NDVI and discharges at the 2nd half of August, 1st half of August, and 2nd half of May. These maps display the correlation patterns with significance at 0.10, 0.05, and 0.01 level. For the 2nd half of August discharge (Fig. 23.6a), the high correlation zone is mainly located in the region upstream of Yukon River. For the 1st half of August discharge, the high correlation zone moved a little more to upstream (Fig. 23.6b). The correlation patterns at the 2nd half of May have a more clear eastward movement and fill almost all the upstream, and enlarge to headwater area, but it is a negative correlation with NDVI (Fig. 23.6c). Relatively to the 2nd half of August, the area of high correlations in the 1st half of August basically maintains same correlation both in significant level and distribution. This may

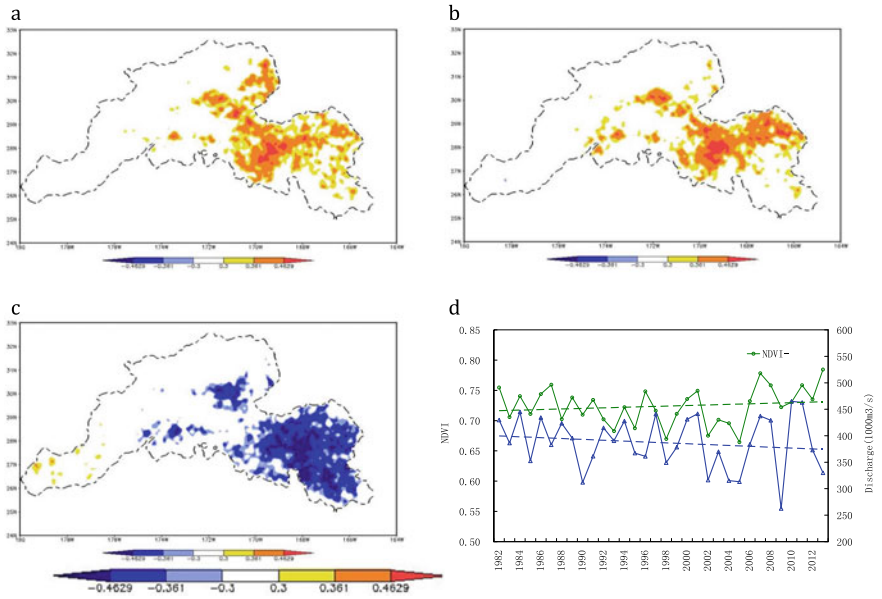

Fig. 23.6 NDVI-discharge correlation maps, **a** NDVI versus discharge, both at the 2nd half of August, **b** 1st half of August and the 2nd half of May, and **c** the 2nd half of August

suggest that the discharge in August would impact vegetation growth in 2nd half of August.

Figure 23.6d displays the 2nd half of August discharge and basin mean NDVI during 1982 to 2013. The interannual fluctuations are very consistent between these two variables before 2010. During 1982 to 2010, the extremely high/low discharge years match exactly with the highest/lowest NDVI years. For example, 2001 and 2007 were the year with higher flow and higher NDVI, and 1998 and 2002 were the year with the lower flow and lower NDVI. This consistency is a good evidence of NDVI association to the river flow. In other words, the precondition of water storage and availability (represented by river flow variations) is the key factor to plant growth and process over the warm season.

23.5 Extreme Flows and NDVI Conditions

We examined the highest and lowest peak flow years during 1982 to 2013 and the corresponding NDVI conditions (Fig. 23.7). Discharge conditions in the extreme years were very different between 1986 and 2008, particularly during the warm season. The flows in 1986 were quite low, with the peak discharge of about 539,100 m^3/s at the 2nd half of June. On the other hand, the flows in 2008 were

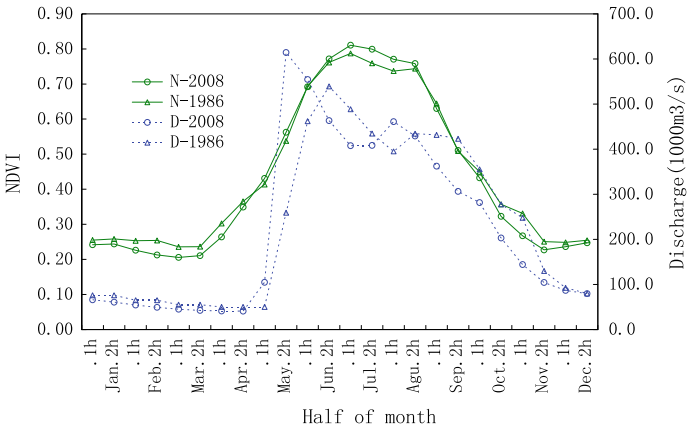

Fig. 23.7 Extreme discharge (D) and basin mean NDVI (N) for 2008 and 1986, respectively

very high, with the peak flow of 614,300 m^3/s at the 2nd half of May. The difference in peak discharge between these two years is about 75,200 m^3/s; relatively, the peak flow in 1986 is about 88% of that in 2008. Summer flow in 1986 was remarkably less than that in 2008; discharge at the 2nd half of May and 1st half of June in 1986 only account for 42 and 83% of that in 2008. In comparison to the mean discharge (see Fig. 23.7), the maximum discharge at the 2nd half of May in 2008 was one half month earlier than the normal year, and was one half month later than in 1986. The huge differences in both the peak flow and its timing (one month) between 1986 and 2008 may affect the vegetation activities over the basin, since there is a close positive correlation between NDVI and discharge at the stage of rapid vegetation growth during spring.

The NDVI patterns were different between 1986 and 2008 over the warm season, particularly during the 1st half of July to 1st half of August. In 2008 with higher flow, the NDVI increased continually and reached the peak (0.81) at the 1st half of July. After that, the NDVI remained higher in 2008 for 3 half months in this summer compared to 1986. It may imply the better water supply with higher flow in the spring may induce a higher vegetation production. The difference in the peak NDVI between the two years is about 0.02; relatively, the peak value in 1986 is about 97% of that in 2008. The period from the 1st half of July to 1st half of August is the key period for vegetation production. Summer NDVI in 1986 was remarkably less than that in 2008; NDVI at the 1st half of July, 2nd half of July, and 1st half of August in 1986 only account for 97, 95, and 96% of that in 2008. The comparisons of extreme flow years support that discharge during spring will directly impact vegetation, i.e., higher discharge will benefit vegetation growth and high production over the basin.

23.6 Discussion and Conclusion

Similar to the Mackenzie river (Xu et al. 2016), analyses of long-term discharge and NDVI data show a strong seasonal consistency between NDVI and discharge over the Yukon rivers. The flow-NDVI association is particularly strong in the early growing season (in May) in both regions. During this period, discharge rapidly rises and reaches the peak, while NDVI increases around the 1st half of May and reaches the maximum in July. In the mid and late summer, both discharge and NDVI decline gradually. Correlation analyses identify May to June as the sensitive period while NDVI significantly responds to discharge variations. This indicates that spring flow has a strong influence on vegetation growth in the early growing season over northern regions. The second sensitive period is different in timing for the basins. NDVI during the 2nd half of August to 1st half of September related to discharge at 2nd half of August in Yukon Basin, the NDVI relates closely to discharge with simultaneous discharge (positive relationship) and the flow in late spring (negative relationship).

Trends analyses suggest that river discharge during 1982 to 2013 increased in most seasons, with the most significant increase by 46 and 23% during the 2 half month in May. Discharge at the 1st half of July decreased by about 16%. The NDVI trends during the growing season from May to September clearly correspond to discharge changes. For example, the NDVI decreased by 4–6% at the 2nd half of June, 1st half of July, 2nd half of July, and 2nd half of August, when discharge had negative changes during the study period. This result clearly indicates that seasonal vegetation change is closely related to discharge variation, and the higher flow in the spring-summer season will lead a better vegetation production over the Yukon Basin. In addition, examination of extreme flow years and corresponding NDVI conditions over the basin also reveals that low runoff year was associated with a lower basin NDVI with an earlier maximum, while the higher flow year was linked with a higher NDVI and a longer growth season. However, in Yukon Basin, the most significant flow decrease by 8, 13, and 15% occurred during the 1st half of June to the 1st half of July. The most significant increase occurred in May, with the total trends of 104.8% and 34.2%, respectively. The NDVI trends during the growing season from May to September reversely correspond to discharge changes.

Basin-scale exploration of vegetation-flow relationship in the northern regions is important to understand that large watershed with diverse climatic, physical, and ecological conditions. The Yukon river is long and flow travel takes weeks from upstream to downstream. It is very important to identify the large-scale linkage between basin flow regime and vegetation patterns. It also closely relates to basin climate and hydrology change analyses, such as Yang et al. (2014a, b) and Woo and Thorne (2003). In order to better understand hydrology and vegetation interactions, it is useful to carry out similar analyses at the sub-basins within a big basin. It is also necessary to link basin/sub-basin study with local/plot scale observations, including snow cover, soil moisture patterns/changes, and their relationship with vegetation processes. Ecosystem modeling and advanced remote sensing techniques

are also powerful tools to advance our understanding of northern hydrology and ecosystems.

The selections of time scale for basin hydrology and climate investigations are also important. A half-month step has been used for the analyses of snow cover and runoff relationship over the large northern basins (Girardin et al. 2014; Wang et al. 2014). We choose the half-month step mainly due to NDVI data availability. The results seem to be reasonable for the large basin. Weekly to decadal time scales may be useful to better relate this work with snowmelt and river flow processes Yang et al. (2009), particularly over the spring season. There are MODIS NDVI or SPOT vegetation products at 10-day time step since 2001 and 1998, respectively. These data are relatively shorter than the NDVI data, and they may be subject to uncertainties especially in the cold regions due to the impact of snow cover. It would be, however, useful to consider the weekly or decade data in the future analyses, so as to compare and validate the result from this work.

The results of this analysis suggest that river flow reflect water availability over a basin. Studies also show river flow is an index for storage changes over a basin (Brutsaert 2008; Ye et al. 2009), although not the best but easy to obtain with long-term records. Regional or basin storage is difficult to measure or determine. In addition to soil moisture, snow cover is important for the northern regions as the main storage. Snow cover affects regional hydrology and vegetation processes (Yang et al. 2009; Yi et al. 2014). GRACE data can determine the total storage changes over large regions (Swenson et al. 2006; Velicogna et al. 2012). Given the total storage, the key challenge is then to determine the amount of water available to plants and trees. It is a critical question as far as how to obtain this information from river discharge records and available GRACE or snow cover (SWE) data. Effort is necessary to study the interactions among basin snow cover, discharge, and vegetation dynamics through coupled models and field observations.

References

Beck PSA, Goetz SJ (2011) Satellite observations of high northern latitude vegetation productivity changes between 1982 and 2008: ecological variability and regional differences. Environ Res Lett 6. https://doi.org/10.1088/1748-3182/6/4/049501

Bertoldi W, Drake NA, Gurnell AM (2011) Interactions between river flows and colonizing vegetation on a braided river: exploring spatial and temporal dynamics in riparian vegetation cover using satellite data. Earth Surf Proc Land 36(11):1474–1486. https://doi.org/10.1002/esp.2166

Bhatt US et al (2010) Circumpolar Arctic Tundra vegetation change is linked to Sea Ice decline. Earth Interact 14(8):1–20. https://doi.org/10.1175/2010ei315.1

Bi J, Xu L, Samanta A, Zhu Z, Myneni R (2013) Divergent Arctic-Boreal vegetation changes between North America and Eurasia over the past 30 years. Remote Sens-Basel 5(5):2093–2112. https://doi.org/10.3390/rs5052093

Bonsal BR, Prowse TD, Duguay CR, Lacroix MP (2006) Impacts of large-scale teleconnections on freshwater-ice break/freeze-up dates over Canada. J Hydrol 330:340–353

Brabets T, Wang B, Meade R (2000) Environmental and hydrologic overview of the Yukon river basin, Alaska and Canada,USGS, Water-Resources Investigation Report 99–4204, 106

Brutsaert W (2008) Long-term groundwater storage trends estimated from streamflow records: climatic perspective. Water Resour Res 44(2):n/a–n/a

Fretwell PT, Convey P, Fleming AH, Peat HJ, Hughes KA (2010) Detecting and mapping vegetation distribution on the Antarctic Peninsula from remote sensing data. Polar Biol 34 (2):273–281. https://doi.org/10.1007/s00300-010-0880-2

Friedlingstein P et al (2006) Climate-carbon cycle feedback analysis: results from the C4MIP model intercomparison. J Clim 19:3337–3353. https://doi.org/10.1175/JCLI3800.1

Girardin MP, Guo XJ, De Jong R, Kinnard C, Bernier P, Raulier F (2014) Unusual forest growth decline in boreal North America covaries with the retreat of Arctic sea ice. Global Change Biol 20(3):851–866. https://doi.org/10.1111/gcb.12400

He YH, Guo XL, Dixon P, Wilmshurst JF (2012) NDVI variation and its relation to climate in Canadian ecozones. Can Geogr-Geogr Can 56(4):492–507. https://doi.org/10.1111/j.1541-0064.2012.00441.x

Hogg EH (1994) Climate and the southern limit of the western Canadian boreal forest. Can J For Res 24:1835–1845

Hogg EH (1997) Temporal scaling of moisture and the forest-grassland boundary in western Canada. Agric For Meteorol 84(1997):115–122

Jiang D, Fu X, Wang K (2013) Vegetation dynamics and their response to freshwater inflow and climate variables in the Yellow River Delta, China. Quatern Int 304:75–84. https://doi.org/10.1016/j.quaint.2012.10.059

Kim Y, Kimball JS, Zhang K, McDonald KC (2012) Satellite detection of increasing northern hemisphere non-frozen seasons from 1979 to 2008: implications for regional vegetation growth. Remote Sens Environ 121:472–487. https://doi.org/10.1016/j.rse.2012.02.014

Kim Y, Kimball JS, Zhang K, Didan K, Velicogna I, McDonald KC (2014) Attribution of divergent northern vegetation growth responses to lengthening non-frozen seasons using satellite optical-NIR and microwave remote sensing. Int J Remote Sens 35(10):3700–3721. https://doi.org/10.1080/01431161.2014.915595

McClelland JW, Déry SJ, Peterson BJ, Holmes RM, Wood EF (2006) A pan-arctic evaluation of changes in river discharge during the latter half of the 20th century. Geophys Res Lett 33 (L06715). https://doi.org/10.1029/2006gl025753

McManus KM, Morton DC, Masek JG, Wang D, Sexton JO, Nagol JR, Ropars P, Boudreau S (2012) Satellite-based evidence for Shrub and Graminoid Tundra expansion in Northern Quebec from 1986 to 2010. Global Change Biol 18:2313–2323. https://doi.org/10.1111/j.1365-2486.2012.02708.x

Myneni RB, Hall FB, Sellers PJ, Marshak AL (1995) The interpretation of spectral vegetation indices. Geosci Remote Sens 33:6–19

Nemani RR, Keeling CD, Hashimoto H, Jolly WM, Piper SC, Tucker CJ, Myneni RB, Running SW (2003) Climate-driven increases in global terrestrial net primary production from 1982 to 1999. Science 300(5625):1560–1563. https://doi.org/10.1126/science.1082750

Olthof I, Latifovic R (2007) Short-term response of arctic vegetation NDVI to temperature anomalies. Int J Remote Sens 28(21):4823–4840. https://doi.org/10.1080/01431160701268996

Peng D, Zhang B, Liu L, Fang H, Chen D, Hu Y, Liu L (2012) Characteristics and drivers of global NDVI-based FPAR from 1982 to 2006. Global Biogeochem Cycle 26. https://doi.org/10.1029/2011gb004060

Peterson BJ, Holmes RM, McClelland JW, Vorosmarty CJ, Lammers RB, Shiklomanov AI, Shiklomanov IA, Rahmstorf S (2002) Increasing river discharge to the Arctic Ocean. Science 298(5601):2171–2173. https://doi.org/10.1126/science.1077445

Pouliot D, Latifovic R, Olthof I (2009) Trends in vegetation NDVI from 1 km AVHRR data over Canada for the period 1985–2006. Int J Remote Sens 30(1):149–168. https://doi.org/10.1080/01431160802302090

Prowse T, Shrestha R, Bonsal B, Dibike Y (2010) Changing spring air temperature gradients along large northern rivers: implications for severity of river-ice floods. Geophys Res Lett 37:201–215

Qian H, Joseph R, Zeng N (2010) Enhanced terrestrial carbon uptake in the Northern high latitudes in the 21st Century from the coupled carbon cycle climate model intercomparison project model projections. Global Change Biol 16:641–656. https://doi.org/10.1111/j.1365-2486.2009.01989.x

Saito K, Zhang T, Yang D, Marchenko S, Barry R, Romanovsky V, Hinzman L (2012) Land-Atmosphere Interactions of Snow and Permafrost Dynamics in the Arctic and Beyond. Ecol Appl 23(8):1778–1797

Swenson S, Yeh PJ-F, Wahr J, Famiglietti J (2006) A comparison of terrestrial water storage variations from GRACE with in situ measurements from Illinois. Geophys Res Lett 33:L16401

Tape KD, Hallinger M, Welker JM, Ruess RW (2012) Landscape heterogeneity of shrub expansion in Arctic Alaska. Ecosystems 15:711–724. https://doi.org/10.1007/s10021-012-9540-4

Velicogna I, Tong J, Zhang T, Kimball JS (2012) Increasing subsurface water storage in discontinuous permafrost areas of the Lena river basin, Eurasia, detected from GRACE. Geophys Res Lett 39:L09403

Wang X, Piao S, Ciais P, Li J, Friedlingstein P, Kovene C, Chen A (2011) Spring temperature change and its implication in the change of vegetation growth in North America from 1982 to 2006. Proc Natl Acad Sci 108(4):1240–1245. https://doi.org/10.1073/pnas.1014425108/-/DCSupplemental

Wang S, Huang J, Yang D, Pavlic G, Li J (2014) An assessment of long-term water budget closures for large drainage basins in Canada. Hydrol Process. https://doi.org/10.1002/hyp.10343

Woo MK, Thorne R (2003) Streamflow in the Mackenzie basin, Canada. Arctic 56(4):328–340

Xu W, Yang D, Li Y, Xiao R (2016) Correlation analysis of Mackenzie river discharge and NDVI relationship. Can J Remote Sens 42(3):292–306. https://doi.org/10.1080/07038992.2016.1171135

Yang D, Kane DL, Hinzman LD, Zhang X, Zhang T, Ye H (2002) Siberian Lena River hydrologic regime and recent change. J Geophys Res 107(D23). https://doi.org/10.1029/2002jd002542

Yang D, Ye B, Kane D (2004a) Streamflow changes over Siberian Yenisei river basin. J Hydrol 296(1–4):59–80

Yang D, Ye B, Shiklomanov AI (2004) Streamflow characteristics and changes over the Ob river watershed in Siberia. J Hydrometeorol 5(4):69–84

Yang D, Zhao Y, Armstrong R, Robsinson D (2009) Yukon river streamflow response to seasonal snowcover changes. Hydrol Process 23:109–121. https://doi.org/10.1002/7216

Yang D, Marsh P, Ge S (2014a) Heat flux calculation and analyses for Mackenzie and Yukon rivers. Polar Sci 8(3):232–241

Yang D, Shi X, Marsh P (2014b) Variability and extreme of Mackenzie River daily discharge during 1973–2011. Quatern Int. https://doi.org/10.1016/j.quaint.2014.09.023

Ye B, Yang D, Zhang Z, Kane DL (2009) Variation of hydrological regime with permafrost coverage over Lena Basin in Siberia. J Geophys Res 114:D07102. https://doi.org/10.1029/2008JD010537

Yi Y, Kimball JS, Reichle RH (2014) Spring hydrology determines summer net carbon uptake in northern ecosystems. Environ Res Lett 9(6):064003. https://doi.org/10.1088/1748-9326/9/6/064003

Zhang K, Kimball JS, Hogg EH, Zhao M, Oechel WC, Cassano JJ, Running SW (2008) Satellite-based model detection of recent climate-driven changes in northern high latitude vegetation productivity. J Geophys Res-Atmos 113(G03033)

Dr. Weixin Xu is a Professor at the Chengdu University of Information Technology, China. His research focuses on vegetation variation and its responses to environment factors in cold regions especially in Qinghai-Tibet Plateau and the northern regions. His current research aims to develop a measurement method of dead grass material in alpine meadow by remote sensing data. He has led numerous research projects and published extensively in various research areas, including monitoring and evaluation of alpine vegetation environment, impact analysis of vegetation variation, and quantitative methods of remote sensing monitoring and parameters identification of alpine vegetation system.

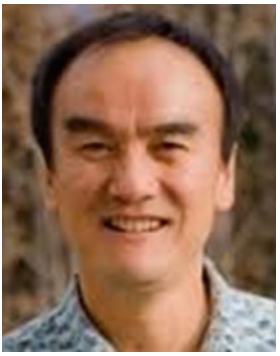

Dr. Daqing Yang is a Research Scientist at the Watershed Hydrology and Ecology Research Division, Environment and Climate Change Canada. He is also Affiliate Research Professor at the International Arctic Research Center, Univ. of Alaska Fairbanks. Over the past 25 years, he has conducted cryosphere system research in China, Canada, Japan, USA, and Norway. His primary research activities/interests include cold region hydrology and climate, particularly Arctic large river streamflow regime and change, snow cover and snowfall measurements, climate change and human impact to regional hydrology, and applications of remote sensing in cold regions. He has served as journal editor and subject editor for IAHS publications (cold region hydrology, northern research basin water balance, and cold/mountain region hydrological systems under climate change), and WMO technical reports (solid precipitation measurement intercomparison, and integrated global observing strategy-cryosphere theme). He also contributed as review and/or author to the IPCC Reports, and the Arctic Council's Snow, Water, Ice and Permafrost in the Arctic (SWIPA 2017 and follow up) assessment. His current research focuses on investigating the impacts of climate variability/change and human activities on hydrologic system across the broader northern regions.

Part V
Cross-System Linkage and Integration

River Freshwater Flux to the Arctic Ocean

24

Alexander Shiklomanov, Stephen Déry, Mikhail Tretiakov, Daqing Yang, Dmitry Magritsky, Alex Georgiadi, and Wenqing Tang

Abstract

Various estimates of freshwater discharge to the Arctic Ocean with different methods and for different drainage areas have shown a good consistency in long-term mean runoff ranging from 200 mm/year to 226 mm/year. Most of the estimates are derived from available discharge measurements at the downstream

A. Shiklomanov (✉)
Earth Systems Research Center, University of New Hampshire, Durham, NH, USA
e-mail: sasha@eos.sr.unh.edu; alex.shiklomanov@unh.eu

A. Shiklomanov · M. Tretiakov
Arctic and Antarctic Research Institute, St. Petersburg, Russian Federation
e-mail: tmv@arri.ru

S. Déry
Environmental Science Program, University of Northern British Colombia, Prince George, BC, Canada
e-mail: sdery@unbc.ca

D. Yang
Watershed Hydrology and Ecology Division, Environment and Climate Change Canada, Victoria, BC, Canada
e-mail: daqing.yang@canada.ca; daqing.yang@gmail.com

D. Magritsky
Moscow State University, Moscow, Russian Federation
e-mail: magdima@yandex.ru

A. Georgiadi
Institute of Geography, Russian Academy of Science, Moscow, Russia
e-mail: galex50@gmail.com

W. Tang
Jet Propulsion Laboratory, California Institute of Technology, Sierra Madre, CA, USA
e-mail: wenqing.tang@jpl.nasa.gov

D. Yang and D. L. Kane (eds.), *Arctic Hydrology, Permafrost and Ecosystems*,
https://doi.org/10.1007/978-3-030-50930-9_24

gauging stations. According to the most recent assessment of the total discharge to the Arctic Ocean is approximately 4300 km^3 $year^{-1}$ and continental contributions to the river input into the Arctic Ocean for Asia, North America, and Europe are 55%, 28%, and 17%, respectively. The river flux to the Arctic Ocean has significantly changed with an increase of 210 km^3 over 1936–2015 across Eurasia, and 36 km^3 over 1964–2015 for northern Canada. These changes were especially pronounced during the last 30-years, associated with most intense warming of air temperature over the northern hemisphere and significant declines in sea ice extent over the Arctic Ocean. The significant increase in annual river flow is mainly due to increases in winter (60%) and spring (33%) discharge. Winter flows have a very consistent and significant increase throughout the Eurasian pan-Arctic. All six largest Eurasian Arctic rivers show a significant increase in winter river flows over the long-term period 1936–2015. Similar but less significant trends in winter and spring discharge were found for Canadian northern rivers. Seasonal discharge has been altered as the result of human activity, particularly reservoir regulation. Eliminating reservoir effect in the largest Arctic rivers of Yenisei, Lena, and Ob, using the hydrograph transformation model, show significant increase in annual discharge, i.e., increase in spring by 49%, winter by 31%, and summer-fall by 20%. These results are different from those obtained from the observational discharge data. Thus, for hydroclimatic analysis to understand possible changes in river flux to the Arctic Ocean, it is necessary to take into account human impact on the discharge regime and change. Sea surface salinity (SSS) links various components of the Arctic freshwater system, including river discharge. Analysis of remote sensed SSS data has shown that SSS distribution pattern in the Arctic Ocean during warm period is partly defined by river flux. There is a great potential of using remote sensing data for a better understanding of variability in the Arctic freshwater system.

24.1 Introduction

The delivery of freshwater from the continental landmass is of special importance to the Arctic Ocean since it contains only 1.0% of the world's ocean water, yet receives 11% of the world's river runoff (Shiklomanov and Shiklomanov 2003). The Arctic Ocean is the most river-influenced and land-locked of all oceans and is the only ocean with a contributing land area greater than its surface area (Ivanov 1976; Vörösmarty et al. 2001). Freshwater inflow contributes as much as 10% to the upper 100 meters of the water column for the entire Arctic Ocean (Serreze and Barry 2000). Thus, river flow to the Arctic Ocean plays a significant role in the oceanic freshwater budget, accounting for about two thirds of the total freshwater flux to the Arctic Ocean (Serreze et al. 2006). Ocean salinity and sea ice formation are critically affected by river input (Rawlins et al. 2009a, b; Tang et al. 2018) and

changes in the freshwater and heat fluxes to the ocean can exert significant control over global ocean circulation via the North Atlantic deep water formation (Manabe and Stouffer 1994; Rahmstorf 2002). River flow from the Arctic drainage basin is thus likely to serve an important role in regulating the heat balance of the planet (Peterson et al. 2006). It also plays an important role as a nutrient supplier to nearshore and estuarine ecosystems of the Arctic Ocean, providing their biological productivity (Carmack et al. 2016).

There is a correspondence between fluctuations of annual river discharge and minimum sea ice extent in the Arctic Ocean with negative correlation $r = -0.7$ (Shiklomanov and Lammers 2009) suggesting that a) both rivers and sea ice are responding to changes in large-scale hemispheric climate patterns (Rawlins et al. 2009a, b) an increasingly ice-free summer in the Arctic Ocean contributed to wetter conditions on the land surface via atmospheric moisture transport from open sea areas. Arctic surface air temperatures are warming at double the rates of the lower latitudes and this phenomenon has widespread implications for all of the components of the Arctic water cycle.

River flow is an important characteristic connecting numerous environmental and anthropogenic processes, and their changes aggregated over large areas. River discharge is one of the most important variables used for observing the hydrological cycle over the land surface. It represents a powerful integrating tool and its monitoring can provide accurate and timely data on responses of the land surface to atmospheric forcing. Streamflow is also one of the most accurately measured components of the hydrological cycle (Shiklomanov et al. 2006), and therefore can serve as an important indicator to reflect changes in the water cycle associated with climate variability and regional human impacts.

In this chapter, we discuss and update long-term variations of various characteristics of river flow to the Arctic Ocean. We present analyses and results of total freshwater input and its variation and change over space and time. We discuss the possible reasons for observed streamflow changes due to climate effect and human impact, and identify knowledge gaps and research challenges for future international collaborations.

24.2 Assessment of River Input to the Arctic Ocean

24.2.1 Terrestrial Domain

To understand variability and changes in the Arctic Ocean freshwater budget, the river flux from the entire Arctic Ocean drainage basin, as well as from the adjacent watersheds contributing runoff to the Arctic Ocean via the north-flowing oceanic currents, should be considered. This Arctic (or pan-Arctic) hydrological domain also includes the drainage basins of Hudson Bay, James Bay, and Bering Strait with a total drainage area of $\sim 3.5 \times 10^6$ km^2 and extending to a latitude of 45°N. An important physical feature of the pan-Arctic drainage basin is that a large majority

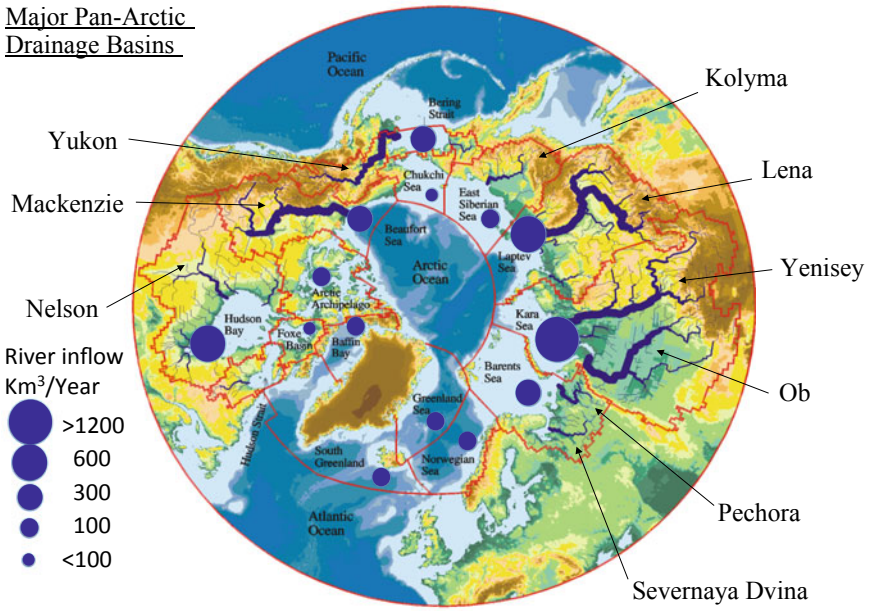

Fig. 24.1 Pan-Arctic drainage basin, major rivers, and sea basins. Blue circles show long-term mean annual river inflow to individual seas based on combinations of observational data and model simulations for unmonitored areas with MERRA2 climate drivers

of the area (77%) lies well south of the Arctic Circle (AC; 66.6°N) (Prowse et al. 2015). A significant part of the domain is located in temperate climate zones and is covered by boreal/taiga forest. The entire pan-Arctic hydrological domain covers a region of ~23.7 million km^2, representing 20% of the total global land area (Milliman and Farnsworth 2011) (Fig. 24.1) and covering several climatic zones from steppes and prairies in the south to a polar desert in the North.

24.2.2 Total River Flow to the Arctic Ocean

Given well-recognized uncertainties in many elements of the Arctic hydrologic cycle (Hinzman et al. 2005; Bring et al. 2016) such as evapotranspiration, precipitation, soil, and groundwater, the value of gauge-based hydrographic measurements is critical. Measurements of river discharge in cold regions have specific peculiarities. Additional uncertainty in streamflow data can arise as result of the complexity of discharge measurements during high flow periods, which are often complicated by ice conditions (Shiklomanov et al. 2006). In addition, during high flows a significant volume of discharge may bypass measurement stations as flow in braided channels, inundated floodplains (Alsdorf and Lettenmaier 2003) or as submarine groundwater seepage (Syed et al. 2007). Despite these issues, river

discharge is one of the most accurately measured components of the water cycle (Grabs et al. 1996) especially in cold regions where observational precipitation and evapotranspiration data also have significant uncertainties (Yang et al. 2005; Bring et al. 2016). Thus, reliable hydrometric information is particularly important to understand and quantify hydrological responses to climatic changes and direct anthropogenic impacts.

The estimates of freshwater discharge from the pan-Arctic drainage region vary considerably (Syed et al. 2007). Much of the variation can be attributed to problems associated with different approaches to river flow evaluation. Most of the estimates are derived from available discharge measurements at the gauging stations (e.g., McClelland et al. 2006; Shiklomanov and Lammers 2009; Déry et al. 2005, 2009, 2011, 2016; Holmes et al. 2018). These estimates, however, do not take into account river discharge to the ocean from extensive unmonitored areas in North America and Eurasia, which are important to understand the variability of total river flux to the Arctic Ocean and oceanic freshwater balance (ACIA 2005). Other approaches are based on model simulations (e.g., Su et al. 2005; Holland et al. 2007; Hamman et al. 2017) or are derived from the synergistic use of modeled and observed streamflow (e.g., Fekete et al. 2002; Shiklomanov and Shiklomanov 2003; Shiklomanov and Lammers 2013). In addition the significant source of variation in discharge evaluations is the result of the different definitions of the geographic extent of the region (Prowse and Flegg 2000). Several geographical definitions of contributing land area to the Arctic Ocean are usually used, ranging from 12×10^6 km^2 to 24×10^6 km^2 with most of the differences found in how various research groups tended to define the drainage system in North America and Greenland (Prowse et al. 2015) (see Table 24.1).

Each of discussed above methods for discharge evaluation has both advantages and disadvantages. Assessment of total freshwater discharge into the Arctic Ocean using only in situ gauge measurements does not take into account discharge from significant portions of unmonitored areas, i.e., about 30–40% of the total pan-Arctic drainage basin (Shiklomanov et al. 2002). For example, the maximum gauged area of the Canadian pan-Arctic was 64% in 1990 before it slowly decreased to 56% in 2008 (Mlynowski et al. 2011). The river flow from the Eurasian pan-Arctic was better monitored, however, the gauged area also declined from almost 80% in 1990 to about 70% in 2012 (Shiklomanov and Lammers 2013) due to the closure or mothballing of several important downstream gauging stations. The method of hydrological analogy is the simplest way to evaluate streamflow for some unmonitored river basins (Shiklomanov and Shiklomanov 2003). This approach provides reasonable results when there are monitored river basins representative for regional hydrological, climatic, and land cover conditions. In this case the runoff data for these rivers can be expanded to the unmonitored territory with similar conditions of runoff formation. However, it is not always possible to find basin analogs with long-term discharge measurements for many small and medium size river basins along the Arctic Ocean coast and over Arctic islands where the conditions for runoff generation are quite different from the monitored part of the Arctic drainage basin. Evaluation of discharge based on various land surface models

Table 24.1 Various assessments of river flow to the Arctic Ocean

References	Method	Discharge, km^3/year	Contributing Area, km^2	Runoff mm/year	Period
Grabs et al. (2000)	Observed	2603	12.8×10^6	203	
Lammers et al. (2001)	Obseved + analogy	4749	22.4×10^6	212	1960–1989
Shiklomanov and Shiklomanov (2003)	Observed + analogy + P-E	4314 5250	18.9×10^6 23.7×10^6	228 222	1921–1999
McClelland et al. (2006)	Observed	2420	12.1×10^6	200	1964–2000
Holmes et al. (2018)	Observed	2310	11.3×10^6	204	1970–2017
Su et al. (2005)	Modeled	3596	16.4×10^6	219	1979–1999
Holland et al. (2007)	Modeled	3162*	15.8×10^6	200	1980–1999
Dai and Trenberth (2002)	Observed + modeled	3658	16.9×10^6	216	
Shiklomanov and Lammers (2013)	Observed + modeled	4300	19.0×10^6	226	1936–2006
Syed et al. (2007)	GRACE	3730	16.7×10^6	223	2003–2005

*Average discharge from 10 GCMs with a range from individual models from 2240 to 4724 km^3/year

strongly depends on the accuracy of the climate drivers used, particularly precipitation, which has a large uncertainty especially during the cold season (Fekete and Vörösmarty 2004; Yang et al. 2005; Biemans et al. 2009). Many models also remain deficient in representing hydrologic processes in regions with perennial-to-intermittent frozen ground, and often significantly overestimate or underestimate river flow in these areas.

During the past few decades remote sensing products were also applied to estimate river flow to the Arctic Ocean. For example, terrestrial water storage (TWS) anomalies from GRACE (Gravity Recovery and Climate Experiment) (Landerer and Swenson 2012), available since 2002, have been used to evaluate changes in water balance across large northern watersheds, to quantify river flows (Frappart et al. 2011; Velicogna et al. 2012; Scanlon et al. 2016) and to improve land surface models (Girotto et al. 2016). Thus the GRACE mass concentration solutions with increased spatial localization and amplitude of recovered TWS anomalies (Scanlon et al. 2016) can significantly improve the assessment of the river flux from large unmonitored Arctic watersheds and can be also applied to better constrain the hydrological models over these regions. Syed et al. (2007) used GRACE TWS estimates along with reanalysis data from the National Centers for Environmental Prediction/National Center for Atmospheric Research (NRA) (Kalnay et al. 1996) to assess the total freshwater inflow to the Arctic Ocean from its drainage area over 2003–2005. The obtained results were quite close to discharge estimates by other methods (Table 24.1). Thus, this relatively new remote sensing

product can significantly improve annual and monthly assessments of river flow, especially from large unmonitored areas. The GRACE-based estimates can also be very useful to evaluate discharge to ocean from large glacierized areas like Greenland or other large Arctic islands.

Most detailed estimates of river flux to the ocean from the entire drainage area (Shiklomanov and Lammers 2013) were made based on a combination of the hydrology analogy method (Shiklomanov and Shiklomanov 2003) and runoff simulated from meteorological data using the UNH water balance/water transport model (WBM) (Wisser et al. 2010, 2013). Simulations of river discharge with a hydrological model significantly improve quantification of river flux from unmonitored areas. Table 24.2 lists estimates of long-term mean annual river flow to different Arctic seas (Fig. 24.1); this information was obtained with a combination of observational data and WBM simulations over 1980–2010 using MERRA reanalysis as climate input data. It also shows estimates made 35 years ago based on observational discharge data and water balance calculations and published in the Russian Arctic Atlas, 1985. It is interesting to notice that both results agree well in spite of different methods and different periods (Table 24.2).

Table 24.2 Long-term mean annual river flow to individual parts of the Arctic Ocean and adjacent sea waters

#	Basin	Discharge*, km^3/year	Discharge**, km^3/year
1	Bering Sea	305	–
2	Chukchi Sea	60	78
3	Beaufort Sea	414	420
4	Arctic Archipelago	188	180
5	Baffin Sea	269	263
6	Foxe Basin	86	65
7	Southern Greenland	169	–
8	Hudson Bay	682	705
9	Hudson Strait	194	215
10	Norwegian Sea	150	145
11	Greenland Sea	148	140
12	Barents Sea	430	478
13	Kara Sea	1330	1350
14	Laptev Sea	760	767
15	East Siberian Sea	229	213
	Total	5414	–
	Without (basins 1 and 7)	4940	5019

*From Shiklomanov and Lammers (2013); average over 1980–2010
**Arctic Atlas, 1985; average over 1950–1980

24.3 Long-Term Variability of River Flux to the Arctic Ocean

24.3.1 Annual Discharge Variability

Multiple observations have shown a significant increase in total annual river discharge to the Arctic Ocean as well as significant spatial and seasonal changes in pan-Arctic river runoff over the last several decades (Shiklomanov and Lammers 2013; Tan and Gan 2015). Observations of combined river discharge from the six largest Russian north flowing rivers have shown an increase of 7% over the period 1936–1999 (Peterson et al. 2002). More recent estimates have shown this increase has continued into the twenty-first century with 2007 setting the new historical maximum (Fig. 24.2; Shiklomanov and Lammers 2009; Holmes et al. 2016) (Fig. 24.2, Table 24.3). River flow has also increased in North America at a rate of 0.9 km^3/year over 1970–2010 for several Arctic rivers: Mackenzie, Yukon, Peel, and Back (Shiklomanov and Lammers 2011) and by 18% over 1989–2013 for rivers in northern Canada (Déry et al. 2016) (Table 24.4). The most recent assessment of the observed river flow to the Arctic Ocean from Eurasia and North America was made based on data from Déry et al. 2016 and Holmes et al. 2018; it shows a 5.1 km^3 per year or 9% increase in total influx over 1964–2015.

The record high annual river flow to the Arctic Ocean from Eurasia over 80 years of observations was 2254 km^3 in 2007, or 25% (454 km^3/year) higher than the long-term mean annual discharge during 1936–2015 (1796 km^3/year) (see Fig. 24.2). This 2007 anomaly was greater than the total annual flow from the Ob

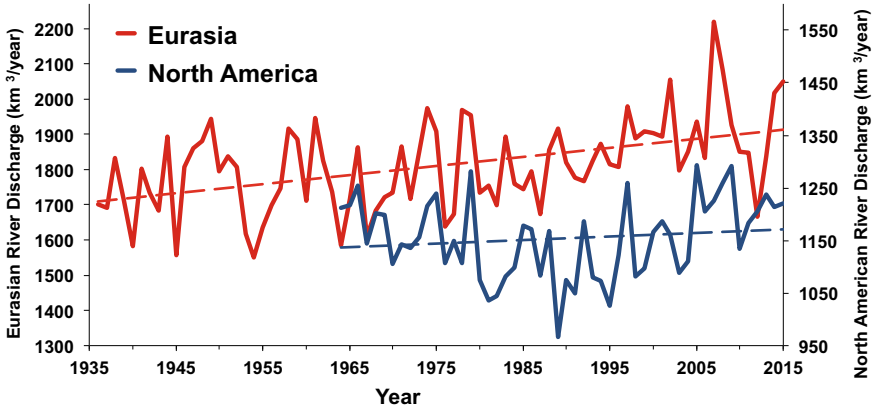

Fig. 24.2 Observed river discharge to the Arctic Ocean represented as total gauged discharge of the 6 largest Eurasian rivers flowing into the Arctic Ocean over 1936–2015, and total gauged discharge to the Arctic Ocean from North America during 1964–2015 (Déry et al. 2016)

Table 24.3 Seasonal and annual discharge of the largest Eurasian rivers flowing into the Arctic Ocean

River, site	Drainage area, mln.km^2	Period years	Annual		Winter (Nov-Mar)		Spring (Apr-Jun)		Summer-Fall (July-Oct)	
			km^3	mm	km^3	mm	km^3	mm	km^3	mm
Northern Dvina-Ust-Pinega	0.348	1936–1979	98	281	15	43	60	170	24	69
		1980–2015	104	299	18	52	61	175	25	73
		2000–2015	100	287	19	55	58	167	23	66
		1936–2015	101	291	**16**	**46**	60	172	25	72
Pechora-Ust-Tsilma	0.248	1936–1979	107	431	11	45	61	246	35	141
		1980–2015	114	462	**13**	**52**	66	267	35	143
		2000–2015	115	463	14	58	66	265	37	150
		1936–2015	**111**	**449**	**12**	**49**	**64**	**258**	209	86
Ob Salekhard	2,99	1936–1979	408	168	**62**	**25**	137	56	210	86
		1980–2015	404	166	72	30	144	59	191	78
		2000–2015	417	172	74	31	147	61	197	81
		1936–2015	406	167	**66**	**27**	**140**	**58**	201	83
Yenisei-Igarka	2,44	1936–1979	581	238	**72**	**30**	302	124	**207**	**85**
		1980–2015	610	250	**119**	**49**	**282**	**115**	**209**	**86**
		2000–2015	615	252	128	53	**252**	**103**	**234**	**96**
		1936–2015	**594**	**243**	**93**	**38**	**293**	**120**	208	85
Lena-Kusur	2,43	1936–1979	527	217	32	13	215	89	280	115
		1980–2015	**574**	**236**	**47**	**19**	**236**	**97**	290	119
		2000–2015	605	249	52	21	251	103	302	124
		1936–2015	**548**	**225**	**39**	**16**	**225**	**92**	285	117

(continued)

Table 24.3 (continued)

River, site	Drainage area, mln.km^2	Period years	Annual		Winter (Nov-Mar)		Spring (Apr-Jun)		Summer-Fall (July-Oct)	
			km^3	mm	km^3	mm	km^3	mm	km^3	mm
Kolyma-Sredne-kolymsk	0.361	1936–1979	71	196	2.0	5.6	33	91	36	100
		1980–2015	**80**	**220**	**5.1**	**14**	**34**	**95**	**40**	**112**
		2000–2015	94	261	6.2	17	40	111	48	133
		1936–2015	**75**	**207**	**3.4**	**9.5**	33	92	38	105
Total for 6 rivers	8,257	1936–1979	1795	217	**194**	**23**	809	98	792	96
		1980–2015	**1829**	**222**	**274**	**33**	**823**	**100**	**790**	**96**
		2000–2015	1815	220	294	36	814	99	839	102
		1936–2015	**1810**	**219**	**230**	**28**	**815**	**99**	791	96

Note Bold red numbers show significant (<0.05) trend over the period

Table 24.4 Annual and seasonal discharge of six North American regional river basins flowing into the Arctic Ocean and surrounding polar seas

River basin	Drainage area, mln.km^2	Period years	Annual		Winter		Spring		Summer		Fall	Fall
			km^3	mm	km^3	mm	km^3	mm	km^3	mm	km^3	mm
Bering Strait*	0.3469	1964–1989	88.1	253.8	4.6	13.2	34.4	99.2	37.9	109.2	11.2	32.2
		1990–2015	88.3	254.4	4.8	13.9	33.5	96.7	37.5	108.0	12.4	35.8
		1964–2015	88.2	254.1	4.7	13.6	34.0	97.9	37.7	108.6	11.8	34.0
Western Arctic Ocean	1.9988	1964–1989	343.5	171.8	31.7	15.9	121.5	60.8	139.9	70.0	56.1	28.1
		1990–2015	355.1	177.6	28.9	14.5	116.8	58.4	142.1	71.1	55.6	27.8
		1964–2015	349.3	174.7	34.5	17.3	126.2	63.1	137.7	68.9	56.6	28.3
Western Hudson Bay	2.2204	1964–1989	313.6	141.2	43.3	19.5	103.8	46.7	93.4	42.1	73.1	32.9
		1990–2015	338.7	152.5	49.2	22.2	104.6	47.1	102.7	46.3	82.1	37.0
		1964–2015	326.2	146.9	46.2	20.8	104.2	46.9	98.1	44.2	77.6	35.0
Eastern Hudson Bay	0.33307	1964–1989	189.9	570.2	25.0	75.2	58.0	174.0	56.2	168.8	50.7	152.3
		1989–2015	211.8	636.0	45.3	136.1	56.4	169.4	52.9	158.9	57.2	171.6
		1964–2015	200.9	603.1	35.2	105.6	57.2	171.7	54.6	163.9	53.9	161.9

(continued)

Table 24.4 (continued)

River basin	Drainage area, mln.km^2	Period years	Annual		Winter		Spring		Summer		Fall	Fall
			km^3	mm	km^3	mm	km^3	mm	km^3	mm	km^3	mm
Eastern Arctic Ocean	0.2339	1964–1989	125.0	534.4	5.5	23.4	53.7	229.7	42.4	181.3	23.4	99.9
		1990–2015	101.5	433.9	4.5	19.1	41.8	178.6	34.0	145.4	21.3	90.9
		1964–2015	113.2	484.1	5.0	21.3	47.7	204.1	38.2	163.4	22.3	95.4
Labrador Sea	0.12227	1964–1989	78.9	645.2	11.9	97.7	28.4	232.0	21.5	176.0	17.1	139.5
		1990–2015	75.1	614.5	15.3	125.0	26.1	213.2	16.4	134.5	17.3	141.8
		1964–2015	77.0	629.9	13.6	111.3	27.2	222.6	19.0	155.2	17.2	140.7
Total for 6 basins	5.25534	1964–1989	1145.0	217.9	120.1	22.9	397.0	75.5	395.4	75.2	232.4	44.2
		1990–2015	1162.9	221.3	152.1	28.9	386.7	73.6	379.6	72.2	244.5	46.5
		1964–2015	1153.9	219.6	136.1	25.9	391.8	74.6	387.5	73.7	238.5	45.4

*Canadian portion of the Yukon River Basin only
**Winter: JFM; Spring: AMJ; Summer: JAS; Fall: OND

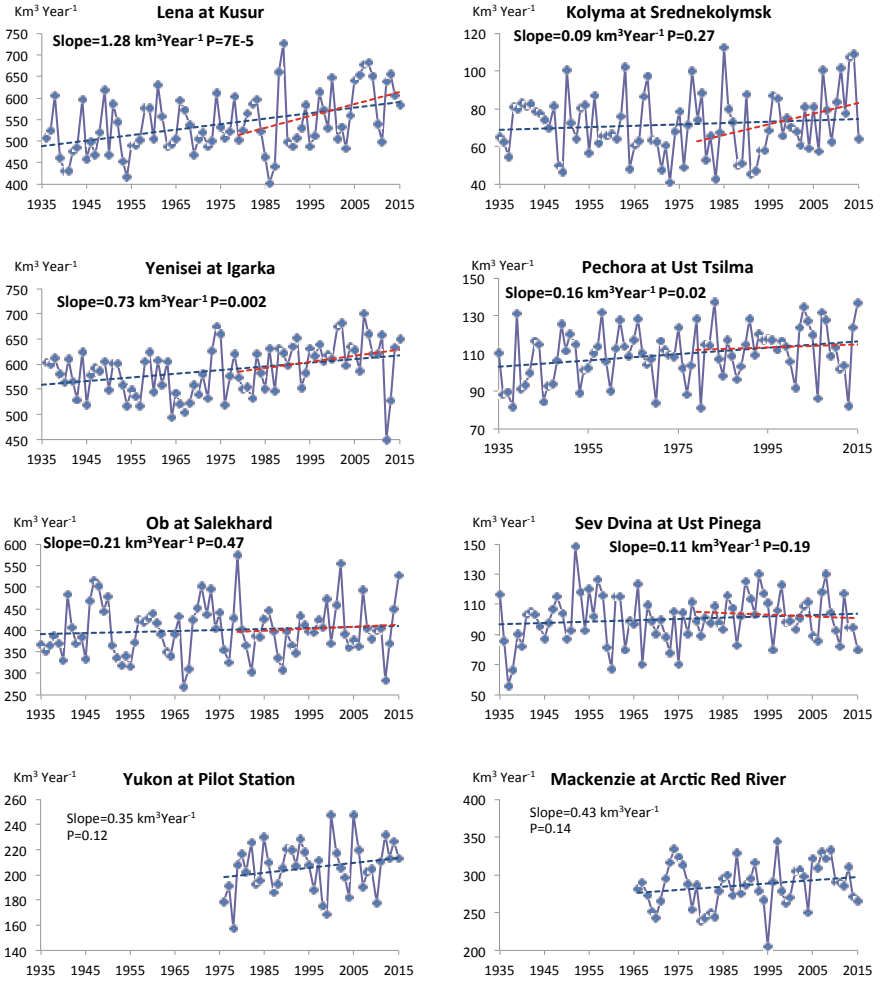

Fig. 24.3 Annual discharge variability of the largest Arctic rivers flowing to the Arctic Ocean over 1936–2015 and long-term annual trends

River basin, the 8th largest basin in the world by drainage area (Vörösmarty et al. 2000), and was approximately equal to the total estimated mean annual Greenland discharge (Mernild et al. 2009). The partitioning of the annual river discharge into the six contributing drainage basins showed record high flows in 2007 in the Pechora and Yenisei basins and very high flows in the Ob, Lena, and Kolyma (Fig. 24.3). Only the Severnaya Dvina experienced flows near the long-term mean. Except for the Kolyma, contributions of individual Eurasian rivers to the 2007 record river discharge were very consistent with the contributions of the river basins to the long-term discharge change, based on linear trends over the entire

observational period 1936–2015 (Shiklomanov and Lammers 2009). This result suggests the 2007 river discharge record reflected the patterns of the long-term changes observed in the Eurasian pan-Arctic over the 1936–2015 period, and the year 2007 was an anomaly in magnitude without major structural changes between basins. The last period (1980–2015) demonstrates an unprecedented rate of change in river discharge to the Arctic Ocean. In spite of the lower river flux from Eurasia during 2011–2013, as the result of both natural and anthropogenic causes (discussed below) and the mean annual slope of linear trend line over 1980–2015, which is about ~ 10 km^3/year, or almost four times higher than that over the entire observational period 1936–2015.

Two largest pan-Arctic rivers in the North America (Mackenzie and Yukon) have shorter observational period (Ge et al. 2012; Yang et al. 2014a, b) and also demonstrate increasing tendencies in river flow to the Arctic Ocean (Fig. 24.3). Perhaps the most comprehensive analysis of changes in river flow to the Arctic Ocean from Canada was compiled by Déry et al. (2016) based on an analysis of discharge data over 1964–2013 for 42 downstream gauging stations. The 1964–2015 discharge to the Arctic Ocean and adjacent polar seas from the North American continent averages 1154 km^3 year^{-1} for a total gauged area of 5.26×10^6 km^2 (Fig. 24.2). There is considerable interannual variability in the flows with the coefficient of variation reaching 7%. Annual flows show a robust linear decline between 1964 and 1989 when a minimum discharge of 966.3 km^3 year^{-1} was observed. This is then followed by strong positive incline marked by two nearly identical peaks of 1292.9 km^3 year^{-1} and 1291.3 km^3 year^{-1} in 2005 and 2009, respectively. Between 1989 and 2013, total annual river discharge to the ocean increased by 208.8 km^3 year^{-1}, equivalent to an 18.1% rise relative to mean annual discharge over the period. This aligns with recent trends in Eurasia (see section above). Mean annual runoff remains low at 220 mm given the relatively cool, dry climate that prevails in the northern United States and Canada.

Partitioning the area into six regional basins shows that rivers draining into Eastern Hudson Bay (including James Bay), Eastern Arctic Ocean (Ungava Bay and Hudson Strait), and Labrador Sea all exhibit relatively high mean annual runoff (from 484.1 mm to 629.9 mm) compared to their western counterparts where it ranges only from 146.9 mm to 254.1 mm. Riverine fluxes are highest to the western Arctic Ocean and western Hudson Bay, which combine to transport 675.5 km^3 year^{-1}. Analysis of annual discharge records for 42 downstream gauging stations on large and medium size rivers flowing to the Arctic Ocean has showed both positive and negative trends in most of Canadian subbasins (Fig. 24.4). There is a general tendency that discharge to the Ocean from the eastern part of the basin shows mostly negative trends and the discharge from the western part demonstrates mostly positive trends over 1964–2013. This can be due both natural and anthropogenic causes, and human impact on discharge of rivers in the western part of the Canadian Arctic significantly greater than on eastern rivers (Fig. 24.4).

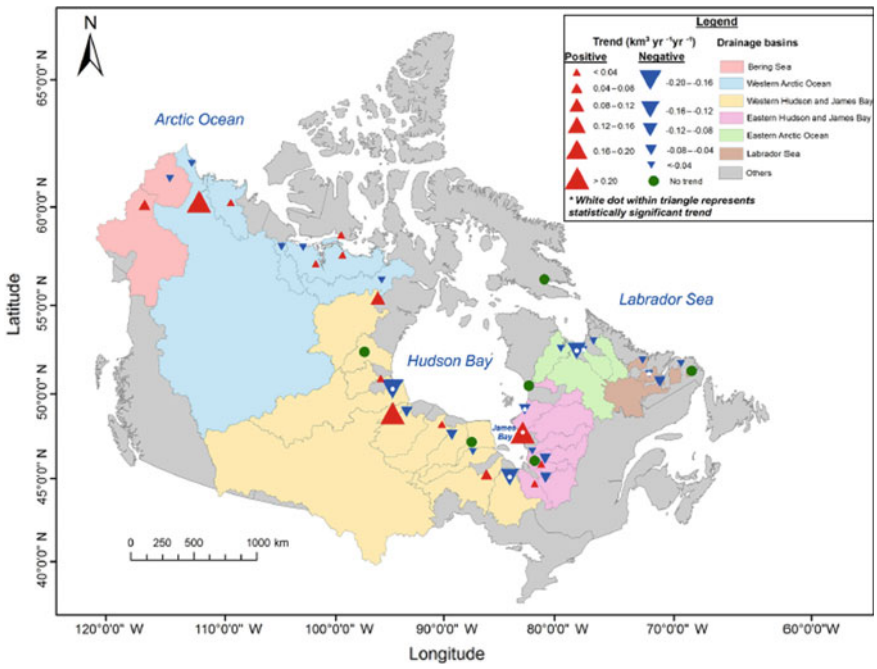

Fig. 24.4 Long-term discharge trends for downstream gauging stations on 42 rivers flowing to the Arctic Ocean from territory of Canada over 1964–2013 (adapted from Déry et al. 2016)

24.3.1.1 Seasonal Discharge Variability

Knowledge of seasonal discharge variability and change is important to better understand reasons and causes responsible for the observed increase in annual river discharge to the Arctic Ocean. The largest portion of the runoff to the seas of the Eurasian Arctic is from snow runoff usually in May–July. The river flow during the freshet can be enriched with melt water from highland snow patches, glaciers, and rainfall. Occasional rainfall flood waves may occur persistently during the warm season. They are caused by intense rainfalls usually during summer-fall and are most characteristic for the rivers of Eastern Siberia (e.g., Lena, Yana, Indigirka, Kolyma). The spring flood period mainly associated with snowmelt usually ends in June–early July on small and medium size rivers of the Eurasian drainage basin and by the end of July–early August on large Arctic rivers (e.g., the Ob, Yenisei, Lena, Kolyma) (Yang et al. 2007). The summer-fall low-flow season is mainly characteristic for small and medium size rivers. Large rivers usually demonstrate more gradual decreases in river flow after spring floods with periodical increases caused by rainfalls. The winter low-flow period usually starts after freeze-up by the end of autumn (October, November). Greater winter discharge is observed in non-permafrost areas of the European part and Western Siberia. Concurrently, even medium size rivers of Central and Eastern Siberia (e.g., Anabar, Olenek, Yana,

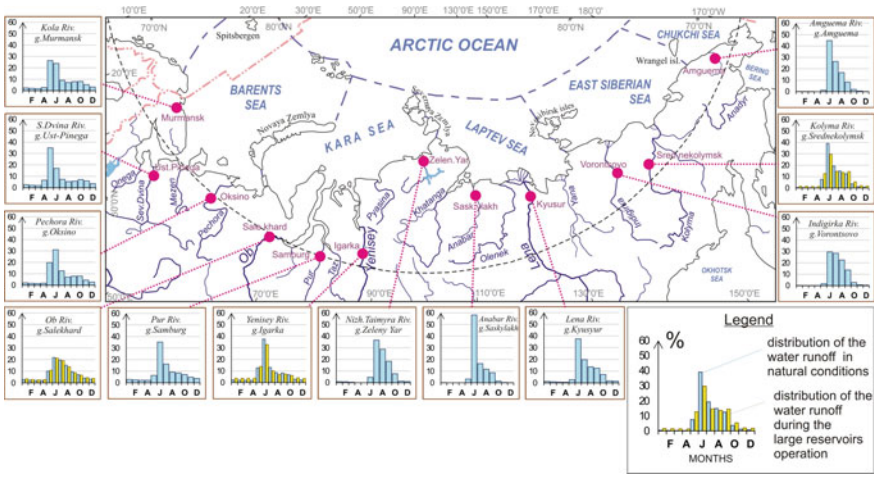

Fig. 24.5 Long-term mean monthly distribution of the monthly discharge of Eurasian rivers to the Arctic Ocean basin, expressed in percent of annual value

Indigirka), where the thick, continuous permafrost is widely distributed, have very low or even no discharge during winters. Figure 24.5 demonstrates long-term mean monthly discharge distribution for downstream gauges of large and medium size rivers in the Eurasian Arctic (from Magritsky et al. 2018). Most of river flow to the Arctic Ocean is generated during spring–summer months and equates to ~60% in European part to ~90% in Eastern Siberia of the total annual discharge (Fig. 24.5). For most rivers, the maximum monthly discharge to the ocean is usually observed in June except rivers flowing to the White Sea where maximum discharge is observed in May and July (rivers of the north-eastern part of the Kara Sea basin and the Alazeya). The river flow during the cold period (November–March) is in the range from 2–5% (Eastern Siberia) to 10–20% (European part and Western Siberia).

Analysis of variations in seasonal discharge to the Arctic Ocean from Eurasia has shown that the observed significant increase in annual river flow is mainly due to increases in winter (60%) and spring (33%) discharge (Fig. 24.6). River flow during winter demonstrates a very consistent and significant increase throughout the Eurasian pan-Arctic. The six largest Eurasian Arctic rivers all show a significant increase in winter flows over the long-term period 1936–2015 (Table 24.3). However, reservoirs operated in several of these river basins may significantly distort winter discharge and complicate the understanding of responses of river flows to climate variability (Shiklomanov and Lammers 2009; Ye et al. 2003, 2009; Yang et al. 2004a, b; Stuefer et al. 2011). Spring discharge has also significantly increased in all basins except Severnaya Dvina although reservoir regulation usually reduces discharge during high flow periods. Significant shifts to earlier snowmelt and freshets found for these river basins (Shiklomanov et al. 2007;

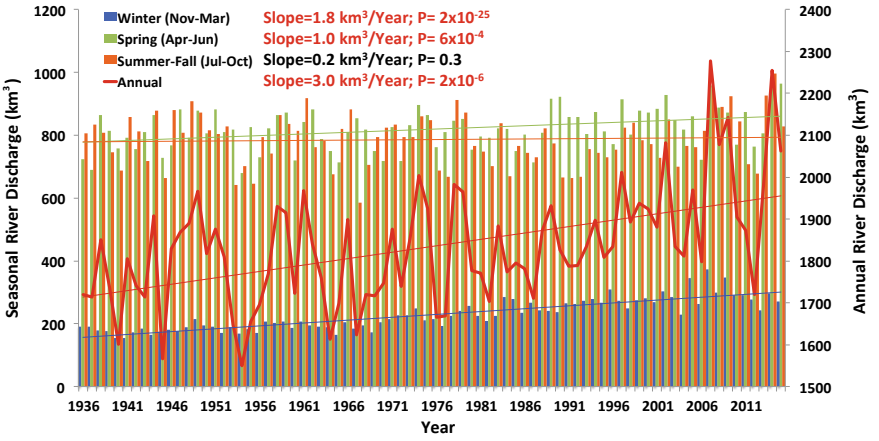

Fig. 24.6 Change in seasonal streamflow based on discharge observation for six largest Eurasian rivers flowing to the Arctic Ocean

Shiklomanov and Lammers 2014) could be partly responsible for increase in spring flow from April to June (Table 24.3).

Snow-dominated river systems draining northern Canada exhibit strong seasonality with low flows during winter when discharge averages 136.1 km^3 $year^{-1}$ and high flows in both spring (391.8 km^3 $year^{-1}$) and summer (387.5 km^3 $year^{-1}$; Table 24.4). Flows decline in autumn but remain moderate at 238.5 km^3 $year^{-1}$, enhanced partly by synoptic-scale storms and their associated rainfall. There are noticeable trends toward greater discharge during winter to Hudson Bay and the Labrador Sea linked to water storage in reservoirs for hydropower production (Déry et al. 2016). Unregulated rivers of northern Canada show only modest changes in seasonality with advances of the spring freshet (Déry et al. 2011) (Fig. 24.7).

24.3.1.2 Human Impact and Natural Variability of Annual and Seasonal Discharge

In addition to climate-induced river streamflow variations, water management such as construction of large reservoirs, inter-basin water diversions, and water withdrawals for various needs can significantly affect discharge variability (Shiklomanov and Lammers 2009; Ye et al. 2003; Yang et al. 2004a, b). Human influence on the hydrological regime of pan-Arctic rivers is usually considered to be minor in comparison with mid- to low-latitude rivers due to lower population, adverse natural conditions, and scarce development (Lammers et al. 2001). Water consumption for human needs in large pan-Arctic river basins does not exceed 1–3% of total river discharge and does not significantly affect annual and seasonal variability of river discharge to the Arctic Ocean (Shiklomanov 2008). At the same time, engineered control of streamflow as the result of reservoir regulation is very important for many large Arctic rivers. Development of the water power potential of the

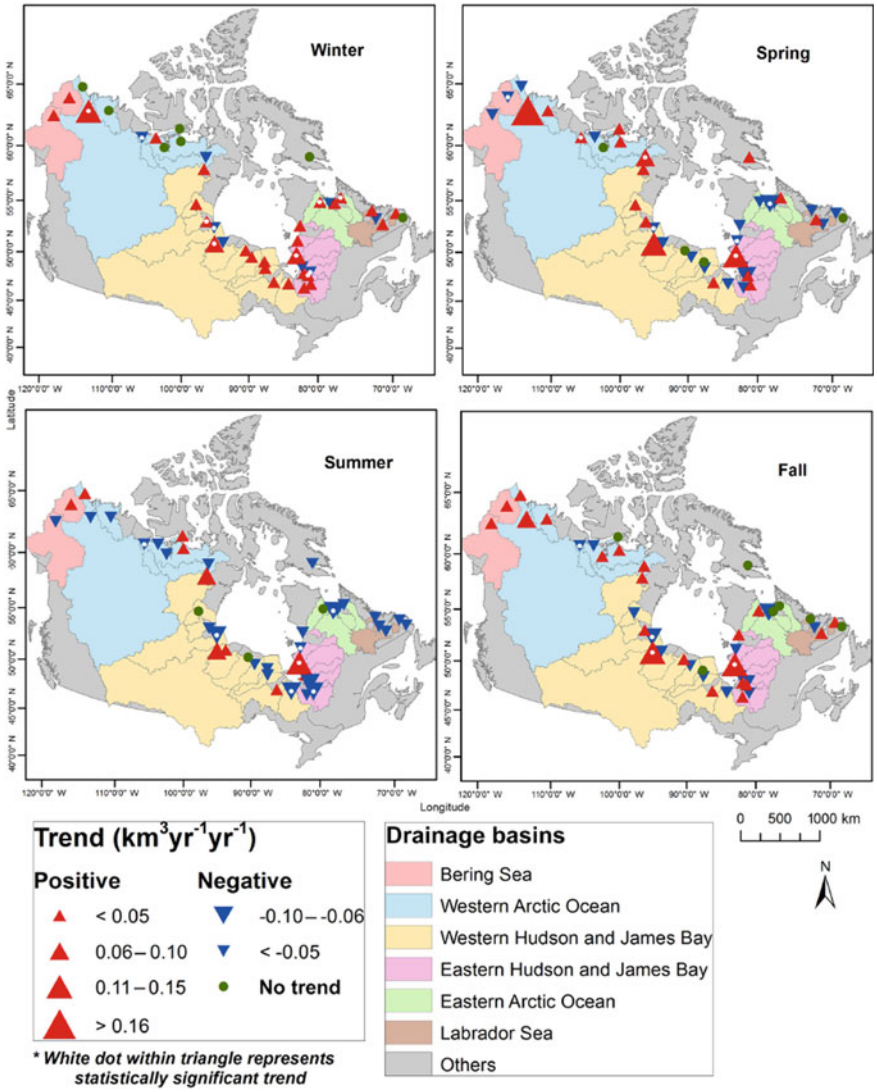

Fig. 24.7 Map of the six major basins draining northern Canada and parts of the northern United States, and spatial trend analysis for the seasonal discharge of 42 downstream gauging stations over 1964–2013 (Map reproduced from Déry et al. 2016)

Russian Arctic rivers began in the late nineteenth century and HPS (Hydroelectric Power Stations) construction peaked in the second half of the twentieth century (Magritsky et al. 2018). Many relatively small HPS are now in operation on rivers of the Kola Peninsula and Karelia (Fig. 24.8). However, the largest reservoirs are

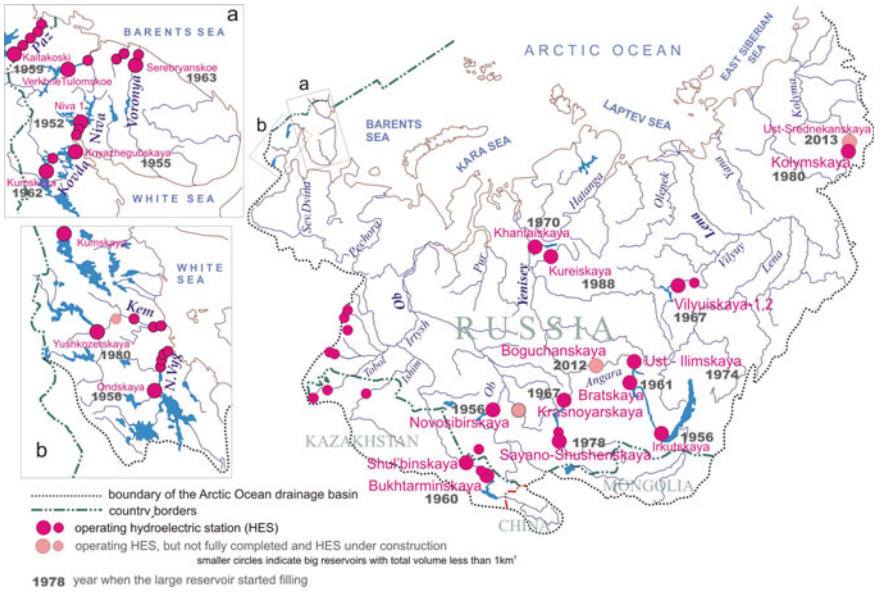

Fig. 24.8 Map of the Russian pan-Arctic including, 1: boundary of the Arctic Ocean drainage basin; 2: boundaries of large river basins; 3: country borders; 4: non-contributing areas; 5: operating hydroelectric station (HES), smaller circles, and all circles indicate reservoirs with total volume less than 1 km^3; 6: operating HES, but not fully completed; 7: HES under construction

located in the Siberian part of the pan-Arctic. There are 17 large reservoirs mainly in the Ob and Yenisei river basins (Fig. 24.8).

The construction of dams and reservoirs in the river systems has the effect of changing the timing of river flows. At higher latitudes, the impoundments are primarily used for hydroelectric power generation and storing water for drier summer seasons. Thus, they redistribute water between the seasons and can significantly change the seasonal hydrological regime, reducing peak discharge during spring and early summer, and increasing discharge during low-flow periods. This effect on seasonal hydrology is widely documented for the Ob, Yenisei, Lena, and Kolyma Rivers (Ye et al. 2003; Yang et al. 2004a, b; Shiklomanov and Lammers 2009; Stuefer et al. 2011; Adam et al. 2007; Georgiadi et al. 2014). The results for these basins demonstrate that reservoir effects can exceed climate-induced hydrological changes even in downstream gauges remotely located from reservoirs. In addition to seasonal discharge distribution, large dams may also affect yearly flow characteristics at the basin scale, particularly during reservoir filling periods immediately after dam construction (Ye et al. 2003; Stueffer et al. 2011; Yang et al. 2004a, b; Shiklomanov and Lammers 2009). There are also several large river dams in the Canadian part of the Arctic drainage basin. Most of them are used for hydroelectric power generation and located in the Eastern part. There are also two large water transfer projects from one river basin to another for hydropower

production in the Hudson Bay drainage area, which completely changed both annual and seasonal discharge regimes on these rivers (Fig. 24.4). Thus, to analyze the climate-induced long-term variability of seasonal discharge to the Arctic Ocean associated with climate change and to better understand the physical mechanisms driving the observed changes in seasonal discharge, it is necessary to eliminate the direct human impact from the observed streamflow records.

Ye et al. (2003) and Yang et al. (2004a, b) used flow regression between upstream and downstream gauges sites to reconstruct flow data for the Lena and Yenisei. Stuefer et al. (2011) and Shiklomanov et al. (2011) applied the Hydrograph Transformation Model to reduce and eliminate reservoir effects over the three largest pan-Arctic river basins—Yenisei, Lena, and Ob. The linear model with concentrated parameters is based on routing of daily discharge hydrographs from the unregulated part of the basin along the river network to the downstream gauge. The optimal parameters for the model were evaluated from the minimization of mean square deviation between the observed and simulated daily discharge values over the pre-dam period. The model has shown less than 10% mean relative errors of modeled daily discharge from observations over the pre-dam period, which are comparable to the accuracy of daily discharge observations on large Siberian rivers (Shiklomanov et al. 2006). Analysis of annual and seasonal naturalized (without direct human impact) river discharge for downstream gauges showed that at annual time steps the trends are less impacted by dam construction, whereas seasonal discharge variability is significantly distorted by reservoir regulation (Fig. 24.9). Total naturalized discharge for the six largest Eurasian Arctic rivers shows similar trends in annual discharge to observed data (2.9 km^3/year) and accompanied with streamflow increases in spring (accounting for 49%), winter (accounting for 31%), and summer-fall (accounting for 20%) (Fig. 24.9). Thus, as reported by Ye et al. (2003), the seasonal trend values associated with only climate variability are

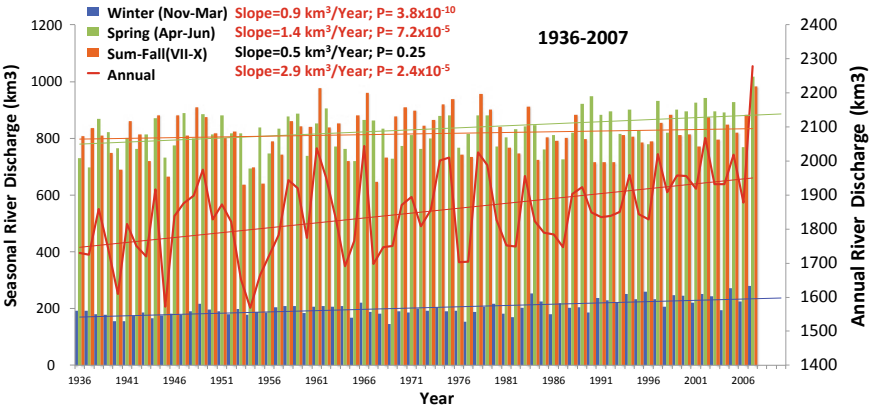

Fig. 24.9 Change in seasonal streamflow based on naturalized discharge with removed human impact for the six largest Eurasian rivers flowing to the Arctic Ocean

significantly different from trends obtained from observational records (Fig. 24.6). However, most of the annual discharge increase (80%) is still due to higher streamflow in spring and winter.

24.4 Discussion About Potential Causes of the River Flow Changes

The Arctic freshwater cycle has been an important focus of research during the last 15 years (White et al. 2007; Smith et al. 2007; Rawlins et al. 2010; Holmes et al. 2013). While a variety of theories have been put forward, the physical mechanisms driving the observed runoff changes are still not yet fully understood (Bring et al. 2016, Shiklomanov et al. 2013). Comprehensive analyses of water balance components (Serreze et al. 2006; Rawlins et al. 2005, 2010; Shiklomanov et al. 2007), human impacts (Ye et al. 2003; Adam et al. 2007; Yang et al. 2002, 2004a, b; McClelland et al. 2004; Shiklomanov and Lammers 2009), and hydrological modeling experiments (Rawlins et al. 2006; Bowling and Lettenmaier 2010; Troy et al. 2012) were not able to resolve the contributions of individual factors to the observed increase in river discharge. McClelland et al. (2004) evaluated direct potential effects of permafrost thaw, dams, and fires on the observed trend in annual river flow and found that it could not be explained by any of these factors. They suggested that increased net atmospheric moisture transport from lower to higher latitudes with a corresponding increase in precipitation as the main cause of changes in river flows. A number of modeling, and observation-based studies show that increased atmospheric moisture transport, may contribute to some increase in precipitation during individual seasons (Zhang et al. 2008, 2013; Rawlins et al. 2009a, b; Troy et al. 2012, Vihma et al. 2016). Later freeze-up in the Arctic Ocean is likely to be a factor for increased moisture content in the atmosphere, warmer temperatures in coastal locations and more snow on the ground, especially early in the winter. The most important processes currently affecting hydrologic conditions on a pan-Arctic scale are overall warming, increased atmospheric moisture content (due to more open water in the Arctic Ocean resulting in possible greater precipitation), and changes in the atmospheric circulation (due to the declining sea ice). It is interesting to notice that until 2011 there was a good correspondence between river discharge to the ocean and minimum sea ice extent with negative correlation $R = -0.7$ (Fig. 24.10, Shiklomanov and Lammers 2009) suggesting that (a) both rivers and sea ice were responding to changes in large-scale hemispheric climate patterns (see Rawlins et al. 2009a, b) and (b) an increasingly ice-free summer in the Arctic Ocean contributed to wetter conditions on the land surface via atmospheric moisture transport from open sea areas. This relationship, however, declined significantly during 2012–2013, when a minimum of sea ice extent corresponded with low discharge values. This discrepancy can be partly result of human activity, namely, filling a new large reservoir on the Angara River (Yenisei basin) during this period with total capacity 58.2 km^3. Minimal annual discharge since 1936 was

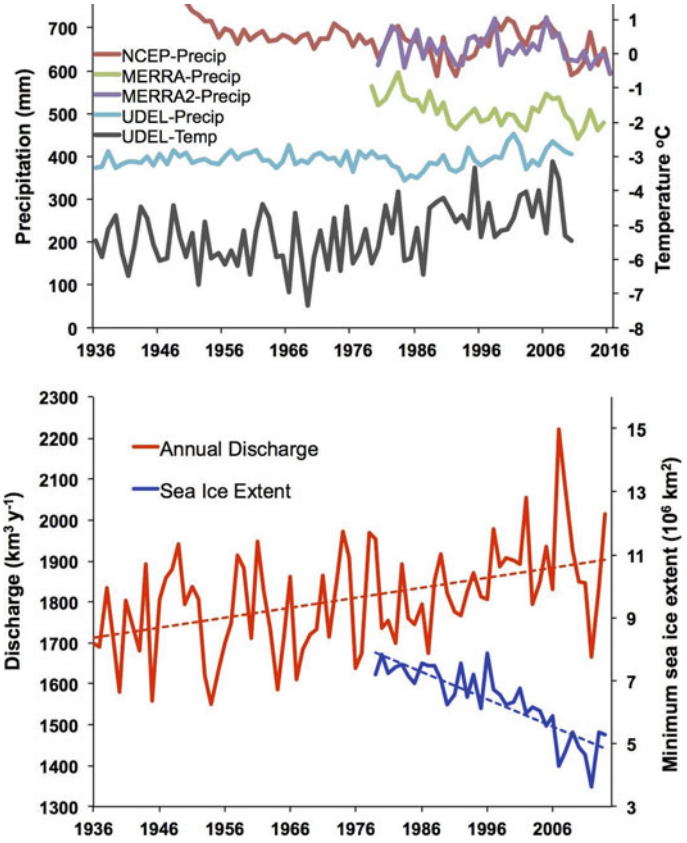

Fig. 24.10 Top: Annual precipitation averaged over 6 largest Eurasian Arctic river basins from stations and reanalysis products and average annual air temperature from Matsuura and Willmott (2012). Lower: annual river discharge to the Arctic Ocean from the six largest rivers in the Eurasian Arctic for the period 1936–2015 (updated from Shiklomanov and Lammers 2009) and annual minimum sea ice extent for 1979–2015

observed on the largest Arctic river, the Yenisei, in 2012 when most of the Boguchany reservoir volume was filled (Fig. 24.3). Moisture transport and associated precipitation patterns play a major role in runoff generation and its changes can significantly alter the hydrological regime of rivers flowing to the Arctic Ocean. Moisture transport into Siberia was analyzed in Zhang et al. (2013), and an increase in moisture convergence over Siberia was offered as a potential source for the multi-decadal increase in the flow of the north flowing large Siberian rivers. However, aggregated over the pan-Arctic and large river basins, annual precipitation, which is typically the most important water balance component for runoff generation, does not show a significant change to support the observed increasing trend in annual river flow (Fig. 24.10; Adam and Lettenmaier 2008; Bring and

Destouni 2011; Bring et al. 2016; Shiklomanov and Lammers 2009; Berezovskaya et al. 2004). There is, however, a tendency toward increasing snowfall during fall and early winter in Western Siberia (Wegmann et al. 2015) and in the Canadian Arctic (Kopec et al. 2016) associated with sea ice decline that is responding to and at the same time contributing to Arctic amplification (Serreze et al. 2009; Stroeve et al. 2011). The changes in winter precipitation and correspondingly in snow accumulation can partly explain increases in spring river flows to the ocean, which is mainly due to snowmelt.

In contrast to precipitation patterns, the increase in air temperature across the pan-Arctic has been widely and consistently documented (Overland et al. 2016) and it is expected to continue with higher rates in the future (IPCC 2014). The air temperature rise leads to significant changes in the regional cryosphere including less frozen soil in winter, deeper annual thaw propagation in the permafrost zone (deeper active layer), and melting of glaciers. Thus, even in the absence of increased precipitation, temperature-driven increased active layer thickness and degraded permafrost as well as decreased thickness of frozen soil in non-permafrost areas, can lead to river flow increases due to changes in the hydrological pathways to the river system and associated decreases in evapotranspiration. The increasing groundwater storage (Muskett and Romanovsky 2009), enhanced subsurface flow connectivity (Watson et al. 2013; Walvoord and Kurylyk 2016) as well as changes in discharge seasonality (Ye et al. 2009; Smith et al. 2007; Shiklomanov and Lammers 2013; Spence et al. 2015; Tananaev et al. 2016) are all probably related to changes in hydrological pathways due to changes in permafrost and seasonally frozen soil. The redistribution of a significant portion of runoff from surface to subsurface and from warm to cold seasons accounts for much less water loss to evapotranspiration and this can provide correspondingly higher total annual river flow.

Several local or regional studies have shown the important influence of changes in different cryospheric components including permafrost thaw (Streletsky et al. 2015; Woo 2012), glacier melt (Bennett et al. 2015), frozen ground (Markov 2003), river ice (Shiklomanov and Lammers 2014; Gurevich 2009) on river runoff generation. Nevertheless, it is still not clear from these studies how these locally observed changes will interact between each other and with spatially varying precipitation changes to affect river flows. There is also considerable uncertainty about how these local changes will scale up to regional and continental scale and their impacts to the significant increases in river fluxes to the Arctic Ocean. Increases in fall and earlier winter snow cover and warmer air temperature, associated with less sea ice in the Arctic Ocean, contribute to improved insulation of unfrozen soil and longer freeze-up of the active layer. This effect can alter streamflow formation during this period. In non-permafrost regions the widely observed significant decrease in frozen soil thickness (Frauenfeld and Zhang 2011) is an important factor in winter runoff change. Experimental investigations on small watersheds in Russia have shown that a 20 cm decrease in thickness of water-saturated frozen soil can contribute up to 60 mm (or 50–200%) to winter runoff (Kaluzhny and Lavrov 2012). However, how this process affects streamflow over larger basins and total river flux to the ocean is still unclear.

24.5 Linkage of River Discharge to Coastal Surface Water Salinity

Sea surface salinity (SSS) links various components of the Arctic freshwater system. SSS responds to freshwater input from river discharge, sea ice change, surface freshwater forcing (precipitation and evaporation), and oceanic circulation and transport. Northern river freshwater influx is expected to be detectable in the SSS field, particularly near the river mouths and over the shallow shelf areas. Tang et al. (2018) examined the SSS response to river discharge variation in the Kara Sea. Figure 24.11 presents the SMAP (NASA Soil Moisture Active Passive) SSS (from the L-band microwave radiometer) evolution over the Kara Sea over the warm season (May to October) in 2015 and 2016. During October to May, SSS was not retrieved when the area was completely covered by sea ice. The first valid SSS retrievals for Kara Sea appeared in June during the study period, but at different locations due to discrepant sea ice conditions, freshet timing, and intensity in 2015 and 2016. The SSS differences between these two years became more dramatic throughout the season. In the summer of 2015, the freshwater anomalies first appeared in June, over the north part east of the northern tip of Novaya Zemlya archipelago (north of Gulf of Ob). It grew and spread to cover almost half of the Kara Sea in August. In contrast, the fresh signature in 2016 was limited in areas near Ob and Yenisei Estuaries. Because the whole region is almost ice-free since July, the impact of freshwater input from sea ice melt is probably minimal. Therefore the dramatic freshening signatures spreading through middle of the Kara Sea from July to September in 2015, and along the Siberia sea coast in 2016 is very likely originated from river flux.

The daily discharge data for the Ob River and Yenisei River (Fig. 24.12) show consistent differences in discharge timing and magnitude during 2015 and 2016. In the first two months of the warm season (May and June), discharge from Ob shows similar magnitude for the two years, while Yenisei discharge peaked early and injected 93.4 km^3 more water in 2015 than 2016. In the following four months from July to October, Ob became the main player, putting 90.9 km^3 more freshwater into the Kara Sea, while Yenisei added another extra 31.5 km^3. During May to Oct., Kara Sea received more than 210 km^3 freshwater from the Ob and Yenisei in 2015 relative to 2016. It is useful to roughly estimate the effect of this extra amount of freshwater on the SSS anomaly. About 3 cm of freshwater are needed to dilute 1 m of seawater by 1 PSU. Assuming the extra $\sim$210 km^3 freshwater spread over half of the Kara Sea (total surface area 926,000 km^2), it may produce 15 PSU salinity anomaly within top 1 m surface water layer, or 7.5 PSU within top 2 m. As seen in Fig. 24.11 (right column), the areas with positive SSS anomaly exceeding 10 PSU covering about half of the Kara Sea, which is in the same order as the freshening effect that may be produced by river discharge anomaly. These results are encouraging, as they demonstrated the great potential of SMAP SSS in understanding Arctic freshwater system during the ice-free (open water) season, although large differences in SSS anomaly may also depend on how the freshwater transported horizontally and vertically in terms of depth and spread of the diluted water body.

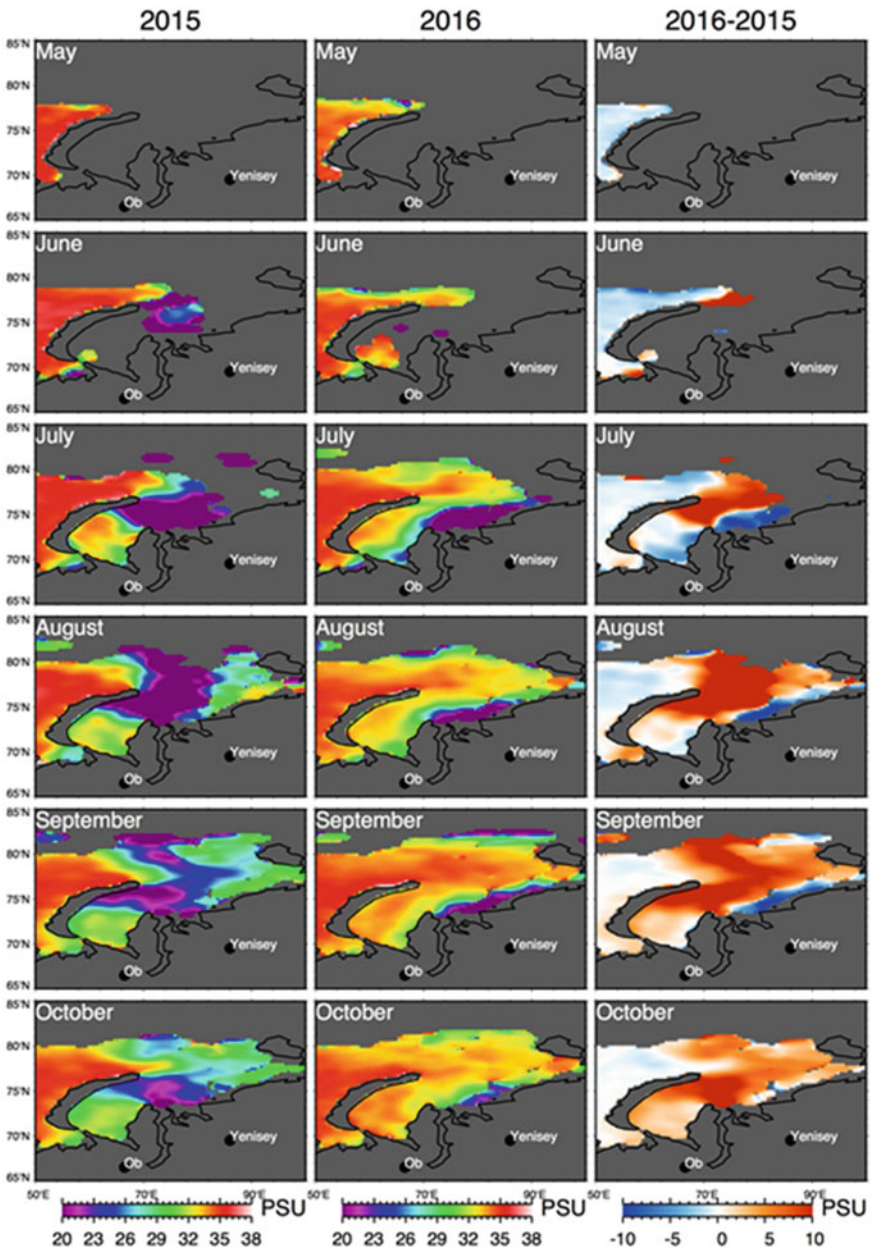

Fig. 24.11 SSS in Kara Sea for the months from May to October (top to bottom) for the year 2015 (left) and 2016 (middle). The corresponding differences (2016 minus 2015) are shown in the right column. Sampling locations of the Ob and Yenisei river are indicated by black circles

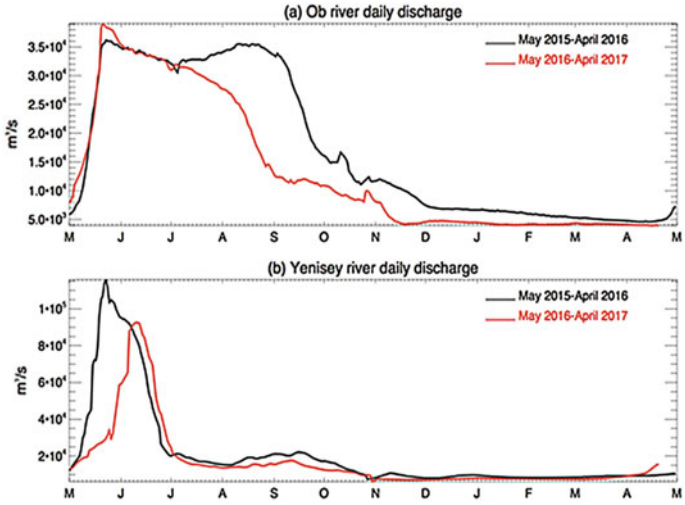

Fig. 24.12 Daily discharge from **a** Ob and **b** Yenisei rivers during May to April, 2015–2017

24.6 Conclusions

Analysis of various estimates of freshwater discharge to the Arctic Ocean with different methods and for different drainage areas has shown a good consistency in long-term mean runoff ranging from 200 mm/year to 226 mm/year. Most discrepancies in estimates of total river discharge to the ocean can be attributed to different drainage areas used for assessment, which vary from 11.3 to 23.7×10^6 km^2. Most of the estimates are derived from available discharge measurements at the downstream gauging stations. According to the most recent contemporary assessment the total discharge to the Arctic Ocean is approximately 4300 km^3 year^{-1} and continental contributions to the river input into the Arctic Ocean for Asia, North America, and Europe are 55%, 28%, and 17%, respectively.

The river flux to the Arctic Ocean has demonstrated significant changes with an increase of 210 km^3 over 1936–2015 across Eurasia and 36 km^3 over 1964–2015 for northern Canada. These changes were especially pronounced during the last 30-years, characterized by the most intense warming of air temperature over the northern hemisphere and significant declines in sea ice extent in the Arctic Ocean.

Analysis of variations in seasonal discharge to the Arctic Ocean from Eurasia has shown that the observed significant increase in annual river flow is mainly due to increases in winter (60%) and spring (33%) discharge. River flows during winter demonstrate a very consistent and significant increase throughout the Eurasian pan-Arctic. All six largest Eurasian Arctic rivers show a significant increase in winter river flows over the long-term observational period 1936–2015. Similar but less significant trends in winter and spring discharge were found for Canadian rivers

flowing to the Arctic Ocean. Seasonal discharge can be however significantly distorted as the result of human activity. Many large rivers flowing to the Arctic Ocean have large reservoirs that can significantly alter the natural hydrological regime. We eliminated effects of large reservoirs for the largest Arctic rivers of Yenisei, Lena, and Ob using the hydrograph transformation model and found that the significant increase in annual discharge is the result of increase in spring (49%), winter (31%), and summer-fall (20%). These results are different from those obtained based on observational discharge data. Thus, for hydroclimatic analysis to understand possible changes in river flux to the Arctic Ocean, it is necessary to take into account human impact on river discharge.

We demonstrate that river flux to the Arctic Ocean has monotonically increased, and river discharge significantly affect Kara Sea salinity patterns in the open water season. The changes in river flux, along with melt of sea ice, and increasing precipitation over the ocean may exert significant control over the North Atlantic meridional overturning (thermohaline) circulation. This is significant for global ocean circulation by controlling the volume of North Atlantic deep water formation with potentially important consequences for climate in the Northern Hemisphere. Accordingly, to project possible extreme anomalies and better adapt to ongoing and oncoming environmental changes, we should expand our knowledge and understanding of these hydrological alterations. The significant increase in river flow to the ocean is probably the result of multiple causes that were briefly discussed here and also in Chaps. 6, 25, and 27. However, detailed large-scale quantitative evaluation of potential causes responsible for observed increases in river flow is still missing.

To better understand the physical mechanisms driving hydrological changes at high latitudes, it is necessary to: (1) extend the regional experimental investigation on interactions between surface and groundwater, especially in the permafrost and transition zones; (2) extend in situ monitoring networks, especially in currently unmonitored basins and regions, and improve international collaboration in data collections and exchanges; (3) expand the scale of remote sensing monitoring efforts; and (4) improve representation of physical processes at different scales in hydrological models; (5) conduct a set of coupled experiments with atmospheric, oceanic, and hydrological/permafrost models to better quantify causes of changes in river flow to the Arctic Ocean. These elements are interrelated and the optimal progress can be reached if development will simultaneously involve all these fundamental aspects.

Acknowledgments We wish to acknowledge the National Science Foundation (grants: 1913962, 1917515) and Russian Foundation for Basic Research (grants: 18-05-60192, 18-05-60240, 18-05-60021) for support and providing results of data analysis and modeling used in the chapter. We also thank the Russian Federal Service for Hydrometeorology—Rosgidromet, United States Geological Survey, and Water Survey of Canada for the discharge data used in the chapter.

References

ACIA (2005) Arctic Climate Impact Assessment Scientific Report. Cambridge University Press, New York, 1042 p

Adam JC, Haddeland I, Su F, Lettenmaier DP (2007) Simulation of reservoir influences on annual and seasonal streamflow changes for the Lena, Yenisei, and Ob' rivers. J Geophys Res 112: D24114. https://doi.org/10.1029/2007JD008525

Adam JC, Lettenmaier DP (2008) Application of new precipitation and reconstructed streamflow products to streamflow trend attribution in northern Eurasia. J Clim 21(8):1807–1828. https://doi.org/10.1175/2007JCLI1535.1

Alsdorf DE, Lettenmaier DP (2003) Tracking fresh water from space. Science 301:1491–1494

Bennett KE, Cannon AJ, Hinzman L (2015) Historical trends and extremes in boreal Alaska river basins. J Hydrol 527:590–607. ISSN 0022-1694. http://dx.doi.org/10.1016/j.jhydrol.2015.04.065

Berezovskaya S, Yang D, Kane DL (2004) Compatibility analysis of precipitation and runoff trends over the large Siberian watersheds. Geophys Res Lett 31:L21502. https://doi.org/10.1029/2004GL021277

Biemans H, Hutjes RW, Kabat P, Strengers BJ, Gerten D, Rost S (2009) Effects of precipitation uncertainty on discharge calculation for main river basins. J Hydrometeorol 10:1011–1025. https://doi.org/10.1175/2008JHM1067.1

Bowling LC, Lettenmaier DP (2010) Modeling the effects of lakes and wetlands on the water balance of Arctic environments. J Hydrometeorol 11:276–295

Bring A, Destouni G (2011) Relevance of hydro-climatic change projection and monitoring for assessment of water cycle changes in the Arctic. G AMBIO 40:361. https://doi.org/10.1007/s13280-010-0109-1

Bring A, Fedorova I, Dibike Y, Hinzman L, Mård J, Mernild SH, Prowse TD, Semenova O, Stuefer S, Woo MK (2016) Arctic terrestrial hydrology: a synthesis of processes, regional effects and research challenges. J Geophys Res Biogeosciences 121:621–649. https://doi.org/10.1002/2015jg003131

Carmack EC, Yamamoto-Kawai M, Haine TWN, Bacon S, Bluhm BA, Lique C, Melling H, Polyakov IV, Straneo M-L, Williams WJ (2016) Freshwater and its role in the Arctic Marine System: Sources, disposition, storage, export, and physical and biogeochemical consequences in the Arctic and global oceans. J Geophys Res Biogeosci 121(3):675–717. https://doi.org/10.1002/2015JG003140

Déry SJ, Stadnyk TA, MacDonald MK, Gauli-Sharma B (2016) Recent trends and variability in river discharge across northern Canada. Hydrol Earth Syst Sci 20:4801–4818. https://doi.org/10.5194/hess-20-1-2016

Déry SJ, Mlynowski TJ, Hernández-Henríquez MA, Straneo F (2011) Interannual variability and interdecadal trends in Hudson Bay streamflow. J Mar Syst 88:341–351

Déry SJ, Hernandez-Henriquez MA, Burford JE, Wood EF (2009) Observational evidence of an intensifying hydrological cycle in northern Canada. Geophys Res Lett 36:L13402

Déry SJ, Stieglitz M, McKenna EC, Wood EF (2005) Characteristics and trends of river discharge into Hudson, James, and Ungava bays, 1964–2000. J Clim 18(14):2540–2557

Dai A, Trenberth KE (2002) Estimates of freshwater discharge from continents: latitudinal and seasonal variations. J Hydrometeorol 3:660–687

Fekete BM, Vorosmarty CJ, Grabs W (2002) High-resolution fields of global runoff combining observed river discharge and simulated water balances. Global Biogeochem Cycles 16 (3):1042. https://doi.org/10.1029/1999GB001254

Fekete BM, Vorosmarty CJ (2004) Uncertainties in precipitation and their impacts on runoff estimates. J Clim 17:294–304. https://doi.org/10.1175/1520-0442(2004)017%3c0294:UIPATI%3e2.0.CO;2

Frappart F, Ramillien G, Famiglietti JS (2011) Water balance of the Arctic drainage system using GRACE gravimetry products. Int J Remote Sensing 32:431–453

Frauenfeld OW, Zhang T (2011) An observational 71-year history of seasonally frozen ground changes in the Eurasian high latitudes. Environ Res Lett 6:044024. https://doi.org/10.1088/1748-9326/6/4/044024

Ge S, Yang D, Kane D (2012) Yukon river basin long-term (1977-2006) hydrologic and climatic analysis. Hydrol Process. https://doi.org/10.1002/hyp.9282

Georgiadi AG, Koronkevich NI, Milyukova IP, Kashutina EA, Barabanova EA (2014) Recent scenario changes in river flow in Russia's largest river basins. Part 2. The Volga and the Don River basins. Maks Press, Moscow, pp 1–214. (In Russian)

Girotto M, De Lannoy GJ, Reichle RH, Rodell M (2016) Assimilation of gridded terrestrial water storage observations from GRACE into a Land Surface Model. Water Resour Res 52:4164–4183. https://doi.org/10.1002/2015wr018417]

Grabs W, De Couet T, Pauler J (1996) Freshwater fluxes from the continents into the world oceans: based on data of the global runoff data base. Glob Runoff Data Centre Rep 10:228

Grabs WE, Portmann F, Couet TD (2000) Discharge observation networks in Arctic regions: computation of the river runoff into the Arctic Ocean, its seasonality and variability. In: Lewis EL et al (eds) Freshwater budget of the Arctic Ocean, NATO Science Series, vol 70. Kluwer Academic, Dordrecht, Netherlands, pp 249–267

Gurevich E (2009) Influence of air temperature on the river runoff in winter (the Aldan river catchment case study). Russ Meteorol Hydrol 34(#9):628–633. https://doi.org/10.3103/s1068373909090088

Hamman J, Nijssen B, Roberts A, Craig A, Maslowski W, Osinski R (2017) The coastal streamflow flux in the regional Arctic system model. J Geophys Res Oceans. https://doi.org/10.1002/2016jc012323

Hinzman L, Bettez N, Bolton WR, Chapin FS, Dyurgerov M, Fastie C, Griffith B, Hollister RD, Hope A, Huntington HP, Jensen A, Jia GJ, Jorgenson T, Kane DL, Klein DR, Kofinas G, Lynch A, Lloyd A, McGuire AD, Nelson FE, Oechel WC, Osterkamp T, Racine C, Romanovsky V, Stone R, Stow D, Sturm M, Tweedie CE, Vourlitis G, Walker M, Walker D, Webber PJ, Welker J, Winker J, Yoshikawa K (2005) Evidence and implications of recent climate change in northern Alaska and other Arctic regions. Clim Change 72:251–298

Holland MM, Finnis J, Barrett AP, Serreze MC (2007) Projected changes in Arctic Ocean freshwater budgets. J Geophys Res 112. https://doi.org/10.1029/2006JG000354

Holmes RM, Shiklomanov AI, Tank SE, McClelland JW, Tretiakov M (2016) River discharge. In state of the climate in 2015. Bull Am Meteor Soc 97:S147–S149

Holmes RM, Coe MT, Fiske GJ, Gurtovaya T, McClelland JW, Shiklomanov AI, Spencer RG, Tank SE, Zhulidov AV (2013) Climate change impacts on the hydrology and biogeochemistry of Arctic rivers. Clim Change Global Warm Inland Waters Impacts Mitig Ecosyst Soc 2013:3–26

Holmes RM, Shiklomanov AI, Suslova A, Tretiakov SM, McClelland JW, Spencer RGM, Tank SE (2018) River discharge, Arctic report card: update for 2018. https://www.arctic.noaa.gov/Report-Card/Report-Card-2018/ArtMID/7878/ArticleID/786/River-Discharge

IPCC (2014) Larsen JN, Anisimov OA, Constable A, Hollowed AB, Maynard N, Prestrud P, Prowse TD, Stone JMR (2014) Polar regions. In: Climate change 2014: impacts, adaptation, and vulnerability. Part B: regional aspects. contribution of working group II to the fifth assessment report of the intergovernmental panel on climate change [Barros VR, Field CB, Dokken DJ, Mastrandrea MD, Mach KJ, Bilir TE, Chatterjee M, Ebi KL, Estrada YO, Genova RC, Girma B, Kissel ES, Levy AN, MacCracken S, Mastrandrea PR, White LL (eds)]. Cambridge University Press, Cambridge, United Kingdom and New York, NY, USA, pp 1567–1612

Ivanov VV (1976) Freshwater balance of the Arctic Ocean, Pr. AARI, 323:138–147. (in Russian)

Kalnay E, Kanamitsu M, Kistler R, Collins W, Deaven D, Gandin L, Iredell M, Saha S, White G, Woollen J, Zhu Y, Chelliah M, Ebisuzaki W, Higgins W, Janowiak J, Mo KC, Ropelewski C, Wang J, Leetmaa A, Reynolds R, Jenne R, Joseph D (1996) The NCEP/NCAR 40-year reanalysis project. Bull Am Met Soc 77(3):437–471

Kaluzhny I, Lavrov A (2012) Basic physical processes and regularities of winter and spring river flow formation under the climate warming. Russ Meteorol Hydrol 1:68–81. https://doi.org/10.3103/S1068373912010074

Kopec B, Feng X, Michel FA, Posmentier E (2016) Influence of sea ice on Arctic precipitation. PNAS 113:46–51. https://doi.org/10.1073/pnas.1504633113

Lammers RB, Shiklomanov AI, Vorosmarty CJ, Fekete BM, Peterson BJ (2001) Assessment of contemporary Arctic river runoff based on observational discharge records. J Geophys Res 106:3321–3334

Landerer FW, Swenson SC (2012) Accuracy of scaled GRACE terrestrial water storage estimates. Water Resour Res 48, W04531, 11 PP. https://doi.org/10.1029/2011wr011453

Magritsky DV, Frolova NL, Evstigneev VM, Povalishnikova ES, Kireeva MB, Pakhomova OM (2018) Long-term changes of river water inflow into the seas of the Russian Arctic sector. Polarforschung 87:177–194. https://doi.org/10.2312/polarforschung.87.2.177

Manabe S, Stouffer RJ (1994) Multiple-century response of a coupled ocean-atmosphere model to an increase of atmospheric carbon dioxide. J Clim 7:5–23

Markov ML (2003) Spatial-temporal dynamic of surface and ground water interaction. In: Proceedings of SHI, Hydrometeoizdat, vol 25, pp 90–104 (in Russian)

McClelland JW, Holmes RM, Peterson BJ, Stieglitz M (2004) Increasing river discharge in the Eurasian Arctic: consideration of dams, permafrost thaw, and fires as potential agents of change. J Geophys Res 109:D18102. https://doi.org/10.1029/2004JD004583

McClelland JW, Dery SJ, Peterson BJ, Holmes RM, Wood EF (2006) A Pan-Arctic evaluation of changes in river discharge during the latter half of the 20th century. Geophys Res Lett 33:L06, 715

Mernild SH, Liston GE, Hiemstra CA, Steffen K (2009) Greenland Ice Sheet surface mass-balance modelling and freshwater flux for 2007, and in a 1995–2007 perspective. Hydrol Process 23:2470–2484. https://doi.org/10.1002/hyp.7354

Milliman JD, Farnsworth KL (2011) River discharge to the Coastal Ocean: a global synthesis. Cambridge University Press, Cambridge, pp 143–144
https://doi.org/10.1017/cbo9780511781247

Mlynowski TJ, Hernández-Henríquez MA, Déry SJ (2011) An evaluation of hydrometric monitoring across the Canadian pan-Arctic region, 1950-2008. Hydrology Research 42:479–490

Muskett RR, Romanovsky VE (2009) Groundwater storage changes in arctic permafrost watersheds from GRACE and in situ measurements. Environ Res Lett 4(4):940–941 Article ID 045009

Overland JE, Hanna E, Hanssen-Bauer I, Kim SJ, Walsh J, Wang M, Bhatt U, Thoman R (2016) Air temperature, in state of the climate in 2015. Bull Am Meteor Soc 97:S132–S134

Peterson BJ, Holmes RM, McClelland JW, Vorosmarty CJ, Lammers RB, Shiklomanov AI, Shiklomanov IA, Rahmstorf S (2002) Increasing river discharge to the Arctic Ocean. Science 298:2171–2173

Peterson BJ, McClelland J, Curry R, Holmes RM, Walsh JE, Aagaard K (2006) Trajectory shifts in the Arctic and Subarctic freshwater cycle. Science 313:1061–1066. https://doi.org/10.1126/science.1122593

Prowse TD, Flegg PO (2000) The magnitude of river flow to the Arctic Ocean: dependence on contributing area. Hydrol Process 14:3185–3188

Prowse T, Bring A, Mård J, Carmack E, Holland M, Instanes A, Vihma T, Wrona FJ (2015) Arctic freshwater synthesis: summary of key emerging issues. J Geophys Res Biogeosci 120:1887–1893. https://doi.org/10.1002/2015JG003128

Rahmstorf S (2002) Ocean circulation and climate during the past 120,000 years. Nature 419:207–214

Rawlins MA, McDonald KC, Frolking S, Lammers RB, Fahnestock M, Kimball JS, Vorosmarty CJ (2005) Remote sensing of snow thaw at the pan-Arctic scale using the SeaWinds scatterometer. J Hydrol 312(1–4):294–311

Rawlins MA, Frolking S, Lammers RB, Vorosmarty CJ (2006) Effects of uncertainty in climate inputs on simulated evapotranspiration and runoff in the Western Arctic. Earth Interact 10:1–18. https://doi.org/10.1175/EI182.1

Rawlins MA, Schroeder R, Zhang X, McDonald KC (2009a) Anomalous atmospheric circulation, moisture flux, and winter snow accumulation in relation to record combined discharge from large Eurasian Rivers in 2007. Environ Res Lett 4:045011. https://doi.org/10.1088/1748-9326/4/4/045011

Rawlins MA, Steele M, Serreze MC, Vorosmarty CJ, Ermold W, Lammers RB, McDonald KC, Pavelsky TM, Shiklomanov A, Zhang J (2009b) Tracing freshwater anomalies through the air-land-ocean system: a case study from the Mackenzie River basin and the Beaufort Gyre. Atmos Ocean 47(1):79–97. https://doi.org/10.3137/OC301.2009

Rawlins MA, Steele M, Holland M, Adam J, Cherry J, Francis J, Groisman P, Hinzman L, Huntington T, Kane D, Kimball J, Kwok R, Lammers R, Lee C, Lettenmaier D, McDonald K, Podest E, Pundsack J, Rudels B, Serreze M, Shiklomanov A, Skagseth O, Troy T, Vorosmarty C, Wensnahan M, Wood E, Woodgate R, Yang D, Zhang K, Zhang T (2010) Analysis of the Arctic system for freshwater cycle intensification: observations and expectations. J Clim. https://doi.org/10.1175/2010JCLI3421.1

Scanlon BR, Zhang Z, Save H, Wiese DN, Landerer FW, Long D, Longuevergne L, Chen J (2016) Global evaluation of new GRACE mascon products for hydrologic applications. Water Resour Res 52:9412–9429. https://doi.org/10.1002/2016WR019494

Serreze MC, Barry RG (2000) Atmospheric components of the Arctic ocean hydrologic budget assessed from rawinsonde data. In: Lewis EL et al (eds)The freshwater budget of the Arctic ocean. Kluwer Academic Publishers, pp. 151–161

Serreze MC, Barrett AP, Slater AG, Woodgate RA, Aagaard K, Lammers RB, Steele M, Moritz R, Meredith M, Lee CM (2006) The large-scale freshwater cycle of the Arctic. J Geophys Res 111:C11010. https://doi.org/10.1029/2005JC003424

Serreze MC, Barrett AP, Stroeve JC, Kindig DM, Holland MM (2009) The emergence of surface-based Arctic amplification. Cryosphere 3:11–19

Shiklomanov AI, Lammers RB, Vörösmarty CJ (2002) Widespread decline in hydrological monitoring threatens Pan-Arctic research. EOS Trans Am Geophys Union 83(2):13, 16, 17

Shiklomanov AI, Yakovleva TI, Lammers RB, Karasev IPh, Vörösmarty CJ, Linder E (2006) Cold region river discharge uncertainty—estimates from large Russian rivers. J Hydrol 326 (2006):231–256

Shiklomanov AI, Lammers RB, Rawlins MA, Smith LC, Pavelsky TM (2007). Temporal and spatial variations in maximum river discharge from a new Russian data set. J Geophys Res 112: G04S53. https://doi.org/10.1029/2006jg000352

Shiklomanov AI, Lammers RB (2009) Record Russian river discharge in 2007 and the limits of analysis. Environ Res Lett 4:045015, 9 p. https://doi.org/10.1088/1748-9326/4/4/045015

Shiklomanov AI, Golovanov O, Lammers RB, Tretjyakov M, Yang D (2011) Dam/reservoir-induced hydrological changes in large Siberian Rivers. Am Geophys Union, Fall Meeting 2011. Abstract #C31B-06

Shiklomanov AI, Lammers RB (2013) Changing discharge patterns of high-latitude rivers. In: Editor-in-Chief Pielke R (ed) Climate vulnerability: understanding and addressing threats to essential resources. Elsevier, pp 161–175. ISBN 9780123847041. http://dx.doi.org/10.1016/B978-0-12-384703-4.00526-8

Shiklomanov AI, Lammers RB, Lettenmaier DR, Polischuk Y et al. (2013) Hydrological changes: historical analysis, contemporary status, and future projections. In: Groisman PY, Gutman G (eds) Regional environmental changes in Siberia and their global consequences. Chapter 4. Springer Environmental Science and Engineering © Springer Science + Business Media Dordrecht, pp 111–154

Shiklomanov AI, Lammers RB (2014) River ice responses to a warming Arctic—recent evidence from Russian rivers. Environ Res Lett 9:035008. https://doi.org/10.1088/1748-9326/9/3/035008

Shiklomanov IA, Shiklomanov AI (2003) Climatic change and dynamics of river discharge into the Arctic Ocean. Water Resour 30:593–601

Shiklomanov IA (ed) (2008) Water resources of Russia and their use. State Hydrological Institute, St. Petersburg, pp 1–600 (In Russian)

Smith LC, Pavelsky TM, MacDonald GM, Shiklomanov AI, Lammers RB (2007) Rising minimum daily flows in northern Eurasian rivers suggest a growing influence of groundwater in the high-latitude water cycle. J Geophys Res Biogeosci 112:G04S47. https://doi.org/10.1029/2006jg000327

Spence S, Kokelj SV, Kokelj SA, McCluskie M, Hedstrom N (2015) Evidence of a change in water chemistry in Canada's subarctic associated with enhanced winter streamflow. J Geophys Res Biogeosci 120(1):113

Stroeve JC et al (2011) Sea ice response to an extreme negative phase of the Arctic oscillation during winter 2009/2010. Geophys Res Lett 38:L02502

Streletskiy D, Tananaev N, Opel T, Shiklomanov N, Nyland K, Streletskaya I, Tokarev I, Shiklomanov A (2015) Permafrost hydrology in changing climatic conditions: seasonal variability of stable isotope composition in rivers in discontinuous Permafrost. Environ Res Lett 10(2015):095003. https://doi.org/10.1088/1748-9326/10/9/095003

Stuefer S, Yang D, Shiklomanov A (2011) Effect of streamflow regulation on mean annual discharge variability of the Yenisei River. In: Yang D, Marsh P, Gelfan A (eds) Cold regions hydrology in a changing climate. IAHS Press, Wallingford, UK, pp 27–32, ISBN 978-1-907161-21-6

Su F, Adam JC, Bowling LC, Lettenmaier DP (2005) Stream-flow simulations of the terrestrial Arctic domain. J Geophys Res 110:D08112. https://www.org/10.1029/2004JD005518

Syed T, Famiglietti J, Zlotnicki V, Rodell M (2007) Contemporary estimates of Pan-Arctic freshwater discharge from GRACE and reanalysis. Geophys Res Lett 34(L19404): 6 p. https://doi.org/10.1029/2007gl031254

Tananaev NI, Makarieva OM, Lebedeva LS (2016) Trends in annual and extreme flows in the Lena River basin, Northern Eurasia. Geophys Res Lett 43:10764–10772. https://doi.org/10.1002/2016GL070796

Tang W, Yueh S, Yang D, Fore A, Hayashi A, Lee T, Fournier S, Holt B (2018) The potential and challenges of using Soil Moisture Active Passive (SMAP) sea surface salinity to monitor Arctic Ocean freshwater changes. Rem Sens 10(6):869

Troy TJ, Sheffield J, Wood EF (2012) The role of winter precipitation and temperature on northern Eurasian streamflow trends. J Geophys Res Atmos 117(D5). https://doi.org/10.1029/2011jd016208

Velicogna I, Tong J, Zhang T, Kimball JS (2012) Increasing subsurface water storage in discontinuous permafrost areas of the Lena River basin, Eurasia, detected from GRACE. Geophys Res Lett 39. http://doi.org/10.1029/2012GL051623

Tan X, Gan TY (2015) Contribution of human and climate change impacts to changes in streamflow of Canada. Sci Rep 5:17767. https://doi.org/10.1038/srep17767

Vihma T, Screen J, Tjernström M, Newton B, Zhang X, Popova V, Deser C, Holland M, Prowse T (2016) The atmospheric role in the Arctic water cycle: a review on processes, past and future changes, and their impacts. J Geophys Res Biogeosci 121:586–620. https://doi.org/10.1002/2015JG003132

Vörösmarty CJ, Fekete BM, Meybeck M, Lammers RB (2000) Global system of rivers: its role in organizing continental land mass and defining land-to-ocean linkages. Glob Biogeochem Cycles 14(2):599–622. https://doi.org/10.1029/1999GB900092

Vörösmarty CJ, Coauthors (2001) The hydrologic cycle and its role in Arctic and global environmental change: a rationale and strategy for synthesis study. ARCUS, 84 p

Walvoord MA, Kurylyk BL (2016) Hydrologic impacts of thawing permafrost—a review. Vadose Zone J 15. https://doi.org/10.2136/vzj2016.01.0010

Wegmann M, Orsolini Y, Vazquez M, Gimeno L, Nieto R, Bulygina O, Jaiser R, Handorf D, Rinke A, Dethloff K, Sterin A, Brönnimann S (2015) Arctic moisture source for Eurasian snow cover variations in autumn. Environ Res Lett 10(5). https://doi.org/10.1088/1748-9326/10/5/054015

White D, Hinzman L, Alessa L, Cassano J, Chambers M, Falkner K, Francis J, Gutowski W, Holland M, Holmes M, Huntington H, Kane D, Kliskey A, Lee C, McClelland J, Peterson B, Rupp TS, Straneo F, Steele M, Woodgate R, Yang D, Yoshikawa K, Zhang T (2007) The arctic freshwater system: changes and impacts. JGR Biogeosci 112:G04S54. https://doi.org/10.1029/2006jg000353

Wisser D, Fekete BM, Vörösmarty CJ, Schumann AH (2010) Reconstructing 20th century global hydrography: a contribution to the Global Terrestrial Network-Hydrology (GTN-H). Hydrol Earth Syst Sci 14:1–24

Wisser D, Frolking S, Hagen S, Bierkens MFP (2013) Beyond peak reservoir storage? a global estimate of declining water storage capacity in large reservoirs. Water Resour Res 49:5732–5739. https://doi.org/10.1002/wrcr.20452

Woo (2012) Permafrost hydrology. Springer-Verlag, Berlin, Germany. https://doi.org/10.1007/978-3-642-23462-0

Yang D, Kane D, Hinzman L et al (2002) Siberian Lena River hydrologic regime and recent change. J Geophys Res 107(D23):4694. https://doi.org/10.1029/2002JD002542

Yang D, Ye B, Kane DL (2004a) Streamflow changes over Siberian Yenisei river basin. J Hydrol 296(1–4): 59–80, 141

Yang D, Ye, B, Shiklomanov A (2004b) Discharge characteristics and changes over the Ob River watershed in Siberia. J Hydrometeorol 5(4):595–610

Yang D, Kane D, Zhang Z, Legates D, Goodison B (2005) Bias corrections of long-term (1973–2004) daily precipitation data over the northern regions. Geophys Res Lett 32(19). https://doi.org/10.1029/2005gl024057

Yang D, Zhao Y, Armstrong R, Robinson D, Brodzik M-J (2007) Streamflow response to seasonal snow cover mass changes over large Siberian watersheds. J Geophys Res 112:F02S22. https://doi.org/10.1029/2006jf000518

Yang D, Shi X, Marsh P (2014a) Variability and extreme of Mackenzie River daily discharge during, 1973–2011. Quat Int. https://doi.org/10.1016/j.quaint.2014.09.023

Yang D, Marsh P, Ge S (2014b) Heat flux calculations for Mackenzie and Yukon Rivers. Polar Sci. https://doi.org/10.1016/j.polar.2014.05.001

Ye B, Yang D, Kane DL (2003) Changes in Lena River streamflow hydrology: human impact versus natural variations. Water Resour Res 39(7):1200–1224

Ye B, Yang D, Zhang Z, Kane DL (2009) Variation of hydrological regime with permafrost coverage over Lena Basin in Siberia. J Geophys Res 114:D07102. https://doi.org/10.1029/2008JD010537

Zhang Y, Carey SK, Quinton WL (2008) Evaluation of the algorithms and parametrizations for ground thawing and freezing simulation in permafrost regions. J Geophys Res 113. https://doi.org/10.1029/2007JD009343

Zhang X, He J, Zhang J, Polyakov I, Gerdes R, Inoue J, Wu P (2013) Enhanced poleward moisture transport and amplified northern high-latitude wetting trend. Nat Clim Change 3:47–51. https://doi.org/10.1038/nclimate1631

Dr. Alexander I. Shiklomanov received M.Sc. (1983) and Ph.D. (1996) degrees from Russian Hydrometeorological State University, St. Petersburg. Since 1983, he has been working at the Arctic and Antarctic Research Institute (AARI), in Saint Petersburg, Russia; and in 1997 he joined the Earth Systems Research Center at the University of New Hampshire, USA. The focuses of his research are on cold region and Eurasian hydroclimatology, hydrological and water management modeling and analysis. Research interests include hydrological monitoring systems; water balance and streamflow routing models; human activity and its influence on hydrology; climate change and hydrological systems; and effect of land cover and land use change on hydrology. He has more than 60 publications including more than 45 in peer-reviewed journals. He is a co-developer of several regional hydrographic databases and a reviewer of multiple national and international scientific journals. He has been a Principal Investigator for many research projects sponsored by NASA and NSF.

Dr. Stephen Déry is Professor in the Environmental Science and Engineering undergraduate program and the Natural Resources and Environmental Studies graduate program at the University of Northern British Columbia (UNBC), Prince George, BC. He also holds the NSERC/Rio Tinto Senior Industrial Research Chair in Climate Change and Water Security with a 5-year program of research focused on the Nechako Watershed. His background is in atmospheric science, hydrometeorology, and applied mathematics, and he has degrees from York University (B.Sc. and M.Sc.) and McGill University (Ph.D.). He has completed postdoctoral positions at the Lamont-Doherty Earth Observatory of Columbia University, New York and held a Visiting Research Scientist position at Princeton University in New Jersey. He investigates the consequences of climate change and water management on the water cycle of northern and alpine regions. A major aspect of this research is to better monitor, understand, and project the water balance and streamflow trends in major watersheds such as the Fraser based on observational data and numerical simulations.

Dr. Mikhail V. Tretiakov is a Head of River Estuaries and Water Resources Department at the Arctic and Antarctic Research Institute in Saint Petersburg, Russia. He got his Ph.D. from Russian State Hydrometeorological University in 2001. His research interests include the development of scientific and methodical bases of monitoring estuarine areas in the cold regions of the world, methods and technologies of hydrothermodynamic process research for river estuaries, numerical modeling in hydrology, and various analyses of hydrometeorological information. He is the author/co-author of numerous (>50) scientific articles that have appeared in a variety of peer-reviewed journals and conference proceedings.

Dr. Daqing Yang is a Research Scientist at the Watershed Hydrology and Ecology Research Division, Environment and Climate Change Canada. He is also Affiliate Research Professor at the International Arctic Research Center, Univ. of Alaska Fairbanks. Over the past 25 years, he has conducted cryosphere system research in China, Canada, Japan, USA, and Norway. His primary research activities/interests include cold region hydrology and climate, particularly Arctic large river streamflow regime and change, snow cover and snowfall measurements, climate change and human impact to regional hydrology, and applications of remote sensing in cold regions. He has served as journal editor and subject editor for IAHS publications (cold region hydrology, northern research basin water balance, and cold/mountain region hydrological systems under climate change), and WMO technical reports (solid precipitation measurement intercomparison and integrated global observing strategy cryosphere theme). He also contributed as review and/or author to the IPCC Reports, and the Arctic Council's Snow, Water, Ice and Permafrost in the Arctic (SWIPA 2017 and follow up) assessment. His current research focuses on investigating the impacts of climate variability/change and human activities on hydrologic system across the broader northern regions.

Dr. Dmitry Magritsky is an Associate Professor at the Department of Land Hydrology, Faculty of Geography, Lomonosov Moscow State University. His research interests are diverse and include the analysis of factors and patterns of spatial and temporal variability of river runoff, the impact of economic activity on water flow, sediment yield, heat flow and hydrological regime of rivers, the study of hydrological processes in river mouths and their climate-related and anthropogenic changes, and the formulation of theoretical foundations for studying and evaluating of dangerous hydrological processes. His first scientific work was devoted to the Arctic rivers of Yakutia. This interest in Arctic hydrology has continued to the present day. He is the author/co-author of about 140 articles, 6 books and 3 atlases (dedicated to the water objects of the Russian Arctic), and 3 textbooks. He directs the educational and scientific activities of students, and participates in hydrological expeditions every year.

Dr. Alexander G. Georgiadi is Leading Scientific Researcher at the Hydrology Department, Institute of Geography RAS. The main areas of his recent projects focus on the assessment of hydrological consequences of global climate change in the past, present, and future for different spatial and temporal scales based on fieldwork, data analysis, and modeling. He has organized and actively participated in several international scientific programs in Russia in different natural zones including Arctic river basins. He is one of the organizers and active participants of several international scientific programs in Russia (international field experiment KUREX, GAME/Siberia program, NEESPI, IPY). He is the author of over 150 scientific publications, including monographs.

Wenqing Tang is a Scientific Applications Software Engineer at the Jet Propulsion Laboratory, California Institute of Technology. Her research activities in earth remote sensing include retrieval algorithms development of microwave radiometer and scatterometer, as well as satellite data validation and application. Her recent work explores the potential and utility of remote sensing sea surface salinity data for large-scale freshwater cycle in the Arctic Ocean and over the Hudson Bay.

River Heat Flux into the Arctic Ocean

25

Daqing Yang, Shaoqing Ge, Hotaek Park, and Richard L. Lammers

Abstract

Long-term observations and data analyses of water temperatures and discharge over the northern regions determine water temperature regimes and quantify river heat flux into the ocean system. This chapter presents an overview of thermal regime and heat flux for the large rivers in northern regions. This chapter compares the results for the Siberian and North American arctic watersheds/regions, and highlights the differences and changes in water temperature and heat flux due to climate variation and human effect. Given the limited water temperature observations, this chapter is unable to discuss the variability and change in river thermal conditions over the northern regions of the North America. There is a knowledge gap in river temperature and heat contribution along the arctic coast of North America. Advanced hydrologic models and remote sensing data have provided opportunities to improve our understanding of river thermal characteristics across the northern regions. There is a need to continue to explore remote sensing data/products in the

D. Yang (✉)
Environment and Climate Change Canada, Watershed Hydrology and Ecology Division, Victoria, BC, Canada
e-mail: daqing.yang@canada.ca; daqing.yang@gmail.com

S. Ge
American Water, Camden, NJ, USA
e-mail: geshaoqing@gmail.com

H. Park
Japan Agency for Marine-Earth Science and Technology, Research Institute for Global Change, Yokohama, Kanagawa, Japan
e-mail: park@jamstec.go.jp

R. L. Lammers
Earth Systems Research Center, University of New Hampshire, Durham, NH, USA
e-mail: richard.lammers@unh.edu

D. Yang and D. L. Kane (eds.), *Arctic Hydrology, Permafrost and Ecosystems*,
https://doi.org/10.1007/978-3-030-50930-9_25

investigations of river water temperature and heat transport processes and to develop coupled land–ocean models, in order to better quantify land–ocean linkage and connections across the northern coastal regions.

25.1 Introduction

Discharge and water temperature are the most important climatic and hydrologic variables, as they directly (or indirectly through combination) reflect river physical and thermal features. River thermal conditions affect biological and ecological processes over the basin and near the coastal regions/shorelines. Stream temperatures usually follow air temperature closely on a seasonal time scale (Sinokrot and Stefan 1993). Due to climate change and human impact, stream temperatures have increased over the USA, Austrian, and Australian rivers. These elevated water temperatures have become an important concern in watersheds where aquatic species such as salmonids are present (Lowney 2000). In the northern regions, discharge and stream temperature significantly impact the freeze-up/break-up processes, thickness of river ice, and thermal erosions along the riverbanks. MacKay and MacKay (1975) analyzed water temperature data at three locations in the Mackenzie River, described the basic thermal regimes, and determined the river heat transport along the Mackenzie Valley. Elshin (1981) calculated the heat runoff (heat flow) for rivers in the European part of the former USSR. Marsh and Prowse (1987) studied the influence of stream heat on overlying ice cover of the Liard River, and discovered large spatial and temporal variations in water temperatures and heat fluxes. Costard et al. (2007) reported that water temperature and discharge are the major factors controlling thermal erosion of the frozen riverbanks in the Siberian Lena basin, and that relatively water temperature is more important than streamflow in these environments. Liu et al. (2005) and Yang et al. (2005) carried out systematic analyses of long-term water temperature records for the Lena basin, and discovered significant changes in river thermal conditions due to climate warming and human impacts (dam regulation). Lammers et al. (2007) conducted a continental-scale river temperature study for the Russian Arctic, they calculated and examined heat energy for the river systems, and found a consistent increase in the decadal maximum temperature for the basins in the European part of Russia.

Discharge, water temperature, and geochemistry data collected near the river mouths are particularly important as they represent the mass and thermal influxes to the ocean system. It is thus critical to examine the fundamental characteristics of discharge and water temperature and geochemistry at the basin outlet, and document any significant variations and changes over space and time. Holmes et al. (2012) and Tank et al. (2012) recently examined the seasonal and annual fluxes of nutrient and organic matter, and DIC flux, respectively, from major Arctic rivers to the Arctic Ocean. Lammers et al. (2007) determined the heat flux to the Arctic Ocean from the large Siberian rivers. The knowledge of heat flux is incomplete for

the large northern rivers in North America. This limits our understanding of total northern river heat transport to the Arctic Ocean. To fill this critical knowledge gap, Yang et al. (2014) compiled and analyzed long-term (40–60 years) downstream discharge and water temperature data for the Yukon and Mackenzie rivers. These two large rivers were chosen because of their distinct cryospheric environments (snow cover, glacier, permafrost), unique climatic (cold and dry) and hydrological features (large lakes, snow, and glacier contribution), minor human impact with little regulations, and close interactions and linkages to the northern seas via freshwater, sediment, and heat transports. The main objectives of that study were to define discharge and water temperature regimes, to quantify heat flux from the northern rivers into the ocean system, and to examine the similarity and difference in thermal conditions between these two watersheds. The results of that investigation are useful in understanding hydrologic and climatic linkages and variations over the northern regions. They are also important for regional hydrology and climate change investigations, such as basin-scale mass/energy balance calculations, and land–ocean interaction, particularly large-scale ocean heat/mass budget and model analyses.

There is a need to link mass and energy data in the investigation of watershed response to climate change over the northern regions. This chapter reviews the regional studies on heat flux into the Arctic Ocean from large rivers and its changes over time due to climate variation and human activities in the northern regions. The goal of this review is to combine and compare the results for the Siberian and North American arctic watersheds/regions, so as to improve our understanding of the river heat transport from the arctic land mass to the ocean systems.

25.2 Methods and Datasets

Based on recent publications, this section reviews/presents the methods and datasets for the heat flux calculations for the northern rivers, and the available discharge and water temperature datasets used for analyses. It also discusses the ice condition and its impact on winter heat flux.

River heat flux can be calculated by the following equation (Elshin 1981):

$$H = 0.3615 \cdot Q \cdot T \cdot n \tag{25.1}$$

where H is the total heat flux in a given month (10^6 MJ), Q and T are the monthly mean discharge (m^3/s), and the monthly mean stream temperature (°C) at the basin outlet, and n is the number of days in a given month. The coefficient, 0.3615, has the dimensions of 10^6 MJs/(°C day m^3) according to unit conversion, and the value of specific heat of water is 4.184 J/(°C g) (Liu et al. 2005). Using the Celsius temperature scale here means the H is not an absolute energy flux, but relative to the freezing point of water (Lammers et al. 2007).

Discharge and water temperature data are necessary to determine heat flux. Chapters 6, 7, and 24 have discussed discharge observations and data availability in the northern regions, while Chap. 10 covered water temperature measurement and modeling in detail. It is important to note that Lammers et al. (2007) developed a river temperature data set covering 20 gauges in 17 unique Arctic Ocean drainage basins in the Russian Arctic (Table 25.1, Fig. 25.1). The warm (open water) season 10 day time step data (decades) were collected from Russian archives for the period 1929–2003, with most data in period from the mid 1930s to the early 1990s. Lammers et al. (2007) produced three versions of river temperature data. In the first version, the errors in the raw data obtained from Russia were fixed or removed. This version was named T0 and it represents the most complete data available. The second version of river temperature data was created based on T0, and some years

Table 25.1 The monitoring stations used for heat flux analyses in the northern regions/watersheds

Monitoring stations (ID)	First year	Last year	Drainage area (km^2)	Latitude	Longitude	Source
Great Bear River (10JC003)	2002–03	2012–13	146400	65.10	123.60	WSC
Klondike River above Bonanza Creek (09EA003)	2010	2012	7810	64.00	139.40	NWS
Liard River at Upper Crossing (10AA001)	1991	2013	32600	60.10	128.90	PYLTM study
Yukon River at Carmacks (09AH001)	1980	1996	81800	62.10	136.30	PYLTM study
Mackenzie River at Arctic Red River (10LC014)	1950	2010	1680000	67.45	−133.74	Yang et al. (2014)
Yukon River at Pilot Station (15565447)	1975	2010	831391	61.93	−162.88	Yang et al. (2014)
Onega at Porog	1937	2003	55700	63.82	38.47	Lammers et al. (2007)
Severnaya Dvina at Ust-Pinega	1936	2003	348000	64.13	41.92	Lammers et al. (2007)
Mezen at Malonisogorskaya	1940	2003	56400	65.00	45.62	Lammers et al. (2007)
Pechora at Ust-Tsilma	1936	2003	248000	65.42	52.28	Lammers et al. (2007)
Pechora at Oksino	1939	2003	312000	67.63	52.18	Lammers et al. (2007)
Ob at Salekhard	1936	1998	2950000	66.63	66.60	Lammers et al. (2007)

(continued)

Table 25.1 (continued)

Monitoring stations (ID)	First year	Last year	Drainage area (km^2)	Latitude	Longitude	Source
Nadym at Nadym	1939	1998	48000	65.62	72.67	Lammers et al. (2007)
Pur at Urengoy	1948	1990	80400	65.97	78.35	Lammers et al. (2007)
Pur at Samburg	1938	1991	95100	67.00	78.22	Lammers et al. (2007)
Taz at Sidorovsk	1951	1995	100000	66.60	82.28	Lammers et al. (2007)
Yenisey at Igarka	1936	2001	2440000	67.43	86.48	Lammers et al. (2007)
Norilka at Valek	1963	2001	19800	69.42	88.32	Lammers et al. (2007)
Khatanga at Khatanga	1961	1992	275000	71.98	102.47	Lammers et al. (2007)
Anabar at Saskulakh	1954	1996	78800	71.97	114.08	Lammers et al. (2007)
Olenek 7.5 km down of Buurs mouth	1964	1992	198000	71.85	123.65	Lammers et al. (2007)
Lena at Kusur	1936	1995	2430000	70.68	127.39	Lammers et al. (2007)
Yana at Ubileinaya	1943	1992	224000	70.77	136.08	Lammers et al. (2007)
Indigirka at Vorontsovo	1939	1992	305000	69.57	147.53	Lammers et al. (2007)
Kolyma at Srednekolymsk	1929	2001	361000	67.47	153.69	Lammers et al. (2007)
Kolyma at Kolymskoye	1965	2001	526000	68.73	158.72	Lammers et al. (2007)

missing data were removed or individual data values were removed or added at the beginning and/or end of the ice-free seasons. This version is called T1 and it was created to perform consistent analysis of ice-free mean temperature values. In the third version, the data were generated from T1 to perform energy calculations. This version was named T2 and all temperature values during the winter period were set to 0 °C, and many years without river discharge data were removed. Since no river temperature data for the winter period were available, there will be a warm season bias giving very different results for time aggregated values and trends when compared to the full record of other studies.

For the Makenzie river in Canada, water temperatures (WT) data have been collected by government agencies irregularly over the basin at various locations and times (dates) of the sediment sampling and during the discharge measurements. The sampling frequency varies from 5 to 35 times per year, but most often in the open

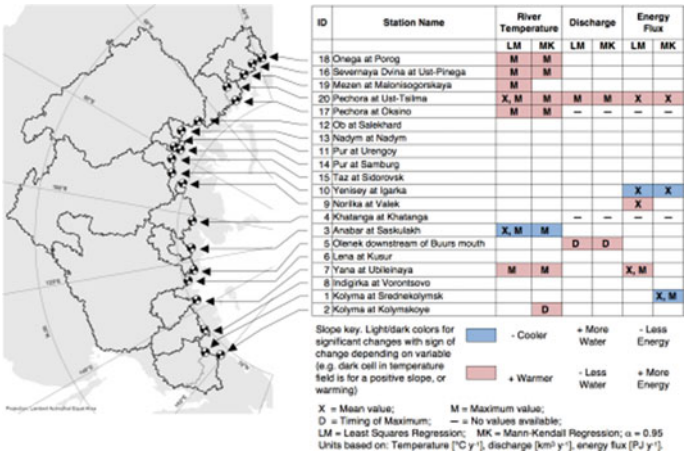

Fig. 25.1 Locations of river temperature gauging stations along the northern Russian pan-Arctic. A total of 20 stations in 17 watersheds cover 85.3% of the Russian Arctic Ocean drainage system. Table also shows significant trends in mean value (X), maximum value (M), and day of maximum (D) for water temperature, river discharge, and energy flux using both linear regression and Mann-Kendall tests. Figure modified from Lammers et al. (2007)

water season. Many samples were taken and available for a given location, although not on fixed dates. Water temperature is instantaneously measured at 0–1 m below water surface (on average around 11:30 a.m. local time, with a standard deviation of 2 h), using a mercury thermometer, battery thermometer, or a conductivity temperature (battery) meter with a precision of 0.1 C (van Vliet et al. 2011). All available WT data collected at the Arctic Red River Station since 1950 have been archived at the UN Environment Programme Global Environment Monitoring System (GEMS/Water) and used for the analyses by Yang et al. (2014). For the Yukon River, the US Geological Survey and Environment Canada maintain a hydrologic network in the basin. The Pilot Station (61.9°N, 162.9°W) is located downstream on the main river valley; this is a gauging site closest to the basin outlet, monitoring a drainage area of 831,400 km^2. Monthly discharge and water temperature records collected at this location since 1975 have been stored at the USGS web site (http://www.usgs.gov/).

Most studies, such as Yang et al. (2014) and Liu et al. (2005), determine the river heat flux on a monthly time scale, using an aggregated average of all water temperature data collected/available in a given month. It is useful to note that WT varies over the open water season, particularly in the early summer of the northern regions (Liu et al. 2005; Yang et al. 2005). Lammers et al. (2007) detected a significant discrepancy between the decadal and monthly mean peak WTs for the Lena river, and emphasized the need for a finer than monthly sampling resolution. Liu et al. (2005) determined monthly mean water temperatures over the Lena basin by averaging 2 observations taken on the 10th and 20th days of a month. They also compared various methods to calculate the monthly means, and found their method

representative and conservative, as it did not overestimate the mean temperatures during the open water season. The use of the aggregated average of all WT data collected on the different dates in a month may not be the most accurate way to determine the monthly mean WT. Given the fact that large numbers of water samples, for example, up to 150 observations for June and total of 680 measurements over the open water season on the Yukon River at the Pilot Station were taken within a given month over the past 40–60 years, monthly scale analysis is useful, in addition to the decadal steps, for the determination of the seasonal cycles of water temperature and heat flux.

25.3 Northern River Heat Flux to the Arctic Ocean

Liu (2004) and Liu et al. (2005) investigated the long-term (1950–1992) heat flux from Lena River watershed into the Arctic Ocean, and reported the mean monthly values between 1922 $\times$ 10^9 MJ in September to 6070 $\times$ 10^9 MJ in July, with the total of 14,281 $\times$ 10^9 MJ during the period June through September (Fig. 25.2). It is important to point out the difference and similarity in seasonal cycles among river discharge, water temperature, and heat flux. The Lena river discharge peaks in June, and the highest water temperature coincides with the maximum heat flux in July. The standard deviations of the monthly heat fluxes vary in a small range from 777 in September to 1258 $\times$ 10^9 MJ in July, while heat flux trends show moderate increases of 311–477 $\times$ 10^9 MJ during June to August and a weak decline of 202 $\times$ 10^9 MJ in September, which are statistically significant at a 45–60% confidence level. The heat flux increase in June is the highest (23% of the long-term mean) owing to the combined effect of peak flow increase (Ye et al. 2003) and stream temperature warming over the Lena basin.

Lammers et al. (2007) found the mean basin-level total energy flux for 17 Russian rivers flowing to the Arctic Ocean was 3500 PJ a^{-1} (0.20 W m^{-2}). Individual drainage basins had total energy flux, ranging from 305 PJ a^{-1} (0.12 W m^{-2}) in the Anabar basin to 15118 PJ a^{-1} in the Lena basin. In terms area averaged

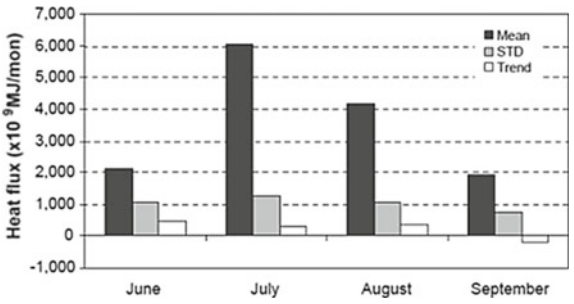

Fig. 25.2 Long-term Lena River heat flux, standard deviation, and trend at the Lean basin outlet, 1950–1992 (Liu 2004)

energy flux the maximum was in the Norilka basin with 0.61 W m^{-2}. Timing of maximum energy flux in these basins ranged from early June in the European (western) Russian basins to the middle of July in the Siberian basins. Significant increases in mean annual energy flux were found for the Pechora, Norilka, and Yana rivers, while the Yenisey and Kolyma (at Srednekolymsk) had decreasing trends. The Yana river also showed increasing total energy flux, both total and decadal maximum values. Both the Yana and Kolyma had significant changes in the maximum value of heat flux, decreasing and increasing, respectively. Slopes of the trend lines for temperature and energy flux for each station are given in Table 25.2. The Yenisey was the only drainage basin of the 3 large Siberian watersheds with any significant changes. The results for the Yana, which had significant trends for both temperature and energy flux, were based on 17 annual values. The Pechora at Ust-Tsilma showed the most significant trends for temperature, discharge, and energy flux. Inspection of the energy flux time series for this gauge showed a step function with a steep rise occurring over a four-year period starting in 1980. The annual temperature and discharge time series suggest the high energy flux is due to a sustained high river temperature during the years in question.

Annual time series for the Russian Arctic aggregate of 16 representative gauges had a mean energy flux of 0.19 W m^{-2}, with no significant trend during 1938–1992 (Fig. 25.3a). However, the subset of the 3 largest basins (Ob, Yenisey, and Lena, Fig. 25.3b) had a mean energy flux of 0.17 W m^{-2} and a significantly decreasing slope of −0.00053 W m^{-2} a^{-1}, representing a total decrease by 0.029 W m^{-2} from 1938 to 1992, or 17% decline relative to the mean for the entire period. Lammers et al. (2007) determined the total energy flux across Russia north to the Arctic Ocean in two ways, a simple extrapolation of the mean energy flux to the entire land area and by applying a latitude correction to river temperature over each ungauged sea basin. Using the mean energy flux from the gauged basins (0.20 W m^{-2}) and assuming this value is representative of the ungauged regions, it is possible to estimate the total energy flux from the entire Russian Arctic drainage area into the Arctic Ocean. Given an area of 12,925,000 km^2, the total flux was estimated to be 8.16×10^{19} J a^{-1} or 82 EJ a^{-1}. A latitude-temperature regression and estimates of discharge were used to calculate the energy flux of the ungauged Russian Arctic. Energy flux from the observed gauges was 63.6 EJ a^{-1} and ungauged energy flux was estimated to be 17.3 EJ a^{-1}, so the total Russian energy flux to the Arctic Ocean to be 80.9 EJ a^{-1}.

Many studies establish relationships between air and water temperatures over various regions (Yang and Peterson 2016; van Vliet et al. 2011; Webb and Nobilis 1995; Davies 1975). For instance, strong positive correlations have been found between the Lena basin mean monthly air and water temperatures during the warm season (Liu et al. 2005). However, Lammers et al. (2007) did not detect river temperature rising with air temperature across the Russian Arctic, and they noticed that river heat flux was not coupled closely to water temperature and discharge. They also found a significant decrease in the aggregated energy flux from the 3 largest Russian rivers (Ob, Yenisey, and Lena); this is not expected given the

Table 25.2 Least squares regression results for river temperature and energy for each monitoring station

		River temperature (T_1)				Energy flux (using T_2)			
Station (Short-hand)	ID	Years	Slope of trend line			Years	Slope of trend line		
			Decadal mean (°C y^{-1})	Decadal maximum (°C y^{-1})	Timing of maximum (decade y^{-1})		Mean value (PJ y^{-1})	Decadal maximum (PJ y^{-1})	Timing of maximum (decade y^{-1})
Oneg	18	47	0.0098	**0.0506**	0.0038	40	1.30	−0.10	−0.0273
Sevr	16	52	0.0068	**0.0397**	−0.0030	48	−5.47	−1.73	−0.0117
Mezn	19	22	0.0014	**0.0578**	−0.0166	20	−0.99	−0.31	−0.0413
PchU	20	53	**0.0190**	**0.0423**	−0.0140	51	**26.74**	2.55	−0.0051
PchO	17	28	0.0101	**0.0668**	−0.0127	1	–	–	–
Ob	12	45	−0.0005	0.0078	−0.0087	45	−14.04	0.67	−0.0194
Nadm	13	35	0.0182	0.0267	−0.0085	23	0.00	0.84	0.0404
PurU	11	29	−0.0026	−0.0013	0.0021	9	3.88	1.71	0.0077
PurS	14	45	0.0090	0.0340	0.0019	41	−0.28	0.04	0.0005
Taz	15	30	−0.0108	−0.0199	−0.0072	20	5.10	2.14	0.0115
Yen	10	59	−0.0107	−0.0066	0.0041	57	**−51.67**	−1.21	−0.0072
Nor	9	31	0.0060	0.0352	−0.0079	29	**2.74**	0.42	−0.0242
Khat	4	32	0.0219	−0.0403	−0.0312	3	–	–	–
Anab	3	34	**−0.0309**	**−0.0736**	0.0047	34	0.29	−0.08	−0.0246
Olnk	5	25	−0.0236	0.0147	−0.0281	25	−0.93	−1.35	−0.0290
Lena	6	50	0.0016	0.0075	−0.0106	50	7.53	−1.42	−0.0088
Yana	7	37	0.0090	**0.0717**	0.0035	17	**34.04**	**9.17**	0.0228
Indk	8	51	−0.0024	0.0102	−0.0024	50	2.38	0.55	0.0072
KolS	1	55	−0.0086	0.0066	0.0109	52	−9.66	−3.32	0.0038
KolK	2	37	−0.0076	0.0110	0.0330	24	−32.30	−5.30	0.0265

Positive slopes in timing of maximum river temperature and energy flux indicate a shift to later in year. Bold, grey cells show significant linear regression slopes ($\alpha = 0.05$). Least squares regression results were not calculated for the energy flux in basins #17 (PchO) and #4 (Khat) due to insufficient number of years of data (1 and 3 years, respectively). Table modified from Lammers et al. (2007)

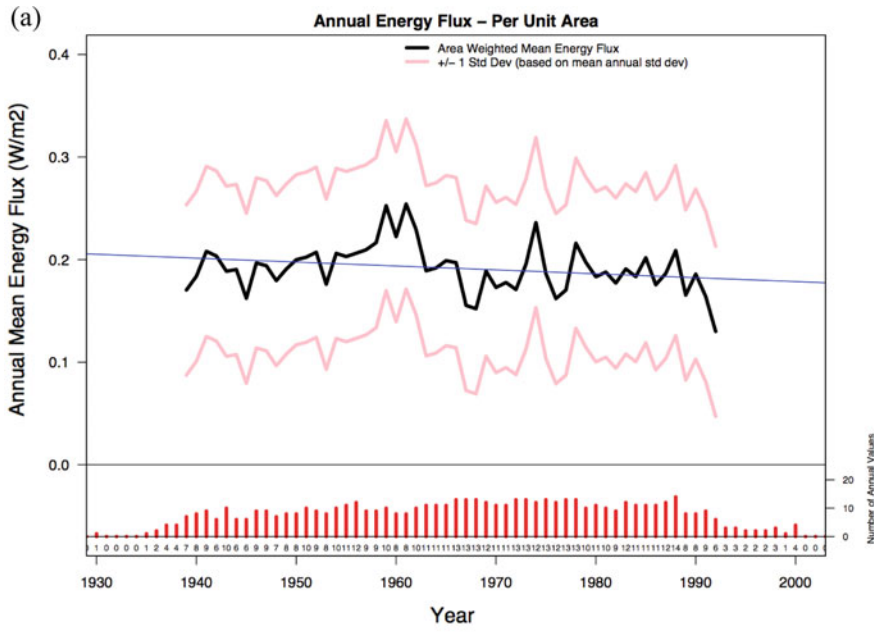
(a)
Annual Energy Flux – Per Unit Area
Area Weighted Mean Energy Flux
+/– 1 Std Dev (based on mean annual std dev)
Annual Mean Energy Flux (W/m2)
0.4
0.3
0.2
0.1
0.0
20
10
0
Number of Annual Values
1930
1940
1950
1960
1970
1980
1990
2000
Year

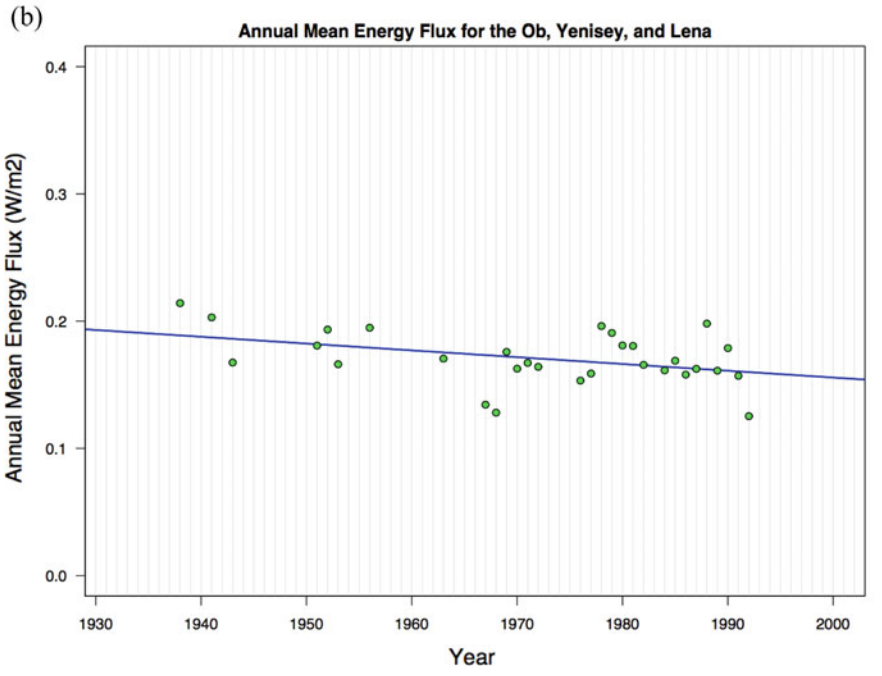
(b)
Annual Mean Energy Flux for the Ob, Yenisey, and Lena
Annual Mean Energy Flux (W/m2)
0.4
0.3
0.2
0.1
0.0
1930
1940
1950
1960
1970
1980
1990
2000
Year

◀ **Fig. 25.3** **a** Aggregate annual time series of energy flux per unit drainage area for 15 gauges. Annual weighted mean energy flux for all basins shown as a thick red line with ±1 standard deviation in light red. Total number of gauges contributing to each annual value shown as histogram at bottom. **b** Aggregate annual mean energy flux for the three largest Russian drainage basins, Ob, Yenisey, and Lena. Only years in which all three basins had values were used. Trend line shows a significant decrease in annual energy flux of 0.00053 W m^{-2} a^{-1}. Figure modified from Lammers et al. (2007)

warming trends over Siberia, but maybe related to large reservoir regulation in these basins, particularly for the Ob and Yenisey rivers (Yang et al. 2004a, b; Ye et al. 2003) where cooler waters are released from the reservoirs during the warmer summer months (Lammers et al. 2007).

Yang et al. (2014) studied the heat flux (HF) regime for the Yukon River and Mackenzie River during 1950–2010 (Fig. 25.4). For the Yukon River, the mean monthly heat fluxes are low in May (about 527 × 10^9 MJ) and very high (2380–2500 × 10^9 MJ) for June and July; then they decrease to 3644 × 10^9 MJ) from August to October. The total HF is about 8590 × 10^9 MJ during May through October. The Mackenzie River shows a similar seasonal HF pattern. The monthly heat transports are relatively low for May, September, and October; and high during June to August, with the highest HF in July. It is interesting to note that, relative to the Yukon River, the Mackenzie WT is slightly cooler and its summer flow is much higher. The Mackenzie monthly HF ranges from 790 × 10^9 to 3100 × 10^9 MJ, with the seasonal total of 10,430 × 10^9 MJ. These values are about 10–50% higher than the Yukon River for May to September, and 21% higher over the entire open

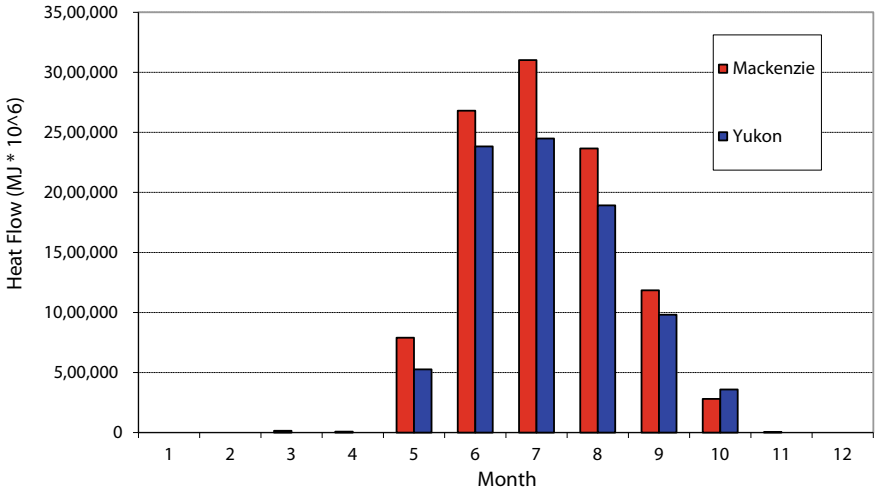

Fig. 25.4 long-term mean monthly heat flux from Yukon and Mackenzie rivers. Figure modified from Yang et al. (2014)

water season. This result suggests that higher summer flows in the Mackenzie River dominate the heat transport to the Arctic Ocean.

It is important to examine the difference and similarity in seasonal cycles among discharge, water temperature, and heat flux over the northern regions. Lammers et al. (2007) report, over the Russian Arctic, the long-term decadal mean water temperature peak around late July, highest discharge in early June, and the maximum heat flux at the end of June. Liu et al. (2005) found that Lena river discharge peaks in June, and the highest water temperature coincides with the maximum heat flux in July. The Yukon discharge peaks in June and the warmest WT occurs in July, while the HF is highest for both June and July. Mackenzie River also has the highest flow in June and warmest WT in July, but the HF reaches the peak in July which lags behind the peak flow by a month. This result is consistent with the Lena River (Liu et al. 2005) and similar to the Russian Arctic regions (Lammers et al. 2007).

Table 25.3, based on long-term observations and recent data analyses, is a summary of heat flux from Arctic rivers into the Arctic Ocean. There is, however, a need to investigate the spatial and temporal distribution of river energy within the large watersheds and over the arctic regions as a whole, particularly thorough model tools and remote sensing technology. Park et al. (2016) used the coupled hydrological and biogeochemical model (CHANGE)] to examine the changes in ice phenology, thickness, and volume of Arctic large rivers during 1979–2009. They found significant changes in river ice characteristics, i.e., a longer ice-free season associated with warmer water temperatures (T_w). Earlier ice breakup likely results in warmer T_w combined with warmer spring surface air temperature (SAT). T_w exhibits abrupt increases following ice breakup. For the Siberian rivers, T_w

Table 25.3 Summary of heat flux of Arctic Rivers into Arctic Ocean in literature

River/basin	Year range studied	Total heat flux (10^9 MJ)	Source
Lena River	1950–1992	14,281	Liu et al. (2005)
Yukon River	1975–2010	8,590	Yang et al. (2014)
Mackenzie River	1973–2010	10,430	Yang et al. (2014)
Seas			
Barents	1929–2003	4,000	Lammers et al. (2007)
Kara	1929–2003	6,900	Lammers et al. (2007)
Laptev	1929–2003	2,400	Lammers et al. (2007)
E. Siberian	1929–2003	2,900	Lammers et al. (2007)
Chukchi	1929–2003	1,100	Lammers et al. (2007)
Total gauged pan-Russia area	1929–2003	63,600	

increased by 1°–2 °C in the first 10 days following ice breakup (Park et al. 2017). Calculations from this result suggest that an increase of 0.2 °C day^{-1} in early spring would enhance the river heat flux by 0.013–0.084 TW under a discharge of 15 000–100 000 m^3 s^{-1}. The heat flux H (W) was calculated by $H = \rho \cdot C_p T_w Q$, where ρ is water density (kg m^{-3}), C_p is specific heat capacity (J $kg^{-1}°C^{-1}$), and Q is river discharge (m^3 s^{-1}). Arctic-flowing monthly mean heat fluxes of Siberian rivers (e.g., Yenisey, Lena, and Kolyma) are <0.1 TW in May (Whitefield et al. 2015). The estimated (0.013–0.084 TW) heat flux increase is expected to contribute to warmer Tw levels and additional energy inputs to the Arctic Ocean, potentially impacting landfast ice and atmosphere dynamics (Yang et al. 2014; Whitefield et al. 2015). SAT records indicate strong warming trends in the spring. Thus, the impact of earlier ice breakup on spring Tw warming is likely larger than what the simulations indicate.

River heat flux discharged into the Arctic shelf seas shows consistently strong seasonal cycles and large regional differences in the amounts, which reflect larger spatio-temporal variations in the Arctic hydroclimates. The heat flux recorded the maximum (i.e., 2–6 TW) in June in all sea basins (Fig. 25.5) due to the largest discharge and warmer Tw (Park et al. 2016). In the Kara Sea basin that is consisted of majorly by Ob and Yenisey rivers, the heat flux in June varied at the range of 4–8 TW, with a mean of 6 TW during 1979–2009. At the same month, the smallest heat flux (<2 TW) is found at East Siberian Sea basin characterized by cold SAT and less river discharge from Kolyma and the neighboring small rivers. Beaufort Sea

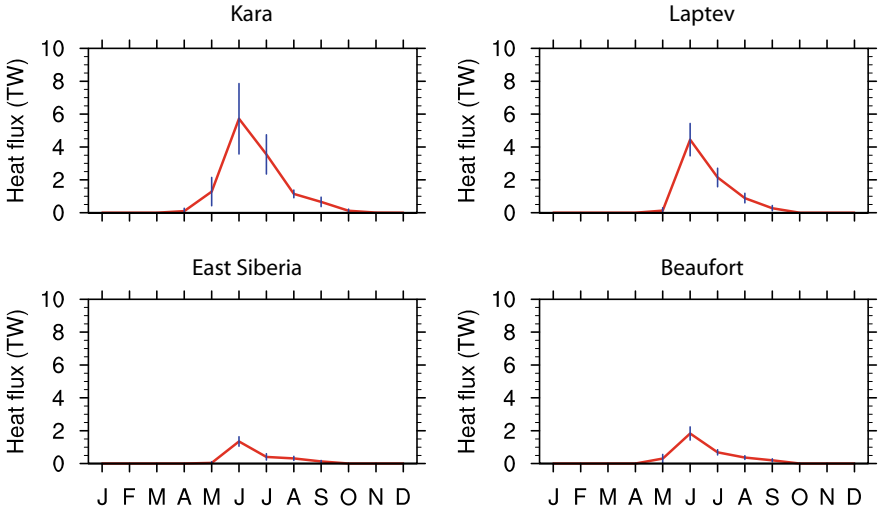

Fig. 25.5 Comparison of modeled river heat flux for the four Arctic Sea basins, defined by Lammers et al. (2001), over seasonal time scale. The vertical lines represent one standard deviation for the model simulation for the period of 1979–2009 (Park et al. 2016 © American Meteorological Society. Used with permission)

basin represented by Mackenzie river has similar magnitude of heat flux with the East Siberian Sea basin. Tw generally exhibits the highest value in August, while the heat flux significantly decreases since June (Fig. 25.5), implicating to the decreasing discharge. There is no heat flux from October over the winter. In reality, a large portion of the heat flux is found in the spring and early summer, indicating the large influence of discharge seasonal cycle. Park et al. (2016) analyzed warmer Tw and increased discharge in the early spring, which suggests the seasonal increases of the heat flux in the recent years and then the impact on the melt of Arctic sea ice. The recent analyses reported increases in the winter river discharge (Smith et al. 2007; Shiklomanov and Lammers 2009). During winter, the Arctic rivers are discharging smaller freshwater close to 0 < °C, flowing under the river ice. However, most models defined the winter Tw to be 0 °C, which is not natural even though the discharge amount is not large.

During the warmer months of the year the timing of river flow, river temperature, and energy flux in the large Russian drainage basins are typically out of phase (Lammers et al. 2007). An example can be seen in the Yenisey River at Igarka from

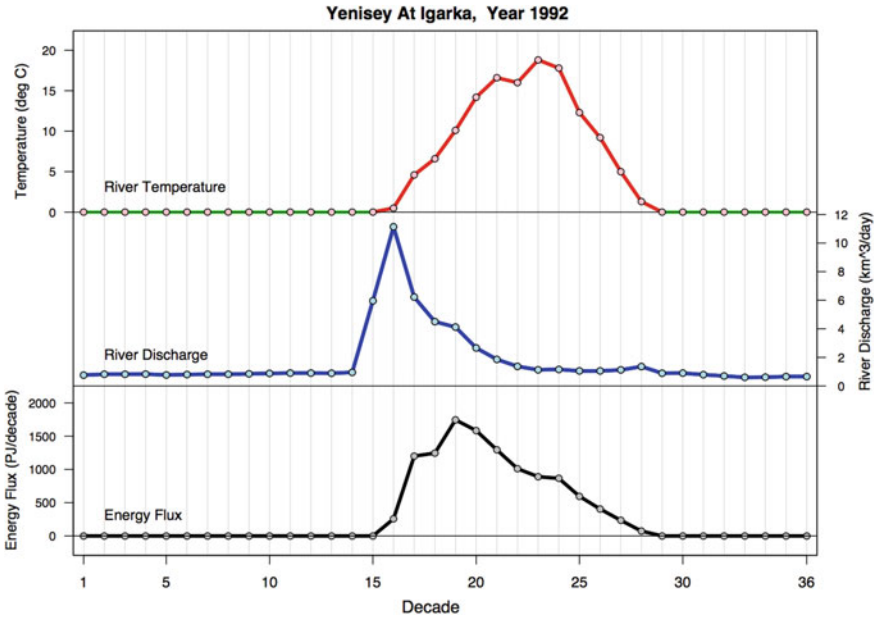

Fig. 25.6 In most gauges and years, river discharge tends to peak first and temperature tends to peak last while the energy flux typically will peak in between these two. This is illustrated for a single year of data, 1992, for the Yenisey drainage basin. River discharge (middle, blue line) peaks a month before the energy flux (bottom, black line), which in turn peaks approximately 40 days before water temperature (top). The top curve also shows two versions of the temperature data T1 (red line) and T2 (green line, values filled in at 0 °C during the cold season). Decade refers to a period of approximately 10 days. Figure modified from Lammers et al. (2007)

1992 (Fig. 25.6). River flow peaks first from the spring freshet in response to the large snowmelt pulse, while river temperature peaks later in the summer as the water continues to warm in response to increasing air temperatures. The maximum energy flux, which is a combination of river flow and water temperature, peaks in early summer between the flow and temperature peaks. The time difference between the flow and temperature peaks in any given year has implications for the maximum energy flux to the Arctic Ocean. As warming occurs in the Arctic, we would expect to see earlier spring river discharge peaks while the maximum river temperature would remain in late summer or occur even later. As the two peaks diverge the maximum energy flux could be lower. This counterintuitive system response can be partly demonstrated by the existing historical data, where increasing the time difference between the flow and temperature peaks reduced maximum energy flux (Fig. 25.7).

25.4 Impact of River Heat Flux to Sea Ice

The Arctic Ocean has experienced unprecedented changes, particularly the loss of sea ice, in recent decades. Freshwater impact to the polar ocean is a main research topic. Prowse et al. (2015) synthesized recent progress and research and pointed out an urgency to closely monitor changes in the Arctic freshwater system via remote sensing technology, including the interactions between northern rivers and the coastal ocean. Nghiem et al. (2014) used satellite observations to investigate the distribution pattern of surface water in the Beaufort Sea. Two different algorithms were used to measure surface temperature from MODIS. To observe the change caused by warm water from the Mackenzie River, open water surface temperature (OWST) in the Beaufort Sea region was compared before and after the landfast sea ice barrier was breached to release the water from the Mackenzie River into the Beaufort Sea.

Clear sky conditions on 14 June in 2012 allowed the use of MODIS satellite data to estimate the Beaufort Sea OWST. The OWST was low while the landfast ice hindered the river discharge (Fig. 25.8a). Warm water was observed to the west of Banks Island, possibly from the inland water runoff. The OWST on 5 July 2012 (Fig. 25.8b) revealed the extrusion of warm water in the Beaufort Sea when the landfast sea ice had disappeared and the river mouths were fully opened for water discharge from the Mackenzie River. The warmest water was observed near the coast of the Mackenzie Delta, 13 °C at 147 km, 10 °C at 287 km, 8 °C at 350 km, and 2 °C as far as 456 km from the Mackenzie River mouth. As the warm river water extended farther out into the Beaufort Sea, the OWST became lower and mixed with cooler water in a complex swirling pattern (Fig. 25.8b). The warm water west of Banks Island also became more extensive and started to connect to the Mackenzie warm water mass.

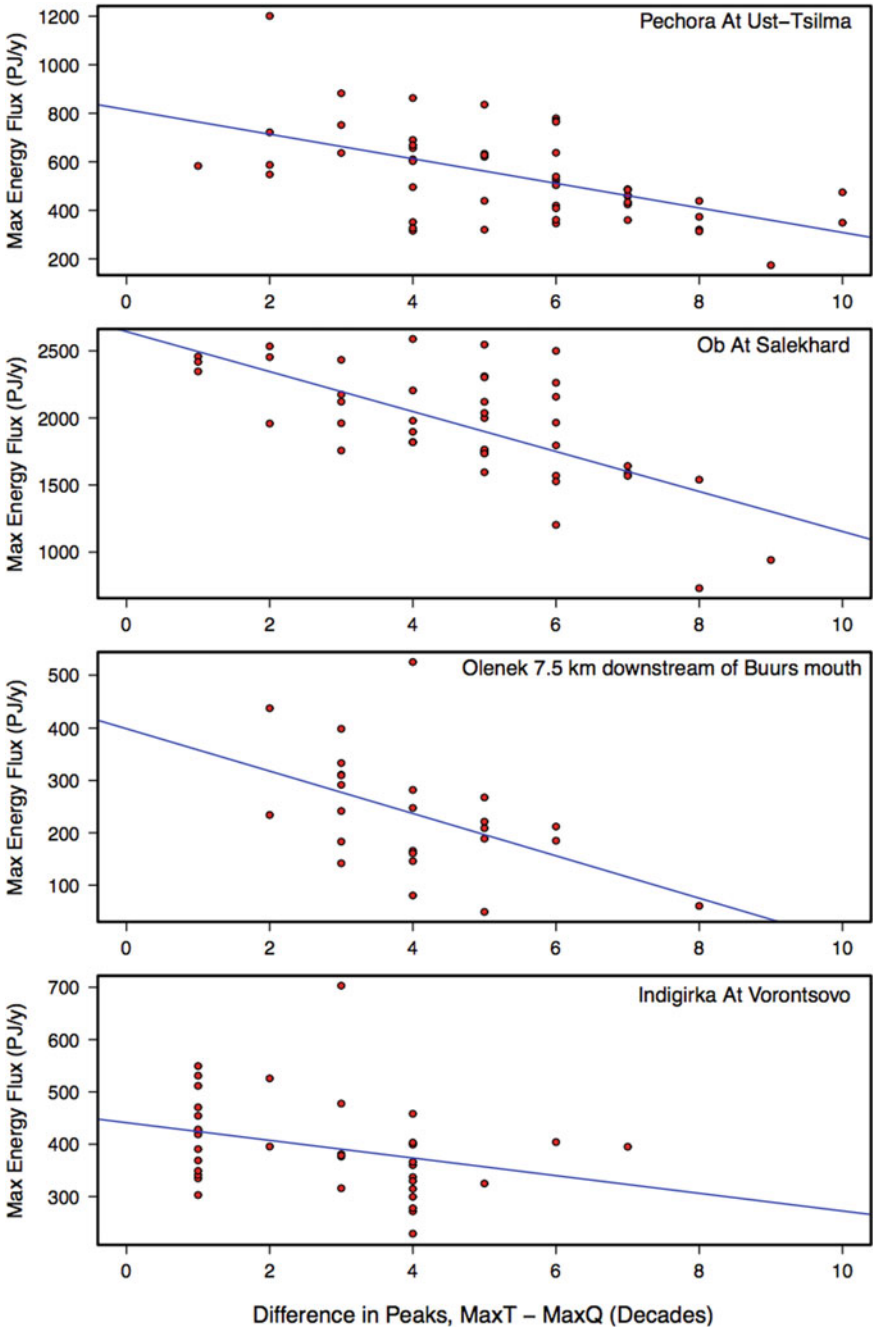
Pechora At Ust−Tsilma
Max Energy Flux (PJ/y)
1200
1000
800
600
400
200
0
2
4
6
8
10
Ob At Salekhard
Max Energy Flux (PJ/y)
2500
2000
1500
1000
Olenek 7.5 km downstream of Buurs mouth
Max Energy Flux (PJ/y)
500
400
300
200
100
Indigirka At Vorontsovo
Max Energy Flux (PJ/y)
700
600
500
400
300
Difference in Peaks, MaxT − MaxQ (Decades)

◀ **Fig. 25.7** Maximum energy flux from the drainage basins appears to be limited by the difference in timing between the peaks in temperature and river discharge. For each gauge-year with a positive difference between maximum decadal temperature and maximum river discharge the annual maximum energy flux is shown for selected watersheds. Blue diagonal lines show the linear regression line. Decade refers to periods of approximately 10 days. Figure modified from Lammers et al. (2007)

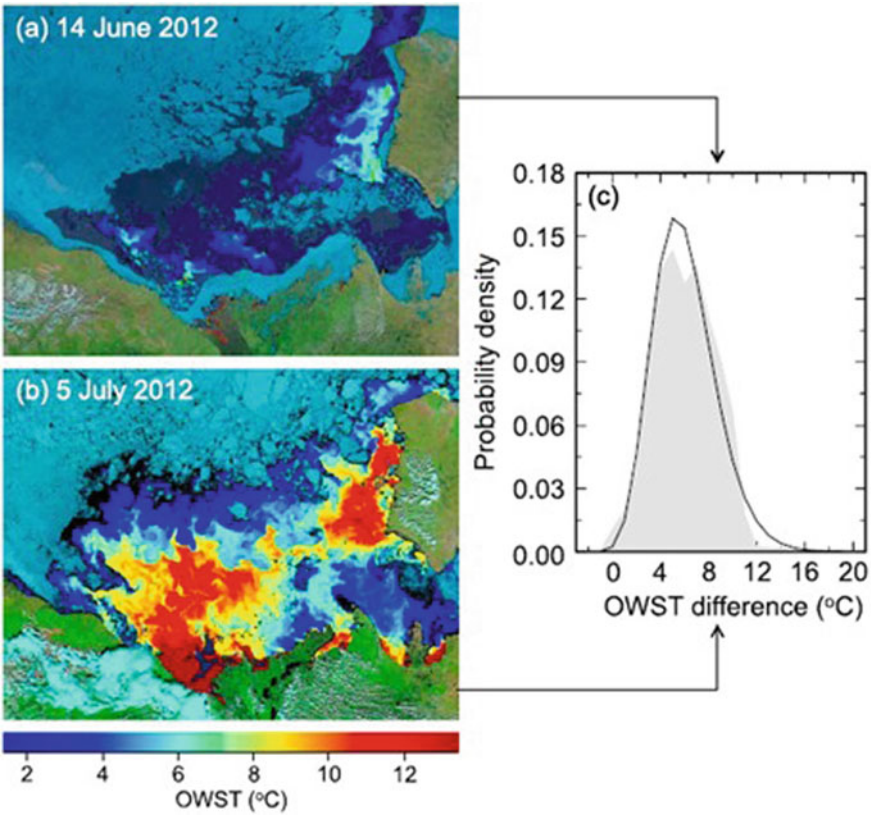

Fig. 25.8 Open water surface temperature (OWST) in °C, measured by MODIS AG1 on 14 June 2012. **a** before the Mackenzie River water broke through the landfast sea ice barrier, and on 5 July 2012, **b** after warm waters from the Mackenzie discharged into the Beaufort Sea. Sea ice is indicated by the steel blue color on the sea surface, and **c** For the measured and calculated histograms of the temperature difference in °C between the two cases in Fig. 25.8a and b. The temperature difference is calculated over each pixel that is open water in both cases (Nghiem et al. 2014)

The histogram of this temperature difference (Fig. 25.8c) shows a mean increase in OWST by 6.5 °C between the two cases before and after the Mackenzie warm water intrusion. Analyses of observation data (Yang et al. 2014) and model simulations (Park et al. 2016) show water temperatures ranging from 13 to 19 °C in the open water season at the downstream reaches of the Mackenzie river, with the heat flux peaking in July. These results in general agree with and support the information derived from the MODIS data. The consistent results between the studies are encouraging and clearly indicating the need to combine in situ observations with remote sensing measurements for northern environmental research and applications.

25.5 Discussion and Conclusion

It is clear that the impact of changes in large northern river thermal flux to the Arctic Ocean needs research attention, although some uncertainty and discrepancy exist in recent analyses of river heat flux. For instance, Liu et al. (2005) found, over the Lena basin, positive changes in stream temperature during the early and mid-June. River discharge also increased in this peak flow period (Ye et al. 2003). As a result, the heat flux increased in June by 23% for the Lena basin. Park et al. (2016) reported, through large-scale model runs, the heat flux increase for Siberian Rivers, in the range of 0.013–0.084 TW, which was expected to contribute to warmer water temperature and additional energy to the Arctic Ocean. They also found significant warming of water temperature and considerable discharge increases during early spring, which may affect the melt of Arctic landfast/sea ice and atmosphere dynamics through albedo and moisture feedbacks (Park et al. 2016). Lammers et al. (2007) detected significant increases in river temperature; however, they do not see a pattern of increases in energy flux for the large Siberian rivers. This discrepancy is perhaps due to the complex nature of a drainage system. Energy flux is a multiplicative combination of both the temperature and discharge. Maximum values in energy flux from the drainage basins occur when the two peaks of the uniform curve of the temperature signal and the asymmetric snowmelt dominated river discharge coincide. If the two peaks diverge, for example, owing to earlier timing of the peak river discharge or a later peak of high water temperature, then overall energy flux may go down.

In the European part of Russia, Lammers et al. (2007) found significant increases in the annual maximum temperatures for four drainage basins (Onega, Severnaya, Mezen, and Pechora). Recent studies of small watersheds with areas less than 50,000 km^2 across the Russian Arctic suggest a shift in the timing of daily maximum discharge to earlier in the spring (Shiklomanov et al. 2007), and increases in trend for minimum discharge were strongest during May and November as the result of a shortening in the cold season (Smith et al. 2007). Therefore, it is likely that increasing temperature, but a shift to earlier peak river flow reduces the overall energy flux in the open water season. There might be a general pattern that appears

to serve as a limit to the flux of area averaged energy from the river systems. As the difference between the decade of maximum temperature and maximum discharge increases (as the timing between the peaks of temperature and discharge diverge), there would be a decrease in the maximum energy flux values. Greater divergence of the peak temperature and discharge creates a tendency toward lower energy flux from the northern basins (Lammers et al. 2007).

Consistent, long-term hydrometric and climatic observations and records are essential for global change research particularly over the vast northern regions with sparse monitoring networks. Hydroclimatic networks have been losing gauges since the mid-1980s in Russia and a delay in the delivery of national agency-collected data to the research community (Shiklomanov et al. 2002). The Russian river temperature data set shows similar features of a decline of available data after 1990 (Lammers et al. 2007). For applications requiring more rapid acquisition of river temperature data, the ongoing collection of discharge and water temperature data is essential. The other option to explore is the use of remote sensing of river (Cherkauer et al. 2005; Handcock et al. 2006) and lake (Bussières and Schertzer 2003) temperatures in combination with near-real time in situ data acquisition over the northern watersheds.

It is clear that numerical modeling, in conjunction with satellite remote sensing and other ancillary data, provides a means for spatial and temporal extrapolation of sparse ground observations and identifying regional hot spots, that require more detailed observations and process investigations. Model simulation experiments also provide an efficient way to diagnose underlying processes and interactive effects driving observed changes. The model framework such as the land process model (CHANGE) coupled with other models of river ice and water temperature dynamics, runoff routing, and discharge, demonstrate progress and advancement that can quantitatively assess changes in river thermal regimes.

This chapter presents a detailed overview of river thermal regime and heat flux for the large rivers in the Siberian regions. Due to the limited water temperature observations and data over the northern regions of the North America, this chapter is not able to discuss the variability and change in river thermal conditions. There is, therefore, a serious knowledge gap in northern river temperature and heat contribution along the arctic coast of North America. Some key questions facing the arctic research communities may include: what are the fundamental water temperature characteristics along the northern coast of Canada and Alaska; what are the amounts and changes in river heat flux to the northern seas; and what are the process and linkage between regional climate change and river thermal features over space and time. To address these issues, it is necessary to: (a) develop regional water temperature dataset and combine them with discharge and climate information across the northern watersheds; (b) apply advanced hydrologic-biological models to simulate and reconstruct the past water temperature and heat flux across the northern regions and basins; (c) continue to explore remote sensing data/products in the investigations of river water temperature and heat transport

processes; (d) develop and improve coupled land–ocean models to better understand land-coastal linkage and connections across the northern coastal regions; and most importantly (e) we call on the hydrometric agencies of the arctic nations to continue regular and comprehensive monitoring of these important river systems.

References

Bussières N, Schertzer WM (2003) The evolution of AVHRR derived water temperature over lakes in the Mackenzie Basin and hydrometeorological applications. J Hydrometeorol 4:660–672

Cherkauer KA, Burges SJ, Handcock RN et al (2005) Assessing satellite-based and aircraft-based thermal infrared remote sensing for monitoring Pacific Northwest River temperature. J Am Water Resour Assoc 41(5):1149–1159

Costard F, Gautier E, Brunstein Yang D et al (2007) Impact of the global warming on the fluvial thermal erosion over the Lena River in Central Siberia. Geophys Res Lett 34(14):L14501. https://doi.org/10.1029/2007GL030212

Davies KF (1975) Mackenzie river input to the Beaufort Sea. Beaufort Sea Technical Report #15. Water Survey of Canada, Department of the Environment. Calgary, Alberta, Canada

Elshin Y (1981) River heat runoff in the European part of Russia. Meteorol Hydrol 9:85–93

Handcock RN, Gillespie AR, Cherkauer KA et al (2006) Accuracy and uncertainty of thermal-infrared remote sensing of stream temperatures at multiple spatial scales. Remote Sens Environ 100:427–440

Holmes RM, McClelland JW, Peterson BJ et al (2012) Seasonal and annual fluxes of nutrients and organic matter from large rivers to the Arctic Ocean and surrounding seas. Estuar. Coasts 35:369–382. http://dx.doi.org/10.1007/s12237-011-9386-6

Lammers R, Shiklomanov A, Vorosmarty C et al (2001) Assessment of contemporary arctic river runoff based on observational discharge records. J Geophys Res 106(D4):3321–3334

Lammers RB, Pundsack JW, Shiklomanov AI (2007) Variability in river temperature, discharge, and energy flux from the Russian pan-Arctic landmass. J Geophys Res 112:G04S59. https://doi.org/10.1029/2006jg000370

Liu B (2004) Siberia Lena river thermal regimes and changes, MS thesis, Water and Environmental Research Center, University of Alaska Fairbanks, 92 p

Liu B, Yang D, Ye B, Berezovskaya S (2005) Long-term open-water season stream temperature variations and changes over Lena River Basin in Siberia. Global Planet Change 48(1–3):96–111. https://doi.org/10.1016/j.gloplacha.2004.12.007

Lowney CL (2000) Stream temperature variation in regulated rivers: evidence for a spatial pattern in daily minimum and maximum magnitudes. Water Resour Res 36(10):2947–2955. https://doi.org/10.1029/2000WR900142

Mackay JR, Mackay DK (1975) Heat energy of the Mackenzie River. In: Further hydrologic studies in the Mackenzie valley, Canada (Environmental-Social Committee Northern Pipelines). Task force on northern oil development report, Ottawa, Information Canada, pp 1–23

Marsh P, Prowse TD (1987) Water temperature and heat flux at the base of river ice covers. Cold Reg Sci Technol 14:33–50

Nghiem SV, Hall DK, Rigor IG et al (2014) Effects of Mackenzie River discharge and bathymetry on sea ice in the Beaufort Sea. Geophys Res Lett 41:873–879. https://doi.org/10.1002/2013GL058956

Park H, Yoshikawa Y, Oshima K et al (2016) Quantification of warming climate-induced changes in terrestrial Arctic river ice thickness and phenology. J Clim 29:1733–1754. https://doi.org/10.1175/JCLI-D-15-0569.1

Prowse T, Bring A, Mård J, Carmack E, Holland M, Instanes A, Vihma T, Wrona FJ (2015) Arctic freshwater synthesis: summary of key emerging issues. J Geophys Res Biogeosci 120:1887–1893. https://doi.org/10.1002/2-15JG003128

Shiklomanov AI, Lammers RB, Vorosmarty CJ (2002) Widespread decline in hydrological monitoring threatens pan-Arctic research. EOS Trans AGU 83(2):13–17

Shiklomanov AI, Lammers RB, Smith L et al (2007) Temporal and spatial variations in maximum discharge from a new river flow data set for the Eurasian pan-Arctic. J Geophys Res 112: G04S53. https://doi.org/10.1029/2006jg000352

Shiklomanov AI, Lammers RB (2009) Record Russian river discharge in 2007 and the limits of analysis. Environ Res Lett 4045015 (9 pp)

Sinokrot BA, Stefan HG (1993) Stream temperature dynamics: Measurement and modeling. Water Resour Res 29(7):2299–2312. https://doi.org/10.1029/93WR00540

Smith L, Pavelsky TM, MacDonald GM et al (2007) Rising minimum flows in northern Eurasian rivers suggest a growing influence of groundwater in the high-latitude water cycle. J Geophys Res. https://doi.org/10.1029/2006JG000327

Tank SE, Raymond PA, Striegl RG et al (2012) A land-to-ocean perspective on the magnitude, source and implication of DIC flux from major Arctic rivers to the Arctic Ocean. Global Biogeochem Cycles 26:GB4018. http://dx.doi.org/10.1029/2011GB004192

van Vliet MTH, Ludwig F, Zwolsman JJG et al (2011) Global river temperatures and sensitivity to atmospheric warming and changes in river flow. Water Resour Res 47(2):W02544. https://doi.org/10.1029/2010WR009198

Webb BE, Nobilis F (1995) Long term water temperature trends in Austrian rivers. Hydrol Sci J 40 (1):83–96

Whitefield J, Winsor P, McClelland J et al (2015) A new river discharge and river temperature climatology data set for the pan-Arctic region. Ocean Modell 88:1–15. https://doi.org/10.1016/j.ocemod.2014.12.012

Yang D, Ye B, Kane D (2004a) Streamflow hydrology changes over Siberian Yenisei river basin. J Hydrol 296(1–4):59–80. https://doi.org/10.1016/j.jhydrol.2004.03.017

Yang D, Ye B, Shiklomanov A (2004b) Discharge characteristics and changes over the Ob river watershed in Siberia. J Hydrometeorol 5(4):595–610. https://doi.org/10.1175/1525-7541(2004)005%3c0595:DCACOT%3e2.0.CO;2

Yang D, Liu B, Ye B (2005) Stream temperature changes over Lena river Basin in Siberia. Geophys Res Lett 32:L15401. https://doi.org/10.1029/2004GL021568

Yang D, Marsh P, Ge S (2014) Heat flux calculations for Mackenzie and Yukon rivers. Polar Sci 8 (3):232–241. https://doi.org/10.1016/j.polar.2014.05.001

Yang D, Peterson A (2016) River water temperature in relation to local air temperature in the Mackenzie and Yukon Basins. Arctic 70(1):47–58. https://doi.org/10.14430/arctic4627

Ye B, Yang D, Kane D (2003) Changes in Lena River streamflow hydrology: human impacts vs. natural variations. Water Resour Res 39(7):1200

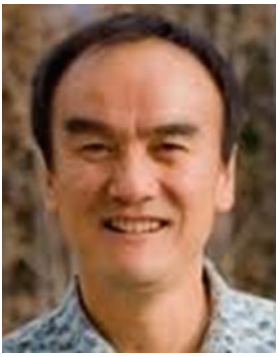

Dr. Daqing Yang is a Research Scientist at the Watershed Hydrology and Ecology Research Division, Environment and Climate Change Canada. He is also Affiliate Research Professor at the International Arctic Research Center, Univ. of Alaska Fairbanks. Over the past 25 years, he has conducted cryosphere system research in China, Canada, Japan, USA, and Norway. His primary research activities/interests include cold region hydrology and climate, particularly Arctic large river streamflow regime and change, snow cover and snowfall measurements, climate change and human impact to regional hydrology, and applications of remote sensing in cold regions. He has served as journal editor and subject editor for IAHS publications (cold region hydrology, northern research basin water balance, and cold/mountain region hydrological systems under climate change), and WMO technical reports (solid precipitation measurement intercomparison and integrated global observing strategy cryosphere theme). He also contributed as review and/or author to the IPCC Reports, and the Arctic Council's Snow, Water, Ice and Permafrost in the Arctic (SWIPA 2017 and follow up) assessment. His current research focuses on investigating the impacts of climate variability/change and human activities on hydrologic system across the broader northern regions.

Dr. Shaoqing Ge is an Engineer in the Engineering Department of American Water and works on buried infrastructure management and water system comprehensive planning studies. His areas of expertise include hydro-climate analysis of watersheds, Prestressed Concrete Cylinder Pipe (PCCP), numerical analysis, pipeline management, asset risk assessment, forensic study of asset failures, and hydraulic analysis of water distribution systems. He received a B.S. in Civil Engineering from China University of Petroleum, an M.S. in Hydraulic Structural Engineering from China Institute of Water Resources and Hydropower Research, an M.S. in Civil Engineering from University of Alaska Fairbanks, and a Ph.D. in Civil Engineering from Virginia Tech. He now serves as a Trustee in the Distribution and Plant Operations Division of AWWA, and the Chair of the Planning Committee for the AWWA Water Infrastructure Conference 2020.

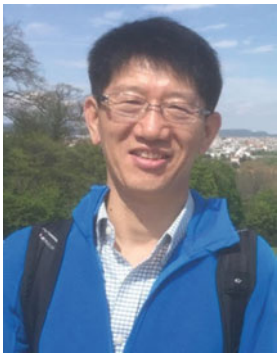

Dr. Hotaek Park is a Senior Scientist at JAMSTEC. He earned his Ph.D. at Graduate School of Bioagricultural Sciences, Nagoya University in 2000. Then, he worked at two Japanese Institutes as postdoctoral fellowship and joined the position of JAMSTEC research scientist in 2007. He is an expert on hydrology, biogeochemistry, and climate researches in cold regions, with interests in evaluating changes in land surface processes under climate changes and predicting future changes using land surface model, remote sensing data, reanalysis products, in site observations, and model outputs. He has the author/co-author of numerous scientific articles that have published on a variety of peer-reviewed journals, conference proceedings, and books. His recent research is focused on assessing impacts of changing snow and permafrost on hydrological processes in the context of climate variability and interactions between declining Arctic sea ice and terrestrial ecohydrologic processes coupling models of land–atmosphere–ocean processes.

Richard L. Lammers is a Research Assistant Professor in the Earth Systems Research Center, Institute for the Study of Earth, Oceans, and Space at the University of New Hampshire. He was one of the founding members of the Water Systems Analysis Group and has been Co-Director since 2008. He received a B.Sc. (Geography and Economics), a M.Sc. and a Ph.D. in 1998 (Physical Geography) from the University of Toronto, Department of Geography. The focus of Dr. Lammers' research is understanding the dynamics of global and regional-scale hydrology with an emphasis on human interactions within the hydrological cycle. His most recent work involves integrating hydrology with power generation systems, economic models and water rights to understand the resilience and vulnerability of water, land, food, and energy systems. His research interests also include understanding the convergence of human and biogeophysical datasets, modeling, and analysis; inter-basin hydrological transfers; tracking glacier water through land surface hydrology; coupling agent-based and physically-based models; the hydrological cycle at high latitudes; future change; spatial datasets and geoprocessing; river networks; and techniques of Internet-based data serving and analysis.

Cold Region Hydrologic Models and Applications

26

Hotaek Park, Yonas Dibike, Fengge Su, and John Xiaogang Shi

Abstract

Over the recent decades, the warming in Arctic has affected changes in the terrestrial hydrologic processes. Unfortunately, the number of hydrometeorological observing stations in the region has decreased. To reduce the limitation in observation, a number of process-based and distributed models have been developed for simulating the hydrological processes in a changing climate. The current generations of models are able to reasonably reproduce the prominent cold region hydrologic processes, such as degrading permafrost, decreasing snow extent, increasing river discharge and evapotranspiration, and increasing streamflow temperature. These models enhance our understanding of the response of Arctic terrestrial processes to climate change and variation. However, the model representations for some of the Arctic hydrological processes are still not yet sufficient and need further improvements. This chapter

H. Park (✉)
Research Institute for Global Change, Japan Agency for Marine-Earth Science and Technology, Yokohama, Kanagawa, Japan
e-mail: park@jamstec.go.jp

Y. Dibike
Watershed Hydrology and Ecology Division, Environment and Climate Change Canada, Victoria, BC, Canada
e-mail: yonas.dibike@canada.ca

F. Su
Institute of Tibetan Plateau Research, Chinese Academy of Sciences, Beijing, China
e-mail: fsu@itpcas.ac.cn

J. X. Shi
School of Interdisciplinary Studies, University of Glasgow, Dumfries, Scotland, UK
e-mail: John.Shi@glasgow.ac.uk

D. Yang and D. L. Kane (eds.), *Arctic Hydrology, Permafrost and Ecosystems*,
https://doi.org/10.1007/978-3-030-50930-9_26

provides an overview of changes in key processes and conditions of the Arctic terrestrial hydrology based on a synthesis of observations and model simulations, and presents recommendations for further development and improvement of cold region hydrologic models.

26.1 Introduction

The Arctic system is composed of various components and processes that are complexly intertwined through interaction and feedback. A change in one of the system components influences the others, hence further amplifying the magnitude of the change through those complex implications. The Arctic is currently undergoing changes never before seen in historic times, such as decreasing sea ice, degrading permafrost, decreasing snow cover, and expanding lake and wetland. These changes are closely connected to the hydrological cycle and the freshwater budget of the Arctic region. The Arctic terrestrial regions are covered by cryospheric components (e.g., glacier and snow) that are very vulnerable to climate warming and the freshwater from this region has the potential to disrupt deep convection of the Arctic Ocean, although the annual amounts are smaller (Prowse et al. 2015). Both observations and simulations have addressed the changes in the Arctic freshwater system, particularly permafrost degradation and increases in river discharge (Peterson et al. 2002). The increase in river discharge was very significant in the recent few decades when the Arctic warming was intensive. These changes have the potential to strongly influence the freshwater and heat budget of the Arctic Ocean and thus the global ocean circulation (Jahn and Holland 2013), sea level rise (Rignot et al. 2011), and the terrestrial carbon cycle (Wrona et al. 2016).

The changes in the Arctic system have been captured through observations. Russia has a long history of hydrological observations in its territory starting from the beginning of the twentieth century. The observations are mostly made at the tributaries as well as the outlet of large rivers, and those measurements have provided evidence showing the increasing discharge from the Russian large rivers (Peterson et al. 2002). However, the number of observational stations began to decrease with the collapse of the old Soviet Union, and the data quality has simultaneously suffered due to the decreasing number of observational experts. In North America, there is a gradual move toward replacing most manual measurements to automatic systems, while the station density is continuously decreasing. In particular, the decrease in northern Canada is worrisome, especially since the end of 1970s (Park et al. 2015). The reduction in the number of measuring stations affects the quality of assessments of the environmental changes. Satellite observations may supplement the reduced number of measuring stations; however, they still have technical limitations in Arctic monitoring, sometimes even increasing uncertainties in the observational records. Hence, it still remains challenging to quantitatively estimate the freshwater budget of the Arctic region from the satellite observations,

and their shorter and more recent observational periods limit the extrapolation of the observations to different time periods and regions.

A large proportion of runoff from the Arctic terrestrial drainage system (up to 41% according to WCRP 1996) originates from ungagged basins and even those that are gaged are based on scattered measurement over large regions and for relatively short time periods. Therefore, models are essential as a means of extrapolating from those available measurements in both space and time, particularly to the ungagged catchments (where measurements are not available) and into the future (where measurements are not possible) to assess the likely impacts of future hydrological change (Beven 2012). Cold region hydrological models can help us to achieve a consistent and representative estimate of the magnitude and spatial distribution of the ever changing Arctic terrestrial water budget for both the contemporary and future time periods. Such models are also an integral and necessary part of the scientific investigation process and provide a powerful tool for developing and testing hypotheses with respect to various hydrologic processes (Lique et al. 2016).

Land surface hydrologic variables were regarded as separable parameters that could be independently prescribed as boundary conditions within climate models. Hence, land surface models (LSMs) were developed to simulate energy, water, and carbon exchanges between the atmosphere and the terrestrial surface over a wide range of time and space scales based on empirical and physical principles. The model simulations helped our understanding of changes of the terrestrial processes in regions with different landscapes and climates. LSMs have been incorporated into climate models (e.g., general circulation models and regional climate models) as the lower boundary of those models. Manabe (1969) developed the first generation of LSM, a bucket model with constant soil depth and water-holding capacity. The model expressed that evaporation is controlled by soil water content and precipitation generates runoff as soil moisture exceeds the saturation level. In 1980s, the radiative, momentum, and heat/mass transfer properties of vegetation surface were parameterized into LSM, including more biophysical control of the vegetation–soil system to evapotranspiration (Dickinson 1984; Sellers et al. 1986). Canadian LSM emphasized the importance of boreal winter processes in the simulation of global climate (Verseghy et al. 1993). LSMs have also treated the surface vegetation as one of the prescribed parameters. During the past few decades, however, various dynamic global vegetation models have been developed and coupled into the land surface model, which made it possible to simulate vegetation change and the associated hydrological and biogeochemical fluxes in responses to climate warming (Foley et al. 1996; Cox et al. 1998; Levis et al. 2004).

However, the description of hydrological processes quite widely varies between LSMs. Hydrologic models are generally simplifications of the real system, and they can be of different levels of complexity and may incorporate different component interactions (Lique et al. 2016). For example, *empirical models* can be built by identifying empirical relationships among different hydrologic process variables based on field observations or laboratory measurements, while *conceptual models* can be designed to illustrate how the different processes across the hydrologic

system link together and interact with each other. The relationships in conceptual model may be more or less complex, but usually employs simple mass balance equations. On the other hand, processed-based hydrological models integrate mathematical relationships describing the dominant fluxes of energy and water in each of the various space and time dependent hydrological processes, such as snow cover evolution, permafrost dynamic, infiltration, etc. While *distributed models* try to solve these mathematical relationships over a uniformly distributed grid with the aim of representing spatial variability and hydrologic connectivity throughout the model domain, *semi-distributed models* lump the various physical processes and their parameters into sub-basins so that they are easier to setup and require relatively shorter running time.

Typical futures of cold region hydrologic models are that they use physically based algorithms to quantify hydrological cycle and cold region hydrological processes, such as blowing snow, snow interception in forest canopies, sublimation, snowmelt, infiltration into frozen soils, permafrost dynamics, actual evaporation, and radiation exchange to complex surfaces (Pomeroy et al. 2007). These processes are strongly intertwined and the effects of any disturbed processes are generally revealed within shorter time scale, while some have longer memory that the effects appear on seasonal and/or annual scales. One particular example is permafrost, where changes to some disturbances may last from over a season to a century scale, strongly affecting the Arctic hydrology. Many LSMs still have some specific problems, such as too shallow soil columns representing the permafrost dynamics (Koven et al. 2013; Slater and Lawrence 2013). However, the models have improved some important dynamical processes such as perched or suprapermafrost water table (Swenson et al. 2012), excess ice (Lee et al. 2014), and hydrological impact of organic soils (Lawrence and Slater 2008). Snow processes are strongly implicated in the permafrost thermal state as well as river discharge. Most LSMs represent the snow processes based on physical principles, which soundly capture earlier snowmelt induced by the warming climates and hence earlier timing of spring peak discharge (Shi et al. 2015; Park et al. 2017). River ice processes were included into LSMs (Park et al. 2016b), which modeled the trend toward shorter ice-cover period and the subsequent warming of river water temperature, consistent with the climate warming (Park et al. 2017). Despite the efforts toward more targeted model development that have been made during the past few decades, models still have limitations and biases in the simulations. However, the models are powerful tools to examine the functioning of the Arctic hydrology system and provide insight on where knowledge is insufficient, motivating past and future research needs (Lique et al. 2016).

The goals of this chapter are to provide an overview of our current knowledge on the functioning of the Arctic hydrology system through modeling perspective and introduce ongoing activities for improving model performance with respect to the various cold region hydrological processes at different time and spatial scales. It also discusses the gaps in our current understanding and the needs and directions of future model developments to better understand the Arctic hydrologic system.

26.2 Historical Background

26.2.1 Major Hydrologic Processes in Arctic Region

The main hydrological processes in the terrestrial Arctic with implications on freshwater storages and fluxes in the northern region are precipitation, evapotranspiration (ET), surface runoff and channel flows, permafrost and groundwater hydrology, and river and lake ice (Bring et al. 2017a). A substantial proportion of Arctic annual precipitation is falling and stored as snow and released to the river network in a relatively short time window during spring snowmelt. The phase of precipitation and the intensity with which precipitation is delivered influences the water balances and runoff generation. The majority of precipitation over most Arctic basins returns to the atmosphere as ET that links the water and energy cycles and couples the land to the atmosphere. River discharge is the other major water flux out of Arctic basins conveying water, heat, sediments, carbon, and nutrients to the coastal domain and to the Arctic Ocean. Most of the rivers flow to the Arctic Ocean during the spring snowmelt and in summer. Permafrost and its active layer dynamics govern a wide range of surface and subsurface processes across permafrost landscapes and control mechanisms of runoff generation. Due to the large extent of the area underlain by permafrost, the active layer thickness and behavior vary across the terrestrial Arctic region, which influences soil moisture and storage. Seasonal changes in river and lake ice-cover are also prominent features of Arctic freshwater systems. The freshwater ice produces numerous effects on various fluxes and flow dynamics in the Arctic regions.

A number of studies have identified changes in the Arctic freshwater system over the recent decades, as warming climate has caused many changes in the terrestrial Arctic freshwater processes. Earlier snowmelt, decreasing snow extent, permafrost degradation with melting of ice-rich surface, expansion of thermokarst lake, increasing vegetation biomass, and northward vegetation movement are some of the changes observed in the region. These changes are also linked to surface and subsurface hydrological processes and river flows, consequently amplifying the complexity of interaction, and feedbacks between the processes. These complexities in turn make it difficult to precisely predict the magnitudes and directions of future changes in hydrologic processes due to climate warming.

26.2.2 Observations Over the Arctic Watersheds

Incomplete knowledge about the magnitude and spatial-temporal pattern of high latitude precipitation has been a big challenge in Arctic hydrologic research over the years and is still a major obstacle to our current efforts to quantify the water and energy budget in the region. The major factors which contribute to uncertainties in the estimation of precipitation in the high latitude regions include: sparseness of the precipitation observation networks; uneven distribution of measurement sites, (i.e.,

biased toward coastal and the low-elevation areas); spatial and temporal discontinuities of precipitation measurements induced by changes in observation methods and by different observation techniques used across national borders, and the biases in gauge measurements, such as wind-induced undercatch, wetting and evaporation losses, and underestimation of trace amount of precipitation (Goodison et al. 1998). Of the above factors, systematic errors in gauge measurements are particularly important, because these biases can reach up to 50–100% of the gauge-measured records at the cold and windy locations (Yang et al. 1998, 1999; Yang 1999; Yang and Ohata 2001). In particular, the reduction of observational stations in high latitudes can affect ground-truthing of satellite observations and the quality of reanalysis datasets, which may in turn influences model projections.

Seasonal snow cover over land area of the Arctic is another component of the terrestrial cryosphere that affects hydrology and provides important feedback to regional climate through its high albedo (e.g., Lemke et al. 2007). However, direct snow observations are very limited across large parts of the terrestrial Arctic with the lowest density of observational stations found at the northern part of Canada (Fig. 26.1). This lack of sufficient observing stations limits proper monitor and quantification of trends in snow cover extent, duration, and snow depth in the region (Rawlins et al. 2007), resulting in larger differences in snow amount between satellite observation and model simulation (Fig. 26.1). In Russia, meteorological stations largely increased since 1950, which contributed to improve model simulation for snow depth (Park et al. 2015) and captured the increasing trend of snow depth at the northern Siberia under the condition of warming temperature (Bulygina et al. 2009). However, the subsequent closing of those stations since 1990s coincides with the beginning of significant changes in the Arctic terrestrial processes and landscapes.

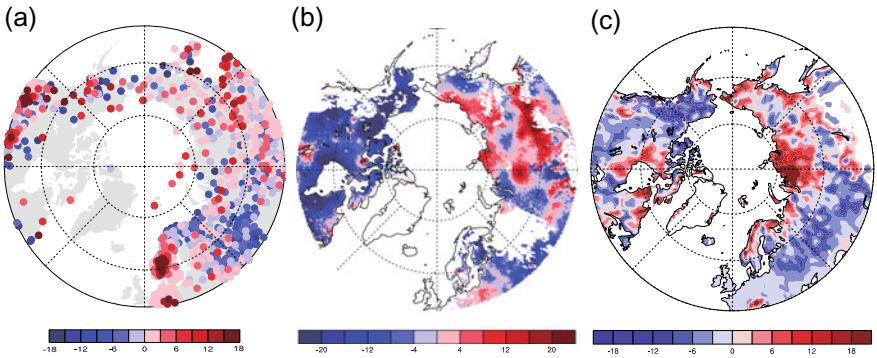

Fig. 26.1 Comparison of decadal anomalies of (**a**) observed mean winter (DJF) snow depth (cm), (**b**) mean winter snow water equivalent (mm) provided by GlobSnow, and (**c**) CHANGE model simulated mean winter snow depth (cm). The anomalies represent differences in 2001–2009 relative to 1991–2000 (Park et al. 2015)

Many river discharge monitoring stations in the Arctic have been closed, resulting in a declining capacity to observe changes in arctic hydrology and northern flowing rivers (Shiklomanov et al. 2006; Déry et al. 2011). Although the reduction in the number of observing stations is followed by specific recommendations on how to modify the monitoring network to make it more efficient (Mishra and Coulibaly 2010), it affects our capacity to identify where and when the greatest changes in river discharge have occurred. Bring et al. (2017b) developed a methodology to identify where monitoring stations should be placed to observe significant changes in river discharge at the pan-Arctic scale and suggested that central and eastern Siberia, Alaska, and central Canada are hot spots for the highest changes.

26.2.3 Changes in Observed and Simulated Hydrological Processes

Increases in snow depth have been observed over northern Siberia in the recent decades (Bulygina et al. 2009), consistent with model simulation (Park et al. 2015). The increase in snow depth was closely associated with an increase in the early winter precipitation (Park et al. 2013). Some studies suggested that the declining Arctic sea ice has resulted in increased precipitation in the form of snow over the Siberian regions (Ghatak et al. 2010; Cohen et al. 2012). On the other hand, Derksen and Brown (2012) have showed that late spring–early summer (May–June) Northern Hemisphere snow cover, which is predominant over the Arctic, decreased significantly over the last four decades. Using the Variable Infiltration Capacity (VIC) model, Shi et al. (2013) have also found that both observed and modeled North American and Eurasian snow cover have statistically significant negative trends from April through June over the period 1972–2006. Holland et al. (2006) found a significantly increasing trend in the ensemble average river runoff to the Arctic Ocean over the twenty century, with the simulated change of 7% increase in the Eurasian runoff; this result is in excellent agreement with the changes during 1936–1999 reported by Peterson et al. (2002). Haine et al. (2015) have also reported that the annual Arctic river discharge increased by 300 km^3 during 2000–2010 relative to 1980–2000. The increases include the contribution of the increased snow water, which is reflected by increases in the spring season river discharge (Park et al. 2017). An assessment of the combined daily discharge of Eurasian Arctic rivers also revealed an earlier and higher spring peak discharge in 2015 relative to the 1980–1989 average (Holmes et al. 2015).

However, with simultaneous changes in air temperature (Hinzman et al. 2005), precipitation (Yang et al. 2003; Rawlins et al. 2010), vegetation (Walker et al. 2010), and active layer thickness (Zhang et al. 2001), and complex interactions among these factors, the actual changes in both the timing and volume of spring streamflow may not be as simple as first expected (Déry et al. 2009). For example, some changes could be expected to result in earlier melt and runoff, while others would delay melt and/or runoff. Using five percentile timing measures of springtime

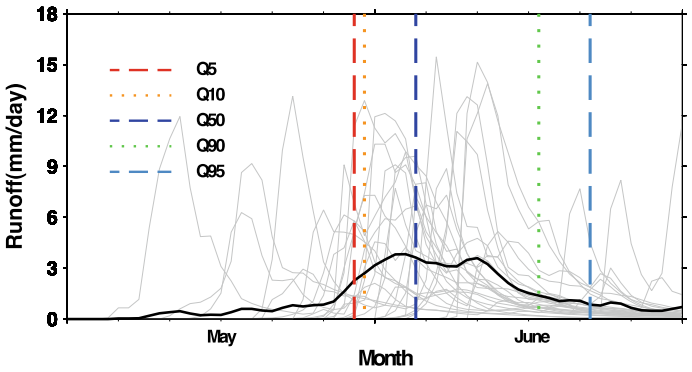

Fig. 26.2 Daily mean runoff (grey lines) for 1985–2011 in Trail Valley Creek, Canada. Five streamflow timing measures (Q5, Q10, Q50, Q90, and Q95) are shown for the spring (May and June) (Reproduced from Shi et al. 2015 Environ. Res. Lett. 10 064003. © IOP Publishing Ltd. CC BY 3.0)

streamflow (Fig. 26.2), Shi et al. (2015) found a general delay in streamflow timing over a small watershed in northern Canada. However, there are stronger trend signals for the high percentiles (Q90 and Q95) of spring runoff than that for the low and middle percentiles (Q5, Q10, and Q50). The results indicate that the differences are due to the contradictory effects of winter-spring air temperature changes, temperature fluctuation during the melting period, and spring rainfall to spring runoff, in addition to the changes in vegetation. Therefore, the effect of climate change may not be the only dominant factor for the changes in spring streamflow regime. Those advancing melt and runoff may include: earlier snowmelt onset resulting from the warming winter/spring air temperature; warmer soil temperature; and shallow snowpack decreasing water storage supply; while those delaying melts and/or runoff may include: increasing tundra shrub cover that would change snow cover distribution with deeper snow in shrub patches and shrub stems shading the surface and reducing wind speed at the snow surface; deeper active layer resulting in greater soil moisture storage and therefore possibly delaying melt runoff. In addition, changing frequency and magnitude of rain-on-snow events, increases in end of winter snow temperature, hillslope runoff controlled by the refreezing of water in the active layer and the storage capacity of the active layer, and streamflow affected by the occurrence of snow dams (Woo and Sauriol 1981) in the stream channel could be other reasons.

Permafrost has experienced warming and degradation during the past decades due to the combined influences of the increased snow depth and warming temperature. Models have simulated the degradation of near-surface permafrost in the last century over the northern regions (Lawrence et al. 2012; Burke et al. 2013; Park

et al. 2015). Increasing active layer thickness (ALT) has been observed at permafrost regions in response to the warming temperature (Park et al. 2016a). The increase in ALT enhances water storage capacity of the soil column, hence temporarily lowering the conversion of soil water into river discharge. On the other hand, later soil freezing and talik formation due to the warming climate would likely increase the connection of soil water to river network during the autumn and winter seasons. Park et al. (2017) examined apparent increases in the Arctic river discharge during the colder months (i.e., October–March), suggesting some implications from the warming permafrost. Tananaev et al. (2016) analyzed permafrost temperature and discharge data in the Lena basin over one century and found higher correlations between winter low flows and air temperature, particularly significant in the southern regions underlain by discontinuous permafrost.

In the Arctic, ET is most active during summer season. Higher summer ET may exceed precipitation, thereby drying soil moisture and lowing contribution of precipitation to river discharge (Park et al. 2008). The warming climate could further reduce the contribution because of increasing ET as it has higher positive correlation with temperature. A process-based land surface model, CHANGE (Park et al. 2011), simulates the increase of ET over the terrestrial Arctic during the period of 1979–2016 (Fig. 26.3). The increase is significant since 2000 when the warming of air temperature was stronger. The increase in simulated ET of 6.3 mm dec^{-1} is comparable to 3.8 mm dec^{-1} of satellite-derived estimation (Zhang et al. 2009). While the influences of soil moisture produced by the degradation of ice-rich permafrost on ET have been highlighted; however, they have not yet been quantitatively assessed.

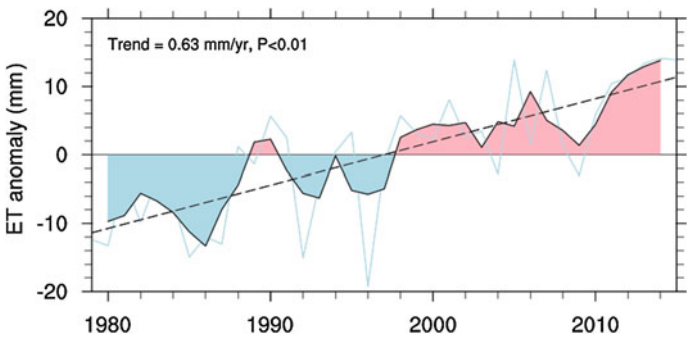

Fig. 26.3 Interannual variability and trend (dashed line) in annual total evapotranspiration anomaly simulated by CHANGE over the pan-Arctic terrestrial region. The dark line represents 3-yr running means of the annual anomaly (light blue line) of the evapotranspiration

26.3 Brief Descriptions of Major Cold Region Hydrologic Models

All mathematical models are by necessity simplifications of complex systems and, as such, they can omit or simplify different processes of relevance to a specific problem. Cold region land surface processes such as sublimation from blowing snow, surface storage in large lakes and wetlands, including those seasonally frozen, and infiltration limitation by frozen soils are still not well represented in some land surface schemes of large-scale models (Bowling et al. 2000, 2003a). For example, Slater and Lawrence (2013) assess the ability of the latest generation of land surface schemes to simulate present day and future permafrost of the terrestrial Arctic and concluded that most of the models still contain structural weaknesses that limit their skill in simulating cold region subsurface processes. While there is a substantial progress in understanding each of these important cold region processes, there is also a lag in up-scaling and incorporating the latest process understanding into the land surface schemes of large-scale models. Moreover, large-scale models are run at quite coarse resolution ($\sim$1 to 10 km) and may not resolve some processes of importance to Arctic hydrology. For example, topographic controls on precipitation are often not well simulated, leading to biases in the regional characterization of rain and snowfall (e.g., Finnis et al. 2008).

One of the most widely used large-scale, cold region models is the Variable Infiltration Capacity (VIC) model. VIC is a semi-distributed macroscale hydrological model (Liang et al. 1994, 1996), which parameterizes the dominant hydrometeorological processes at the land surface-atmosphere interface and solves both surface water and energy balances over a grid mesh. Distinguishing characteristics of the VIC model include: subgrid variability in land surface vegetation classes; subgrid variability in the soil moisture storage capacity; drainage from the lower soil moisture zone (base flow) as a nonlinear recession. To simulate streamflow, VIC results are typically post-processed with a separate routing model (Lohmann, et al. 1996, 1998) based on a linear transfer function to simulate the streamflow. The critical elements in the model that are particularly relevant for implementation in cold regions include a two-layer energy balance snow model (Cherkauer and Lettenmaier 1999), frozen soil and permafrost algorithm (Cherkauer and Lettenmaier 1999, 2003), blowing snow algorithm (Bowling et al. 2004), and effects of lake and wetlands on moisture storage and evaporation, which are particularly important for runoff at high latitudes (Bowling et al. 2003a). VIC has participated in the WCRP Intercomparison of Land Surface Parameterization Schemes (PILPS) project and the North American Land Data Assimilation System (NLDAS), where it has performed well relative to other schemes and to available observations (Bowling et al. 2003b; Lohmann et al. 2004; Nijssen et al. 2003). Consequently, VIC has been used to conduct hydrologic studies over the Pan-arctic region (Su et al. 2005, 2006). The VIC model included lake and wetland algorithm, and a simulation of runoff from Putuligayuk watershed on the Alaskan arctic coastal plain indicated that up to 80% of snow meltwater did go into storage each year,

meaning temporarily negative contribution to streamflow (Bowling and Lettenmaier 2010). A major ability of VIC can calculate the global freshwater discharge to the oceans. The VIC model estimated that discharge from Eurasian rivers portioned 37% of flows to the world oceans (Clark et al. 2015).

The coupled hydrological and biogeochemical model (CHANGE, Park et al. 2011) is another process-based cold region model that is combined with sub-models of soil thermal and hydrologic states, snow hydrology, and plant stomatal physiology and photosynthesis to calculate heat, water, and carbon fluxes in the atmosphere-land system. The model solves the heat and hydraulic conduction equations and represents permafrost dynamics including an explicit treatment of soil freezing/thawing phase changes. The snow sub-model includes energy and mass budgets to express changes of heat and water contents in the snowpack, so that it simulates snow accumulation and snowmelt at the land surface. The vertical water flux between soil column layers is solved by Darcy's law. Excess water at the soil surface is determined as surface runoff. At the bottom soil layer, the excess moisture is defined as subsurface runoff that flows to the river network. If permafrost is present within the soil column, water infiltration to lower soil layers is considerably impeded, which is calculated by a parameterization representing the ice impedance. The excess water at the permafrost table is substituted to subsurface runoff. CHANGE couples the river routing scheme TRIP2 (Total Runoff Integrating Pathways) to represent basin runoff routing and river discharge dynamics (Park et al. 2016b). Surface and subsurface runoffs calculated by CHANGE are directly passed to individual storage reservoirs of TRIP2, in which water is routed to the river mouth through a prescribed channel network. The discharge processes consider the contribution of groundwater to streamflow, which is represented by a linear function of outflow with a groundwater delay parameter. The discharge scheme also includes stream temperature model where water temperature (T_w) is calculated based on the inflow of upstream heat into the stream segment within the drainage network, the dominant heat exchange at the air–water surface, and the inflow of heat and water from tributaries (Park et al. 2017). The calculated T_w is also used to simulate river ice thickness on the basis of heat exchanges between atmosphere–snow–ice–frazil ice–water boundaries (Park et al. 2016b).

The Community Land Model (CLM4) (Lawrence et al. 2011), on the other hand, is the land component of the Community Climate System Model (Gent et al. 2011) that simulates water, energy, and carbon fluxes in the atmosphere–vegetation–soil system, and the export of freshwater to the oceans using a streamflow routing sub-model called the River Transport Model (RTM). Each grid runoff calculated by CLM4 is transported to the oceans along the river network by RTM based on linear reservoirs (Oleson et al. 2010). The presence of frozen surface soils and permafrost front reduce infiltration rates of soils with high ice contents in such a way that much of the snowmelt water and rainfall can be converted to runoff. The impedance effect of ice on water is expressed by the soil hydraulic properties in the model, thereby improving the runoff hydrographs and soil moisture profiles (Swenson et al. 2012).

Another cold region hydrologic modeling approach for simulation of river discharge by combining land surface model and streamflow routing model is that of the Joint UK Land Surface Simulator (JULES) (Finney et al. 2012) and Jena Scheme for Biosphere–Atmosphere Coupling in Hamburg (JSBACH) model (Ekici et al. 2014). JULES contains a version of TOPMODEL to account for subgrid heterogeneity of soil moisture using surface topography within the calculation of surface and subsurface runoff. The influence of frozen soils on the hydraulic conductivity is also included in JULES in the same way as it is represented in CHANGE and CLM4. JSBACH also represents freeze/thaw processes coupling hydrological processes in a layered soil scheme.

26.4 Current Research and Model Applications

26.4.1 Factors Affecting Cold Region Hydrologic Modeling

Most cold region land surface models represent the process of phase change to correctly simulate permafrost dynamics, including effects of soil organic carbon on soil thermal and hydraulic properties and vegetation dynamics. The models should be able to simulate permafrost degradation and the deepening active layer thickness under a warming climate. While the directions of simulated changes are generally consistent between models, their magnitudes usually have quite larger differences. This is mainly because of the differences in model structures, parameters, forcing data, and possibly the depth of the bottom soil boundary that the models define for the simulations. For example, most of the models that had participated in the Coupled Model Intercomparison Project Phase 5 (CMIP5) confined the bottom boundary to a depth of <15 m, simulating permafrost extents for the year 2005 ranging between 1.4 and 17.4 million km^2 (Koven et al. 2013). Larger soil depth reduces the heat conductive rates from the surface, consequently limiting the speed of permafrost degradation. Alexeev et al. (2007) suggested that a soil depth of at least 30 m is needed to simulate annual and decadal cycles of temperature dynamics for the permafrost. A simulation experiment conducted by setting the lower soil boundary to 3.6 m and 50.5 m reported the early twenty-first century near surface-permafrost areas of 1.2 and 2.9 million km^2, respectively, for the two experiments (Park et al. 2015). This difference emphasizes that a shallower soil boundary could underestimate the permafrost extent, which can inductively increase uncertainties of permafrost-associated interactions and feedbacks.

The quality of the forcing data is probably the primary source of uncertainty in model simulation; in particular, simulation results are greatly dependent on the quality of precipitation. In the Arctic rivers, a considerable amount of the discharge is generated from southern mountainous regions. The quantity of mountainous precipitation is characterized by high negative biases that may result in underestimation of the discharge. Adam et al. (2006) produced a bias-corrected global precipitation dataset, separating mean monthly catch ratios for rainfall and snowfall

and also adjusting precipitation for orography effect. Simulation of the VIC model using the bias-corrected precipitation exhibited appropriate model performance for the seasonal and interannual variations of the discharge over the pan-arctic land area, highlighting the precipitation-related uncertainties in simulating for Arctic river discharge (Su et al. 2005). Tian et al. (2007) conducted model simulations forced with and without precipitation-bias corrections from 1973 to 2004 and found that the enhanced snowfall induced by the bias corrections increased streamflow by 5–25% for most major rivers in the northern latitudes.

Cold region land surface processes such as sublimation from blowing snow, surface storage in large lakes and wetlands, including those seasonally frozen, and infiltration limitation by frozen soils are still not well represented in some of the large-scale cold region hydrologic models (Bowling et al. 2000, 2003a). Hostetler et al. (2000) developed a model for multiple lakes within one grid cell representing dynamic lake area as a function of water storage. The model was further improved the storage dynamics as linking directly lakes to the channel network (Gao et al. 2011). However, most of models do not yet include the processes of lake and wetland. This deficiency tended to reproduce seasonal hydrographs deviated from observations, peaking too much in spring, especially in Ob and Mackenzie rivers (Slater et al. 2007) where a large proportion of the basin area (11% for Ob and 49% for Mackenzie) is covered by lakes and wetlands that can temporarily store snow-melted water in the spring, reducing runoff and peak discharge rates. The fifth generation Canadian Regional Climate Model (CRCM5) coupled a one-dimensional lake model included interflow, i.e., lateral flow of water in the soil layers (Huziy and Sushama 2017). Comparison of CRCM5 simulations with and without lakes suggested that adding the interflow process led to increased streamflow during summer and fall seasons for the majority of the northeast Canadian rivers.

26.4.2 Recent Improvements in Representing Cold Region Hydrological Processes

As an important component of cold regions processes, frozen soil infiltration plays a very dominant role in the hydrology of the terrestrial Arctic regions. Both seasonally frozen ground and permafrost directly affect infiltration while they indirectly affect the heat transfer to and from the overlying snowpack (Kane and Chacho 1990). To improve spring peak flow predictions, the VIC model has developed a parameterization of the spatial distribution of soil frost (Cherkauer and Lettenmaier 2003). Adam (2007) described some significant modifications to the frozen soil algorithm, including the bottom boundary specification, the exponential thermal node distribution, the implicit solver using the Newton-Raphson method, and an excess ground ice and ground subsidence algorithm. This is good for simulating permafrost, for which it is often necessary to specify a maximum depth of as much as 30 m (Alexeev et al. 2007). By adding the ice content component in the heat flux equation, the impact of frozen soil on moisture transport can be

simulated by the moisture flux algorithm. One way the ice content in the frozen soil affects the moisture transport is through available moisture storage. Each of the three soil layers in VIC is divided into thawed, frozen, and unfrozen sublayers. The thickness of these sublayers depends on the soil temperatures at the nodes. When there is a frozen layer present, the ice content is based on the average temperature of the sublayer. The second way the ice content affects soil moisture transport is through its effect on infiltration and drainage. When a soil layer has high ice content, it will be nearly saturated to the runoff calculations; but at the same time, there is little moisture that can be allowed to drain to the lower layer. The model implementation for permafrost by Shi et al. (2016) uses a depth of 15 m with 18 soil thermal nodes exponentially distributed with depth and a no flux bottom boundary condition. When the no flux bottom boundary condition is selected for the soil column, the VIC model solves the ground heat fluxes using the finite difference method. This means that the soil temperature at the bottom boundary can change, but there is no loss or gain of heat energy through the boundary. To evaluate the model ability to replicate observed trends in frozen soils simulations, Fig. 26.4 compares modeled and observed soil temperature anomalies averaged over 146 observation sites across the former Soviet Union for the period of 1970–1990 at the depths of 0.2 m, 0.8 m, 1.6 m, and 3.2 m, respectively. The results reveal that the model captures the interannual variability of the soil temperature dynamics. In addition, Fig. 26.4 also shows the correlation coefficients between modeled and

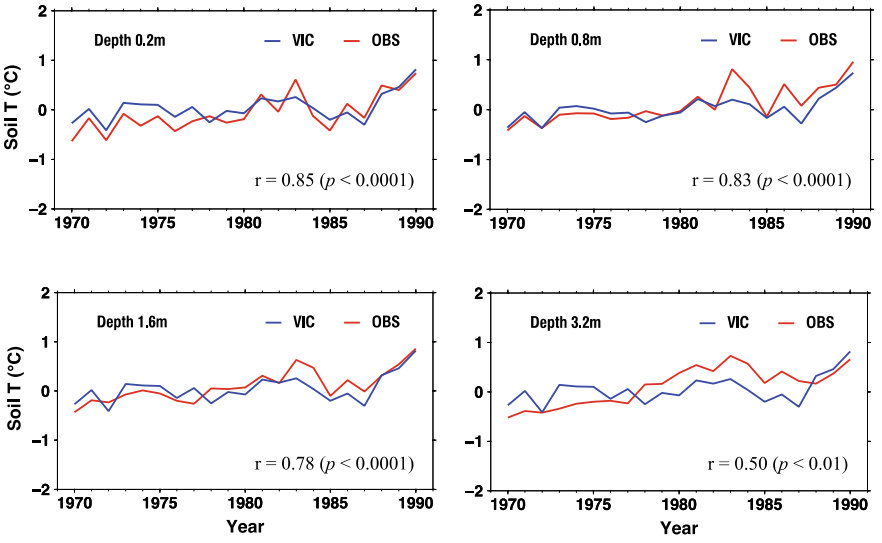

Fig. 26.4 Comparisons between observed and modeled soil temperature anomalies averaged over 146 observation sites across the former Soviet Union for the period of 1970–1990 at the depths of 0.2 m, 0.8 m, 1.6 m, and 3.2 m, respectively. The correlation is statistically significant at a level of $p < 0.025$ (from Shi et al. 2016)

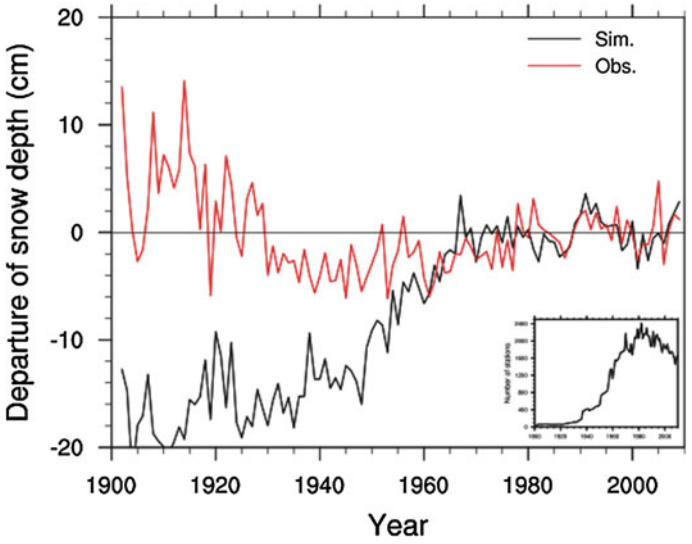

Fig. 26.5 Comparison of interannual anomalies (relative to 1971–2000) between observed and simulated winter snow depths over the pan-Arctic terrestrial region. The inner graph represents the number of observation stations used for the analysis (modified from Park et al. 2015)

observed time series for the period from 1970 to 1990. The VIC and observed soil temperature time series at 0.2, 0.8, 1.6, and 3.2 m are highly correlated (two-sided $p < 0.01$), indicating that VIC is able to reproduce soil temperature profiles and provides a surrogate for scarce observations for estimation of long-term changes in permafrost at high latitudes.

Lakes are other important component of the terrestrial Arctic drainage basins through the storage and flux exchange of heat and moisture that are affected by the presence and nature of snow and ice-cover. Similarly, most Arctic rivers are ice-covered for significant part (six to eight months) of the year and the freezing and breakup of river ice-cover significantly affect the magnitude of discharge and water levels throughout the river system. There is a significant growth in the study of lake and river ice modeling in recent years, though mostly at local scale. However, lake and river ice processes are rarely included in cold region hydrologic models (Ma and Fukushima 2002). Recently, the CHANGE coupled a river ice algorithm into the river routing and discharge scheme, enabling explicit representation of river ice and water temperature dynamics based on surface energy exchange with the atmosphere (Park et al. 2016b). The simulated mean total Arctic river ice volume was 54.1 km^3 based on the annual maximum ice thickness, while the volume decreased by 2.8 km^3 over the period of 1979–2009 in response to the warming air temperature. Brooks et al. (2013), using a degree-day ice growth model, estimated January peak river ice volume of 140 km^3 over the Northern Hemisphere, and reported a decreasing trend in the estimated ice volume during 1957–2002

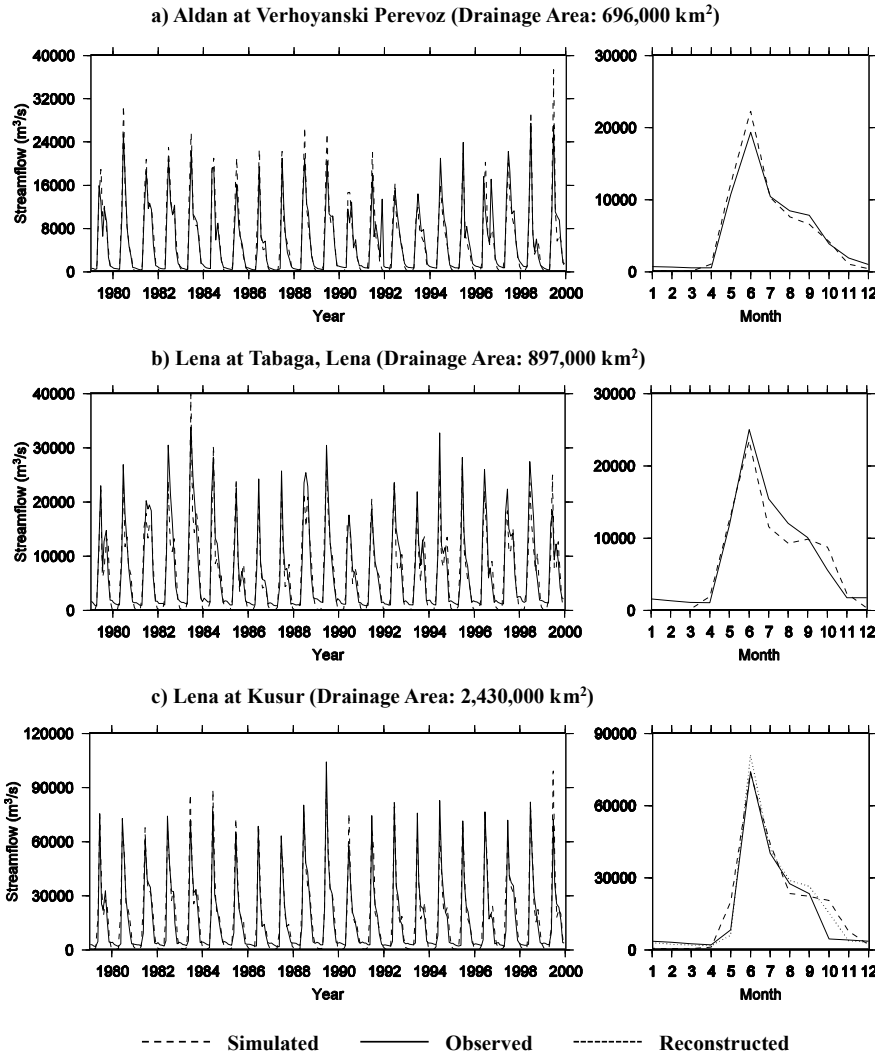

Fig. 26.6 Observed versus VIC simulated hydrographs at three locations within the Lena River basin: **a** Aldan at Verkhoyanskiy Perevoz, **b** Lena at Tabaga, and **c** Lena at Kusur (the mouth of the Lena River). The left column of the figure presents time series of monthly streamflow for 1979–1999, and the right column of the figure displays mean monthly streamflow for 1979–1999 (modified from Su et al. 2005)

(-0.075 km^3 yr^{-1}). A lake-ice modeling study by Dibike et al. (2011), using a one-dimensional lake simulation model, also indicated that future warming will result in an overall decrease in lake ice-cover duration by about 15–50 days and maximum lake-ice thickness by about 10–50 cm, on average, by the end of this

century. A one-dimensional dynamic lake model was also implemented for simulating small lakes within a land surface scheme of a Canadian regional climate model (MacKay 2012). This model is based largely on well-established process algorithms and a complete nonlinear surface energy balance including turbulent mixing in the surface mixed layer. However, this approach is still not implemented in any of the uncoupled land surface schemes and cold region hydrologic models.

The Arctic rivers are frozen during the winter, which decreases heat exchanges with the atmosphere. The ice formation reduces water storage within the river channel, and thus decreases the winter low flow. When the river ice is melted, the energy exchange between the river surface and atmosphere becomes strong. The river water temperature is warmer and reaches the maximum value in summer season alongside the seasonal variation of air temperature. Models that had considered the heat exchanges between the river surface and atmosphere and the heat movement from upstreams well simulated the seasonal and interannual variability of water temperature in the Arctic rivers (van Vliet et al. 2012; Park et al. 2017). Model simulation results by Park et al. (2017) indicated a warming trend of river water temperature by 0.16 °C dec^{-1} at the outlets of the pan-Arctic rivers, including widespread spatial warming consistent with the warming air temperature. The warming of water temperatures in the Arctic rivers induced by climate warming suggests the supply of warmer freshwater along with increasing river discharge (Fig. 26.7) result in an overall increase in heat supply to the Arctic Ocean. This change in river heat flux would most likely impact seasonal sea ice retreat and the warming of sea waters along the shelf regions.

The CHANGE model simulation shows increase in winter snow depth since 1901 and deeper snow after 1980 (Fig. 26.5). Large differences in snow depth between the observation and simulation are found for the period before 1960, which is likely attributable to the small number of available observation stations during that period. Since 1960, the simulated anomalous snow depth displays a similar time series with the observation ($r = 0.38$, $p < 0.1$). The higher level of snow depth

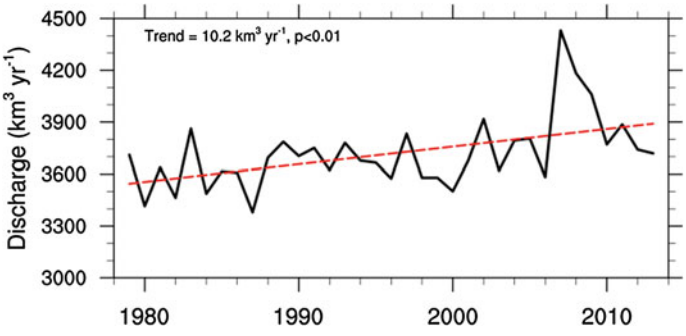

Fig. 26.7 Interannual variability and trend (dashed line) in total annual discharge at the outlets of Arctic rivers, simulated by the CHANGE model

since 1970 is probably due to relatively large contribution of the increased snow over the Eurasian region (Bulygina et al. 2009; Park et al. 2013). The increase of the Eurasian winter snow was closely correlated to the increase of snow in the autumn and early winter season (Park et al. 2015). Observations had captured wetting surface humidity in the autumn at the northern Siberia regions (Cohen et al. 2012). The increased snow depth contributed to permafrost warming trough the higher insulation (Park et al. 2015) and the decrease of river ice thickness (Park et al. 2016b).

Long-term monitoring of river discharge and water chemistry in northern basins is essential for identifying and understanding changes in the Arctic freshwater system. However, the simultaneous observations are not common in the Arctic regions. As a result, the long-term water chemistry in the Arctic is considerably rare relative to the discharge. Only recently, parallel sampling programs, called as the Pan-Arctic River Transport of Nutrients Organic matter and suspended Sediments (PARTNERS) project in 2003 and continued as the Arctic Great Rivers Observatory (Arctic-GRO) in 2008, have been operated on the Arctic major rivers (Tank et al. 2012; McClelland et al. 2015). Results of the projects contributed to capture characteristics of seasonal and geographical variations in water chemistry that is associated with watershed properties. This knowledge has established a framework for tracking future changes in river hydrological processes through the water chemistry. However, model developments on the river water chemistry are considerably delayed relative to the river discharge models. Very few studies have therefore provided quantitative assessments of changes in water chemistry in Arctic rivers, addressing the potential changes caused by the warming climate. Li Yung Lung et al. (2018) assessed the chemical composition of a broad suite of rivers draining to the Canadian Arctic Ocean and Hudson Bay using previously observed data. However, they found larger data gap in the observations and suggested a modeling approach to extrapolated the fluxes to the full Canadian Arctic drainage basin.

26.4.3 Freshwater Inflow to the Arctic Ocean

Historically, observations have indicated increases of discharge over much of the pan-Arctic (Peterson et al. 2002, 2006; Shiklomanov and Lammers 2009). In particular, the annual flow during 2000–2010 has increased by about 300 km^3 relative to the 3900 km^3 during 1980–2000 (Haine et al. 2015). The Russian river discharge, constituting about 80% of the Arctic discharge, increased 3.0 $km^3\ yr^{-1}$ during the same period, which is comparable to the increase 2.9 $km^3\ yr^{-1}$ from the major Russian rivers over 1936–2008 (Shiklomanov 2010). Discharge from North America northern rivers shows insignificant increase; earlier studies reported decreasing flows for North America high latitudes (Déry and Wood 2005), while recent analyses suggest flow increases (Ge et al. 2013; Déry et al. 2016). The VIC model with cold region land process updates was applied to the entire pan-Arctic domain at a 100-km to evaluate the representation of Arctic terrestrial hydrologic

processes and to provide a consistent baseline hydroclimatology for the region (Su et al. 2005). The model simulations of key hydrologic processes for the periods of 1979–1999 were evaluated using streamflow records, snow cover extent, dates of lake freeze-up and breakup, and permafrost active layer thickness. The pan-Arctic drainage basin was partitioned into 12 regions for model calibration and parameter transfer according to geographical definitions and hydroclimatology. Twenty-seven individual sub-basins within different regions were chosen for model calibration and validation. Results indicated that the VIC model was able to reproduce the seasonal and interannual variations in streamflow quite well (for 19 basins out of 27 monthly Nash efficiency exceeded 0.75, and for 13 it exceeds 0.8) (Fig. 26.6). However, comparison of multi-model simulations of the pan-Arctic river discharge shows large deviation from the observations, particularly in the spring peak discharge with earlier timing and larger amount (Slater et al. 2007). The deviation was later improved by coupling river ice processes to the discharge model where the breakup of river ice in the spring causes the delay of snowmelt-peak discharge and underestimate the flow volumes, thus improving the seasonal variability of discharge in model simulations (Park et al. 2016b). Swenson et al. (2012) also improved the parameterization of the hydraulic properties of frozen soil limiting the infiltration of soil water, which increased summer discharge in two large Siberian rivers compared to simulation results without the parameterization.

The discharge simulated by the VIC model at the farthest downstream sites was used to estimate the total circumpolar river inflow to the Arctic Ocean. As such, a 21-year (1979–1999) average river inflow to the Arctic Ocean was estimated as 3354 km^3/year; and 3596 km^3/year with the inclusion of the Canadian Archipelago. On the other hand, the total Arctic discharge, excluding the Yukon River, simulated by the CHANGE model over 1979–2013 was averaged to be around 3717.3 $km^3\ yr^{-1}$ (Fig. 26.7), which is comparable with the VIC simulation and 3900–4200 $km^3\ yr^{-1}$ for the observation over 1980–2010 (Haine et al. 2015). The differences in the annual Arctic river discharge between observation and simulation are attributable to the different estimations of discharges from the Canadian Arctic Archipelago and Baffin Bay that have lower observational stations. Haine et al. (2015) estimated the annual discharge of 500 km^3 for this region, while models (e.g., VIC and CHANGE) simulated 250–300 $km^3\ yr^{-1}$ (Su et al. 2005; Park et al. 2017). The relationship between the inflow volume and contributing area resulting from various data sources and VIC simulations indicated that the VIC model was comparable to the previous estimates derived from the observed data (Su et al. 2005). However, the wide range of Arctic freshwater discharge estimates, when adjusted for differences in drainage areas, were quite similar despite of the differences in drainage areas used in the individual studies.

26.4.4 Long-Term Hydrologic Model Simulations of Pan-Arctic River Basins

Using the Variable Infiltration Capacity (VIC) macroscale land surface model forced with gridded climatic observations, Shi et al. (2013) have reproduced spatial and temporal variations of snow cover extent (SCE) reported by the National Oceanic and Atmospheric Administration (NOAA) Northern Hemisphere weekly satellite SCE data. They have found that both observed and modeled North American and Eurasian snow cover in the pan-Arctic have statistically significant negative trends from April through June over the period 1972–2006. A number of studies (Bowling et al. 2000; Rawlins et al. 2003; Su et al. 2005) have also demonstrated the potential of different cold region hydrologic models to reproduce seasonal variations in freshwater discharge to the Arctic. However, results from multi-model simulation of pan-arctic hydrology by Slater et al. (2007) showed up to 30% difference in annual partitioning of precipitation between evaporation and runoff over a major Arctic watershed such as the Lena. Therefore, there seems to be still more work to be done in terms of both good quality forcing data and improved parametrization of land surface processes to arrive at a better model estimates of the historical variability and change within terrestrial components of arctic freshwater system. Similarly, the CHANGE model simulates an increasing trend (10.2 km^3 yr^{-1}, $p > 0.1$) of the entire Arctic river discharge over the past four decades (Fig. 26.7), consistent with the increasing precipitation under the warming climate. The combination of observations and general circulation models estimated a positive trend of 5.3 km^3 yr^{-2} for annual pan-Arctic discharge from 1950 to 2004 (Rawlins et al. 2010). A synthesis for earlier simulations with global hydrological models, with inputs from climate models, estimated overall increases of 10–20% over the pan-Arctic rivers (Walsh et al. 2005). Recent such simulations generally show increases on the order of 25–50% (Shiklomanov et al. 2013; van Vliet et al. 2013; Koirala et al. 2014). Decreases are mostly concentrated to the southern interior of the pan-Arctic drainage basin (van Vliet et al. 2013; Koirala et al. 2014).

Using future climate projections from six climate models and two emissions scenarios and a macroscale hydrological model, Arnell (2005) has found increases of up to 31% in river inflows to the Arctic by the 2080s under high emissions and up to 24% under lower emissions, with large differences between models. He has also demonstrated that future runoff projection using such uncoupled model is more sensitivity to the input data used to drive the models than to the terrestrial hydrologic model form and parameterization. The sign of projected changes of seasonal snowfall and snow water equivalent (SWE) with respect to the present is spatially variable as it depends on the present local climate conditions: in very cold regions, climate warming will lead to overall increased winter snowfall due to increased winter precipitation and thus to a thicker snow cover, while in warmer regions, the higher temperatures will lead to the opposite (Räisänen 2008). However, other snow-related variables, such as snow cover extent (SCE), exhibit a more direct relationship to temperature. Under CMIP3 B2 scenario of climate change, a regional climate model coupled a large-scale hydrological model simulated a 25%

increase in the future freshwater runoff from rivers in Northern Europe to the Barents Sea (Dankers and Middelkoop 2008). As the snow season is 30–50 days shorter, the simulation revealed the shift of about 2–3 weeks in the spring discharge peak.

26.5 Future Research Needs

While there is a substantial progress in understanding important cold region processes (e.g., sublimation from blowing snow, permafrost degradation and surface storage in lakes and wetlands, infiltration in frozen soils, etc.), there is a lag in up-scaling and incorporating the latest process understanding into the cold region hydrologic models. The long-term impact of permafrost degradation on local and regional hydrology is poorly understood, but is absolutely critical in terms of predicting future Arctic soil moisture states and river discharge and associated changes in biogeochemical cycling (Holland et al. 2007). The frozen soil and presence of permafrost reduce infiltration rates of snow-melted water and rainfall, consequently increasing surface runoff in the spring and subsurface drainage runoff. The impedance effects of permafrost were parameterized, and the models coupling the parameter generally simulated the observed Arctic river discharges (Swenson et al. 2012; Park et al. 2016b). On the other hand, the warming climates derive the melting of the ice-rich surface permafrost, subsequently forming thermokarst lakes. Observations identified the expansion of the thermokarst lake under the recent warming climates (Ulrich et al. 2017). Models physically represented the processes that form thermokarst lakes and subsidence of the ground surface following thawing of ice-rich soil (Lee et al. 2014; Westermann et al. 2016). The improved model had applied to the pan-Arctic scale and addressed that the expansion of thermokarst lakes are effective to more releases of carbon dioxide and methane to the atmosphere, enhancing positive feedbacks to the climate changes (Lee et al. 2014). Furthermore, the channeling between thermokarst lakes formed during the melting makes it easy the transport of lake water to river network (Turner et al. 2014; Ala-aho et al. 2018). This process likely affects river discharge at smaller or local scale, but is uncertain at larger scale.

One other area that needs more research effort in cold region hydrologic modeling is on how to get more representative precipitation data over the Arctic terrestrial watersheds. The difficulty to estimate the magnitude and special variability of cold season precipitation because of the uncertainty in snowfall measurement at high latitude resulting from gauge undercatch of solid precipitation, low precipitation amounts, sparsely distributed observations with the location of observing stations mostly biased toward low elevations and coastal regions, and rare long-term records, are some of the challenges that should be addressed by exploring new approach including enhancing methods to assimilate remote sensing products. (Behrangi et al. 2018; Serreze and Hurst 2000; Adam and Lettenmaier 2003; Yang et al. 2005).

The warming climates are effective to higher photosynthesis by vegetation, increasing the biomass productivity. The vegetation growths can both intercept more precipitation and access to soil waters produced by the permafrost thawing, consequently reducing the contribution rates of both permafrost-induced water and precipitation to river discharge. Model experiments based on various scenarios can provide quantitative values involving changes in water cycle/budget following ecosystem changes in the context of the warming climates. However, most models have a consistent deficiency in representing the physical processes of the ground ice in permafrost, as mentioned before. Therefore, even though river discharge is increased under the permafrost change, the deficiency makes it hard to separate the contribution rate of the permafrost-induced water to the discharge. This is because the increase of discharge includes the contribution of precipitation that is projected to be increased under the warming climate. A useful way to solve this problem is to incorporate isotope module into the models that can simulate a back trajectory to sources of the discharged water.

The recent warming temperature resulted in the earlier melting of the Arctic river ice. Models well reproduced the changes in the observed river ice phenology (Park et al. 2016b). When river ice is broken in the spring, the broken ice gradually melts as it flows down the river. In the process that ice floes move downstream, ice jam occasionally occur and can induce flooding. Although most models have still considerable deficiency in describing the ice jam, there were efforts of model development to project ice jam flooding in northern rivers (Lindenschmidt et al. 2012; Eliasson and Gröndal 2018). One of the biggest issues in the Arctic terrestrial regions is to know when and where ice jams form and release, because the ice-induced hazards greatly affect people's life in the Arctic community (Rokaya et al. 2018). The projected changes in future climate are big enough to alter the ice jam processes and the severity of breakup event. Therefore, more improvements are needed in representing ice-jam-related processes in cold region models. Moreover, the Arctic rivers convey heat and geochemical constituents to the Arctic Ocean and influence sea ice and biogeochemical dynamics. Observations estimated the total river delivery of nutrients, sediment, and carbon under the current climate (Holmes et al. 2011; Tank et al. 2012). Frey and McClelland (2009) highlighted linkages between permafrost changes and the Arctic river biogeochemistry, because the warming-induced permafrost changes could influence the delivery of biogeochemical constituents. There is also a real possibility that the Arctic freshwater system is likely to undergo transition from a surface water to a groundwater dominant as the result of permafrost thawing (e.g., Brutsaert and Hiyama 2012). However, models representing the river conveyance of biogeochemical constituents in the Arctic are still insufficient and incomplete. In general, more research is needed toward better understanding and representation of all the different cold region processes.

26.6 Conclusion

The hydrological system of cold regions is represented by the unique seasonality; the freezing of the cold season increases the terrestrial water storage as snow and ice, while the melting and thawing as a result of warmer temperature produce larger fluxes of water and heat during the summer season. Those fluxes are further amplified by the warming climate, which subsequently results in changes in the Arctic hydrological processes, such as earlier timing of peak river discharge by earlier snow melt, increasing active layer, and earlier greening with higher vegetation productivity. These changes have certain influences on the freshwater and biogeochemical cycles in the Arctic system with considerable climate implications, ultimately impacting human life in the Arctic regions. This also indicates the need for increased understanding of the changes that are happening in the Arctic hydrological system. However, we are still lacking detailed knowledge of some cold region processes to have a comprehensive picture on how the Arctic hydrologic system respond to the projected change in climate and increased anthropogenic activities across the terrestrial Arctic regions. As an example, operation of dams constructed in the major Arctic rivers has changed the seasonality of discharge; control of flow during spring and early summer has reduced peak discharge, while release of water from the reservoirs has increased discharge during winter (Ye et al. 2003; McClelland et al. 2004). Construction and operation of dams likely enhance evaporation from reservoir surfaces and water usages for agricultural and municipal practices. Climatic warming may increase such water loss. Knowing how the missing water does affect the Arctic hydrologic system is an important concern in the future climates (McClelland et al. 2004).

Land surface models that are based on physical, hydrological, and biogeochemical principles are useful tools that can increase our understanding for the Arctic hydrological system across time and space, through various experimental designs and analysis. Although the models have different levels of complexity and coupled interactions, the simulation results at pan-Arctic scale generally show similar trends in most of the hydrological processes that are consistent with observations. The models project permafrost degradation and the subsequent more vigorous hydrological cycle caused by a warmer and wetter surface. However, the magnitude of permafrost degradation shows large variability between the models due to differences in model structure, parameterization, etc. This variability further increases the uncertainty in the models' projection of the other related processes (e.g., freshwater discharge and biogeochemical cycles), indicating a need to further improve those model processes. As discussed above, model improvement works have been conducted on many aspects of cold region hydrology, including the incorporation of new components and new feedback and interactions (e.g., Swenson et al. 2012; Lee et al. 2014). However, the models still have uncertainty that needs further improvement. For continued progress in understanding the Arctic hydrological system, future research should include the use of innovative strategies, such as the incorporation of assimilation of satellite data within hydrological

models (e.g., Lique et al. 2016), more widespread use of multi-model ensembles, parameterization development through better collaboration between the observational and process modeling community, and development of high quality forcing dataset.

References

Adam JC (2007) Understanding the causes of streamflow changes in the Eurasian Arctic. Ph.D thesis 174 pp, University of Washington, Seattle, WA

Adam JC, Lettenmaier DP (2003) Adjustment of global gridded precipitation for systematic bias. J Geophys Res 108:4257. https://doi.org/10.1029/2002JD002499

Adam JC, Clark EA, Lettenmaier DP, Wood EF (2006) Correction of global precipitation products for orographic effects. J Clim 19:15–38. https://doi.org/10.1175/JCLI3604.1

Ala-aho P, Soulsby C, Pokrovsky OS, Kirpotin SN, Karlsson J, Serikova S, Manasypov R, Lim A, Krickov I, Kolesnichenko LG, Laudon H, Tetzlaff D (2018) Permafrost and lakes control river isotope composition across a boreal Arctic transect in the Western Siberian lowlands. Environ Res Lett 13:034028. https://doi.org/10.1088/1748-9326/aaa4fe

Alexeev VA, Nicolsky DJ, Romanovsky VE, Lawrence DM (2007) An evaluation of deep soil configurations in the CLM3 for improved representation of permafrost. Geophys Res Lett 34: L09502. https://doi.org/10.1029/2007GL029536

Arnell NW (2005) Implications of climate change for freshwater inflows to the Arctic Ocean. J Geophys Res 110:D07105. https://doi.org/10.1029/2004JD005348

Behrangi A, Gardner A, Reager JT, Fisher JB, Yang D, Huffman GJ, Adler RF (2018) Using GRACE to estimate snowfall accumulation and assess gauge undercatch corrections in high latitudes. J Clim 31:8689–8704. https://doi.org/10.1175/JCLI-D-18-0163.1

Beven K (2012) Rainfall-runoff modelling: the primer. John Wiley & Sons, Ltd. https://doi.org/10.1002/9781119951001

Bowling LC, Lettenmaier DP (2010) Modeling the effects of lakes and wetlands on the water balance of Arctic environments. J Hydrometeorol 11:276–295

Bowling LC, Lettenmaier DP, Matheussen BV (2000) Hydroclimatology of the arctic drainage basin. In: Lewis EL et al (eds) The freshwater budget of the arctic ocean. Springer, New York, pp 57–90

Bowling LC, Kane DL, Gieck RE, Hinzman LD, Lettenmaier DP (2003a) The role of surface storage in a low-gradient arctic watershed. Water Resour Res 39:1087. https://doi.org/10.1029/2002WR001466

Bowling LC et al (2003b) Simulation of high-latitude hydrological processes in the Torne-Kalix basin: PILPS phase 2(e) - 1: Experiment description and summary intercomparisons. Global Planet Change 38:1–30

Bowling LC, Pomeroy JW, Lettenmaier DP (2004) Parameterization of blowing snow sublimation in a macroscale hydrology model. J Hydrometeorol 5(5):745–762

Bring A, Fedorova I, Dibike Y, Hinzman L, Mård J, Mernild SH, Prowse T, Semenova O, Stuefer SL, Woo M-K (2017a) Arctic terrestrial hydrology: a synthesis of processes, regional effects and research challenges. J Geophys Res Biogeosci 121(3):621–649. https://doi.org/10.1002/2015JG003131

Bring A, Shiklomanov A, Lammers RB (2017b) Pan-Arctic river discharge: prioritizing monitoring of future climate change hot spots. Earth Future 5:72–92

Brooks RN, Prowse TD, O'Connell IJ (2013) Quantifying northern hemisphere freshwater ice. Geophys Res Lett 40:1128–1131. https://doi.org/10.1002/grl.50238

Brutsaert W, Hiyama T (2012) The determination of permafrost thawing trends from long-term streamflow measurements with an application in eastern Siberia. J Geophys Res 117:D22110. https://doi.org/10.1029/2012JD018344

Bulygina ON, Razuvaev V, Korshunova N (2009) Change in snow cover northern Eurasia in the last decades. Environ Res Lett 4:045026. https://doi.org/10.1088/17489326/14/4/045026
Burke EJ, Kankers R, Jones CD, Wiltshire AJ (2013) A retrospective analysis of pan Arctic permafrost using the JULES land surface model. Clim Dyn. https://doi.org/10.1007/s00382-012-1648-x
Cherkauer KA, Lettenmaier DP (1999) Hydrologic effects of frozen soils in the upper Mississippi River basin. J Geophys Res 104(D16):19599–19610
Cherkauer KA, Lettenmaier DP (2003) Simulation of spatial variability in snow and frozen soil. J Geophys Res 108(D22):8858. https://doi.org/10.1029/2003JD003575
Clark EA, Sheffield J, van Vliet MTH, Nussen B, Lettenmaier DP (2015) Continental runoff into the oceans (1950–2008). J Hydrometeorol 16:1502–1520
Cohen J, Furtado J, Barlow M, Alexeev V, Cherry J (2012) Arctic warming, increasing snow cover and widespread boreal winter cooling. Environ Res Lett 7:014007. https://doi.org/10.1088/1748-9326/1/1/014007
Cox PM, Huntingford C, Harding RJ (1998) A canopy conductance and photosynthesis model for use in a GCM land surface scheme. J Hydrol 212–213:79–94
Dankers R, Middelkoop H (2008) River discharge and freshwater runoff to the Barents Sea under present and future climate conditions. Clim Change 87:131–153
Derksen C, Brown R (2012) Spring snow cover extent reductions in the 2008–2012 period exceeding climate model projections. Geophys Res Lett 39:L19504. https://doi.org/10.1029/2012GL053387
Déry S J, Stahl K, Moore RD, Whitfield PH, Menounos B, Burford JE (2009) Detection of runoff timing changes in pluvial nival and glacial rivers of Western Canada. Water Resour Res 45. https://doi.org101029/2008WR006975
Déry SJ, Wood EF (2005) Decreasing river discharge in northern Canada. Geophys Res Lett 32: L10401. https://doi.org/10.1029/2005GL022845
Déry SJ, Mlynowski TJ, Hernandez-Henriquez MA, Straneo F (2011) Interannual variability and interdecadal trends in Hudson Bay streamflow. J Mar Syst 88:341–351
Déry SJ, Stadnyk TA, MacDonald MK, Gauli-Sharma B (2016) Recent trends and variability in river discharge across northern Canada. Hydrol Earth Syst Sci 20:4801–4818
Dibike YB, Prowse T, Saloranta T, Ahmed R (2011) Response of Northern Hemisphere lake-ice cover and lake-water thermal structure patterns to a changing climate. Hydrol Process 25:2942–2953. https://doi.org/10.1002/hyp.8068
Dickinson RE (1984) Modeling evapotranspiration for three-dimensional global climate models. In: Hansen JE and T Takahashi (eds), Climate processes and climate sensitivity, geophysical monograph, 29, Amer Geophys Union, Washington, DC, pp 58–72
Ekici A, Beer C, Hagemann S, Boike J, Langer M, Hauck C (2014) Simulating high-latitude permafrost regions by the JSBACH terrestrial ecosystem model. Geosci Model Dev 7:631–647
Eliasson J, Gröndal GO (2018) Development of a river ice jam by a combined heat loss and hydraulic model. Hydrol Earth Syst Sci 12:1249–1256
Finney DL, Blyth E, Ellis R (2012) Improved modelling of Siberian river flow through the use of an alternative frozen soil hydrology scheme in a land surface model. Cryosphere 6:859–870
Finnis J, Cassano J, Holland M, Serreze M, Uotila P (2008) Synoptically forced hydroclimatology of major Arctic watersheds in general circulation models; Part 1: the Mackenzie River Basin. Int J Climatol 29*:1226–1243
Foley JA, Prentice IC, Ramankutty N, Levis S, Pollard D, Sitch S, Haxeltine A (1996) An integrated biosphere model of land surface processes, terrestrial carbon balance, and vegetation dynamics. Global Biogeochem Cycles 10(4):603–628
Frey KE, McClelland JW (2009) Impacts of permafrost degradation on arctic river biogeochemistry. Hydrol Process 23:169–182
Gao H, Bohn TJ, Podest E, McDonald KC, Lettenmaier DP (2011) On the causes of the shrinking of Lake Chad. Environ Res Lett 6:034021. https://doi.org/10.1088/1748-9326/6/3/034021

Ge S, Yang D, Kane DL (2013) Yukon River Basin long-term (1977–2006) hydrologic and climatic analysis. Hydrol Process 27(17):2475–2484

Gent PR et al (2011) The community climate system model version 4. J Clim 24:4973–4991. https://doi.org/10.1175/2011JCLI4083.1

Ghatak D, Frei A, Gong G, Stroeve J, Robinson D (2010) On the emergence of an Arctic amplification signal in terrestrial Arctic snow extent. J Geophys Res 11:D24105. https://doi.org/10.1029/2010JD014007

Goodison BE, Louie PYT, Yang D (1998) WMO solid precipitation measurement intercomparison, Final Rep (WMO TE-872). World Meteorol Org, 212 pp

Haine TWN et al (2015) Arctic freshwater export: status, mechanisms, and prospects. Global Planet Change 124:13–35. https://doi.org/10.1016/j.gloplacha.2014.11.013

Hinzman LD et al (2005) Evidence and implications of recent climate change in northern Alaska and other arctic regions. Clim Change 72:251–298

Holland MM, Finnis J, Serreze MC (2006) Simulated Arctic Ocean freshwater budgets in the 20th and 21st centuries. J Clim 19:6221–6242

Holland MM, Finnis J, Barrett AP, Serreze MC (2007) Projected changes in Arctic Ocean freshwater budgets. J Geophys Res 112:G04S55, https://doi.org/10.1029/2006jg000354

Holmes RM et al (2011) Seasonal and annual fluxes of nutrients and organic matter from large rivers to the Arctic Ocean and surrounding seas. Estuaries Coasts 35(2):369–382

Holmes RM, Shiklomanov AI, Tank SE, McClelland JW, Tretiakov M (2015) River Discharge, NOAA Arctic Report Card. http://www.arctic.noaa.gov/Report-Card/Report-Card-2015/ArtMID/5037/ArticleID/227/River-Discharge

Hostetler SW, Bartlein PJ, Clark PU, Small EE, Soloman AM (2000) Simulated influences of Lake Agassiz on the climate of central North America 11000 years ago. Nature 405:334–337

Huziy O, Sushama L (2017) Impact of lake–river connectivity and interflow on the Canadian RCM simulated regional climate and hydrology for Northeast Canada. Clim Dyn 48:709–725

Jahn A, Holland MM (2013) Implications of Arctic sea ice changes for North Atlantic deep convection and the meridional overturning circulation in CCSM4-CMIP5 simulations. Geophys Res Lett 40:1206–1211. https://doi.org/10.1002/grl.50183

Kane DL, Chacho EF (1990) Frozen ground effects on infiltration and runoff. Cold Regions Hydrol Hydraul 259–300

Koirala S, Hirabayashi Y, Mahendran R, Kanae S (2014) Global assessment of agreement among streamflow projections using CMIP5 model outputs. Environ Res Lett 9(6):064017. https://doi.org/10.1088/1748-9326/9/6/064017

Koven CD, Riley WJ, Stern A (2013) Analysis of permafrost thermal dynamics and response to climate change in the CMIP5 earth system models. J Clim 26:1877–1900. https://doi.org/10.1175/JCLI-D-12-00228.1

Lawrence DM, Slater AG (2008) Incorporating organic soil into a global climate model. Clim Dyn 30:145–160. https://doi.org/10.1007/s00382-007-0278-1

Lawrence D et al (2011) Parameterization improvements and functional and structural advances in version 4 of the community land model. J Adv Model Earth Syst 3:M03001. https://doi.org/10.1029/2011MS000045

Lawrence DM, Slater AG, Swenson SC (2012) Simulation of present-day and future permafrost and seasonally frozen ground conditions in CCSM4. J Clim 25:2207–2225. https://doi.org/10.1175/JCLI-D-11-00334.1

Lee H, Swenson SC, Slater AG, Lawrence DM (2014) Effects of excess ground ice on projections of permafrost in a warming climate. Environ Res Lett 9:124006. https://doi.org/10.1088/1748-9326/9/12/124006

Lemke P et al (2007) Observations: changes in snow, ice and frozen ground. In: Solomon S et al (eds) Climate change 2007: the physical science basis. Cambridge Univ Press, New York, pp 337–383

Levis, SG, Bonan B, Vertenstein M, Oleson KW (2004) The community land model's dynamic global vegetation model (CLM-DGVM): technical description and user's guide, NCAR Tech. Note TN-459+lA, 50 pp, National Center for Atmospheric Research, Boulder, Colorado

Li Yung Lung JYS, Tank SE, Spence C, Yang D, Bonsal B, McClelland JW, Holmes RM (2018) Seasonal and geographic variation in dissolved carbon biogeochemistry of rivers draining to the Canadian Arctic Ocean and Hudson Bay. J Geophys Res: Biogeosci 123. https://doi.org/10.1029/2018jg004659

Liang X, Lettenmaier DP, Wood EF, Burges SJ (1994) A simple hydrologically based model of land surface water and energy fluxes for general circulation models. J Geophys Res 105 (D17):14415–14428

Liang X, Wood EF, Lettenmaier DP (1996) Surface soil moisture parameterization of the VIC-2L model: evaluation and modifications. Glob Planet Change 13:195–206

Lindenschmidt K, Sydor M, Carson R, Harrison R (2012) Ice jam modelling of the Lower Red River. J Water Resour Protect 4:16739. https://doi.org/10.4236/jwarp.2012.41001

Lique C, Holland MM, Dibike YB, Lawrence DM, Screen JA (2016) Modeling the arctic freshwater system and its integration in the global system: lessons learned and future challenges. J Geophys Res Biogeosci 121:540–566. https://doi.org/10.1002/2015JG003120

Lohmann D, Nolte-Holube R, Raschke E (1996) A large scale horizontal routing model to be coupled to land surface parameterization schemes. Tellus 48A:708–721

Lohmann D, Raschke E, Nijssen B, Lettenmaier DP (1998) Regional scale hydrology: I. Formulation of the VIC-2L model coupled to a routing model. Hydrol Sci J 43:131–141

Lohmann D et al (2004) Streamflow and water balance intercomparisons of four land surface models in the North American land data assimilation system project. J Geophys Res 109 (D7):22

Ma X, Fukushima Y (2002) A numerical model of the river freezing process and its application to the Lena River. Hydrol Processes 16:2131–2140

MacKay MD (2012) A process-oriented small lake scheme for coupled climate modelling applications. J Hydrometeorol 13:1911–1924. https://doi.org/10.1175/JHM-D-11-0116.1

Manabe S (1969) Climate and the ocean circulation: 1, the atmospheric circulation and the hydrology of the Earth's surface. Monthly Weather Rev 97:739–805

McClelland JW, Holmes RM, Peterson BJ, Stieglitz M (2004) Increasing river discharge in the Eurasian Arctic: Consideration of dams, permafrost thaw, and fires as potential agents of change. J Geophys Res 109:D18102. https://doi.org/10.1029/2004JD004583

McClelland JW, Tank SE, Spencer RGM, Shiklomanov AI (2015) Coordination and sustainability of river observing activities in the Arctic. Arctic 68, https://doi.org/10.14430/arctic4448

Mishra AK, Coulibaly P (2010) Hydrometric network evaluation for Canadian watersheds. J Hydrol 380:420–437

Nijssen B et al (2003) Simulation of high latitude hydrological processes in the Torne-Kalix basin: PILPS phase 2(e): 2. Comparison of model results with observations. Glob Planet Change 38:31–53

Oleson KW et al (2010) Technical description of version 4.0 of the Community Land Model. NCAR Tech Note NCAR/TN-478+STR, Natl Cent For Atmos Res, Boulder, Colo

Park H, Yamazaki T, Yamamoto K, Ohta T (2008) Tempo-spatial characteristics of energy budget and evapotranspiration in the eastern Siberia. Agric For Meteorol 148:1990–2005. https://doi.org/10.1016/j.agrformet.2008.06.018

Park H, Iijima Y, Yabuki H, Ohta T, Walsh J, Kodama Y, Ohata T (2011) The application of a coupled hydrological and biogeochemical model (CHANGE) for modeling of energy, water, and CO_2 exchanges over a larch forest in eastern Siberia. J Geophys Res 116:D15102. https://doi.org/10.1029/2010JD01586

Park H, Walsh J, Fedorov AN, Sherstiukov AB, Iijima Y, Ohata T (2013) The influence of climate and hydrological variables on opposite anomaly in active-layer thickness between Eurasian and North American watersheds. Cryosphere 7:631–645. https://doi.org/10.5194/tc-7-631-2013

Park H, Fedorov AN, Zheleznyak MN, Konstantinov PY, Walsh JE (2015) Effect of snow cover on pan-Arctic permafrost thermal regimes. Clim Dyn 44:2873–2895
Park H, Kim Y, Kimball JS (2016a) Widespread permafrost vulnerability and soil active layer increases over the high northern latitudes inferred from satellite remote sensing and process model assessments. Remote Sens Environ 175:349–358. https://doi.org/10.1016/j.rse.2015.12.046
Park H, Yoshikawa Y, Oshima K, Kim Y, Ngo-Duc T, Kimball JS, Yang D (2016b) Quantification of warming climate-induced changes in terrestrial Arctic river ice thickness and phenology. J Clim 29:1733–1754. https://doi.org/10.1175/JCLI-D-15-0569-1
Park H, Yoshikawa Y, Yang D, Oshima K (2017) Warming water in Arctic terrestrial rivers under climate change. J Hydrometeorol. https://doi.org/10.1175/JHM-D-16-0260.1
Peterson BJ et al (2002) Increasing river discharge to the Arctic Ocean. Science 298:2171–2173
Peterson BJ, McClelland J, Curry R, Holmes RM, Walsh JE, Aagaard K (2006) Trajectory shifts in the Arctic and subarctic freshwater cycle. Science 313(5790):1061–1066
Pomeroy JW, Gray DM, Brown T, Hedstrom NR, Quinton WL, Granger RJ, Carey SK (2007) The cold regions hydrological model, a platform for basing process representation and model structure on physical evidence. Hydrol Process 21:2650–2667. https://doi.org/10.1002/hyp.6787
Prowse T, Bring A, Mard J, Carmack E, Holland M, Instanes A, Vihma T, Wrona FJ (2015) Arctic freshwater synthesis: summary of key emerging issues. J Geophys Res Biogeosci 120:1887–1893. https://doi.org/10.1002/2015JG003128
Räisänen J (2008) Warmer climate: less or more snow? Clim Dyn 30. https://doi.org/10.1007/s00382-007-0289-y
Rawlins MA, Lammers RB, Frolking S, Fekete BM, Vorosmarty CJ (2003) Simulating pan-Arctic runoff with a macro-scale terrestrial water balance model. Hydrol Process 17:2521–2539
Rawlins MA, Fahnestock M, Frolking S, Vörösmarty CJ (2007) On the evaluation of snow water equivalent estimates over the terrestrial Arctic drainage basin. Hydrol Process 21:1616–1623. https://doi.org/10.1002/hyp.6724
Rawlins MA et al (2010) Analysis of the Arctic system for freshwater cycle intensification: observations and expectations. J Clim 23:5715–5737. https://doi.org/10.1175/2010JCLI3421.1
Rignot E, Velicogna I, Van den Broeke MR, Monaghanand A, Lenaerts JTM (2011) Acceleration of the contribution of the Greenland and Antarctic ice sheets to sea level rise. Geophys Res Lett 38:L05503. https://doi.org/10.1029/2011GL046583
Rokaya P, Budhathoki S, Lindenschmidt K (2018) Trends in the timing and magnitude of ice-jam floods in Canada. Sci Rep 8:5834. https://doi.org/10.1038/s41598-018-24057-z
Sellers PJ, Mintz Y, Sud YC, Dalcher A (1986) A simple biosphere model (SiB) for use within general circulation models. J Atmos Sci 43:505–531
Serreze MC, Hurst CM (2000) Representation of mean Arctic precipitation from NCEP-NCAR and ERA reanalyses. J Clim 13(1):182–201
Shi X, Déry SJ, Groisman PY, Lettenmaier DP (2013) Relationships between recent hydroclimate trends. J Clim 26:2048–2064. https://doi.org/10.1175/JCLI-D-12-00044.1
Shi X, Marsh P, Yang D (2015) Warming spring air temperatures, but delayed spring streamflow in an Arctic headwater basin. Environ Res Lett 10:064003
Shi X, Troy TJ, Lettenmaier DP (2016) Effects of pan-Arctic snow cover and air temperature changes on soil heat content. The Cryosphere Discuss. https://doi.org/10.5194/tc-2016-70
Shiklomanov AI (2010) River discharge. In: Richter-Menge J, Overland JE (eds), Arctic Report Card 2010, NOAA, pp 38–40
Shiklomanov AI, Lammers RB (2009) Record Russian river discharge in 2007 and the limits of analysis. Environ Res Lett 4(4):045015. https://doi.org/10.1088/1748-9326/4/4/045015
Shiklomanov AI, Yakovleva TI, Lammers RB, Karasev IP, Vorosmarty CJ, Linder E (2006) Cold region river discharge uncertainty – Estimates from large Russian rivers. J Hydrol 326:231–256
Shiklomanov AI, Lammers RB, Lettenmaier DP, Polischuk YM, Savichev OG, Smith LC, Chernokulsky AV (2013) Hydrological changes: historical analysis, contemporary status, and

future projections. Regional environmental changes in siberia and their global consequences. Springer, Dordrecht, The Netherlands, pp 111–154
Slater AG, Lawrence DM (2013) Diagnosing present and future permafrost from climate models. J Clim 26:5608–5623
Slater AG, Bohn TJ, McCreight JL, Serreze MC, Lettenmaier DP (2007) A multimodel simulation of pan-Arctic hydrology. J Geophys Res 112:G04S45, https://doi.org/10.1029/2006jg000303
Su F, Adam JC, Bowling LC, Lettenmaier DP (2005) Streamflow simulations of the terrestrial Arctic domain. J Geophys Res 110:D08112. https://doi.org/10.1029/2004JD005518
Su F, Adam JC, Trenberth KE, Lettenmaier DP (2006) Evaluation of surface water fluxes of the pan-Arctic land region with a land surface model and ERA-40 reanalysis. J Geophys Res 11: D05110. https://doi.org/10.1029/2005JD006387
Swenson SC, Lawrence DM, Lee H (2012) Improved simulation of the terrestrial hydrological cycle in permafrost regions by the community land model. J Adv Model Earth Syst 4:M08002. https://doi.org/10.1029/2012MS000165
Tananaev NI, Makarieva OM, Lebedeva LS (2016) Trends in annual and extreme flows in the Lena River basin, Northern Eurasia. Geophys Res Lett 43:10764–10772. https://doi.org/10.1002/2016GL070796
Tank SE et al (2012) A land-to-ocean perspective on the magnitude, source and implication of DIC flux from major Arctic rivers to the Arctic Ocean. Global Biogeochem Cycles 26:GB4018. https://doi.org/10.1029/2011gb004192
Tian X, Dai A, Yang D, Xie Z (2007) Effects of precipitation-bias corrections on surface hydrology over northern latitudes. J Geophys Res 112:D14101. https://doi.org/10.1029/2007JD008420
Turner KW, Edwards TWD, Wolfe BB (2014) Characterising runoff generation processes in a lake-rich thermokarst landscape (Old Crow Flats, Yukon, Canada) using δ18O, δ2H and d-excess measurements. Permafrost Periglac Process 25:53–59
Ulrich M, Matthes H, Schirrmeister L, Schutze J, Park H, Iijima Y, Fedorov AN (2017) Differences in behaviour and distribution of permafrost-related lakes in Central Yakutia and their response to climatic drivers. Water Resour Res 53. https://doi.org/10.1002/2016wr019267
van Vliet MTH, Yearsley JR, Franssen WHP, Ludwig F, Haddeland I, Lettenmaier DP, Kabat P (2012) Coupled daily streamflow and water temperature modelling in large river basins. Hydrol Earth Syst Sci 16:4303–4321. https://doi.org/10.5194/hess-16-4303-2012
van Vliet MTH, Franssen WHP, Yearsley JR, Ludwig F, Haddeland I, Lettenmaier DP, Kabat P (2013) Global river discharge and water temperature under climate change. Global Environ Change 23(2):450–464
Verseghy DL, McFarland NA, Lazare M (1993) CLASS -A Canadian land surface scheme for GCMs, Part II: vegetation model and coupled runs. Int J Climatol 13:347–370
Walker DA et al (2010) Vegetation Special Supplement to B. Am Meteorol Soc 91:S115–S116
Walsh J et al (2005) Cryosphere and hydrology. Arctic climate impact assessment. Cambridge Univ Press, Cambridge, U.K, pp 183–242
WCRP (1996) Report of the fourth session of the WCRP ACSYS scientific steering group. Toronto, Canada, October 11–14, 1995, WCRP informal report N10
Westermann S, Langer M, Boike J, Heikenfeld M, Peter M, Etzelmuller B, Krinner G (2016) Simulating the thermal regime and thaw processes of ice-rich permafrost ground with the land-surface model CryoGrid 3. Geosci Model Dev 9:523–546
Woo MK, Sauriol J (1981) Effects of snow jams on fluvial activities in the High Arctic. Phys Geog 2:83–98
Wrona FJ et al (2016) The atmospheric role in the transitions in Arctic ecosystems: ecological implications of a changing hydrological regime. J Geophys Res Biogeosci 121. https://doi.org/10.1002/2015jg003133
Yang D (1999) An improved precipitation climatology for the Arctic Ocean. Geophys Res Lett 26:1525–1528

Yang D, Goodison BE, Benson CS, Ishida S (1998) Adjustment of daily precipitation at 10 climate stations in Alaska: application of WMO Intercomparison results. Water Resour Res 34(2):241–256

Yang D, Ishida S, Goodison BE, Gunther T (1999) Bias correction of daily precipitation measurements for Greenland. J Geophys Res 105(D6):6171–6182

Yang D, Ohata T (2001) A bias corrected Siberian regional precipitation climatology. J Hydrometeorol 2:122–139

Yang D, Robinson D, Zhao Y, Estilow T, Ye B (2003) Streamflow response to seasonal snow cover extent changes in large Siberian watersheds. J Geophys Res 108:4578

Yang D, Kane D, Zhang Z, Legates D, Goodison B (2005) Bias corrections of long-term (1973–2004) daily precipitation data over the northern regions. Geophys Res Lett 32:L19501. https://doi.org/10.1029/2005GL024057

Ye B, Yang D, Kane DL (2003) Changes in Lena River streamflow hydrology: human impacts versus natural variations. Water Resour Res 39(7):1200. https://doi.org/10.1029/2003WR001991

Zhang T, Barry RG, Gilichinsky D, Bykhovets SS, Sorokovikov VA, Ye JP (2001) An amplified signal of climatic change in soil temperatures during the last century at Irkutsk, Russia. Clim Change 49:41–76

Zhang K, Kimball JS, Mu Q, Jones LA, Goetz SJ, Running SW (2009) Satellite based analysis of northern ET trends and associated changes in the regional water balance from 1983 to 2005. J Hydrol 379:92–110. https://doi.org/10.1016/j.jhydrol.2009.09.047

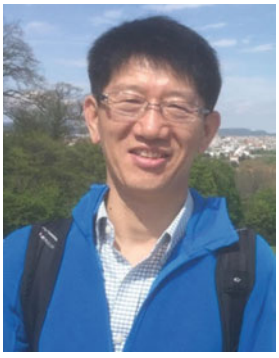

Dr. Hotaek Park is a Senior Scientist at JAMSTEC. He earned his Ph.D. at Graduate School of Bioagricultural Sciences, Nagoya University in 2000. Then, he worked at two Japanese Institutes as postdoctoral fellowship and joined the position of JAMSTEC research scientist in 2007. He is an expert on hydrology, biogeochemistry, and climate researches in cold regions, with interests in evaluating changes in land surface processes under climate changes and predicting future changes using land surface model, remote sensing data, reanalysis products, in site observations, and model outputs. He has the author/co-author of numerous scientific articles that have published on a variety of peer-reviewed journals, conference proceedings, and books. His recent research is focused on assessing impacts of changing snow and permafrost on hydrological processes in the context of climate variability and interactions between declining Arctic sea ice and terrestrial ecohydrologic processes coupling models of land–atmosphere–ocean processes.

Dr. Yonas Dibike is a Research Scientist at Environment and Climate Change Canada, Watershed Hydrology and Ecology Research Division at the University of Victoria. His research interests include hydrological, hydrodynamic, and transport modeling as well as hydro-climate analysis and climate change impact studies in cold region watersheds. He also holds adjunct faculty appointments at McMaster University and the University of Victoria in Canada. He is the author/co-author of numerous (>70) scientific articles that have appeared in a variety of peer-reviewed journals and conference proceedings. He is actively involved in Departmental and University-based researches and has co-supervised several graduate students and postdoctoral fellows.

Dr. Fengge Su is currently a Research Professor at the Institute of Tibetan Plateau, Chinese Academy of Sciences (ITP/CAS). She received her doctoral degree in 2001 from the Hohai University. She had been working in Dennis Lettenmaier's group at the University of Washington during 2003–2009. In 2010, she joined ITP/CAS. Her background is hydrology and water resources, specializing in large-scale land surface hydrological modeling. Her current research interests are mostly Tibetan Plateau-related Glacier/snow runoff modeling, runoff response to climate and glacier changes, high mountain precipitations, etc.

Dr. John Xiaogang Shi is a Senior Lecturer in hydrology at the University of Glasgow. He earned his Ph.D. from the Department of Civil and Environmental Engineering at the University of Washington in 2013. Then, he was awarded the Natural Sciences and Engineering Research Council of Canada (NSERC) postdoctoral fellowship and worked at Environment Canada's National Hydrology Research Centre. Prior to joining the University of Glasgow in 2018, he has previously worked as a Lecturer at Lancaster University and Xi'an Jiaotong-Liverpool University, and a Research Scientist in the Commonwealth Scientific and Industrial Research Organisation (CSIRO) in Australia. In 2015, he received the Research Innovation Award of Australian Water Association. He is an expert on water resources and climate research, with interests on modeling and predicting the role of water resources in the climate system and understanding the nature of hydrologic variability and change under changing climate at local, regional, continental, and global scales. His research has been focused on land surface hydrologic

model development, the analysis and modeling of hydrometeorological hazards (e.g., floods and droughts), hydrological forecasting, groundwater and surface–water interactions, snow and permafrost hydrology, and coupled modeling of land–atmosphere interactions in the context of climate variability and change by using remote sensing data, reanalysis products and in situ observations, as well as model outputs.

Regional Climate Modeling in the Northern Regions

27

Zhenhua Li, Yanping Li, Daqing Yang, and Rajesh R. Shrestha

Abstract

Regional climate models (RCMs) are indispensable tools for dynamically downscaling climate projections to regional scales. Compared to statistical downscaling, RCMs provide a tool to investigate how regional scale climate evolves without assuming stationarity by explicitly representing the physical processes resolved by the RCMs. Studies using RCMs have investigated the climate change's impacts on precipitation, temperature, floods, permafrost, wildfire, etc., over the northern regions of North America. As the computing capacity increases, RCMs with grid spacing less than 5 km can directly resolve convection and eliminate the need to parameterize one important process in the generation of precipitation and improves the simulation of convective precipitation. As the need for regional climate dynamical downscaling increases, further improvements of RCMs and incorporation of other components of eco-climate system are needed.

Z. Li (✉) · Y. Li
Global Institute for Water Security, University of Saskatchewan, Saskatoon, SK, Canada
e-mail: zhenhua.li@usask.ca

D. Yang · R. R. Shrestha
Watershed Hydrology and Ecology Division, Environment and Climate Change Canada, Victoria, BC, Canada
e-mail: Daqing.Yang@gmail.com; daqing.yang@canada.ca

D. Yang and D. L. Kane (eds.), *Arctic Hydrology, Permafrost and Ecosystems*,
https://doi.org/10.1007/978-3-030-50930-9_27

27.1 Introduction

Regional climate models (RCMs) are high-resolution climate system models that simulate the climate system of regions typically covering a domain from thousands of square kilometres to a continent. RCMs have many applications in the field of climate science, hydrology, and ecosystem due to their fine resolution to better represent processes that are unresolved by Global Climate Models (GCMs). The projection of future climate is often conducted by large-scale GCMs that are forced by projected radiative forcing by greenhouse gas emission. To connect the large-scale climate projection to local and regional climate impacts when shifting climate regimes are bound to change the statistical distribution of climate variables, dynamical downscaling is indispensable. For the regional climate projection and the assessments of the impacts of climate change on hydrological processes and eco-systems, many small-scale processes in the climate system cannot be properly represented by large-scale climate models. RCMs are computationally more feasible for high-resolution simulation because of their limited domains compared to GCMs. Typical horizontal resolution of RCMs is several kilometres to 25 kilometres whereas the horizontal spacing of GCM is usually larger than 100 km. As shown in Fig. 27.1, the higher resolution of RCMs makes them better at resolving fine-scale atmospheric processes such as convective cells, local topography, land-sea contrast, local scale hydrological, and terrestrial processes compared to GCMs (Leung 2012; Feser et al. 2011).

RCMs are developed from mesoscale atmospheric models that were designed for weather forecasting and short-term simulation of a few days. Unlike global climate models, weather forecasting models lack proper representation of radiative transfer and biosphere–atmosphere exchange near the land surface that governs the energy and water balance of the climate system, which make weather forecasting model unsuitable for long term climate simulation (Leung 2012). By adapting the physics parameterization from GCMs, RCM can be run at long duration for climate simulations (Giorgi et al. 1993a, b). Most RCMs include atmospheric model and the coupled land surface models (LSMs) for the underlying boundary. More sophisticated models may have model components of ocean, sea ice, hydrology, and atmospheric chemistry as well.

The added value of RCM simulations relative to its driving GCMs are widely accepted especially in regions of strong heterogeneous underlying boundary and for mesoscale atmospheric processes in particular when the RCM is constrained at the large spatial scales through boundary condition and spectral nudging (Feser et al. 2011). This is especially true for variables, such as near-surface temperature, humidity that are strongly affected by the representation of near-surface processes. The mesoscale phenomena such as polar lows (Feser et al. 2011) and mesoscale convective systems (Prein et al. 2017) can be represented more realistically in high-resolution RCM simulations. Because of RCMs' ability to resolve subgrid-scale processes in GCMs that are important to water cycles and ecosystem,

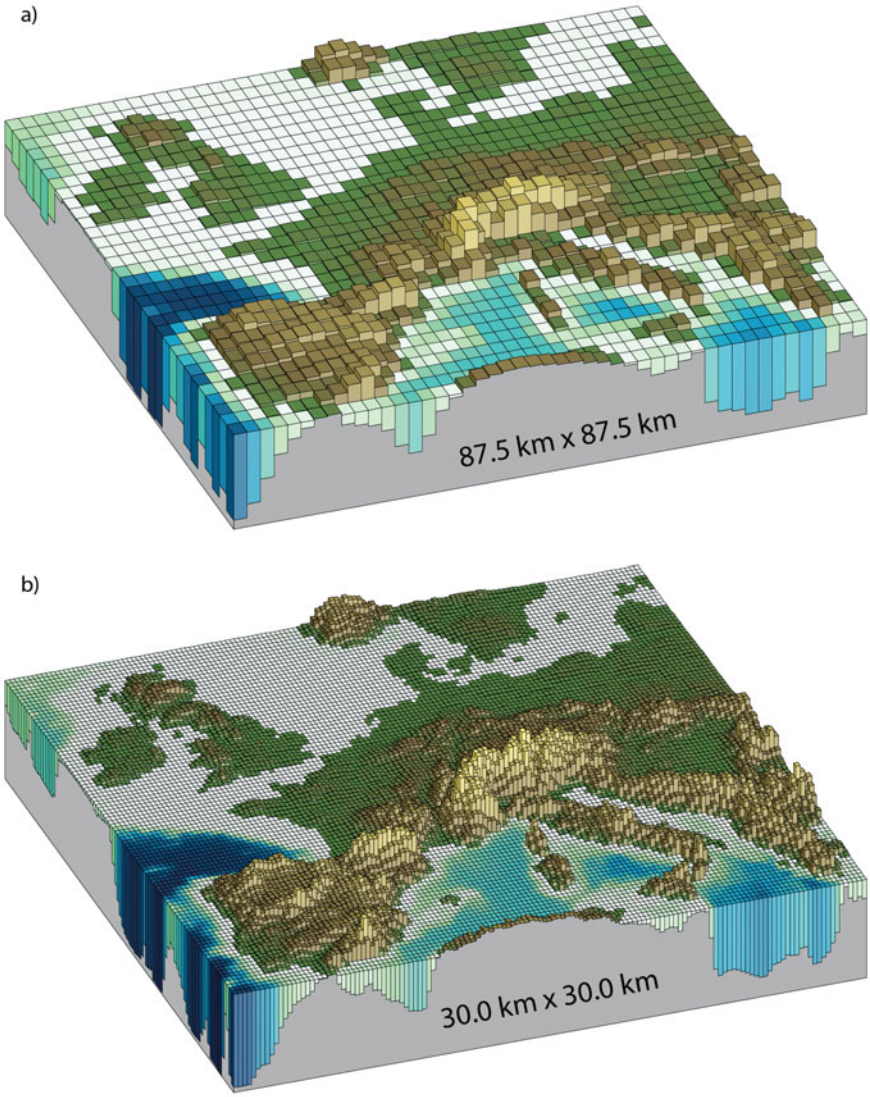

Fig. 27.1 Horizontal resolutions considered in today's higher resolution models and in the very high-resolution models now being tested: **a** Illustration of the European topography at a resolution of 87.5 × 87.5 km; **b** same as (a) but for a resolution of 30.0 × 30.0 km (Adapted from IPCC http://www.climatechange2013.org/images/report/WG1AR5_Chapter01_FINAL.pdf Fig. 1.14)

RCMs are widely used to provide detailed projections of future climate scenarios and downscaling information for impact studies, especially those associated with the aforementioned fine-scale processes.

27.2 Regional Climate Modeling in Canada

RCMs in principle can be used as a dynamical downscaling tool in vastly different geographical regions because the general dynamics of the atmosphere and climate is the same across the globe. However, the difference in the driving GCMs and RCM physics have significant impacts on regional climate change projection (Elía and Hélène 2010). RCMs developed by many institutions from the US, Europe, and Canada have been applied in the northern part of North America for climate downscaling and impact studies. Two major Canadian models are CRCM (Canadian Regional Climate Model, current version 5), developed by Université du Québec à Montréal (UQAM)'s Centre pour l'étude et la simulation du climat à l'échelle régionale (ESCER), in collaboration with Environment and Climate Change Canada (ECCC) (Caya and Laprise 1999; Laprise 2008) and the Canadian Regional Climate Model (CanRCM current version 4) developed by Canadian Centre for Climate Modelling and Analysis (CCCma), ECCC (Scinocca et al. 2016). These RCMs have been applied to downscale climate (e.g., temperature, precipitation) projections over the North America individually and under several intercomparison frameworks.

CRCM has been used by several researchers to downscale climate projection in the twenty-first century with special interest in the cold region hydrology. Using 45 km resolution CRCM4 forced by CGCM3 (Canadian Centre for Climate Modelling and Analysis Coupled Global Climate Model 3) with IS92a emission scenario that specifies effective CO_2 concentration increasing at 1% per year, Sushama et al. (2006) projected that the average annual precipitation in the Mackenzie, Yukon, and Fraser River basins will increase by 6–10% by 2070. They also projected a general decrease of snow water equivalent in the above basins and decrease of runoff. Sushama et al. (2007) used the same configuration of CRCM4 to study the impact of climate change on permafrost in North America under the Special Report on Emissions Scenarios (SRES) A2 scenario. Permafrost is categorized into isolated, sporadic, discontinuous, or continuous distributed across northern Canada. In all four zones, the temperature of the soil near the surface showed a marked increase, especially the temperature of the continuous permafrost by mid-century (2041–2070) will increase by 4–6 °C. Precipitation in all zones is projected to increase in all months. By the middle of this century, the average annual precipitation will increase by 15–20%.

Climate change's impact on hydrological cycle in Canada has also been studied with focus on the attribution of changes to different spatial and temporal scale processes. Bresson and Laprise (2009) used CRCM4 driven by CGCM to simulate current conditions for 1961–1990 and SRES A2 scenario (2041–2070) over North America. The moisture flux divergence is decomposed in terms of three scales of wind and moisture which provide nine interaction terms that separate small scales resolved exclusive by the high-resolution CRCM from larger scales. Future climate projection showed an overall intensification of the hydrological cycle in winter and mixed trend in summer. They also found a significant contribution of small-scale

terms to time variability both in the current and future climate. Mailhot et al. (2007) used the CRCM4 simulations under control (1961–1990) and future (2041–2070) climates to investigate the change in the intensity–duration–frequency curve of May to October annual maximum rainfall for different duration from 2-h to 24-h. The return periods of 2- and 6-h extreme events will approximately halve in future climate and will decrease by a third for 12- and 24-h events. These extreme precipitations will come more from convective and localized weather systems in the future. Similarly, Mladjic et al. (2011) using a 10 member CRCM4 ensemble-driven by CGCM 3 with the A2 SRES scenario showed an increase in extreme precipitation events with different durations in Canada.

27.3 NARCCAP and CORDEX

RCM simulations are strongly affected by the representation of dynamics and physics in the model as well as boundary conditions. Because the sensitivity of RCM simulation to the driving GCMs and model physics, two major frameworks for intercomparison of RCM downscaling efforts, NARCCAP and CORDEX-NA corresponding to Coupled Model Intercomparison Project, Phase 3 (CMIP3) and Phase 5 (CMIP5) GCMs, respectively, were constructed for North America in the last decade. Both Intercomparison projects enhanced the knowledge of model performance in many aspects of regional climate simulation and the uncertainty of dynamical downscaling.

The North American Regional Climate Change Assessment Program (NARCCAP) produced high-resolution (50 km) climate scenario projection for North America (the US, Canada, and northern Mexico) with RCMs coupled with Atmosphere-Ocean General Circulation Models (AOGCM)s and time-slice experiments (Mearns et al. 2009). RCMs from the US, Canada, and Europe were forced by AOGCM output for the historical period 1971–2000 and for the future period 2041–2070 with A2 SRES (Nakicenovic et al. 2000) of future emissions scenarios. The A2 SRES, an emissions scenario at the higher end of the SRES, was chosen to provide more insights on the impact and adaptation to a larger climate change in the next century. It is also close to the actual trajectory of emissions from 1990s to present (Mearns et al. 2012).

In addition to continuous AOGCM simulation from current to the future, time-slice experiments that use projected boundary conditions applied to the atmospheric models are also performed in NARCCAP. In a time-slice experiment, the atmospheric component of an AOGCM is forced with observed sea surface temperatures and sea ice boundaries for the historical run, while those same observations combined with perturbations from the future AOGCM to represent a warmer boundary condition for the scenario run. The two time-slice simulations are coupled with the Geophysical Fluid Dynamics Laboratory (GFDL) atmospheric model (AM2.1) and the National Center for Atmospheric Research (NCAR) CCSM atmospheric model (CAM3) each (Mearns et al. 2012).

Table 27.1 The participating models of NARCCAP

Model	Institute	Coupled GCMs, reanalysis	Resolution (km)	Land surface	Boundary layer	Cumulus parameterization
CRCM	UQAM	CCSM, CGCM3, NCEP	50	CLASS	Local K, gradient Richardson number formulation	Mass flux
ECP2	UC San Diego/Scripps	GFDL, HadCM3, NCEP	50	NOAH	Hong-Pan non-local K	Simplified Arawaka-Schubert
HRM3	Hadley Centre	GFDL, HadCM3, NCEP	50	MOSES	First order turbulent mixing	Mass Flux, including downdraft
MM5I	Iowa State University	CCSM, HadCM3, NCEP	50	NOAH	Hong-Pan (MRF) counter-gradient, non-local K	Kain-Fritsch2 mass flux
RCM3	UC Santa Cruz	CGCM3, GFDL, NCEP	50	BATS	Non-local K, counter-gradient flux	Grell with Fritsch-Chappell closure
WRFG	NCAR	CCSM, CGCM3, NCEP	50	NOAH	Yonsei Univ. (explicit entrainment)	Grell

Table 27.1 shows the summary of the participating models and basic configuration of the simulations for NARCCAP. These RCM simulations have been used for climate impact analysis, further downscaling experiments, analysis and comparison of model performance and uncertainty at regional scales to project future climate. Researches based on the data from NARCCAP provide many insights on the regional climate change projection in North America, including extreme precipitation, drought characteristics, snow covers, etc. Using RCMs driven by NCEP reanalysis, Wehner (2013) showed that there is large variability between models' projection of extreme precipitation statistics. From the same study, using AOGCM driven RCM results from NARCCAP, statistically significant precipitation increases are projected for most of the northern US and Canada in the winter and in most of Canada for the other three seasons. Future changes in the seasonal maxima precipitation and their 20-year return values follow the same general spatial pattern though less statistically significant. Masud et al. (2017) assessed the projected changes of drought in Alberta, Saskatchewan, and Manitoba through Standardized Precipitation Index (SPI) and the Standardized Precipitation Evapotranspiration Index (SPEI) using six RCMs driven by NCEP reanalysis and four RCMs driven by AOGCM. The projected changes in the six RCMs ensemble-averaged drought characteristics in terms of the mean and 20- and 50-year return levels show increases over the southern and south-western parts of the prairie provinces. McCrary et al. (2017) compared snow water equivalent (SWE) from six RCMs driven by reanalysis from NARCCAP to SWE from a new ensemble observational product which is from 14 sources to assess the RCMs' capability in simulating the magnitude, spatial distribution, duration, and timing of the snow season. MM5I is

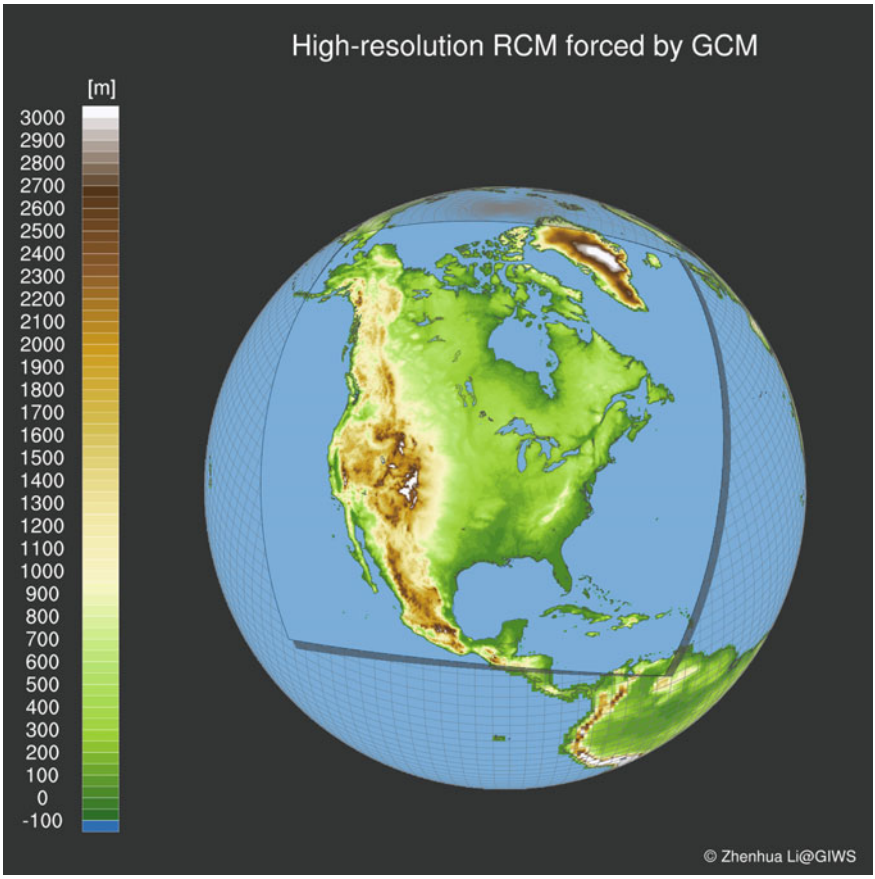

Fig. 27.2 The common simulation domain for NA-CORDEX

found to best capture SWE features despite its use of the Noah land surface model. RCM3 overestimates SWE due to its excessive precipitation in snow season. CRCM produces more SWE due to cold temperature biases and surface temperature parameterization options. Warm biases in HRM3 causes an underestimate in SWE. The Noah land surface model plays the major role in causing misrepresented SWE in WRFG and ECP2.

NA-CORDEX (https://na-cordex.org), the North American branch of Coordinated Regional Climate Downscaling Experiment (CORDEX, Giorgi et al. 2009) is the more recent and on-going coordinated regional climate downscaling efforts in North America. As shown in Fig. 27.2, NA-CORDEX archives RCM runs over a domain covering most of North America driven by boundary conditions from GCM simulations in the CMIP5 archive and CMIP6 in the future. The Arctic-CORDEX domain also covers the northern Canada and Alaska. CORDEX has both hindcast

(ERA-Interim and GCM-driven historical simulations) and scenario (GCM-driven rcp4.5, rcp8.5 simulations) simulations. These simulations run from 1950–2100 with a spatial resolution of 0.22°/25 km or 0.44°/50 km. The higher spatial resolution of CORDEX compared to NARCCAP is a reflection of the advancement in the computing capacity of the climate modeling community in recent years. More detailed information about NA-CORDEX simulations can be found on NA-CORDEX website (https://na-cordex.org).

Over Canada, the one of the model participant of CORDEX-NA is the fifth-generation Canadian Regional Climate Model (CRCM5), and several studies have been conducted focusing on model evaluation and improvements. As part of the CORDEX project, Takhsha et al. (2017) used CRCM5 over the Arctic domain driven by reanalyses and by the MPI-ESM-MR coupled global climate model (CGCM) under the RCP8.5 scenario to study the sensitivity of the downscaling results to spectral nudging and SST correction. Spectral nudging in the hindcast simulation driven by reanalysis reduced the mean sea level pressure bias in spring. The CRCM5 run driven by CGCM with empirically corrected SST provides similar projection for temperature but different projection for precipitation than those driven by CGCM with simulated SST.

In comparison with several observation datasets, Martynov et al. (2013) evaluated the performance of the reanalysis-driven CRCM5 in capturing the present climate over the NA-CORDEX domain for the 1989–2008 period. Their results show that CRCM5 captured the general pattern of surface temperature and precipitation well, though winter precipitation in coastal mountainous regions is overestimated. Martynov et al. (2013) also concluded that CRCM5 is substantially improved compared to CRCM3 and CRCM4 in terms of seasonal mean statistics. Eparović et al. (2013) used CRCM5 driven by the CanESM2 and MPI-ESM-LR CGCM simulations to conduct dynamical downscaling for the historical (1850–2005) and future (2006–2100) RCP4.5 scenario. The CRCM5 projected a general warming for the whole NA-CORDEX domain in the twenty-first century, especially over the northern regions in winter. The CRCM5 runs also showed a reduction in the frequency and intensity of cold spells. In general, the projected annual precipitation increases over the continent, except over central America where less precipitation is projected by CRCM5.

Whan and Zwiers (2016) evaluated the simulation of North American climate extremes by these two CORDEX generation Canadian RCMs: CRCM5 and CanRCM4, with lateral boundary conditions derived from the ERA-Interim reanalysis. They found that annual cycle and spatial patterns of extreme temperature indices were generally well reproduced by both models but the magnitude varies. However, varying amount of biases were present in both RCMs. Furthermore, CanRCM4 simulates too little convective rainfall, while over-estimating largescale rainfall. CRCM5 simulates more large-scale rainfall throughout the year on the west coast and in winter in other regions. Nevertheless, the spatial extent, intensity, and location of atmospheric river (AR) landfall were well reproduced by the RCMs, as is the fraction of winter rainfall from AR days.

The fourth generation Canadian Regional Climate Model (CanRCM4) (Scinocca et al. 2016) also participated in the CORDEX-NA with a large ensemble. The novelty of CanRCM4 stems from a new philosophy of coordinating the development and application of RCMs and GCMs. CanRCM4 shares exactly the same package of physical parameterizations with CCCma's global atmospheric climate model (CanAM4; von Salzen et al. 2013). Further, by employing a spectral nudging procedure in CanESM2 designed to constrain its evolution to follow any large-scale driving data, CanRCM4 can be driven by its parent GCM for all downscaling applications. A 50-member large ensemble of CanRCM4 (CanRCM-LE) has been set up by initializing five CMIP5 CanESM2 historical simulations, and randomly perturbing the initial conditions in the year 1950 and performing 10 runs for each CMIP5 ensemble member (Kirchmeier-Young et al. 2017).

Focusing on western Canada, Fig. 27.3 compares the ensemble mean of 50-member CanRCM4-LE simulations of temperature and precipitation with the observation-based dataset (Pacific Northwest North-American meteorological (PNWNAmet) gridded climate data; Werner et al. 2019). The climatology (1986–2010) plots that include the two Arctic flowing Mackenzie and Yukon basins indicate a good representation of the spatial variability of temperature and precipitation, although, compared to the PNWNA dataset, CanRCM4-LE mean is colder for the Yukon and warmer for the Mackenzie basin, and wetter for both basins.

Climate change's impact on wildfire is an important application of RCMs in Canada, where vast area of boreal forests are vulnerable to wildfire in a warmer climate. Kirchmeier-Young et al. (2017) used CanRCM4-LE under an event attribution framework to quantify the influence of anthropogenic forcings on extreme wildfire risk in a region of western Canada that includes Fort McMurray.

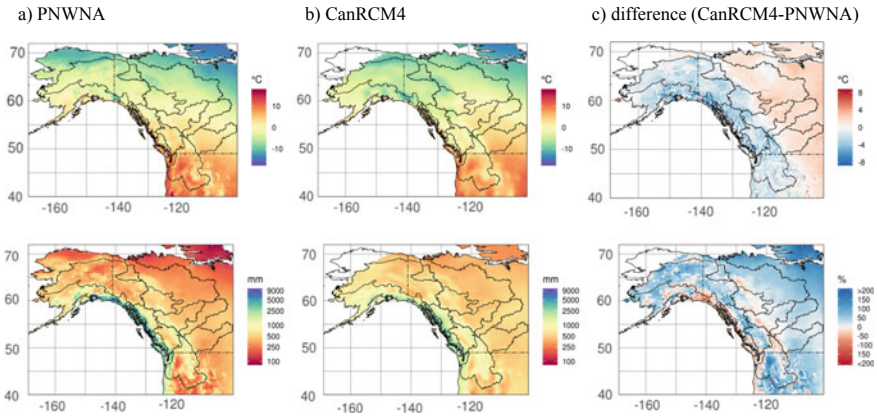

Fig. 27.3 Comparison of the CanRCM4-LE ensemble mean 1986–2010 climatology with the observation-based PNWNA dataset. The upper and lower panels depict the annual mean temperature and precipitation, with differences expressed as °C and %, respectively

Based on the fourteen metrics from the Canadian Forest Fire Danger Rating System derived from CanRCM-LE data, they found that due to the combined effect of anthropogenic and natural forcing, extreme fire risk events in the region likely has increased by 1.5–6 times compared to a climate that would have been with natural forcings alone. Further, Kirchmeier-Young et al. (2019) using CanRCM4-LE showed that the fire risk factors affecting the event, and the area burned itself, were made substantially greater by anthropogenic climate change.

27.4 Convection-Permitting RCMs

A major source of uncertainty in future climate projection is the representation of convective precipitation in the RCMs. Even though most RCMs have finer resolution than GCMs, they still cannot resolve convection and have to rely on convective parameterization schemes to represent the convective storms in the model. A convective parameterization scheme, either bulk mass-flux schemes or spectral schemes, calculate the estimated statistically averaged effects of convection over model grid and modify the vertical profile of model variables on the grid to deduce the redistribution of the heat, mass, moisture, and momentum associated with the subgrid convective processes that cannot be resolved at coarse resolution (Yu and Lee 2010). Because deep convection contributes disproportionately to precipitation amount and extremes in summer, convective parameterization causes substantial bias in simulated hydrological cycle in terms of underestimated dry days and misrepresentation of the diurnal cycles of convective precipitation.

In recent years the resolution of RCMs has been increasing together with the growth of computing power. Another problem occurs when the grid size of RCMs is reduced to fine scales of 10–40 km, which are comparable to the size of average thunderstorm and common resolution in both NARCCAP and CODEX. At these resolutions, the models attempt to resolve convection cells explicitly on the grid when their relatively coarse resolution generate updrafts that are too large and physically unrealistic. To reduce the convective instability and prevent the spurious convection, the convection parameterization has to be tuned to be more active, which actually enhances the deficiency in the convective schemes (Westra et al. 2014).

The assumptions that the grid square size is much larger than convective cells, on which mass-flux convection scheme is based on, often break down at these “grey zone” resolutions (Yu and Lee 2010) when the area of convection becomes comparable to the area of the grid (Swann 2001). RCMs using grid spacing less than 4 km are able to represent the convection on the grid sufficiently well without the use of a convection parameterization (Westra et al. 2014). Regional climate modeling using convection-permitting models (CPMs), sometimes referred as cloud resolving models, emerges as a promising framework to generate more realistic regional to local scales climatic information compared to models with coarser resolution and convective parameterization (Prein et al. 2015). In addition to

explicitly representing deep convection, CPMs also permit a more accurate representation of underlying surface and topography.

Though CPMs require higher computational resources compared to large-scale models, CPMs can simulate mesoscale convective systems more realistically, produce better convective precipitation, and orographic precipitation (Prein et al. 2015, 2017; Weusthoff et al. 2010). Liu et al. (2017) conducted convection-permitting simulation with 4-km grid spacing over much of North America using the WRF model. Two 13-year simulations were performed over contiguous US (WRF-CONUS) for a retrospective simulation (October 2000–September 2013) driven by ERA-interim reanalysis (Dee et al. 2011) and a future climate sensitivity simulation with reanalysis-derived initial and boundary conditions perturbed with changes in filed variables from the CMIP5 ensemble-mean high-end emission scenario (RCP8.5) climate. The retrospective CPM simulation of WRF-CONUS has been evaluated to reproduce the characteristics observed mesoscale convective systems (MCSs) (Prein et al. 2017a), a significant improvement over GCMs and RCMs employing cumulus parameterizations. As shown in Fig. 27.4, Prein et al. (2017) analyzed the MCSs in WRF-CONUS simulation using an objective tracking algorithm and found larger rain volumes, higher rainrates, larger rain areas, and faster translation of MCSs by the end of twenty-first century.

27.5 Challenge for RCMs in Canada

The first challenge for climate simulation in Arctic Canada stems from the lack of comprehensive observation network covering the whole country. Canada's meteorological observation network is heavily concentrated in the southern part of the country and over the plains because of its population density distribution and logistics factors. There are far less observation stations in the sparsely populated area in the north and over the mountainous regions. The lack of observation presents unique challenges for regional climate modeling in several aspects. The sparse observation network in the sparsely populated region provides less reliable and representative observation data for the development and validation of regional climate models in the region (Hofstra et al. 2009; Takhsha et al. 2017).

The unique geographical features of Canada and Arctic also pose special challenges for model development. The mountainous terrain and large numbers of lakes make interpolation of observation data to gridded data-sets difficult. The cold region hydrological cycle and treatment of the snow cover in the land surface model component of RCMs also poses great challenge to simulate the characteristics of surface temperature and hydrological processes in the region (Niu et al. 2011; Casati and de Elía 2014). In total, there are more than one million lakes of various kinds and sizes covering Canada. About 8% of Canada's surface is covered by lakes (tundra ponds, glacial lakes, and reservoirs). Lakes influence the regional climate through thermal moderation, enhanced evaporation, changing local wind, and precipitation patterns such as lake-effect snow, etc. In turn, lakes are also affected

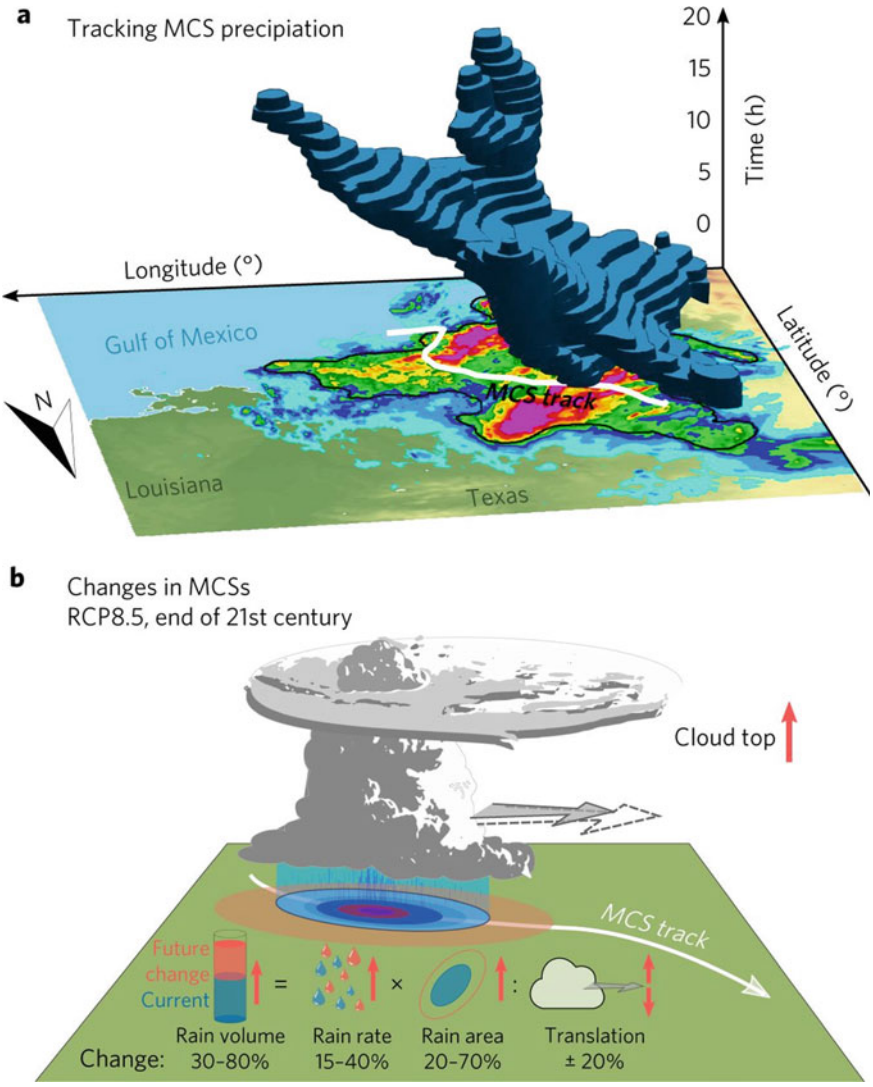

Fig. 27.4 Using objective tracking algorithm in a retrospective and RCP8.5 pseudo-global warming simulation, Prein et al. (2017b) show MCSs in the US will have larger rain volume, higher rainrates, larger rain areas, and faster translations by the end of twenty-first century. Copyright: Nature Climate Change 2017 Prein et al. Fig. 27.1

by hydrological changes caused by climate change. Many efforts have been put into improving the representation of lakes and wetland in RCMs. Some preliminary work aims to improve CRCM5 by including lake–river interaction and interflow is presented by Huziy and Sushama (2016), Goyette et al. (2000), and shows that the

impact of lakes–river interaction is important on the regional hydrology, particularly streamflows.

Cold region hydrometerology is also strongly affected by snow processes. The representation of snow pack and cover in the mountainous region is a challenging obstacle to overcome in order to realistically reproduce the hydroclimatic condition in the Canadian Rockies (Niu et al. 2011; Pomeroy et al. 2007). Casati and de Elía (2014) demonstrate the importance of snow cover and sea ice for daily minimum temperature and soil moisture for daily maximum temperature. In the recent paper by McCrary et al. (2017), the snow water equivalent (SWE) from six reanalysis driven NARCCAP RCMs is evaluated against the observational ensemble. The simulated SWE is affected by both the precipitation and temperature biases in the models and the different treatments of snow cover and snow layer in the LSMs in the RCMs. Even though the MM5I produces less bias than other models, McCrary et al. (2017) note the SWE is not well represented by the Noah LSM used in MM5I. CRCM uses CLASS LSM that allows snowmelt to refreeze in the snowpack, which contributes to the high SWE values and long SWE retention in CRCM on top of cold temperature bias.

For long term climate projection, the permafrost zones in Canada provide further challenges. The huge amount of soil organic carbon storage in the permafrost poses the most important feedback mechanism to escalate global warming (Koven et al. 2011; Schuur et al. 2008; Tarnocai et al. 2009; MacDougall et al. 2012). The representation of permafrost in the RCMs is generally crude and only account for shallow soil layers. Sushama et al. (2007) use CRCM4 with a three-layer Canadian Land Surface Scheme (CLASS) to study the soil thermal and moisture regimes for permafrost regions in North America. Paquin and Sushama (2014) studied the sensitivity of simulated Arctic soil temperature and moisture for near-surface permafrost to soil layer configuration and soil organic carbon using offline simulation with CLASS and CRCM5 experiments with 0.5 degree resolution. They found substantial improvements in the representation of soil thermal and moisture regimes by using a deeper soil column, implementing soil organic carbon, and modification of snow thermal conductivity. Due to the high heterogeneity of soil organic carbon distribution (i.e., high in valleys and low in ridges), high-resolution RCMs with better representation of soil layers in permafrost in the LSMs are needed to realistically simulate the thermal and moisture regimes and the decomposition of soil organic carbon.

Besides these challenges in the physical process representation, RCMs are affected by biases in GCMs. Since GCMs are not designed to represent regional and local scale climatology, the biases that arise from driving GCMs propagate into RCMs, and the biases may be reduced or amplified by RCMs (Gao et al. 2011). After all, small deviations in the boundary and initial conditions provided by GCMs for the RCMs can be amplified by the internal regional and local scale dynamics of RCMs and various parameterization schemes that only approximate the physical processes in the boundary layer and atmosphere. For instance, Shrestha et al. (2014) evaluated hydroclimatic change signals from CRCM4 (Music and Caya 2009) with statistically downscaled GCMs and hydrologic models (Schnorbus et al. 2014).

The comparisons were made for the Peace River basin in Western Canada that flow onto Mackenzie River. They found that CRCM-simulated temperature, precipitation, snow water equivalent, and runoff differ substantially when compared to statistically downscaled GCMs and hydrologic model simulations. Specifically, CRCM4 simulated precipitation and temperature were found to be drier and colder, respectively, with annual precipitation $\sim$18% lower and annual temperature $\sim$6 °C colder than observed. The differences were attributed to the biases that propagate through the CRCM model system. Nevertheless, the projected changes in the future period (2050s) relative to the historical period (1970s) were qualitatively similar for precipitation and temperature, although substantially different for snow water equivalent and runoff.

Enhancements such as reduction of biases and better representation of the land surface processes have been achieved in the current generation of RCMs through the increase of resolution and improvements in the parameterization schemes and land surface models. For instance, 52% and 79% of grid points in the CanRCM4 ensemble mean are within $\pm$1 °C and $\pm$2 °C, respectively, compared to PNWNAmet dataset (Fig. 27.3). However, precipitation biases still appear to persist with only about 40% of grid points in the CanRCM4 ensemble mean are within $\pm$30% of the PNWNAmet dataset. The difficulty in precipitation simulation compared to temperature is due to the challenges to represent the complex subgrid processes involved in precipitation generation such as cumulus clouds, cloud micro-physics schemes, and boundary-layer processes. Nevertheless, with continued enhancements, the RCMs can be expected to provide improved representations of basin scale hydroclimatology. Furthermore, with the recent advancement in computation capability in climate science, higher resolution models have been used more widely to achieve better representation of these subgrid processes of GCMs. Higher resolution RCMs also make the direct comparison of model simulation to in situ observation more realistic and provide means to discover model deficiencies in representing small-scale physical processes, which can contribute back to the improvement of parameterizations in large-scale models. Therefore, downscaling climate projection over Canada with convection-permitting RCMs is urgently needed to provide better representation of convection over warm seasons, better representation of cold region hydrometerology in the LSMs, especially in the mountainous regions in western Canada.

27.6 Summary and Discussion

Great advances have been achieved by the regional climate modeling community to better simulate the hydroclimatic and meteorological phenomena in the northern regions of North America. Many inter-model comparisons have been conducted

under the two frameworks for RCM evaluation and projection. These studies have provided insights on the abilities and deficiencies of current RCMs and projections on how the future climates under different emission scenarios are going to manifest over North America's cold regions.

The challenges for the regional climate modeling in the northern regions can be categorized into three main aspects. One is the difficulty to obtain high quality high-resolution meteorological data for evaluation of the models in the harsh climates, sparsely populated areas, and over highly heterogenous geographical features. This can be partly remedied through the utilization of remote sensing data from space and ground and relies on the improvements in the reanalysis datasets. One example is the high-temporal and spatial resolution precipitation products such as Stage IV (Lin and Mitchell 2005) that enables the comparison between high-resolution RCM precipitation with observation. The second challenge is to properly represent subgrid-scale processes at higher resolution compared to GCMs. For example, as RCMs go into convection-permitting resolution and directly resolve cumulus clouds and convection, the relative importance of cloud microphysics increases for properly simulating precipitation. Adapting and improving these schemes involved in precipitation in the cold regions are urgently needed to properly represent the hydrological cycles. Thirdly, as the application of regional climate modeling expends in many areas of ecosystem, the incorporation of additional processes in RCMs requires cross-discipline cooperation. Such examples include the coupling of ocean, sea ice, and lake model, the development of dynamic vegetation component in the land surface models, the addition of deep soil layers represents permafrost and carbon cycle, etc.

References

Bresson R, Laprise R (2009). Scale-decomposed atmospheric water budget over North America as simulated by the Canadian regional climate model for current and future climates. Clim Dyn 36 (1–2):365–84. https://doi.org/10.1007/s00382-009-0695-4. Springer Nature

Casati B, de Elía R (2014) Temperature extremes from Canadian regional climate model (CRCM) climate change projections. Atmos-Ocean 52(3):191–210. https://doi.org/10.1080/07055900.2014.886179. Informa UK Limited

Caya D, Laprise R (1999) A semi-implicit semi-lagrangian regional climate model: the Canadian RCM. Month Weather Rev 127(3):341–62. https://doi.org/10.1175/1520-0493(1999)127%3c0341:asislr%3e2.0.co;2. American Meteorological Society

Dee DP, Uppala SM, Simmons AJ, Berrisford P, Poli P, Kobayashi S, Andrae U et al (2011) The ERA-interim reanalysis: configuration and performance of the data assimilation system. Quart J Royal Meteorol Soc 137(656):553–597. https://doi.org/10.1002/qj.828

de Elía R, Hélène C (2010) Climate and climate change sensitivity to model configuration in the Canadian RCM over North America. Meteorol Z 19 (4):325–39. https://doi.org/10.1127/0941-2948/2010/0469. Stuttgart, Germany: Schweizerbart Science Publishers

Eparović L, Alexandru A, Laprise R, Martynov A, Sushama L, Winger K, Tete K, Valin M (2013) Present climate and climate change over North America as simulated by the fifth-generation Canadian regional climate model. Clim Dyn 41(11-12):3167–3201. https://doi.org/10.1007/s00382-013-1737-5. Springer Nature

Feser Frauke, Rockel Burkhardt, von Storch Hans, Winterfeldt Jörg, Zahn Matthias (2011) Regional climate models add value to global model data: a review and selected examples. Bull Am Meteor Soc 92(9):1181–1192. https://doi.org/10.1175/2011bams3061.1

Gao Y, Vano JA, Zhu C, Lettenmaier DP (2011) Evaluating climate change over the Colorado River basin using regional climate models. J Geophys Res 116:D13104. https://doi.org/10.1029/2010JD015278

Giorgi F, Jones C, Asrar GR (2009) Addressing climate information needs at the regional level: the CORDEX framework. WMO Bull 58(3):175

Giorgi F, Marinucci MR, Bates GT (1993a) Development of a second-generation regional climate model (Regcm2). Part I: boundary-layer and radiative transfer processes. Mon Weather Rev 121(10):2794–2813. https://doi.org/10.1175/1520-0493(1993)121$%3c$2794:DOASGR%3e2.0.CO;2

Giorgi F, Marinucci MR, Bates GT, De Canio G (1993b) Development of a second-generation regional climate model (RegCM2). Part II: convective processes and assimilation of lateral boundary conditions. Mon Weather Rev 121(10):2814–32. https://doi.org/10.1175/1520-0493(1993)121$$%3c$$2814:DOASGR%3e2.0.CO;2. American Meteorological Society

Goyette S, McFarlane NA, Flato G (2000) Application of the Canadian regional climate model to the laurentian great lakes regions. Implementation of a lake model. Atmos-Ocean 38:481

Hofstra Nynke, New Mark, McSweeney Carol (2009) The influence of interpolation and station network density on the distributions and trends of climate variables in gridded daily data. Clim Dyn 35(5):841–858. https://doi.org/10.1007/s00382-009-0698-1

Huziy O, Sushama L (2016) Impact of lakeriver connectivity and interflow on the Canadian RCM simulated regional climate and hydrology for northeast Canada. Clim Dyn 48(3):709–25. https://doi.org/10.1007/s00382-016-3104-9. Springer Berlin Heidelberg

Kirchmeier-Young MC, Zwiers FW, Gillett NP, Cannon AJ (2017) Attributing extreme fire risk in Western Canada to human emissions. Clim Change 144(2):365–379

Kirchmeier-Young MC, Gillett NP, Zwiers FW, Cannon AJ, Anslow FS (2019) Attribution ofthe influence of human-induced climate change on an extreme fire season. Earth's Future 7. https://doi.org/10.1029/2018EF001050

Koven CD, Ringeval B, Friedlingstein P, Ciais P, Cadule P, Khvorostyanov D, Krinner G, Tarnocai C (2011) Permafrost carbon-climate feedbacks accelerate global warming. Proc Natl Acad Sci 108(36):14769–14774. https://doi.org/10.1073/pnas.1103910108

Laprise R (2008) Regional climate modelling. J Comput Physics 227(7):3641–66. https://doi.org/10.1016/j.jcp.2006.10.024. Elsevier BV

Leung LR (2012) Regional climate models regional climate model. In: Encyclopedia of sustainability science and technology. Springer, New York, NY, pp 8902–8919. https://doi.org/10.1007/978-1-4419-0851-3_363

Lin Y, Mitchell KE (2005) The NCEP stage II/IV hourly precipitation analyses: development and applications. In: 19th conference hydrology. August 2019. https://ams.confex.com/ams/pdfpapers/83847.pdf

Liu C, Ikeda K, Rasmussen R, Barlage M, Newman AJ, Prein AF, Chen F et al (2017) Continental-scale convection-permitting modeling of the current and future climate of North America. Clim Dyn 49(1):71–95. https://doi.org/10.1007/s00382-016-3327-9. Springer Berlin Heidelberg

MacDougall AH, Avis CA, Weaver AJ (2012) Significant contribution to climate warming from the permafrost carbon feedback. Nat Geosci 5(10):719–721. https://doi.org/10.1038/ngeo1573

Mailhot A, Duchesne S, Caya D, Talbot G (2007) Assessment of future change in intensity-duration-frequency (IDF) curves for southern quebec using the Canadian regional

climate model (CRCM). J Hydrol 347(1-2):197–210. https://doi.org/10.1016/j.jhydrol.2007.09.019. Elsevier BV

Martynov A, Laprise R, Sushamarc L, Winger K, Šeparović L, Dugas B (2013) Reanalysis-driven climate simulation over CORDEX North America domain using the Canadian regional climate model, version 5: model performance evaluation. Clim Dyn 41(11):2973–3005. https://doi.org/10.1007/s00382-013-1778-9

Masud MB, Khaliq MN, Wheater HS (2017) Future changes to drought characteristics over the Canadian prairie provinces based on NARCCAP Multi-RCM ensemble. Clim Dyn 48(7):2685–2705. https://doi.org/10.1007/s00382-016-3232-2

McCrary RR, McGinnis Seth, Mearns LO (2017) Evaluation of snow water equivalent in NARCCAP simulations, including measures of observational uncertainty. J Hydrometeor 18(9):2425–2452. https://doi.org/10.1175/JHM-D-16-0264.1

Mearns LO, Flory D, Gutowski W, Moufouma-Okia W, McDaniel L, Qian Y, Roads J et al (2012) The North American regional climate change assessment program: overview of phase I results. Bull Am Meteorol Soc 93(9):1337–1362. https://doi.org/10.1175/BAMS-D-11-00223.1. American Meteorological Society

Mearns LO, Gutowski W, Jones R, Leung R, McGinnis S, Nunes A, and Qian Y (2009) A regional climate change assessment program for North America. Eos, Trans Am Geophys Union 90(36):311–11. https://doi.org/10.1029/2009EO360002. Wiley-Blackwell

Mladjic B, Sushama L, Khaliq MN, Laprise R, Caya D, Roy R (2011) Canadian RCM projected changes to extreme precipitation characteristics over Canada. J Clim 24(10):2565–2584. https://doi.org/10.1175/2010jcli3937.1. American Meteorological Society

Music B, Caya D (2009) Investigation of the sensitivity of water cycle components simulated by the Canadian regional climate model to the land surface parameterization, the lateral boundary data, and the internal variability. J Hydrometeor 10:3–21. https://doi.org/10.1175/2008JHM979.1

Nakicenovic N, Alcamo J, Grubler A, Riahi K, Roehrl RA, Rogner H-H, Victor N (2000) Special Report on Emissions Scenarios (SRES), a special report of working group III of the intergovernmental panel on climate change. Cambridge University Press, Cambridge. http://pure.iiasa.ac.at/id/eprint/6101/

Niu G-Y, Yang Z-L, Mitchell KE, Chen F, Ek MB, Barlage M, Kumar A et al (2011) The community noah land surface model with multiparameterization options (Noah-Mp): 1. Model description and evaluation with local-scale measurements. J Geophys Res 116 (D12). https://doi.org/10.1029/2010jd015139. American Geophysical Union (AGU)

Paquin J-P, Sushama L (2014) On the arctic near-surface permafrost and climate sensitivities to soil and snow model formulations in climate models. Clim Dyn 44(1–2):203–228. https://doi.org/10.1007/s00382-014-2185-6

Pomeroy JW, Gray DM, Brown T, Hedstrom NR, Quinton WL, Granger RJ, Carey SK (2007) The cold regions hydrological model: a platform for basing process representation and model structure on physical evidence. Hydrol Process 21(19):2650–2667. https://doi.org/10.1002/hyp.6787

Prein AF, Langhans W, Fosser G, Ferrone A, Ban N, Goergen K, Keller M et al (2015) A review on regional convection-permitting climate modeling: demonstrations, prospects, and challenges. Rev Geophys 53(2):323–361. https://doi.org/10.1002/2014RG000475

Prein AF, Liu C, Ikeda K, Bullock R, Rasmussen RM, Holland GJ, Clark M (2017a) Simulating North American mesoscale convective systems with a convection-permitting climate model. Clim Dyn. https://doi.org/10.1007/s00382-017-3993-2

Prein AF, Liu C, Ikeda K, Trier SB, Rasmussen RM, Holland GJ, Clark MP (2017b) Increased rainfall volume from future convective storms in the US. Nature Climate Change 7(12):880

Schuur EAG, Bockheim J, Canadell JG, Euskirchen E, Field CB, Goryachkin SV, Hagemann S et al (2008) Vulnerability of permafrost carbon to climate change: implications for the global carbon cycle. Bioscience 58(8):701–714. https://doi.org/10.1641/b580807

Schnorbus M, Werner A, Bennett K (2014) Impacts of climate change in three hydrologic regimes in British Columbia, Canada. Hydrol Process 28:1170–1189. https://doi.org/10.1002/hyp.9661

Scinocca JF, Kharin VV, Jiao Y, Qian MW, Lazare M, Solheim L, Flato GM, Biner S, Desgagne M, Dugas B (2016) Coordinated global and regional climate modeling. J Clim 29:17–35. https://doi.org/10.1175/JCLI-D-15-0161.1

Shrestha RR, Schnorbus MA, Werner AT, Zwiers FW (2014) Evaluating hydroclimatic change signals from statistically and dynamically downscaled GCMs and hydrologic models. J Hydrometeorol 15(2):844–860. https://doi.org/10.1175/JHM-D-13-030.1

Sushama L, Laprise R, Caya D, Frigon A, Slivitzky M (2006) Canadian RCM projected climate-change signal and its sensitivity to model errors. Int J Climatol 26(15):2141–2159. https://doi.org/10.1002/joc.1362. Wiley-Blackwell

Sushama L, Laprise R, Caya D, Verseghy D, Allard M (2007) An RCM projection of soil thermal and moisture regimes for North American permafrost zones. Geophys Res Lett 34(20). https://doi.org/10.1029/2007gl031385

Swann H (2001) Evaluation of the mass-flux approach to parametrizing deep convection. Quart J Royal Meteorolog Soc 127(574):1239–1260. https://doi.org/10.1002/qj.49712757406

Takhsha M, Nikiéma O, Lucas-Picher P, Laprise R, Hernández-Díaz L, Winger K (2017) Dynamical downscaling with the fifth-generation Canadian regional climate model (CRCM5) over the CORDEX arctic domain: effect of large-scale spectral nudging and of empirical correction of sea-surface temperature. Clim Dyn, October. https://doi.org/10.1007/s00382-017-3912-6

Tarnocai C, Canadell JG, Schuur EAG, Kuhry P, Mazhitova G, Zimov S (2009) Soil organic carbon pools in the northern circumpolar permafrost region. Global Biogeochem Cycles 23 (2): n/a–n/a. https://doi.org/10.1029/2008gb003327

von Salzen K, Scinocca JF, McFarlane NA, Li J, Cole JN, Plummer D, Verseghy D, Reader MC, Ma X, Lazare M, Solheim L (2013) The Canadian fourth generation atmospheric global climate model (CanAM4). Part I: representation of physical processes. Atmos-Ocean 51 (1):104-125

Wehner M (2013) Very extreme seasonal precipitation in the narccap ensemble: model performance and projections. Clim Dyn 40(1–2):59–80. https://doi.org/10.1007/s00382-012-1393-1

Westra S, Fowler HJ, Evans JP, Alexander LV, Berg P, Johnson F, Kendon EJ, Lenderink G, Roberts NM (2014) Future changes to the intensity and frequency of short-duration extreme rainfall. Rev Geophys 52(3):522–555. https://doi.org/10.1002/2014rg000464

Werner AT, Schnorbus MA, Shrestha RR, Cannon AJ, Zwiers FW, Dayon G, Anslow F (2019) A long-term, temporally consistent, gridded daily meteorological dataset for northwest North America. Nat Sci Data 6:180299. https://doi.org/10.1038/sdata.2018.299

Weusthoff T, Ament F, Arpagaus M, Rotach MW (2010) Assessing the benefits of convection-permitting models by neighborhood verification: examples from map d-phase. Mon Weather Rev 138(9):3418–3433. https://doi.org/10.1175/2010mwr3380.1

Whan K, Zwiers F (2016) Evaluation of extreme rainfall and temperature over North America in CanRCM4 and CRCM5. Clim Dyn 46(11–12):3821–3843

Yu X, Lee T-Y (2010) Role of convective parameterization in simulations of a convection band at grey-zone resolutions. Tellus A: Dyn Meteorol Oceanogr 62(5):617–632. https://doi.org/10.1111/j.1600-0870.2010.00470.x

Dr. Zhenhua Li is a Research Scientist at the Global Institute for Water Security at the University of Saskatchewan, Canada. He obtained his Ph.D. in Atmospheric Science from the University of Illinois at Urbana-Champaign (UIUC), USA. His research interests are atmospheric dynamics, regional climate modeling, drought study, etc. In particular, he is interested in looking at the interaction between climate change and regional land cover change, and interface between climate change and adaptive decision-makings over long timescales.

Dr. Yanping Li is an Associate Professor at the School of Environment and Sustainability and the Global Institute for Water Security at the University of Saskatchewan, Canada. She obtained her Ph.D. from Yale University, USA in Atmosphere, Ocean and Climate Dynamics. Her research interests are inter-disciplinary regarding high-resolution regional climate modeling, extreme weather, and land–atmosphere interaction to inform climate adaptations.

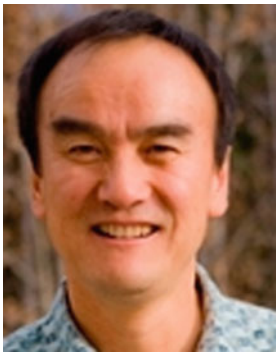

Dr. Daqing Yang is a Research Scientist at the Watershed Hydrology and Ecology Research Division, Environment and Climate Change Canada. He is also Affiliate Research Professor at the International Arctic Research Center, University of Alaska Fairbanks. Over the past 25 years, he has conducted cryosphere system research in China, Canada, Japan, USA, and Norway. His primary research activities/interests include cold region hydrology and climate, particularly Arctic large river streamflow regime and change, snow cover and snowfall measurements, climate change and human impact to regional hydrology, and applications of remote sensing in cold regions. He has served as journal editor and subject editor for IAHS publications (cold region hydrology, northern research basin water balance, and cold/mountain region hydrological systems under climate change), and WMO technical reports (solid precipitation measurement intercomparison and integrated global observing strategy cryosphere theme). He also contributed as review and/or author to the IPCC Reports, and the Arctic Council's Snow, Water, Ice and Permafrost in the Arctic (SWIPA 2017 and follow up) assessment. His current research focuses on investigating the impacts of climate variability/change and human activities on hydrologic system across the broader northern regions.

Dr. Rajesh R. Shrestha is a Research Scientist at the Watershed Hydrology and Ecology Research Division, Environment and Climate Change Canada, and holds an Adjunct Professor appointment at the University of Victoria. His current research focuses primarily on assessing the impacts of climate variability and change on hydrologic systems, including methods to characterize interactions and uncertainties in hydrologic projections, and nonstationarity of extreme events. He is active in the development and application of snow and hydrologic models, and observation-based and statistically downscaled climate data products.

28

High-Resolution Weather Research Forecasting (WRF) Modeling and Projection Over Western Canada, Including Mackenzie Watershed

Yanping Li and Zhenhua Li

Abstract

Weather Research Forecasting (WRF) model was run at a Convection-Permitting (CP) 4-km resolution to dynamically downscale the 19-member CMIP5 ensemble mean projection to assess the hydroclimatic risks in Western Canada under high-end emission scenario RCP8.5 by the end of twenty-first century. A retrospective simulation (CTL, 2000–2015) forced by ERA-Interim and a Pseudo-Global Warming (PGW) forced with the reanalysis plus the climate change forcing (2071-2100–1976-2005) were derived using CMIP5 ensemble. The surface air temperature of WRF-CTL, evaluated against gridded analysis ANUSPLIN, shows good agreements in the geographical distribution. There are cold biases east of the Canadian Rockies, especially in spring. WRF-CTL's precipitation resembles the geographical distribution of CaPA and ANUSPLIN. The wet bias mainly resides near the British Columbia coast in winter and over on the eastern side of the Canadian Rockies in summer. WRF-PGW shows much larger warming over the polar region in the northeast during the cold season relative to WRF-CTL. Precipitation increases in most areas in spring and autumn, whereas unchanged or decreased precipitation in summer occurs in the Saskatchewan River Basin and southern Canadian Prairies. The flat precipitation changes cannot compensate the enhanced evapotranspiration over the region causing the water stress for the rain-fed agriculture during the growing season in the future. WRF-PGW projects lower warming than that by the CMIP5 ensemble throughout the year. The CMIP5 ensemble projects a much drier future over the

Y. Li (✉)
School of Environment and Sustainability, Global Institute for Water Security, University of Saskatchewan, Saskatoon, SK, Canada
e-mail: yanping.li@usask.ca

Z. Li
Global Institute for Water Security, University of Saskatchewan, Saskatoon, SK, Canada
e-mail: zhenhua.li@usask.ca

D. Yang and D. L. Kane (eds.), *Arctic Hydrology, Permafrost and Ecosystems*,
https://doi.org/10.1007/978-3-030-50930-9_28

Canadian Prairies with a 10–20% decrease of summer precipitation. The CMIP5 ensemble mean generally agrees with WRF-PGW except for regions with significant terrain, which may be due to WRF's higher resolution can represent small-scale summer convection and orographic lifting better. A larger increase of high-intensity precipitation events compared to lower intensity events, which indicates a higher risk for extreme events and lower effective rainfall for agriculture. New bias correction methods need to be developed to capture the shift in the precipitation intensity distribution in the future. The study also reveals the urgent need for high-quality meteorological observation to provide forcing data and evaluation benchmarks in Western Canada. The high-resolution dynamical downscaling over Western Canada provides opportunities for studying local-scale atmospheric dynamics and providing hydroclimatic data for cold region ecosystems, agriculture, and hydrology.

28.1 Introduction

Since the beginning of instrument records in the nineteenth century, the global mean surface temperature has been rising, and many fingerprint changes in the climate system indicate that climate change is associated with greenhouse gas emission and accelerating (Bindoff et al. 2013; IPCC 2013). For the foreseeable future, greenhouse gas emissions will continue to increase, the global average temperatures will rise, and extreme weather events will increase (Easterling et al. 2000; Sugiyama et al. 2009), which will affect many aspects of ecosystems, environment, and society. While there is a consensus on anthropogenic climate change, it is unclear how regional climate systems will respond to potential greenhouse gas emissions due to the complexity of the climate system and uncertainty about future emissions. The challenge of predicting regional climate responses is not only due to the complexity of the atmosphere, oceans, surface, and hydrological processes but also because of the many interrelated, interactive, and feedback processes in the climate system.

Climate models are indispensable tools for improving our understanding and prediction of climate systems. Global Climate Models (GCMs) have been widely used to predict future climates under different emission scenarios and to assess the impacts of human activity on climate change since the Industrial Revolution. To represent complex climate systems in climate models, parameterization must be adopted to represent subgrid-scale processes. To faithfully represent the Earth's basic energy balance, GCM needs to simulate planetary-scale climate processes that transmit heat and mass through ocean currents and meandering jet streams. In addition to large-scales advection by mean atmospheric and ocean flows, GCM also needs to simulate atmospheric and ocean eddies embedded in the flow and transmit large amounts of heat and momentum. These eddies rise from the thermal gradient, and as global temperatures rise, the thermal gradient between the tropical and polar

regions changes, which are bound to affect these processes. Due to the complexity of the climate system, different numerical representation methods of climate processes bring great inter-model variability between climate centers (Deser et al. 2012; Mearns et al. 2013). Climate intercomparison projects show that the projections by GCMs have significant uncertainty depending on models, which often requires using ensemble mean to reduce uncertainty. For example, the Coupling Model Interaction Project Phase 5 (CMIP5) uses a common set of model simulations to evaluate GCMs from multiple countries.

The impact of climate change on ecosystems and human society, however, often occurs at local and regional levels. For instance, surface air temperature is strongly influenced by the properties of the underlying surface and local-scale circulation. To bridge the gap between large-scale projection and regional-scale impacts, climate projections from GCMs need to be downscaled. Statistical downscaling has the advantages of low computing cost and relatively easy implementation, but it is affected by the stationarity hypothesis of the statistical distribution of hydroclimatic variables. In the ever evolving climate and earth system, the stationarity hypothesis is never true. Using regional climate models to dynamically downscale GCM projection can explicitly represent small-scale processes that are important to regional ecoclimatic system but are parameterized in GCMs, thus providing added values for understanding regional climate change (Castro 2005).

Because of its geographical characteristics, the dynamical downscaling of GCM outputs in Western Canada has many benefits compared to the original simulation and statistical downscaling. Most notably, steep terrains and small-scale atmospheric processes such as wave dynamics and mountain meteorology play important roles in the Canadian Rockies. During the cold season, atmospheric, hydrological, and snow processes are tightly integrated through small-scale boundary processes, including snow cover, snow melting, and blowing snow. Western Canada, on the other hand, also includes the Canadian Prairie, where the summer convection's contribution to the growing season precipitation is the largest. These subgrid-scale convections in GCM simulation are poorly represented, and need high-resolution convection-permitting model to adequately simulate them.

To provide high-resolution convection-permitting regional climate downscaling for Western Canada, two sets of 4-km Weather Research and Forecasting (WRF) model simulations were performed for the current climate and high-end emission scenarios (Li et al. 2019) RCP8.5. The retrospective simulation (CTL, October 2000–September 2015) is forced by ERA-Interim reanalysis (Dee et al. 2011). The future climate sensitivity simulations were forced by the same reanalysis as the CTL with additional changes by the end of twenty-first century derived from the CMIP5 high-end emission scenario (RCP8.5) ensemble mean, known as Pseudo-Global Warming (PGW) method. This chapter evaluates the performance of the retrospective simulation and examines regional climate change projection in Western Canada, particularly the dynamic downscaling temperature and precipitation of the Mackenzie River Basin (MRB) and Saskatchewan River Basin (Saskatchewan). We assess the ability of modern RCMs, such as WRF, to run at the convection-permitting resolution to reproduce precipitation and temperature

characteristics that are critical to hydrology and water applications in Western Canada, including the northern regions.

28.2 Model Setup and Data

28.2.1 Model Setup

The historical (2000–2015) and projected climate (RCP8.5) over Western Canada were simulated with the WRF model Version 3.6.1 with a convection-permitting resolution. The WRF model, using the Advanced Research WRF (ARW) dynamical solvers, is fully compressible and nonhydrostatic. The model domain, composed of 699 × 639 grid points, covers Western Canada as shown in Fig. 28.1 with 4-km horizontal resolution. In total, the model domain extends 2800 km in the east–west direction and 2560 km in the north–south direction. The vertical coordinate has 37 stretched vertical levels that top at 50 hPa in the lower stratosphere. The model

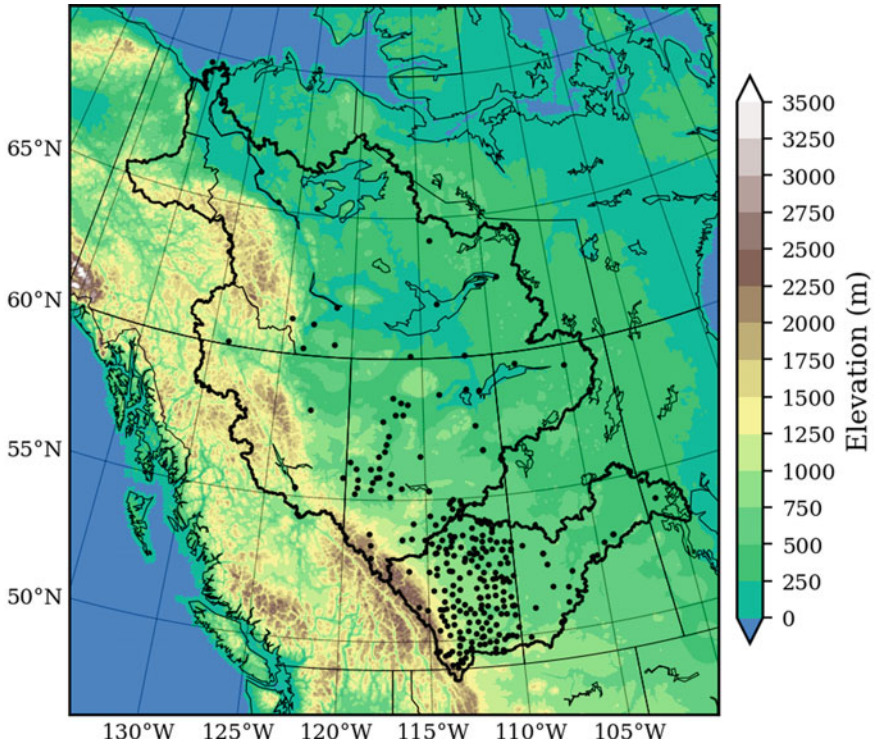

Fig. 28.1 The WRF simulation domain. Each black dot indicates an observation stations used in the evaluation of the simulations

simulations employed the Thompson microphysics scheme (Thompson et al. 2008), the Yonsei University (YSU) planetary boundary layer scheme, the Noah land surface model (Chen and Dudhia 2001), and the CAM3 radiative transfer scheme (Collins et al. 2004). We have chosen these physics schemes based on past performances using these schemes in cold regions in the literature (Liu et al. 2011; Rasmussen et al. 2014; Liu et al. 2017; Li et al. 2017). Liu et al. (2011) conducted a comprehensive sensitivity test with various microphysics schemes for the simulation of winter precipitation in the headwater region of Colorado river and found that the Thompson et al. (2008) and Morrison et al. (2009) microphysics schemes, with comparable skills to each other, are superior to others. The dependence of performance on other schemes such as radiation parameterizations, Planetary Boundary Layer (PBL), and land surface scheme is moderate or weak because of the weak solar radiative heating, shallow PBL, and weak land surface coupling in winter (Liu et al. 2011). The deep cumulus parameterization was turned off to explicitly resolve deep convection and simulate convective storms using the 4-km resolution and avoid unrealistic parameterized convection (Westra et al. 2014). The subgrid cloud cover was also switched off.

28.2.2 Numerical Experiments

The control experiment (CTL), a retrospective/historical simulation, aimed to reproduce the current climate statistics from October 1, 2000, to September 30, 2015, was forced using the ERA-Interim reanalysis data (Dee et al. 2011). The climate projection simulation was a climate perturbation experiment similar to the Pseudo-Global Warming (PGW) approach by Rasmussen et al. (2014). Substantial inter-model variability among GCMs climate projections (Deser et al. 2012; Mearns et al. 2013) can obscure the climate change response solely due to global warming. Using the PGW approach with GCM ensemble mean can overcome the inter-model variability and isolate radiative forcing and related circulation changes as the sole cause for the regional climate response. Using PGW methodology for a future period by the end of the century also requires less computation resources than a continuous simulation spanning a century. PGW method also has its limitations and drawbacks. The climate change signals added may cause an imbalance to the lateral boundary forcing because the nonlinear terms in the signals are not guaranteed additive to satisfy the dynamical balance. PGW cannot fully include the nonlinear interaction between atmospheric circulation changes and global warming due to GHG emissions, thus, fail to estimate the changes in future storm intensity, storm frequency, and storm track locations, all of which interact with the large-scale climate system beyond the regional model boundary and could hardly be represented by simple addition of thermodynamic and kinetic change to current reanalysis (Sato et al. 2007).

Using convection-permitting models has a range of advantages over using models that rely on convection parameterization in regional climate dynamical downscaling. Convection-permitting PGW simulation over the contiguous United

States (CONUS) (Liu et al. 2017) has been used in several recent studies to investigate the decrease of overall precipitation frequency and light-moderate precipitation events (Dai et al. 2017), the intensification of precipitation extremes (Prein et al. 2017), the change of cloud population (Rusmussen et al. 2017), and the increase of rain-on-snow events in western North America (Musselman et al. 2018). In our simulation, the PGW forcing's climate change signals were derived from a 19-member ensemble mean of CMIP5 models (Liu et al. 2017). In particular, PGW simulation was forced with the identical 6-h ERA-Interim reanalysis as in CTL with the modification by a climate change perturbation from the ensemble CMIP5 RCP8.5 projection (2071-2100–1976-2005):

$$\mathrm{PGW\_forcing} = \mathrm{ERA} - \mathrm{Interim} - \mathrm{CMIP5rcp8.5} \tag{28.1}$$

where ΔCMIP5rcp8.5 is the change derived from the CMIP5 multi-model ensemble mean (19 ensemble members) under the RCP8.5 scenario from 2071–2100 relative to 1976–2005. The list and description of the 19 CMIP5 models can be found in Liu et al. (2017). Climate change signals were interpolated onto each calendar date using the monthly ΔCMIP5rcp8.5 data for essential field variables such as temperature, geopotential height, wind. The initial and boundary conditions of CTL forcing derived from the ERA-Interim reanalysis were added with the pseudo-warming signals to form the PGW forcing.

28.2.3 Verification Data

When conducting intercomparison between models, reanalyses, and observation, the spatial distribution of observation and resolution of the data need to be considered. The gridded observation dataset ANUSPLIN (Xu and Hutchinson 2013; Hutchinson et al. 2009) makes interpolations from observation sites, which makes it unrepresentative in complex terrains such as in the Canadian Rockies and regions with sparse observations as in the northern territories. Most atmospheric reanalyses generate prognostic precipitation and do not assimilate precipitation observation. Though precipitation is assimilated in NARR (Mesinger et al. 2006), the poor observation coverage in Canada makes it much less reliable in less populated regions in the north as most population concentrated in southern Canada. Consequently, NARR performs worse than both CaPA and ANUSPLIN over Western Canada, especially in cold seasons (Wong et al. 2017). CaPA (Canadian Precipitation Analysis, Mahfouf et al. 2007) incorporates both station and radar observation, which generates a better spatial distribution of precipitation than ANUSPLIN (Fortin et al. 2018). Additionally, the different horizontal resolutions among data also introduce differences in elevation in mountains and valleys. The comparison of temperature and precipitation on a common grid is difficult because the elevation difference can induce large precipitation and temperature biases. Finally, due to the lack of physical representation of terrain induced processes, ANUSPLIN and CaPA cannot represent precipitation features associated with

mountain weather processes well. The sparse observation network in the mountainous region and the elevation placement of sites tend to be at lower elevation, which cannot adequately provide coverage to delineate the sharp change in precipitation and temperature across terrains. Observation is also difficult for both remote sensing and in situ instrument in the region: Radar observation is hindered by mountains; In situ precipitation in cold seasons often suffers under catchment. Therefore, we must consider these limitations when evaluating WRF-CTL with datasets based on limited observation.

28.3 Evaluation of CTL Experiment

The datasets with coarser resolutions are interpolated to WRF's 4 km grid. The interpolated observation and reanalyses have surface elevation much smoother than that of the WRF simulation due to their coarser resolution. High-resolution WRF has higher peaks and lower valleys, which can cause elevation-related temperature difference and orographic precipitation differences. The 4 km WRF simulation provides finer geographical details for temperature and precipitation, especially over complex terrains. However, lack of high-resolution precipitation observation, such as those provided by NCEP Stage IV (Nelson et al. 2016) in the US, makes it difficult to conduct a thorough evaluation of the spatial features of WRF against coarse resolution datasets over Western Canada.

28.3.1 Near-Surface Temperature

Surface air temperature directly affects the daily life of people, evapotranspiration physiological development of field crops, agricultural product quality. The effects of very cold temperatures range from a minor inconvenience for some to severe infrastructure damage and increased mortality for vulnerable populations. Extreme and persistent hot days in summer can cause heat-related illness, especially for vulnerable populations such as elderly people and those without air conditioning. For agriculture, extreme hot spells can significantly reduce crop yields. The extreme distribution of temperature also changes substantially as the mean temperature rises, sometimes more than in the mean. Surface air temperature is also crucial to estimate evapotranspiration, energy fluxes between the surface and atmosphere, and the flux and phase transition of water near the ground. Thus, evaluating the surface air temperature simulation is critical in laying the foundation for applying the WRF-CTL and PGW simulations to climate change impact analysis and hydrological modeling.

The surface air temperature (2 m) from CTL and ANUSPLIN is shown in Fig. 28.2 indicating that WRF-CTL simulation of daily mean temperature agrees well with ANUSPLIN temperature in terms of the geographical distribution. Cold biases exist east of the Canadian Rockies, especially in spring. The strong cold bias

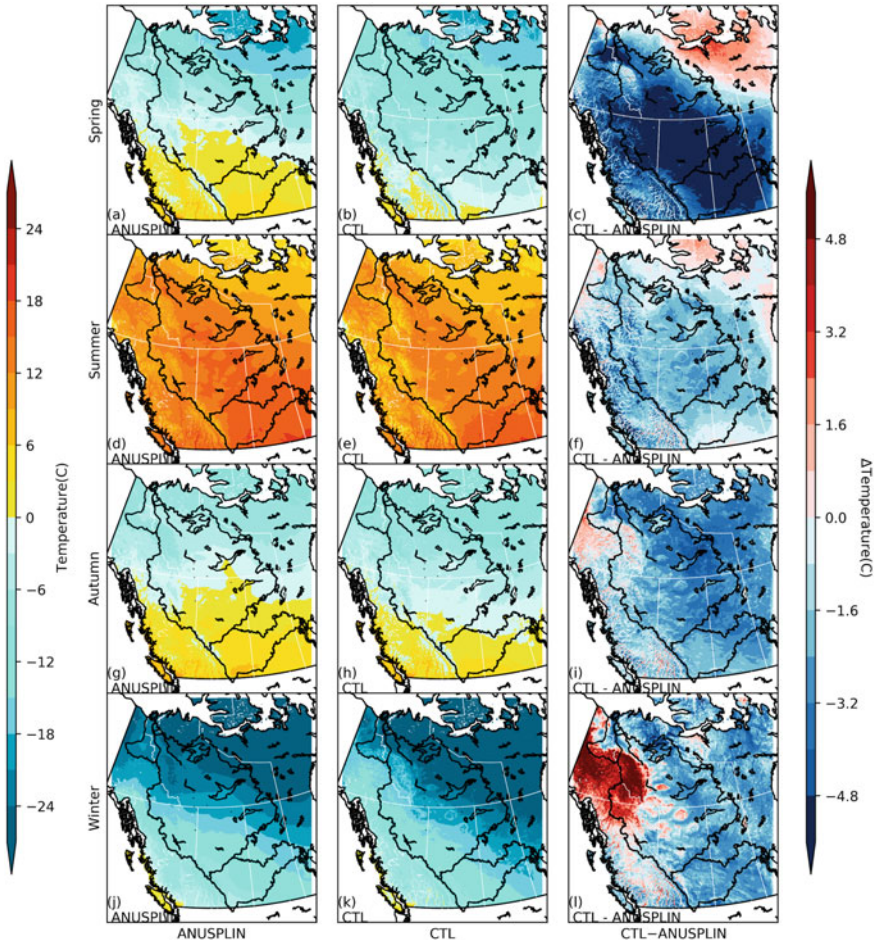

Fig. 28.2 From top to bottom: spring (MAM), summer (JJA), autumn (SON), and winter (DJF) daily mean temperature from 2000 to 2015 of ANUSPLIN (left), WRF-CTL (middle) and the difference (WRF-CTL—ANUSPLIN, right). The Δ sign indicates the difference of WRF-CTL relative to ANUSPLIN

(about −5 °C) in spring over the Canadian Prairies is accompanied with a small warm bias of 1–2 °C in the northeast domain. In winter near the Yukon and western Northwest Territories, a warm bias (about 3–4 °C) is likely inherited from the reanalysis because it is also present in ERA-Interim (2 °C) as in Fig. 28.3. Warm biases (about 2 °C) also occur in northern and central British Columbia. To the east of the Canadian Rockies, there are small cold biases (−1 to −2 °C) in summer, autumn, and winter, where the ERA-Interim has warm biases (about 1 °C) instead. Although regional climate models are forced by reanalysis data on the boundary

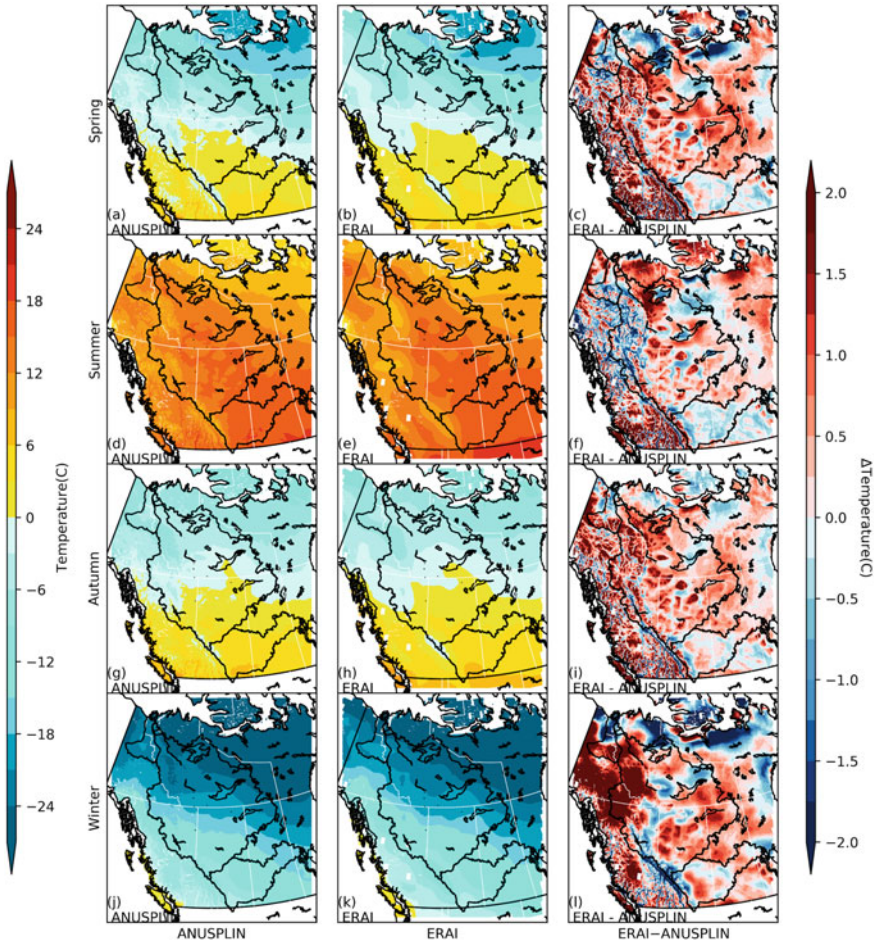

Fig. 28.3 ERA-Interim surface air temperature compared to ANUSPLIN over 2000–2015

and underlying surface, changes can be introduced by internal processes in the models, especially the near-surface temperature is strongly influenced by the parameterization of surface processes and boundary layer energy exchange. The cold bias in spring over the Canadian Prairies is likely due to the following factors: a wet precipitation bias and cold bias in temperature during winter, and the over-estimation of snow cover in the region, which causes the cold bias in spring through snow-albedo feedback. WRF-CTL also has a small warm bias in the valleys of southern BC where WRF's high-resolution grid has lower elevations than both ANUSPLIN and ERA-Interim. ERA-Interim shows a cold bias in the region due to its coarser resolution ($\sim$75 km) than ANUSPLIN (10 km) and the inability to resolve the valleys.

28.3.2 Precipitation

Capturing the observed temporal-spatial characteristics of precipitation is crucial for climate models to provide input data for hydrological models. Precipitation simulation is one of the most challenging tasks for modelers as precipitation processes compose of many subgrid scale processes that have to be parameterized. Due to the limit in spatial resolution, GCM's precipitation has to downscale to be useful in hydrological and ecological studies that are at regional and local scales. Using a convection-permitting resolution, the WRF model avoids using convection or cumulus parameterization, which can introduce large biases in simulating convective precipitation systems. The comparison of the CMIP5 19-member GCM ensemble mean precipitation with observation presents marked differences from the observed pattern of precipitation distribution: the high precipitation region near the BC coast is much broader in CMIP5 due to coarse resolution; the dry belt between mountain ranges and a secondary peak to the east of the Canadian Rockies are missing (not shown, see the supplementary of Li et al. 2019). These two features are well captured by WRF-CTL. Thus, a full evaluation of the WRF-CTL precipitation against GCM output or reanalysis with coarse resolution (>25 km) is not performed because the performances of GCM precipitation simulation and coarse resolution reanalysis are poor.

New methods to infer and merge precipitation and the increasing coverage of satellite have increased the number of gridded precipitation analyses in recent years. However, due to large uncertainties/errors in remote sensing data, the quality of precipitation analysis is still limited by the density and distribution of ground observatories throughout Canada. This is particularly true in the Canadian Rockies and the northern part of the country, where only a few observation sites are scattered over a wide area. Wong et al. (2017) evaluated a variety of precipitation products for their statistics in different climate zones and river basins in Canada with station observations and found that CaPA and ANUSPLIN were closer to observation than other data sets. Albeit the two data sets still perform poorly in the mountains and the northern regions. Specifically, ANUSPLIN's coverage of northern Western Canada relies on a very limited number of stations and shows dry bias in these areas. CaPA is a reanalysis dataset that has been proven that its overall spatial distribution of precipitation is superior to that of ANUSPLIN (Fortin et al. 2018; Wong et al. 2017). With these in mind, we evaluated WRF-CTL precipitation based on two observational precipitation analysis data sets (ANUSPLIN and CaPA).

As shown in Figs. 28.4 and 28.5, the WRF-CTL simulation captures the main precipitation distribution patterns in the precipitation observed by CaPA and ANUSPLIN, respectively: higher precipitation in the vicinity of the BC coast in winter and the near-term areas of the Canadian Rockies. The spatial pattern of WRF-CTL is more similar to CaPA and is significantly different from that of ANUSPLIN, especially within the eastern range of the Canadian Rockies. Both CaPA and WRF-CTL are more humid than ANUSPLIN, especially in the mountains and northern regions. Compared to ANUSPLIN in Fig. 28.4, WRF-CTL's wet

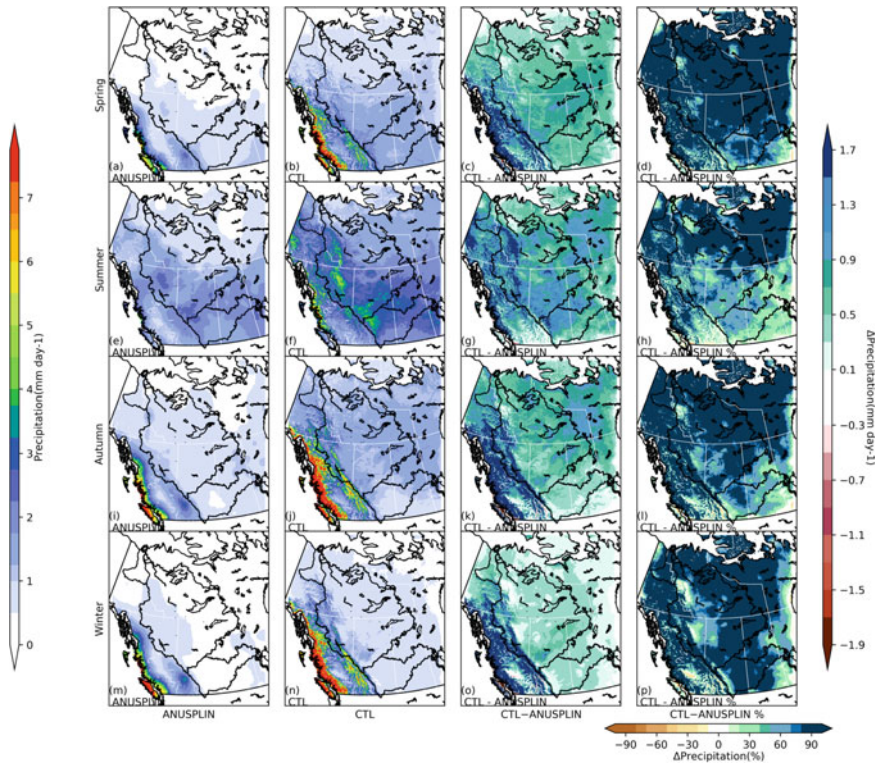

Fig. 28.4 The daily mean precipitation from ANUSPLIN (1st column) and WRF-CTL (2nd column), and their absolute (3rd column) and relative differences in percentage (4th column) in spring (MAM, 1st row), summer (JJA, 2nd row), and autumn (SON, 3rd row), and winter (DJF, 4th row). The Δ sign indicates the bias of WRF-CTL relative to CaPA

bias is located mainly in the pacific and Canadian Rockies mountains. This terrain-related wet bias is up to 1.7 mm/day and is more prominent in winter and spring. However, it must be taken into account that gridded observational analysis often underestimates the precipitation of mountainous areas with scarce data through the interpolation of existing low-altitude observations. East of the Canadian Rockies, grasslands, and northern forests have a moderate wet bias (about 0.5–0.9 mm/day). In terms of the relative deviation of WRF-CTL relative to ANUSPLIN, there is a significant wet deviation (−90%) in the northern sector, including MRB in all seasons. For SBBs, due to the low precipitation observed during the season, there will be a large dry relative deviation in winter. However, according to Wong et al. (2017), ANUSPLIN estimates that annual precipitation in Western Canada has decreased by 10–50% compared to observations in the region from 2002 to 2012. As a result, WRF-CTL has a large wet bias relative to the NORTHERN ANUSPLIN, mainly because the ANUSPLIN there has a large dry bias.

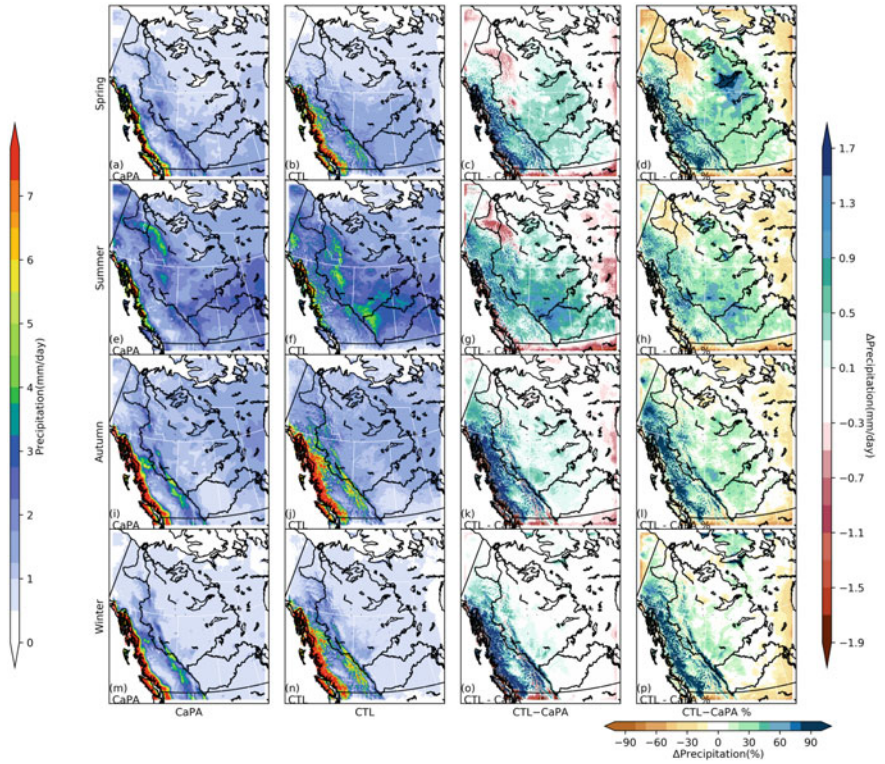

Fig. 28.5 Seasonal mean daily precipitation from CaPA (1st column) and WRF-CTL (2nd column), and their absolute (3rd column) and relative differences in percentage (4th column), from top to bottom: spring, summer, autumn, and winter

Compared to CaPA, WRF-CTL typically has less bias and its bias is less correlated with terrain because CaPA absorbs GEM forecasts and remote sensing data to better represent orographic precipitati +on than analysis data, which relies heavily on rain gauges at lower altitudes. Wet precipitation bias in the coastal mountains of British Columbia and the Canadian Rockies is prominent in spring, autumn, and winter. East of the Canadian Rockies, wet bias is mainly in spring and summer in SRB and southern MRB. In spring, summer, and autumn, areas around MRB and SRB also have dry bias areas. In winter, the difference between CTL and CaPA is small in east of the Canadian Rockies as winter precipitation amount is low. It is important to note that, according to Wong et al. (2017), the WRF-CTL wet bias from WRF-CTL in the eastern Canadian Rockies may be due in part to CaPA's dry bias (10%) relative to the station observation (Fig. 28.5).

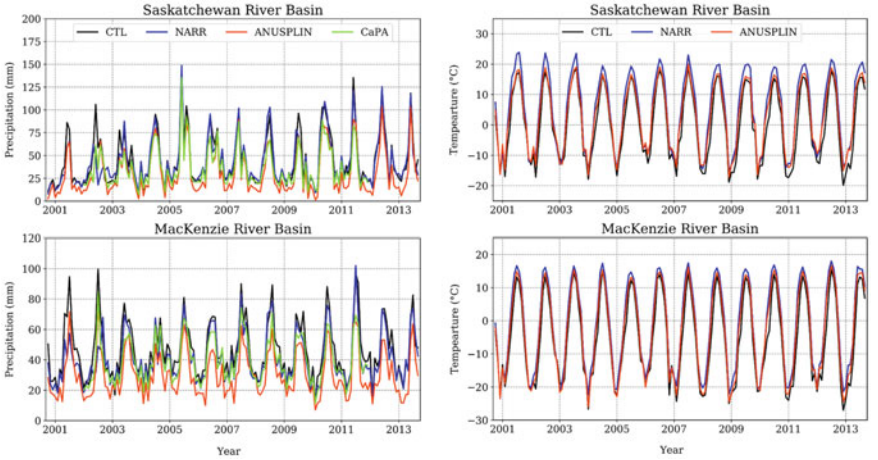

Fig. 28.6 The monthly mean precipitation/temperature averaged over the Saskatchewan River Basin (top) and Mackenzie River Basin (bottom) from 2000 to 2015 from WRF-CTL (black curve) and an ensemble of observation/reanalyses of temperature (NARR, blue; ANUSPLIN, red) and precipitation (NARR, blue; ANUSPLIN, red; CaPA, green)

28.3.3 Basin Mean Statistics

The WRF simulation faithfully reproduces the seasonal and interannual variations in temperature observation in MRB. Compared to the observations in MRB, the WRF temperature simulation is within the range of observation analysis/reanalysis datasets, but mostly at the lower end. In summer NARR is generally much warmer than ANUSPLIN and WRF-CTL. The WRF-CTL simulation shows cold biases throughout the year, especially from March to July, compared to ANUSLIN. The average precipitation in WRF-CTL in the MRB is consistent with observations in terms of interannual changes and seasonal cycles. This good match shows that WRF-CTL's ability to capture key features of precipitation variations from year to year with large-scale forcing provided by the ERA-Interim reanalysis, but with a difference in total precipitation amount. ANUSPLIN shows that its average annual precipitation in the MRB is much lower than others, in line with previous assessments (e.g., Wong et al. 2017). Simulated precipitation in WRF-CTL shows a wet bias since the WRF-CTL curve is almost always at the top of the observation envelope, especially in spring and summer. In Fig. 28.7, the average annual MRB precipitation cycles were compared between WRF-CTL, CaPA, NARR, and ANUSPLIN. WRF-CTL precipitation simulation and observation all peak in July. WRF-CTL precipitation is higher than ANUSPLIN in each month, very close to NARR and CaPA with a wet bias in summer. The average summer precipitation in WRF-CTL is 5 mm/month higher compared to NARR and CaPA.

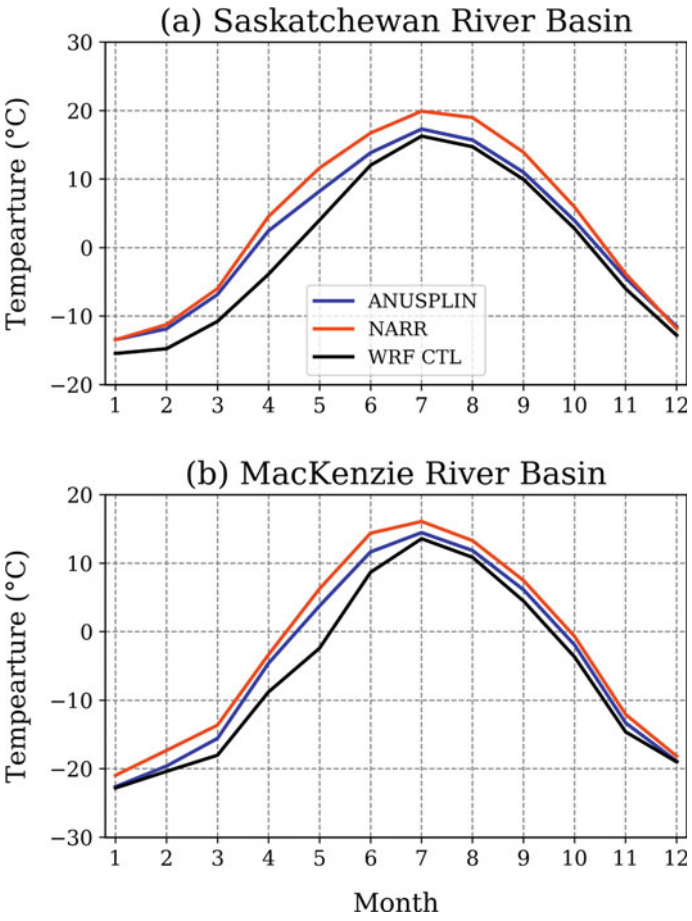

Fig. 28.7 The mean annual cycle of temperature for WRF-CTL (black), NARR (red), and ANUSPLIN (blue) over the Mackenzie River Basin (bottom) and Saskatchewan River Basin (top)

WRF simulation captures the seasonal and interannual variations in temperature in the SRB. Compared to observation analysis and reanalyses, the WRF simulation is closer to ANUSPLIN, with cold bias in spring and smaller cold bias in other seasons. The annual temperature cycles of WRF, NARR, and ANUSPLIN show good consistency in SRB (Fig. 28.8). In warm seasons, NARR is much warmer than WRF-CTL and ANUSPLIN, with average bias as high as 5 °C in the SRB. The WRF-CTL simulation shows a cold bias relative to ANUSPLIN throughout the year, especially from March to July. The cold bias of SRB is greater than the cold bias of MRB, which is consistent with the spatial distribution of temperature bias in Fig. 28.3, where the cold bias during spring in the SRB and the Canadian Prairies is stronger.

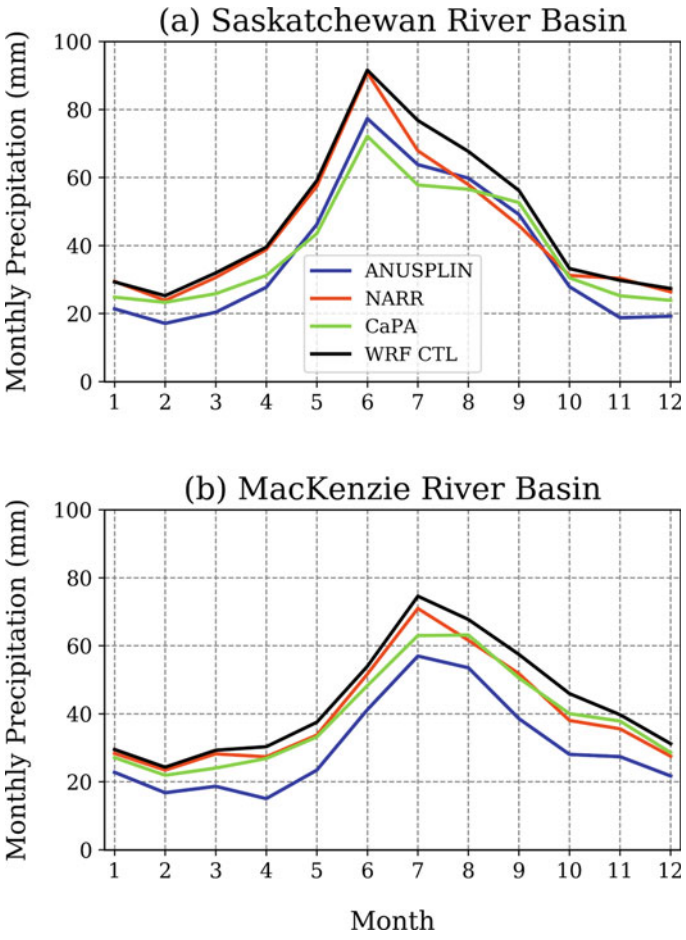

Fig. 28.8 The mean annual cycle of monthly precipitation for WRF-CTL (black), NARR (red), CaPA (green) and ANUSPLIN (blue) over the Mackenzie River Basin (bottom) and Saskatchewan River Basin (top)

Figure 28.7 shows the simulated monthly precipitation of WRF-CTL from 2001 to 2013 among gridded observation analysis, ANUSPLIN, and reanalyses, CaPA, and NARR. WRF-CTL precipitation is comparable to that of NARR, ANUSPLIN, and CaPA in SRB. In the summer of 2002–2003, when the Canadian Prairies were in drought, WRF-CTL was much wetter than other data sets. The average precipitation in WRF-CTL shows similar seasonal cycles and interannual variations to the analysis and reanalyses (Fig. 28.8). Simulation and analysis/reanalyses' June precipitation peak at about 60–90 mm and indicates that winter precipitation amount is small, with approximately 20–30 mm. ANUSPLIN is drier than other data, especially during cold seasons. Similarly, WRF-CTL is closer to the precipitation of

NARR and CaPA than ANUSPLIN precipitation in SRB. Compared to CaPA and ANUSPLIN, simulated precipitation in WRF-CTL has wet biases in all seasons, and the WRF-CTL simulation curve is almost always at the top of the observation envelope (Fig. 28.8).

28.4 Pseudo-Global Warming Simulation

Dynamical downscaling using regional climate models generates not only higher spatial resolution climate projections but also oftentimes different hydroclimatic regimes from GCMs. These improvements or differences can be attributed to the enhanced or explicit representation of fine-scale processes in the lower boundary conditions and atmosphere. In this section, we discuss the changes in WRF-PGW relative to WRF-CTL and the CMIP5 ensemble.

28.4.1 Near-Surface Temperature

The average daily temperature modeled by WRF-CTL and WRF-PGW, the warming of WRF-PGW relative to CTL, and the predicted warming in the CMIP5 ensemble (2071-2100–1976-2005) are shown in Fig. 28.9. The temperature in the northeast increases greatly, whereas the southwest region's warming is small, and the northeast–southwest temperature gradients in the four seasons are generally reduced, especially in winter. Warming is the strongest in winter, with the northeast quadrant increasing by about 10 °C. In spring, the Canadian Prairies experience the largest warming, which is associated with the rise in average daily temperatures from below freezing to above freezing in the early and mid-spring seasons, in turn, leads to enhanced warming due to snow-albedo feedback. Average temperatures in the Yukon and the Northwest Territories will be similar to current spring and summer temperatures in Saskatchewan and Alberta, which will have a significant impact on the length of the growing season in the northern regions. Winter temperatures in the coldest parts of the region will be as warm as the grasslands of central Canada in the current climate. Rising temperatures in northern forest areas will significantly increase the likelihood of wildfires, water stress, and pests, threatening the boreal forest ecosystem and could eventually be replaced by grasslands and parks (Stralberg et al. 2018). The overall projection of CMIP5 shows that the warming range is higher for all seasons than the WRF projection, and the spatial patterns are different in spring and summer. In summer, WRF shows that, except for the northeast corner (the warming is around 6 °C), the warming in most areas is 5 °C. CMIP5 shows that the warming intensity south of 55 N is about 7 °C in summer. CMIP5 ensemble mean shows stronger warming in the southern region in summer, in line with the larger reduction of summer precipitation in the region.

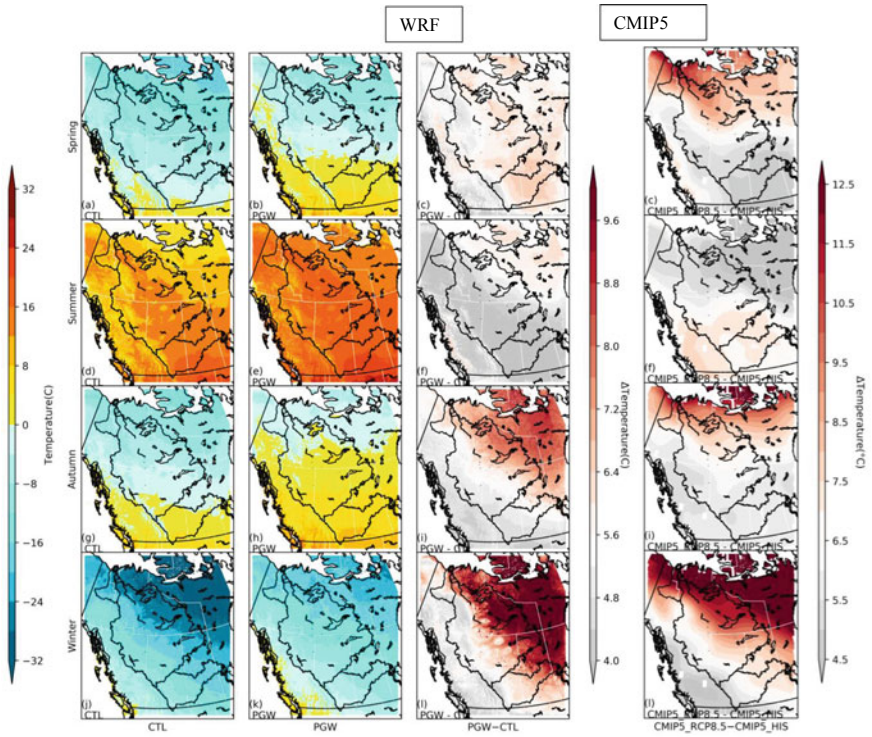

Fig. 28.9 The spring (1st row), summer (2nd row), autumn (3rd row), and winter (4th row) daily mean temperature from WRF-CTL (1st column) and WRF-PGW (2nd column), the difference (PGW—CTL, 3rd column), and the projected warming from CMIP5 ensemble (2071-2100–1976-2005, 4th column)

28.4.2 Precipitation

Figure 28.10 shows the comparison of WRF-PGW and WRF-CTL precipitation. In general, precipitation will increase in most areas. In most places, WRF-PGW shows that precipitation increased by about 15–30% in all seasons compared to WRF-CTL. Near the coast of British Columbia, up to 2 mm of rain is received every day. Significant increases in precipitation in the coastal mountains of British Columbia are associated with a large water vapor load in PGW. The change of precipitation in summer is the least, and the PGW precipitation in parts of Canadian Prairies is less than CTL. With a slight increase in summer precipitation, much more evaporation in PGW than CTL, the amount of available water during the growing season will be a challenge for the Canadian Prairies. Compared with the CMIP5 ensemble mean prediction in Fig. 28.10, the dynamical downscaling of WRF-PGW is not as pessimistic about the amount of water in the Canadian grassland growing season. CMIP5 shows a significant decline (−10–20%) in the

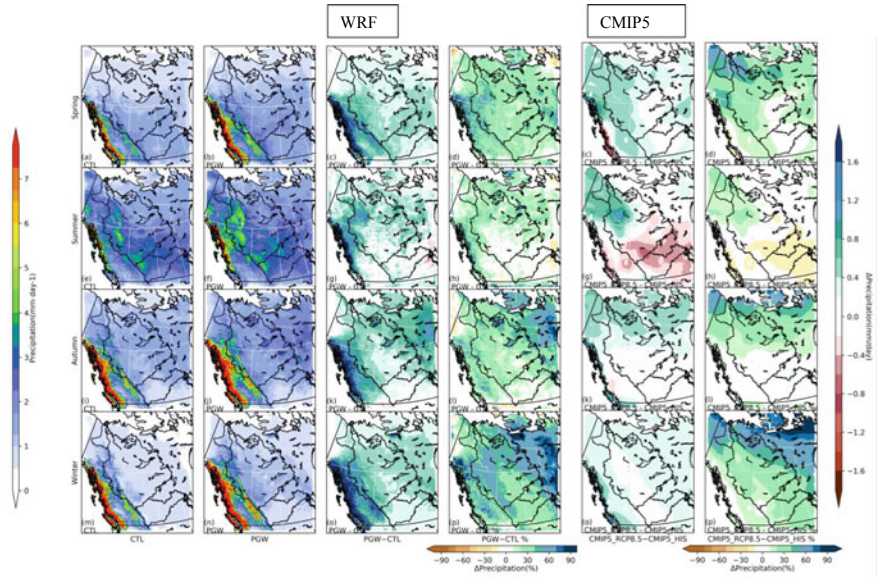

Fig. 28.10 The seasonal mean daily precipitation of spring, summer, autumn, and winter for WRF-CTL (1st column), WRF-PGW (2nd column), the difference (PGW—CTL, 3rd column), and percentage difference over CTL (4th column). On the right hand side, the projected changes from CMIP5 ensemble for precipitation are shown

southern summer precipitation, including SRB and southern MRB. In northern Manitoba and the Northwest Territory, precipitation increases by 0.5–1 mm per day and by about 40 % in autumn and winter. In the Yukon and northern British Columbia, winter precipitation is expected to increase by 40 % due to increased water vapor load as the climate warms. In addition to the wetter summer projection for the Canadian Prairies, the WRF projection also shows a significant increase in precipitation near the BC coast and the Canadian Rockies. These areas have significant terrains, which are represented better by high-resolution WRF than GCMs, which initiate convection and orographic precipitation and more effectively convert higher concentrations of water vapor in warm climates into higher precipitation. Poor GCM orographic representation may cause poor precipitation estimation, especially the lower increase in precipitation over these terrains in CMIP5 ensemble mean.

28.4.3 Changes in Water Balance

The comparison of surface water budget components (precipitation, P; evapotranspiration, ET; runoff, Q; storage, S) in WRF-PGW with WRF-CTL are shown in Figs. 28.11 and 28.12. Relative to WRF-CTL, the magnitudes of the P and ET seasonal cycles in both basins are larger in WRF-PGW mainly due to the summer

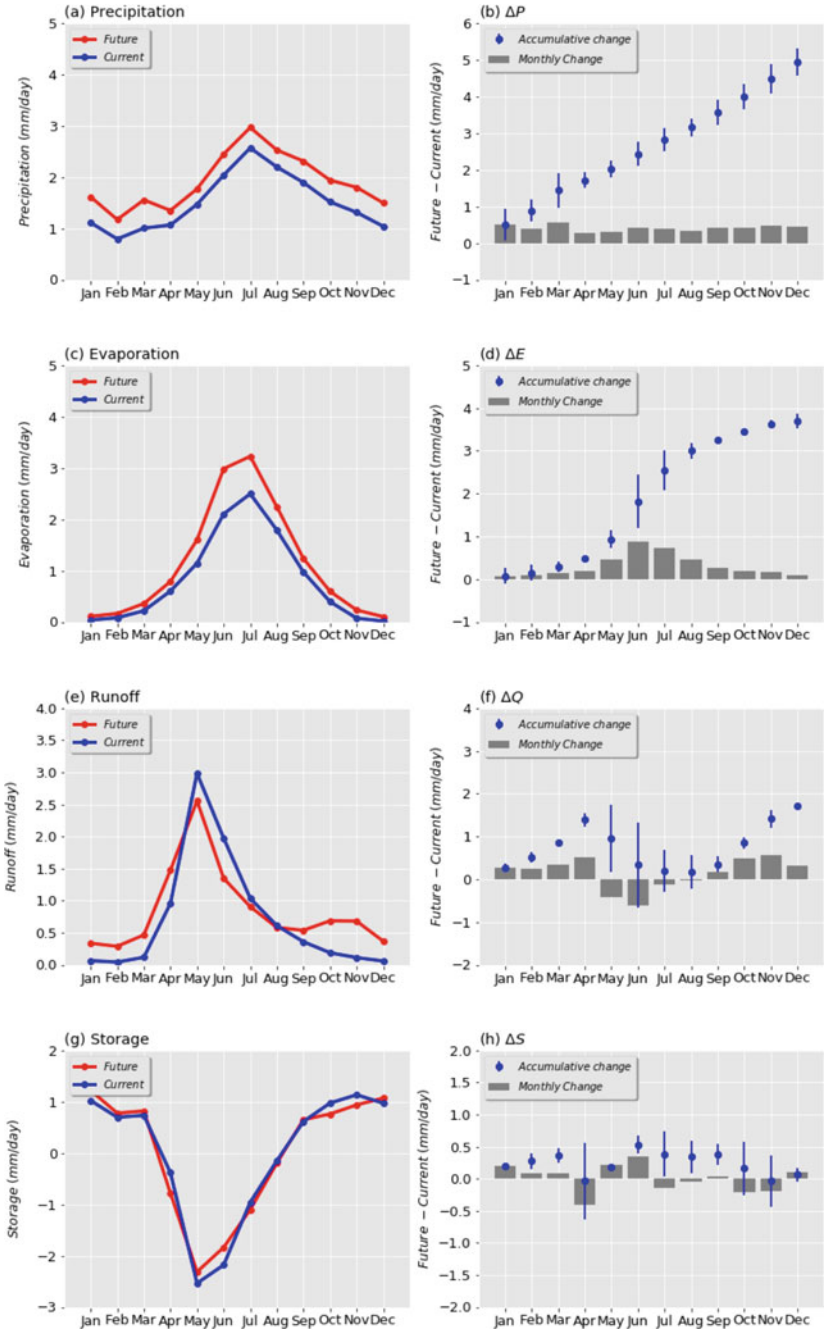

Fig. 28.11 The surface water budget (mm day^{-1}) in MRB for the WRF-CTL and the WRF-PGW simulations: **a** P, **b** changes in P and its accumulated changes in P; **c** ET, **d** changes in ET and its accumulated changes in ET; **e** runoff, **f** changes in runoff and its accumulated changes in runoff; **g** storage and **h** changes in storage and its accumulated change; **g** storage and **h** changes in storage and its accumulated change. Adapted from Kurkute et al. (2019)

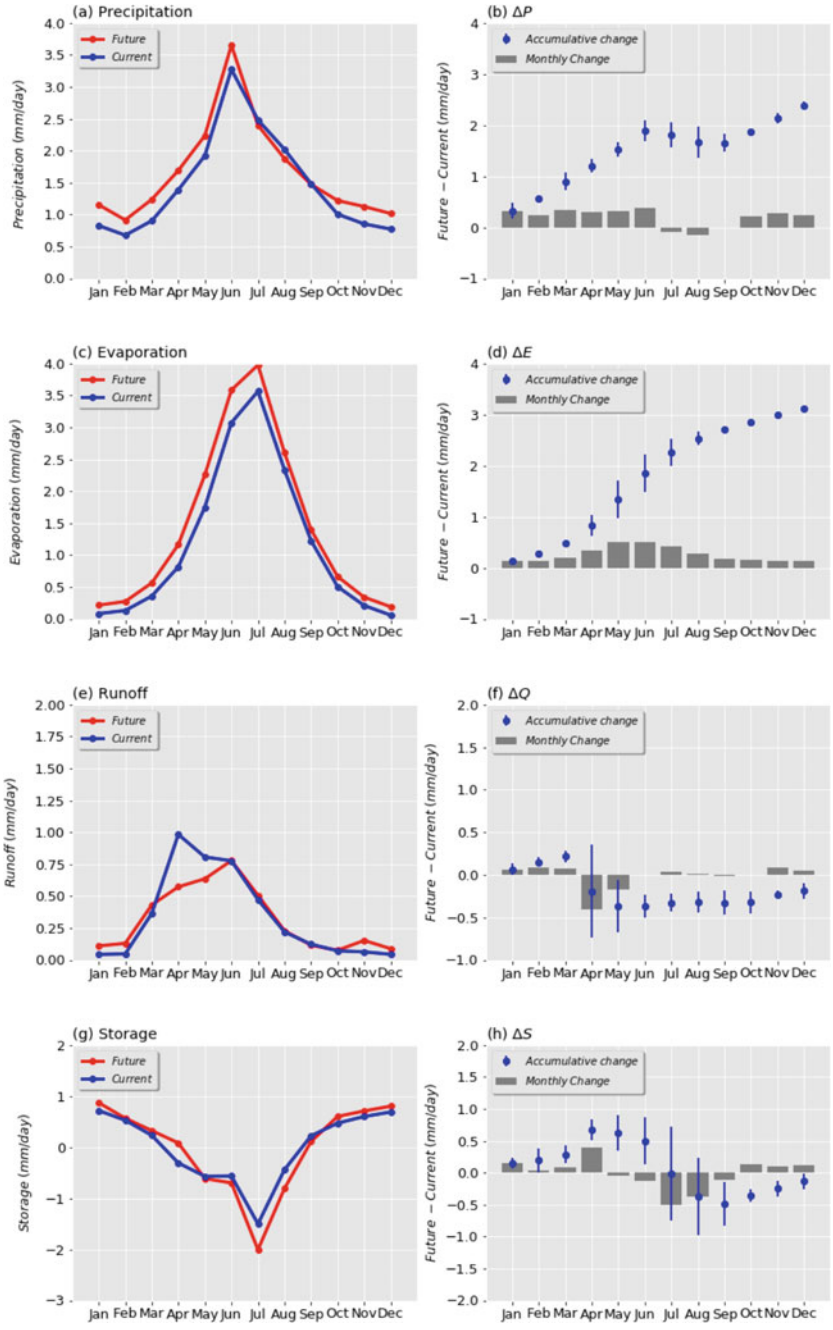

Fig. 28.12 The same as in Fig. 28.10 except for SRB. Adapted from Kurkute et al. (2019)

increases of P and ET and winter enhancement of precipitation, signaling an enhanced water cycle in both basins. MRB shows a decrease of runoff from May to July, almost no change in August, and an increase from September to April. The increase of winter precipitation in MRB exceeds the additional storage term in WRF-PGW and more precipitation falling in the form of rain in a warmer climate, which causes a small increase in winter runoff and decline in spring and early summer runoff. SRB shows a decrease of runoff from April to May, almost no change from June to October, and an increase from November to March. The peak runoff for SRB occurs in April in WRF-CTL and in June in WRF-PGW. The storage change term in SRB significantly decreases in summer due to the deficit in P-ET in WRF-PGW, which is also consistent with a decrease of runoff. These changes are due to that in a warmer climate, P increases during winter causing larger snow water equivalent, providing more snowmelt and rain for the fall and early spring; and ET increases more than P in summer, which causes less water storage is converted to runoff during late spring and summer.

The atmospheric moisture budget provides an additional way for the evaluation of (P–ET) in the simulation. The spatially averaged water budget of atmosphere and the surface water budget can be represented in the following way:

$$\frac{dW}{dt} = E - P - \nabla \mathrm{MF} \tag{28.2}$$

Here, ∇ is the horizontal divergence operator, W is the total liquid content per unit area, and MF is the vertically integrated moisture flux (kg $m^{-1}s^{-1}$) given by

$$MF = \frac{1}{g} \int_{psurf}^{ptop} qVdp \tag{28.3}$$

where g is the gravitational acceleration constant, q is the specific humidity, dp is the change in pressure per model layer, and V is the vector wind. The horizontal divergence of the vertically integrated moisture flux ∇ MF is the atmospheric moisture divergence, which corresponds to a net gain of moisture when it is negative.

The MRB moisture divergence increases in summer and declines in winter and autumn as shown in Fig. 28.13, which means MRB gains more water vapor during cold seasons and loses more in summer in PGW compared to CTL. June sees the largest enhancement in moisture divergence in MRB because the evapotranspiration increases more in the eastern MRB than precipitation. As a result, the accumulative change of moisture divergence in WRF-PGW decreases throughout the year in MRB compared to WRF-CTL. The SRB moisture divergence increases moderately during warm months (May–September) and shows little change over cold months. The change in divergence in WRF-PGW over SRB peaks in July. The annual accumulative change in the moisture divergence over SRB shows an enhancement of about 2 mm day^{-1}, which is mainly accounted for by the large accumulative

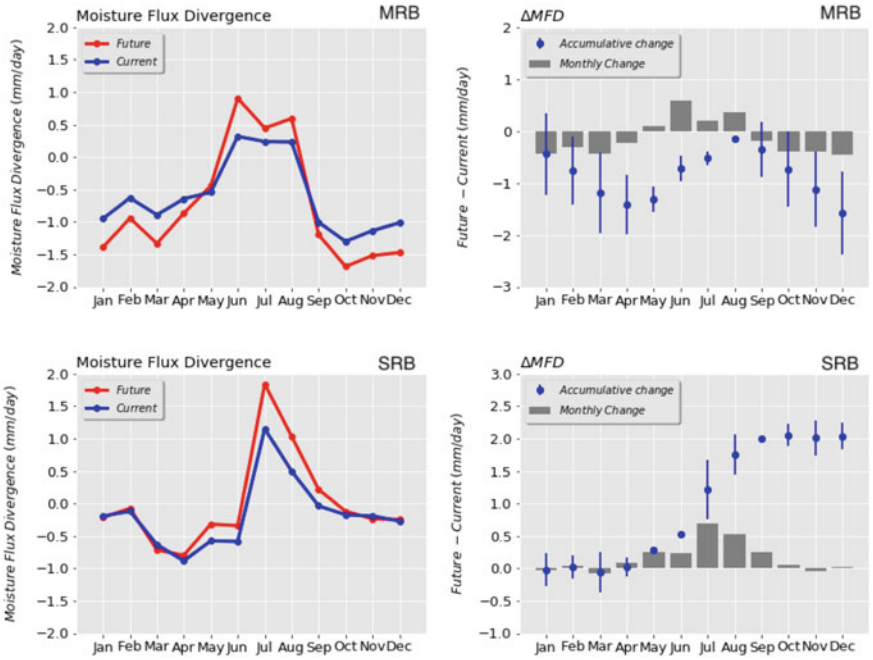

Fig. 28.13 Changes in atmospheric water vapour divergence (mm day^{-1}) for each calendar month between WRF-PGW and WRF-CTL over MRB (top) and SRB (bottom). Adapted from Kurkute et al. (2019)

increase of ET in SRB, especially in summer. The storage term barely changes in WRF-PGW during cold season in SRB until spring (April, May) when larger amount of snowmelt and precipitation increase water storage in the land surface. The vapor divergence enhancement in summer is supplied by the larger amount of water draw-down from soil moisture and reduction in runoff in both basins.

28.4.4 Hourly Precipitation Extremes

To further investigate precipitation extremes on an hourly time scale, the hourly precipitation rate distribution from station observation, WRF-CTL, and WRF-PGW in two basins was compared and the changes in the distribution of precipitation rate per hour were studied. Figure 28.14 shows the change in the distribution of precipitation per hour at a one-hour interval between surface observations and WRF simulations. The black curve represents observations collected from 232 ground stations of the SRB and MRB from the Environment and Climate Change Canada (ECCC, http://climate.weather.gc.ca/index_e.html). The blue and red lines are the closest grid points to station observation, and these stations are extracted every hour

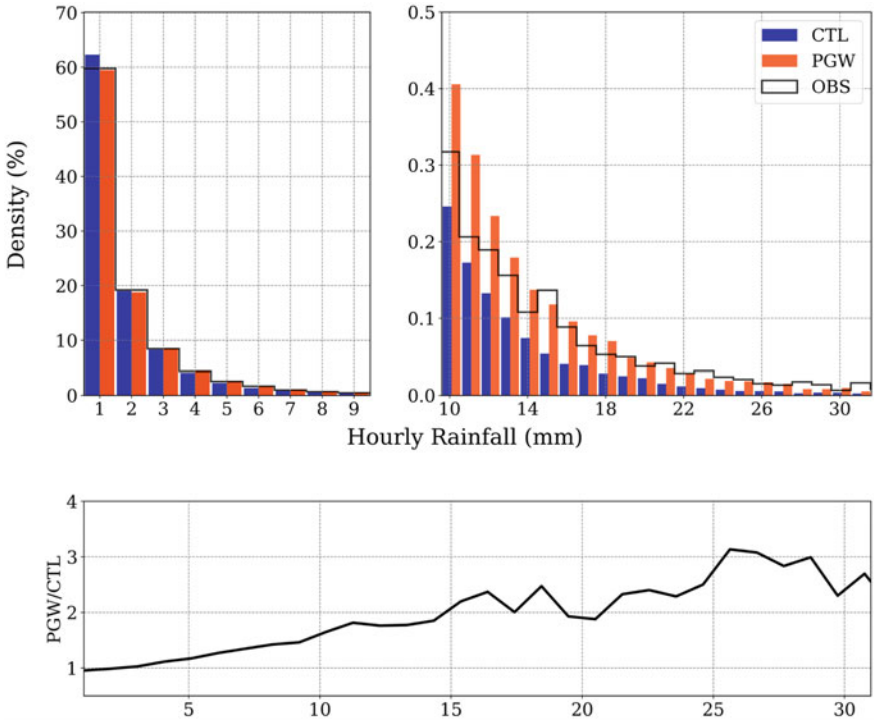

Fig. 28.14 Hourly extreme precipitation frequency density over western Canada from station observation, WRF-CTL (blue) and PGW (orange). The bottom plot shows the ratio between PGW and CTL for events with different intensities (mm hr^{-1})

(113,952 time steps over 13 years) for WRF domains for both CTL and PGW, respectively. Despite the spatial scarcity and data quality associated with station observations, the results do provide a good assessment of WRF simulations of hourly rainfall, from small to extreme. Most of the hourly precipitation simulated by the WRF-CTL simulation is close to the observed value, in the precipitation rate range of 1–10 mm/hr. Within this range, future rainfall has barely increased, or even decreased slightly, compared with the current climate. High-level hourly rainfall is high, and although only 0.5% of the total event density is at the extreme precipitation rate, the probability of a significant increase in frequency in warmer climates in the future is 1.5–3 times. It is worth noting that the density of the high-end distribution is much higher than that of CTL in station observations, because the denominator of the observation density (total number of events) is significantly less in observations, although the absolute number of high-intensity events in WRF-CTL is comparable or higher. In addition to the higher likelihood of extreme precipitation events, light precipitation has also decreased, supporting previous findings in other modeling studies (Cubasch et al. 2013; Easterling et al. 2000).

28.5 Extreme Temperature and Precipitation

The number of high-temperature extreme weather events in Canada has increased in recent decades, especially as the average global temperature has risen. Both extremely cold and hot days have great impacts on the economy, society. Changes in the high/low percentiles of WRF-PGW and CTL daily maximum and minimum temperatures are used to assess future changes in summer extreme hot weather and cold winter weather in Western Canada. The 95th (5th) percentile of the daily highest (lowest) temperature of the CTL and PGW and its change in summer (winter) are shown in Fig. 28.15. Only the 95th (5th) percentile is shown here, as the warming pattern of the 90th (1st)–99th (10th) percentiles in summer (winter) is similar. The least warming place is the central part of the boreal forest, mainly within MRB, with a magnitude of about 2.5 °C. In the surrounding area, the temperature rises at 4–5 °C. The change in the 5th percentile of the WRF-PGW winter minimum temperature compared to the WRF-CTL is shown in the bottom row of Fig. 28.15. In winter, the strongest warming of low percentiles occurs in the eastern region, where general warming is also stronger.

The distribution of high percentile daily precipitation in CTL and PGW simulations shows different geographic patterns for different percentiles in summer. Typical values of the 90th, 95th, and 99th percentiles are around 10, 18, 36 mm/day in high precipitation areas, respectively. For the 90 percentiles of daily precipitation, the change in PGW relative to CTL is mostly homogeneous, except for the

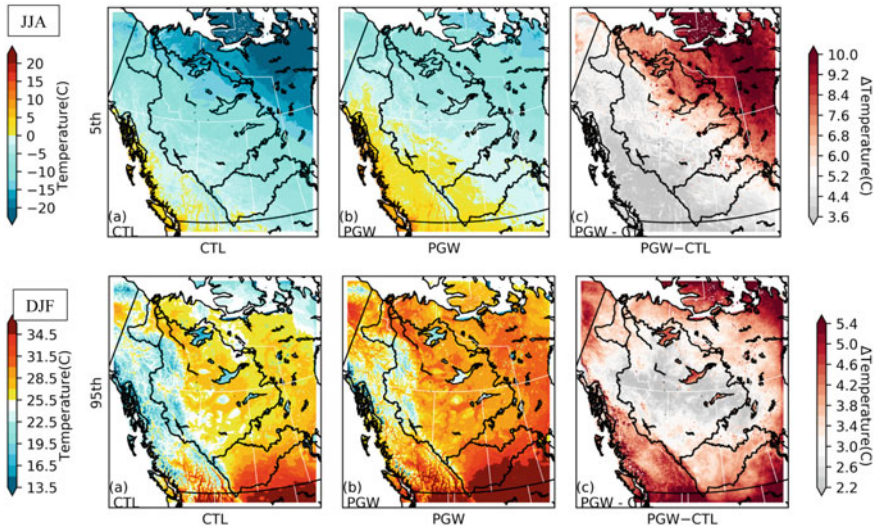

Fig. 28.15 Top: Extreme daily maximum temperature distribution in summer at the 95th percentile, WRF-CTL versus WRF-PGW. Bottom: Extreme statistics of daily minimum temperature in winter WRF-CTL versus WRF-PGW, 5th percentile

Yukon and western MRB which increases (1.5–3 mm/day) and the southeastern region (−1.5 mm/day), as shown in the first row of Fig. 28.16a. PGW's 95th percentile precipitation generally increases by 1–3 mm/day compared to CTL, but

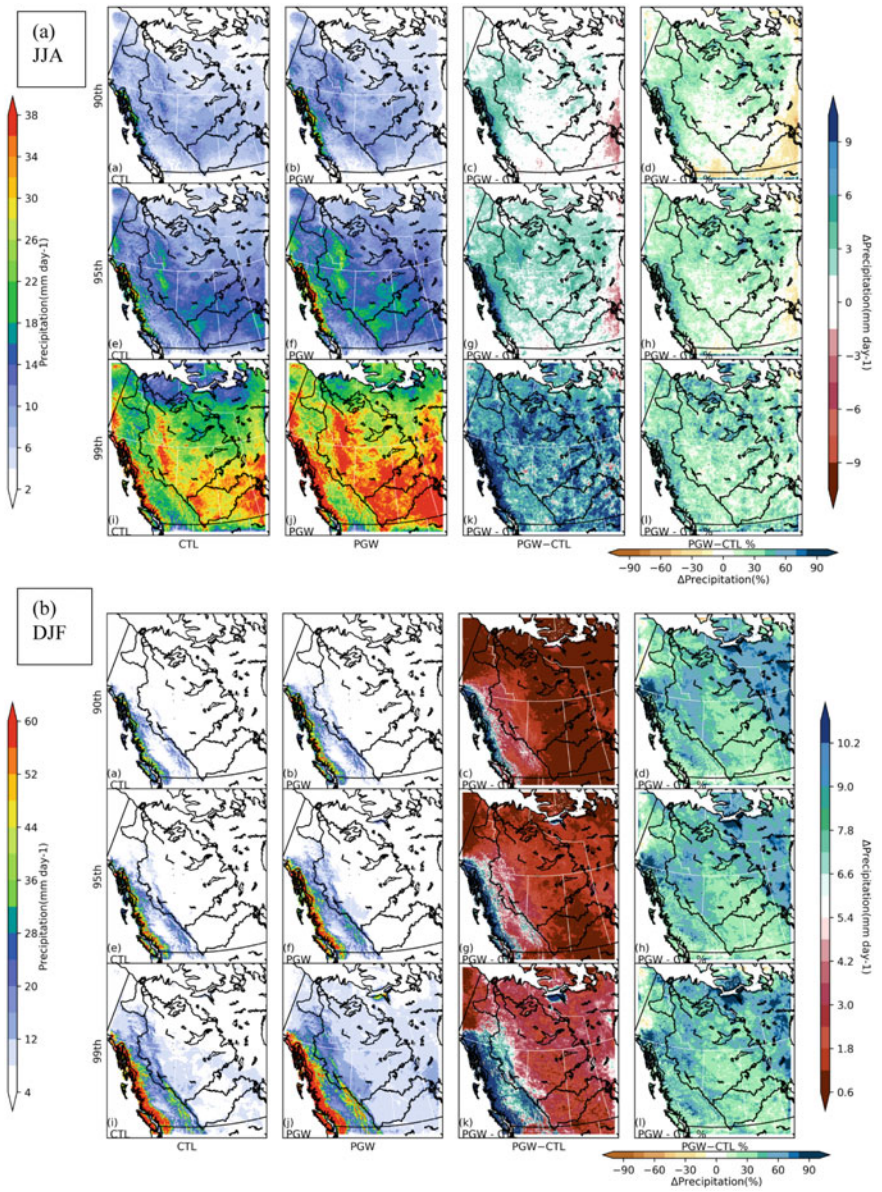

Fig. 28.16 Extreme statistics of daily precipitation distribution in summer (**a**) and winter(**b**) for WRF-CTL versus WRF-PGW, from top to bottom at each plot: 90th, 95th, and 99th percentile

slightly decreases east of SRB, as shown in the second line of Fig. 28.16a. The 99th percentile of summer precipitation shows that precipitation increasing by 6–9 mm/day, or about 15–30% over the region. High percentiles, such as the 99th percentile, are usually associated with large-scale weather systems. The increase in the 99th percentile precipitation is more uniform within the domain because it is associated with large-scale systems and proportional to the water vapor loading over a large area. The 90th percentile of summer precipitation (CTL is about 6–10 mm/day over the Canadian Prairies) may be associated with strong local thunderstorms, which is affected by future boundary layer changes and lower atmospheric conditions. The availability of local water and the division between sensible and latent heat flux can alter convective inhibition and convective available potential energy, which in turn affects convective precipitation. As a result, the 90th percentiles summer precipitation changes have significant geographical variation in the domain compared to higher percentiles.

28.6 Discussion

Lack of observation is the main obstacle to regional climate modeling in several ways. Mountainous terrain and numerous lakes make it difficult to interpolate observations into gridded data sets. Due to high population density and logistical factors, Canada's meteorological observation network is concentrated in the southern part of the country and over the plains. In sparsely populated areas and mountainous areas in the north, there are far fewer ground-based observatories. Sparse observation networks in low-density areas provide less reliable and representative observations for the development and validation of regional climate models in the region (Hofstra et al. 2009; Takhsha et al. 2017). As a result, model performance evaluation relative to gridded observational datasets such as ANUSPLIN is less reliable in mountainous and polar regions.

Hydrological cycles and snow cover treatment in the components of the land surface model at the regional to local scales also pose a major challenge to correctly simulate surface temperature and hydrological processes in the region (Casati and de Elía 2014). For example, hydrometeorology in cold areas is strongly influenced by snowfall processes, which in turn are affected by fine terrain and wind direction. The representation of mountain snow processes and snow cover is a challenging obstacle to be overcome in the Canadian Rockies to reproduce hydrologic climate conditions (Casati and de Elía 2014). In our case, because the near-surface temperature in spring is highly sensitive to the representation of spring snow cover, the snow-albedo feedback amplifies the bias of winter snow to a significant spring cold bias. The convection-permitting high-resolution WRF-CTL shows the geographical distribution of precipitation in line with CaPA, with small wet bias in the northern and mountainous regions of the domain. However, it is worth noting that

WRF-CTL shows that areas of wet bias are also affected by the scarcity of observational data and poor representation of topographic precipitation due to site locations. WRF-PGW projections produce less warming compared to the CMIP5 ensemble, especially in the eastern region. WRF-PGW also predicts that the Canadian Prairies will have less summer precipitation change than the CMIP5 ensemble mean, which means that high-resolution simulations tend to produce more summer precipitation in the Canadian Prairies than GCMs. In the WRF-PGW simulation, unlike other regions, the total summer precipitation in the Canadian Prairies decreases or only changes slightly compared to CTL, especially with moderate intensity precipitation. One reason for the small or no increase in summer precipitation may be the decline in relative humidity in the region both in PGW forcing and in PGW simulation. Dai et al. (2017) showed that a smaller increase in specific humidity than the increase in temperature would result in a decrease in relative humidity, and a much smaller increase in precipitation. Detailed mechanisms for curbing summer precipitation in the Prairies compared to the surrounding area are to be further investigated.

Under RCP 8.5, high-intensity precipitation events are expected to increase by the end of the twenty-first century. High-intensity precipitation in MRB and SRB in WRF-PGW is expected to increase significantly. Extreme precipitation is affected by changes in the amount of water vapor and vertical velocity in the atmosphere, storm size, storm translational speed, etc. Extreme precipitations are more affected by water vapor loading than local-scale circulation, which is consistent with the relative uniformity of the 99 percentiles of daily precipitation changes in each season. In contrast, there are large regional differences in the 90th percentile of precipitation associated with less intense storms in summer. The histogram of precipitation per hour shows a larger increase in the number of heavy precipitation events (about 300%) than light precipitation (about 150%).

Various bias correction methods have been used to correct RCM outputs against bias before their application. For many hydrological and agricultural applications, the temperature and precipitation bias correction of RCM output often bases on quantile mapping. Quantile mapping, which matches the simulation's distribution with and distribution of observations, assumes the stationarity of statistical distribution of hydrometeorological variables. Because of the cold bias in spring and MRB wet bias in the east of the Canadian Rockies, it is recommended that applications of WRF simulation should be calibrated with the observed hydrologic climate. However, due to the change of precipitation intensity's probability distribution in WRF-PGW relative to WRF-CTL, the quantile mapping of PGW simulation would change the original precipitation change signal between WRF-PGW and WRF-CTL. To retain the climate change signals in bias correction and generate appropriate bias correction for summer precipitation for future scenarios, consideration needs to be given to the physical processes involved in the change.

28.7 Summary

Dynamical downscaling of current and future climates (RCP8.5) using 4 km WRF provides valuable high-resolution regional climate data for hydrological applications and climate impact studies. For the current climate (CTL, 2000–2015), a high-resolution convective regional climate simulation (CTL, 2000–2015) was performed using WRF with 4 km grid spacing in Western Canada, and a high-end emission scenario RCP8.5 was simulated using the PGW method. WRF-CTL simulation is forced by a reanalysis (ERA-Interim) on the boundaries at 6-h intervals. WRF-PGW is forced in the same way as CTL, in addition to climate change signals from an ensemble mean of 19 CMIP5 members between 2070–2100 and 1976–2005. At a horizontal resolution of 4 km, convection is explicitly represented in the model and the convection parameterization scheme is disabled.

The WRF-CTL assessments against the reanalyses (such as CaPA and NARR) based on grid observation datasets show that WRF-CTL agrees with them in terms of geographical distribution, seasonal cycle, and interannual variation. For temperature biases, the largest bias occurs on the plains east of the Canadian Rockies in spring. In general, WRF-CTL produces more precipitation than both ANUSPLIN and CaPA, especially in the northern part of the domain, where observations are also few and most observation analysis has a dry bias relative to station observation. WRF-CTL's precipitation bias for CaPA is smaller than the bias with ANUSPLIN, which has been shown to be too dry in the north and SRB (Wong et al. 2017). The assessment reminds us that many of the differences are due to low coverage of observational data from interpolation from sparse observation. This indicates that high-quality meteorological observation with reasonable geographical coverage over Western Canada is urgently needed to provide forcing for RCM simulations and reference for model evaluations.

In the future warming scenario of RCP8.5, WRF-PGW shows that Western Canada will experience significant warming, although warming will be slightly lower than the CMIP5 ensemble projection. During the cold season, the warming is stronger, especially in the north-eastern polar regions in winter, and in the Canadian Prairies in spring. Although the CTL precipitation of PGW varies with the seasons, the precipitation in the two basins in spring and late autumn increased more, while the precipitation in summer did not increase much or decrease. The smallest change in precipitation occurred in summer when PGW precipitation in some parts of the grassland was less than CTL. With little precipitation and PGW evaporation in summer, which is much larger than CTL, Canadian grasslands will face water supply challenges during the growing season. With the increase in temperature and the potential increase of evaporation, the slight increase in summer precipitation indicates a slight decrease in effective summer precipitation in Canadian grassland and northern forest biomes, which may have a significant impact on soil moisture and forest fires in agricultural fields. This dynamic decrease in WRF is also different from CMIP5's overall average forecast SRB and southern MRB, where summer precipitation is expected to decrease significantly. Because convection plays an

important role in summer precipitation in the Canadian grasslands, the difference between the 4 km WRF and GCM combinations may be due to differences in simulated convection. Precipitation changes in the BC coast and the Canadian Rockies are also expected to be higher than CMIP5 due to the representation of the underlying terrain and the elevation of the GCM to the 4 km WRF terrain.

Future changes in water budget components as indicated by the change in WRF-PGW (RCP8.5) relative to WRF-CTL show a general enhancement of water cycle in both basins. Evapotranspiration increases consistently throughout the region and more so during warm seasons. Because the warmer atmosphere holds more water vapor, WRF-PGW shows an increase in atmospheric moisture transport and precipitation than WRF-CTL. The increase in severe precipitation events exceeded moderate and light precipitation events as the distribution of precipitation events shift to higher intensity in all seasons except summer. In summer, light to moderate precipitation (5–10 mm/3 h) in WRF-PGW is smaller than WRF-CTL in MRB and SRB. In the north-eastern region where warming is strongest, precipitation increases significantly during the cold season. With the shift of PGW simulated precipitation events to the higher intensity end, the total summer precipitation in the two basins only increases slightly, which may not reflect the actual changes in agricultural flood risk and water supply, as evapotranspiration increases greatly in growing season and the frequency of extreme precipitation events increases disproportionately, which produces less effective precipitation. Changes in the distribution of precipitation intensity in WRF-PGW also pose challenges to bias correction, which often relies on fitting to the distribution of observations assuming statistical stationarity.

In summary, high-resolution convection-permitting WRF simulations reproduce the general characteristics of the climate in the western Canadian region. The model results not only provide a wealth of opportunities for atmospheric and climate scientists interested in local and regional-scale meteorological phenomena and climate dynamics and circulation changes under global warming, but also offer new opportunities for hydrology stakeholders and agricultural experts for their need for high-resolution climate information and detailed global warming projections in Western Canada, including some large watersheds.

Acknowledgments The research described in this chapter is funded by Changing Cold Region Network.

References

Bindoff N, Stott P, Achuta Rao K, Allen M, Gillett N, Gutzler D, Hansingo K, Hegerl G, Hu Y, Jain S, Mokhov I, Overland J, Perlwitz J, Sebbari R, Zhang X (2013) Detection and attribution of climate change: from global to regional, in climate change 2013: the physical science basis. In: Stocker T, Qin D, Plattner G-K, Tignor M, Allen S, Boschung J, Nauels A, Xia Y, Bex V, Midgley P (eds) Contribution of working group I to the fifth assessment report of the intergovernmental panel on climate change. Cambridge University Press, Cambridge, United Kingdom; New York, NY, USA, pp 867–952

Casati B, de Elía R (2014) Temperature extremes from Canadian regional climate model (CRCM) climate change projections. Atmos Ocean 52(3):191–210. https://doi.org/10.1080/07055900.2014.886179

Castro CL (2005) Dynamical downscaling: assessment of value retained and added using the regional atmospheric modeling system (rams). J Geophys Res 110(D5):D05108. https://doi.org/10.1029/2004jd004721

Chen F, Dudhia J (2001) Coupling an advanced land surface-hydrology model with the penn state-ncar mm5 modeling system. Part I: model implementation and sensitivity. Mon Weather Rev 129(4):569–585. 10.1175/1520-0493(2001)129<0569:CAALSH>2.0.CO;2

Collins WD, Rasch P, Boville B, Hack J, McCaa J, Williamson D, Kiehl J, Briegleb B, Bitz C, Lin S-J, Zhang M, Dai Y (2004) Description of the NCAR community atmosphere model (cam 3.0). In: Natational Centre for Atmospheric Research, Boulder, Colorado

Cubasch U, Wuebbles D, Chen D, Facchini M, Frame D, Mahowald N, Winther J-G (2013) Introduction. In: Stocker T, Qin D, Plattner G-K, Tignor M, Allen S, Boschung J, Nauels A, Xia Y, Bex V, Midgley P (eds) Climate change 2013: The physical science basis. Contribution of working group I to the fifth assessment report of the intergovernmental panel on climate change. Cambridge University Press, Cambridge, United Kingdom; New York, NY, USA, pp 119–158

Dai A, Rasmussen RM, Liu C, Ikeda K, Prein AF (2017) A new mechanism for warm-season precipitation response to global warming based on convection-permitting simulations. Clim Dyn. https://doi.org/10.1007/s00382-017-3787-6

Dee DP, Uppala SM, Simmons AJ, Berrisford P, Poli P, Kobayashi S, Andrae U, Balmaseda MA, Balsamo G, Bauer P, Bechtold P, Beljaars ACM, van de Berg L, Bidlot J, Bormann N, Delsol C, Dragani R, Fuentes M, Geer AJ, Haimberger L, Healy SB, Hersbach H, Hólm EV, Isaksen L, Kållberg P, Köhler M, Matricardi M, McNally AP, Monge-Sanz BM, Morcrette J-J, Park B-K, Peubey C, de Rosnay P, Tavolato C, Thépaut J-N, Vitart F (2011) The ERA-Interim reanalysis: configuration and performance of the data assimilation system. Quart J Royal Meteorolog Soc 137(656):553–597. https://doi.org/10.1002/qj.828

Deser C, Phillips A, Bourdette V, Teng H (2012) Uncertainty in climate change projections: the role of internal variability. Clim Dyn 38(3–4):527–546. https://doi.org/10.1007/s00382-010-0977-x

Easterling DR, Meehl GA, Parmesan C, Changnon SA, Karl TR, Mearns LO (2000) Climate extremes: observations, modeling, and impacts. Science289:5487, 2068–74

Feser F, Rockel B, von Storch H, Winterfeldt J, Zahn M (2011) Regional climate models add value to global model data: a review and selected examples. Bull Am Meteor Soc 92(9):1181–1192. https://doi.org/10.1175/2011bams3061.1

Fortin V, Roy G, Stadnyk T, Koenig K, Gasset N, Mahidjiba A (2018) Ten years of science based on the Canadian precipitation analysis: a CaPA system overview and literature review. Atmos Ocean 56(3):178–196. https://doi.org/10.1080/07055900.2018.1474728

Giorgi F, Jones C, Asrar GR (2009) Addressing climate information needs at the regional level: the cordex framework. WMO Bull 58(3):175

Hofstra N, New M, McSweeney C (2009) The influence of interpolation and station network density on the distributions and trends of climate variables in gridded daily data. Clim Dyn 35(5):841–858. https://doi.org/10.1007/s00382-009-0698-1

Hopkinson RF, McKenney DW, Milewska EJ, Hutchinson MF, Papadopol P, Vincent LA (2011) Impact of aligning climatological day on gridding daily maximum–minimum temperature and precipitation over canada. J Appl Meteorol Climatol 50(8):1654–1665. https://doi.org/10.1175/2011jamc2684.1

Hutchinson MF, McKenney DW, Lawrence K, Pedlar JH, Hopkinson RF, Milewska E, Papadopol P (2009) Development and testing of canada-wide interpolated spatial models of daily minimum-maximum temperature and precipitation for 1961-2003. J Appl Meteorol Climatol 48(4):725–741. https://doi.org/10.1175/2008jamc1979.1

IPCC (2013) Climate change 2013: the physical science basis. Contribution of working group I to the fifth assessment report of the intergovernmental panel on climate change, Book, Cambridge University Press, Cambridge, United Kingdom; New York, NY, USA

Karl TR, Meehl GA, Miller CD, Hassol SJ, Waple A, Murray W (2006) Weather and climate extremes in a changing cimate. Regions of focus, North America, Hawaii, Caribbean, and U.S. Pacific islands

Kurkute S, Li Z, Li Y, Huo F (2019) Assessment and projection of water budget over western canada using convection permitting WRF simulations. Hydrol Earth Syst Sci Dis 1–32:2019. https://doi.org/10.5194/hess-2019-522

Li Y, Szeto K, Stewart RE, Thériault JM, Chen L, Kochtubajda B, Liu A, Boodoo S, Goodson R, Mooney C, Kurkute S (2017) A numerical study of the june 2013 flood-producing extreme rainstorm over southern Alberta. J Hydrometeor 18:2057–2078. https://doi.org/10.1175/JHM-D-15-0176.1

Li Y, Li Z, Zhang Z, Chen L, Kurkute S, Scaff L, Pan X (2019) High-resolution regional climate modeling and projection over western Canada using a weather research forecasting model with a pseudo-global warming approach. Hydrol Earth Syst Sci 23:4635–4659. https://doi.org/10.5194/hess-23-4635-2019

Liu C, Ikeda K, Thompson G, Rasmussen R, Dudhia J (2011) High-resolution simulations of wintertime precipitation in the colorado headwaters region: sensitivity to physics parameterizations, Month Weather Rev 139(11):3533–3553. http://dx.doi.org/10.1175/MWR-D-11-00009.1

Liu C, Ikeda K, Rasmussen R, Barlage M, Newman AJ, Prein AF, Chen F, Chen L, Clark M, Dai A, Dudhia J, Eidhammer T, Gochis D, Gutmann E, Kurkute S, Li Y, Thompson G, Yates D (2017) Continental-scale convection-permitting modeling of the current and future climate of North America. Clim Dyn 49(1):71–95. https://doi.org/10.1007/s00382-016-3327-9

Mahfouf J-F, Brasnett B, Gagnon S (2007) A Canadian precipitation analysis (CaPA) project: description and preliminary results. Atmos-Ocean 45(1), 1–17. https://doi.org/10.3137/ao.450101

Mearns LO, Sain S, Leung LR, Bukovsky MS, McGinnis S, Biner S, Caya D, Arritt RW, Gutowski W, Takle E, Snyder M, Jones RG, Nunes AMB, Tucker S, Herzmann D, McDaniel L, Sloan L (2013) Climate change projections of the North American regional climate change assessment program (narccap). Clim Change 120(4):965–975. https://doi.org/10.1007/s10584-013-0831-3

Mearns LO, Lettenmaier DP, McGinnis S (2015) Uses of results of regional climate model experiments for impacts and adaptation studies: the example of NARCCAP. Curr Clim Change Rep 1(1):1–9. https://doi.org/10.1007/s40641-015-0004-8

Meng X, Lyu S, Zhang T, Zhao L, Li Z, Han B, Li S, Ma D, Chen H, Ao Y, Luo S, Shen Y, Guo J, Wen L (2018) Simulated cold bias being improved by using modis time-varying albedo in the tibetan plateau in WRF model. Environ Res Lett. 13(4):044028. http://stacks.iop.org/1748-9326/13/i=4/a=044028

Mesinger F, DiMego G, Kalnay E, Mitchell K, Shafran PC, Ebisuzaki W, Jović D, Woollen J, Rogers E, Berbery EH, et al (2006) North American regional reanalysis. Bull Am Meteorol Soc 87(3):343–360. https://doi.org/10.1175/bams-87-3-343

Misra V, Kanamitsu M (2004) Anomaly nesting: a methodology to downscale seasonal climate simulations from agcms. J Clim 17(17):3249–3262. http://dx.doi.org/10.1175/1520-0442(2004)017$<$3249:anamtd>2.0.co;2

Morrison H, Thompson G, Tatarskii V (2009) Impact of cloud microphysics on the development of trailing stratiform precipitation in a simulated squall line: comparison of one- and two-moment schemes. Month Weather Rev 137(3):991–1007. http://dx.doi.org/10.1175/2008mwr2556.1

Musselman KN, Lehner F, Ikeda K, Clark MP, Prein AF, Liu C, Barlage M, Rasmussen R (2018) Projected increases and shifts in rain-on-snow flood risk over western North America. Nat Clim Change 8(9):808–812. https://doi.org/10.1038/s41558-018-0236-4

Nelson BR, Prat OP, Seo D, Habib E (2016) Assessment and Implications of NCEP Stage IV Quantitative Precipitation Estimates for Product Intercomparisons. Weather Forecast 31:371–394. https://doi.org/10.1175/WAF-D-14-00112.1

Prein AF, Rasmussen RM, Ikeda K, Liu C, Clark MP, Holland GJ (2017) The future intensification of hourly precipitation extremes. Nat Clim Change 7(1):48–52. https://doi.org/10.1038/nclimate3168

Rasmussen R, Ikeda K, Liu C, Gochis D, Clark M, Dai A, Gutmann E, Dudhia J, Chen F, Barlage M, Yates D, Zhang G (2014) Climate change impacts on the water balance of the colorado headwaters: high-resolution regional climate model simulations. J Hydrometeorol 15 (3):1091–1116. https://doi.org/10.1175/jhm-d-13-0118.1

Rasmussen KL, Prein AF, Rasmussen RM, Ikeda K, Liu C (2017) Changes in the convective population and thermodynamic environments in convection-permitting regional climate simulations over the united states. Clim Dynamic. http://dx.doi.org/10.1007/s00382-017-4000-7

Sato T, Kimura F, Kitoh A (2007) Projection of global warming onto regional precipitation over mongolia using a regional climate model. J Hydrol 333(1):144–154. http://dx.doi.org/10.1016/j.jhydrol.2006.07.023

Stralberg D, Wang X, Parisien M-A, Robinne F-N, Sólymos P, Mahon CL, Nielsen SE, Bayne EM (2018) Wildfire-mediated vegetation change in boreal forests of alberta, canada. Ecosphere 9 (3):e02156. https://doi.org/10.1002/ecs2.2156

Sugiyama M, Shiogama H, Emori S (2009) Precipitation extreme changes exceeding moisture content increases in miroc and IPCC climate models. Proc Natl Acad Sci 107(2):571–575. https://doi.org/10.1073/pnas.0903186107

Takhsha M, Nikiéma O, Lucas-Picher P, Laprise R, Hernández-Díaz L, Winger K (2017) Dynamical downscaling with the fifth-generation Canadian regional climate model (crcm5) over the cordex arctic domain: effect of large-scale spectral nudging and of empirical correction of sea-surface temperature. Clim Dyn. https://doi.org/10.1007/s00382-017-3912-6

Thompson G, Field PR, Rasmussen RM, Hall WD (2008) Explicit forecasts of winter precipitation using an improved bulk microphysics scheme. Part II: implementation of a new snow parameterization. Mon Weather Rev 136(12):5095–5115. https://doi.org/10.1175/2008mwr2387.1

Westra S, Fowler HJ, Evans JP, Alexander LV, Berg P, Johnson F, Kendon EJ, Lenderink G, Roberts NM (2014) Future changes to the intensity and frequency of short-duration extreme rainfall. Rev Geophys 52(3):522–555. https://doi.org/10.1002/2014rg000464

Wong JS, Razavi S, Bonsal BR, Wheater HS, Asong ZE (2017) Inter-comparison of daily precipitation products for large-scale hydro-climatic applications over Canada. Hydrol Earth Syst Sci 21(4):2163–2185. https://doi.org/10.5194/hess-21-2163-2017

Xu T, Hutchinson MF (2013) New developments and applications in the ANUCLIM spatial climatic and bioclimatic modelling package. Environ Modell Softw 40:267–279. https://doi.org/10.1016/j.envsoft.2012.10.003

Dr. Yanping Li is an Associate Professor at the School of Environment and Sustainability and the Global Institute for Water Security at the University of Saskatchewan, Canada. She obtained her Ph.D. from Yale University, USA in Atmosphere, Ocean and Climate Dynamics. Her research interests are interdisciplinary regarding high-resolution regional climate modeling, extreme weather, and land–atmosphere interaction to inform climate adaptations.

Dr. Zhenhua Li is a Research Scientist at the Global Institute for Water Security at the University of Saskatchewan, Canada. He obtained his Ph.D. in Atmospheric Science from the University of Illinois at Urbana-Champaign (UIUC), USA. His research interests are atmospheric dynamics, regional climate modeling, drought study, etc. In particular, he is interested in looking at the interaction between climate change and regional land cover change, and interface between climate change and adaptive decision-makings over long timescales.

Responses of Boreal Forest Ecosystems and Permafrost to Climate Change and Disturbances: A Modeling Perspective

29

Shuhua Yi and Fengming Yuan

Abstract

The north circumpolar region contains a large amount of carbon. This carbon storage is vulnerable due to permafrost degradation and wildfire disturbances under ongoing and projected climate change. Climate warming and wildfires change soil organic horizons gradually or abruptly, and modify permafrost thermal-hydrology and biogeochemistry, ecosystem structures, functions, and capability of sequestrating rising atmospheric CO_2. Land models do not fully take accounts of these interactions and its complexity in the high latitude. This chapter describes a terrestrial ecosystem model with dynamic organic soil module (DOS-TEM) and its unique freezing-thawing algorithm, and presents key results of its applications mainly in boreal forests of Alaska. The DOS-TEM explicitly considers interactions of soil thermal and hydrological processes, permafrost degradation and the direct and indirect effects of wildfire disturbances, in addition to soil–plant C and N cycles. We first introduce four modules of DOS-TEM, focusing on its disturbance module and coupling with a dynamic organic soil module. Then we describe and validate DOS-TEM's freezing-thawing algorithm and development based on two-directional Stefan algorithm (TDSA). Finally, we apply the DOS-TEM at site and region scales, with a focus on model ability to dynamically simulate soil organic thickness under warming and wildfires, and consequent impacts on permafrost in the Yukon River Basin. We conclude that land surface model development is

S. Yi (✉)
School of Geographic Sciences, Nantong University, 999 Tongjing Road, Nantong 226007, China
e-mail: yis@ntu.edu.cn

F. Yuan
Environmental Science Division, Oak Ridge National Laboratory, Climate Change Science Institute, Oak Ridge, TN 37831, USA
e-mail: yuanf@ornl.gov

D. Yang and D. L. Kane (eds.), *Arctic Hydrology, Permafrost and Ecosystems*,
https://doi.org/10.1007/978-3-030-50930-9_29

urgently needed to include other critical landscape processes, such as thermalkarst and other disturbances, to synchronize thermal-hydrological-biogeochemical processes, and to incorporate an advanced understanding of biospheric feedbacks to atmosphere and ecosystems. Such a complexity of modeling scope is plausible with advancement of high performance computing.

29.1 Overview

Permafrost is defined as ground (soil or rock) that remains at or below 0 °C for at least two consecutive years. Permafrost covers about 1/4 of the land area of the North Hemisphere (Zhang et al. 1999). There is about 1400–1850 PgC/60–90 PgC stored in permafrost soils/vegetation over the northern circumpolar region (Schuur et al. 2008; Tarnocai et al. 2009; McGuire et al. 2009). Since ongoing and projected climate warming has been recorded or estimated to be the strongest in the high latitudes, the northern regions have experienced pronounced warming and consequences during the last century (ACIA 2004). For example, very likely this strong warming, in combination of subsequent changes of environment, will make a large amount of carbon vulnerable and turn northern ecosystem from C sinks to sources (McGuire et al. 2018). Once thawed, the organic carbons previously protected at depth in frozen soils are subject to decomposition (Goulden et al. 1998). Regional analyzes indicate that recent increases in wildfires, associated with climate warming, could release substantial amounts of soil C from boreal forests and/or arctic tundra in the future (Zhuang et al. 2006; Balshi et al. 2009a, b; Schaefer et al. 2011; Schneider von Deimling et al. 2012). Meanwhile warming and CO_2 fertilization effects likely benefit plant productivity. Changes in soil temperature and moisture due to climate warming can also affect nutrient availability (van Cleve et al. 1983) and plant phenology (van Wijk et al. 2003), which further enhance plant biomass production and subsequently soil sequestration of CO_2. However, plant biomass production in the long term would provide more fuels for wildfires (Rupp et al. 2016). In general, warming would potentially alter structures and functions of terrestrial ecosystems and impact C storage in permafrost, its unique functions in sequestration of atmospheric C, and its highly interacted thermal-hydrological-biogeochemical processes.

To properly understand and project carbon dynamics of the northern circumpolar region, it is critical to consider the responses to climate change of soil thermal and hydrological factors, permafrost degradation, vegetation dynamics, wildfire disturbances, and their interactions. However, one limitation of regional and global model analyzes to date, is the treatment of soil organic horizons as static, in terms of thickness and composition, and thus of thermal-hydrological properties. Historically, highly depending upon progressive mechanic understanding of terrestrial ecosystems and computing techniques, modeling interactions between soil thermal-hydrological dynamics and interaction with other processes were generally

implemented only since the third generation land surface models. In General Circulation Models (GCM) or Earth System Models (ESM), to simulate the lower boundary water, heat and momentum fluxes, and greenhouse gas exchanges between atmosphere and biosphere was one of the critical but usually a small component, until presently (Verseghy 1991; Bonan 1996; Oleson et al. 2004). These interactions were initially simplified in most single disciplinary ecosystem models where bucket of soils might be enough to represent soil abiotic factors in their applications (e.g., Sitch et al. 2003), and simple analytical or empirical functions were adopted to model relevant soil processes (e.g., Bond-Lamberty et al. 2005). Gradually large-scale ecosystem models have considered vertical soil thermal or hydrological dynamics due to its importance in biogeochemical processes, e.g., the Terrestrial Ecosystem Model (TEM) (Zhuang et al. 2001, 2004; Euskirchen et al. 2006), DAYCENT (Parton et al. 2001), etc. But there are rarely models with fully and synchronized coupling of thermal and hydrological processes (e.g., Wang et al. 2017). On the other hand, soil physical and hydrological studies have developed very complicated models for agricultural and natural soil systems initially, e.g., HYDRUS (Šimůnek et al.), Ecosys (Grant et al.), Endrizzi et al. (2014), etc., and then widely have been applied for in other managed or natural ecosystems, but there are not yet incorporated into large scale ESMs or even regional level models. It appears that what really missing are multidisciplinary or cross-disciplinary model coupling of whole soil-vegetation-atmospheric transports (SVAT), with each of processes reasonably well represented physically and biogeochemically. There exist variable-resolution models in atmospheric (e.g., Huang et al. 2016) and ocean or ice sheet components in ESMs, but rarely in their soil systems due to priority and computing limitation.

For high latitude ecosystems, soil temperature and moisture are considered as the most important environmental factors affecting soil organic matter decomposition (Davidson and Janssens 2006) and plant productivity in the Arctic and boreal regions. Unlike other areas, soil thermal and hydrological processes are highly coupled, due to seasonal freezing-thawing cycles in permafrost, which is one of the grand challenges for modeling thermal-hydrology and tightly coupled C and N biogeochemistry in cold regions (e.g., Painter and Karra, 2014). There are two primary ways in which soil water can influence its thermal dynamics: (1) the thermal conductivity of dry organic soil horizons, i.e., usually of greater than 18% organic C, is substantially lower than that of wet organic soil, which makes dry organic soil a good heat insulator (Yi et al. 2007); (2) the seasonal amplitude of soil temperature is damped through the release and absorption of latent heat. Conversely, thermal states and properties of partially frozen soils can also influence its hydrology locally and laterally: (1) frozen soils have limited infiltration capacity, which results in a large runoff during spring snowmelt (Shanley and Chalmers 1999); and (2) baseflow depends on the extent of unfrozen soil in the hydrologically active zone. For example, deeper unfrozen soil layers are expected to contribute to the increase in winter discharge from northern rivers into the Arctic Ocean (Oelke

et al. 2004). Unfortunately those strongly linked heat and water processes, controlled by mechanisms including phase changes, advections, and/or transports, are either not fully taken into account or not really synchronously coupled in the most land surface models of ESMs until recently (Cuntz and Haverd 2018).

One of the modeling challenges in terms of computing is likely the numerical difficulties in fully and explicitly simulating permafrost thermal-hydrology (Painter 2010; Dall'Amico et al. 2011; Painter et al. 2012; Kurylyk and Watanabe 2013; Endrizzi et al. 2014), and various simplifications had to be adopted with rational assumptions. When soil thermal-hydrology itself is part of large scale landscape hydrological processes, including surface and groundwater, challenges even become more (Bring et al. 2016; Painter et al. 2016; Jan et al. 2018; Jafarov et al. 2018). There are a number of different techniques used to simulate permafrost dynamics (Riseborough et al. 2008; Kurylyk and Watanabe 2013). A wide range of numerical models exists, and have been applied in either stand-alone permafrost simulations or land surface schemes. Numerical solutions for permafrost dynamics in large scale models are commonly obtained by solving finite difference equations. One category of the numerical solution, referred by Zhang et al. (2008) as "decoupled energy conservation parameterization," assumes that the soil water is homogeneous and freezes or thaws at exactly 0 °C. Soil temperature is calculated for each layer and if the temperature of a particular layer is greater than 0 °C, some or all of any ice present will melt and the temperature is then recalculated, and vice versa. This is an efficient method and is commonly used in land surface models (Zhang et al. 2003; Oleson et al. 2004). However, the lower layers in land surface models are usually thick and the freezing or thawing fronts derived from soil temperature interpolation are not realistic (Yi et al. 2006).

The second category of numerical methods, referred by Zhang et al. (2008) as "apparent heat capacity parameterization," assumes that soil water freezes or thaws over a range of temperatures below 0 °C and simulates both the unfrozen soil water content and the temperature, simultaneously. Since small changes in soil temperature within the freeze/thaw range will result in a large change in apparent heat capacity, an iterative procedure is required to ensure that only small temperature changes occur during each time interval (Nicolsky et al. 2007). This method is commonly applied in permafrost models (Goodrich 1978; Nicolsky et al. 2007; Hipp et al. 2012: Langer et al. 2013) and has also recently been applied in a land surface model (Ringeval et al. 2012). Although the method is more physically realistic it has several disadvantages: (1) it requires greater computing resources, which may lead to limitations in the spatial resolution, the length of time that can be modeled, and the number of simulated land surface classes, etc. (2) static frozen and unfrozen soil physical properties are used, e.g., thermal conductivity.

Both categories of numerical models have their disadvantages when they are applied for regional permafrost simulations. Apart from numerical models, analytical solutions also exist that can be used for solving phase change problems. For example, exact Neumann solutions to freezing and thawing problems exist for

idealized cases, such as for infinite or semi-infinite homogeneous material, steady upper boundary conditions, etc. (Lunardini 1981). Stefan's equation, which was originally used to predict the thickness of sea ice, is widely used due to its simple form (Lunardini 1981); an algorithm for applying Stefan's equation to a layered system (e.g., soil) was developed by Jumikis (1977) and applied in a hydrological model by Fox (1992). However, predictions from the Stefan algorithm usually overestimate the depths of freeze/thaw fronts as it neglects any heat transport beneath the front. In order to mitigate this problem of overestimation, Woo et al. (2004) developed a two-directional Stefan algorithm (TDSA). Yi et al. (2009a, b) integrated a TDSA within the Terrestrial Ecosystem Model (TEM) in order to first simulate the depths of freezing or thawing fronts, and then update the soil temperatures for layers above the uppermost front, beneath the lowermost front, and between these two fronts. This is an efficient method and is able to track the positions of fronts within thick soil layers, meanwhile soil properties change depending on the changes in soil water content and thermal state.

Another feature distinguishing high latitude system from the rest is its soil organic horizons. Due to its unique thermal and hydrological properties of those organic layers in permafrost, any novel change of their thickness and/or bulk density is likely to influence many aspects of cold region hydrology and biogeochemistry. It's especially of importance for assessing long-term effects of warming and its consequent environment changes and/or abrupt disturbances. In short-term initial warming and rising CO_2 should benefit plant production and thus littering which could add near-surface organic horizons, while deepening active layer allowed lower organic horizon thinning physically and C loss biogeochemically. Thus in a long time soil structure changes are expected and consequently soil thermal, hydrological, and biogeochemical properties, locally and across landscape (e.g., thermalkarst).

Recently enhanced wildfires in terms of frequency and severity took places not only in boreal forest ecosystems of North America (Kasischke et al. 2007) but also in tundra (Mack et al. 2011). It is projected to increase further throughout this century in response to projected climate warming (Flannigan et al. 2005; Balshi et al. 2009b). A growing number of studies indicate that wildfire plays an important role in the carbon dynamics of northern high latitude ecosystems (Zimov et al. 1999; Harden et al. 2000; Bond-Lamberty et al. 2007; Balshi et al. 2007, 2009a). In contrast to gradual climate change effects, fires especially severe ones destroy near-surface soil organic layers, and change the soil's physical and chemical properties abruptly, which indirectly impact ecosystems through the changes of surface energy balance (Liu et al. 2005), soil thermal and hydrological regimes (MacKay 1995; Burn 1998; O'Neill et al. 2002; Kasischke and Johnstone 2005; Liljedahl et al. 2007), and vegetation succession (Johnstone and Kasischke 2005; Johnstone and Chapin 2006), at short-term or decade or century time-scales.

At the regional scale, direct effects of fire occurrence have received much attention (Thonicke et al. 2001; Arora and Boer 2005; Balshi et al. 2007). But the evaluation of the indirect effects of fire has been limited because appropriate tools

have not yet been fully developed for application at the regional scale. With an increase in understanding importance of organic soil on thermal and hydrological regimes, regional land surface and terrestrial ecosystem models have begun to implement organic matter horizons into their representations of the soil profile (Zhuang et al. 2001; Zhang et al. 2003; Yi et al. 2006; Lawrence and Slater 2008). Some site-specific modeling studies have represented changes in thickness of organic horizons after fire based on the balance between litter input and soil C decomposition (Carrasco et al. 2006; Fan et al. 2008; also see Frolking et al. 2001), but these studies did not consider how those changes affect soil temperature and moisture dynamics.

Furthermore, the thickness and composition of soil organic horizons are quite variable in both space and time (Johnson et al. 2011; Barrett et al. 2011). In addition to initially biomass increasing, warming (and rising CO_2) enhanced vegetation growth, litterfall, and root mortality into soil organic horizons may benefit permafrost stability, because of ground surface cover (mulching) of newly added materials with different density and its thermal-hydrological properties. Meanwhile deep organic matter C respiration (release) may also change the total soil thermal-hydrological properties (including thickness). On the other hand, burning removal of soil organic horizons by fires not only exposes permafrost to thaw by modifying surface energy balance and soil thermal conditions, but also in a warming climate permafrost may undergo long-term thaw from this exposure (Yoshikawa et al. 2003; Yi et al. 2009b, 2010). These will challenge experimental investigations, e.g., measurement of thermal and hydraulic characteristics of organic materials, under freezing-thawing and/or wetting-drying conditions, still remains as grand difficulties. They also require model developments in terms of variable-resolution spatially and temporally (i.e., discretization), and very likely mathematical solutions or schemes are urgently needed.

One of the key challenges to assess high latitude regional changes in terrestrial ecosystem carbon stocks and its functions and services is to explicitly represent how the structure and composition of soil organic horizons responding to climate warming and other environmental changes. To our knowledge, none of the modeling efforts to date have dynamically represented such soil dynamics. It's still unknown how this would influence soil thermal, hydrological, biogeochemical, and vegetation dynamics spatially and temporally. For this reason, in the last 10 years the Dynamic Organic Soil version of the Terrestrial Ecosystem Model (DOS-TEM) (Yi et al. 2009a, b, 2010; Yuan et al. 2012, 2013; Kelly et al. 2015; Euskirchen et al. 2016; Genet et al. 2013, 2018) has been developed, calibrated, assessed, and applied for as a tool to understand the relative roles of climate warming, changes in fire regime, and other landscape-level changes on the dynamics of forest ecosystem C in high latitude mainly in Alaska. In this chapter we will (1) specifically overview initial development of DOS-TEM, which was designed to represent thermal-hydrological-biogeochemical processes for targeting soil-vegetation-atmosphere systems; (2) demonstrate its capability to simulate soil-vegetation dynamics of a

typical boreal black spruce forest; and (3) apply for DOS-TEM in northern high latitude terrestrial ecosystems under historical and projected warming and fire regimes at watershed scales, i.e., the Yukon River Basins (YRB).

29.2 Dynamic Organic Soil-Terrestrial Ecosystem Model

The Terrestrial Ecosystem Model (TEM) is a process-based ecosystem model designed to simulate the carbon and nitrogen pools of vegetation and soil, and carbon and nitrogen fluxes among vegetation, soil, and atmosphere (Raich et al. 1991; McGuire et al. 1992). While previous model development efforts have improved the soil thermal and hydrological processes in TEM for application in high latitude regions (Zhuang et al. 2001, 2002, 2003, 2004; Euskirchen et al. 2006), soil thermal and hydrological processes are not comprehensively coupled, and fire disturbance reduced the amount of soil carbon without affecting organic soil thickness and associated changes in the thermal and hydrological properties of organic soil (e.g., see Balshi et al. 2007). Zhuang et al. (2002) conducted model experiments that demonstrated that changes in organic matter horizons during and after fire potentially have important influences on soil temperature and moisture, but subsequent modeling efforts have not dealt with the issue of dynamic changes in organic horizons.

Therefore, the model development research reported here is focused on the explicit coupling of soil thermal and hydrological processes in the context of a changing organic horizon, which is a necessary step toward dynamically simulating how changes in organic matter horizons during and after fire influence the interactions among soil thermal, hydrologic, and biogeochemical processes.

29.2.1 Modules of DOS-TEM

In the following parts, we described the main features modified in or unique to Dynamic Organic Soil version of TEM (DOS-TEM), including environmental (EnvM), ecological (EcoM), dynamic organic soil (DOSM), and fire disturbance effects modules (FEM) (Fig. 29.1).

29.2.1.1 The Environmental Module (EnvM)

In the EnvM, ground/soil column is represented by a snow horizon, three soil organic horizons, two mineral soil horizons, and a rock horizon. Each horizon is further divided into variable numbers of layers that are explicitly treated with respect to energy and moisture exchange. Specifically, snow horizon can consist of up to five snow layers, organic soil horizons up to seven layers, while five mineral and five rock layers. Obviously thickness of snow and organic soil layers are dynamical spatially and temporally. Generally layer thickness is thicker downward, with a total mineral soil of 3.8 m and total soil-rock column of around 50 m.

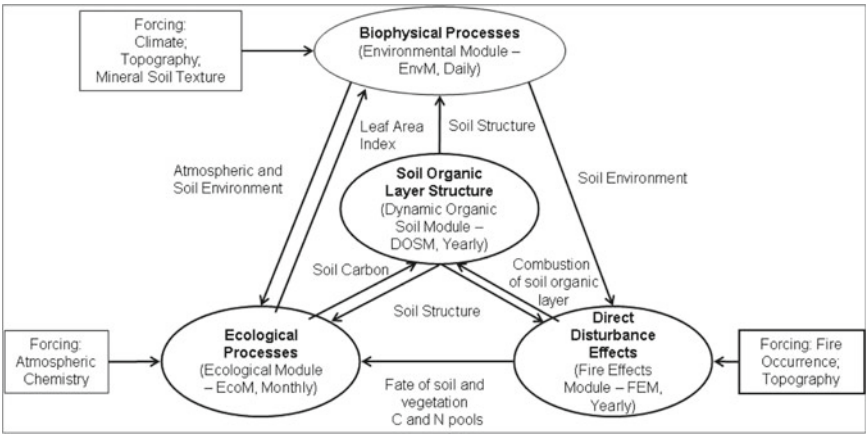

Fig. 29.1 Interactions among modules of the dynamic organic soil version of the Terrestrial Ecosystem Model (DOS-TEM). Modules include the daily environmental module (EnvM), the monthly ecological module (EcoM), the annual fire effects module (FEM), and the dynamic organic soil module (DOSM)

The organic soil horizons include types of live moss, fibrous organic soil, and amorphous organic soil. For accurate simulation of soil temperature and moisture, the soil horizons near the surface are divided into thin layers (e.g., layers are a few centimeters thick in the live moss horizon), and layers become thicker as the distance from the surface gets deeper (e.g., layers are approximately 10 m thick in the rock horizon). Following the method used in land surface models, e.g., the Canadian Land Surface Scheme (Verseghy 1991), the EnvM considers upper and lower mineral soil horizons. Each mineral soil horizon is 1 of 11 mineral soil types as defined in Beringer et al. (2001).

The EnvM operates at a daily time step using daily air temperature, vapor pressure, surface solar radiation and precipitation, downscaled from monthly input data. The EnvM considers the radiation and water fluxes among the atmosphere, canopy, snowpack, and soil. A Two-Directional Stefan Algorithm (TDSA) (Woo et al. 2004) is used to predict the positions of freezing/thawing fronts (FTFs) in soil column. Soil moistures are only updated for unfrozen layers by solving Richard equation. Both the thermal and hydraulic properties of soil layers are affected by its water content. The simulated estimates of daily evapotranspiration, soil temperature, and moisture are integrated to monthly values, as abiotic factors to EcoM. Most of the processes simulated in EnvM are similar to those of land surface models, e.g., Community Land Model (Oleson et al. 2004). In the following part, we only introduced the soil freezing/thawing scheme, which is unique to DOS-TEM. In EnvM, the TDSA can satisfactorily simulate the positions of FTFs in a land surface model when proper surface forcing is provided (Yi et al. 2006).

Soil freezing and thawing fronts (FTFs)

In EnvM, the positions of FTFs are first determined at a daily time step using the TDSA. The TDSA first processes layers from top to bottom, using ground surface temperature as the forcing for the surface layer, until all the energy (degree days) is used up, or the front meet the bottom boundary of soil. The temperature at the bottom of the first rock layer is then used as the forcing for the bottom boundary to force the deepest FTF upwards. An FTF separates a layer into homogeneous frozen and unfrozen parts. Then snow/soil column can be treated as a set of homogeneous frozen and unfrozen sublayers.

Take a positive driving temperature in summer as an example. At the beginning of the TDSA estimates dd_{left}, the available degree days for phase change (°C day), as follows

$$dd_{\text{left}} = T_0 d \tag{29.1}$$

where T_0 is the ground surface temperature (°C), d is in unit of day.

If a layer is frozen, then phase change will happen in this layer. TDSA calculates:

$$dd_{\text{need},i} = \theta_i \lambda d_i \left(R_{\text{sum},i} + \frac{R_i}{2}\right) \tag{29.2}$$

where $dd_{\text{need},i}$ is the degree-day (°C day) needed to completely thaw layer i, θ_i is the volumetric water content of layer i (m^3/m^3), λ is latent heat of fusion (J/m^3), d_i is the thickness of layer i (m), R_i is the thermal resistance of layer i (Ks/J), $R_{\text{sum},i}$ is the sum of thermal resistance above layer i (Ks/J). R_i is defined as

$$R_i = d_i / k_{\text{unf},i} \tag{29.3}$$

where $k_{\text{unf},i}$ is the unfrozen thermal conductivity ($W \cdot m^{-1} \cdot K^{-1}$) of layer i, which is calculated following the method of Johansen (1975):

$$k_{\text{unf},i} = (k_{\text{sat},i} - k_{\text{dry},i}) K_e + K_{\text{dry},i} \tag{29.4}$$

where, K_e is Kersten number, which is related to soil water content. The parameters $k_{\text{sat},i}$ and $k_{\text{dry},i}$ are saturated and dry thermal conductivities of a soil layer, which are specified for each soil layer type.

If $dd_{\text{need},i}$ is less than dd_{left}, the frozen state is changed to unfrozen, and a thawing front is moved to the top of the next layer, and dd_{left} is recalculated:

$$dd_{\text{left}} = dd_{\text{left}} - dd_{\text{need},i} \tag{29.5}$$

$R_{\text{sum},i}$ is then updated by adding the thermal resistivity of the current layer to the old value of $R_{\text{sum},i}$ and the TDSA then proceeds to the next layer if it is not rock.

If $dd_{\text{need},i}$ is greater than dd_{left}, partial depth that can be thawed,d_{part}, calculated as:

$$d_{\text{part}} = -k_{\text{unf},i}R_{\text{sum},i} + \sqrt{k_{\text{unf},i}^2 R_{\text{sum},i}^2 + \frac{2k_{\text{frz},i}dd_{\text{left}}}{\lambda\theta_i}} \tag{29.6}$$

where, and $k_{\text{frz},i}$ is the frozen thermal conductivity of layer i (J/Kms). A thawing front will be created at a depth d_{part} relative to the top of layer i. The dd_{left} is set to zero and the iteration stops. If a layer is unfrozen, the dd_{left} is kept unchanged, $R_{sum,i}$ is updated, and the TDSA then proceeds to the next layer if the layer is not rock. After the movement of thawing front downwards, the same procedure is used to adjust the deepest front upwards.

Temperatures of all layers

After the positions of FTFs are determined, the temperature of each layer will be updated. If there is no front in the whole ground column, the temperature of each layer will be updated by solving finite difference equations of all layers, with the derived ground surface temperature from air temperature as the top boundary condition. Because the heat flux around 50–100 m can be neglected for a time period of centuries (Nicolsky et al. 2007), we assumed a zero heat flux as the lower boundary condition. If there is one front in whole ground column, the layers above and below the front will be updated separately by solving two different sets of equations assuming no phase change. If there are two or more fronts in the whole soil column, the temperatures of layers above the first front will be updated by solving the finite difference equation of layers above the first front, and a similar method will be used to update temperatures below the last front. For layers between first and last front, the temperatures are assumed to be 0 °C.

The Crank–Nicholson scheme is used to solve the finite difference equations of ground temperatures. To keep the calculation stable, an adaptive step-size integration approach is used. The initial time step is a half day. After advancing one time step, if the change of a layer's temperature is greater than a specified threshold (0.1 °C in this study), the time step will be halved. Iteration continues until the calculation covers a full day.

29.2.1.2 The Ecological Module (EcoM)

The EcoM simulates the C and N pools of vegetation and soil, and the C and N fluxes among vegetation, soil, and atmosphere, as summarized in Fig. 29.2. In contrast to previous versions of TEM, DOS-TEM simulates the dynamics of three different soil C horizons (the fibrous, amorphous, and mineral soil horizons). Because the decomposition parameters used in the model are defined separately for each horizon, DOS-TEM is capable of representing multiple soils of different quality that is stratified vertically. And also vegetative litterfall is divided into aboveground and belowground, with the former only to the first layer of the fibrous horizon, while the latter to different layers based on the fractional distribution of fine

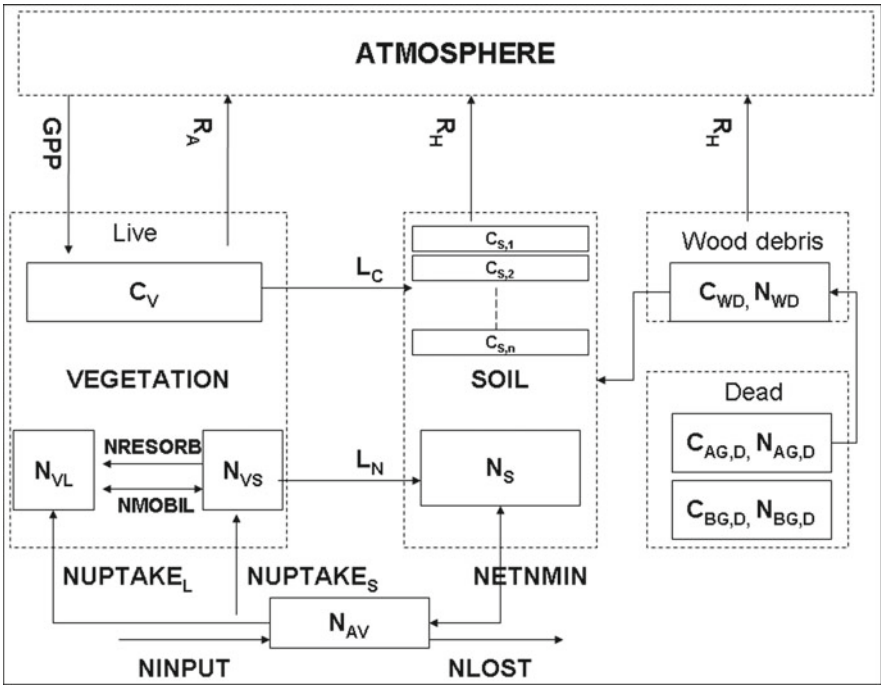

Fig. 29.2 The carbon and nitrogen pools and fluxes of the ecological module in the dynamic organic soil version of the Terrestrial Ecosystem Model (DOS-TEM). R_A: autotrophic respiration; GPP: gross primary production; R_H: heterotrophic respiration; C_V: vegetation carbon; N_{VL}: labile vegetation nitrogen; N_{VS}: structural vegetation nitrogen; L_C: litterfall carbon; L_N: litterfall nitrogen; $C_{S,i}$: soil carbon of layer i; N_S: soil organic nitrogen; N_{AV}: available soil inorganic nitrogen; WD: woody debris; AG: aboveground; BG: belowground; D: dead; $NUPTAKE_L$: N uptake into the labile N pool of the vegetation; $NUPTAKE_S$: N uptake into the structural N pool of the vegetation; NETNMIN: net N mineralization of soil organic N; NINPUT: N inputs from outside the ecosystem; and NLOST: N losses from the ecosystem

roots with depth. The dynamics of coarse woody debris, an important C pool associated with fire disturbance in the boreal forest (Manies et al. 2005), is also considered in DOS-TEM.

As the previous version of TEM, the EcoM operates at monthly time step driven by monthly atmospheric climate input data and simulated environmental soil conditions. Monthly leaf area index (LAI) is estimated in EcoM, and feedback to EnvM at end of each month for surface biophysical processes. The fibrous and amorphous organic horizon thicknesses are updated at the end of each year, based on the simulated soil C in each horizon, and re-structure columns in DOSM.

Freezing–thawing modulated Gross Primary Production (GPP)

GPP is calculated at a monthly timestep and is affected by several factors (Zhuang et al. 2003):

$$GPP = C_{\max} f(PAR) f(PHENOLOGY) f(FOLIAGE) f(T) f(C_a, G_v) f(NA) f(FT) \quad (29.7)$$

where $C_{\max}$ is the maximum rate of C assimilation; PAR is photosynthetically active radiation, $f(PHENOLOGY)$ is monthly leaf area relative to leaf area during the month of maximum leaf area; $f(FOLIAGE)$ represents the ratio of canopy leaf biomass relative to maximum leaf biomass; $f(T)$ represents the effect of air temperature;C_a and G_v are atmospheric CO_2 concentration and relative canopy conductance, respectively, $f(C_a, G_v)$ represents the effect of stomatal regulation on atmospheric CO_2 uptake; $f(NA)$ represents the limiting effect of available inorganic N on GPP; and $f(FT)$ represents the effect of freeze and thaw on photosynthetic activity. Except for $C_{\max}$, others range from 0 to 1.

The positions of the FTFs are used to calculate a daily $f(FT)$. It is assumed that if the thawing front penetrates 5 cm of the soil column (excluding living moss), then $f(FT)$ of that day is 1, otherwise it is 0. The monthly value $f(FT)$ is calculated as the mean of the daily values. For various plant function types, $f(FOLIAGE)$ is modified as a function of total vegetation C so that representing the plant life cycle (Yuan et al. 2012).

Litter input and soil carbon dynamics

As briefly discussed above C litter input is distinguished as aboveground and belowground root litterfall. We assume that the ratio of aboveground to total litter input is similar to the ratio of root NPP to total NPP. Studies estimate that root NPP contributes approximately 40–60% of total NPP for black spruce in the boreal forest of North America (Steele et al. 1997; Ruess et al. 2003). We define those litters as coarse plant materials, which follow similar decomposition process as three soil organic matters (SOM), but with different respiration rates (Yuan et al. 2012). Namely, SOMs are distinguished as active, physically resistant, and chemically resistant SOM, similarly as those by Jenkinson and Rayner (1977).

When each of those four organic matters decomposed, fractioning occurs and, according to Jenkinson and Rayner (1977), approximately 0.0955, 0.1571, and 0.0044 gC g^{-1} CO_2 is transformed to active, physically and chemically resistant SOM, respectively. To mimic various forms of SOM vertical mixing and transport, e.g., cryoturbation in permafrost active layers, it's assumed that (1) all decomposition products in top fibrous horizon deposit into the underlying amorphous horizon; and (2) a portion (currently 7.5%) of those in the amorphous horizon are transferred and mixed into the top 25 cm mineral horizon. In this way stratification of naturally observed SOM profile may be simulated reasonably.

Woody debris

Woody debris C and N dynamics were included in DOS-TEM. Woody debris originates from aboveground dead vegetation. After fire disturbance, dead aboveground vegetation is completely converted to wood debris in about nine years based

on Manies et al. (2005). The rate-limiting parameter for decomposition K_d of wood debris is assumed to be the same as that for the amorphous organic horizon. The soil temperature and moisture of the first organic layer are used to drive decomposition of wood debris.

29.2.1.3 The Fire Effects Module (FEM)

The FEM simulates how fire affects C and N pools of vegetation and soil, including combustion emissions to the atmosphere, the fate of uncombusted C and N, and the flux of N from the atmosphere to soil via deposition in the years following a fire (Fig. 29.3).

Combustion of Vegetation biomass and surface soil organic layers

The FEM calculates an index of burn severity that ranges from 0 to 1, based on the fire season, area burned in a fire year (termed as fire size), and soil drainage (Table 29.1). Fire season is broadly classified into two categories: early season (July and months before July), and late season (August and months after August).

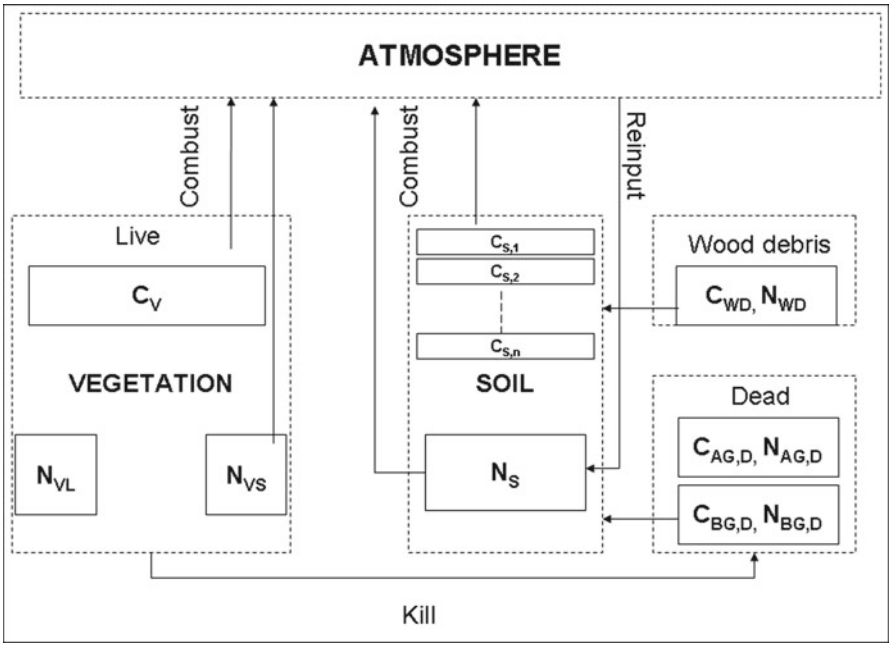

Fig. 29.3 The fate of carbon and nitrogen at the time of fire as defined by the fire effects module of the dynamic organic soil version of Terrestrial Ecosystem Model (DOS-TEM). C_V: vegetation carbon; N_{VL}: labile vegetation nitrogen; N_{VS}: structural vegetation nitrogen; $C_{S,i}$: soil carbon of layer i; N_S: soil organic nitrogen; WD: woody debris; AG: aboveground; BG: belowground; D: dead

Table 29.1 The fire severity category, fraction of aboveground vegetation biomass and soil organic horizons (moss, fibrous, and amorphous) combusted during a fire based on and the type of soil drainage, the season of burning, and the relative area burned in a particular year

Soil drainage	Fire season	Relative area burned (size)	Fire severity category	Combusted vegetation fraction	Burned fraction of organic soil
Dry	Early	Small to Intermediate	Low	0.16	0.54
		Large to Ultra-Large	Moderate	0.24	0.69
	Late	All sizes	High	0.32	0.80
Wet	All seasons	All sizes	N.A.	0.16	0.48

The area burned in Alaska is broadly classified into four categories: small fire years (less than 1% of interior Alaska), large fire years (1–2% of interior Alaska burned), very large fire years (2–3% of interior Alaska burned), and ultra-large fire years (>3% of interior Alaska burned). The relative amount of area burned is determined through analysis of records for area burned in Alaska between 1950 and 2006 (Kasischke et al. 2010). For application of the model to years before 1950, the influence of area burned on burn severity is generated randomly.

At a fire event, aboveground and root vegetation C and N is divided into three components: combusted, aboveground dead (slashed), and aboveground live. Based on field investigations, the percentage of pre-fire aboveground biomass combusted, fire severity, depends upon drainage conditions and fire season and size, e.g., about 16% in dry upland black spruce ecosystems in small fire size years (Table 29.1). Assuming $\sim$1% live, the rest is dead, leaving a large portion as woody debris.

The depth of burn of the surface organic soil is calculated by multiplying burn severity from Table 29.1 by the total thickness of the moss, fibrous, and amorphous horizons in the soil column. Based on the calculated depth of burn, all soil C in combusted layers is emitted to the atmosphere. The dead belowground root C is assigned, as amorphous SOM, to each of the remaining soil layers based on the distribution of fine root fraction.

Retention and Reinput of Burned Nitrogen

Due to fire it's reasonable to assume dead vegetation N as with amorphous SOM. The combusted N from both vegetation and organic soil are either volatized into atmosphere or retained in ecosystem. It is assumed that 85% of combusted N is retained based on Harden et al. (2004). For mass conservation, the volatized N is then reinput into the ecosystem, as a form of deposition, in equal annual amendments in subsequent years within a fire return interval (FRI, years).

29.2.1.4 The Dynamic Organic Soil Module (DOSM)

DOSM updates organic soil structure at the time of fire and at the end of each year, based soil C content of the fibrous and amorphous horizons. The thicknesses of fibrous and amorphous layers are calculated using the simulated soil C content of each horizon and the equation:

$$C = ad^b \tag{29.8}$$

where C is C content (gC/cm^2) of an organic horizon, d is organic horizon thickness (cm), and a and b are fitted coefficients for the fibrous or amorphous horizons.

As the fibrous organic horizon grows thicker, the bottom layer of the fibrous organic horizon is transferred to the amorphous organic horizon. In this study, a threshold method is used to mimic this process of humification. For example, the threshold is 16 and 33 cm for dry and wet black spruce stands, respectively, which approximately mean value plus one standard deviation of fibrous organic horizons based on a soil horizon data set from numerous Canadian black spruce stands (Yi et al. 2009b).

In DOSM it is important to define or re-define structure of soil organic horizons for the purpose of maintaining stability and efficiency of soil temperature and moisture calculations when the thickness of organic soil C is altered by either wildfire disturbance or ecological processes. The soil column consists of a maximum of one moss layer, three fibrous organic layers, and three amorphous organic layers.

It is assumed that the minimum soil layer thickness for each horizon is 2 cm. If the thickness of a layer is less than 2 cm, a layer will be combined with other layers of the same horizon. The rationale is that upper layers in the soil column should be thinner than deeper layers, following the common practice of land surface models and ecosystem models in simulation soil thermal and moisture dynamics. But the upper layer may not so thin that it leads to instability and inefficiency of soil thermal-hydrological algorithm. For fibrous horizon, therefore, layer numbers and thickness are determined in a look-up table (Table 29.2).

Table 29.2 The configuration of soil layers within the fibrous organic horizon, based on total organic thicknesses (cm)

Total thickness (DZ, cm)	Layer 1 (top)	Layer 2	Layer 3
0–4	DZ (>=2)		
4–6	2	DZ-2	
6–10	3	DZ-3	
10–15	2	4	DZ-6
15–20	3	6	DZ-9
20–28	4	8	DZ-12
28–33	5	10	DZ-15

And for amorphous organic horizon, number of layers in the (n_{amp}) are based the thickness of the deepest fibrous horizon layer ($d_{fib,bot}$) and the total thickness of amorphous organic horizon (d_{amp}), as following

$$n_{amp} = \begin{cases} 1 & d_{amp} < 3d_{fib,bot} \\ 2 & 3d_{fib,bot} \le d_{amp} < 6d_{fib,bot} \\ 3 & d_{amp} \ge 6d_{fib,bot} \end{cases} \tag{29.9}$$

Then, for the 2-layer amorphous horizon, layer thicknesses are 1/3 and 2/3 of total horizon thickness, respectively; while for 3-layer horizon, thicknesses are 1/6, 2/6, and 3/6 of the total downwardly, respectively.

When fire occurs the unburned fibrous organic layer is converted to the amorphous organic layer, following Harden et al. (2000). A 2 cm fibrous organic layer is immediately added on top of the amorphous organic layer. In this way, the fibrous organic layer can start accumulating litterfall and grow.

When the thickness of live moss increases to 2 cm, a new moss layer is added on top of the first fibrous organic layer. The growth of moss is determined by a number of factors, including moss type, radiation, wind speed, and precipitation (Bisbee et al. 2001). In DOS-TEM, the biomass and NPP of moss are not simulated explicitly, as they are considered as part of overall vegetation biomass and NPP. However, the thickness of moss is explicitly considered for the purposes of soil temperature and moisture calculations. Moss thickness is simulated as an empirical function of years since last fire based on Yi et al. (2009b):

$$d_{moss} = d_{moss,max} \frac{y_{sf}}{y_{sf} + y_{half}} \tag{29.10}$$

where d_{moss} is the thickness of moss (cm), $d_{moss,max}$ is the maximum thickness of moss (m), y_{sf} is the number of years since last fire (year), and y_{half} is the number of years which was the need for moss to reach half of $d_{moss,max}$. In this study, we assigned 3.5 cm to $d_{moss,max}$ and 5.0 cm to Y_{half} according to Yi et al. (2009b).

Each time the soil column structure created or redefined, the temperature of each new layer is determined by linear interpolation of the nearest soil temperatures in an old organic soil column. Soil FTFs positions are reassigned with the relative distance to the top of a type of horizon (moss, fibrous, amorphous) unchanged. Soil total water content of each new organic soil layer is first retrieved from its previous, and then summed or divided, upon how the new layer formed either by merge or division. Then soil liquid and ice contents are recalculated according to FTFs position in a layer.

29.2.2 Model Validation and Numerical Verification

It is critical to perform model verification or validation before its application. DOS-TEM simulated soil temperature, moistures, active layer depths, and ecosystem carbon and nitrogen pools have been validated using field measured datasets over boreal forests, the tundra of Alaska, the tundra of Siberia, and alpine grassland of the Qinghai–Tibetan Plateau (Yi et al. 2009b, 2013, 2014a, b).

Soil freezing and thawing processes simulated by DOS-TEM were also verified against numerical solutions under idealized conditions, which were seldom done by other modeling studies (Yi et al. 2014b). In the following part, we only present the verifications against an analytical solution.

Three different materials were tested in this study, i.e., water, minerals (sand), and organic soil. The properties of these materials are listed in Table 29.3. The initial temperature of each material at different depths (up to 5000 m in the DOS-TEM) was set to −10 °C, and the temperature at the upper boundary of each material was set to 5 °C over the whole simulation period (100 yrs). We assumed zero heat flux conditions at the lower boundary, i.e., at 5000 m depth. The temperatures and the depth of the thawing front obtained from the DOS-TEM were compared with those from analytical solutions and those obtained using the one-directional Stefan's equation. For the DOS-TEM, the temperature at a specific depth was calculated by linear interpolation between the temperatures of overlying and underlying layers. To test the sensitivity of the model to the depth used for the bottom-up forcing, we tried bottom-up forcing at different depths below the thawing front (i.e., at 50 cm, 1 m, 2 m, 5 m, and 20 m). In order to test the effects of total soil/water thickness, we also evaluated the DOS-TEM using different depths for the lower boundary (50, 500, and 5000 m). The maximal thickness of the soil/water layer was set to 1, 10, and 100 m for runs with the lower boundary at 50 m, 500 m, and 5000 m depth, so that the total number of layers was constant for each run.

Results showed that the bottom-up forcing in the DOS-TEM is very important for accurate simulation of the position of the thawing front using Stefan's algorithm (Fig. 29.5). For all cases of water, mineral soil, and organic soil, the thawing fronts simulated without bottom-up forcing were very close to those calculated using Stefan's equation. The root mean squared errors (RMSEs, n = 36,500) between

Table 29.3 The thermal conductivity, volumetric heat capacity, volumetric water content, and porosity used in idealized runs for water, mineral soils, and organic soils

	Thermal conductivity (J/mKs)		Volumetric Heat capacity (10^6 J/m^3)		Volumetric water content (%)	Porosity (%)
	Frozen	Unfrozen	Frozen	Unfrozen		
Water	2.29	0.6	2.12	4.19	100	100
Mineral	2.69	1.71	2.06	2.79	33.28	39
Organic	0.37	0.21	0.99	1.84	36.25	90

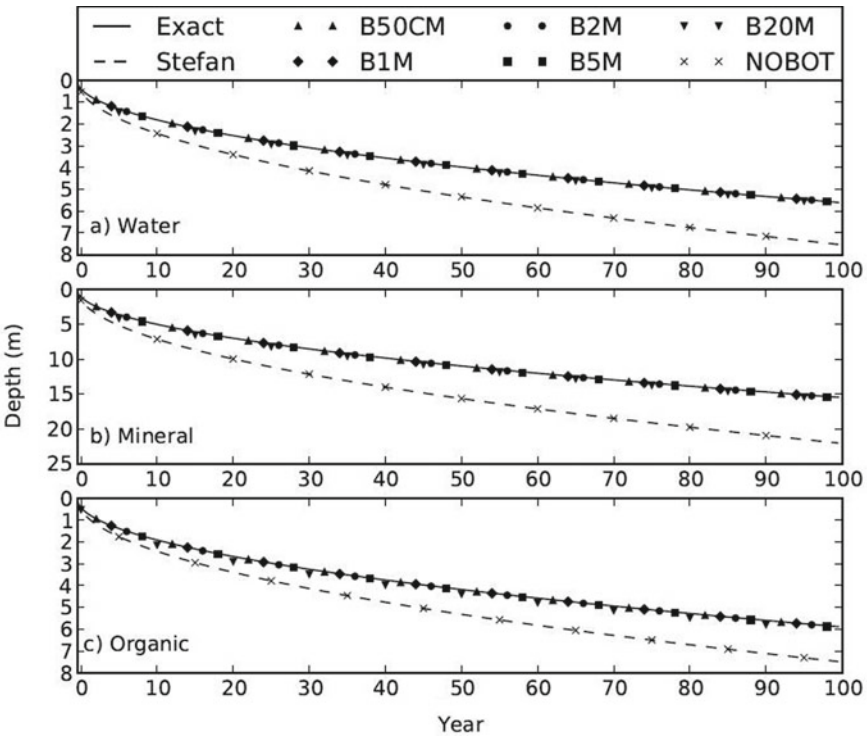

Fig. 29.5 Comparisons of outputs from DOS-TEM simulations, exact Neumann solutions (Exact), and Stefan's equation (Stefan) for **a** water, **b** mineral soil, and **c** organic soil over a one hundred year period. The term B50CM means simulations from the DOS-TEM with bottom-up forcing at 50 cm beneath the lowest freezing or thawing front, and likewise for other similar terms. NOBOT means no bottom-up forcing. The outputs from the DOS-TEM have been plotted for the middle of every tenth year and different cases have been started from different years in order to make the figures more readable

thawing fronts simulated without bottom-up forcing and those from exact Neumann solutions for three different idealized cases were greater than 1.128 m. In contrast, the RMSEs between the thawing fronts simulated with bottom-up forcing and those from exact Neumann solutions were less than 0.047 m (Table 29.4).

The simulated water or soil temperatures and thawing fronts were not sensitive to the depth of bottom-up forcing (Fig. 29.5). For example, there was almost no difference between the thawing fronts simulated for bottom-up forcing at depths of between 0.5 m and 20 m, in all three cases (water, mineral soil, and organic soil). The differences between thawing front simulations using bottom-up forcing and those from Neumann solutions were also very small (Fig. 29.5). Taking bottom-up forcing at a depth of 1 m beneath the thawing front as an example, most of the

Table 29.4 The root mean squared error (n = 36,500) between the thawing fronts (m) from exact Neumann solutions and simulated thawing fronts from the DOS-TEM, with different combinations of the total thickness (50, 500, and 5000 m) and bottom-up forcing (b1m: bottom-up forcing at 1 m below front; nobot: no bottom-up forcing) for different materials

	5000 m, b1m	5000 m, nobot	500 m, b1m	50 m, b1m
Water	0.004	1.253	0.032	0.274
Mineral	0.062	4.645	0.177	1.899
Organic	0.012	1.128	0.047	0.065

RMSEs for temperatures at depths shallower than 1 m were less than 0.01 °C, and approximately 0.1 °C for depths greater than 1 m (Fig. 29.6 and Table 29.5).

The simulated temperatures were sensitive to the total thicknesses of the various materials, especially that of mineral soil which has the highest thermal conductivity and the lowest water content (Table 29.5).

In conclusion, the DOS-TEM performed very well in both simulated freezing/thawing fronts and temperatures under idealized conditions.

29.3 Dynamics of a Typical Black Spruce and Permafrost and Fires

Black spruce forest is one of the typical ecosystems in boreal, usually associated with peats which under ongoing warming conditions and subsequent changes like fires. There are two types of black spruce: (1) the "dry" black spruce, which represents a gradient of black spruce forest stands between well-drained and intermediately drained landscape positions in interior Alaska; (2) the "wet" black spruce, which represents stands with somewhat poorly and very poorly drained landscape (i.e., with a high water table) (Harden et al. 2003).

To assess the ability of DOS-TEM to simulate organic soils in high latitude, we evaluated it in a dry black spruce forest at two sites with well-drained soils without underlying permafrost, and another two sites with intermediately drained soils with permafrost, near the Delta Junction, Alaska (65°53′N, 145°44′W). The well-drained sites are the Donnelly Flats tower control site (DFTC) last burned around 1921, and the Donnelly Flats tower burn site (DFTB) recently burned in 1999 (Liu and Randerson 2008). The intermediately drained sites are the Donnelly Flats Creek Control site (DFCC), which last burned around 1886, and the Donnelly Flats Creek burn site (DFCB), which burned in 1999. We did not evaluate it in wet black spruce because there have not been any studies conducted in interior Alaska that would allow to evaluate the effects of fire on the re-accumulation of organic matter.

In this study DOS-TEM was driven by monthly climate data, including air temperature, precipitation, vapor pressure, and surface solar radiation, retrieved from the Climate Research Unit (CRU) datasets (Mitchell and Jones 2005) for the period 1901–2002. The CRU datasets do not include the period 2003–2006, so the

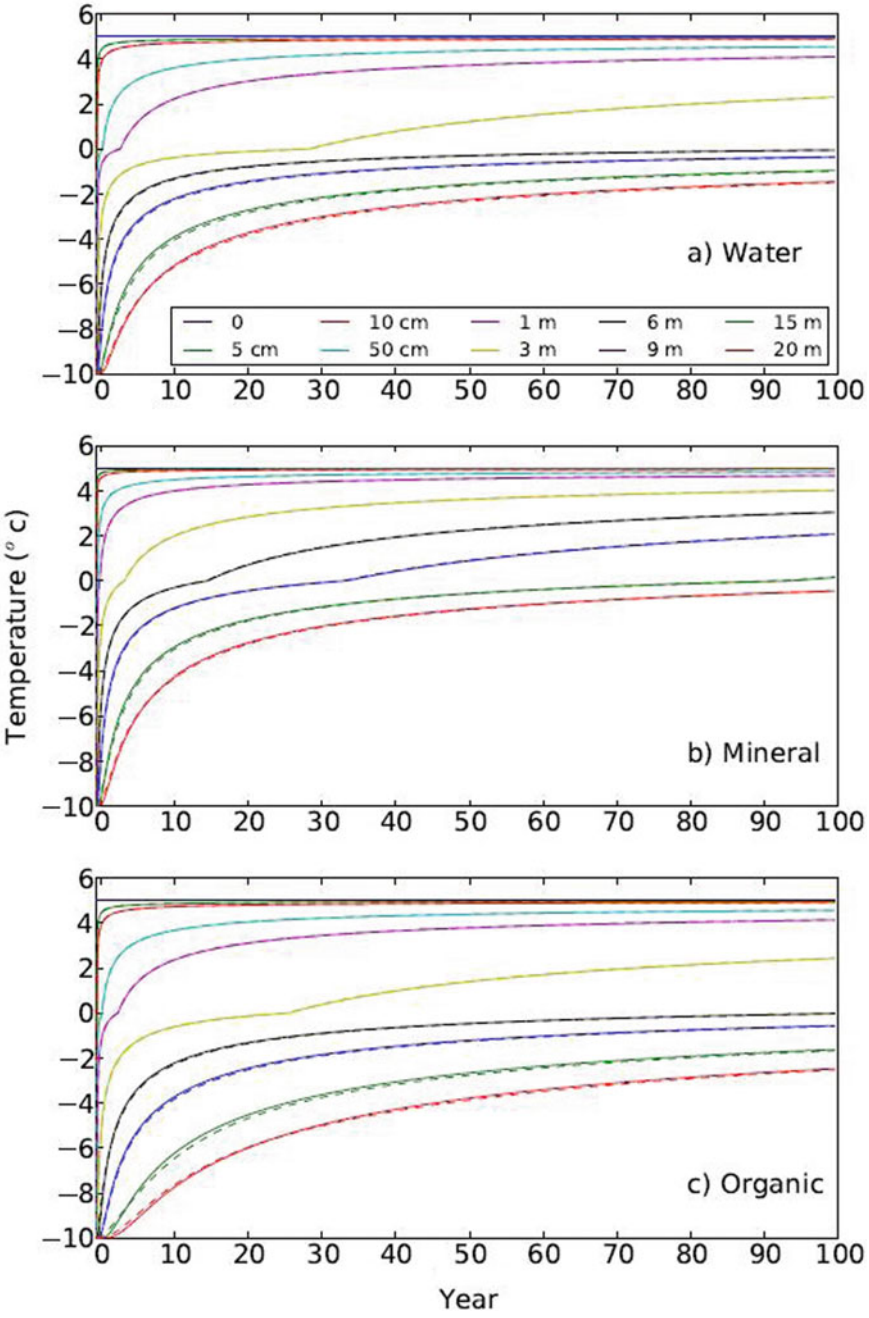

Fig. 29.6 Comparisons of outputs from DOS-TEM simulations (dashed lines) and exact Neumann solutions (solid lines) for **a** water, **b** mineral soil, and **c** organic soil over a period of one hundred years, at depths from 0 cm to 20 m

Table 29.5 The root mean squared error (n = 36,500) between the temperatures (°C) from exact Neumann solutions and simulated temperatures from the DOS-TEM for different materials, with 5000 m total thickness and bottom-up forcing at 1 m below the thawing front, at depths of between 0.05 and 20 m

	0.05	0.1	0.5	1	3	6	9	15	20
Water	0.018	0.017	0.044	0.054	0.039	0.039	0.041	0.087	0.071
Mineral	0.011	0.018	0.014	0.010	0.016	0.027	0.030	0.057	0.062
Organic	0.019	0.016	0.009	0.009	0.024	0.042	0.047	0.111	0.110

anomalies of the National Center for Environmental Prediction (NCEP) reanalysis datasets (Kanamitsu et al. 2002) were used to extend CRU data sets through 2006 (Hayes et al. 2009). We modified this CRU/reanalysis data set by replacing the temperature and precipitation data with data from meteorological stations of Delta Junction (from 1941 to 2006) and Fairbanks (from 1930 to 2006). The atmospheric CO_2 data used to drive the simulations were obtained from the Mauna Loa station (Keeling and Whorf 2005).

29.3.1 Model Calibration for a Specific Ecosystem

With DOS-TEM model, a Java interface (https://github.com/fmyuan/dostem2.0-runner) was developed via JNI can be used to calibrate or parameterize it for a specific ecosystem. Later this interface was rewritten in python and tools (https://github.com/ua-snap/dvm-dos-tem/blob/master/calibration/CalibratorREADME.md).

As previous TEM, we calibrated the rate-limiting parameters (maximum rate of C assimilation, respiration of vegetation per unit carbon at 0 °C, C and N litterfall rate, maximum rate of N uptake by vegetation, the ratio between N immobilized and C respired by heterotrophs, heterotrophic respiration) for "target" values of pools and fluxes of a mature "generalized" ecosystem. In this study, those target states or fluxes, i.e., for black spruce stands based on estimates derived from studies conducted in Alaska, USA, and Manitoba, Canada, available in the literature. The calibration process is similar as before (Clein et al. 2002), but for DOS-TEM, the rate-limiting decomposition constants for each of two organic (fibrous, amorphous) and mineral horizons have to be calibrated. For detrending warming and other climate forcing, mean monthly climate data from Fairbanks only from 1901–1930 were used in calibration, assuming that soil organic matter mainly accumulated prior modern era.

29.3.2 Model Configuration

Initially DOS-TEM runs to equilibrium at around year 1000 or more, a.k.a. model equilibrium stage, using mean monthly climate of 1901–1930 for Delta Junction. Then model spinup for as long as enough, with mean monthly climate of the 1901–1930 time period repeatedly. Fire disturbances were backcast prior to the earliest known fire event based on FRI, assumed 80 years at DFTC and DFTB, and 150 years at DFCC and DFCB, respectively, based on a fire dataset from Manitoba, Canada. Finally, we ran the model over the 1901–2006 time period for analysis, driven by monthly climate from the modified CRU/reanalysis data set. Since unknown vegetation type history, it's assumed that the sites are self-replacing black spruce stands all the time.

We performed two sets of simulations, one used the DOSM (i.e., with dynamic organic soil, DOS), versus that kept organic soil thickness static (SOS). For DOS simulations, organic soil thickness is changed at the time of fire disturbance and during post-fire succession. In the SOS simulations, C pools are reduced at the time of fire disturbance, but the thickness of organic soil is not changed.

29.3.3 Organic Soil Dynamics During Fires and Post-fire Transition

We compared the simulated (with DOS and with SOS) thickness of organic soil, and C of organic soil and mineral soil with measurements at the four sites in the year 2001 (Harden et al. 2006). The deepest measurement of C in mineral soil at DFTC was 82 cm, at DFTB was 67 cm, at DFCC was 22 cm, and at DFCB was 35 cm. The organic layer thicknesses of DOS simulations were all within one standard deviation of the mean of the measurements at all four sites, while those of SOS simulations were at 22.8 cm. The estimated C of organic soils in both the DOS and SOS simulations were within one standard deviation of the mean of the measurements at all four sites. However, mineral soil C by SOS simulations were approximately 70% larger than those in the DOS simulations (Fig. 29.7).

DOS-TEM simulations (Fig. 29.7) demonstrate that fire causes organic soil C reduced abruptly at least half of pre-fire stocks, and recovered during succession at speed apparently upon fire return interval (FRI) and black spruce growth. By dynamically associating these C stocks, organic soil thickness changes correspondingly. Due to unique organic soil thermal-hydrological properties, post-fire active layer depth initially increases sharply as well, as seen in Fig. 29.7, compared to slight variation in the SOS simulations. It's also simulated for water table depth to rise remarkably after fire and drop when organic soil horizons recovering to some thickness, but never down to water table assuming constant in the SOS simulations.

In both DOS and SOS simulations, fire decreased vegetation C, and net primary production (NPP) immediately, and recovered more quickly than soil C. The heterotrophic respiration (RH) recovery after fire appeared quicker than both organic and mineral soil C, likely due to warmer soil conditions after fires. Otherwise RH in

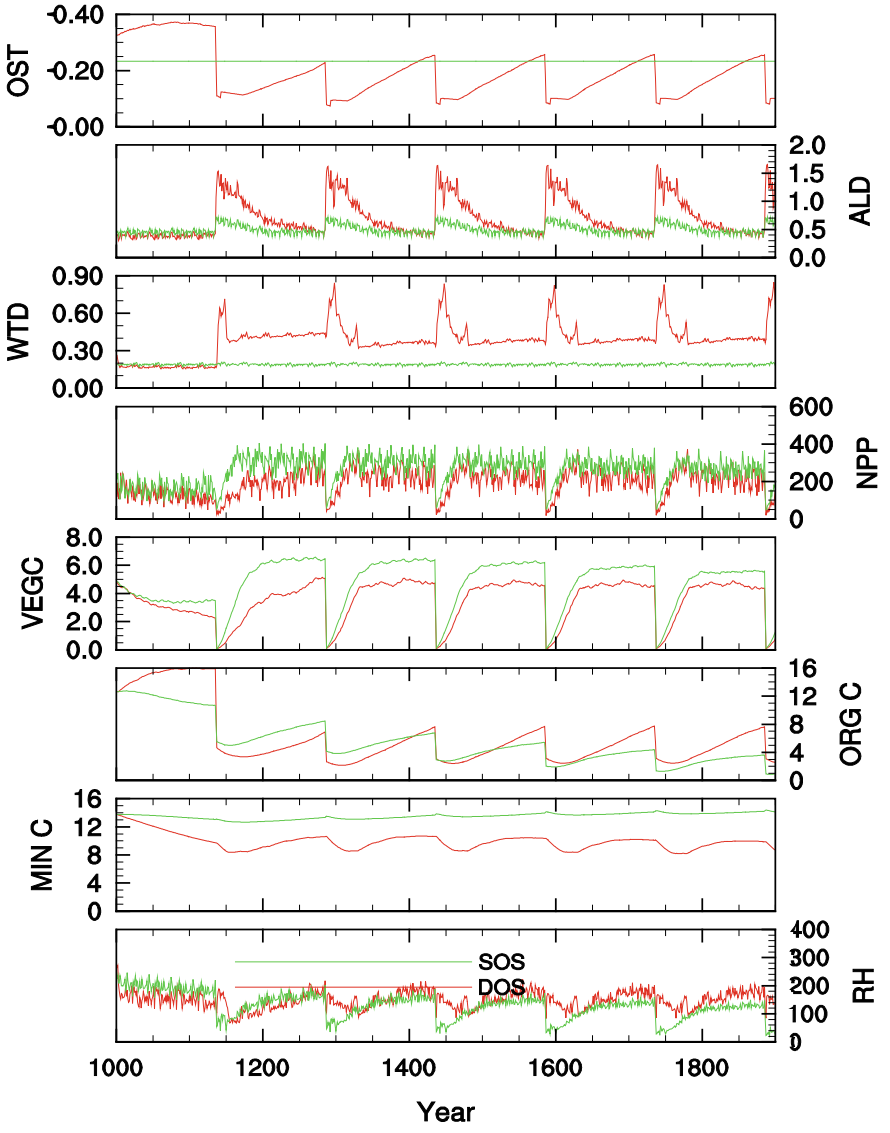

Fig. 29.7 Comparisons of various aspects of ecosystem dynamics between the application of DOS-TEM with a dynamic organic soil (DOS) and a static organic soil (SOS) for a site typical of the intermediately drained sites near Delta Junction (Donnelly Flats Creek Control and Burn sites) with a 150-year fire return interval. Variables compared include organic soil thickness (OST; m), active layer depth (ALD; m), water table depth (WTD; m), net primary production (NPP; gC/m^2yr), vegetation carbon (VEGC), organic soil carbon (ORG C; kgC/m^2), mineral soil carbon (MIN C; kgC/m^2) and heterotrophic respiration (RH; gC/m^2yr)

the SOS simulation remained low because of the cold wet soil conditions, nearly following all respirable SOM C dynamics. For similar causes, the C in mineral soil of SOS simulation was approximately 5 kgC m^{-2} greater than that of DOS, due to colder soil temperature.

As mentioned above, post-fire organic soil recovery in the DOS to pre-burn levels takes approximately 80 years after the fire, but apparently both thickness and C stocks not yet reaches equilibrium when the fire returns (80–150 years in this dry to intermediate-drain black spruce stands). Water table depth may be stabilized after about 40 years. And vegetation NPP and C in both DOS and SOS simulations can reach maximum approximately 30 and 70 years after the fire, respectively.

29.3.4 Model Sensitivity to Soil Drainage Conditions and Fire Return Interval

Our goal in developing DOS-TEM is to better represent and understand the effects of fire and other disturbances on soil C dynamics of forests in boreal regions. There are two important factors that control spatial heterogeneity of soil C responses to fire in boreal forests, soil drainage, and fire frequency. So here we conducted simulations with DOS-TEM to understand the sensitivity of ecosystem C dynamics to them. The model in these sensitivity analyzes was generally configured as above.

To evaluate the sensitivity of C dynamics to soil moisture as it is influenced by depth to permafrost and soil drainage class, we performed three sets of simulations: (1) a simulation for the dry black spruce parameterization with FRI of 100 years and moderate belowground burn severity (69% organic soil depth), (2) simulations of wet black spruce parameterization with FRI of 200, and (3) same configuration as (2) but with FRI of 100 years. As mentioned briefly above, FRIs of 100 and 200 years would be appropriate for dry and wet black spruces, respectively, in interior Alaska. An extra simulation of wet black spruces with FRI of 100 years was conducted to separate out the effects of drainage from FRI in these ecosystems.

To evaluate model sensitivity of C dynamics to fire frequency, we performed three simulations, with dry black spruces undergoing three FRIs of 150, 100, and 60 years, all with moderate belowground burn severity (69% of the organic soil depth was combusted).

Effects of drainage

For all simulations in the drainage sensitivity analysis, the thickness of organic soil, NPP, vegetation C, and organic soil C declined immediately at the time of fire disturbance, and the active layer depth, water table depth, and RH increased (Fig. 29.8). During succession, all these variables almost recovered to pre-fire states. As expected, in dry upland black spruce stands water table was deep (about 0.8 m after the fire, and 0.4 m before the fire), while in wet drainage conditions was shallow. It's surprising that active layer depth could be dropping to a similar level after long enough since fires.

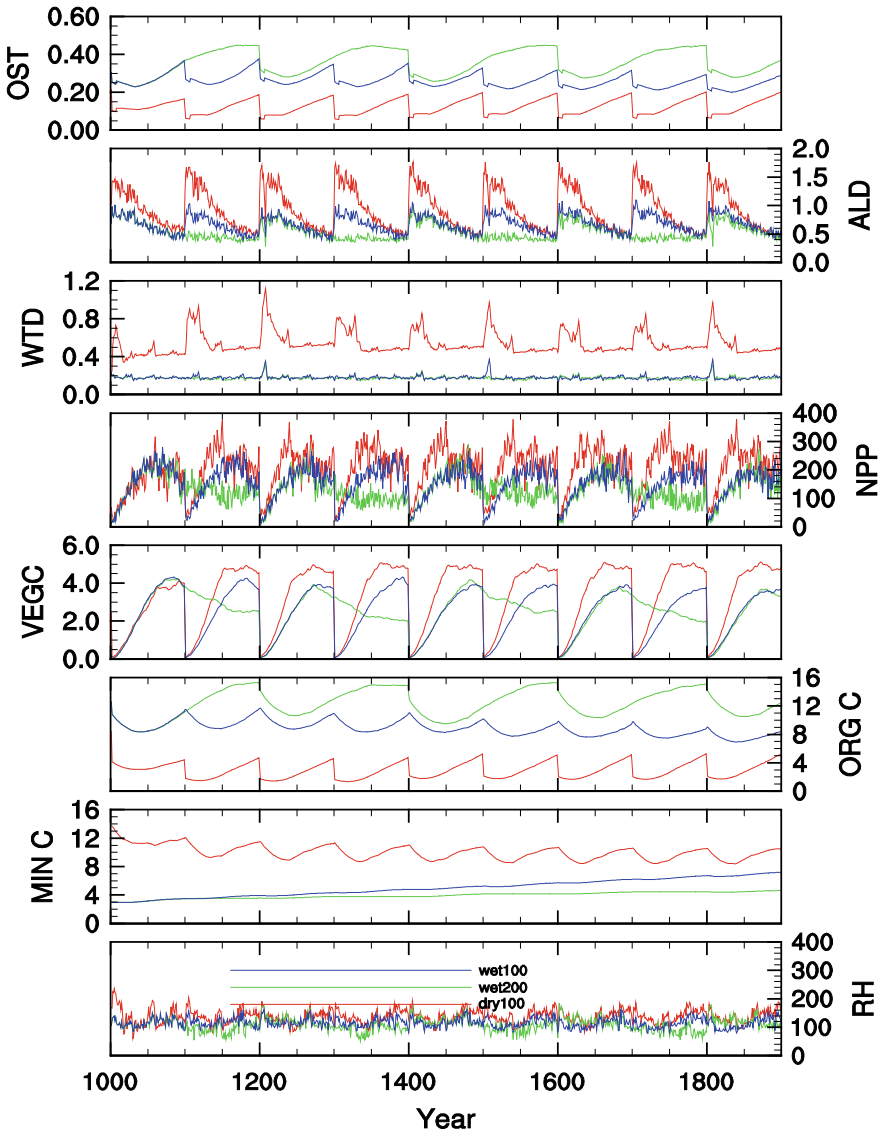

Fig. 29.8 Comparisons of various aspects of ecosystem dynamics between the application of DOS-TEM for wet (wet100: with 100-year fire return interval; wet200: with 200-year fire return interval) and dry (with 100-year fire return interval) black spruce parameterizations. Variables compared include organic soil thickness (OST; m), active layer depth (ALD; m), water table depth (WTD; m), net primary production (NPP; gC/m^2yr), vegetation carbon (VEGC), organic soil carbon (ORG C; kgC/m^2), mineral soil carbon (MIN C; kgC/m^2), and heterotrophic respiration (RH; gC/m^2yr)

The model showed that well-drained stands (dry condition) had higher maximum NPP than in wet conditions. Thus, vegetation C of dry drainage simulation reached a maximum ($\sim$5.0 kgC/m^2) after about 50 years, while for vegetation Cs of wet drainage simulations did not reach a maximum ($\sim$4 kgC/m^2) until after 70 years.

The organic soil C in dry black spruce stands was consistently lower than those of wet conditions, due to higher fire severity defined in dry drainage simulation and relatively higher decomposition (RH), although it's higher productivity. The mineral soil C in dry simulations was consistently greater than in wet conditions. This occurred because litter input of C into the soil is based on static fine root distribution, implying that thinner organic soil horizons of dry black spruce stands could have more root litter mortality into mineral horizons. This is also why mineral C in dry conditions more sensitive to fire cycles. However in our simulation the mineral C in wet conditions appeared not yet at equilibrium, by which mineral C stocks may be larger.

Effects of fire frequency

Under both wet (Fig. 29.8) and dry (Fig. 29.9) drainage conditions, simulations with longer fire return interval (FRI) had thicker organic soils and more organic soil C storage, as expected. In the wet drainage simulations, the longer FRI simulation had less mineral soil C. In contrast, the 150- and 100-year FRI simulations in the dry drainage conditions had more mineral soil C than the 60-year FRI simulation, while the difference between 150 and 100-year FRI simulations was small.

For both dry and wet condition simulations, the pre-fire NPP with the shorter FRI tended to be greater than those with longer FRI. The colder soil environment in the longer FRI simulations led to lower NPP just before the fire. For example, the active layer of the 150-year FRI simulation was about 40 cm shallower than that of 60-year FRI simulation. It implied that old-growth black spruce might show reduced productivity when soil getting colder and colder with thicker organic soils.

29.4 Landscape-Scale Interactions of Climate, Fires, and Vegetation on Terrestrial Ecosystem and Permafrost in Yukon River Basin (YRB)

As demonstrated in Sect. 29.3, site-specific modeling analyzes have indicated that the thickness and structure of soil organic horizons have important influences on soil thermal dynamics that affect biogeochemical responses to soil warming and wildfire (Yi et al. 2007, 2009a). Apparently they were mostly focused on the black spruce forest ecosystem, characterized by underlying peats with seasonal frozen-thawing cycle. For other major taiga forest types in interior Alaska, DOS-TEM was calibrated or parameterized as well (Yuan et al. 2012). Fortunately in those study cases fire history was either recorded or investigated well.

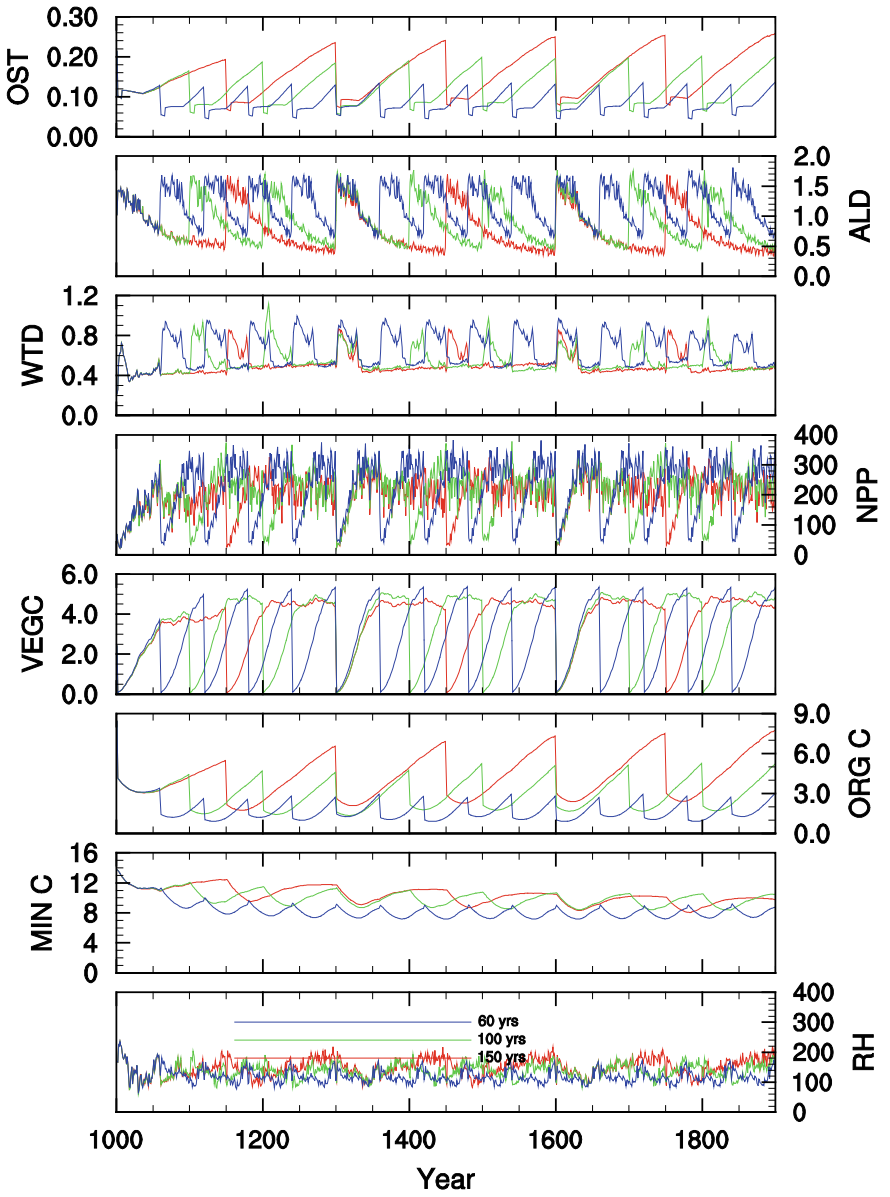

Fig. 29.9 Comparisons of various aspects of ecosystem dynamics among the application of DOS-TEM for fire return intervals of 60, 100, and 150 years. Variables compared include organic soil thickness (OST; m), active layer depth (ALD; m), water table depth (WTD; m), net primary production (NPP; gC/m^2yr), vegetation carbon (VEGC), organic soil carbon (ORG C; kgC/m^2), mineral soil carbon (MIN C; kgC/m^2), and heterotrophic respiration (RH; gC/m^2yr)

In contrast to broadleaf deciduous trees, coniferous species, especially black spruces, are more flammable due to its fluffy branches and foliage, understory materials including shrubs, mosses and litters, and peats. Thus, equally as important as organic dynamics to permafrost integrity (vulnerability) and/or whole ecological ecosystem responses and feedbacks is vegetation dynamics across regions and in long runs. Johnsone et al. (2011) found that generally more severe fires tend to increase the fraction of less flammable deciduous forest at the expense of more flammable coniferous forest. This type of shift in the composition of the boreal forest may already have been taking place (Barrett et al. 2011). Thus such a change in the long term across regions can be slowing increases in fire activity associated with climate warming. Those dependencies of wildfire regime in interior Alaska highly on the complexity of interactions among climate, fire ignitions, and fuel stocks and its flammability, indicates that effects on ecosystem and feedbacks may be in complexity way that DOS-TEM alone could be incomplete for regional applications especially for purpose of projection.

To evaluate this issue, regional or national fire databases could be hooked into DOS-TEM for past and current analysis (Yuan et al. 2012). Further in this study, outputs from a landscape-level ecosystem model, Alaska FRame-based EcoSystem Code (ALFRESCO), that represents interactions between fire regime and vegetation composition in addition to climate, topography and other critical factors (Rupp et al. 2016), were asynchronously incorporated into DOS-TEM. Then soil thermal-hydrology and biogeochemical cycles could be more realistically analyzed across the landscape and in future (Fig. 29.10).

In this section, thus, this model framework of ALFRESCO-DOSTEM was applied for the Alaska portion of Yukon River Basin (AKYRB) for the historic period of 1950–2007 and throughout the twenty-first century with forcing data from two of the most suitable GCMs for Alaska with A1B scenario. After a brief overview of climate and fire regimes in the region and results of a series of DOS-TEM studies on C storages, we are focusing on the complexity of interactions of warming, fires, vegetation dynamics and their effects on organic soil horizons and active layer depths, unique features in permafrost.

29.4.1 Historical and Projected Climate Warming and Fire Regime Changes in YRB

In the Yukon River Basin, climate warming like other high latitude regions has been remarkable, and appears continuing into future. CRU data showed that warming approximately started since the late 1960s or early 1970s at about 0.47 °C per decade, with a slight variation (0.44–0.56 °C per decade) across sub-basins of YRB (Yuan et al. 2012). Under IPCC A1B scenarios, MPI ECHAM5 models (referred to as “echam5” hereafter) projected this warming trends continuously in the region, while CCCMA-CGCM3.1 (referred to as “cccma” hereafter) projected similarly only until the late 2030s and then slightly declining warming trend

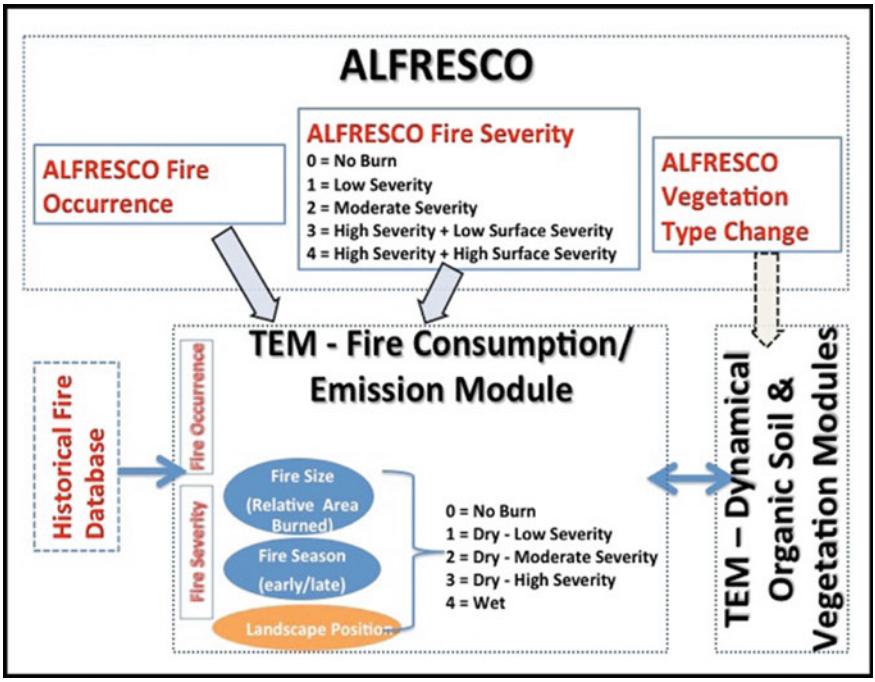

Fig. 29.10 A schematic of the coupling of ALFRESCO fire occurrence and severity outputs with the fire emissions module of DOS-TEM in this study. The DOS-TEM can also be driven by fire occurrence from the historical database of fire occurrence

(Fig. 29.11). In other words, "echam5" projection appears warmer than that by "cccma" for the region.

The YRB has also experienced substantial increases in wildfire extent and severity over the period of 1950–2006 (Kasischke et al. 2010; Barrett et al. 2011). Alaska historical fire database showed that both fire frequency and severity in YRB had remarkably increased in1990s and abnormally very active since the late 2000s (Fig. 29.12). It apparently had reduced thickness of insulating soil organic horizons to allow more efficient conduction of heat into underlying permafrost during the summer, which in a warming climate can make permafrost more vulnerable to degradation.

In Fig. 29.12 we summarize and compare historical fire occurrences (1950–2006) and future fire regimes (2007–2099) simulated by the ALFRESCO model driven by downscaled GCM climate outputs from "cccma" and "echam5" under the A1B scenario at 1 km × 1 km resolution for the region. ALFRESCO predicts that fire activity, which has already increased since the 1990s in the region and abnormally active in the last decade, would continue through the middle of the twenty-first Century. Then fire activity will revert to pre-1990 levels (Fig. 29.12 upper panel). As briefly stated above, this is because the increased fire activity has

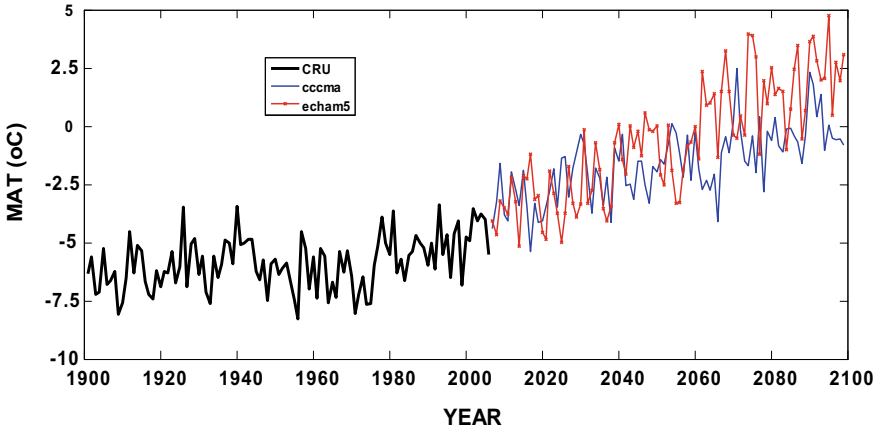

Fig. 29.11 Mean annual temperature (MAT, °C) over the Yukon River Basin (YRB) region during 1900–2006 historical period and 2007–2099 projected period. Historical temperature is based on downscaled data from the Climate Research Unit (CRU), and the projections are based on the downscaled GCM data, for Alaska and a small portion of Canada, from simulations by the CCCMA-CGCM3.1 ("cccma") and MPI ECHAM5 ("echam5") models for the A1B emissions scenario *Data Source* SNAP, Scenarios Network for Alaska and Arctic Planning, http://ckan.snap.uaf.edu/dataset?tags=IEM

caused the proportion of the landscape occupied by less flammable deciduous forest compared to conifers, which then tends to slow down fire activity. The distribution of annual burned area for 2007–2099 (Fig. 29.12 bottom panel) indicates that there will be fewer small fire years (<0.5% area burned) and more intermediate fire years (0.5–1.0% area burned), compared to the historical wildfires (1950–2006). For large fire years (i.e., greater than 1% area burned), under warmer "echam5" ALFRESCO predicted remarkably more years of 1.0–1.5% area burned than the historical record, while under "cccma" projection it simulated just slightly more years of 1.5–2.0% area burned. Under both warming climates, fire years of greater than 2% area burned were less than historical record. Because of the complexity and dynamics of feedbacks between fire regime and vegetation composition, it is not clear the degree to which soil organic horizons and permafrost integrity in this region are vulnerable to climate warming in future. Modeling analysis likely provides perspectives on it as below.

29.4.2 Relative Roles of Warming and Fire Regime Changes on YRB Boreal Forest C Stocks

Among the most warming regions in high latitude, YRB boreal forest experienced large and observable biomass productions, while meantime enhanced soil C losses at a delayed but accelerated speed. However it's difficult for data collections and

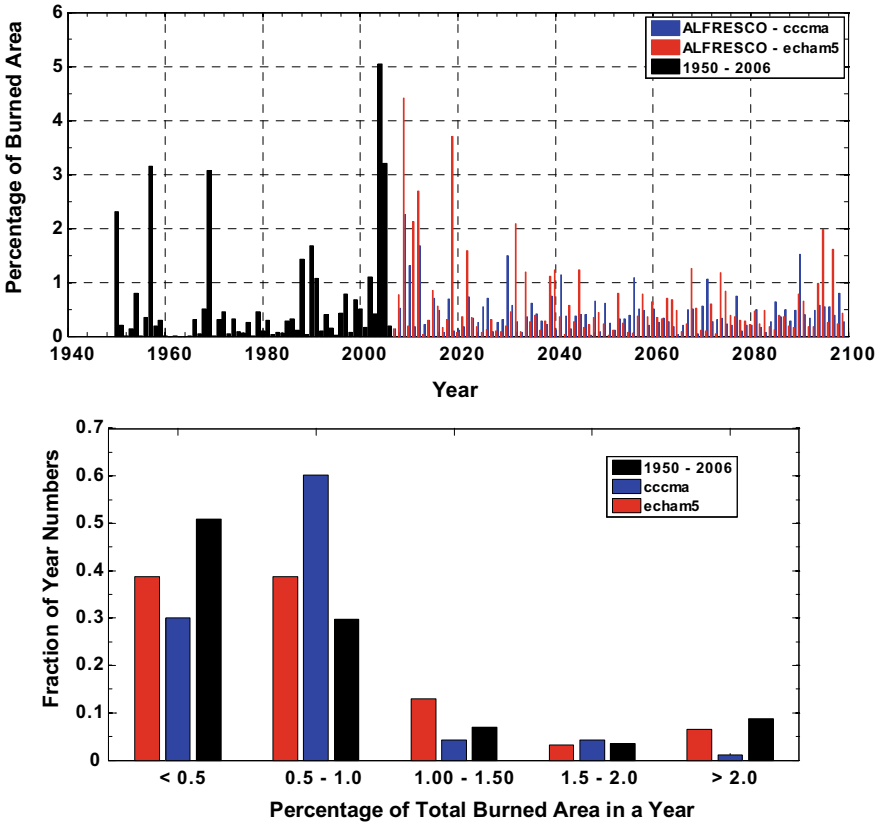

Fig. 29.12 Comparison of fire burned areas and its distribution of the relative frequency of annually burned percentage in bins of <0.5%, 0.5–1.0%, 1.0–1.5%, 1.5–2.0%, and >2.0%, over AKYRB region from the historical database (1950–2006) and ALFRESCO simulations for the projected period (2007–2099). Note that there are two ALFRESCO fire projections driven by GCM outputs of CCCMA-CGCM3.1 ("cccma") and MPI ECHAM5 models ("echam5") for the A1B emissions scenario *Data Source* SNAP, Scenarios Network for Alaska & Arctic Planning, http://ckan.snap.uaf.edu/dataset?tags=IEM

analysis alone to distinguish or weight controlling driving forces of boreal forest C dynamics under ongoing environmental changes without model tools, and vice versa.

For regional application, as mentioned above the DOS-TEM model is parameterized and calibrated for black spruce, white spruce and deciduous forest types based on soil C pools from a soil C database for interior Alaska and based on estimates of vegetation biomass C and N pools and fluxes from studies conducted by the Bonanza Creek Long-Term Ecological Research (LTER) forest sites located near Fairbanks, Alaska (Yuan et al. 2012). The model was validated by comparing simulated estimates of forest aboveground biomass and soil organic horizon

thickness to those of a forest inventory database in Alaska. Such a series of calibration, validation, and applications have been progressively extended into the rest of Alaska including tundra (Euskirch et al. 2016).

We applied the model to analyze changes in forest vegetation and soil C stocks of the YRB from 1960 to 2006, driven by historical climate (monthly from 1900–2006) and a historical fire database (from 1960–2006) ("historical simulation") (Yuan et al. 2012). DOS-TEM analysis showed that response of changes in estimated C stocks of 13 sub-basins of the YRB to warming and fire regimes appeared spatially varied very much (Fig. 29.13), even though that sub-basin warming ranged from about 0.4–0.6 °C per decade, and annual burn area varied from essentially no fire to 1.1% only. Generally warming increased vegetation biomass in majority of sub-basins, but may or not benefited soil organic C stocks implying more complexity response to warming, compared to vegetation (Fig. 29.13a). It's because of the immediate and sensitive response of plants to warming and rising atmospheric CO_2. But in more fire active areas both vegetation biomass and soil C changes could be greatly decreased (with statistically high regression coefficients), and actually if a sub-basin forest was burned over about 0.7% annually, the ecosystems turned from C sink to source (Fig. 29.13b).

Baselined with pre-1990s fire regimes and detrended climate in the past century, DOS-TEM analysis indicated that warming and more active fires in the past two decades played approximately equivalent roles in their effects on soil C storage (Yuan et al. 2012). This conclusion was apparently upon how model set up or forced by fire regimes. In a more recent study using DOS-TEM, driven by a paleorecord of reconstructed fire frequency in Yukon Flats and paleoclimate from the MPI-ESM model, Kelly et al. (2015) argued that fire variability during the past few decades could dominate over climate warming and CO_2 rising in regarding

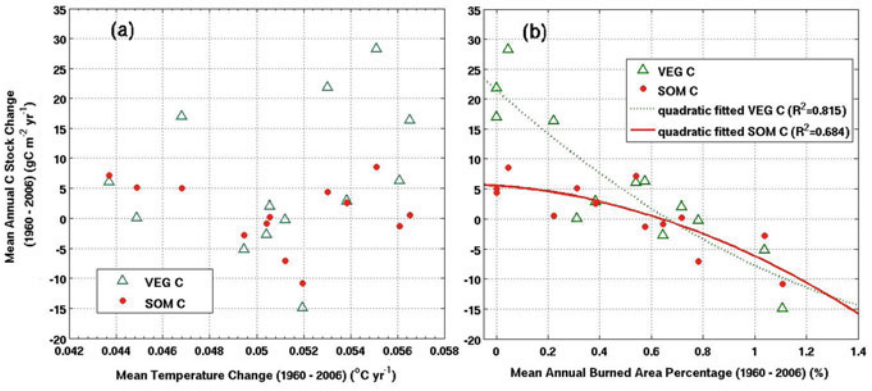

Fig. 29.13 Relationships of spatially averaged annual forest vegetation and soil C stock changes in 13 sub-basins simulated by DOS-TEM from 1960–2006 with **a** mean annual air temperature change and **b** percentage of mean annual burned forested areas in the Yukon River Basin (YRB)

Alaska boreal forest (mostly in YRB) C stock variability (about 84%). It implied that fire regime over much large spatial content and extremely long temporal scale, compared to the other relative gradual environmental changes, appears playing a role beyond most current model concepts of equilibrium.

29.4.3 Complexity of Warming, Fires and Vegetation Dynamics Interaction on Permafrost

According to Rupp et al. (2016), ALFRESCO wildfire model for forests generally trajectories burned (black or white) spruce forest transitions into the early successional deciduous forest, within transition times differing probabilistically between climax black and white spruce trajectories. The amount of this transition times is also probabilistically determined until climax spruce stage dominates again. Burned deciduous forest self-replaces until repeating fire or climate condition preclude transition to climax spruce. That is to say, upon climate conditions and statistical rationales of post-fire vegetation successions, spruces, especially for fire-prone black spruces, can be replaced by less flammable deciduous. One of the reasons for the higher probability of black spruces may include its usually old-aged biomass with fluffy and low canopy and ignitable understory materials like moss/litter/fibrous under drought. Such conditions may satisfy the deep burning of peats as well, which cause substantial consumption of soil organic matters, i.e., severe fires.

Based on those mechanisms and historical fire occurrences and projections from ALFRESCO, DOS-TEM simulated that the fibrous organic horizon of the AKYRB decreased drastically in response to the very large fire years in the 2000s (Fig. 29.14 cf. Fig. 29.12 upper panel). This undergoing consumption of near-surface organic horizons at present continued until around 2020 under the "cccma" GCM simulated climate or around 2050 under the "echam5" simulation.

The steady organic thickness increasing from 1950 to around 2000 apparently was due to warming and rising CO_2 caused vegetation productivity, however with three large observable organic horizon thinning immediately following large fires.

The fibrous organic layer continued to increase through the remainder of the twenty-first century as ALFRESCO projected fire regime returned to pre-1990 levels of annual area burned (Fig. 29.14 left panel). By 2100, the fibrous organic layer had increased by 3.5 cm with the "cccma" projection and by 1 cm with the relatively warmer "echam5" projection, in comparison to the 1950 thickness. It implies that effects of a warmer climate on soil organic matter decomposition and/or fire consumption appeared over that on soil C inputs from vegetation production in the future.

In contrast to a fibrous increasing trend, the thickness of the deeper amorphous organic horizon varied less than 0.5 cm of about 10 cm total thickness between 1950 and 2100 by DOS-TEM (Fig. 29.14 right panel). In general, the thickness of the amorphous horizon increases very slowly due to the conversion of a very slow process of this type of organic matter formation. It showed an abrupt increase

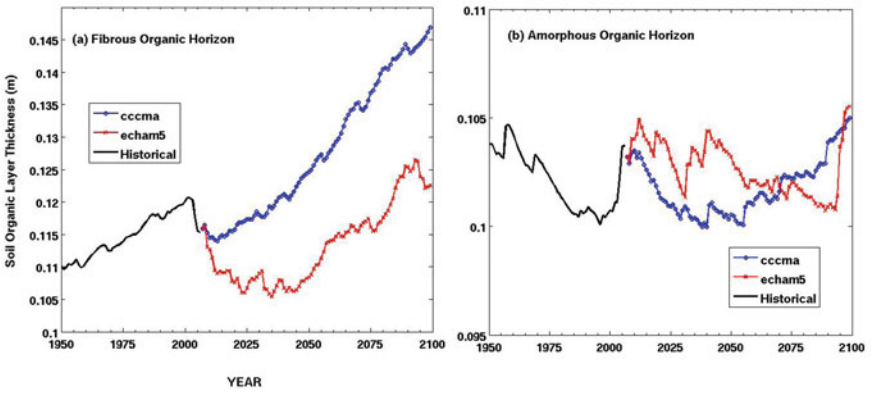

Fig. 29.14 Simulation by DOS-TEM of the mean thickness of **a** fibrous and **b** amorphous organic soil horizons over the AKYRB region from 1950 to 2006 (driven by historical climate) and 2007–2099 (driven by cccma and echam5 projected climate)

during large fire years as the remaining fibrous organic matter and dead roots are converted to amorphous organic matter. However, the thickness of this horizon decreases after large fire years as decomposition is greater than inputs into the horizon.

Apparently soil organic layer thickness was not changing substantially, but its effects on thermal and hydrological processes may be of significantly critical, since its very contrasted thermal and hydraulic properties, such as high porosity, high heat capacity, low water conductivity, etc. Due to organic layers' thermal insulation, generally, the DOS-TEM simulations indicate that the active layer depth of permafrost increases slightly across the AKYRB since the late 1970s when warming trending became observable. However this trend of deepening active layer of permafrost showed the complexity of interacted warming, fire occurrence and other factors, due to somewhat opposite effects on organic layer changing when newly littering materials added into soils while decomposition was enhanced. Those changes not only occur with layer thickness, but also with properties. For example, newly added plant materials contribute more into coarser organic matters and near-surface soils. Warming effects on soil C decomposition may initially be very significant to deeper soils, due to essentially extremely slow process of recently sequestrated organic C. But the unusual fire occurrences and concurrent enhanced ongoing warming since 2000s, which substantially thinned organic horizons (ref. Fig. 29.14), would likely deepen permafrost active layer from about 1 m to about 1.5 m by 2040 if driven by the "cccma" projection, or to about 1.7 m by 2020 if by the warmer "echam5" projections (Fig. 29.15).

However, our model results indicate that, after reaching maximum depths, the active layer would then recover to approximately its late twentieth Century depth by the end of the twenty-first Century (Fig. 29.15). It's probably due to organic

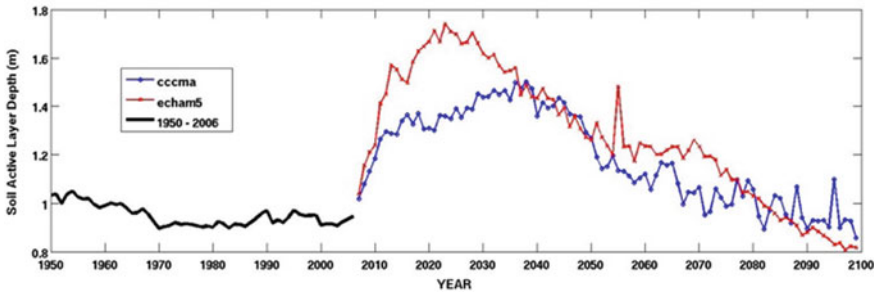

Fig. 29.15 Mean active layer depth of shallow permafrost (within 5.4 m of the surface) in the AKYRB as simulated by DOS-TEM driven by the historical and projected climate changes and fire occurrences

horizons gradually recovering from the increased fire activity early in the century even though warming will be continuing. Although there could be existed other uncertainty in this model simulation and analysis, it's apparent that soil organic matter horizons and its dynamics under warming and its consequent changes in the environment could be critical to underlying permafrost stability in a long term. It has been evaluated that Current warming and rising CO_2 and consequently induced disturbances such as active wildfires could probably turn present boreal forest ecosystems from an initially large C sink to source in the coming century or earlier, upon how fast warming trends going (e.g., McGuire et al. 2018). Unfortunately most modeling projections rarely took accounts of permafrost soil organic layer thickness dynamics with simultaneous enhancements of newly added littering and old soil C. This is especially of importance when fire regime changed along with vegetation dynamics across landscapes, as demonstrated in this DOS-TEM model analysis.

29.5 Future Directions

Due to observed changes in fire regimes in the last decades in the YRB, as discussed in Sects. 29.3 and 29.4, relevant studies indicated that fire effects on ecosystems and feedbacks to climate (e.g. albedo) could be profound and complex. In DOS-TEM, AFRESCO was loosely coupled, implying that vegetation dynamics could be asynchronized into the modeling framework. Under the Alaska Integrated Ecosystem Model Project (AIEM), Dynamical Vegetation Module (DVM)-DOS-TEM model has actively been developed and assessed (https://github.com/ua-snap/dvm-dos-tem). In such a way, the model can be synchronously and seamlessly coupled with other landscape models like ALFRESCO and deep permafrost model (GIPL, Geophysical Institute Permafrost Laboratory Model) for a long-term analysis of the high latitude ecosystem. Such a model framework can further provide

foundation to analyze and evaluate qualities and quantities of ecosystem services across sectors, such as other natural resources and wildlife (Fig. 29.16). These motivations and urgent needs, including applications into managed ecosystems and synchronous feedbacks to the atmosphere, will likely promote more complexity and better integration of modeling earth systems.

Thermalkarst in ice-rich permafrost over high latitude impacts permafrost stability across the landscape (Olefeldt et al. 2016). Such a geomorphological change over centuries time-scale might be accelerated and/or abrupted under ongoing and projected environmental changes. For example, lowland boreal forests with underlying discontinuous permafrost might have been in transition to wetlands during the past few decades likely relevant to warming caused thermalkarst (Lara et al. 2016). Another example may be ice-wedge featured polygonal tundra degradation (Jorgenson et al. 2006). Projected warming and/or drying may cause frost lowland tundra collapsing along troughs, due to underlying ice-wedges formed by seasonal thawing-freezing, and later evolving into rising high-centered polygons and thus exposing old soil C for decomposition. Models featuring those geo-mechanical changes should be developed and coupled into the framework in order to evaluate its effects. Based on the DOS-TEM, dynamical soil module can be

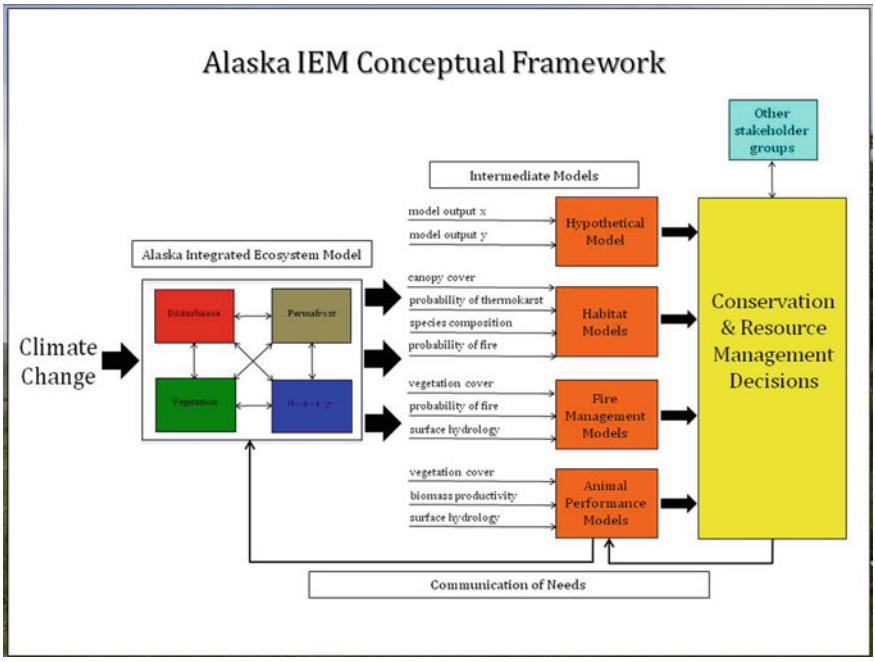

Fig. 29.16 Conceptual framework of coupling DOS-TEM with other landscape models and its extension for evaluating ecosystem services, adopted by Alaska Integrated Ecosystem Models (AIEM)

developed to include other types of soil horizons, such as Alaska Thermalkarst Model (ATM) (https://casc.alaska.edu/resource/modeling-thermokarst-dynamics-boreal-and-arctic-regions-alaska-and-northwest-canada-white).

Although terrestrial ecosystems' responses to or impacts by climate warming have been extensively investigated both spatially and temporarily, it's a challenge to quantify the feedbacks of changing ecosystems to climate, especially in a synchronous way, so that both climate and land surface systems may be co-evolving. For example, Euskirchen et al. (2016) assessed that snow cover reduction in Alaska and northwest Canada from 2010 to 2099 under "echam5" and "cccma" projections could provide larger positive feedbacks to climate, compared to smaller negative feedbacks due to changes in vegetation cover, using ALFRESCO-DOSTEM modeling framework. However, such kinds of detailed feedbacks from land surfaces to atmosphere might not be synchronously fed into GCM or ESM models, although most GCMs may have taken accounts of similar mechanisms in much coarse spatial contents. One of the obstacles could be slow or delayed progress in incorporating most advanced knowledges in terrestrial ecosystem sciences into the GCMs or ESMs, partially due to relatively small portions of land surface processes in the entire ESM traditionally. However, when ESM advance toward high resolution or regional scale, the roles of land surface systems would be more important.

In this chapter, computing difficulties in fully coupled and even 3-D explicit thermal-hydrological-biogeochemical modeling systems were merely mentioned or discussed. In fact, freezing-thawing physics itself is a grand challenge to compute due to phase changes and water property dynamics. In a natural system, with high spatiotemporal ground surface heterogeneity (e.g., vegetations, snow, ice, water) and soil property diversity with variable top/bottom/lateral boundaries, thermal-hydrological models often exhibit instability. For example, diurnal oscillation around freezing point, during either freezing or thawing days, multiple fronts in soil columns often cause algorithm in trouble. Vertical resolutions have always been an issue with soil freezing-thawing. Variable resolutions of dynamical soil models would probably be adopted in the next generation of the freezing-thawing model, which plausible in the near future for high-performance computing (HPC). In HPC, in addition to parallelism, standard discretization (mesh) of the structured or unstructured domain, modern mathematical libraries, PDE solvers, and other tools benefit very much to those problems.

Acknowledgments S.-H. Yi received support for this study through grants as part of the National Key Research and Development Program of China (2017YFA0604801). A portion of this work was conducted as part of Alaska Integrated Ecological Model Project phase I, funded jointly by the U.S. Geological Survey and U.S. Fish and Wildlife Service, through Alaska Climate Science Center. Manuscript preparation by F.-M. Yuan is supported through the Next-Generation Ecosystem Experiments (NGEE) Arctic project, supported by the Office of Biological and Environmental Research in the Department of Energy Office of Science. Oak Ridge National Laboratory (ORNL) is managed by UT-Battelle LLC for the Department of Energy under contract DE-AC05-00OR22725.

References

ACIA (2004) Arctic climate impact assessment. Cambridge University Press, Cambridge, UK

Arora V, Boer GJ (2005) Fire as an interactive component of dynamic vegetation models. J Geophys Res 110:G02008. https://doi.org/10.1029/2005JG000042

Balshi MS, McGuire AD, Zhuang Q, Melillo J, Kicklighter DW, Kasischke E, Wirth C, Flannigan M, Harden J, Clein JS, Burnside TJ (2007) The role of fire disturbance in the carbon dynamics of the pan-boreal region: a process-based analysis. J Geophys Res Biogeosci 112: G02029. https://doi.org/10.1029/2006jg000380

Balshi MS, McGuire AD, Duffy P, Kicklighter DW, Melillo J (2009a) Vulnerability of carbon storage in North American boreal forests to wildfires during the 21st Century. Global Change Biol 15:1491–1510. https://doi.org/10.1111/j.1365-2486.2009.01877.x

Balshi MS, McGuire AD, Duffy P, Flannigan M, Walsh J, Melillo J (2009b) Assessing the response of area burned to changing climate in western boreal North America using a Multivariate Adaptive Regression Splines (MARS) approach. Global Change Biol 15:578–600. https://doi.org/10.1111/j.1365-2486.2008.01679.x

Barrett K, McGuire AD, Hoy E, Kasischke E (2011) Potential shifts in dominant forest cover in interior Alaska driven by variations in fire severity. Ecol Appl 21:2380–2396

Beringer J, Lynch AH, Stuart Chapin III F, Mack M, Bonan GB (2001) The representation of Arctic soils in the land surface model: the importance of mosses. J Clim 14:3324–3335

Bonan GB (1996) A land surface model (LSM Version 1.0) for ecological, hydrological, and atmospheric studies: technical description and users guide. NCAR, University Corporation for Atmospheric Research, NCAR/Tn-417 + STR

Bond-Lamberty B, Wang C, Gower ST (2005) Spatiotemporal measurement and modeling of stand-level boreal forest soil temperatures. Agr For Meteorol 131:27–40

Bond-Lamberty B, Gower ST, Ahl DE (2007) Improved simulation of poorly drained forests using Biome-BGC. Tree Physiol 27:703–715

Bring A, Fedorova I, Dibike Y, Hinzman L, Mård J, Mernild SH, Prowse T, Semenova O, Stuefer SL, Woo MK (2016) Arctic terrestrial hydrology: a synthesis of processes, regional effects, and research challenges. J Geophys Res Biogeosci 121:621–649

Burn CR (1998) The response (1958-1997) of permafrost and near-surface ground temperatures to forest fire, Takhini River valley, southern Yukon Territory. Can J Earth Sci 35:184–199

Bisbee KE, Gower ST, Norman JM, Nordheim EV (2001) Environmental controls on ground cover species composition and productivity in a boreal black spruce forest. Oecologia 129:261–270

Carrasco JJ, Neff JC, Harden J (2006) Modeling physical and biogeochemical controls over carbon accumulation in a boreal forest soil. J Geophys Res 111:G02004. https://doi.org/10.1029/2005JG00087

Clein JS, McGuire AD, Zhang X, Kicklighter D, Melillo J, Wofsy SC, Jarvis PG, Massheder JM (2002) Historical and projected carbon balance of mature black spruce ecosystems across North-America: the role of carbon-nitrogen interactions. Plant Soil 242:15–32

Cuntz M, Haverd V (2018) Physically Accurate Soil Freeze-Thaw Processes in a Global Land Surface Scheme. J Adv Model Earth Syst 10(1):54–77

Dall'Amico M et al (2011) A robust and energy-conserving model of freezing variably-saturated soil. The Cryosphere 5(2):469–484

Davidson EA, Janssens IA (2006) Temperature sensitivity of soil carbon decomposition and feedbacks to climate change. Nature 440:165–173

Deimling TS, Meinshausen M, Levermann A, Huber V, Frieler K, Lawrence DM, Brovkin V (2012) Estimating the near-surface permafrost-carbon feedback on global warming. Biogeosciences 9:649–665

Endrizzi S et al (2014) GEOtop 2.0: simulating the combined energy and water balance at and below the land surface accounting for soil freezing, snow cover and terrain effects. Geosci Model Dev 7(6):2831–2857

Euskirchen SE, McGuire AD, Kicklighter DW, Zhuang Q, Clein JS, Dargaville RJ, Dye DG, Kimball JS, McDonald KC, Melillo JM, Romanovsky VE, Smith NV (2006) Importance of recent shifts in soil thermal dynamics on growing season length, productivity, and carbon sequestration in terrestrial high-latitude ecosystems. Global Change Biol 12:731–750

Euskirchen ES et al (2016) Consequences of changes in vegetation and snow cover for climate feedbacks in Alaska and northwest Canada. Environ Res Lett 11(10)

Fan Z, Neff JC, Harden JW, Wickland KP (2008) Boreal soil carbon dynamics under a changing climate: a model inversion approach. J Geophys Res G04016. https://doi.org/10.1029/2008JG000723

Flannigan M, Logan KA, Amiro BD, Skinner WR, Stocks BJ (2005) Future area burned in Canada. Climatic Change 77(1-2):1–16

Fox JD (1992) Incorporating Freeze-Thaw calculations into a water balance model. Water Resour Res 28(9):2229–2244

Frolking S, Roulet NT, Moore TR, Richard PJ, Lavoie M, Muller SD (2001) Modeling northern peatland decomposition and peat accumulation. Ecosystems 4:479–498

Genet H et al (2013) Modeling the effects of fire severity and climate warming on active layer thickness and soil carbon storage of black spruce forests across the landscape in interior Alaska. Environ Res Lett 8(4):045016

Genet H et al (2018) The role of driving factors in historical and projected carbon dynamics of upland ecosystems in Alaska. Ecol Appl 28(1):5–27

Goodrich EL (1978) Efficient numerical technique for one-dimensional thermal problems with phase change. Int J Heat Mass Transfer 21:615–621

Goulden ML, Wofsy SC, Harden J, Trumbore SE, Crill MP, Gower ST, Fries T, Daube BC, Fan S, Sutton JD, Bazzaz A, Munger WJ (1998) Sensitivity of boreal forest carbon balance to soil thaw. Science 279:214–216

Harden J, Trumbore SE, Stocks BJ, Hirsch AI, Gower ST, ONeill KP, Kasischke E (2000) The role of fire in the boreal carbon budget. Global Change Biol 6(Suppl. 1):174–184

Harden JW, Meier R, Silapaswan C, Swanson DK, McGuire AD (2003) Soil drainage and its potential for influencing wildfire in Alaska. In: Galloway J (ed) studies in Alaska by the U.S. Geological Survey. U.S. Geological Survey Professional Paper 1678

Harden JW, Neff JC, Sandberg DV, Turetsky MV, Ottmar R, Gleixner G, Fries TL, Manies KL (2004) Chemistry of burning the forest floor during the FROSTFIRE experimental burn, interior Alaska, 1999. Global Biogeochem. Cycles 18:GB3014. https://doi.org/10.1029/2003gb002194

Harden JW, Manies KL, Neff JC, Turetsky MR (2006) Effects of wildfire and permafrost on soil organic matter and soil climate in interior Alaska. Glob Change Biol 12:1–13. https://doi.org/10.1111/j.1365-2486.2006.01255.x

Hayes DJ, McGuire AD, Kicklighter DW, Burnside TJ, Melillo JM (2009) The effects of land cover and land use change on the contemporary carbon balance of the arctic and boreal ecosystems of northern Eurasia. In: Chapter 5 G. Gutman (ed) Arctic land cover and land use in a changing climate

Hipp T, Etzelmuller B, Farbrot H, Schuler TV, Westermann S (2012) Modeling borehole temperatures in Southern Norway—insights into permafrost dynamics during the 20th and 21st century. The Cryosphere 6:553–571

Huang Y, Rhoades AM, Ullrich PA, Zarzycki CM (2016) Evaluation of the variable-resolution CESM for modeling California's climate. J Adv Model Earth Syst 8:345–369

Jan A, Coon ET, Painter SL, Garimella R, Multon JD (2018) Comput Geosci 22(1):163–177

Jafarov EE, Coon ET, Harp DR, Wilson CJ, Painter SL, Atchley AL, Romanovsky VE (2018) Modeling the role of preferential snow accumulation in through talik development and hillslope groundwater flow in a transitional permafrost landscape. Environ Res Lett 13 (2018):105006

Jenkinson DS, Rayner JH (1977) The turnerover of soil organic matter in some of the Rothamsted classical experiments. Soil Sci 123:298–305

Johansen O (1975) Thermal conductivity of soils, Ph.D. thesis, University of Trondheim, Trondheim, Norway
Johnson KD, Harden JW, McGuire AD, Norman NB, Bockheim JG, Clark M, Nettleton-Hollingsworth T, Jorgenson TT, Kane ES, Mack M, O'Donnell J, Ping C-L, Shuur EAG, Turetsky MR, Valentine DW (2011) Soil carbon distribution in Alaska in relation to soil-forming factors. Geoderma 167–168:71–84
Johnstone JF, Kasischke E (2005) Stand-level effects of soil burn severity on postfire regeneration in a recently burned black spruce forest. Can J For Res 35:2151–2163
Johnstone JF, Chapin SF (2006) Effects of soil burn severity on post-fire tree recruitment in Boreal Forest. Ecosystems 9:14–31
Jorgenson MT et al (2006) Abrupt increase in permafrost degradation in Arctic Alaska. Geophys Res Lett 33(2)
Jumikis AR (1977) Thermal geotechnics. Rutgers University Press, New Brunswick, NJ, 375 p
Kanamitsu M, Ebisuzaki W, Woollen J et al (2002) NCEP-DOE AMIP-II Reanalysis (R-2). B Am Meteorol Soc 83:1631–1643
Kasischke ES, Johnstone JF (2005) Variation in postfire organic layer thickness in a black spruce forest complex in interia Alaska and its effects on soil temperature and moisture. Can J For Res 35:2164–2177
Kasischke E, Bourgeau-Chavez LL, Johnstone JF (2007) Assessing spatial and temporal variations in surface soil moisture in fire-disturbed black spruce forests in Interior Alaska using spaceborne synthetic aperture radar imagery - Implications for post-fire tree recruitment. Remote Sens Environ 108:42–58
Kasischke ES, Verbyla D, Rupp TS, McGuire AD, Murphy KA, Allen JL, Hoy EE, Jandt R, Duffy P, Calef M, Turetsky MR (2010) Alaska's changing fire regime—implications for the vulnerability of its boreal forests. Can J For Res 40(7):1313–1324
Keeling CD, Whorf TP (2005) Atmospheric CO_2 records from sites in the SIO air sampling network, in trends: a compendium of data on global change, carbon dioxide. Information Analysis Center, Oak Ridge National Laboratory, U.S. Department of Energy, Oak Ridge, Tennessee
Kelly R et al (2015) Palaeodata-informed modelling of large carbon losses from recent burning of Boreal forests. Nat Clim Change 6(1):79–82
Kurylyk BL, Watanabe K (2013) The mathematical representation of freezing and thawing processes in variably-saturated, non-deformable soils. Adv Water Resour 60:160–177
Langer M, Westermann S, Heikenfeld M, Dorn W, Boike J (2013) Satellite-based modeling of permafrost temperatures in a tundra lowland landscape. Remote Sens Environ 135:12–24
Lara MJ, Genet H, McGuire AD, Euskirchen ES, Zhang Y-J, Brown DRN, Jorgenson MT, Romanovsky V, Breen A, Bolton WR (2016) Thermokarst rates intensify due to climate change and forest fragmentation in an Alaskan boreal forest lowland. Glob Chang Biol 22 (2):816–829
Lawrence DM, Slater AG (2008) Incorporating organic soil into a global climate model. Clim Dyn. https://doi.org/10.1007/s00382-007-0278-1
Liljedahl A, Hinzman LD, Busey R, Yoshikawa K (2007) Physical short-term changes after a Tussock Tundra Fire, Seward Peninusula, Alaska. J Geophys Res 112:F02S07. https://doi.org/10.1029/2006jf000554
Liu H, Randerson JT, Lindfors J, Chapin FS III (2005) Changes in the surface energy budget after fire in boreal ecosystems of interior Alaska: an annual perspective. J Geophys Res 110: D13101. https://doi.org/10.1029/2004JD005158
Liu H, Randerson JT (2008) Interannual variability of surface energy exchange depends on stand age in a boreal forest fire chronosequence. J Geophys Res 113:G01006. https://doi.org/10.1029/2007JG000483
Lunardini VJ (1981) Heat transfer in cold climates. Van Nostrand Reinhold, New York
Mack MC et al (2011) Carbon loss from an unprecedented Arctic tundra wildfire. Nature 475 (7357):489–492

Manies KL, Harden J, Bond-Lamberty B, ONeill KP (2005) Woody debris along an upland chronosequence in boreal Manitoba and its impact on long-term carbon storage. Can J For Res 35:472–482

MacKay JR (1995) Active layer changes (1968 to 1993) following the Forest-Tundra Fire near Inuvik, N.W.T, Canada. Arct Alp Res 27:323–336

McGuire AD, Melillo J, Jobbagy EG, Kicklighter D, Grace AL, Moore B, Vorosmarty CJ (1992) Interactions between carbon and nitrogen dynamics in estimating net primary productivity for potential vegetation in North America. Global Biogeochem Cycles 6:101–124

McGuire AD, Anderson LG, Christensen TR, Dallimore S, Guo L, Hayes DJ, Heimann M, Lorenson TD, Macdonald RW, Roulet N (2009) Sensitivity of the carbon cycle in the Arctic to climate change. Ecol Monogr 79:523–555

McGuire AD et al (2018) Dependence of the evolution of carbon dynamics in the northern permafrost region on the trajectory of climate change. Proc Natl Acad Sci USA 115(15):3882–3887

Mitchell TD, Jones PD (2005) An improved method of constructing a database of monthly climate observations and associated high-resolution grids. Int J Clim 25:693–712

Nicolsky DJ, Romanovsky VE, Alexeev VA, Lawrence DM (2007) Improved modeling of permafrost dynamics in a GCM land-surface scheme. Geophys Res Lett 34:L08501. https://doi.org/10.1029/2007GL029525

Oelke C, Zhang T, Serreze MC (2004) Modeling evidence for recent warming of the Arctic soil thermal regime. Geophys Res Lett 31:L07208. https://doi.org/10.1029/2003GL019300

Olefeldt D et al (2016) Circumpolar distribution and carbon storage of thermokarst landscapes. Nat Commun 7:13043

Oleson KW, Dai Y, Bonan GB, Bosilovich GM, Dickinson RE, Dirmeyer P, Hoffman F, Houser RP, Levis S, Niu G-Y, Thornton P, Vertenstein M, Yang Z-L, Zeng X (2004) Technical description of the Community Land Model (CLM). NCAR, University Corporation for Atmospheric Research, NCAR/TN-461 + STR

O'Neill KP, Kasischke E, Richter DD (2002) Environmental controls on soil CO_2 flux following fire in black spruce, white spruce, and aspen stands of interial Alaska. Can J For Res 32:1525–1541

Painter SL (2010) Three-phase numerical model of water migration in partially frozen geological media: model formulation, validation, and applications. Comput Geosci 15(1):69–85

Painter SL et al (2012) Modeling challenges for predicting hydrologic response to degrading permafrost. Hydrogeol J 21(1):221–224

Painter SL, Karra S (2014) Constitutive model for unfrozen water content in subfreezing unsaturated soils. Vadose Zone J 13(4)

Painter SL et al (2016) Integrated surface/subsurface permafrost thermal hydrology: Model formulation and proof-of-concept simulations. Water Resour Res 52:6062–6077

Parton WJ et al (2001) Generalized model for NOx and N2O emissions from soils. J Geophys Res Atmos 106(D15):17403–17419

Raich JW, Rastetter EB, Melillo J, Kicklighter D, Steudler PA, Peterson BJ, Grace AL, Moore B, Vorosmarty CJ (1991) Potential net primary productivity in South America: application of a global model. Ecol Appl 1:399–429

Ringeval B, Decharme B, Piao S, Ciais P, Papa P, Noblet-Ducoudre N, Prigent C, Friedlingstein P, Gouttevin I, Koven CD (2012) Modelling sub-grid wetland in the ORCHIDEE global land surface model: evaluation against river discharges and remotely sensed data. Geosci Model Dev 5:941–962

Riseborough DW, Shiklomanov NI, Etzelmuller B, Gruber S, Marchenko S (2008) Recent advances in permafrost modelling. Permafrost Periglac 19:137–156

Ruess RW, Hendrick RL, Burton AJ, Pregitzer KS, Sveinbjornsson B, Allen MF, Maurer GE (2003) Coupling fine root dynamics with ecosystem carbon cycling in black spruce forests of interior Alaska. Ecol Monogr 73:643–662

Rupp TS et al (2016) Chapter 2. Climate simulations, land cover, and wildfire. In: Zhu Z, McGuire AD (eds) Baseline and projected future carbon storage and greenhouse gas fluxes in ecosystems of Alaska, Reston, VA, U.S. Geological Survey. Professional Paper 1826

Schaefer K, Zhang T, Bruhwiler LP, Barret AP (2011) Amount and timing of permafrost carbon release in response to climate warming. Tellus B 63B:65–180

Schuur EAG, Bockheim J, Canadell JG, Euskirchen E, Field CB, Goryachkin SV, Hagemann S, Kuhry P, Lafleur PM, Lee H, Mazhitova G, Nelson FE, Rinke A, Romanovsky VE, Shiklomanov N, Tarnocai C, Venesky S, Vogel JG, Zimov SA (2008) Vulnerability of permafrost carbon to climate change: implications for the global carbon cycle. Bioscience 58:701–714

Shanley JB, Chalmers A (1999) The effect of frozen soil on snowmelt runoff at Sleepers River, Vermont. Hydrol Process 13:1843–1857

Sitch S, Smith B, Prentice CI, Arneth A, Bondeau A, Cramer W, Kaplan A, Levis S, Lucht W, Sykes M, Thonicke K, Venevsky S (2003) Evaluation of ecosystem dynamics, plant geography and terrestrial carbon cycling in the LPJ dynamic global vegetation model. Global Change Biol 9:161–185

Steele SJ, Gower ST, Vogel JG, Norman JM (1997) Root mass, net primary production and turnover in aspen, jack pine and black spruce forests in Saskatchewan and Manitoba, Canada. Tree Physiol 17:577–587

Tarnocai C, Canadell JG, Mazhitova G, Schuur EAG, Kuhry P, Zimov S (2009) Soil organic carbon pools in the northern circumpolar permafrost region. Global Biogeochem. Cycles 23: GB2023. https://doi.org/10.1029/2008gb003327

Thonicke K, Venevsky S, Sitch S, Cramer W (2001) The role of fire disturbance for global vegetation dynamics: coupling fire into a Dynamic Global Vegetation Model. Global Ecol Biogeogr 10:661–677

van Cleve K, Dyrness CT, Viereck LA, Fox JF, Chapin FS III, Oechel W (1983) Taiga ecosystems in interior Alaska. Bioscience 33:39–44

van Wijk TM, Williams M, Laundre JA, Shaver GR (2003) Interannual variability of plant phenology in tussock tundra: modelling interactions of plant productivity, plant phenology, snowmelt and soil thaw. Global Change Biol 9:743–758

Verseghy DL (1991) CLASS-A Canadian land surface scheme for GCMs I: soil model. Int J Climat 11:111–133

Wang L, Zhou J, Qi J, Sun L, Yang K, Tian L, Lin Y, Liu W, Shrestha M, Xue Y, Koike T, Ma Y, Li X, Chen Y, Chen D, Piao S, Lu H (2017) Development of a land surface model with coupled snow and frozen soil physics. Water Resour Res 53:5085–5103

Woo M-K, Arain AM, Mollinga M, Yi S (2004) A two-directional freeze and thaw algorithm for hydrologic and land surface modelling. Geophys Res Lett 31:L12501. https://doi.org/10.1029/2004GL019475

Yi S, Arain AM, Woo M-K (2006) Modifications of a land surface scheme for improved simulation of ground freeze-thaw in northern environments. Geophys Res Lett 33:L13501. https://doi.org/10.1029/2006GL026340

Yi S, Woo M-K, Arain AM (2007) Impacts of peat and vegetation on permafrost degradation under climate warming. Geophys Res Lett 34:L16504. https://doi.org/10.1029/2007/GL030550

Yi S, Manies KL, Harden J, McGuire AD (2009a) The characteristics of organic soil in black spruce forests: Implications for the application of land surface and ecosystem models in cold regions. Geophys Res Lett 36:L05501. https://doi.org/10.1029/2008GL037014

Yi S, McGuire AD, Harden J, Kasischke E, Manies KL, Hinzman LD, Liljedahl A, Randerson JT, Liu H, Romanovsky VE, Marchenko S, Kim Y (2009b) Interactions between soil thermal and hydrological dynamics in the response of Alaska ecosystems to fire disturbance. J Geophys Res 114:G02015. https://doi.org/10.1029/2008JG000841

Yi S, McGuire AD, Kasischke E, Harden J, Manies KL, Mack M, Turetsky MR (2010) A Dynamic organic soil biogeochemical model for simulating the effects of wildfire on soil

environmental conditions and carbon dynamics of black spruce forests. J Geophys Res 115: G04015. https://doi.org/10.1029/2010JG001302

Yi S, Li N, Xiang B, Wang X, Ye B, McGuire AD (2013) Representing the effects of alpine grassland vegetation cover on the simulation of soil thermal dynamics by ecosystem models applied to the Qinghai-Tibetan Plateau. J Geophys Res 118:1186–1199

Yi S, Wischnewski K, Langer M, Muster S, Boike J (2014a) Freeze/thaw processes of complex permafrost landscape of Northern Siberia simulated using the TEM ecosystem model: impact of thermokarst ponds and lakes. Geosci Model Dev 7(4):1671–1689

Yi S, Wang X, Qin Y, Xiang B, Ding Y (2014b) Responses of alpine grassland on Qinghai-Tibetan Plateau to climate warming and permafrost degradation: a modeling perspective. Environ Res Lett 9:074014. https://doi.org/10.1088/1748-9326/9/7/074014

Yoshikawa K, Bolton WR, Romanovsky VE, Fukuda M, Hinzman LD (2003) Impacts of wildfire on the permafrost in the boreal forests of Interior Alaska. J Geophys Res 108(D1):8148. https://doi.org/10.1029/2001JD000438

Yuan FM et al (2012) Assessment of boreal forest historical C dynamics in the Yukon River Basin: relative roles of warming and fire regime change. Ecol Appl 22(8):2091–2109

Zhang T, Barry RG, Knowles K, Heginbottom JA, Brown J (1999) Statistics and characteristics of permafrost and ground ice distribution in the Northern Hemisphere. Polar Geogr 23(2):147–169

Zhang Y, Chen W, Cihlar J (2003) A process-based model for quantifying the impact of climate change on permafrost thermal regimes. J Geophys Res Atmos 108(D22):4695. https://doi.org/10.1029/2002JD003354

Zhang Y, Carey SK, Quinton WL (2008) Evaluation of the algorithms and parameterizations for ground thawing and freezing simulation in permafrost regions. J Geophys Res 113:D17116. https://doi.org/10.1029/2007JD009343

Zhuang Q, Romanovsky VE, McGuire AD (2001) Incorporation of a permafrost model into a large-scale ecosystem model: Evaluation of temporal and spatial scaling issues in simulating soil thermal dynamics. J Geophys Res Atmos 106(D24):33649–33670

Zhuang Q, McGuire AD, Harden J, O'Neill KP, Romanovsky VE, Yarie J (2002) Modeling soil thermal and carbon dynamics of a fire chronosequence in interior Alaska. J Geophys Res Atmos 107:8147. https://doi.org/10.1029/2001jd001244. [printed 108(D1), 2003]

Zhuang Q, McGuire AD, Melillo JM, Clein JS, Dargaville RJ, Kicklighter DW, Myneni RB, Dong J, Romanovsky VE, Harden J, Hobbie JE (2003) Carbon cycling in extratropical terrestrial ecosystems of the Northern Hemisphere during the 20th century: a modeling analysis of the influences of soil thermal dynamics. Tellus 55B:51–776

Zhuang Q, Melillo J, Kicklighter D, Prinn RG, McGuire AD, Steudler PA, Felzer BS, Hu S (2004) Methane fluxes between terrestrial ecosystems and the atmosphere at northern high latitudes during the past century: a retrospective analysis with a process-based biogeochemistry model. Global Biogeochem Cycle 18:GB3010. https://doi.org/10.1029/2004gb002239

Zhuang Q, Melillo J, Sarofim MC, Kicklighter D, McGuire AD, Felzer BS, Sokolov A, Prinn RG, Steudler PA, Hu S (2006) CO2 and CH4 exchanges between land ecosystems and the atmosphere in northern high latitudes over the 21st century. Geophys Res Lett 33L(17):403. https://doi.org/10.1029/2006GL026972

Zimov SA, Davidov SP, Zimova GM, Davidova AI, Chapin FS, Chapin MC, Reynolds JF (1999) Contribution of disturbance to increasing seasonal amplitude of atmospheric CO_2. Science 284:1973–1976

Dr. Shuhua Yi is a Professor of Institute of Fragile Ecosystem and Environment, School of Geographic Science, Nantong University. He focuses on the studies of cold region ecosystem, including alpine grassland of the Qinghai-Tibetan Plateau, Boreal forest and Arctic tundra, using numerical modeling and unmanned aerial vehicle. He developed a dynamic organic soil version of Terrestrial Ecosystem Model when he was a postdoc at University of Alaska Fairbanks and a Research Professor at Cold and Arid Regions Environment and Engineering Research Institute, Chinese Academy of Sciences. The model can simulate the interactions among the thermal, hydrological and ecological processes to investigate the effects of wild fire disturbance and permafrost degradation on Boreal forest. He now focuses on the application of small unmanned aerial vehicle to study the distribution of Plateau Pika and its role in Alpine grassland.

Dr. Fengming Yuan is a Professional Technical Staff at Climate Change Science Institute/Environmental Science Division, Oak Ridge National Laboratory (ORNL). He is a thermal-hydrology and biogeochemical modeler for terrestrial ecosystems, focusing on northern high-latitude regions, with background in field experiments (soil sciences). His research interests include supercomputing (HPC) application in modeling complexity of water, energy, carbon and nitrogen cycling in agricultural, forest and other terrestrial ecosystems, within framework of Earth System Models at various scales. He earned his B.S. in Soil Sciences and Plant Nutrition from the Central-China Agricultural University, M. S. in Soil Sciences from the Chinese Academy of Agricultural Sciences, and Ph.D. in Soil Sciences from the University of Wisconsin-Madison. Before joining ORNL, He was at the University of Alaska Fairbanks conducting research on fire disturbances on boreal forest carbon stock dynamics using the Terrestrial Ecological Model (TEM). He had also worked on DAYCENT and HYDRUS applications for the Southern California natural ecosystems under atmospheric nitrogen depositions, and on development and application of the Carbon and Nitrogen coupled Canadian Land Surface Scheme (CN-CLASS) for FLUXNET-Canada.

Future Trajectory of Arctic System Evolution

30

Kazuyuki Saito, John E. Walsh, Arvid Bring, Ross Brown, Alexander Shiklomanov, and Daqing Yang

Abstract

The Arctic climate system is undergoing changes in its multiple components, including its hydrologic cycle, as documented in the preceding chapters. The future trajectory of the Arctic climate system becomes a major issue for adapting to anticipated impacts ranging from local-scale impacts on water security (hydropower, infrastructure, and human health), to global-scale impacts such as greenhouse gas releases and sea level rise. Here we highlight projections of

K. Saito (✉)
Research Institute for Global Change, Japan Agency for Marine-Earth Science and Technology, Yokohama, Kanagawa, Japan
e-mail: ksaito@jamstec.go.jp

J. E. Walsh
International Arctic Research Center, University of Alaska, Fairbanks, Alaska, USA
e-mail: jewalsh@alaska.edu

A. Bring
Department of Physical Geography, Stockholm University, Stockholm, Sweden
e-mail: arvid.bring@natgeo.su.se

R. Brown
Climate Research Division, Environment and Climate Change Canada, Montreal, Quebec, Canada
e-mail: rdbrown@videotron.ca

A. Shiklomanov
Earth Systems Research Center, University of New Hampshire, Durham, NH, USA
e-mail: sasha@eos.sr.unh.edu

D. Yang
Watershed Hydrology and Ecology Division, Environment and Climate Change Canada, Victoria, British Columbia, Canada
e-mail: daqing.yang@gmail.com; daqing.yang@canada.ca

D. Yang and D. L. Kane (eds.), *Arctic Hydrology, Permafrost and Ecosystems*,
https://doi.org/10.1007/978-3-030-50930-9_30

changes in key Arctic variables relevant to the Arctic freshwater cycle: precipitation, evapotranspiration, snow, river discharge, surface- and ground-water, and permafrost. We highlight key uncertainties arising from the future emission scenarios and across-model differences. Precipitation and evapotranspiration are both projected to increase, consistent with atmospheric warming and the Clausius–Clapeyron equation. The percentage increases of precipitation projected for the Arctic are among the largest in the world. Evapotranspiration is also projected to increase, although not enough to offset the increase in precipitation, so the freshwater runoff as river discharge is also projected to increase. The projected change signal of the river discharge increase is much greater than the model uncertainty. Projected changes in soil moisture are highly uncertain because of interactions with vegetation, topography, and permafrost, together with uncertainties in local net precipitation minus evapotranspiration. Snow cover duration and maximum accumulation are projected to decrease across most regions of the Arctic, with increased annual maximum accumulations only in high latitudes where increased snowfall dominates the decrease of snow season length. Near-surface permafrost is projected to thaw over large portions of the Arctic, with timing dependent on the rate of warming (emission scenario) and the effects of changes in snow cover. Projected changes become more sensitive to emission trajectories after about the middle of the twenty-first century with projected changes in many variables accelerating under a business as usual scenario in contrast to much slower rates of change where efforts are made to limit GHG emissions.

30.1 Introduction

The Arctic climate system, including hydrological and ecological components, is comprised of many different elements which are interwoven through different linkages and pathways (Bring et al. 2016; Vihma et al. 2016; Wrona et al. 2016; Hinzman et al. 2013; Saito et al. 2013). As described in the previous chapters, most arctic system components have changed in response to rapid climate warming in recent decades (Box et al. 2019), and are projected to continue to change. The Arctic is changing at a much more rapid rate than the rest of the globe from a number of positive feedback mechanisms contributing to Arctic amplification (Serreze and Francis 2006; Screen and Simmonds 2010; Taylor et al. 2013; Pithan and Mauritsen 2014; Franzke et al. 2016; Dai et al. 2019). Even under a modest scenario (i.e., RCP4.5), the arctic system will take about a century to stabilize at a new level. In addition, the Arctic cryosphere is characterized as temperature threshold dependent (0 °C, by phase change of water) with tipping points that can generate periods of large, rapid, and/or irreversible change in physical and biological systems, ranging from a large-scale ocean–atmosphere–sea ice system and Greenland ice sheets to smaller-scale subsystems, e.g., the loss of perennial ice

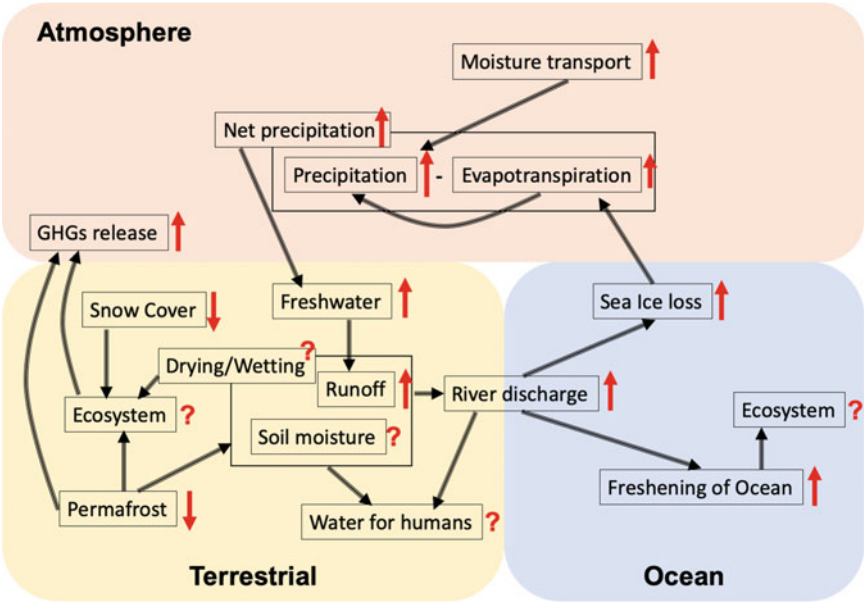

Fig. 30.1 The key elements in the Arctic hydrological trajectories under climate warming. Red arrows denote increasing (upward) or decreasing (downward) changes whereas the red question marks imply uncertainty in the direction. Black arrows indicate drivers or influences

cover on northern lakes, and degradation of ice-rich permafrost (Wassmann and Lenton 2012; Lenton 2012; Lehnherr et al. 2018; Strauss et al. 2017).

This chapter highlights projections of changes in key Arctic variables relevant to the Arctic hydrological cycle (Fig. 30.1): especially, precipitation, river discharge, snow, and permafrost. It also discusses issues related with future water for northern society, as well as gaps and key uncertainties in future trajectory, including those arising from the future emission scenarios and across-model differences (Lique et al. 2016).

30.2 Water Cycle

A future warmer climate will lead to an intensification of hydrological cycle in the Arctic. Precipitation will keep its increasing trend in high latitudes during this century (Figs. 11.12 and 12.22, in IPCC (2013); Lique et al. 2016). Precipitation will increase by about 50% from the current value in the Arctic, with the seasonal peak in late autumn to winter. Mean precipitation, as well as the extremes (such as heavy rain days, or maximum rainfall in 1- or 5-days), are projected to increase (Lader et al. 2017; Kusunoki et al. 2015). The precipitation increase is partly

associated with warming of the atmosphere and the oceans. The major contributions to the projected increase in Arctic precipitation are primarily increased local evaporation from sea ice retreat (Bintanja and Selten 2014), and secondly, moisture transport from mid-latitudes (peaking in late summer to autumn).

Recent model simulations under different greenhouse gas emission scenarios (such as business as usual (RCP8.5), or reduced emissions (RCP4.5)) show that, in high latitudes, the projected mean change in precipitation is larger than the natural variability, leading to a higher confidence in the precipitation change projections unlike other regions of the globe where natural variability dominates the climate change signal. These projections further show increase in evapotranspiration (E) and near-surface specific humidity in the twenty-first century, consistent with projected overall temperature increase. However, relative humidity may decrease; air from the oceans, possibly close to saturation at the sea surface temperature, move inland, where the projected temperature increase is higher than in the ocean, hence leading to reductions in the relative humidity near the terrestrial surface (Sherwood et al. 2010). Precipitation minus evapotranspiration (P-E) will be projected to increase for the Arctic (IPCC 2013; Lique et al. 2016); for the land areas, it likely implies increase in runoff and river discharge. The projected mean increase of runoff was larger than the inter-model variability, with the areas of statistically significant changes are proportional to the higher GHG emission among the scenarios.

In general, a unit of air mass with higher temperature can hold more moisture in it. The conversion rate from moisture to precipitation, whose theoretical upper bound is given by the Clausius–Clapeyron relationship as 7–7.5%/K, depending on the range considered, is projected to be 1–3%/K by global climate models (Lambert and Webb 2008; Lu and Cai 2009; Kusunoki et al. 2015). Hydrological sensitivity —defined as percent increase of precipitation against one degree of temperature warming—of mean precipitation for the Arctic (4.5%/K) is estimated from modeling studies to be much larger than that for the entire globe (1.6–1.9%/K) in response to the enhanced surface evaporation from retreating winter sea ice (Bintanja and Selten 2014). Break-down analysis shows that the sensitivity varies among different precipitation regime: it is lower for heavy precipitation (1.5–3.5%/K, for average precipitation on rainy days, or maximum in 5 days) than the annual mean precipitation (4.5%/K). Kusunoki et al. (2015) show that future increases in moisture transport to the Arctic (northward of 50 N) are associated more with transient eddies (such as cyclonic activities or storm truck intensity) than to the stationary field (i.e., the location and strength of the subpolar jet stream) for all seasons. Projected decreases in the meridional temperature gradient under warming will shift the subpolar jet to the north, while it may change the location and magnitude of the baroclinic instabilities.

Precipitation changes influence many different aspects of the Arctic hydrology such as snow and ice on land and sea ice (Charalampidis et al. 2015; Mernild et al. 2014; Tedesco et al. 2011; Brown et al. 2017), rapid land ice buildup (Doyle et al. 2015), and the insulation effects on the subsurface thermal regime (Westermann et al. 2011). Further, the fraction of total precipitation falling as rain will increase

over most regions of the Arctic (Bintanja and Andry 2017). Along with overall wetter and warmer trend in the Arctic, rain-on-snow (ROS) events are also projected to increase (Forbes et al. 2016; Hansen et al. 2014; Pan et al. 2018) with impacts on Arctic flora and fauna (Hansen et al. 2014), and sea ice growth and ice-ocean feedback (Screen and Simmonds 2010; Bintanja and Selten 2014). Freshening of the Arctic Ocean, observed in this century (Haine et al. 2015) may continue with contributions from increased river discharge, net precipitation (P-E), and oceanic transport (e.g., freshwater through Barents Sea Opening and Bering Strait) in addition to sea ice melting (Shu et al. 2018). Climate modeling studies indicate that declining sea ice and increasing humidity provides a positive cloud-sea ice feedback from strengthened cloud radiative effects that emerge during non-summer months (Morrison et al. 2019; Jun et al. 2016). Loss of the Arctic sea ice can induce changes in mid-latitude weather patterns, such as severe winter weather occurred in 2013–14 in North Pacific and North America (Lee et al. 2015), or droughts in California during 2012–16, as a part of wider impacts on precipitation (Cvijanovic et al. 2017) through dynamical linkages, which may occur more frequently in the future with continuing loss of sea ice.

Projection of soil moisture changes (in the top 10 cm layer) is still highly uncertain partly because of the complexity of the physical processes involved (for example, infiltration and runoff, which are highly dependent on local vegetation, soil texture, and micro-topography), and the different representations of soils in climate models (e.g., depth of soil columns and thickness of the layers, presence of organic material, and treatment of physical processes). In the Arctic region, the presence of permafrost, and freeze/thaw cycles with phase changes further complicate the thermos-hydrological processes involved in subsurface water dynamics. It is unclear whether the Arctic land will be drier or wetter partly stemming from uncertainties in projected changes in permafrost (see later in this chapter), as well as in the modulations of the environmental conditions (such as longer snow-free period, increase in rain-to-snowfall ratio, and additional meltwater from glaciers).

30.3 Freshwater/River Discharge

As noted in Chaps. 6 and 24, river discharge to the Arctic Ocean has increased over the past 4–5 decades, particularly from the Eurasian part of the Arctic domain (Peterson et al. 2002; Berezovskaya et al. 2005; Ye et al. 2003, 2004a, b; Georgiadi et al. 2008; Shiklomanov and Lammers 2009). Discharge from the North American basins also showed an increasing trend in the recent 3–4 decades (Déry et al. 2016; Ge et al. 2013). Projections of future changes in river discharge and total river flux to the Arctic Ocean due to global warming have been made by many studies, including Arnell (2004). Some investigations and results during the 1990s were summarized by Shiklomanov and Shiklomanov (2003). At that time most studies used climate scenarios with GCMs for doubled atmospheric CO_2 concentrations. Future climate scenarios were used as inputs to hydrological models of varying

complexity for individual river basins to estimate the effects of climate change on regional hydrological regime (Shiklomanov and Lins 1991).

Table 30.1 shows a summary of recent studies on the future discharge for the large Arctic rivers due to climate change. These studies, mainly based on the CMIP 5 outcomes, use individual and multi-model average climate projections to evaluate expected changes in the northern hydrology. Despite the diversity of models and approaches, the results from these studies are qualitatively consistent. They suggest that increases in annual runoff are expected in the twenty-first century for most large rivers. Relative to the period 1976–2005, the annual mean flows during 2027–2090

Table 30.1 Projected changes in river discharge of large northern rivers under the impact of climate change

River basin	Annual discharge change (%)	Climate scenario	Source
Mackenzie	21%	Comparing CMIP5 historical runoff data (1976–2005) to future projections under RCP 8.5 (2070–2099)	Ferguson et al. (2018)
Lena	34%		
Ob	15%		
Don	−16%		
Western Hudson Bay	5–7%	19 CMIP5 GCMs ensemble average for RCP 4.5-8.5 by 2070.	MacDonald et al., (2008)
Eastern Hudson Bay	9–12%		
Ungava Bay & Hudson Strait	12–16%		
Foxe Basin	40–45%		
Eastern Siberia, Northern Alaska	+50–80%	6 CMIP5 GCMs ensemble, average for RCP 4.5-8.5 by 2080	Bring et al. (2017)
Western Siberia, Central Canada	−15–+15%		
Major Siberian rivers	80%	Voeikov Main Geophysical Observatory 30 member ensemble under RCP 8.5	Shkolnik et al. (2018)
Northern Eurasia in general	20–40%		
Total annual river runoff and freshwater input into the Arctic Basin	(none given, but Fig. 17 shows increasing runoff from 1860–2100)	CMIP 5 EC-Earth 2.3 simulation ensemble means for RCP 2.6, 4.5, 6.0, and 8.5 up to 2100	Koenigk et al. (2013)
Yenisey	6	6 CMIP3 GCMs for A2 by 2035	Shiklomanov et al. (2008)
Lena	11		
Ob	3		
Yenisey	16	19 models ensemble 2081–2100; A1b emissions	Nohara et al. (2006)
Lena	24		
Ob	10		
Yenisey	13	IS92a by 2035–2065	Manabe et al. (2004)
Lena	12		
Ob	21		
Total flow to Arctic Ocean for A2/B2	24/18	6 model ensemble to 2080; A2 & B2 emissions	Arnell (2004)

would increase by 15–35% for the Lena and Ob basins, and about 21% for the Mackenzie river. Similarly, 19 GCM ensemble average indicate flows increases of 5–7% for western Hudson Bay and 9–12% for the eastern Hudson Bay by 2070 (MacDonald et al. 2008). Six GCM ensemble average shows flow changes (by 2080) around 50–80% for eastern Siberia and northern Alaska, and −15–15% for western Siberia and central Canada (Bring et al. 2017). Although the rates of changes reported vary depending on the models and the time scale of interest, they, however, show a common feature, i.e., a significant shift to earlier dates in spring peak flow, as result of rising spring air temperatures and earlier snowmelt.

30.4 Snow Cover

Because snow has major impacts on the atmosphere, subsurface thermal state, and hydrology, assessments of changes in snow cover are essential to an understanding of the present and future trajectory of the Arctic system. There is increasing awareness that Arctic snow cover is responding to multiple environmental drivers such as warming, increased moisture availability, changing atmospheric circulation, increased frequency of winter thaws, and rain-on-snow events. As shown in Chap. 3, there is widespread multi-dataset evidence of recent reductions in Arctic snow cover. The annual duration of snow on the ground has decreased by 2–4 days per decade since the 1970s, with the largest negative trends occurring at high latitudes and high elevations. Trends in annual maximum snow accumulation are more uncertain and vary by region, elevation, and data source. However, the aggregate evidence points to declining annual maximum snow accumulation in the pan-Arctic average.

Projected changes in Arctic snow cover by the CMIP5 model ensemble are generally consistent with current trends. The pan-Arctic mean annual snow cover duration (SCD) is projected to decrease at a rate of 2–4% per decade (Brown et al. 2017) over the coming decades, with the rate of change in the latter half of the twenty-first century differing noticeably between the RCP 4.5 and RCP 8.5 scenarios (Fig. 30.2). The RCP 4.5 projections show a stabilization of the annual Arctic SCD losses at a level about 10% below current values by 2100, while the RCP 8.5 projections show accelerating losses of snow cover through the end of the twenty-first century. Regionally, the relative decreases in SCD are largest in the warmer more southern sectors of the Arctic primarily because the historical baseline values of mean annual SCD are smaller in these regions (Fig. 30.3b, d). The projected end of century decrease in annual SCD of 10–20% over large areas of Arctic seems modest but represents 30–60 days less snow cover.

Projected change in end of century annual maximum snow accumulation (SWEmax) over the Arctic (Fig. 30.3c) exhibits a contrasting regional pattern with important relative decreases exceeding 50% over warmer sectors such as Scandinavia and coastal Alaska, with increases exceeding 30% over the coldest sectors (Siberia and Canadian Arctic Archipelago). This contrasting pattern arises from the

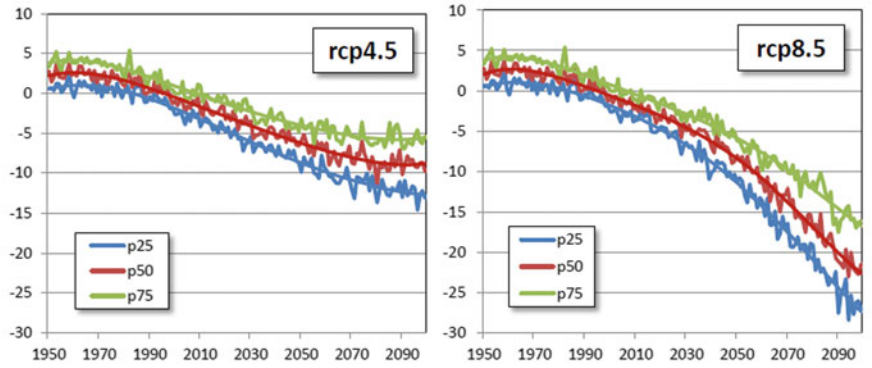

Fig. 30.2 Projected percentage change in annual snow cover duration over Arctic non-glaciated land areas under the RCP 4.5 (left) and RCP 8.5 (right) emission scenarios relative to the period 1986–2005. The plots show the 25th, 50th, and 75th percentiles of 16 CMIP5 model simulations

interplay between warming (generating a shorter accumulation period and a reduction in the solid fraction of total precipitation) and increased winter precipitation. Arctic regions with the warmest winter air temperatures and highest winter precipitation (e.g., Scandinavia and coastal Alaska) are most at risk of experiencing large reductions in winter snowpack in response to global warming. The regions with projected increases in SWEmax coincide with areas of continuous permafrost, so the model simulations imply an increased potential for insulation of cold permafrost soils during the winter months. The extent to which this increased insulation will augment the direct effect of atmospheric warming needs to be addressed in assessments of the future changes in permafrost. The seasonal patterns of projected changes in SCD and SWEmax are largest in the shoulder seasons which has important implications for energy exchanges and ecosystems (Niittynen and Luoto 2018).

While clear spatial and temporal signals are apparent in the CMIP5 future trajectories of Arctic snow cover depicted here, there are large differences among climate models in the timing and characteristics of the future changes. These differences arise in part because of each model's internal climate variability, but they are also related to different representations of snow physical processes, and to biases in snowpack driving variables such as atmospheric temperature and precipitation. Incorporating spatial heterogeneity and snow-vegetation dynamics in climate models remain important challenges for reducing uncertainties in Arctic snow cover change scenarios. The challenges may be even more complex in Arctic marine areas where realistic simulation of snow on sea ice requires accurate timing of sea ice formation and disappearance, the simulation of local-scale Arctic winter precipitation processes associated with open water bodies such as polynyas, and the treatment of processes such as blowing snow and slushing that impact the depth and thermal properties of the snow layer.

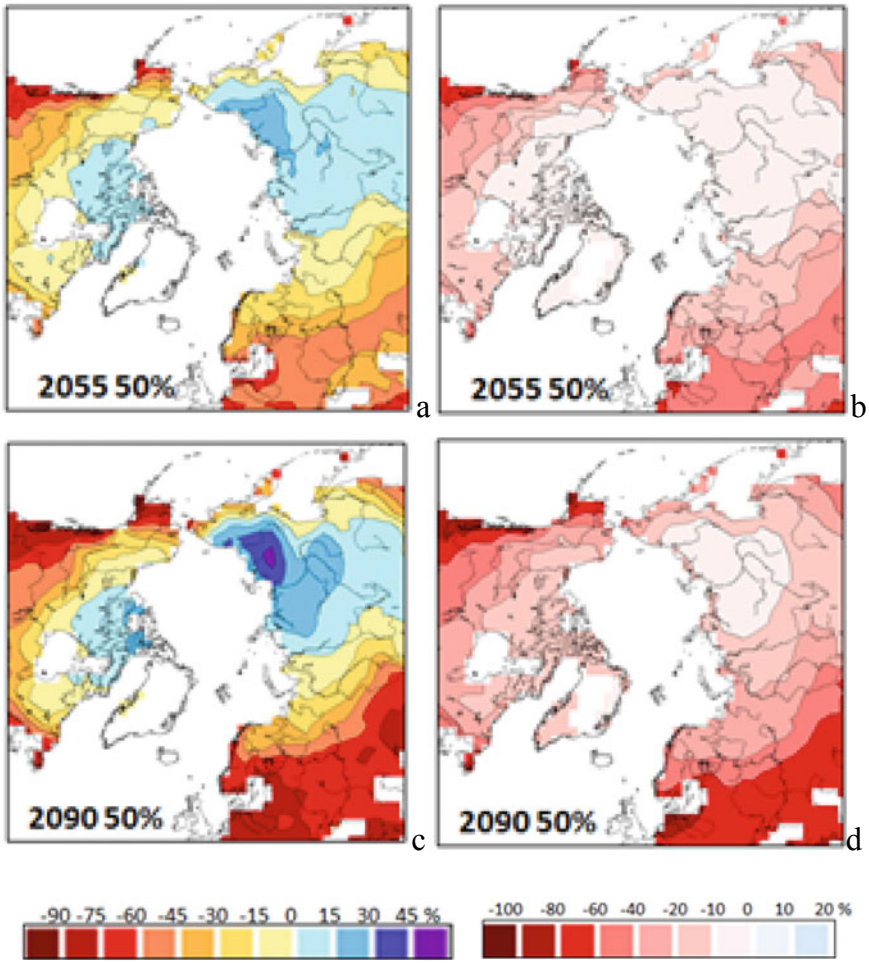

Fig. 30.3 Regional patterns of projected change in mean annual maximum monthly SWE and mean annual SCD. **a** 2055 projected median % change in annual maximum monthly SWE from 16 CMIP5 GCMs for RCP8.5 scenario (2046–2065 minus 1986–2005); **b** same for annual snow cover duration; **c** same as a) for 2090 (2081–2100 minus 1986–2005); **d** same as b) for 2090. Details of the model ensemble are provided in Brown et al. 2017

30.5 Permafrost

Recent observations and instrumental measurements have shown warming trends in the circum-Arctic permafrost conditions, e.g., increased temperatures of permafrost, and deepening of active layers (Biskaborn et al. 2019; SWIPA 2011, 2017; IPCC 2013; ACIA 2007; Romanovsky et al. 2010a, b; Smith et al. 2010; Christiansen

Table 30.2 Simulated changes in the areal extent of near-surface permafrost until 2099, and degradation sensitivity

Target	RCP4.5	RCP8.5	Remarks
Loss of permafrost [10^6 km^2]	3–5	6–16	McGuire et al. (2018)
Loss of permafrost [%]	15–87	30–99	Slater and Lawrence (2013)
Loss of high-latitude permafrost [%]	49	79	Guo and Wang (2016)
degradation sensitivity of permafrost [10^6 $km^2°C^{-1}$]	–	0.8–2.3	Slater and Lawrence (2013)
Mean degradation sensitivity of permafrost [% $°C^{-1}$]	−13	−10	Guo and Wang (2016)

et al. 2010), as already described in the previous chapters in detail. This tendency is projected to continue in this century under various warming scenarios of different greenhouse gas (GHG) emission levels. The most comprehensive projection of the permafrost extent changes in this and coming centuries were carried out by the state-of-the-art Earth System Models (ESMs), or some of their suits (Table 30.2). McGuire et al. (2018) showed, using the land process models of the ESMs and two radiation scenarios (i.e., RCP4.5 for a moderate emission case, and RCP8.5 for a high emission case), that the area of near-surface permafrost (defined as the area with less-than-3-meter active layer depth) would decrease by 3–5 million km^2 under the medium emission scenario, while it would decrease by three to five times larger under the high emission scenario from the current simulated area. The spread of the simulations is, however, large among the models even for the current extent, which vary from 7.6 to 21.1 million km^2 (uncoupled terrestrial simulations; McGuire et al. 2018), 5–27 million km^2 (coupled ESMs simulations in the CMIP5; Slater and Lawrence 2013), or 14.22 million km^2 with a spread of 19.8% (indirect, physico-statistical modeling; Guo and Wang 2016).

Continuing permafrost degradation will increase the thickness of active layer, leading to larger space for seasonal and longer-term water mobility, possible increase in water storage capacity, and enhanced connectivity between surface and ground water. These subsurface hydrological changes may facilitate shift from a surface water-dominated one to a groundwater-dominated (Bring et al. 2016; Wrona et al. 2016), affecting the terrestrial Arctic wetter or drier (SWIPA 2017) with wider impacts on atmospheric, geomorphologic, and ecosystem processes. Wetter slope is more prone to landslide or thaw slump, possibly supplying more sediments and nutrients into the riverine system. The changes in balance of sensible to latent heat flux will lead to energy and water exchange between the atmosphere. The ecosystem will also be impacted with respect to habitat changes, change from terrestrial to aquatic ecosystem, and its productivity (Wrona et al. 2016).

One of the largest uncertainties on future Arctic trajectory related to permafrost is the interactions between permafrost degradation and carbon dynamics. Arctic biomes have been acting as a carbon sink in the global carbon budget (SWIPA 2011). Thawing permafrost will enhance release of greenhouse gases (CO_2, CH_4) from the

formerly frozen carbon pool through various pathways (Schuur et al. 2015; Strauss et al. 2017; Koven et al. 2013; Walther Anthony et al. 2018; Schneider von Deimling et al. 2012, 2015); e.g., conductive warming, and consequential deepening and extension of thawed layer; more abrupt exposure of deeper (older) carbon resulting from melting large amount of ground ice in ice-rich permafrost (e.g., Yedoma). Near-surface hydrological condition will also play an important role in determining either aerobic (e.g., dry surfaces, favoring productions of carbon dioxide) 2016or anaerobic (e.g., wetland and lake bed, favoring productions of methane) conditions (van Huissteden and Dolman 2012; Jorgenson et al. 2013; Schädel et al.2016 ; Zheng et al. 2019). Such a change may lead the Arctic ecosystem to a source of GHGs. While, warmer climate can favor growth of plants and expansion of forests into tundra areas, which may enhance carbon uptake from the terrestrial ecosystem. This permafrost-carbon feedback is definitely a key for the future trajectory.

Large-scale model projections, such as those by ESMs in CMIP5, are useful in drawing larger pictures of the future changes in permafrost distribution and the consequential fate of carbon stored in permafrost, as well as its hemispheric to global influences through dynamical and thermodynamical pathways. However, computational limitations currently limit the spatial and temporal resolution required to adequately represent the key processes and interactions at local scales described in this section. In addition, relevant processes such as ground subsidence, drainage network changes, terrestrial and lacustrine ecosystem including microbes, and human activities and infrastructure, are not yet adequately parameterized and validated for implementation in climate models. Offline simulations with standalone permafrost models (see Sect. 4.3.2 of SWIPA 2017) are one way to provide information on permafrost response to a changing climate but this does not incorporate important feedbacks from the changing ground thermal state. Examples of issues that are not yet readily treated in large-scale climate models include melting of massive ground ice producing irreversible changes on the overlying ground and landscapes, such as subsidence or erosions (SWIPA 2017; Strauss et al. 2017), which can alter the hydrological conditions. Changes in timing and places of ground freezing may cause contamination of freshwater resources by release of previously frozen materials (both natural, such as mercury, and industrial, such as chemicals. E.g., Schuster et al. 2018; St Pierre et al. 2018), and human waste (such as sewage and drainage).

30.6 Water for Humans and Society

With rapid changes to Arctic hydroclimate, effects are likely to be strongly noticeable across human society, not only in the Arctic but also outside it, through various feedbacks such as altering storm tracks and greenhouse reinforcement through methane release from thawing permafrost. Considering primarily the effects within the Arctic, we focus here on three key aspects of human impacts of a changing water system: water security; hydropower and infrastructure; and water and human health. A more in-depth analysis of human adaptation options to climate

change in the Arctic can be found in the recent reports of the Adaptation Actions for a Changing Arctic project, carried out under the Arctic Council's Arctic Monitoring and Assessment Programme.

As noted above and in Chaps. 6 and 24, there is a general agreement among models that annual water flows in Arctic rivers will increase. However, sub-annual changes are less certain, and will likely involve decreasing river flows in the summer, at least for some regions (Bring et al. 2016; van Vliet et al. 2013). Furthermore, in some regions the models tend to agree on substantial changes, but not on the direction of change (Bring et al. 2017). In the next decade, some high Arctic communities may face decreasing water levels in reservoirs they depend on for water supply (Bakaic and Medeiros 2016), requiring investment in increased storage capacity or water saving measures to ensure a continuous supply of drinking water. Similarly, several regions in the boreal and northern temperate latitudes have recently experienced declining surface water and groundwater levels (Bouchard et al. 2013; Nygren et al. 2018; Rodell et al. 2018). This is a relatively new phenomenon on timescales up to the last century (Bouchard et al. 2013; Nygren et al. 2018), and the development will likely get worse, as projections indicate drying of soils and decrease in soil moisture over the interior parts of the pan-Arctic drainage basin (Collins et al. 2013; Swain and Hayhoe 2015). Overall, there have not been any coordinate studies of the water security situation for various types of settlements and community types in the Arctic, which indicates that the magnitude of the problem on a pan-Arctic scale is largely unknown.

The factors that are likely to impact hydropower and infrastructure are changing hydroclimatic regime and the thawing of permafrost. Most reservoirs in the Arctic were built and used for hydropower generation; they regulate flows and redistribute water between seasons (Ye et al. 2003; McClelland et al. 2004; Yang et al. (2004a, b). If the capacity or safety margins of dams are not limiting factors, there should therefore be an opportunity to, in general, increase power production due to the overall increase in precipitation and river flow (Instanes et al. 2016). The increase in runoff, together with an increasing demand for energy, is likely to result in continued expansion of hydropower in the relatively sparsely populated parts of the Arctic. For example, in Greenland there has been 45 MW of hydropower capacity installed since 2006, a number equal in size to the island's first and largest plant, with a capacity of 45 MW (Mortensen 2014). However, for older dams built several decades ago, the increasing precipitation and changing flow regimes may also incur costs for redesign in order to comply with existing or reinforced safety regulations (Cherry et al. 2017). Infrastructure will also be affected by both hydroclimatic change and permafrost thaw. Due to a shorter season of frozen ground, operations on ice roads and on lake and river ice, important for ground transportation to remote communities, will be less stable (Prowse et al. 2009). Also, roads and buildings constructed on permafrost will be subject to risks of subsidence or collapse as frozen ground starts to thaw.

With an increasing intensity of heavy rainfall events, as projected particularly for the Arctic region (Collins et al. 2013; Hansen et al. 2014), there is generally a tendency for an increased amount of pathogens in surface water (Delpla et al. 2009;

Hunter 2003). Furthermore, as climate changes, pathogens that are presently not established locally may migrate to the Arctic region from the lower latitudes (Greer et al. 2008). It is not yet well established which waterborne diseases that are climate sensitive and may become established in Arctic regions. However, one example shows that outbreaks of Tularemia in Sweden are controlled by mosquito abundance, which in turn depends, among other factors, on summer precipitation and river flows (Rydén et al. 2011). Therefore, outbreak patterns of Tularemia and other insect-borne diseases, such as tick-borne encephalitis (TBE, Tokarevich et al. 2017) may change with an evolving hydroclimate regime. In general, while large impacts on human health from hydroclimatic changes are not certain in temperate and highly developed countries (Hunter 2003), they seem inevitable in the Arctic (Greer et al. 2008), where climate changes are faster and human communities are more vulnerable.

30.7 Summary and Future Steps

The Arctic is a system with many interwoven processes through multiple feedbacks and pathways operating over a wide range of spatial and temporal scales. To adequately capture future possible trajectories of the Arctic hydrologic system, it is important that climate models resolve key physical and bio-physical processes, as well as their interactions and feedbacks. Lack of reliable observational datasets of key variables such as precipitation, snow water equivalent, soil moisture, and evapotranspiration for validation and calibration of process models is a fundamental obstacle to further improve the representation of the Arctic climate system in earth system models. Part of this problem is related to the remoteness and harshness of the Arctic environment that imposes constraints on surface observing systems (Yang et al. 2005; Bring et al. 2016; Wrona et al. 2016). Satellite observation will be utilized more skillfully for calibrating models, as well as bridging scales between the site observations to basin-wide, and regional scales. However, the implementation of water-related processes in climate models is also more complex and challenging in the Arctic than mid-latitudes (Lique et al. 2016; Schoof 2012; Brutsaert 2005).

Some of the largest uncertainties in simulating future trajectories of the Arctic hydrologic system are net precipitation (P-E), snow water equivalent, permafrost degradation, wetting and drying of land surface, and the lateral fluxes of fresh water, including river transport. Important processes above the ground that need more research and development include rain-on-snow, sublimation from and redistribution by blowing snow, and realistic simulation of snowpack physical properties, such as wind- or sun-crust and depth hoar that can significantly impact the thermal conductivity of snow pack. As for the surface water processes, wetland and lake dynamics are crucial not only for water storage but also for carbon budget and aquatic ecosystems. Processes involving phase change of water are essential in, and many of them are specific to, the region. Thawing and subsequent degradation of

permafrost still need to be improved; it affects water holding capacity of soil layer, drainage networks by changing subsurface water connectivity, and stability of the ground. Subsidence and geomorphological changes after thermokarst and thermo-mechanical erosion can facilitate mobility of formerly frozen soils and sediments to wider areas, and/or accelerate decomposition of old carbons to release additional greenhouse gases.

Understanding the interactions between the hydrologic system and biological and human systems (including agriculture and other water resource uses) is essential. The consequence of increased river flow, and increased transport of energy, nutrients, and sediments will affect physical, thermodynamic, and biogeochemical state of the Arctic Ocean. Coordinated cross-disciplinary research and monitoring are necessary to tackle those issues (Wrona et al. 2016). There are also a large number of important cross-cutting issues involved in better understanding the future trajectory of the Arctic hydrologic system and the ecological implications. These include atmospheric moisture transport to the polar regions (Zhang et al. 2012), coupled ice-ocean-ecosystem modeling (ABA 2013; ABT 2010), freshwater ecology (Wrona et al. 2016), river sediments (Syvitski 2002), nutrients and biogeochemistry (Amon and Meon 2004), and linkages or interactions between permafrost and ecology (Schuur and Mack 2018; Martin et al. 2009). Other knowledge gaps pertain to hydrologic and ecological regime shifts in the northern regional and the degree of warming affecting these shifts. Examples include the sustainability of the boreal forest, the fate of Arctic sea ice and the Greenland Ice Sheet, and the Atlantic Meridional Overturning Circulation.

References

ABA (2013) Arctic biodiversity assessment—Status and trends in Arctic biodiversity, Conservation of Arctic Flora and Fauna (CAFF), Akureyri, Iceland, pp 674

ABT (2010) Arctic biodiversity trends 2010—Selected indicators of change. CAFF, Akureyri, Iceland, pp 124

ACIA (2007) Arctic climate impact assessment. Cambridge University Press

AMAP (2011) Snow, Water, Ice and Permafrost in the Arctic (SWIPA): climate change and the cryosphere. Arctic Monitoring and Assessment Programme (AMAP), Oslo, Norway. xii+ 538 pp

AMAP (2017) Snow, Water, Ice and Permafrost in the Arctic (SWIPA) 2017. Arctic Monitoring and Assessment Programme (AMAP), Oslo, Norway. xiv+ 269 pp

Amon RMW, Meon B (2004) The biogeochemistry of dissolved organic matter and nutrients in two large Arctic estuaries and potential implications for our understanding of the Arctic Ocean system. Mar Chem 92:311–330

Arnell NW (2004) Climate change and global water resources: SRES emissions and socio-economic scenarios. Global Environmental Change 14(1):31–52

Bakaic M, Medeiros AS (2016) Vulnerability of northern water supply lakes to changing climate and demand. Arct Sci 3:1–16. https://doi.org/10.1139/AS-2016-0029

Berezovskaya S, Yang D, Hinzman L (2005) Long-term annual water balance analysis of the Lena River. Global and Planetary Change 48:84–95

Bintanja R, Andry O (2017) Towards a rain-dominated Arctic. Nat Clim Change 7:263–267

Bintanja R, Selten FM (2014) Future increases in Arctic precipitation linked to local evaporation and sea-ice retreat. Nature 509:479–482

Biskaborn BK, Smith SL, Noetzli J, Matthes H, Vieira G, Streletskiy DA, Schoeneich P, Romanovsky VE, Lewkowicz AG, Abramov A, Allard M, Boike J, Cable WL, Christiansen HH, Delaloye R, Diekmann B, Drozdov D, Etzelmüller B, Grosse G, Guglielmin M, Ingeman-Nielsen T, Isaksen K, Ishikawa M, Johansson M, Johannsson H, Joo A, Kaverin D, Kholodov A, Konstantinov P, Kröger T, Lambiel C, Lanckman J-P, Luo D, Malkova G, Meiklejohn I, Moskalenko N, Oliva M, Phillips M, Ramos M, Sannel ABK, Sergeev D, Seybold C, Skryabin P, Vasiliev A, Wu Q, Yoshikawa K, Zheleznyak M, Lantuit H (2019) Permafrost is warming at a global scale. Nat Commun 10:264. https://doi.org/10.1038/s41467-018-08240-4

Bouchard F, Turner KW, MacDonald LA, Deakin C, White H, Farquharson N, Medeiros AS, Wolfe BB, Hall RI, Pienitz R, Edwards TWD (2013) Vulnerability of shallow subarctic lakes to evaporate and desiccate when snowmelt runoff is low. Geophys Res Lett 40. https://doi.org/10.1002/2013GL058635

Box JE, Colgan WT, Christensen TR, Schmidt NM, Lund M, Parmentier FJW, Brown R, Bhatt US, Euskirchen ES, Romanovsky VE, Walsh JE (2019) Key indicators of Arctic climate change: 1971–2017. Environ Res Lett 14(4):045010

Bring A, Fedorova I, Dibike Y, Hinzman L, Mård J, Mernild SH, Prowse TD, Semenova O, Stuefer S, Woo M-K (2016) Arctic terrestrial hydrology: a synthesis of processes, regional effects and research challenges. J Geophys Res Biogeosci 121:621–649. https://doi.org/10.1002/2015JG003131

Bring A, Shiklomanov A, Lammers RB (2017) Pan-Arctic river discharge: prioritizing monitoring of future climate change hot spots. Earths Future 5:72–92. https://doi.org/10.1002/2016EF000434

Brown R, Schuler D, Bulygina O, Derksen C, Luojus K, Mudryk L, Wang L, Yang D (2017) Arctic terrestrial snow. In: Snow, Water, Ice and Permafrost in the Arctic (SWIPA), Arctic Monitoring and Assessment Program (AMAP), Oslo, Norway, pp 25–64

Brutsaert W (2005) Hydrology. Cambridge University Press, New York, p 605

Pan GC, Kirchner PB, SKimball J, Kim Y, Du J (2018) Rain-on-snow events in Alaska, their frequency and distribution from satellite observations. Environ Res Lett 13:075004

Charalampidis C, van As D, Box JE, van den Broeke MR, Colgan WT, Doyle SH, Hubbard AL, MacFerrin M, Machguth H, Smeets CJPP (2015) Changing surface–atmosphere energy exchange and refreezing capacity of the lower accumulation area. West Greenland. -e Cryosphere 9:2163–2181

Cherry JE, Knapp C, Trainor S, Ray AJ, Tedesche M, Walker S (2017) Planning for climate change impacts on hydropower in the Far North. Hydrol Earth Syst Sci 21:133

Christiansen HH, Etzelmu¨ller B, Isaksen K, Juliussen H, Farbrot H, Humlum O, Johansson M, Ingeman-Nielsen T, Kristensen L, Hjort J, Holmlund P, Sannel ABK, Sigsgaard C, A˚kerman HJ, Foged N, Blikra LH, Pernosky MA, Ødega˚rd R (2010) The thermal state of permafrost in the Nordic area during IPY 2007–2009. Permafrost Periglac Process 21:156–181

Collins M, Knutti R, Arblaster J, Dufresne J-L, Fichefet T, Friedlingstein P, Gao X, Gutowski WJ, Johns T, Krinner G, Shongwe M, Tebaldi C, Weaver AJ, Wehner M (2013) Long-term climate change: projections, commitments and irreversibility. In: Stocker TF, Qin D, Plattner G-K, Tignor M, Allen SK, Boschung J, Nauels A, Xia Y, Bex V, Midgley PM (eds) Climate Change 2013: the physical science basis. contribution of working group I to the fifth assessment report of the intergovernmental panel on climate change. Cambridge University Press, Cambridge, United Kingdom and New York, NY, USA, pp 1029–1136

Cvijanovic I, Santer BD, Bonfils C, Lucas DD, Chiang JCH, Zimmerman S (2017) Future loss of Arctic sea-ice cover could drive a substantial decrease in California's rainfall. Nat Commun. https://doi.org/10.1038/s41467-017-01907-4

Dai A, Luo D, Song M, Liu J (2019) Arctic amplification is caused by sea-ice loss under increasing CO2. Nat Commun 10:121. https://doi.org/10.1038/s41467-018-0795

Delpla I, Jung A-V, Baures E, Clement M, Thomas O (2009) Impacts of climate change on surface water quality in relation to drinking water production. Environ Int 35:1225–1233. https://doi.org/10.1016/j.envint.2009.07.001

Déry SJ, Stadnyk TA, MacDonald MK, Gauli-Sharma B (2016) Recent trends and variability in river discharge across northern Canada. Hydrol Earth Syst Sci 20:4801–4818. https://doi.org/10.5194/hess-20-4801-2016

Doyle SH, Hubbard A, van de Wal RSW, Box JE, van As D, Scharrer K, Meierbachtol TW, Smeets PCJP, Harper JT, Johansson E, Mottram RH, Mikkelsen AB, Wilhelms F, Patton H, Christoffersen P, Hubbard B (2015) Amplified melt and flow of the Greenland ice sheet driven by late-summer cyclonic rainfall. Nat Geosci 8:647–653

Ferguson CR, Pan M, Oki T (2018) The Effect of Global Warming on Future Water Availability: CMIP5 Synthesis. Water Resources Research 54(10):7791–7819

Forbes BC et al (2016) Sea ice, rain-on-snow and tundra reindeer nomadism in Arctic Russia. Biol Lett 12:20160466. https://doi.org/10.1098/rsbl.2016.0466

Franzke CLE, Lee S, *Feldstein SB (2016) Evaluating Arctic warming mechanisms in CMIP5 models. Clim Dyn 48:3247–3260

Ge S, Yang D, Kane D (2013) Yukon River Basin Long-term (1977-2006) hydrologic and climatic analysis. Hydrol Process. https://doi.org/10.1002/hyp.9282

Georgiadi AG, Milyukova IP, Kashutina EA (2008) Recent and Projected River Runoff Changes in Permafrost Regions of Eastern Siberia (Lena River Basin). Proceeding of the Ninth International Conference on Permafrost. Fairbanks, Alaska, pp 511–515

Greer A, Ng V, Fisman D (2008) Climate change and infectious diseases in North America: the road ahead. Can Med Assoc J 178:715–722

Guo D, Wang H (2016) Permafrost degradation and associated ground settlement estimation under 2°C global warming. Clim Dyn. https://doi.org/10.1007/s00382-016-3469-9

Haine TWN, Curry B, Gerdes R, Hansen E, Karcher M, Lee C, Rudels B, Spreen G, de Steur L, Stewart KD, Woodgate R (2015) Arctic freshwater export: Status, mechanisms, and prospects. Global and Planetary Change 125:13–35

Hansen BB, Isaksen K, Benestad RE, Kohler J, Pedersen ÅØ, Loe LE, Coulson SJ, Larsen JO, Varpe Ø (2014) Warmer and wetter winters: characteristics and implications of an extreme weather event in the High Arctic. Environ Res Lett 9:114021. https://doi.org/10.1088/1748-9326/9/11/114021

Hinzman LD, Deal CJ, McGuire AD, Mernild SH, Polyakov IV, Walsh JE (2013) Trajectory of the Arctic as an integrated system. Ecol Appl 23(8):1837–1868. https://doi.org/10.1890/11-1498.1

Hunter PR (2003) Climate change and waterborne and vector-borne disease. J Appl Microbiol 94:37–46. https://doi.org/10.1046/j.1365-2672.94.s1.5.x

Instanes A, Kokorev V, Janowicz R, Bruland O, Sand K, Prowse TD (2016) Changes to freshwater systems affecting Arctic infrastructure and natural resources. J Geophys Res Biogeosci 121:567–585. https://doi.org/10.1002/2015JG003125

IPCC (2013) Climate change 2013: the physical science basis. Contribution of working group I to the fifth assessment report of the intergovernmental panel on climate change. In: Stocker TF, Qin D, Plattner G-K, Tignor M, Allen SK, Boschung J, Nauels A, Xia Y, Bex V, Midgley PM (eds). Cambridge University Press

Jorgenson MT, Harden J, Kanevskiy M, O'Donnell J, Wickland K, Ewing S, Manies K, Zhuang Q, Shur Y, Striegl R (2013) Reorganization of vegetation, hydrology and soil carbon after permafrost degradation across heterogeneous boreal landscapes. ERL 8:035017

Jun SY, Ho CH, Jeong JH, Choi YS, Kim BM (2016) Recent changes in winter Arctic clouds and their relationships with sea ice and atmospheric conditions. Tellus A 68:1. https://doi.org/10.3402/tellusa.v68.29130

Koenigk T, Brodeau L, Graversen RG, Karlsson J, Svensson G, Tjernström M, Willén U, Wyser K (2013) Arctic climate change in 21st century CMIP5 simulations with EC-Earth. Clim Dyn 40:2719–2743. https://doi.org/10.1007/s00382-012-1505-y

Koven CD, Riley WJ, Stern A (2013) Analysis of permafrost thermal dynamics and response to climate change in the CMIP5 earth system models. J Clim 26:1877–1900

Kusunoki S, Mizuta R, Hosaka M (2015) Future changes in precipitation intensity over the Arctic projected by a global atmospheric model with a 60-km grid size. Polar Sci 9:277–292

Lader R, Walsh JE, Bhatt US, Bieniek PA (2017) Projections of twenty-first-century climate extremes for Alaska via dynamical downscaling and quantile mapping. J Appl Meteorol Climatol 56:2393–2409

Lambert FH, Webb MJ (2008) Dependency of global mean precipitation on surface temperature. Geophys Res Lett 35:L16706

Lee M-Y, Hong C-C, Hsu H-H (2015) Compounding effects of warm sea surface temperature and reduced sea ice on the extreme circulation over the extratropical North Pacific and North America during the 2013–2014 boreal winter. Geophys Res Lett 42:1612–1618. https://doi.org/10.1002/2014GL062956

Lehnherr I, Louis VLS, Sharp M, Gardner AS, Smol JP, Schiff SL, Muir DC, Mortimer CA, Michelutti N, Tarnocai C, Pierre KAS (2018) The world's largest high Arctic lake responds rapidly to climate warming. Nat Commun 9(1):1290

Lenton TM (2012) Arctic climate tipping points. Ambio 41(1):10–22. https://doi.org/10.1007/s13280-011-0221-x

Lique C, Holland MM, Dibike Y, Lawrence DM, Screen J (2016) Modeling the Arctic freshwater system and its integration in the global system: lessons learned and future challenges. J Geophys Res Biogeosci 121. https://doi.org/10.1002/2015jg003120

Lu J, Cai M (2009) Seasonality of polar surface warming amplification in climate simulations. Geophys Res Lett 36:L16704

MacDonald MK, Stadnyk TA, Déry SJ, Braun M, Gustafsson D, Isberg K, Arheimer B (2008) Impacts of 1.5 and 2.0°C Warming on Pan-Arctic River Discharge Into the Hudson Bay Complex Through 2070. GRL 45(15):7561-7570

Manabe S, Milly PCD, Wetherald R (2004) Simulated long-term changes in river discharge and soil moisture due to global warming / Simulations à long termede changements d'écoulement fluvial et d'humidité du sol causés par le réchauffement global. Hydrological Sciences Journal 49(4):625–642. https://doi.org/10.1623/hysj.49.4.625.5442

Martin PD, Jenkins JL, Adams FJ, Jorgenson MT, Matz AC, Payer DC, Reynolds PE, Tidwell AC, Zelenak JR (2009) Wildlife response to environmental Arctic change: predicting future habitats of Arctic Alaska. Report of the Wildlife Response to Environmental Arctic Change (WildREACH): predicting future habitats of Arctic Alaska workshop, 17–18 November 2008. Fairbanks, Alaska: U.S. Fish and Wildlife Service. pp 138

McClelland JW, Holmes RM, Peterson BJ, Stieglitz M (2004) Increasing river discharge in the Eurasian Arctic: consideration of dams, permafrost thaw, and fires as potential agents of change. J Geophys Res 109:D18102. https://doi.org/10.1029/2004JD004583

McGuire DA, Lawrence DM, Koven C, Clein JS, Burke E, Chen G, Jafarov E, MacDougall AH, Marchenko S, Nicolsky D, Peng S, Rinke A, Ciais P, Gouttevin I, Hayes DJ, Ji D, Krinner G, Moore JC, Romanovsky V, Schädel C, Schaefer K, Schuur EAG, Zhuang Q (2018) Dependence of the evolution of carbon dynamics in the northern permafrost region on the trajectory of climate change. PNAS 115:3882–3887

Mernild SH, Liston GE, Hiemstra CA (2014) Northern Hemisphere glaciers and ice caps surface mass balance and contribution to sea-level rise. J Clim 27:6051–6073

Morrison AL, Kay JE, Frey WR, Chepfer H, Guzman R (2019) Cloud response to Arctic sea ice loss and implications for future feedback in the CESM1 climate model. J Geophys Res: Atmos 124(2):1003–1020

Mortensen BOG (2014) Exploiting hydropower in greenland: climate, security of supply, environmental risks and energy-intensive industries. Yearb. Polar Law 6:36

Niittynen P, Luoto M (2018) The importance of snow in species distribution models of arctic vegetation. Ecography 41(6):1024–1037

Nohara D, Kitoh A, Hosaka M, Oki T (2006) Impact of climate change on river discharge projected by multi-model ensemble. J. Hydrometeorol. 7:1076–1089

Nygren M, Haaf E, Rossi P, Kløve B, Barthel R (2018) Investigating hydrogeologic controls on groundwater drought hazard in Sweden and Finland

Pan CG, Kirchner PB, Kimball JS, Kim Y, Du J (2018) Rain-on-snow events in Alaska, their frequency and distribution from satellite observations. Environ Res Lett 13:075004

Peterson BJ, Holmes RM, McClelland JW, Vörösmarty CJ, Lammers RB, Shiklomanov AI, Shiklomanov IA, Rahmstorf S (2002) Increasing River Discharge to the Arctic Ocean. Science 298:2171–2173

Pithan F, Mauritsen T (2014) Arctic amplification dominated by temperature feedbacks in contemporary climate models. Nat Geosci 7(3):181

Prowse TD, Furgal C, Chouinard R, Melling H, Milburn D, Smith SL (2009) Implications of climate change for economic development in Northern Canada: energy, resource, and transportation sectors. AMBIO J Hum Environ 38:272–281. https://doi.org/10.1579/0044-7447-38.5.272

Rodell M, Famiglietti JS, Wiese DN, Reager JT, Beaudoing HK, Landerer FW, Lo M-H (2018) Emerging trends in global freshwater availability. Nature 557:651. https://doi.org/10.1038/s41586-018-0123-1

Romanovsky V, Smith SL, Christiansen HH (2010a) Permafrost thermal state in the polar northern hemisphere during the international polar year 2007–2009: a synthesis. Permafrost Periglac Process 21:106–116

Romanovsky VE, Drozdov DS, Oberman NG, Malkova GV, Kholodov AL, Marchenko SS, Moskalenko NG, Sergeev DO, Ukraintseva NG, Abramov AA, Gilichinsky DA, Vasiliev AA (2010b) Thermal state of permafrost in Russia. Permafrost Periglac Process 21:106–116. https://doi.org/10.1002/ppp.683

Rydén P, Björk R, Schäfer ML, Lundström JO, Petersén B, Lindblom A, Forsman M, Sjöstedt A, Johansson A (2011) Outbreaks of tularemia in a boreal forest region depends on mosquito prevalence. J Infect Dis 205:297–304

Saito K, Zhang T, Yang D, Marchenko S, Barry RG, Romanovsky V, Hinzman L (2013) Influence of the physical terrestrial Arctic in the eco-climate system. Ecol Appl 23(8):1778–1797

Schädel C, Bader M, Schuur E et al (2016) Potential carbon emissions dominated by carbon dioxide from thawed permafrost soils. Nature Clim Change 6:950–953. https://doi.org/10.1038/nclimate3054

Shiklomanov IA, Georgievsky VYu, Shalygin AL, Georgievsky MV, Golovanov OPh, Shiklomanov AI (2008) Chapter 11: Water Resources in Future in monograph: Water Resources of Russia and their Use. Shiklomanov IA (ed.) Nauka, St.Petersburg, 441-489 (In Russian)

Shiklomanov AI, Lammers RB (2009) Record Russian river discharge in 2007 and the limits of analysis. Environ. Res. Lett. 4:045015

Shiklomanov IA, Lins G (1991) Effect of climate changes on hydrology and water management. Meteorology and Hydrology 4:51–66 (in Russian)

Shiklomanov IA, Shiklomanov AI (2003) Climatic change and the dynamics of river runoff into the Arctic Ocean. Water Resour 30:593–601

Shkolnik I, Pavlova T, Efimov S, Zhuravlev S (2018) Future changes in peak river flows across northern Eurasia as inferred from an ensemble of regional climate projections under the IPCC RCP8.5 scenario. Clim Dyn 50:215–230. https://doi.org/10.1007/s00382-017-3600-6

Schneider von Deimling T, Meinshausen M, Levermann A, Huber V, Frieler K, Lawrence DM, Brovkin V (2012) Estimating the near-surface permafrost-carbon feedback on global warming. Biogeosciences 9:649–665

Schneider von Deimling T, Grosse G, Strauss J, Schirrmeister L, Morgenstern A, Schaphoff S, Meinshausen M, Boike J (2015) Observation-based modelling of permafrost carbon fluxes with accounting for deep carbon deposits and thermokarst activity. Biogeosciences 12:3469–3488

Schoof JT (2012) Scale issues in the development of future precipitation scenarios. J Contemp Water Res Educ 147:8–16
Schuster PF, Schaefer KM, Aiken GR, Antweiler RC, Dewild JF, Gryziec JD … Zhang T (2018) Permafrost stores a globally significant amount of mercury. Geophys Res Lett 45:1463–1471. https://doi.org/10.1002/2017gl075571
Schuur EAG, Mack MC (2018) Ecological response to permafrost thaw and consequences for local and global ecosystem services. Annu Rev Ecol Evol Syst 49:279–301
Schuur EAG, McGuire AD, Schädel C, Grosse G, Harden JW, Hayes DJ, Hugelius G, Koven CD, Kuhry P, Lawrence DM, Natali SM, Olefeldt D, Romanovsky VE, Schaefer K, Turetsky MR, Treat CC, Vonk JE (2015) Climate change and the permafrost carbon feedback. Nature 520:171–179. https://doi.org/10.1038/nature14338
Screen JA, Simmonds I (2010) The central role of diminishing sea ice in recent Arctic temperature amplification. Nature 464:1334–1337
Serreze MC, Francis JA (2006) The Arctic amplification debate. Clim Change 76:241–264
Sherwood SC, Roca R, Weckwerth TM (2010) Tropospheric water vapor, convection, and climate. Rev Geophys 48:RG2001
Shu Q, Qiao F, Song Z, Zhao J, Li X (2018) Projected freshening of the Arctic Ocean in the 21st century. JGR Oceans 123:9232–9244. https://doi.org/10.1029/2018JC014036
Slater AG, Lawrence DM (2013) Diagnosing present and future permafrost from climate models. J Clim 26:5608–5623
Smith SL, Romanovsky VE, Lewkowicz AG, Burn CR, Allard M, Clow GD, Yoshikawa K, Throop J (2010) Thermal state of permafrost in North America: a contribution to the international polar year. Permafrost Periglac Process 21:117–135. https://doi.org/10.1002/ppp.690
St. Pierre KA, Zolkos S, Shakil S, Tank SE, St. Louis VL, Kokelj SV (2018) Unprecedented increases in total and methyl mercury concentrations downstream of retrogressive thaw slumps in the western Canadian Arctic. Environ Sci Technol 52:14099–14109
Strauss J, Schirrmeister L, Grosse G, Fortier D, Hugelius G, Knoblauch C, Romanovsky V, Schädel C, Schneider von Deimling T, Schuur EAG, Shmelev D, Ulrich M, Veremeeva A (2017) Deep Yedoma permafrost: a synthesis of depositional characteristics and carbon vulnerability. Earth-Sci Revi 172:75–86
Swain S, Hayhoe K (2015) CMIP5 projected changes in spring and summer drought and wet conditions over North America. Clim Dyn 44:2737–2750. https://doi.org/10.1007/s00382-014-2255-9
Syvitski J (2002) Sediment discharge variability in Arctic rivers: implications for a warmer future. Polar Res 21(2):323–330. https://doi.org/10.3402/polar.v21i2.6494
Taylor PC et al (2013) A decomposition of feedback contributions to polarwarming amplification. J Clim 26:7023–7043
Tedesco M, Fettweis X, van den Broeke MR, van de Wal RSW, Smeets CJPP, van de Berg WJ, Serreze MC, Box JE (2011) e role of albedo and accumulation in the 2010 melting record in Greenland. Environ Res Lett 6:014005. https://doi.org/10.1088/1748-9326/6/1/014005
Tokarevich N, Tronin A, Gnativ B, Revich B, Blinova O, Evengard B (2017) Impact of air temperature variation on the ixodid ticks habitat and tick-borne encephalitis incidence in the Russian Arctic: the case of the Komi Republic. Int J Circumpolar Health 76:1298882
van Huissteden J, Dolman AJ (2012) Soil carbon in the Arctic and the permafrost carbon feedback. Current Opinion in Environmental Sustainability 4(5):545–551
van Vliet MTH, Franssen WHP, Yearsley JR, Ludwig F, Haddeland I, Lettenmaier DP, Kabat P (2013) Global river discharge and water temperature under climate change. Glob Environ Change 23:450–464. https://doi.org/10.1016/j.gloenvcha.2012.11.002
Vihma T, Screen J, Tjernström M, Newton B, Zhang X, Popova V, Deser C, Holland M, Prowse T (2016) The atmospheric role in the Arctic water cycle: a review on processes, past and future changes, and their impacts. J Geophys Res Biogeosci 121:586–620. https://doi.org/10.1002/2015JG003132

Walther Anthony K, von Deimling TS, Nitze I, Frolking S, Emond A, Daanen R, Anthony P, Lindgren P, Jones P, Grosse G (2018) 21st-century modeled permafrost carbon emissions accelerated by abrupt thaw beneath lakes. Nat Commun 9:3262. https://doi.org/10.1038/s41467-018-05738-9

Wassmann P, Lenton TM (2012) Arctic tipping points in an Earth system perspective. Ambio 41 (1):1–9. https://doi.org/10.1007/s13280-011-0230-9

Westermann S, Boike J, Langer M, Schuler TV, Etzelmüller B (2011) Modeling the impact of wintertime rain events on the thermal regime of permafrost. -e Cryosphere 5:945–959

Wrona FJ, Johansson M, Culp JM, Jenkins A, Mård J, Myers-Smith IH, Prowse TD, Vincent WF, Wookey PA (2016) Transitions in Arctic ecosystems: ecological implications of a changing hydrological regime. J Geophys Res Biogeosci 121:650–674. https://doi.org/10.1002/2015JG003133

Yang D, Ye B, Kane DL (2004a) Streamflow changes over Siberian Yenisei river basin. J Hydrol 296(1–4):59–80

Yang D, Ye B, Shiklomanov A (2004b) Discharge characteristics and changes over the Ob River watershed in Siberia. J Hydrometeorol 5(4):595–610

Yang D, Kane D, Zhang Z, Legates D, Goodison B (2005) Bias corrections of long-term (1973–2004) daily precipitation data over the northern regions. Geophys Res Lett 32(19). https://doi.org/10.1029/2005gl024057

Ye B, Yang D, Kane DL (2003) Changes in Lena River streamflow hydrology: human impacts versus natural variations. Water Resour Res 39(7):1–14. https://doi.org/10.1029/2003WR001991

Zhang X, He J, Zhang J, Polyakov I, Gerdes R, Inoue J, Wu P (2012) Enhanced poleward moisture transport and amplified northern high-latitude wetting trend. Nat Clim Change 3:47–51

Zheng J, Thornton PE, Painter SL, Gu B, Wullschleger SD, Graham DE (2019) Modeling anaerobic soil organic carbon decomposition in Arctic polygon tundra: insights into soil geochemical influences on carbon mineralization. Biogeosciences 16:663–680. https://doi.org/10.5194/bg-16-663-2019

Dr. Kazuyuki Saito is a Senior Research Scientist of Japan Agency for Marine-Earth Science and Technology (JAMSTEC), Yokohama, Japan. His primary research interest is in the land–climate interactions of the cryosphere over seasonal to glacial–interglacial timescales. His more recent research has addressed permafrost variability and functionality, in the Arctic and other cold regions. He received a B.E. and M.E. in Mathematical Engineering from the University of Tokyo, an M.S. in Climate Physics and Chemistry from the Massachusetts Institute of Technology, and a Ph.D. in the Atmospheric Science from Nagoya University.

Dr. John E. Walsh is the Chief Scientist of the International Research Center and President's Professor of Global Change at the University of Alaska, Fairbanks, USA. He is also an emeritus faculty member of the University of Illinois. He has been involved in Arctic research and education for more than 40 years. His more recent research has addressed Arctic climate and weather variability, with an emphasis on the drivers of cryospheric variations over seasonal to multidecadal timescales. He has served as lead author for assessment reports of the Intergovernmental Panel on Climate Change, the Arctic Monitoring and Assessment Programme, and the U.S. National Climate Assessment. He has also co-authored a textbook, Severe and Hazardous Weather. He received a B.S. in Mathematics from Dartmouth College and a Ph.D. in Meteorology from the Massachusetts Institute of Technology.

Dr. Arvid Bring has been a Senior Researcher at the Department of Physical Geography at Stockholm University until 2019. He is presently at Formas, a Swedish Research Council for Sustainable Development. He has authored over 25 peer-reviewed publications in scientific journals, with an emphasis on climate, water, and water information in the Arctic. He has also been responsible for the Master's program in Hydrology, Hydrogeology and Water Resources at Stockholm University, and acted as leader for the research area for Hydrosphere, Cryosphere and Climate at the Bolin Centre for Climate Research. He received an M.Sc. in Environmental Engineering from KTH Royal Institute of Technology and a Ph.D. in Physical Geography from Stockholm University.

Ross Brown is a recently retired climate scientist from the Climate Research Division of Environment and Climate Change Canada (ECCC), with more than 30 years of experience investigating variability and change in snow cover, and over 70 publications as lead or co-author in refereed journals and proceedings. He was the lead author of the Arctic terrestrial snow cover chapter in the Arctic Council's Snow, Water, Ice and Permafrost in the Arctic (SWIPA) 2017 assessment report, and a contributing author for several Intergovernmental Panel on Climate Change (IPCC) Assessment Reports between 1995 and 2013. He graduated from McGill University in 1980 with an M. Sc. in Physical Geography with specialization in climatology. He is currently working part-time for ECCC until December 2020 and is located at the Ouranos Climate Change Consortium in Montreal where he has collaborated in Ouranos projects since 2005, most notably the ArcticNet Integrated Regional Impact Studies for the Canadian Arctic.

Dr. Alexander I. Shiklomanov received M.Sc. (1983) and Ph.D. (1996) degrees from Russian Hydrometeorological State University, St. Petersburg. Since 1983, he has been working at the Arctic and Antarctic Research Institute (AARI), in Saint Petersburg, Russia; and in 1997 he joined the Earth Systems Research Center at the University of New Hampshire, USA. The focuses of his research are on cold region and Eurasian hydroclimatology, hydrological and water management modeling and analysis. Research interests include hydrological monitoring systems; water balance and streamflow routing models; human activity and its influence on hydrology; climate change and hydrological systems; and effect of land cover and land use change on hydrology. He has more than 60 publications including more than 45 in peer-reviewed journals. He is a co-developer of several regional hydrographic databases and a reviewer of multiple national and international scientific journals. Dr. Shiklomanov has been a Principal Investigator for many research projects sponsored by NASA and NSF.

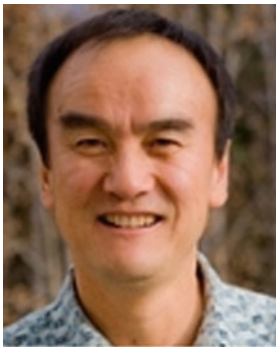

Dr. Daqing Yang is a Research Scientist at the Watershed Hydrology and Ecology Research Division, Environment and Climate Change Canada. He is also Affiliate Research Professor at the International Arctic Research Center, Univ. of Alaska Fairbanks. Over the past 25 years, he has conducted cryosphere system research in China, Canada, Japan, USA, and Norway. His primary research activities/interests include cold region hydrology and climate, particularly Arctic large river streamflow regime and change, snow cover and snowfall measurements, climate change and human impact to regional hydrology, and applications of remote sensing in cold regions. He has served as journal editor and subject editor for IAHS publications (cold region hydrology, northern research basin water balance, and cold/mountain region hydrological systems under climate change), and WMO technical reports (solid precipitation measurement intercomparison and integrated global observing strategy cryosphere theme). He also contributed as review and/or author to the IPCC Reports, and the Arctic Council's Snow, Water, Ice and Permafrost in the Arctic (SWIPA 2017 and follow up) assessment. His current research focuses on investigating the impacts of climate variability/change and human activities on hydrologic system across the broader northern regions.

Correction to: Arctic Hydrology, Permafrost and Ecosystems

Daqing Yang and Douglas L. Kane

Correction to:
D. Yang and D. L. Kane (eds.), *Arctic Hydrology, Permafrost and Ecosystems*,
https://doi.org/10.1007/978-3-030-50930-9

In an earlier version of this book, the affiliation of the volume editor "Daqing Yang" was incorrect. This has been corrected. Correct Affiliations is Daqing Yang, Watershed Hydrology and Ecology, Research Division, Water Science and Technology Directorate, Environment and Climate Change Canada, Victoria, BC, Canada.

The updated version of the book can be found at
https://doi.org/10.1007/978-3-030-50930-9

D. Yang and D. L. Kane (eds.), *Arctic Hydrology, Permafrost and Ecosystems*,
https://doi.org/10.1007/978-3-030-50930-9_31